THE SOVIET-AMERICAN CONFERENCE ON COSMOCHEMISTRY OF THE MOON AND PLANETS

CASE FILE
COPY



NATIONAL AERONAUTICS AND SPACE ADMINISTRATION

NASA SP-370
Part 1

THE SOVIET-AMERICAN CONFERENCE ON COSMOCHEMISTRY OF THE MOON AND PLANETS

Edited by
John H. Pomeroy
NASA Headquarters
and
Norman J. Hubbard
NASA Johnson Space Center

A conference held in Moscow, U.S.S.R.,
June 4-8, 1974

Scientific and Technical Information Office 1977
NATIONAL AERONAUTICS AND SPACE ADMINISTRATION
Washington, D.C.

For sale by the Superintendent of Documents,

U.S. Government Printing Office, Washington, D.C. 20402
(2-Part Set; Sold in Sets Only) Stock Number 033–000–00633–1
Library of Congress Catalog Card Number 75–600013

The joint Soviet-American Conference on the Cosmochemistry of the Moon and Planets was held in Moscow, June 4–8, 1974. It was proposed by the Soviets, primarily as a conference on the chemistry of the Moon, and was agreed to by the United States during the joint meeting on cooperation in space held in August 1971. At that time, we envisioned that it would occur within one to two years. Several factors led to delaying the date of the Conference, the main ones being a problem of scheduling around the annual Houston Lunar Science Conferences and, more important, a desire to wait until the end of the Apollo program so that the scientific contributions might not become outdated within a few months. During the gestation period between 1971 and 1973, it became evident to both the United States and the USSR that data from the successful U.S. Mariner 9 mission to Mars and the Soviet Venera mission to Venus were not only pertinent but essential to the lunar discussions, as were new data and theories on Jupiter, comets, and meteorites. Thus, the content of the Conference was expanded to become "cosmochemical" and to include the planets in the broadest sense. I believe that this format, emphasizing comparative planetology, will become the norm for all similar future conferences.

I judge the Conference to have been a success. Papers were lucidly presented, most visual material was prepared especially for the Conference, the Soviet interpreters and translators were excellent, and significant exchanges of ideas and data did occur on the personal level. A key ingredient in this, evident in the preparatory work leading up to and continuing at the Conference, was a clear recognition by all concerned of the scientific contributions by both the United States and the USSR and a gratifying lack of protocol and paperwork. The tone for this was admirably set by Academician A. P. Vinogradov.

The formal papers of the Conference, contained in this volume and in a companion volume printed in the USSR, should stand for many years as one of the best consolidated treatises on the state of our knowledge of planetology and cosmochemistry. The other benefits of the joint Conference, such as an increased respect for each other's ideas and capabilities, cannot be similarly committed to paper but may, in the long run, be the more valuable.

NOEL W. HINNERS
Associate Administrator
for Space Science

Page intentionally left blank

Page intentionally left blank

Foreword

In the course of the last several years the possibility has developed for extensive studies of the material of the Moon, thanks to samples brought back from the Moon's surface by man or with the help of automatic space stations. Samples of soil and rocks have been returned from five maria: Mare Tranquillitatis, Oceanus Procellarum, Mare Imbrium, Mare Serenitatis, and Mare Fecunditatis; and from three terra regions of the Moon's nearside: the Fra Mauro region, the central highlands near the crater Descartes, and the highland region between Mare Fecunditatis and Mare Crisium. Through extensive study of these samples by scientists of many countries, a huge quantity of data has been accumulated about the physical, chemical, petrographic, mineralogical, and geochemical features of lunar rocks. Along with the great general similarity of some surface rocks of the Moon, especially lunar basalts, to basic igneous rocks of the Earth's crust, i.e., tholeiitic basalts, differences also have been found between the character of lunar rocks and that of terrestrial rocks. Many cardinal questions arise on comprehensive examination of all the extensive data that have resulted from study of the material of the Moon and planets.

The present volumes contain papers presented at the Soviet-American Conference on the Cosmochemistry of the Moon and Planets held in Moscow from the 4th to the 8th of June, 1974. The basic goal of the conference was consideration of the origin of the planets of the solar system, based on the physical and chemical data obtained by study of the material of the Moon and planets.

Papers at the conference were presented in the following sessions:

1. Differentiation of the material of the Moon and planets
2. The thermal history of the Moon
3. Lunar gravitation and magnetism
4. Chronology of the Moon, planets, and meteorites
5. The role of exogenic factors in the formation of the lunar surface
6. Cosmochemical hypotheses about the origin and evolution of the Moon and planets
7. New data about the planets Mercury, Venus, Mars, and Jupiter

The results presented in the papers are of exceptional scientific interest since on the one hand they contain new knowledge about the matter of the Moon and planets, while on the other they summarize significant material accumulated during recent years as the result of spacecraft missions to the Moon, Venus, Mars, Mercury, and Jupiter.

During consideration of the problem of accretion of the Moon and other planets, attention has turned to the possibility of an inhomogeneous protoplanetary nebula. Differentiation of the matter of the Moon into concentric layers, and especially the formation of a lunar crust, has directed

much attention to the mechanism of formation, composition, and thickness of the lunar crust. Hypotheses about the formation of the mascons of the circular maria on the Moon were reviewed during the conference.

Significant material about the mineralogical, petrographic, and chemical composition of igneous lunar rocks (basalts, norites, anorthosites) as well as the lunar regolith, permitted the presentation of ideas about their formation to be based on comparison with analogous terrestrial rocks.

Significant interest was aroused by consideration of questions about the composition of rocks, particularly those within the interior of the Moon. Numerous data give no indication of a metallic core in the Moon. Problems of magnetic, gravitational, and thermal fields of the Moon were considered. Papers also dealt with the role of exogenic factors in the transformation of rocks on the lunar surface and in the development of the lunar landscape. Especially memorable were the new images of the surface of Mars, which is significantly more complex than the lunar surface, and the images of the surface of Mercury, whose relief is analogous to that of the lunar surface.

A view was given of "lunar" topography found on Venus by Earth based observations, and a movie was shown which illustrated the dynamics of the cloud layer of Venus. Finally, from the results of an American automatic spacecraft, scientists acquired the first data on the possible composition of the outer layers of Jupiter.

All of this taken together permitted participants of the conference to gain a fuller understanding of, and to propose models for, the origin and evolution of the Moon and planets of the solar system.

The work presented at the conference contains extensive and original information about the cosmochemistry of the Moon and planets.

Academician A. P. Vinogradov
Academy of Sciences of the USSR

Contents

Page

Preface ---- iii
Noel W. Hinners

Foreword ---- v
Vinogradov

DIFFERENTIATION OF LUNAR AND PLANETARY MATTER

Differentiation of the Matter of the Moon ---- 5
A. P. Vinogradov

A Survey of Lunar Rock Types and Comparison of the Crusts of Earth and Moon ---- 35
John A. Wood

Geochemical Zoning and Early Differentiation in the Moon ---- 55
S. R. Taylor and P. Jakeš

Evolution of the Moon: the 1974 Model ---- 63
Harrison H. Schmitt

Petrogenesis of Lunar Rocks: Rb-Sr Constraints and Lack of H_2O ---- 81
Arden L. Albee and Alexander J. Gancarz

Lunar Highland Rock Types: Their Implications for Impact-Induced Fractionation ---- 91
W. C. Phinney, J. L. Warner, and C. H. Simonds

Lunar Igneous Rocks and the Nature of the Lunar Interior ---- 127
James Fred Hays and David Walker

A Chemical Model for Lunar Non-Mare Rocks ---- 137
Norman J. Hubbard and J. Michael Rhodes

Lunar Elemental Analysis Obtained from the Apollo Gamma-Ray and X-Ray Remote Sensing Experiment ---- 153
J. I. Trombka, J. R. Arnold, I. Adler, A. E. Metzger, and R. C. Reedy

Comparison of Lunar Rocks and Meteorites: Implications to Histories of the Moon and Parent Meteorite Bodies ---- 183
Martin Prinz, R. V. Fodor, and Klaus Keil

Radioactivity of the Moon, Planets, and Meteorites ---- 201
Yu. A. Surkov and G. A. Fedoseyev

The Effect of Temperature and Pressure on the Distribution of Iron Group Elements Between Metal and Olivine Phases in the Process of Differentiation of Protoplanetary Material ---- 219
A. P. Vinogradov, N. P. Il'yin, and L. N. Kolomeytseva

The Chemical Composition of the Cores of the Terrestrial Planets and the Moon ---- 231
O. L. Kuskov and N. I. Khitarov

Page

To the Problem About the Origin of Lunar Maria and Continents (Mössbauer Investigations) ---- 243
T. V. Malysheva

The Surface Abundance and Stratigraphy of Lunar Rocks from Data About Their Albedo ---- 253
V. V. Shevchenko

New Data for the Luna 20 Core and a Survey of Published Chemical Data ---- 259
N. J. Hubbard, A. P. Vinogradov, G. I. Ramendik, and M. S. Chupakhin

Chemical Composition of Crystalline Rock Fragments from Luna 16 and Luna 20 Fines ---- 263
A. Cimbálníková, M. Palivcová, J. Fŕana, and A. Maśtalka

Investigation of the Composition of the Luna 16 Lunar Sample ---- 277
L. Bakos, M. Chayka, L. Cher, A. Cheke, N. N. Dogadkin, A. Elek, K. Kulchar, A. Nagy, D. L. Nagy, E. Szabo, B. Forzats, and E. Zemplen

THERMAL HISTORY OF THE MOON

In-Situ Measurements of Lunar Heat Flow ---- 283
Marcus G. Langseth and Stephen J. Keihm

The Evolution of the Moon and the Terrestrial Planets ---- 295
M. Nafi Toksöz and David H. Johnston

Heat Flow and Thermal History of the Moon ---- 329
Ye. A. Lyubimova

Calculations of the Moon's Thermal History at Different Concentrations of Radioactive Elements, Taking Into Account Differentiation on Melting ---- 347
O. I. Ornatskaya, Ya. I. Al'ber, and I. L. Ryanzantseva

Riddles About the Origin and Thermal History of the Moon ---- 367
B. Yu. Levin and S. V. Mayeva

LUNAR MAGNETISM AND GRAVITY

Results From the Apollo Passive Seismic Experiment ---- 389
Gary Latham, Yosio Nakamura, James Dorman, Frederick Duennebier, Maurice Ewing, and David Lammlein

Lunar Mascons ---- 403
V. N. Zharkov and A. P. Trubitsyn

Some Geologic Observations Concerning Lunar Geophysical Models ---- 407
James W. Head

Magnetic and Dielectric Properties of Lunar Samples ---- 417
D. W. Strangway, G. W. Pearce, and G. R. Olhoeft

Magnetic Field in Le Monnier Bay According to Data of Lunokhod 2 ---- 433
Sh. Sh. Dolginov, Ye. G. Yeroshenko, L. N. Zhuzgov, V. A. Sharova, G. A. Vnuchkov, B. A. Okulessky, and A. T. Bazilevsky

Deep Electromagnetic Sounding of the Moon with Lunokhod 2 Data ---- 443
L. L. Van'yan, I. V. Yegorov, and E. B. Faynberg

Lunar Electrical Conductivity, Permeability, and Temperature from Apollo Magnetometer Experiments ---- 447
P. Dyal, C. W. Parkin, and W. D. Daily

Page

On the Mechanism of the Magnetic Dynamo of the Planets ---- 493
Sh. Sh. Dolginov

The Intensity of the Ancient Lunar Field from Magnetic Studies on Lunar Samples ---- 499
A. Stephenson, D. W. Collinson, and S. K. Runcorn

CHRONOLOGY OF THE MOON, PLANETS, AND METEORITES

Early History of the Moon: Implications of U-Th-Pb and Rb-Sr Systematics ---- 507
Mitsunobu Tatsumoto, Paul D. Nunes, and Daniel M. Uhruh

^{39}Ar–^{40}Ar Dating of Basalts and Rock Breccias from Apollo 17 and the Malvern Achondrite ---- 525
T. Kirsten and P. Horn

The Exposure History of the Apollo 16 Site: An Assessment Based on Methane and Hydrolysable Carbon Measurements ---- 541
C. T. Pillinger, G. Eglinton, A. P. Gowar, A. J. T. Jull, and J. R. Maxwell

Pre-Mare Cratering and Early Solar System History ---- 553
G. W. Wetherill

THE ROLE OF EXOGENIC FACTORS IN THE FORMATION OF THE LUNAR SURFACE

The Role of Exogenic Factors in the Formation of the Lunar Surface ---- 571
K. P. Florenskiy, A. T. Bazilevskiy, and A. V. Ivanov

Microcraters on Lunar Samples ---- 585
H. Fechtig, W. Gentner, J. B. Hartung, K. Nagel, G. Neukum, E. Schneider, and D. Storzer

The Micrometeoroid Complex and Evolution of the Lunar Regolith ---- 605
F. Hörz, D. A. Morrison, D. E. Gault, V. R. Oberbeck, W. L. Quaide, and J. F. Vedder, D. E. Brownlee, and J. B. Hartung

Lunar Highlands Breccias Generated by Major Impacts ---- 637
Odette B. James

Meteoritic Material on the Moon ---- 659
John W. Morgan, R. Ganapathy, Hideo Higuchi, and Edward Anders

Primary Cosmic Rays on the Lunar Surface ---- 691
S. N. Vernov and A. K. Lavrukhina

Results of Special Mechanical Analyses of Luna 16 Material ---- 697
H. Stiller, H. Vollstädt, R. Wäsch, P. Bankwitz, E. Bankwitz, F. C. Wagner, and J. Schön

The Analysis of Various Size, Visually Selected and Density and Magnetically Separated Fractions of Luna 16 and 20 Samples ---- 703
The Royal Society Lunar Sample Investigation Team (G. Eglinton, A. P. Gowar, A. J. T. Jull, C. T. Pillinger, S. O. Agrell, J. E. Agrell, J. V. P. Long, S. H. U. Bowie, P. R. Simpson, R. D. Beckinsale, J. J. Durham, G. Turner, P. H. Cadogan, T. C. Gibb, R. Greatrex, N. N. Greenwood, D. W. Collinson, S. K. Runcorn, A. Stephenson, S. A. Durrani, J. H. Fremlin, F. S. W. Hwang, and H. A. Khan)

Mössbauer Spectroscopy of Iron in the Luna 20 Regolith ---- 729
T. Zemcík and K. Raclavsky

The Main Pecularities of the Urocesses of the Deformation and Destruction of Lunar Soil ---- 735
A. K. Leonovich, V. V. Gromov, A. D. Dmitriyev, V. N. Penetrigov, P. S. Semenov, and V. V. Shvarev

Page

The Radiation History of Matter Returned by the Soviet Automatic Stations Luna 16 and Luna 20, According to Track Studies ---- 745
L. L. Kashkarov, L. I. Genayeva, and A. K. Lavrukhina

Antipodes on the Moon ---- 755
Yu. N. Lipsky and Zh. F. Rodionova

Measurement of the Optical Properties of Lunar Rocks in the Transition Zone, Resulting from Observations Made by Lunokhod–2 ---- 763
Yu. N. Lipskiy and V. V. Shevchenko

COSMOCHEMICAL HYPOTHESES OF THE ORIGIN AND EVOLUTION OF THE MOON AND PLANETS

Clues in the Rare Gas Isotopes to Early Solar System History ---- 771
John H. Reynolds

Heterogeneities in the Solar Nebula ---- 781
Robert N. Clayton, Lawrence Grossman, Toshiko K. Mayeda, and Naoki Onuma

Chemical Fractionation in the Solar Nebula ---- 787
Lawrence Grossman

Time Scale for the Formation of the Earth and Planets and Its Role in Their Geochemical Evolution ---- 797
V. S. Safronov

Mechanical Processes Affecting Differentiation of Proto-Lunar Material ---- 805
W. M. Kaula

The Origin of the Moon ---- 815
Ye. L. Ruskol

Formation and Composition of the Moon ---- 823
Don L. Anderson

NEW DATA ON THE PLANETS

The Interior Structure of Jupiter (Consequences of Pioneer 10 Data) ---- 849
R. Smoluchowski

The Magnetic Field of Mars Estimated from the Data of Plasma Measurements by Soviet Artificial Satellites of Mars ---- 859
K. I. Gringauz, V. V. Bezrukikh, T. K. Breus, M. I. Verigin, and A. P. Remizov

Television Observations of Mercury by Mariner 10 ---- 865
Bruce C. Murray, Michael J. S. Belton, G. Edward Danielson, Merton E. Davies, Donald E. Gault, Bruce Hapke, Brian O'Leary, Robert G. Strom, Verner Suomi, and Newell Trask

Studies of Chemical Abundances in the Outer Solar System ---- 887
Tobias Owen

The Use of Ground-Based Telescopes in Determining the Composition of the Surfaces of Solar System Objects ---- 893
Thomas B. McCord and John B. Adams

Comets: Data, Problems, and Objectives ---- 923
Fred L. Whipple

part 1

Page intentionally left blank

Page intentionally left blank

section 1

Differentiation of Lunar and Planetary Matter

Page intentionally left blank

Page intentionally left blank

Differentiation of the Matter of the Moon

A. P. Vinogradov
V. I. Vernadskiy Institute of Geochemistry
and Analytical Chemistry
Academy of Sciences,
Moscow, U.S.S.R.

In the past few years it has become possible to study lunar materials directly because surface rocks of the Moon have been returned by man and by automatic spacecraft. A tremendous number of new facts have been accumulated about the properties and composition of lunar crustal rocks. There is a great general similarity between the surface rocks of the Moon and the basic rocks of the Earth's crust, such as tholeiitic basalts, although certain differences have been found between lunar and terrestrial rocks. It is the differences between lunar and terrestrial rocks to which the current report essentially addresses itself. From comprehensively studying laboratory materials, the scientific literature on the composition of lunar rocks, and hypotheses concerning the formation of the matter of the Moon, etc., we have been forced involuntarily to turn to the cardinal question, which is of exceptional significance for our understanding of the evolution of the solar system: are the differences observed in the surface rocks of the Moon the result of the uniqueness of the differentiation of lunar material into concentric layers, or a result of the early preplanetary separation of the matter of the Sun, which occurred in the protoplanetary cloud? We have available only surface rocks from the Moon. Is it possible, by studying the surface rocks of the Moon and the other planets, to gain an idea of the chemical structure of the matter within the Moon? This will be determined later. In any case, a comparative physical and chemical study of surface and near-surface rocks of the Earth and Moon and various types of meteorites, as well as a search for possible genetical processes, forms the main approach to answering the question stated above.

I must recall some of the basic physical-chemical data concerning the terrestrial planets. Apparently, all of the terrestrial planets and the Moon have concentric layered structures. Some of them—the Earth, Venus, and Mercury—have dense cores, probably of an alloy of Fe and Ni with admixtures of certain other siderophilic elements. This affirmation is based, as we will see later, on the wide distribution of iron, on studies of its behavior during the evolution of the solar plasma, and on studies of the metallic phase of various meteorites. On the other hand, attempts to replace these concepts of the FeNi core of the planets with a silicate core or any other core have not been successful because, for example, no jump in density occurred when silicates were compressed under pressures of millions of atmospheres. The ratio $FeNi_{met}$/silicate (metal/silicate), as we know, differs rather widely for different terrestrial planets and, as a result, so do the densities of the planets. Here we first encounter a sharp difference between the composition of the planets and the composition of the Sun, at least for Fe and the siderophile elements. We will return to this question later in our analysis of ways to form the FeNi cores of planets. The mantles of the planets represent the silicate phase of planetary material. We can assume that the mantle is either "whole" solar material, not subjected to separation in

the protoplanetary cloud, or that it represents some portion of the solar plasma. Doubtless, this is an ultrabasic substance similar in composition to stony meteorites. However, we have never studied it directly in any objective way, since very little has been obtained. From beneath the Earth's crust and from the rift valleys of the midoceanic ridges, rock has been obtained (from the upper mantle of the Earth) which is ultrabasic in nature (rich in Mg and Fe and with little Al), i.e., harzburgites and lherzolites (ref. 1). Possibly the composition of the mantles of the planets varies somewhat like the compositional variations of rocky chondritic meteorites of various types, but doubtless the composition remains similar to terrestrial ultrabasic rocks. However, flows of basic rock similar to terrestrial primitive tholeiitic basalts apparently occur on all terrestrial planets. This follows directly from data for the Earth and Moon. Based on photographs of the landscape of Mars (polar caps with CO_2) and particularly remarkable of Mercury, the same type of planetary surface has been observed, i.e., with tremendous craters. Finally, we cannot imagine the absence of lava flows on Venus where the atmosphere, due to the "greenhouse effect," contains (according to our calculations) all of the probable "reserve" of carbon of the entire planet in the form of CO_2, which could have resulted only from volcanism. Consequently, the phenomena of magmatism, effusion of basaltic lava, and accompanying degassing, occur on all planets. In other words, basaltic crusts form on all of the planets. The thickness and composition of these crusts are only just now beginning to be studied. The landscape of all terrestrial planets is surprisingly similar. In addition to volcanic craters, a tremendous mass of craters of all sizes has been produced as a result of meteorite impacts. People first became familiar with the "lunar" landscape on the Moon. It was then discovered on Mars, and recently on Mercury. On Earth, meteorite craters have been partially (particularly before the atmospheric age) eroded, and are presently hidden beneath thick sediments. Some have been retained and are well known, as, for example, the huge Canyon Diablo meteorite crater in the United States and the Alae Crater in Hawaii and many others. Finally, under the influence of various factors on the various planets, layers of fine-grained materials have developed on their surfaces and cover the planets: soil on Earth, regolith on the Moon, and dust on Mars. The Moon's regolith, which was formed by thermal explosions caused by meteorite impacts, reaches several meters in thickness. On Venus there are probably thick sediments covering its surface as a result of the corrosive influence of the carbon dioxide atmosphere and the "greenhouse effect" on the destruction of magmatic rock. Radar studies of Venus show altitude differences of not over one kilometer. Craters 33–160 km in diameter, with depths of up to 400 m, have been discovered on Venus (ref. 2). Mountains on the Moon, Mars, and Earth, however, reach 10 km in height. The nature of the landscape is influenced by many factors. Also, depending on the mass of the planet and its distance from the Sun, on life, on solar, cosmic, and galactic radiation, and on many other factors, various atmospheres develop or are finally lost.

The seismic observations of Apollos 14, 15, and 16 have indicated that, by analogy with the structure of the Earth, the lunar crust is ~ 25 km thick. We recall that the thickness of the Earth's crust is ~ 40 km on the continents and 6–8 km beneath the ocean floor, amounting to ~ 1 percent of the thickness of the entire silicate mantle of the Earth (ref. 3). There is therefore considerable interest in the seismic data recently produced by Apollo 17, indicating that, for example, the thickness of the basaltic rocks in the Taurus-Littrow Valley is only a little more than one kilometer, totaling 1860 meters. The problem of the thickness of the crust remains open. Reflections of seismic waves were received from deeper horizons as well, but their significance is not sufficiently clear. The central portion of the Moon is apparently melted and does not transmit seismic shear waves. Many are inclined to believe that the entire area of

the core is like the asthenosphere of the Earth, with low seismic conductivity (ref. 4).

There is every reason to believe that the Moon has no FeNi core. Let us begin with the fact that the density of the Moon is 3.34 (10 percent of the density is probably a result of gravitational compression). The density of stony meteorites (chondrites containing ~ 12 percent metallic alloy) is ~ 3.58–3.6, i.e., higher than that of the Moon. The solar plasma flowing around the Moon is not perturbed. The Moon has no global magnetic field. Later, we will show that the Moon was formed in a cloud with reduced quantities of FeNi and therefore the Moon not only has no FeNi alloy at its center, but also contains significantly lower quantities of the 10 siderophilic elements that ordinarily accompany metallic iron than, for example, the rocks of the Earth.

It should be recalled that the metallic iron contained in stony meteorites is not sufficient to form the iron-nickel cores of the planets. A solid addition of tremendous fragments of metallic iron—iron meteorites—is required.

The Moon has an asymmetrical surface structure. About 30 percent of its visible area is occupied by so-called lunar maria and the remaining area by a mountainous continental portion. On the back side of the Moon only ~ 2.5 percent of the area consists of maria and all of the rest is mountainous relief. The force of gravity on the Moon is one-sixth that of the Earth, which is of particular interest in connection with the process of upthrusting of lunar magma to the surface. The temperature at the center of the Moon, according to various extrapolations (for example, based on the electrical conductivity of "dry" lunar rock), is probably not presently over 1000°–1500°C. The expected heat flux at the surface of the Moon would be about one-sixth of the mean heat flux on the Earth. However, measurements have yielded a heat flux from the surface of the Moon that is one-half that of the Earth (ref. 5). The temperature gradient differs significantly from the terrestrial gradient (Moon, 1°–4°C/meter; crust, 0.01°C/meter).

On the Moon, the terrestrial factors of rock weathering are absent. Water has participated little in geological processes on the Moon. On the Moon quite different factors cause the destruction of rock: variations in temperature between lunar day and night; the solar wind; the cosmic, solar, and galactic radiation; and meteorite and micrometeorite impacts. Finally, the surface relief of the Moon is changed by volcanism and lava flows, which were most intensive during the first billions of years, up to 3.0 billion years ago. Some of the circular lunar maria such as Mare Imbrium, Serenitatis, Humorum, Nectaris, and Crisium have positive gravity anomalies (ref. 6). It is assumed that below these maria at depths of ~ 100 km there are denser rocks, the so-called mascons. According to the thinking of many scientists they are of extralunar origin, i.e., planetesimals which struck the Moon during the last stage of its accretion. The surface of the Moon, particularly its highland portions, is covered with many craters. There are no lines of mountains on the Moon, the mountainous relief being created by circles of mountains, crater walls, over 10 km high.

Craters on the Moon have been caused by two different processes. One is ancient volcanic activity, which was confirmed after man visited the Moon and found that the surface rocks are of magmatic origin. There are direct observations of frozen lava flows on the Moon, for example, in the crater Aristarchus and elsewhere. Other craters were formed as a result of meteorite impacts or the impacts of stones ejected by explosive volcanism. The impact nature of craters has been proven by the finding of fragmental meteoritic material on the surface of the Moon, and by direct observation in our own time of the formation of a crater on the Moon, which was observed upon impact of a meteorite two years ago (ref. 7).

However, there is no generally accepted visual evaluation of craters as to their origin. Obviously, the small craters of precise circular shape, up to 1 km in diameter and surrounded frequently by rock fragments, are of impact origin. On the other hand, the

impact mechanism is credited with the formation of certain circular lunar maria by impact of planetesimals. The influence of meteorite impacts on changes in rocks on the surface of the Moon is tremendous. On the lunar surface, particularly in the continental areas, we have encountered large numbers of primary magmatic lunar rocks that have been crushed and metamorphized by impact mechanisms, particularly basalt-type rocks, to form various types of breccia, slag, and, finally, the fine-grained powder called regolith, which covers the entire surface of the Moon in a layer reaching a thickness of several meters in places. The grains of rocks in the regolith are melted, or have glass-covered surfaces, or are in the form of drops. The glass has various compositions and colors. The impact of meteorites causes a thermal explosion and temperatures reach several thousands of degrees C. Lunar rocks have properties quite unusual for terrestrial rock, i.e., tremendous density, the appearance of nonrusting iron, etc. The rock fragments take on remarkable forms due to micrometeorite impacts. The metamorphism of surface rocks on the Moon arises under the influence of meteorite and micrometeorite impacts, greatly complicates the surface processes, and causes complete or partial remelting of the primary magmatic rocks of the Moon, with subsequent formation of breccia, etc.

As a result of the continuous study of lunar rocks, the possibility has arisen of determining unique petrologic provinces on the Moon; and by determining the absolute age of rocks from various areas of the Moon, it has become possible to determine the more ancient and younger petrographic areas of the Moon. For example, it has been found that rocks from the Fra Mauro province are older that the material from Mare Imbrium.

In order to approach the solution of the problem of which process was predominant in the formation of lunar rocks, and in their composition (either separation of matter in the protoplanetary nebula or fractional differentiation of lunar material during formation of the Moon's crust), we must first of all obtain comprehensive data on the nature of the most ancient, unchanged primary crystalline magmatic rocks of the Moon. Therefore, our attention will next be concentrated primarily on (1) analysis of the composition of just these unchanged or little changed magmatic surface rocks of the Moon and (2) comparison with the tholeiitic basalts of the Earth and feldspar achondrites. The lunar mare basalts have many features in common with the tholeiitic basalts of the Earth. They also poured out directly from the underlying layer of ultrabasic "meteoritic" rock. However, breccias, regolith, and other clastic material, of course, are of considerable interest in light of the problem at hand.

The Lunar Rock Collection

Let us briefly recall the nature of the lunar surface rocks returned by Apollos 11, 12, 14, 15, 16, and 17 and by Luna 16 and Luna 20.

MARE SAMPLES

Apollo 11 — Mare Tranquillitatis, southwestern portion, 10 km from the Crater Sabine D, 0°41′15″ N.; 23°26′ E.

They are magmatic rocks in the form of two varieties of basalt, one with subophitic texture, basalt type A, and one with granular texture, basalt type B (microgabbro). They differ slightly in mineralogical and chemical composition (see table 1). Basalt type A is richer in Rb, REE, Y, and other trace elements (see table 1). These basalts are also rich in FeO and TiO_2 (almost 11 percent) and contain low concentrations of alkalies in comparison with primitive terrestrial tholeiitic basalts (see table 1). Fragments of anorthosite were found in the Apollo 11 regolith. We will return to the rocks of the anorthositic series somewhat later.

Apollo 12 — Oceanus Procellarum, northwestern edge, near Surveyer Crater: 23°4′ W., 3.2° S., 120 km from the crater Lansberg.

Fine-grained and medium-grained basalts are encountered. However, these basalts are less differentiated than the Apollo 11 basalts and contain still more FeO, but less TiO_2. In addition, the regolith contains a variety of nonmare basaltic fragments (with increased content of Al_2O_3 and CaO) and grains of anorthositic rock.

Apollo 15 — On the edge of Mare Imbrium in the bay Palus Putredinis; 26°06′04″ N. and 3°39′10″ E. between the Apennine Front and Hadley Rille.

The Mare basalts are like those of Mare Imbrium and Serenitatis. Various types of basalts are found, some rich in dark-colored pyroxenes, and others with olivine. This mission discovered a flow of mare basalt lava 30 feet thick (rille edge) (see table 1). Here also were certain basaltic fragments containing larger quantities of Al_2O_3 and CaO and less FeO and MgO in comparison with typical mare basalts from Apollo 11, 12, and 15, i.e., the so-called nonmare basalts (see table 1), as well as fragments of anorthositic rock.

Apollo 17 — Southeastern edge of Mare Serenitatis, south of Littrow Crater and the Taurus Mountains; 20°10′ N., 30°46′58″ E., in a valley.

These are a complex group of rocks, of pulverized and clastic type. The crystalline basalts have textures similar to the basalts of Apollo 11 type B (see table 1), i.e., they repeat the mare basalt compositions from other mare areas.

Luna 16 — Mare Fecunditatis, northeastern portion, 13°41′ S. and 56°18′ E.; 100 km west of Webb Crater.

Regolith with varied grain size was retuned. Among the fused regolith grains, there are angular fragments of fresh-looking, unfused basalt. In composition, they are also typical mare basalts. Rare grains of anorthositic rock also occur.

CONTINENTAL SAMPLES

Apollo 14 — Shore of Mare Imbrium and Fra Mauro Ridge, 3°40′24″ S., 17°27′55″ W.

Rocks were returned from a continental area of the Moon. These were highly altered, clastic rocks. Their composition and history are exceptionally complex. Only one ~ 50–g rock was found to be a fragment with the texture of primary basalt. The basalts are distinguished by their high content of Al_2O_3 and CaO and their low content of FeO and TiO_2. Some of them contain significant quantities of K, REE, and P and are called KREEP basalts (or norites). The material contained primarily light-colored rocks of the anorthositic series.

Apollo 16 — Highland area, region of the old Descartes Crater (8°59′ 34″ S. and 15°30′47″ E.).

These rocks are quite varied, of complex composition, and clastic in nature. The breccias are fused and recrystallized. All rocks were divided into four types: (1) cataclastic anorthosites, (2) partially fused breccias, (3) polymict breccias, and (4) igneous rocks with a high degree of metamorphism. Our attention is currently drawn to the last type of rock. These are crystalline rocks with various degrees of homogeneity. Their composition varies. Plagioclase predominates. On the other hand, KREEP basalts were returned (see table 1).

Luna 20 — Highland area between Mare Fecunditatis and Mare Crisium; 3°32′ N. and 56°23′ E.

Luna 20 returned soil from a continental area in which particles of light anorthositic-type rock predominated. Particles with good basaltic texture were also found.

A petrological classification of the lunar gabbro-basalts is not yet agreed upon, and the same types of basalts continue to be called by different names, for example, nonmare basalts or norites. Apparently the lunar gabbro-basalts can be separated into 8 or 10

Table 1.—*Lunar Basalts From Various Sites: Chemical Composition in Weight Percent (data from various authors)*

Type of Rocks	SiO_2	TiO_2	Al_2O_3	FeO	MnO	MgO	CaO	Na_2O	K_2O	P_2O_5	Cr_2O_3
Mare Basalts											
Mare Tranquillitatis, Apollo 11 (1)	40.3	10.8	7.52	18.06	0.2	6.97	11.76	0.40	0.22	—	—
Mare Tranquillitatis, Apollo 11 (2)	42.8	10.5	11.84	17.15	0.2	6.47	7.34	0.48	0.10	—	—
Oceanus Procellarum, Apollo 12 (3)	45.0	2.97	9.76	19.7	0.27	10.9	9.97	0.33	0.05	0.09	0.50
Mare Imbrium, Palus Putredinus, Apollo 15 (4)	45.0	2.54	8.9	22.21	0.30	9.08	10.27	0.28	0.03	0.08	—
Mare Serenitatis, Taurus-Littrow, Apollo 17 (5)	37.19	13.14	8.7	19.62	0.28	8.52	10.43	0.32	0.04	0.09	0.42
Mare Fecunditatis, Luna 16 (6)	42.95	5.5	13.88	20.17	0.21	6.05	10.8	0.23	0.16	0.14	0.24
Highland Basalts											
Fra Mauro, Apollo 14 (7)	48	1.5	12.0	16	0.29	8.4	12	0.58	0.14	—	0.44
Crater Descartes, Apollo 16 (8)	45.40	0.32	28.63	4.25	0.06	4.38	16.39	0.41	0.06	0.07	—
Taurus-Littrow, Apollo 17 (9)	48.5	0.95	17.2	11.4	—	8.94	11.6	0.40	0.25	—	—
KREEP Basalts											
Fra Mauro, Apollo 14 (10)	50	1.3	20	7.7	0.14	8	11	0.63	0.53	—	—
Crater Descartes, Apollo 16 (11)	47.18	1.04	19.98	7.91	0.12	10.34	12.03	0.44	0.32	0.40	—
Earth Basalts											
Oceanic Tholeiitic Basalts (276 cases)	49.15	2.09	15.09	7.58 (+Fe_2O_3 3.35)	0.17	7.75	10.61	2.23	0.3	0.23	—
Meteorites											
Basaltic achondrites (12 cases) (12)	49.0	0.61	11.95	18.05	0.52	9.73	9.03	0.40	0.05	0.11	0.48
Chondrites (94 cases)	38.04	0.11	2.50	12.45	0.25	22.84	1.95	0.98	0.17	0.21	0.36

NOTES: (1) Data of Wänke (see bibliography) (refs. 8–11)
(2) Data of Wänke (refs. 8–11)
(3) Data of Cuttitta et al. (refs. 12 and 13)
(4) Data of A Preliminary Description (ref. 17)
(5) Preliminary Exploration Team (70215,2) (refs. 15–17)
(6) Data of Vinogradov (refs. 3, and 18–28)
(7) Data of Preliminary Scientific Report (14053) (refs. 29 and 30)
(8) Data of Preliminary Exploration Team (68415,6) (refs. 15–17)
(9) Data of Taylor (77275) (refs. 31–35)
(10) Data of Preliminary Scientific Report (14310) (refs. 29 and 30)
(11) Data of Hubbard et al. (65016,45) (refs. 36–38)
(12) According to calculations performed for the author by G. P. Vdovykin.

groups. However, this has not yet been done. Therefore, we will use the mineralogical and chemical composition for comparison, and compare the lunar gabbro-basalts on the one hand with the achondrites, rich in Ca and feldspar; and, on the other hand, with primitive terrestrial tholeiitic basalts-oceanic olivine-basalt associations. There is a tendency to classify basalts—more precisely—to divide them into groups or types, according to the content of FeO, TiO_2 or Al_2O_3, etc.

The texture of basalts depends on the conditions of crystallization, primarily temperature and time. It varies as a function of pressure, content of volatiles in the magma, etc.

Chemical compositions are presented in

table 1. They are nonaveraged individual data for various basalt types according to various authors. First, the primary attention of researchers was drawn to material from the lunar mare. Attention was given to the high content of FeO and TiO_2 in various types of mare basalts, as well as to the very low content of alkalies. The content of FeO is over 25 percent, approximately double the mean content of FeO in terrestrial tholeiitic basalts. One can consider that the content of FeO in all mare basalts is distinctly higher than in terrestrial tholeiitic basalts, as well as in the Ca-rich feldspar achondrites. Therefore, the ratio (100 Mg/Mg + Fe) is higher on Earth. The presence of Fe_2O_3 in lunar basalts is doubtful. The fugacity of O_2 for lunar rocks is 10^{-13}, and for terrestrial basalts is 10^{-11}. The Ca-rich feldspar achondrites occupy an intermediate position.

In order for Fe_2O_3 or Fe_3O_4 to form in the protoplanetary cloud, the partial pressure of O_2 would have to be changed by several orders of magnitude in comparison with the P_{O_2} (partial O_2 pressure) for the formation of FeO, which would also greatly influence the valency states of many other metals.

Furthermore, the rocks of the Moon and their minerals contain metallic Fe as well as Ti and Cr in trivalent form, etc., indicating the deeply reducing conditions during accretion of the Moon.

The presence of large quantities of FeO in the mare basalts has a considerable influence on the physical properties of the magma. First of all, Fe^{2+} significantly reduces the melting point of minerals, and consequently of basalts, due to the exceptional ease with which Fe^{2+} isomorphically replaces many divalent and other ions. Secondly, due to the presence of large quantities of FeO a series of iron minerals is formed. Further, a still more interesting effect occurs in the lunar basalts because of the large quantities of TiO_2, which also forms a number of minerals which are unusual for terrestrial basalts, ortho- and para-armacolite, tranquillityite, zirkelite, pseudobrookite, etc., a compound with Cr, -spinel, and with ZrO_2 and other of its analogues. The primary Ti mineral in the lunar basalts is ilmenite. The content of TiO_2 in the mare basalts reaches 13 percent, i.e., 100 times its content in the chondrites. Since ilmenite easily exchanges, many other minerals containing Ti are also found, and interesting processes occur. For example, it has been experimentally proven that plagioclase and olivine do not form liquids, but with high contents of TiO_2 and clinopyroxene, a silicate fluid is formed. All together, this results in a group of minerals in the lunar basalts which would be unusual for their terrestrial analogues. In the tholeiitic basalts the average TiO_2 concentration $\cong$ 2 percent, and in the Ca-feldspar achondrites there is very little, $\cong$ 0.5 percent TiO_2, indicating the peculiarities of the genesis of these achondrites.

The lunar basalts have at least an order of magnitude less alkali, particularly K, than the tholeiites. The Ca-feldspar achondrites contain still less K than the lunar basalts. This deficiency of K and, as we will see below, of other alkalies is explained by their loss either in the process of accretion or in the process of differentiation of lunar material. Since a similar loss is noted for many other easily volatilized chemical compounds and elements, we will return to this question specially somewhat later. We must recall that there are no hydrate minerals. A number of the peculiarities of the process of formation of lunar basalts indicate the slight participation of water in them, or its total absence, which also differentiates the magmatic processes on the Moon from those of terrestrial magmatism.

The content of other primary oxides in mare basalts is to some extent monotonous. I have in mind here SiO_2, MgO, CaO, and to some extent Al_2O_3. This is also true of the nonmare basalts from the highland areas of the Moon (norites). These highland nonmare basalts (norites) have been significantly less studied; however, it is these rocks which create the primary background for the composition of the surface rocks of the Moon, since highland areas occupy its entire backside—in all, over 70 percent of the surface.

The nonmare basalts (norites) have significantly higher contents of the feldspar

molecule and therefore much higher contents of Al_2O_3, and particularly of CaO, than the lunar mare basalts; and at the same time, lower contents of FeO and TiO_2. The remaining primary elements—SiO_2, MgO, Cr, Na, K, and Mn—are found in the nonmare basalts in quantities comparable to those of mare basalts, and with the known variations and tendencies. Among the rocks obtained from the Fra Mauro province and in the samples from other areas as well the so-called KREEP basalt was found, particularly in samples from Mare Procellarum. They differ in composition, structure, and texture from the other basalts. The composition and method of their formation will be discussed later as we study the behavior of trace elements in lunar rocks.

The nonmare basalts (norites) show a tendency toward enrichment with the feldspar molecule and, consequently, higher contents of Al_2O_3 and CaO, a characteristic which is still more completely realized by the formation on monomineralic anorthosite in the highland areas. The process of melting and raising basalt magma to the surface of the Moon and the formation of the basalt crust is basically similar to such processes on Earth. However, some of the conditions of formation and rise of magma and its crystallization on the Moon show significant differences. As indicated by a study of magma crystallization, the precipitation of various minerals occurs primarily in the range of 1025–1310° C. According to direct determinations lava usually solidified at $\sim$ 1200° C $\pm$ 50°. Because of the low gravitational force and low viscosity, the magma rose quickly. Xenoliths are practically absent. The pressure at which magma crystallized on the Moon was only a few kbar (3–10 kbar); H_2O and the volatiles common in terrestrial magmatic processes were significantly less abundant, i.e., a "dryer" process occurred. There are few vesicles in the lunar rocks, because of the tremendous vacuum on the surface of the Moon. However, we cannot exclude the participation of traces of H_2O in the processes of lunar differentiation. Magma rose from a depth of several hundreds of kilometers, depending on the nature of the basalts (content of Ti, Al_2O_3, olivine, etc.). It is assumed that with the high Al_2O_3 content, basalts must have risen from depths of over 400 kilometers in order to provide for the extraction of Al_2O_3 from depths in large quantities. On the other hand, the presence of large quantities of olivine in the basalts indicates a shallow depth of origin because olivine breaks down at 3 kbar. The presence of tridymite and cristobalite in some lunar rocks indicates high temperatures and low pressures and, consequently, the depth of the magma sources. Cooling must have occurred quite rapidly, as indicated by the texture of the complex basalts, the disordered nature of the plagioclase, and other factors. Under the near-surface conditions, the depth of crystallization differentiation could not have been great. Probably, the variety of basalt types is most closely related to the temperature and depth of melting. Some variety in the composition of the basaltic rocks resulted from meteorite impacts which caused remelting or partial melting of the lunar material and the formation of various types of breccia. Our attention is drawn to the unusually high content of Ni for certain crystalline magmatic rocks, for example, in the specimens of KREEP basalts, etc. We should also note that the maximum of the magmatic process occurred in time intervals of 4.5 to 3 $\times$ 10^9 years, when the young Moon was producing heat as a result of the decay of K^{40}, primarily U^{235}, and also U^{238} and Th^{232} by approximately one half an order of magnitude higher than today. The absolute ages of lunar rocks indicate that volcanism practically stopped on the Moon by 3 to 2.5 $\times$ 10^9 years. We will return once more to the reason for this sharp reduction in magmatism and thickness of the basaltic crust of the Moon, when we study the behavior of the radioactive elements in lunar rocks.

Anorthosites

Anorthosites were discovered on the Moon primarily in the lunar highlands, and accord-

Table 2.—*Anorthositic Rocks From Various Sites on the Moon: Chemical Composition in Weight Percent (data from various authors)*

	SiO_2	TiO_2	Al_2O_3	FeO	MnO	MgO	CaO	Na_2O	K_2O	P_2O_5	Cr_2O_3
Apollo 11 [1]	46.0	0.3	27.3	6.2	0.1	7.9	14.1	0.3	tr.	—	0.2
Apollo 14 [2] [3]	43.50	0.19	23.29	4.56	0.06	15.82	12.27	0.28	0.06	0.03	—
Apollo 15 [3]	44.08	0.02	36.49	0.29	0.60	0.09	19.68	0.34	0.01	0.01	—
Apollo 16 [4]	43.97	0.02	35.83	0.36	0.00	0.25	18.95	0.34	0.01	—	tr.
Apollo 17 [5]	42.7	0.0	34.9	0.2	—	0.1	19.1	0.01	0.1	0.2	—
Luna 16 [6]	42.9	0.02	36.0	1.99	0.01	2.52	18.1	0.36	0.02	0.03	0.01
Luna 20 [7] [8]	44.2	0.32	19.1	6.91	0.12	13.37	13.3	0.48	0.47	0.17	0.18
Terrestrial Anorthosite	54.54	0.52	25.72	1.72	0.02	0.85	9.62	4.66	1.06	0.11	—

NOTES: (1) Wood et al. (refs. 40–42)
(2) Chao et al. (ref. 43)
(3) Preliminary Description (ref. 17)
(4) Juan et al. (ref. 44)
(5) Stoeser et al. (ref. 45)
(6) Keil et al. (ref. 46)
(7) Vinogradov (refs. 3 and 18–28)
(8) Troctolite

ingly the old concepts concerning a primary terrestrial anorthosite crust were extended to the Moon (ref. 39).

Lunar anorthosites were found at a number of landing sites (see table 2). Anorthosites have not been found in meteorites. These are usually light-colored rocks of practically monomineralic composition. Lunar anorthosites contain Ca-rich anorthite, AN 96–98. They contain a great deal of Al_2O_3, up to 35 percent, and CaO up to 20 percent. Their content of FeO is quite low in comparison with the basalts. Alkalies are generally sparse and less than in terrestrial anorthosites, particularly K_2O and Na_2O. The content of all trace elements is also lower. However, exceptions are known—for example, the rocks from the Apollo 16 collection.

The anorthosites of the Moon have an anomalously high content of Eu. The content of all other REE is presented in the table (see table 2). The texture of lunar anorthosites is reminiscent of the texture of the massive stratoform anorthosites on Earth. They have cumulative structure and there is no orientation of crystals. Norites and anorthosites are found in joint association. However, contact of anorthosites with other rocks on the Moon has not been described as a layered structure. Thus on the Moon, and probably particularly on its far side, we find a unique series of rocks; gabbro-basalts-norites-anorthosites. The age of the anorthosites is great, from 3.5 to 4.2×10^9 years (refs. 43, 47, and 48). Anorthosites are generated when tremendous masses of gabbro-basalts are melted under high heat flow conditions and anorthite crystals float upward from the magma. Yoder studied the phase diagram of diopside-anorthite-water and showed the possibility of accumulating floating anorthite to form anorthositic rocks (ref. 49).

Anorthositic rocks are somewhat varied in composition and are subdivided into anorthosites, gabbroic anorthosites, anorthositic gabbros, and troctolites. The magmatic origin of these rocks follows from the high formation temperatures of their pyroxenes and pigeonites. This is also confirmed by their association with rocks with lower melting points and slight enrichment with O^{18} ($\Delta O^{18} \cong 6$ parts per mil).

On Earth, anorthosites are found in an-

Table 3.—*Mean Content of Siderophile Trace Elements in Lunar Basalts (ppm)*[1]

	Ga	Ge	As	Sn	Sb	Cu	Co	Ni
Mare Basalts								
Apollo 11 A	3.92	0.73	0.046	0.5	0.0056	10	45.3	11.46
	(22)[2]	(8)	(5)	(2)	(1)	(20)	(24)	(7)
Apollo 11 B	4.12	0.63	0.036	1.2	0.0072	—	13.25	11.5
	(15)	(2)	(2)	(1)	(1)	—	(22)	(9)
Apollo 12	4.2	0.00	0.013	0.2	0.08	9.6	47.2	46
	(37)	(14)	(12)	(5)	(8)	(37)	(63)	(31)
Apollo 15	3.86	0.012	—	0.19	0.00032	11	55	65
	(29)	(11)	—	(1)	(7)	(16)	(33)	(25)
Apollo 17	—	0.00147	—	—	0.00011	3	25	1
	—	(2)	—	—	(2)	(3)	(5)	(2)
Luna 16	4.4	1.8	1.6	2.3	0.35	19	19.5	113
	(6)	(2)	(2)	(2)	(2)	(2)	(4)	(2)
Highland Basalts								
Apollo 14	3.8	0.47	0.86	—	1.7	17.3	30.5	161
	(8)	(1)	(3)		(3)	(16)	(25)	(22)
Apollo 16	3.0	0.022	—	—	0.00021	6.7	29.6	343.4
	(11)	(1)	—	—	(1)	(10)	(15)	(24)
KREEP Basalts								
Apollo 14	4.25	0.086	—	—	—	11	23.5	175
	(2)	(1)	—	—	—	(1)	(2)	(3)
Apollo 16	4.17	—	—	—	—	10.8	48	890
	(2)					(1)	(2)	(2)
Terrestrial Basalts								
Tholeiitic Basalts	18.5	1.46	—	1	—	97	42	114
	(50)	(13)		(10)		(94)	(87)	(116)
Meteorites								
Ca-Achondrites	1.85	0.25	0.05	—	0.01	8.0	12.36	1
	(21)	(5)	(1)		(1)	(16)	(39)	-- -- -- --
Chondrites	5.0	10	2	5	0.1	120	700	145

NOTES: (1) Data used for specimens of various missions were taken from the following references:
Apollo 11: 8 and 50–62
Apollo 12: 9, 12, 32, 50, 59, and 63–71
Apollo 14: 10, 30, 37, 58, 68, and 72–79
Apollo 15: 13, 34, 47, 58, and 80–86
Apollo 16: 15 and 87–93
Apollo 17: 34, 35, and 94–96
Luna 16: 20, 21, 28, and 97
(2) Each figure in parentheses indicates number of determinations.

cient shields (around platforms and in the base of platforms) of Precambrian age, for example in the Ukraine, in Canada, etc. They are also found in gabbros, which are often layered, and in which the light portion frequently corresponds in composition to anorthosite. The thickness of rock associated with anorthosites on the Earth is several kilometers and only ~ 10 percent actually consists of anorthosites. All of this forces me to think that the thickness of anorthosite layers on the Moon is not great.

Trace Elements

The content of trace elements in lunar rocks, in comparison with the content of these elements in meteorites and tholeiite basalts of the Earth, represents a significant

Table 4.—*Partial Pressure of Oxygen (PO_2) in the Reversible Equilibrium of Metals With Their Oxides (at the melting temperature of Fe, 1803 K)*

Elements	PO_2 (atmospheres)	Elements	PO_2 (atmospheres)
$La–La_2O_3$	3.2×10^{60}	$Mn–MnO$	4×10^{-15}
$Ta–Ta_2O_5$	2×10^{-41}	$Y–Y_2O_3$	4×10^{-14}
$Nb–NbO_2$	6.3×10^{-34}	$Cr–Cr_2O_3$	1×10^{-13}
$Th–ThO_2$	2×10^{-28}	$Zn–ZnO$	3.2×10^{-12}
$Be–BeO$	1×10^{-25}	$W–WO_2$	1×10^{-11}
$U–UO_2$	1.2×10^{-24}	$Mo–MoO_2$	7.4×10^{-9}
$Ba–BaO$	2×10^{-23}	$Fe–FeO$	4×10^{-9}
$Sc–Sc_2O_3$	5×10^{-23}	$Ga–Ga_3O_3$	$n \times 10^{-9}$
$Al–Al_2O_3$	5×10^{-22}	$As–As_2O_3$	3.2×10^{-8} (542K)
$Zr–ZrO_2$	1×10^{-22}	$In–In_2O_3$	3.2×10^{-8}
$Ti–TiO_2$	7.9×10^{-19}	$Sn–SnO_2$	7×10^{-7}
$Si–SiO_2$	6.3×10^{-17}	$Ge–GeO_2$	2×10^{-7}
		$Ni–NiO$	2×10^{-5}
		$Sb–Sb_2O_3$	1.3×10^{-5}
		$Co–CoO$	6.3×10^{-4}
		$Cu–Cu_2O$	2×10^{-4}
		(Pt,Pd,Ir,Os, Ru,Rh,Au)	

fund of information about the formation conditions of lunar material. In the process of condensation and agglomeration of the matter of the protoplanetary cloud, definite phases occur, which we encounter, for example, in meteoritic material, namely metallic FeNi, which contains a characteristic set of siderophilic trace elements (Ga, Ge, As, Sb, Sn, Cu, Co, Ni, and Au) and platinoids, a silicate phase, and a sulfide phase, as well as gases and volatile substances with high vapor pressure (In, Tl, Hb, Pb, Bi, etc.). During differentiation of the silicate material of planets (mantles) refractory elements such as Ba, Zr, Nb, Hf, Y, REE, Sc, Ta, Ti, and Be are differentiated into the gas phase and the easily melted phase. Obviously, the behavior of these groups of chemical elements must also be studied in the processes of formation of a celestial body, i.e., in the processes of accretion and then in the crystallization differentiation of planetary and lunar material.

Siderophile Elements

Iron is found in lunar rocks, chondrites, and other meteorites in the form of metallic Fe (primarily in meteorites) and in the form of FeO. In lunar rocks and meteorites (chondrites) Fe is not in higher oxidation states, for example Fe_3O_4 and Fe_2O_3, since oxidation of Fe to this valence would require an O_2 partial pressure and order of magnitude higher than that required for the production of FeO. This characterizes the protoplanetary cloud. Metallic iron forms continuous solid solutions with almost 70 chemical elements. However, metallic Fe in meteorites is always accompanied by a more limited composition of these elements (ref. 22).

We can see from table 3 that many siderophilic elements are converted to oxides by a quite negligible shift to the left in the equilibrium $H_2O/H_2 = 1$ in the protoplanetary cloud. These include all elements located in table 4 above the Fe-FeO system. Because of this characteristic, these oxides are not dissolved in vapors, liquids, or metallic iron and are not encountered in them. Those chemical elements which dissolve in Fe are located below the Fe-FeO system in the table, i.e., Ga, Ge, As, Sn, Sb, Co, Ni, the platinoids, Au, and certain others, which actually are systematically strongly concen-

trated in all metallic phases of meteorites, and obviously so in the FeNi cores of the planets. This is why such widespread siderophilic elements as Ti, Mn, Cr, V, and many others are not concentrated in the metallic iron of the meteorites. Therefore, for example, it is impossible to imagine that the initial iron in celestial bodies was in the form of FeO and that it was substantially reduced by CO or other means within the planets to Fe, since FeO does not concentrate the many siderophile elements mentioned above, including Ni particularly; and therefore reduction of FeO would produce only pure metallic Fe without the siderophile trace elements. However, such pure metallic Fe is completely unknown in meteorites. Naturally, the metallic FeNi alloy in celestial bodies might to some extent be subjected to oxidation, as a result of various processes, with the result that the siderophile trace elements concentrated in the metallic Fe would enrich the other phases of the cosmic material. The silicate phases of meteorites are many times poorer in these siderophile elements than the metallic FeNi phase.

Before us is a table giving the contents of these siderophilic elements in the basaltic rocks of the Moon, the Earth, and various meteorites. There is no doubt about the lower content of all of these elements in the crystalline basalts of the Moon in comparison with the tholeiitic basalts of the Earth, and, of course, the chondrites. For example, the content of Ni is higher in terrestrial olivines, etc. The stability of the parallel increase of MnO and FeO is surprising. As concerns the nonmare basalts and KREEP basalts, as we have already mentioned, the presence of large quantities of Ni and other siderophile elements and Pt is obviously a result of contamination with nonlunar meteorite matter. The content of siderophile trace elements in Ca-rich feldspar achondrites is still lower. They are closer in this respect to the lunar basaltic rocks.

The low content of siderophile elements that accompany metallic iron indicates a deficit of metallic iron in the lunar material in comparison with analogous terrestrial rocks. On the other hand, lunar rocks contain approximately 1.5 to 2 times more FeO than do terrestrial tholeiitic basalts. This also characterizes the evolution of conditions in the protoplanetary cloud where the center of accretion of lunar material arose. We will return to this question later.

The Platinoids and Gold

The platinoids and gold are also typical siderophile elements; they dissolve in Fe and are concentrated in it. One needs only to examine table 5 to become convinced that their content in crystalline lunar rocks is extremely low. We see that the content of the platinoids and Au in the metallic iron of the meteorites is thousands of times higher than in the silicate crystalline rocks of the Moon and Earth. The platinoids and Au are distributed approximately 70 percent in the iron phase, 20 percent in tollite, and 10 percent in the silicate phase in the meteorites. The even platinoids predominate. Suffice it to say that the content of FeS in the lunar rocks is negligible. The higher content of platinoids and Au in the regolith, in comparison with crystalline rocks in the lunar regolith, is explained by the addition of meteoritic material. Calculations show that approximately 2.5 percent of the material of stony meteorites is present in the lunar regolith (which is equivalent to 0.25 percent meteoritic FeNi) (ref. 28). The content of platinoids and Au in the regolith and breccias of mare origin is higher than that of the regolith from the highland areas. The content of platinoids and Au in terrestrial tholeiites and Ca-rich feldspar achondrites is on the same order of magnitude as in lunar basalts. The lower content of platinoids and Au in the lunar basalts also indicates a deficit of metallic iron on the Moon, as do the other siderophile elements.

Refractory Oxides

Table 6 presents those refractory microelements for which reliable concentration data are available for lunar basalts. All of

Table 5.—*Mean Content of Platinoids and Gold in Lunar Basalts (ppb)*[1]

	Ir	Pd	Os	Rh	Ru	Pt	Au
Mare Basalts							
Apollo 11 A	0.68	56	0.42	—	—	—	0.72
	(13)[2]	(5)	(4)				(18)
Apollo 11 B	0.11	2.2	0.26	—	—	—	0.25
	(5)	(5)	(2)				(13)
Apollo 12	0.44	<1	0.65	0.21	70		0.598
	(20)	(5)	(19)	(4)	(10)		(20)
Apollo 15	0.04	—	—	—	—		0.094
	(9)					—	(9)
Luna 16	—	27	—	—	—		—
		(1)					
Apollo 17	0.002	—	—	—	—	—	0.017
	(2)						(2)
Highland Basalts							
Apollo 14	1.99	0.1	—	—	—	—	1.48
	(4)	(1)					(3)
Apollo 16	0.081	—	—	—	—	—	0.127
	(4)						(4)
Terrestrial Basalts							
Tholeiitic Basalts	0.4						7.7
	(13)						(16)
Meteorites							
Ca-Achondrites	1.2	1.0	0.5	0.2	1.0	2.0	10.0
	(21)						(21)
Chondrites	630	950	700	200	880	1350	180
	(25)	(19)	(21)	—	(17)	(18)	(24)
Troilite	1320	3190	1540		3410	3740	1196
	(15)	(15)	(15)		(15)	(18)	(16)
Metallic phase of chondrites	3660	4610	3300	—	4675	8770	1120
	(17)	(17)	(16)		(16)	(17)	(16)

NOTES: (1) Data used for various missions were taken from the following references:
Apollo 11: 8, 50, 52–54, 58–60, 62, 63, 98, and 99
Apollo 12: 9, 50, 56, 58, 63–65, 68, 99, and 100
Apollo 14: 10, 58, 68, and 72
Apollo 15: 58, 80, 83, 90, 91, 96
Apollo 16: 34, 35, and 94–96
Luna 16: 20, 21, and 28
(2) Each figure in parentheses indicate number of determinations.

these metals and their oxides melt at temperatures of over 2000° C and boil at temperatures up to 5000° C. Within this range of temperatures, they condense from vapor in the protoplanetary cloud. They are all easily oxidized at very low O_2 pressures (in the table they fall above the Fe-FeO system). The table gives us an idea of the content of these oxides in the lunar rocks, terrestrial tholeiites, and meteorites. The refractory elements (oxides) are found predominantly in the basaltic rocks of the Moon. We have already mentioned the accumulation of TiO_2 in the lunar basalts. In terrestrial tholeiites, the content of refractory elements is significantly lower. In the achondrites, it is practically identical to that of the terrestrial basalts. However, the degree of enrichment with rare refractory elements varies. The concentration of Sc and Y, for example, is low. The concentrations of Ba, Ti, REE, Nb, Be, and other elements are

Table 6.—*Mean Content of Refractory Trace Elements in Lunar Rocks (ppm)*[1]

	Ba	Zr	Nb	Y	Sc	Ta	Hf	Ti (percent)	Be
Mare Basalts									
Apollo 11 A	285.5	617.8	29.9	155.8	74.83	2.0	17.4	6.0	2.7
	(37)[2]	(18)	(9)	(13)	(24)	(17)	(20)	(13)	(8)
Apollo 11 B	158.8	412.4	26.86	135.4	103.6	2.0	16.6	5.6	4.1
	(34)	(20)	(7)	(14)	(26)	(18)	(23)	(12)	(4)
Apollo 12	102.7	146.5	9.7	53.0	51	0.42	3.62	2.0	1.32
	(59)	(34)	(29)	(25)	(60)	(26)	(43)	(32)	(16)
Apollo 15	65.59	91.3	8.6	27.0	40.4	0.45	2.50	1.4	1.0
	(32)	(34)	(29)	(27)	(28)	(14)	(20)	(14)	(19)
Apollo 17	57				—	—	—	7.8	—
	(1)							(1)	
Luna 16	220	300	15	89.0	39	—	3.00	3.0	1.2
	(11)	(3)	(1)	(2)	(7)		(5)	(3)	(1)
Highland Basalts									
Apollo 14	534	807.8	43.6	182.3	34	3.1	16.7	1.2	3.3
	(11)	(17)	(16)	(16)	(21)	(3)	(6)	(4)	(6)
Apollo 16	223	500.5	27.4	76.4	9.8	1.3	29.4	0.51	3.7
	(17)	(19)	(14)	(15)	(14)	(5)	(14)	(1)	(3)
Apollo 17 (1)	150.0	250	11	31	11	—	3	0.3	—
	(1)	(1)	(1)	(1)	(1)		(1)	(1)	
KREEP Basalts									
Apollo 14	808	911.5	43	170	—	—	21	—	—
	(3)	(2)	(1)	(2)	—	—	(1)	—	—
Apollo 15	686	—	—	—	—	—	—	—	—
	(1)								
Apollo 16	466	840	33	120	14.2	—	16.2	0.7	5.2
	(1)	(1)	(1)	(1)	(2)		(2)	(1)	(512)
Terrestrial Basalts									
Tholeiitic Basalts	23.3	105	<30	31.7	43	—	20	1.25	—
	(88)	(51)	(10)	(64)	(23)			(276)	
Meteorites									
Ca–Achondrites	35	46	<30	22	26	0.1	0.8	0.46	0.1
Chondrites			(10)	(4)	(40)				
	6	7	0.3	2	8	002	0.2	0.065	0.04

NOTES: (1) See following references regarding specimens of various missions:
Appolo 11: 8, 31, 51, 54–61, and 101–107
Apollo 12: 9, 12, 32, 36, 56, 58, 59, 64–67, 69, 71, 106, and 108
Apollo 14: 10, 30, 33, 37, 58, 73–75, 77–79, 109, and 110
Apollo 15: 13, 34, 38, 47, 58, 82, 86, 91, and 111
Apollo 16: 15, 87–89, 91–93, and 111–114
Apollo 17: 34, 35, 94, and 96
Luna 16: 20, 21, 28, 97, and 115–118
(2) Each figure in parentheses indicates number of determinations.

more than a hundred times greater than their concentrations in chondrites. The question arises as to whether rapid extrusion and cooling of the magma on the Moon could cause this enrichment. According to all available data, the nonmare basalts of the Moon are quite rich in these refractory substances. However, it is interesting to note that the content of refractory oxides in the basalt returned by Apollo 15 is practically identical to that of terrestrial tholeiitic basalts and Ca achondrites. Lunar basalts contain TiO_2 at levels of up to 13 percent, primarily in the form of the ilmenite. Zr and Hf follow the Ti minerals, such as $FeTiO_3$, to a significant extent. However, they contain 6 to 8 times

more Zr than terrestrial ilmenite (0.058 percent Zr). Ba is concentrated in the feldspars of lunar basalts. The ratios of Zr/Hf and Nb/Ta, and of similar pairs of isomorphic elements are similar to their ratios in terrestrial basalts. Nb and Ta are enriched in Fe minerals and are also distributed in MgFe minerals. Nb and Zr do not form their own minerals in lunar rocks. The entire range of rare earths must also be considered refractory. Table 7 shows the significant excess of rare earths in lunar rocks in comparison with terrestrial rocks and Ca achondrites. The last two contain practically identical low contents of the rare earths.

In comparison with the chondrites, the basalts of the Moon have a relatively higher content of the heavier rare earths. The anomalous behavior of Eu among the other rare earths is now well known. Its content is decreased in pyroxenes and increased in plagioclases (see anorthosites). This indicates once more that the magma was liquid. Here also the increase in the content of rare earths reaches 100 fold or more—for example, for La, Ce, Nd, and others. The rare earths, like the other refractory oxides, are more abundant in nonmare basalts. One should note that the refractory elements and their oxides are not concentrated in the regolith. Also, on the average, a single-event process (melting of tholeiitic basalts of the Earth, etc.) causes up to twentyfold enrichments of some elements. Consequently, enrichment by 100 times in lunar rocks requires a content of refractory elements in the Moon 3 to 5 times higher than in chondrites.

Radioactive Elements

Because of the many absolute age determinations of lunar rocks by the U-Pb and U-He method, a number of determinations of U, Th, and K have been made (see table 8). The mean data indicate a significant excess in the content of U and Th in lunar basalts of various types, in comparison with terrestrial tholeiitic basalts and Ca achondrites. The content of U and Th is particularly high in the nonmare basalts (norites) and KREEP basalts. Therefore, the K/U ratio for nonmare basalts is $\sim$ 1500 and for the mare territories $\sim$ 2000. U and Th are unevenly distributed in lunar rocks. We consider it probable that the minimum content of U in mare basalts is 0.20 ppm, i.e., some 20 times higher than in chondrites. The arithmetic mean content in all basalts of the Moon is higher, up to 0.6 ppm. Many data indicate 0.1 to 0.2 ppm U in terrestrial tholeiitic basalts. On the Earth, the effusion of primitive tholeiitic basalts is reminiscent of the single-event melting process that produced mare basalts on the Moon. The content of U and Th in the lunar rocks parallels the increase of other lithophile elements, for example, in the nonmare basalts. However, what process increased the U content to 3.5 ppm and higher, as has occurred in certain provinces on the Moon, remains unclear. In the continental areas of the Earth the first stage of U concentration (production of basalts) is followed by a second stage of enrichment, i.e., granitization. Granitization increases the U content to 3 ppm and higher in granites (produced by conversion at depth of a portion of the basaltic substrate of the basalts during the complex process of granitization), i.e., it is increased by another 10 times in the crust of the Earth, a total of $\sim$ 100 times. Processes occur in the Earth's crust with fluxing agents (CO_2, H_2O, etc.) not present on the Moon, where the processes are more primitive. Th increases in the lunar basalts in parallel with U. The redistribution of U, Th, and K into the various rocks of the Moon, and particularly the accumulation of U and Th at the periphery in the lunar crust, as we will see below, has significantly disrupted the primitive thermal balance of the Moon and allows us to draw certain important conclusions. These will be discussed later.

The Loss of Volatiles from the Moon (Deficient Elements)

We see the greatest deficit of elements, generally volatile at elevated temperatures,

Table 7.—*Mean Content of Rare Earth Elements in Lunar Rocks (ppm)*[1]

	La	Ce	Nd	Sm	Eu	Gd	Tb	Dy	Ho	Er	Tm	Yb	Lu	Pr
Mare Basalts														
Apollo 11 A	22.7	70.64	62.68	21.4	2.48	26.9	4.9	37.5	5.9	20.9	2.3	18.0	2.8	14.52
	(31)[2]	(29)	(16)	(27)	(28)	(14)	(19)	(17)	(16)	(14)	(4)	(28)	(26)	(5)
Apollo 11 B	12.4	43.4	47.2	16.2	2.3	21.8	3.2	30.2	6.0	13.8	1.8	15.3	2.2	11.68
	(22)	(21)	(16)	(21)	(21)	(14)	(14)	(15)	(10)	(14)	(2)	(20)	(18)	(4)
Apollo 12	7.7	22.4	15.6	4.8	1.2	7.1	1.55	9.0	1.75	5.9	0.93	5.2	0.77	3.46
	(48)	(48)	(34)	(54)	(54)	(27)	(38)	(42)	(29)	(30)	(12)	(54)	(43)	(20)
Apollo 15	5.54	16.9	11.65	3.78	0.96	5.24	0.74	5.48	3.45	3.2	0.4	2.4	0.36	2.0
	(28)	(14)	(13)	(29)	(29)	(1)	(15)	(13)	(2)	(13)	(1)	(29)	(24)	(1)
Apollo 17	5.1	—	—	8.7	1.6	—	2.2	13	—	—	—	—	—	—
	(1)			(1)	(1)		(1)	(1)						
Luna 16	15.6	43.4	32.6	9.18	2.8	12.3	2.0	12.78	3.0	3.9	0.9	6.43	1.04	16.00
	(5)	(10)	(5)	(10)	(10)	(7)	(4)	(10)	(6)	(7)	(1)	(10)	(9)	(1)
Highland Basalts														
Apollo 14	46.7	51.5	36	8.9	1.3	12.7	1.7	14.7	1.9	4.7	—	12.2	0.81	4.3
	(19)	(7)	(4)	(7)	(5)	(5)	(3)	(5)	(3)	(4)	—	(7)	(8)	(3)
Apollo 16	52.6	67.4	36.9	11.14	1.6	4.43	2.54	26.7	3.28	6.84	—	7.2	1.2	—
	(9)	(11)	(10)	(11)	(11)	(7)	(4)	(11)	(4)	(6)	—	(11)	(10)	—
Apollo 17	11.0	31	15	4.5	1.5	5.4	0.85	5.4	1.3	3.6	0.5	3.4	0.4	4.0
	(1)	(1)	(1)	(1)	(1)	(1)	(1)	(1)	(1)	(1)	(1)	(1)	(1)	(1)
KREEP Basalts														
Apollo 14	60.8	173.6	90	26.7	2.2	34.5	5.5	32.2	7.6	22.4	3.0	20.0	2.9	23
	(9)	(6)	(4)	(5)	(6)	(2)	(3)	(5)	(3)	(4)	(1)	(6)	(5)	(1)
Apollo 15	75.2	191.2	116	32.4	2.65	39.2	—	42.3	—	25.3	—	22.2	3.4	—
	(4)	(6)	(6)	(6)	(6)	(4)		(5)		(6)		(6)	(3)	
Apollo 16	48.0	139.2	74.7	23.0	1.87	25.6	4.40	29.65	5.2	17.84	1.4	15.82	2.31	—
	(6)	(6)	(6)	(6)	(6)	(6)	(2)	(6)	(2)	(5)	(1)	(5)	(3)	
Terrestrial Basalts														
Tholeiitic Basalts (64)	3.36	10.3	9.87	3.49	1.26	5.05	0.86	5.22	1.24	3.48	0.53	3.20	0.49	1.87
Meteorites														
Ca-Achondrites (4)	3.7	9.7	7.0	2.3	0.72	3.1	0.57	3.8	0.80	2.3	0.38	2.0	0.35	1.4
Chondrites (20)	0.3	0.84	0.58	0.21	0.074	0.32	0.05	0.31	0.073	0.21	0.053	0.17	0.031	0.12

NOTES: (1) See following references for data on specimens of various missions.
Apollo 11: 8, 54–57, 59, 61, 102, and 105
Apollo 12: 36, 56, 64, 65, and 70
Apollo 15: 34, 38, 77, 82, 86, and 91
Apollo 16: 38, 89, 91, 92, and 114
Apollo 17: 34, 35, 89, 94, and 96
Luna 16: 20, 21, 28, 116, 118, and 119
(2) Each figure in parentheses indicates numbers of determinations.

Table 8.—*Mean Content of U,Th,K in Lunar Rocks (ppm)* [1]

	U	Th	K	K/U
Mare Basalts				
Apollo 11 A	0.55	2.7	2140	3890
	(35) [2]	(30)	(11)	
Apollo 11 B	0.33	1.63	1330	4030
	(22)	(24)	(9)	
Apollo 12	0.641	1.39	501	783
	(70)	(54)	(38)	
Apollo 15	0.153	0.5	375	2451
	(14)	(2)	(7)	
Apollo 17	0.14	0.4	507	3620
	(11)	(9)	(8)	
Highland Basalts				
Apollo 14	0.58	2.3	2444	4214
	(4)	(3)	(3)	
Apollo 16	1.18	5.09	238	200
	(15)	(11)	(1)	
Apollo 17	0.5	1.8	900	1800
	(1)	(1)	(1)	
KREEP Basalts				
Apollo 14	3.2	10.6	3924	1226
	(9)	(10)	(5)	
Apollo 15	3.39	—	—	—
	(6)			
Apollo 16	2.09	9.2	3100	1550
	(6)	(1)	(1)	
Terrestrial Basalts				
Tholeiitic Basalts	0.20	0.62	2490	12 450
Ca-Achondrites	0.1	0.41	400	4000
Chondrites	0.012	0.04	850	70 833

NOTES: (1) Data regarding various missions were taken from the following references:
Apollo 11: 8, 55, 57–59, 60, 61, 101, 106, and 120–123
Apollo 12: 9, 32, 56, 58, 59, 64, 65, 67, 69–71, 100, 124, and 125
Apollo 14: 10, 33, 37, 58, 73, 75, 77, and 126
Apollo 15: 34, 38, 58, 83, and 86
Apollo 16: 15, 38, 87, 90–92, and 127
Apollo 17: 34, 35, and 94–96
(2) Each figure in parentheses indicates numbers of determinations.

in the lunar basalts—a deficit greater than that in the tholeiitic basalts of the Earth or even the ordinary chondrites. The deficit in lunar rocks has been noted for the following groups of chemical elements or their compounds, in comparison with terrestrial basalts and meteorites:

1. H_2O, CO_2, H_2S, and many other gases
2. Alkalies: K, Na, Rb, and others
3. Halogens: F, Cl, and others
4. Metals with high vapor pressure: In, Ti, Pb, Bi, Hg, and others

GROUP 1

Kinetic calculations show that practically all gases up to mass 40 are lost from the Moon into space. However, the nuclei of neutral gases, N_2 and others, are implanted in the rocks of the Moon by the solar wind.

H_2O, CO_2, and other gases: A multitude of available data make it easy to see that the Moon contains a markedly lower quantity of H_2O, CO_2, S, and other ordinary gases in comparison with their content in the terrestrial rocks. The vesicles of lunar rocks have been found to contain CO_2, H_2, and N_2 in negligible quantities. Traces of H_2O have not been found with sufficient accuracy. This does not mean that H_2O and the other gases are totally absent in the lunar rocks. In the basalts of the Moon, the content of H_2O is generally considered to be on the order of 0.01 to 0.1 percent. This is markedly less than the content of H_2O in the magmatic rocks of Earth. However, the entire course of chemical reactions in the crust of the Moon directly indicates the deficit of H_2O. The regolith does not accumulate H_2O in comparison with the crystalline rocks. This means that the shortage of H_2O, C, N, and other elements is not a result of their loss during the differentiation of lunar material, but more probably is related to the accretion of lunar material, where the loss of H_2O occurred during the condensation and agglomeration of lunar material. The basic reasons might be the high temperature of accretion and an H_2O/H_2 ratio less than 1.

GROUP 2

The second group consists of the alkalies Na, K, Rb, and others. As we can see from

Table 9.—*Mean Content of Elements With High Vapor Pressure in Lunar Rocks (ppb)* [1]

	In	Tl	Hg	Pb (ppm)	Bi
Mare Basalts					
Apollo 11 A	13.0	0.80	9.01		0.38
	(6) [2]	(3)	(2)	1.0	(3)
Apollo 11 B	86	0.45	0.60		0.16
	(4)	(2)	(1)	(16)	(1)
Apollo 12	2.1	0.36	6.0	1.14	0.55
	(31)	(16)	(8)	(17)	(5)
Apollo 15	1.06	0.46	—	0.5	0.24
	(11)	(7)		(1)	(7)
Apollo 17	—	0.23	—		0.07
		(2)			(2)
Luna 16	12		—	0.33	—
	(1)			(1)	
Highland Basalts					
Apollo 14	10.75	1.4	—	10.2	0.28
	(2)	(1)		(4)	(1)
Apollo 16	40	0.36	—	3	0.08
	(2)	(1)		(1)	(1)
Apollo 17	—	—	—	1.7	—
				(1)	
KREEP Basalts					
Apollo 12	1.25	6.0	—	—	4.6
	(1)	(1)			(1)
Apollo 14	75	10	—	—	0.39
	(2)	(1)			
Terrestrial Basalts					
Tholeiitic Basalts	77	—	—	2	—
	(13)			(20)	
Meteorites					
Ca-Achondrites	5.0	11.0	—	0.5	3.14
	(25)	(20)		(?)	(19)
Chondrites	1.0	1.0	—	0.3	3.0

NOTES: (1) Data used were taken from the following references:
Apollo 11: 8, 52, 54, 62, 106, 123, and 128
Apollo 12: 9, 50, 63–65, 68–70, 100, and 125
Apollo 14: 10, 33, 68, 72, 78, and 79
Apollo 15: 34, 80, 83, and 84
Apollo 16: 87, 90, and 92
Apollo 17: 34, 35, and 96
Luna 16: 20, 21, and 28
(2) Each figure in parentheses indicates numbers of determinations.

table 1, the content of alkalies, particularly K, is significantly lower in lunar basalts than in terrestrial tholeiitic basalts or even in ordinary chondrites. Only the Ca-feldspar achondrites have lower contents of alkalies than lunar basalts. On the other hand, the regolith overall does not accumulate alkalies in all known cases, but rather shows the same slight variations as the crystalline lunar basalts. It is of course possible to assume a loss of alkalies during the thermal events that accompany the formation of fragments of regolith, glasses, etc., as well as breccia. These losses, however, could not be compar-

able with the quantities which might have been present in lunar rock by analogy with terrestrial rocks. It is well known from everyday experimental experience that when basalts and other rocks are heated they lose primarily alkalies, namely K and others. All of this together indicates that it is most probable that the alkali losses result from conditions of the accretionary process, not from differentiation of the lunar material. At the same time, we should note the local fact of increased K content in the KREEP basalts during formation of lunar crustal rocks.

GROUP 3

The third group is the halogens F, Cl, and others. Their contents vary in the crystalline rocks of the Moon. A number of data indicate that their concentrations are sometimes significant. For example, F and Cl parallel the contents of other volatile elements, such as Ge, in the mare regoliths and particularly in the highland regoliths (even those consisting primarily of grains of anorthositic rock, e.g., Apollo 16). It is of interest that the content of all halogens, as a rule, increases several fold in the regolith (ref. 127); therefore, their loss occurs upon breakup of crystalline basalts and their hydrogen compounds in the volcanic exhalations of ancient lunar volcanism.

GROUP 4

Group 4 consists of metals such as In, Tl, Hg, Pb, Bi and others (table 9) that have high vapor pressures (see table 10). This group is interesting in that Tl, Hg, Pb, and Bi do not produce solid solutions with metallic Fe. The element In alloys only to a limited extent with Fe. On the other hand, group 4 metals require higher O_2 partial pressures for oxidation than does metallic Fe. Therefore, under reducing conditions in the accretionary process, and also in the chemical differentiation of lunar material and formation of a lunar crust, these elements are scattered among the various phases and are generally easily mobile at elevated temperatures. In any case, it has been noted that the regolith, particularly from the highland areas, contains Tl, Zn, Hg, Pb, and other similar elements in significantly higher quantities than do the crystalline rocks from which it was formed. This means that they are dispersed in a fashion similar to the dispersion of Hg and I on Earth. This does not exclude the possibility of loss of these elements in the accretionary stage as well, but it seems to me today difficult to determine the share of these losses in each individual process.

Thus, it seems to me that some of the volatile elements or their compounds were primarily lost in the process of accretion, for

Table 10.—*Melting Points, Boiling Points, and Vapor Pressures of the Metals* In, Tl, Pb, Hg, *and* Bi *(*Fe *for comparison) at 25° C and 1500° C*

Metals	Melting Point		Boiling Point		Vapor Pressure (atm)	
	°C	K	°C	K	T = 25° C (298 K)	T = 1500°C (1773 K)
In	156	429	2000	2273	3.3×10^{-37}	3.5×10^{-2}
Tl	303	576	1457	1730	8.2×10^{-26}	1.3
Pb	327	600	1725	1998	2.7×10^{-29}	2.2×10^{-1}
Hg	−38	235	357	630	4.2×10^{-6}	1.1×10^{-3}
Bi	271	544	1560	1833	1.3×10^{-27}	6.3×10^{-1}
(Fe	1539	1812	2857	3130	6.3×10^{-66}	1.4×10^{-5})

example, H_2O and alkalies; while other elements were probably lost in both processes, for example, the inert gases, halogens, and elements with high vapor pressures. However, this loss did not cause them to escape from the Moon in significant quantities.

Brief Conclusions

Thus, in comparing the basaltic surface rocks of the Moon with terrestrial tholeiitic basalts and ordinary chondrites we have discovered a number of facts important in principle:

1. There is an excess of the so-called refractory chemical elements, including the group of truly refractory elements, the rare earths, U, and Th, in comparison with their content in primitive terrestrial basalts and chondrites.
2. The so-called siderophilic elements have lower contents in the lunar surface rocks than in terrestrial rocks.
3. The low alkali content (Na, K, Rb) in lunar rocks is established.
4. There is a low content of H_2O and the ordinary gases CO_2, halides, etc.
5. The low content of metals with high vapor pressure, (In, Tl, etc.) has been established. The primary question is, which processes have caused in one case an abundance and in another case a deficit of certain chemical elements in the lunar surface rocks?

As is well known, the mean composition of the Sun is similar if not identical to that of stony meteorites, i.e., chondrites, if we exclude the mass of ordinary gases. Because of this, many scientists have developed the so-called chondritic model of the Earth and the other planets: in other words, it is considered that all of the matter of the Sun, without separation, is included in the composition of the terrestrial planets. However, the differences already known in the contents of metals in the cores of the planets have caused critical discussion. The chondritic model also includes other unanswered questions, such as the sharp difference in the Sr^{86}/Sr^{87} ratio between chondrites (0.7480), terrestrial rocks (tholeiite basalts), and lunar basalts (norites, anorthosites) (0.6990–0.7036). Furthermore, particular attention has been drawn to the huge lunar deficit of K, etc. As we have just seen, dissimilarities in the chemical composition of the rocks of the Moon and the Earth, and of chondrites are still greater. If we exclude from consideration the influence of the meteoritic and planetesimal impacts, which have caused tremendous destruction of the structures of lunar surface rocks during the formation of regolith and breccias, and the influence of impact metamorphism on lunar rocks, which however has relatively little changed their mean compositions, then two main processes may be responsible for changes in the composition of lunar rocks: (1) the very process of accretion of lunar material, and (2) the process of differentiation of the substance of the Moon into concentric layers (formation of the crust). It seems to us that study of the process of accretion makes sense only if we relate the origin of the Moon to that of the Earth, namely to the Earth-Moon system. Otherwise, everything becomes quite abstract. Therefore, we suggest that the center of condensation of lunar material arose near the Earth. Every celestial body in this system developed according to two different models—the Earth with its heavy inner metal core and the Moon without a heavy metal core.

Let us examine what conditions must be satisfied by the formation of the Moon from a protoplanetary cloud, having in mind our preliminary geochemical analysis. According to all data mentioned above, the protoplanetary cloud was rather homogeneous. The first condition for formation and growth of the Moon would have to be its formation near a large celestial body, under whose influence it was born, evolved, and had its growth interrupted. Most probably, such a body is either the Sun or the Earth. I would prefer not to discuss here the problems of celestial mechanics that arise, nor other hypotheses about the formation of the Moon, based purely on mechanics. Why did the

Moon, if it was near the Sun, avoid capture by the Sun, and subsequent death? Further, what caused it to move away from the tremendous mass of the Sun and approach the Earth? Its capture by the Earth would require deceleration of the Moon near the Earth and its transition into an elliptical orbit around the Earth, and so forth.

Secondly, for the preferential condensation of refractory chemical elements or their compounds (they are 3 to 5 times greater on the Moon than in chondrites) during the process of the Moon's accretion requires very high temperatures of the gases in the protoplanetary cloud—on the order of at least 1500° to 2000° C at the center of accretion of the Moon. This could occur easily only near the Sun, at a certain distance. However, the temperature of the area of accretion of the Moon must have evolved rather quickly, as did the Moon itself, reaching a rather low temperature by the end of accretion, generally markedly below 1500° C. The Sun, however, had only just begun to heat up, and could not have provided this sort of temperature variation. The temperature of the protoplanetary cloud near the Sun could not have fallen at the rate with which the Moon grew. Therefore, formation and growth of the Moon near the Earth and under its influence, is more acceptable (ref. 129).

In this case, the initial high temperature of the protoplanetary cloud at the center of accretion of the Moon can be easily explained by a somewhat earlier beginning of condensation of lunar material than the beginning of condensation of the Earth and the other planets, or by effects which cause local temperature increases in the protoplanetary cloud at the center of accretion of the Moon, which is near the Earth.

We suggest (ref. 22) that the core of the Earth and the other terrestrial planets arose at first independently and directly from the vapor phase of the protoplanetary cloud and condensed at a temperature of less than 1500° C. With global separation of matter in the protoplanetary cloud, the magnetic field would have a significant influence on the separation of ferromagnetic particles from dielectrics. We must not forget here that the past magnetic field between the planets of the solar system had an intensity thousands of times greater. Further, Fe particles easily fuse together upon collision, because of the great thermal conductivity of the alloy, and form larger fragments. Recall that at the present time such chunks of FeNi, meteorites weighing up to hundreds of tons, are still falling on the Earth, whereas silicate matter —stony meteorites—reaches the Earth with masses of not over a few kilograms. It was these very chunks of alloy which formed the cores of the planets. We do not share the common opinion that all of the matter of the planets participated in the process of differentiation of the planets into concentric layers. Only the silicate portion (mantle) participated; the metal core already existed. Otherwise, as the process is usually imagined, the silicate material from the central parts of the planet would rise to the periphery while the FeNi alloy moved to the center of the planet, and temperatures for the Earth would reach, for example, $\sim$ 3000° C. There is no known method to carry away this heat. Furthermore, such differentiation temperatures of the Earth have never been observed, either directly or indirectly. As argued above, we suggest a model of the Moon without a heavy metal core. To some extent, to answer the question of why the Moon has no metal core is to answer a similar question: How have the Ca-poor (ordinary) achondrites been formed? They contain little or no metallic iron or FeS and have lost their structure. It seems to us that enrichment of refractory elements and impoverishment in siderophilic elements and the loss of volatile substances are all aspects of a single process of accretion in a system of two celestial bodies—a process that uninterruptedly occurred in time and space at different stages of development in the evolution of the Earth-Moon system.

Thus, two centers of accretion, one near the other, arose almost simultaneously—the Earth with its metal core and the Moon with no core. The temperature of condensation of the lunar material was higher. Probably at a temperature of 2000° C or higher, the oxides

of the refractory elements condensed preferentially. The ratio $H_2O/H_2 = 1$ in the cloud was shifted to the left negligibly, but sufficiently to convert all of these and many other metals into oxides. Thus, solid dust was formed at significantly lower temperatures in comparison with the higher temperatures of the surrounding gas. The difference in temperature of the solid particles and gas reached several hundreds of degrees (ref. 130). At the same time, a similar process occurred at the center of accretion of the Earth, either in a shorter period of time or at a comparatively lower temperature. Thus, refractory elements and their oxides condensed during the accretion of the Moon, accompanied by the loss of gases, H_2O, volatile alkalies, and elements of high vapor pressure at the relatively high temperatures near the Earth. During this time, as the temperature of accretion of the Moon dropped, the metallic Fe in the lunar cloud condensed and was lost by magnetic separation. Because of the other properties of FeNi, it came under the influence of Earth's gravity. The growth of the Earth probably occurred more rapidly than the growth of the Moon, and as soon as the Earth accumulated significant mass it began to have a great influence on the accretion of the Moon. The second stage of accretion of the Moon occurred at relatively low temperatures and higher O_2 partial pressures, and under the influence of the gravitational force of the Earth, which significantly limited the accretion of the Moon. Thus, the Moon was deprived of volatile materials from the beginning of its accretion, particularly since the accretion of the Moon soon stopped due to the formation of the nearby massive Earth.

During the first stage, the condensing Fe vapors dissolved the siderophile elements from the dust particles because the partial pressure of O_2 was insufficient for their oxidation.

Thus, the accretion of the Moon occurred under the influence of the accretion of the Earth. During the first, high-temperature stage, this resulted in the accretion of refractory elements into the body of the Moon.

During the second stage, the dimensions of the Earth reached many hundreds of kilometers and the gravitational force of the Earth increased significantly, interfered with the accretion of the Moon, and caused the loss of Fe and many siderophile elements. Lower accretion temperatures caused a greatly decreased intensity of accumulation of volatile substances by the Moon.

During the third stage, growth occurred such that condensation occurred significantly below 1500° C. The Moon returned to conditions of the protoplanetary cloud that were in common with those for the Earth. Then, growth of the Moon decreased and stopped completely.

I do not doubt that a great deal of what occurred in the Earth-Moon system can be calculated when our considerations become more quantitative.

Let us now see how the differentiation of lunar material could be reflected in the composition of the surface rocks of the Moon. According to various estimates, the thickness of the lunar crust is ~ 25 km (ref. 4). Deeper, there is a layer with low seismic velocity. We have examined the crust of the Moon in a somewhat one-sided manner, mainly from the history of the lunar mare, even though the continental crust predominates in the lunar exterior. We have characterized the continental crust as a profile of mare gabbro-basalts—norites—anorthosites. In connection with this, the behavior of individual elements in this profile has definite tendencies (for example, Fe, Ti, Cr, Al, Ca, etc.) as we saw above. We share the opinion of many researchers that the formation of anorthosites was a result of cumulation and flotation of feldspar crystals from norite-type rock.

If we held to the strictly condritic model for the Moon, in other words, starting with a primary substance with the composition of the Sun, the enrichment of various elements in lunar rocks (sometimes by hundreds of times relative to chondrites) would force us to consider the thickness of the crust to be but a few kilometers. We now assume, for a number of elements, that the entire Moon is

rich in these elements relative to chondrites, and this conflict is removed. Magmatic activity on the Moon leads to lava flows and the formation of gabbro-basalts similiar to the magmatic rocks of the Earth. The known variety of these rocks is related to the enrichment of the Moon with lithophile refractory elements and the loss of a portion of the siderophile elements. At the same time, the depth of formation of magma on the Moon, its rate of rise, the temperature of the magma, and, finally—very importantly—the variety of conditions of surface crystallization of the magma, are reflected primarily in the structure and texture of the rock, and expand this variety. We have turned our attention to the significance of the high content of FeO, TiO_2, etc., in reducing the temperature of crystallization of the magma. The ratios of isomorphic pairs of chemical elements K/Rb, Ca/Sr, REE/Y, Zr/Hf, Nb/Ta, Th/U, and many others approach the ratio in the tholeiite basalts of the Earth, with small deviations. There are no deviations in the even-odd behavior of the rare earth elements or of the platinoids. The isotopic ratios for the chemical elements are not disturbed, except for similar changes in the rocks of the Earth (changes in D/H_2 ratio or O^{16}/O^{18} ratio, due to various reactions at low temperatures). The geological and geochemical processes on the Moon are significantly more primitive than the processes involved in formation of the crust of the Earth and processes within the Earth's crust itself. A full petrological model of the crust of the Moon can be produced by development of a quaternary diagram for silicates, plus TiO_2.

The thermal history of the Moon was exceptionally significant.

According to our ideas set forth above, U and Th were carried from the internal areas to the peripheral rocks of the Moon (see table 8) during magmatic activity, i.e., up to 3 billion years, when the production of heat was $\sim \frac{1}{2}$ greater. This redistribution of U and Th leads to their concentration in narrow surface and near-surface layers of the Moon, and the heat which they generated was lost primarily into surrounding space. Actually, the Moon, which conducts heat poorly, has a high thermal gradient for rock. Therefore, one expects a heat flux from the surface of the Moon of $\sim \frac{1}{6}$ the heat flux of the Earth, whereas the measured heat flux was found to be $\sim \frac{1}{2}$ that of the Earth (ref. 5). All of this forces us to believe that intensive magmatic activity on the Moon ended some 3×10^9 years ago. Incidentally, ~ 500 volcanoes are still active on Earth.

We have come to the conclusion that in order to understand the processes on the Moon, we cannot use the chondritic model even though it retains its significance for the study of the planets of our solar system. In this regard, I would like to note that the rejection of the chondritic model for the Moon will doubtless influence our conceptions of the processes of condensation of other celestial bodies in the protoplanetary solar cloud as well.

References

1. DMITRIYEV, L. B., *Geochemistry and Petrochemistry of Bedrock of the Middle Ocean Ridges.* Doctoral Dissertation, 1974.
2. DRISCOLL, E. Our Cratered Sister Planet. *Science News*, Vol. 104, 1973, p. 72.
3. VINOGRADOV, A. P., *Chemical Evolution of the Earth (Zone Melting).* Academy of Sciences, 1959.
4. NAKAMURA, Y. D. LAMMLEIN, G. LATHAM, M. EWING, J. DORMAN, F. PRESS AND N. TOKSÖZ, New Seismic Data on the State of the Deep Lunar Interior. *Science*, Vol. 181, 1973, p. 49.
5. LANGSETH, M. G., S. P. CLARK, J. L. CHUTE, S. KEIHM AND A. E. WECHSLER, The Apollo 15 Lunar Heat-Flow Measurement. *The Moon*, Vol. 4, Nos. 3 and 4, 1972, p. 390.
6. MULLER, P. M. AND W. L. SJOGREN, Mascons Mass Concentrations. *Science*, Vol. 161, 1968, p. 680.
7. *Meteorite on the Moon*, Smithsonian Institution Event Notification Card 1392, May 13, 1972.
8. WÄNKE, H., R. RIEDER, H. BADDENHAUSEN, B. SPETTEL, F. TESCHKE, M. QUIJANO-RICO AND A. BALACESCU, Major and Trace Elements in Lunar Material. *Proceedings of the Apollo 11 Lunar Science Conference*, Vol. 2, 1970, p. 1719.
9. WÄNKE, H. et al., Apollo 12 Samples: Chemical Composition and Its Relation to Sample Locations and Exposure. *Proceedings of the*

Second Lunar 2 Science Conference, Vol. 2, 1971, p. 1187.

10. WÄNKE, H., H. BADDENHAUSEN, A. BALACESCU, F. TESCHKE, B. SPETTEL, G. DREIBUS, H. PALME, M. QUIJANO-RICO, H. KRUSE, F. WLOTZKA AND A. BEGEMANN, Multielement Analyses of Lunar Samples and Some Implications of the Results. *Proceedings of the Third Lunar Science Conference*, Vol. 2, 1972, p. 1251.
11. WÄNKE, H., H. BADDENHAUSEN, G. DREIBUS, E. JAGOUTZ, H. KRUSE, H. PALME, B. SPETTEL AND F. TESCHKE, Multielement Analyses of Apollo 15, 16 and 17 Samples. *Proceedings of the Fourth Lunar Science Conference*, Vol. 2, 1973, p. 1461.
12. CUTTITTA, F., H. J. ROSE, C. S. ANNELL, M. K. CARRON, R. P. CHRISTIAN, E. J. DWORNIK, L. P. GREENLAND, A. W. HELZ AND D. T. LIGON, Elemental Composition of Some Apollo 12 Lunar Rocks and Soil. *Proceedings of the Second Lunar Science Conference*, Vol. 2, 1971, p. 1217.
13. CUTTITTA, F., H. J. ROSE, C. S. ANNELL, M. K. CARRON, R. P. CHRISTIAN, D. T. LIGON, E. J. DWORNIK, T. L. WRIGHT AND L. P. GREENLAND, Chemistry of 21 Igneous Rocks and Soils Retrieved by the Apollo 15 Mission. *Proceedings of the Fourth Lunar Science Conference*, Vol. 2, 1973, p. 1081.
14. Preliminary Examination of Lunar Samples From Apollo 11. *Science*, Vol. 165, 1969, p. 1211.
15. The Apollo 16 Lunar Samples: Petrographic and Chemical Description. Apollo 16 Preliminary Examination Team. *Science*, Vol. 179, 1973, p. 23.
16. Apollo 17 Lunar Samples: Chemical and Petrographic Description. Apollo 17 Preliminary Examination Team. *Science*, Vol. 182, 1973, p. 639.
17. The Apollo 15 Preliminary Examination Team, Lunar Samples: A Preliminary Description. *Science*, No. 175, 1972, p. 363.
18. VINOGRADOV, A. P., Substance of Meteorites. *Geokhimiya*, No. 11, 1965, p. 1275.
19. VINOGRADOV, A. P., et al., Physical and Chemical Model of the Division of Elements During the Differentiation of the Substance of the Mantle. *Geokhimiya*, No. 4, 1970, p. 389.
20. VINOGRADOV, A. P., Preliminary Data on the Lunar Soil Returned by the Luna 16 Automatic Station. *Geokhimiya*, No. 7, 1972, p. 261 and *Lunar Soil from the Sea of Fertility*, 1974.
21. VINOGRADOV, A. P., Preliminary Data on Lunar Ground Brought to Earth by Automatic Probe Luna 16. *Proceedings of the Second Lunar Science Conference, Geochimica et Cosmochimia Acta*, Supplement 2, 1971, p. 1.
22. VINOGRADOV, A. P., High-Temperature Protoplanetary Processes. *Geokhimiya*, No. 11, 1971, p. 1283.
23. VINOGRADOV, A. P., Preliminary Data on the Lunar Soil Returned by the Luna 20 Automatic Station. *Geokhimiya*, No. 7, 1972, p. 763.
24. VINOGRADOV, A. P., Preliminary Data on Lunar Ground Brought to Earth by Automatic Probe Luna 20. *Geochimica et Cosmochimica Acta*, Vol. 37, 1973, p. 721.
25. VINOGRADOV, A. P., A. K. LAVRUKHINA, A. G. GANIYEV, YU. A. SIL'VANOVICH and KH. R. RAKHIMOV, Distribution of Platinoids and Gold Between Various Phases of Meteoritic Substance–Report 1. *Geokhimiya*, No. 12, 1972, p. 1461.
26. VINOGRADOV, A. P., A. K. LAVRUKHINA, A. G. GANIYEV, YU. A. SIL'VANOVICH AND KH. R. RAKHIMOV, Distribution of Platinoids and Gold Between Various Phases of Meteoritic Substance–Report 2. *Geokhimiya*, No. 1, 1973, p. 963.
27. VINOGRADOV, A. P., Brief Report on the Moon. *Vestnik Moskovskogo Universiteta*, No. 6, 1973, p. 3.
28. VINOGRADOV, A. P., M. S. CHUPAKNIN, I. D. SHEVALEVSKIY AND YU. I. BELYAYEV, Chemical Composition of the Lunar Regolith from Luna 16. In *Lunar Soil From the Sea of Fertility*, 1974.
29. Apollo 12: Preliminary Science Report. *National Aeronautics and Space Administration*, 1970.
30. Apollo 14: Preliminary Science Report. *National Aeronautics and Space Administration*, 1971.
31. TAYLOR, S. R., P. H. JOHNSON, R. MARTIN, D. BENNETT, J. ALLEN AND W. NANCE, *Preliminary Chemical Analysis of Apollo 11 Lunar Samples. Proceedings of the Apollo 11 Lunar Science Conference*, Vol. 2, 1970, p. 1627.
32. TAYLOR, S. R., R. RUDOWSKI, P. MUIR AND A. GRAHAM, *Trace Element Chemistry of Lunar Samples From the Ocean of Storms. Proceedings of the Second Lunar Science Conference*, Vol. 2, 1971, p. 1083.
33. TAYLOR, S. R., M. KAYE, P. MUIR, W. NANCE, R. RUDOWSKI AND N. WARE, Composition of the Lunar Upland Chemistry of Apollo 14 Samples From Framauro. *Proceedings of the Third Lunar Science Conference*, Vol. 2, p. 1231.
34. TAYLOR, S. R., M. P. GORTON, P. MUIR, W. NANCE, R. RUDOWSKI, AND N. WARE, Lunar Highland Composition: Apennine Front. *Proceedings of the Fourth Lunar Science Conference*, Vol. 2, 1973, p. 1445.
35. TAYLOR, S. R., M. P. GORTON, P. MUIR, W. NANCE, R. RUDOWSKI, AND N. WARE, Lunar

Highland Composition. *Lunar Science, Abstracts and Papers*, Vol. V, 1974, p. 789.

36. HUBBARD, N. J. AND P. W. GAST, Chemical Composition and Origin of Non Mare Basalts. *Proceedings of the Second Lunar Science Conference*, Vol. 2, 1971, p. 999.
37. HUBBARD, N. J., P. W. GAST, J. M. RHODES, P. M. BANSAL, H. WIESMANN AND S. E. CHURCH, Nonmare Basalts: Part II. *Proceedings of the Third Lunar Science Conference*, Vol. 2, 1972, p. 1161.
38. HUBBARD, N. J., J. M. RHODES, P. W. GAST, B. M. BANSAL, CHI-YU SHIN, H. WIESMANN AND L. E. NYGUIST, Lunar Rock Types. *Proceedings of the Fourth Lunar Science Conference*, Vol. 2, 1973, p. 1297.
39. HASKIN, L. A., P. A. HELMKE, D. P. BLANCHARD, J. W. JACOBS AND K. TELANDER, Major and Trace Element Abundances in Samples From the Lunar Highland. *Proceedings of the Fourth Lunar Science Conference*, Vol. 2, 1973, p. 1273.
40. WOOD, J. A. AND COLLABORATOR, *Mineralogy and Petrology of the Apollo 11 Lunar Sample*. Smithsonian Astrophysical Observatory, Spec. Report 397, 1970.
41. WOOD, J. A. AND COLLABORATOR, *Mineralogy and Petrology of the Apollo 12 Lunar Sample*. Smithsonian Astrophysical Observatory, Spec. Report 333, 1971.
42. WOOD, J. A., J. S. DICKEY, U. B. MARVIN AND B. N. POWELL, Lunar Anorthosites and a Geophysical Model of the Moon. *Geochimica et Cosmochimica Acta*, Supplement 1, 1970, p. 965.
43. CHAO, E. C. T., J. B. BEST AND J. A. MINKIN, Apollo 14 Glasses of Impact Origin and Their Parent Rock Types. *Proceedings of the Third Lunar Science Conference*, Vol. 1, 1972, p. 907.
44. JUAN, V. C. ET AL., Petrology and Chemistry of Some Apollo 16 Lunar Samples. *Lunar Science*, Abstracts and Papers: Part I, Vol. V, 1974, p. 394.
45. STOESER, D. B. ET AL., Petrographic Studies of A Boulder From the South Massif. *Lunar Science*, Abstracts and Papers: Part II, Vol. V, 1974, p. 743.
46. KEIL, K., G. KURAT, M. PRINS AND J. A. GRAN, *Lithic Fragments, Glasses and Chondrules from Luna 16 fines*.
47. CHAPELL, B. W., AND D. H. GREEN, Chemical Compositions and Petrogenetic Relationships in Apollo 15 Mare Basalts. *Earth Planet. Science Letters*, Vol. 18, No. 2, 1973, p. 237.
48. CHEMINEE, J. L., *Contribution a L'etude des Comprotements du K de U et du Th dans L'evolution des Magmas (These)*, 1973.
49. Yoder, The System Diopside-Anorthite-Water. *Origin Anorthosite and Related Rocks*, 1969.
50. ANDERS, E., R. GANAPATHY, R. R. KEAYS, J. C. LAUL AND J. W. MORGAN, Volative and Siderophile Elements in Lunar Rocks. *Proceedings of the Second Lunar Science Conference*, Vol. 2, 1971, p. 1021.
51. ANNELL, C. S. AND A. W. HELZ, Emission Spectrographic Determination of Trace Elements in Lunar Samples from Apollo 11. *Proceedings of the Apollo 11 Lunar Science Conference*, Vol. 2, 1970, p. 991.
52. GANAPATHY, R., R. R. KEAYS, J. C. LAUL AND E. ANDERS, Trace Elements in Apollo 11 Lunar Rocks. *Proceedings of the Apollo 11 Lunar Science Conference*, Vol. 2, 1970, p. 1117.
53. HASKIN, L. A., F. A. FREY, R. A. SCHMITT AND R. H. SMITH, *Meteoritic, Solar and Terrestrial Rare-Earth Distributions*, 1966.
54. HASKIN, L. A., R. O. ALLEN, P. A. HELMKE, T. P. PASTER, M. R. ANDERSON, R. L. KOROTEV AND K. A. ZWEIFEL, Rare-Earth and Other Trace Elements in Apollo 11 Lunar Samples. *Proceedings of the Apollo 11 Lunar Science Conference*, Vol. 2, 1970, p. 1213.
55. GOLES, G. G., K. RANDLE AND M. OSAWA, Elemental Abundances by Instrumental Activation Analyses in Chip From 27 Lunar Rocks. *Proceedings of the Apollo 11 Lunar Science Conference*, Vol. 2, 1970, p. 1165.
56. KHARKAR, D. P. AND K. K. TUREKIAN, Analyses of Apollo 11 and Apollo 12 Rocks and Soils by Neutron Activity. *Proceedings of the Second Lunar Science Conference*, Vol. 2, 1971, p. 1301.
57. MORRISON, G. H., J. T. GERALD, A. T. KASHUBA, E. V. GANGATHARAM, A. M. ROTHENBERG, N. M. POTTER AND G. B. MILLER, Elemental Abundance of Lunar Soil and Rocks. *Proceedings of the Apollo 11 Lunar Science Conference*, Vol. 2, 1970, p. 1383.
58. SCHONFELD, E. AND CH. MEYER, The Abundance of Components of the Lunar Soils by a Least-Squares Mixing Model. *Proceedings of the Third Lunar Science Conference*, Vol. 2, 1972, p. 1397.
59. SMALES, A. A., D. MAPPER, M. S. W. WEBB, R. K. WEBSTER AND J. D. WILSON, Elemental Composition of Lunar Surface Material. *Proceedings of the Apollo 11 Lunar Science Conference*, Vol. 2, 1970, p. 1575.
60. TUREKIAN, K. K. AND D. P. KHARKAR, Neutron Activation Analysis of Major Quantities of Apollo 11 Lunar Rocks and Soil. *Proceedings of the Apollo 11 Lunar Science Conference*, Vol. 2, 1970, p. 1659.
61. WAKITA, H., R. A. SCHMITT AND P. REY, Elemental Abundance of Major, Minor and Trace Elements in Apollo 11 Lunar Rocks. *Proceedings of the Apollo 11 Lunar Science Conference*, Vol. 2, 1970, p. 1685.

62. WASSON, J. T., AND P. A. BAEDECKER, Ga, Ge, Zn, Zr and Au in Lunar Terrestrial and Meteoritic Basalts. *Proceedings of the Apollo 11 Lunar Science Conference*, Vol. 2, 1970, p. 1741.
63. BAEDECKER, P. A., R. SCHANDY, J. L. ELZIE, J. KIMBERLIN AND J. WASSON, Trace Element Studies of Rocks and Soils From Oceanus Procellarum and Mare Tranquillitatis. *Proceedings of the Second Lunar Science Conference*, Vol. 2, 1971, p. 1037.
64. BOUCHET, M., G. KAPLAN, A. VOUDON AND MARIE-JEANNE BERTOLCTTI, Spark Mass Spectrometric Analysis of Major and Minor Elements in Six Lunar Samples. *Proceedings of the Second Lunar Science Conference*, Vol. 2, p. 1247.
65. BRUNFELT, A. O., K. S. HEIER AND E. STEINNES, Determination of 40 Elements in Apollo 12 Materials. *Proceedings of the Second Lunar Science Conference*, Vol. 2, 1971, p. 1281.
66. EHMANN, W. D. AND J. W. MORGAN, Major Element Abundances in Apollo 12 Rocks. *Proceedings of the Second Lunar Science Conference*, Vol. 2, 1971, p. 1237.
67. GOLES, G. G., A. R. DUNCAN, D. J. LINDSTROM, M. R. MARTIN, R. L. BEYER, M. OSAWA, K. RANDLE, L. T. MEEK, T. L. STEINBORN AND S. M. MCKAY, Analyses of Apollo 12 Specimens. *Proceedings of the Second Lunar Science Conference*, Vol. 2, 1971, p. 1063.
68. MORGAN, J. W., J. C. LAUL, U. KRÄHENBÜHL, R. GANAPATHY AND E. ANDERS, Major Impacts on the Moon. *Proceedings of the Third Lunar Science Conference*, Vol. 2, 1972, p. 1277.
69. MORRISON, G. H., J. T. GERARD, N. M. POTTER, E. V. GANGADHARAM, A. M. ROTHENBERG AND R. A. BURDO, Elemental Abundance of Lunar Soil and Rocks From Apollo 12. *Proceedings of the Second Lunar Science Conference*, Vol. 2, 1971, p. 1169.
70. WAKITA, H. AND R. A. SCHMITT, Bulk Elemental Composition of Apollo 12 Samples. *Proceedings of the Second Lunar Science Conference*, Vol. 2, 1971, p. 1231.
71. WILLIS, J. P., L. H. AHRENS, R. V. DANCHIN, A. J. ERLANK, J. J. GURNEY, P. K. HOFMEYR, T. S. MCCARTHY AND M. JORREN, Some Interelement Relationships Between Lunar Rocks and Fines and Stony Meteorites. *Proceedings of the Second Lunar Science Conference*, 1971, Vol. 2, p. 1123.
72. BAEDECKER, P. A., CHEN-LIN-CHOU AND J. T. WASSON, The Extralunar Component in Lunar Soils and Breccia. *Proceedings of the Third Lunar Science Conference*, Vol. 2, 1972, p. 1343.
73. BRUNFELT, A. O., K. S. HEIER, B. NILSSEN AND B. SUNDVOLL, Distribution of Elements Between Different Phases of Apollo 14 Rocks. *Proceedings of the Third Lunar Science Conference*, Vol. 2, 1972, p. 1133.
74. HELMKE, P. A., L. A. HASKIN, R. L. KOROTEV AND K. E. ZIEGE, Rare-Earth and Other Trace Elements in Apollo 14 Samples. *Proceedings of the Third Lunar Science Conference*, Vol. 2, 1972, p. 1275.
75. JANGHORBANI, M., M. D. MILLER, MAN-SUEN MA, L. L. CHYI AND W. D. EHMANN, Oxygen and Other Elemental Abundance Data From Apollo 14, 15, 16 and 17 Samples. *Proceedings of the Fourth Lunar Science Conference*, Vol. 2, 1973, p. 1115.
76. LAUL, J. C., R. REID, R. KEAYS, R. GANAPATHY, E. ANDERS AND J. W. MORGAN, Chemical Fractionation in Meteorites. *Geochimica et Cosmochimica Acta*, Vol. 35, No. 4, 1971, pp. 337–365.
77. LAUL, J. C., H. WAKITA, D. L. SHOWALTER, W. V. BOYTON AND R. A. SCHMITT, Bulk, Rare-Earth and Other Trace Elements in Apollo 14 and 15 and Luna 16 Samples. *Proceedings of the Third Lunar Science Conference*, Vol. 2, 1972, p. 1181.
78. ROSE, H. J., F. CUTTITTA, C. S. ANNELL, M. K. CARRON, R. P. CHRISTIAN, E. J. DWORNIK, L. P. GREENLAND AND D. T. LIGON, Compositional Data for 21 Fra Mauro Lunar Materials. *Proceedings of the Third Lunar Science Conference*, Vol. 2, 1972, p. 1215.
79. STRASHEIM, A., P. F. S. JACKSON, K. T. WYBENGA, A. J. GRICIUS, M. L. KOKOT AND R. H. SCOTT, Analysis of Lunar Samples 14163, 14259 and 14321. *Proceedings of the Third Lunar Science Conference*, Vol. 2, 1972, 1337.
80. BAEDECKER, P. A., CHEN-LIN-CHOU, E. B. GRUDEWITZ AND J. T. WASSON, Volative and Siderophille Trace Elements in Apollo 15 Samples. *Proceedings of the Fourth Lunar Science Conference*, Vol. 2, 1973, p. 1177.
81. BAEDECKER, P. A., CHEN-LIN-CHOU, E. B. GRUDEWITZ, L. L. SUNDBERG AND J. T. WASSON, Extralunar Materials in Lunar Soils and Rocks. *Lunar Science*, Abstracts and Papers, Vol. V, 1974, p. 28.
82. FRUCHTER, J. S., J. W. STOESER, M. M. LINDSTROM AND G. G. GOLES, Apollo 15 Clastic Materials and Their Relationship to Local Geologic Features. Proceedings of the Fourth *Lunar Science Conference*, Vol. 2, 1973, p. 1227.
83. GANAPATHY, R., J. W. MORGAN, U. KRÄHENBÜHL AND E. ANDERS, Ancient Meteoritic Components in Lunar Highland Rocks. *Proceedings of the Fourth Lunar Science Conference*, Vol. 2, 1973, p. 1239.
84. MORGAN, J. W., U. KRÄHENBÜHL, R. GANAPATHY AND E. ANDERS, Trace Elements in Apollo 15 Samples. *Proceedings of the Third Lunar Science Conference*, Vol. 2, 1972, p.

1361.
85. MORGAN, J. W., U. KRÄHENBÜHL, R. GANAPATHY, E. ANDERS AND U. B. MARVIN, Trace Element Abundance and Petrology of Separates From Apollo 15 Soils. *Proceedings of the Fourth Lunar Science Conference*, Vol. 2, 1973, p. 1379.
86. RHODES, J. M. AND N. J. HUBBARD, Chemistry, Classification and Petrogenesis of Apollo 15 Mare Basalts. *Proceedings of the Fourth Lunar Science Conference*, Vol. 2, 1973, p. 1127.
87. BRUNFELT, A. O., K. S. HEIER, B. NILSSEN AND B. SUNDVOLL, Geochemistry of Apollo 15 and 16 Materials. *Proceedings of the Fourth Lunar Science Conference*, Vol. 2, 1973, p. 1209.
88. DUNCAN, A. R., A. J. ERLANK, J. B. WILLIS, M. K. SHER AND L. H. AHRENS, Trace Element Evidence For a Two-Stage Origin of High-Titanium Mare Basalts. *Lunar Science*, Abstracts and Papers, Vol. V, 1974, p. 187.
89. HASKIN, L. A., D. P. BLANCHARD, J. W. JACOBS, R. L. KOROTEV, A. G. HERRMAN AND R. REID, Rare-Earth and Other Trace Elements in Some Individual 1-21m Fines From Apollo 16 and 17. *Lunar Science*, Abstracts and Papers, Vol. V, 1974, p. 310.
90. KRÄHENBÜHL, U., R. GANAPATHY, J. W. MORGAN AND S. ANDERS, Volative Elements in Apollo 16 Samples. *Geochimica et Cosmochimica Acta*, Supplement 4, 1973, p. 1325.
91. LAUL, J. C. AND R. A. SCHMITT, Chemical Composition of Apollo 15, 16 and 17 Samples. *Proceedings of the Fourth Lunar Science Conference*, Vol. 2, 1973, p. 1349.
92. MORRISON, G. H., R. A. NADKARNI, J. YAWORSKI, R. I. BOTTO AND J. R. ROTH, Elemental Abundances of Apollo 16 Samples. *Proceedings of the Fourth Lunar Science Conference*, Vol. 2, 1973, p. 1399.
93. ROSE, H. J., F. CUTTITTA, S. BESMAN, M. K. CARRON, R. P. CHRISTIAN, E. J. DWORNIK, L. P. GREENLAND AND D. T. LIGON, Compositional Data For 22 Apollo 16 Samples. *Proceedings of the Fourth Lunar Science Conference*, Vol. 2, 1973, p. 1149.
94. BRUNFELT, A. O., K. S. HEIER, B. NILSSEN, E. STEINNES AND B. SUNDVOLL, Elemental Composition of Apollo 17 Fines. *Lunar Science*, Abstracts and Papers, Vol. V, 1974, p. 92.
95. ELDRIDGE, J. S., G. D. O'KELLY AND K. J. NORTHCUTT, Primordial Radio-Element Concentrations from Taurus Littrow. *Lunar Science*, Abstracts and Papers, Vol. V, 1974, p. 206.
96. MORGAN, J. W., R. GANAPATHY, H. HIGUCHI, U. KRÄHENBÜHL AND E. ANDERS, Lunar Basins. *Lunar Science*, Abstracts and Papers, Vol. V, 1974, p. 526.
97. GRIEVE, R. A. F., G. A. MCKAY AND D. F. WEILL, Microprobe Studies of Three Luna 16 Basalt Fragments. *Earth Planet. Science Letters*, Vol. 13, No. 2, 1972, p. 233.
98. LOVERING, J. F. AND D. BUTTERFIELD, Neutron Activation Analysis of Rhenium and Osmium Apollo 11 Lunar Material. *Proceedings of the Apollo 11 Lunar Science Conference*, Vol. 2, 1970, p. 1351.
99. LOVERING, J. F. AND T. C. HUGHES, Re and Os Abundance Determination and Meteoritic Contamination Levels in Apollo 11 and 12 Lunar Samples. *Proceedings of the Second Lunar Science Conference*, Vol. 2, 1971, p. 1331.
100. REED, G. W. AND S. JOVANOVIC, The Halogens and Other Trace Elements in Apollo 12 Samples. *Proceedings of the Second Lunar Science Conference*, Vol. 2, 1971, p. 1261.
101. COMPSTON, W., B. W. CHAPPELL, P. A. ARRIENS AND M. J. VERNON, The Chemistry and Age of Apollo 11 Lunar Material. *Proceedings of the Apollo 11 Lunar Science Conference*, Vol. 2, 1970, p. 1007.
102. GAST, P. W., N. J. HUBBARD AND H. WIESMANN, Chemical Composition and Petrogenesis of Basalts from Tranquillity Base. *Proceedings of the Apollo 11 Lunar Science Conference*, Vol. 2, 1970.
103. MAXWELL, J. A., L. C. PECK AND H .B. WIIK, Chemical Composition of Apollo 11 Lunar Samples 10017, 10020, 10072 and 10084. *Proceedings of the Apollo 11 Lunar Science Conference*, Vol. 2, 1970, p. 1369.
104. MURTHY, R., N. M. EVENSEN AND M. R. COSCIO, Distribution of K, Rb, Sr and Ba and Rb-Sr Isotopic Relations in Apollo 11 Lunar Samples. *Proceedings of the Apollo 11 Lunar Science Conference*, Vol. 2, 1970, p. 1393.
105. PHILPOTTS, J. A. AND C. C. SCHNETZLER, Apollo 11 Lunar Samples: K, Rb, Sr, Ba and Rare-Earth Concentrations in Some Rocks and Separate Phases. *Proceedings of the Apollo 11 Lunar Science Conference*, Vol. 2, 1970, p. 1471.
106. SILVER, L. T., Uranium-Thorium-Lead Isotopes in Some Tranquility Base Samples. *Proceedings of the Apollo 11 Lunar Science Conference*, Vol. 2, 1970, p. 1533.
107. TERA, F., O. EUGSTER, D. S. BURNETT AND G. J. WASSERBUBG, Comparative Study of Li, Na, K, Rb, Cs, Ca, Sr and Ba Abundance in Achondrites and in Apollo 11 Samples. *Proceedings of the Apollo 11 Lunar Science Conference*, Vol. 2, 1970, p. 1637.
108. WAKITA, H., P. REY AND R. A. SCHMITT, Abundance of the 14 Rare Earth Elements and 12 Other Trace Elements in Apollo 12 Samples. *Proceedings of the Second Lunar Science Conference*, Vol. 2, 1971, p. 1319.
109. EISENTRAUT, K. J., M. S. BLACK, F. D. HILE-

MAN AND R. E. SILVERS, Be and Cr Abundances in Fra Mauro and Haddley-Apennine Lunar Samples. *Proceedings of the Third Lunar Science Conference,* Vol. 2, 1972, p. 1327.

110. PHILPOTTS, J. A., C. C. SCHNETZLER, D. F. NAVA, M. L. BOTTINO, P. D. FULLAGAR, H. H. THOMAS, S. SCHUNMANN AND C. W. KOUNS, Apollo 14: Some Geochemical Aspects. *Proceedings of the Third Lunar Science Conference,* Vol. 2, 1972, p. 1293.
111. CHYI, L. L. AND W. D. EHMANN, Zr and Hf Abundances in Some Lunar Materials and Implications of Their Ratios. *Proceedings of the Fourth Lunar Science Conference,* Vol. 2, 1973, p. 1219.
112. CHYI, L. L. AND W. D. EHMANN, Implication of Zr and Hf Abundances and Their Ratios in Lunar Materials. *Lunar Science,* Abstracts and Papers, Vol. V, 1974, p. 118.
113. NAKAMURA, N. AND A. MASUDA, Chemical Composition and Rare-Earth Features of Four Apollo 16 Samples. *Proceedings of the Fourth Lunar Science Conference,* Vol. 2, 1973, p. 1407.
114. PHILPOTTS, J. A., S. SCHUINMANN, C. W. KOUNS, R. K. L. LUM, A. L. BICKEL AND C. C. SCHNETZLER, Apollo 16 Returned Lunar Samples. *Proceedings of the Fourth Lunar Science Conference,* Vol. 2, 1973, p. 1427.
115. ALBEE, A. L., A. A. CHODOS, A. J. GANCARZ, E. L. HAINES, D. A. PAPANASTASSIOU, L. RAG, F. TERA, G. J. WASSERBURG AND T. WEN, Mineralogy, Petrology and Chemistry of a Luna 16 Basalts Fragment, Sample B–I. *Earth Planet. Science Letters,* Vol. 73, No. 2, 1972, p. 353.
116. ALLEGRE, C., *Rb-Sr Age and K, Rb, Sr, Ba Rare Earth Contents in the Sea of Fertility Soil.* C. R. Acad. Sci. Paris, Series D, t. 273, s. 779, 1971.
117. EYSTER, O., Contents of Li, Be, B and Ti and the Isotopic Composition of Li, B and Mg in the Luna 16 Regolith Probe. *Lunar Solar from the Sea of Fertility,* 1974, p. 370.
118. HELMKE, P. A. AND L. A. HASKIN, Rare-Earth and Other Trace Elements in Luna 16 Soil. *Earth Planet, Science Letters,* Vol. 13, No. 2, 1972, p. 441.
119. PHILPOTTS, J. A., C. C. SCHNETZLER, M. L. BOTTINO, S. SCHUMANN AND H. H. THOMAS, Luna 16: Some Li, K, Rb, Sr, Ba Rare-Earth, Zr and Hf Concentrations. *Earth Planet. Science Letters,* Vol. 13, No. 2, 1972, p. 429.
120. GOPALAN, K., S. KAUSHAL, C. LEE-HU AND G. W. WETHERILL, Rb-Sr and U, Th-Pb Ages of Lunar Materials. *Proceedings of the Apollo 11 Lunar Science Conference,* Vol. 2, 1970, p. 1195.
121. HERZOG, G. F. AND G. F. HERMAN, Na^{22}, Al^{21}, Th and U in Apollo 11 Lunar Samples. *Proceedings of the Apollo 11 Lunar Science Conference,* Vol. 2, 1970, p. 1239.
122. O'KELLEY, G. D., J. ELDRIDGE, E. SCHONFELD AND P. R. BELL, Primordial Radionuclide Abundance and Ages of Apollo 11 Lunar Samples. *Proceedings of the Apollo 11 Lunar Science Conference,* Vol. 2, 1970, p. 1415.
123. TATSUMOTO, M., Age of the Moon. *Proceedings of the Apollo 11 Lunar Science Conference,* Vol. 2, p. 1595.
124. O'KELLEY, G. D. AND J. S. ELDRIDGE, Abundance of the Primordial Radionuclides K, Th and U in Apollo 12. *Proceedings of the Second Lunar Science Conference,* Vol. 2, 1971, p. 1159.
125. TATSUMOTO, M., R. J. KNIGHT AND B. R. DOE, U-Th-Rb Systematics of Apollo 12 Lunar Samples. *Proceedings of the Second Lunar Science Conference,* Vol. 2, 1971, p. 1521.
126. TATSUMOTO, M., C. E. HEDGE, B. R. DOE AND D. M. UNRUH, U-Th-Pb and Rb-Sr Measurements on Some Apollo 14 Lunar Samples. *Proceedings of the Third Lunar Science Conference,* Vol. 2, 1972, p. 1531.
127. JOVANOVIC, S. AND G. W. REED, Volative Trace Elements and the Characterization of the Cayley Form and the Primitive Lunar Crust. *Proceedings of the Fourth Lunar Science Conference,* Vol. 2, 1973, p. 1313.
128. REED, G. W., JR. AND S. JOVANOVIC, Hologens, Mercury, Lithium and Osmium in Apollo 11 Samples. *Proceedings of the Apollo Lunar Science Conference,* Vol. 2, 1970, p. 1487.
129. *Symposium sur l'Origine du Systeme Solaire.* Centre National de la Recherche Scientifique, Nice, April 3–7, 1972.
130. ARRHENINS, G. AND H. ALFV'EN, Fractionation and Condensation in space. *Earth Planet. Science Letters,* Vol. 10, 1971, p. 253.
131. ALLEN, R. O., S. JOVANOVIC, D. SHOWALTER AND G. W. REED, Pb^{204}, Bi, Tl, and Zn in Apollo 16 Samples and Inferences on the Lunar Geochemistry, Etc. *Lunar Science,* Abstracts and Papers, Vol. V, 1974, p. 12.
132. BALASHEV, YU. A., *Geochemistry of Rare-Earth Elements in Magmatic and Sedimentary Rocks.* Doctoral Dissertation, 1974.
133. CAMPSIE, J., J. C. BAILEY, M. RASMUSSEN AND F. DITTMER, Chemistry of Tholeiites From the Reykjanes Ridge and Charlie Gibbs Fracture Zone. *Nature,* Vol. 244, No. 135, 1973, p. 71.
134. CHOU-CHEN-LIN AND A. J. COHEN, Ga and Ge in the Metal and Silicates of L and LL-Chondrites. *Geochimica et Cosmochimica Acta,* Vol. 37, 1973, p. 315.
135. CHOU-CHEN-LIN, P. A. BAEDECKER, R. W. BILD, K. L. ROBINSON AND J. T. WASSON, *Lunar Science,* Abstracts and Papers, Vol. V, 1974,

p. 115.
136. COMPSTON, W., H. BERRY, M. J. VERNON, B. W. CHAPPELL AND M. J. KAYE, Rb-Sr Chronology and Chemistry of Lunar Materials From the Ocean of Storms. *Proceedings of the Second Lunar Science Conference*, Vol. 2, 1971, p. 1471.
137. ENGEL, A. E., ET AL., Chemical Characteristics of Oceanic Basalts and the Upper Mantle. *Bull. Geol. Soc. Am.* Vol. 76, No. 7, 1965.
138. FISHER, D. E., Achondritic Uranium. *Earth Planet. Science Letters*, Vol. 20, No. 1, 1973, p. 151.
139. GANAPATHY, R., J. W. MORGAN, H. HOGUCHI, E. ANDERS AND A. T. ANDERSON, Meteoritic and Volative Elements in Apollo 16 Rocks in Separated Phase From 14306. *Lunar Science*, Abstracts and Papers, Vol. V, 1974, p. 257.
140. HART, E., K. H. SCHMIDT AND K. N. VASUDEVAN, Apollo 17 Seismic Profiling. *Science*, Vol. 180, 1973, p. 1063.
141. HASKIN, L. A., P. A. HELMKE, R. O. ALLEN, M. R. ANDERSON, R. L. KOROTEVA AND K. A. ZWEIFEL, Rare-Earth Elements in Apollo 12 Lunar Materials. *Proceedings of the Second Lunar Science Conference*, Vol. 2, 1971, p. 1307.
142. HODGES, C. A., W. R. MUCHLBERGER AND G. E. ULRICH, Geologic Setting of Apollo 16. *Proceedings of the Fourth Lunar Science Conference*, Vol. 1, 1973, p. 1.
143. JAKES, P. J. AND A. J. R. WHITE, U-Bearing Minerals of Lunar Rock 12013. *Earth Planet. Science Letters*, Vol. 12, No. 2, 1973, p. 145.
144. JOVANOVIC, S. AND G. W. REED, Labile Trace Elements in Apollo 17 Samples. *Lunar Science*, Abstracts and Papers, Vol. V, 1974, p. 391.
145. KUTOLIN, V. A., *Statistical Study of the Chemism of Basalts*, 1969.
146. LAUL, J. C. AND R. A. SCHMITT, Chemical Composition of Apollo 17 Boulder-2 Rocks and Soils. *Lunar Science*, Abstracts and Papers, Vol. V, 1974, p. 438.
147. MASON, B. AND W. G. MELSON, The Lunar Rocks. *Eucrites*, 1970, p. 117.
148. MASON, B., (ed.), *Elemental Abundances in Meteorites*. Gordon and Breach, 1971.
149. NUNES, P. D., M. TATSUMOTO, R. J. KNIGHT, D. M. UNRUH AND B. R. DOE, U-Th-Pb Systematics of Some Apollo 16 Lunar Samples. *Proceedings of the Fourth Lunar Science Conference*, Vol. 2, p. 1797.
150. PHILPOTTS, J. A., S. SCHUMANN, C. W. KOUNS AND R. K. L. LUM, Lithophile Trace Elements in Apollo 17 Soils. *Lunar Science*, Abstracts and Papers, Vol. V, 1974, p. 599.
151. REED, G. W., S. JOVANOVIC AND L. FUCHS, Trace Element Relation Between Apollo 14 and 15. *Proceedings of the Third Lunar Science Conference*, Vol. 2, 1972, p. 1989.
152. REED, S. J. B., Determination of Ni, Ga and Ge in Iron Meteorites by X-ray Fluorescence Analysis. *Meteoritics*, Vol. 7, No. 3, 1972, p. 257.
153. REID, A. M. AND P. JAKES, Luna 16 Revisited: The Case for Aluminous Mare Basalts. *Lunar Science*, Abstracts and Papers, Vol. V, 1974, p. 627.
154. ROSE, H. J., F. W. BROWN, M. K. CARRON, R. P. CHRISTIAN, F. CUTTITTA, E. J. DWORNIK AND D. T. LIGON, Composition of Some Apollo 17 Samples. *Lunar Science*, Abstracts and Papers, Vol. V, 1974, p. 645.
155. SCHMITT, R. A., G. GOLES, R. H. SMITH AND T. W. OSBORN, Elemental Abundances in Stone Meteorites. *Meteoritics*, Vol. 7, No. 2, 1972, p. 131.
156. SIEVERS, R. E. ET AL., Variations in Be and Cr Contents in Lunar Fines Compared with Crystalline Rocks. *Proceedings of the Second Lunar Science Conference*, Vol. 2, p. 1451.
157. UREY, H. C. AND H. CRAIG, The Composition of the Stone Meteorites and the Origin of the Meteorites. *Geochimica et Cosmochimica Acta*, Vol. 4, 1953, p. 36.
158. WOLFE, E. W. AND COLLABORATOR, Apollo 17: Exploration at Taurus-Littrow. *Geotimes*, Vol. 17, No. 11, 1972, p. 14.

Page intentionally left blank

Page intentionally left blank

A Survey of Lunar Rock Types and Comparison of the Crusts of Earth and Moon

John A. Wood
Center for Astrophysics
Harvard College Observatory and
Smithsonian Astrophysical Observatory
Cambridge, Massachusetts

The principal known types of lunar rocks are briefly reviewed, and their chemical relationships discussed.

In the suite of low-KREEP highland rocks, Fe/(Fe + Mg) in the normative mafic minerals increases and the albite content of normative plagioclase decreases as the total amount of normative plagioclase increases, the opposite of the trend predicted by the Bowen reaction principle. Lunar highland samples analyzed are uniformly distributed in this sequence, in which normative plagioclase contents range from ~ 40 percent to ~ 100 percent. The distribution of compositions of rocks from terrestrial layered mafic intrusives is substantially different: here the analyses fall in several discrete clusters (anorthositic rocks, norites, granophyres and ferrogabbros, ultramafics), and the chemical trends noted above are not reproduced.

It is suggested that the observed trends in lunar highland rocks could be produced by crystal fractionation in a deep global surface magma system if (1) plagioclase tended to float, upon crystallization, and (2) the magma was kept agitated and well mixed (probably by thermal convection) until crystallization was far advanced and relatively little residual liquid was left. When such a system was finally immobilized, the Fe-, Na-rich residual liquid would produce Fe-rich mafic minerals in the upper levels of the system, but could not much alter the composition of abundant calcic plagioclase. Conversely, the same liquid would produce sodic plagioclase deep in the sequence, but could not much alter the composition of abundant magnesian mafic minerals.

After the crustal system solidified, but before extensive cooling had developed a thick, strong lithosphere, mantle convection was able to draw portions of the lunar anorthositic crust down into the mantle in a manner analogous to the present-day behavior of the terrestrial mantle and crust. At depth, the crustal material was heated; KREEP-rich norite was extracted by partial melting and erupted at the surface as a lava, analogous to terrestrial andesite eruptions.

Five years have passed since Eagle, the Lunar Module of the Apollo 11 mission, landed at Tranquillity Base. In the time since, samples of lunar material returned by six Apollo and two Luna missions to the Moon have been studied intensively, and thousands of pages of descriptive material have been published. The samples collected at the eight sites are not totally different from one another: in many cases, essentially the same rock type has been observed among the collections returned from two or more sites. The tendency for certain rock types to occur at several widely separated points on the Moon is sufficiently great to make us confident that we have obtained a fairly good sampling of the surface layers of the lunar nearside.

In reading the literature, it is not easy to gain an impression of the total range of compositions of lunar materials encountered, or their frequency of occurrence in the samples returned. Papers descriptive of lunar samples

are typically specialized and detailed, and present only the results from a single laboratory, employing a single technique of analysis. Sometimes data from the samples of other missions, or data obtained by other workers, are shown for comparison, but the body of data included for comparison tends to be small and highly selective. The need exists for a broad comparison of the properties of all lunar materials studied to date.

The chemical composition of its major element is the most fundamental property of a lunar rock, and the one most useful for separating categories of lunar rocks and understanding the relationship of the various categories to one another. Petrographic textural information is, in my opinion, of secondary importance. In the case of highland rocks, textures record a history of relatively superficial processes (brecciation, mixing, thermal recrystallization) that are less important than the large-scale internal geochemical processes that largely determined the chemical compositions of the lunar rocks. It might be argued that textural information is essential in order to distinguish between pristine igneous rocks and polymict breccias in which several rock types with different chemical compositions have been mixed; but, unfortunately, major impacts are capable of remelting complex breccias on the Moon and giving them igneous textures. For few, if any, crystalline igneous rocks from the lunar highlands can one exclude, on petrographic grounds, the possibility of derivation from an impact melt, in which the parent material melted was a complex mixture of earlier rock types.

There are three major categories of lunar samples, the analyses of which might be expected to inform us of the major lunar rock types. The first of these is lunar rocks of hand specimen size, which are usually analyzed by traditional wet-chemical or X-ray fluorescence techniques. The second is smaller lithic fragments from soil samples and discrete clasts from complex breccias. These can be analyzed by a variety of techniques, including neutron activation analysis and electron-microprobe analysis of fused beads; but the great majority of lithic fragment and clast analyses reported in the literature were obtained by using an electron microprobe with a broad (defocused) beam to analyze a large number of spots on a polished section surface. The third category consists of fragments or globules of glass from the lunar soil samples, which are analyzed individually by the traditional electron-microprobe method.

Each of these three categories of material, including its method of analysis, has its own strengths and weaknesses, which are summarized in table 1. Here the comment that studies of lithic fragments from soils (and clasts) are least accurate alludes to the fact that most such analyses reported in the liter-

Table 1.—*Sources of Information About Lunar Rock Compositions*

	Advantages	Disadvantages	No. of Analyses in SAO Library
Large Rocks	Most accurate Representative (?) Petrography, other properties known	Small number of samples analyzed Integrates polymict breccias	156
Lithic Fragments From Soils	Petrography known Large number analyzed	Least accurate Poorly representative (?)	530
Glass Particles From Soils	Accurate Probably very representative (well-mixed) Large number analyzed	Petrography not known; parent may be polymict	2389

ature were made by the defocused-beam technique. The traditional procedure for reducing and correcting electron-microprobe analyses assumes a homogeneous target volume and is not strictly applicable when the microprobe beam is enlarged to embrace many mineral grains of differing compositions simultaneously. For this reason, it is recognized that defocused-beam analyses (DBA) provide no more than an approximation of the true composition of the material analyzed, although the approximation can be a very good one, if the data reduction is carried out thoughtfully.

In table 1, the question of which type of sample is most representative of its parent rock is not so straightforward as it might seem. Clearly, a large rock can be sampled and analyzed in a much more representative way than a 1-mm lithic fragment, especially when only a section surface through the lithic fragment is accessible for DBA sampling. However, this assumes that the large rock, or a substantial fraction of it, was homogenized and properly sampled to obtain an aliquot for chemical analysis. In fact, with a handful of exceptions, this procedure was not carried out for lunar hand specimens because of the wish to consume as little of them as possible, retaining the great bulk of each specimen intact and uncontaminated for study by future generations of scientists. Typically, rock in the amount of 0.5 g was allocated to an investigator for major element chemical analysis, and this was delivered in the form of a single chip, rather than as a powder representative of a much larger mass of material. If the rock was coarse grained or otherwise heterogeneous on a large scale, the sample analyzed may have been a poor representative of the whole.

In the case of lithic fragments, the volume sampled is undeniably smaller by a large factor; yet for very fine grained rocks, the sample volume may be adequate. Many of the lunar highland rocks are, in fact, fine grained; presumably responsible investigators would not report or attempt analyses of lithic fragments in which the grain size is too coarse to permit adequate sampling. The DBA technique has an advantage that should be weighed against the disadvantage of the small volume sampled, i.e., the fact that lithic fragments can be assessed petrographically, in thin section, at the time the analysis is performed. Thus, materials that are obviously polymict in character can be avoided, and analyses can be limited to fragments or clasts of uniform lithology.

During the past year, my group has assembled from the literature a library of chemical analyses of lunar materials from all three categories. The current number of entries is shown in table 1. These come from many different sources, too many for each to be referenced explicitly. The library includes all analyses reported in the *Proceedings* of the first through fourth Lunar Science Conferences, in *Lunar Science I* through *IV*, and in the Apollo 15, 16, and 17 Preliminary Science Reports. The largest contributors to the library were the group headed by K. Keil (DBA's of lithic fragments and point microprobe analyses of glass particles) and the Apollo Soil Survey (A. M. Reid and coworkers; point analyses of glass particles from soil samples). No analyses of bulk soil samples were included in the library.

My objective was to plot large bodies of lunar data in a number of types of chemical and mineralogical variation diagrams, and to seek broad trends and clusterings of compositions. A conscious effort was made to escape the detailed relationships between individual analyses that have dominated lunar science, and to try to see "the forest instead of the trees." A computer plotting routine was developed that samples the library and enters the appropriate analyses in a three-variable orthogonal reference frame, the axes of which can be made to correspond to three chosen variables. An orthographically projected view of the reference frame and up to 500 plotted data points are drawn by a CalComp plotter. Each data point is represented as the head of a pin, the shaft of which projects down to the plane defined by the two horizontal axes of the reference frame. This intersection of the "pin" with the base of the reference frame gives the

viewer an impression of its depth in the three-dimensional volume portrayed. The assembly of a single plot takes about 1 minute of central processor time on a CDC 6400 computer, and the plot is drafted in approximately 1 hour by a CalComp model 564.

It should be stressed that when the content or composition of minerals is plotted in these diagrams, the reference is to normative mineralogy, computed from major element chemical compositions. Actual modal mineralogies and compositions are not stored in the analysis library.

Use of the data library and plotting routine is illustrated in figure 1, a plot of three chemical parameters that might be expected to discriminate effectively between lunar mare basalts and highland samples. The library of analyses was sampled randomly, in such a way as to provide approximately equal numbers of data points from the three categories of analyses discussed above. Included are 152 whole-rock analyses, 177 analyses of lithic fragments, and 171 analyses of glass particles. The plot distinguishes fairly cleanly between mare and highland materials. However, it also illustrates some of the shortcomings of lithic fragment and glass analyses alluded to in table 1. The highland data points form an extremely compact and well-defined grouping, except for a number of DBA stragglers, which seem to contain anomalously high levels of Al_2O_3 and/or $K_2O + P_2O_5$ (D, figure 1). The "stragglers" appear only on the high Al_2O_3 side of the highland grouping. It is likely that their position is false; the DBA technique systematically overreports Al and P, unless special corrections are

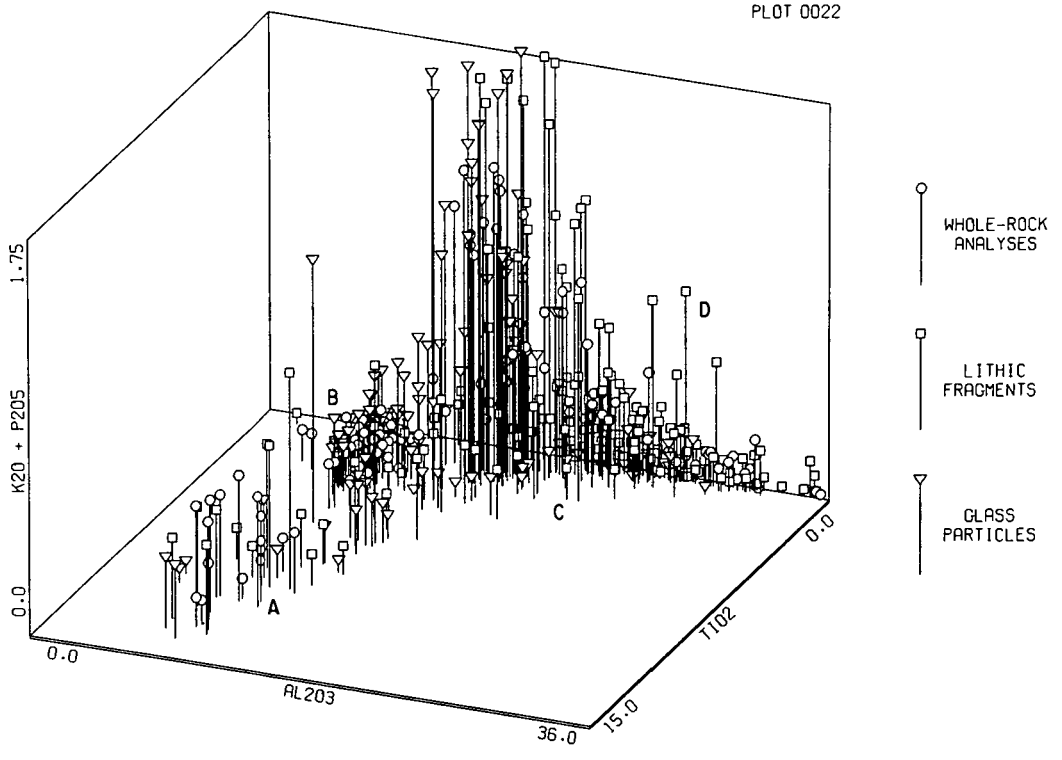


Figure 1.—*Approximately equal numbers of lunar whole-rock, lithic fragment, and glass analyses, in a type of plot that attempts to discriminate clearly between mare and highland samples. A: high-Ti mare basalts from the Apollo 11 and 17 missions. B: Apollo 12 and 15 basalts and green glasses (chiefly from Apollo 15). C: highland materials. D: defocused-beam analyses of highland materials, probably reporting spuriously high levels of Al_2O_3 and/or KREEP.*

made. Again, there is an almost continuous row of data points representing glass analyses extending from A (mare basalts) to C (highland compositions). This does not represent a spectrum of real lunar lithic types; it is undoubtedly a mixing line. These glasses were derived from soil or breccia parent materials that contained a mechanical mixture of mare and highland rock types. The crucial distinction between mare and highland rock types is blurred here, and also in the gap between cluster B and the main body of highland rock compositions, by glass analyses. Because of this obscuring effect of the glass data, I have omitted glass analyses from most of the other plots in this paper. Possibly this is an overreaction to the deficiencies of the glass data; the consideration of plots of large numbers of glass particle compositions has led to the appreciation of several important lunar rock types (ref. 1), and it is also the case that several important lunar materials (the green and orange glasses) have no known crystalline equivalents.

Figure 2 is a replot of figure 1, containing 156 whole-rock analyses and 348 lithic fragment analyses. Here and in most other plots of this paper, shapes of pinheads are no longer used to identify the categories of lunar samples plotted, but rather their sources on the Moon. The distinction between mare and highland rock compositions can be drawn somewhat more clearly in this figure than in figure 1. Two entries that occupy an equivocal position between the mare and highland groupings of analyses are identified in the caption of figure 2. The "highland/mare" boundary drawn on the floor of the plot illus-

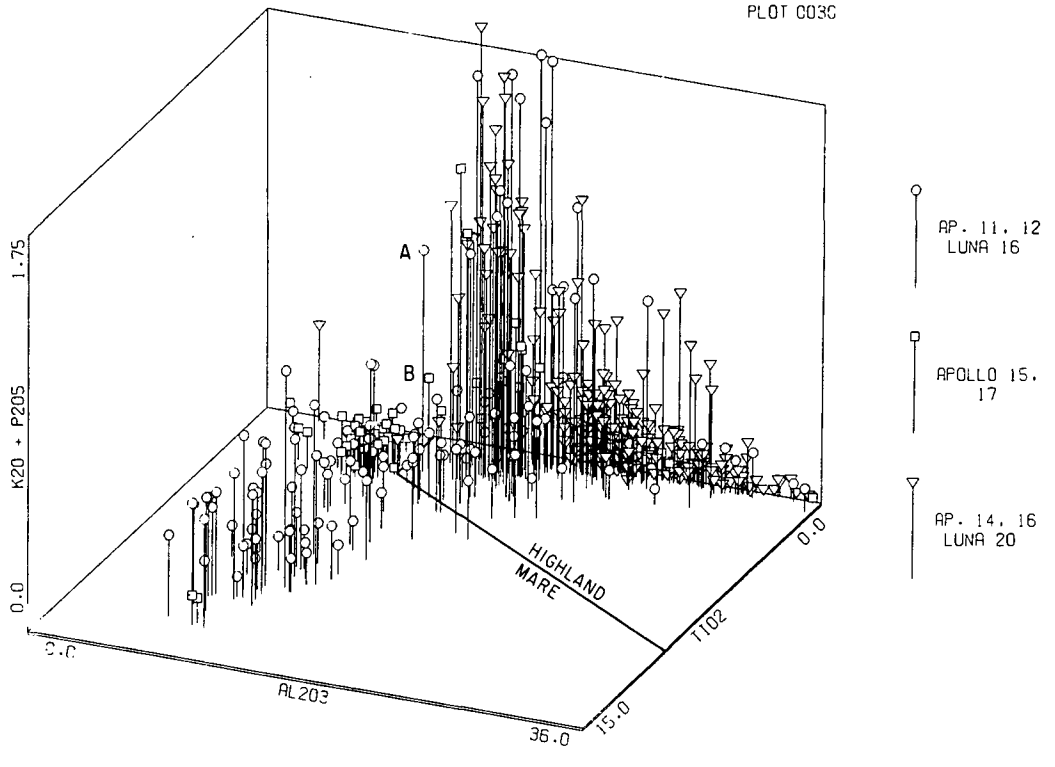


Figure 2.—*Plot similar to figure 1, except that glass analyses have been eliminated; pinhead shapes now denote sources of samples on the Moon. "Highland/Mare" boundary drawn on floor illustrates chemical criteria used to separate these two classes of lunar rocks in succeeding plots. The separation is generally clean; A and B occupy equivocal positions. A is a DBA of an "igneous" lithic fragment from soil 12057 (Bunch et al., ref 2); B is soil breccia 15558, which contains both mare and highland components.*

trates the chemical criteria used elsewhere in this paper to arbitrarily separate mare from highland samples. The rule adopted was that if

$Al_2O_3 > 11\%$ and $(0.3 \times Al_2O_3 - 1.1) > TiO_2$,

a sample was considered to be a highland rock type.

The two discrete categories of lunar rocks —mare basalts and highland rocks of various types—will be discussed separately below.

Mare Basalts

Crystalline mare materials can be separated into four categories—three major and one minor—by plotting TiO_2 against K_2O (fig. 3). The plot also displays the proportion of olivine among normative mafic minerals, a measure of the degree of undersaturation of the rock. Categories C, D, E, and F of figure 3 have been further subdivided petrographically, as follows.

Group C consists of Apollo 12 and 15 basalts. James and Wright (ref. 3) subdivide the Apollo 12 basalts into three categories: olivine-pigeonite basalts and gabbros, ilmenite-bearing basalts and gabbros, and feldspathic basalts. Brown et al. (ref. 4) subdivide the Apollo 15 mare basalts into three additional groups: pyroxene-rich tridymite gabbros, porphyritic vitrophyres, and olivine basalts.

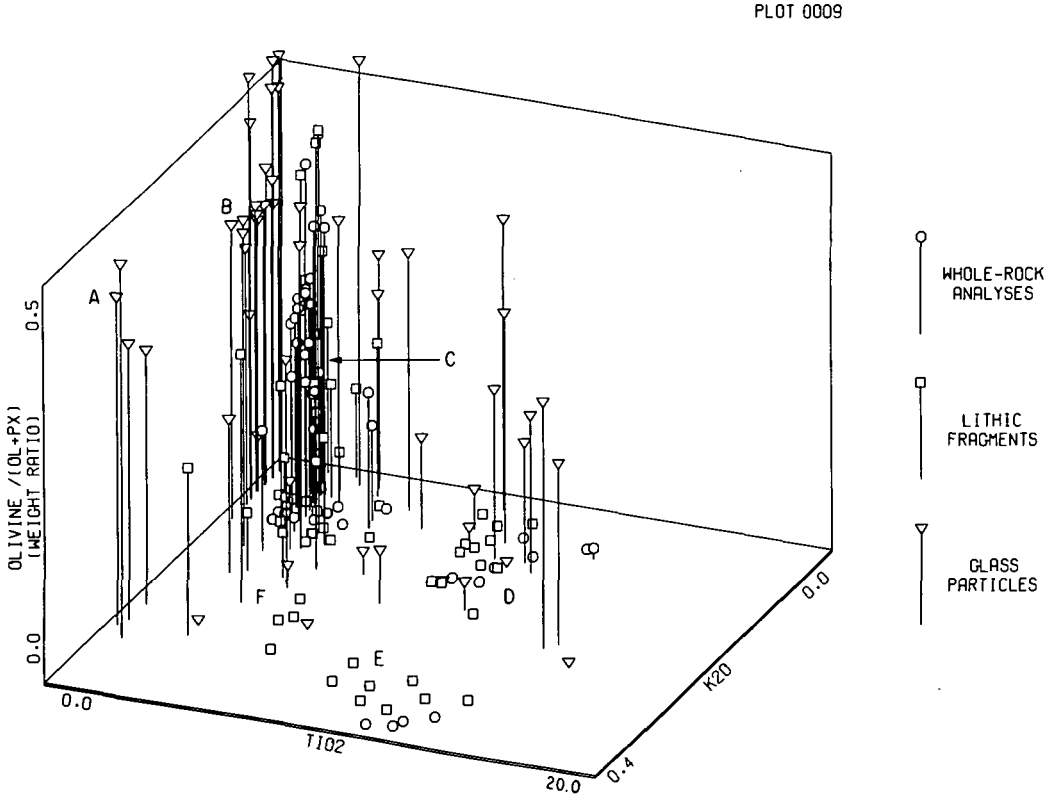


Figure 3.—*Plot of parameters that tend to separate the recognized categories of lunar mare basalts. The criteria of figure 2 were used to reject highland materials from the plot, but the separation is not perfect; points at A (Apollo 14 and 15 glasses) are unlikely to be pure rock types. The array of low-TiO_2 entries at B is composed of green glasses, mostly from Apollo 15. C is a column of Apollo 21 and 15 mare basalts; both missions are represented along the entire sequence of olivine contents. D represents Apollo 11 and 17 low-K basalts; E, Apollo 11 high-K basalts. At F, several of the entries are Luna 16 basalts, which tend to span the gap between E and C.*

Group D comprises the Apollo 11 ophitic ilmenite basalts (low-K basalts) recognized by James and Wright (ref. 3) and others, and all the Apollo 17 mare basalts. Brown et al. (ref. 5) subdivide the latter into three categories: olivine basalts, ferrobasalts, and basalts transitional between these two.

Group E consists of the Apollo 11 intersertal ilmenite basalts (high-K basalts) recognized by James and Wright (ref. 3) and other authors.

The ophitic pigeonite basalt fragments from the Luna 16 soil sample appear in group C. In terms of the parameters plotted, the Luna 16 basalt is intermediate in character between groups C and E; however, in other respects, including its content of trace elements (e.g., ref. 6), the Luna 16 basalt cannot be regarded as a simple mixture of the two end members indicated.

Chemical compositions of representatives of most of the mare basalt subcategories discussed are presented in table 2.

Highland Rocks

The frequency of occurrence of different types of highland rock is highly variable in figure 2. In this figure, a dense mass of entries occurs in the interval of Al_2O_3 content between 21 and 32 percent. These are the anorthositic rocks of the lunar highlands; they are anorthositic gabbros and gabbroic anorthosites according to traditional terrestrial nomenclature. The KREEP content of this group of rocks is probably extremely sharply bounded; as previously noted, the half-dozen entries that rise to KREEP contents substantially higher than those of the great mass of lunar anorthositic rocks are probably the result of inaccurate defocused-beam analyses. The density of entries seems to fall off very sharply above 32 percent Al_2O_3.

The central column of "pins" in figure 2 represents the lunar norites. This cluster of entries appears discontinuous with the low-plagioclase end of the anorthositic distribution. This may signify that the two families of highland rocks formed by fundamentally different processes, a conclusion that has gained wide currency in the lunar science community for other reasons; but it is important to recognize that the exceptional density of data points in the Al_2O_3 range from 21 to 32 percent in figure 2 is largely due to the heroic project of defocused-beam analysis of lithic fragments from the Luna 20 sample carried out by Conrad et al. (ref. 15). Thus, the apparent discontinuity between abundances of noritic and anorthositic gabbro compositions may occur only in the vicinity of Mare Crisium, and may not be a property of the lunar highlands as a whole.

Entries appear to be unevenly distributed along the vertical extent of the norite column. When the entries in this column are plotted in a simple histogram, three peaks appear: a low-KREEP peak centered about 0.3 percent $K_2O + P_2O_5$; a high-KREEP peak centered on 1 percent $K_2O + P_2O_5$; and a smaller extra-high-KREEP peak at 1.6 percent $K_2O + P_2O_5$. The extra-high-KREEP cluster consists entirely of DBA's of lithic fragments from Apollo 12 and 14 soil samples; several were reported by my own group. It now appears that these analyses systematically overreported P_2O_5, so it is likely that the extra-high-KREEP group is spurious. Unfortunately, the total number of high- and low-KREEP points plotted is not large enough to resolve with confidence the important question of whether the distribution of KREEP contents is continuous or bimodal.

Table 3 presents analyses of lunar highland rocks representative of the major classes discussed above. One other minor but potentially important rock class, the spinel troctolites, is also represented. Spinel troctolite entries in figure 2 would be hidden behind the mare basalt cluster beneath B. They are excluded from plots containing highland samples only, by the chemical criteria that separate out mare basalt analyses.

In figure 4, 156 whole-rock analyses and 530 lithic fragment analyses of highland materials are plotted against three indices of igneous fractionation. The assemblage of "pins" falls into two distinct groups. At the left of the plot (A–B), a group of entries

Table 2.—*Chemical Compositions of Mare Basalts Representative of of Major Recognized Classes*

Group	C					D			E	F
	Apollo 12			Apollo 15		Apollo 11	Apollo 17		Apollo 11	Luna 16
Petrographic Type	Olivine-Pigeonite Basalt	Ilmenite-bearing Basalt	Feldspathic Basalt	Pyroxene-rich Tridymite Gabbro	Olivine Basalt	Ophitic Ilmenite Basalt	Olivine Basalt	Olivine Ferro-basalt	Intersertal Ilmenite Basalt	Ophitic Pigeonite Basalt
Example	12009[a]	12022[b]	12038[c]	15058[d]	15016[e]	10020[f]	70215[g]	70017[g]	10072[f]	21012, B-1[h]
SiO_2	45.03	43.20	47.1	47.81	44.30	41.00	37.91	38.37	40.20	45.50
Al_2O_3	8.59	9.04	12.8	8.87	8.39	9.83	8.86	8.78	7.78	13.95
TiO_2	2.90	5.16	3.17	1.77	2.27	10.28	13.08	12.83	12.28	4.04
MgO	11.55	10.43	6.80	9.01	11.65	7.77	7.99	9.41	8.06	5.95
FeO	21.03	21.44	17.4	19.97	22.95	19.03	19.96	18.71	19.77	17.77
MnO	0.28	0.25	0.24	0.28	0.29	0.27	0.26	0.25	0.22	0.26
CaO	9.42	9.56	11.4	10.32	9.20	11.96	10.77	10.43	10.27	11.96
Na_2O	0.23	0.47	0.64	0.28	0.32	0.37	0.38	0.43	0.52	0.63
K_2O	0.06	0.07	0.07	0.03	0.05	0.05	0.04	0.05	0.29	0.21
P_2O_5	0.07	0.13	0.17	0.08	0.06	0.07	0.11	0.05	0.18	0.15
SUM	99.16	99.75	99.79	98.42	99.48	100.63	99.36	99.31	99.57	100.42

NOTES: [a] Compston et al. (ref. 7).
[b] Engel et al. (ref. 8).
[c] Cuttitta et al. (ref. 9).
[d] Rhodes and Hubbard (ref. 10).
[e] Cuttitta et al. (ref. 11).
[f] Maxwell et al. (ref. 12).
[g] Duncan et al. (ref. 13).
[h] Albee et al. (ref. 14).

Table 3.—*Compositions of Highland Rocks Representative of Major Chemical Classes*

	Anorthositic Gabbro	Gabbroic Anorthosite	Anorthosite (cataclastic)	Low-KREEP Norite	High-KREEP Norite	Spinel Troctolite
Example	60335[a]	68415[a]	60015[b]	76055[c]	14303[d]	62295[e]
SiO_2	46.33	45.30	43.97	45.7	47.90	45.16
Al_2O_3	25.01	28.70	35.83	15.84	15.6	20.05
TiO_2	0.57	0.29	0.02	1.38	1.80	0.70
MgO	7.70	4.35	0.25	17.89	10.93	14.85
FeO	4.60	4.12	0.36	9.27	10.74	6.40
MnO	0.08	0.05	0.00	0.12	0.15	0.09
CaO	14.23	16.24	18.95	9.13	9.90	11.85
Na_2O	0.62	0.50	0.34	0.55	0.78	0.48
K_2O	0.27	0.09	0.01	0.22	0.52	0.11
P_2O_5	0.21	0.06	—	0.22	0.60	0.15
SUM	99.62	99.70	99.73	100.32	98.92	99.84

NOTES: [a] Rose et al. (ref. 16).
[b] Juan et al. (ref. 17).
[c] Nava (ref. 18).
[d] Wiik et al. (ref. 19).
[e] Rose et al. (ref. 20).

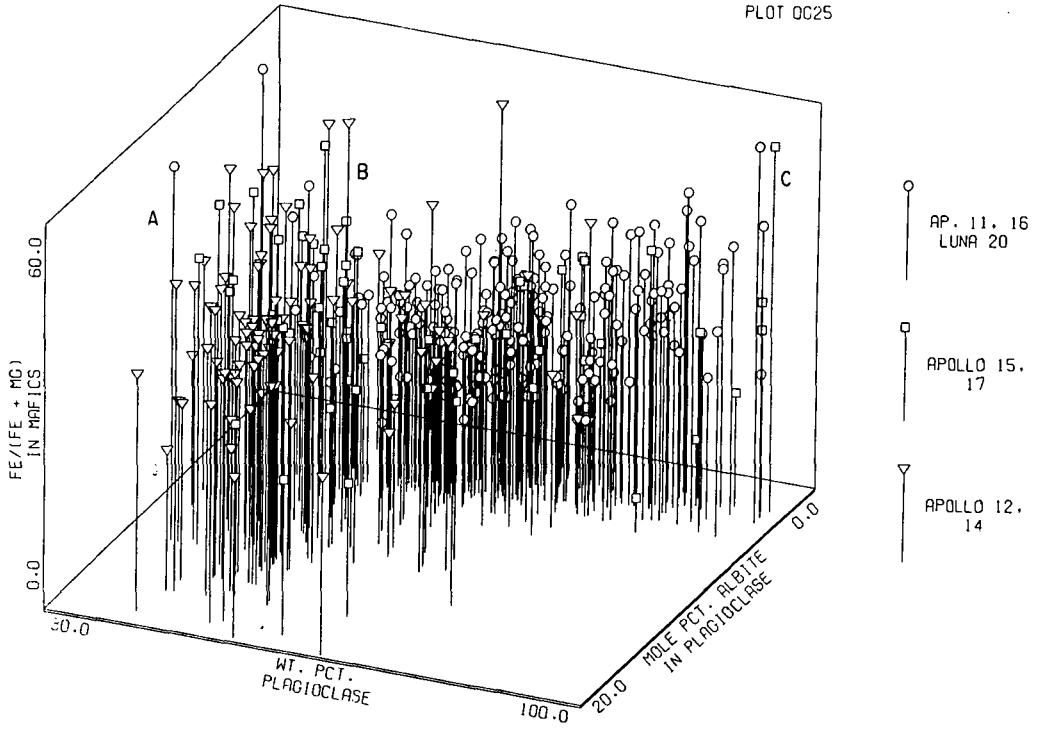


Figure 4.—*Lunar highland samples only (whole-rock and lithic fragments analyses), plotted against three indicators of the degree of differentiation. Group between A and B: noritic materials; B through C: sequence ranging from anorthositic gabbro to anorthosite.*

has an approximately constant (40- to 50-percent) content of normative plagioclase, but the plagioclase has variable albite content; these are the lunar norites. It is not possible in this figure to discriminate between high- and low-KREEP norites. The other group of "pins" (B–C) is the anorthositic sequence, ranging from anorthositic gabbro near B to anorthosites proper at C. Here, the albite content of the plagioclase varies very little, while the content of normative plagioclase ranges from 50 percent to almost 100 percent.

This plot provides an opportunity to test the observation of Steele and Smith (ref. 21), that the relationship between the fayalite content of olivine and the albite content of coexisting plagioclase in highland rocks is the inverse of that predicted by the Bowen reaction principle; i.e., as the plagioclase content of highland materials increases, the albite content of plagioclase decreases, but Fe/(Fe + Mg) in olivine (and presumably also in pyroxene) increases. Figure 4 confirms this relationship, although the variation of the albite content of plagioclase is extremely small compared with the general scatter of albite content plotted for anorthositic samples. (The small range of Ab content compared with that of Fo in coexisting olivines was also noted by Steele and Smith (ref. 21).)

Comparison of the Crusts of Earth and Moon

It would appear interesting to draw a direct comparison between the crustal materials of the Earth and Moon. However, we are conscious by now that the crusts of the two bodies are the products of very different processes. Because of the thinness of the Earth's lithosphere and the thermal and convective activity of its interior, the crust of the Earth is continually being drawn down into its mantle (fig. 5). In the process, certain easily meltable and low-density constituents are selectively removed from the descending crustal material and sent back to the surface

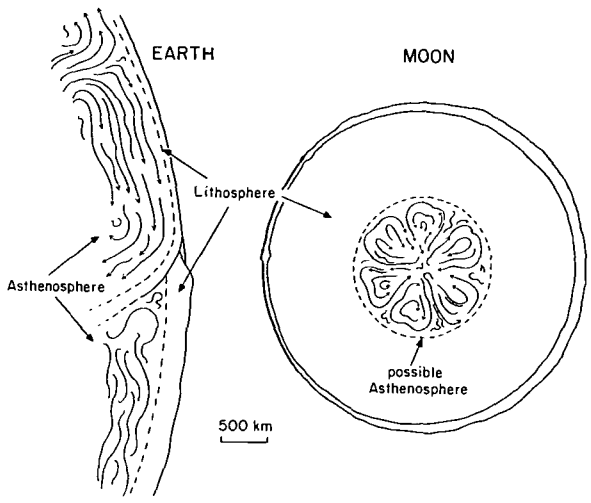


Figure 5.—*Differences in thickness of lithospheres of the Earth and Moon; to scale. Because Earth's lithosphere is less than 100 km thick beneath ocean basins, it is not strong enough to resist being moved and subducted by mantle convection. The Moon's lithosphere is 1000 km thick and highly stable. A weaker zone (attenuating seismic S-waves), which may or may not be in convective motion, exists beneath 1000 km.*

in the form of volcanic rocks. These low-temperature, low-density constituents have, in this way, become concentrated near the surface of the Earth over the course of geologic time and have come to dominate the composition of Earth's crust. The Moon has a very much thicker lithosphere than does the Earth, for two reasons. First, the temperature increase with depth is smaller in the Moon than in the Earth, because of the Moon's greater surface-to-volume ratio, which compromises its ability to conserve internal heat; and, second, the water content of the Moon is effectively zero, and the plasticity of mantle rocks at a given temperature is greatly enhanced by the presence of water. Because of the thickness and rigidity of the Moon's lithosphere, internal mantle convection (if it occurs at all) does not act to draw lunar crustal material down into the depths of the Moon and selectively recycle its easily meltable constituents. The pre-mare crust of the Moon is generally felt to be the product of a great cycle of geochemical differentiation that affected the outermost hundreds of

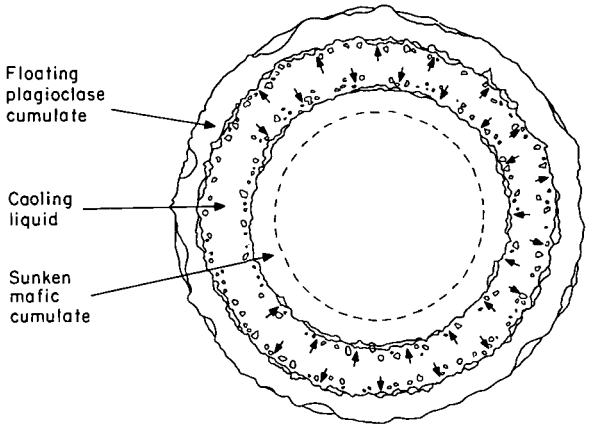


Figure 6.—*Model for early large-scale differentiation of the Moon's outer layers (schematic; radial scale exaggerated). Accretional heating melted the primordial lunar material to a depth suggested by the dashed line. During subsequent cooling and crystallization, dense mafic minerals sank and plagioclase floated to form an anorthositic crust.*

kilometers of the Moon immediately after its formation (fig. 6).

Because of these fundamental differences, there is little point in making a straightforward chemical comparison between the lithic constituents of the crusts of Earth and Moon. It is more profitable to draw a comparison between lunar rocks and selected terrestrial rock systems in which the processes of geochemical fractionation that have operated are similar to those believed to have affected the lunar crust. The Earth's crust contains a number of layered mafic intrusives, in which gravity crystal fractionation has produced a range of different rock types from a (presumably) homogeneous parent magma. This is the process that, on a much larger scale, is believed to have differentiated the premare crust of the Moon. It is interesting to compare the array of rock types found in terrestrial mafic layered intrusives with those from the lunar crustal system. To com-

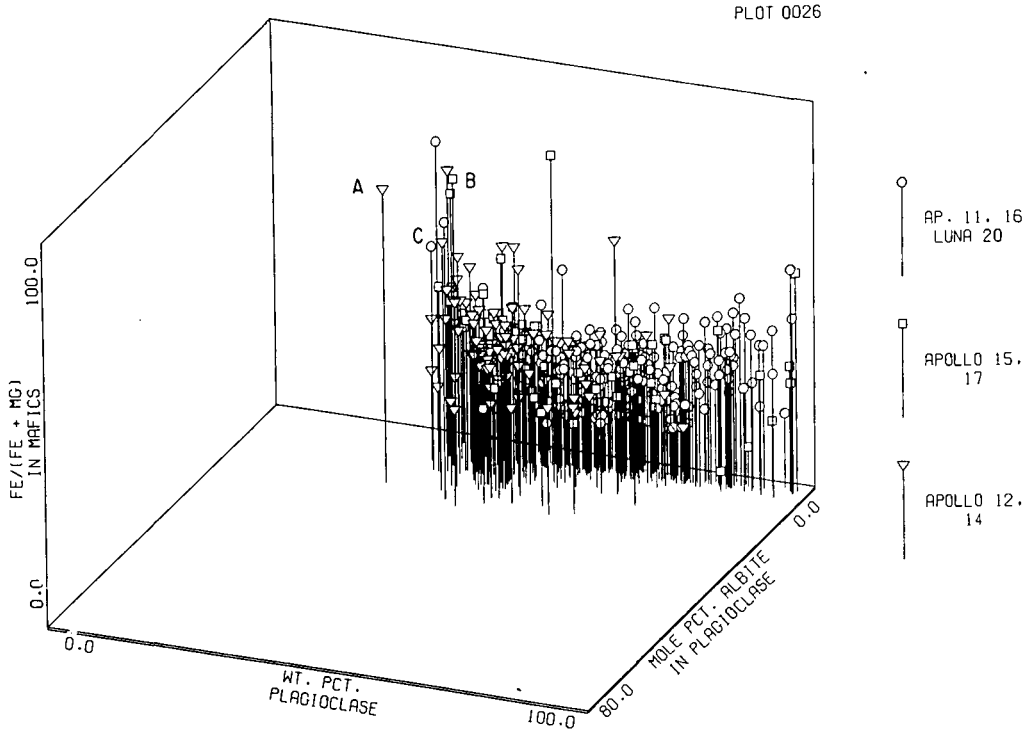


Figure 7.—*Data of figure 4, plotted on an expanded scale. Entries with highest Fe/(Fe+Mg) and low plagioclase (A, B, C) are not actually highland materials, reflecting the limitations of the arbitrary criteria for discrimination shown in figure 2.*

pare the data of figure 4 with terrestrial systems, the scale of the axes must be expanded to accommodate the greater range of rock compositions found in terrestrial systems. This is done in figure 7, where the data of figure 4 are replotted. Emphasis in this figure is upon the tendency of the total array of data to reach minimum Fe/(Fe + Mg) values for mafic minerals at intermediate contents of plagioclase, and to rise to higher values of mafic Fe/(Fe + Mg) at the low-plagioclase and high-plagioclase ends of the array. (The entries displaying the highest values of Fe/ (Fe + Mg) at the low-plagioclase end of the array are probably not highland rocks; but the general tendency of the array to rise to higher values of Fe/ (Fe + Mg) below the letter C in the diagram is definitely attributable to non-mare samples.)

Analyses of 317 rock samples from nine terrestrial mafic layered intrusives are plotted in figure 8. To jumble analyses of rocks from three widely separated and petrologically unrelated intrusives on the Earth in this fashion, and to lose sight of the known spatial relationships between the rocks analyzed, might be deplored; however, precisely such a situation exists for the collection of lunar highland samples we have access to, so a similarly indiscriminate mixture of terrestrial analyses (of rocks from appropriate geologic structures) provides the most valid basis for a comparison between the Earth and the Moon available to us.

Figures 7 and 8 appear totally dissimilar. To make a fair comparison, however, allowance must be made for several things. First, it is well known by now that the Moon is depleted in Na, along with all the other volatile elements, relative to Earth. For this reason, the plagioclase in terrestrial rocks of all types should contain a greater albite component than do their lunar equivalents. Consequently, the "pins" of figure 8 stand

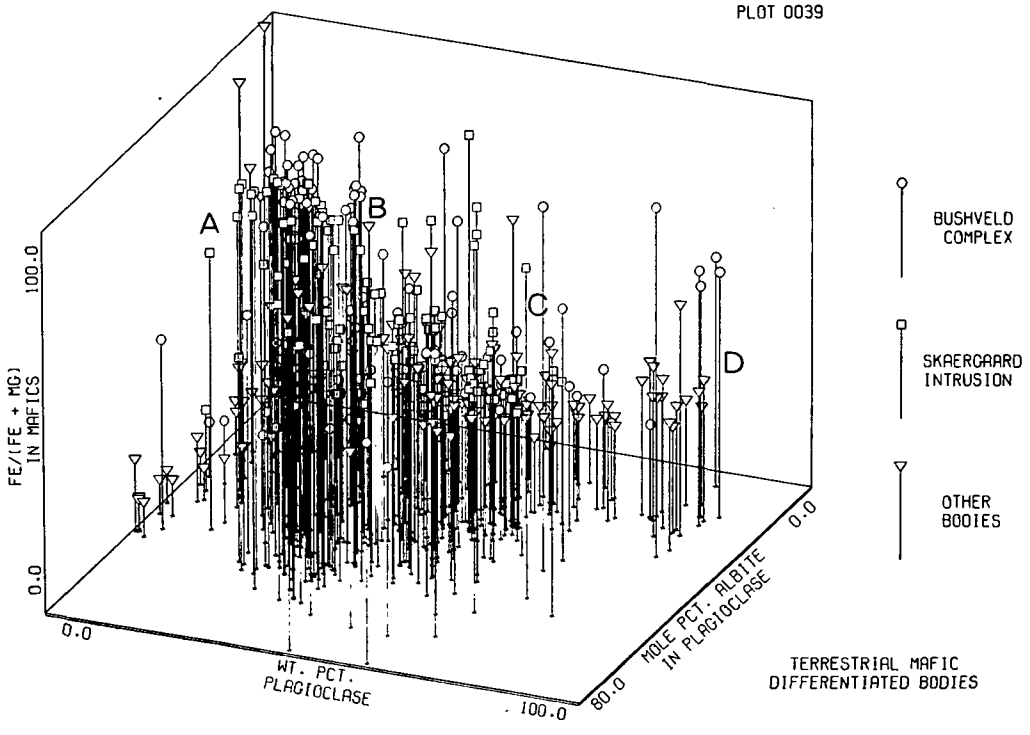


Figure 8.—*Rock analyses from nine terrestrial differentiated mafic igneous bodies, plotted on the same base as figure 7. Group between A and B: chiefly ferrogabbros and granophyres. Between B and C: norites and gabbroic rocks. C and D: anorthositic sequence. Analyses of samples from the Stillwater, Rhum, Guadalupe, Duluth, Bay of Islands, Usushwana, and Fethiye complexes are lumped under "other bodies."*

farther forward in the plot than do those of figure 7. Second, a number of the entries in figure 8 are ultramafic cumulates. (Most of these occur near the origin of the plot, largely hidden behind the major cluster of "pins" between A and B.) Ultramafic rocks are rare among the lunar samples (but not absent), presumably because we have access only to the uppermost layers of the great differentiated sequence that composes the crust of the Moon, and ultramafic cumulates would be expected to occur near its base. Such ultramafic rocks as do occur in our library of analyses were excluded from figure 7 by the chemical criteria that were used to separate highland from mare rocks. Third, figure 8 contains a massive cluster of entries displaying very high values of Fe/(Fe + Mg), between A and B, which has no equivalent in figure 7. These represent the ferrogabbros and granophyres that are abundant in terrestrial mafic layered intrusives and that appear to comprise the late-stage residua after extensive crystal fractionation has removed other components from the melt. Rocks of this type are also rare on the Moon but not nonexistent, although our analysis library has not incorporated any. Fragments of granophyric material in which Fe/(Fe + Mg) for the mafics present is very high have been found in soils and breccias by a number of authors (e.g., refs. 22 and 23). If plotted in figure 7, they would occupy a position analogous to the A–B grouping in figure 8, although the density of the cluster in figure 8 could not be matched. After allowance is made for these discrepancies, the entries corresponding to noritic and anorthositic rock types (B–C–D) form an array somewhat similar to that of figure 7, in that the Fe/(Fe + Mg) content of mafic minerals reaches a minimum value of approximately 0.3 in the intermediate or anorthositic gabbro range of plagioclase contents while higher values (approximately 0.5) obtain for rock types that contain greater and lesser amounts of plagioclase.

In an earlier version of the present article that was distributed as a preprint, I attached importance to this similarity and suggested that the suite of lunar feldspathic rocks was formed by processes analogous to those that operate in terrestrial mafic intrusives, including the tendency of plagioclase to sink rather than float. However, further investigation of the compositional trends among lunar rocks has diminished the apparent similarity of the two rock types.

In particular, it is widely believed for both petrologic and geochemical reasons (refs. 24 and 25) that KREEP-rich lunar norites do not sample the liquid residuum after separation of anorthositic rocks, nor do they represent differentiates complementary to the anorthosites; instead, they appear to be products of a different magma system that was produced by remelting of some suitable parent rock, which may have been the anorthositic sequence itself. In the terrestrial systems plotted, on the other hand, it is clear from field relationships that the noritic rocks are part of the same differentiation sequence that contains the anorthositic members, and have not been introduced to the sequence by some late act of magma generation. Thus, the KREEP-rich norites would need to be excluded from figure 7 in order to reveal trends attributable solely to those lunar differentiation processes thought to be analogous to processes operating in terrestrial layered mafic intrusives. When this is done (by excluding all analyses for which $K_2O + P_2O_5 > 0.5$ percent), the high-Fe/(Fe + Mg) peak at the left end of the sequence in figures 4 and 7 disappears (ref. 26). Low-KREEP norites are still present in the sequence, but Fe/(Fe + Mg) in their mafic minerals is small, ~ 0.25. The overall trend among low-KREEP lunar crustal rocks is for Fe/(Fe + Mg) to increase monotonically, and for the albite content of plagioclase to decrease monotonically, with increasing content of plagioclase. This is still consistent with the trend noted by Steele and Smith (ref. 21), but it bears very little resemblance to trends in terrestrial mafic intrusives.

For crystal fractionation to produce a suite of rocks that appear to violate the Bowen reaction principle, it is necessary for the two principal mineral groups to move in

opposite directions (i.e., if mafic minerals sink, feldspar must float). In a magma where plagioclase floats, early-formed calcic plagioclase will accumulate at the top of the system in company with relatively unfractionated intercumulus liquid, which will crystallize mafic minerals of intermediate Fe/(Fe + Mg). Early-formed magnesian mafic minerals will accumulate on the floor of the system in company with relatively unfractionated intercumulus liquid, which will crystallize plagioclase of intermediate composition. Thus, at the top and bottom of the system, compositions are qualitatively similar to those found at the right and left ends of the trend shown in figure 4.

The difficulty lies in what occurs between the end members. Straightforward application of principles of phase equilibrium indicates that both Fe/(Fe + Mg) in mafic minerals and albite in plagioclase should increase downward in the floating anorthositic layer, and upward in the sunken mafic layer. These trends are not reflected by figure 4. Further, it is unlikely that bulk plagioclase content would decrease smoothly with depth in the anorthositic and mafic layers, as is suggested by the even distribution of entries in the sequence of figure 4. Terrestrial experience suggests that units of mafic-poor anorthosite and plagioclase-poor ultramafic rock would be produced, probably separated by a residual magma rich in Fe and Na. (Note the clusters of "pins" corresponding to these three compositions in figure 8). These discontinuities of composition are not apparent among the lunar rocks, and there are no samples corresponding to an Fe-, Na-rich residual liquid. (It might appear that the KREEP-rich norites fill this role; but, as already noted, there are compelling reasons for believing that this class of rocks was formed by partial melting, not as a residuum after crystal fractionation. In the simplest terms, degrees of enhancement of Fe/(Fe + Mg) and enrichment of large-ion-lithophile (LIL) elements are incongruous if the rock type was formed by crystal fractionation. The ratio Fe/(Fe + Mg) reflects only a modest degree of fractionation, while a very large percentage of the original magma would have to be removed as crystals to effect the observed enrichment of LIL elements.)

The seriousness of the difficulty just noted depends upon the mechanics of crystal fractionation. The problem is at its worst if the lunar surface magma system was quiescent and cooled slowly. Under these circumstances, thick units of anorthositic and ultramafic cumulate rocks could be expected to form, and the crystals added last to these units should be richer in Fe and Na than the first-formed crystals. On the other hand, the problem diminishes if we contemplate a dynamically active system in which magma motions kept crystals well stirred until crystallization was far advanced. As magma motions slowed and the solidifying system approached stability, some degree of gravitational separation of the crystals would occur, but clean separation of plagioclase from mafic minerals would be impossible (except at the extremities of the system) because of the crowding of crystals in the magma. The rocks of the sequence would be left with a continuous spectrum of plagioclase contents. The suspended minerals would be relatively uniform in composition at the time when the system immobilized, because of stirring during the previous period when they crystallized. Subsequent crystallization of the Fe-, Na-rich intercumulus liquid in the upper, plagioclase-rich levels of the system would increase the mean value of Fe/(Fe + Mg) in the mafic minerals substantially, since few early-crystallized Mg-rich crystals would be present to lower Fe/(Fe + Mg); on the other hand, the amount of early-formed calcic plagioclase present would be so great that the contribution of Na from the intercumulus liquid could do little to enhance the mean value of albite content of the plagioclase.

Conversely, crystallization of the same Fe-, Na-rich intercumulus liquid in a mafic-rich cumulate deep in the system would effect a great increase in the mean albite content of the small amount of plagioclase present, but could not importantly increase Fe/

(Fe + Mg) in the abundant mafic minerals. The process should operate to intermediate degrees at intermediate positions in the differentiated sequence, and continuous compositional trends similar to those of figure 4 would be produced.

Is it reasonable to suppose that the lunar surface magma system was more dynamically active than terrestrial mafic intrusives during the first phase of its cooling history? There are several reasons for thinking so.

1. The outer surface of the lunar magma system was exposed to space; hence, heat losses at this surface were vastly greater than at the walls of a terrestrial plutonic intrusive. The steep thermal gradient established in the lunar case would be more likely to promote convective motion, which would act to stir the magma. Surface heat losses would be cut when the system began to crust over, as in the case of a lava flow, but it is likely that the intensity of the early meteoroid bombardment of the Moon thwarted formation of a crust for some time.
2. Because of the Moon's small mass, the pressure gradient in the Moon is only one-sixth as steep as the terrestrial pressure gradient. As a consequence, the vertical thermal gradient in a magma system needed to produce convective motion would only need to be one-sixth as steep on the Moon as on Earth.
3. Because of the small value of lunar gravity, crystals are less rapidly separated from a lunar magma by specific gravity differences, and hence would be more readily held suspended by a convecting magma, than would be the case on Earth. (The small value of lunar gravity also works against this model, however, by providing less energy for a convecting system to use to overcome viscous drag.)
4. Plagioclase crystals, in particular, could be kept well mixed with the lunar magma even by sluggish convective motions, since the specific gravity contrast between calcic plagioclase and a residual magma of reasonable composition is extremely small. Plagioclase crystallization would act principally to increase the effective viscosity of the cooling system, until the latter stabilized.

The question of the origin of high-KREEP norite has tormented lunar petrologists since this lithology was recognized. Its content of large-ion-lithophile elements and its position in the quartz-olivine-anorthite pseudo-ternary phase diagram seem to require that it was generated by partial melting of a parent similar to lunar anorthositic rocks. An objection I have raised to this interpretation (ref. 27) is that once the surface layers of the Moon had solidified and their content of heat-generating radionuclides had been immobilized, this part of the system would have cooled monotonically. Temperatures in a subcrustal layer or zone should not rise again (as is required in order to remelt the material) unless some new external source of energy were involved. The question of a source of heat to effect remelting of KREEP norite has been a serious one.

One possible resolution of this problem has been overlooked, however. Earlier in this paper it was remarked that the Moon's thick lithosphere prevents interior convection from subducting crustal material into its mantle. But this was not necessarily always the case. If the initially hot outer layers of the Moon cooled from the surface inward, there must have been a time, after the crustal magma system had completely solidified, when the lunar lithosphere was still thin and weak. If mantle convective motion occurred during this early and transient phase of lunar history, it is possible that the primordial anorthositic crustal material was dragged down into the lunar mantle. There, higher temperatures would have occasioned partial melting of the crustal material, producing a melt having many of the properties of KREEP-rich norite, which would have

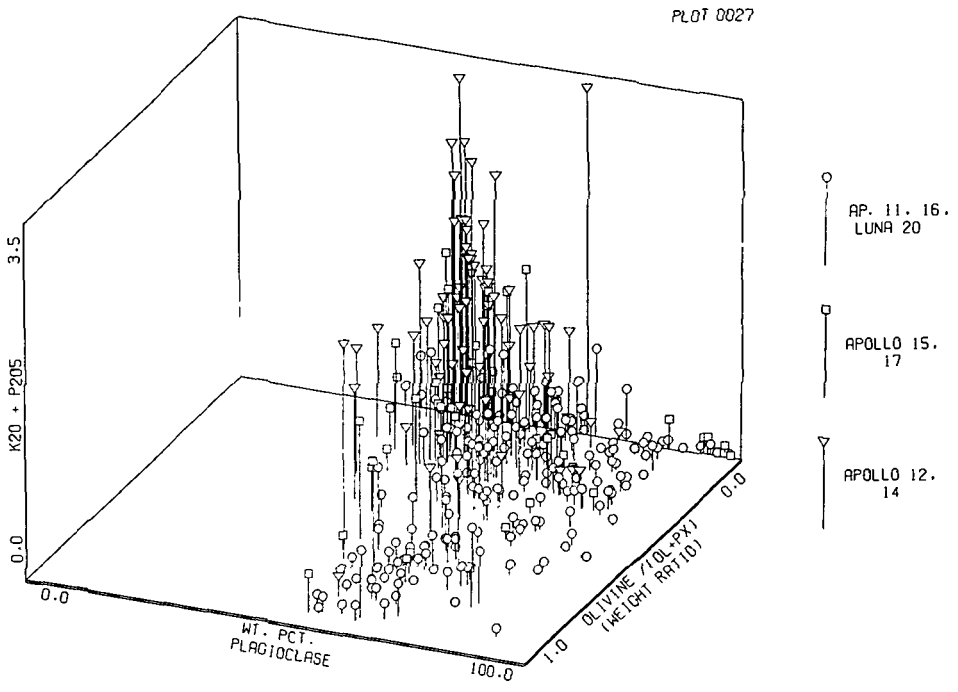


Figure 9.—*Lunar highland samples only (whole-rock and lithic fragment analyses), plotted against KREEP content ($K_2O+P_2O_5$) and degree of silica saturation (expressed as normative olivine/(ol + px)).*

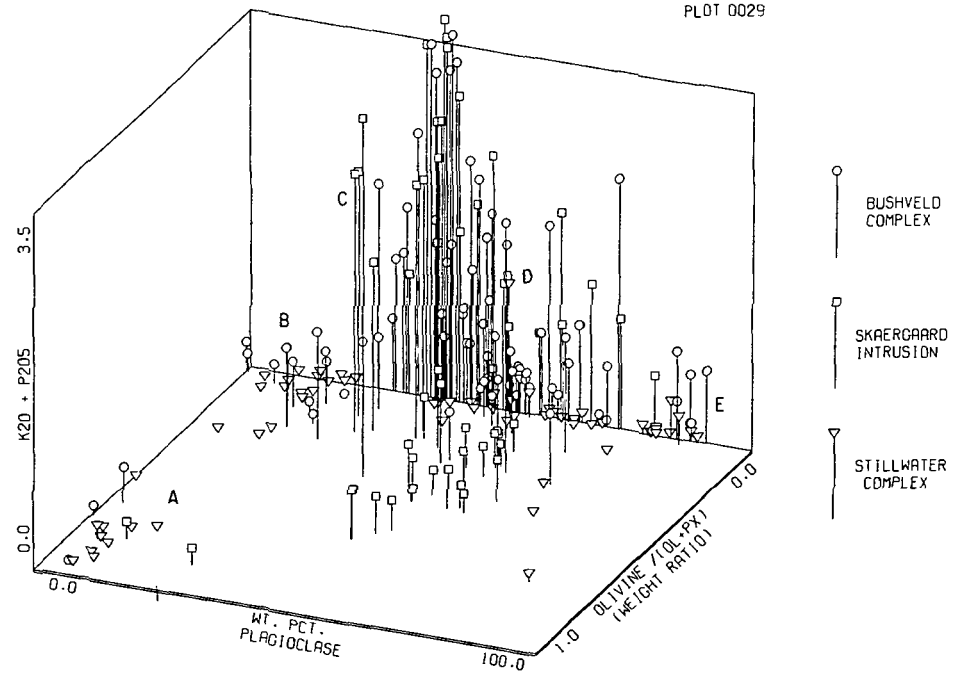


Figure 10.—*Rock analyses from three classic terrestrial differentiated mafic igneous boaies, plotted on the same base as figure 9. A: peridotites, dunites; B: pyroxenites. Olivine-free rocks range from ferrogabbros at C through norites and gabbros near D, to anorthosites at E.*

erupted to the surface as a lava. In this case, the KREEP-rich norites could be regarded as the lunar equivalents of terrestrial andesites.

In figures 9 and 10, a comparison is drawn between the lunar highland rocks and samples from the three classic terrestrial basic differentiated bodies, for several other parameters of petrologic interest. Entries representing granophyric rocks are largely missing from figure 10, because their content of K_2O is too great to be accommodated by the axes defined. Of greatest interest is the difference in olivine content of the rocks of the two series. Lunar highland rocks, especially those of the anorthositic series, are often troctolitic in character. The terrestrial differentiates are much less likely to contain olivine.

The difference may be due to the fundamentally dissimilar modes of origin of the parent magmas of the two systems. The terrestrial gabbroic magmas were presumably generated by a small degree of melting in the mantle of the Earth and escaped from their source before the temperature of the system had risen high enough to melt substantial amounts of any olivine present in the source region. If the lunar surface magma system was melted by accretional energy during the assembly of the Moon, on the other hand, this control on melt composition would not have existed. The injection of large amounts of energy during accretional impact would have tended to melt the primordial material of the Moon completely. Presumably this primordial material included a substantial component of chondrite-like material (refs. 28 and 29); chondritic meteorites are substantially undersaturated and contain a large proportion of normative olivine, all of which would have been included in magmas formed by the total melting of primordial lunar material.

In conclusion, while no valid comparison can be drawn between the properties of the lunar crust and the present terrestrial crust, it is possible that the Moon preserves an accurate and informative record of the properties of the crust that *initially* formed on the Earth. If the Earth began its existence with a plagioclase-rich crust analogous to the Moon's, formed by crystal flotation in an extensive early global magma system, this crust would not have been thicker than the Moon's in proportion to the greater size of the Earth. Paradoxically, it may have been thinner. Since the acceleration due to gravity is six times greater on the Earth than on the Moon, the pressure gradient inside the Earth is six times steeper (fig. 11). Plagioclase is unstable in mafic rock systems at pressures in excess of approximately 12 kb. In the Moon, plagioclase could have crystallized stably from a cooling mafic magma system to depths in excess of 200 km. For magmas of reasonable composition, this volume of magma could have crystallized enough plagioclase to form a crustal cumulate up to 100 km thick. In the case of the Earth, plagioclase instability begins at less than a 50-km depth. A layer thicker than this could not have formed.

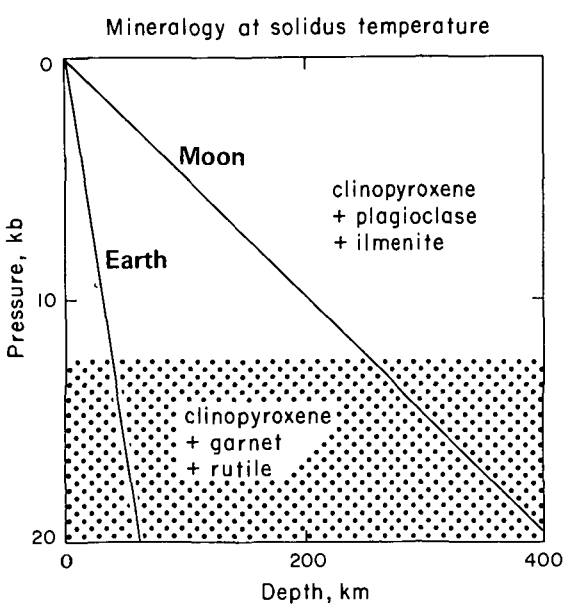


Figure 11.—*Relationship between depth and pressure in Earth and Moon. At greater than ~ 12 kb of pressure, plagioclase in crystallizing mafic rocks is unstable relative to denser garnet-bearing assemblages (Ringwood and Essene, reference 30).*

References

1. Reid, A. M., J. Warner, W. I. Ridley, D. A. Johnston, R. S. Harmon, P. Jakes, and R. W. Brown, The Major Element Compositions of Lunar Rocks as Inferred From Glass Compositions in the Lunar Soils. *Proc. Third Lunar Science Conference, Geochimica et Cosmochimica Acta,* Supplement 3, Vol. 1, 1972, pp. 363–378.
2. Bunch, T. E., M. Prinz, and K. Keil, *Electron Microprobe Analyses of Lithic Fragments and Glasses From Apollo 12 Lunar Samples.* Univ. New Mexico, Institute of Meteoritics, Spec. Publication No. 4, 1972.
3. James, O. B., and T. L. Wright, Apollo 11 and 12 Mare Basalts and Gabbros: Classification, Compositional Variations and Possible Petrogenic Relations. *Geol. Soc. Am. Bull.,* Vol. 83, 1972, pp. 2357–2382.
4. Brown, G. M., C. H. Emeleus, J. G. Holland, A. Peckett, and R. Phillips, Petrology, Mineralogy and Classification of Apollo 15 Mare Basalts. *The Apollo 15 Lunar Samples,* Lunar Science Institute, Houston, 1972, pp. 40–44.
5. Brown, G. M., A. Peckett, C. H. Emeleus, and R. Phillips, Mineral-Chemical Properties of Apollo 17 Mare Basalts and Terra Fragments. *Lunar Science,* Vol. V, Lunar Science Institute, Houston, 1974, pp. 89–91.
6. Hubbard, N. J., L. E. Nyquist, J. M. Rhodes, B. M. Bansal, H. Weismann, and S. E. Church, Chemical Features of the Luna 16 Regolith Sample. *Earth Planet. Sci. Letters,* Vol. 13, 1972, pp. 423–428.
7. Compston, W., H. Berry, and M. J. Vernon, Rubidium-Strontium Chronology and Chemistry of Lunar Material From the Ocean of Storms. *Proc. Second Lunar Science Conference, Geochimica et Cosmochimica Acta,* Supplement 2, Vol. 2, 1971, pp. 1471–1485.
8. Engel, A. E. J., C. G. Engel, A. L. Sutton, and A. T. Myers, Composition of Five Apollo 11 and Apollo 12 Rocks and One Apollo 11 Soil and Some Petrographic Considerations. *Proc. Second Lunar Science Conference, Geochimica et Cosmochimica Acta,* Supplement 2, Vol. 1, 1971, pp. 439–448.
9. Cuttitta, F., H. J. Rose, Jr., C. S. Annell, M. K. Carron, R. P. Christian, E. J. Dwornik, L. P. Greenland, A. W. Helz, and D. T. Ligon, Jr., Elemental Composition of Some Apollo 12 Lunar Rocks and Soils. *Proc. Second Lunar Science Conference, Geochimica et Cosmochimica Acta,* Supplement 2, Vol. 2, 1971, pp. 1217–1229.
10. Rhodes, J. M., and N. J. Hubbard, Chemistry, Classification, and Petrogenesis of Apollo 15 Mare Basalts. *Proc. Fourth Lunar Science Conference, Geochimica et Cosmochimica Acta,* Supplement 4, Vol. 2, 1973, pp. 1127–1148.
11. Cuttitta, F., H. J. Rose, Jr., C. S. Annell, M. K. Carron, R. P. Christian, D. T. Ligon, Jr., E. J. Dwornik, T. L. Wright, and L. P. Greenland, Chemistry of Twenty-One Igneous Rocks and Soils Returned by the Apollo 15 Mission. *Proc. Fourth Lunar Science Conference, Geochimica et Cosmochimica Acta,* Supplement 4, Vol. 2, 1973, pp. 1081–1096.
12. Maxwell, J. A., L. C. Peck, and H. B. Wiik, Chemical Composition of Apollo 11 Lunar Samples 10017, 10020, and 10084. *Proc. Apollo 11 Lunar Science Conference,* Vol. 2, 1970, pp. 1369–1374.
13. Duncan, A. R., A. J. Erlank, J. P. Willis, M. K. Sher, and L. H. Ahrens, Trace Element Evidence for a Two-Stage Origin of High-Titanium Mare Basalts. *Lunar Science,* Vol. V, Lunar Science Institute, Houston, 1974, pp. 187–189.
14. Albee, A. L., A. A. Chodos, A. J. Gancarz, E. L. Haines, D. A. Papanastassiou, L. Ray, F. Tera, J. Wasserburg, and T. Wen, Mineralogy, Petrology, and Chemistry of a Luna 16 Basaltic Fragment, Sample B–1. *Earth Planet. Sci. Letters,* Vol. 13, 1972, pp. 353–367.
15. Conrad, G. H., P. F. Hlava, J. H. Green, R. B. Moore, G. Moreland, E. Dowty, M. Prinz, K. Keil, C. E. Nehru, and T. E. Bunch, *Electron Microprobe Analyses of Lithic Fragments and Their Minerals From Luna 20 Fines.* Univ. New Mexico, Institute of Meteoritics, Spec. Publication No. 12, 1973.
16. Rose, H. J., Jr., M. K. Carron, R. P. Christian, F. Cuttitta, E. J. Dwornik, and D. T. Ligon, Jr., Elemental Analysis of Some Apollo 16 Samples. *Lunar Science,* Vol. IV, Lunar Science Institute, Houston, 1973, pp. 631–633.
17. Juan, V. C., J. C. Chen, C. K. Huang, P. Y. Chen, and C. M. Wang Lee, Petrology and Chemistry of Some Apollo 16 Lunar Samples. *Lunar Science,* Vol. V, Lunar Science Institute, Houston, 1974, pp. 394–396.
18. Nava, D. F., Chemistry of Some Rock Types and Soils From the Apollo 15, 16, and 17 Lunar Sites. *Lunar Science,* Vol. V, Lunar Science Institute, Houston, 1974, pp. 547–549.
19. Wiik, H. B., J. A. Maxwell, and J. L. Bouvier, Chemical Composition of Some Apollo 14 Lunar Samples. *Earth Planet. Sci. Letters,* Vol. 17, 1973, pp. 365–368.
20. Rose, H. J., Jr., F. Cuttitta, S. Berman, M. K. Carron, R. P. Christian, E. J. Dwornik, L. P. Greenland, and D. T. Ligon, Jr., Compositional Data for Twenty-Two Apollo 16 Samples. *Proc. Fourth Lunar Science Conference, Geochimica et Cosmochimica Acta,* Supplement 4, Vol. 2, 1973, pp. 1149–1158.
21. Steele, I. M., and J. V. Smith, Mineralogy and

Petrology of Some Apollo 16 Rocks and Fines: General Petrologic Model of Moon. *Proc. Fourth Lunar Science Conference, Geochimica et Cosmochimica Acta,* Supplement 4, Vol. 1, 1973, pp. 519–536.

22. WOOD, J. A., U. B. MARVIN, J. B. REID, JR., G. J. TAYLOR., J. F. BOWER, B. N. POWELL, AND J. S. DICKEY, JR., *Mineralogy and Petrology of the Apollo 12 Lunar Sample.* Smithsonian Astrophysical Observatory, Spec. Report No. 333, 1971.
23. STOESER, D. B., R. W. WOLFE, J. A. WOOD, AND J. F. BOWER, Petrology. *Consortium Indomitabile, Interdisciplinary Studies of Samples from Boulder 1, Station 2, Apollo 17,* Vol. 1, 1974, pp. 35–109.
24. WALKER, D., J. LONGHI, AND J. F. HAYES, Experimental Petrology and Origin of Fra Mauro Rocks and Soil. *Proc. Third Lunar Science Conference, Geochimica et Cosmochimica Acta,* Supplement 3, Vol. 1, 1972, pp. 797–817.
25. HUBBARD, N. J., P. W. GAST, C. MEYER, L. E. NYQUIST, C. SHIH, AND H. WEISMANN, Chemical Composition of Lunar Anorthosites and Their Parent Liquids. *Earth Planet. Sci. Letters,* Vol. 13, 1971, pp. 71–75.
26. WOOD, J. A., The Lunar Rocks: A Chemical Classification. *Rev. Geophys. Space Phys.,* in press, 1975.
27. LSAPT (Lunar Sample Analyses Planning Team.) Fourth Lunar Science Conference. *Science,* Vol. 181, 1973, pp. 615–622.
28. GANAPATHY, R., AND E. ANDERS, Bulk Compositions of the Moon and Earth, Estimated from Meteorites. *Lunar Science,* Vol. V, Lunar Science Institute, Houston, 1974, pp. 254–256.
29. WÄNKE, H., H. PALME, H. BADDENHAUSEN, G. DREIBUS, E. JAGOUTZ, H. DRUSE, B. SPETTEL, AND F. TESCHKE, Composition of the Moon and Major Lunar Differentiation Processes. *Lunar Science,* Vol. V, Lunar Science Institute, Houston, 1974, pp. 820–822.
30. RINGWOOD, A. E., AND E. ESSENE, Petrogenesis of Apollo 11 Basalts, Internal Constitution and Origin of the Moon. *Proc. Apollo 11 Lunar Science Conference,* Vol. 1, 1970, pp. 769–799.

Page intentionally left blank

Page intentionally left blank

Geochemical Zoning and Early Differentiation in the Moon [1]

S. R. Taylor and P. Jakeš
The Lunar Science Institute
Houston, Texas

The large volume of geochemical, petrological, and geophysical data (refs. 1 and 2) now available place many constraints on the composition and evolution of the Moon. For example, one of the first-order facts that appears to be well established is that the volatile elements (e.g., Rb, Pb, Tl, Bi, Cs) had already been depleted (refs. 3 and 4) at the time of accretion. Accordingly, it may be assumed that the Moon initially accreted from refractory material. Whether the siderophile elements (e.g., Ir, Au, Ni) were depleted before accretion is a current question.

The good correlation between volatile/involatile element ratios (e.g., Cs/U, K/La, K/Zr) in both highland and maria samples means that element distribution in lunar crustal rocks is not governed by volatility differences. This and other evidence (refs. 5, 6, and 7) encourages the view that the Moon was accreted homogeneously. Theories that the highlands represented a late addition of chemically distinct refractory material have been abandoned.

A consequence of homogeneous accretion theories is that very efficient large-scale element fractionation is required to account both for the high near-surface concentrations of refractory elements (e.g., Th, U, REE, Zr, Ba, etc.) and for the Ca-Al-rich crust.

There are several independent constraints of varying severity that indicate a high refractory trace element abundance for the Moon:

(1) Near-surface concentrations of many refractory elements are two orders of magnitude higher than those in primitive (Type I carbonaceous chondrite) meteorites (CCI). The latter are taken to represent a good approximation of the abundances of nonvolatile elements in the solar nebula (ref. 8).

(2) The high heat flow (~ 0.7 HFU) (HFU $= 10^{-6}$ cal cm^{-2} s^{-1}) indicates that the total lunar abundance of uranium is about 60 ± 15 ppb (ref. 9). The abundance of U in CCI is variable (ref. 10), but generally estimated at about 12 ppb. On this basis the Moon is enriched at least five times over the CCI abundances. Even the extreme value of 17 ppb (ref. 10) still requires about $4 \times$ CCI levels.

(3) The orbital gamma ray value for Th averages about 1.5 ppm (ref. 11). If the 60-km-thick crust (10 percent of the Moon) has this value, then $4 \times$ CCI levels (35 ppb) are required just to provide for the crustal concentrations. In addition there must have been some Th in the lunar interior to provide radioactive heating during the period 3.8 to 3.2 aeons in order to produce the maria basalts.

(4) The highland element trace abun-

[1] This paper constitutes Lunar Science Institute Contribution No. 229.

dances (refs. 5 and 12) set further limits. If the concentration levels are representative of the 60-km-thick crust and not some thinner surficial zone, then 3 to 4 × CCI abundances are required to provide enough Ba and light REE. Maria basalts, derived from deeper levels by partial melting after the highland crust was formed, also contain high levels of Ba, U, Th, REE, Zr, Hf, Nb, etc. (relative to CCI abundances), increasing the abundance problem.

(5) The uniform interelement ratios in lunar samples (e.g., K/La, K/Ba, K/Th, K/Ar, etc.) (refs. 7 and 13) set limits for the lunar abundance of K. Assuming 5 × CCI for the *involatile* elements, the K concentration is ~ 100 ppm. On this basis, about 80 percent of the K (and associated Rb and Cs) is in the highland crust.

Some of these arguments depend on the vertical element distribution in the lunar crust. It is assumed here that the overall 60-km-thick crust has similar element abundances. The 40 observed ringed basin-forming events (ref. 14) must have effectively overturned large segments of the deep crust. Many lunar models predict somewhat exhanced KREEP-type components with depth, so that the abundance problem is likely to be exacerbated rather than alleviated by lack of thorough mixing.

In summary, some limits can be set. The lower limit of 4 × CCI appears well established by the element abundance levels. The heat flow values set upper limits of perhaps 7 × CCI. An overall lunar average for the involatile elements of about 5 × CCI appears reasonable and is adopted here.

The major element abundances in the Moon may then be estimated as follows. The refractory elements Ca, Al, and Ti are taken as 5 × CCI. The iron content is set at 10.5 percent FeO to accommodate density and magnetic requirements (ref. 15). The Si/Mg ratio in chondrites is used to obtain Si and Mg concentrations (table 1). This composition is very close to that proposed by Ganapathy and Anders (ref. 17).

The Moon's moment of inertia (0.3953 ± 0.0045) suggests a nearly uniform density distribution with depth (ref. 18). This and the low bulk density of the Moon (3.34 g/cm^3) rules out the existence of dense (eclogitic) phases at depth (refs. 16 and 19). Thus, neither the highlands anorthosites nor the maria basalts are suitable compositions for the deep lunar interior. The lack of major

Table 1.—*Major Element Compositions*

	(1)	(2)	(3)	(4)	(5)	(6)	(7)	(8)
SiO_2	44.0	44.3	45.2	44.9	43.3	53.1	48.9	42.73
TiO_2	0.3	—	0.6	0.56	0.7	1.0	0.15	0.42
Al_2O_3	8.2	0.6	16.9	24.6	14.4	5.0	3.6	8.21
FeO	10.5	9.9	6.8	6.6	12.6	13.5	10.5	10.95
MgO	31.0	44.7	18.3	8.6	17.7	22.5	34.2	30.70
CaO	6.0	0.7	12.5	14.2	11.3	4.0	2.7	7.68

Explanation of column headings:
(1) Bulk Moon (this study).
(2) Composition of 300 to 1000 km of Moon (this study).
(3) Composition of upper 300 km of Moon.
(4) Average highlands, composition of upper 60 km of Moon (ref. 12).
(5) Composition of 60 to 300 km of Moon (including source of maria basalts).
(6) Composition of source of maria basalts (200 to 400 km pyroxenite, ref. 16).
(7) Carbonaceous chondrite (CCl-Orgueil); volatile and siderophile elements subtracted and Fe taken as in column 1.
(8) Bulk Moon (ref. 17).

seismic discontinuities between the base of the crust at 60 km and a depth of 1000 km suggests a rather uniform interior with gradational boundaries in mineralogy and chemical composition. The interior of the Moon is divided into (a) crust (upper 60-km), (b) lithosphere (60–1000 km), and (c) asthenosphere (1000–1738 km), with at least the upper portion of this zone partially liquid (refs. 9 and 20). The presence of orthopyroxene (with some Al and Ca) below 300 km is inferred from P-wave velocities that fit an olivine-orthopyroxene mixture better than olivine alone.

Experimental petrology studies indicate that the source region of the maria basalts lies between depths of 100 to 300 km (refs. 16 and 21). Among the maria basalts, several types are distinguished using major and trace element criteria; their common feature is a high Ca/Al ratio, relatively low Mg/Fe, varying degrees of REE enrichment with Eu depletion, and varying but low contents of Ni. Although the maria basalts could be related by petrological schemes involving different degrees of partial melting, the TiO_2 and Al_2O_3 contents (accompanied by Eu anomalies) and the Fe/Ni ratios suggest as well that partial melting of slightly different mineralogies involving a combination of pyroxene, olivine, Fe-Ti phases, and plagioclase (and sulphides) has taken place. The REE abundances in maria basalts suggest that plagioclase was removed from their source region (refs. 22 and 23).

The highland rocks contain three distinct and incompatible geochemical components: (a) high Ca, Al, Sr, and Eu (anorthite); (b) high Mg and Cr contents; and (c) high abundances of REE, Th, U, Zr, Hf, etc. Conventional theories involving crystal fractionation cannot account for this association.

We now attempt to reconcile this geochemical information with the geophysical constraints, derive the composition of the deep lunar interior, and correlate the overall composition with the sequence of geological events, beginning with a homogeneously accreted Moon that underwent partial or total melting due to accretional heating. Toksöz et al. (ref. 9) have shown that early heating and melting of large parts of the Moon are compatible with the later thermal history of the Moon. Melting of a large part of the Moon can be achieved if short accretional times of order 100 to 1000 yr are considered (ref. 24).

Three alternative models may account for the deep lunar interior (asthenosphere) (below 1000 km):

(1) An immiscible Fe-FeS liquid sinks to form a core effectively removing most siderophile and chalcophile elements (ref. 25). The core radius is restricted to less than 700 km by the moment of inertia (0.395). Enough sulfur ($\sim$ 0.5 percent) is retained in the whole Moon to form FeS. The partially liquid zone as suggested by the seismic evidence below 1000 km is interpreted as due to dispersed Fe-FeS in an olivine-orthopyroxene matrix. The magnetic field appearing in remanently magnetized rocks results from a core dynamo mechanism.

(2) The initial melting did not extend below 1000 km. The central part of the Moon is formed of primitive unfractionated material now in a partially molten state from heating due to trapped initial K, U, and Th. The seismic data are satisfied by 0.5- to 1-percent partial melting. This model precludes core formation, since sinking Fe-FeS will drive these incompatible elements upward. In this model, the remanent magnetism of lunar rocks is caused by external magnetic fields (ref. 26).

(3) The molten zone is a relic of early melting. The choice between these models for the lunar interior depends critically on the amount of the early siderophile and chalcophile element depletion. If the siderophile elements were accreted, even in the amounts corresponding to low bulk Fe content of the Moon, a lunar core is required

to remove them in a very efficient manner. The evidence at present for a chemically distinct core is equivocal (ref. 27).

We assume in the following discussion that a core did not form and that an inner zone 700 km thick (10 percent volume) was not melted initially (model 2). Following accretional melting of 90 percent of the Moon, the first silicate phase to separate from the primitive molten Moon is Mg-rich olivine. The early precipitation of olivine removes Ni^{2+} and lesser amounts of Cr^{2+} and Co^{2+}.

The surface of the Moon cools rapidly forming a "frozen crust," although this is continually broken up by the declining meteoritic bombardment. This frozen surface layer, analogous to the chilled margins of terrestrial intrusions, retained high concentrations of Mg, Cr, etc., in near-surface regions. Thus, its composition is probably representative of the melt composition during the early stages of crystallization of the lower interior. This chilled early lunar crust is later incorporated into the overall highland composition and contributes the Mg and Cr "primitive" component. If this model is correct, the high Cr/Ni ratios in the highlands indicate that the primitive lunar composition was deficient in siderophile elements.

As crystallization proceeds and Si/Mg changes, orthopyroxene precipitates. This has a similar effect on the composition of the residual melt, as does olivine, except for Si/Mg ratios. Most cations, except Mg, Fe, Ni, Co, and Cr^{2+}, are excluded from the olivine and orthopyroxene lattice sites and migrate upward, concentrating in the still voluminous residual melt. These include Ca and Al. The high Cr^{3+} abundances in most accessible lunar materials indicate that separation of clinopyroxene, if any, was minor, and that olivine and orthopyroxene were probably the major components.

The density and seismic properties and the Si/Mg ratio in the deep lunar interior are satisfied by 80-percent olivine ($\geq Fo_{85}$) and 20-percent orthopyroxene ($\leq En_{85}$). The composition of the lower part of the Moon below 300 km (assuming 2.2 percent Al_2O_3 and 2.5 percent CaO in the orthopyroxene) is given in table 1, column 2. The model requires, however, that even the lower parts of the Moon are compositionally and mineralogically zoned. Orthopyroxene with Al_2O_3 and CaO content is present at shallower depths, together with olivine, whereas Mg-rich olivine is present in deeper parts.

Increasing crystallization of Mg-rich olivine, later accompanied by orthopyroxene at depth, leads to an increasing concentration of refractory elements (Ca-Al) trapped between the already crystallized lower (Ol-Opx) lunar interior and the chilled surface layer. The composition of this zone (the upper 300 km of the Moon) is given in table 1, column 3. When the concentration of Al reaches 12- to 17-percent Al_2O_3, An-rich plagioclase precipitates and concentrates or remains suspended beneath the frozen surface, whereas the Mg-Fe phases continue to crystallize and sink (ref. 28). The Ca-Al-rich region (plagioclase) incorporates Sr^{2+} and Eu^{2+}, but most other elements are unable to enter the Ca^{2+} sites in significant amounts.

Experimental petrology provides constraints on the Al_2O_3 content of melts to precipitate plagioclase together with Fe-Mg silicates (olivine and pyroxene). Values above 12-percent Al_2O_3 are necessary (ref. 29). If the Moon has initially the Ca/Al ratio of meteorites, the corresponding value for CaO at that stage is 9.0 percent or higher. The composition of the highland crust is given in table 1, column 4. The composition of the zone from 60 to 300 km is given in table 1, column 5.

The removal of plagioclase from the source region of maria basalts explains the high Ca/Al ratios, negative Eu anomalies, low content of Al in maria basalts, and relative depletion of larger REE (ref. 23). Plagioclase is not a liquidus phase in maria basalts (ref. 30) (note the exception of high Al mare basalts such as 14053 and 12038) (ref. 31), and prior removal of plagioclase is required to account for the above-mentioned features.. We suggest therefore that the

source region of maria basalts is zoned in respect of Ca-Al and also Mg/Fe and, consequently, in mineralogy (ref. 23).

The high-Al maria basalts come from plagioclase-bearing regions shallower than other maria basalts (ref. 32); our model suggests that the content of plagioclase decreases from the base of the crust (60 km) downward, whereas the contents of Fe-Mg silicates increase. These silicates become more Mg-rich with depth. Pockets or zones of Fe-Ti oxides and FeS in shallower regions account for the high Ti and S contents of the Apollo 11 and 17 basalts (ref. 33). The source region of 15555 (Great Scott) and the green glass (ref. 34) may represent a lower boundary of plagioclase precipitation. We assume that plagioclase separation commenced when a large part ($\simeq$40 percent) of the Moon was still molten, i.e., during formation of the source region of maria basalts above 300 km depth. The composition of the source region of the maria basalts (200 to 300 km) is given in table 1, column 6.

As crystallization of the source region of maria basalts and crust proceeds, elements unable to enter the Ca-Al sites in plagioclase (above) or the Mg-Fe sites (below) are trapped between. In this trapped or residual zone, all the remaining elements concentrate. These include K, Ba, Rb, Cs, REE, Th, U, Zr, and Nb. It is a geochemical characteristic of great importance that the principal lunar mineral phases do not readily accommodate the refractory trace elements. The evidence of high concentrations of these elements near the surface of the Moon is a dramatic consequence of this crystal chemical fact. Thus, following the primordial fractionation, a chemically zoned Moon is produced, with residual phases enriched below chilled margin and plagioclase crust and above the source region of maria basalts.

This crustal zonation established at about 4.5 aeons is changed very quickly. The declining stages of the meteoritic bombardment pulverize the chilled zone, and larger impacts mix in the underlying anorthosite. The high concentration of heat-producing elements K, U, and Th (and Zr, Hf, REE, etc.) trapped beneath the plagioclase zone provide the high element abundances for the Fra Mauro or KREEP basalts. Possibly this zone did not solidify, but residual liquids invaded the crust where impact mixing of the primitive surface layer, the Ca-Al plagioclase-rich layer, and the residual liquids beneath produced the parent material for the anorthositic gabbro (highland basalt) and the Fra Mauro basalts. The average composition of the highland crust is given in table 1, column 4. The activity continues to 3.9 aeons, culminating in the production of the ringed basins and the cessation of the intense highland cratering.

Partial melting next occurs in successively deeper layers as the smaller amounts of the heat producing elements induce partial melting and a succession of "maria-type" basalts are erupted. The high-Al maria basalts formed in this model at shallow depths beneath the crust. This emplacement of basalts overlaps with the later stages of the bombardment and predates the Imbrium collision in part, as shown by their presence in Fra Mauro breccias. Some of the high-Al maria basalts were emplaced later ($\approx$ 3.4 aeons), suggesting that partial melting in shallower zones was not limited to early periods of maria formation (Luna 16 rocks, 12038).

Following these, the Ti-rich Apollo 11 and 17 basalts were extruded during the period 3.8 to 3.6 aeons from a zone where Fe-Ti oxides and FeS accumulated. They have about 1 ppm Ni. Later (3.4 to 3.2 aeons), the Apollo 12 and 15 quartz and olivine normative basalts were extruded. These contain nickel, indicating extensive partial melting involving olivine, and many show evidence of near-surface fractionation. A negative Eu anomaly is characteristic of all maria basalts and contrasts with the deepest material erupted, the Apollo 15 emerald green glass (15426) (refs. 34 and 35) with 180-ppm Ni and primitive REE patterns, low total REE (3 to 5 times chondrites), and a small Eu anomaly (ref. 36). This material is the least fractionated lunar material that has been sampled (ref. 37). The thickness of the crust

above this zone, as well as the residual high melting point material and lack of heat sources due to the upward concentration of K, U, and Th, causes cessation of lunar vulcanism at 3.2 aeons. A diagrammatic view of the model proposed here is given in figure 1.

Acknowledgment

The authors express their gratitude to many colleagues at the Earth and Planetary Sciences Division, NASA/Johnson Space Center, Houston, for stimulating discussions, and to Dr. Robin Brett for constructive criticism of this manuscript. This paper was written at the Lunar Science Institute, which is operated by the Universities Space Research Association under NASA Contract No. NSR 09–051–001.

References

1. *Proc. Fourth Lunar Science Conference, Geochimica et Cosmochimica Acta*, Lunar Supplement 4, Vols. 1–3, 1973.
2. *Lunar Science*, Vol. V, Lunar Science Institute, Houston, 1974.
3. PAPANASTASSIOU, D. A., G. J. WASSERBURG, AND D. S. BURNETT, *Earth Planet. Sci. Letters*, Vol. 8, 1970, p. 1.
4. WETHERILL, G., *Science*, Vol. 173; 1971, p. 383.
5. TAYLOR, S. R., *Nature*, Vol. 245, 1973, p. 203.
6. BRETT, R., *Geochimica et Cosmochimica Acta*, Vol. 37, 1973, p. 2697.
7. DUNCAN, A. R., A. J. ERLANK, J. P. WILLIS, AND L. H. AHRENS, *Proc. Fourth Lunar Science Conference*, 1973, p. 1097.
8. ANDERS, E., *Geochimica et Cosmochimica Acta*, Vol. 35, 1971, p. 516.
9. TOKSÖZ, N. M., A. M. DAINTY, S. C. SOLOMON, AND K. R. ANDERSON, *Proc. Fourth Lunar Science Conference*, 1973, p. 2529.
10. MASON, B. H., *Elemental Abundances in Meteorites*, Gordon and Breach, 1970.
11. TROMBKA, J. I., J. R. ARNOLD, R. C. REEDY, L. E. PETERSON, AND A. E. METZGER, *Proc. Fourth Lunar Science Conference*, 1973, p. 2847.
12. TAYLOR, S. R., M. P. GORTON, P. MUIR, W. B. NANCE, AND R. RUDOWSKI, *Geochimica et Cosmochimica Acta*, Vol. 37, 1973, p. 2665.
13. WÄNKE, H., H. BADDENHAUSEN, G. DREIBUS, E. JAGOUTZ, H. KRUSE, H. PALME, B. SPETTEL, AND F. TESCHKE, *Proc. Fourth Lunar Science Conference*, 1973, p. 1461.
14. STUART-ALEXANDER, D., AND K. A. HOWARD, *Icarus*, Vol. 12, 1970, p. 440.
15. PARKIN, C. W., P. DYAL, AND W. D. DAILY, *Proc. Fourth Lunar Science Conference*, 1974, p. 2947.
16. RINGWOOD, A. E., AND E. ESSENE, *Proc. Apollo 11 Lunar Science Conference*, 1970, p. 769.
17. GANAPATHY, R., AND E. ANDERS, *Lunar Science*, Vol. V, Lunar Science Institute, Houston, 1974, p. 254.
18. KAULA, W. M., G. SCHUBERT, R. E. LINGENFELTER, W. L. SJORGEN, AND W. R. WOLLENHAUPT, *Lunar Science*, Vol. V, Lunar Science Institute, Houston, 1974, p. 399.
19. WETHERILL, G. W., *Science*, Vol. 160, 1968, p. 1256.
20. LATHAM, G. J., DORMAN, F. DUENNEBIER, E. EWING, D. LAMMLEIN, AND Y. NAKAMURA, *Proc. Fourth Lunar Science Conference*, 1974, p. 2515.
21. WALKER, D., J. LONGHI, E. STOLPER, T. GROVE, AND J. F. HAYS, *Lunar Science*, Vol. V, Lunar Science Institute, Houston, 1974, p. 814.
22. SCHNETZLER, C. C., AND J. A. PHILPOTTS, *Proc. Second Lunar Science Conference*, 1971, p. 1101.

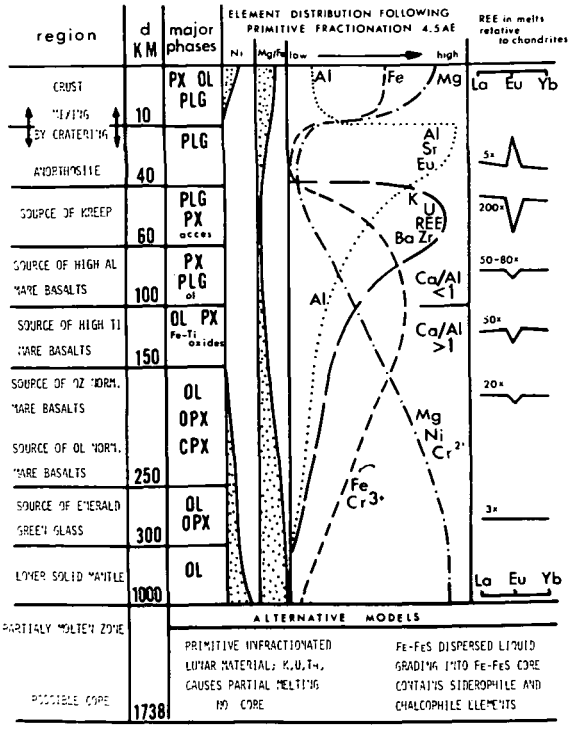


Figure 1.—*Geochemical model of the lunar interior at about 4.4 aeons.*

23. SCHNETZLER, C. C., J. A. PHILPOTTS, D. F. NAVA, S. SCHUHMANN, AND H. H. THOMAS, *Science*, Vol. 175, 1972, p. 426.
24. MIZUTANI, H., T. MATSUI, AND H. TAKEUCHI, *The Moon*, Vol. 4, 1972, p. 658.
25. BRETT, R., *Geochimica et Cosmochimica Acta*, Vol. 37, 1973, p. 165.
26. STRANGWAY, D. W., AND H. A. SHARPE, *Lunar Science*, Vol. V, Lunar Science Institute, Houston, 1974, p. 755.
27. LATHAM, G., Y. NAKAMURA, D. LAMMLEIN, J. DORMAN, AND F. DUENNEBIER, *Lunar Science*, Vol. V, Lunar Science Institute, Houston, 1974, p. 434.
28. WOOD, J. A., *Abstr. 36th Annual Meeting Meteoritical Soc.*, Davos, 1973, p. 164.
29. WALKER, D., T. L. GROVE, J. LONGHI, E. M. STOLPER, AND J. F. HAYS, *Earth Planet. Sci. Letters*, Vol. 20, 1973, p. 325.
30. GREEN, D. H., A. E. RINGWOOD, N. G. WARE, W. O. HIBBERSON, A. MAJOR, AND E. KISS, *Proc. Second Lunar Science Conference*, 1971, p. 601.
31. BIGGAR, G. M., M. J. O'HARA, A. PECKETT, AND D. J. HUMPHRIES, *Proc. Second Lunar Science Conference*, 1971, p. 617.
32. REID, A. M., AND P. JAKEŠ, *Lunar Science*, Vol. V, Lunar Science Institute, Houston, 1974, p. 627.
33. LSPET (Lunar Science Preliminary Examination Team), *Science*, Vol. 182, 1973, p. 659.
34. RIDLEY, W. I., A. M. REID, J. L. WARNER, AND R. W. BROWN, *Phys. Earth Planet. Interiors*, Vol. 7, 1972, p. 133.
35. GREEN, D. H., AND A. E. RINGWOOD, *Earth Planet. Sci. Letters*, Vol. 19, 1973, p. 1.
36. TAYLOR, S. R., M. P. GORTON, P. MUIR, W. NANCE, R. RUDOWSKI, AND N. WARE, *Proc. Fourth Lunar Science Conference*, 1973, p. 1445.
37. GREEN, D. H., AND A. E. RINGWOOD, *Earth Planet. Sci. Letters*, Vol. 19, 1973, p. 1.

Page intentionally left blank

Page intentionally left blank

Evolution of the Moon: The 1974 Model [1]

Harrison H. Schmitt
Astronaut, Apollo 17[2]

The geology of the decade of Apollo and Luna probably will become one of the fundamental turning points in the history of all science. For the first time, the scientists of the Earth have been presented with the opportunity to interpret their home planet through the direct investigations of another. Mankind can be proud and take heart in this fact.

The interpretive evolution of the Moon can be divided now into seven major stages beginning sometime near the end of the formation of the solar system. These stages and their approximate durations in time are as follows:

1. The Beginning: 4.6 billion years ago
2. The Melted Shell: 4.6 to 4.4 billion years ago
3. The Cratered Highlands: 4.4 to 4.1 billion years ago
4. The Large Basins: 4.1 to 3.9 billion years ago
5. The Light-colored Plains: 3.9 to 3.8 billion years ago
6. The Basaltic Maria: 3.8 to 3.0 (?) billion years ago
7. The Quiet Crust: 3.0 (?) billion years ago to the present

The Apollo and Luna explorations that permit us to study these stages of evolution each have contributed in progressive and significant ways. Through them we now can look with new insight into the early differentiation of the Earth, the nature of the Earth's protocrust, the influence of the formation of large impact basins in that crust, the effects of early partial melting of the protomantle, and possibly the earliest stages of the breakup of the protocrust into continents and ocean basins.

The probability is very great that the synthesis of the geological discoveries of Apollo and Luna will become one of the fundamental turning points in the history of all science. For the first time, men have been presented with the opportunity to interpret their own Earth through an understanding of a second planet. This second planet, the Moon, is now a pitted and dusty window into the Earth's own origins and evolution.

The view through this window is new and at present incomplete. On the other hand, at the close of the decade of Apollo and Luna, we can speak with considerable confidence about the internal structure of the Moon, the composition of its crust, the past processes that formed that crust, and the evolutionary sequence through which major portions of that small planet have passed. This paper will review the new limits on our interpretive understanding of the Moon and the sequence of events by which we gained this understanding. It also will suggest some of the new directions we can follow in search for understanding of the Earth as we attempt to apply our new vision of the Moon.

The summary of lunar science contained in this paper draws upon a broad spectrum of ideas and investigations performed by what has become known internationally as "The Lunar Science Team." One of the major difficulties inherent in such a large joint

[1] This paper is a revision and augmentation of a paper prepared for the Soviet-American Conference on Cosmochemistry of the Moon and Planets, Moscow, U.S.S.R., June 4–8, 1974. Adapted from "The Geology of Apollo," William Smith Lecture, Geological Society of London, London, England, 19 December 1973, Contribution No. 2480, Division of Geological and Planetary Science, California Institute of Technology, Pasadena, California.

effort and in the intimate verbal contact among those involved is the nearly impossible task of properly acknowledging all contributors to a given idea or area of discussion. This is manifestly more difficult in a review paper such as this. For the present work, I hope that it will suffice to include some general references and to say that what the reader finds he can agree with should be credited to the lunar science team as a whole; what he finds he cannot agree with should be blamed on the author.

The Moon and Its Evolution

THE BEGINNING

Mysterious events were taking place around our youthful Sun about 4.6 billion years ago. The materials left over from the birth of that Sun were combining in systematic ways, but by largely unknown processes, to form the planets and their satellites. The specific beginning of the Moon remains unclear, as is the case for all the planets and satellites in the solar system; however, there appears to be no reason to doubt that the beginning occurred about 4.6 billion years ago. On the other hand, the rate at which new information is being provided by the space investigations of the Soviet Union and the United States makes it almost certain that an internally consistent model for the origin of the solar system will appear in the not too distant future. It is this very rate by which we are learning, plus the vast detail that now constrains the possible models, that has presently saturated our collective ability to find a satisfactory model. A return to fundamental principles, extrapolated under the new constraints, has begun. However, the first new, generally accepted model for the evolution of the solar system has not appeared.

THE MELTED SHELL

Sunset on the farside of the Moon was not always so starkly tranquil as it is now. About 4.6 billion years ago, when the growing Moon was approximately its present size, the Sun probably set on a glowing, splashing sea of molten rock. Storms of debris still swept this sea, mixing, quenching, outgassing, and remelting a primitive melted shell. This outer shell, and possibly the entire Moon, appear to have been melted by the great thermal energy released by the last violent stages of the formation of terrestrial planets. The actual processes by which this energy was released and, in fact, the processes by which the seemingly closely related materials of the Moon and Earth came together in space remain subjects of heated debate.

Inside the melted shell the crust and upper mantle of the Moon were gradually taking form through processes associated with the fractional separation of phases on a planetary scale. At the base of the melted shell or possibly in the center of the completely melted Moon, an immiscible, dense liquid of iron and sulfur probably accumulated as the melting took place. The initial separation of silicate minerals in the outer melted shell then produced a combined crust and upper mantle a few hundred kilometers thick; the crust rich in calcium and aluminum (anorthitic plagioclase), the upper mantle rich in magnesium and iron (pyroxene and olivine).

Our lunar samples indicate that, in addition to calcium-feldspar, about 30 percent of the volume of material of the outer 25 kilometers of the crust is made up of minerals rich in magnesium and iron. Seismic information from beneath the area of our nearside net of seismometers indicates that the lower crust, that is, a zone between depths of about 25 and 65 kilometers, is similar in mineralogical composition to the outer crust; however, it appears to be of a much more coherent and more uniform structure. Below 65 kilometers and at least to about 200 kilometers beneath the Moon's surface, our seismic evidence indicates that the upper lunar mantle is probably composed largely of pyroxene and olivine. Both the upper mantle and crust, however, have been greatly modified by later events and materials.

Most of the major chemical differentiation we have observed on the Moon may have been established with the formation and cooling of the outer melted shell. This differentiation included the fractionation of siderophile and chalcophile elements into the immiscible iron-sulfur liquid; the fractionation of many major, minor, and trace elements between the crust and upper mantle during the fractional crystallization of silicate minerals; and the loss of volatile elements from the crust and upper mantle as the continued rain of primordial debris mixed and splashed the outer melted shell in the vacuum of space.

The distributions of rare earth elements presently form one of the major tests of the validity of arguments for the existence of an early melted shell as well as other events during the evolution of the Moon. We can assume that differences and similarities in the valence state and ionic radii of the rare earth elements, as compared with themselves and other elements, would exercise the major controls over the effect of various lunar processes on specific element distribution. The now obvious reduced oxidation state of the Moon and the systematic decrease in ionic radius with increasing atomic number of the rare earth elements offer some simplifications to problems of interpretation. However, the uncertainties in the nature of lunar evolutionary processes and in critical distribution coefficients for these elements leave much room for alternative explanations of the observed distributions.

An additional uncertainty is the average or beginning abundances of the rare earth elements in the Moon. In the absence of these data, the abundances in chondrites are used as a standard for comparison; however, it is clear that the initial abundances and variations in those initial abundances can affect some interpretations.

The period of crystallization of the melted shell appears to have been dominated by the simultaneous formation of calcium-feldspar and one or more magnesium- and iron-rich minerals. The dense magesium- and iron-rich minerals would sink in response to gravity to form a cumulate at the base of the melted shell. It is probable that the less dense calcium-feldspar floated upward in the shell, for there has occurred a great enrichment of that mineral in the upper 60 km of the Moon. The dominant effects of these crystallization processes on the rare earth elements of the Moon were the gradual enrichment of rare earths in the residual liquid and the relative depletion of europium in that liquid as it was extracted preferentially by the calcium-feldspar.

As our confidence grows in the "melted shell" interpretation of the second phase of lunar evolution, we must emphasize the concept of early crustal melting and differentiation in our thinking about the early history of the Earth. In addition to the creation of the protoforms ("proto" means "first") of a crust, mantle, and possibly a core at this time, the earth probably also had accumulated a fluidsphere by virtue of a gravitational field strong enough to hold volatile components that would have been lost from the less massive Moon. The extreme depletion of the Moon's crust in components more volatile than sodium relative to the Earth seems to reflect this difference in mass. On Earth as on the Moon, it is probable that the major radial controls on the distribution of the elements were established at the very start of the planet's evolution.

It may be of interest to note at this point that in the oldest complexes on Earth there are rocks called anorthosites, which are rich in calcium and aluminum, as are the very old crustal rocks on the moon. The early differentiation of a plagioclase-rich crust on earth may account for at least the initial concentration of elements composing these mysterious rocks. Understanding their origin and evolution is not a trivial problem, as most of our known titanium resources are found in such rocks.

The early fluidsphere of the Earth is also of great interest. It can be assumed to have contained nitrogen, water, and carbon because of the present great abundance of these components in the atmosphere and hydrosphere. They are also abundant in meteor-

ites of the carbonaceous chondrite variety. The analysis of lunar volatile components that are indigenous (in contrast to solar-wind-derived components) indicates that the early fluidsphere of the earth probably also contained significant sulfur and chlorine. The exact chemical and physical nature of this fluidsphere would be greatly dependent on temperatures that are presently unknown.

The formation of a core is one of the most important planetary phenomena that may have occurred at or soon after the time of the melted shell. There is geochemical, magnetic, and seismic evidence suggesting that a core of a liquid solution of sulfur and iron accumulated in the Moon at or prior to 3.9 billion years ago. This would have occurred early in lunar history if the entire Moon was once molten, or somewhat later if there was a gradual gravitational migration of the immiscible liquid from the melted shell period through an always solid mantle.

Whenever the core formed, a remarkable and still little understood phenomenon apparently occurred: an electric dynamo probably came into existence, began to perpetuate itself, and produced a magnetic field about 1/25th the strength of that presently associated with the Earth. Other alternatives for the creation of this field presently exist; however, its previous presence is unquestioned. Although the field is not presently active, regional magnetic anomalies left in crustal rocks persist. The anomalies have dimensions on the order of 100 kilometers and the strongest known is, appropriately, near the crater Van de Graaff. The presence of hard remanent magnetism in soil breccias formed only a few tens of millions of years ago suggests the possibility that the lunar magnetic field is only temporarily inactive.

If the creation of a lunar magnetic field was dependent on the formation of a conducting core, as seems most likely, then such a core was present at least 3.9 billion years ago, the age of the oldest rock that has been examined for remanent magnetic evidence of an ancient field. It also seems likely that a protective magnetic field existed around the Earth at least as far into the past as that of the Moon. The nature of the influence of this field on ancient climatic and biological processes on Earth is not yet known, but there are many reasons to believe that this influence would have been considerable. Further delineations of the history and origin of the magnetic fields of the Moon and other planets will bear heavily on our understanding of these terrestrial processes and their significance.

THE CRATERED HIGHLANDS

By about 4.4 billion years ago the surface of the Moon's outer crust was solid and must have looked not unlike the cratered highland areas we see today. As the debris storms continued their declining but still violent ways, this cratered and broken outer crust was saturated by craters 50 to 100 kilometers in diameter. It is now composed largely of impact-pulverized, shock-melted, and reaggregated plagioclase feldspar, a silicate mineral rich in calcium and aluminum. The intensity and depth of the disturbance of the outer crust cannot be overemphasized. By about 4.1 billion years ago, a debris zone formed that was at least 10 kilometers thick. The size of the craters with which the surface is saturated and the seismic data we have accumulated, indicate that the total disturbance extended to about 25 kilometers below the surface. It is not yet certain that the infall of debris declined in a continuous way or that this decline may have occurred in pulses of varying intensity.

The four- to five-hundred million years during which the cratered highlands were being profoundly modified by impacting debris may have resulted in changes in the characteristics of the rare earth element distributions established during the melted shell stage. Such changes would have been most extensive in the upper 10 kilometers of the cratered highlands. The first obvious possibility is that new material with different rare earth characteristics from those in the early crust may have been added either from deep or extralunar sources. In addition,

selective volatilization and redeposition of the light rare earth elements may have occurred. Possibly most important, however, was the regional homogenization of the outer crust over areas on the scale of a few hundred kilometers in diameter. Presently observed geochemical heterogeneities on scales less than this must be the result of late additions of new material. In particular, the most obvious geochemical anomalies appear to be the result of the additions of material derived from depth through excavation or magmatic activity.

It is highly probable that the protocrust of the Earth underwent disturbance comparable to that of the Moon. There is no clear evidence of this yet recognized on Earth; however, we should begin to consider the implications of the occurrence of such intense cratering. For example, the rates of mechanical and chemical weathering of the protocrust in the environments of the fluidsphere probably were greatly accelerated, with a resulting increase in the rates and degree of geochemical differentiation at the Earth's surface. The rates of early biological evolution also may have been greatly enhanced by the availability of nutrients and thermal energy and by the continuous mixing caused by impacting debris. That debris also may have continuously supplied the early organic building blocks of life which are present even now in some meteorites and in the interstellar medium.

THE LARGE BASINS

As the residue of creation was consumed by Earth and Moon alike, the debris storms decreased in frequency, although not without occasional unusually massive reminders of the past. Some time prior to about 4.1 billion years ago, large basins began to be formed by major impact events at a time when they could not be obliterated by smaller collisions or by a subsequent period of large collisions. Most of these basins are now partially filled by younger materials such as the basaltic maria; however, certain generalizations can be made.

The relatively young large basins, such as Serenitatis, are circular in shape and have deep original floors. Variations in gravitational accelerations measured from lunar orbit show that these young basins overlie large concentrations of mass (mascons) and have roughly concentric deficiencies of mass just inside their rims. The older large basins, such as Tranquillitatis, are irregular in shape, have shallow original floors, and contain no large concentrations or deficiencies of mass within them. Although all of the great basins appear to have been formed by major impact events, the general differences between them suggest a major change in the mechanical properties of the crust about 4.0 billion years ago. The final upward migration and crystallization of the highly fractionated residual liquids of the melted shell may have occurred at this time.

The mechanics of the formation of the large basins and the detailed physical and chemical processes associated with their formation are poorly understood. Most of our terrestrial experience with impact and explosion cratering has been on a scale where local shock effects, hemispherical excavation, ballistic ejection, and limited movement of shock-melted material have been dominant. We must now try to understand events that occur on scales ten to a hundred times more energetic, and which will interact with large portions of an entire planet. Regional or global shock waves, large-scale lateral excavation, fluidized ejection and transport of pulverized debris, and regional movement and deep crustal injection of shock-melted material are phenomena that may need to dominate our thinking about the formation and effects of the large basins.

Samples from the lunar surface and data from orbital sensors indicate that rocks possibly formed from the residual liquids of the melted shell, and rich in alkalies, radioactive isotopes, rare earth elements, and phosphorus, are now present in varying amounts in the debris on the Moon's surface. They have been referred to as the "KREEP" basalts. Their major known distribution limits are between longitudes 5° E and about 60° W.

They appear to be spatially associated with the southern portion of the Imbrium Basin and its ejecta blanket to the south and southwest.

The separation of large volumes of calcium-feldspar and magnesium- and iron-rich minerals from the residual liquid of the melted shell appears to be the most likely origin for at least the parent materials of the KREEP basalts. In addition to the great enrichment of all the rare earth elements and the greatly accented depletion of europium in these materials, we find the expected relative enrichment of the light over the heavy elements, imposed by differences in ionic radii.

With the completion of the formation of the large basins and prior to their partial filling by younger materials, a major lunar surface formation existed that is now largely covered by light-colored plains materials and basaltic maria. This formation is now extensively exposed only inside the outer mountain ring of the Orientale Basin where it consists of a hummocky, cracked, and locally draped layer that appears to have been shock-melted lava that flowed within the basin just after the impact event that created it. Although now largely covered elsewhere on the Moon, impacts into this surface may have contributed significant amounts of its material to the debris that was forming on the surrounding highland regions.

There are many good reasons to believe that the early crust of the Earth suffered the same violent indignities of large basin formation as did the Moon's crust. Although the subsequent 4 billion years of dynamic Earth history have masked the effects of this violence, there are now many new things to look for and many new lines of interpretation to pursue. For example, the distribution of the early ocean basins may have been determined by the distribution of large impact basins and groups of basins. Also, throughout the Earth's crust there have long been recognized regional provinces that are rich in certain elements and which are the loci of ore deposits of those elements. For example, the southwestern United States is one such geochemical province rich in copper. Our present understanding of the origin and structure of these provinces is very limited even though much time, effort, and money have been spent in endeavoring to understand. Locked in the mechanics of the formation of the very large lunar basins, and their penetration into the crust, and in the distribution of ejecta around such basins, may be much of the understanding we seek.

THE LIGHT-COLORED PLAINS

The first event possibly generated by the Moon's interior processes about 3.9 billion years ago was the surface deposition of light-colored, plains-forming materials. Visual and geochemical studies conducted from lunar orbit indicate that these light-colored materials are composed largely of the pulverized, but possibly annealed, remnants of the ancient feldspar-rich crust. The surface features of the plains that fill large basins on the far-side of the Moon suggest that the materials underlying the plains are eruptive and have partially filled all the great basins that then existed. These surface features include irregular, nearly rimless maar-like craters and low, finely hummocky terrain overlain locally by smooth, ponded material. The eruption of such light-colored plains materials may have been driven by the first internal melting of the lunar mantle. These early melts probably were rich in gaseous components. Through additional partial melting of the mantle, less gaseous and more magnesium- and iron-rich basaltic melts would later concentrate in much larger volumes to form the maria.

There are other light-colored plains in old, irregular depressions on the Moon's surface. Many of these, particularly those that are roughly circumferential to the large basins near the limits of their ejecta blankets, may have formed from the ponding of fine debris ejected or remobilized by the impacts that formed the basins. Still other plains as yet have no obvious origins. It is probable that both eruptive and impact processes created light-colored plains during this period of time.

THE BASALTIC MARIA

Just after the last of the large basins were created about 3.9 billion years ago, the final major internally generated episode of evolution took place. This chapter of lunar history consists of the flooding of all the great basins on the frontside of the Moon by vast, now frozen "oceans" of dark basalt. Only the very deepest of basins on the farside, such as Tsiolkovsky, were affected by the formation of the maria. To some degree, however, all portions of the broken outer crust must have been permeated up to a general mare "sea-level."

The tremendous upwellings and extrusions of the basaltic maria were perpetuated by heat from radioisotopic decay, and, in this case, geochemical and petrogenetic arguments suggest that portions of the Moon's upper mantle or even deeper inner mantle probably melted. The radioisotopic heat accumulation was probably accentuated by at least one of four factors: (1) the insulative properties of the outer crustal regolith produced during the cratered highland period, (2) the additional insulative properties of regional blankets of hot ejecta from large basins, (3) the possible heat contribution from the less differentiated inner mantle, and (4) in some cases of the earliest maria eruptions, the local release of pressure caused by the formation of the large basins.

The extrusions of the products of the melting appear to have been in pulses each of which is now represented by the basaltic filling of many of the large basins and of other topographically low areas. The distribution of different chemical varieties appears to be roughly concentric to the Tranquillitatis region. This suggests that successive surface eruptions of the maria may have been controlled by the interaction of the equipotential surfaces of the lunar gravitational field with an offset lunar figure and the borders of impermeable crust beneath older mare eruptive areas. The limits of the large basins would be the dominant lateral modifier of this idealized pattern of eruption.

The early extrusion of each major pulse of mare basalt may have been very rapid through the intensely and deeply broken outer crust of the preceding cratered highland stage. If this was true, then each local basalt-filled basin may be a single cooling unit and similar in internal structure to our own planet's basaltic and ultramafic stratiform sheets. Most of the upper visible portions of these basins, however, are now composed of extensive lava flows, 10 to 100 meters thick, and, in some cases, several hundred kilometers long. These flows, along with some pyroclastic debris, appear to have erupted from late-stage, localized centers and then spread over vast areas in and around the large basins.

Variations in the internal composition of the Moon or in temperatures as a function of depth caused the period of mare basin flooding to span at least the time from 3.8 to 3.0 billion years ago. Such variations in composition or depth of origin also caused major differences in the contents of titanium and certain minor and trace elements in the basalts that were produced as this time passed. Finally, near the end of each of several periods of mare flooding, mantles of chemically distinct, orange, black, red, and green basaltic material were deposited as pyroclastic debris over large areas. This debris is unusually rich in magnesium, iron, some volatiles, and primitive lead isotopes, and may have been derived from the very deep, less differentiated interior of the Moon.

The details of the rare earth element distribution after the crystallization of the melted shell may offer some clues to the depths of origin of the mare basalts. As the magnesium- and iron-rich cumulate formed at the base of the shell, the lunar mantle was gradually formed. In an extremely simplistic model, the cumulate as it formed would trap and isolate an intercumulate liquid. Because of the progressive concentration of the rare earth elements in the residual liquids, the intercumulate liquid would tend to have progressively higher concentrations of these elements with decreasing depth and age of accumulation in the mantle. In addition, the separation of calcium-feld-

spar from the residual liquid would cause the intercumulate liquid to have a progressively greater depletion of europium relative to other rare earths with decreasing depth in the mantle.

A large number of the characteristics of the basaltic maria indicate that they originated by the partial melting of selected portions of the lunar mantle. In particular, the nearly complete remelting of localized intercumulate material is suggested by the model ages (approximately 4.5 billion years) of many mare basalts. The characteristics of the rare earth abundances in the various mare basalts suggest a depth-dependent sequence of remelting of the mantle to produce the magmas from which they crystallized. This sequence is based on the expected increases with decreasing depth in (1) the total rare earth abundances, and (2) the relative depletion of europium relative to other rare earths. The probable sequence of maria sampled to date in order of decreasing depth of origin is Apollo 15 (3.2 b.y.), Apollo 12 (3.1 b.y.), possibly Luna 16 (3.4 b.y.), Apollo 17 (3.8 b.y.), and Apollo 11 (3.7 b.y.). As is indicated by the apparent ages of the maria, the remelting of the mantle was generally from the outside in, as has been suggested by many workers based on geophysical arguments.

There is a further suggestion in this sequence that the titanium-rich portions of the original mantle, from which came the Apollo 17 and 11 basalts, were formed relatively late (shallow mantle depths) in the crystallization of the melted shell. The remelting of titanium- and iron-rich oxides in addition to the intercumulate material may account for the enrichment of the heavy rare earths relative to the light rare earths in the Apollo 17 and Apollo 11 titanium-rich basalts.

With the completion of the eruptions of the maria, a relative quiet settled forever on the surface of the Moon. When the waves and currents in the surface flows of the maria had finally been arrested, the Moon's appearance differed only slightly from that of today.

We perhaps should note at this point that the oldest rock terrains on Earth also contain vast layered rock sheets which in aggregate are basaltic or ultramafic in composition. Their resemblance to the lunar maria may be more than coincidental. The possibly higher rate of radioisotopic heat accumulation in the Earth due to its larger volume to surface area ratio would have accelerated and prolonged any internal melting that might have produced mare-like materials. Again, as with the anorthosites, the question of the existence of terrestrial maria is not of trivial interest because large portions of the nickel, chromium, and platinum-group metal resources of our planet are located within these sheets of rock. In addition, the eruption and weathering of terrestrial basaltic maria may have produced a "geochemical pulse" at the Earth's surface, of presently undefined significance.

THE QUIET CRUST

About 3 billion years ago, except for faint rumblings and occasional sharp ringings we hear now as seismic reminders of the past, the storied Moon apparently completed the visible record of its tale. There are indications of a brief period of later internal activity, possibly a convective overturn of the mantle, but nothing like the continuing activity of Earth and, apparently, of Mars. The stratigraphically young ridge and volcanic system in Mare Procellarum, the great regional graben systems across the southeast quadrant of the frontside of the Moon, and the light-colored swirls of apparent alteration scattered around the whole Moon may reflect the embryonic stresses of aborted evolution.

Thus, we bring ourselves to the Moon as it is at present. In many respects, the Moon is as chemically and structurally differentiated as the Earth, lacking only the continued refinements of mantle melting and convection and crustal weathering and metamorphism. In other respects, the Moon moves through space as an ancient text, related to the history of the Earth only through the

interpretations of our minds, and as the modern archive of our Sun, recording in its soils much of immediate importance to man's future well-being. Our only means of reading the text and using the archive is to study what we now have and, most importantly, to continue to go there.

The History of Apollo's and Luna's Science

TRANQUILLITY BASE—APOLLO 11

(July 20, 1969)

What was the history of events of Apollo and Luna that have led us to this first-order interpretation of the evolution of another planet? The most important of those events occurred in the southern region of Mare Tranquillitatis. That region holds a unique place in the annals of science and of mankind. The event which history will remember as having changed forever the course of that same history was the landing of Apollo 11 by Armstrong, Aldrin, and Collins.

Science for its part finally had real and factual insight into the temporal dimensions, if not all of the actualities, of the evolution of our sister planet. The ages of at least major portions of the rocks in the lunar crust were found to be very old relative to known terrestrial rocks and to most previous estimates of the probable ages of lunar rocks. Support for the arrested evolution of the Moon was also illustrated by the lack of significant internal seismic activity. The fact that the relatively young-appearing Tranquillitatis mare was 3.7 *billion* years old seemed to confirm that we would be studying our own past along with that of the Moon. As a consequence of comparing the very highly cratered highlands of the Moon with the relatively uncratered but nonetheless very old maria, it was necessary to conclude that a major change in the frequency of large impact events occurred prior to 3.7 billion years ago. This conclusion caused major revisions in our stratigraphic interpretations related to the time scale of lunar and, therefore, terrestrial evolution.

The rocks of the maria were found to be basaltic, as predicted; however, they were not only unusually rich in iron and titanium and poor in sodium, carbon, and water by terrestrial standards, but were highly differentiated chemically, relative to solar and meteoritic elemental abundances. Because of this and other new factors, the isotope and trace element chemistry of the Moon was obviously not to be a straightforward application of fact and prejudice gained from studies of the Earth and meteorites. Within the basalts as a whole, we began to see that the crust of the Moon was much richer in uranium and thorium than would be expected from accepted solar abundances. The basalts also appeared to make up several flow units that in turn appeared to be locally differentiated through fractional crystallization. Related to this crystallization is a still incompletely identified, immiscible sulphur-rich gas phase that produced spherical holes and vugs in most of the basalt samples. The detailed nature of this gas phase in these and many other rocks from all other landing sites remains a mystery.

Tranquillity Base gave us our first direct exposure to the complexities and puzzles of the lunar soils, or what became known as the "lunar regolith." As had been supposed from previous investigations, including Ranger, Surveyor, and early Luna missions, most of the material in these soils appeared to have been derived by the pulverization, shock metamorphism, shock melting, and local reaggregation of the underlying basalts. The reaggreation process produced dark matrix breccias that are chemically and texturally nearly equivalent to the soils. Within the soils and soil breccias there were found to be small amounts of exotic materials including not only basaltic material from distant or now covered maria, but also anorthositic and granitic non-mare debris apparently derived from the cratered highlands to the south. Meteoritic debris, migrant volatiles from other regions, gases derived from the

solar wind, and the effects of galactic cosmic rays were also identified. The debris that may have come from the cratered highlands seemed to confirm the Surveyor VII results at Tycho that the southern lunar highlands, and, therefore, the lunar crust, were rich in calcium and aluminum silicates.

Possibly most important to science, Apollo 11 confirmed that much of our intellectual experience in geoscience was applicable to our studies of the Moon; however, it also confirmed that our intellectual insight was in great need of expansion.

MARE COGNITUM—APOLLO 12

(November 19, 1969)

Conrad, Bean, and Gordon on Apollo 12 landed within a few hundred meters of a previously landed Surveyor III automated spacecraft in Mare Cognitum southwest of Imbrium. Their mission returned obvious complexity to lunar science after the emotional early simplifications following the results from Apollo 11. The structure of the gardened upper few meters of the lunar surface became a complex history book not only recording solar and cosmic events, but showing that the relative mobility of volatile elements in high vacuum would be of great significance in interpreting geochemical measurements. Representatives were uncovered of heretofore unsuspected rocks rich in potassium, rare earth elements, and phosphorus (KREEP basalts) apparently recording a fractionation event that occurred about 4.5 billion years ago in the melted shell. The range of ages of the basaltic maria was extended downward to about 3.2 billion years; that is, the formation of the mare basalts covered at least half a billion years. It also was found that the major chemical variability in basaltic maria extended to varieties with relatively low quantities of titanium. The surface units of the maria were confirmed to be differentiated flows on the order of several tens of meters thick.

Of considerable importance to lunar stratigraphy was the fact that the landing site was located on a ray of debris from the crater Copernicus. Rays were thus seen to consist of large masses of material and not just disruptions of the surface by relatively small amounts of ejecta. Material from this ray was used to determine that the event that formed Copernicus probably occurred 0.9 billion years ago. This date now provides an anchor to much of the stratigraphic correlation of events that occurred after the formation of the basaltic maria.

The geophysical data from Apollo 12, taken in concert with the strange findings from Apollo 11, began to establish their own special surprises. The seismometer showed us that the upper crust of the Moon rings like a bell when hit. It has the unusual and unexpected combined properties of very low attenuation (high Q) and very intense wave scattering. Such properties probably are the result of a dry, pervasively fractured crust in which individual blocks have well-seated contact points against one another.

Magnetometers onboard automated orbital spacecraft had previously shown that the Moon presently has essentially no global magnetic field (less than 1 gamma). In contrast, the Apollo 12 surface magnetometer showed that local, low-intensity fields (around 100 gammas) were present. This, combined with the presence of hard remanent magnetism in the rocks, indicated that there had been a strong ancient global magnetic field (2000–3000 gammas).

MARE FECUNDITATIS—LUNA 16

(September 20, 1970)

The sample return from the northwestern part of Mare Fecunditatis by Luna 16 demonstrated an important new dimension to the previous Luna and Surveyor automated study of the Moon's surface. The data from the materials of the upper surface of this great eastern plain permitted further generalizations to be made concerning the character of the basaltic maria previously

sampled by Apollo 11 and Apollo 12 in Mare Tranquillitatis and Mare Cognitum. Although each mission had sampled only a very small part of the vast region contained in these three, widely separated maria, the internal consistency of the results of various investigations on the samples increased the confidence that many of the data from an individual mission were representative of broad regions.

The crystallization age of a fragment of the local Fecunditatis basalt was determined to be about 3.4 billion years, intermediate to the 3.7- and 3.2-billion-year crystallization ages measured for Tranquillitatis and Cognitum mare basalts, respectively. Some other characteristics of the Fecunditatis basaltic material also are intermediate relative to Tranquillitatis and Cognitum, including the titanium and silicon contents. On the other hand, new ranges in the variability of basaltic compositions were established by the Luna 16 analyses; rare earth element concentrations are lower than found for earlier missions, and the depletion of europium relative to chondrites is less.

The investigation of the regolith characteristics at the Luna 16 site indicates broad similarities with those of Tranquillity Base; however, the non-mare components of the regolith show many distinctive features relative to both the Apollo 11 and 12 sites. In particular, the chemistry of the non-mare components indicates that the cratered highlands (surrounding Fecunditatis) that have contributed to the regolith, have retained their own distinctive provincial character, as has been seen at all Apollo and Luna landing sites.

FRA MAURO—APOLLOS 13 AND 14

(February 5, 1971)

To the east of the Mare Cognitum landing site of Apollo 12, and in the highlands south of the crater Copernicus, we planned the landing of the Apollo 13 mission. We were anticipating that through study of the Imbrium Basin ejecta blanket, we would receive insight into the intensity and timing of the event that formed the basin. Instead, we received new insight into ourselves. The courage of Lovell, Haise, and Swigert, as well as the resourcefulness of the ground controllers of their mission following the explosive destruction of the Service Module, provided one of history's most graphic examples of man's potential in the face of extreme adversity.

Apollo 14 and Shepard, Mitchell, and Roosa inherited Apollo 13's exploration plan for Fra Mauro. The mission told us that not only did the Imbrium event occur barely 100 million years before the oldest mare basalt extrusions, but that such massive collisions cause much more geologic disruption and transfer much more heat energy into a planet's surface than we had ever before imagined. In fact, it now appears that much of the pulverized crustal material ejected from the large basins moved many hundreds of kilometers across the Moon's surface and had many of the mechanical, dynamic, and metamorphic characteristics of volcanic ash flows.

The Apollo 14 mission also confirmed the extreme chemical differences between the highlands and the maria detected on previous missions. On the other hand, the abundance of rocks richer in alkalies, radioactive isotopes, rare earth elements, and phosphorus than were other known highland rocks suggested a well-defined provincial nature to the distribution of at least some lunar materials other than the maria.

With Apollo 14 we finally established the baseline of a net of seismometers. In conjunction with the Apollo 12 seismometer, it became possible to look at the structure and physical properties of the lunar crust through the analysis of data from natural and manmade seismic (impact) events. Most importantly, evidence appeared that at least the outer portions of the Moon are layered. Also, the first evidence of moonquakes began to accumulate, indicating that, although very quiet, the Moon was not yet completely dead internally.

HADLEY-APENNINES—APOLLO 15

(July 30, 1971)

The Apollo 15 mission to Hadley Rille at the foot of the lunar Apennine Mountains introduced a new scale to lunar exploration. First, Scott, Irwin, and Worden began to look at the whole planet through the eyes of precision cameras and electronics as well as the eyes of man. Then, on the Moon's surface they reached beyond our earlier hopes and were the first to use a powered surface vehicle to rove and observe the wide variety of features available for investigation.

The varied samples and observations from the vicinity of Hadley Rille and the mountain ring of Imbrium pushed our knowledge of lunar time and processes back past the 3.9-billion-year barrier we had seemed to see on previous missions. We discovered, however, that our interpretations of lunar history behind this barrier would have to come through the mask of multiple cycles of impact brecciation. Nevertheless, through the clasts in the breccias we began to vaguely see into the first half-billion years of lunar evolution and into some of the details of the melted shell period. In addition, we expanded our delineation of the complex volcanic processes that created the present surfaces of the maria. These processes now were seen to include not only internally differentiated lava flows but possible processes of volcanic erosion that could create the lunar sinuous rilles. We also saw once again how pervasive are the effects of contamination of surface materials by the rays of distant impact events.

With Apollo 15, we finally established a geophysical net, particularly a seismic net, by which we began to see into the inside of a second planet; the structure of that planet as partly described earlier had begun to be deciphered. This net and correlations of its information with other facts have shown that the general structure of at least major portions of the Moon's interior is as follows: an upper, broken, calcium- and aluminum-rich silicate crust extending from 0 to 25 kilometers; a lower, coherent, calcium- and aluminum-rich silicate crust from 25 to 65 kilometers; an upper, magnesium- and iron-rich silicate mantle from 65 to about 200 or 300 kilometers; an inner, probably chondritic and volatile-bearing silicate mantle from about 300 to about 600 kilometers; a lower, also probably chondritic and volatile-bearing, seismically active, locally melted mantle from about 600 to about 1100 kilometers; and an at least partially fluid, possibly iron-sulfur core from about 1100 kilometers to the Moon's center at 1735 kilometers.

Our geophysical station at Hadley-Appennines also told us that the flow of heat from the Moon was possibly two times that expected for a Moon of the approximate radioisotopic composition of the Earth's mantle. If true, this tended to confirm earlier suggestions that much of the radioisotopic materials in the Moon were concentrated in its crust. Otherwise, the interior of the Moon would be more fluid and active than the record of the seismometers indicates.

We began to be able to correlate our landing areas around the whole Moon by virtue of geochemical X-ray and gamma-ray mapping from orbit. These remote sensing investigations disclosed the provincial nature of lunar chemistry, particularly by highlighting differences in the ratios of aluminum to silicon and of magnesium to silicon within the maria and the highlands. By outlining anomalies in the distribution of uranium, thorium, and potassium, the gamma-ray information suggested that large basin-forming events were capable of creating surface geochemical provinces through the ejection of deep-seated material.

From our orbital investigations, we also greatly expanded our knowledge of the distribution and geological correlation of gravitational and magnetic anomalies in the Moon's crust. This was accomplished by use of a small satellite ejected by Apollo 15 prior to leaving lunar orbit for the return to Earth.

Possibly of equal importance with all these discoveries by Apollo 15 was the realization, by ourselves and through television by millions of people around the world, that

there yet existed beauty and majesty in views of nature previously outside human experience.

APOLLONIUS REGION—LUNA 20

(February 21, 1972)

The second automated sample return mission from the Moon, Luna 20, landed in the Apollonius region south of the large basin Crisium and 120 kilometers north of the Mare Fecunditatis landing site of Luna 16. As with Luna 16's data on the basaltic maria, the most important aspect of the Luna 20 sample was the increased global perspective it gave us with respect to the character of lunar highlands. When compared with the investigation of cratered highland material sampled on Apollos 14 and 15 and later on Apollos 16 and 17, the Luna 20 materials emphasize the homogenization effects of the half-billion years of cratering that formed the highland regions we now see. It is in the remaining traces of heterogeneity which reflect ancient highland provinces that we see the extent of the homogenization.

The materials of the Apollonius region appear to be similar to the materials returned slightly later by Apollo 16 from the Descartes region. The major exceptions to this similarity are the significantly lower aluminum contents of debris probably representative of the Apollonius region, and the abundance of fragments representing a distinctive suite of crystalline rocks known as the anorthosite-norite-troctolite suite. This suite first became recognized after Apollo 15 as possibly being the much reworked remnants of at least portions of the ancient lunar crust. Luna 20 confirmed its importance. In addition to these major distinctions, the Luna 20 material show differences in their trace element concentrations relative to other highland areas. In particular, the rare earth elements are present in clearly lower abundances than in materials from Apollos 14, 15, and 16.

The last crystallization age of some of the Luna 20 rocks appears to be about 3.9 billion years, and continued to point up this age as reflecting a major age limit in lunar history. The same general age for the cooling of highland or highlandlike materials had been determined for the ejecta blanket of the Imbrium Basin at Fra Mauro and for the rocks of the Apennines, and soon would be determined for the highland rocks at Descartes. This age limit was now seen to represent one of the following occurrences: (1) a major thermal event associated with the formation of several of the large basins over a relatively short time period, (2) a major thermal event associated with the formation of the light-colored plains, or (3) the rapid cessation of the period of major cratering that had continually reworked the cratered highlands until most vestiges of original ages had disappeared and only the last local impact event was recorded. As we attempt to explain the absence of very old rocks on Earth, we also should not forget these possibilities.

DESCARTES—APOLLO 16

(April 21, 1972)

Apollo 16 found that we were not yet ready to understand the earliest chapters of lunar history exposed in the southern highlands. In the samples returned by Young, Duke, and Mattingly from the Descartes area, we seem to see that the major central events of that history were compressed in time far more than we had guessed. There are indications that the formation of the youngest major lunar basins, the eruption of light-colored plains materials, and the earliest extrusions of basaltic maria took place over about 100 million years of time around 3.9 billion years ago. In addition, indications are present at Descartes that the light-colored plains may be the loci of many of the observed regional magnetic anomalies, suggesting that the plains formed as single cooling units that were initially above the Curie point.

The extreme complexity of the problem of interpreting the lunar highland rocks and

processes became clearly evident even as the Apollo 16 mission progressed. Rather than revealing materials of clearly volcanic origin as had been expected, most information suggests that the samples from the Descartes regolith had been subjected to an interlocking sequence of igneous and impact processes. Some of these samples may have been derived from the distant, now covered surface layer of shock-melted lava in the large basins, as well as from bedrock beneath the Descartes highland region. A new chemical rock group known as "very high aluminum basalts" could be defined although their ancestry relative to other lunar materials has been obscured by the final events that gave the cratered highlands their present form. The results of Apollo 16 have within them an integrated look at almost all previously and subsequently identified highland rock types. With this complexity comes a unique opportunity to understand the formation and modification of the Moon's, and potentially the Earth's, early crust.

Apollo 16 continued the broad-scale geological, geochemical, and geophysical mapping of the Moon's crust from orbit. This mapping greatly expanded our knowledge of geochemical provinces and geophysical anomalies, and has helped to lead to many of the generalizations it is now possible to make about the evolution of the crust.

TAURUS-LITTROW—APOLLO 17

(December 11, 1972)

Near the coast of the great frozen sea of Serenitatis, Apollo 17 carried Cernan, Evans, and me to visit the valley of Taurus-Littrow. The unique scientific character of this valley helps to mitigate the sadness that with our visit the Apollo explorations ended. If this end had to be, it would have been difficult to find a better locality to synthesize and expand our ideas on the evolution of the Moon.

At Taurus-Littrow we have looked at and sampled the ancient lunar record ranging back from the extrusion of the oldest known basaltic maria, through the formation of the breccias of the Serenitatis mountain ring, and thence back into clasts in these breccias that may reflect the very origins of the lunar crust itself. Also, we have found and are studying volcanic materials and debris-forming processes that range forward from the formation of the earliest basaltic maria surface and through 3.8 billion years of modification of that surface.

The pre-mare events in the Taurus-Littrow region that culminated in the formation of the Serenitatis Basin produced at least three major and distinctive units of multilithic breccias. The oldest of these breccia units contains distinctive clasts of crystalline mafic and ultramafic rocks that appear to be the remains of the fractional crystallization of portions of the melted shell. This conclusion is supported by one of these distinctive clasts, a crushed rock of magnesium olivine, which has an apparent crystallization age of 4.6 billion years. The old breccia unit containing these clasts has been intruded and locally metamorphosed by another breccia unit which was partially molten at the time of intrusion. This intrusive event appears to have occurred about 3.9 billion years ago. Such intrusive breccias are probably the direct result of the massive impact event that formed the nearby large basin of Serenitatis; however, an internal eruptive origin cannot yet be ruled out. The third unit appears to partially cap the tops of the mountains and it may be another old ejecta unit from one of the several large basins within range of the valley. This breccia contains a wide variety of clasts of mafic crystalline material plus other, previously unrecognized material that includes barium-rich granitic rock.

The valley of Taurus-Littrow and other nearby low areas appear to be a coincidental structural window that exposes some of the oldest, if not the oldest, basaltic maria extrusives on the Moon. With an age of 3.8 billion years, they are 50 to 100 million years older than the basalts at Tranquillity Base. Like the Tranquillity Base basalts, the Taurus-Littrow rocks are titanium-rich with up to 13 weight percent TiO_2. Except for near-surface, fine-grained varieties, the tex-

ture and composition of the Taurus-Littrow basalt appears to be essentially uniform to depths of at least 120 meters. This suggests that the valley may be the top of a very thick cooling unit of basaltic material. Geophysical evidence indicates that this unit of basaltic material may be as thick as two kilometers indicating also that, when taken with the present height of the surrounding massifs, the valley may have had an original depth of over four kilometers.

One of the many major remaining puzzles of potentially great significance is that of the tectonic history of the valley and the massifs surrounding it. Several facts suggest that the structural boundary between the valley and the massifs has been active throughout most of its existence. A young scarp strongly resembling that of a fault suggests recent activity. Also, there are no debris accumulations at the bases of the steep (20°–25°) slopes of the massifs; in fact, there tends to be a continuous shallow moat instead. In addition, the soils and rocks that are present at the bases of the massifs are all tens to hundreds of millions of years old rather than having the imprint of the presumed 3.9-billion-year age of the massifs. All of these considerations suggest that blocks of the lunar crust may be in continuous, but episodic motion in spite of the obvious general strength and quiescence of that crust. Recently identified, but rare near-surface moonquakes may also relate to this phenomenon.

Relatively recent modifications of the lunar surface as a result of internal processes also are indicated by the visual and photographic data on the mysterious light-colored swirls that were obtained by Apollo 17 from orbit. The swirls, of which Riner Gamma in Oceanus Procellarum is the most well-known example, are much more widely distributed than previously thought, particularly in broad regions to the north and east of Mare Smythii. In all known instances, the swirls have no discernable topographic relief and are superimposed on all associated features. In addition, many swirls are zoned, with light-colored zones bordering an inner dark-colored zone that is darker than the surrounding, unaffected surface. These characteristics suggest that fluidized alteration processes have formed the swirls. The fluids in turn may have their origin in the continued, gradual degassing of the lunar interior.

The modifications of the surface of the valley basalt included the addition of mantles of beads of chemically distinctive orange glass and black devitrified glass. These glasses may have been formed as the result of processes once active within the deep interior of the Moon. The titanium-rich, basaltic to ultramafic glasses surprised us once again; their 10- to 30-million-year exposure age is young and was expected for the dark mantling deposits seen in photographs; but their 3.5- to 3.7-*billion*-year cooling age was not expected. The explanation for this difference is complex and not yet completely understood. The glasses also have an unusual complement of trace elements, including lead, zinc, sulfur, chlorine, and others. Some of the more volatile trace components are present as relatively low-temperature absorbed material. The volatile lead in the orange glasses is extremely enriched in primitive lead isotopes and has other isotopic characteristics that indicate early isolation from the rock systems that produced other lunar materials examined to date. Green glass beads found at Hadley-Apennines on Apollo 15 have similar but less definitive characteristics. The characteristics of the glass beads strongly suggest a volcanic source and a parent material in or below the mantle of the Moon and different in major respects from the parent of the mare basalts.

As a followup to the recognition of orange and black pyroclastic materials on the lunar surface at Taurus-Littrow, Apollo 17 also provided visual and photographic data from orbit that have permitted the identification and interpretation of broad areas of similar materials around the southwestern, southern, and southeastern borders of the Serenitatis Basin. It is now clear that the previously identified and mapped "dark-mantle materials" in these areas (and most probably elsewhere on the Moon) are indeed volcanic deposits made up of various combinations of

layers of orange, black, red, and green glass and devitrified glass.

THE FUTURE

For all of our Apollo missions we left the Moon before the lunar sunrise had progressed into the vast regions of the lunar west: Mare Procellarum, where the young mysterious features of that region's central ridge system still await the crew of a mission diverted after Apollo 13; Mare Orientale, whose stark Alpine rings have been viewed closely by man only in the subdued blue light of the Earth. The promise of the story in these regions has not diminished, but seemingly watches for the progression of the sunrises and the landing craft of another generation of explorers. When that time comes and we merge the scientific revolution brought about by Apollo and Luna on the Moon with the simultaneous revolution brought about by new insight into the origins of ocean basins and continents on the Earth, we may begin to understand the great stresses and strains within our planet's crust as ocean floors grow and continents move. Within future understanding of features like the basalts of Mare Procellarum and its vast ridge and volcanic system may lie further inspiration for all of us.

References

CONFERENCE PROCEEDINGS

Proc. Apollo 11 Lunar Science Conference, A. A. Levinson, ed., Pergamon Press, 1970; *Geochimica et Cosmochimica Acta*, Supplement 1.

Proc. Second Lunar Science Conference, A. A. Levinson, ed., MIT Press, 1971; *Geochimica et Cosmochimica Acta*, Supplement 2.

Proc. Third Lunar Science Conference, Elbert A. King, Jr., Dieter Heymann, and David R. Criswell, eds., MIT Press, 1972; *Geochimica et Cosmochimica Acta*, Supplement 3.

Proc. Fourth Lunar Science Conference, Wulf A. Gose, ed., Pergamon Press, 1973; *Geochimica et Cosmochimica Acta*, Supplement 4.

Proc. Fifth Lunar Science Conference, Wulf A. Gose, ed., Pergamon Press, 1974; *Geochimica et Cosmochimica Acta*, Supplement 5.

PRELIMINARY SCIENCE REPORTS

Apollo 11 Preliminary Science Report, NASA SP-214, U.S. Government Printing Office, 1969.

Apollo 12 Preliminary Science Report, NASA SP-235, U.S. Government Printing Office, 1970.

Apollo 14 Preliminary Science Report, NASA SP-272, U.S. Government Printing Office, 1971.

Apollo 15 Preliminary Science Report, NASA SP-289, U.S. Government Printing Office, 1972.

Apollo 16 Preliminary Science Report, NASA SP-315, U.S. Government Printing Office, 1972.

Apollo 17 Preliminary Science Report, NASA SP-330, U.S. Government Printing Office, 1974.

REPORTS IN SCIENCE

Lunar Sample Preliminary Examination Team, Preliminary Examination of Lunar Samples From Apollo 11. *Science*, Vol. 165, September 19, 1969, pp. 1211–1227.

Lunar Sample Preliminary Examination Team, Preliminary Examination of Lunar Samples From Apollo 12. *Science*, Vol. 167, March 6, 1970, pp. 1325–1339.

Lunar Sample Preliminary Examination Team, Preliminary Examination of Lunar Samples From Apollo 14. *Science*, Vol. 173, August 20, 1971, pp. 681–693.

Apollo 15 Preliminary Examination Team, The Apollo 15 Lunar Samples: A Preliminary Description. *Science*, Vol. 175, January 28, 1972, pp. 363–375.

Apollo 16 Preliminary Examination Team, The Apollo 16 Lunar Samples: Petrographic and Chemical Description. *Science*, Vol. 179, January 5, 1973, pp. 23–24.

Apollo 17 Preliminary Examination Team, Apollo 17 Lunar Samples: Chemical and Petrographic Description. *Science*, Vol. 182, November 16, 1973, pp. 659–672.

Apollo Field Geology Investigation Team, Geologic Exploration of Taurus-Littrow: Apollo 17 Landing Site. *Science*, Vol. 182, November 16, 1973, pp. 672–680.

SCHMITT, H. H., Apollo 17 Report on the Valley of Taurus-Littrow. *Science*, Vol. 182, November 16, 1973, pp. 681–690.

COMPILATIONS OF ABSTRACTS

54th Annual Meeting, April 16–20, 1972, abstracts and program in *EOS, Trans. Am. Geophys. Union*, Vol. 54, April 1973, pp. 218–520.

Fall Annual Meeting, December 10–13, 1973, abstracts and program in *EOS, Trans. Am. Geophys. Union*, Vol. 54, November 1973, pp. 1060–1236.

GSA Meeting, Dallas, Texas, 1973, Symposium on Geology and Geochemistry of the Moon, W. R. Muehlberger and Harrison H. Schmitt, presiding, abstracts published in *Geological Society of America*, Vol. 5, October 1973; summary of symposium published in *Geology*, Vol. 2, March 1974, pp. 136–137.

OTHER ARTICLES

HINNERS, N. W., The New Moon: A View. *Rev. Geophys. and Space Phys.*, Vol. 9, August 1971, pp. 447–522.

WASSERBURG, G. J., The Moon and Sixpence of Science. *Astronautics and Aeronautics*, Vol. 10, April 1972, pp. 16–21.

Luna 16 Issue, *Earth Planet. Sci. Letters*, Vol. 13, January 1972, pp. 223–446.

Luna 20 Issue, *Earth Planet. Sci. Letters*, Vol. 17, December 1972, pp. 3–63.

Luna 20 Issue, E. Anders and A. L. Albee, eds., *Geochimica et Cosmochimica Acta*, Vol. 37, April 1973, pp. 719–1109.

U.S. GEOLOGICAL SURVEY APOLLO GEOLOGY TEAM REPORTS

Apollo 11 geologic setting included in PET article, *Science*, Vol. 165, September 19, 1969, pp. 1221–1227.

Apollo 12 geologic setting included in PET article, *Science*, Vol. 167, March 6, 1970, pp. 1325–1339.

SWANN, G. A., N. J. TRASK, M. H. HAIR, AND R. L. SUTTON, Geologic Setting of the Apollo 14 Samples. *Science*, Vol. 173, August 20, 1971, pp. 716–719.

Apollo Lunar Geology Investigation Team, Geologic Setting of the Apollo 15 Samples. *Science*, Vol. 175, January 28, 1972, pp. 407–417.

Apollo Field Geology Investigation Team, Apollo 16 Exploration of Descartes: A Geologic Summary. *Science*, Vol. 179, January 5, 1973, pp. 62–69.

Apollo Field Geology Investigation Team, Geologic Exploration of Taurus-Littrow: Apollo 17 Landing Site. *Science*, Vol. 182, November 16, 1972, pp. 672–680.

APOLLO 11

U.S. Geological Survey, *Interagency Report: Astrogeology 20*. David Schleicher, ed., geologic transcript from Apollo 11 mission, December 1969.

APOLLO 12

U.S. Geological Survey, *Interagency Report: Astrogeology 21*. David Schleicher, ed., paraphrased geologic excerpts from Apollo 12 mission, June 1970.

Information of the USGS sample location and orientation for Apollo 11 and 12 is also in R. L. Sutton and G. C. Schaber, Lunar Locations and Orientations of Rock Samples from Apollo 11 and 12. *Proc. Second Lunar Science Conference*, Vol. 1, MIT Press, 1971, pp. 17–26.

APOLLO 14

U.S. Geological Survey, *Interagency Report: Astrogeology 25*. R. M. Batson, et al., preliminary log of 70mm pictures taken on the lunar surface during the Apollo 14 mission (magazines II, JJ, KK, LL, MM), March 1971.

U.S. Geological Survey, *Interagency Report: Astrogeology 28*. R. L. Sutton, et al., documentation of the Apollo 14 samples, May 1971 (supercedes Astrogeology 27).

U.S. Geological Survey, *Interagency Report: Astrogeology 29*. G. A. Swann, et al., preliminary geologic investigations of the Apollo 14 landing site, March 1971.

APOLLO 15

U.S. Geological Survey, *Interagency Report: Astrogeology 32*. Apollo Lunar Geology Investigation Team, preliminary report on the geology and field petrology at the Apollo 15 landing site, August 1971.

U.S. Geological Survey, *Interagency Report: Astrogeology 34*. R. L. Sutton, et al., preliminary documentation of the Apollo 15 samples, August 1971.

U.S. Geological Survey, *Interagency Report: Astrogeology 35*. R. M. Batson, et al., preliminary catalog of pictures taken on the lunar surface during the Apollo 15 mission, August 1971.

U.S. Geological Survey, *Interagency Report: Astrogeology 36*. G. A. Swann, et al., preliminary description of Apollo 15 sample environments, September 1971.

U.S. Geological Survey, *Interagency Report: Astrogeology 47*. R. L. Sutton, et al., documentation of Apollo 15 samples, April 1972.

APOLLO 16

U.S. Geological Survey, *Interagency Report: Astrogeology 48*. Apollo Lunar Geology Investigation Team, preliminary report on the geology and field petrology at the Apollo 16 landing site, April 1972.

U.S. Geological Survey, *Interagency Report: Astrogeology 49*. Apollo Lunar Geology Investigation

Team, progress report: Apollo 16 sample documentation, May 1972.

U.S. Geological Survey, *Interagency Report: Astrogeology 50.* R. M. Batson, et al., preliminary catalog of pictures taken on the lunar surface during the Apollo 16 mission, May 1972.

U.S. Geological Survey, *Interagency Report: Astrogeology 51.* Apollo Lunar Geology Investigation Team, documentation and environment of the Apollo 16 samples: a preliminary report, May 1972.

APOLLO 17

U.S. Geological Survey, *Interagency Report: Astrogeology 69.* Apollo Lunar Geology Investigation Team, preliminary report on the geology and field petrology at the Apollo 17 landing site, December 1972.

U.S. Geological Survey, *Interagency Report: Astrogeology 70.* K. B. Larson, et. al., preliminary catalog of pictures taken on the lunar surface during the Apollo 17 mission, January 1972.

U.S. Geological Survey, *Interagency Report: Astrogeology 71.* Apollo Lunar Geology Investigation Team, documentation and environment of the Apollo 17 samples: a preliminary report, January 1973.

U.S. Geological Survey, *Interagency Report: Astrogeology 72.* Apollo Lunar Geology Investigation Team, preliminary geologic analysis of the Apollo 17 site, March 1973.

Petrogenesis of Lunar Rocks: Rb-Sr Constraints and Lack of H_2O [1]

Arden L. Albee and Alexander J. Gancarz
Division of Geological and Planetary Sciences
California Institute of Technology
Pasadena, California

Rb and Sr isotopic data and other chemical data indicate major lunar differentiation at about 4.6 AE (AE = 10^9 years) and very limited subsequent differentiation. The constraints of limited differentiation after 4.6 AE and the apparent lack of H_2O on the Moon, when applied to the derivation and petrogenesis of lunar samples, suggest the following: (1) soil samples, breccias, metaclastic rocks, and feldspathic basalts represent mixtures of repeatedly modified clastic material, which was ultimately derived from materials formed during the ~ 4.6 AE differentiation; and (2) mare basalts crystallized from melts which formed by partial melting, and which developed without equilibration between the melt and crystalline residuum.

Rb-Sr mineral isochrons currently provide the basic chronology of lunar evolution (refs. 1–14). Rb/Sr data also impose rigorous constraints on lunar petrogenetic models. This paper will discuss these constraints, emphasize the important role of large-scale differentiation which occurred at about 4.6 AE, and show that only limited chemical fractionation occurred during the subsequent evolution of most lunar rocks. Regardless of other types of evidence, no petrogenetic theory for the origin of lunar rocks can invoke extensive fractionation later than about 4.6 AE as a dominant part of the theory. The lack of H_2O on the Moon may be the critical physical-chemical factor limiting subsequent fractionation in many processes.

Rb-Sr Systematics and Fractionation Factors

Measurements of the isotopic abundance of Rb and Sr in the various mineral phases of a rock provide information not only on the time of crystallization and equilibration (T_x), but also on the fractionation history of the rock prior to this most recent crystallization and equilibration. As illustrated in figure 1, cogenetic systems, either consanguineous total rocks or the various minerals in a single rock, attain identical values of $^{87}Sr/^{86}Sr$, but during equilibration at T_x, different values of $^{87}Rb/^{86}Sr$. On the Rb-Sr evolution diagram these different compositions subsequently evolve along straight line trajectories with a slope of -1. If the systems were closed to gain or loss of Rb and Sr since T_x, then the cognetic systems measured at any time form a linear array on the Rb–Sr evolution diagram. An array based on minerals from a single rock is a mineral or internal isochron, and one based on cogenetic rocks is a total-rock isochron. The isochron has a slope indicative of the time since equilibration (slope = $\exp(\lambda T_x - 1)$) and an $^{87}Sr/^{86}Sr$ intercept, $(^{87}Sr/^{86}Sr)_I$, equal to the Sr isotopic composition at time T_x (ref. 15).

The deviation of $(^{87}Sr/^{86}Sr)_I$ from that assumed to have existed at some time prior to T_x, coupled with the $^{87}Rb/^{86}Sr$, provides

[1] Contribution number 2474.

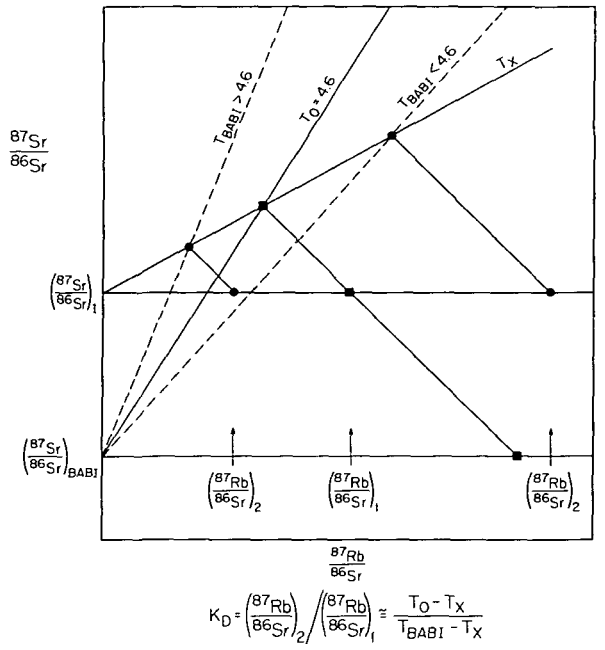


Figure 1.—*Rb-Sr evolution diagram. Material formed at T_o with $(^{87}Sr/^{86}Sr)$ equal to $(^{87}Sr/^{86}Sr)_{BABI}$ is represented by a square. Fractionation at time T_x results in a portion enriched and a portion depleted in Rb relative to Sr (circles) and an unfractionated portion (square), all of which lie along the T_x isochron. The unfractionated portion yields a model age, T_{BABI}, equal to T_o, whereas fractionated portions yield model ages different from T_o.*

an integrated measure of the Rb/Sr fractionation history of the rock. This fractionation history can be parameterized by a two-stage model as illustrated in figure 1. The model assumes that a source material originated at reference time $T_o = 4.6$ AE with the "BABI" value of $^{87}Sr/^{86}Sr$ ($(^{87}Sr/^{86}Sr)_{BABI} = 0.69898$) (ref 16). Fractionation at time T_x resulted in three fractions, one enriched in Rb relative to Sr, one unfractionated, and one depleted in Rb relative to Sr. Mineral isochrons on all three rocks would yield identical ages (T_x) and the same $(^{87}Sr/^{86}Sr)_1$. However, they would have different model ages, T_{BABI}, which is the time required for the $^{87}Sr/^{86}Sr$ of the total rock with its measured $^{87}Rb/^{86}Sr$ to evolve from $(^{87}Sr/^{86}Sr)_{BABI}$. The unfractionated rock will have $T_{BABI} = 4.6$ AE, the enriched rock will have $T_{BABI} < 4.6$ AE, and the depleted rock will have $T_{BABI} > 4.6$ AE. Thus, any deviation of T_{BABI} from 4.6 AE indicates a fractionation history prior to T_x.

The fractionation factor for this two-stage model is (ref. 10)

$$K_D \equiv \frac{(^{87}Rb/^{86}Sr)_2}{(^{87}Rb/^{86}Sr)_1} \cong \frac{T_o - T_x}{T_{BABI} - T_x}$$

This approximation is quite accurate since the decay constant for Rb is small. During the time interval from T_o to T_x numerous episodes of fractionation could have affected the rock as opposed to the simple two-stage model illustrated. However, $(^{87}Rb/^{86}Sr)_1$ is still the integrated $^{87}Rb/^{86}Sr$ in the interval from T_o to T_x.

As noted previously $T_o = 4.6$ AE and $(^{87}Sr/^{86}Sr)_{T_o} = 0.69898$ are reference values, and the subsequent conclusions drawn in this paper are basically independent of their precise value. In fact, the time of major differentiation is probably not 4.6 AE, but may be as low as 4.5 AE or even 4.4 AE (ref. 13).

Lunar Rock Groups

On the basis of petrologic characteristics seven different groups of lunar rocks are recognized. Each of these groups has a distinctive Rb-Sr isotopic pattern. The Rb-Sr data are summarized in figure 2, which shows T_x, T_{BABI}, and K_D for representative members of each group. Most of the type examples shown are those on which we have made detailed petrographic and electron probe studies in conjunction with the Rb-Sr isotopic studies of Papanastassiou and Wasserburg. Figure 2 indicates that six of these groups are characterized by T_{BABI} close to 4.6 and $K_D < 2$. The seven groups are as follows:

1. Soils with $T_{BABI} = 4.6 \pm 0.3$ AE

Clots from the soil samples and friable soil-breccia samples, as well as bulk soil samples, have model ages of about 4.6 AE. This group includes samples from all landing sites and has a wide range of Rb/Sr (ref. 10). To a large extent many of these model ages

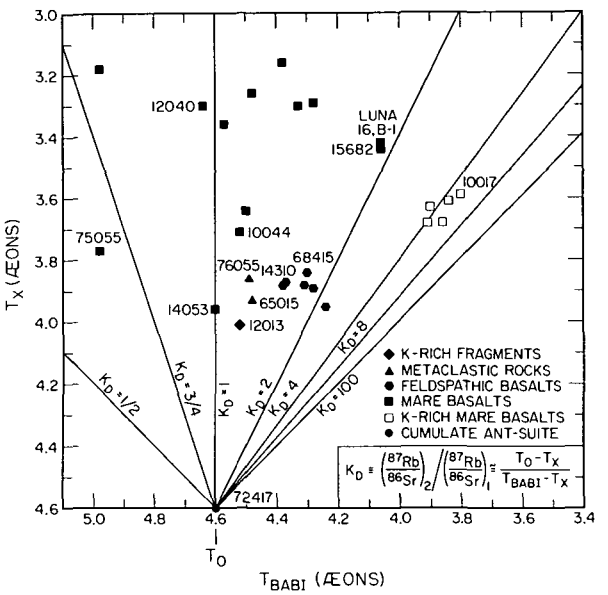


Figure 2.—T_{BABI} *versus* T_x. *Despite the variety of rock types represented, nearly all samples indicate less than a factor of 2 fractionation of Rb relative to Sr subsequent to* T_o = *4.6 AE. Only the K-rich mare basalts indicate a greater degree of fractionation.*

are dominated by a small fraction of very high Rb/Sr material with a model age of about 4.6 AE (ref. 10).

2. K-rich fragments with T_{BABI} = 4.3 to 4.6 AE

These fragments, the so-called "KREEP" rocks (ref. 17), include glass-rich agglutinates and metaclastic rocks, and have been found in the soils at all landing sites. Most are small fragments such as Lunar Rock 1 (ref. 18), and no internal isochrons have been measured on them. Nyquist et al. (ref. 19), however, showed that by grouping such fragments by chemical composition and location, Rb and Sr data yield linear arrays, which, if interpreted as total-rock isochrons, indicate ages ranging from 4.1 to 4.4 AE. Sample 12013 is the only large sample which we would place in this group. It is a heterogeneous metaclastic rock with K, Th, and U concentration a factor of 40 greater than typical mare basalts and a factor of 10 greater than Apollo 11 K-rich basalts (ref. 20). Fragments of 12013 have a model age of 4.52 AE and a recrystallization age (T_x) of 4.01 AE (ref. 2).

3. Metaclastic rocks with $T_x \approx$ 3.95 AE and $T_{BABI} \approx$ 4.5 AE

This group includes a large proportion of the Lunar Highlands samples and also constitutes a large proportion of the lithic fragments in soil samples from all landing sites. These clastic rocks, composed predominantly of plagioclase, have been extensively recrystallized by metamorphic and/or partial melting processes (ref. 21). Typical examples are 65015 and 76055, both of which display isotopic and petrologic evidence for extensive, but not complete, equilibration at 3.95 AE (refs. 10, 13, 21, and 22). Step-wise heating ^{40}Ar-^{39}Ar studies on 65015 suggest that the cores of the larger plagioclase clasts have an age greater than 4.46 AE (ref. 22). This is also suggested by Rb-Sr isotopic data (ref. 10).

4. Feldspathic basalts with $T_x \approx$ 3.85 AE and $T_{BABI} \approx$ 4.3 AE

This group includes a number of samples of intersertal, plagioclase-rich basalts from the Apollo 14 and 16 landing sites (e.g., 14310, 14276, and 68415). In addition to the high plagioclase content (60 to 80 percent) they are characterized by high K, rare earth element, P, Ba, U, and Th contents (ref. 23), and a high content of siderophile elements (ref. 24). Even in these rocks, which almost certainly crystallized from a melt, plagioclase grains are present which, on the basis of electron probe data, have not completely equilibrated with the melt (ref. 23). ^{40}Ar-^{39}Ar studies also indicate older relict plagioclase and provide evidence for an older event (refs. 25 and 26).

5. Mare basalts with T_x = 3.16 to 3.95 AE and T_{BABI} = 4.1 to 5.0 AE

This group includes all of the mare basalts with the exception of those in Group 6. Samples from each landing site have similar T_x and T_{BABI}, but $(^{87}Sr/^{86}Sr)_I$ values and trace element concentrations differ for samples from an individual landing site (refs. 6, 11, 12, 13, and 27). This suggests derivation of individual samples (and flows) from different sources (ref. 27) or differing degrees

of assimilation of country rock (ref. 6). Typical well-characterized samples from the various landing sites include:

10044 (refs. 1, 28, and 29)
12040 (refs. 6, 30, and 31)
14053 (refs. 7, 32, and 33)
15682 (refs. 11 and 34)
75055 (refs. 13, 21, and 26)
Luna 16, B–1 (refs. 8, 35, and 36).

6. Mare basalts with $T_x = 3.65$ AE and $T_{BABI} = 3.85$ AE

Although grossly similar to the Apollo 11 low-K basalts included in Group 5, these samples from the Apollo 11 landing site are higher in K and other incompatible elements, and have much younger model ages. A typical well-characterized example is 10017 (refs. 1, 29, and 37).

7. "ANT" rocks with $T_{BABI} = 4.6$ AE

"The "ANT" rock suite includes the coarse-grained rocks of the anorthosite-norite-troctolite-dunite suite. In general they display magmatic cumulate textures, but are extensively modified by shock processes. Dunite sample 72417 has both an isochron age and a model age of about 4.6 AE (ref. 3). No mineral isochron ages have been measured on anorthosite samples such as 15415 (refs. 38 and 39), or on troctolite samples such as 76535 (ref. 40). However, low $^{87}Sr/^{86}Sr$ ratios indicate that these rocks cannot have equilibrated and resided in a higher Rb/Sr environment for any extended length of time (ref. 14; and Papanastassiou, personal communication).

Nature of Major Differentiation at ~4.6 AE

Many types of chemical, isotopic, and physical evidence are consistent with the hypothesis of primitive, large-scale, crustal differentiation (refs. 1, 41, 42, and 43). The presence of a "magic component" (ref. 5), with T_{BABI} of 4.6 AE and a high $^{87}Rb/^{86}Sr$ which dominates the model age of many lunar soil samples, indicates that this differentiation occurred at about 4.6 AE and produced rocks with very high Rb/Sr ratios. The existence of high Rb/Sr material with relatively old model ages was confirmed by the discovery of the K-rich rock 12013 (ref. 2) and other fragments (refs. 17 and 18). The existence of material complementary to the Rb/Sr-rich material is indicated by dunite sample 72417, which has crystallization and model ages of 4.6 AE (ref. 3).

Rb-Sr data also indicate that only limited fractionation occurred, subsequent to the primitive differentiation, and furthermore suggest that most of the observed chemical characteristics were produced during the primitive differentiation. That most of the chemical differences observed in the lunar rocks are consistent with primitive differentiation at ~ 4.6 AE, rather than subsequent fractionation processes, is illustrated in figure 3. Sm/Eu, a parameter sensitive to frac-

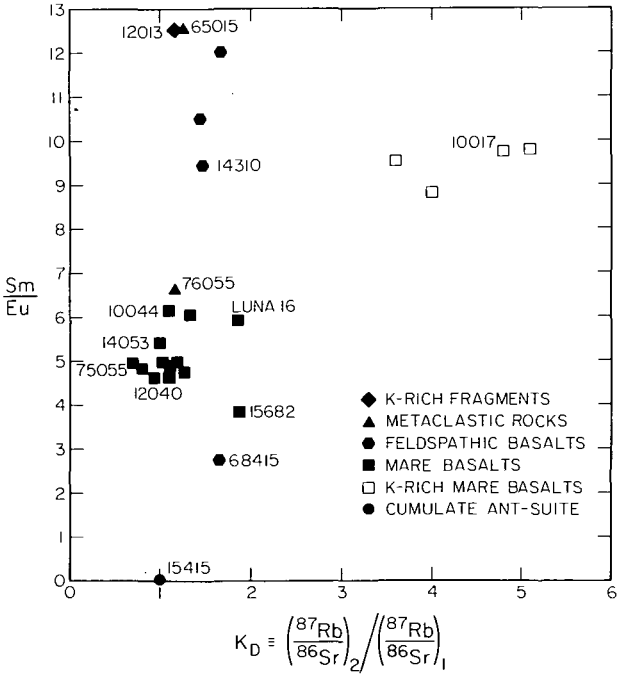


Figure 3.—*Sm/Eu versus* K_D. *The large range of Sm/Eu, indicative of extensive fractionation, is not commensurate with the fractionation of Rb relative to Sr as indicated by the small range of* K_D. *This indicates that the fractionation of Sm and Eu occurred prior to* T_x; *and, from additional data, most likely occurred during the large-scale lunar differentiation at ~4.6 AE. Data on Sm and Eu are from the following: refs. 17 and 44–58.*

tionation, varies by a factor of ~ 200, whereas K_D, a measure of fractionation after the differentiation at ~ 4.6 AE, varies only by a factor of about 2. The strong fractionation indicated by Sm/Eu must have occurred prior to the time of crystallization. Although neither K_D nor Sm/Eu is particularly sensitive to olivine or Ca-poor pyroxene fractionation, both are extremely sensitive to fractionation of plagioclase or of late-stage K-rich material. The large range of Rb/Sr observed between samples, approximately a factor of 1000, is comparable to the range of Sm/Eu. Hence, we conclude that the Sm/Eu differences must have been a characteristic of the source from which the rocks were derived and that most chemical differences in lunar rocks are a result of primitive differentation at about 4.6 AE.

Regardless of physical details, this primitive differentiation process resulted in a fraction rich in K (Rb, Ba, U, Th, trivalent rare earth elements), a Ca-Al-Si-rich fraction (anorthosite and anorthositic gabbro), and a Mg-Fe-rich fraction (dunite, troctolite, and norite). Samples of the Ca-Al-Si-rich fraction and the Mg-Fe-rich fraction have survived subsequent excavation by meteorite impact, but exhibit a wide range of modification. Less modified samples suggest that these fractions cooled slowly enough to produce rocks with coarse-grained, homogeneous phases. The original nature of the K-rich fraction is not clear as no samples have been recognized which have not been extensively modified.

Possible Petrogenetic Processes Involving Limited Fractionation

The Rb-Sr constraint on the amount of fractionation, as well as constraints imposed by many other kinds of data, are satisfied if we hypothesize that soils, glass-agglutinate fragments, friable breccias, and progenitors of metaclastic rocks and feldspathic basalts (Groups 1–4) are all basically mixtures of clastic material, which have been subsequently modified by a variety of processes, including fragmentation, metamorphism, partial melting, and complete melting. Rb and Sr would not be fractionated if the formation of the clastic mixture involved only fragmentation of preexistent rocks from one or many sources, even if fragmentation occurred repeatedly over a long period of time. Consequently, if the source regions of a clastic mixture are primary, unmodified materials formed during the primitive differentiation at ~ 4.6 AE, or if they themselves are clastic mixtures repeatedly modified either by continued fragmentation and mixing, or by processes characterized below, then Rb and Sr will remain unfractionated and the model age of the mixture will still reflect the time of primitive differentiation.

Preservation of the old model age of such a mixture would be accomplished during subsequent modification by processes with the following characteristics, even if repeated many times:

1. Volatile loss of Rb was in general not significant.
2. Metamorphism, in the absence of H_2O, was strictly controlled by solid-state and grain-surface diffusion and resulted in lithification by sintering at grain boundaries with only short-range migration and limited segregation of elements.
3. Partial melting in the metaclastic rocks of Group 3, and in the K-rich fragments of Group 2, was characterized by extensive reaction between an intersitial melt and larger clastic grains. Lack of Rb-Sr fractionation dictates very limited mobility of the melt and only short-range migration of elements within the melt. These characteristics can be partially attributed to the absence of H_2O and to the fine-scale homogeneity of the fragmental mixture. Local segregation of Rb-rich material and partial Sr equilibration are suggested by the Rb/Sr data of Nyquist et al. (ref. 19) on small chemically defined groups of samples from single sites. The Rb/Sr data on these sam-

ples have been interpreted as total-rock isochrons representing distinct events at times ranging from 4.1 AE to 4.4 AE. These may alternatively be interpreted as the result of local segregation of K-rich, Rb-rich material without total Sr equilibration at 3.95 AE.

4. Impact-produced melts, which formed by nearly *total* melting of soil, breccia, or metaclastic rocks, crystallized as the feldspathic basalts of Group 4. Such an origin would preserve the old model age of the source and would satisfy several other geochemical constraints on these rocks, such as the high content of siderophile elements. However, the Rb-Sr constraint could also be satisfied if these rocks formed by partial melting of plagioclase-rich source rocks with the additional restrictions described below for mare basalts.

The Rb-Sr constraint limiting fractionation is satisfied if the ultimate source of the clastic mixture formed during the large-scale differentiation at ~ 4.6 AE. If the modification process or processes retain the characteristics described above, or if modification is a simple fragmentation process, then fractionation does not basically occur and old model ages are preserved. This is true regardless of either the order or the number of times this clastic mixture is modified.

Mare basalts with near 4.6 AE model ages (Group 5) must also have been derived without substantial fractionation of Rb and Sr, either during formation of the parent magma or during the ascent and crystallization. All other chemical parameters suggestive of a greater degree of fractionation must be a characteristic of the source region. The origin of the mare basalts is further restricted by the $(^{87}Sr/^{86}Sr)_I$ values, which suggest that rocks of the same age were derived from a number of different sources. A magma meeting these requirements could be produced by several mechanisms (ref. 23):

1. *Total* melting of a source rock which has an Rb-Sr model age of 4.6 AE and also meets all other chemical and isotopic constraints would form a rock satisfying the Rb-Sr constraints. Although total melting is generally regarded as an unlikely terrestrial event, it is possible that, in the absence of H_2O and tectonic activity, instability and separation of a melt from a source region would be delayed until complete melting occurs. *Total* melting could also occur as a result of impact processes.
2. Uniform contamination of relatively low Rb/Sr melts by assimilation of Rb-rich crustal material with a model age of 4.6 AE is the mechanism invoked by Papanastassiou and Wasserburg (ref. 6).
3. Our preferred hypothesis is that, in the absence of H_2O, partial melting occurs by incremental melting of integral volumes of solid phases with little or no equilibration between melt and crystalline residuum. Thus, the low-temperature phases rich in Rb and ^{87}Sr would melt totally and grains of higher temperature phases would melt peripherally, but the solid residuum would not equilibrate with the melt. As pointed out by Graham and Ringwood (ref. 59), the resulting melt would have the same model age as the source region. Any crystallization and separation of Ca-rich pyroxene and/or plagioclase during the ascent of the melt to the surface would result in Rb-Sr fractionation. However, silicate melt curves typically have a positive slope $(\Delta P/\Delta T > O)$ in the absence of H_2O, and under these circumstances the melt may become superheated as it moves upward, effectively preventing crystallization and consequent Rb-Sr fractionation. Production of a superheated magma is also an important consideration in the contamination hypothesis, since it would facilitate assimilation and homogenization.

The Apollo 11 K-rich mare basalts (Group 6) could also form by this process, but the younger model ages require a greater degree

of equilibration between the melt and residuum or of some fractional crystallization before extrusion onto the surface.

Conclusion

An intriguing feature of these explanations for deriving lunar rocks without fractionation of Rb and Sr is the linking of this special characteristic to another characteristic lunar feature—the apparent lack of indigenous H_2O. The hypotheses outlined here differ from other models of lunar petrogenesis in that many rock types would be derived by near-surface modification of rocks formed during primitive crustal differentiation. This can be accomplished with energy derived partially from impacting bodies rather than totally from internal heat sources.

Acknowledgment

Most of the Rb-Sr patterns summarized here are based on mineral isochron data from G. J. Wasserburg and D. A. Papanastassiou. Furthermore, many of the arguments incorporated into these hypotheses have been expressed in their published papers and expressed even more vociferously in numerous discussions during the course of our cooperative work since July 1969. Unpublished Sm and Eu data were provided by N. J. Hubbard and by J. A. Philpotts. This paper has been supported by NASA grants NGL–05–002–188 and NGL–05–002–338.

References

1. ALBEE, A. L., D. S. BURNETT, A. A. CHODOS, O. J. EUGSTER, J. C. HUNEKE, D. A. PAPANASTASSIOU, F. A. PODOSEK, G. P. RUSS, III, H. G. SANZ, F. TERA, AND G. J. WASSERBURG, Ages, Irradiation History, and Chemical Composition of Lunar Rocks From the Sea of Tranquility. *Science*, Vol. 167, 1970, pp. 463–466.
2. ALBEE, A. L., D. S. BURNETT, A. A. CHODOS, E. L. HAINES, J. C. HUNEKE, D. A. PAPANASTASSIOU, F. A. PODOSEK, G. P. RUSS, III, AND G. J. WASSERBURG, Mineralogic and Isotopic Investigations on Lunar Rock 12013. *Earth Planet. Sci. Letters*, Vol. 9, 1970, pp. 137–163.
3. ALBEE, A. L., A. A. CHODOS, R. F. DYMEK, A. J. GANCARZ, D. S. GOLDMAN, D. A. PAPANASTASSIOU, AND G. J. WASSERBURG, Dunite From the Lunar Highlands: Petrography, Deformation History, Rb-Sr Age. *Lunar Science*, Vol. V, Lunar Science Institute, Houston, 1974, pp. 3–5.
4. PAPANASTASSIOU, D. A., G. J. WASSERBURG, AND D. S. BURNETT, Rb-Sr Ages of Lunar Rocks From the Sea of Tranquillity. *Earth Planet. Sci. Letters*, Vol. 8, 1970, pp. 1–19.
5. PAPANASTASSIOU, D. A., AND G. J. WASSERBURG, Rb-Sr Ages From the Ocean of Storms. *Earth Planet. Sci. Letters*. Vol. 8, 1970, pp. 269–278.
6. PAPANASTASSIOU, D. A., AND G. J. WASSERBURG, Lunar Chronology and Evolution From Rb-Sr Studies of Apollo 11 and 12 Samples. *Earth Planet. Sci. Letters*, Vol. 11, 1971, pp. 37–62.
7. PAPANASTASSIOU, D. A., AND G. J. WASSERBURG, Rb-Sr Ages of Igneous Rocks From the Apollo 14 Mission and the Age of the Fra Mauro Formation. *Earth Planet. Sci. Letters*, Vol. 12, 1971, pp. 36–48.
8. PAPANASTASSIOU, D. A., AND G. J. WASSERBURG, Rb-Sr Age of a Luna 16 Basalt and the Model Age of Lunar Soils. *Earth Planet. Sci. Letters*, Vol. 13, 1972, pp. 368–374.
9. PAPANASTASSIOU, D. A., AND G. J. WASSERBURG, The Rb-Sr Age of a Crystalline Rock From Apollo 16. *Earth Planet. Sci. Letters*, Vol. 16, 1972, pp. 289–298.
10. PAPANASTASSIOU, D. A., AND G. J. WASSERBURG, Rb-Sr Systematics of Luna 20 and Apollo 16 Samples. *Earth Planet. Sci. Letters*, Vol. 17, pp. 52–63.
11. PAPANASTASSIOU, D. A., AND G. J. WASSERBURG, Rb-Sr Ages and Initial Strontium in Basalts From Apollo 15. *Earth Planet. Sci. Letters*, Vol. 17, 1973, pp. 324–337.
12. TERA, F., D. A. PAPANASTASSIOU, AND G. J. WASSERBURG, The Lunar Time Scale and a Summary of Isotopic Evidence for a Terminal Lunar Cataclysm. *Lunar Science*, Vol. V, Lunar Science Institute, Houston, 1974, pp. 792–794.
13. TERA, F., D. A. PAPANASTASSIOU, AND G. J. WASSERBURG, Isotopic Evidence for a Terminal Lunar Cataclysm. *Earth Planet. Sci. Letters*, Vol. 22, 1974, pp. 1–21.
14. WASSERBURG, G. J., AND D. A. PAPANASTASSIOU, Age of an Apollo 15 Mare Basalt; Lunar Crust and Mantle Evolution. *Earth Planet. Sci. Letters*, Vol. 13, 1971, pp. 97–104.
15. LANPHERE, M. A., G. J. F. WASSERBURG, A. L. ALBEE, AND G. R. TILTON, Redistribution of Strontium and Rubidium Isotopes During

Metamorphism, World Beater Complex, Panamint Range, California. In *Isotopic and Cosmic Chemistry*, H. Craig, S. L. Miller, and G. J. Wasserburg, eds., North-Holland, Amsterdam, 1964.

16. PAPANASTASSIOU, D. A., AND G. J. WASSERBURG, Initial Strontium Isotopic Abundances and the Resolution of Small Time Differences in the Formation of Planetary Objects. *Earth Planet. Sci. Letters*, Vol. 5, 1969, pp. 361–376.
17. HUBBARD, N. J., C. MEYER, JR., P. W. GAST, AND H. WIESMANN, The Composition and Derivation of Apollo 12 Soils. *Earth Planet. Sci. Letters*, Vol. 10, 1971, pp. 341–350.
18. ALBEE, A. L., AND A. A. CHODOS, Microprobe Investigations on Apollo 11 Samples. *Proc. Apollo 11 Lunar Science Conference, Geochimica et Cosmochimica Acta*, Supplement 1, Vol. 1, 1970, pp. 135–157.
19. NYQUIST, L. E., N. J. HUBBARD, P. W. GAST, B. M. BANSAL, H. WEISMANN, AND B. JAHN, Rb-Sr Systematics for Chemically Defined Apollo 15 and 16 Materials. *Proc. Fourth Lunar Science Conference, Geochimica et Cosmochimica Acta*, Supplement 4, Vol. 2, 1973, pp. 1823–1846.
20. ANDERSON, D. H., The Preliminary Examination and Preparation of Lunar Sample 12013. *Earth Planet. Sci. Letters*, Vol. 9, 1970, pp. 94–102.
21. ALBEE, A. L., A. J. GANCARZ, AND A. A. CHODOS, Metamorphism of Apollo 16 and 17 and Luna 20 Metaclastic Rocks at About 3.95 AE: Samples 61156, 64423,14–2, 65015, 67483,15–2, 76055, 22006, and 22007. *Proc. Fourth Lunar Science Conference, Geochimica et Cosmochimica Acta*, Supplement 4, Vol. 1, 1973, pp. 569–595.
22. JESSBERGER, E. K., J. C. HUNEKE, AND G. J. WASSERBURG, Evidence for a ~ 4.5 Aeon Age of Plagioclase Clasts in a Lunar Highland Breccia. *Nature*, Vol. 248, 1974, pp. 199–202.
23. GANCARZ, A. J., A. L. ALBEE, AND A. A. CHODOS, Comparative Petrology of Apollo 16 Sample 68415 and Apollo 14 Samples 14276 and 14310. *Earth Plant. Sci. Letters*, Vol. 16, 1972, pp. 307–330.
24. MORGAN, J. W., J. C. LAUL, U. KRÄHENBÜHL, R. GANAPATHY, AND E. ANDERS, Major Impacts on the Moon: Characterization From Trace Elements in Apollo 12 and 14 Samples. *Proc. Third Lunar Science Conference, Geochimica et Cosmochimica Acta*, Supplement 3, Vol. 2, 1972, pp. 1377–1395.
25. HUNEKE, J. C., F. A. PODOSEK, AND G. J. WASSERBURG, An Argon Bouillabaisse Including Ages From the Luna 20 Site. *Lunar Science*, Vol. IV, Lunar Science Institute, Houston, 1972, pp. 403–405.
26. HUNEKE, J. C., E. K. JESSBERGER, F. A. PODOSEK, AND G. J. WASSERBURG, $^{40}Ar/^{39}Ar$ Measurements in Apollo 16 and 17 Samples and the Chronology of Metamorphic and Volcanic Activity in the Taurus-Littrow Region. *Proc. Fourth Lunar Science Conference, Geochimica et Cosmochimica Acta*, Supplement 4, Vol. 2, 1973, pp. 1725–1756.
27. SCHMITT, R. A., AND J. C. LAUL, A survey of the Selenochemistry of Major, Minor and Trace Elements. *The Moon*, Vol. 8, 1973, pp. 182–209.
28. AGRELL, S. O., J. H. SCOON, I. D. MUIR, J. V. P. LONG, J. D. C. MCCONNELL, AND A. PECKETT, Observations on the Chemistry, Mineralogy, and Petrology of Some Apollo 11 Lunar Samples. *Proc. Apollo 11 Lunar Science Conference, Geochimica et Cosmochimica Acta*, Supplement 1, Vol. 1, 1970, pp. 93–128.
29. TURNER, G., Argon-40/Argon-39 Dating of Lunar Rock Samples. *Proc. Apollo 11 Lunar Science Conference, Geochimica et Cosmochimica Acta*, Supplement 1, Vol. 2, 1970, pp. 1665–1684.
30. FRENCH, B. M., L. S. WALTER, K. F. J. HEINRICH, P. D. LOMAN, JR., A. S. DOAN, JR., AND I. ADLER, *Compositions of Major and Minor Minerals in Five Apollo 12 Crystalline Rocks.* National Aeronautics and Space Administration, SP–306, 1972.
31. REID, M. J., A. J. GANCARZ, AND A. L. ALBEE, Constrained Least-Squares Analysis of Petrologic Problems With an Application to Lunar Sample 12040. *Earth Planet. Sci. Letters*, Vol. 17, 1973, pp. 433–445.
32. GANCARZ, A. J., A. L. ALBEE, AND A. A. CHODOS, Petrologic and Mineralogic Investigation of Some Crystalline Rocks Returned by the Apollo 14 Mission. *Earth Planet. Sci. Letters*, Vol. 12, 1971, pp. 1–18.
33. TURNER, G., J. C. HUNEKE, F. A. PODOSEK, AND G. J. WASSERBURG, ^{40}Ar-^{39}Ar Ages and Cosmic Ray Exposure Ages of Apollo 14 Samples. *Earth Planet. Sci. Letters*, Vol. 12, 1971, pp. 19–35.
34. DOWTY, E., M. PRINZ, AND K. KEIL, Composition, Mineralogy, and Petrology of 28 Mare Basalts From Apollo 15 Rake Samples, *Proc. Fourth Lunar Science Conference, Geochimica et Cosmochimica Acta*, Supplement 4, Vol. 1, 1973, pp. 423–444.
35. ALBEE, A. L., A. A. CHODOS, A. J. GANCARZ, E. L. HAINES, D. A. PAPANASTASSIOU, L. RAY, F. TERA, G. J. WASSERBURG, AND T. WEN, Mineralogy, Petrology, and Chemistry of a Luna 16 Basaltic Fragment, Sample B–1. *Earth Planet. Sci. Letters*, Vol. 13, 1972, pp. 353–367.
36. HUNEKE, J. C., F. A. PODOSEK, AND G. J. WASSERBURG, Gas Retention and Cosmic-Ray Exposure Ages of a Basalt Fragment From

Mare Fecunditatis. *Earth Planet. Sci. Letters*, Vol. 13, 1972, pp. 375–383.

37. ADLER, I., L. S. WALTER, P. D. LOWMAN, B. P. GLASS, B. M., FRENCH, J. A. PHILPOTTS, K. J. F. HEINRICH, AND J. I. GOLDSTEIN, Electron Microprobe Analysis of Apollo 11 Lunar Samples. *Proc. Apollo 11 Lunar Science Conference, Geochimica et Cosmochimica Acta*, Supplement 1, Vol. 1, 1970, pp. 87–92.
38. JAMES, O. B., Lunar Anorthosite 15415: Texture, Mineralogy, and Metamorphic History. *Science*, Vol. 175, 1972, pp. 434–438.
39. TURNER, G., ^{40}Ar-^{39}Ar Age and Cosmic Ray Irradiation History of the Apollo 15 Anorthosite, 15415. *Earth Planet. Sci. Letters*, Vol. 14, 1972, pp. 169–175.
40. GOOLEY, R., R. BRETT, J. WARNER, AND J. R. SMYTH, Sample 76535, A Deep Lunar Crustal Rock. *Geochimica et Cosmochimica Acta*, in press, 1974.
41. RINGWOOD, A. E., AND E. ESSENE, Petrogenesis of Apollo 11 Basalts, Internal Constitution and Origin of the Moon. *Proc. Apollo 11 Lunar Science Conference, Geochimica et Cosmochimica Acta*, Supplement 1, Vol. 1, 1970, pp. 769–799.
42. SMITH, J. V., A. T. ANDERSON, R. C. NEWTON, E. J. OLSEN, AND P. J. WYLLIE, A Petrologic Model for the Moon Based on Petrogenesis, Experimental Petrology, and Physical Properties. *J. Geology*, Vol. 78, 1970, pp. 381–405.
43. WOOD, J. A., J. S. DICKY, JR., U. B. MARVIN, AND B. N. POWELL, Lunar Anorthosites and a Geophysical Model of the Moon. *Proc. Apollo 11 Lunar Science Conference, Geochimica et Cosmochimica Acta*, Supplement 1, Vol. 1, 1970, pp. 965–988.
44. BRUNFELT, A. O., K. S. HEIER, B. NILSSEN, B. SUNDVOLL, AND E. STEINNES, Distribution of Elements Between Different Phases of Apollo 14 Rocks and Soils. *Proc. Third Lunar Science Conference, Geochimica et Cosmochimica Acta*, Supplement 3, Vol. 2, 1972, pp. 1133–1147.
45. GAST, P. W., N. J. HUBBARD, AND H. WIESMANN, Chemical Composition and Petrogenesis of Basalts From Tranquillity Base. *Proc. Apollo 11 Lunar Science Conference, Geochimica et Cosmochimica Acta*, Supplement 1, Vol. 2, 1970, pp. 1143–1163.
46. GOLES, G. G., K. RANDLE, M. OSAWA, D. J. LINDSTROM, D. Y. JEROME, T. L. STEINBORN, R. L. BEYER, M. R. MARTIN, AND S. M. MCKAY, Interpretations and Speculations on Elemental Abundances in Lunar Samples. *Proc. Apollo 11 Lunar Science Conference, Geochimica et Cosmochimica Acta*, Supplement 1, Vol. 2, 1970, pp. 1177–1194.
47. GOLES, G. G., A. R. DUNCAN, D. J. LINDSTROM, M. R. MARTIN, R. L. BEYER, M. OSAWA, K. RANDLE, L. T. MEEK, T. L. STEINBORN, AND S. M. MCKAY, Analyses of Apollo 12 Specimens: Compositional Variations, Differentiation Processes, and Lunar Soil Mixing Models. *Proc. Second Lunar Science Conference, Geochimica et Cosmochimica Acta*, Supplement 2, Vol. 2, 1971, pp. 1063–1081.
48. HASKIN, L. A., R. O. ALLEN, P. A. HELMKE, T. P. PASTER, M. R. ANDERSON, R. L. KOROTEV, AND K. A. ZWEIFEL, Rare Earths and Other Trace Elements in Apollo 11 Lunar Samples. *Proc. Apollo 11 Lunar Science Conference, Geochimica et Cosmochimica Acta*, Supplement 1, Vol. 2, 1970, pp. 1213–1231.
49. HASKIN, L. A., P. A. HELMKE, D. P. BLANCHARD, J. W. JACOBS, AND K. TELANDER, Major and Trace Element Abundances in Samples From the Lunar Highlands. *Proc. Fourth Lunar Science Conference, Geochimica et Cosmochimica Acta*, Supplement 4, Vol. 2, 1973, pp. 1275–1296.
50. HUBBARD, N. J., AND P. W. GAST, Chemical Composition and Origin of Nonmare Lunar Basalts. *Proc. Second Lunar Science Conference, Geochimica et Cosmochimica Acta*, Supplement 2, Vol. 2, 1971, pp. 999–1020.
51. HUBBARD, N. J., P. W. GAST, AND C. MEYER, JR., Chemical Composition of Lunar Anorthosites and Their Parent Liquids. *Lunar Science*, Vol. III, Lunar Science Institute, Houston, 1972, pp. 404–406.
52. HUBBARD, N. J., P. W. GAST, J. M. RHODES, B. M. BANSAL, H. WIESMANN, AND S. E. CHURCH, Nonmare Basalts: Part II. *Proc. Third Lunar Science Conference, Geochimica et Cosmochimica Acta*, Supplement 3, Vol. 2, 1972, pp. 1161–1179.
53. LAUL, J. C., H. WAKITA, D. L. SHOWALTER, W. V. BOYNTON, AND R. A. SCHMITT, Bulk, Rare Earth, and Other Trace Elements in Apollo 14 and 15 and Luna 16 Samples. *Proc. Third Lunar Science Conference, Geochimica et Cosmochimica Acta*, Supplement 3, Vol. 2, 1972, pp. 1181–1200.
54. MORRISON, G. H., J. T. GERARD, N. M. POTTER, E. V. GANGADHARAM, A. M. ROTHENBERG, AND R. A. BURDO, Elemental Abundances of Lunar Soil and Rocks From Apollo 12. *Proc. Second Lunar Science Conference, Geochimica et Cosmochimica Acta*, Supplement 2, Vol. 2, 1971, pp. 1169–1185.
55. PHILPOTTS, J. A., C. C. SCHNETZLER, D. F. NAVA, S. SCHUMANN, C. W. KOUNS, R. K. L. LUM, AND A. L. BICKEL, Apollo 16: Large Ion Lithophile Trace Element Abundances in Some Fines, a Basalt and an Anorthosite. *Lunar Science*, Vol. IV, Lunar Science Institute, Houston, 1973, pp. 592–594.
56. RHODES, J. M., AND N. J. HUBBARD, Chemistry, Classification, and Petrogenesis of Apollo 15

Mare Basalts. *Proc. Fourth Lunar Science Conference, Geochimica et Cosmochimica Acta,* Supplement 4, Vol. 2, 1973, pp. 1127–1148.

57. VINOGRADOV, A. P., Preliminary Data on Lunar Ground Brought to Earth by Automatic Probe "Luna-16." *Proc. Second Lunar Science Conference, Geochimica et Cosmochimica Acta,* Supplement 2, Vol. 1, 1971, pp. 1–16.

58. WAKITA, H., AND R. A. SCHMITT, Elemental Abundances in Seven Fragments From Lunar Rock 12013. *Earth Planet. Sci. Letters,* Vol. 9, 1970, pp. 169–176.

59. GRAHAM, A. L. AND A. E. RINGWOOD, Lunar Basalt Genesis: The Origin of the Europium Anomaly. *Earth Planet. Sci. Letters,* Vol. 13, 1971, pp. 105–115.

Lunar Highland Rock Types: Their Implications for Impact-Induced Fractionation [1]

W. C. Phinney and J. L. Warner
NASA/Johnson Space Center
Houston, Texas
C. H. Simonds
Lunar Science Institute
Houston, Texas

The first step in a petrologic study must be a classification based on observed textures and mineralogy. Lunar rocks may be classified into three major groups: (I) coarse-grained igneous rocks, (II) fine-grained igneous rocks, and (III) breccias. Group I is interpreted as primitive lunar crustal rocks that display various degrees of crushing and/or annealing. Group II is interpreted as volcanic rocks. Group III is interpreted as resulting from impacts on the lunar surface and is subdivided on the basis of matrix textures into fragmental breccias, crystalline breccias that have been annealed, and crystalline breccias with igneous matrices.

A synthesis of the relevant data concerning lunar highlands polymict breccias from the fields of petrography, chemistry, photogeology, and impact studies compels the prediction that the breccias should have homogenous matrices from rock to rock within regions of the highlands of limited size where impact mixing has been efficient and extensive. But the returned breccias, even from one landing site, display a wide range in composition. This incompatibility between prediction and observation is a paradox that may be resolved by a process that acts after impact mixing to cause a differentiation of the breccia compositions. Partial melting of the local average crustal composition (as modeled by the average soil composition for each site) and separation of melt and residue in ejecta and/or fall-back blankets are compatible with the reviewed data and may resolve the paradox.

Lunar samples have now been returned by eight missions, Apollo 11, 12, 14, 15, 16, and 17 and Luna 16 and 20. From many hand-specimen-sized rocks, but mostly from smaller fragments separated from soils, thousands of thin sections of lithic fragments have been made and studied (see refs. 1 through 7). Lithic types returned from mare areas are largely Fe-Ti-rich basalts or breccias comprised largely of such basalts. Those returned from highland areas are more complex; most are breccias of various types, and a small number are partially crushed and annealed, coarser grained igneous rocks. An initial attempt is made in this paper to classify the highland lithologies and explain their petrogenesis. Previous studies of limited suites of samples from individual missions have resulted in several lithologic classifications; commonly these are based on objective and interpretive combinations of chemical, mineralogic, and textural criteria. Although a thorough understanding of lunar rocks should eventually include a wide variety of petrogenetically significant criteria, the first step in a petrologic study must be a classification based on observed textures and mineralogy as was historically developed for terrestrial rocks. Further refinements may include chemical, experimental, or other data. Table 1 is a classification based solely

[1] Lunar Science Institute Contribution No. 230.

Table 1.—*Petrographic Classification of Lunar Rocks*

Groups and Subgroups	Interpretation
I. Coarse-Grained Igneous Rocks (intergrown crystals, >1 mm, typical of terrestrial equivalents)	Early crustal cumulate rocks, some of which have been partly crushed and/or annealed.
A. Plutonic Rocks (anorthosite, troctolite, etc.)	
B. Cataclastic Rocks (cataclastic anorthosite, etc.)	
C. Granulitic Rocks (granulitic troctolite, etc.)	
II. Fine-Grained Igneous Rocks (glassy to fine-grained (<1 mm) intergrown, crystalline textures typical of terrestrial equivalents)	
A. Mare Basalts[1] (ferromagnesian silicates plus opaques comprise >50% and plagioclase <50% of minerals, essentially no orthopyroxene)	Melts from the lunar interior.
B. Pyroclastic Rocks (aggregates of vitric to devitrified ash)	
C. (?) Feldspathic Basalts (?) (plagioclase comprises >50% of minerals, orthopyroxene is common, e.g., 14310, Apollo 15 KREEP, 68415)	
III. Breccias (angular to rounded relic fragments in a fragmental, crystalline or glassy matrix; polymict)	
A. Fragmental Matrix Breccias (no sutured or interlocking minerals in matrix as in crystalline textures)	
1. Light Matrix Breccias (seriate distribution of lithic and mineral fragments)	
2. Vitric Matrix Breccias (matrix is largely 0.5 to 2.0μm glass fragments)	
B. Crystalline Matrix Breccias	Nonmelted, crushed, and mixed breccias formed directly from impact events. (Matrix never consisted of coherent melt, although matrix may have contained many fragments of glass.) Some may have undergone one or more subsequent heating events.
1. Crystalline Matrix Breccias With Equant Feldspar in Matrix	
a. Low-Grade Breccias (grain-size distribution is discontinuous; no obvious mosaic pattern to minerals)	
b. High-Grade Breccias (grain-size distribution is discontinuous; minerals form mosaic pattern; silicates as regular polyhedra)	
c. Poikilitic Breccias	
2. Crystalline Matrix Breccias with tabular feldspar in matrix	
a. Basaltic Matrix Breccias	
i. Mesostasis-rich Basaltic Breccias (matrix contains plagioclase, olivine, >10% cryptocrystalline mesostasis of glass, phosphates, opaque minerals, pyroxene, and other accessory minerals)	Melt-derived breccias formed directly from impact events. (Matrix at some stage consisted of reasonably coherent melt.)
ii. Ophitic Basaltic Breccias	
iii. Porphyritic Basaltic Breccias	
iv. Micronoritic Breccias	
v. (?) Feldspathic Basalts (?)	
b. Poikilitic Matrix Breccias	
C. Glassy Matrix Breccias (primarily agglutinates; matrix consists of coherent glass)	
D. Devitrified Glass-Matrix Breccias	

NOTE: [1] Mare basalts may be further subdivided, but this paper is concerned more with highland rock types.

on petrographic observations. Because there are gradations between most groups, the divisions between groups are somewhat arbitrary. The texture of an individual thin section may overlap more than one group and not be clearly assignable to one group or the other. Some rocks may contain more than one distinct petrographic type, and the proximity of these various types may be petrogenetically significant. For example, the black and white rocks of Apollo 15 and 16 are irregularly banded mixtures of basaltic-textured breccias and light matrix breccias or cataclastic rocks. In spite of this complex-

ity, the groupings in this classification represent reasonably well the major rock types required to describe the returned highland samples.

Several ground rules were used in developing this classification:

1. Terminology is based primarily on study of thin sections.
2. Existing terrestrial or lunar rock names and terminology are used when possible.
3. When several terms have been used to classify a particular rock type, the term having the least ambiguity in the literature is utilized.
4. New names are not invented.
5. Although it is impossible to avoid some degree of genetic connotation in many rock terms, the terms utilized are those considered as having the least genetic connotation.
6. Assignment to a group in the classification must be possible on the basis of binocular and petrographic microscope examinations and not require chemical or isotopic data available for only a small fraction of the samples for which thin sections exist.

Classification

The rocks are divided into three major groups: coarse-grained igneous rocks, fine-grained igneous rocks, and breccias. Each of the three major groups is further subdivided into several subgroups.

GROUP I. COARSE-GRAINED IGNEOUS ROCKS

Grain sizes in this group are generally greater than 1 mm and occur in various in-

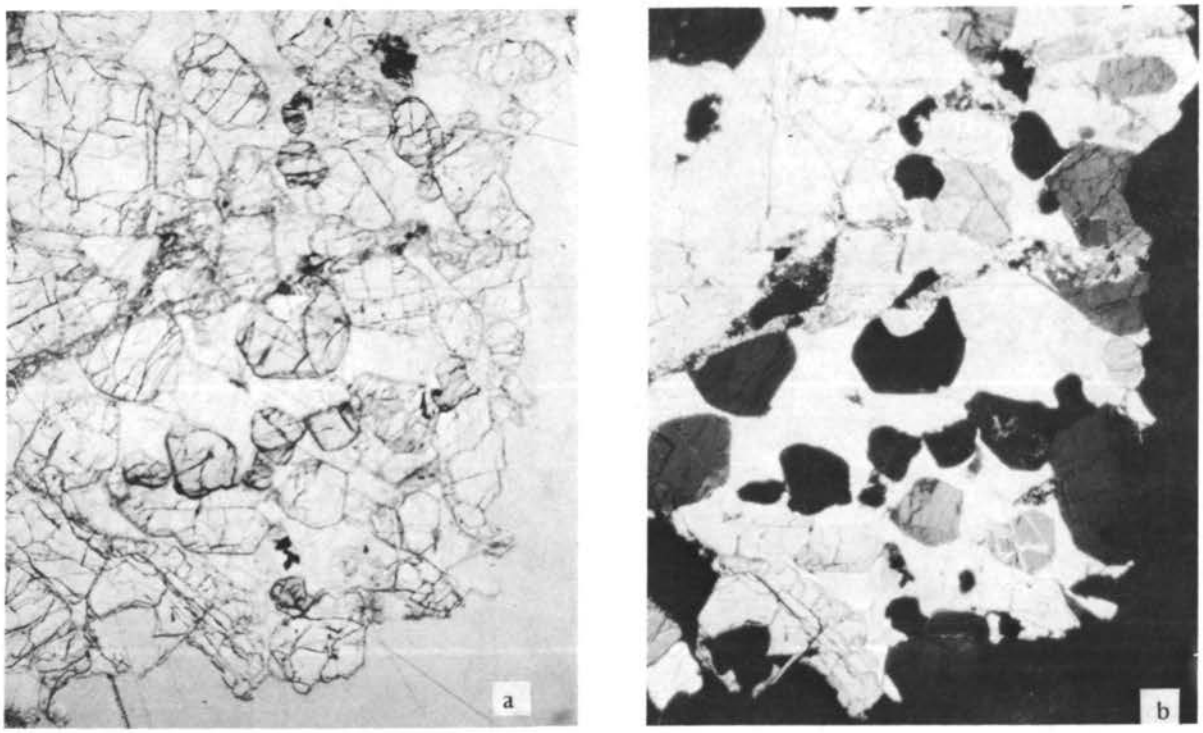


Figure 1.—*Clast of spinel-bearing troctolite from 67435 which is a poikilitic matrix breccia with tabular feldspar. (a) Plane light view of plagioclase (very light gray), subhedral olivine (light gray), and subhedral spinel (gray); (b) cross polars view illustrating isotropic nature of spinel and poikilitic nature of plagioclase. The troctolite has the cumulative texture of igneous rocks (long dimension = 2.4 mm).*

tergrowths of euhedral to subhedral minerals as in terrestrial gabbroic and granitic rocks (fig. 1). Applicable terrestrial terms such as troctolite and anorthositic gabbro are appropriate for these coarse igneous lithologies that are more common as clasts in breccias than as separate rock fragments. A few coarse mare basalts attain dominant, or average, grain sizes of up to 1 to 2 mm, thus overlapping with the coarse-grained group. However, they contain less than 35-percent plagioclase, significant augite and ilmenite, continuous gradations to much finer grained or vitrophyric textures, and greater than 14-percent FeO, all of which are characteristic of mare basalts that are classed as fine-grained igneous rocks.

Most of the coarse-grained igneous rocks have been partly to extensively crushed. If there are petrographically recognizable remnants of previous coarse-grained igneous textures, the rock is classified as the cataclastic equivalent of the appropriate predecessor, e.g., cataclastic gabbro, cataclastic anorthosite. As in the terrestrial equivalents, the greater the degree of crushing the more difficult it is to deduce a coarse-grained igneous origin. To be a cataclastic igneous rock, the minerals may be crushed but not mixed with material from other source rocks. Lithologies that are most clearly in this category are those with seriate monomineralic matrices enclosing multigrain clasts of the same mineral (fig. 2a). Monomineralic matrices with large single mineral grains of the same mineral (fig. 2b) are also included in this group.

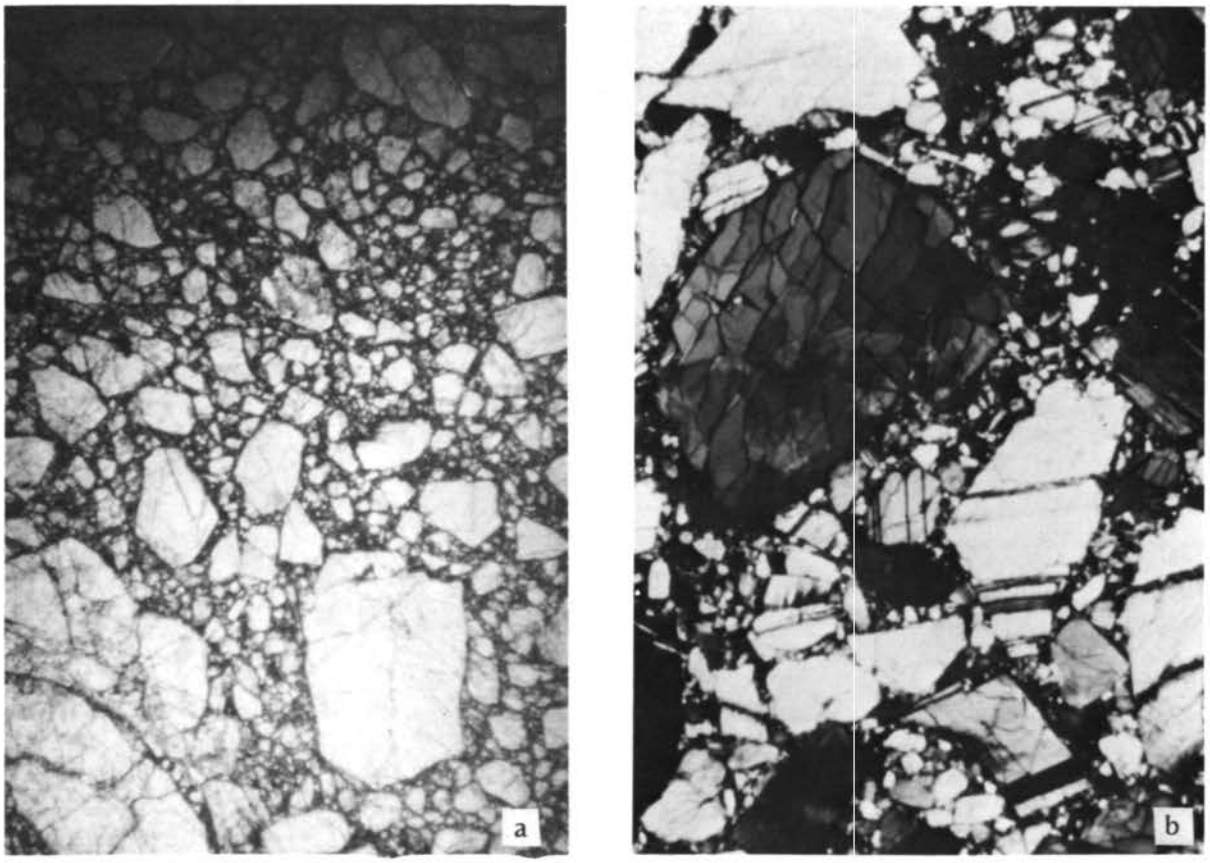


Figure 2(a).—*Cataclastic dunite, 72415,56 (plane light). This rock is essentially all olivine in seriate grain size distribution. Note clast of multigrain olivine at lower left (long dimension = 7.2 mm); (b) cataclastic anorthosite, 60025,110 (crossed polars). This rock is essentially all plagioclase both as large grains and fine-grained matrix (long dimension = 1.8 mm).*

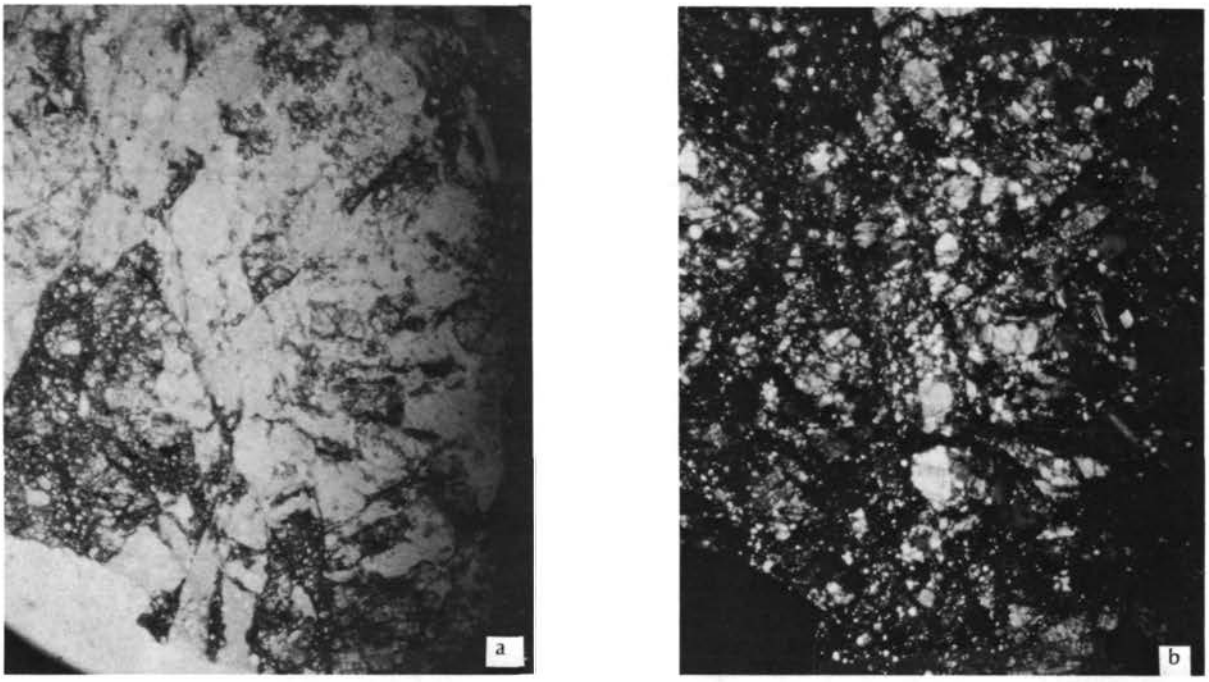
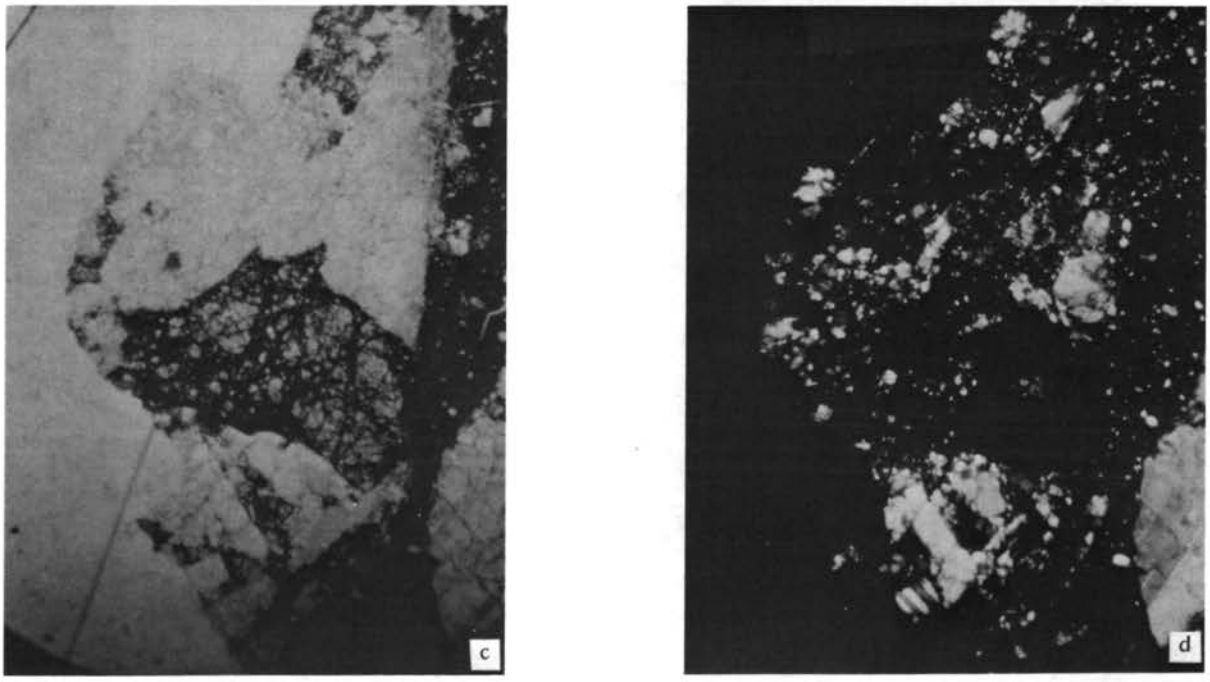


Figure 3.—*White area of black and white breccia 15455 showing plane light view (a) of zones of crushed plagioclase (light gray) containing larger fragments of plagioclase (white) enclosing zones of crushed orthopyroxene (black) and larger fragments of orthopyroxene (medium gray, high relief). Crossed polars view of same area (b) shows continuity of twinning from one plagioclase fragment to another, especially at right center and lower center. Similar pair of plane light (c) and crossed polars views (d) show that orthopyroxene fragments (medium gray in c) in crushed orthopyroxene (dark gray in c) form one optically continuous grain as shown by their simultaneous extinction in (d) (long dimension = 7.2 mm).*



Lithologies containing seriate polymineralic matrices enclosing multigrain clasts, all of which have the same coarse-grained lithology and minerals as those in the matrix, would also be placed in this group. More equivocal are those textures in which crushed zones are irregularly interspersed with coarse grains which are themselves fractured and partly crushed (fig. 3). If no relic igneous texture remains, then the rock would be categorized as a breccia.

In other coarse-grained igneous rocks, partial to extensive annealing, or recrystallization, has resulted in granulitic textures. The grains display equigranular, polyhedral morphology with triple junctions of 120°. The rock may have been a coarse-grained igneous rock that has been intensely crushed and then recrystallized (fig. 3). Such histories can commonly be verified by studies of textural variations in both hand specimens and thin sections. If remnants of a coarse-grained igneous precursor are present, the rock may be classed as a granulitic troctolite, granulitic anorthosite, etc. The hand specimen may clearly show the rock to have a coarse-grained, cumulus texture, yet the thin section may show granulitic texture as is the case with troctolite 76535 and anorthosite 15415 (fig. 4). Again, as in terrestrial equivalents, the more extensive the recrystallization the more equivocal the initial rock type. In cases where the rock initially may have been a polymict or detrital breccia and then recrystallized, there may be some heterogeneities or relic clasts suggesting such an origin, and the rock would be termed a high-grade breccia under the crystalline matrix category. In the absence of any petrographic evidence of an igneous or detrital origin (fig. 5), it is suggested that the rock be termed a granulite with constituent mineral

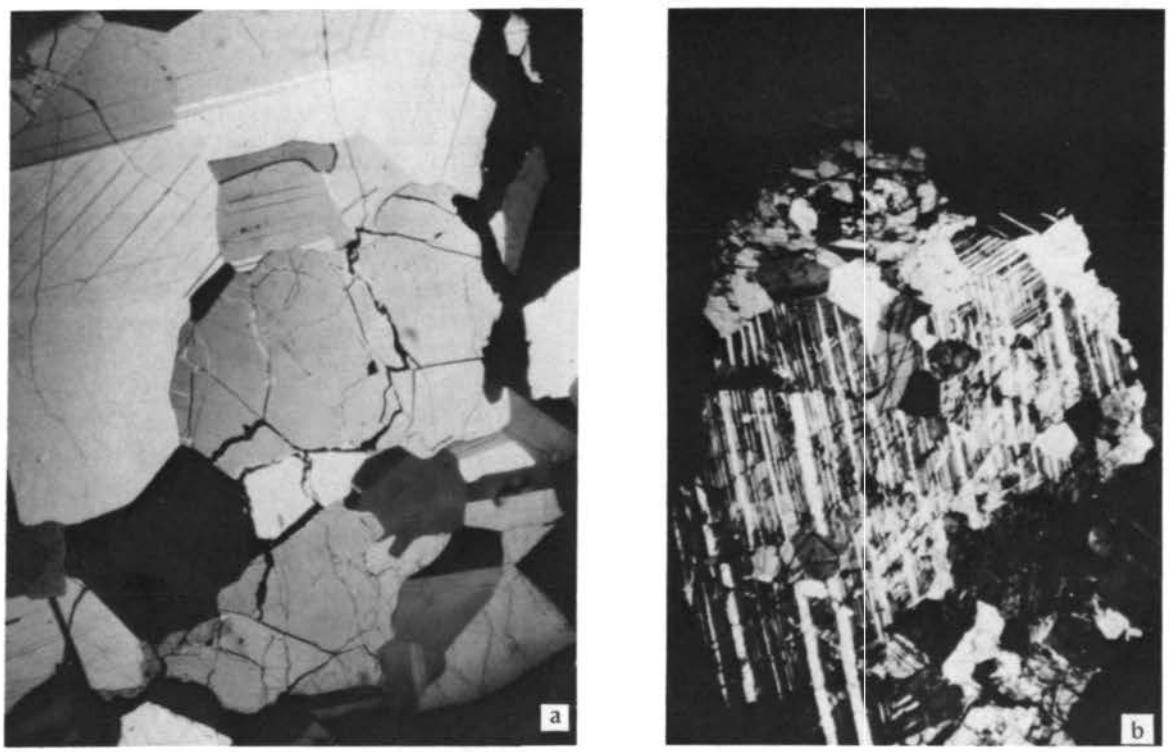


Figure 4(a).—*Crossed polars view of troctolite 76535,51 showing polyhedral grain development with triple junctions. Gray, irregularly cracked grains are olivine; remainder is plagioclase (long dimension = 7.2 mm); (b) crossed polars view of chip from anorthosite 15415,30 showing polyhedral grain development of smaller plagioclase grains within much larger plagioclase grains (long dimension = 7.2 mm).*

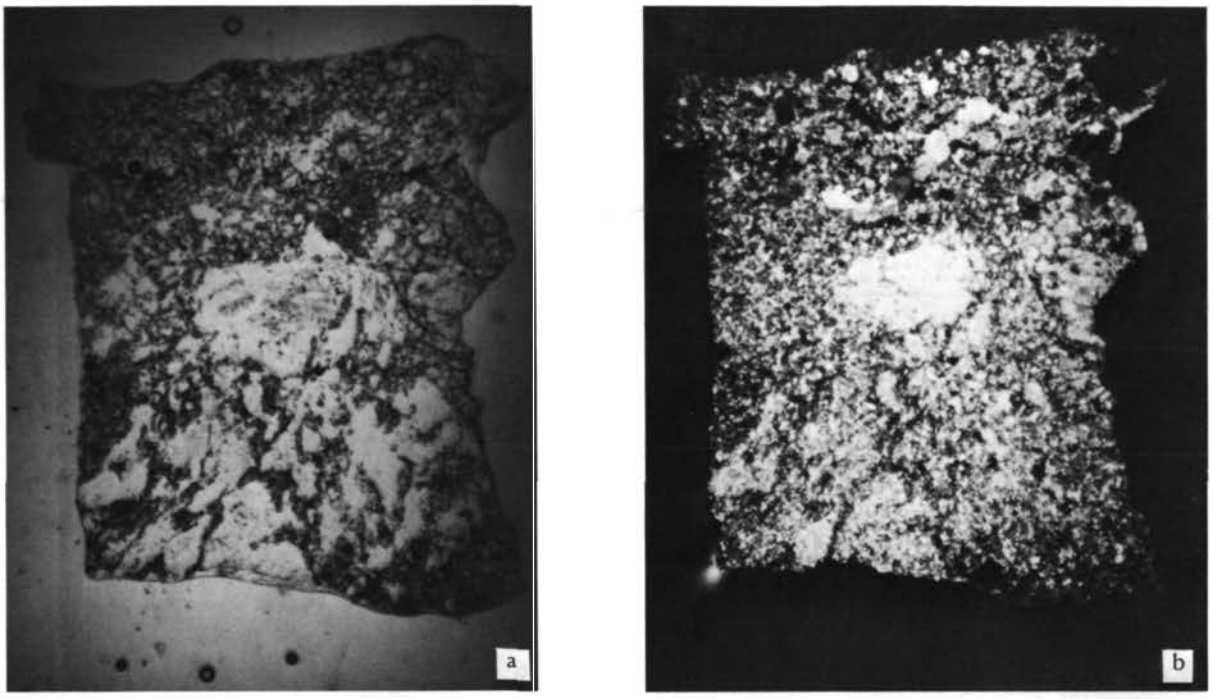
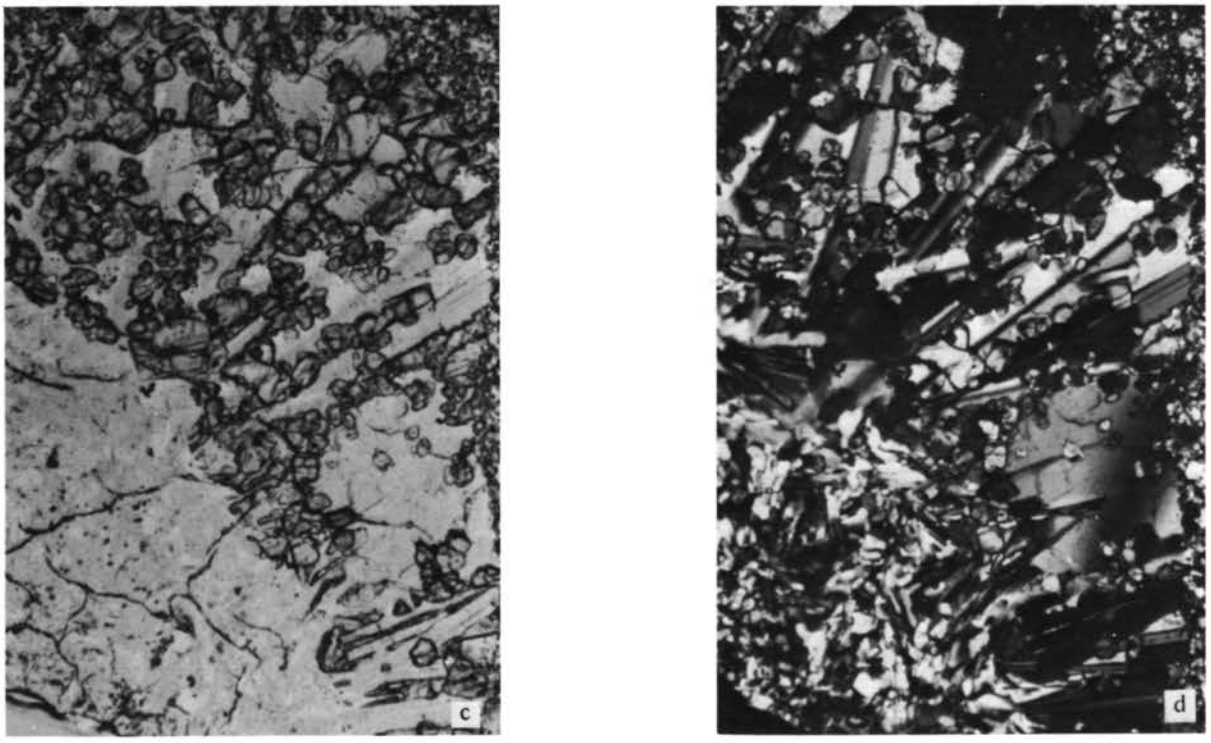


Figure 5.—*(a) Plane light and (b) crossed polar views of 79215,58. Light area in center is large plagioclase grain that has developed extensive small polyhedral grains in its outer zone. Top left and top right are similar zones of polyhedral grains but entirely of olivine. Light areas in lower half of fragment consist of polyhedral plagioclase grains (long dimensions = 7.2 mm). (c) Plane light and (d) crossed polars views of another thin section of 79215,50 at lower magnification showing polyhedral grain development from a large plagioclase (lower left) and in zones of olivine between plagioclase crystals (upper right) (long dimension = 1.8 mm).*



names as adjectives (e.g., plagioclase-olivine granulite). Further studies of petrologic, chemical, and physical properties might allow a more definitive determination of origin.

GROUP II. FINE-GRAINED IGNEOUS ROCKS

This group consists of vitrophyric to fine-grained (< 1 mm) crystalline rocks with ophitic, subophitic, diabasic, intersertal, and porphyritic textures similar to those of terrestrial volcanic rocks. Most of the returned fine-grained igneous rocks are mare basalts containing less than 50-percent feldspar, greater than 50-percent ferromagnesian silicates, several percent opaque minerals largely as ilmenite, significant amounts of augite or other clinopyroxenes, and essentially no orthopyroxenes (fig. 6). The high content of ferromagnesian minerals is reflected in the high FeO content (> 14 percent of the chemical analyses of mare basalts).

Pyroclastic rocks consist of aggregates of small (< 1 mm) glassy to devitrified fragments, most of which are spheroids or fragments of spheroids. The fragments are extremely homogeneous, some contain phenocrysts, many are composite, and a few contain vesicles (fig. 7). A review of these materials from Apollo 17 (ref. 8) presents the arguments for a pyroclastic origin. The green rocks of Apollo 15 (15425, 15426, and 15427),

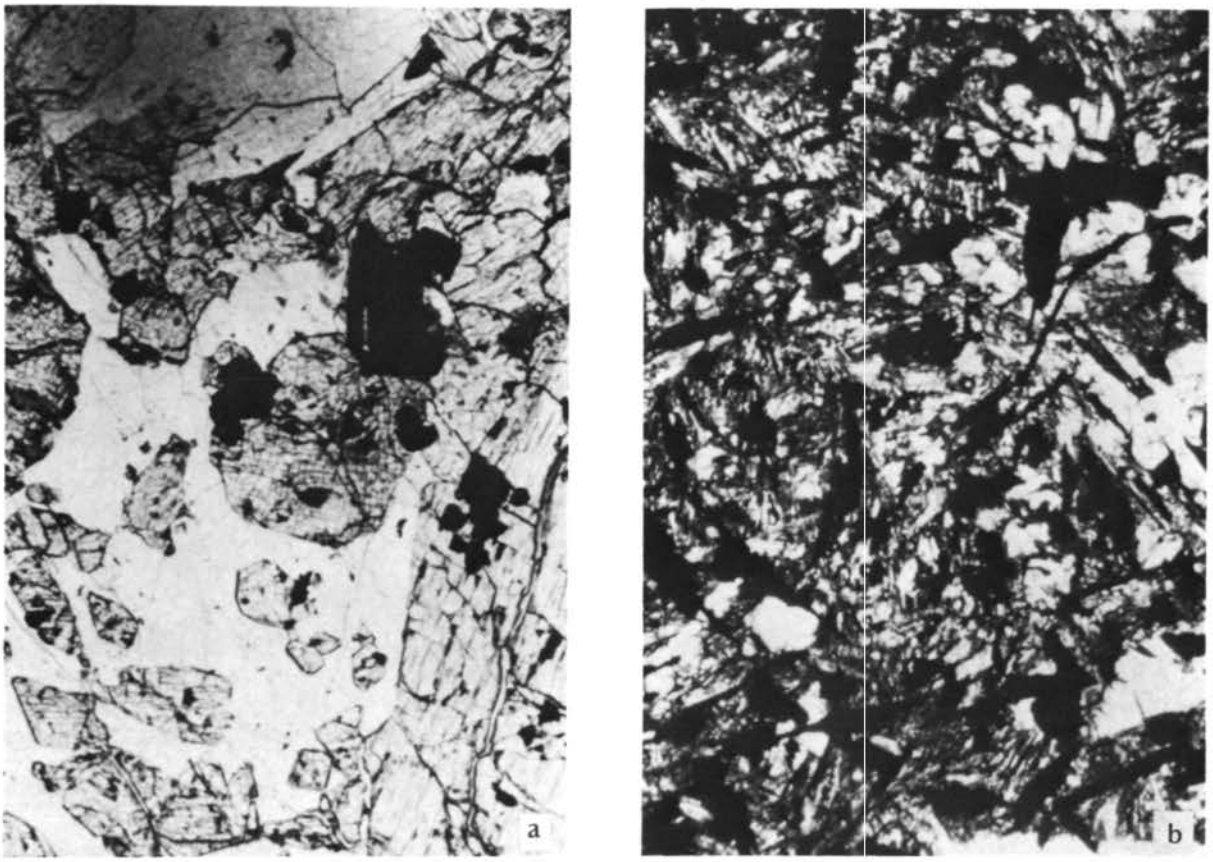


Figure 6.—*Plane light views of mare basalts. (a) Coarse-grained basalt 15555,206 showing olivines and clinopyroxenes (gray) poikilitically enclosed in plagioclase. Opaque minerals are primarily ilmenite. Large clinopyroxene grain with opaque inclusions occurs along right margin. (b) Crystals of armalcolite or ilmenite (black) and pyroxene (white) in matrix of glass and spherulitic crystals in 70215,160 (long dimension = 1.8 mm).*

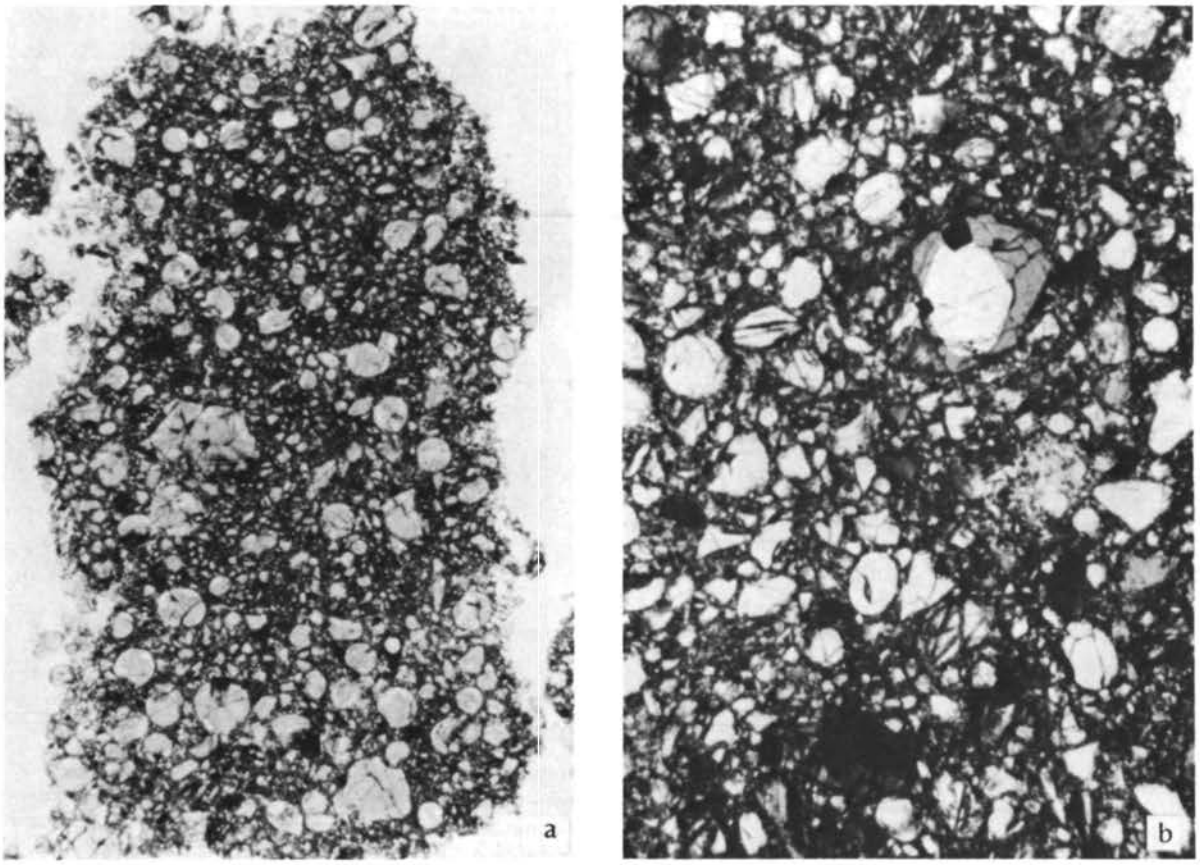


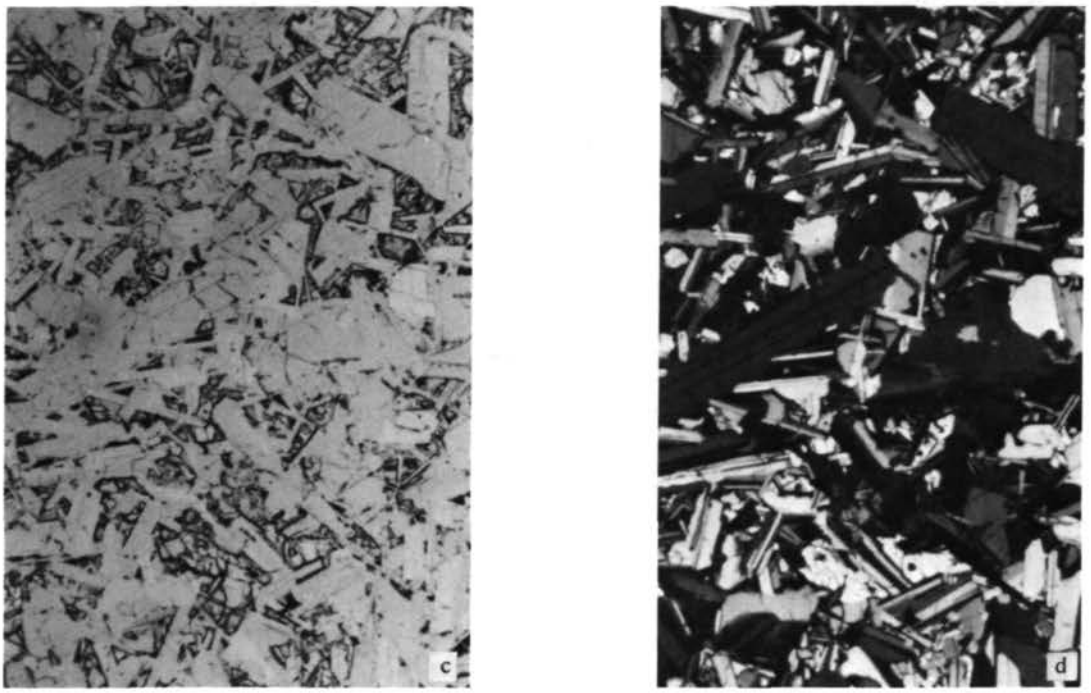
Figure 7.—*Plane light views of (a) orange clod 74220,78 and (b) green rock 15427,29. Both are very similar in that they contain spheroids or fragments of spheroids that are primarily glass, but also a few that are divitrified. The gray matrix is mostly finer fragments of the same material. Note the euhedral olivine grain in the large glass fragment in the upper right of 15427.*

the orange clods and soil of Apollo 17 (74220), and the black soil of Apollo 17 (74001) are all in this group.

Rocks with basaltic texture, 50-percent plagioclase, predominantly Ca-poor pyroxene including orthopyroxene, about 1- to 2- percent opaques, and no obvious relic fragments are termed feldspathic basalts (fig. 7). In some cases they have been considered as volcanic in origin, but some may be impact units representing totally melted matrices that contain fragments on a scale too large (cm to m) to observe in the returned samples, and certainly too large to observe in a single thin section. Therefore, this group appears with queries in two places on table 1. For example, thin sections of a 370-g feldspathic basalt from the Apollo 16 site (68415), contain no obvious relic fragments, yet the lunar surface photos show this to be a sample of the matrix from a fragment-laden rock, and the description of the overall specimen in the Apollo 16 lunar sample catalog contains the following comment: "No clear-cut inclusions and clasts observed; however, patchy distribution of light and dark colored parts is suggestive of almost completely resorbed clasts." Although another feldspathic basalt (68416) was collected from the matrix of the same boulder only 20 to 30 cm from 68415, it has different mineral compositions and textures (refs. 9, 10, and 11) indicating significant meterogeneity in the matrix. Crystalline KREEP basalt fragments



Figure 8 a–d.—*(a) Plane light and (b) crossed polars views of KREEP feldspathic basalt 15434,37, consisting of elongate plagioclase laths (white) some of which are slightly curved, tabular orthopyroxene (gray), and fine-grained mesostasis (dark gray) containing glass, opaques, phosphates, and other accessories. (c) Plane light and (d) crossed polars views of feldspathic basalt 68415,130, consisting mostly of feldspar laths and irregularly shaped, interstitial grains of pyroxene, much of which is orthopyroxene.*



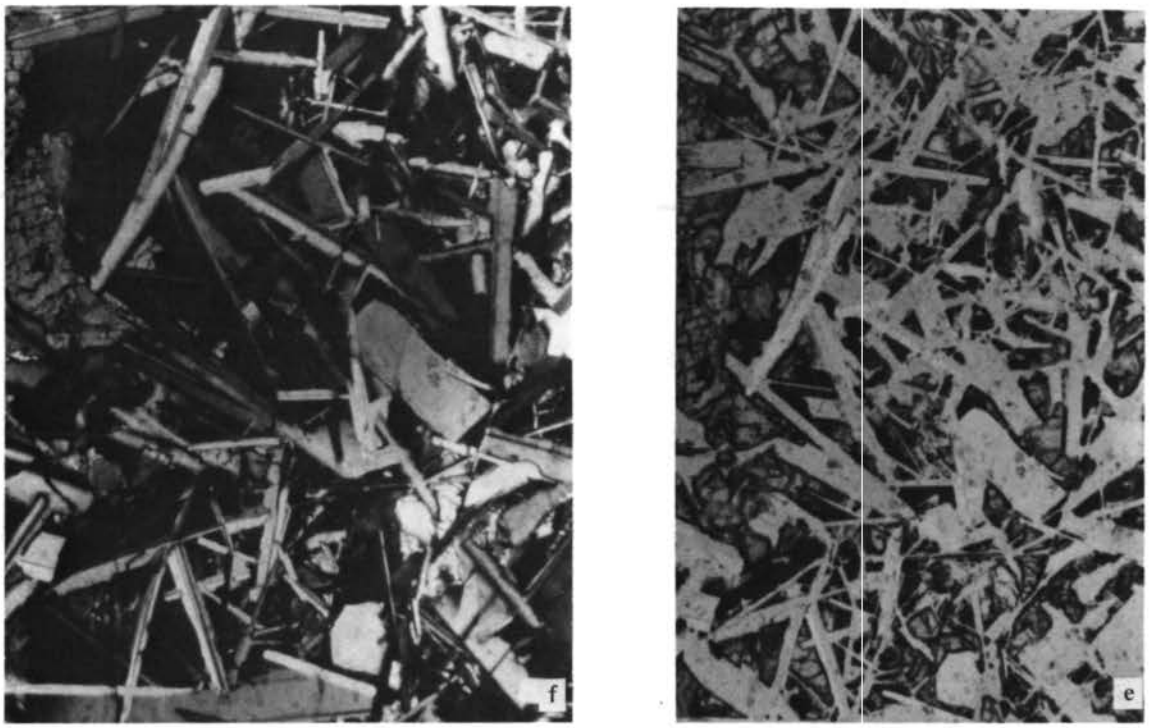


Figure 8 e,f.—*(e) Plane light and (f) crossed polars views of feldspathic basalt 14310,183, consisting of plagioclase laths (white), orthopyroxene phenocryst (light gray, upper left), interstitial pyroxene (light gray), opaques (black), and a trace of fine-grained mesostasis (dark gray in e) (long dimension = 1.8 mm).*

(ref. 12) from the Apollo 15 site contain no obvious clasts but are all less than 2 cm across and could also be breccia matrix fragments. The much larger but similar feldspathic, or KREEP, basalt from the Fra Mauro site (14310) has been interpreted both as of volcanic origin (ref. 13) and as an impact melt derived from the lunar regolith (refs. 14, 15, and 16). Such rocks might be placed in either the fine-grained igneous rock or basaltic matrix breccia groups during the initial petrographic observations, but further study of petrologic, chemical, and physical properties may allow a more definite assignment to a group.

GROUP III. BRECCIAS

As with terrestrial equivalents, the breccias consist of various sized, angular to rounded, clastic fragments from more than one source rock set in a finer grained matrix of either clastic or igneous origin. The ratio of clasts to matrix may vary considerably, and the clastic fragments represent a polymict source. Clast types may vary from one geographic area to another or with depth of origin, making them important in provenance studies. Information about the processes that formed breccias is best preserved in the matrix and reactions between clasts and matrix. Temperatures, cooling rates, fugacities of certain volatile components such as O_2 and CO_2, pressures, and mechanical processes involved in the lithification of breccias are best deduced from the mineralogy, texture, composition, and physical properties of the matrix. Therefore, the breccia groups of table 1 are based on the petrography of matrices. Further modifications of these groups to include clast content could be accomplished by having clast terms precede the matrix name: e.g., troctolite and gabbro-bearing vitric matrix breccia.

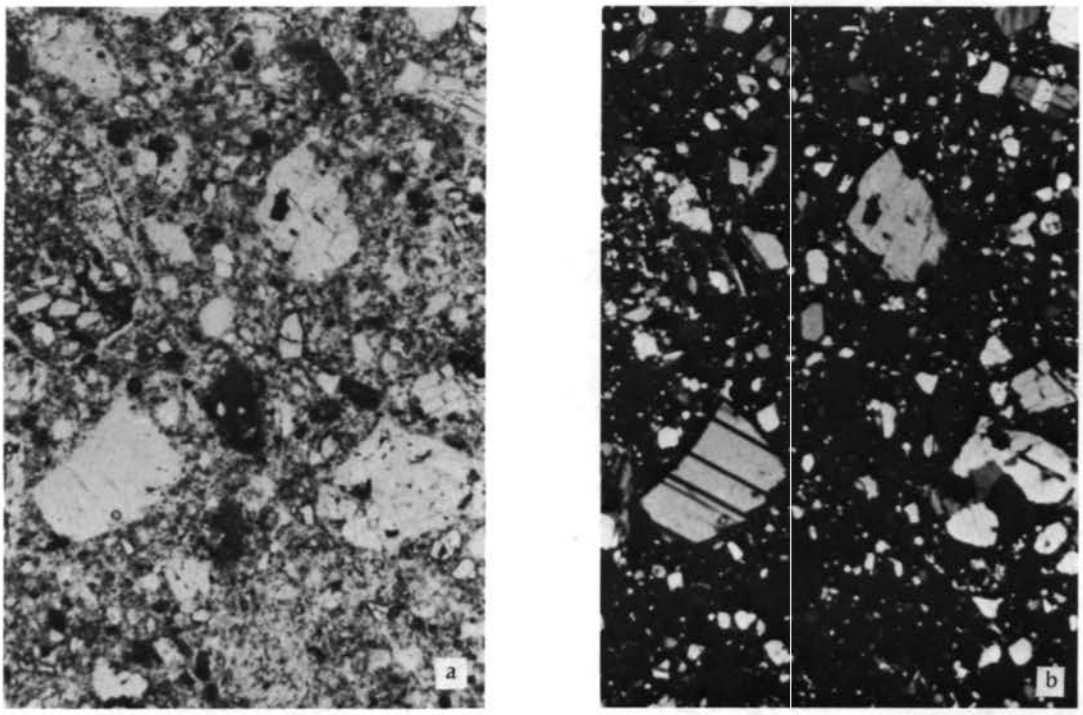
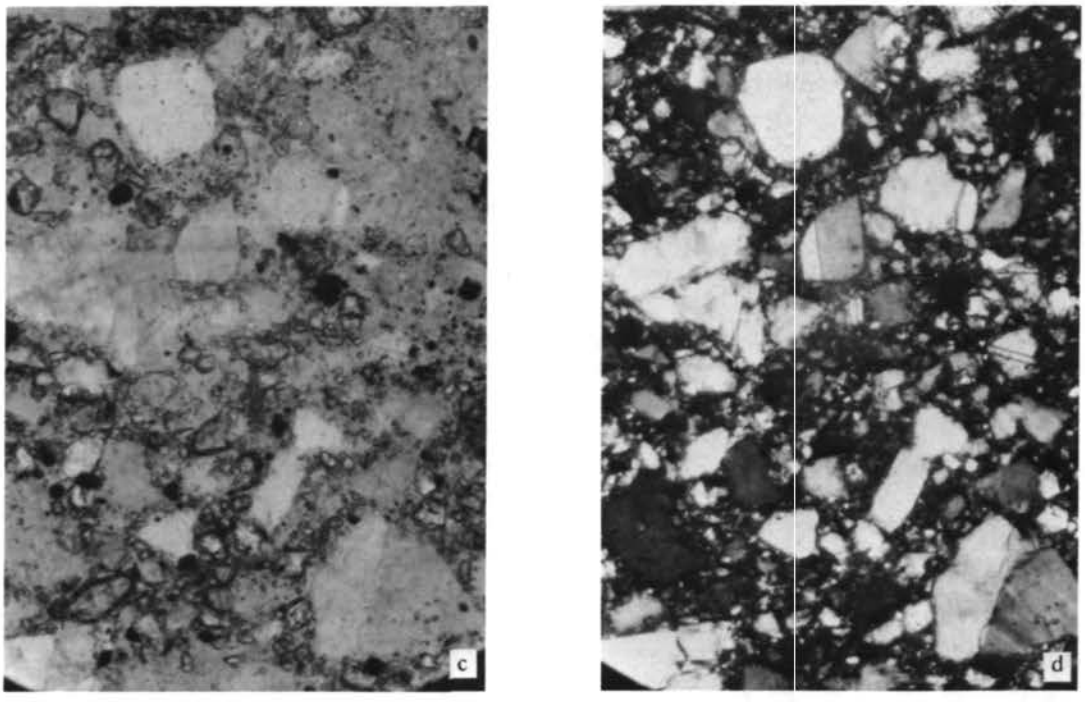


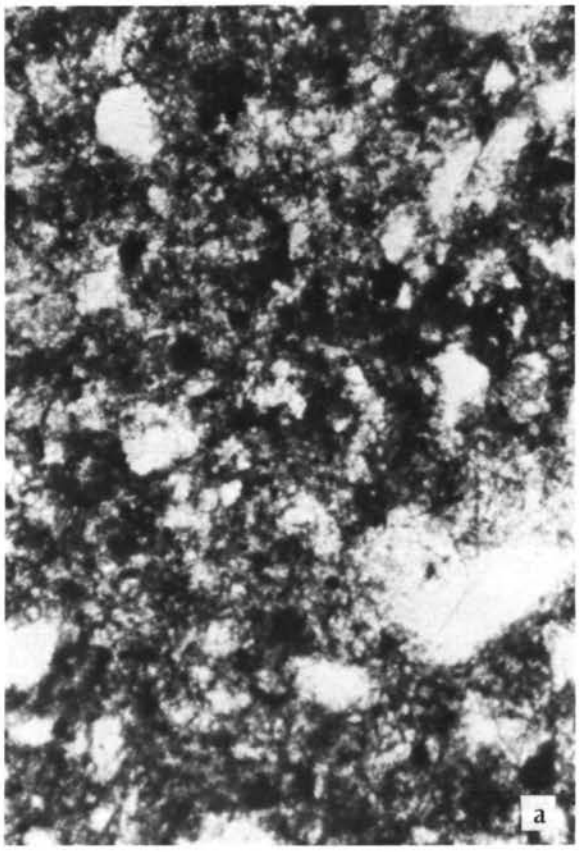
Figure 9.—*(a) Plane light and (b) crossed polars views of light matrix breccia 61516,4, showing seriate grain size distribution and crystalline nature of fragments (long dimension = 1.8 mm) (c) Plane light and (d) crossed polars views of light matrix breccia 14082,10 at much greater magnification than (a) and (b), showing seriate grains and their crystalline nature in the very fine fraction (long dimension = 0.44 mm).*



Fragmental, crystalline, and glassy matrix breccias are common. Because of the great variety of breccias and their importance to interpretation of the evolution of the lunar highlands, the classification of this major group is subdivided more extensively than were the other major groups.

Among the fragmental breccias there are two subdivisions: (1) light matrix breccias containing a seriate distribution of mineral, lithic, and, rarely, glass fragments and (2) vitric matrix breccias containing a large proportion of tiny glass fragments in their matrices (fig. 9). The light matrix breccias consist of crushed and mixed mineral and lithic debris with minor amounts of glass in some samples. There is no clear-cut distinction between matrix and clasts because of a continuous gradation in grain size as though comminution and accumulation were the major processes involved in formation. There are varying degrees of coherence in the light matrix breccias ranging from crumbly, clod-like lumps to quite coherent fragments that may be partly cemented by very small amounts of glass at the grain boundaries causing fritting of the grains. The fine-grained, crushed silicate debris imparts a light gray color to the matrix.

The vitric matrix breccias are dark brown. The matrix consists largely of small, brown glass fragments about 0.5 to 2 μm in longest dimension (fig. 10). Waters et al. (ref. 17) showed that these glass particles are mostly irregular to stubby in shape, although rod-like and platy forms are also common. The particles are molded plastically against one another and against mineral, lithic, and



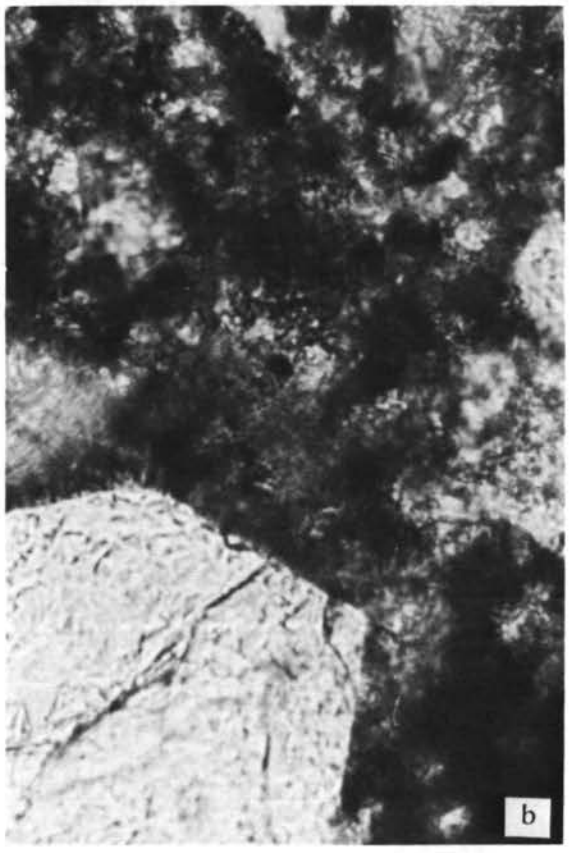


Figure 10.—*Plane light views of vitric matrix breccias at (a) intermediate magnification (long dimension = 0.44 mm) of 14042,7 and (b) high magnification (long dimension = 0.18 mm) of 15314,45. Matrix consists of micromillimeter-sized particles of brown glass which can be resolved in (b).*

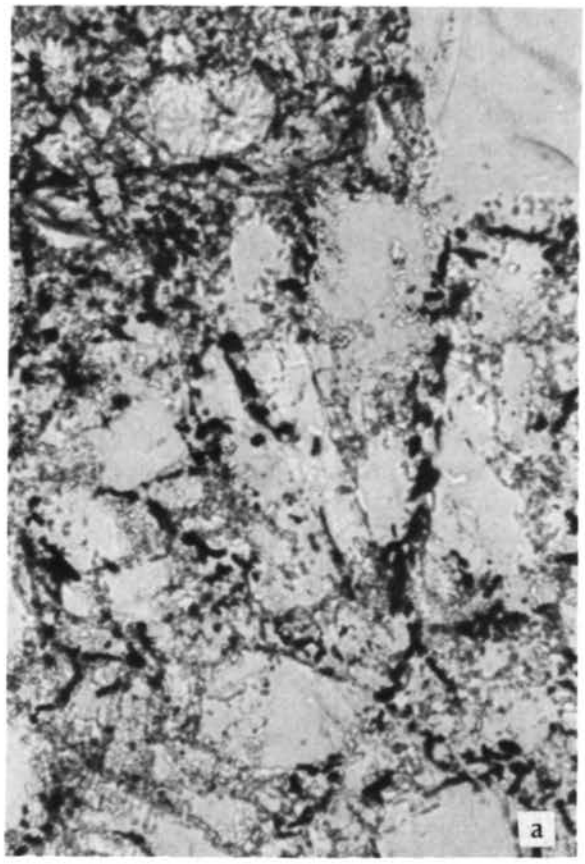


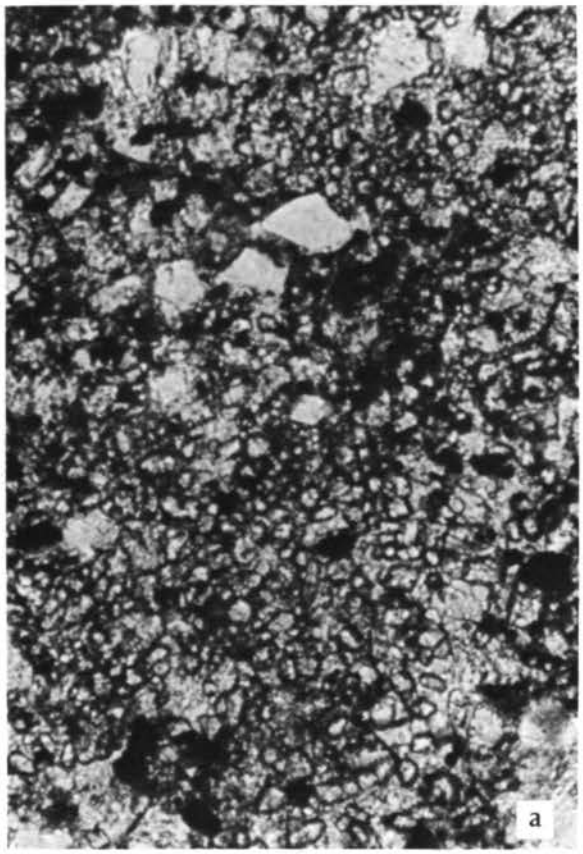
Figure 11.—*Low-grade crystalline matrix breccia 15314,43, showing (a) lack of regular pattern and restricted grain size range of matrix in plane light and (b) crystalline nature of matrix in cross polars (long dimension = 0.44 mm).*

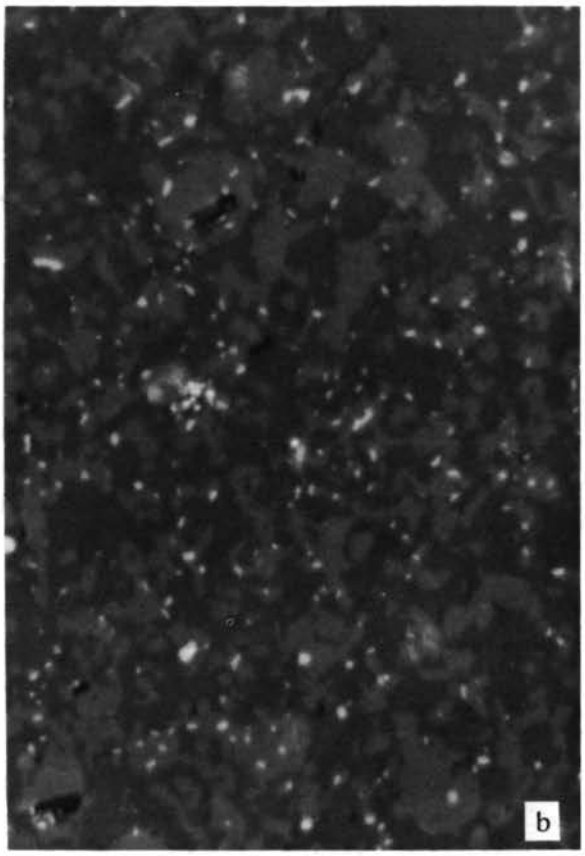
glass clasts indicating that the material accumulated while still reasonably soft and hot. Mineral and lithic fragments occur in seriate distribution ranging from fine debris mixed with the minute glass fragments to much larger discrete clasts.

Crystalline matrix breccias are subdivided into two groups based on crystal morphology in the matrix. Feldspars are particularly useful because of their distinct flat-sided, lathy to tabular forms when euhedral, in contrast to their more equant, rounded to polygonal forms when anhedral. Pyroxenes have similar but less distinctive contrasts in morphology, while olivine is roughly equidimensional in both its euhedral and anhedral forms. Because feldspars have the most distinctive morphology the crystalline breccias are divided into two groups, one with equant feldspar and the other with tabular to lathy feldspar in the matrix. Irregularly shaped mineral clasts of predominantly plagioclase with subordinate olivine, pyroxene, spinel, and a variety of lithic clasts are generally present in both groups in quantities ranging from 5 to 45 percent of the total rock.

Crystalline matrix breccias with equant feldspar display distinct discontinuities in grain size distribution for each mineral in the matrix; i.e., each matrix mineral has a fairly restricted size range. For example, in some Apollo 14 breccias (ref. 5) the plagioclase and pyroxene of the matrix are restricted to the range 3 to 6 μm. For mineral fragments greater than 25 μm there is a seriate distribution. Warner (ref. 5) suggested that this distribution resulted from

Figure 12.—*High-grade crystalline matrix breccias showing (a) development of equant matrix grains in plane light, sample 14311,13 (long dimension = 0.44 mm), and (b) mosaic arrangement of polygonal grains in a small area of matrix in reflected light, sample 14305,95 (long dimension = 0.18 mm).*





recrystallization of the finest grained material (< 25 μm) in an originally detrital matrix.

Further textural distinctions allow three subdivisions of the crystalline matrices containing equant feldspar: low grade, high grade, and poikilitic. Low-grade breccias (fig. 11) display no particular pattern in the matrix minerals; i.e., there is no mosaic pattern of polygonal grains as in the high-grade breccias nor poikilitic mineral development as in the poikilitic breccias. There is less than 5-percent glass in the low-grade breccias corresponding to grades 3 and 4 of Warner (ref. 5). High-grade breccias contain silicate minerals as regular polygons in a mosaic pattern with 120° triple junctions. Figure 12 shows some fine-grained versions of this texture which may also be much coarser grained. There is no glass in the matrix of high-grade breccias corresponding to grades 5 and 6 of Warner (ref. 5). When the original rock cannot be shown to have been a breccia, it may be equivalent to the granulitic igneous rocks of Group I. Poikilitic breccias contain ferromagnesian silicates, particularly low-calcium pyroxenes, as oikocrysts enclosing rounded, equant-to-irregular chadacrysts of plagioclase and ferromagnesian silicates (fig. 13). This texture is quite distinct from the polygonal mosaics of high grade breccias.

Crystalline matrix breccias containing tabular plagioclase in their matrix display poikilitic texture and several varieties of basaltic textures (refs. 3 and 18). The matrices of the mesostasis-rich basaltic breccias

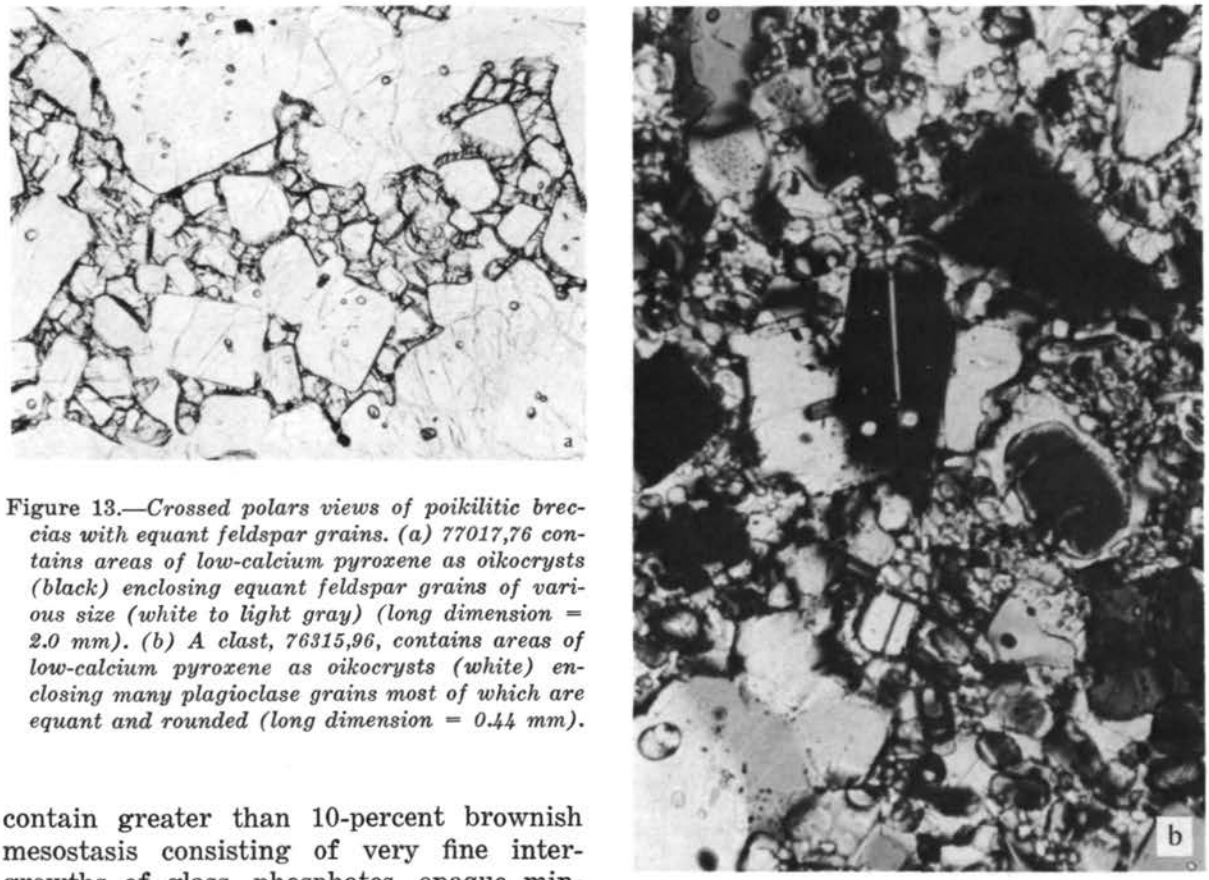


Figure 13.—*Crossed polars views of poikilitic breccias with equant feldspar grains. (a) 77017,76 contains areas of low-calcium pyroxene as oikocrysts (black) enclosing equant feldspar grains of various size (white to light gray) (long dimension = 2.0 mm). (b) A clast, 76315,96, contains areas of low-calcium pyroxene as oikocrysts (white) enclosing many plagioclase grains most of which are equant and rounded (long dimension = 0.44 mm).*

contain greater than 10-percent brownish mesostasis consisting of very fine intergrowths of glass, phosphates, opaque minerals, pyroxene, and accessory minerals (fig. 14). With increasing content of mesostasis, these grade into devitrified glass matrix breccias. At about 50-percent mesostasis, most of the crystal development is in the spherulitic or dendritic patterns typical of the devitrified glass matrix breccias. The plagioclase of mesostasis-rich basaltic breccias ranges from H-shaped to tabular, commonly with hollow cores. Olivine is the most common mafic mineral and displays a subophitic relationship with plagioclase. Pyroxene is rather rare outside the mesostasis, and the subophitic texture occurs in olivine-plagioclase combinations rather than in clinopyroxene-plagioclase as is usually required by the term ophitic. Ophitic basaltic breccias contain matrices of plagioclase, olivine, augite, and pigeonite in subophitic to ophitic textures (fig. 15). A few percent of the mesostasis described above may be present in this subgroup. These textures are dominated by an interlocking network of tabular plagioclase with interstices occupied by pyroxene and olivine crystals that extend over areas two to four times as large as the plagioclase tablets. Grain sizes of each mineral are usually restricted to a fairly narrow range varying little more than a factor of 2 to 3. Porphyritic basaltic breccias are similar to the ophitic basaltic breccias except for the presence of plagioclase phenocrysts (fig. 16). Grain sizes vary considerably more than in the ophitic basaltic breccias. Some of the basaltic textures contain orthopyroxene as the predominant ferromagnesian silicate (refs. 3, 18, and 19). To distinguish these from the previously discussed basaltic matrices, they are termed micronoritic breccias (fig. 17). Feldspathic basalts which may represent extensively melted breccia matrices were discussed under fine-grained igneous rocks.

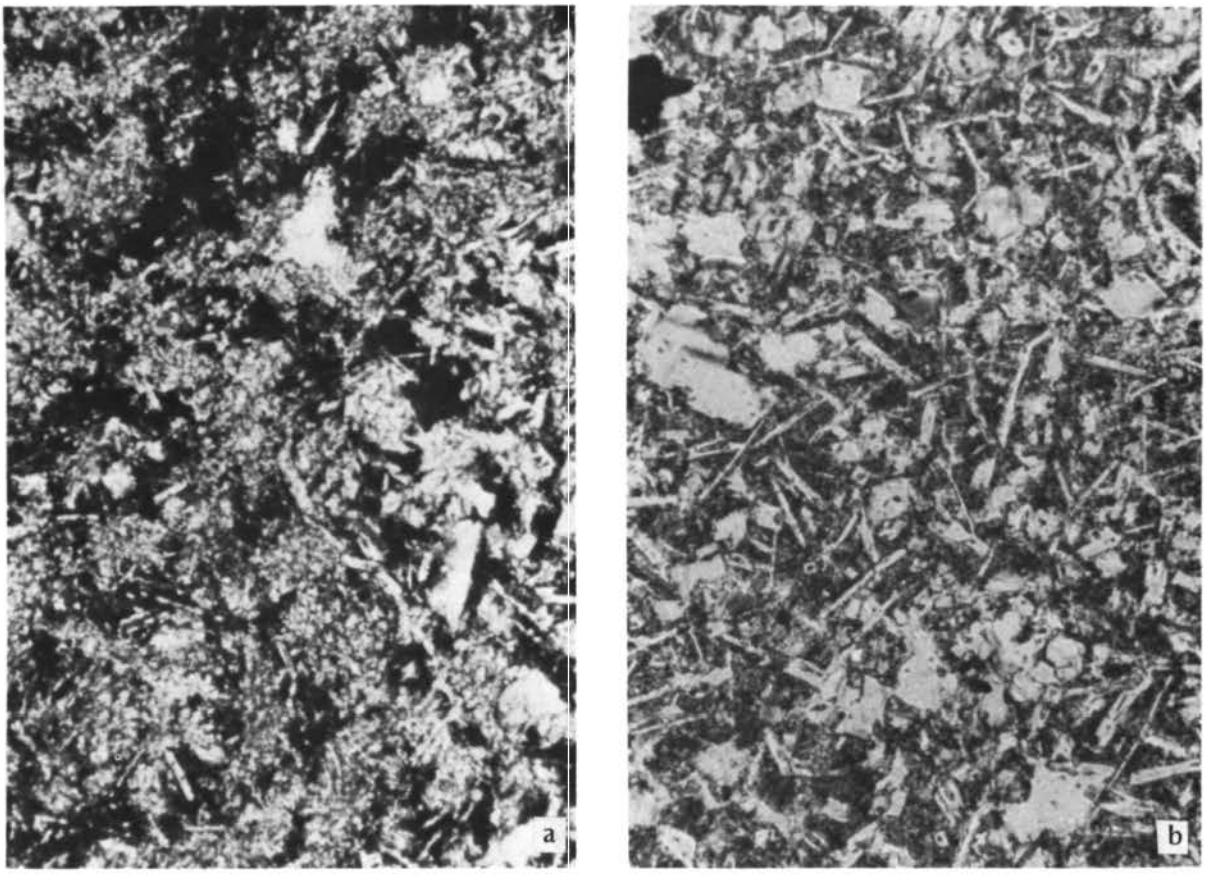


Figure 14.—*Plane light views of mesostasis-rich basaltic breccias. (a) 64477,13 shows mesostasis (black) amid clusters of small equant olivine grains (gray) and elongate plagioclase laths (white to light gray). A few larger mineral clasts are visible (b) 15314,40 contains a greater proportion of mesostasis (gray) with equant olivine (light gray) and lathy plagioclase (light gray) grains (long dimension = 0.44 mm).*

Poikilitic matrix breccias contain poikilitic ferromagnesian minerals, usually low-calcium pyroxene but also high-calcium pyroxene and olivine (refs. 7, 20, and 21). They consist of oikocrysts, generally of orthopyroxene or pigeonite, but also of olivine, up to 3 mm across, enclosing up to 50 percent of their volume as chadacrysts, consisting predominantly of plagioclase tablets, but also of a few mafic silicates (fig. 18). The regions between oikocrysts contain the same minerals as occur in the chadacrysts, plus accessory minerals such as potassium feldspar, apatite, and opaques. In some cases the plagioclase tablets are well aligned both in and around the oikocrysts (fig. 18d).

Glassy matrix breccias contain a coherent, usually vesicular, mass of glass that forms a bonding medium for mineral and lithic clasts (fig. 19). This contrasts with the vitric matrix breccias that contain tiny fragments rather than coherent masses of glass in their matrices. Because cooling of relatively large fragments ($>$ a few cm) from melt temperatures ($\sim$ 1300° C) to 600° or 700° C would take tens of minutes to hours, these larger fragments would be expected to commence crystallizing (or devitrifying) and not remain as glass. Therefore, the glassy matrix breccias occur as small fragments, primarily as agglutinates, rarely larger than a few centimeters across.

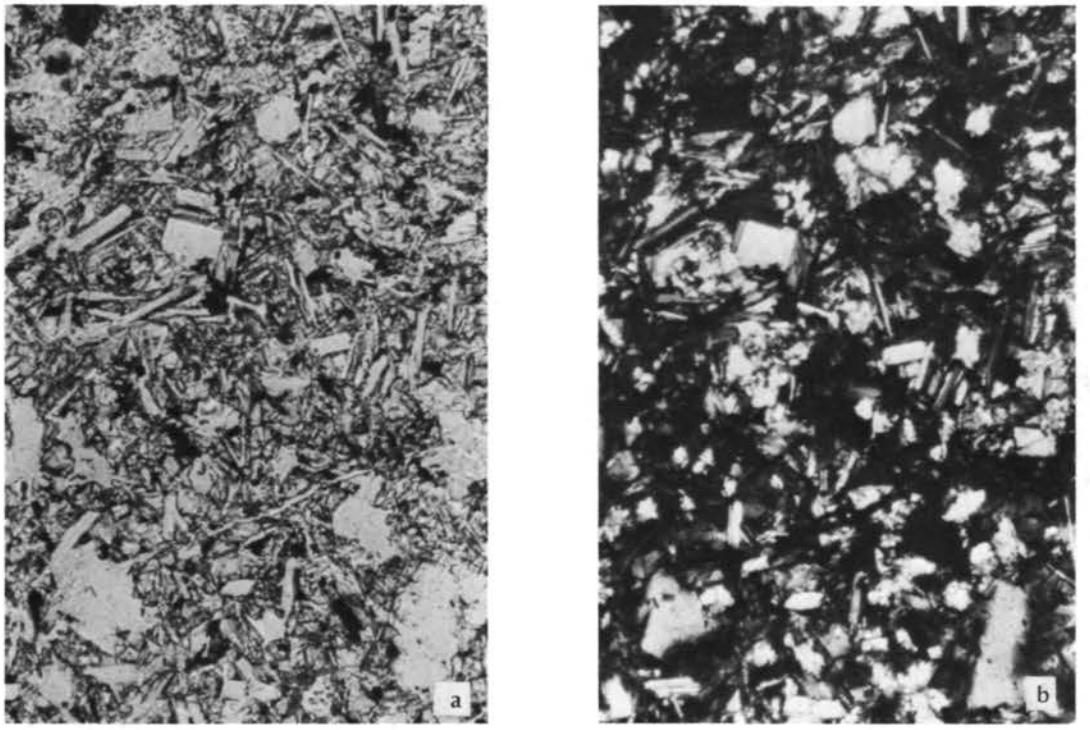
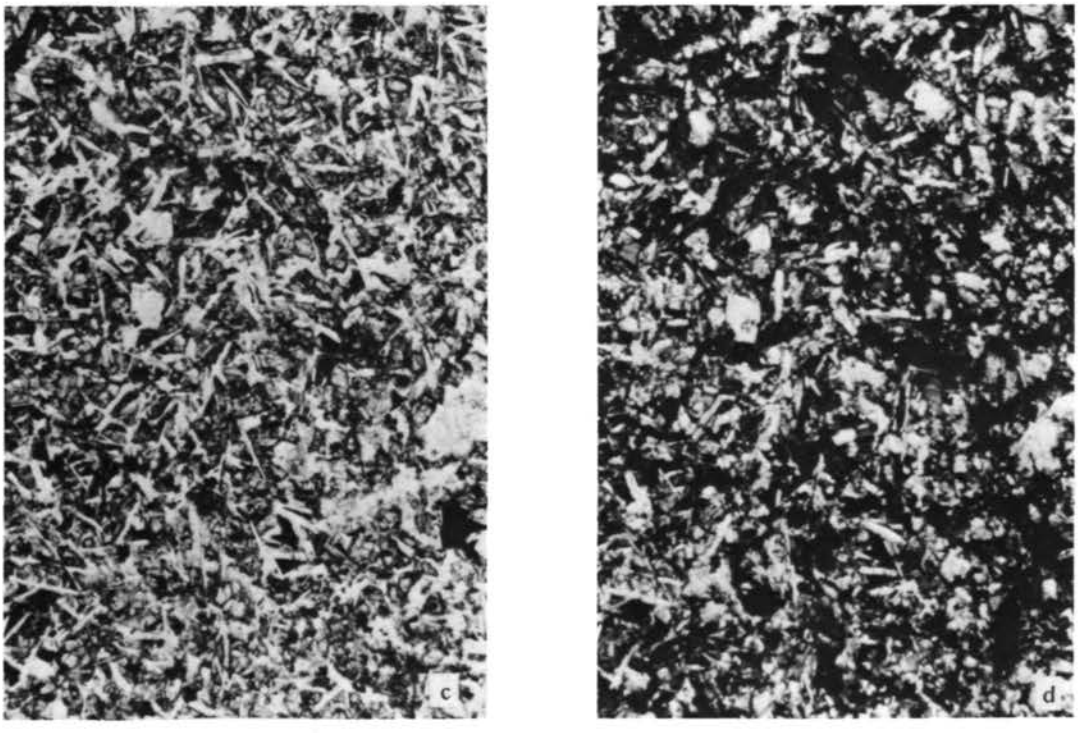


Figure 15.—*Ophitic basaltic breccias. (a) Plane light view of 66095,86, showing tabular plagioclase (light gray), equant olivine and pyroxene (gray), and opaques (black). Large irregular grains in lower half are clasts. (b) Crossed polars view of (a) to show ophitic texture. Upper half of photo shows several ophitic pyroxenes (larger irregular white patches) containing a few plagioclase laths (long dimension = 0.44 mm). (c) Plane light and (d) crossed polars views of 63585,4, one of the coarser grained versions of this group showing the relatively uniform grain size distribution (long dimension = 1.8 mm).*



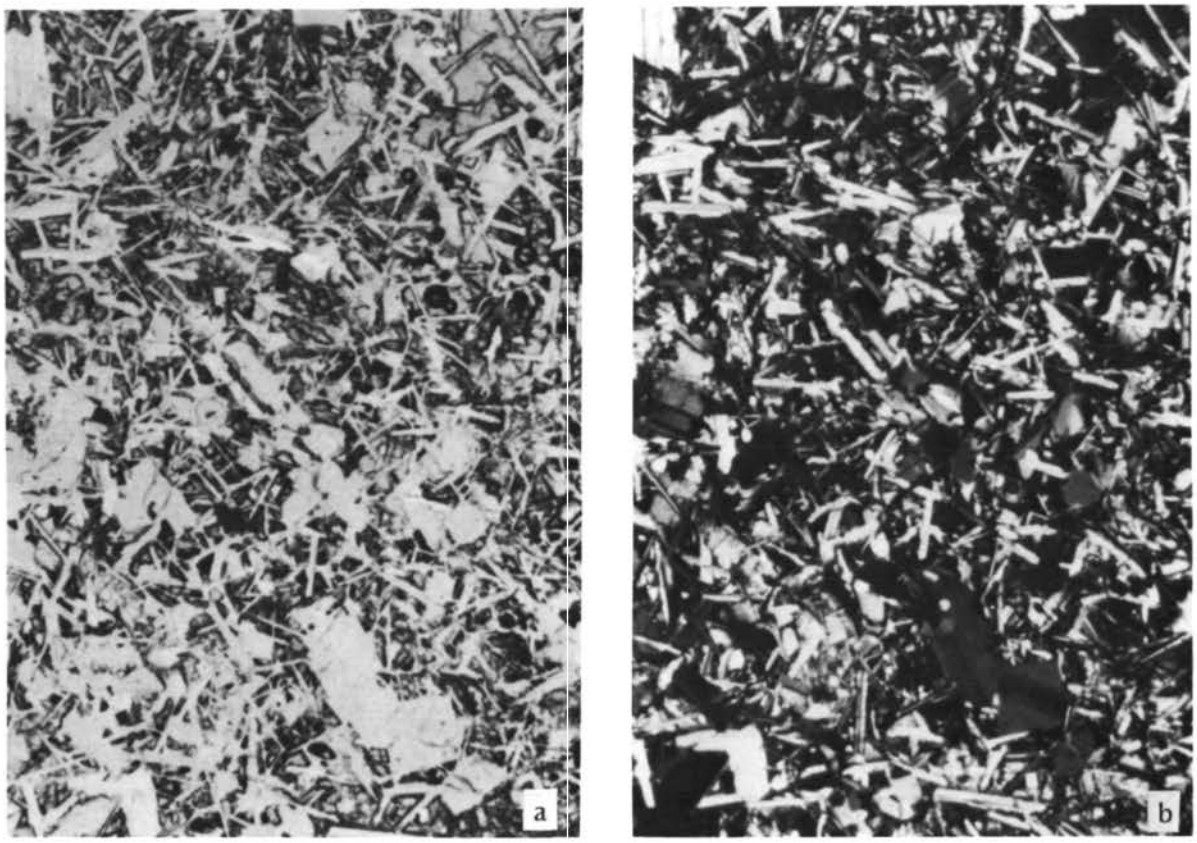


Figure 16.—*Porphyritic basaltic breccia 64817,3 (a) plane light and (b) crossed polars, showing the larger plagioclase grains developing a porphyritic texture. Note the much greater variation in grain size than in the ophitic basalts of figure 15 (long dimension = 1.8 mm).*

Devitrified glass-matrix breccias consist of intergrowths of very fine dendritic to spherulitic crystals and glass (fig. 20). The crystals often develop in fan and bow-tie patterns nucleated on relic grains. As the crystalline development becomes more extensive, this group grades into the basaltic matrix types of crystalline matrix breccias.

Interpretation

On the basis of our knowledge of previous studies plus our studies of textures and mineralogy, the summary interpretations of various lunar rock groups are shown in the right-hand column of table 1. In combination with chemical data, the textural diversity of breccias is attributed to various degrees of metamorphism or annealing in the nonmelted group (ref. 5) and various peak temperatures and cooling rates in the melt-derived group (ref. 3).

The remainder of this paper examines the possibility that the chemical diversity of lunar highland polymict breccias is the result of impact processes. Petrographic observations, combined with photogeologic and geochemical results, show that the lunar highlands have been subjected to continuous, extensive meteorite bombardment that has crushed, ground, and mixed the autochthonous and allochthonous material into a series of polymict breccias. We use petrologic and geologic arguments to suggest that those processes should have produced breccias with relatively homogeneous matrix compositions. Since the matrices, even within one landing site, are

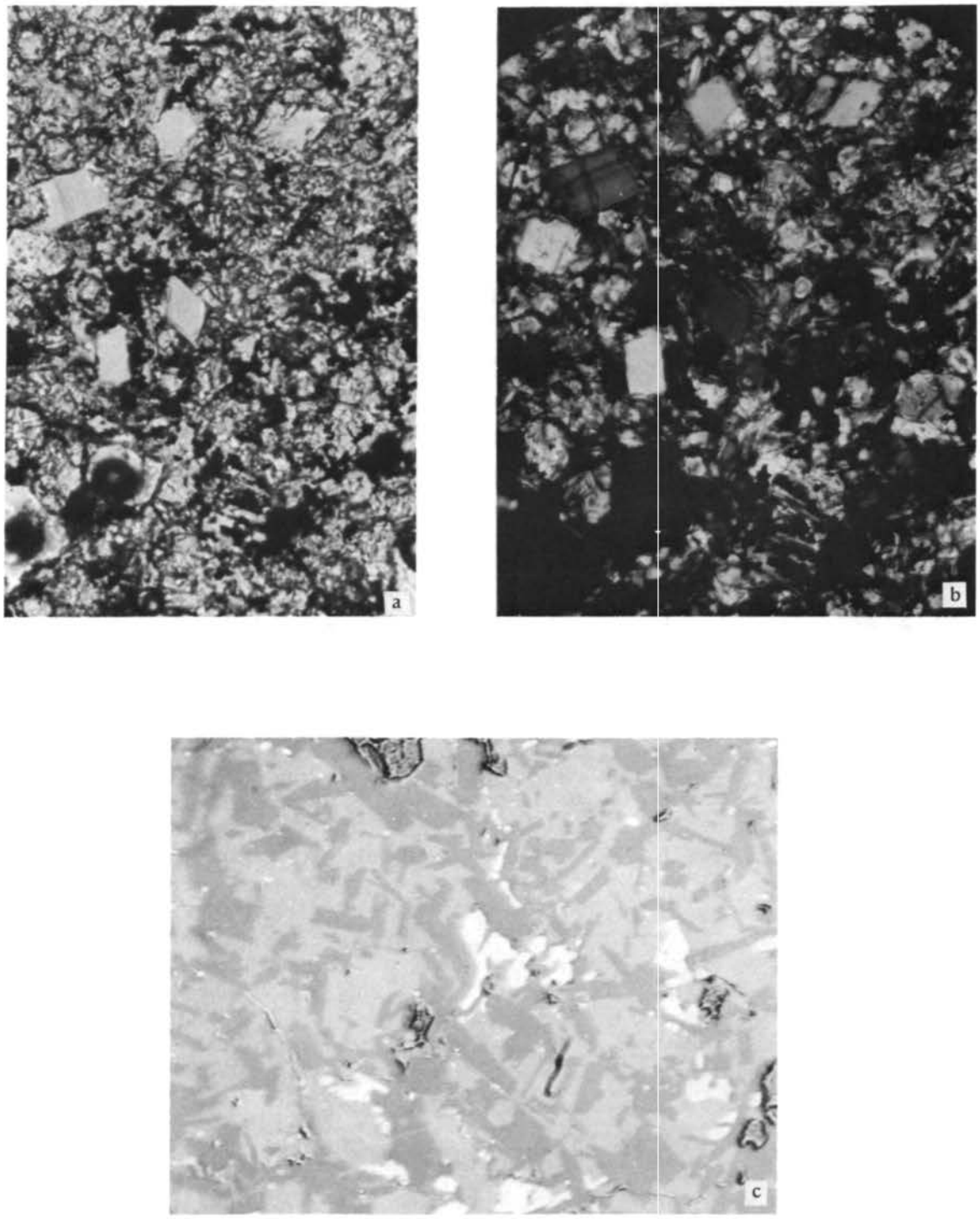


Figure 17.—*(a) Plane light and (b) crossed polars views of noritic breccia 63598,4. Note the barely resolvable to clearly seen laths of plagioclase (light gray) throughout the matrix. Most of the remaining light gray material is orthopyroxene. A few large plagioclase clasts are present (long dimension = 0.44 mm). (c) The lath-shaped plagioclase is best seen in high magnification under reflected light as in 72435,7 (long dimension = 0.18 mm). Dark gray is plagioclase and light gray is largely orthopyroxene.*

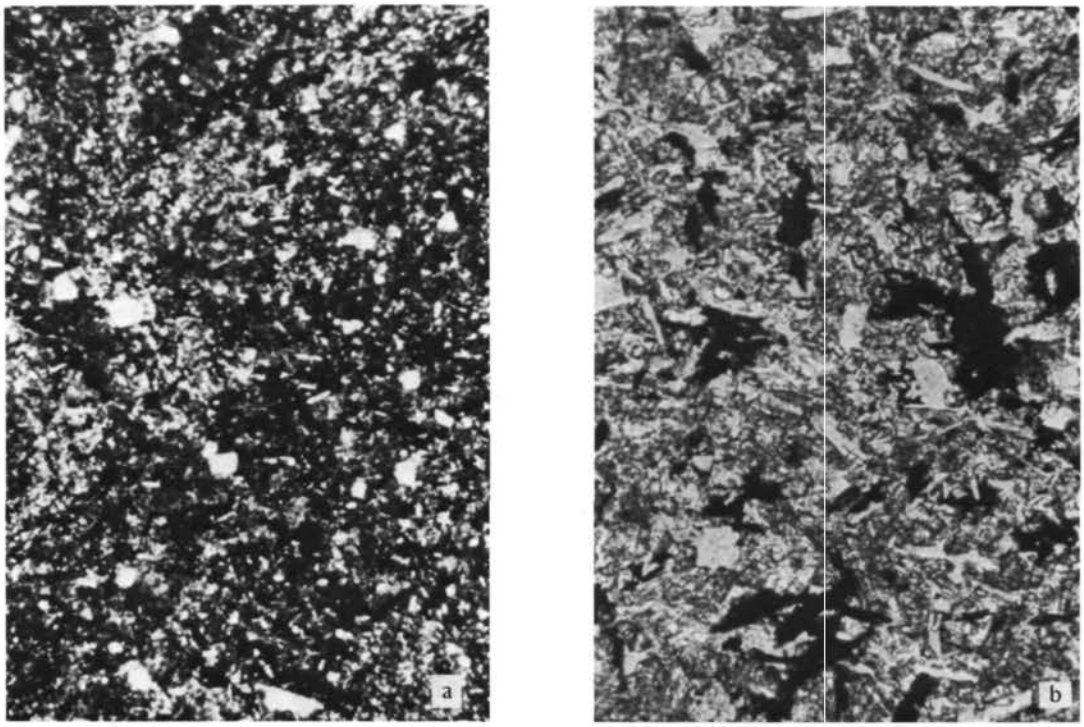
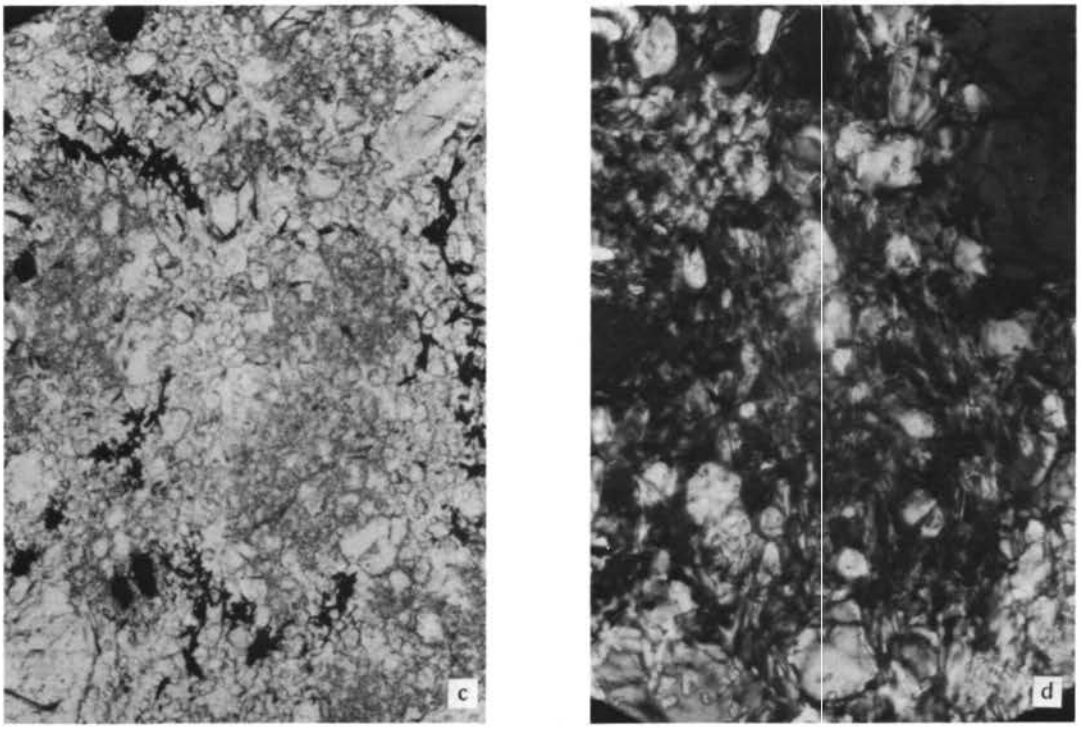


Figure 18a–d.—*Poikilitic matrix breccia 15414,11 (a) in crossed polars showing the pyroxene oikocrysts (large light gray and dark gray patches) (long dimension = 1.8 mm) and (b) in plane light at higher magnification showing the tabular to lathy forms of plagioclase (long dimension = 0.44 mm). Similar texture occurs in 76055,13 (c) in plane light showing oikocrysts (light gray and medium gray patches) (long dimension = 1.8 mm) and (d) in crossed polars showing the plagioclase laths in one of the oikocrysts. Note the alignment of plagioclase grains (long dimension = 0.44 mm).*



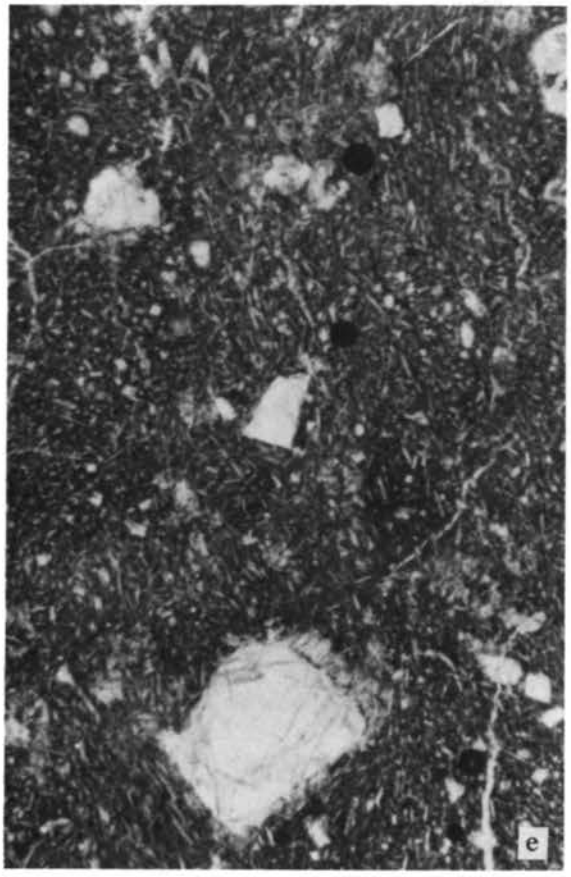
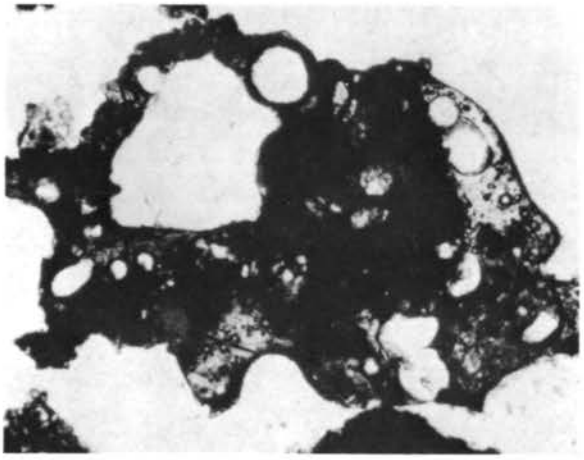


Figure 18e.—*(e) Sample 66035,2 in crossed polars showing several oikocrysts with plagioclase laths having consistent alignment through all of them (long dimension = 1.8 mm).*



not homogeneous, there must be a differentiation process that accompanies the crushing, grinding, and mixing of the impact process. Using phase equilibrium and geochemical data as support, we suggest that partial melting, accompanied by some separation of melt from residue, takes place within ejecta and/or fall-back blankets or in the wall rock of craters. This partial melting can account for the geochemical trends and the fact that the polymict breccias at each landing site have diverse compositions.

Petrographic Observations

Petrographic study of most lunar highlands breccias that have been thin sectioned (refs. 3, 5, 6, 18, and 22) yields several generalizations: (1) the breccias are polymict; (2) most breccias show evidence of multiple impact events; (3) the matrix of each breccia is homogeneous; and (4) breccias were deposited hot.

BRECCIAS ARE POLYMICT

The multiparent origin of highlands breccias may be established from mineral, glass,

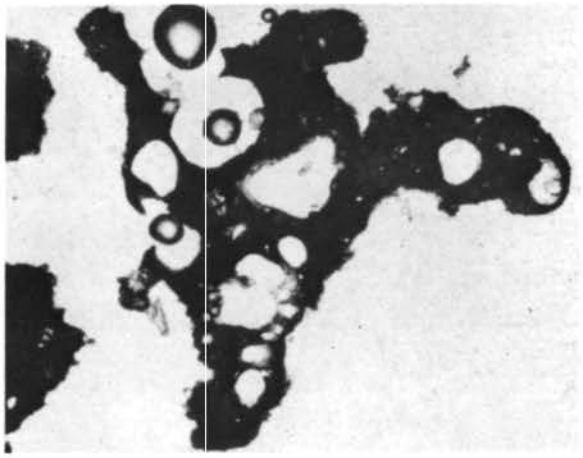


Figure 19.—*Plane light views of glassy matrix breccias from 14003,28. Dark areas are brown glass, white areas are vesicles, and gray areas are clasts (long dimension = 0.34 mm).*

and lithic clasts. The mineral clasts in any one breccia show a wide range of composition that would not be expected in a single igneous rock (ref. 5). One example of this diversity is found in rock 76255, a fragmental matrix breccia clast in a basaltic matrix breccia from Station 6 at Apollo 17. This rock contains clasts of inverted pigeonite alongside clasts of orthopyroxene, pigeonite, and augite (ref. 22).

Lithic clasts are not as numerous as mineral and glass clasts, especially in a single thin section, and therefore evidence from lithic clasts that lunar breccias are polymict is more difficult to obtain. However, it is common to find lithic clasts of both coarse-grained igneous rock and one or more different types of breccia in a single thin section. The lithic clast population has been studied in many thin sections of melt-rock breccias 76015 and 76315. Results are presented in reference 22 and indicate that each sample contains clasts that represent a wide range of lunar highlands rock types. Similar results have been obtained from a Station 2 boulder (ref. 23) and from Apollo 14 breccias (ref. 24).

Vitric breccias contain glass clasts ranging in color from yellow to brown to red. Moreover, the glass clasts generally do not display a continuum of colors, but rather exhibit several discrete colors. For example, 15294, from the Apennine front, contains yellow, deep orange, green, light brown, and tan glasses. These glasses, of different colors and compositions, must have formed from different parents.





Figure 20.—*Plane light views of divitrified glass-matrix breccias. (a) 67435,17 shows glass (light gray) at bottom left and various spherulitic crystal growths. (b) 64579,4 shows nucleation around margins of clasts (long dimension = 1.8 mm).*

The matrices of vitric breccias contain fragments of the same minerals, glasses, and rock types as found in the clasts, except the proportion of these materials is different. Lithic fragments are more abundant as clasts, whereas glass fragments are more abundant in the matrix. The similarity in types of material in clasts and matrix and the seriate grain-size distribution of the matrix and clasts suggest that the matrix and the clasts are derived from the same set of parents. The extremely fine grain size of the matrix of fragmental matrix polymict breccias (on the order of < 1 to 5 μ) illustrates the pervasiveness, extent, and multiplicity of impact comminution.

EVIDENCE FOR MULTIPLE EVENTS

Petrographic evidence that many breccias represent multiple events has been well documented by Wilshire and Jackson (ref. 24). They found that breccia clasts within breccia clasts within the main breccia were common, and in rare cases they documented occurrences of breccia within breccia within breccia within breccia. Each generation of breccia clasts has different compositions and textures which indicate different parents and thermal histories. The number of observed breccia-in-breccia relations must be taken as a minimum number of brecciation cycles for a given rock because the intense recrystallization and melting that the current, and preexisting, breccias underwent would obscure the recognition of prexisting breccia clasts. Breccia-in-breccia texture is observed in single impact events (e.g., at the Reis Crater). However, the scale of Reis breccia-in-breccia texture is meters (ref. 25), whereas in the lunar case the scale is millimeters.

BRECCIA MATRIX IS HOMOGENEOUS

The matrices of polymict breccias are petrographically homogeneous on the scale of millimeters. That is, the texture, grain sizes, mineral abundances, and mineral compositions are the same within several 1-mm-square areas across a single thin section, and from thin section to thin section of one rock (e.g., ref. 5). Homogeneity studies have been carried out on the matrices of two samples (76015 and 76315), from a large boulder and reported in detail by Phinney et al. (ref. 26) and Simonds et al. (ref. 22). These studies include major element chemistry, minor element chemistry, trace element chemistry, mineral chemistry, and petrographic observations of the texture and modal abundances of minerals. Data from several samples separated by several centimeters in each rock yield essentially identical results, indicating that the matrix of each sample is homogeneous on the scale of the aliquots studied—30 mm^3 for chemistry and 1 mm^2 for petrography. The chemistry of 76015 and 76315 is nearly the same, indicating chemical homogeneity on a scale of meters between two textural units of a large boulder. That the matrix of breccias is homogeneous is not surprising in view of the fact that analyses of many lunar breccias performed by different laboratories, on different aliquots of the same rock, for a variety of elements, are about the same. For example, there are nine determinations of Al_2O_3 from sample 14310 which range from 20.0 to 21.7 wt%, and eight from sample 60315 range from 16.4 to 17.8 wt% (data from the Lunar Sample Curator's data base).

BRECCIAS WERE DEPOSITED HOT

Analysis of petrologic and geochemical data for vitric and recrystallized breccias (ref. 27), combined with the experimental sintering data of Simonds (ref. 20), suggests that vitric breccias were deposited at temperatures on the order of 700°C and the recrystallized breccias at progressively higher temperatures up to approximately 1000°C. Warner et al. (refs. 3 and 18) and Simonds et al. (ref. 28) demonstrated that many of the Apollo 16 breccias contain matrices that were clast-laden liquids. Statistical studies of 2- to 4-mm soil fragments by Delano et al.

(ref. 1) indicate that melt-rock breccias constitute about one-third of the Apollo 16 site. Bence et al. (ref. 29) show that a similar fraction of the Apollo 17 highlands are melt-rock breccias. Phase equilibrium studies on these compositions by Walker et al. (ref. 30) and Hodges and Kushiro (ref. 9) show that the matrices of these breccias must have reached 1200° or 1300°C. Although the details of processes that heat ejecta and fall-back blankets are not understood, the data are irrefutable that the breccias were formed in hot-ejecta blankets. This suggests that abundant thermal energy is available in ejecta blankets.

Extent of Mixing in the Lunar Highlands

Petrographic evidence indicates that lunar breccias, which comprise about 90 percent of the returned lunar highlands rocks, were formed by multiple meteorite impacts from many parents. The physical processes involved are crushing, grinding, and mixing. The rarity of nonmixed (i.e., fine-grained and coarse-grained igneous) rocks, the wide range of lithic clasts types found in several breccias, and the chemical and petrographic homogeneity of breccia matrices suggest that impact mixing has been an extensive and efficient process in the lunar highlands. This is not surprising in view of supporting data from photogeology, cratering studies, geochemistry, and the abundance of mixed versus unmixed rocks.

The numerous overlapping meteorite impact craters observed on any photograph of the lunar highlands attests to the pervasiveness of impact-induced mixing. Head (ref. 31) has emphasized the importance of the many local 10 km and larger craters to the Apollo 16 samples. Hartmann (ref. 32) has shown that the cratering rate prior to the deposition of the Fra Mauro formation was 1.5 to 2 orders of magnitude greater than since Fra Mauro time. Short and Foreman's (ref. 33) calculations show that ejecta from only the visible craters average out to a uniform layer 1 to 2 km thick. Secondary impacts will enhance the mixing effects of primary impact. Oberbeck (ref. 34) and Oberbeck et al. (ref. 35) show that the total mass of material moved by the secondaries may be larger than the mass moved by the primary impact. Thus, virtually all material in the upper few kilometers of the Moon should be thoroughly mixed.

Siderophile element (e.g., Au) concentrations in the polymict breccias and soils are 1 to 2 orders of magnitude higher than equivalent values for fine-grained and coarse-grained igneous rocks (refs. 36 and 37). Following Ganapathy et al. (ref. 38), the Au content of igneous rocks is a measure of the siderophile element concentrations that are indigenous to the Moon, and the higher values in soils and polymict breccias represent contamination by meteorites. Thus, siderophile element concentrations may be used as an index to the mixed versus the nonmixed rocks. The uniformly high concentration of Au and other siderophile elements in all analyzed polymict breccias (except 15205 (ref. 39)) is further corroborative evidence that the highlands have been extensively mixed by impacts.

At the Apollo 14 and 16 sites where there is no nearby mare material, the rocks show a wider composition range than the soils (table 2). Soils are about 95-percent degraded local bedrock, and the rocks are samples of the local bedrock. The narrower range of soil compositions is thus an indication of the effectiveness of the mixing process during the last 10^9 yr, when the impact rate has been much less intense than during the time of formation of highland rocks. Further, because the soils appear to be well-mixed local material, they are used to approximate the composition of the local crust.

The Apollo 15 and 17 sites straddle mare-highland boundaries, and the rock-soil relations are obscured. The soils define a linear trend from the field of mare rocks to the field of highland rocks (as illustrated in fig. 21 for Apollo 17). This is due to recent mixing between a "mare average" and a "highland average." The "highland average" com-

Table 2.—*Range of Composition of Selected Elements and Oxides in Highland Polymict Breccias and Soils*

	Apollo 14		Apollo 15		Apollo 16		Apollo 17	
	Breccias[1]	Soils[1]	Breccias[1]	Soils[1, 2]	Breccias[1]	Soils[1]	Breccias[1]	Soils[2, 3]
TiO (%)	1.4–1.7	1.6–1.8	.3–1.4	1.27	0.3–1.7	0.4–0.7	0.2–1.5	1.24
Al_2O_3 (%)	14.8–22.2	16.2–17.7	15.2–23.5	17.38	17.2–31.2	26.0–29.0	17.0–27.0	21.42
FeO (%)	6.7–11.0	10.0–10.9	5.9–15.0	11.65	3.2–10.5	4.1–6.2	5.1–11.6	8.14
MgO (%)	8.3–13.7	9.2–10.2	9.4–13.3	10.36	2.3–15.1	4.2–6.3	6.1–16.3	9.94
CaO (%)	9.1–12.8	10.2–11.3	10.3–13.7	11.52	10.4–18.3	15.0–16.5	9.9–15.2	13.06
K_2O (%)	0.15–0.87	0.50–0.60	0.08–0.17	0.17	0.03–0.49	0.05–0.16	0.06–0.30	0.15
P_2O_5 (%)	0.22–0.63	0.40–0.58	0.02–0.55	0.13	0.02–0.48	0.06–0.15	0.03–0.35	0.12
Sm (ppm)	20–42	29–31	3–13	~10	2–27	3–7	2–25	—
Sr (ppm)	180–230	177–181	113–268	142	139–235	167–188	111–177	151

NOTES: (1) Data from Curator's data base, Curator's Office, Johnson Space Center, Houston.
(2) Data presented are "highlands average" as described in text.
(3) Data from LSPET (ref. 40) and Rhodes et al. (ref. 41).

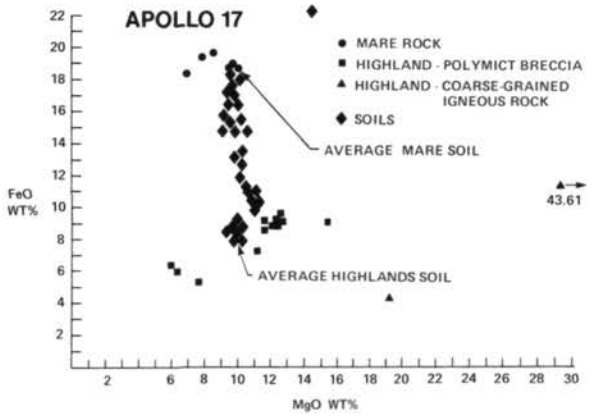


Figure 21.—*FeO-MgO plot of Apollo 17 rock and soil analyses. "Average mare" and "average highlands" soils are described in the text. Data are from the Curator's data base.*

position, as set out in table 2, may be used to approximate the local highland crust at Apollo 15 and 17.

The abundance of various highland rock types also provides supporting evidence as to the extent of highland impact mixing. The only nonmixed highlands samples are the fine-grained and coarse-grained igneous rocks. Nonmixed materials (both as individual rocks and as clasts in polymict breccias) make up less than 15 percent of the mass of returned highlands samples. Further, the nonmixed rocks themselves are generally small—a few centimeters across or less (sample 61016, a black and white rock, is an exception—the cataclastic anorthosite part is about 10 cm thick).

The extent of impact mixing in the lunar highlands suggests *a low probability that large amounts of nonmixed rock could survive on or near the surface of the lunar highlands for a long time.* This does not imply that no nonmixed rock can survive. Impact comminution is a random process and a few nonmixed rocks can survive numerous impact events, but nonmixed rocks cannot form a major proportion of the highlands samples. One exception, which should be rare and local, is if the formation and/or emplacement of the nonmixed rock onto the lunar surface was near the end of the evolution of the highlands.

The petrographic and chemical homogeneity studies suggest that the upper limit for effective mixing is greater than tens of cubic meters, and the lower limit is less than a cubic centimeter. Obviously a few grains at a time, taken in sets, should not be homogeneous. The lower limit thus appears to be less than a cubic centimeter but more than a few grains, probably a few thousand grains.

Because soils at each highland landing site are very similar in composition and thus

relatively homogenized (except for later local mixing at contacts with nearby mare material), the upper limit for effective mixing must be larger than a landing site (which is on the order of several square kilometers). Without a doubt there are major lateral heterogeneities in the lunar highlands as evidenced by the orbital XRF and γ-ray experiments (refs. 42 and 43). Because the local average crust (soil) composition is different at each landing site, the limit must be less than the inter-landing-site distances (which are on the order of 10^3 km). The resolution element of the orbital XRF and γ-ray experiments is not clearly defined, but it is on the order of tens of kilometers across, and the orbital data as plotted (refs. 42 and 43) suggest that these resolutions are close to the scale of lunar surface homogeneity. The upper limit of effective mixing thus appears to be about tens of kilometers across.

The arguments and data cited in this section suggest that within most regions of the lunar highlands that are on the order of several hundred square kilometers, there should have been adequate impact mixing to produce polymict breccias with relatively homogeneous matrices. That is, we predict that within any small area (up to 100 km^2) of the lunar highlands that is chosen at random the bedrock will consist of polymict breccias that are all of about the same composition. Reference to table 2 shows that this prediction is wrong.

Paradox and a Solution

The diversity of breccia compositions at each highland landing site has been well established (refs. 40, 44, 45, and 46). We use Apollo 16 as an example since it contains the most diverse highlands rock compositions and the landing site lies well within the lunar highlands. Figure 22 shows that the diversity of Apollo 16 rock compositions forms a linear trend from aluminous basalt (KREEP) (CaO = 10–12 wt%; Al_2O_3 = 17 wt%) to anorthosite (CaO = 19–20 wt%; Al_2O_3 = 35 wt%). The one sample that plots

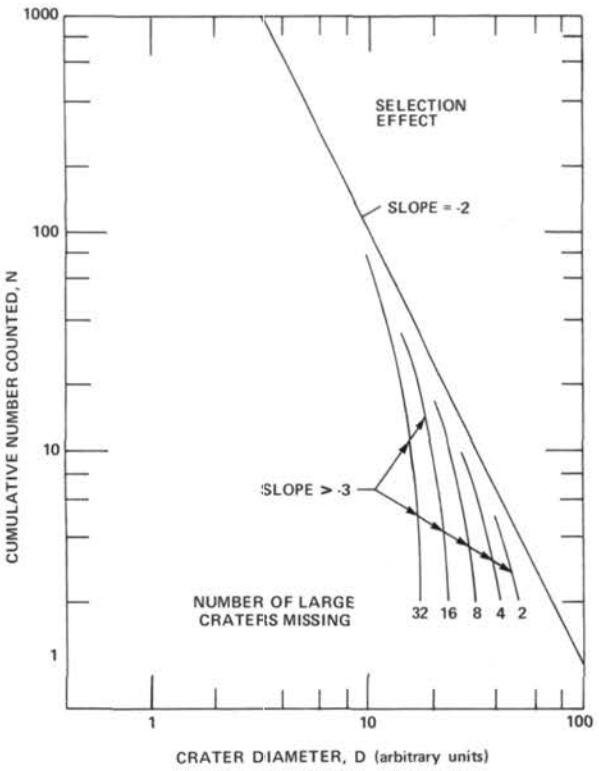


Figure 22.—*CaO-Al_2O_3 plot of Apollo 16 rock and soil analyses. Data are from the Curator's data base.*

off this trend at 6 wt% CaO and 16 wt% Al_2O_3 (a spinel troctolite (ref. 47)) and several of the rocks at the anorthositic end are coarse-grained igneous rocks; the remainder are polymict breccias (ref. 18). Soil compositions lie on the rock trend, but with a much narrower composition range (15–16.5 wt% CaO; 26–29 wt% Al_2O_3). The average soil composition is taken to approximate the local average crustal material and is used as the starting point for petrochemical processes that take place after impact mixing.

We have shown above that meteorite impacts crush, grind, and mix material; that this material is deposited hot; and that it lithifies into polymict breccias. We argue that impact mixing is so efficient it compels the prediction that breccia matrices should be homogeneous from rock to rock within some ill-defined-sized region of the lunar highlands. Yet the rock analyses (which are

essentially matrix analyses because clasts larger than about 2 mm are separated from the analyzed material) from any landing site are not homogeneous. This incompatibility between prediction and observation presents a paradox.

There are two explanations for this paradox: the prediction that the highland breccias are well mixed is wrong or the diversity of breccia compositions is due to some differentiation process that takes place after impact mixing.

The first explanation that impact mixing is not extensive has two alternatives: (1) the diversity of rock compositions is old (it either dates from crustal formation or pre-4.3 AE volcanism) and the subsequent impact events have not caused significant chemical mixing or (2) the diversity of rock compositions is young (3.9–4.3 AE volcanism) and the breccia petrography is due to contamination with, and/or partial assimilation of, regolith. The evidence for mixing set out above makes alternative (1) unlikely. If alternative (2) were the explanation, we would expect to find volcanic rocks that were not contaminated by regolith; and essentially none have been found in the highlands. The even distribution of mineral and lithic clasts does not suggest that they are xenoliths and xenocrysts. If the melt-rock breccias were volcanic, we would expect some coarser grained equivalents; the latter are not found, and, in fact, the breccias are an order of magnitude finer grained than the mare basalts, suggesting a formational process other than volcanism. For these reasons, and others discussed in the last paragraph of the section on the definition of rock types, we do not accept the first explanation for the paradox.

The second and favored explanation for the paradox calls for a differentiation process to take place during formation of the breccias so that the repeated mixing is partially undone. The fact that the breccias were formed between 700° and 1300°C suggests the presence of adequate thermal energy (within ejecta and fall-back blankets and in the heated wall rock of craters) to drive petrochemical processes. Processes that may be associated with impacts and could cause differentiation are selective volatilization, crystal fractionation in pools of impact melt, and partial melting.

Volatilization does not appear to be a significant process, since the trend in the breccia compositions is not the trend of vaporization. Volatilization would selectively remove alkali elements, but the breccias show a covariant trend in CaO and Al_2O_3 and no evidence of alkali loss. Furthermore, the alkali element concentrations are so low in lunar material (even KREEP) that volatilization loss should not be a major process of highland petrogenesis. The necessity of bringing a large fraction of lunar surface material to within 1 mm of the lunar vacuum while that material is hot in order for volatilization to be effective seems impossible.

Crystal fractionation in a pool of impact melt of the local average crustal composition could adequately account for the chemistry of the breccias; the observed trend is essentially due to feldspar enrichment plus minor Fe/Mg variation. A major problem with crystal settling is that an impact melt would not be a conducive environment for such a process to take place. Melt-rock breccias are glassy to very fine grained, which suggests cooling rates so rapid that crystal settling could not be effective. Terrestrial basalts, which are coarser grained and thus may have cooled more slowly, do not show crystal settling in lava lakes tens of meters thick. Also, impact melts are laden with mineral and lithic clasts which would hinder crystal settling and, in fact, should themselves settle.

Partial melting processes are controlled by the phases melted: the first melt from the Apollo 16 local average crustal composition should appear at the olivine-pyroxene-feldspar peritectic. Walker et al. (ref. 48) have shown that the peritectic has an aluminous basalt (KREEP) major element composition ($CaO \approx 12$; $Al_2O_3 \approx 16$ wt%) which plots at one end of the trend in figure 22. Further partial melting will produce melts along the olivine-plagioclase cotectic and toward the local average crust; the rocks that

fall in this range are melt-rock breccias. The residue will be more anorthositic, and that is where the potential residue candidates among the Apollo 16 rocks lie on figure 22.

STATEMENT OF THE MODEL

The model we propose to explain the variety of breccia compositions is illustrated in figure 23 and outlined below:

1. Continuous grinding, crushing, and mixing of surface and near-surface materials occur as a result of primary and secondary impacts from the time of crustal formation to about 3.85 AE. This step is represented in figure 23 by the MIXING oval and the arrows leading into it. The product is a homogeneous mixture of fine-grained and coarse-grained igneous rocks, preexisting polymict breccias, and regolith material deposited in ejecta and fall-back blankets. This mixture, which approximates the LOCAL AVERAGE LUNAR CRUST in composition, is the material that further processes act upon.
2. Those parts of the mixed deposits that do not attain temperatures of about 700°C form regolith or SOIL.
3. Those parts of the mixed deposits that attain temperatures above 700°C but below 1200°C lithify into VITRIC BRECCIAS and RECRYSTALLIZED BRECCIAS.
4. Those parts of the mixed deposits that attain temperatures above about 1200° will start MELTING following the normal rules of phase equilibrium. There will be at least a partial separation of MELT (with included mineral and lithic clasts) from RESIDUE. The melt will crystallize into basaltic matrix and poikilitic matrix (MELT-ROCK) breccias, and the residue will form some sort of breccia, perhaps a LIGHT MATRIX BRECCIA.
5. There will be many impacts that aid in homogenizing the deposits, whereas there will be relatively few impacts that are accompanied by partial melting and separation of melt and residue.
6. The partial melting may take place in an ejecta blanket, a fall-back blanket, or within the deposits that form the wall rock of craters.

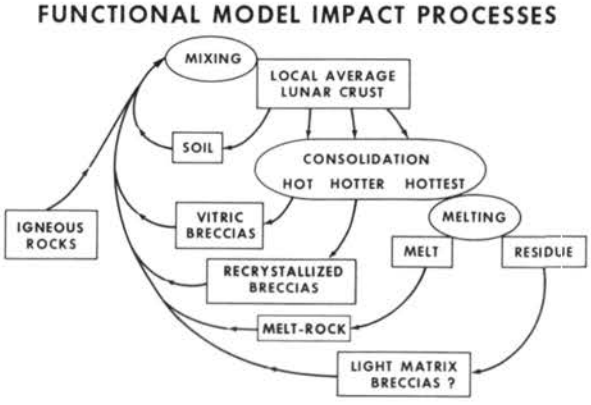


Figure 23.—*Schematic representation of the impact mixing and partial melting model that explains the diversity of polymict breccia compositions. Boxes represent various spinel-bearing microtroctolites.*

Such a partial melting process can explain the observed diversity of breccia compositions. Below we examine if partial melting of the local average crustal composition is consistent with the chemical data and discuss evidence bearing on the problem of separation of melt from residue and identification of the residue. As is pointed out below, there are problems with this model, especially in regard to Fe/Mg ratio evolution. Although some details of the model are surely wrong, we stress that the data demand that some sort of chemical fractionation process must take place in ejecta and fall-back blankets.

Chemical Tests of Partial Melting

There are six points of chemical data used to test impact partial melting. None of these prove that impact partial melting is the major process responsible for the diversity of highland breccia compositions. Rather, they

show that a low-pressure partial melting model is consistent with the chemical data.

The range of rock compositions at each highland site has some major similarities. The local crustal average composition would yield an aluminous basalt (KREEP) as the first liquid during partial melting, and rocks with that composition are found at each site. Two sites, Apollo 16 (see figure 22) and Luna 20 (ref. 4), have rocks that are more aluminous than the first melt but less aluminous than the parent composition. Those rocks may have formed by larger amounts of partial melting than that required to form the aluminous basalt. Finally, each site contains rocks that are more aluminous than the parent composition. These rocks may be residues.

The general major element variations that would be expected in this series are not completely present. The Fe/Mg ratio decreases from the aluminous basalts to the rocks formed by larger amounts of partial melting, but the decrease does not continue through the local average crustal composition to the residue. This problem could be explained if impact crushing and grinding systematically biased the finer grain-size fractions to more mafic compositions, and this finer fraction were the first material melted. There is evidence that mafic minerals (refs. 49 and 50) and trace elements (ref. 51) are fractionated into finer grain sizes.

The aluminous basalt at each landing site is different in detail in both major and trace elements (ref. 52). This difference shows up in the Fe/Mg ratio and the trivalent lithophile trace elements. In the impact-generated partial melting model, these small but significant differences may be accounted for by corresponding differences in the trace element content and Fe/Mg ratio of the local average crust and different partial melting histories.

There is a correlation between the trivalent lithophile trace elements and major elements at each site as shown by Haskin et al. (ref. 53) and Hubbard et al. (ref. 52) for Apollo 16. For example, the total rare earth element content decreases with increasing Al_2O_3 content in the breccias. Since the trivalent lithophile trace elements occur in accessory minerals, the first liquid generated during partial melting will contain most of these elements, and the first liquid contains the lowest Al_2O_3, yielding a liquid with high trace elements and low Al_2O_3. If we use local soil as a model of the material that was partially melted, an enrichment factor of only 5 or less is needed to produce the trace element concentrations in the low Al_2O_3 breccias. With increased partial melting, the Al_2O_3 content of the liquid increases, and the trace element contents are lowered by dilution.

Taylor et al. (ref. 54) have demonstrated that highland-wide, positive, one-to-one correlations exist among total rare earth elements, Ba, Hf, Nb, Th, and Zr. Hubbard (ref. 52) and Haskin et al. (ref. 53) have pointed out the consistency of the slope of the rare earth elements when normalized to chondrites, which corresponds to the one-to-one correlations found by Taylor et al. (ref. 54). Because these elements occur in the accessory minerals, the first melt will contain most of them and there will be no differential fractionation of the trivalent lithophile trace elements. Further partial melting will simply dilute the abundances that occur in the first liquid. The partial melting model does not specify the slope of the rare earth elements, but once that slope is established as characteristic of the lunar highlands, the partial melting model propagates it.

Although these interelement correlations between major and trivalent lithophile trace elements do not constitute proof of the proposed impact partial melting, the relations are so striking that they demonstrate a general genetic relationship among the highland breccias. The weight of geochemical evidence argues for partial melting as the basic process. If the diversity of compositions of highland breccias was due to partial melting of different source regions in the lunar interior, the chemical relations would be expected to show discontinuities in the correlations, and these discontinuities do not exist. Partial melting in homogenized ejecta

blankets would not produce discontinuities.

The Ar^{39}–^{40} and Rb-Sr data for highland breccias yield crystallization ages between 3.85 and 4.05 AE for the majority of the samples, with a few measurements as old as 4.25 AE (refs. 55, 56, and 57). This spectrum of ages would be expected for continuous impact mixing and partial melting in ejecta blankets. The sharp cutoff of ages at 3.85 AE indicates the time that meteorites large enough to cause extensive mixing and partial melting stopped impacting the Moon on a regular basis. The range in ages of about 200 m.y. suggest that toward the end of highland formation meterorites large enough to cause partial melting impacted the Moon with a frequency such that there was an effective thermal cycle time in the highlands of about 200 m.y.

Rb-Sr and U-Pb data on highland breccias yield "whole rock isochrons" of about 4.3 to 4.4 AE (refs. 57 and 58). Nyquist has suggested that these model ages indicate a major lunar differentiation at that time. Tera et al. (ref. 58) give two explanations for the data. Either the model age is the age of the lunar crust for a simple two-stage model, or ". . . about one-half of the crust formed between 4.6 to 4.5 AE, and the remainder evolved uniformly down to ~ 3.9 AE." In the latter case the initial ratios (of both Pb and Sr) and the age would "represent an average of the rocks sampled and mixed during . . . impacts." This latter interpretation is consistent with our model of continuous impact mixing and partial melting.

We have performed calculations of Rb-Sr evolution to test our geologic model. Visualize that all Rb^{87}, Sr^{86}, and Sr^{87} are contained in one or more "pots." The calculations start with one "pot" that contains $Sr^{87}/Sr^{86} = 0.6990$ (BABI) and $Rb^{87}/Sr^{86} = 0.05$ at 4.6 AE. The calculations iterate every 0.1 AE from 4.6 AE to 3.9 AE. Within each iteration the following processes are calculated:

1. All existing "pots" are allowed to age for 0.1 AE.
2. The mechanical aspects of impact are simulated by sampling all existing "pots" and combining the sampled material into one "temporary pot." The sampling algorithm removes half of the material in 0.1 AE old "pots," half of the remaining material in 0.2 AE old "pots," and all the remaining material in 0.3 AE old "pots." Thus, at any time there are "pots" of three ages with a spread of 200 m.y. to agree with the spread in observed crystallization ages.
3. The chemical aspects of impact (i.e., partial melting) are simulated by fractionating the "temporary pot" into a new Rb-rich (melt) "pot" and a new Rb-poor (residue) "pot." This part of the calculation contains two variables: the partitioning of Rb between the two new "pots" and the partitioning of Sr between the two new "pots." There is no Sr isotopic fractionation.

At this stage of the calculation the formation of the highlands is essentially complete, and the systems are allowed to age for 3.9 AE to the present. We have calculated models that use various expressions for the Rb and Sr partition variables, and many of these yield similar results (fig. 24). Although the results do not provide a perfect match to the observed data, they show that no major problems exist with our model of impact partial melting. For example, the calculations demonstrate that the residues will not have extremely high (> 5.0 AE) model ages with BABI.

Separation of Melt and Residue

Physical separation of partial melt and residue is necessary for the proposed model to be effective. However, the reader should keep in mind that the mechanical details of separation are not really understood for the case of terrestrial migmatites or basalts, although evidence is exceedingly strong that such separations do take place. We hope that this model will not be judged on how well the separation process is specified. The scale of separation of partial melt within an ejecta

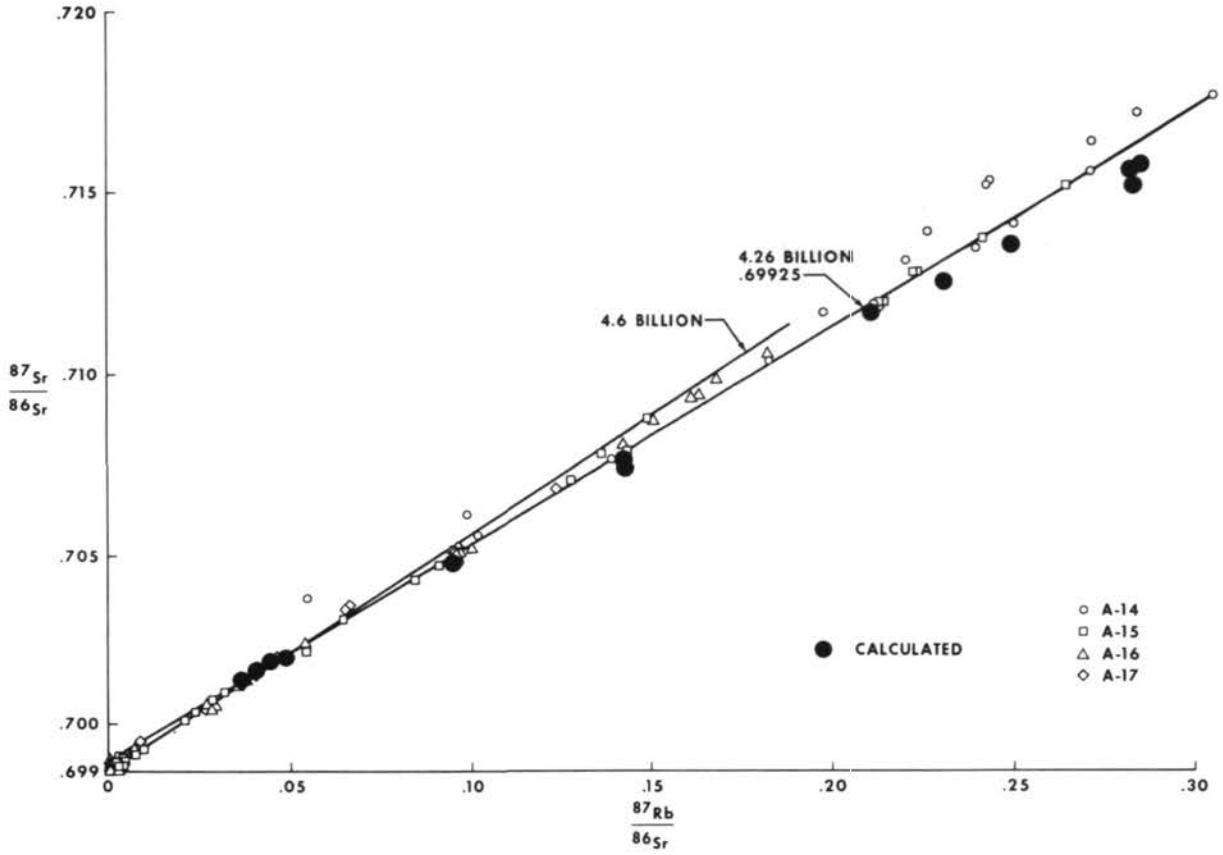


Figure 24.—*Rb-Sr evolution diagram showing whole-rock data for lunar highlands rocks. The results of our calculated Rb-Sr evolution are shown for comparison. The calculations are based on the impact mixing and partial melting model and are described in the text. Data are taken from Nyquist et al. (refs. 58 and 59), Papanastassiou and Wasserburg (refs. 60, 61, and 62), and Tera et al. (ref. 63).*

blanket is small compared to separating basaltic magma from the Earth's mantle; the largest known mass of rock that could be considered formed by impact partial melting is the boulder at Station 6 on Apollo 17. That boulder represents about 10 stratigraphic meters and contains three layers (ref. 64), perhaps suggesting that each layer represents a separate event. Calculations by Brett (ref. 65) based on petrologically derived cooling rates indicate that layers of melt-rock breccia were not more than several meters thick.

Returned samples display partial melts (presumably formed during impact) that have separated. Samples 64455 and 65075 show partial melting and separation of the melt on the millimeter scale (ref. 66). Similar separation of partial melt and residue has been documented by Phinney et al. (ref. 6) from KREEP fragments found at Station 7 on Apollo 15. Segregation of a partial melt into small pods and 100-μ veins has been suggested for 67075 by Lunar Sample Preliminary Examination Team (LSPET) (ref. 46).

The black and white rocks from Apollo 15 and 16 consist of angular veins of clast-laden melt-rock breccia (black) that intrude cataclastic anorthosites and cataclastic norites (white) and are examples where melt has migrated some unknown distance (but at least 1 cm) and injected a fractured, refractory rock.

The small size of returned lunar samples precludes finding examples of separation on the meter scale. Pools of melt on the kilo-

meter scale occur on the floors and ejecta blankets of highland craters (e.g., the King and Tycho craters (ref. 67)). These pools may be total impact melts or separated partial melts, but in any case they occur in an ejecta environment.

Finally, if there were mechanical fractionation of the lower melting material into the finer grain sizes as was suggested above, that process would accomplish much of the required separation of partial melt and residue.

Identification of the Residue

The residue from the proposed partial melting in an ejecta blanket must meet well-defined chemical criteria. Phase equilibrium relations dictate that the residue must be higher in Al_2O_3 and CaO and lower in TiO_2, K_2O, Fe/Mg ratio, and all trivalent lithophile trace elements.

We cannot predict what the texture of the residue should be. Rocks that meet the chemical criteria include cataclastic anorthosites (e.g., 61016), light matrix breccias (e.g., 67955), melt rocks (e.g., 68815), and metamorphosed breccias (e.g., 61295). Hubbard et al. (ref. 68) have suggested that there are two types of anorthosites with higher and lower Sr^{87}/Sr^{86}. Perhaps the low Sr^{87}/Sr^{86} anorthosites are derived from the Moon's original crust and the high Sr^{87}/Sr^{86} anorthosites are partial melting residues. However, the monomict nature of the anorthosites is not consistent with their being the residue from the impact partial melting of a polymict breccia, unless they were the clasts. We suggest that the residue is probably a polymict breccia or granulite of some type—the light matrix breccias appear to be prime candidates. This is a subject that demands considerable study.

Conclusions

The general petrogenesis of the Moon is best understood by the interpretation of primary rock types returned by the Apollo and Luna missions. It is therefore imperative that we can unambiguously identify the primary rocks. This paper shows how difficult that problem is. Although fine-grained and coarse-grained igneous rocks are probably primary, the bulk of the returned highland rocks are polymict breccias, and this paper demonstrates that the polymict breccias are not primary rocks. Polymict breccias were formed in impacts, and the crushing, grinding, and especially mixing that take place during impact do not allow the preservation of original chemistry, but should produce homogeneous breccias.

There is a paradox between compelling evidence that the breccias should be about the same composition and the wide range of compositions displayed by the returned highland breccias. This paradox demands a differentiation process after the impact mixing. A process that may explain the heterogeneity is partial melting and separation of melt and residue in ejecta and fall-back blankets or in the wall rock of craters. We are now investigating the possibility of even better fits of chemical, petrographic, and impact data resulting from a mechanical concentration of mafic and accessory minerals into the finer grained fraction of regolith and preferential melting of this lower melting temperature material.

Finally, the processes that we discuss are not of major importance on Earth, but seem to be on the Moon. Recent photographs of the surface of Mars and Mercury show those planets to be intensely cratered like the Moon. Perhaps the processes discussed in this paper will have application to those planets.

Acknowledgment

The authors have greatly benefited from stimulating discussions with their colleagues, especially A. Albee, G. Heiken, F. Hörz, G. Lofgren, and L. Nyquist. However, any errors are those of the authors. Mr. Simonds is a Staff Scientist at the Lunar Science Institute which is operated by the Universities Space Research Association under NASA Contract No. NSR 09–051–001.

References

1. DELANO, J. W., A. E. BENCE, J. J. PAPIKE, AND K. L. CAMERON, Petrology of the 2–4 mm Soil Fraction From the Descartes Region of the Moon and Stratigraphic Implications. *Proc. Fourth Lunar Science Conference, Geochimica et Cosmochimica Acta*, Supplement 4, Vol. 1, 1973, pp. 537–551.
2. TAYLOR, G. J., M. J. DRAKE, J. A. WOOD, AND U. B. MARVIN, The Luna 20 Lithic Fragments, and the Composition and Origin of the Lunar Highlands. *Geochimica et Cosmochimica Acta*, Vol. 37, 1973, pp. 1087–1106.
3. WARNER, J. L., C. H. SIMONDS, AND W. C. PHINNEY, Apollo 16 Rocks: Classification and Petrogenetic Model. *Proc. Fourth Lunar Science Conference, Geochimica et Cosmochimica Acta*, Supplement 4, Vol. 1, 1973, pp. 481–504.
4. PRINZ, M., E. DOWTY, K. KEIL, AND T. E. BUNCH, Mineralogy, Petrology and Chemistry of Lithic Fragments From Luna 20 Fines: Origin of the Cumulate ANT Suite and Its Relationship to High-Alumina Basalts. *Geochimica et Cosmochimica Acta*, Vol. 37, 1973, pp. 979–1006.
5. WARNER, J. L., Metamorphism of Apollo 14 Breccias. *Proc. Third Lunar Science Conference, Geochimica et Cosmochimica Acta*, Supplement 3, Vol. 1, 1972, pp. 623–643.
6. PHINNEY, W. C., J. L. WARNER, C. H. SIMONDS, AND G. E. LOFGREN, Classification and Distribution of Rock Types at Spur Crater. *Apollo 15 Lunar Samples*, Lunar Science Institute, Houston, 1972, pp. 149–153.
7. BENCE, A. E., J. H. PAPIKE, S. SUENO, AND J. W. DELANO, Pyroxene Poikiloblastic Rocks From the Lunar Highlands. *Proc. Fourth Lunar Science Conference, Geochimica et Cosmochimica Acta*, Supplement 4, Vol. 1, 1973, pp. 597–611.
8. HEIKEN, G., D. S. MCKAY, AND R. W. BROWN, Lunar Deposits of Possible Pyroclastic Origin. *Geochimica et Cosmochimica Acta*, in press, 1974.
9. HODGES, F. N. AND I. KUSHIRO, Petrology of Apollo 16 Lunar Highland Rocks. *Proc. Fourth Lunar Science Conference, Geochimica et Cosmochimica Acta*, Supplement 4, Vol. 1, 1973, pp. 1033–1048.
10. HELZ, R. T., AND D. E. APPLEMAN, Mineralogy, Petrology, and Crystallization History of Apollo 16 Rock 68415. *Proc. Fourth Lunar Science Conference, Geochimica et Cosmochimica Acta*, Supplement 4, Vol. 1, 1973, pp. 643–659.
11. GANCARZ, A. J., A. L. ALBEE, AND A. A. CHODOS, Comparative Petrology of Apollo 16 Samples 68415 and Apollo 14 Samples 14276 and 14310. *Earth Planet. Sci. Letters*, Vol. 16, No. 3, 1972, pp. 307–330.
12. MEYER, C., Mineral Assemblages and the Origin of Non-Mare Lunar Rock Types. (abs.). *Lunar Science*, Vol. III, Lunar Science Institute, Houston, 1972, pp. 542–544.
13. BROWN, G. M., C. H. EMELEUS, J. G. HOLLAND, A. PECKETT, AND P. PHILLIPS, Mineral-Chemical Variations in Apollo 14 and Apollo 15 Basalts and Granitic Fractions. *Proc. Third Lunar Science Conference, Geochimica et Cosmochimica Acta*, Supplement 3, Vol. 1, 1972, pp. 141–147.
14. JAMES, O. B., *Crystallization History of Lunar Feldspathic Basalt 14310*. USGS Prof. Paper 841, 1973.
15. DENCE, M. R., AND A. G. PLANT, Analysis of Fra Mauro Samples and the Origin of the Imbrium Basin. *Proc. Third Lunar Science Conference, Geochimica et Cosmochimica Acta*, Supplement 3, Vol. 1, 1972, pp. 379–399.
16. LSAPT (Lunar Sample Analyses Planning Team), Third Lunar Science Conference, *Science*, Vol. 176, No. 4038, 1972, pp. 975–981.
17. WATERS, A. C., R. V. FISHER, R. E. GARRISON, AND D. WAX, Matrix Characteristics and Origin of Lunar Breccia Samples 12034 and 12073. *Proc. Second Lunar Science Conference, Geochimica et Cosmochimica Acta*, Supplement 2, Vol. 1, 1971, pp. 893–907.
18. WARNER, J. L., C. H. SIMONDS, W. C. PHINNEY, AND R. GOOLEY, Petrology and Genesis of Two "Igneous" Rocks from Apollo 17 (76055 and 77135). EOS Transactions, *Am. Geophys. Union*, Vol. 54, 1973, pp. 620–621.
19. CHAO, E. C. T., The Petrology of 76055,10, a Thermally Metamorphosed Fragment-Laden Olivine Micronorite Hornfels. *Proc. Fourth Lunar Science Conference, Geochimica et Cosmochimica Acta*, Supplement 4, Vol. 1, 1973, pp. 719–732.
20. SIMONDS, C. H., Sintering and Hot Pressing of Fra Mauro Composition Glass and the Lithification of Lunar Breccias. *Am. J. Sci.*, Vol. 273, 1973, pp. 428–439.
21. CHAO, E. C. T., AND J. A. MINKIN, The Petrogenesis of 77135, a Fragment-Laden Pigeonite Feldspathic Basalt—A Major Highland Rock Type (abs.). *Lunar Science*, Vol. V, Lunar Science Institute, Houston, 1974, pp. 112–114.
22. SIMONDS, C. H., W. C. PHINNEY, AND J. L. WARNER, Petrography and Classification of Apollo 17 Non-Mare Rocks With Emphasis on Samples From the Station 6 Boulder. *Proc. Fifth Lunar Science Conference, Geochimica et Cosmochimica Acta*, Supplement 5, Vol. 1, 1974.
23. STOESER, D. B., R. W. WOLFE, U. M. MARVIN, J. A. WOOD, AND J. F. BOWER, Petrographic

Studies of a Boulder From the South Massif (abs). *Lunar Science*, Vol. V, Lunar Science Institute, Houston, 1974, pp. 743–745.

24. WILSHIRE, H. G., AND E. D. JACKSON, *Petrology and Stratigraphy of the Fra Mauro Formation at the Apollo 14 Site*. U.S. Geol. Survey Prof. Paper 785, 1972, pp. 1–26.
25. HÜTTNER, R., Bunte Trümmermassen und Suevit. *Geologica Bavarica*, Vol. 61, 1969, pp. 142–200.
26. PHINNEY, W. C., E. ANDERS, D. BOGARD, P. BUTLER, E. GIBSON, W. GOSE, G. HEIKEN, C. HOHENBERG, L. NYQUIST, W. PEARCE, M. RHODES, L. SILVER, C. SIMONDS, D. STRANGWAY, C. TURNER, R. WALKER, J. WARNER, AND D. YUHAS, Progress Report: Apollo 17, Station 6 Boulder Consortium. *Lunar Science*, Vol. V, Supplement A, Lunar Science Institute, Houston, 1974, pp. 7–13.
27. WILLIAMS, R. J., The Lithification of Metamorphism of Lunar Breccias. *Earth Planet. Sci. Letters*, Vol. 16, 1972, pp. 250–256.
28. SIMONDS, C. H., J. L. WARNER, AND W. C. PHINNEY, Petrology of Apollo 16 Poikilitic Rocks. *Proc. Fourth Lunar Science Conference, Geochimica et Cosmochimica Acta*, Supplement 4, Vol. 1, 1973, pp. 613–632.
29. BENCE, A. E., J. W. DELANO, AND J. J. PAPIKE, Nature of the Highland Massifs at Taurus Littrow: An Analysis of 2–4 mm Soil Fraction (abs.). *Lunar Science*, Vol. V, Lunar Science Institute, Houston, 1974, pp. 51–53.
30. WALKER, D., J. LONGHI, T. L. GROVE, E. STOLPER, AND J. F. HAYS, Experimental Petrology and Origin of Rocks From the Descartes Highlands. *Proc. Fourth Lunar Science Conference, Geochimica et Cosmochimica Acta*, Supplement 4, Vol. 1, 1973, pp. 1013–1032.
31. HEAD, J. W., Stratigraphy of the Descartes Region (Apollo 16): Implications for the Origin of Samples. *The Moon*, in press, 1974.
32. HARTMANN, W. K., Paleocratering of the Moon: Review of Post-Apollo Data. *Astrophys. and Space Sci.*, Vol. 12, 1972, pp. 183–199.
33. SHORT, N. M., AND M. L. FOREMAN, Thickness of Impact Crater Ejecta on the Lunar Surface. *Modern Geol.*, Vol. 3, 1972, pp. 69–91.
34. OBERBECK, V. R., A Mechanism for the Production of Lunar Crater Rays. *The Moon*, Vol. 2, 1971, pp. 263–278.
35. OBERBECK, V. R., R. H. MORRISON, F. HÖRZ, W. L. QUAIDE, AND D. E. GAULT, Smooth Plains and Continuous Deposits of Craters and Basins. *Proc. Fifth Lunar Science Conference, Geochimica et Cosmochimica Acta*, Supplement 5, Vol. 3, 1974.
36. MORGAN, J. W., U. KRÄHENBÜHL, R. GANAPATHY, E. ANDERS, AND U. B. MARVIN, Trace Element Abundances and Petrology of Separates From Apollo 15 Soils. *Proc. Fourth Lunar Science Conference, Geochimica et Cosmochimica Acta*, Supplement 4, Vol. 2, 1973, pp. 1379–1398.
37. MORGAN, J. W., R. GANAPATHY, H. HIGUCHI, U. KRÄHENBÜHL, AND E. ANDERS, Lunar Basins: Tentative Characterization of Projectiles, From Meteoritic Elements in Apollo 17 Boulders (abs.). *Lunar Science*, Vol. V, Lunar Science Institute, Houston, 1974, pp. 526–528.
38. GANAPATHY, R., J. W. MORGAN, U. KRÄHENBÜHL, AND E. ANDERS, Ancient Meteorite Components in Lunar Highland Rocks: Clues From Trace Elements in Apollo 15 and 16 Samples. *Proc. Fourth Lunar Science Conference, Geochimica et Cosmochimica Acta*, Supplement 4, Vol. 2, 1973, pp. 1239–1261.
39. BAEDECKER, P. A., C. L. CHOU, E. B. GRUDEWICZ, AND J. T. WASSON, Volatile and Siderophilic Trace Elements in Apollo 15 Samples: Geochemical Implications and Characterization of the Long-Lived and Short-Lived Extralunar Materials. *Proc. Fourth Lunar Science Conference, Geochimica et Cosmochimica Acta*, Supplement 4, Vol. 2, 1973, pp. 1177–1195.
40. LSPET (Lunar Sample Preliminary Examination Team), Apollo 17 Lunar Samples: Chemical and Petrographic Description. *Science*, Vol. 182, 1973, pp. 659–672.
41. RHODES, J. M., K. V. RODGERS, C. SHIH, B. M. BANSAL, L. E. NYQUIST, AND H. WIESMANN, The Relationship Between Geology and Soil Chemistry at the Apollo 17 Landing Site. (abs.). *Lunar Science*, Vol. V, Lunar Science Institute, Houston, 1974, pp. 630–632.
42. ADLER, I., J. I. TROMBKA, R. SCHMADEBECK, P. LOWMAN, H. BLODGET, L. YIN, E. ELLER, M. PODWYSOCKI, J. R. WEIDNER, A. L. BICKEL, R. K. L. LUM, J. GERARD, P. GORENSTEIN, P. BJORKHOLM, AND B. HARRIS, Results of the Apollo 15 and 16 X-Ray Experiment. *Proc. Fourth Lunar Science Conference, Geochimica et Cosmochimica Acta*, Supplement 4, Vol. 3, 1973, pp. 2783–2791.
43. METZGER, A. E., J. I. TROMBKA, L. E. PETERSON, R. C. REEDY, AND J. R. ARNOLD, Lunar Surface Radioactivity: Preliminary Results of the Apollo 15 and Apollo 16 Gamma-Ray Spectrometer Experiments. *Science*, Vol. 179, 1973, pp. 800–803.
44. LSPET (Lunar Sample Preliminary Examination Team), Preliminary Examination of Lunar Samples From Apollo 14. *Science*, Vol. 173, 1971, pp. 681–693.
45. LSPET (Lunar Sample Preliminary Examination Team), The Apollo 15 Lunar Samples: A Preliminary Description. *Science*, Vol. 175, 1972, pp. 363–374.
46. LSPET (Lunar Sample Preliminary Examination Team), The Apollo 16 Lunar Samples: Petrographic and Chemical Description. *Science*, Vol. 179, 1973, pp. 23–34.
47. PRINZ, M., E. DOWTY, K. KEIL, AND T. E.

BUNCH, Spinel Troctolite and Anorthosite in Apollo 16 Samples. *Science*, Vol. 179, 1973, pp. 74–76.

48. WALKER, D., T. L. GROVE, J. LONGHI, E. M. STOLPER, AND J. F. HAYS, Origin of Lunar Feldspathic Rocks. *Earth Planet. Sci. Letters*, Vol. 20, 1973, pp. 325–336.
49. BUTLER, J. C., G. M. GREENE, AND E. A. KING, JR., Grain Size Frequency Distribution and Modal Analysis of Apollo 16 Fines. *Proc. Fourth Lunar Science Conference, Geochimica et Cosmochimica Acta*, Supplement 4, Vol. 1, 1973, pp. 267–278.
50. FINKELMAN, R. B., Analysis of the Ultrafine Fraction of the Apollo 14 Regolith. *Proc. Fourth Lunar Science Conference, Geochimica et Cosmochimica Acta*, Supplement 4, Vol. 1, 1973, pp. 179–189.
51. EVENSEN, N. M., V. R. MURTHY, AND M. R. COSCIO, JR., Rb-Sr Ages of Some Mare Basalts and the Isotopic and Trace Element Systematics in Lunar Fines. *Proc. Fourth Lunar Science Conference, Geochimica et Cosmochimica Acta*, Supplement 4, Vol. 2, 1973, pp. 1707–1724.
52. HUBBARD, N. J., J. M. RHODES, P. W. GAST, B. M. BANSAL, C. Y. SHIH, H. WIESMANN, AND L. E. NYQUIST, Lunar Rock Types: The Role of Plagioclase in Non-Mare and Highland Rock Types. *Proc. Fourth Lunar Science Conference, Geochimica et Cosmochimica Acta*, Supplement 4, Vol, 2, 1973, pp. 1297–1312.
53. HASKIN, L. A., P. A. HELMKE, D. P. BLANCHARD, J. W. JACOBS, AND K. TELANDER, Major and Trace Element Abundances in Samples for the Lunar Highlands. *Proc. Fourth Lunar Science Conference, Geochimica et Cosmochimica Acta*, Supplement 4, Vol. 2, 1973, pp. 1275–1296.
54. TAYLOR, S. R., M. P. GORTON, P. MUIR, W. NANCE, R. RUDOWSKI, AND N. WARE, Lunar Highlands Composition: Apennine Front. *Proc. Fourth Lunar Science Conference, Geochimica et Cosmochimica Acta*, Supplement 4, Vol. 2, 1973, pp. 1445–1459.
55. SCHAFFER, O. A., AND L. HUSIAN, Early Lunar History: Ages of 2 to 4 mm Soil Fragments From the Lunar Highlands. *Proc. Fourth Lunar Science Conference, Geochimica et Cosmochimica Acta*, Supplement 4, Vol. 2, 1973, pp. 1847–1863.
56. SCHAEFFER, O. A., AND L. HUSIAN, Chronology of Lunar Basin Formation and Ages of Lunar Anorthositic Rocks (abs.). *Lunar Science*, Vol. V, Lunar Science Institute, Houston, 1974, pp. 663–665.
57. TERA, F., D. A. PAPANASTASSIOU, AND G. J. WASSERBURG, The Lunar Time Scale and a Summary of Isotopic Evidence for a Terminal Lunar Cataclysm (abs.). *Lunar Science*, Vol. V, Lunar Science Institute, Houston, 1974, pp. 792–794.
58. NYQUIST, L. E., N. J. HUBBARD, P. W. GAST, B. M. BANSAL, H. WIESMANN, AND B. JAHN, Rb-Sr Systematics for Chemically Defined Apollo 15 and 16 Materials. *Proc. Fourth Lunar Science Conference, Geochimica et Cosmochimica Acta*, Supplement 4, Vol. 2, 1973, pp. 1823–1846.
59. NYQUIST, L. E., N. J. HUBBARD, P. W. GAST, S. E. CHURCH, B. M. BANSAL, AND H. WIESMANN, Rb-Sr Systematics for Chemically Defined Apollo 14 Breccias. *Proc. Third Lunar Science Conference, Geochimica et Cosmochimica Acta*, Supplement 3, Vol. 2, 1972, pp. 1515–1530.
60. PAPANASTASSIOU, D. A., AND G. J. WASSERBURG, Rb-Sr Ages of Igneous Rocks From the Apollo 14 Mission and the Age of the Fra Mauro Formation. *Earth Planet. Sci. Letters*, Vol. 12, 1971, pp. 36–48.
61. PAPANASTASSIOU, D. A., AND G. J. WASSERBURG, The Rb-Sr Age of a Crystalline Rock From Apollo 16. *Earth Planet. Sci. Letters*, Vol. 16, 1972, pp. 289–298.
62. PAPANASTASSIOU, D. A., AND G. J. WASSERBURG, Rb-Sr Systematics of Luna 20 and Apollo 16 Samples. *Earth Planet. Sci. Letters*, Vol. 17, 1972, pp. 52–63.
63. TERA, F., D. A. PAPANASTASSIOU, AND G. J. WASSERBURG, A Lunar Cataclysm at 3.95 AE and the Structure of the Lunar Crust (abs.). *Lunar Science*, Vol. IV, Lunar Science Institute, Houston, 1973, pp. 723–725.
64. HEIKEN, G., P. BUTLER, JR., C. H. SIMONDS, W. C. PHINNEY, J. L. WARNER, H. H. SCHMITT, D. D. BOGARD, AND W. G. PEARCE, *Preliminary Data on Boulders at Station 6, Apollo 17 Landing Site*. National Aeronautics and Space Administration, TM X–58116, 1973, pp. 1–56.
65. BRETT, R., AND W. MENDELL, Thickness of Some Lunar Mare Basalt Flows and Ejecta Blankets Based on Chemical Kinetics (abs.). *Meteoritics*, in press, 1974.
66. GRIEVE, R. A. F., AND A. G. PLANT, Partial Melting on the Lunar Surface, as Observed in Glass Coated Apollo 16 Samples. *Proc. Fourth Lunar Science Conference, Geochimica et Cosmochimica Acta*, Supplement 4, Vol. 1, 1973, pp. 667–679.
67. HOWARD, K. A., Ejecta Blankets of Large Craters Exemplified by King Crater. *Apollo 16 Preliminary Science Report*, Chapter 29, NASA SP–315, 1972, pp. 70–77.
68. HUBBARD, N. J., P. W. GAST, C. MEYER, L. E., NYQUIST, C. SHIH, AND H. WEISMANN, Chemical Composition of Lunar Anorthosites and Their Parent Liquids. *Earth Planet. Sci. Letters*, Vol. 13, 1971, pp. 71–75.

Lunar Igneous Rocks and the Nature of the Lunar Interior

James Fred Hays and David Walker
Center for Earth and Planetary Physics
Harvard University, Cambridge, Massachusetts

Lunar igneous rocks, properly interpreted, can give useful information about mineral assemblages and mineral chemistry as a function of depth in the lunar interior. Though intensely brecciated, terra rocks reveal, in their chemistry, evidence for a magmatic history. Partial melting of feldspathic lunar crustal material occurred in the interval 4.6 to 3.9 Gy. Melting of ilmenite-bearing cumulates at depths near 100 km produced parent magmas for Apollo 11 and 17 titaniferous mare basalts in the interval 3.8 to 3.6 Gy. Melting of ilmenite-free olivine pyroxenites (also cumulates?) at depths greater than 200 km produced low-titanium mare basalts in the interval 3.4 to 3.1 Gy. No younger igneous rocks have yet been recognized among the lunar samples, and present-day melting seems to be limited to depths greater than 1000 km.

Returned lunar samples from six Apollo and two Luna landing sites, remote chemical analyses from Lunokhod and Surveyor space vehicles, and orbital spectrographic observations have given us a reasonably comprehensive view of the chemistry and mineralogy of the lunar surface (refs. 1–8). Unfortunately, very few of the returned lunar samples seem to be of deep-seated origin. Gooley et al. (ref. 9) have described a coarse-grained plagioclase-bearing rock (76535) which they interpret as a product of slow cooling at a depth of at least 10 km. Several ultramafic clasts in breccias have been interpreted as deep-seated cumulates although the evidence is not unambiguous (refs. 10, 11, and 12). The great majority of returned lunar samples, however, appear to have been formed at the lunar surface or within a few kilometers of it. Thus our knowledge of the mineralogy and chemistry of the lunar interior remains indirect and unsatisfactory.

Nevertheless, isotopic studies, geophysical evidence, and geochemical arguments all lead to a growing consensus that at least the outer several hundred kilometers of the Moon were subjected to partial or complete melting at a very early stage in lunar history (refs. 13–17). If this view is correct, then the outer portion of the Moon and perhaps the entire Moon should consist of layers of cumulus crystals combined with the crystallization products of trapped residual liquids. The chemical and petrological character of these layers, the initial composition of the magmatic system, the proportion of the lunar mass involved, and the nature of the differentiation process are among the major unsolved problems of lunar science, and, by implication, of the early history of other planetary bodies as well.

In the absence of more than fragmentary direct evidence from geophysics, the petrographic, geochemical, and experimental study of lunar igneous rocks is the best available approach to the solution of these problems.

Method of Approach

Let us suppose that a certain primary magma originates by partial melting within the lunar interior and is then transported

directly to the lunar surface without modification of its chemistry (major element, minor element, or isotopic). If a lunar rock sample can be shown to be the crystalline or glassy equivalent of such a primary liquid, then careful geochemical and experimental study of this sample will reveal the depth of origin of the primary liquid and the mineralogy and mineral chemistry of the residuum left after partial melting. Lunar igneous rocks, therefore, are potentially a most powerful probe to explore the nature of the lunar interior. This tool was first exploited with respect to the moon by Ringwood and Essene (ref. 18). Unfortunately, most lunar igneous rocks show clear-cut evidence either of contamination by lunar soil, including meteoritic debris, or of near-surface crystal-liquid fractionation processes that cause the chemistry of the final rock product to differ significantly from that of the parental liquid.

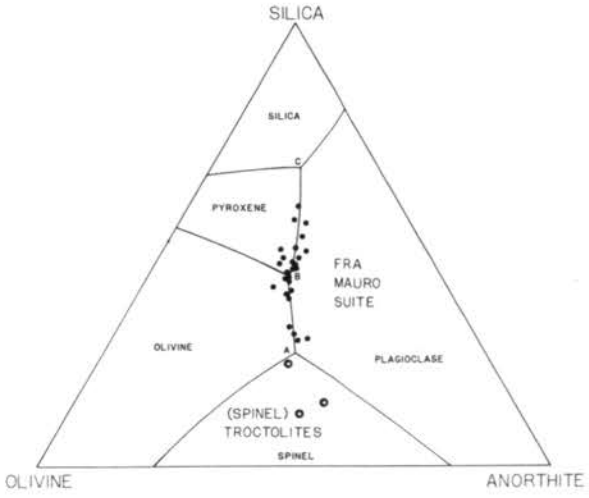


Figure 1.—*Pseudoternary liquidus projection for feldspathic lunar rocks. The liquidus field of plagioclase occupies the right portion of the composition plane adjacent to anorthite. The liquidus fields of olivine and silica are in the lower left and top, respectively. The liquidus field of low-calcium pyroxene occurs in the left center between those of olivine, silica, and plagioclase. The spinel liquidus field occupies the bottom central region of the plane. Details of the projection may be found in reference 32. Solid circles represent compositions of the Fra Mauro suite interpreted to be partial melts of the feldspathic lunar crust. Open circles represent various spinel-bearing microtroctolites.*

In applying this approach, therefore, it is important to detect and allow for the effects of possible near-surface contamination or fractionation processes.

We have used the quenching technique to study low-pressure equilibrium crystallization behavior of various lunar compositions at the very low oxygen fugacities appropriate for lunar surface conditions. By means of electron microprobe analyses of coexisting crystals and liquid at various stages of the crystallization process, we have mappped out the low-pressure "liquid lines of descent" for lunar magmas and the loci of multiple saturated liquids within the complex chemical system to which the lunar rocks belong. Results of these studies and details of the methods used are given in references 19–23. These results are combined with petrographic observations in the interpretation of the origins and crystallization histories of the specific samples studied and in the evaluation of their potential as probes of the lunar interior (refs. 23–27). High-pressure phase equilibrium studies of promising compositions are carried out in the manner pioneered by Ringwood and Essene (ref. 18), and O'Hara et al. (ref. 28).

Terra Samples and the Lunar Crust

Lunar samples from terra (highland) sites have been intensely brecciated and texturally modified by surface impact processes. Multiple generations of brecciation, thermal metamorphism, and partial melting are common (refs. 6 and 7). The few rocks showing unquestioned igneous textures may well have crystallized from pools of impact melt. Nevertheless, chemical variations from site to site and within the sample suites from individual sites are present, indicating that chemical evidence for early magmatic activity may have survived the impact mixing process. This is especially clear in statistical studies of glass and lithic fragment compositions in the coarse soil samples (e.g., refs. 29, 30, and 31).

Figure 1 (ref. 27) is a plot of "preferred compositions" recognized by various groups

from glass or lithic fragment studies. Each point represents the average of a large number of individual analyses that cluster about that point. Clusters that obviously represent compositions of mare basalts or anorthositic rocks are excluded, but otherwise all "preferred compositions" reported in the literature are shown. These compositions are projected onto the pseudoternary liquidus for the system olivine (Fo^{70})-anorthite-silica (refs. 19 and 20). The tendency of these preferred compositions to lie along the curves of twofold saturation and to cluster about the two peritectic points, A and B, is apparent. We interpret this to mean that these recurrent chemical types among the terra rocks are related by the crystal-liquid equilibria indicated. We have argued at length (ref. 27) that KREEP and KREEP-related compositions near point B are produced by partial melting of rocks consisting of plagioclase, olivine, and low-calcium pyroxene, and that some of the "very-high alumina basalts" of Apollo 16 and Luna 20, with compositions near point A, and some so-called "spinel troctolites," may be produced by partial melting of rocks consisting of anorthite, olivine (Fo_{93}), and spinel (Mg, Fe)(Al, Cr)$_2O_4$ (ref. 32).

Since the crystal-liquid equilibria shown in figure 1 were determined at low pressures, and the equilibrium curves shift position with increasing pressure, the inferred partial melting events must have occurred at relatively shallow depths (≤ 60 km), i.e., within the lunar crust. Thus, the crust contains rocks having the mineral assemblages of anorthositic gabbro or norite (ANT) and of pink-spinel troctolite (PST). Presumably both these materials are among the crystal cumulate products of the early crust-forming event. Phase relationships do not allow us to say if these contrasting crustal materials represent widespread layers at different depths, but if they do, the abundance of ANT rocks at the surface, and the paucity of PST rocks, suggest that the latter would represent a deeper level within the crust. Isotopic studies indicate that the crustal melting processes, whether the energy sources were external (impact) or internal, took place prior to 3.8 Gy, and possibly much earlier (ref. 33).

Mare Basalts and the Deep Lunar Interior

The dark, iron-rich, alumina-poor basaltic rocks from the mare basins present a different problem. Their textures and isotopic ages leave little doubt that they crystallized from internally generated lavas that reached the lunar surface after the intense bombardment recorded by the highland rocks had largely subsided (refs. 4, 5, 8, and 34). There has been much debate, however, about the degree to which their compositions have been affected by near-surface fractionation processes (refs. 28, 35, and 37). It is not yet clear which, if any, mare basalt compositions represent primary unmodified melts from the lunar interior, and may therefore be used to infer the nature of the interior.

In order to discuss these questions, we divide the mare basalts into two groups: the old (3.6 to 3.8 Gy), titaniferous ($TiO_2 > 8$ percent) basalts from Mare Tranquilitatis (Apollo 11) and Mare Serenitatis (Apollo 17); and the younger (3.1 to 3.4 Gy), low-titanium ($TiO_2 < 5$ percent) basalts from Oceanus Procellarum (Apollo 12), Mare Imbrium (Apollo 15), and Mare Fecunditatis (Luna 16). It is not yet certain whether this distinction based on TiO_2 content is a real one or whether it is an artifact of the small number of sampling localities. Among the titaniferous group the rapidly cooled members tend to have high TiO_2 values, while rocks with TiO_2 near the lower limit of 8 percent appear on textural grounds to have cooled more slowly with consequent opportunity for loss of FeTi oxides by crystal settling. The compositional gap may, therefore, be even larger than it appears. We tentatively conclude that it is real, and attribute the marked difference in TiO_2 content between the groups to the presence or absence of a titanium-rich phase (ilmenite?) in their respective source materials.

The low-titanium basalts are, for the most part, porphyritic, and show systematic chemical variations that can be accounted for by simple low-pressure fractionation of observed phenocryst and matrix compositions (refs. 5, 34, 37, 38, and 39). These rocks are, therefore, widely acknowledged to have been subjected to near-surface fractional crystallization. Nevertheless, certain compositions (e.g., 12009) appear to have existed at the surface as liquids, have compositions not obviously related to low-pressure cotectics, and are capable of serving as parent to related rock compositions by means of low-pressure fractional crystallization. These arguments have been presented by Green et al. (refs. 40 and 41), Kushiro et al. (ref. 38), and Grove et al. (ref 26). (For a contrary view, however, see Biggar et al. (ref. 42) and O'Hara and Biggar (ref. 43).)

If these authors are correct in their interpretation that the basalts they studied accurately represent the compositions of primary liquids generated by partial melting in the lunar interior, then high-pressure phase-equilibrium studies on the compositions will reveal the nature and depth of the source region. The argument follows: (1) a liquid produced by equilibrium partial melting must be saturated with all crystalline phases remaining in the residue; (2) these crystalline phases will, therefore, appear simultaneously on the liquidus of the basalt composition at the pressure corresponding to magma generation (or to last equilibrium of liquid with residual crystals); (3) if a pressure range exists where several crystalline phases appear simultaneously on the liquidus, this pressure range yields the inferred depth of origin, and the nature and chemical compositions of the observed liquidus crystals yield the nature and chemistry of the residual crystals in the source region. If the degree of partial melting is small, the residual crystals will not differ greatly from those present prior to the partial melting event, although their proportions will ordinarily be changed.

By following this line of reasoning, Green et al. (refs. 40 and 41), Kushiro et al. (ref. 38), Green and Ringwood (ref. 44), Longhi et al. (ref. 25), and Chappell and Green (ref. 45), have all concluded that low-titanium mare basalts are ultimately derived by partial melting of olivine pyroxenite (typically spinel-bearing) at various depths ranging from 150 to 400 km. Reported variations in source depth and mineral chemistry may reflect real heterogeneities in the lunar interior and differences in the depths of melting or simply varying degrees of deviation from the initial assumption that the basalt compositions studied represent unmodified primary liquids.

Unfortunately, this method yields only the nature and mineral chemistry of the phases present in the source region. The proportions of the various crystalline phases present (and hence the bulk chemistry of the source region) do not greatly affect the major element chemistry of the liquid produced as long as no crystalline phase is completely consumed (ref. 46). Minor element chemistry of the liquid, however, *is* sensitive to the proportions of phases initially present as shown by Gast (ref. 47) and Shaw (ref. 48). Full, quantitative exploitation of this powerful tool remains to be done.

Isotopic age determinations on the low-titanium mare basalts indicate crystallization ages of 3.1 to 3.4 Gy. Presumably this is the time of partial melting at depths of 200 to 400 km. It should be noted that these basalts have Rb-Sr model ages near 4.6 Gy (ref. 15), requiring that the inferred partial melting event quantitatively extracted Rb and Sr from the source region (or at least extracted these elements without significant fractionation). This observation apparently precludes the presence of plagioclase or any other Sr-bearing phase from the residual assemblage unless elaborate processes are invoked to prevent Sr homogenization (e.g., ref. 49).

High-Titanium Mare Basalts

The titaniferous mare basalts returned by Apollo 11 and Apollo 17 are nearly free of

phenocrysts and form tight compositional groupings, within which compositional trends are not conspicuous. It has been argued by Ringwood and his colleagues that these rocks represent insignificantly modified primary melts from the lunar interior (refs. 18, 35, 50, and 51). O'Hara has argued, to the contrary, that these compositions represent low-pressure cotectic compositions, and that the rocks are therefore products of extensive, near-surface, fractional crystallization possibly accompanied by large-scale loss of volatiles (refs. 28, 42, and 52).

In order to resolve this apparent conflict, we have traced the course of residual liquids produced during the equilibrium crystallization of two Apollo 17 titaniferous mare basalts. Because the CaO/Al_2O_3 molar ratio of mare basalts differs from unity, and because the TiO_2 content cannot be neglected, the simplified system used to discuss melting and crystallization behavior in terra compositions is not adequate for the study of mare basalt compositions. Excess CaO is expressed by the presence of high-calcium pyroxenes, and high TiO_2 content results in early saturation with an FeTi-oxide phase—armalcolite or ilmenite. Figure 2 attempts to represent compositions within this complex system in two-dimensional projections; several different projections are required to display all of the significant variables. Details of the projection scheme will be published elsewhere (ref. 23). The lower right-hand portion of figure 2 shows a portion of the FeTi-oxide saturated liquidus surface for the complex natural system; curves shown were

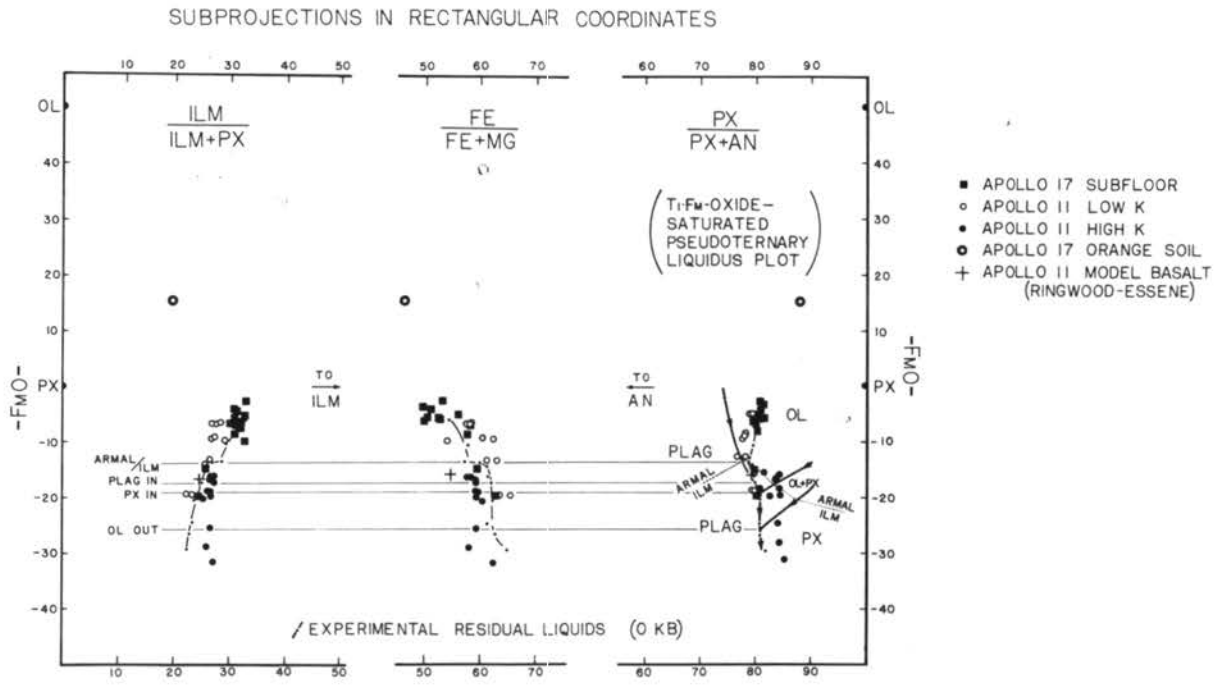


Figure 2.—*Subprojections in FmO-$CaAl_2Si_2O_8$ $-FmTiO_3$ $-(FmSiO_3 + CaFmSi_2O_6)$ composition space. Molar units are used throughout. $FmO = FeO + MgO$. All subprojections have FmO as the ordinate. Decreasing FmO correlates with increasing silica saturation and with decreasing temperature of the experiments (range 1200–1125° C). The first subprojection is from $CaAl_2Si_2O_8$ and can be used to visualize the locus of titaniferous oxide saturation. Armalcolite and ilmenite saturation volumes are to the right. The second subprojection shows variation with respect to $Fe/Fe + Mg$. The third subprojection is from $FmTiO_3$ and behaves as if it were a pseudoternary liquidus diagram. Silicate saturation volumes coexisting with armalcolite or ilmenite are located on this composition plane. Details of the experiments and the projection method are discussed in reference 23.*

located by microprobe analyses of glasses quenched from liquids saturated with an FeTi-oxide (armalcolite or ilmenite, as indicated) and one or more additional crystalline phases.

On each portion of figure 2 is plotted the locus of residual liquids produced during the equilibrium crystallization of two Apollo 17 high-titanium basalts (70215 and 70017). Also plotted are the compositions of analyzed Apollo 11 and Apollo 17 basaltic rocks. Apollo 11 ophitic rock compositions fall along the trend of Apollo 17 residual liquids in confirmation of their inferred crystallization sequence: FeTi-oxide—olivine—plagioclase—pyroxene (ref. 53). Apollo 11 intersertal rocks show a parallel trend, but lie off the curves of plagioclase saturation, confirming the petrographically inferred and experimentally demonstrated late appearance of plagioclase in these rocks.

It seems clear that the contention that these rock compositions bear no relation to low-pressure fractionation trends is false; it is also clear, however, that these compositions cannot all have been produced by simple near-surface fractional crystallization. It seems to us that the proximity of titaniferous mare basalt compositions to the path of residual liquids and the parallelism of the compositional trends is strong circumstantial evidence that these rocks, like most of the low-titanium mare basalts, have been affected to some extent by near-surface crystal liquid fractionation processes. Obviously, if a primary magma is to be sought among this group, care must be taken in its identification. Absence of liquidus plagioclase is not a sufficient criterion.

Among the titaniferous suite, one of the compositions most remote from low-pressure multiple saturation (and hence most likely to be a primitive partial melt) is the vitrophyre 70215. A liquid of this composition is in near-liquidus equilibrium with olivine, pigeonite, ilmenite, and spinel at 5 kb (ref. 23) and could, therefore, be produced by partial melting of an olivine-pigeonite-ilmenite-spinel assemblage at a depth of 100 km. The inferred time of melting at this depth would

The shallow source depth inferred for Apollo 17 basaltic magma, the Eu anomaly (ref. 55), and the high TiO_2 content of the magmas, all point to a source within the zone of mafic cumulates believed to lie beneath the feldspathic lunar crust. Partial remelting of cumulates consisting of olivine, pigeonite, spinel, and ilmenite plus variable amounts of the crystallization products of trapped residual liquids (plagioclase-saturated and rich in incompatible trace-elements) would produce most of the observed characteristics of the titaniferous mare basalt suite (ref. 22).

Speculations on Magmatic Time Sequence and Implied Lunar Thermal History

The inferred source depths for magma generation reported here show an inverse correlation with radiometric age of the resulting crystalline rocks. It is tempting to speculate on a model for lunar structure and history that would be consistent with the observed sequence of magmatic activity.

We recognize the difficulty of accounting for a heat source adequate to remelt refractory cumulates once crystallized. We are also aware of telescopic observations suggesting the presence on the lunar surface of young (2.5 Gy?), titanium-rich mare basalts that have not yet been recognized among the returned lunar samples. Despite these reservations, we present the following highly speculative model compatible with studies of lunar igneous rocks.

The Moon now has a crust consisting of a (floating) cumulus of plagioclase with entrapped olivine, low-calcium pyroxene, and MgAl-rich spinel. It overlies a (sinking) layered cumulus of olivine, low- and high-Ca pyroxene, and FeCr-rich spinel, with an intermediate zone rich in FeTi-oxide and fractionated residual liquid or its crystallization product. From 4.7 to 3.8 Gy, lunar petrologic history was dominated by impact brecciation and metamorphism and intracrustal

melting (< 60 km). In the interval from 3.8 to 3.6 Gy, titaniferous mare basalts were produced by partial melting in the subcrustal Ti-rich zone (~ 100 km). From 3.4 to 3.1 Gy, low-titanium mare basalts, produced by deep melting (200–400 km) reached the surface after varying degrees of en route crystallization. Present-day lunar melting is limited to depths below 1000 km, and lavas produced in the interval from 3 Gy to the present have not yet been identified among the lunar samples.

Acknowledgment

This work was supported by the National Aeronautics and Space Administration under grant NGL 22–007–247, and by the Committee on Experimental Geology and Geophysics of Harvard University. John Longhi, Timothy Grove, and Edward Stolper collaborated on much of the experimental work. The authors are grateful to them and to many other colleagues for helpful discussions.

References

1. TURKEVICH, A. L., Average Chemical Composition of the Lunar Surface. *Lunar Science IV*, J. W. Chamberlain and C. Watkins, eds., Lunar Science Institute, Houston, 1973, pp. 740–742.
2. TAYLOR, S. R., Geochemistry of the Lunar Highlands. *The Moon*, Vol. 7, 1973, pp. 181–195.
3. ADLER, I., J. I. TROMBKA, P. LOWMAN, R. SCHMADEBECK, H. BLODGET, E. ELLER, L. YIN, R. LAMOTHE, G. OSSWALD, J. GERARD, P. GORENSTEIN, P. BJORKHOLM, H. GURSKY, B. HARRIS, J. ARNOLD, A. METZGER, AND R. REEDY, Apollo 15 and 16 Results of the Integrated Geochemical Experiment. *The Moon*, Vol. 7, 1973, pp. 487–504.
4. LSPET (Lunar Sample Preliminary Examination Team), Preliminary Examination of Lunar Samples From Apollo 11. *Science*, Vol. 165, 1969, pp. 1211–1227.
5. LSPET (Lunar Sample Preliminary Examination Team), Preliminary Examination of Lunar Samples From Apollo 12. *Science*, Vol. 167, 1970, pp. 1325–1339.
6. LSPET (Lunar Sample Preliminary Examination Team), Preliminary Examination of Lunar Samples From Apollo 14. *Science*, Vol. 173, 1971, pp. 681–693.
7. LSPET (Lunar Sample Preliminary Examination Team), The Apollo 16 Lunar Samples: Petrographic and Chemical Description. *Science*, Vol. 179, 1973, pp. 23–34.
8. LSPET (Lunar Sample Preliminary Examination Team), Apollo 17 Lunar Samples: Petrographic and Chemical Description. *Science*, Vol. 182, 1973, pp. 659–690.
9. GOOLEY, R., R. BRETT, J. WARNER, AND J. R. SMYTH, Sample 76535, a Deep Lunar Crustal Rock. *Geochimica et Cosmochimica Acta*, in press, 1974.
10. ANDERSON, A. T., The Texture and Mineralogy of Lunar Peridotite 15445, 10. *J. Geol.*, Vol. 81, 1973, pp. 219–226.
11. RIDLEY, W. I., N. J. HUBBARD, J. M. RHODES, H. WEISMANN, AND B. BANSAL, Petrology of Lunar Breccia 15445 and Petrogenetic Implications. *J. Geol.*, Vol. 81, 1973, pp. 621–631.
12. ALBEE, A. L., A. A. CHODOS, R. F. DYMEK, A. J. GANCARZ, D. S. GOLDMAN, D. A. PAPANASTASSIOU, AND G. J. WASSERBURG, Dunite From the Lunar Highlands: Petrographic Deformational History, Rb-Sr Age. *Lunar Science*, Vol. V, Lunar Science Institute, Houston, 1974, pp. 3–5.
13. SMITH, J. V., A. T. ANDERSON, R. C. NEWTON, E. J. OLSEN, P. J. WYLIE, A. V. CREWE, M. S. ISAACSON, AND D. JOHNSON, Petrologic History of the Moon Inferred from Petrography, Mineralogy and Petrogenesis of Apollo 11 Rocks. *Proc. Apollo 11 Lunar Science Conference, Geochimica et Cosmochimica Acta*, Supplement 1, Vol. 1, 1970, pp. 897–925.
14. WOOD, J. A., Petrology of the Lunar Soil and Geophysical Implications. *J. Geophys. Res.*, Vol. 75, 1970, pp. 6497–6513.
15. PAPANASTASSIOU, D. A., AND G. J. WASSERBURG, Lunar Chronology and Evolution From Rb-Sr Studies of Apollo 11 and 12 Samples. *Earth Planet. Sci. Letters*, Vol. 11, 1971, pp. 37–62.
16. LSAPT (Lunar Sample Analyses Planning Team), Third Lunar Science Conference. *Science*, Vol. 176, 1972, pp. 975–981.
17. BRETT, R., The Lunar Crust: A Product of Heterogeneous Accretion or Differentiation of a Homogeneous Moon? *Geochimica et Cosmochimica Acta*, Vol. 37, 1973, pp. 2697–2703.
18. RINGWOOD, A. E., AND E. ESSENE, Petrogenesis of Apollo 11 Basalts, Internal Constitution and Origin of the Moon. *Proc. Apollo 11 Lunar Science Conference, Geochimica et Cosmochimica Acta*, Supplement 1, Vol. 1, 1970, pp. 769–799.
19. WALKER, D., J. LONGHI, AND J. F. HAYS, Experimental Petrology and Origin of Fra Mauro Rocks and Soil. *Proc. Third Lunar Science Conference, Geochimica et Cosmochimica Acta*,

Supplement 3, Vol. 1, 1972, pp. 797–817.

20. WALKER, D., J. LONGHI, T. L. GROVE, E. M. STOLPER, AND J. F. HAYS, Experimental Petrology and Origin of Rocks from the Descartes Highlands *Geochimica et Cosmochimica Acta*, Supplement 4, Vol. 1, 1973, pp. 1013–1032.
21. WALKER, D., J. LONGHI, E. STOLPER, T. GROVE, AND J. F. HAYS, Experimental Petrology of Titaniferous Lunar Basalts. *Lunar Science*, Vol. V, Lunar Science Institute, Houston, 1974, pp. 814–816.
22. WALKER, D., J. LONGHI, E. STOLPER, T. GROVE, AND J. F. HAYS, Origin of Titaniferous Lunar Basalts. Submitted for publication, 1974.
23. LONGHI, J., D. WALKER, T. L. GROVE, E. STOLPER, AND J. F. HAYS, The Petrology of the Apollo 17 Mare Basalts. *Proc. Fifth Lunar Science Conference*, in press, 1974.
24. LONGHI, J., D. WALKER, AND J. F. HAYS, Petrography and Crystallization History of Basalts 14310 and 14072. *Proc. Third Lunar Science Conference, Geochimica et Cosmochimica Acta*, Supplement 3, Vol. 1, 1972, pp. 131–139.
25. LONGHI, J., D. WALKER, E. STOLPER, T. L. GROVE, AND J. F. HAYS, Petrology of Mare/Rille Basalts 15555 and 15065. *The Apollo 15 Lunar Samples*, J. W. Chamberlain and C. Watkins, eds., Lunar Science Institute, Houston, 1972, pp. 131–134.
26. GROVE, T. L., D. WALKER, J. LONGHI, E. N. STOLPER, AND J. F. HAYS, Petrology of Rock 12002 From Oceanus Procellarum. *Proc. Fourth Lunar Science Conference, Geochimica et Cosmochimica Acta*, Supplement 4, Vol. 1, 1973, pp. 995–1011.
27. WALKER, D., T. L. GROVE, J. LONGHI, E. STOLPER, AND J. F. HAYS, Origin of Lunar Feldspathic Rocks. *Earth Planet. Sci. Letters*, Vol. 20, 1973, pp. 325–336.
28. O'HARA, M. J., G. M. BIGGAR, S. W. RICHARDSON, C. E. FORD, AND B. G. JAMIESON, The Nature of Seas, Mascons and the Lunar Interior in the Light of Experimental Studies. *Proc. Apollo 11 Lunar Science Conference, Geochimica et Cosmochimica Acta*, Supplement 1, Vol. 1, 1970, pp. 695–710.
29. REID, A. M., J. WARNER, W. I. RIDLEY, D. A. JOHNSTON, R. S. HARMON, P. JAKES, AND R. W. BROWN, The Major Element Composition of Lunar Rocks as Inferred From Glass Compositions in the Lunar Soils. *Proc. Third Lunar Science Conference, Geochimica et Cosmochimica Acta*, Supplement 3, Vol. 1, 1972, pp. 363–378.
30. PRINZ, M., E. DOWTY, K. KEIL, AND T. E. BUNCH, Spinel Troctolite and Anorthosite in Apollo 16 Samples. *Science*, Vol. 179, 1973, pp. 74–76.
31. TAYLOR, G. J., U. B. MARVIN, J. B. REID, JR., AND J. A. WOODS, Noritic Fragments in the Apollo 14 and 12 Soils and the Origin of Oceanus Procellarum. *Geochimica et Cosmochimica Acta*, Supplement 3, Vol. 1, 1972, pp. 995–1014.
32. PRINZ, M., E. DOWTY, K. KEIL, AND T. E. BUNCH, Mineralogy, Petrology and Chemistry of Lithic Fragments From Luna 20 Fines: Origin of the Cumulate ANT Silute and its Relation to High Alumina and Mare Basalts. *Geochimica et Cosmochimica Acta*, Luna 20 Vol. 37, 1973, pp. 979–1006.
33. NYQUIST, L. E., N. J. HUBBARD, P. W. GAST, B. M. BANSAL, H. WEISMANN, AND B. JAHN, Rb-Sr Systematics for Chemically Defined Apollo 15 and 16 Materials. *Proc. Fourth Lunar Science Conference, Geochimica et Cosmochimica Acta*, Supplement 4, Vol. 2, 1973, pp. 1823–1846.
34. LSPET (Lunar Sample Preliminary Examination Team), Apollo 15 Lunar Samples: A Preliminary Description. *Science*, Vol. 175, 1972, pp. 363–375.
35. RINGWOOD, A. E., Petrogenesis of Apollo 11 Basalts and Implications for Lunar Origin. *J. Geophys. Res.*, Vol. 75, 1970, pp. 6453–6479.
36. BIGGAR, G. M., M. J. O'HARA, A. PECKETT, AND D. J. HUMPHRIES, Lunar Lavas and the Achondrites: Petrogenesis of Protohypersthene Basalts in the Maria Lava Lakes. *Proc. Second Lunar Science Conference, Geochimica et Cosmochimica Acta*, Supplement 2, Vol. 1, 1971, pp. 617–643.
37. KUSHIRO, I., AND H. HARAMURA, Major Element Variation and Possible Source Materials of Apollo 12 Crystalline Rocks. *Science*, Vol. 171, 1971, pp. 1235–1237.
38. KUSHIRO, I., Y. NAKAMURA, K. KITAYAMA, AND S. AKIMOTO, Petrology of Some Apollo 12 Crystalline Rocks. *Proc. Second Lunar Science Conference, Geochimica et Cosmochimica Acta*, Supplement 2, Vol. 1, 1971, pp. 481–495.
39. MASON, B., E. JAROSEWICH, W. G. MELSON, AND G. THOMPSON, Mineralogy, Petrology and Chemical Composition of Lunar Samples 15085, 15256, 15271, 15471, 15475, 15476, 15535, 15553, 15556. *Proc. Third Lunar Science Conference, Geochimica et Cosmochimica Acta*, Supplement 3, Vol. 1, 1972, pp. 785–796.
40. GREEN, D. H., A. E. RINGWOOD, N. G. WARE, W. O. HIBBERSON, A. MAJOR, AND E. KISS, Experimental Petrology and Petrogenesis of Apollo 12 Basalts. *Proc. Second Lunar Science Conference, Geochimica et Cosmochimica Acta*, Supplement 2, Vol. 1, 1971, pp. 601–615.
41. GREEN, D. H., N. G. WARE, W. O. HIBBERSON, AND A. MAJOR, Experimental Petrology of Apollo 12 Basalts: Part 1, Sample 12009. *Earth Planet. Sci. Letters*, Vol. 13, 1971, pp. 85–96.
42. BIGGAR, G. M., M. J. O'HARA, D. J. HUMPHRIES,

AND A. PECKETT, Maria Lavas, Mascons, Layered Complexes, Achondrites and the Lunar Mantle. *The Moon*, H. Urey and S. K. Runcorn, eds., I.A.U., 1972, pp. 129–164.

43. O'HARA, M. J., AND G. M. BIGGAR, A Point of Phase Equilibrium Interpretation in Connection with Lavas From Apollo 12 Site. *Earth Planet. Sci. Letters*, Vol. 16, 1972, pp. 388–390.
44. GREEN, D. H., AND A. E. RINGWOOD, Significance of Apollo 15 Mare Basalts and "Primitive" Green Glass in Lunar Petrogenesis. *The Apollo 15 Lunar Samples*, Lunar Science Institute, Houston, 1972, pp. 82–84.
45. CHAPPELL, B. W., AND D. H. GREEN, Chemical Compositions and Petrogenetic Relationships in Apollo 15 Mare Basalts. *Earth Planet. Sci. Letters*, Vol. 18, 1973, pp. 237–246.
46. PRESNALL, D. C., The Geometrical Analysis of Partial Fusion. *Amer. J. Sci.*, Vol. 267, 1969, pp. 1178–1194.
47. GAST, P. W., Trace Element Fractionation and the Origin of Tholeitic and Alkaline Magma Types. *Geochimica et Cosmochimica Acta*, Vol. 32, 1968, pp. 1057–1086.
48. SHAW, D. M., Trace Element Fractionation During Anatexis. *Geochimica et Cosmochimica Acta*, Vol. 34, 1970, pp. 237–243.
49. RINGWOOD, A. E., Minor Element Chemistry of Maria Basalts. *Lunar Science*, Vol. V, Lunar Science Institute, Houston, 1974, pp. 633–635.
50. RINGWOOD, A. E., AND D. H. GREEN, Crystallization of Plagioclase in Lunar Basalts and its Significance. *Earth Planet. Sci. Letters*, Vol. 14, 1972, pp. 14–18.
51. GREEN, D. H., A. E. RINGWOOD, N. G. WARE, AND W. O. HIBBERSON, Petrology and Petrogenesis of Apollo 17 Basalts and Apollo 17 Orange Glass. *Lunar Science*, Vol. V, Lunar Science Institute, Houston, 1974, pp. 287–289.
52. O'HARA, M. J., G. M. BIGGAR, D. J. HUMPHRIES, AND P. SAHA, Experimental Petrology of High Titanium Basalt. *Lunar Science*, Vol. V, Lunar Science Institute, Houston, 1974, pp. 571–573.
53. JAMES, O. B., AND E. D. JACKSON, Petrology of the Apollo 11 Ilmenite Basalts. *J. Geophys. Res.*, Vol. 75, 1970, pp. 5793–5824.
54. TERA, F., D. A. PAPANASTASSIOU, AND G. J. WASSERBURG, The Lunar Time Scale and a Summary of Isotopic Evidence for a Terminal Lunar Cataclysm. *Lunar Science*, Vol. V, Lunar Science Institute, Houston, 1974, pp. 792–794.
55. PHILPOTTS, J. A., S. SCHUHMANN, C. C. SCHNETZLER, C. W. KOUNS, A. S. DOAN, F. M. WOOD, A. L. BICKEL, AND R. K. L. LUM STAAB, Apollo 17: Geochemical Aspects of Some Soils, Basalts, and Breccia. *EOS*, Vol. 54, 1973, pp. 603–604.

Page intentionally left blank

Page intentionally left blank

A Chemical Model for Lunar Non-Mare Rocks

Norman J. Hubbard
NASA/Johnson Space Center
Houston, Texas

J. Michael Rhodes
Lockheed Electronics Corporation
Houston, Texas

Nearly all rocks returned from the Moon are readily divided into three broad categories on the basis of their chemical compositions: (1) mare basalts, (2) non-mare rocks of basaltic composition (KREEP, VHA), and (3) anorthositic rocks. Only mare basalts may unambiguously be considered to have original igneous textures and are widely understood to have an igneous origin. Nearly all other lunar rocks have lost their original textures during metamorphic and impact processes. For these rocks one must work primarily with chemical data in order to recognize and define rock groups and their possible modes of origin. Non-mare rocks of basaltic composition have chemical compositions consistent with an origin by partial melting of the lunar interior. The simplest origin for rocks of anorthositic chemical composition is the crystallization and removal of ferromagnesian minerals. We propose that the rock groups of anorthositic and non-mare basaltic chemical composition could have been generated from a single series of original, but not necessarily primitive, lunar materials.

Lunar rock samples can be subdivided according to three important types of criteria: the physiographic or geologic province where the sample was collected, the petrographic features of the sample, and its chemical composition. The lunar rocks thus far collected have come from three physiographic regions: (1) mare regions (Apollo 11 and 12), (2) a non-mare area (Apollo 14), and (3) a highland area (Apollo 16). The Apollo 15 and 17 sites were chosen to sample mare boundaries. In the broadest sense, two petrographic types of rocks have been returned: rocks with igneous textures and brecciated and metamorphosed rocks that are often visually polymict. Rocks with igneous textures were collected from all three physiographic regions but are scarce among the samples returned from the non-mare and highland regions. They are common, even characteristic, of the mare regions. Using chemical data, lunar rocks are readily separated into three major groups: (1) mare basalts, including a more aluminous feldspathic subcategory sometimes called "mare-like" basalts (ref. 1); (2) rocks with basaltic chemical composition, but distinct from the chemical compositions of mare basalts and characteristically brecciated; and (3) a group of rocks with broadly anorthositic chemical compositions.

The mare basalts, as the name implies, are typical of mare regions and have not been returned as large rocks from any other regions. In this paper the term "mare basalt" will be used to denote a combination of physiographic or geologic province, chemical composition, and basaltic igneous texture, i.e., as commonly used. Mare basalts are not a major topic in this paper and have been included for contrast and comparson with other lunar rocks of basaltic chemical composition.

Other rocks of basaltic chemical composition have been returned as large rocks from the Apollo 14, 16, and 17 sites, and were re-

turned from the Apollo 12 and 15 sites as large fragments (rake fragments and coarse fines). The term non-mare basalt will be used to denote this group of samples because a prominant member of this group, KREEP, is typical of the non-mare Apollo 14 site. This group is identical to the KREEP plus VHA compositions defined earlier (refs. 2 and 3). This usage broadens the range of chemical compositions indicated by Hubbard and Gast (ref. 2) when they introduced the term "non-mare basalt," but continues to denote a group of lunar rocks with basaltic chemical composition which we believe records some of the earliest magmatic activity on the Moon. The non-mare basaltic group contains three groups of samples that we have kept separate in earlier publications. They are the common Apollo 14 KREEP group at lower Al_2O_3 values, the Apollo 16/17 KREEP group at intermediate Al_2O_3 values, and the VHA group at higher Al_2O_3 values. They are grouped together here because the purposes of this general paper are better served by emphasizing the similarities within the non-mare basaltic group of samples and the differences between this group and the mare basalt and anorthositic groups.

Large rocks with anorthositic chemical compositions have been returned from Apollo 15, 16, and 17 and are present as small fragments in the samples returned by Apollo 11, 12, and 14 and Luna 20. A predominant subset of this group of rocks will be referred to as the Low-K Anorthositic Series (LKAS) (ref. 4). These rocks may be samples of the oldest chemical compositions returned from the Moon, and appear to have been a major component in the lunar crust for at least the last 4.0×10^9 yr (ref. 5).

The approach of this paper is to start with the returned rocks and to work backward in an attempt to deduce the chemical composition of the outer part of the Moon before these rocks were formed. In doing this, no assumptions are made about the material that formed the Moon or about an early lunar differentiation.

Presentation of Data

The chemical data used in this report were all obtained on samples of large rocks, large

Table 1.—*Precision of Major Element Data for Lunar Soils*

	10084 N = 9		12070 N = 6		14163 N = 6		15101 N = 4		66081 N = 3		72701 N = 4	
	Mean	Rel. Dev.(1)	Mean	Rel. Dev.(1)	Mean	Rel. Dev.(1)	Mean	Rel. Dev.(1)	Mean	Rel. Dev.(1)	Mean	Rel. Dev.(1)
SiO_2	41.98	0.6	45.83	0.2	47.66	0.9	46.21	0.3	44.97	0.9	45.13	0.6
TiO_2	7.49	1.7	2.81	0.7	1.80	2.6	1.31	5.2	0.67	0.9	1.53	2.5
Al_2O_3	13.75	2.1	12.71	1.6	17.45	1.6	17.55	0.7	25.99	0.8	20.64	0.4
FeO	15.83	0.8	16.52	1.2	10.26	1.3	11.61	0.9	5.99	2.5	8.84	1.7
MnO	0.21	3.7	0.22	2.3	0.14	2.9	0.16	0.0	0.08	0.0	0.12	5.3
MgO	7.90	1.6	10.14	3.3	9.29	0.9	10.32	1.9	6.40	0.6	9.95	0.6
CaO	12.02	0.8	10.45	0.4	10.95	2.0	11.63	0.9	15.17	1.1	12.77	0.5
Na_2O	0.44	8.4	0.45	9.7	0.70	9.1	0.40	6.5	0.48	21.5	0.46	10.8
K_2O	0.14	10.4	0.25	6.2	0.57	2.7	0.18	5.4	0.14	8.5	0.16	4.8
P_2O_5	0.10	26.5	0.31	6.9	0.50	4.8	0.16	15.4	0.13	15.4	0.15	4.0
S	0.13	8.4	0.09	29.4	0.09	9.1	0.07	20.8	–	–	0.07	16.4
Cr_2O_3	0.30	7.9	0.41	13.0	0.21	13.5	0.29	21.0	0.13	–	0.22	11.4
Total	100.29		100.19		99.62		99.89		100.15		100.04	

NOTE: (1) Standard deviation (1σ) expressed as a percentage of the mean.
Sources of data:
10084: References 6 through 12.
12070: References 9, 13, 14, and 15.
14163: References 9, 12, and 16 through 19.
15101: References 9, 12, 20, and 21.
66081: References 22, 23, and 24.
72701: References 10, 25, 26, and 27.

breccia clasts, or rake samples. (Data for soil samples are given in figures 1, 2, 4, and 5 for comparison.) The major element data are largely from X-ray fluorescence analyses, and the trace element data are predominantly from stable isotope dilution mass spectrometric analyses done in our laboratory and reported in numerous papers by Hubbard and coauthors. Neutron activation and X-ray fluorescence data have been included when needed to fill critical gaps for the elements Eu and Sr.

DATA QUALITY

The quality of data from a purely analytical standpoint is best assessed using analyses of lunar soils. The chief advantage of this approach is that samples covering a broad range of chemical compositions were analyzed in an analytical environment that was "real" in the sense that these analyses were made in order to supply scientists with chemical data for research purposes rather than to obtain data on rock standards for the purpose of interlaboratory comparison. The analyses were commonly performed without the knowledge of other analyses of the same samples. In table 1 we list the means and percent-relative deviations for one soil sample with three or more chemical analyses from each Apollo mission. This comparison extends over the entire Apollo program and includes results from eight research groups. In an earlier paper (ref. 28), we documented the degradation of chemical data for mare basalts that resulted from the allocation of excessively small subsamples (commonly only 0.5 g) of coarse-grained Apollo 15 mare basalts. This sampling problem is severe when attempting to use such analyses to interpret the detailed petrogenesis of individual coarse-grained mare basalts, but less troublesome when studying mare basalts as a chemical group. In contrast, lunar rocks of non-mare and anorthositic chemical compositions contain so many complexities that it has not proven feasible to interrelate individual samples; their study is therefore largely limited to consideration of the chemical groups. The analysis of a large clast in a breccia of different composition is treated as a separate sample. The chemical analyses often reflect the heterogeneities due to the intimate but incomplete mixing of two different rocks with two widely different chemical compositions (e.g., 61016), and also reflect variability in the plagioclase/ferromagnesian ratio (e.g., 67075, 14310, 65015).

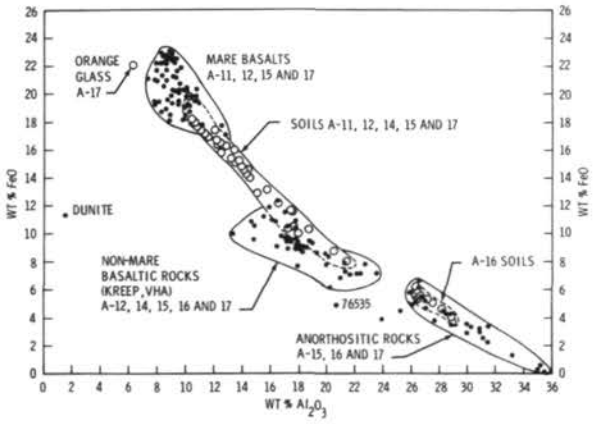
In order to test the reproducibility of our trace element data we recently reanalyzed the very first lunar sample analyzed by us (10084) and the first Apollo 12 sample analyzed by us (12070). In all cases the new values are within 12 percent of the original values, and about 80 percent of the new values are within 5 percent of the first values. This comparison covers a 4-year period and a total change of laboratory, equipment, and materials.

In view of the above results, we conclude that the chemical data used in this paper are fully adequate to support detailed study, with due respect for sampling problems, and are free of analytical error for the types of interelement comparisons and correlations made in this study.

THE DATA

Chemical data for soils are included in some figures for comparison and to demonstrate that lunar soils from the Apollo sites are composed of varying proportions of material, chemically similar or identical to the material found in the local rocks. However, estimates of the relative abundances of these rock types based on soil composition may differ drastically from their relative abundances in the returned sample collection (ref. 26). The three main chemical groups used in this paper have been recognized on several bases, including the chemical one used in this paper. Individual samples that are inconsistent with this broad chemical classification will be noted where considered appropriate.

In figure 1 we have plotted data for FeO versus Al_2O_3, which, with the exception of



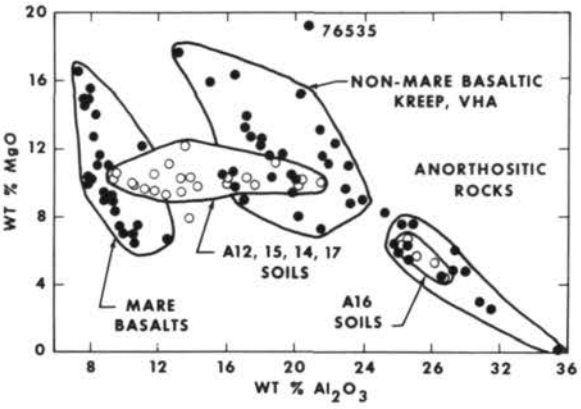


Figure 2.—*MgO versus Al_2O_3 for lunar rock and soils. Data are from the same sources as for figure 1.*

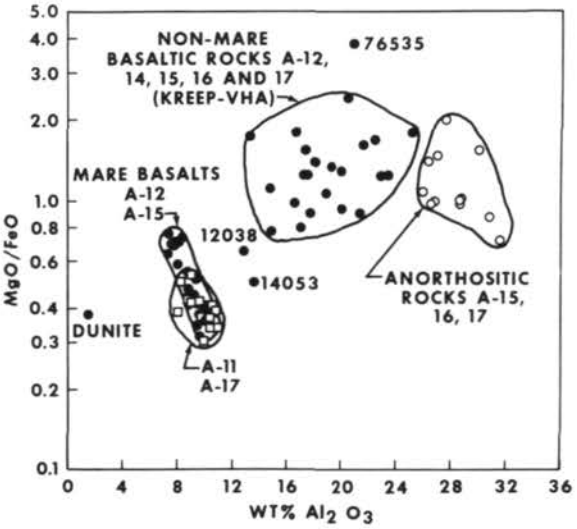


Figure 3.—*MgO/FeO ratio versus Al_2O_3 for lunar rocks. Note that the rocks with the highest Al_2O_3 concentrations have the widest range in MgO/FeO ratios. Data are from the same sources as for figure 1.*

Figure 1.—*FeO versus Al_2O_3 for lunar rocks and soils. Data are from references 4, 9, 10, 12 through 15, 17, 23, 24, 26, and 28 through 31.*

Ti, are the major elements that show the most variance in lunar rocks. The anorthositic rocks have a relatively well-defined inverse variation of FeO and Al_2O_3. Extrapolation of the FeO-Al_2O_3 trend seen in these rocks toward the non-mare basaltic rocks shows that the non-mare basaltic rocks generally have less FeO for a given Al_2O_3 value than predicted from the extrapolation. This demonstrates that non-mare basaltic rocks and anorthositic rocks are two populations and not simply one population with internal variation in plagioclase abundance. The mare basalts have, on the contrary, more FeO than expected from the extrapolation. In figure 2, MgO is plotted versus Al_2O_3, where it is shown by extrapolating from the data for anorthositic rocks that mare basalts have far less MgO than expected. Non-mare basaltic rocks show a wide range in MgO and Al_2O_3 concentrations, with their range in MgO concentrations nearly identical to the range in MgO concentrations for mare basalts. Figure 3 shows MgO/FeO ratios versus Al_2O_3 and demonstrates that anorthositic rocks have the widest range of MgO/FeO ratios of any group of lunar rocks and that the ranges of MgO/FeO ratios for non-mare and mare basalts are similar even though mare basalts have much lower MgO/FeO ratios. The range in MgO/FeO ratios in mare basalts suggests that the similar variations in the non-mare basalt group may also be due to fractional crystallization even though these samples have lost any original igneous textures. Figure 4 illustrates the variation of TiO_2 relative to Al_2O_3. The major features of this diagram are the steady rise in average TiO_2 concentrations in the series anor-

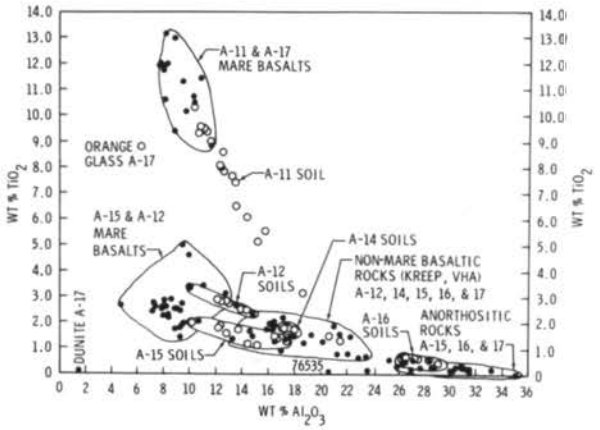
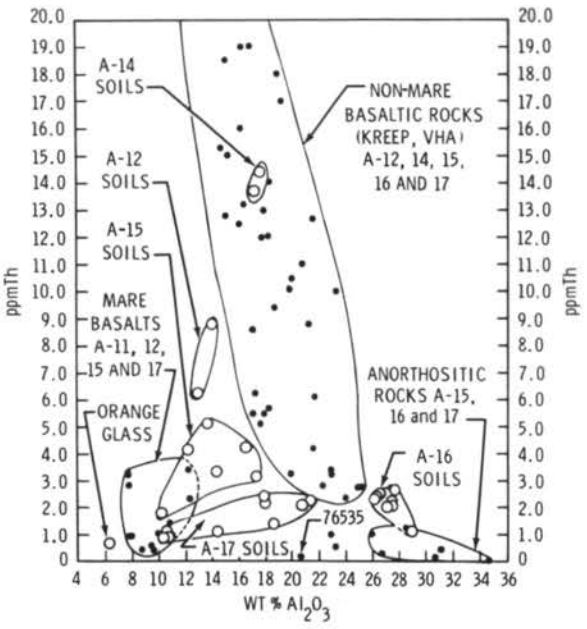


Figure 5.—*Th versus Al_2O_3 for lunar rocks and soils. This plot serves to demonstrate that it is the non-mare basaltic group of rocks that has high concentrations of lithophile trace elements such as Th, U, rare earths, Ba, Zr, etc. Data are from the same sources as for figure 1, plus numerous other papers published in the Lunar Science Conference volumes.*

Figure 4.—*TiO_2 versus Al_2O_3 for lunar rocks and soils. Note that only the Apollo 11 and 17 mare basalts and associated soils have TiO_2 values greater than 6 percent. Data are from the same sources as for figure 1.*



thositic rocks → non-mare basaltic rocks → Apollo 12 and 15 mare basalts and the threefold to fourfold higher TiO_2 concentrations of the Apollo 11 and 17 mare basalts.

Figure 5 shows the variation of Th relative to Al_2O_3 and serves to make the transition between major element and trace element data, and identifies the non-mare basaltic rocks as the group of rocks that have high concentrations of lithophilic trace elements such as Th, U, REE, Ba, Zr, etc.

The data for one set of lithophilic trace elements, the REE, and Ba are summarized in figure 6 for a wide range of Apollo 15, 16, and 17 non-mare basaltic rocks and anorthositic rocks. The data in this diagram can be divided into two major groups: (1) rocks with deep negative Eu anomalies and high concentrations of REE and Ba and (2) rocks with almost no Eu anomalies or positive Eu anomalies and low REE concentrations. Not surprisingly, the samples in group 2 have anorthositic major element chemistry and are the anorthositic samples in figures 1 through 5. The samples in group 1 are the non-mare basaltic rocks (KREEP, VHA) that cluster together in terms of major element variables (figures 1 through 5). Taken together, the data in figures 1 and 6 amply demonstrate that non-mare basaltic rocks and anorthositic rocks are two separate chemical groups.

Rare Earth, Ba, U, and Sr data are presented in figure 7 for anorthositic rocks only. There is a high degree of regularity in the REE, Ba, and U abundance patterns of these rocks, in that the concentrations of REE, Ba, and U generally decrease with increasing Al_2O_3 concentrations, suggesting that we may be dealing with a series of anorthositic rocks where the major chemical variations are a function of plagioclase concentration. However, some samples deviate from the simple requirements of an anorthositic series—in this case, a specific correlation of REE

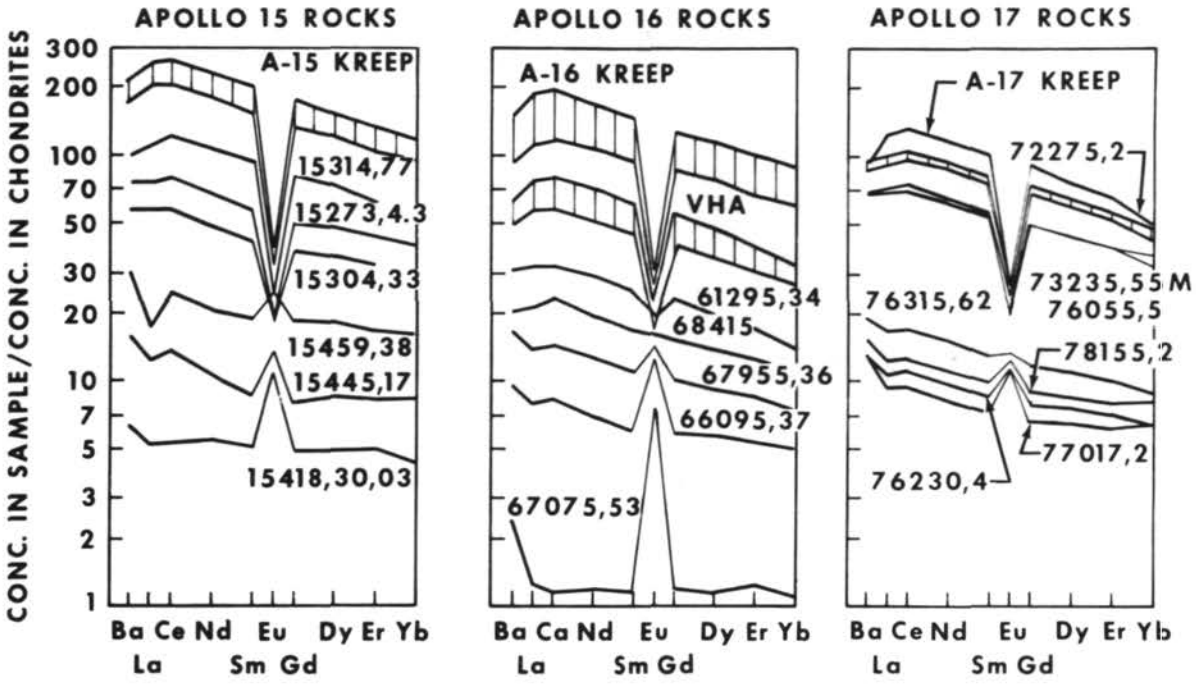


Figure 6.—*Rare earth and Ba data for a large number of Apollo 15, 16, and 17 rocks. The main features of these data are that the rocks with deep negative Eu anomalies belong to the group of nonmare basaltic rocks in figures 1 through 5, and the rocks with positive Eu anomalies belong to the anorthositic group in figures 1 through 5, as do samples 68415 and 61295. All of the data are from publications by Hubbard and coworkers.*

abundance patterns with Al_2O_3 versus Eu, Sr, and Sm (ref. 4). Further subdivision or reduction to conditional membership in the main subgroup is made on other chemical parameters such as the slope of the trivalent rare earth abundance patterns, MgO/FeO ratio, and abnormally low or high concentrations of any rock-forming element like Si, K, Ti, Cr, etc. On this basis we can immediately reject 63335,36, 15459,38, 61295,34, 68415,10 and 63549,2 from the rest of the samples because 63335,36 has an abnormal Eu anomaly and 15459,38, 61295,34, 68415,10, and 63549,2 have too much Eu, Sr, and Sm for their Al_2O_3 concentrations. Samples 15418, 67075, and 15445,17 are conditionally retained with the majority of samples even though sample 15418 has low Sm for its Al_2O_3 value of 26 percent and also has a flatter trivalent rare earth pattern. Sample 67075,53 also has a flat trivalent rare earth pattern and has the lowest MgO/FeO ratio of anorthositic samples included in this study. Sample 15445, 17 has low Al_2O_3, a high MgO/FeO ratio, and a high SiO_2 concentration. The white portion of sample 15445 (ref. 32) has not been included in the LKAS group because of its high MgO/FeO ratio, low TiO_2, very high Eu concentration, and the steep slope of its trivalent rare earth pattern. There are more than 10 samples remaining, after the deletions, with a simple and regular pattern of major and trace element chemical compositions. These have been named the Low-K Anorthositic Series (LKAS). This series has been proposed to be a major subset of anorthositic lunar rocks (ref. 4).

A thorough consideration of the behavior of Eu in lunar rocks requires accurate knowledge of the $Eu^{+3/+2}$ ratio during petrogenesis. Lunar rocks formed in rather reducing conditions, i.e., about 10^{-13} atm of oxygen partial pressure at temperatures about 1200°C (ref. 33), and it is reasonable to assume, as is commonly done, that Eu is largely

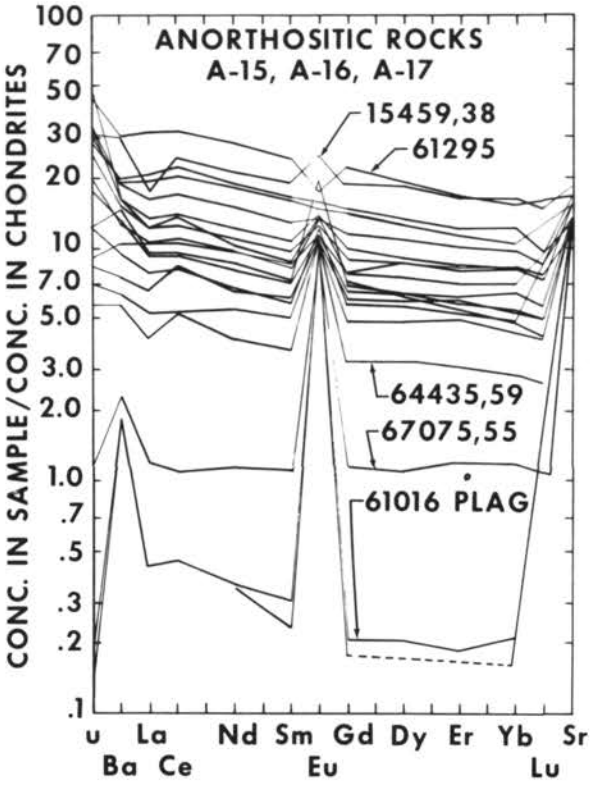
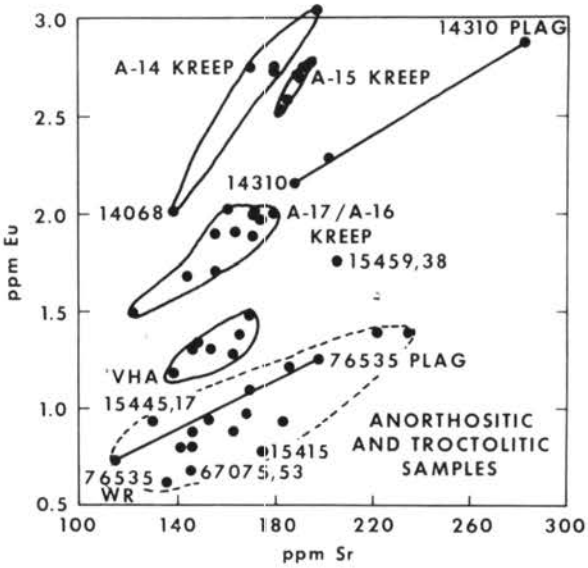


Figure 8.—*Eu versus Sr for the entire range of non-mare basaltic and anorthositic lunar rocks. If Eu were entirely divalent and the lunar rocks were formed from a common parent with a single Eu/Sr ratio, this Eu versus Sr plot should be very nearly a single narrow band of data points. Instead, for a twofold range in Sr concentration there is a fourfold range in Eu concentrations. As discussed in the text, this greater range in Eu concentrations is explained as the result of 10 to 20 percent of the Eu having been in the trivalent oxidation state during magma genesis.*

Figure 7.—*Rare earth, Ba, U, and Sr data for anorthositic rocks from Apollo 15, 16, and 17. Nearly all of the data are from Hubbard et al. (1974). The remainder are from earlier publications. In order of increasing Sm concentrations, the samples plotted are 61016, plag, 67075,53, 64435,59, 15418,30,03, 66095,37, 15418,30,07A, 76230,4, 63335,36, 61016,3, 77017,2, 15445,17, 78155,2, 67955,56, 76315,62, 68415,10, 63549,2, 15459,38, and 61295.*



divalent. A plot of Eu versus Sr (fig. 8) and the overall rare earth data shown in figure 6 provide fundamental information about the ratio of $Eu^{+3/+2}$ in the lunar petrogenetic environment for non-mare and anorthositic rocks. If Eu was entirely divalent during lunar petrogenesis, then Eu should closely follow Sr. Instead, Eu has a much wider range of concentration than Sr in lunar non-mare and highland rocks. If one considers that this is due to the presence of substantial Eu^{+3}, then the rare earth data in figure 6 allow one to estimate that the percentage of Eu that is trivalent is 10 to 20 percent, on the assumption that trivalent Eu is intermediate between trivalent Sm and Gd in its chemical behavior. Some recent experimental work is directly relevant to this question. Morris and Haskin (ref. 34) found that for a fixed pO_2, the $Eu^{+3/+2}$ ratio is strongly dependent on the bulk composition for glasses in the compositional range from anorthite to Ca-Mg pyroxene. Specifically, the nearer the glass composition to the pyroxene

end member the higher the $Eu^{+3/+2}$ ratio. Related research by Morris et al. (ref. 35) found that even in glass of anorthite composition ($CaAl_2Si_2O_8$) at 1370 to 1600°C the Eu^{+3} was about 10 percent of the total Eu at $pO_2 = 10^{-12}$, and about 4 percent of the total at $pO_2 = 10^{-14}$. Thus, even a pure anorthite liquid at lunar pO_2 may have a few percent of trivalent Eu. Glass of diopside composition ($CaMgSi_2O_2$) at 1450°C at $pO_2 = 10^{-14}$ was found to have $Eu^{+3/+2} \sim 0.5$. These experimental data suggest that silicate liquids on the Moon of non-mare basaltic composition (KREEP, VHA), i.e., 50 percent or less pyroxene, will have about one-fourth or less of their Eu in the trivalent oxidation state, thus substantiating the above interpretation of the chemical data for lunar rocks.

The Chemical Model

INTRODUCTORY REMARKS

This model is primarily concerned with the origin of the non-mare basaltic and anorthositic rocks. There will be no attempt to further decipher the genesis of mare basalts. With both non-mare basaltic and anorthositic rocks there is a fundamental need to directly determine which rocks have had their chemical compositions seriously contaminated by material from non-cogenetic rocks and the nature and extent of such contamination. Typically for current studies of lunar rocks, such data are almost nonexistent for the chips of samples used in this study. It is expected that accurate and verifiable knowledge of such contamination will result in a sharper view of the chemical processes described in this paper because the "noise" introduced by contamination will be reduced and seriously contaminated rocks can be excluded from this type of study. Impact-related mixing processes are the accepted means of mixing (i.e., contaminating) non-cogenetic lunar rocks, as well as mixing the members of a cogenetic suite of rocks.

There is an apparent paradox in that there is an extensive cratering history in the lunar highlands (ref. 36) which is consistent with the brecciated nature of nearly all lunar samples except mare basalts. Yet, the bulk of the chemical data shown in this paper is compatible with igneous processes, suggesting that igneous processes have produced a wide range of chemical compositions. From this we conclude that igneous processes were either more effective or lasted longer than the homogenizing effect of impact processes, or, perhaps, simply that impact mixing was not adequately efficient to erase the chemical record. This apparent paradox between the extensive cratering record and the extensive range of chemical compositions seen among the non-mare and highland rocks, as well as the existence of preferred chemical groups, has led one group of researchers (ref. 37) to propose that the impacts both homogenize (through mixing) and differentiate (through partial fusion) the material involved in the impact. We find it difficult to accept the hypothesis that impact events can produce the observed abundance of material that has an apparent igneous origin because of a lack of evidence that impact processes cause significantly more igneous differentiation than mixing. Since mixing reverses the processes of differentiation, Warner et al. (ref. 37) are dependent on an unproven efficiency of impact-related differentiation.

Mixing processes must operate on existing material and, if mixing processes are of any importance, that material must have initially had at least as wide a range of chemical composition as presently observed, because mixing processes will decrease the probable range of chemical compositions available for sampling. The observed range of chemical compositions was either produced on the Moon, already existed in the material that accreted to form the outer tens to hundreds of kilometers of the Moon, or some combination of the two possibilities. At least one model (ref. 38) proposes that the Moon was made from partially disrupted preexisting planetary bodies and thus provides for lunar material that has a prelunar igneous history. In the absence of unambiguous data to the contrary, and for simplicity, we presume that

igneous differentiation on the Moon was the cause of the range of chemical compositions observed in the non-mare basaltic and anorthositic rocks and that homogenization due to impact-related mixing has been minimal. We will describe what we consider to be the general features of that differentiation. We believe that the hypothesis we have chosen to emphasize has the greatest potential for revealing fundamental internal lunar processes and evolution. In this paper we will not consider heat sources that could have caused the inferred igneous differentiation. If an igneous interpretation of the chemical data is correct, then an adequate heat source must have existed. Current interpretations of the Rb-Sr data (refs. 5, 39, and 40) suggest that the heat source was adequate about 4.3×10^9 years ago.

THE MODEL

We will first consider the non-mare basaltic and anorthositic groups independently and then combine the requirements of these groups in order to arrive at an overall model. The genesis of mare basalts will not be discussed below. Interested readers are referred to reference 4 and earlier papers where we have presented arguments for the generation of mare basalts from a different source material than non-mare basaltic rocks and proposed that much of the inferred chemical differences were the result of heterogeneous accretion of the outer part of the Moon.

Non-Mare Basaltic Rocks

This group of rocks is identical with the KREEP and VHA rocks described earlier (refs. 1 through 4, 30, and 31). The recent experimental paper of Walker et al. (ref. 41) provides the clearest insight into the origin of the non-mare basaltic rock types so far as major elements are concerned. Briefly, they are the result of partially melting any of a wide range of rocks having variable amounts of plagioclase, pyroxene, olivine, and, for the VHA samples, sometimes spinel. The deep negative Eu (also Sr) anomalies of these rocks are explained as the result of partially melting plagioclase-bearing source rocks that retain significant plagioclase in the residue after the partial melting episode (ref. 2). These samples have a characteristic slope in their trivalent rare earth abundance patterns (chondrite normalized $La/Yb \simeq 2.0$). This was initially explained (ref. 2) as the result of partially melting a plagioclase, clinopyroxene, olivine source rock to a very limited extent (only a few percent liquid generated). This specific partial melting model depended on the combination of clinopyroxene and small amounts of liquid to produce the observed La/Yb slope from material that had the rare earths in absolutely chondritic relative abundances. Even with the enrichments provided by the small amounts of liquid produced, this model requires the source to have about tenfold chondritic concentrations. However, clinopyroxene is absent or of minor importance in both non-mare basaltic and anorthositic rocks, as well as in their probable source materials and their P–T conditions of origin (refs. 41 and 42), thus invalidating partial melting models that depend on clinopyroxene for fractionation of the La/Yb ratio. Recently Hubbard and Shih (refs. 43 and 44) considered partial melting models that are more realistic for lunar non-mare basaltic samples, i.e., no clinopyroxene. In addition, distribution coefficient data obtained using phenocrysts were preferred to those obtained using high-pressure metamorphic mineral pairs. The resulting model, using only plagioclase, olivine, and orthopyroxene does very little differentiation of La/Yb ratio, essentially transmitting the trivalent rare earth abundance pattern of the unmelted source material into the liquid. It is possible to use an orthopyroxene-rich source material (fig. 9) to produce La/Yb ratios approaching the observed ratios from a source material with chondritic relative abundances of the rare earths, but only with the generation of 1 percent or less liquid. Increasing the plag/opx ratio of the source reduces the La/Yb ratio of the liquid, as does the generation of larger

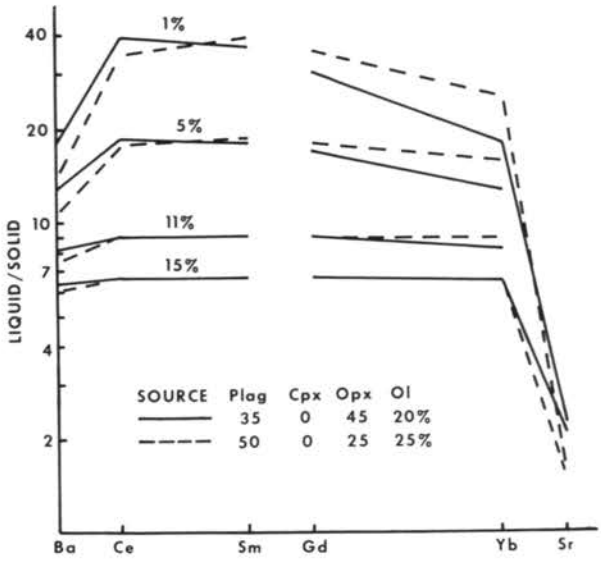


Figure 9.—*Two partial melting models that are capable of producing the range of trivalent rare earth concentrations observed in the non-mare basaltic group of rocks. See Gast (ref. 45) for the most recent version of the old clinopyroxene bearing models. Sr serves to indicate the behavior of* Eu^{+2}*, which is not plotted in order to emphasize the trivalent rare earths.*

percentages of melt. This model requires that the observed La/Yb ratio and the characteristic slope of the trivalent rare earth abundance pattern must have already been in the source material. The deviation from absolutely chondritic relative abundances for the rare earths is not large, in fact only requiring La to be 1.35 × and Yb 0.675 × chondritic. Since the chemical compositions of the returned lunar samples are grossly nonchondritic, this deviation is quite permissible. Partial melting events that produce about 4 to 5 percent of liquid (fig. 9) have about twentyfold more rare earths, etc., in the liquid than in the initial material, and can thus produce even the rare earth concentrations in Apollo 14 KREEP if the initial material had tenfold chondrite concentrations of these elements.

There is an inverse correlation between Al_2O_3 and Eu and the trivalent rare earths within the non-mare basaltic group of rocks for the series VHA through Apollo 16/17 KREEP to Apollo 14 common KREEP (figs. 1, 6, and 8 and ref. 4). This can be explained by coupling the pseudoternary silica-anorthite-olivine diagram of Walker et al. (ref. 41) with trace-element-derived partial melting model calculations. On the pseudoternary diagram the series of compositions from Apollo 14 common KREEP to Apollo 16/17 KREEP to VHA becomes more aluminous and moves toward higher liquidus temperatures. The Eu and trivalent rare earths decrease in this series, implying, in terms of partial melting models, increasing percentages of liquid (melting). This in turn is consistent with the higher liquidus temperatures of the more Al_2O_3-rich compositions. This is not meant to imply that the entire series of chemical compositions within the non-mare basaltic group was generated from a single source material, but rather that many of the predictable chemical features are consistent with this concept, even though some allowance must be made for the MgO/FeO ratio differences (ref. 41). Schemes that properly combine partial melting models and experimental data require that partial melting models be tuned to produce the observed variations in major element chemical composition and attendant changes in the permissible mineralogical composition of the source material. This is presently very difficult to do for the observed wide range in MgO/FeO ratios, but has been taken into consideration for plagioclase/orthopyroxene/olivine ratios.

The Anorthositic Group

The LKAS subset of the anorthositic samples was anticipated by Hubbard et al. (ref. 1) when they calculated the REE, Ba, and Sr concentration in a hypothetical silicate liquid in equilibrium with anorthosite sample 15415. The crystal plus equilibrium liquid model behind those calculations is still the most satisfactory chemical explanation of the internal, plagioclase-related chemical variations. Samples like 77017 and 66095,37 have major and trace element compositions

approximating the equilibrium liquid of the model.

It is easier to say, with qualifications, how the group of rocks with anorthositic chemical compositions were not formed than how they were formed. Although the major cause of internal chemical variations is clearly a result of plagioclase control, the anorthositic group itself is probably not the result of plagioclase fractional crystallization because of the consistent lack of negative Eu and Sr anomalies for this group. One could avoid this constraint by assuming a precursor with positive Eu and Sr anomalies; that is, by assuming an even more Al_2O_3- and plagioclase-rich precursor and further increasing the difficulty of accounting for these rocks. The consistent lack of negative Eu and Sr anomalies also rules against the production of this group by partial melting because again negative anomalies in the observed rocks and more Al_2O_3 and plagioclase precursors are the predicted result. If the process is to be igneous, we are left with either plagioclase accumulation or fractional crystallization of ferromagnesian minerals. Plagioclase accumulation due to flotation of plagioclase has been popular (refs. 46 and 47), but it remains unproven that plagioclase will float in feldspathic silicate liquids. On the other hand, ferromagnesian minerals will almost surely sink unless there is a prohibitive mesh of earlier crystallizing plagioclase. A prohibitive mesh of plagioclase crystals is increasingly likely as the Al_2O_3 concentration increases, thus progressively reducing the efficiency of this process as more feldspathic compositions are reached. So long as sinking of ferromagnesian minerals is the proposed mechanism for generating the anorthositic group, plagioclase does not move relative to the liquid, and we have no knowledge of the olivine/pyroxene ratio, the MgO/FeO ratio of the parental material is very poorly defined. Although likely, it is not essential that the parent material have plagioclase on the liquidus, but it must have had an even higher MgO/FeO ratio than presently found in anorthositic lunar rocks in order to allow removal of ferromagnesian minerals, especially extensive removal. If extensive removal of orthopyroxene occurred, then the La/Yb ratio would have been increased somewhat, but probably no higher than one and one-half times the initial ratio in the source material (ref. 44). Also, if large volumes of material were removed by the fractional crystallization of ferromagnesian minerals, then the initial Eu and Sr concentrations would have been lower and the early crystallizing plagioclase crystals would have had to completely reequilibrate in order to produce the observed consistent minimum concentrations of Eu and Sr. This difficulty decreases as the amount of ferromagnesian minerals removed decreases after the onset of plagioclase crystallization. In summary, we consider the removal of ferromagnesian minerals to be the most reasonable means of making the anorthositic rocks on the Moon, or any other similar planetary body, mainly because the alternate means considered here are even less probable. Another alternative is to provide a precursor that has a chemical composition very near to or within the field of compositions for anorthositic rocks.

A Common Precursor

The chemical similarities of the parental materials inferred for the non-mare basaltic and anorthositic chemical groups is suggestive of a common precursor for these groups. It does not seem possible to describe material with a single chemical composition because some of the requirements of the two groups are mutually inconsistent, in particular the inferred initial concentrations of rare earths and related lithophile trace elements. However, definition of a series of closely related precursors seems appropriate and possible at the present time. The goal is to define the limits of a probable set of lunar materials that could have been parental to the chemical groups observed in the returned lunar samples. The result of this exercise is expected to change, perhaps radically, as further data are obtained and the approach is further developed.

First, the materials do not have to be plagioclase rich. Thirty percent plagioclase is adequate to produce the observed deep negative Eu and Sr anomalies of the non-mare basaltic group, and the ferromagnesian fractional crystallization deduced for the anorthositic group can produce the required plagioclase enrichments. Conversely, nothing prohibits a plagioclase-rich material so long as the requirements imposed by large percentages of plagioclase are not considered prohibitive. The natural limit on plagioclase enrichment is reached when it becomes prohibitively difficult to produce an adequate volume of the non-mare basaltic composition liquid, probably around 70 percent plagioclase.

Second, the pyroxene/olivine ratio is not very well determined and neither is the MgO/FeO ratio, although the MgO/FeO ratio must be greater than about 1.5 in order to produce liquids with MgO/FeO greater than 1.5. Ratios of MgO/FeO increasingly greater than 1.5 are probably compatible with decreasing pyroxene/olivine ratios.

Third, there is no independent way of postulating the trace element concentrations and ratios of these lunar materials unless one adopts a specific model for making the material that was later incorporated into the Moon. We have adopted no such model because we are attempting to work backwards from the chemical compositions of analyzed lunar rocks. If the REE concentrations are to be produced by single-stage partial melting and the problems of extracting very small percentages ($\sim$ 1 percent) of liquid are to be avoided, this approach requires that the parental material for the non-mare basaltic group had at least tenfold chondritic concentrations of REE for the Apollo 14-type KREEP and perhaps as little as threefold to fourfold for the VHA compositions. A source with tenfold chondritic concentrations of REE can also be used as the source for the Apollo 16/17-type KREEP and VHA basaltic compositions. The anorthositic rocks require parental material with less than tenfold chondritic concentration for the LKAS subgroup and similar concentrations for the other samples. Threefold to fivefold lower concentrations are possible if extensive fractional crystalization occurred during the genesis of these rocks.

In summary, the plausible outer bounds for a set of precursors that could have been parental to the non-mare basaltic group and the anorthositic group are quite far apart. The plagioclase concentration could be as low as about 30 percent or as high as about 75 percent. The Al_2O_3 concentration could be as low as about 10 percent or as high as about 26 percent. The MgO/FeO ratio can only be constrained to be greater than 1.5 and can be highly variable. Concentrations of lithophile trace elements may be as low as threefold chondritic values or as high as more than tenfold. This wide range in chemical composition is easily converted into a set or spectrum of compositions if the realistic assumption is made that the concentration of lithophile trace elements is inversely correlated with plagioclase concentration. However, if the anorthositic rocks require a plagioclase-rich source material with nearly tenfold chondritic concentrations of rare earths, etc., then the series cannot be so simple as just suggested. Although we consider it improbable that the precursor for non-mare lunar rocks was as simple as deduced here, we do consider a precursor consisting of a related series of chemical compositions to be much more reasonable than one with a single chemical composition. The old Rb-Sr model ages of the KREEP rocks and the low initial $Sr^{87/86}$ ratios of some anorthositic samples suggests that this precursor may be original lunar material (refs. 5, 39, and 40).

If the type of precursor suggested here is basically correct, the hypothesized increase of rare earths, etc., with ferromagnesian content implies that it was not produced by crystal accumulation because the relevant minerals, orthopyroxene, olivine, and plagioclase, all reject rare earths (except Eu^{+2}) to a very similar extent. We are left with two poorly defined possibilities: (1) the precursor was a residual liquid produced by extensive differentiation of the Moon or (2) the precursor was the material that accumu-

lated to form the outer part of the Moon, altered by thermal metamorphism prior to melting. In view of the inferred old ages for the chemical compositions of lunar nonmare rocks (refs. 5, 39, and 40), this approach may get us as close as any to the chemical composition of original lunar crustal material and is certainly more comprehensive than approaches using individual and unique lunar rocks such as 76535, 72415, or 15415.

References

1. HUBBARD, N. J., P. W. GAST, C. MEYER, L. E. NYQUIST, C. SHIH, AND M. WIESMANN, Chemical Composition of Lunar Anorthosites and Their Parent Liquids. *Earth Planet. Sci. Letters*, Vol. 13, 1971, pp. 71–75.
2. HUBBARD, N. J., AND P. W. GAST, Chemical Composition and Origin of Nonmare Lunar Basalts. *Proc. Second Lunar Science Conference, Geochimica et Cosmochimica Acta*, Supplement 2, Vol. 2, 1971, pp. 999–1020.
3. HUBBARD, N. J., J. M. RHODES, AND P. W. GAST, Chemistry of Very High Al_2O_3 Lunar Basalts. *Science*, Vol. 181, 1973, pp. 339–342.
4. HUBBARD, N. J., H. WIESMANN, C. SHIH, B. BANSAL, AND J. M. RHODES, The Chemical Definition and Interpretation of Rock Types Returned From the Non-Mare and Highland Regions of the Moon. *Proc. Fifth Lunar Science Conference, Geochimica et Cosmochimica Acta*, Supplement 5, Vol. 2, in press, 1974.
5. NYQUIST, L. E., B. M. BANSAL, H. WIESMANN, AND B. JAHN, Taurus Littrow Chronology: Some Constraints on Early Lunar Crustal Development. *Proc. Fifth Lunar Science Conference, Geochimica et Cosmochimica Acta*, Supplement 5, Vol. 2, in press, 1974.
6. AGRELL, S. O., J. H. SCOON, I. D. MUIR, J. V. P. LONG, J. D. C. MCCONNEL, AND A. PECKETT, Observations on the Chemistry, Mineralogy and Petrology of Some Apollo 11 Lunar Samples. *Proc. Apollo 11 Lunar Science Conference, Geochimica et Cosmochimica Acta*, Supplement 1, Vol. 1, 1970, pp. 93–128.
7. COMPSTON, W., B. W. CHAPPELL, P. A. ARRIENS, AND M. J. VERNON, The Chemistry and Age of Apollo 11 Lunar Material. *Proc. Apollo 11 Lunar Science Conference, Geochimica et Cosmochimica Acta*, Supplement 1, Vol. 2, 1970, pp. 1007–1027.
8. ENGEL, A. E. J., AND C. G. ENGEL, Lunar Rock Compositions and Some Interpretations. *Proc. Apollo 11 Lunar Science Conference, Geochimica et Cosmochimica Acta*, Supplement 1, Vol. 2, 1970, pp. 1081–1084.
9. LSPET (Lunar Sample Preliminary Examination Team), The Apollo 15 Lunar Samples: A Preliminary Description. *Science*, Vol. 175, 1972, pp. 363–375.
10. LSPET (Lunar Sample Preliminary Examination Team), Apollo 17 Lunar Samples: Chemical and Petrographic Description. *Science*, Vol. 182, 1973, pp. 659–674.
11. MAXWELL, J. A., L. C. PECK, AND H. B. WIIK, Chemical Composition of Apollo 11 Lunar Samples 10017, 10020, 10072 and 10084. *Proc. Apollo 11 Lunar Science Conference, Geochimica et Cosmochimica Acta*, Supplement 1, Vol. 2, 1970, pp. 1369–1374.
12. WILLIS, J. P., A. J. ERLANK, J. J. GURNEY, R. H. THEIL, AND L. H. AHRENS, Major, Minor and Trace Element Data for Some Apollo 11, 12, 14 and 15 Samples. *Proc. Third Lunar Science Conference, Geochimica et Cosmochimica Acta*, Supplement 3, Vol. 2, 1972, pp. 1269–1274.
13. COMPSTON, W., H. BERRY, M. J. VERNON, B. W. CHAPPELL, AND M. J. KAYE, Rubidium-Strontium Chronology and Chemistry of Lunar Material From the Ocean of Storms. *Proc. Second Lunar Science Conference, Geochimica et Cosmochimica Acta*, Supplement 2, Vol. 2, 1971, pp. 1471–1486.
14. CUTTITTA, F., H. J. ROSE, JR., C. S. ANNELL, M. K. CARRON, R. P. CHRISTIAN, E. J. DWORNIK, L. P. GREENLAND, A. W. HELZ, AND D. T. LIGON, JR., Elemental Composition of Some Apollo 12 Lunar Rocks and Soils. *Proc. Second Lunar Science Conference, Geochimica et Cosmochimica Acta*, Supplement 2, Vol. 2, 1971, pp. 1217–1320.
15. WILLIS, J. P., L. H. AHRENS, R. V. DANCHIN, A. J. ERLANK, J. J. GURNEY, P. K. HOFMEYR, T. S. MCCARTHY, AND M. J. ORREN, Some Inter-Element Relationships Between Lunar Rocks and Fines, and Stony Meteorites. *Proc. Second Lunar Science Conference, Geochimica et Cosmochimica Acta*, Supplement 2, Vol. 2, 1971, pp. 1123–1138.
16. CHAPPELL, B. W., Personal communication, 1972.
17. ROSE, H. J., JR., F. CUTTITTA, C. S. ANNELL, M. K. CARRON, R. P. CHRISTIAN, E. J. DWORNIK, L. P. GREENLAND, AND D. T. LIGON, JR., Compositional Data for Twenty-One Fra Mauro Lunar Materials. *Proc. Third Lunar Science Conference, Geochimica et Cosmochimica Acta*, Supplement 3, Vol. 2, 1972, pp. 1215–1230.
18. SCHNETZLER, C. C., AND D. F. NAVA, Chemical Composition of Apollo 14 Soils 14163 and 14259. *Earth Planet. Sci. Letters*, Vol. 11, 1971, pp. 345–350.
19. WIIK, H. B., J. A. MAXWELL, AND J. L. BOUVIER,

Chemical Composition of Some Apollo 14 Lunar Samples. *Earth Planet. Sci. Letters*, Vol. 17, 1973, pp. 365–368.

20. CARRON, M. K., C. S. ANNELL, R. P. CHRISTIAN, F. CUTTITTA, E. J. DWORNIK, D. T. LIGON, JR., AND H. J. ROSE, JR., Elemental Analyses of Lunar Soil Samples From Apollo 15 Mission. *The Apollo 15 Lunar Samples*, Lunar Science Institute, Houston, 1972, pp. 198–200.
21. SCOON, J. H., Chemical Analysis of Lunar Samples 15101,65 and 15211,6. *The Apollo 15 Lunar Samples*, Lunar Science Institute, Houston, 1972, pp. 255–256.
22. COMPSTON, W., M. J. VERNON, B. W. CHAPPELL, AND R. FREEMAN, Rb-Sr Model Ages and Chemical Composition of Nine Apollo 16 Soils (abs.). *Lunar Science*, Vol. IV, Lunar Science Institute, Houston, 1973, pp. 158–158b.
23. LSPET (Lunar Sample Preliminary Examination Team), The Apollo 16 Lunar Samples: Petrographic and Chemical Description. *Science*, Vol. 179, 1973, pp. 23–34.
24. ROSE, H. J., JR., F. CUTTITTA, S. BERMAN, M. K. CARRON, R. P. CHRISTIAN, E. J. DWORNIK, L. P. GREENLAND, AND D. T. LIGON, JR., Compositional Data for Twenty-Two Apollo 16 Samples. *Proc. Fourth Lunar Science Conference, Geochimica et Cosmochimica Acta*, Supplement 4, Vol. 2, 1973, pp. 1149–1158.
25. DUNCAN, A. R., A. J. ERLANK, J. P. WILLIS, AND M. K. SHER, Compositional Characteristics of the Apollo 17 Regolith (abs.). *Lunar Science*, Vol. V, Lunar Science Institute, Houston, 1974, pp. 184–186.
26. RHODES, J. M., K. V. RODGERS, C. SHIH, B. M. BANSAL, L. E. NYQUIST, H. WIESMANN, AND N. J. HUBBARD, The Relationship Between Geology and Soil Chemistry at the Apollo 17 Landing Site. Submitted to *Proc. Fifth Lunar Science Conference.*
27. SCOON, J. H., Chemical Analysis of Lunar Samples From the Apollo 16 and 17 Collections (abs.). *Lunar Science*, Vol. V, Lunar Science Institute, Houston, 1974, pp. 690–692.
28. RHODES, J. M., AND N. J. HUBBARD, Chemistry, Classification and Petrogenesis of Apollo 15 Mare Basalts. *Proc. Fourth Lunar Science Conference, Geochimica et Cosmochimica Acta*, Supplement 4, Vol. 2, 1973, pp. 1127–1148.
29. DUNCAN, A. R., A. J. ERLANK, J. P. WILLIS, AND L. H. AHRENS, Composition and Inter-Relationships of Some Apollo 16 Samples. *Proc. Fourth Lunar Science Conference, Geochimica et Cosmochimica Acta*, Supplement 4, Vol. 2, 1973, pp. 1097–1114.
30. HUBBARD, N. J., P. W. GAST, J. M. RHODES, B. M. BANSAL, H. WIESMANN, AND S. E. CHURCH, Nonmare Basalts: Part II. *Proc. Third Lunar Conference, Geochimica et Cosmochimica Acta*, Supplement 3, Vol. 2, 1972, pp. 1161–1179.
31. HUBBARD, N. J., J. M. RHODES, P. W. GAST, B. M. BANSAL, C. Y. SHIH, H. WIESMAN, AND L. E. NYQUIST, Lunar Rock Types: The Role of Plagioclase in Non-Mare and Highland Rock Types. *Proc. Fourth Lunar Science Conference, Geochimica et Cosmochimica Acta*, Supplement 4, Vol. 2, 1973, pp. 1297–1312.
32. TAYLOR, S. R., M. P. GROTON, P. MUIR, W. NANCE, R. RUDOWSKI, AND N. WARE, Lunar Highlands Composition: Apennine Front. *Proc. Fourth Lunar Science Conference, Geochimica et Cosmochimica Acta*, Supplement 4, Vol. 2, 1973, pp. 1445–1460.
33. SATO, M., N. L. HICKLING, AND J. E. MCLANE, Oxygen Fugacity Values of Apollo 12, 14 and 15 Lunar Samples and Reduced State of Lunar Magmas. *Proc. Fourth Lunar Science Conference, Geochimica et Cosmochimica Acta*, Supplement 4, Vol. 1, 1973, 1066–1079.
34. MORRIS, R. V. AND L. A. HASKIN, EPR Measurement of the Effect of Glass Composition on the Oxidation States of Europium. *Geochimica et Cosmochimica Acta*, in press, 1974.
35. MORRIS, R. V., L. A. HASKIN, G. M. BIGGARS, AND M. J. O'HARA, Measurement of the Effects of Temperature and Partial Pressure of Oxygen on the Oxidation States of Europium in Silicate Glasses. *Geochimica et Cosmochimica Acta*, in press, 1974.
36. SHORT, N. M., AND M. L. FORMAN, Thickness of Impact Crater Ejecta on the Lunar Surface. *Modern Geology*, Vol. 3., 1972, pp. 69–91.
37. WARNER, J. L., C. H. SIMONDS, AND W. C. PHINNEY, Impact Induced Fractionation in the Highlands. *Lunar Science*, Vol. V, 1974, pp. 823–825.
38. WOOD, J. A., AND H. E. MITLER, Origin of the Moon by Modified Capture Mechanism, or Half a Loaf Is Better Than a Whole One. *Lunar Science*, Vol. V, 1974, pp. 851–853.
39. NYQUIST, L. E., N. J. HUBBARD, P. W. GAST, S. E. CHURCH, B. M. BANSAL, AND H. WIESMANN, Rb-Sr Systematics for Chemically Defined Apollo 14 Breccias. *Proc. Third Lunar Science Conference, Geochimica et Cosmochimica Acta*, Supplement 3, Vol. 2, 1972, pp. 1515–1530.
40. NYQUIST, L. E., N. J. HUBBARD, P. W. GAST, B. M. BANSAL, H. WIESMANN, AND B. JAHN, Rb-Sr Systematics for Chemically Defined Apollo 15 and 16 Materials. *Proc. Fourth Lunar Science Conference, Geochimica et Cosmochimica Acta*, Supplement 4, Vol. 2, 1973, pp. 1823–1846.
41. WALKER, D., T. L. GROVE, J. LONGHI, E. M. STOLPER, AND J. F. HAYS, Origin of Lunar Feldspathic Rocks. *Earth Planet. Sci. Letters*, Vol. 20, 1973, pp. 325–336.
42. WALKER, D., J. LONGHI, T. L. GROVE, E. STOLPER, AND J. F. HAYS, Experimental Petrology and

Origin of Rocks From the Descartes Highlands. *Proc. Fourth Lunar Science Conference, Geochimica et Cosmochimica Acta,* Supplement 4, Vol. 1, 1973, pp. 1013–1032.

43. HUBBARD, N. J., AND C. SHIH, Opposing Partial Melting Models and the Genesis of Some Lunar Magmas (abs.). *36th Annual Meeting Meteoritical Society,* 1973, pp. 72–73.
44. HUBBARD, N. J., AND C. SHIH, *Partial Melting Models and the Precursors of Lunar Non-Mare Magmas.* In preparation.
45. GAST, P. W., The Chemical Composition and Structure of the Moon. *The Moon,* Vol. 5, 1972, pp. 121–148.
46. WOOD, J. A., J. S. DICKEY, JR., U. B. MARVIN, AND B. N. POWELL, Lunar Anorthosites and a Geophysical Model of the Moon. *Proc. Apollo 11 Lunar Science Conference, Geochimica et Cosmochimica Acta,* Supplement 1, Vol. 1, 1970, pp. 965–988.
47. SMITH, J. V., A. T. ANDERSON, R. C. NEWTON, E. J. OLSEN, P. J. WYLLIE, A. V. CREWE, M. S. ISAACSON, AND D. JOHNSON, Petrologic History of the Moon Inferred From Petrography, Mineralogy and Petrogenesis of Apollo 11 Rocks. *Proc. Apollo 11 Lunar Science Conference, Geochimica et Cosmochimica Acta,* Supplement 1, Vol. 1, 1970, pp. 897–925.

Page intentionally left blank

Page intentionally left blank

Lunar Elemental Analysis Obtained From the Apollo Gamma-Ray and X-Ray Remote Sensing Experiment

J. I. Trombka
Goddard Space Flight Center
Greenbelt, Maryland

J. R. Arnold
University of California, San Diego
La Jolla, California

I. Adler
University of Maryland
College Park, Maryland

A. E. Metzger
Jet Propulsion Laboratory
Pasadena, California

R. C. Reedy
Los Alamos Scientific Laboratory
Los Alamos, New Mexico

Gamma-ray and X-ray spectrometers carried in the Service Modules of the Apollo 15 and Apollo 16 spacecraft were employed for compositional mapping of the lunar surface. The measurements involved the observation of the intensity and characteristic energy distribution of gamma rays and X-rays emitted from the lunar surface. A large-scale compositional map of over 10 percent of the lunar surface was obtained from an analysis of the observed spectra. The Apollo 15 flight was at a lunar orbital inclination of 29 degrees as compared with a 9-degree inclination of the Apollo 16 flight; thus, the projected ground track of the Apollo 15 flight covered a larger projected surface area than that of the Apollo 16 flight.

The objective of the X-ray experiment was to measure the K spectral lines from Mg, Al, and Si. Spectra were obtained and the data were reduced to Al/Si and Mg/Si intensity ratios and ultimately to chemical ratios. Analyses of the results have indicated (1) that the Al/Si ratios are highest in the lunar highlands and considerably lower in the maria, and (2) that the Mg/Si concentrations generally show the opposite relationship. There is a tendency for the Al/Si values to increase from the western mare areas to the eastern limb highlands. There are distinct chemical contrasts between such features as the small mare basins and the highland rims.

The objective of the gamma-ray experiment was to measure the natural and cosmic-ray-induced activity emission spectrum. At this time, the elemental abundances for Th, U, K, Fe, Ti, Si, and O have been determined over a number of major lunar regions. Regions of relatively high natural radioactivity were found in the Mare Imbrium and Oceanus Procellarum regions. High spots of natural radioactivity were also found south of Fra Mauro, somewhat southwest of Archimedes, and south of Aristarchus. An enhanced region of natural radioactivity was found around Van de Graaff on the far side of the Moon. In regions other than Mare Imbrium and Oceanus Procellarum, an anticorrelation between natural radioactivity and lunar elevation, as determined from the Apollo laser altimeter, has been found.

From the combined results of the gamma-ray and X-ray spectrometer experiments almost complete information concerning the major element composition of over 10 percent of the lunar surface has been obtained. Distributions have also been mapped for K, Th, and Ti. Interesting correlations between lunar topography and magnetic and gravitational properties have been found.

Gamma-ray and X-ray fluorescent spectrometers carried in the Service Modules of the Apollo 15 and Apollo 16 spacecraft were employed for compositional mapping of the lunar surface. The measurements involved the observation of the intensity and characteristic energy distribution of gamma rays and X-rays emitted from the lunar surface. The objective of the X-ray experiment was to measure the K spectral lines from Mg, Al, and Si, while that of the gamma-ray experiment was to measure the natural and cosmic-ray-induced emission spectrum. At this time it is possible to obtain large-scale compositional maps of over 10 percent of the lunar surface for Al, Mg, Th and U, K, Fe, Ti, Si, and O. The Apollo 15 flight was at a lunar orbital inclination of about 29 degrees as compared with about a 9-degree inclination of the Apollo 16 flight; thus, the projected ground track of the Apollo 15 flight covered a larger surface area than that of the Apollo 16 flight.

Over the past two years, certain results of these Apollo gamma-ray and X-ray remote sensing experiments have appeared in the literature. This report will present a summary of the results and indicate the present methods employed in the analysis of the data. It is hoped that this summary of both the analytic methods and results will enable other investigators in planetology to make optimum use of the results.

Instrumentation and Data Analysis, Gamma-Ray Experiment

The gamma-ray spectrometer consisted of a 7- by 7-cm right cylindrical NaI (Tl) crystal detector with a plastic anticoincidence mantle to suppress response to charged particles, and a 512-channel, pulse-height analyzer including an amplifier, but no memory. The information was transmitted event by event in real time or, if necessary, was stored on a magnetic tape for later transmission to Earth. Spectra were obtained by accumulating the pulses received on Earth for various periods of time. Details of the experimental system are described in Arnold et al. (ref. 1) and Harrington et al. (ref. 2). The instrument was mounted on a boom capable of extending 7.6 m from the spacecraft in order to minimize background interference due to gamma-ray emission from the spacecraft.

The model on which the data analysis is based can be found in a research paper by Reedy, Arnold, and Trombka (ref. 3). The experimental data as received from the Johnson Space Center were processed for analysis by eliminating those data having parity errors and other problems and analytically shifting to a constant level of gain. (The overall instrument gain decreased over 40 percent on Apollo 15 and about 10 percent on Apollo 16 during the lunar phase of the mission.) The gain as adjusted for analysis was about 19 keV/channel. The spectra were then corrected for solid angle to a constant height of 110 km above the lunar surface. All data obtained over each region to be analyzed were then accumulated into master spectra. An initial background correction was made for the general sky background of gamma radiation, for natural gamma-ray emission, and for cosmic-ray-induced gamma-ray emission from the spacecraft, local mass around the detector, and the detector itself. The background level was determined from measurements made during the trans-Earth flights of Apollo 15 and Apollo 16, returning from the Moon. Shown in figure 1 is a pulse-height spectrum obtained during trans-Earth flight.

Two types of data analyses were carried out: (1) Integral counts in the $\sim$ 0.6- to $\sim$ 2.7-MeV region were used to determine the

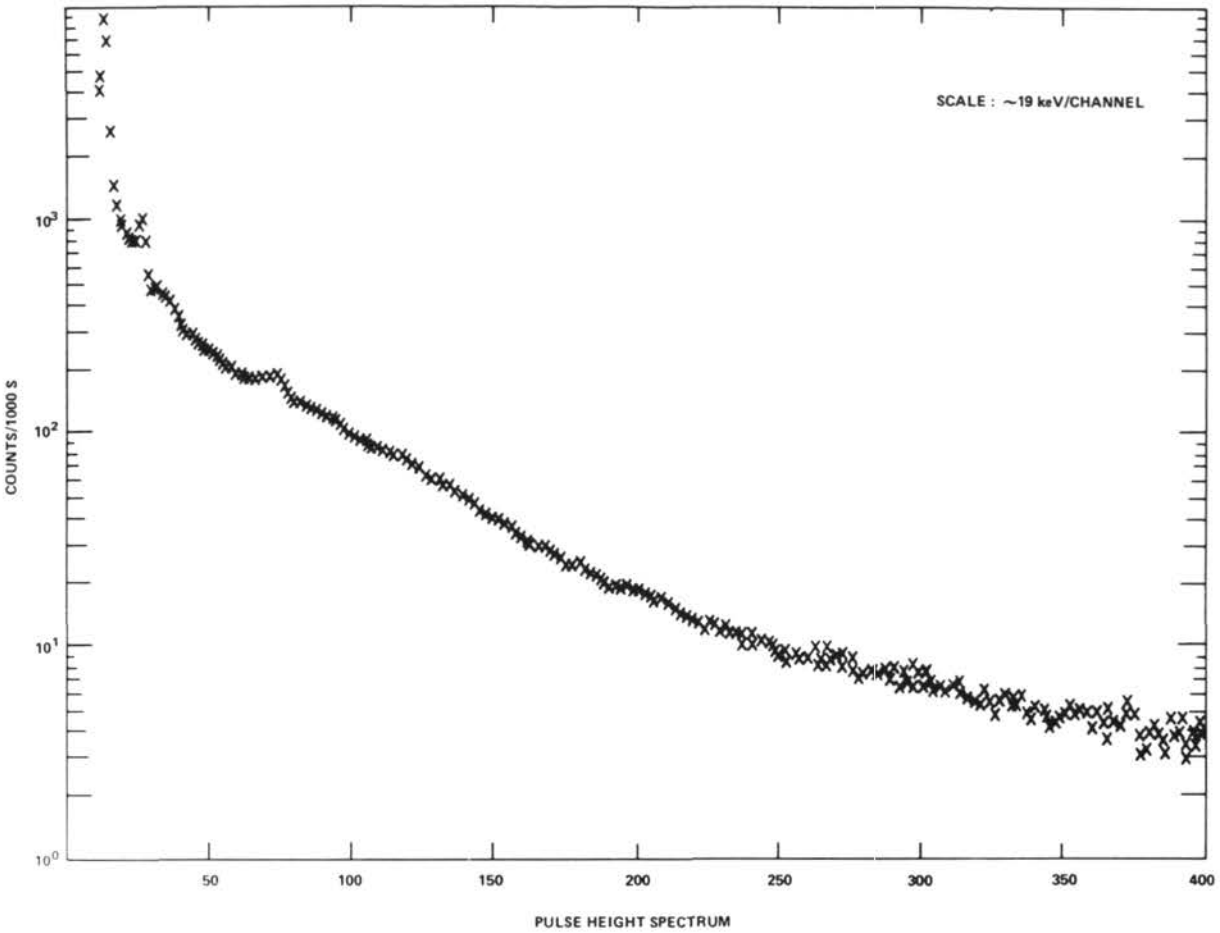


Figure 1.—*Pulse height spectrum obtained with a 7-cm by 7-cm NaI(Tl) detector, on a boom 7.6 m from the Apollo spacecraft. The measurement was made during the trans-Earth phase of the Apollo 15 mission. Scale is ~ 19 keV/channel.*

variation of the counts due to the natural emitters K, U, and Th; and (2) detailed spectral analysis was performed to separate the elemental components enabling quantitative analyses to be obtained for Th + U, K, Fe, Ti, Mg, Si, and O. With use of the methods described by Reedy, Arnold, and Trombka (ref. 3), a minimum of 30 to 40 minutes of counting was required for these quantitative analyses; for smaller data blocks, statistical errors produce unacceptable scatter. Much shorter time periods of data were used with the integral counting method for determining the natural radioactivity distribution. This integral count method works well in determining natural radioactivity. It was found that for the most part the variation in the count rate in the 0.6- to 2.7-MeV region can be attributed to gamma emission from K, Th, and U (ref. 4).

The quantitative analyses were carried out with interactive matrix inversion procedures described schematically by Reedy, Arnold, and Trombka (ref. 3). The most difficult analysis was the derivation of the lunar gamma-ray continuum, that is, the portion of the flux in the 0.5- to 10-MeV region which does not contain characteristic lines. The continuum was found to produce about 85 percent of the counts in the detector. While its general shape is understood, the continuum must be derived from the

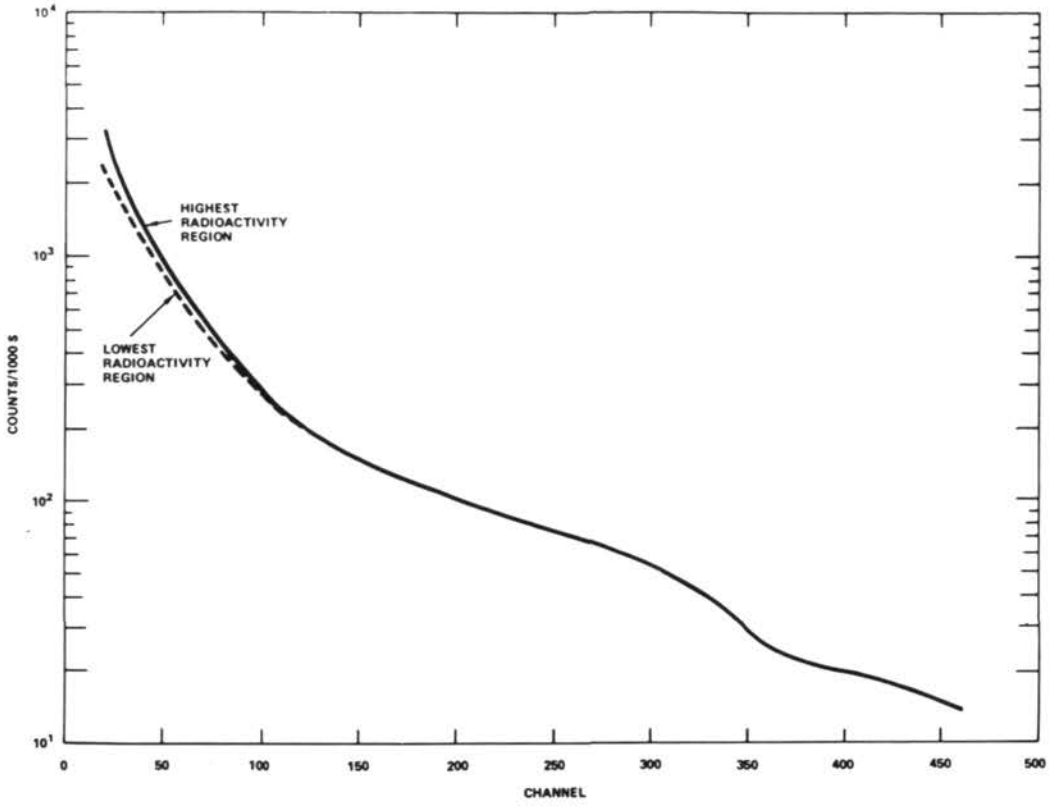


Figure 2.—*Lowest and highest background used in the analysis of the Apollo 15 lunar spectrum. Crystal detector is 7 cm by 7 cm and at a boom position 7.6 m from the spacecraft. Scale is ~ 19 keV/channel.*

data. The continuum shape and magnitude are not constant over the whole Moon. Below 3 MeV, the lines due to the radioactive elements K, Th, and U make an important contribution to this continuum by Compton scattering in the lunar material. In this manner, the continuum was separated into two components; one component was found to be constant over the lunar surface, while a second component varied as a function of the concentration of the radioactive elements K, Th, and U. The constant portion of the lunar background was derived from an analysis of lunar regions where the minimum natural radioactivity is found. The increase above this minimum level was then derived by taking differences between regions of higher activity and their low-activity regions. Empirical methods were developed to determine the magnitude and shape of the scatter

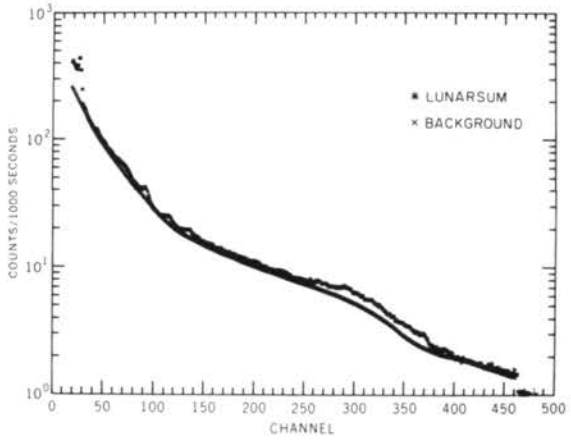


Figure 3.—*Pulse height spectrum corresponding to an average lunar spectrum for the Apollo 15 orbital mission. The derived average lunar background is also indicated. The pulse height spectra were obtained with the Apollo 15 gamma-ray spectrometer. Scale is ~ 19 keV/channel.*

buildup as a function of Th, U, and K concentration. Figure 2 shows the lowest magnitude background and the highest magnitude background used in the analysis of the Apollo 15 data. Figure 3 shows the measured lunar pulse-height spectrum obtained by integrating the spectrum over a number of hours of measurement, thus representing an average composition, over the Apollo 15 ground track and the derived lunar background for this same average spectrum. The difference pulse-height spectrum corresponding to the lunar discrete line emission pulse-height spectrum is indicated in figure 4. Also shown are the various elemental components used in the matrix analysis method (ref. 3) and the best least squares fit obtained by synthesizing these elemental components with respect to the difference spectrum.

The results to be presented in this paper were obtained from an analysis of the net discrete line spectrum from Apollo 15 and Apollo 16. The background shapes were derived from the Apollo 15 data and were used for both Apollo 15 and Apollo 16. Good agreement for elemental concentration was achieved except for the Ti calculated from the high-energy (n,γ) line in the overlap region of Apollo 15 and Apollo 16. The improved energy resolution of the Apollo 16 instrument and differences in proton-induced activation may be responsible for the changes

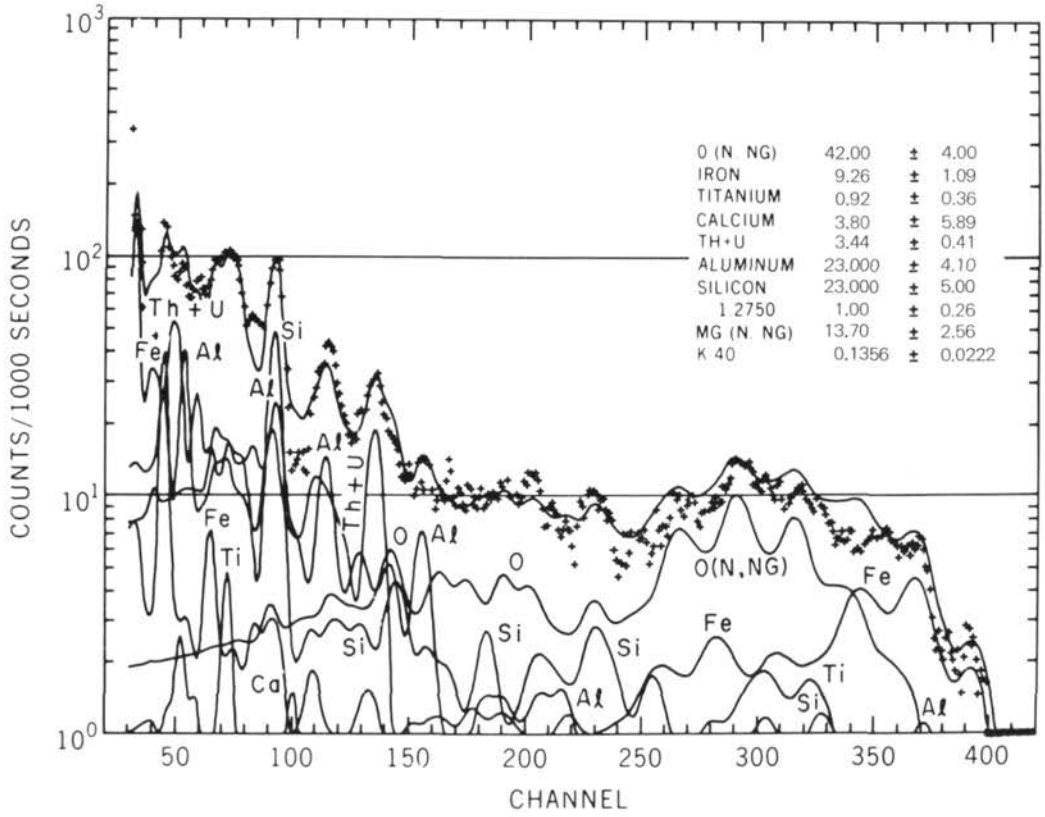


Figure 4.—*Difference pulse height spectra or discrete line lunar emission pulse height spectrum obtained with the Apollo 15 gamma-ray spectrometer over the whole ground track. The elemental components for O, Fe, Ti, Co, Th + U, Al, Si, Mg, and K are also indicated. The components were used for the least squares analysis of the difference curve. The synthesized curve obtained from least squares analysis is also shown. Scale is ~ 19 keV/channel.*

in the Apollo 16 versus Apollo 15 high-energy portion of the background which affect the Ti calculation. Separate background continua for Apollo 16 are presently being calculated.

Some changes have been made in the procedure described by Reedy, Arnold, and Trombka (ref. 3). It has been found useful to perform the analysis in two stages. In the first stage, only the spectrum from 5 to 9 MeV is analyzed; in this region, as can be seen in figure 4, only Fe, O, Si, and Ti contribute significant intensity. In the second stage of analysis, the component intensities derived by matrix inversion in stage one were subtracted from the spectrum, and all the remaining components were then used to analyze the difference spectrum in the lower energy region.

Another change in the analytical procedure involved the calculation of the iron component. Iron produces a line spectrum in the $>$ 0.8-MeV region due to inelastic scatter of neutrons (the (n,n′,γ) process), and a second line spectrum in the $>$ 5-MeV region due to prompt capture of neutrons by the (n,γ) process. Because of the good statistics for determining the distributions for this element, the two iron components were analyzed separately. The difference in the ratio of the number flux of the (n,γ) emission with respect to the (n,n′,γ) process can be used as an indicator for the presence of strong thermal neutron absorbers (such as Gd and other rare earths). This can be done because the (n,γ) gamma-ray number flux is approximately proportional to the neutron flux near thermal energies (below 1 eV). The (n,n′,γ) number flux is proportional to the fast flux (above 1 MeV). Since the rare earth group includes several large thermal neutron absorbers, their presence in large concentrations will depress the magnitude of the thermal flux without significantly perturbing the fast flux. This has been seen in the analysis under consideration here. For the other elements, such as Si, which have important lines of both types, the library spectra were combined into a single component. Thorium and uranium were also combined into a single component, an estimate of the U being based on an assumption that the abundance ratio of Th/U is 3.8. This was necessary because the uranium lines, although contributing significantly to the emission spectrum, are significantly masked by other lines in the discrete line spectrum. This masking is due to the poor energy resolution of NaI (Tl) detectors. Rather precise determination of the thorium component is possible because the 2.62-MeV emission line for this element is easily discernible in the discrete line pulse-height spectra (fig. 4).

The elements which can be usefully analyzed fall into two groups. For the natural radioactivities, K and (Th + U), the elemental concentrations can be derived from the decay schemes and the properties of the detector, using theory and laboratory calibrations, with no ambiguity in principle. Concentration values for these elements were derived in this way, without adjustable parameters. The elements that depend on cosmic-ray excitation, O, Si, Fe, Mg, and Ti, require input information from nuclear and cosmic-ray physics whose combined accuracy is not yet very high. The agreement to be expected is no better than that for the parent models as proposed by Reedy and Arnold (ref. 7) for the production of cosmogenic nuclides in the Moon, and that of Lingenfelter, Canfield, and Hampel (ref. 8) for low-energy neutrons. The depth variations of induced radioactivity observed in the lunar soil are in rather good agreement (ref. 9), with Reedy and Arnold's calculations, but the absolute amounts depart by $\pm$ 25 percent from calculated values from Apollo gamma-ray data. The experiment of Woolum and Burnett (ref. 10) on Apollo 17 confirms to some extent the calculations of Lingenfelter et al. (ref. 8) of the lunar neutron flux, but suggests a somewhat harder neutron spectrum. The deviations observed from the Reedy, Arnold, and Trombka calculations (ref. 3) also suggest a harder neutron spectrum.

The best way to treat the data for O, Si, Fe, Mg, and Ti is to use "ground-truth" data,

normalizing the orbital data to the surface samples at one or more selected points. While there are many mapped areas that include several sites from which samples have been returned, most of these are unsuitable because of local variability of the soil chemistry, as, for example, the Apollo 15 landing site. The two best sites are Mare Tranquillitatis, where the Apollo 11 analyses are supplemented by the results of the Surveyor 5 experiment (ref. 11), and the Apollo 16 landing site near the Descartes region. The Apollo 15 and 16 spectrometer Fe, Mg, and Ti data were normalized to the ground-truth data for Mare Tranquillitatis, and the Descartes region ground-truth data were used as a check. Another check was performed by comparing regions overflown by both Apollo 15 and Apollo 16.

Table 1 gives the ground-truth element concentrations used for the region of Mare Tranquillitatis to derive the published values for the soil sample 10084. The exception is Ti, with a somewhat lower assumed value. The reason for this exception is that the count rates for the spectral region in which Ti is important (5.97 to 6.37 MeV) show a variation that is far outside the counting error over the Tranquillitatis region. The Apollo and Surveyor sites are in the two regions of highest observed counting rate. Because O, Si, and Fe appear to be constant in this region, the assumption is that any variation in integrated intensity is due to Ti. The conclusion drawn is that the true mean Ti concentration over the region is lower by a factor of 0.65 than that observed on the ground. This correction of course increases the uncertainty of the Ti values.

In the work to be reported, errors are not quoted because, in complex interactive analyses of the present type, the magnitude of random and systematic errors is difficult to evaluate. The main sources of error are (1) statistical counting mistakes, (2) uncertainties in the shape of the subtracted continuum, (3) unknown interactions between components, and (4) where applicable, the ground-truth normalization. At the present stage of analysis, the ground-truth comparisons and comparisons on the overlap regions of Apollo 15 and Apollo 16 give an indication of the uncertainties.

Finally, with regard to the data analysis, the compositions determined reflect the average composition down to about 20 cm in depth.

All data in table 1 (below) and in later tables are in percent or ppm element by weight. The values of Th and K are given for convenience; they are not used for renormalization. The data are for soil 10084 (refs. 12 and 13).

Table 1.—*Ground-Truth Values, Mare Tranquillitasis*

Element	Value
O	40.8%
Si	19.6%
Fe	12.1%
Mg	4.8%
Ti	2.9% (1)
Th	2.1 ppm
K	1100 ppm

NOTE: (1) This is 0.65 times the soil 10084 concentration. See text for discussion.

The X-Ray Experiment

The X-ray spectrometer consists of three large-area proportional detectors; a set of large-area filters for energy discrimination among the characteristic X-rays of Al, Si, and Mg; collimators; and data-handling electronics for obtaining eight-channel pulse-height spectra. These three detectors pointed at the lunar surface while taking measurements. A fourth proportional counter that looked in the direction opposite to the three large-area proportional counters was used as a solar monitor. The three proportional counters used to monitor the lunar X-ray flux were identical, each having an effective window area of ~ 21 cm^2. The window consisted of Be 0.0025 cm in thickness. The proportional counters were filled to a pressure of 1 atm with the standard P–10 mix-

ture of 90 percent argon (A), 9.5 percent carbon dioxide (CO_2), and 0.5 percent helium (He). To change the energy response, filters were mounted across the Be window aperture on two of the proportional counters. The filters consisted of an Mg foil (5.08×10^{-4} cm thick) and an Al foil (1.27×10^{-3} cm thick). The collimator consisted of multicellular baffles that defined a field-of-view of the three detectors to $\sim$ 44 degrees full width at half maximum. Details of the systems can be found in Adler et al. (ref. 14).

In the X-ray fluorescence experiment, the production of characteristic X-rays followed the interaction of solar X-rays with the lunar surface. The typical solar X-ray is energetically capable of producing measurable amounts of characteristic X-ray from all the abundant elements with atomic members of approximately 14 (Si) or less. The spectral characteristics and magnitude of the incident solar X-ray flux greatly affected the analysis of the data. For a detailed discussion of this problem see Adler et al. (ref. 14).

Figure 5 shows characteristic pulse-height spectra taken over Mare Crisium for the three detectors aboard Apollo 15. The spectra were normalized so that the area under the spectrum corresponding to the base detector is taken as unity. The effects of the Mg and Al filters can be seen in figures 5b and 5c. An integral count method employing the characteristics of the filters was used to determine the intensity of the characteristic lines due to Mg, Al, and Si. The relative magnitude and absolute intensity of these lines depend on the magnitude and spectral quality of the incident solar spectrum, the angle of incidence of the solar flux with respect to the look direction of the X-ray detectors, the local altitude of the detectors with respect to the lunar surface, and the surface composition and physical characteristics. If the solar spectral shape is constant, it is found that the other correction factors having to do with detector-spacecraft geometry and physical characteristics of the surface material cancel out in the calculation ratios of the abundance ratios Al/Si and Mg/Si. Further, if it is assumed that the Si concentration is constant over the lunar surface sampled (an assumption supported to good accuracy by sample analyses to date), then these ratios reflect the changes in the Al and Mg concentration over the lunar surface. Actual concentrations were obtained by an approach that is both theoretical and empirical. The theoretical calculations are based on the assumption of a quiet Sun and a coronal temperature of 4×10^6 K. These conditions give an X-ray energy distribution, consisting of both a continuum and characteristic lines, that is consistent with the solar-monitor observations. The X-ray energy distribution and various soil compositions, as determined from the analysis of lunar samples, were used to calculate a relationship between Al/Si intensity ratios as a function of chemical ratios. The empirical approach involves the assumption that the soil values from the Apollo 11 site at Mare Tranquillitatis and the Luna 16 soil values from Mare Fecunditatis are ground-truth values. With these values and the theoretically calculated slopes, values of Al/Si concentrations for

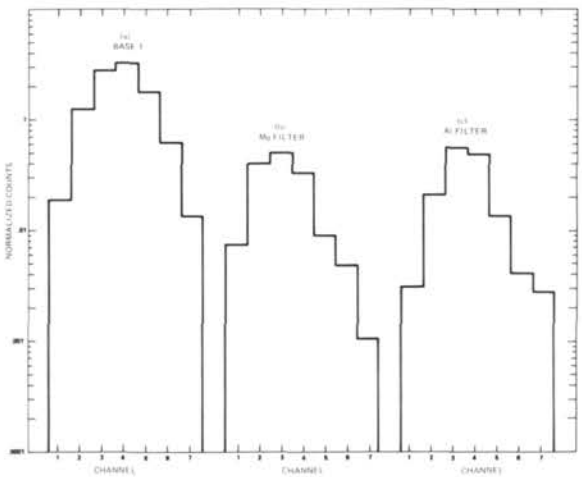


Figure 5a–c.—*Pulse height spectra obtained with the Apollo 15 X-ray spectrometer. The spectrum was taken over Mare Crisium. Spectra shown are from the base detector (a), the detector with the Mg filter (b), and the detector with the Al filter (c). The scale as shown has a lower level of 0.75 keV and is about 0.33 keV/channel. The data have been normalized so that the area under the base detector peak is unity.*

various parts of the lunar surface along the ground track were determined. The X-ray fluorescence experiment measured surface composition down to a depth of approximately 0.1 mm. Because of the gardening (mixing) of the lunar regolith by meteorite impact, no difference in composition is expected between the X-ray and gamma-ray experiments because of the different depths sampled.

The first results of the X-ray fluorescence experiments were used to map the ratios Al/Si and Mg/Si on a broad scale across the lunar surface. Recently attempts have been made (refs. 15 and 16) to prepare more detailed maps relating the X-ray results to small lunar morphological features and to various parameters independently determined, such as photogeologic observations, gravitational anomalies, and the electromagnetic sounder results.

Various methods of contouring have been considered. One approach which seems to be rather successful has been to perform trend surface studies of the lunar data (refs. 16 and 17). Surfaces described by different order polynomial expressions are fitted to the observed data by a least-squares technique. The significance of the surface is tested by statistical means. A regional model surface which is shown to be statistically valid is assumed to be the proper model for the particular region. Differences between the observed values and the model values that are statistically significant are plotted as residuals and are interpreted as local anomalies with respect to the model. It must be remembered that in all of these analyses it has been assumed that Si is constant and that the variations can be attributed to changes in either Al or Mg composition.

Experimental Results and Interpretations

GAMMA-RAY SPECTROMETER

The first results available from the gamma-ray experiment concerned the distribution of the radioactive elements of Th, U, and K (refs. 5, 18, and 19). In the spectral region above the 0.51-MeV line and up to and including the highest energy line, the 2.61-MeV line due to Th, the regional differences in count rate are overwhelmingly due to the varying intensities of the lines of Th, U, and K. This is a fortunate circumstance because the statistical precision of the total count in this region (the integrated intensities from 0.55 to 2.75 MeV) is excellent, and good area resolution can thus be obtained. In the *Proceedings of the Fourth Lunar Science Conference* (ref. 19), the count rate data are presented for 2- by 2-degree resolution elements on the lunar surface, which corresponds to a square approximately 60 km on edge. The data were adjusted to correspond to a nominal altitude of 100 km. Count rates in the energy range 0.55 to 2.75 MeV were obtained in the regions traversed by both Apollo 15 and Apollo 16, and were compared. The Apollo 16 average rate in this region is 4.6 percent greater than that from Apollo 15. This difference can be attributed to differences in particle radiation fluxes and differences in induced activity due to different trajectories through the Earth's radiation belts and the influence on Apollo 15 as compared with Apollo 16. The main results of this portion of the analysis are shown on the Moon's near and far sides, respectively.

The range of the corrected counting rates is from about 73 to 94 counts per second, or about 25 percent. The standard deviation for a typical counting time of 300 seconds per 5-degree square is about 0.5 counts per second (cps) based on counting statistics alone; it is about 1 cps for the shortest counting times used. The data from areas overflown several times on successive passes and from regions overflown on both missions provide good correlation.

The data obtained during observation periods allow some definite conclusions to be reached, even at the present early stage of data analysis.

1. On both missions, all 5-degree regions

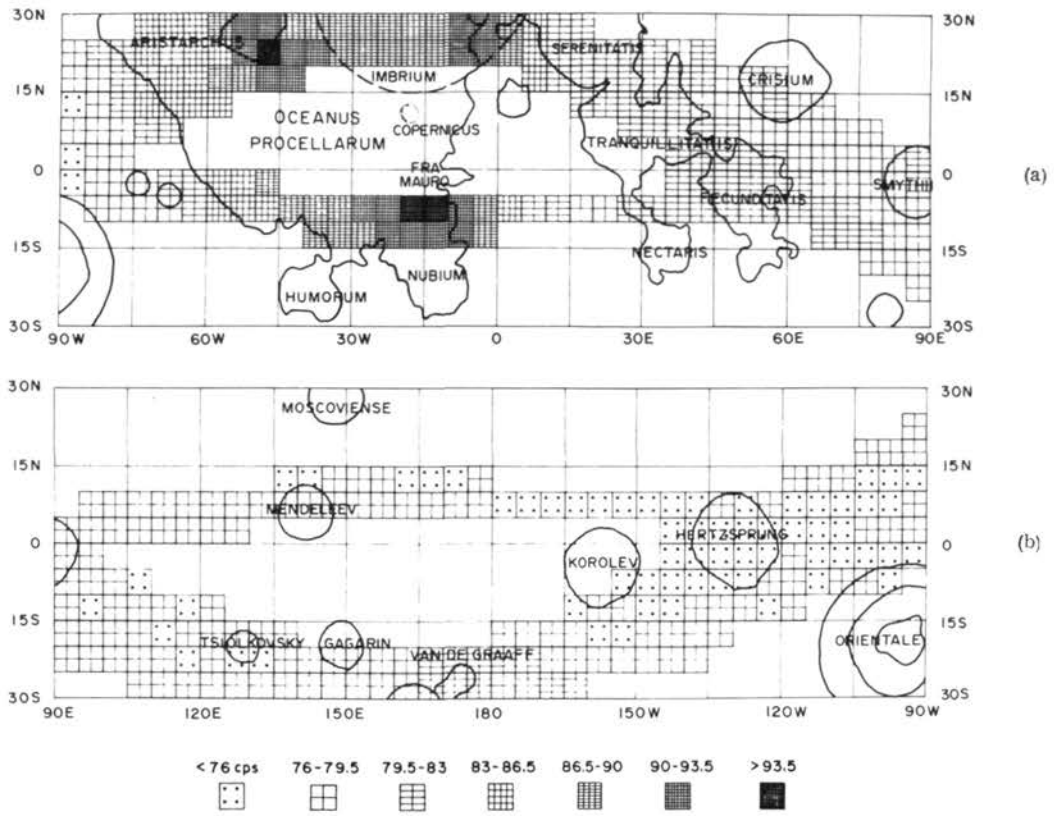


Figure 6.—*Distribution of lunar radioactivity in the energy region 0.55–2.75 MeV over the Apollo 15 and Apollo 16 ground tracks. The data are presented on a 5- by 5-degree scale over a base map freely adapted from one furnished by Dr. Farouk El Baz.*

within and bounding the overflown western maria show higher levels of radioactivity than any 5-degree region elsewhere. The contrast between this region and the rest of the observed Moon is striking, particularly as it extends to a comparison with the eastern maria. It is reasonable to infer that in most instances, the western mare regions not overflown are also highly radioactive and that other regions of the Moon are generally less radioactive. With reference to the radioactive elements, the boundaries between Oceanus Procellarum and named mare regions contiguous to Oceanus Procellarum, such as Mare Nubium, do not correspond to boundaries of composition. These observations, when combined with the radioactive content found in samples from the Apollo 12 and 14 sites (ref. 20), imply a geochemical relationship for the entire Mare Imbrium-Oceanus Procellarum Region.

2. There is detailed structure within the high-radioactivity region. The highest concentrations observed are in the Aristarchus area, in high ground west of the Apollo 15 landing site and south of Archimedes, and in the area south of the crater Fra Mauro. The Fra Mauro area overflown is about 7 degrees south of the Apollo 14 landing site, soil from which showed comparable levels of radioactive concentration. The data from this area indicate

that the Fra Mauro is, surficially at least, related to the western maria rather than the adjacent highlands as has sometimes been inferred from the albedo and topography.

3. The eastern maria show evidence of having locally enhanced radioactivity which is lower than that of the western maria. Higher intensities of radioactivity, relative to the surrounding highlands, are visible in Mare Tranquillitatis, Mare Fecunditatis, Mare Crisium, and Mare Smythii. This intensity has not been seen in Mare Serenitatis, but its accessibility to ejecta from Mare Imbrium tends to "wash out" any inherent difference. From a numerical analysis, Mare Crisium shows more contrast in radioactivity relative to its surroundings than the other eastern maria observed by the Apollo spectrometers.
4. The highland regions show low radioactivity, except on the borders of the western maria where lateral mixing seems to have occurred. On the lunar farside, the highlands to the east (180 to 90 degrees east longitude) are perceptibly more radioactive than those of the west (90 to 180 degrees west longitude) along both the Apollo 15 and 16 ground tracks. The same is true for the limb areas (compare the highland area 60 to 105 degrees east longitude to the area 90 to 120 degrees west longitude). There is a small radioactive maximum on the lunar farside near Van de Graaff (where a major magnetic anomaly is also seen); no increase is observed at these longitudes between 8 to 10 degrees north latitude.
5. Figure 7 shows a profile of the lunar topography observed below the Command Service Module (CSM) by the laser altimeter for single orbits of the Apollo 15 and 16 missions (ref. 21). Superimposed on figure 7 are points representing the relative natural radioactivity. Ignoring the region of highest radioactivity in the Mare Imbrium-Oceanus Procellarum area, a strong inverse correlation between ele-

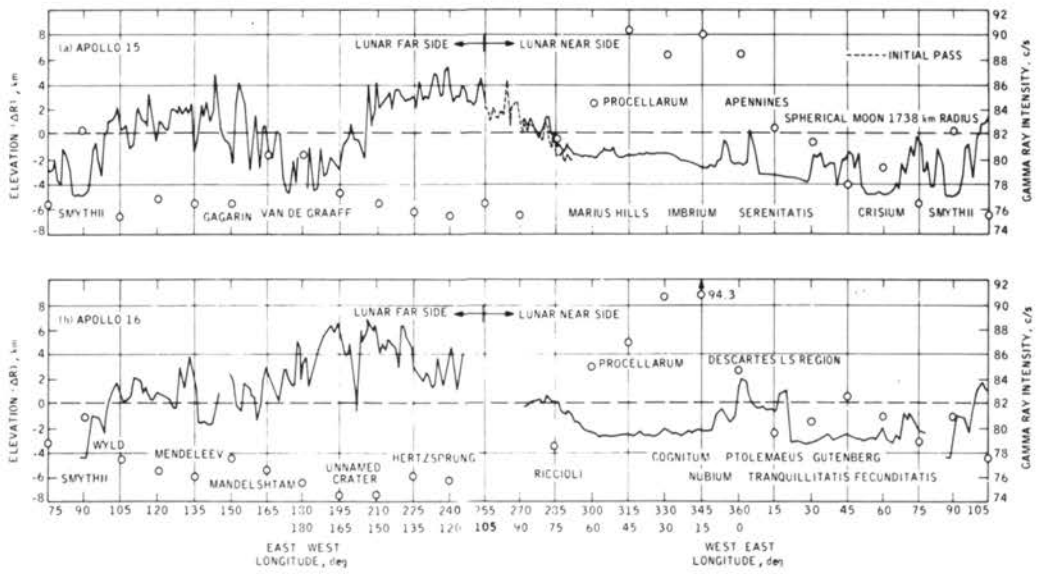


Figure 7.—*Profile of lunar topography and natural radioactivity across the Apollo 15 and Apollo 16 ground tracks as measured by the laser altimeter and gamma-ray spectrometer. The deviation is represented by the line; radioactivity plus the underlying continuum, by the points.*

vation and natural radioactivity is displayed over the remaining 360-degree track. Regions of high elevation are characterized by low material radioactivity and vice versa. While this inverse relationship is observed in the Mare Imbrium-Oceanus Procellarum region, there is structure in the radioactivity which does not correlate with changes in topography. On the lunar farside, this inverse correlation extends to an observation of greater east-west asymmetry around 180 degrees for the Apollo 16 trajectory than that of Apollo 15—an asymmetry which exists for both elevation and natural radioactivity. This inverse correlation does not appear consistently in intercomparisons among maria but rather appears to be reflecting both the nature and extent of major lunar differentiation processes. If the Moon is in isostatic equilibrium, the more extensive the early anorthositic differentiation, as characterized by lower densities and lower concentrations of the naturally radioactive nuclides than are found in mare regions, the higher the elevation and the lower the radioactivity expected.

The major lunar depression occurs in the vicinity of the crater Van de Graaff and exhibits the sharpest contrast in elevation with adjacent highlands along either ground track, that is, about 8 km. This depression

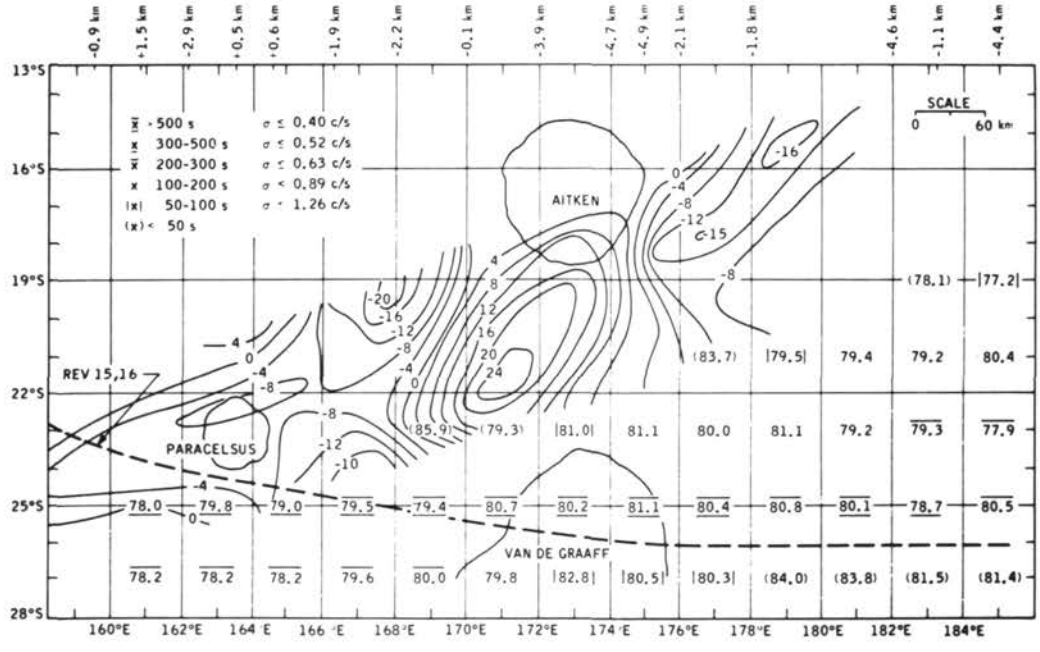


Figure 8.—*The region around the crater Van de Graaff, showing the altitude-corrected, gamma-ray intensities between 0.55 MeV and 2.75 MeV in 2- by 2-degree areas, the location of the laser altimeter ground track with elevation given at the top, and a contour map of the lunar contribution to the solar-directed component of the magnetic field from an elevation of 67 km. The subsatellite magnetometer values are in tenths of gammas. The insert gives the coding which represents the observation time within the 2- by 2-degree area, and the maximum 1σ standard deviation corresponding to that period.*

is also the site of the only major farside enhancement in natural radioactivity. The depression extends some 30 degrees in longitude on either side of 180 degrees longitude, and the gamma-ray feature is of comparable extent. Figure 8 shows the Van de Graaff area in detail. The gamma-ray intensities (counts/second) between 0.55 MeV and 2.75 MeV are calculated in 2- by 2-degree segments of area north and south of the laser altimeter track. In this case, the gamma-ray data have been corrected for spacecraft altitude but not for differences in elevation of the lunar surface. Also shown is the lunar surface magnetic field as mapped by the Apollo 15 subsatellite magnetometer with contours given in tenths of gammas (ref. 22). The elevation track is shown by the dotted line with variations from a mean radius of 1738 km tabulated at the top (ref. 21). The magnetic feature shown is the strongest observed by either the Apollo 15 or 16 subsatellite magnetometers (ref. 22). Ignoring values based on less than 50 seconds of counting time, the highest gamma-ray intensity location is identical to the minimum elevation in the Van de Graaff region. No trace of this enhanced radioactivity was found at regions north of this feature by Apollo 16. Thus, over that portion of the lunar surface scanned to date, the largest surface remanent magnetic field, one of the deepest depressions, and the only significant farside enhancement in radioactivity have all been observed within about 5 degrees (150 km) of each other. This Van de Graaff area is a notable and, to date, quite singular exception to the general conditions prevailing on the lunar farside. When understood, the area is likely to contribute significantly to comprehension of lunar evolutionary processes. This will be considered further after the following discussion of elemental composition maps.

Because of statistical problems in performing the detailed chemical analyses, the mission ground track was divided into a series of regions. Table 2 gives the number, assigned name, and lunar coordinates for each region. Figure 9 shows the actual regions in outline form. In the case of Apollo 15, the data for early revolutions have not been used in this synthesis; hence, the western portions (southwestern or northwestern in east and west longitudes, respectively, except those near 0 and 180 degrees longitude) of regions observed by Apollo 15 are heavily weighted. These regions were chosen by considering major topographic boundaries, the density of high-quality data in a given region, and the contrasts observed in the radioactivity maps (fig. 6). The smallest regions, such as Mendeleev, were chosen in order to determine the minimum area in which useful data can be derived; the errors in these regions are so large that no statistically meaningful concentrations can be derived. In this paper, the analysis used only data with sufficient total counts above background, indicating significantly low statistical errors; thus complex border regions were assigned either to mare or to highland. Doubtless, this reduced the true chemical contrasts in some regions.

Table 3 presents the results of the analysis for Apollo 15 data, normalizing Fe, Mg, and Ti as described above. The values for Fe are weighted means for the two modes of analysis. Starred values note regions where the values determined from neutron capture (low energy) are well below those from inelastic scatter (MeV neutrons). These regions appear to have high concentrations of K, Rare Earths, and P (KREEP), whose rare earth content should depress the thermal flux. In such places the true Fe content may be up to a few percent higher than shown here.

Table 4 gives the Apollo 16 results. The Apollo 15 continuum was used for this work, with very good consistency except for the Ti results, which are omitted. Here again, Fra Mauro gives evidence of a depressed thermal neutron flux; the apparent depression in a few highland regions is not yet understood.

In table 5 a number of instructive comparisons are presented. In the crossover region near the east limb, the regions analyzed on the two missions are roughly the same, and the comparison should give good agree-

Table 2.—*Lunar Regions Analyzed*

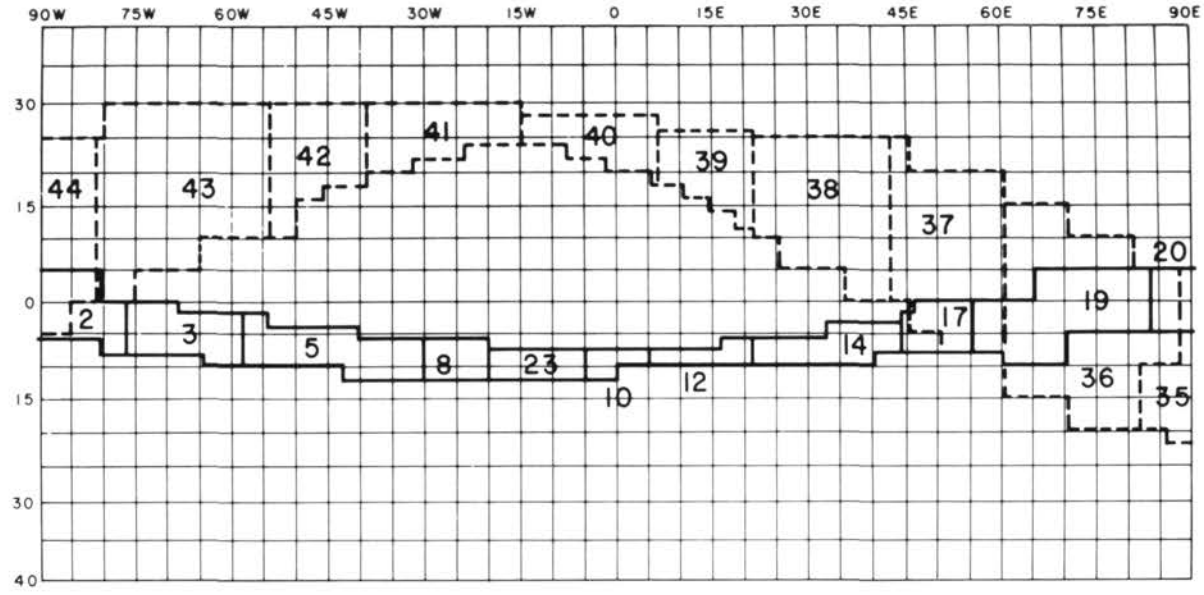
Number	Assigned Name	Coordinates Boundary Regions
	Apollo 15:	
34	Van de Graaff Region	168°W–168°E
35	Highland East Farside	168°E–82°E (south of 10°S) 168°E–88°E (north of 10°S)
36	Highland East Nearside	from (Region 35) to 60°E
37	Mare Fecunditatis	60°E–42°E
38	Mare Tranquillitatis	42°E–21°E
39	Mare Serenitatis	21°E–6°E
40	Archimedes Region	6°E–15°W
41	Mare Imbrium	15°W–39°W
42	Aristarchus Region	39°W–54°W
43	Oceanus Procellarum (north)	54°W–81°W
44	Highland West Farside	81°W–168°W
	Apollo 16:	
26	Highland East Farside	180°–142°E
22	Mendeleev	142°E–138°E
28	Highland East Limb	138°E–92°E
20	Mare Smythii	92°E–83°E
19	Highland East Nearside	83°E–55°E
17	Mare Fecunditatis	55°E–44°E
14	Intermediate Mare-Eastern Highland	44°E–21°E
12	Highland Nearside Center	21°E–5°E
10	Ptolemaeus-Albategnius	5°E–5°W
23	Fra Mauro Region	5°W–20°W
8	Mare Cognitum	20°W–30°W
5	Oceanus Procellarum (south)	30°W–50°W
3	Grimaldi Region	50°W–76°W
2	Orientale Rings	76°W–105°W
29	Highland West Limb	105°W–119°W
1	Hertzsprung Region	119°W–136°W
27	Highland West Farside	136°W–180°

ment. The highland region from 5 to 21 degrees east longitude, which includes the Descartes region, is compared with the soil analysis. The deviations seen are in the expected direction if more mare and KREEP materials are mixed in near the margins of the region.

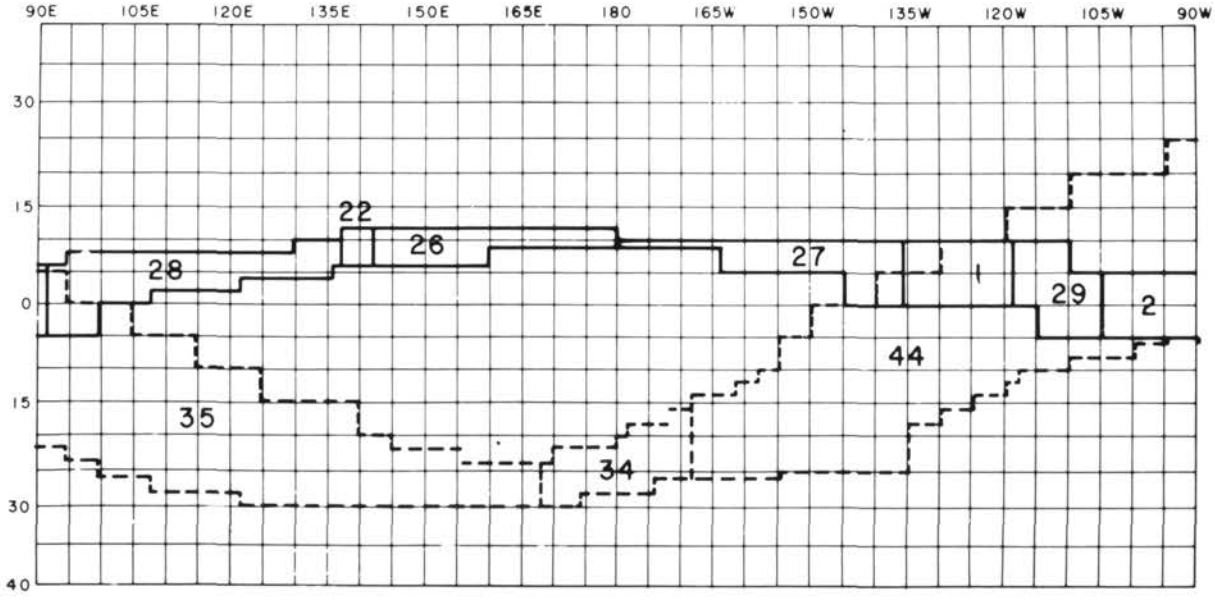
A plausible comparison is possible at two landing sites that were not overflown. Apollo 14 observed the northern end of the Fra Mauro formation; Apollo 16 overflew the southern end. Whatever the origin of this feature, similarities are to be expected throughout. Apollo 12 sampled an area of Oceanus Procellarum not very far from, and topographically similar to, the area overflown by Apollo 16. These comparisons are shown in parts (c) and (d) of table 5.

All these comparisons seem generally satisfactory and serve to confirm the validity of the analysis. There is room for further work in a number of areas and this in underway. However, no substantial modification of the values reported here is expected.

An implication of the results just obtained is that the contrasts between mare and high-



LUNAR NEAR SIDE



LUNAR FAR SIDE

Figure 9.—*Areas on the Moon used in the lunar data analysis (see table 2 for key).*

Table 3.—*Apollo 15: Element Concentrations by Regions*

Region	Fe(%)	Mg(%)	Ti(%)	Th(ppm)	K(ppm)
34	7.7	3.8	0.1	2.3	1600
35	6.5	4.5	1.3	1.0	940
36	9.3	5.7	0.8	1.4	1200
37	11.3	7.0	2.2	1.2	1400
38 [1]	(12.1)	(4.8)	(2.9)	1.7	1200
39	10.7	6.6	2.6	2.3	1700
40	8.4 [2]	6.3	0.8	6.8	3100
41	13.6	6.2	1.4	5.8	1700
42	9.6 [2]	4.9	2.2	6.9	2500
43	10.5	4.6	2.0	3.9	1700
44	5.7	3.5	1.5	0.4	950
All Data	8.7	4.8	1.45	2.2	1230

NOTES: (1) Values in parentheses are ground-truth data used to normalize concentrations for these elements in all regions.
(2) Region of apparent depressed thermal neutron flux (see text).

Table 4.—*Apollo 16: Element Concentrations by Regions*

Region	Fe(%)	Mg(%)	Th(ppm)	K(ppm)
26	6.2	3.4	0.6	920
22	4.3	3.0	0.5	960
28	7.2	2.9	0.5	840
20	8.8	2.8	1.3	1900
19	8.6	4.5	1.3	980
17	9.0	4.6	2.1	1100
14	9.0	3.5	1.5	1300
12	5.9	4.0	2.1	1400
10	4.8 [1]	5.2	5.0	2700
23	9.7 [1]	5.7	10.5	3900
8	12.1	4.9	8.4	3600
5	12.2	5.0	5.0	2300
3	4.4 [1]	3.6	2.4	1100
2	4.7	2.9	0.8	1000
29	3.5 [1]	2.1	0.4	1200
1	3.6 [1]	3.6	0.6	720
27	5.2	2.7	0.5	730
All Data	7.2	3.6	2.1	1300

NOTE: (1) Region of apparent depressed thermal neutron flux (see text).

land regions are as expected nearly everywhere. In the maria, Fe (and, less strikingly, Mg) is relatively enriched. The radioactive elements show the same pattern except for one place.

The Van de Graaff region (table 3, Region 34) shows a chemical composition different from any thus far observed on the Moon. The major elements are highland-like, though Fe content is a little high for this. The concentrations of K and Th are very similar to those of Mare Tranquillitatis and are typical for a mare. The Ti concentration is significantly below that of any region analyzed. Such a composition could not be formed by mixing the major components as observed elsewhere.

The most exciting possibility concerning the composition of the remarkable "granitic" rock 12013 is that Van de Graaff or some chemically similar unmapped region is its source. The K/Th ratios are compatible (ref. 25) and about 5 percent of material of 12013 chemistry, added to highland soil, could produce the observed radioactivity. The major elements are also compatible, though this is not a useful check at the 5-percent level. The Van de Graaff region is very far from all the landing sites; it is thus expected that such material would be uncommon among the returned samples.

The large highland regions are not entirely uniform. Most notable is an east-west asymmetry in the lunar farside. The iron concentration is higher in the eastern regions, which are lower topographically (ref. 21), and this effect extends to the limb and near to the mare edges. The radioactivity

Table 5.—*Comparisons of Orbital Data with Returned Lunar Samples*

Some Comparisons

	a. East Crossover		b. Ground Truth	
	Apollo 15 Region 36	Apollo 16 Region 19	Apollo 16 Region 12	Descartes Soil [3]
Fe(%)	9.3	8.6	5.9	4.0
Mg(%)	5.7	4.5	4.0	3.3
Th(ppm)	1.4	1.3	2.1	2.0
K(ppm)	1200.	980.	1400.	940.

Ground Analogies

	c. Fra Mauro		d. Oceanus Procellarum	
	Apollo 16 Region 23	Apollo 14 Soil [2]	Apollo 16 Region 5	Apollo 12 Soil [3]
Fe(%)	9.7	8.1	12.2	12.5
Mg(%)	5.7	5.6	5.0	6.2
Th(ppm)	10.5	11.6	5.0	7.6
K(ppm)	3900.	4400.	2300.	2600.

NOTES: (1) Fe and Mg: Average of soil analysis, taken from five papers, Third Lunar Science Conference and PET report. K and Th from Eldridge et al. (ref. 23).

(2) Fe and Mg: Average of soil analysis, taken from five papers, Third Lunar Science Conference, and PET report. K and Th from Eldridge et al. (ref. 24).

(3) Fe and Mg: Average of analyses of bulk soil 12070 and related samples in five papers, Second Lunar Science Conference. K and Th from O'Kelley et al. (ref. 25).

maps show more detail (fig. 6). The dry basins like Mendeleev give typical highland analyses within a rather large experimental error.

The values of Ti found in the farside highlands from Apollo 15 data are unexpectedly high and are another example of inhomogeneity in broad highland areas.

There are also differences among maria and KREEP-rich regions. The variability in Ti has been well documented in the mare samples and is well displayed in the comparison of Mare Imbrium (Region 41) with Oceanus Procellarum (Region 43). The Archimedes and Aristarchus regions also differ in Ti and probably in Fe.

The most interesting element ratio is K/Th (and its assumed close correlate K/U). In both missions this ratio rises from something like 400 in the KREEP-rich regions to ratios of 1000–2000 in the highlands. Figure 10 shows plots of the two-element concentrations for the two Apollo missions (15 and 16), as a function of longitude. The errors for both elements are of course larger at the lowest concentrations, but the trend is unmistakable.

Earlier, interpretations of radioactivity maps were presented in terms of a three-component model: mare basalt, KREEP, and a low-radioactivity highland component (ref. 6). Clearly, this preliminary model is inadequate for the detailed information now available, as evidenced at Van de Graaff, where material not prominently displayed in lunar samples so far described is observed. However, no broad regions dominated by radically different chemistry (basic rocks or granites) are observed in the present analysis. If such regions exist, they lie in areas so far unmapped.

X-RAY SPECTROMETER

With the gamma-ray spectrometer results in mind, the results of the X-ray spectrometer are summarized (refs. 14–17, and 26–28). These results will add Al to the elemental composition obtained with the gamma-ray spectrometer. Furthermore, much more detailed information on areal distribution for both Al and Mg is obtainable because of the superior spatial resolution of the X-ray detector.

Figures 11a, 11b, 12a, and 12b show Al/Si and Mg/Si profiles along a northern and a southern track observed by the Apollo 15 mission. Figures 13a and 13b show the Al/Si profile along a track of the Apollo 16 mission. Because of the greater area covered by Apollo 15, two paths for the Apollo 15 mission are included.

The method of calculation of the Al/Si

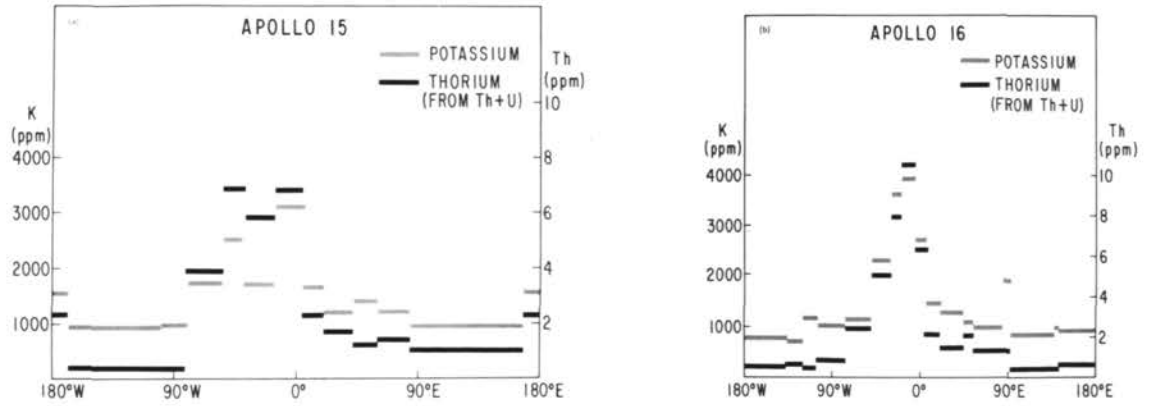


Figure 10.—*(a) Potassium and thorium on the lunar surface, plotted against longitude on the Apollo 15 ground track. (b) A similar plot for Apollo 16, with different thorium scale.*

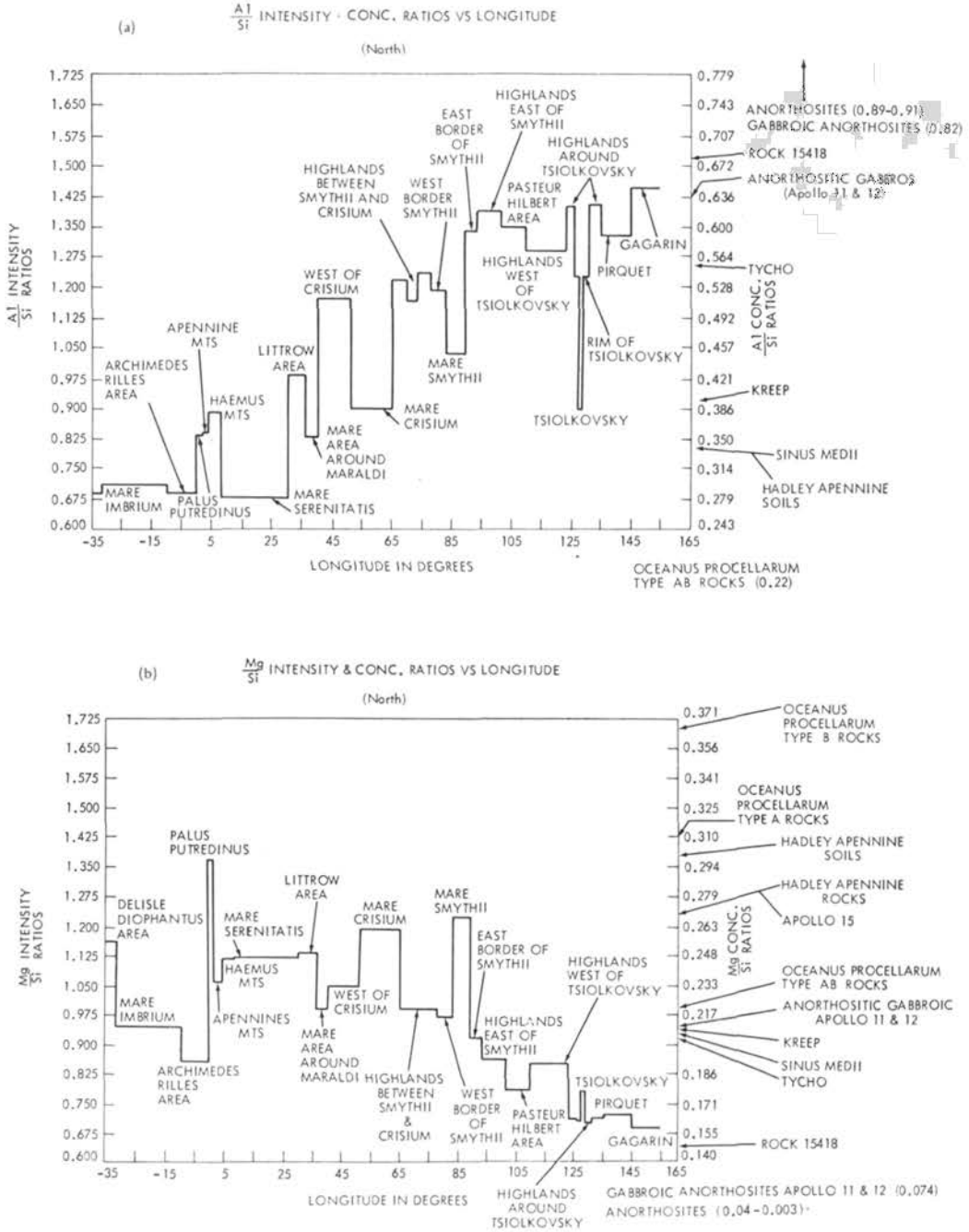


Figure 11.—*(a) Al/Si ratio versus longitude for the Apollo 15 ground northern track. The values for some reference material are shown. (b) Mg/Si ratios for the same tracks as northerly track above.*

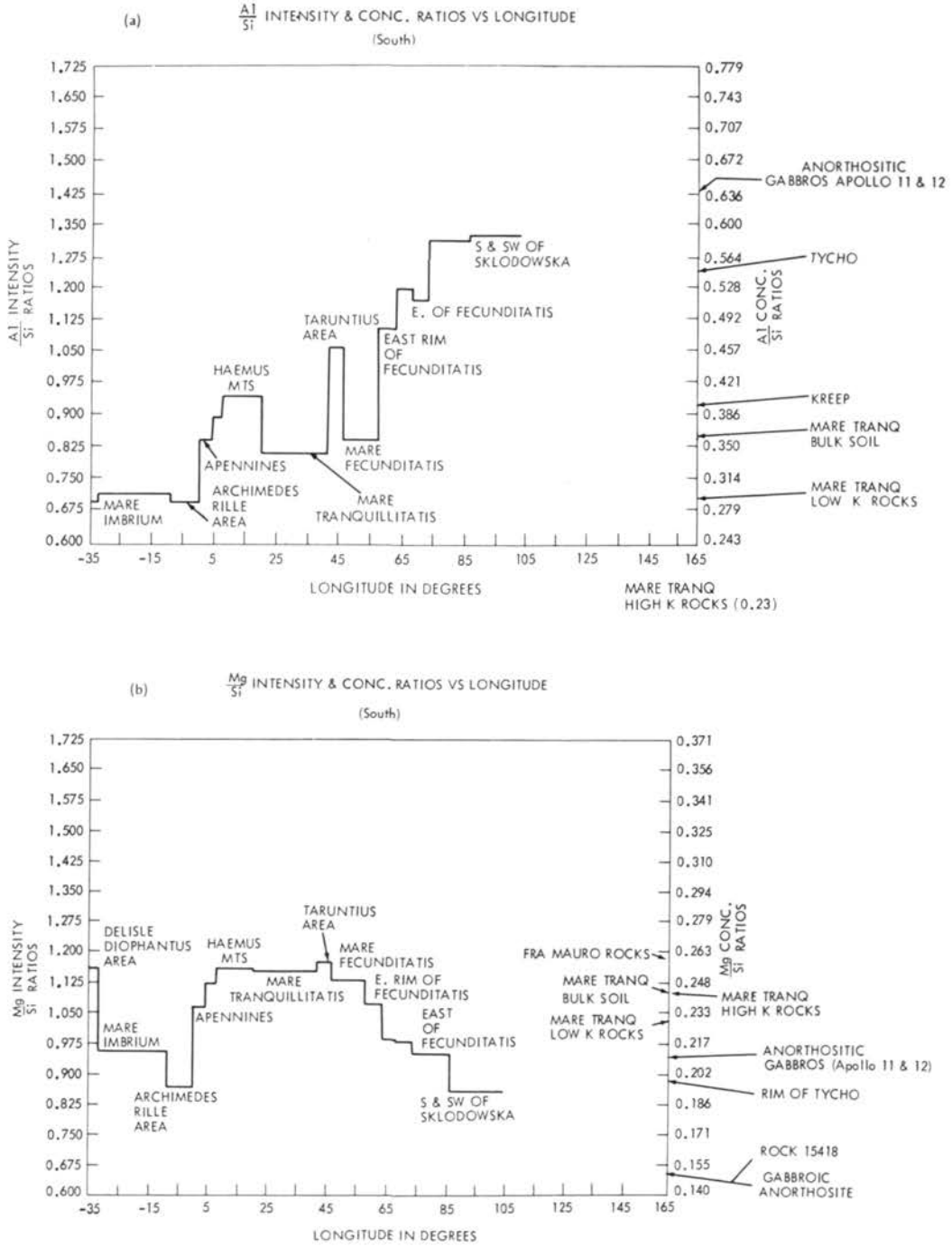


Figure 12.—*(a) Al/Si for the Apollo 15 southern ground track; (b) Mg/Si for the same southern track.*

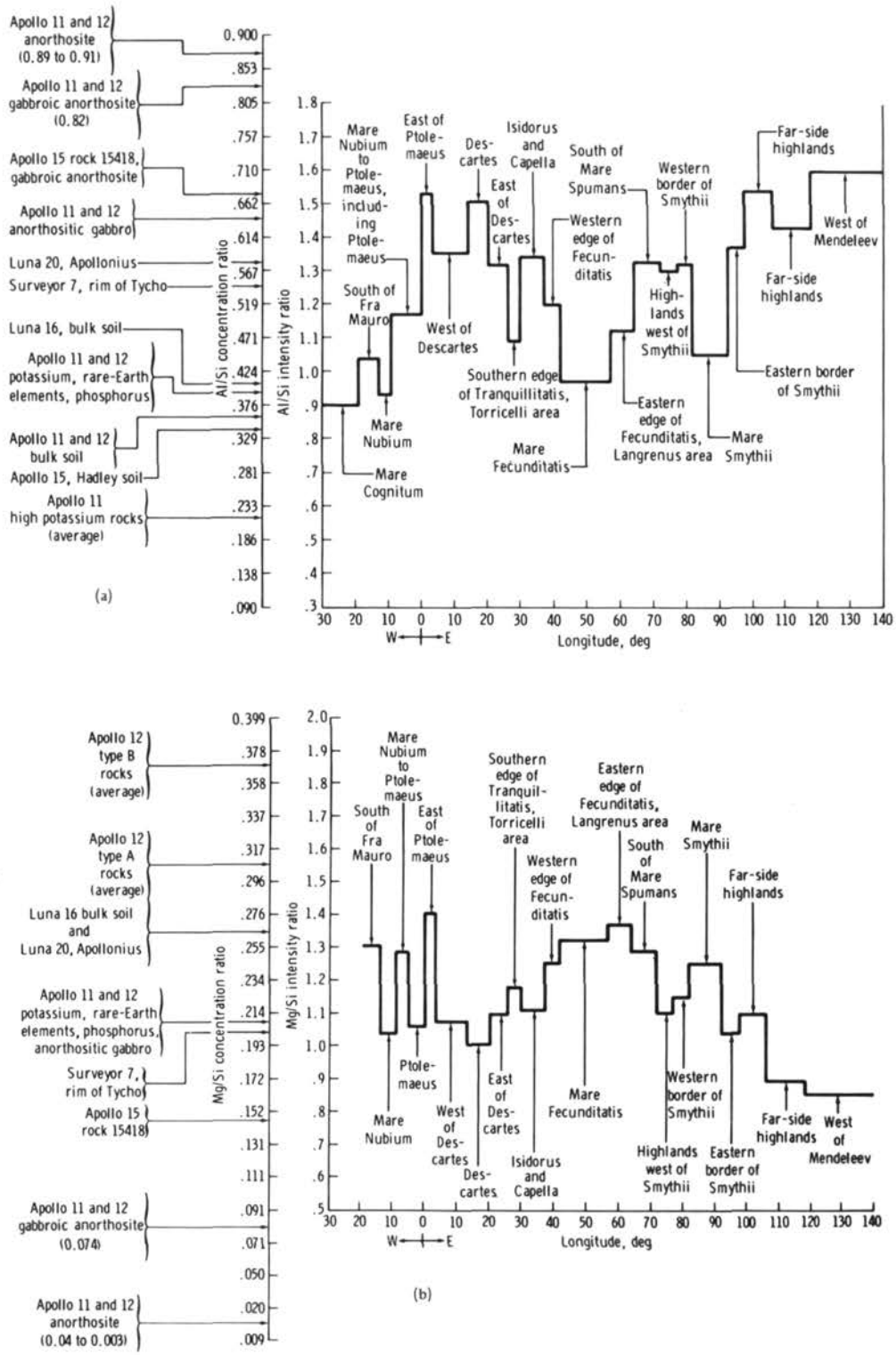


Figure 13.—*(a) Al/Si for the Apollo 16 ground track; (b) Mg/Si for the same track.*

and Mg/Si concentration ratios was previously discussed, and the results are shown in tables 6, 7, and 8. Table 6 shows the consistency in measurement between the Apollo missions. Tables 7 and 8 give results obtained over a number of lunar features. The results are obtained by integrating the spectra obtained through a number of passes over the same feature.

The data show some striking regularities:

1. The Al/Si ratios are highest in the eastern limb highlands and considerably lower in the mare areas. The extreme variation is about a factor of 2, the lowest value occurring in the Imbrium basin region. The Mg/Si concentration ratios generally show the opposite relationship. If the gamma-ray results reported above for the Fe concentration are considered, it is found that Fe is high, in low-Al regions, and the converse is also found. Also, in those regions where the Mg does remain constant, in comparison with the spatial resolution of the gamma-ray detector, there is good agreement between Mg/Si concentrations calculated from the X-ray and gamma-ray measurements. The Al/Si and Mg/Si chemical ratios for the highlands correspond to that for anorthositic gabbro through gabbroic anorthosites or feldspathic basalts. By contrast, the chemical ratios for the mare areas correspond to the mare basalts. This result is consistent with the gamma-ray results on Fe, Th, U, and K reported above.
2. Our early reports (while the Apollo 16 mission was in progress) of very high Al/Si ratios in the Descartes area were confirmed by the analysis of the lunar samples brought back from the site. The values reported of 26.5 percent aluminum oxide agree very well with the estimates in table 6. It appears reasonable from the data that some material sampled at Descartes is similar to that of the eastern limb and farside highlands. This conclusion is further justified by the fact the Mg/Si concentration ratios for some of the returned materials is about 0.18, close to the values reported here of 0.19 ± 0.05. The eastern limb highlands and farside highlands as shown in table 6, are about 0.16 to 0.21.
3. In both Apollo 15 and Apollo 16 missions, the Al and Mg values derived show an inverse relationship in most instances. The inverse relationship between Al obtained from the X-ray results and Fe obtained from the gamma-ray results is even more striking.
4. There are distinct chemical contrasts

Table 6.—*Comparison of Overlap Between Apollo 15 and Apollo 16 Ground Tracks*

Feature (1)	Apollo 16 Concentration Ratio		Apollo 15 Concentration Ratio	
	Al/Si $\pm$ 1σ	Mg/Si $\pm$ 1σ	Al/Si $\pm$ 1σ	Mg/Si $\pm$ 1σ
Mare Fecunditatis	0.41 $\pm$ 0.05	0.26 $\pm$ 0.05	0.36 $\pm$ 0.06	0.25 $\pm$ 0.03
Mare Smythii	0.45 $\pm$ 0.08	0.25 $\pm$ 0.05	0.45 $\pm$ 0.06	0.27 $\pm$ 0.06
Langrenus area	0.48 $\pm$ 0.07	0.27 $\pm$ 0.06	0.48 $\pm$ 0.11	0.24 $\pm$ 0.06
Highlands west of Smythii	0.57 $\pm$ 0.07	0.21 $\pm$ 0.03	0.55 $\pm$ 0.06	0.22 $\pm$ 0.03
Western border of Smythii	0.58 $\pm$ 0.08	0.22 $\pm$ 0.04	0.52 $\pm$ 0.06	0.22 $\pm$ 0.06
Eastern border of Smythii	0.61 $\pm$ 0.09	0.20 $\pm$ 0.06	0.60 $\pm$ 0.10	0.21 $\pm$ 0.03

NOTE: (1) The overlap between corresponding areas of the Apollo 16 and 15 ground tracks is not exact, and therefore differences for the same area may be real.

Table 7.—*Concentration Ratios of Al/Si and Mg/Si for the Various Features Overflown During Apollo 15 Mission*

Feature	Concentration Ratios	
	Al/Si ± 1σ	Mg/Si ± 1σ
West of Diophantus and Delisle,	0.26 ± 0.13	0.21 ± 0.06
northeast of Schröters Valley	0.28 ± 0.08	0.21 ± 0.06
Mare Serenitatis	0.29 ± 0.10	0.26 ± 0.07
Diophantus and Delisle area	0.29 ± 0.08	0.19 ± 0.05
Archimedes Rille area	0.30 ± 0.10	0.21 ± 0.06
Mare Imbrium	0.34 ± 0.06	0.25 ± 0.04
Mare Tranquillitatis	0.35 ± 0.08	0.22 ± 0.04
Mare east of Littrow (Maraldi)	0.35 ± 0.09	0.30 ± 0.03
Palus Putredinus	0.36 ± 0.06	0.25 ± 0.03
Mare Fecunditatis	0.36 ± 0.09	0.23 ± 0.05
Apennine Mountains		
Haemus Mountains, west border of	0.38 ± 0.10	0.25 ± 0.05
Serenitatis	0.39 ± 0.08	0.26 ± 0.05
Mare Crisium	0.39 ± 0.11	0.18 ± 0.02
Tsiolkovsky		
Haemus Mountains, south-south-	0.40 ± 0.07	0.26 ± 0.04
west of Serenitatis	0.42 ± 0.10	0.25 ± 0.06
Littrow area	0.45 ± 0.06	0.27 ± 0.06
Mare Smythii		
Taruntius area, between Tranquillitatis and Fecunditatis	0.45 ± 0.07	0.26 ± 0.02
Langrenus area, east of Fecunditatis to 62.5°E	0.48 ± 0.11	0.24 ± 0.06
Highlands between Crisium and Smythii (Mare Spumans and Mare Undarum area)	0.51 ± 0.06	0.22 ± 0.05
Highlands east of Fecunditatis,	0.51 ± 0.10	0.22 ± 0.05
Kapteyn area 68°–73°E 7.5°–15°S	0.51 ± 0.10	0.23 ± 0.05
Highlands west of Crisium		
Highlands east of Fecunditatis 62.5°–68°E, 4°–12.5°S	0.52 ± 0.10	0.22 ± 0.05
West border of Smythii to 4°–5° out from Rim	0.52 ± 0.06	0.22 ± 0.03
South of Crisium, Apollonius area, to Fecunditatis, 50°–60°E	0.53 ± 0.06	0.23 ± 0.03
East border of Crisium out to 6° from Rim	0.54 ± 0.09	0.22 ± 0.04
	0.54 ± 0.12	0.16 ± 0.02
Tsiolkovsky—Rim		
Highlands between Crisium and Smythii, 2.5°S 69°E, 5°S 76°E, 12°N 80°E, 10°N 83°E	0.55 ± 0.06	0.22 ± 0.03
Highlands west of Tsiolkovsky, 110°–124°E to 9°–21°S	0.57 ± 0.11	0.19 ± 0.04
Highlands east of Fecunditatis 73°–85°E, 10°–19°S	0.58 ± 0.13	0.21 ± 0.05
South and southwest of Sklodowska,	0.59 ± 0.14	0.19 ± 0.07
86°–101°E, 18°–23°S	0.59 ± 0.15	0.16 ± 0.05
Pirquet, 135°–145°E, 18°–23°S	0.60 ± 0.10	0.21 ± 0.03
East border of Smythii, out to 4°–5°		
Pasteur Hilbert highlands area, 101.5°–110°E, 7°–18°S	0.60 ± 0.10	0.18 ± 0.04
Hirayama, highlands east of Smythii, 89°E 12°S,	0.62 ± 0.07	0.19 ± 0.04
100°E 15°S, 98°E 2°S, 103°E 5°S	0.62 ± 0.12	0.15 ± 0.06
Highlands around Tsiolkovsky		
South part of Gagarin, 144°–153°E, 21°–23°S	0.65 ± 0.24	0.14 ± 0.05

Table 8.—*Concentration Ratios of Al/Si and Mg/Si for the Various Features Overflown During Apollo 16 Mission*

Feature	Concentration Ratios	
	Al/Si ± 1σ	Mg/Si ± 1σ
Mare Cognitum	0.38 ± 0.11	0.40 ± 0.29
Upper part of Sea of Clouds, 9°–13°W	0.39 ± 0.12	0.20 ± 0.05
Mare Fecunditatis, 42°–57°E	0.41 ± 0.05	0.26 ± 0.05
South of Fra Mauro, 13°–19°W	0.45 ± 0.07	0.26 ± 0.04
Mare Smythii, 82°–92.5°E	0.45 ± 0.08	0.25 ± 0.05
Southern edge of Mare Tranquillitatis, Torricelli area, 26°–30°E	0.47 ± 0.09	0.23 ± 0.05
Eastern edge of Fecunditatis, Langrenus area, 57°–64°E	0.48 ± 0.07	0.27 ± 0.06
Ptolemaeus, 4°W–0.5°E	0.51 ± 0.07	0.21 ± 0.04
Highlands west of Ptolemaeus to Mare Nubium, 4°–9°W	0.51 ± 0.11	0.25 ± 0.12
Highlands west of Mare Fecunditatis, 37.5°–42°E	0.52 ± 0.07	0.24 ± 0.05
Highlands west of Smythii, 72°–77°E	0.57 ± 0.07	0.21 ± 0.03
Western border of Smythii, 77°–82°E	0.58 ± 0.08	0.22 ± 0.04
Highlands east of Descartes, 20.5°–26°E	0.58 ± 0.07	0.21 ± 0.04
South of Mare Spumans, 64°–72°E	0.58 ± 0.07	0.25 ± 0.04
Isidorus and Capella, 30°–37.5°E	0.59 ± 0.11	0.21 ± 0.05
Highlands west of Descartes, 3°–14°E	0.59 ± 0.11	0.21 ± 0.05
Eastern border of Mare Smythii, 92.5°–97.5°E	0.61 ± 0.09	0.20 ± 0.06
Farside highlands, 106°–118°E	0.63 ± 0.08	0.16 ± 0.05
Descartes area, highlands, Apollo 16 landing site, 14°–20.5°E	0.67 ± 0.11	0.19 ± 0.05
East of Ptolemaeus, 0.5°–3°E	0.68 ± 0.14	0.28 ± 0.09
Highlands, 97.5°–106°E	0.68 ± 0.11	0.21 ± 0.05
Farside highlands west of Mendeleev, 118°–141°E	0.71 ± 0.11	0.16 ± 0.04

between such features as the small mare basins and the highland rims (note, for example, the crater Tsiolkovsky in figures 11a and 11b).

An interesting use of the data was to compare the Al/Si intensity ratios to optical albedo values. These observations are particularly significant in view of the longstanding discussions about whether these albedo differences represent topographic differences solely or also reflect compositional differences among surface materials. Early workers such as Whitaker (ref. 29) and others recognized convincing evidence for compositional changes where sharp albedo changes occur. However, it remained for the later Surveyor, Apollo, Luna, and Lunokhod missions to provide quantitive compositional data. Chemical differences related to albedo variations were first confirmed by the alpha backscattering experiment carried on Surveyors 5, 6, and 7 (ref. 30). The Surveyor 5 and Surveyor 6 experiment data were used to analyze widely separated mare sites, and chemically similar surface materials in each site were reported. The Surveyor 7 experiment, on the other hand, observed a highland site and data analysis found a significant chemical difference between that region and the two mare locations. The Surveyor results and the analyses of returned lunar samples confirmed that albedo is indeed affected by composition as well as topographic differerences. The X-ray fluorescence experiments on Apollo 15 and Apollo 16 now have provided the data for correlation of regional albedo with surface composition for these selected chemical elements.

The data from both Apollo flights exhibit an excellent correspondence between Al/Si values and the optical albedo values. An ex-

ample from the Apollo 16 flight is shown in figure 14. There is positive correlation between the albedo and the Al/Si values, although the rate of change is not always similar. In the Apollo 15 data, the main anomalies were observed where an occasional small Copernican-type crater occurred and produced an abnormally high albedo value. This was considered to be due to the highly reflective, finely divided ejecta rather than to compositional changes. A similar anomaly is noted in the Apollo 16 data around 27 degrees west longitude in a Tranquillitatis embayment north of Theophilus. Four Apollo 16 orbits are plotted. Orbits 58 and 60 show the expected decrease in Al/Si with decreasing albedo. Orbits 55 and 59, on the other hand, show an occasional increase in Al/Si although the albedo decreases. This may record the existence of an old "weathered" ray consisting of aluminum-rich, highland-derived ray material which has lost its high reflectivity. This loss is thus attributed to chemical rather than physical change.

The X-ray fluorescence experiment is especially well suited to look at the problem of horizontal transport and, particularly, the question of whether or not the mare fill is highland material carried by electrostatic forces. To appreciate this, one must keep in

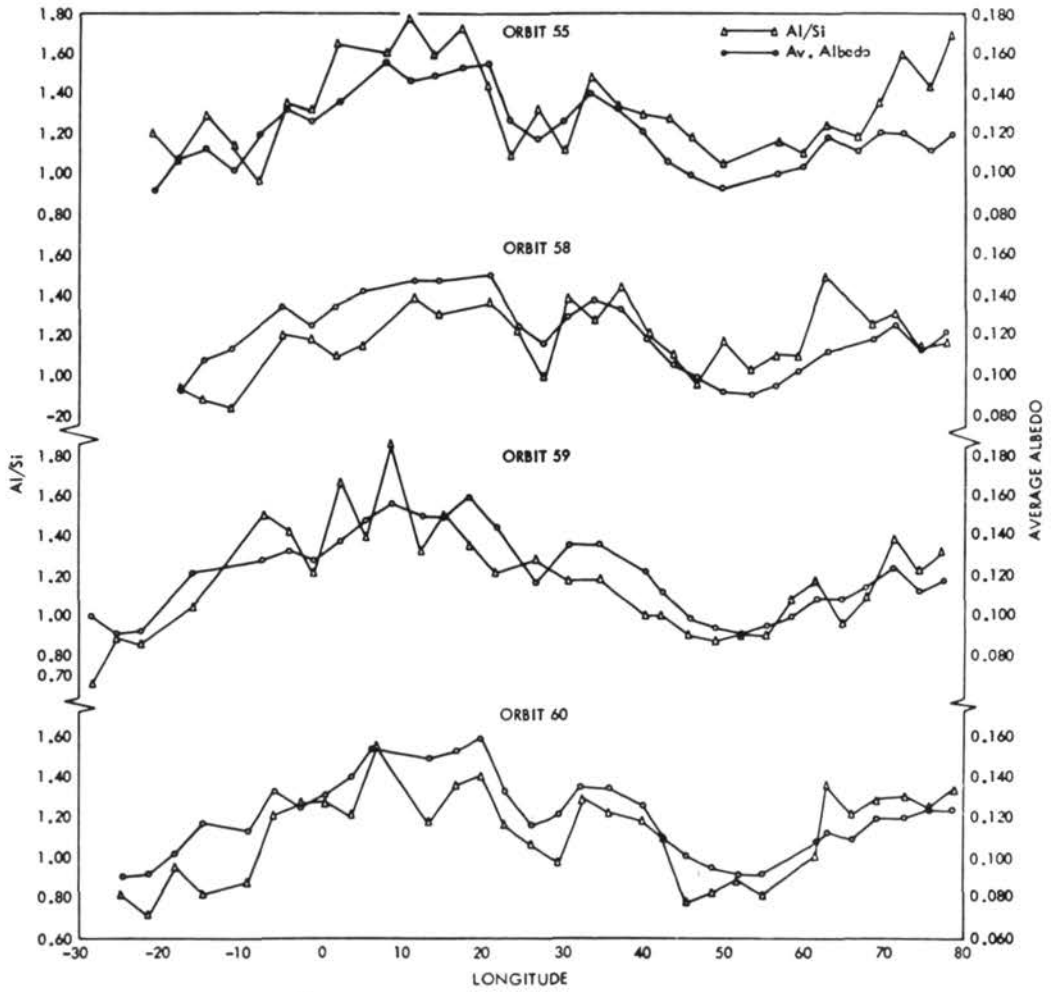


Figure 14.—*A comparison of Al/Si intensity ratios versus optional albedo values for various Apollo 16 orbits.*

mind that the X-ray measurements are extremely shallow. A 0.1-mm layer of basalt or feldspar would represent effectively infinite thickness. This is equivalent to about 3×10^{-4} g/cm^2 of material.

In a recent paper (ref. 31), it was proposed that horizontal transport by such mechanisms as electrostatic charging has played a large role in the formation of the flat mare basins. It is obvious that if highland material had drifted into the basins to any extent, the differences between the mare and the surrounding highlands would not be perceived. In fact, very marked differences have been found and are demonstrated. There are outstanding examples such as the crater Tsiolkovsky. The ratio of aluminum in the rim area to that of the basin is about 2:1. Further, real differences can be discerned in such relatively homogeneous sites as the Serenitatis-Tranquillitatis zones and in the Tranquillitatis basin itself. There is additional substantiation in the recent paper of Kocharov and Viktorov (ref. 32) on the results obtained by the Lunokhod 2 in the crater Le Monnier. From the analysis of returned lunar samples, it has been found that the soils in the highland regions are generally like the highland rocks; and similarly in maria regions the soils are generally like the maria rocks. Thus it seems highly unlikely that these chemical differences arise because one type of rock is more easily broken up than another or more easily transported. It

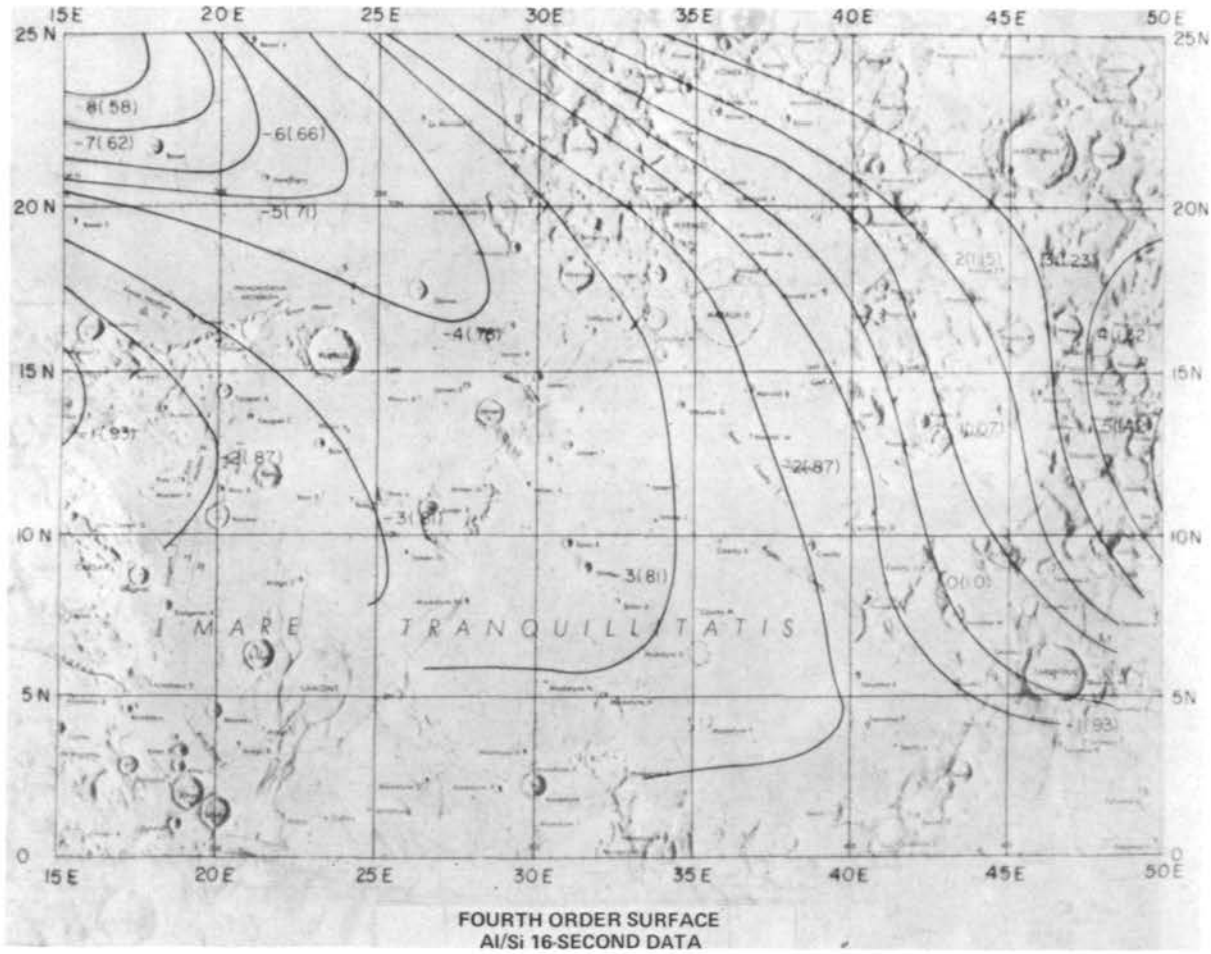


Figure 15.—*Fourth order trend surface map for Al/S intensity ratios using 16-second data (ref. 17).*

is questionable, therefore, whether small-scale, continuous, horizontal transport has played a large role in the formation of the flat maria basin.

Finally, short-time (8- and 16-second) X-ray fluorescence data were analyzed to determine their capability for mapping relatively small lunar features. Fluctuation in the solar spectral shape and variation of the look angle with spacecraft altitude make this type of analysis rather difficult, but some analysis can be performed and preliminary results have been obtained (ref. 17). Spatial mapping using trend surface analysis demonstrated that a usable signal could be abstracted from Al/Si intensity ratios compiled over short time periods. Residuals from the trend surface allowed isolation of similar areas. For details of the analytic method, see (ref. 17).

In this work a portion of Mare Serenitatis and Mare Tranquillitatis and their adjacent highlands observed during the Apollo 15 mission were chosen. On the basis of the analysis of variance interpretation using trend surface analysis of 16-second Al/Si ratio data, a fourth-order surface is the highest order which shows the proper level of significant improvement. Figure 15 (ref. 17) shows the derived model. Ratios are highest in the highlands to the northeast, and become progressively lower toward the mare. Low ratios are associated with the maria proper; the lowest values occur in Mare Serenitatis in the northwest portion of the mapped area. A high ratio is indicated by the Haemus Mountains in the western part of the map. The general model conforms well to the results discussed, in which the highlands have higher Al/Si intensity ratios than maria (figs. 11, 12, and 13).

Figure 16 (ref. 17) illustrates some selected anomalies based on the residuals from the fourth-order surface for the Al/Si ratio data.

Areas 10 and 11 and Area 3, representing Taurus-Littrow and Haemus highlands, respectively, show quite similar Al/Si ratios. Morris and Wilhelms (ref. 33) and Carr (ref. 34) mapped the Haemus highlands as Imbrian-age Fra Mauro formation, while the Taurus-Littrow highlands have been mapped as pre-Imbrian in age. As mentioned above, X-rays of the energy level measured during the Apollo missions have a penetration capability of 10μm; thus only surficial materials are mapped. Hence, it might be argued that Imbrian ejecta is being mapped in the Taurus-Littrow highlands, although it may form only a thin blanket. The crater Proclus covered in Area 21 displays considerably different Al/Si and Mg/Si ratios as compared with Area 20 ejecta material (refs. 35 and 36) derived from Proclus. These disparate results for materials of the same provenance may indicate stratigraphic variations within Proclus and the highlands.

Area 5, containing the crater Plinius, shows up as a distant positive anomaly from the maria materials as exemplified by Areas 4 and 6. The crater occupies an area interpreted as an impact crater (ref. 33) in an area of relatively thin mare materials at the transition between Mare Tranquillitatis and Mare Serenitatis. Crater excavation due to impact has most likely excavated and exposed highland material from the subsurface. Topographic data indicate that the crater was excavated to approximately 1200 meters below the mare floor. This sets a maximum limit for the mare thickness, which De Hon (ref. 37) estimates as 500 to 600 meters in this area.

Two additional positive mare anomalies which may be of significance are Areas 7 and 2. Area 7 corresponds to a wrinkle ridge and high albedo mare material as mapped by Carr (ref. 34). Examination of Apollo 15 metric photography indicates some features which might be interpreted as volcanic terrain or extrusive features. Both Young et al. (ref. 38) and Hodges (ref. 39) report possible extrusive igneous features in the same general vicinity. Low-albedo Mare Serenitatis materials are typified by ratios such as those in the negative residual of Area 1. This suggests that at least two types of substantially different mare basalts are present within Mare Serenitatis. Lowman (ref. 40)

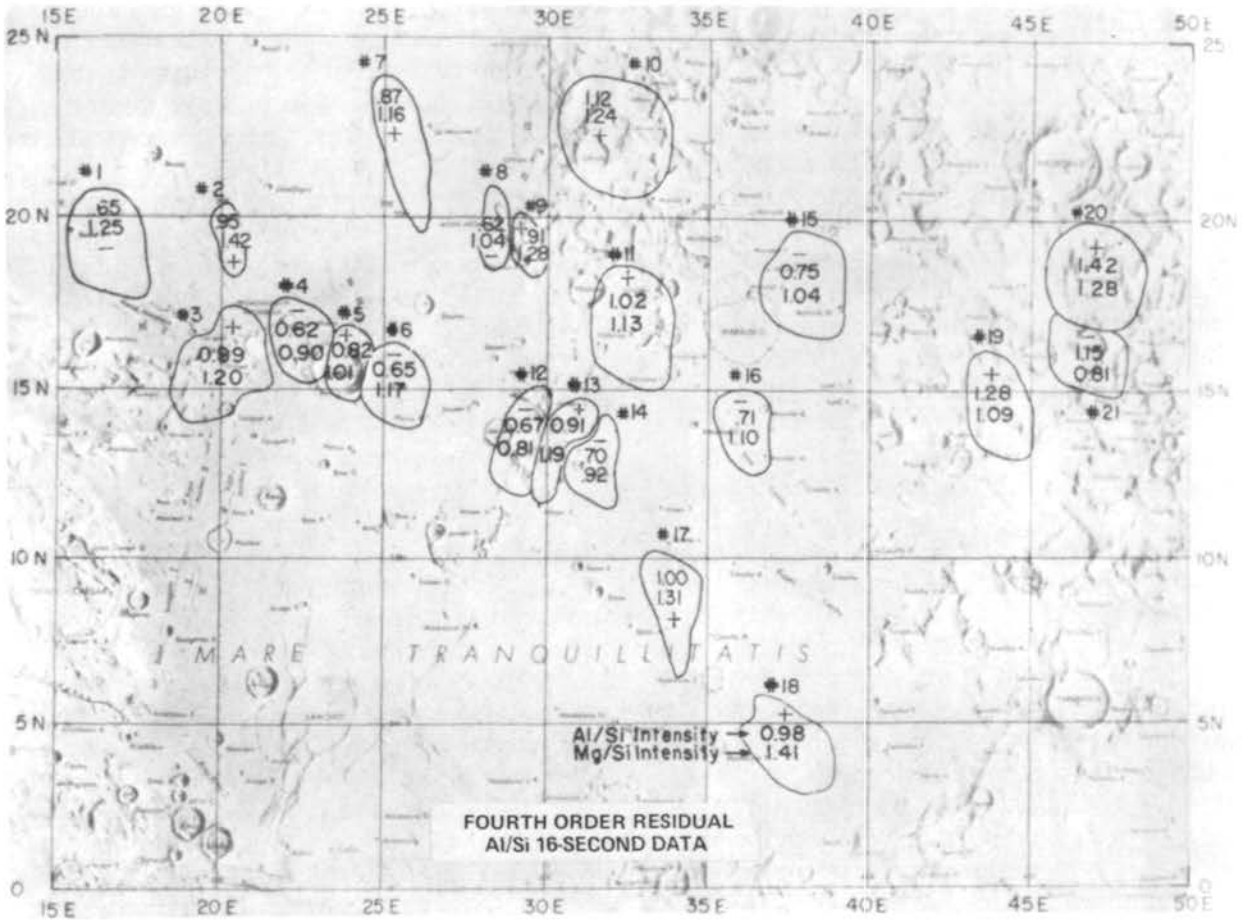


Figure 16.—*Residuals from the fourth order trend surface for Al/Si intensity ratios. Departures or deviations are based on normalized data. A plus sign denotes a positive residual; a negative sign indicates a negative residual. Calculated intensity ratios are given in original units for ease of interpretation (ref. 17).*

suggests that these wrinkle ridge areas may contain the final differentiation products of a large basaltic body and should contain higher alumina concentrations. Area 2, associated with a rectilinear junction of four mare ridges forming a parallelogram, also displays a similar positive anomaly.

Positive residuals associated with Areas 17 and 18 appear to be associated with zones of the highest albedo mare materials within Mare Tranquillitatis as mapped by Wilhelms (ref. 36). The positive residual associated with Area 13 is perplexing, for it is not associated with the Jansen craters as might be expected, but is located to their east. The only explanation for this anomaly at this time may be the concentration of ray materials as mapped by Morris and Wilhelms (ref. 33).

Conclusions

It is hoped that this summary and interpretation of results obtained from the Apollo X-ray and gamma-ray spectrometer experiment data presented here, will be helpful to investigators in the field of planetology. As can be seen from the results reported, the work is not yet completed, but much information was obtained. There is still much to be completed in the future.

Acknowledgment

The results reported in this work represent the efforts of persons too numerous to mention here. Appreciation is expressed to all these individuals for their help in the development, implementation, analysis, and interpretation of project results.

References

1. ARNOLD, J. R., L. E. PETERSON, A. E. METZGER, AND J. I. TROMBKA, *Preliminary Science Report*, NASA SP–289, 1972.
2. HARRINGTON, T. M., J. H. MARSHALL, J. R. ARNOLD, L. E. PETERSON, J. I. TROMBKA, AND A. E. METZGER, The Apollo Gamma-Ray Spectrometer. *Nuc. Instruments and Methods*, in press, 1974.
3. REEDY, R. C., J. R. ARNOLD, AND J. I. TROMBKA, Expected Gamma-Ray Emission Spectra From the Lunar Surface as a Function of Chemical Composition. *J. Geophys. Res.*, Vol. 78, 1973, pp. 5847–5866.
4. METZGER, A. E., J. I. TROMBKA, L. E. PETERSON, R. C. REEDY, AND J. R. ARNOLD, A First Look at the Lunar Orbital Gamma-Ray Data. *Proc. Third Lunar Science Conference, Geochimica et Cosmochimica Acta*, Supplement 3, Vol. 3, 1972, frontispiece.
5. METZGER, A. E., Lunar Surface Radioactivity: Preliminary Results of the Apollo 15 and Apollo 16 Gamma-Ray Spectrometer Experiments, *Science*, Vol. 179, 1973, pp. 800–803.
6. METZGER, A. E., J. I. TROMBKA, L. E. PETERSON, R. C. REEDY, AND J. R. ARNOLD, Element Concentration From Lunar Orbital Gamma-Ray Measurements. *Proc. Fifth Lunar Science Conference, Geochimica et Cosmochimica Acta*, in press, 1974.
7. REEDY, R. C., AND J. R. ARNOLD, Interaction of Solar and Galactic Cosmic Ray Particles With the Moon. *J. Geophys. Res.*, Vol. 77, 1972, p. 537.
8. LINGENFELTER, R. E., E. H. CANFIELD, AND V. E. HAMPEL, The Lunar Flux Revisited. *Earth Planet. Sci. Letters*, Vol. 16, 1972, p. 355.
9. FINKEL, R. C., M. IMAMURA, M. HONDA, K. NISHIIZUM', C. P. KOHL, S. M. KOCIMSKI, AND J. R. ARNOLD, Cosmic Ray Produced Mn and Be Radionuclides in the Lunar Regolith. *Proc. Fifth Lunar Science Conference, Geochimica et Cosmochimica Acta*, in press, 1974.
10. WOOLUM, D. S., AND D. S. BURNETT, In-Situ Measurement of the Rate of ^{235}U Fission Induced by Lunar Neutrons. *Earth Planet. Sci. Letters*, Vol. 21, 1974, p. 153.
11. TURKEVICH, A. L., E. J. FRANZGROTE, AND J. H. PATTERSON, Chemical Composition of the Lunar Surface in Mare Tranquillitatis. *Science*, Vol. 165, 1969, p. 277.
12. WAKITA, H., R. A. SCHMITT, AND P. REY, Elemental Abundances of Major, Minor and Trace Elements in Apollo 11 Lunar Rocks. *Apollo 11 First Lunar Science Conference, Geochimica et Cosmochimica Acta*, Supplement 1, Vol. 2, 1970, p. 1685.
13. SCHONFELD, E., AND C. MEYER, The Abundances of Components of the Lunar Soils by a Least Squares Mixing Model and the Formation Age of KREEP. *Proc. Third Lunar Science Conference, Geochimica et Cosmochimica Acta*, Supplement 3, Vol. 2, 1972, pp. 1397–1420.
14. ADLER, I., J. I. TROMBKA, J. GERARD, R. SCHMADEBECK, ET AL., X-Ray Fluorescence Experiment. *Apollo 15 Preliminary Science Report*, NASA SP–289, 1972.
15. ADLER, I., J. I. TROMBKA, R. SCHMADEBECK, P. LOWMAN, H. BLODGET, L. YIN, E. ELLER, M. PODWYSOCKI, J. R. WEIDNER, A. L. BICKEL, R. K. L. LUM, J. GERARD, P. GORENSTEIN, P. BJORKHOLM, AND B. HARRIS, Results of the Apollo 15 and 16 X-Ray Experiment. *Proc. Fourth Lunar Science Conference, Geochimica et Cosmochimica Acta*, Supplement 4, Vol. 3, 1973, pp. 2783–2791.
16. ADLER, I., M. PODWYSOCKI, C. ANDRE, J. I. TROMBKA, AND R. SCHMADEBECK, The Role of Horizontal Transport—As Evaluated From the Apollo 15 and 16 Orbital Experiments. *Proc. Fifth Lunar Science Conference, Geochimica et Cosmochimica Acta*, in press, 1974.
17. PODWYSOCKI, M. H., J. R. WEIDNER, C. G. ANDRE, A. L. BECKEL, R. S. LUM, I. ADLER, AND J. I. TROMBKA, An Analysis of the Apollo 15 X-Ray Fluorescence Experiment for Detailed Lunar Morphological and Geochemical Parameters. *Proc. Fifth Lunar Science Conference, Geochimica et Cosmochimica Acta*, in press, 1974.
18. TROMBKA, J. I., J. R. ARNOLD, R. C. REEDY, L. E. PETERSON, AND A. E. METZGER, Some Correlations Between Measurements by the Apollo Gamma-Ray Spectrometer and Other Lunar Observations. *Proc. Fourth Lunar Science Conference, Geochimica et Cosmochimica Acta*, Supplement 4, Vol. 3, 1973, pp. 2847–2853.
19. *Proc. Fourth Lunar Science Conference, Geochimica et Cosmochimica Acta*, Supplement 4, Vol. 1, 1973, frontispiece, plate II.
20. LSPET (Lunar Sample Preliminary Examination Team), *Science*, Vol. 173, 1971, p. 681.
21. SJOGREN, W. L., AND W. R. WOLLENHAUPT, Lunar Shape Via the Apollo Laser Altimeter. *Science*, Vol. 179, 1973, pp. 275–278.
22. COLEMAN, P. F., B. R. LICHTENSTEIN, C. T.

RUSSEL, G. SCHUBERT, AND L. R. SHARP, The Particles and Fields Subsatellite Magnetometer Experiment. *Apollo 16 Preliminary Science Report*, NASA SP–315, 1973.

23. ELDRIDGE, J. S., G. D. O'KELLEY, AND K. J. NORTHCUTT, Radionuclide Concentrations in Apollo 16 Samples. *Proc. Fourth Lunar Science Conference, Geochimica et Cosmochimica Acta*, Supplement 4, Vol. 2, 1973, p. 2115.
24. ELDRIDGE, J. S., G. D. O'KELLEY, AND K. J. NORTHCUTT, Abundances of Primordial and Cosmogenic Nuclides in Apollo 14 Rocks and Fines. *Proc. Third Lunar Science Conference, Geochimica et Cosmochimica Acta*, Supplement 3, Vol. 2, 1972, p. 1651.
25. O'KELLEY, G. D., J. S. ELDRIDGE, E. SCHONFELD, AND P. R. BELL, Abundances of the Primordial Radionuclides K, Th, and U in Apollo 12 Lunar Samples by Non-Destructive Gamma-Ray Spectrometry; Implications for Origin of Lunar Soils. *Proc. Second Lunar Science Conference, Geochimica et Cosmochimica Acta*, Supplement 2, Vol. 2, 1971, p. 1159.
26. ADLER, I., J. GERARD, J. I. TROMBKA, R. SCHMADEBECK, ET AL., The Apollo 15 X-Ray Fluorescence Experiment. *Proc. Third Lunar Science Conference, Geochimica et Cosmochimica Acta*, Vol. 3, David R. Criswell, ed., 1972, pp. 2157–2178.
27. ADLER, I., J. I. TROMBKA, J. GERARD, P. LOWMAN, R. SCHMADEBECK, H. BLODGETT, E. ELLER, L. YIN, R. LAMOTHE, P. GORENSTEIN, AND P. BJORKHOLM, Apollo 15 Geochemical X-Ray Fluorescence Experiment: Preliminary Report. *Science*, Vol. 175, 1972, pp. 436–440.
28. ADLER, I., J. I. TROMBKA, J. GERALD, P. LOWMAN, R. SCHMADEBECK, H. BLODGETT, E. ELLER, L. YIN, R. LAMOTHE, G. OSSWALD, P. GORENSTEIN, P. BJORKHOLM, H. GURSKY, AND B. HARRIS, Apollo 16 Geochemical X-Ray Fluorescence Experiment: Preliminary Report. *Science*, Vol. 177, 1972, pp. 256–259.
29. WHITAKER, E. A., *The Nature of the Lunar Surface, The Surface of the Moon*. Hess, Menzel, and O'Keefe, eds., The Johns Hopkins Press, 1965, p. 79.
30. PATTERSON, JAMES H., ANTHONY L. TURKEVITCH, E. J. FRANZGROTE, T. E. ECONOMOU, AND E. P. SOWINSKI, *Science*, Vol. 168, 1972, p. 825.
31. GOLD, T., *The Moon*. Vol. 7, Nos. 3 and 4, 1973.
32. KOCHAROV, G. E., AND S. V. VIKTOROV, Doklady, Akad. Nauk USSR, in press, 1974.
33. MORRIS, E. C., AND D. E. WILHELMS, Geologic Map of the Julius Caesar Quadrangle of the Moon. U.S. Geol. Survey, Map I–510, 1967.
34. CARR, M. H., Geologic Map of the Mare Serenitatis Region of the Moon, U.S. Geological Survey, Map I–489, 1966.
35. SCOTT, P. H., AND H. A. POHN, Geologic Map of the Macrobius Quadrangle of the Moon. U.S. Geol. Survey, Map I–799, 1972.
36. WILHELMS, D. E., Geologic Map of the Taruntius Quadrangle of the Moon. U.S. Geol. Survey, Map I–722, 1972.
37. DE HON, R. A., Thickness of Mare Material in the Tranquillitatis and Nectaris Basins. *Proc. Fifth Lunar Science Conference, Geochimica et Cosmochimica Acta*, in press, 1974.
38. YOUNG, R. A., W. J. BRENNAN, R. W. WOLFE, AND D. J. NICHOLS, Volcanism in the Lunar Maria. *Apollo 17 Preliminary Science Report*, NASA SP–330, 1973, pp. 31–1 and 31–11.
39. HODGES, C. A., Mare Ridges and Lava Lakes. *Apollo 17 Preliminary Science Report*, NASA SP–330, 1973, pp. 31–12 to 31–21.
40. LOWMAN, P., The Geologic Evolution of the Moon. *J. Geology*, Vol. 80, No. 2, 1972, pp. 125–166.

Comparison of Lunar Rocks and Meteorites: Implications to Histories of the Moon and Parent Meteorite Bodies

Martin Prinz, R. V. Fodor, and Klaus Keil
Department of Geology and Institute of Meteoritics
University of New Mexico
Albuquerque, New Mexico

There are many similarities between lunar samples and stone meteorites. Lunar samples, especially from the highlands, indicate that they have been affected by complex and repeated impact processes that can result in breccias with a wide variety of features produced by crushing; grinding; comminution; cataclasis; mixing (with other rock types and meteorites); partial or complete melting and mobilization; production of glass as matrix, agglutinates, spherules, fragments, and chondrules; solid-state recrystallization; impact melt as matrix or as essentially wholly new igneous rocks with ophitic, intersertal, poikilitic, or other textures; etc. Similar complex and repeated impact processes have also been operative on the achondritic and chondritic meteorites, but there has been much less detailed study of the effects of these processes and discussion of their implications. In this study, we draw attention to a number of similarities between lunar and meteoritic rocks and suggest that this comparison is essential for a clear understanding of meteorites as probes of the early history of the solar systems. (1) Monomict and polymict breccias occur in lunar rocks, as well as in achondritic and chondritic meteorites, having resulted from complex and repeated impact processes. (2) Chondrules are present in lunar meteorites, as well as in a few achondritic and most chondritic meteorites. They apparently crystallized spontaneously from molten highly supercooled droplets which may have formed from impact melts or, perhaps, volcanic processes (as well as from the solar nebula, in the case of meteoritic chondrites). It is pointed out that because chondrules may form in several different ways and in different environments, a distinction between the different modes of origin and an estimate of their relative abundance is important if their significance as sources of information on the early history of the solar system is to be clearly understood. (3) Lithic fragments are very useful in attempts to understand the preimpact and postimpact history of lunar and meteoritic breccias. They vary from little modified (relative to the apparent original texture) to partly or completely melted and recrystallized lithic fragments. Their detailed study allows conclusions to be drawn about their parent rock types and their origin, thereby gaining insight into preimpact histories of lunar and meteoritic breccias. There is considerable evidence that cumulate rocks were involved in the early history of both the Moon and parent meteorite bodies. In the light of knowledge derived from the lunar program and by continued study of meteoritic samples, we should learn more about the preimpact history of both rock groups and thereby be better prepared to make comparative studies of planetary bodies, particularly regarding their early histories.

One of the most important characteristics of lunar rocks, particularly from the lunar highlands, is that they have been greatly altered by intense, repeated impact bombardment. The histories of these rocks, both preimpact and postimpact, are difficult to decipher, and interpretation of their genesis is a major goal of lunar research. There is general agreement that the lunar highland rocks originated as cumulates, although very few

original textures have survived the impact processes without major obliteration. About 90 percent of the highland rocks are polymict breccias (ref. 1) which are the result of complex impact processes. These breccias were produced by crushing; grinding; comminution; cataclasis; mixing (with other rock types as well as meteorites); partial or complete melting and mobilization; production of glass as matrix, agglutinates, spherules, fragments, and chondrules; solid-state recrystallization; crystallization of impact melt as matrix or as essentially wholly new igneous rocks with ophitic, intersertal, poikilitic, or other textures; etc. In spite of all these complications, some aspects of the preimpact history of the cumulate rocks have been deciphered, and great progress has been made in interpreting their origins, although there is still much to be learned and some basic problems are yet to be resolved.

In the case of meteorites, particularly the ordinary chondrites, there is much less general agreement as to whether the textural features observed are "primary," i.e., were established during condensation from a solar nebula; whether they are "secondary," having been formed on a parent body or bodies by secondary (i.e., impact, volcanic, etc.) processes; or whether they formed by some combination of the two. There is much evidence and general agreement that many meteorites have been involved in impact events. However, there are only a few studies of meteorites in terms of deciphering their preimpact and postimpact histories: Fredriksson et al. (ref. 2) pointed out that black veins in stone meteorites are shock-wave produced; Fredriksson and Keil (ref. 3) showed that the light-dark structures in the Kapoeta achondrite and the Pantar chondrite are due to impact brecciation; Fredriksson (refs. 4 and 5), Fredriksson and Reid (ref. 6), Urey (ref. 7), and Kurat et al. (ref. 8) maintained that ordinary chondrites formed in large-scale impact events on parent meteorite bodies. If impact processes were indeed involved with formation of chondrites and achondrites, one should expect to find the features observed in shock-modified lunar rocks (if meteorites constitute a representative sample).

At this writing, we are only at the beginning of an era of comparative research of lunar and meteorite samples, and this type of work holds much promise for the future. We have studied both lunar rocks and meteorites (refs. 9 through 16), and other workers have identified impact-produced features in stone meteorites (e.g., refs. 17 through 23).

Since meteorites may have originated on small parent bodies with essentially no atmospheric cushion, many of their textural features must be impact- and regolith-produced, similar to what can be seen in lunar samples. In the present paper we draw attention to some of the similarities between lunar and meteoritic samples, mostly in the form of photographic analogs. It is hoped that some of the analogies will provoke other workers into studies whereby lunar and meteoritic samples will be used together in deciphering the histories of both groups of rocks and the processes that were effective on their parent bodies.

There are, of course, many ways of comparing lunar and meteoritic samples, but for the purpose of this paper we shall limit our examination to only three general areas: (1) evidence of impact brecciation, either monomict or polymict; (2) modes of origin of chondrules; and (3) origin and history of lithic fragments and their host breccias.

Lunar and Meteoritic Breccias

Many lunar highland rocks are complex monomict and polymict breccias and exhibit many of the characteristics associated with impact metamorphism. Several excellent examples of monomict breccias were found in the lunar highlands. One of the best known is anorthosite 15415, the "genesis rock" (see ref. 24). A group of eight other very similar rocks termed ferroan anorthosites were found in the Apollo 16 rake samples (ref. 25), indicating a widespread distribution of this rock type. Another important monomict breccia is dunite 72415, described by Albee

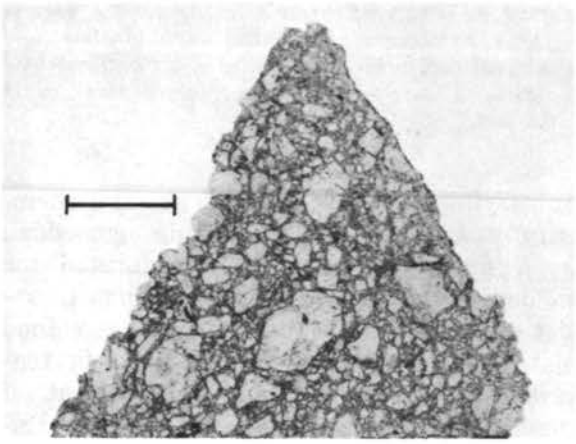


Figure 1.—*Monomict brecciated lunar dunite (72415). Plane polarized light; scale bar equals 0.25 cm. (Photo by A. Albee)*

et al. (ref. 26) and shown in figure 1. The matrix of the dunite formed as the result of crushing (without recrystallization) of the parent rock; other deformational characteristics are also present.

Several meteoritic analogs to lunar monomict breccias exist, particularly in achondritic meteorites. There, the enstatite achondrites and bronzite achondrites (terminology of Keil, ref. 27) consist mainly of what appear to be monomict breccias of enstatitite and bronzitite (orthopyroxenites). One example of a bronzite achondrite, or bronzitite, is Johnstown (fig. 2), which is texturally very similar to the lunar dunite (fig. 1). Portions of the Johnstown meteorite are unbrecciated and retain a preimpact, coarsely recrystallized texture with triple-point junctions between the bronzite grains. Brecciated and unbrecciated portions of this meteorite have identical bulk chemical compositions (ref. 28), indicating that, at least in this one case, the mineralogy and bulk chemistry of a monomict brecciated rock is the same as its preimpact parent.

Most lunar highland samples, however, are polymict breccias. They are particularly abundant at the Apollo 16 (ref. 29) and Apollo 14 sites (ref. 30). One such polymict breccia (14318), with a chondritic texture, has been described by Kurat et al. (ref. 31). This rock differs, of course, from a meteoritic chondrite in its mineral and bulk chemistry and especially in its paucity of metal and troilite, but is very similar to chondrites in its texture. It consists of a fine-grained matrix into which are embedded lithic fragments, glasses, and chondrules of ANT suite, high-alumina basalt, and dunite composition. The rock is annealed and has a partly glassy matrix analogous to many relatively unrecrystallized chondrites. A similar Apollo 14 breccia, 14315, is shown in figure 3.

Analogs to this rock type exist in both achondritic and chondritic meteorites. Among the achondritic meteorites, the best examples of polymict breccias are the howardites. These have previously been considered to be polymict breccias by numerous workers (e.g., Duke and Silver, ref. 32), and the analogy to lunar breccias has reinforced the conclusion that they are impact-produced breccias from meteorite parent-body regoliths (refs. 21 and 33). Bunch (ref. 21) finds lithic fragments ranging from anorthositic gabbro to basalt to ferrobasalt in five howardites, which would appear to indicate stronger mineralogical and chemical similarity to lunar rocks than previously realized. An example of one of these howardites, Malvern, is shown in figure 4.

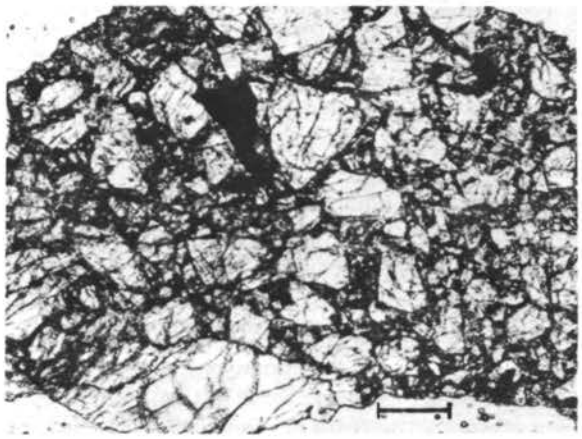


Figure 2.—*Monomict brecciated Johnstown bronzite achondrite or bronzitite. Note similarity in texture to lunar brecciated dunite (fig. 1). Plane polarized light; scale bar equals 0.5 mm.*

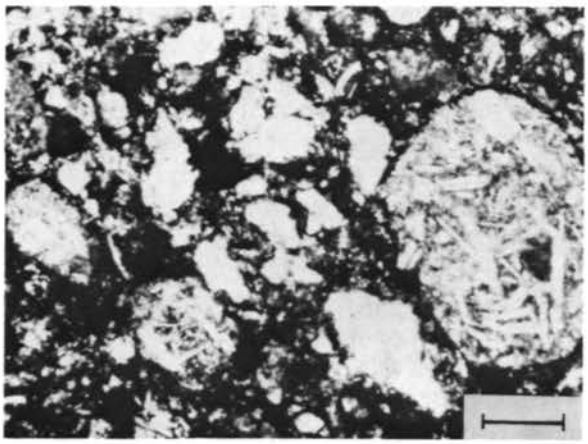


Figure 3.—*Polymict brecciated Apollo 14 breccia 14315, containing chondrules, angular glass, and mineral and lithic fragments in a tightly welded matrix. Plane polarized light; scale bare equals 0.5 mm.*

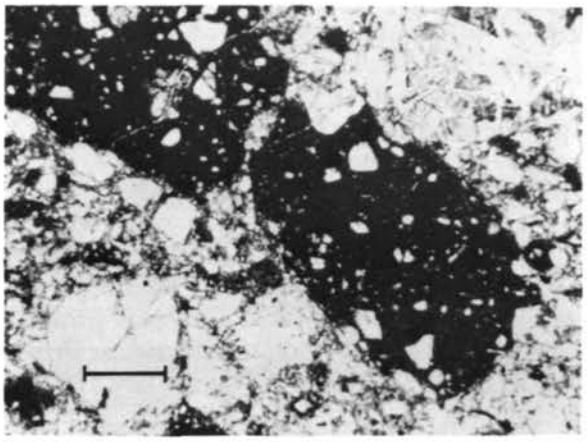


Figure 4.—*Polymict brecciated achondrite Malvern, a howardite, containing dark angular breccia fragments, glass, mineral, and igneous lithic fragments in a tightly welded matrix. Plane polarized light; scale bar equals 0.5 mm.*

Many chondrites, particularly those of the LL-group, are also brecciated, and it is sometimes difficult to determine whether they are monomict or polymict. One such example, Soko-Banja, is shown in figure 5. In some cases, the complex impact-produced relationships are further obscured by metamorphism which causes recrystallization and may be a late stage of the impact event or a later event superimposed on the impact features. The clearly brecciated chondrites exhibit these textures on the hand specimen level, and microscopic studies indicate lithic fragments of varying textures, mineralogy, and chemistry associated with chondrules embedded in a finer grained, highly indurated, or welded matrix. Since many chondrites consist of chondrules embedded in fine-grained matrices and show evidence of shock features in the minerals, it is possible that all chondrites are breccias and that those without a visibly brecciated texture were originally comminuted on a finer scale and metamorphosed. Thus, there are many unresolved major problems with regard to the interpretation of the history of chondrites, as seen by the petrologist. These histories must then be correlated with studies of many types before final interpretations are possible.

Wahl (ref. 34) stressed the importance of polymict brecciated meteorites, but his descriptions were based largely on petrographic studies without chemical data. Nevertheless, there are now some well-established examples of polymict brecciated chondrites. Some of the more recent descriptions are given in references 5, 10, 12, 13, 14, 16, 17, 20, 35, and 36.

One of the best known examples of a meteoritic polymict breccia is Cumberland Falls, which consists of an enstatite achondrite host into which are embedded fragments of chondritic material. However, Fodor et al. (ref. 13) recently showed that achondritic material may be present in a chondrite: the Adams Co. chondrite contains a large lithic fragment of regolithic material consisting of smaller lithic and mineral fragments apparently derived from ureilites and enstatite achondrites. A photo of this fragment is shown in figure 6. Another group of polymict breccias currently receiving wide attention are C3 chondrites, such as Allende, which contain white Ca-Al-rich inclusions.

Even now it is already apparent that me-

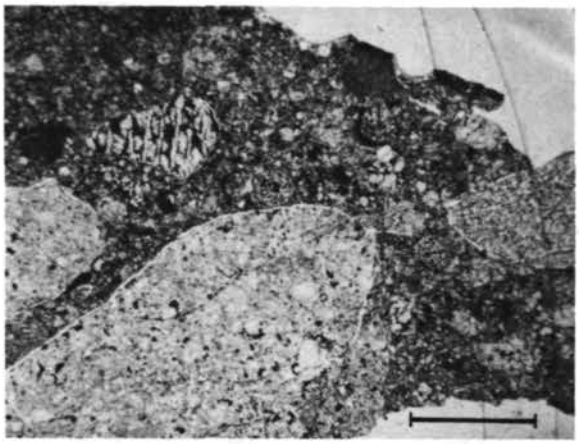


Figure 5.—*Brecciated LL-group chondrite Soko Banja, showing lithic fragments of various sizes, shapes, and textures. White lines around some fragments are fractures. Plane polarized light; scale bar equals 3 mm.*

teorites, both achondrites and chondrites, show many of the impact features seen in lunar highland rocks. The conclusion appears therefore inescapable; namely, that parent meteorite bodies have been severely affected by impact processes, and that many of the textural features in achondrites and chondrites are the result of these complex and repeated impact processes, similar to the lunar case. It will be an important task of future lunar and meteoritic research to clearly describe these "secondary" features and distinguish them from "primary" features. Inevitably, this will lead to a clearer understanding of the history of parent meteorite bodies and to a better appreciation of what meteorites can tell us regarding the early history of the solar system.

Origin of Chondrules

Chondrules are characteristic features of chondritic stone meteorites and are thought by some to be primary bodies that condensed from a nebula of solar composition and then agglomerated to form parent meteorite bodies (refs. 37 through 40). They are thought by others to be secondary objects that formed from preexisting material by either volcanism (refs. 41 through 44), lightning discharge (ref. 45), shock melting of primitive dust (ref. 46), or impact splattering (refs. 4 through 8).

Lunar chondrules were found in some breccias and soils from most Apollo and Luna sites (e.g., ref. 47). Their textures are similar to those found in some meteorites, especially in unequilibrated ordinary chondrites which often have chondrules with glassy matrices. The lunar chondrules have textures that often appear to be due to a greater amount of supercooling as compared to those in chondrites, but quantification of

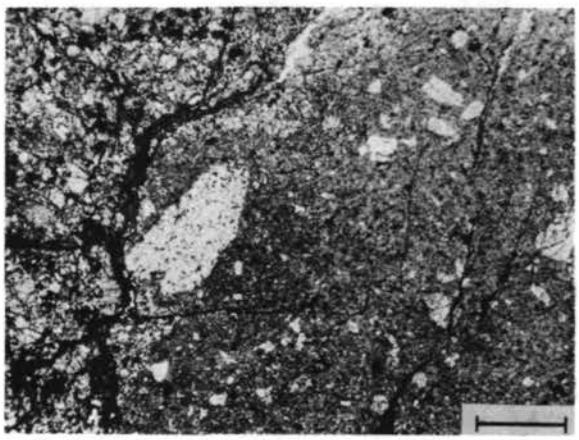
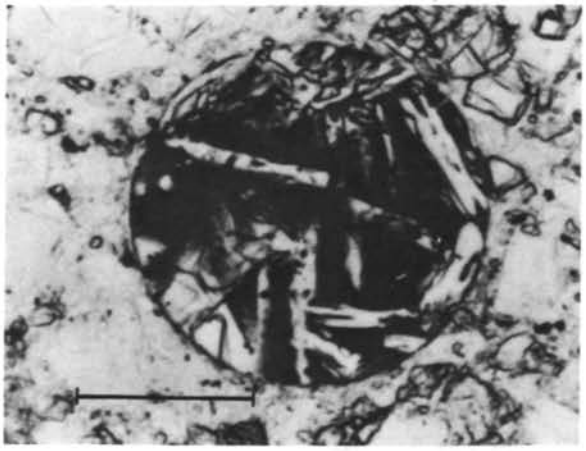


Figure 6.—*Polymict brecciated H-group chondrite, Adams Co. Regolithic achondritic breccia fragment is right-hand two-thirds of photo (dark line is boundary). Left one-third of photo is chondritic host. Achondritic breccia fragment contains enstatite achondrite or enstatite subfragment (large white area) and smaller ureilite fragments. Plane polarized light; scale bar equals 1 mm.*

this difference is difficult because of bulk compositions. Lunar and meteoritic chondrules are interpreted by most workers as being produced from molten droplets that have spontaneously crystallized from the highly supercooled state. However, the critical and controversial question is the origin of the molten droplets, especially in the case of meteorites. Recent experimental work has contributed significantly to an understanding of the origin of chondrules. In this work, sili-



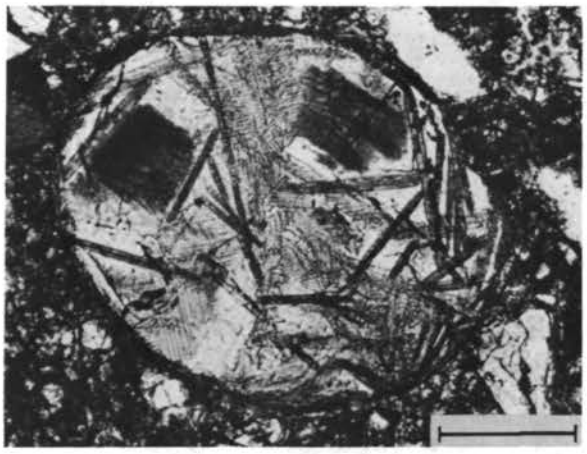


Figure 8.—*An Apollo 15 green glass chondrule containing crystals of olivine and dark microcrystalline areas, in sample 15425. Plane polarized light; scale bar equals 0.15 mm.*

cates were melted with the use of a CO_2 laser and allowed to fall freely into a variety of atmospheres. The freely falling molten droplets supercooled highly and crystallized spontaneously from the highly supercooled state, with the resulting spherules having typical chondrule textures (refs. 48 and 49). It is therefore concluded that both meteoritic and lunar chondrules formed by spontaneous crystallization of highly supercooled molten droplets, but nothing can be said from the experiments as to the origin of the molten droplets (i.e., whether they formed by condensation or by secondary processes such as volcanism or impact splattering).

Figure 7.—*An Apollo 16 chondrule, with plagioclase microphenocrysts, in a light matrix breccia (66036). Plane polarized light; scale bar equals 0.5 mm.*

In the case of some lunar chondrules, the mode of origin of the molten droplets is uncontroversial, being interpreted as having formed by impact splattering (ref. 47). An example of an impact-produced lunar chondrule is shown in figure 7. All gradations between glass spherules and chondrules, with microcratered surfaces indicative of repeated impact processes, were found in the lunar samples. Although some workers do not refer to these objects as chondrules and use such terms as "devitrified glass spherules," there is little or no disagreement that the crystallization in the chondrules occurred in the same event that formed the molten droplet; thus, the apparent difference in interpretation is merely a matter of terminology.

However, the origin of two other lunar chondrule types is somewhat uncertain and controversial. This is the green glass (one example of a great variety of textures is shown in fig. 8), which is most abundant at the Apollo 15 site, and the orange glass (one example is shown in fig. 9), which was found at the Apollo 11 and 17 sites. Most workers argue that orange glass was formed by a volcanic process (e.g., refs. 50, 51, and 52), such as fire-fountaining; we have suggested (ref. 53) that the volcanic event may have been triggered by a major impact event because the composition implies a major amount of partial melting of the same source rock as for high-Ti mare basalts. It has also been suggested that the orange glass may have formed by impact into a lava lake (ref. 54). Cameron et al. (ref. 55) suggested that green glass may be of volcanic origin, and Bunch et al. (ref. 56) stressed their ultramafic character, distribution at other sites, and abundance of chondrules. Since green glass has many of the same unique characteristics as orange glass, most workers would probably now assume a similar mode of origin. The character of the ill-defined volcanic

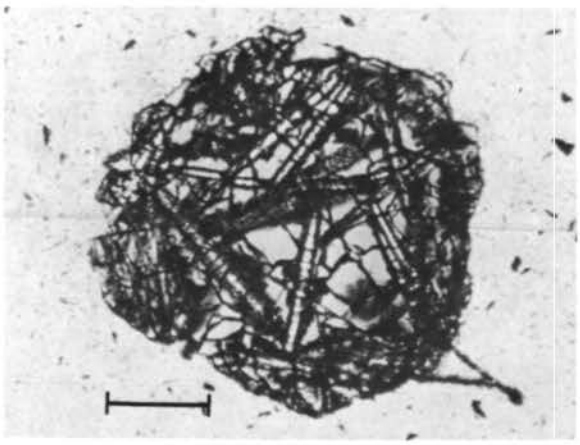


Figure 9.—*An Apollo 17 orange glass chondrule containing crystals of olivine and an Fe-Ti phase (probably ilmenite), in sample 74220. Plane polarized light; scale bar equals 0.05 mm.*

process responsible for green and orange glass is of critical importance to the interpretation of lunar history. Adams et al. (ref. 52) have shown that orange glass has a wide distribution on the lunar surface and is found in belts along the edges of major mare basins. The distribution of green glass deposits is not yet known. If these chondrules are indeed of volcanic origin, then this process must be reexamined for a possible mode of origin of at least some meteoritic chondrules.

In case of meteoritic chondrules, the problem is even more complicated. Only a few chondritic meteorites, namely the howardites, contain chondrule-like glass spherules, presumably of impact origin. One example from Bununu is shown in figure 10. If impact-produced glass spherules are found, then a small percentage of chondrules should also be present. Brownlee and Rajan (ref. 57) have indeed found such objects with microcratered surfaces in the howardite Kapoeta, a gas-rich meteorite formed as an impact-produced regolith breccia similar to the lunar regolith breccias. Noonan et al. (ref. 58) also found glass spherules in Bununu and Kapoeta and, in addition, in Malvern.

Chondrules, often with glassy matrices, are an important constituent of chondritic meteorites. Also, some chondrites contain glass spherules, especially unequilibrated ordinary chondrites. One example of a glass spherule in Chainpur is shown in figure 11. Two chondrules from the same meteorite are pictured in figure 12, and their textural similarity to the lunar orange-glass chondrule (fig. 9) should be noted. Thus, these similarities in texture for glass spherules and

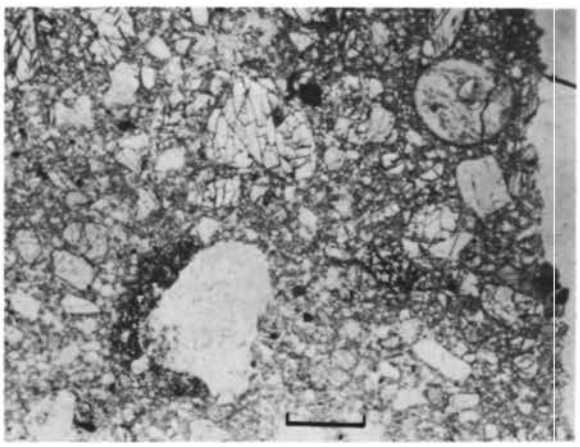


Figure 10.—*Polymict brecciated achondrite Bununu, a howardite, with an impact-produced glass spherule (upper right), together with glass, mineral, and lithic fragments in an indurated matrix. Plane polarized light; scale bar equals 0.25 mm.*

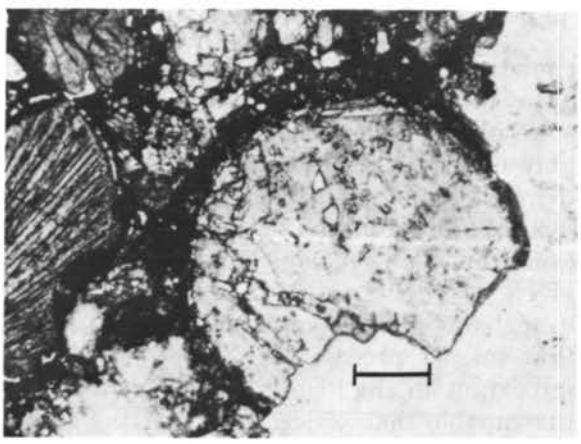


Figure 11.—*A glass spherule in the unequilibrated LL-group chondrite, Chainpur. Fragmental material in spherule suggests that the spherule was impact-produced. Plane polarized light; scale bar equals 0.5 mm.*

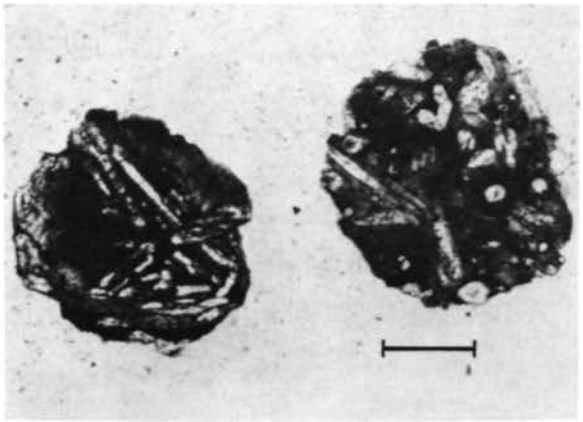


Figure 12.—*Two chondrules from the unequilibrated LL-group chondrite, Chainpur. Chondrules are similar in texture to the orange glass chondrule (fig. 9). Plane polarized light; scale bar equals 0.2 mm.*

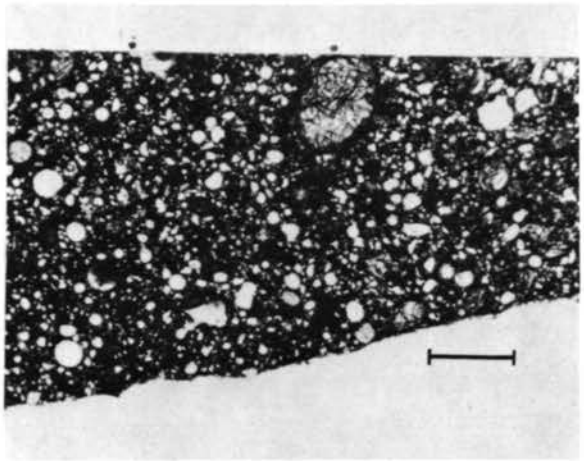


Figure 13.—*Apollo 15 green-glass breccia 15427, consisting largely of green glass spherules and chondrules. Note one large chondrule at top. The texture of this breccia is similar to that of many chondrule-rich chondrites, except for paucity of metal and troilite and differences in chemical composition. Plane polarized light; scale bare equals 1 mm.*

chondrules in meteoritic and lunar samples appear to imply that at least some of the spherules and chondrules in some meteorites may be the result of impact splattering (as in most lunar spherules) or volcanism (as possibly in green and orange glasses). However, this does not imply that chondrules derived by other processes are not also present in meteorites. However, since we have shown that impact processes have been extremely important in the history of chondrites, it is inescapable that at least some of the spherules and chondrules must have been derived by this process. It should be noted that McDougall et al. (ref. 59) recently reported evidence that the H-group chondrite Fayetteville probably formed as a regolith on a parent meteorite body.

It is also interesting to note that Fredriksson et al. (ref. 60) have shown that regolithic breccias, impact glasses, and glass spherules can form terrestrially in terrestrial meteorite impact events. Also, chondrules were found in glassy microtektites from a sea floor core in the Venezuela basin (ref. 61). These additional occurrences confirm our earlier conclusion that chondrules are not unique to chondrites, but that they may form in a number of different ways and in different environments.

One of the arguments against lunar chondrules having an origin which may be relevant to meteorite chondrules has been that impact-produced chondrules make up only a small proportion of a lunar breccia, whereas meteoritic chondrules often constitute a very large proportion of a chondrite. While this argument does appear to be a strong one with regard to impact-produced glass, it is not the case for presumably volcanic-produced lunar chondrules, such as green and orange glass. A breccia consisting largely of green glass spherules and chondrules is shown in low magnification in figure 13. There is a strong similarity in texture with that of many chondrites, although the abundance of glass is much greater and there is very little metal and troilite, compared to chondrites. Although it is not necessarily implied that chondrites formed in a manner analogous to green and orange glass breccias, it should be recognized that the mode of origin of green and orange glass has not previously been recognized as a process for making meteoritic chondrules.

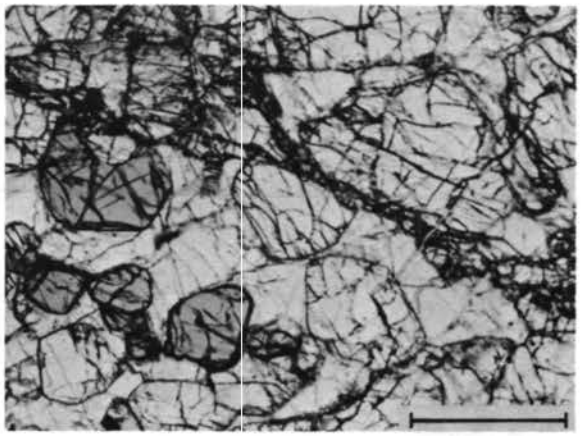


Figure 14.—*Apollo 16 spinel troctolite 67435 lithic fragment. Dark euhedral crystals are Mg-Al spinel; light gray crystals are euhedral olivine; and both are poikilitically set in light-colored plagioclase matrix. Plane polarized light; scale bar equals 0.5 mm.*

In summary, it may be said that chondrules and glass spherules in lunar rocks, meteorites, and on Earth can form in a variety of ways. All that is required is a process that produces molten silicate droplets which are given a chance to supercool and crystallize spontaneously from the highly supercooled state. In the case of lunar chondrules and glass spherules, this process is largely impact splattering, but volcanism or impact into a liquid cannot be ruled out. Because of the many indications for impact modification of chondrites and achondrites (e.g., brecciation), some meteoritic chondrules and glass spherules must have formed by impact as well. It is the subject of future studies to derive parameters that will allow one to distinguish between impact-produced meteoritic chondrules and those that may have formed by other processes (e.g., condensation, volcanism).

Lithic Fragments and Their Parent Material

Lithic fragments in lunar breccias and soils vary widely in textures; some appear to be only little modified, retaining their original (sometimes cumulate) textures, whereas others have partly modified textures, such as the cataclastic textures of monomict breccias, or are partly or completely melted or recrystallized. The lithic fragments are daughter products of an original parent rock or rocks (perhaps mixed together) and are sometimes in a matrix that may or may not be directly related to the parent. This makes any interpretation of the nature of the parental rocks an exceedingly difficult task, although some progress has been made.

One example of a possible parent in a parent-daughter relationship is that of spinel

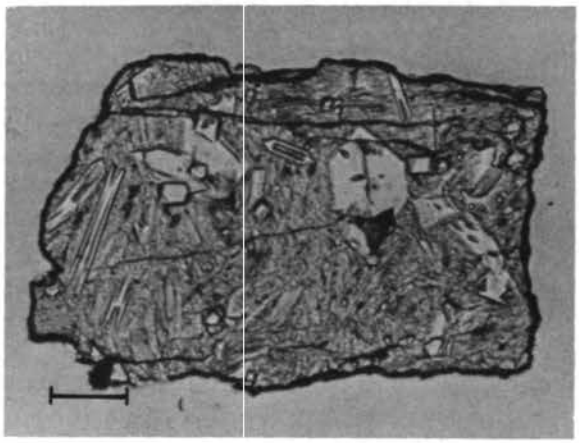


Figure 15.—*Impact melt-rock lithic fragment in the Luna 20 fines, containing quench crystals of olivine (Fo_{95}) and Mg-Al spinel in a glassy matrix. Bulk chemistry is that of spinel troctolite. Plane polarized light; scale bar equals 0.025 mm.*

troctolite 67435 (fig. 14), described by Prinz et al. (ref. 62). This is an important lunar rock type, but one that has rarely survived impact processes without major textural alterations. A large number of lithic fragments derived from spinel troctolites (perhaps with some addition of KREEP and/or ANT component) were found in the Luna 20 sample (ref. 63) and have a wide variety of textures. One example of a spinel-troctolite daughter derived by total melting and quenching is shown in figure 15; it consists of spinel, olivine, and glass with the bulk chemistry of a spinel troctolite.

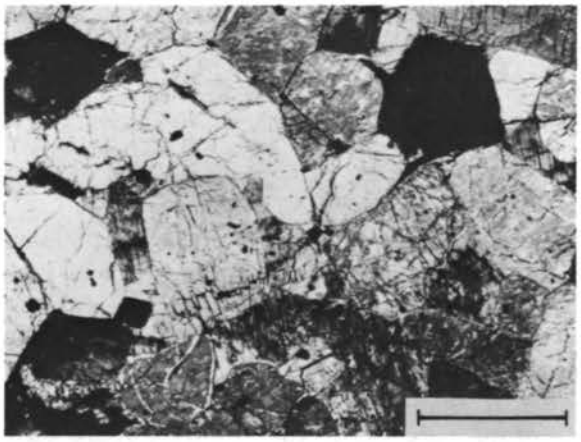


Figure 16.—*The meteorite Chassigny, an olivine achondrite, or dunite, consisting mainly of olivine crystals poikilitically included in exsolved pyroxene (striped areas), constituting a cumulate texture. In part, olivine crystals have triple junctions, indicating subsolidus recrystallization, probably immediately following igneous crystallization. Plane polarized light; scale bar equals 1 mm.*

Analogs to this lunar situation also exist in meteorites. Some lithic fragments found in brecciated achondrites and chondrites may have been derived from cumulate parent rocks, such as the olivine achondrite, or dunite, Chassigny (ref. 64; fig. 16) and the bronzite achondrite, or bronzitite, Johnstown (ref. 28; fig. 2). Chassigny is shocked and unbrecciated and basically retains its partly igneous, partly recrystallized metamorphic (not by impact) texture; whereas Johnstown is mostly brecciated (monomict), but retains some of its originally coarsely recrystallized texture. The LL-group polymict-brecciated chondrite Olivenza contains numerous lithic fragments (unpublished data), two of which may be of interest because their parent rocks may be similar to Chassigny or Johnstown. One coarse-grained fragment (fig. 17) is olivine-rich and could have been derived from a rock such as Chassigny. The other fragment (fig. 18) consists almost entirely of orthopyroxene and could have been derived from a meteorite such as Johnstown. The orthopyroxene-rich fragment has a bulk composition of SiO_2, 52.3 percent; FeO, 16.9 percent; MgO, 24.5 percent; and Cr_2O_3, 0.35 percent (ref. 65). A comparison with the bulk chemistry of Johnstown (ref. 66) shows a striking similarity; Cr_2O_3 is somewhat lower, but Johnstown has more chromiferous orthopyroxene than the other bronzite achondrites. However, the possibility that these two fragments may have been derived from their host chondrite should not be discounted.

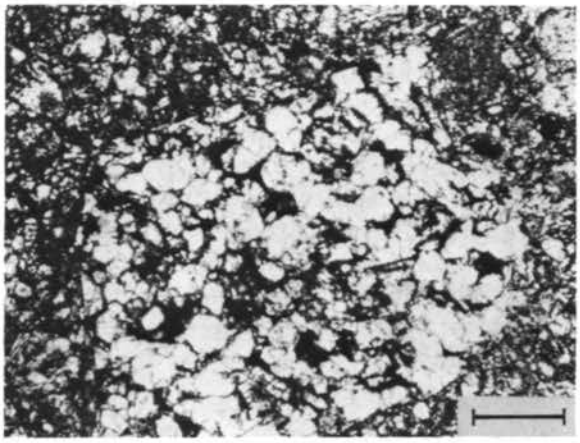


Figure 17.—*A subrounded olivine-rich (dunite) lithic fragment in the brecciated LL-group chondrite, Olivenza. Plane polarized light; scale bar equals 1 mm.*

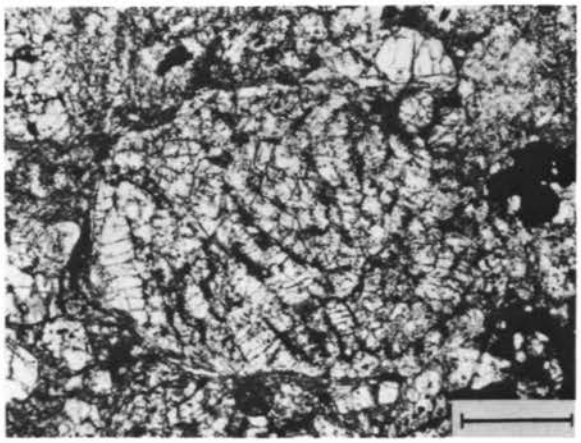


Figure 18.—*A subrounded orthopyroxene-rich (bronzitite) lithic fragment in the brecciated LL-group chondrite, Olivenza. Plane polarized light; scale bar equals 0.5 mm.*

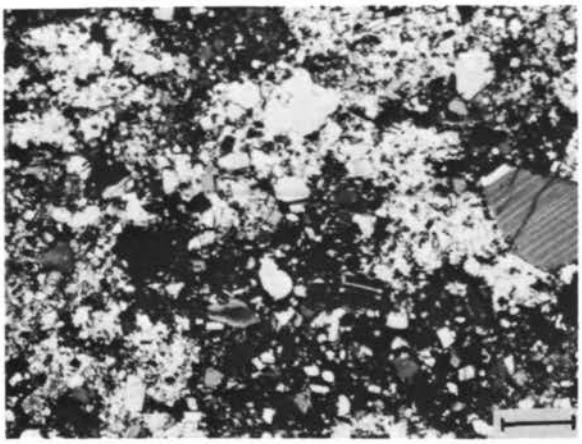


Figure 19.—*An Apollo 16 polymict breccia 65778 with relict crystals and lithic fragments in a poikilitic matrix of low-Ca pyroxene oikocrysts. Crossed nicols; scale bar equals 0.25 mm.*

Sometimes the parent rock or rocks were only partly melted and relicts of the parent rock(s) are retained in a matrix of molten material. This appears to be the case in some of the lunar breccias which have a poikilitic-textured matrix with unmelted relict crystals (fig. 19). In meteorites, unmelted relict crystals in an igneous matrix are also found. One such meteorite (fig. 20), the H-group chondrite Plainview, shows a lithic fragment with relict olivine crystals (and minor pyroxene) in a fine-grained igneous groundmass that represents impact melt. In some cases the impact-derived melt rocks represent a melt formed from a mixture of two or more rock types. Some examples were cited by Dowty et al. (refs. 25 and 67), and further work is planned to check this hypothesis with regard to these and other samples. Melt rocks derived from mixtures of various rock types should be common products from regoliths on the Moon and on parent meteorite bodies. One meteoritic example of a possible mixture of two or more rock types to produce an igneous-textured lithic fragment is shown in figure 21. This fragment is from the LL-group chondrite Bhola which contains numerous fragments of this type. The fragments consist predominantly of olivine set in a groundmass of K_2O-rich glass (5 percent) with minor pyroxene crystallites; the texture is similar to those of the most supercooled lunar pyroxene-phyric rocks (ref. 68). Fredriksson et al. (ref. 22) suggest that these fragments indicate that the chondrite is probably a polymict breccia. Fodor et al. (ref. 14) suggest that the fragments are most rea-

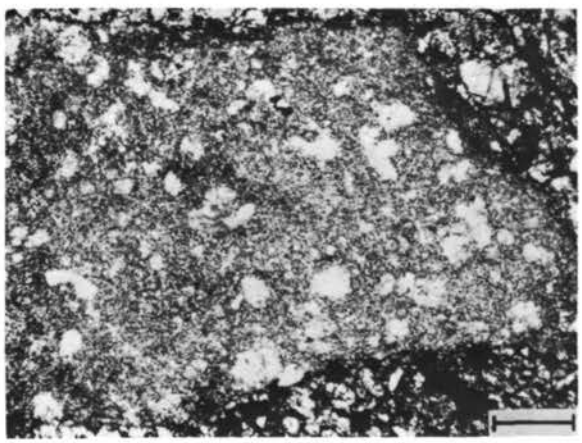


Figure 20.—*A lithic fragment is the polymict brecciated H-group chondrite, Plainview, consisting of partly melted relict olivine crystals in a fine-grained olivine-feldspar (melt) matrix. Plane polarized light; scale bar equals 0.5 mm.*

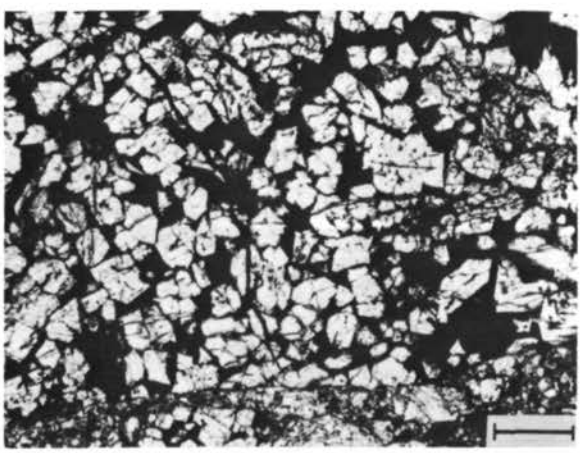


Figure 21.—*A large lithic fragment in the brecciated LL-group chondrite Bhola consisting mostly of euhedral olivine crystals in a dark matrix of pyroxene crystallites and high K_2O (~ 5 percent) glass. Porphyritic texture is the result of supercooling of the igneous melt. Plane polarized light; scale bar equals 0.5 mm.*

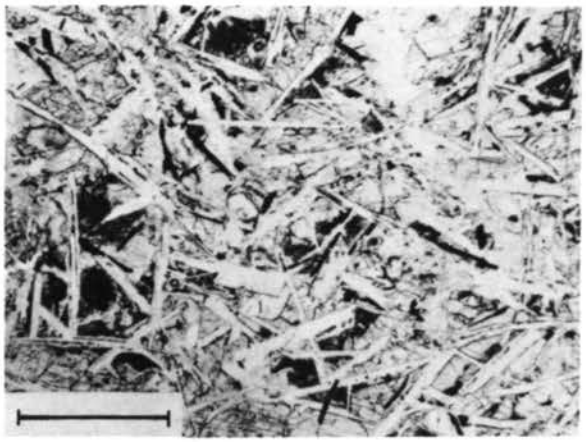


Figure 22.—*A lunar melt rock (15382) with ophitic texture, having alkalic high-alumina basalt (KREEP) composition. Plane polarized light; scale bar equals 1 mm.*

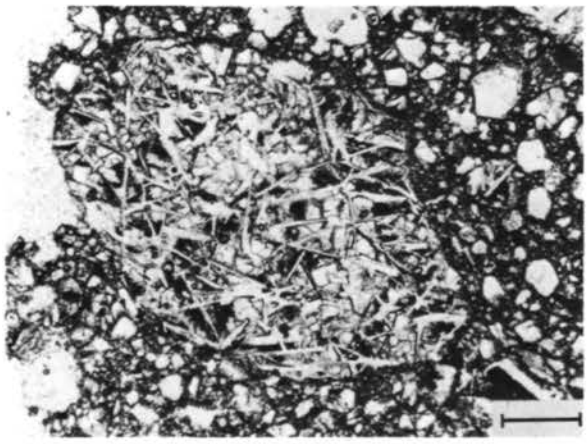


Figure 23.—*A lithic fragment with ophitic texture, a probable impact melt rock, in the eucrite Pasamonte. Plane polarized light; scale bar equals 0.5 mm.*

sonably explained as having crystallized from impact shock melts into an olivine-rich rock such as dunite (a chondrite is less reasonable because the fragments are essentially free of metal and troilite) and a K_2O-rich rock such as granite (chondrites have very low K_2O contents). Thus, these fragments, which are also present in other meteorites (unpublished data), may represent impact melting of a regolith with at least these two major rock components represented.

One of the most important results of the lunar program has been the realization that impact melting can produce abundant quantities of igneous-textured rocks which are very difficult to distinguish texturally from internally generated igneous rocks. One of the best examples is 14310, although this conclusion remains controversial with some workers. A very similar lunar rock is 15382 (ref. 69), which is shown in figure 22. Even for rocks of this type, meteoritic analogs exist: a lithic fragment with a very similar texture from the eucrite Pasamonte is shown in figure 23. Although it is not certain at this time that either the lunar or meteoritic examples given here are really impact melts, their textures are strikingly similar to some rocks that have been interpreted as impact melts on the Moon, based on compositional data and evidence of meteoritic contamination. More quantitative criteria for distinguishing internally derived from externally generated melts are badly needed.

Another type of texture commonly seen in lunar lithic fragments and larger samples is granoblastic or equigranular. This is commonly seen in entire samples, or in matrices of samples, especially in feldspathic rocks. These rocks may retain relict, unrecrystallized crystals, but sometimes these are difficult to distinguish from newly crystallized grains. An example is shown in figure 24. This type of texture is also observed in lithic fragments in meteoritic breccias such as howardites and eucrites. One example of such a lithic fragment from the eucrite Bialystok is shown in figure 25. The fragment appears to be feldspar-rich, but has not yet been studied in detail.

Finally, there are similarities between lunar and meteoritic lithic fragments in the case of poikilitic or poikiloblastic textures. Detailed studies of poikilitic- or poikiloblastic-textured rocks with relict crystals, taken from the Apollo 16 site, were published by Simonds et al. (ref. 70), Bence et al. (ref. 71), Albee (ref. 72), and others. There is still some controversy as to the de-

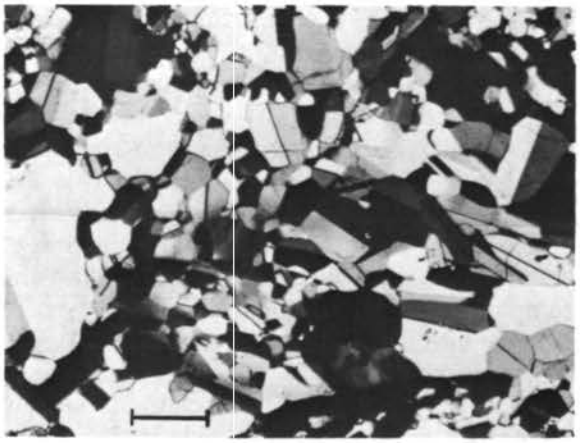


Figure 24.—*An Apollo 16 anorthosite (60619) with granoblastic texture. Crossed nicols; scale bar equals 0.5 mm.*

tails of the processes involved, although most workers agree that the textures are related to impact events. An example of one of these rocks is shown in figure 19. Similar textures are also found in lithic fragments in meteorites. We have found such fragments in several LL-group chondrites (ref. 15), and one example, from the H-group chondrite Plainview, is shown in figure 26. Impacted melt rocks with poikilitic textures have also been identified in terrestrial impact structures, such as at Lake Mistasin, Canada (ref. 73). There, the target rock is known to be anorthositic, and the poikilitic melt rock is clearly an impact-generated derivative. Although it can be said with some confidence that some poikilitic- or poikiloblastic-textured rocks or fragments were derived as the result of impact processes, it should not be concluded that all material with these textures, especially meteoritic examples, formed in such a way. Some could have been derived from internally generated melts as well. Again, more criteria are needed that allow us to distinguish between the two processes.



Figure 25.—*A feldspar-rich granoblastic-textured lithic fragment in the eucrite, Bialystok. Compare with figure 24. Crossed nicols; scale bar equals 0.5 mm.*

Conclusions

By comparing structures and textures of lunar rocks and meteorites, it can be shown that monomict and polymict brecciation caused by complex and repeated impacts is recorded in both rock types. Sometimes the brecciation may be so intense, resulting in such fine-grained rocks, that it is difficult to recognize the brecciated nature. In meteorites, this includes both achondrites and chondrites. A very important part of future research is

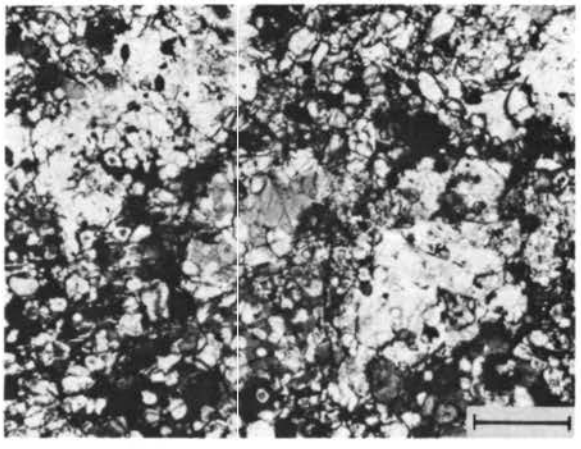


Figure 26.—*A large poikilitic-textured lithic fragment in the polymict brecciated H-group chondrite, Plainview, consisting mainly of olivine grains poikilitically enclosed in orthopyroxene. Crossed nicols; scale bar equals 0.25 mm.*

to disentangle the features that impact events left on meteorites from features caused by previous histories (i.e., planetary accretion, igneous differentiation), or from possibly still later histories, such as metamorphic recrystallization and reequilibration. We emphasize that any interpretation of the origin and history of meteorites and their parent bodies that does not take into account the complexities of their impact histories (which may or may not be easily recognizable) may be in serious error.

The origin of chondrules, both lunar and meteoritic, is not yet resolved. It does seem certain, however, that more than one process has been responsible for the chondrules present in both lunar and meteoritic rocks. On the Moon, chondrules appear to have formed by supercooling of molten droplets derived by impact and possibly volcanic processes (perhaps triggered by impact processes). In places they are very abundant, such as at green glass and orange glass sites. In meteorites, it seems clear that at least some chondrules and chondrule-like objects must have formed by impact processes; these are present in both achondrites and chondrites. Possibly some chondrules are also of volcanic origin, and others may have developed by remelting condensates from the solar nebula. The task for future research is to develop criteria for distinguishing between chondrules of different modes of origin and to estimate their relative abundances. This is a very important task indeed, if the significance of stone meteorites and, particularly, chondrites as probes into the early history of the solar system is to be clearly understood.

Impact processes can produce a variety of rock types from a parent rock. Applying the same type of interpretations as used for the Moon, it appears that polymict brecciated achondrites contain lithic fragments which preserve some history of their igneous (often cumulate) origin. Other brecciated achondrites are made up entirely of this material, some of which are monomict breccias. The cumulates are olivine-rich, pyroxene-rich, plagioclase-rich and, in fact, involve generally the same mineralogy as lunar rocks. Some achondrites contain lithic fragments of mafic rock types which obviously crystallized from melts, but the origin of these melts, either from within the planet, by impact melting of a rock, or by impact melting of a mechanical mixture in the regolith, has not yet been established. After this question has been solved, we can begin to better reconstruct the history of the parent body or bodies. Chondrites are also brecciated and, therefore, could not have escaped some of the inevitable effects of an impact history. Some lithic fragments may have been derived by impact brecciation and melting or brecciation of cumulate rocks, but this is not at all certain yet. Detailed studies of individual chondrites, especially brecciated ones, are necessary to determine the effects of the variety of processes that have been operative.

Thus, the time has come to take a new look at meteorites, taking into account the results of the lunar programs. It is already apparent that meteorite parent bodies, just like the Moon, have been affected by complex and repeated impact processes, and all the complexities that such processes have caused in lunar rocks appear to be present in meteorites. It is therefore of the utmost importance that workers from many different disciplines unite in an effort to decipher these complex histories in stone meteorites and compare them to lunar rocks. Only when these processes and their resulting textural and compositional features are clearly understood can the significance of meteorites as probes for the early history of small planetesimals in the solar system be clearly recognized.

Acknowledgment

The authors wish to express appreciation to personnel of the Smithsonian Institution, Washington, D.C., and the Center for Meteorite Studies, Arizona State University, Tempe, Arizona, who have generously provided meteorite samples and meteorite polished thin sections. In addition, they wish to

thank Dave Lewis for assistance in preparing the photomicrographs and the National Aeronautics and Space Administration for a travel grant to attend the Soviet-American Conference on Cosmochemistry of the Moon and the Planets, Moscow, U.S.S.R. This work is supported in part by NASA grants NGL 32–004–063 and NGL 32–004–064.

References

1. WARNER, J. L., C. H. SIMONDS, AND W. C. PHINNEY, Impact Induced Fractionation in the Lunar Highlands. *Proc. Fifth Lunar Science Conference, Geochimica et Cosmochimica Acta*, Supplement 5, Vol. 1, 1974, pp. 379–397.
2. FREDRIKSSON, K., P. S. DE CARLI, AND A. AARAMAE, Shock-Induced Veins in Chondrites. *Space Sci. III (COSPAR)*, North Holland Pub. Co., 1962.
3. FREDRIKSSON, K., AND K. KEIL, The Light-Dark Structure in the Pantar and Kapoeta Stone Meteorites. *Geochimica et Cosmochimica Acta*, Vol. 27, 1963, pp. 717–739.
4. FREDRIKSSON, K., Chondrules and the Meteorite Parent Bodies. *Trans. N.Y. Acad. Sci.*, Series 11, Vol. 25, 1963, pp. 756–769.
5. FREDRIKSSON, K., E. JAROSEWICH, AND J. NELEN, The Sharps Chondrite—New Evidence on the Origin of Chondrules and Chondrites. *Meteorite Research*, P. Millman, ed., D. Reidel Pub. Co., Drodrecht, Holland, 1969, pp. 155–165.
6. FREDRIKSSON, K., AND A. M. REID, A Chondrule in the Chainpur Meteorite. *Science*, Vol. 149, 1965, pp. 856–860.
7. UREY, H. C., Parent Bodies of the Meteorites. *Icarus*, Vol. 7, 1967, pp. 350–359.
8. KURAT, G., K. FREDRIKSSON, AND J. NELEN, Der Meteorit von Siena. *Geochimica et Cosmochimica Acta*, Vol. 33, 1969, pp. 765–773.
9. FODOR, R. V., K. KEIL, AND E. JAROSEWICH, The Oro Grande, New Mexico, Chondrite and its Lithic Inclusion. *Meteoritics*, Vol. 7, 1972, pp. 495–507.
10. FODOR, R. V., AND K. KEIL, Carbonaceous and Non-Carbonaceous Lithic Inclusions in the Plainview, Texas, Chondrite (abs.). *Meteoritics*, Vol. 8, 1973, p. 33.
11. KEIL, K., AND R. V. FODOR, Composition and Origins of Lithic Fragments in LL-Group Chondrites (abs). *Meteoritics*, Vol. 8, 1973, pp. 394–396.
12. FODOR, R. V., AND K. KEIL, Composition and Origin of Lithic Fragments in L- and H-Group Chondrites (abs.). *Meteoritics*, Vol. 8, 1973, pp. 366–367.
13. FODOR, R. V., M. PRINZ, M. G. BROWN, AND K. KEIL, A Chondrite With a Regolith Fragment Containing Non-Chondritic Material (abs.). *Meteoritics*, Vol. 9, 1974, pp. 337–338.
14. FODOR, R. V., M. PRINZ, AND K. KEIL, Implications of K-Rich Lithic Fragments and Chondrules in the Bhola Brecciated Chondrite. *Program, 87th Geol. Soc. Amer. Annual Meeting*, 1974, pp. 739–740.
15. FODOR, R. V., AND K. KEIL, Composition and Origin of Lithic Fragments in LL-Group Chondrites. *Geochimica et Cosmochimica Acta*, in preparation, 1974.
16. FODOR, R. V., AND K. KEIL, Carbonaceous and Non-Carbonaceous Lithic Inclusions in the Plainview, Texas, Chondrite: Origin and History. *Geochimica et Cosmochimica Acta*, in press.
17. VAN SCHMUS, W. R., Polymict Structure of the Mesö-Madaras Chondrite. *Geochimica et Cosmochimica Acta*, Vol. 31, 1967, pp. 2027–2042.
18. BUNCH, T. E., AND D. STÖFFLER, The Kelly Chondrite: A Parent Body Surface Metabreccia. *Contr. Mineral. Petrol.*, Vol. 44, 1974, pp. 157–171.
19. WILKENING, L. L., Foreign Inclusions in Stony Meteorites: I. Chondritic Xenoliths in the Kapoeta Howardite. *Geochimica et Cosmochimica Acta*, Vol. 37, 1973, pp. 1985–1989.
20. WILKENING, L. L., AND R. N. CLAYTON, Foreign Inclusions in Stony Meteorites: II. Rare Gases and Oxygen Isotopes in a Carbonaceous Chondritic Xenolith in the Plainview Gas-Rich Meteorite. *Geochimica et Cosmochimica Acta*, Vol. 38, 1974, pp. 937–945.
21. BUNCH, T. E., Howardites: Parent Body Surface Breccias (abs.). *Meteoritics*, Vol. 10, 1975, pp. 91–92.
22. FREDRIKSSON, K., A. F. NOONAN, AND J. A. NELEN, The Bhola Stone—A True Polymict Breccia? (abs.). *Meteoritics*, Vol. 9, 1974, pp. 334–335.
23. DODD, R. T., St. Mesmin: A Petrologic Overview (abs.). *Meteoritics*, Vol. 9, in press, 1974.
24. JAMES, O. B., Lunar Anorthosite 15415: Texture, Mineralogy and Metamorphic History. *Science*, Vol. 175, pp. 432–434.
25. DOWTY, E., K. KEIL, AND M. PRINZ, Igneous Rocks From Apollo 16 Rake Samples. *Proc. Fifth Lunar Science Conference, Geochimica et Cosmochimica Acta*, Supplement 5, Vol. 1, 1974, pp. 431–445.
26. ALBEE, A. C., A. A. CHODOS, R. F. DYMEK, A. J. GANCARZ, D. J. GOLDMAN, D. A. PAPANASTASSIOU, AND G. J. WASSERBURG, Dunite From the Lunar Highlands: Petrography Deformational History, Rb/Sr Age. *Proc. Fifth Lunar Science Conference, Abstracts*, 1974, pp. 3–5.
27. KEIL, K., Meteorite Composition. *Handbook of*

Geochemistry, Vol. 1, Springer-Verlag, 1969, pp. 78–115.

28. PRINZ, M., P. H. HLAVA, AND K. KEIL, Petrology of the Johnstown Achondrite, an Orthoproxenite. In preparation, 1974.
29. WARNER, J. L., C. H. SIMONDS, AND W. C. PHINNEY, Apollo 16 Rocks: Classification and Petrogenetic Model. *Proc. Fourth Lunar Science Conference, Geochimica et Cosmochimica Acta*, Supplement 4, Vol. 1, 1973, pp. 481–504.
30. WARNER, J. C., Metamorphism of Apollo 14 Breccias. *Proc. Third Lunar Science Conference, Geochimica et Cosmochimica Acta*, Supplement 3, Vol. 1, 1972, pp. 623–643.
31. KURAT, G., K. KEIL, AND M. PRINZ, Rock 14318: A Polymict Lunar Breccia With Chondritic Texture. *Geochimica et Cosmochimica Acta*, Vol. 38, 1974, pp. 1133–1146.
32. DUKE, M. B., AND L. T. SILVER, Petrology of Eucrites, Howardites and Mesosiderites. *Geochimica et Cosmochimica Acta*, Vol. 31, 1967, pp. 1637–1665.
33. REID, A. M., The Macibini Meteorite and Some Thoughts on the Origin of Basaltic Achondrites (abs.). *Meteoritics*, Vol. 9, 1974, pp. 398–399.
34. WAHL, W., The Brecciated Stony Meteorites and Meteorites Containing Foreign Fragments. *Geochimica et Cosmochimica Acta*, Vol. 2, 1952, pp. 91–117.
35. KURAT, G., Zur Genese des kohligen Materials im Meteoriten von Tieschitz. *Earth Planet. Sci Letters*, Vol. 7, 1970, pp. 317–324.
36. DODD, R. T., H-Group Xenoliths in the St. Mesmin LL-Group Chondrite. *Geochimica et Cosmochimica Acta*, in press, 1974.
37. SUESS, H. E., Zur Chemie der Planeten-und Meteoritenbildung. *Z. Elektrochem.*, Vol. 53, 1949, pp. 237–241.
38. WOOD, J. A., Metamorphism in Chondrites. *Geochimica et Cosmochimica Acta*, Vol. 26, 1962, pp. 739–749.
39. BLANDER, M., AND J. L. KATZ, Condensation of Primordial Dust. *Geochimica et Cosmochimica Acta*, Vol. 31, 1967, pp. 1025–1034.
40. BLANDER, M., AND M. ABDEL-GAWAD, The Origin of Meteorites and the Constrained Equilibrium Theory. *Geochimica et Cosmochimica Acta*, Vol. 33, 1969, pp. 701–716.
41. TSCHERMAK, G., Die Bildung der Meteoriten und der Vulcanismus. *Sitzungsber. Akad. Wiss. Wein*, Vol. 71, 1875, pp. 661–673.
42. MERRILL, G. P., On Chondrules and Chondritic Structure in Meteorites. *Proc. Nat. Acad. Sci.*, Vol. 6, 1920, pp. 449–472.
43. RINGWOOD, A. E., Chemical and Genetic Relationships Among Meteorites. *Geochimica et Cosmochimica Acta*, Vol. 24, 1961, pp. 159–197.
44. FREDRIKSSON, K., AND A. E. RINGWOOD, Origin of Meteoritic Chondrules. *Geochimica et Cosmochimica Acta*, Vol. 27, 1963, pp. 639–641.
45. WHIPPLE, F. L., Chondrules: Suggestion Concerning Their Origin. *Science*, Vol. 153, 1966, p. 54.
46. WOOD, J. A., On the Origin of Chondrules and Chondrites. *Icarus*, Vol. 2, 1963, pp. 152–180.
47. KURAT, G., K. KEIL, M. PRINZ, AND C. E. NEHRU, Chondrules of Lunar Origin. *Proc. Third Lunar Science Conference*, Vol. 1, 1972, pp. 707–721.
48. NELSON, L. S., M. BLANDER, S. R. SKAGGS, AND K. KEIL, Use of a CO_2 Laser To Prepare Chondrule-Like Spherules From Supercooled Molten Oxide and Silicate Droplets. *Earth Planet. Sci. Letters*, Vol. 14, 1972, pp. 338–344.
49. KEIL, K., M. PRINZ, H. N. PLANNER, S. R. SKAGGS, E. DOWTY, L. S. NELSON, N. L. RICHARDSON, AND M. BLANDER, *A Qualitative Comparison of Textures in Lunar Chondrules and CO_2 Laser-Formed Synthetic Chondrule-Like Spherules*. Univ. of New Mexico, Inst. of Meteoritics, Spec. Pub. 7, 1973.
50. REID, A. M., G. E. LOFGREN, G. H. HEIKEN, R. W. BROWN, AND G. MORELAND, Apollo 17 Orange Glass, Apollo 15 Green Glass and Hawaiian Lava Fountain Glass. *EOS, Trans. Am. Geophys. Union*, Vol. 54, 1973, pp. 606–607.
51. HEIKEN, G., D. S. MCKAY, AND R. W. BROWN, Lunar Deposits of Possible Pyroclastic Origin. *Geochimica et Cosmochimica Acta*, in press, 1974.
52. ADAMS, J. B., C. PIETERS, AND T. B. MCCORD, Orange Glass: Evidence for Regional Deposits of Pyroclastic Origin on the Moon. *Proc. Fifth Lunar Science Conference, Geochimica et Cosmochimica Acta*, Supplement 5, Vol. 1, 1974, pp. 171–186.
53. PRINZ, M., E. DOWTY, AND K. KEIL, A Model for the Origin of Orange and Green Glasses and the Filling of Mare Basins. *EOS, Trans. Am. Geophys. Union*, Vol. 54, 1973, pp. 605–606.
54. ROEDDER, E., AND P. W. WEIBLEN, Origin of Orange Glass Spherules in Apollo 17 Sample 74220. *EOS, Trans. Am. Geophys. Union*, Vol. 54, 1973, pp. 612–613.
55. CAMERON, K. L., J. W. DELANO, A. E. BENCE, AND J. J. PAPIKE, Petrology of the 2–4 mm Soil Fraction From the Hadley-Apennine Region of the Moon. *Earth Planet. Sci. Letters*, Vol. 19, 1973, pp. 9-21.
56. BUNCH, T. E., W. QUAIDE, M. PRINZ, K. KEIL, AND E. DOWTY, Lunar Ultramafic Glasses, Chondrules, and Rocks. *Nature Phy. Sci.*, Vol. 239, 1972, pp. 57–59.
57. BROWNLEE, D. E., AND R. S. RAJAN, Micrometeorite Craters Discovered on Chondrule-Like

Objects From Kapoeta. *Science*, Vol. 182, 1973, pp. 1341–1344.

58. NOONAN, A. F., R. S. RAJAN, AND A. A. CHODOS, Microprobe Analyses of Glassy Particles From Howardites (abs.). *Meteoritics*, Vol. 9, 1974, pp. 385–386.
59. MCDOUGALL, D., R. S. RAJAN, AND P. B. PRICE, Gas-Rich Meteorites: Possible Evidence for Origin in a Regolith. *Science*, Vol. 183, 1974, p. 73.
60. FREDRIKSSON, K., A. DUBE, AND D. MILTON, Microbreccias, Impact Glasses, and Spherules From Lunar Crater, India; Lunar Analogs (abs.). *Meteoritics*, Vol. 8, 1973, p. 34.
61. JOHN, C., AND B. GLASS, Clinopyroxene-Bearing Glass Spherules Associated With North American Microtektites. *Geology*, Vol. 2, 1974, pp. 599–602.
62. PRINZ, M., E. DOWTY, K. KEIL, AND T. E. BUNCH, Spinel Troctolite and Anorthosite in Apollo 16 Samples. *Science*, Vol. 179, 1973, pp. 74–76.
63. PRINZ, M., E. DOWTY, K. KEIL, AND T. E. BUNCH, Mineralogy, Petrology and Chemistry of Lithic Fragments From Luna 20 Fines: Origin of the Cumulate ANT Suite and its Relationship to High-Alumina and Mare Basalts. *Geochimica et Cosmochimica Acta*, Vol. 37, 1973, pp. 979–1006.
64. PRINZ, M., P. H. HLAVA, AND K. KEIL, The Chassigny Meteorite: A Relatively Iron-Rich Cumulate Dunite (abs.). *Meteoritics*, Vol. 9, 1974, pp. 393–394.
65. FODOR, R. V., AND K. KEIL, Catalogue of Lithic Fragments in 20 LL-Group Chondrites. Univ. of New Mexico, Spec. Pub., in preparation, 1974.
66. MASON, B., AND E. JAROSEWICH, The Composition of the Johnstown Meteorite. *Meteoritics*, Vol. 4, 1971, pp. 241–245.
67. DOWTY, E., M. PRINZ, AND K. KEIL, Very High Alumina Basalt: A Mixture and Not a Magma Type. *Science*, Vol. 183, 1974, pp. 1214–1215.
68. DOWTY, E., K. KEIL, AND M. PRINZ, Lunar Pyroxene-Phyric Basalts: Crystallization Under Supercooled Conditions. *J. Petrology*, Vol. 15, 1974, pp. 419–453.
69. DOWTY, E., M. PRINZ, K. KEIL, AND T. E. BUNCH, Non-Mare Rock Types in Apollo 15 Rake Samples (abs.). *Geol. Soc. Am. Abstracts*, Vol. 4, 1972, pp. 491–492.
70. SIMONDS, C. H., J. C. WARNER, AND W. C. PHINNEY, Petrology of Apollo 16 Poikilitic Rocks. *Proc. Fourth Lunar Science Conference, Geochimica et Cosmochimica Acta*, Supplement 4, Vol. 1, 1973, pp. 613–632.
71. BENCE, A. E., J. J. PAPIKE, S. SUENO, AND J. W. DELANO, Pyroxene Poikiloblastic Rocks From the Lunar Highlands. *Proc. Fourth Lunar Science Conference, Geochimica et Cosmochimica Acta*, Supplement 4, Vol. 1, 1973, pp. 597–612.
72. ALBEE, A. L., A. J. GANCARZ, AND A. A. CHODOS, Metamorphism of Apollo 16 and 17 and Luna 20 Metaclastic Rocks at About 3.95 AE: Samples 61156, 64423,14–2, 65015, 67483,15–2, 76055, 22006 and 22007. *Proc. Fourth Lunar Science Conference, Geochimica et Cosmochimica Acta*, Supplement 4, Vol. 1, 1973, pp. 569–596.
73. GRIEVE, R. A. F., A. G. PLANT, AND M. R. DENCE, Lunar Impact Melts and Terrestrial Analogs: Their Characteristics, Formations, and Implications for Lunar Crustal Evolution. *Proc. Fifth Lunar Science Conference, Geochimica et Cosmochimica Acta*, Supplement 5, Vol. 1, 1974, pp. 261–273.

Page intentionally left blank

Page intentionally left blank

Radioactivity of the Moon, Planets, and Meteorites

Yu. A. Surkov and G. A. Fedoseyev
V. I. Vernadskiy Institute of Geochemistry
and Analytical Chemistry
Academy of Sciences,
Moscow, U.S.S.R.

This paper reviews and summarizes analytical data for the content of natural radioactive elements in meteorites, eruptive terrestrial rocks, and also in lunar samples returned by Apollo missions and the Luna series of automatic stations.

The K-U systematics of samples analyzed in the laboratory are combined with data for orbital gamma-ray measurements for Mars (Mars 5) and with the results of direct gamma-ray measurements of the surface of Venus by the Venera 8 lander.

Using information about the radioactivity of solar system bodies and evaluations of the content of K, U, and Th in the terrestrial planets, we examine certain aspects of the evolution of material in the protoplanetary gas-dust cloud and then in the planets of the solar system.

As we know, radioactive elements play a special role in the history of the solar system. The study of their abundance in various celestial bodies is a key to the development of our concepts of the solar system. However, the small number of thoroughly studied extraterrestrial objects creates certain difficulties in an attempt at quantitative estimation of the abundance of radioactive elements in the solar system.

In recent years the study of this problem has been influenced by a stream of new information on the celestial bodies, particularly the Moon.

Measurements of the gamma radiation of the Moon were performed by the Luna 10 automatic spacecraft in 1966 and first established that lunar rocks are similar to terrestrial basalts in their content of natural radioactive elements (refs. 1 and 2).

Many further investigations of lunar specimens returned by automatic and manned spacecraft have shown that for natural radioactive elements and a number of other aspects of their chemical compositions, lunar rocks from the mare regions are similar to terrestrial tholeiitic basalts (and to stony meteorites—the Ca achondrites), while the lunar continents are similar to anorthositic rocks (refs. 3 through 8).

In 1972, the Venera 8 automatic spacecraft produced the first data on the natural radioactivity of Venus, and allowed certain conclusions about the nature of Venusian rocks and their formation (refs. 9 and 10).

In 1974, the Mars 4 and Mars 5 automatic spacecraft first measured the intensity and spectral composition of the gamma radiation of Mars (ref. 11).

Combination of all this information on the radioactivity of solar system bodies expands our ability to understand certain aspects of the evolution of material both in the protoplanetary gas-dust cloud and in the planets of the solar system.

The history of the radioactive elements is closely related to the history of all chemical elements. However, as we know, radioactive

elements play a special role in the evolution of the material of the solar system. In this work we study the cosmochemical aspect of the history of the natural radioactive elements from their formation to the present.

We can imagine that during the earliest stage of formation of the solar nebula radioactive elements were homogeneously distributed in the gas cloud whose density decreased with increasing distance from its center to its periphery. The entire subsequent evolution of solar system material and, in particular, the history of the natural radioactive elements can be divided into two main periods: the preplanetary stage when the material was in a gas-dust state and the planetary stage when the material was concentrated into the large bodies of the solar system.

At the present time, the radioactivity of planetary material is due primarily to U, Th, and K. The mean content of these elements in the Earth is either estimated on the basis of the current heat flux from the interior of the planet (ref. 12) or is assumed equal to the mean content of these substances in chondritic meteorites (ref. 13). The radioactivity of the planets in the distant past was significantly higher, due not only to the higher content of these elements at that time, but also to the decay of more short-lived elements with half-lives on the order of 10^6 to 10^8 yr. These elements were made during nuclear synthesis and later became part of the young bodies of the solar system.

Finally, it is possible that during the preplanetary stage and the early stage of formation of the planets, super-heavy transuranium elements existed ($Z \sim 106$–116, $N \sim 284$), since fission tracks of these elements have been found in some meteorites and lunar rock specimens (ref. 14).

In addition to the natural radioactivity, the surface layers of all celestial bodies have a radioactivity that results from interaction with cosmic rays. Most cosmogenic isotopes are short lived (of the longer lived, Na^{22} and Al^{26} are most common) and are retained only in extremely small quantities. Cosmogenic isotopes were mostly witnesses of, while the natural isotopes were participants in, the formation of the solar system material during the various stages of its existence (ref. 15).

Natural Radioactive Elements on the Earth

We know that in the Earth's crust U, Th, and K are quite unevenly distributed. They are present in the greatest quantities in acid rocks, in lesser quantities in intermediate rocks, still less in basic rocks, and, finally, in extremely small quantities in ultrabasic rocks. Table 1 presents the mean contents of natural radioactive elements in the most common rocks of the Earth (ref. 16). Data on individual rocks have also been collected in the work of Yermolayev and Sobornov (ref. 17), as well as that of Smyslov (ref. 18). Given a general concept of the processes leading to the formation of these rocks, we can imagine the behavior of natural radioactive elements and their role in the evolution of our planet.

Figure 1 is a K-U plot showing data for the most representative terrestrial rocks. This sort of systematization using log-log plots is widely used in geochemical and cosmochemical studies. At the present time, data on the natural radioactivity of basic and ultrabasic rocks of the Earth have been significantly supplemented and refined, primarily as a result of intensive investigations of the crustal rocks of the rift zones of the oceans. In particular, there is great interest in specimens of rock collected from the central oceanic ridges where the rock complexes are formed in a single process of differentiation of the primitive material of the mantle. The central ridges are of interest for study of the composition of mantle material, the process of formation of the basalt magma, and the formation of the most primitive crust, which can serve as a prototype of the primitive crust formed in the early stage of development of the Earth, the Moon, and the other terrestrial planets. These data on deep crustal rocks have also been considered in the composition of this diagram.

Table 1.—*Content of Natural Radioactive Elements in Various Types of Terrestrial Rock*

Rock Classes	Rock Types	Contents of Radioactive Elements		
		K.10⁴, g/t	U, g/t	Th, g/t
Acid	granites, granodiorities (quartz porphyries, rhyolites, dacities)	3.4 1–6	3.5 1–20	18 6–40
Intermediate	diorites (andesites)	2.3 1–4	1.8 1–3	7 6–30
Basic	gabbros (basalts), anorthosites	0.8 0.05–3.0	0.5 0.03–4	3.0 0.05–10
Ultrabasic	dunite, peridotite, harzburgite (picrite)	0.03 0.001–0.1	0.003 0.001–0.8	0.005 0.001–1.0

Petrographic and petrochemical study of specimens of oceanic rocks allowed Dmitriyev and Udintsev (ref. 19) to analyze the nature of the genetic relationship between basalts and ultrabasalts which are divided into two main groups of rocks: lherzolites and harzburgites. They classified lherzolites as upper mantle material and harzburgites as the residue following production of the primitive basalts. These opinions are apparently confirmed by the K-U systematics.

Figure 1 shows that the mean values of the K/U ratio for lherzolite nodules of the oceanic areas occupy a narrow band within limits of (2–3) $\times$ 10^3; i.e., fall significantly below the K/U ratios for the sequence of tholeiite basalts (K/U $\sim$ 7 $\times$ 10^3) and the main mass of alkaline basalts (K/U = (1–2) $\times$ 10^4). It is natural to propose that the increase of the K/U ratio in these rocks should be accompanied by a decrease in this ratio in other samples that are related to them by genetical processes. Obviously, the harzburgites are such rocks. Thus, in analyzing the data on the K/U ratios our attention is drawn by the branching of the K/U ratio for lherzolites into two series that are significantly different from each other. The upper series begins with the oceanic tholeiite basalts and is characterized by a higher K/U ratio, while the lower series is represented by the harzburgites and has lower K/U ratios.

Among the rocks and formations of the continental crust, local reductions of the K/U ratio are not uncommon and are, as a rule, related to increased uranium concentrations that arise during the geochemical cycle for uranium. Among the oceanic formations, the group of rocks with a decreased K/U ratio is of particular interest.

In this sense, the second series, outlined by the data on harzburgites and serpentinized lherzolites and located below the continuation of the band of moderate K/U ratio values (which are strictly characteristic of the lherzolites of the mantle), is itself somewhat supplementary to the series of oceanic tholeiite basalts.

The decreased K/U ratios in the harzburgite rocks of the rift zones are due to a uranium content that is quite high for ultrabasic rocks. Based on a number of factors, we can assume that such high uranium contents result from secondary enrichment that

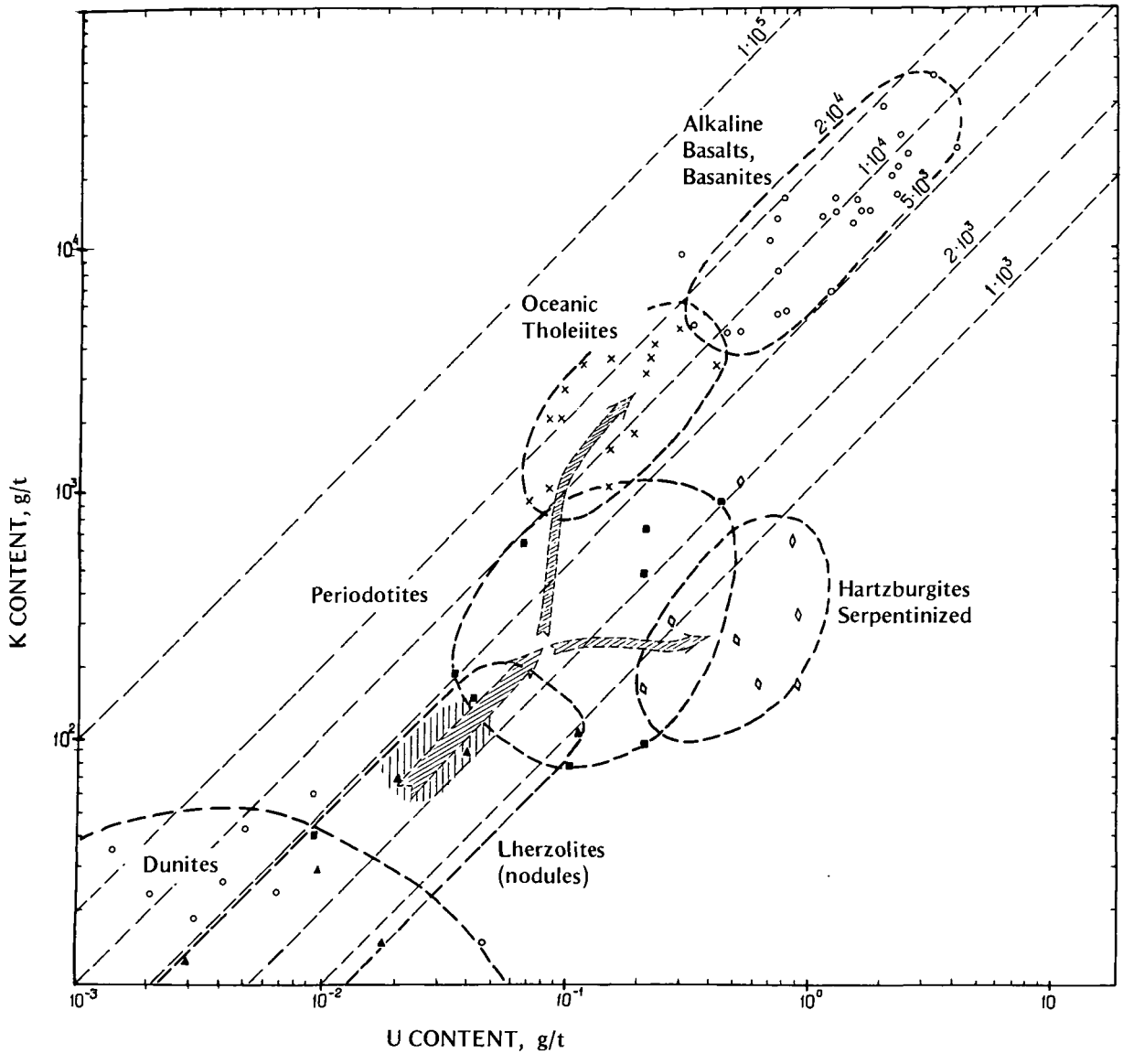


Figure 1.—*Potassium-uranium system of magmatic rocks of the earth.*

occurred when these rocks were reworked by the products of degassing of the mantle. In this case it is important that the rocks enriched by uranium were directly related to the mantle. In the rift zones there could have been no influences of the continental crust, and the variation in K/U ratios resulted only from differentiation in mantle material and its products.

Thus, using the proposal first set forth by Wakita et al. (ref. 20) that lherzolite nodules are material from the upper mantle and keeping in mind the distribution of K-U contents presented in figure 1, we can assume that in the primitive mantle material the potassium content is not over 300 g/t, and the uranium content is not over 0.1 g/t.

In estimating the mean contents of U, Th, and K for the Earth as a whole, one ordinarily starts with the following assumptions:

1. The mean heat flux at the surface of the Earth is 1.5×10^{-6} cal/cm^2 s.

2. The ratio of radioactive elements in the rocks of the upper mantle is true for the entire Earth.

3. The limits of the potassium content in the Earth are estimated on the basis of K^{40}, which is derived from the content of daughter Ar^{40} in the atmosphere of the planet (lower limit), and the established minimum possible value (50 percent) of fractional release of Ar^{40} (upper limit) (refs. 21 and 22).

Assuming that the heat flux is in equilibrium with heat formation and considering that most of the heat is generated by the decay of uranium and thorium, MacDonald (ref. 12) obtained a mean U content for the Earth of 0.031 g/t. Similar estimates using thermodynamic calculations have been made by others; particularly, Tera et al. (ref. 23) obtained a mean value (assuming that there are no radioactive elements in the core of the Earth) of U = 0.035 g/t, Th = 0.14 g/t, with Th/U = 4.

As concerns estimates of the mean content of potassium for the Earth, the value of 100 g/t, obtained from a K/U ratio of $\sim 3 \times 10^3$, seems to us preferable to the value of ~350 g/t calculated from the generally accepted ratio K/U $\sim 10^4$. Furthermore, the value of 100 g/t corresponds better to the range of possible contents of potassium of 90 to 170 g/t, estimated from data on daughter Ar^{40} (ref. 22).

As we will see later, the mean contents of U and Th in the Earth occupy an intermediate position between the corresponding quantities characteristic of ordinary chondrites and of basaltic achondrites, while potassium is several times less than in the chondrites and achondrites.

Natural Radioactive Elements on the Moon

At the present time, material has already been acquired and analyzed for eight regions of the Moon: three maria (Mare Fecunditatis, Mare Tranquillitatis, and Oceanus Procellarum); three continental areas (around the crater Apollonius-C and the Cayley-Descartes and Taurus-Littrow mountain systems); and two intermediate regions (around Fra Mauro Crater and the Hadley-Apennine formations). It is of interest to systematize and summarize the data produced.

Table 2 presents data on the mean contents of K, U, and Th, as well as their ratios (K/U and Th/U) for 400 specimens of crystalline rocks, breccias, and fine fractions of regolith from all eight regions studied.

A comparison of the abundance of the radioactive elements in the specimens of igneous rock, breccia, and fine regolith fractions shows a rather wide range in K, U, and Th contents for the various collection of specimens returned by the following missions: Apollo 11, 12, 14, 15, 16, and 17 and Luna 16 and 20. The main mass of specimens studied has the following limits of radioactive element content: for potassium, 0.03 to 0.7 percent; for uranium, 0.1 to 5 g/t; for thorium, 0.4 to 18 g/t. The K/U ratio varies from 1×10^3 to 5×10^3. However, for individual specimens, the data produced go significantly beyond these limits. For example, one of the breccia specimens collected by Apollo 12 (12013) is rich in a high silica-feldspar differentiate and contains 10.7 g/t uranium and 34.3 g/t thorium. These values are even higher than the U and Th contents in most terrestrial granites which, characteristically, have the highest content of the radioactive elements.

Also distinguished by their high values of K/U ratio (around 7×10^3) are specimens of anorthosite (62236) and basalt (63335) from the Apollo 16 collection, as well as specimens 15415 (Apollo 15) and 62275 (Apollo 16), which have K/U ratios of over 10^4. On the other hand, such specimens of crystalline rock as 62295 (Apollo 16) and 10062 (Apollo 11) have K/U ratio of $< 10^3$. Our attention is drawn by the similarity of K/U ratios (but decreased contents of potassium (200 g/t), uranium (0.07 g/t), and thorium (0.28 g/t), as compared with the main mass of lunar specimens) to the group of breccias from the collection of Apollo 15 and Apollo 16 (15418, 60135, 62237, 64435, 67455, and 69955).

Table 2.—*Content of Radioactive*

Element	Lunar Sample	Mare Tranquillitatis Apollo 11	Oceanus Procellarum Apollo 12	Mare Fecundatatis Luna 16
K, g/t	Crystalline rocks	1460 230–2515	500 260–670	1500
	Breccia	1330 940–1600	2310 1040–4360	—
	Soil	1100	2200 1700–3100	910
U, g/t	Crystalline rocks	0.48 0.18–0.78	0.24 0.21–0.31	0.3
	Breccia	0.50 0.29–0.63	2.1 0.6–3.46	—
	Soil	0.5	1.47 0.72–2.35	0.3
Th, g/t	Crystalline rocks	2.4 0.86–3.54	0.91 0.77–1.2	1.15
	Breccia	2.2 1.4–2.8	8.1 2.5–13.6	—
	Soil	2.3	5.9 3.52–8.8	1.1
Th/U	Crystalline rocks	4.6 3.4–5.5	3.6 1.9–4.0	3.8
	Breccia	4.4 3.8–5.0	4.0 3.2–4.2	—
	Soil	4.6	3.9 3.3–4.9	3.7
K/U	Crystalline rocks	3000 820–4650	2340 1760–4290	4700
	Breccia	2760 2280–3420	1470 1260–1740	—
	Soil	2200	1660 1240–2360	3640

Elements in Lunar Samples

Fra Mauro Apollo 14	Hadley-Apennines Apollo 15	Apollonius-C Lune 20	Cayley-Descartes Apollo 16	Taurus-Litthrow Apollo 17
3030 / 880–4150	400 / 120–500	1370 / 1000–1740	1170 / 90–4000	1610 / 410–3000
4370 / 1100–4780	1890 / 86–4780	715	1000 / 50–2000	2800
4520 / 3570–5300	1410 / 750–1860	645	940 / 425–1230	800 / 600–1330
2.14 / 0.6–3.2	0.14 / 0.003–0.16	0.7 / 0.5–0.9	0.76 / 0.016–3.0	1.02 / 0.11–2.0
3.34 / 1.0–4.5	1.18 / 0.04–3.14	0.7	0.57 / 0.03–1.00	0.6
3.69 / 3.1–4.0	1.0 / 0.42–1.69	0.29	0.56 / 0.18–0.74	0.3 / 0.15–1.0
8.44 / 2.24–21.1	0.49 / 0.028–0.6	2.55 / 1.7–3.4	2.84 / 0.1–9.4	3.96 / 0.31–8.0
12.7 / 4.4–15.6	4.53 / 0.12–12.3	1.2	2.1 / 0.1–4.85	2.32
13.6 / 12.0–14.4	3.74 / 1.73–6.34	1.0	2.08 / 0.6–2.74	1.25 / 0.3–2.4
3.8 / 3.5–4.2	3.63 / 2.9–4.3	3.6 / 3.4–3.8	3.58 / 2.82–4.84	3.46 / 2.50–4.0
3.63 / 3.3–3.9	3.78 / 3.0–4.2	1.7	3.73 / 3.33–4.86	3.87
3.7 / 3.6–3.9	3.79 / 3.4–4.5	3.45	3.75 / 2.81–4.45	3.3 / 2.0–3.92
1400 / 1280–1560	3000 / 2220–4.10⁴	1970 / 1930–2000	2070 / 740–7200	2410 / 1290–418
1330 / 830–1760	1700 / 1470–2150	1020	2070 / 1270–3470	4700
1250 / 1120–1390	1520 / 1230–2050	2220	1730 / 1300–2900	2500 / 1750–4200

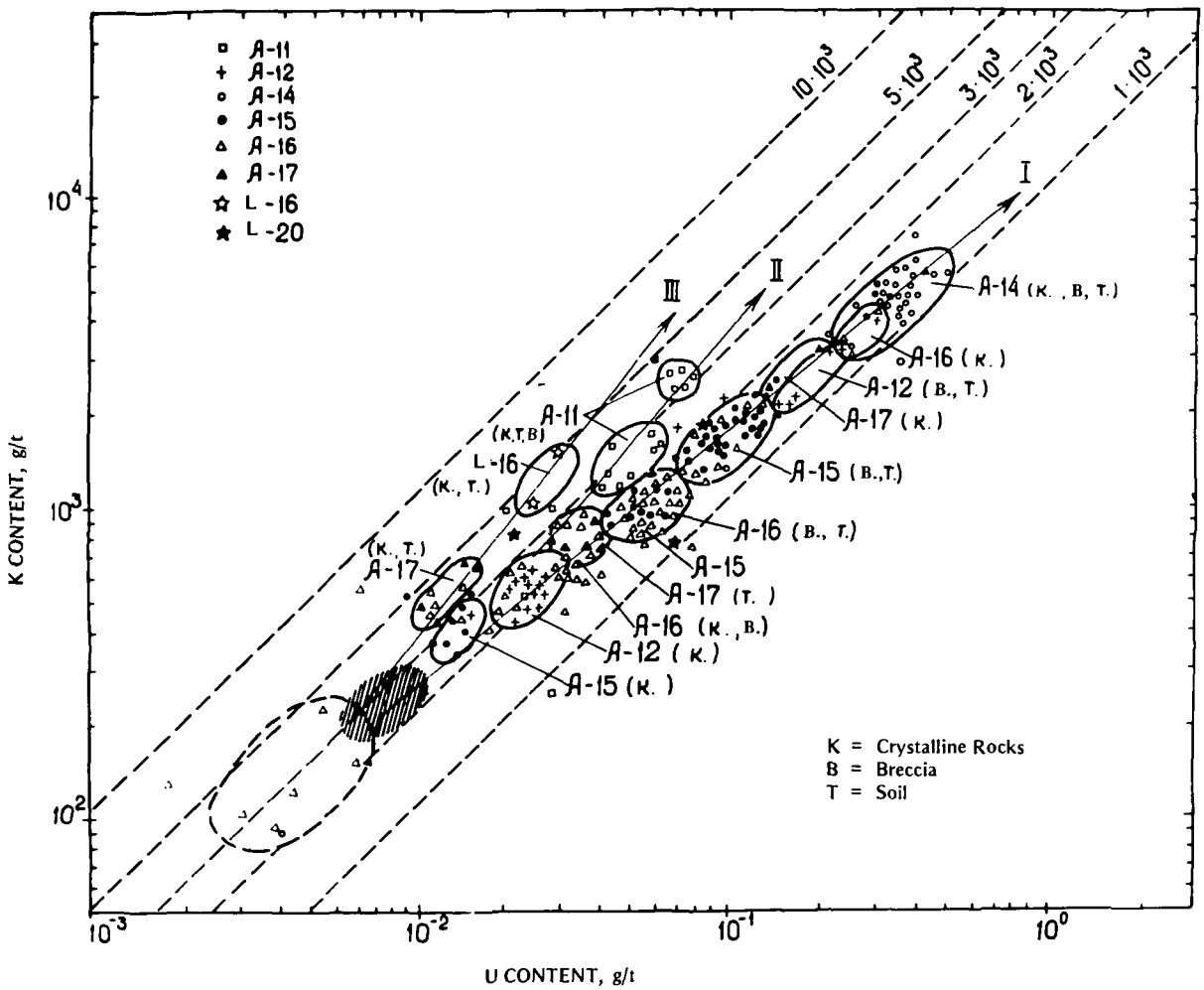


Figure 2.—*Potassium-uranium system of lunar specimens.*

Analysis shows that regions of the Moon such as Mare Tranquillitatis, Mare Fecunditatis, and the Fra Mauro region are characterized within each region by similar potassium-uranium contents and K/U ratios for specimens of various types (crystalline rocks, breccias, fine regolith fractions). This fact apparently indicates that the formation of the regolith in these regions was basically local in nature. At the same time, the increased content of radioactive elements in the regolith of the Oceanus Procellarum and the Hadley-Apennine formation in comparison with the original rocks of these regions is related to horizontal movement of the substance over the surface of the Moon. In particular, the lunar soil and breccias in these regions are a mixture of local basalt and a foreign component with high K, U, and Th content. This material could not have been anorthosite, which has low contents of K, U, and Th and would act as a diluting agent to decrease the K–U content in comparison with those for the soil and breccia. The most probable component is the material called KREEP (UTh), which is characterized by a high content of natural radioactive elements, rare earths, and phosphorous.

Figure 2 presents the analytical results of all known lunar specimens on a K-U plot. As we can see from the figure, most lunar specimens from the regions studied can be

differentiated by their contents of potassium, uranium, and K/U ratio into a number of areas with more or less clearly defined boundaries. These areas are partially overlapping and form the links in several more or less clearly pronounced chains that connect the zone of low content of radioactive elements with several higher zones that have differing K/U ratios.

First, we see a long chain with K/U ratios of (1–3) $\times$ 10^3. The lowest link in this chain is formed by the mare basalts of Apollo 15, which have the lowest content of natural radioactive elements. The highest link is formed by the KREEP (UTh) material of the Apollo 14 collection from the Fra Mauro region. In the middle portion of the chain are the links that characterize the regolith from various regions and the links that correspond to crystalline rocks from the Taurus-Littrow, Cayley-Descartes, and Apennine Mountain regions. The same values of K and U content were found by analysis of the individual fragments of crystalline rock from the Luna 20 core sample.

Obviously, formal placement of several links characterizing specimens from widely varied parts of the Moon in a single chain does not mean that they belong to a single sequence or related series of rock formed in the process of magmatic differentiation. Nevertheless, the great similarity in distribution within the very same chain of specimens from different collections such as those of Apollo 12, 15, and 16 allows us to speak of general trends manifested in the origin and evolution of the material of these regions.

The second chain, not so clearly expressed as the first and having K/U ratios in the range (2–4) $\times$ 10^3, can be traced for links that include specimens from the mare regions of the Moon, particularly from the Mare Tranquillitatis. We can support that this chain also has its origin in the zone where we find the links that characterize the low-potassium basalts of the Oceanus Procellorum (Apollo 12) and the Hadley region (Apollo 15), as well as basalt 10003 from Mare Tranquillitatis (Apollo 11). Apparently, this very same chain should include the link from the Apollo 17 series, which includes regolith specimens from Mare Serenitatis, particularly since in their content of both major and rare-earth elements these specimens are similar to the regolith specimens from the Mare Tranquillitatis.

Comparison of these two chains and their individual links leads to the conclusion that the rock specimens characteristic of mountain regions lie basically in the range of K/U ratios that are lower when compared with the range of K/U ratios characteristic of mare basalts. This enrichment of igneous rocks with uranium relative to potassium, as shown by Taylor (ref. 24), might result from fractional crystallization of melts because the physiochemical properties of these elements are different, particularly in their ionic radii and charges. According to the calculations of the author, the content of potassium in the continental crust relative to the mean content in the entire Moon is 32 percent, whereas for uranium this figure is 54 percent and for thorium 56 percent.

The third chain presented in figure 2 is less obvious and statistically weaker. It includes a number of specimens of the Apollo 17 series (coarse-grained basalts 70135 and 79155, regolith specimens 74220 and 75081, and breccia 76255, which is distinguished by comparatively high contents of potassium and uranium with K/U $\sim$ 4700) ; the Apollo 16 series of breccias collected at one station (67035, 67115, and 67915) ; the Apollo 11 series (specimens 10056 and 10058) ; as well as regolith and basalt fragment specimens from the Luna 16 series. In any case, the presence of a whole group of specimens distributed in the diagram along the area of elevated K/U ratios gives us reason to consider this chain as well.

These chains can be represented as approximating regression lines with different slopes relative to the straight lines for K/U = const. and probably intersecting the values of potassium-uranium content corresponding to the material of the lunar mantle. Obviously, this material should be poorer in radioactive elements than the lunar surface

rocks, since otherwise the radiogenic heat released by the Moon should have maintained it in the melted state.

As we know, zone melting of the substance of the mantle is accompanied by accumulation of a number of elements, including lithophilic K, U, and Th in the upper zone of the melt, and the corresponding impoverishment of the mantle in the zone of formation of the melt. As noted above, the presence in the collection of lunar specimens of a group of breccias of deep origin with extremely low contents of radioactive elements (area outlined by dashed line on fig. 2) allows us to affirm more reliably the existence of deep magmatic zones poor in K, U, and Th.

In order to define the initial matter of the Moon, we must establish the genetic affinity of rocks formed in a single process of mantle differentiation. This could be confirmed by the complementary nature of their chemical compositions and by data on the distribution of trace elements in them.

The difference in the approximately straight slopes that characterize various "families" of lunar specimens in a K-U plot apparently indicates the existence of complementary parts of these families that were formed as a result of magmatic differentiation in an early stage of lunar development (ref. 25).

Certainly, for the Moon, the picture of differentiation and the genetic relationship of rocks formed in a single process is not as clear as for the Earth. This is explained by the fact that the process of differentiation on the Moon was probably not as intensive as on the Earth. However, it is interesting that the primary undifferentiated material of both the Earth and Moon apparently had approximately the same ratio of natural radioactive elements $K/U \simeq 2.8 \times 10^3$ (ref. 26).

Obviously the order of magnitude difference in K/U ratios between the Moon and Earth, as used in a number of papers about similar systematics of the data, has no definite meaning because it results from comparing only secondary, differentiated rocks and not from considering the average composition of the entire planet.

We can estimate the mean content of U, Th, and K on the Moon as 0.07, 0.25, and 180 grams per ton of lunar material, respectively. This is accomplished by keeping in mind the ratios $K/U \sim 2.8 \times 10^3$ and $Th/U \sim 3.6$ and the mean heat flux values of 30–40 erg/cm^{2}s (determined by a radio-astronomy method) (ref. 27) or 28–31 erg/cm^{2}s (measured directly on the Moon by Apollo 15 and 17) (ref. 28).

It should be noted that these contents of natural radioactive elements for the primitive material of the internal zones of the Moon, which have been subjected to radiogenic heating and chemical differentiation, are close to the contents produced by Wanke et al. (ref. 29) in calculating the chemical composition of their two-component model of the Moon (U = 0.086, Th = 0.32, and K = 250 g/t). Finally, these data for the Moon are also close to the mean values of U, Th, and K contents in achondrites–data that will be considered below.

With these data for the mean content of the natural radioactive elements on the Moon and data on the mean content of lunar specimens (see table 2) that characterize the lunar crust, we can make a few statements concerning the thickness of the lunar crust.

For example, if we assume that at the present time practically all of the uranium has been concentrated and rather evenly distributed in the lunar crust with a mean content of ~ 0.5 g/t, then its thickness should be 60 to 70 km. If uranium has remained partially in the mantle, the crust should be thinner; if its content in the crust is uneven and decreases with depth, the crust should be thicker.

Comparing the content of radioactive elements on the Moon and the Earth, we note the following. The mean content of radioactive elements in the Moon is twofold higher than in the Earth, while the mean content of radioactive elements in the lunar crust is lower than on the Earth (e.g., for uranium ~ 0.5 g/t and ~ 2 g/t, respectively). This means that the processes of differentiation of matter on the Moon have not been as intensive as on the Earth, and as a result the en-

richment of radioactive elements in the lunar crust has been at least an order of magnitude lower than on the Earth. This might also be the reason why we do not observe Moon rocks that are highly enriched with potassium, as is the case for certain igneous terrestrial rocks that have K/U ratios of $\sim 10^4$.

Natural Radioactive Elements in Meteorites

The peculiarities of the composition of meteorites agree with their formation as a result of condensation and fractionation of the matter of the solar nebula as it cooled. This process has been thermodynamically studied in detail (refs. 30, 31, and 32). The early condensate was rich in elements (Al, Ca, Ti) that formed refactory compounds, after which the silicates and iron condensed, followed by the condensation of the more volatile elements that enter into the composition of the low-temperature phases. The fractionation of solar nebula matter led to the formation of carbonaceous, ordinary (bronzite, hypersthene, amphoterite), and enstatic chondrites and achondrites, including basaltic achondrites (eucrites and howardites). After their formation, some meteorites were subjected to secondary heating and recrystallization.

In the process of condensation of meteoritic matter, fractionation of the radioactive elements U, Th, and K obviously occurred.

The first two of these elements are relatively refractory and apparently condensed in one of the early stages of cooling. The early condensate was doubtless poor in volatile compounds, including K_2O. The contemporary distribution of the radioactive elements in various groups of meteorites is probably the result of these processes and occurred in the early existence of the solar system.

Table 3 and figure 3 show data on the distribution of K, U, and Th in stony meteorites. Naturally, the greatest quantity of published data on the content of radioactive elements in the meteorites relates to the most representative and numerous chondrite group. For the achondrite group, statistically significant radioactivity data (for comparison of individual classes of meteorites), are available mostly for eucrites, which amount to 45 percent, and howardites, which amount to 27 percent of all known achondrites.

What are the distinguishing features of the K-U and U-Th systems of the meteorites? As regards the chondrite group, there is particular interest in data on carbonaceous chondrites whose material is generally throught to be closest to the protoplanetary matter of which the planets and asteroids were formed. More precisely, the carbonaceous chondrites are divided into three types (C1, C2, C3); what we have said relates to type C1 chondrites, whose chemical composition has atomic ratios and amounts of volatile substances that are most similar to the chemical composition of the Sun. In particular, types C2 and C3 carbonaceous chondrites are poorer in volatile elements than type C1. The content of potassium relative to silicon in C1, C2, and C3 carbonaceous chondrites is 3200, 2100, and 1700 atoms/10^6 atoms of Si, respectively; i.e., C2 and C3 are poorer in potassium than C1 by 0.63 and 0.52 times, respectively (ref. 30).

The mean values of the K/U ratio for all three types of carbonaceous chondrites differ significantly: $\simeq 4.3 \times 10^4$ for C1; $\simeq 3 \times 10^4$ for C2; and $\simeq 2.3 \times 10^4$ for C3. Unfortunately, the insufficiency of statistical material, particularly for type C1 and C3 carbonaceous chondrites, and the possibility of their contamination on Earth, forces us to approach with caution estimates of the mean values of K, U, and Th contents characteristic of any given class of meteorites.

Nevertheless, the content of potassium in ordinary chondrites is greater than in carbonaceous chondrites, although they are rather similar to type C1 carbonaceous chondrites in K/U ratio. As we can see from figure 3, the separate fields that characterize individual classes of ordinary chondrites overlap each other significantly and fall

Table 3.—*Content of Radioactive Elements in Stony Meteorites*

	Meteorites	K, g/t	U, 10^{-3} g/t	Th 10^{-3} g/t	Th/U	K/U, 10^4
Chondrites	Carbonaceous C1	510 380–580	11.0 8.7–14.0	39 29–59	3.5 2.8–4.2	4.8 3.9–6.7
	Carbonaceous C2	415 130–1100	12.6 10.8–15	44 38–61	3.5 3.1–4.3	3.0 1.5–4.1
	Carbonaceous C3	500 100–1400	18 14–24	85 57–120	4.4 4.0–5.0	2.3 1.6–2.8
	Amphoterite	840 700–1240	16.5 10.5–25.5	45 43–50	3.6 3.0–3.9	5.2 3.3–8.1
	Hypersthene	900 640–1660	16 8.6–25	42 38–49	3.4 2.5–3.9	5.3 3.5–11.6
	Bronzite	850 500–1580	13.6 9.0–24.5	40 36–42	3.4 2.9–3.8	6.5 4.4–9.1
	Enstatite	850 500–1740	10 6.0–16	34 29–42	3.7 2.6–7.0	8.4 4.4–11.2
Achondrites	Eucrites	360 150–650	93 15.9–200	350 53–590	3.8 2.9–6.1	0.4 0.37–0.76
	Howardites	250 170–400	52 23–89	167 63–312	3.1 2.6–3.45	0.4 0.34–0.48

within a rather limited area of potassium-uranium contents (K from 600 to 1000 g/t, U from 0.1 to 0.25 g/t). The range of uranium contents for enstatite chondrites is shifted somewhat into the area of lower U concentrations (from 0.06 to 0.16 g/t).

Achondrites of various classes have rather wide variations in potassium and uranium contents. Although due to the small number of such chondrites as aubrites, ureilites, angrites, nakhlites, and shergottites, it is difficult to draw any conclusions concerning genetic relationships; most of the calcium-rich achondrites—eucrites and howardites—show a number of common characteristics. This conclusion can be made on the basis of both structural peculiarities and mineralogical composition. As concerns radioactive elements, we can state that howardites and eucrites have practically identical mean values of K/U ratio ($\sim 4 \times 10^3$), but differ in absolute uranium and potassium contents. Whereas in figure 3 the field defined by the howardites Frankfurt and Kapoeta lies near the point with coordinates K = 200 g/t and U = 0.05 g/t, the area of eucrites extends to values of 0.2 g/t uranium and 700 g/t potassium. This point of the diagram corresponds to the eucrite Stannern, the basaltic achondrite richest in radioactive elements, and agrees with the conclusion of Ahrens (ref. 33) that Stannern is possibly an end product of the differentiation of achondritic matter.

Of the achondrites poor in calcium, our attention is drawn primarily by the group of diogenites shown in the graph. Schnetzler

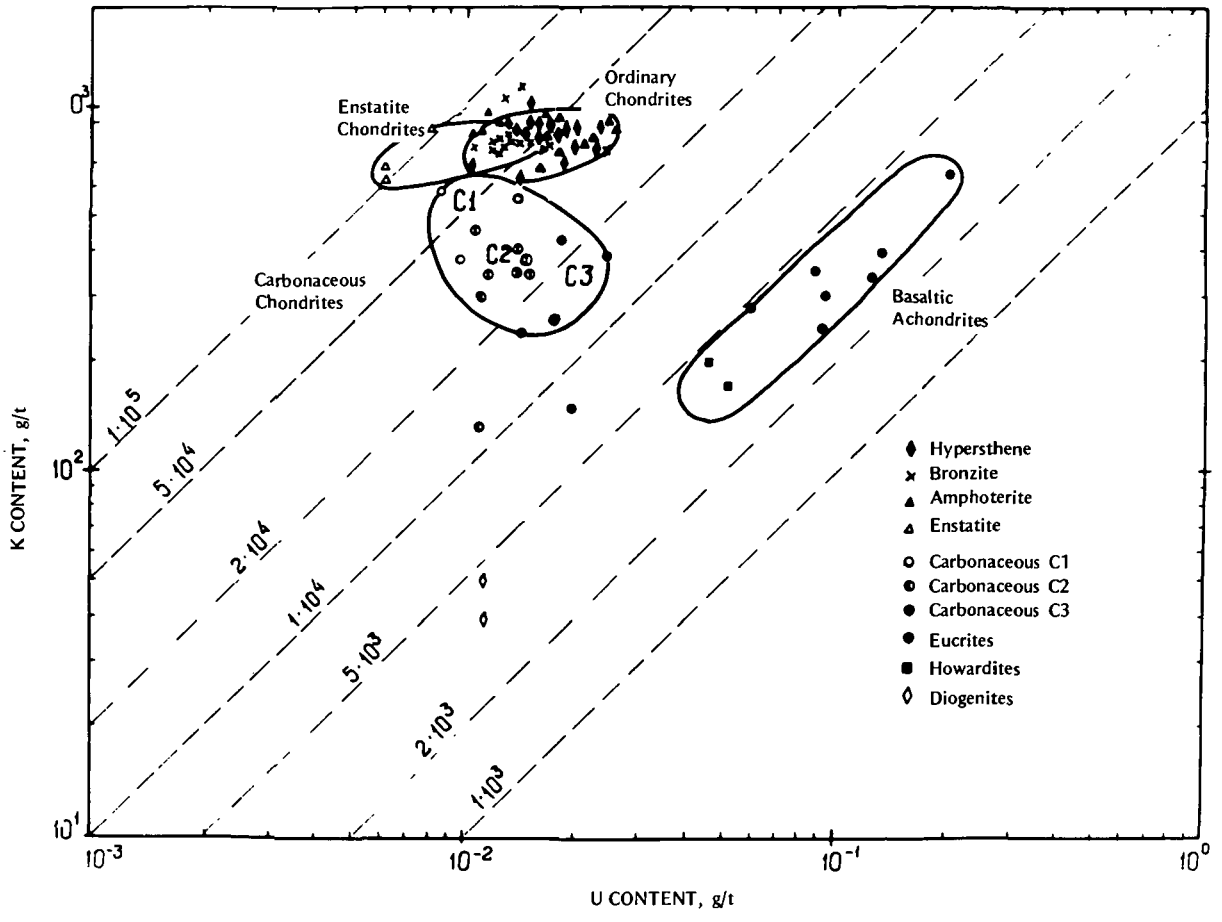


Figure 3.—*Potassium-uranium system of rocky meteorites.*

and Philpotts (ref. 34) believed that the diogenites are a residual product produced by the melting of calcium-rich achondrites out of chondrite matter. On the other hand, based on their similarity to hypersthene chondrites, the opinion has been stated (ref. 35) that diogenites were formed from iron-poor chondrites as a result of intensive metamorphism. As follows from figure 3, radioactivity data do not contradict this idea. Actually, some diogenites (Johnston and Shalka) are quite poor in potassium (by approximately one order of magnitude) in comparison with the chondrites and at the same time have K/U ratios similar to the Ca achondrites ($\sim 4 \times 10^3$), but significantly lower K and U contents.

In contrast to K/U ratios, the Th/U ratio for these classes of meteorites is less subject to fluctuations, although the actual content of Th and U in the stony meteorites is distributed over broad limits. For example, the main mass of chondrites falls within 0.03 to 0.06 g/t and 0.016 g/t for Th and U contents. Most eucrites for which thorium and uranium were determined are concentrated in the area of relatively high contents: Th = $\sim$ 0.4 g/t and U $\sim$ 0.1 g/t.

At the same time, howardites (Frankfurt, Kapoeta) occupy an intermediate area and even fall adjacent (Binda) to the Moore County and Serra de Mage eucrites in the lower area of Th and U contents, corresponding to the chondrite group of materials. Still poorer in U and Th are the diogenites; in particular, the Ellemeet diogenite has the

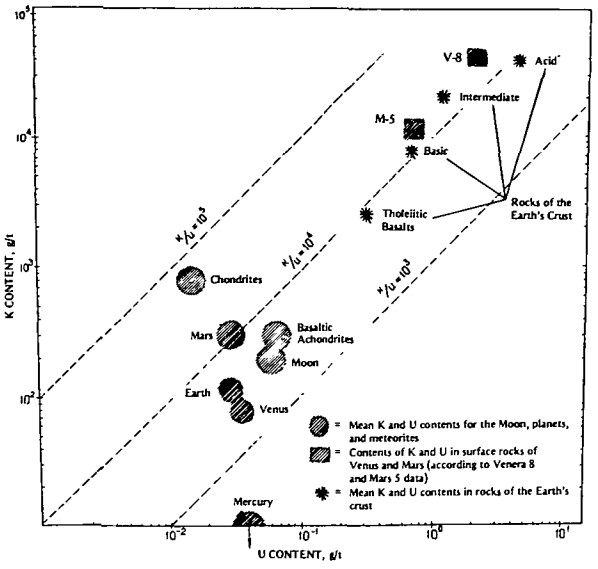


Figure 4.—*Potassium-Uranium system of bodies of the solar system.*

lowest radioactivity, with U = 0.0015 g/t and Th = 0.0038 g/t.

Nevertheless, as can be seen from table 3, the mean Th/U ratios for meteorites of various classes and types fall in a relatively narrow band of 3.6 ± 0.5, which agrees well with the value of 3.8 ± 0.3 calculated indirectly for the solar system by Fowler and Hoyle (ref. 36).

Natural Radioactive Elements in the Solar System

Whereas the fractionation of volatile elements and compounds between the terrestrial planets and the giant planets is beyond doubt and results from the variation in temperatures at various distances from the Sun, the question of fractionation dependent on heliocentric distance within the limits of the terrestrial planets remains open. However, an impression of this fractionation can be gained by analysis of both the various condensation models of planetary formation from the protoplanetary cloud and indirect data on the structure of the planets.

We will study the abundance of natural radioactive elements in the solar system, using the previously discussed data on the Earth, Moon, and meteorites, and supplementing them with some estimates on the content of U, Th, and K in the planets. Assuming that the relationship of U and Th changes little or remains completely unchanged within at least 4 AU, we will study only the content and ratio of U and K.

Figure 4 presents the mean contents of radioactive elements on the Moon and planets and in meteorites, as well as the mean content in rocks of the crust of the Earth, Venus, and Mars.

What considerations can be used to estimate the mean contents of U, Th, and K on the planets? Obviously, the determining factors will be placement in the solar system, size and density, and current internal structure. Let us consider these characteristics.

VENUS

According to these considerations, Venus, probably more than the other planets, is similar to the Earth. It is currently known that the content of volatile components (particularly CO_2, N_2, O_2, etc.) on Venus is close to that of Earth, and only the difference in temperatures on the surface of the planets determines the quantity of these substances in the atmosphere or in the bonded state in the rocks of the planets. The presence on Venus of an atmosphere consisting of components which, as on the Earth, can be released only in the process of degassing of melted crustal material indicates that Venus should be a differentiated planet.

Finally, the contents of U, Th, and K in the Venusian rock measured by the Venera 8 spacecraft amount to 2.2, 6.5, and 4×10^4 g/t, respectively (point V–8 on fig. 4), and indicate the existence of igneous rock on the surface of Venus. Even if we assume that these initial data may not be representative of the distribution of radioactive elements throughout the crust of the planet, this point, in our opinion, is quite indicative when we compare it with the K/U data for the other

planets of the solar system. It is not difficult to see that these contents correspond to those of high-potassium acidic rocks on Earth.

Vinogradov et al. (ref. 37) studied possible processes leading to the enrichment of the surface Venusian rock with natural radioactive elements. One reason for the stability of high-potassium material in particular might be related to the acid-alkaline properties of melts flowing on the surface of the planet. Korzhinskiy (ref. 38) and Yakovlev et al. (ref. 39) showed that as the acidity of a melt increases the resistance to evaporation of the alkaline components of such melts also increases. This, apparently, is the reason for the high concentration of potassium in the Venusian rocks.

Thus, everything indicates that Venus is a differentiated planet. The process of differentiation on Venus apparently occurred quite intensively, as indicated by the high contents of U, Th, and K in the Venusian rock as measured by Venera 8.

If we also keep in mind the high temperatures on the surface of the planet (ref. 40), the mountainous relief (ref. 41), and the dense atmosphere consisting of gases liberated as a result of volcanic activity (refs. 37 and 42), we can imagine that the process of differentiation is still continuing, the interior of the planet is still quite hot, and the heat flux at the present time is obviously higher than that of Earth.

Since with identical initial data (and particularly identical contents of radioactive elements) Venus should have a slightly lower heat flux, it is reasonable to assume that Venus has a slightly higher content of uranium than the Earth's 0.035 g/t. The K/U ratio for Venus might be somewhat lower than for Earth.

MARS

Quite a bit is now also known about Mars. Its mass and moment of inertia indicate a significant increase in density with depth and the possible existence of a dense core. This is also indicated by the weak dipole magnetic field of Mars (ref. 43). However, everything that we now know concerning the surface of Mars, based on the photographs of Mariner 9 (volcanism, tectonic phenomena, high mountain regions, etc.), indicates the possible existence of a Martian crust consisting of igneous rocks (ref. 44). Finally, recent measurements of the gamma radiation of Mars by Mars 5 (ref. 11) indicate a comparatively high content of natural radioactive elements in the surface rock of Mars in comparison with the possible mean content of these elements on Mars. (In fig. 4, the point corresponding to the K-U content in the Martian rock is represented by the index M–5.)

In a number of its characteristics, Mars occupies a middle position between the Earth and the Moon. At the present time it is not as active as the Earth, but not as cold as the Moon. It can be assumed that the heat flux of Mars is now intermediate between the values for the Moon and the Earth, i.e., ~ 40 erg/cm^{2}s.

Based on analysis of the internal structure of Mars, Binder and Davis (ref. 45) indicated that the composition of the Martian mantle is similar to that of the Earth; i.e., the content of olivine and fosterite should amount to 65 to 80 percent. The mass of the core of Mars should be ~ 10 percent of the mass of the entire planet, and the radius of the core is approximately 1250 km.

Mars was formed in an area of the cloud where the temperature was ~ 500 K (i.e., significantly lower than the condensation temperature of potassium and the other volatile elements and compounds). As such, we should expect that Mars has retained these volatile substances, though perhaps not to the same extent as the chondrites whose accretion occurred in the temperature range 350 to 500K (ref. 46), but obviously more than Earth.

Therefore, based on these considerations we can assume that the mean content of U on Mars is no less than on Earth and that Mars has a K/U ratio of $\sim 10^4$. The value of K/U for Mars is intermediate between the corresponding values for Earth (K/U ~ 3

$\times 10^3$) and the chondrites (K/U = (2.4–8.4) $\times 10^4$), which are determined by their position at 1.5 AU from the Sun.

MERCURY

There is somewhat less information available concerning Mercury. The presence of regions broken by craters and of lower, smooth regions similar to the continents and mare of the Moon (ref. 47) may indicate volcanic activity in the past and the possible existence of a crust at present. The presence of a weak magnetic field, as shown by Mariner 10 (ref. 48), probably indicates the existence of at least a partially melted core. Thus, we can assume that Mercury is also a differentiated planet. Mercury apparently is richer in refractory elements than the other planets and has little or no volatile elements, including potassium. For Mercury we can assume very approximately a K content of < 1 g/t and a U content of ~ 0.04 g/t.

All these peculiarities in the abundance of the radioactive elements on the Moon, planets, and meteorites fit into our general concept of the evolution of the matter in the solar system (refs. 49, 50, and 51).

According to these concepts, the protoplanetary matter, of which all bodies in the solar system were later formed, took on significant heterogeneity in the course of its chemical evolution, as is reflected in the composition of the Moon, planets, and meteorites. This compositional heterogeneity of the protoplanetary mass was determined primarily by the relationship between volatile and refractory elements and their compounds.

During the evolution of protoplanetary matter, the volatile elements and compounds moved to the periphery of the cloud (in the area of lower temperatures), while the refractory elements moved closer to the Sun (in the area of higher temperatures). This process of differentiation in the preplanetary period was naturally reflected in the abundance of radioactive elements (particularly their relationships) in the solar system. For example, as the distance changes from Mercury (~ 0.4 AU) to the asteroid belt (~ 2–4 AU), the K/U ratio changes by almost five orders of magnitude.

Thus, the various bodies of the solar system that formed later inherited those quantities and relationships of radioactive elements which existed in the formation region of each body.

The formation of the planetary Earth-Moon system is somewhat more complex. In spite of the identical nature of the preplanetary matter in the zone which fed these two bodies, differences in their condensation conditions (pressure, temperature) have resulted in differences in their chemical compositions. According to condensation models, the metallic core of the Earth was able to form before the beginning of the condensation of low-temperature magnesium silicates. Due to this, the relative shortage of iron on the Moon may be related to the fact that during its accretion a significant portion consisted of high-temperature condensates enriched in refractory elements (including U and Th).

On the other hand, the mechanism of interaction of the solar wind with particles of the forming swarm must have played a significant role in the shortage of volatile elements on the Earth and the Moon. According to the model developed by Ruskol (ref. 52), the influence of the solar wind should have been particularly strong for the Moon during the final stage of accretion of its surface layers. During this period, at the periphery of the cluster around the Earth the transparency was sufficiently great that the atoms of the volatile elements, released by evaporation of matter during the processes of collision of solid particles and bodies, were partially removed from the swarm under the influence of the solar wind.

After the formation of the planets, further evolution occurred. As we know, during the course of differentiation of the matter of the planets, the crust was enriched with natural radioactive elements, particularly potassium.

Whereas in the lunar rocks the differentiation was relatively slight, Earth, Venus, and Mars underwent a long process of differ-

entiation during their thermal history, which is indicated particularly by the high K/U ratio of the surface magmatic rock in comparison to the assumed relationship of mean contents of these radioactive elements in the planets.

References

1. VINOGRADOV, A. P., YU. A. SURKOV, G. M. CHERNOV, F. F. KIRNOZOV, AND G. B. NAZARKINA, *Kosmich. Issled.*, Vol. 4, 1966, p. 874.
2. VINOGRADOV, A. P., YU. A. SURKOV, G. M. CHERNOV, F. F. KIRNOZOV, AND G. B. NAZARKINA, *Kosmich. Issled.*, Vol. 5, 1967, p. 871.
3. LSPET, *Science*, Vol. 165, 1969, p. 1211.
4. LSPET, *Science*, Vol. 167, 1970, p. 1325.
5. LSPET, *Science*, Vol. 173, 1971, p. 681.
6. LSPET, *Science*, Vol. 175, 1972, p. 363.
7. LSPET, *Science*, Vol. 179, 1973, p. 23.
8. LSPET, *Science*, Vol. 182, 1973, p. 659.
9. VINOGRADOV, A. P., YU. A. SURKOV, F. F. KIRNOZOV, AND V. N. GLAZOV, *Dokl. AN SSSR*, Vol. 208, 1972, p. 723.
10. SURKOV, YU, A., F. F. KIRNOZOV, O. P. SOBORNOV, G. A. FEDOSEYEV, L. N. MYASNIKOVA, B. N. KONONOV, S. S. KUROCHKIN, AND D. YE. FERTMAN, *Kosmich. Issled*, Vol. II, 1973, p. 781.
11. SURKOV, YU. A. et al., *Kosmich. Issled*, In press, 1974.
12. MACDONALD, G. J. F., *J. Geophys. Res.*, Vol. 69, 1964, p. 2933.
13. UREY, H. S., *Proc. Natl. Acad. Sci. U.S.*, Vol. 41, 1955, p. 127.
14. BHANDARI, H. S. BHAT, D. LAI, G. RAJAGOPLAN, A. S. IHAMHANE, AND V. S. VENKATAVARADEN, *Nature*, Vol. 230, No. 5291, 1971.
15. VERNOV, S. N., AND A. K. LAVRUKHINA. *Soviet-American Conference on Cosmochemistry of the Moon and Planets*, Summary of Reports, 1974, p. 129.
16. VINOGRADOV, A. P., *Geokhimiya*, No. 7, 1962, p. 555.
17. YERMOLAYEV, N. P., AND O. P. SOBORNOV, *Geokhimiya*, No. 6, 1973, p. 803.
18. SMYSLOV, A. A., *Trudy VSEGEI*, Vol. 164, 1968.
19. DMITRIYEV, L. V., AND G. B. UDINTSEV, *Studies on the Problem of the Rift Zones of the World Ocean*, Collection of Works, Vol. 1, Nauka Press, Moscow, 1972.
20. WAKITA, H., H. NAGASAWA, S. UYEDA, AND H. KUNO, *Earth Planet. Sci. Letters*, Vol. 2, 1967, p. 377.
21. HURLEY, P. M., *Geochimica et Cosmochimica Acta*, Vol. 32, 1968, p. 273.
22. LARIMER, J. W., *Geochimica et Cosmochimica Acta*, Vol. 35, 1971, p. 769.
23. TERA, F., D. A. PAPANASTASSIOU, AND G. J. WASSERBURG, *Earth Planet. Sci. Letters*, Vol. 22, 1974, p. 1.
24. TAYLOR, S. P., *Nature*, Vol. 245, 1973, p. 203.
25. FANALE, F. P., AND D. B. NASH, *Science*, Vol. 171, 1971, p. 282.
26. SURKOV, YU. A., G. A. FEDOSEYEV, O. P. SOBORNOV, AND L. S. TARASOV, *Kosmich. Issled*, Vol. II, 1973, p. 926.
27. TIHONOVA, T. V., AND V. S. TROITSKIY, *Fizika Luny i Planet*, Collection of Works, Nauka Press, Moscow, 1972, p. 178.
28. LANGSETH, M. G., S. P. CLARK, J. L. CHUTE, S. J. KHEIM AND A. E. WECHSTER, *The Moon*, Vol. 4, 1973, p. 390.
29. WANKE, H., H. BADDENHAUSEN, G. DREIBUS, E. JAGOUTZ, H. KRUSE, H. PALME, B. SPETTEL AND F. TESCHKE, *Proc. Fourth Lunar Science Conference, Geochimica et Cosmochimica Acta*, Supplement 4, Vol. 2, 1973, p. 1461.
30. LARIMER, J. W., AND E. ANDERS, *Geochimica et Cosmochimica Acta*, Vol. 31, 1967, p. 1239.
31. LARIMER, J. W., AND E. ANDERS, *Geochimica et Cosmochimica Acta*, Vol. 34, 1970, p. 367.
32. ANDERS, E., *Ann. Rev. Astron. Astrophys.*, Vol. 9, 1971, p. 1.
33. AHRENS, L. H., *International Symposium on the Chemistry and Mineralogy of Meteorites and Extraterrestrial Matter*, London, April 6–8, 1970.
34. SCHNETZLER, C. C., AND J. A. PHILPOTTS, *Meteorite Research*, 1969, p. 206.
35. DODD, R. T., *Trans. Am. Geophys. Union*, Vol. 52, No. 7, 1971.
36. FOWLER, W., AND F. HOYLE, *Ann. Phys.*, Vol. 10, 1960, p. 280.
37. VINOGRADOV, A. P., YU. A. SURKOV, AND B. M. ANDREYCHIKOV, *Dokl. AN SSSR*, Vol. 190, 1970, p. 552.
38. KORZHINSKIY, D. S., *Geokhimiya*, No. 7, 1956.
39. YAKOVLEV, O. I., A. I. KOSOLAPOV, A. V. KUSNETSOV, AND M. D. NUSINOV, *Vestnik MGU Ser. Geol.*, No. 5, 1973, p. 85.
40. MAROV, M. YA., V. S. AVDUYEVSKIY, M. K. ROZHDESTVENSKIY, N. F. BORODIN, AND V. V. KERZHANOVICH, *Kosmich. Issled.*, Vol. 9, 1971, p. 570.
41. CAMPBELL, D. B., R. B. DYCE, R. P. INGALLS, G. H. PETTENGILL, AND I. I. SHAPIRO, *Science, Vol.* 175, 1972, p. 514.
42. VINOGRADOV, A. P., YU. A. SURKOV, K. P. FLOPENSKIY, AND B. M. ANDREYCHIKOV, *Dokl AN SSSR*, Vol. 179, 1968, p. 37.
43. DOLGINOV, SH. SH., *Soviet-American Conference on Cosmochemistry of the Moon and Planets*, Summary of Reports, 1974, p. 177.
44. MASURSKY, H., *J. Geophys. Res.*, Vol. 78, 1973, p. 4009.
45. BINDER, A., AND D. DAVIS, No more information available, 1973.

46. LARIMER, J. W., *Space Science Reviews*, Vol. 15, 1973, p. 103.
47. TRASK, N. J., *Trans. Am. Geophys. Union*, Vol. 55, 1974, p. 340.
48. BEHANNON, K. W., R. P. LEPPING, N. F. NESS, K. H. SCHATTEN, AND Y. C. WHANG, *Trans. Am. Geophys. Union*, Vol. 55, 1974, p. 340.
49. LEWIS, J. S., *Earth Planet. Sci Letters*, Vol. 15, 1972, p. 286.
50. ANDERSON, D. L., *Earth Planet. Sci. Letters*, Vol. 18, 1973, p. 301.
51. GROSSMAN, L., AND J. W. LARIMER, *Rev. Geophys. and Space Phys.*, Vol. 12, 1974, p. 71.
52. RUSKOL, YE. L., *Izv. AN SSSR, Fizika Zemli*, No. 7, 1972, p. 99.

The Effect of Temperature and Pressure on the Distribution of Iron Group Elements Between Metal and Olivine Phases in the Process of Differentiation of Protoplanetary Material

A. P. Vinogradov, N. P. Il'yin, and L. N. Kolomeytseva
V. I. Vernadskiy Institute of Geochemistry and Analytical Chemistry Committee on Meteorites Academy of Sciences, Moscow, U.S.S.R.

The distribution patterns of Ni, Co, Mn, and Cr were studied in olivines of various origins: from meteorites (chondrites, achondrites, pallasites), which are likely analogs of the protoplanetary material, to peridotite inclusions in kimberlite pipes, which are analogs of mantle material.

According to X-ray microanalysis data, each genetic group of olivines is characterized by a specific concentration of these elements. Nickel is concentrated (up to 0.34 percent) in peridotite olivines, while manganese is concentrated in meteoritic olivines. The maximum chromium content (0.2 percent) was found in ureilites, which were formed under reducing conditions.

Experiments at pressures of 20 to 70 kbar and temperatures of 1100 to 2000°C have shown that in a mixture of olivine and Ni metal or NiO nickel enters the silicate phase (up to 4 percent), displacing Fe into the metallic phase.

Equilibrium temperatures were estimated from the Fe, Ni distribution coefficients between the metal and olivine: 1500 K for pallasites, 1600 K for olivine-bronzite H6 chondrites, 1200 K for olivine-hypersthene L6, 900 K for LL6, and 1900 K for ureilites (at P = 1 atm). The equilibrium conditions of peridotites are close to T = 1800 K and P over 100 kbar.

The distribution patterns of the transition elements are explained on the basis of physical-chemical properties. It is concluded that there is a sharp difference between the conditions of differentiation of the protoplanetary material at the time meteorites were formed and the conditions of differentiation of the planets into concentric layers.

It is important to study the reactions of metallic and silicate phases under conditions of varying P and T in order to analyze the process of differentiation of the protoplanetary material during the early stages of formation of the planets and asteroids after accretion. The most significant aspect of this interaction is the exchange of the transition metals, iron, nickel, cobalt, and chromium, that enter into the composition of the silicate and metallic phases in meteorites, as well as in silicate minerals of deep terrestrial and lunar rocks.

The transition metals of the iron group are characterized by variable valence states, due to structural features of their electron shells. Changes in valence and, consequently, the appearance of lithophilic, siderophilic,

Table 1.—*Transition Metal Content in Olivines From Meteorites, Lunar Rocks, and Ultrabasic Terrestrial Rocks*

Samples	Number of Samples	Fe wt.%	Mn wt.%	Ni ppm	Cr ppm	Co ppm
Pallasites	8	8.4–9.8	0.16–0.28	50	160–200	40
H6 Olivine-Bronzite	3	13.6–15.0	0.33–0.35	90	110	30
Olivine-Hypersthene						
L 6	4	17.1–18.0	0.36–0.38	70	210–290	30
LL 6	2	20.9–21.8	0.40–0.42	70	380–410	40
Ureilites	1	17.5	0.35	70	2000	40
Chassignites	1	24.2	0.43	300	250	60
Nakhlites	1	37.4	0.49	80	150	80
Lunar Regolith	3					
Peridotites			0.19–0.26	40	280–470	40
Inclusions in Kimberlite Pipes	15	5.2–6.2	0.06–0.08	2800–3400	40	40–90
Alpine-Type Ultrabasites	4	5.5–6.5	0.08–0.09	2600–3000	30	70–90

and chalcophilic properties in these elements are in conformance with the conditions of mineral formation. The equilibrium constants for the distribution of transition metals between the silicate and metallic phases depend on the temperature of the process, as well as on the pressure, as is indicated by significant volumetric effects when cations in the olivine structure are replaced by transition metals.

Attempts to calculate the conditions of equilibrium in meteorites using the distribution of iron and nickel between the silicate and metal phases in meteorites have been previously attempted (refs. 1 and 2). However, the authors did the calculations using excessive nickel contents for the silicate phase of the meteorites and, in addition, they used experimental equilibrium constants determined for the metal-pyroxene reaction. Therefore, they obtained equilibrium conditions in meteorites corresponding to a temperature of 2000 K and a pressure on the order of 100 kbar. Such parameters cannot be acknowledged to be real for the parent bodies of meteorites. In this work the task is to define more precisely the content of transition metal trace elements in olivine meteorites, to compare olivines of different origins, to conduct an experimental study of the distribution of these elements between the metal and olivine phases, and to model the processes of differentiation at various pressures and temperatures. Based on the chondrite model of the mantle of the Earth proposed by Vinogradov (ref. 3), the main comparison has been drawn between meteorites, which are most likely similar to the primary matter of the protoplanetary nebula, and peridotites from kimberlite pipes, which are assumed to be analogs of mantle material. For a comparison of the processes taking place under the conditions of the Earth and bodies of smaller sizes such as the Moon and asteroids, samples of lunar rocks and achondrites also were studied. All samples were analyzed in an X-ray microanalyzer under identical conditions and using single standards.

Samples Studied and the Analytical Procedure

In order to perform the tasks set forth, 42 samples were analyzed: eight pallasites; nine olivine-hypersthene and olivine-bronzite chondrites; three achondrites; 15 garnet and spinel peridotites from the Mir, Udachnaya vostochnaya, Dama, Novinka, and Obnazhyennaya kimberlite pipes; and four terrestrial harzburgites and three olivines from the lunar regolith (Luna 16).

Sample preparation for the majority of samples, excluding the chondrites and achondrites, consisted of selecting a monomineralic fraction mounted in epoxy resin, with subsequent sectioning and polishing of the minerals. Polishing was done only with diamond powder. The usual crystal dimensions were from 30 to 40 μ for lunar and chondrite olivines and up to 2 to 3 mm for ultrabasic rocks.

Olivines from the Pavlodar and Mar'yalakhti pallasites, as well as olivines from peridotites, were used as standards.

The standard samples were prepared particularly carefully. A portion of the crystals analyzed for uniformity was then used for chemical analysis of the content of trace elements. Analysis of the standard samples was carried out by several methods. Initially, iron, manganese, nickel, chromium, and cobalt were determined by the method of total silicate analysis of homogenized samples. Subsequently, the same elements were determined on 20- to 30-mg samples by atomic absorption spectrophotometry. In addition, the nickel and cobalt concentrations were precisely determined, by highly sensitive methods, using special methods of organic solvent extraction (ref. 4) of nickel with α-furyl-dioxime and cobalt with β-nitroso-α-naphthol.

Determination of the concentrations of Ni, Cr, Mn, and Co, as well as iron, in the olivines was carried out by X-ray spectral microanalysis using an XMA–5V microanalyzer. A previously developed method of trace element analysis, with increased sensitivity of determination of these elements, was used. The limits of detection for Ni and Mn were 10 ppm and, for Cr and Co, 20 ppm at the 3-sigma level.

Counting times for one measurement of line intensity and background was 1 to 2 min. At least five points in each microregion, 200 to 300 μm in size, were analyzed: for chondrites and lunar olivines the microregion was 30 to 50 μm. In this manner a statistically significant number of measured counts (3 000 to 10 000 counts) was collected in one olivine grain. For each sample the number of olivine grains was usually 3 to 5; it was 10 in some cases, such as in analyses of cobalt and nickel in pallasites and chondrites. The values presented in the tables are averages of 30 to 50 determinations of a given element in each sample. Analysis for uniformity showed that for the majority of samples the deviation from the mean was within the limits of statistical error, 2 to 3 percent for terrestrial samples and pallasites, 5 to 6 percent for lunar olivines and achondrites, 3 to 5 percent for the chondrites, and up to 5 percent for synthetic samples.

Results for Natural Olivines

The concentrations of the transition elements, iron, nickel, cobalt, manganese, and chromium in olivines of different origins are presented in table 1.

Within each of the groups studied there are no sharp differences in trace elements contents. All groups, with the exception of the achondrites and lunar regolith, are quite uniform in trace element contents. Small differences in concentrations are practically within the maximum permissible error of measurement. The variations observed in manganese contents are regular, as is nickel within the peridotite group.

The observed similarities in content of transition trace elements is evidence of the genetic similarities of the samples within each of the groups analyzed.

A completely different picture emerges on comparison of olivines from different genetic groups. As seen from table 1, the quantity

Table 2.—*Scheme for the Two-Stage Olivine Synthesis*

Apparatus	Initial Charge	Synthesis Conditions P(kbar)	T(°C)	(min)	Processes	Mineral	Natural Analog
High-frequency heating unit	Oxide mixture	10^{-3}	1600–1900	10	Melting and crystallization	Olivine (1)	Olivines of pallasites
Modified Bridgman anvil-type high-pressure unit	Olivine (1) + Ni or NiO	20–70	1100 1500 2000	30–50	Recrystallization	Olivine (2)	Olivines of the Earth's mantle

NOTES: (1) Synthetic olivine not containing Ni (<0.004 percent).
(2) Olivine synthesized from olivine (1) plus nickel.

of trace elements changes regularly when going from one group of samples to another. Thus, the greatest concentrations of manganese are in olivines from achondrites and chondrites (up to 0.42 percent) in olivine-hypesthene chondrites and up to 0.49 percent in achondrite-nakhlites). The lowest Mn content is observed in ultrabasic terrestrial rocks, especially in peridotite inclusions in kimberlite pipes (up to 0.06 percent).

In contrast to manganese, nickel is concentrated in deep terrestrial rocks—up to 0.34 percent in olivines from peridotites—and its content is almost two orders of magnitude less in pallasite olivine (40 ppm). Low nickel concentrations are found in olivines of the lunar rocks (30 to 50 ppm).

The behavior of chromium is quite convincing: its maximum concentrations were measured in carbon- and diamond-containing achondrites (up to 0.2 percent in ureilites). The chromium content is considerable in olivines from lunar mare rocks and chondrites.

Samples of different origin differ little from one another in cobalt content. Some increase in cobalt concentrations is noted in ultrabasic terrestrial rocks and in achondrite-nakhlites. Iron is one of the principal major elements in olivines, but it does not have typical concentrations for each group. There is only a general increase of this element in going from ultrabasic terrestrial rocks · to chondrites and achondrites.

Experimental Investigation of the Distribution of Elements Between Metal and Olivine Phases at High Pressures and Temperatures

To confirm the regularities found in analysis of natural samples, experiments were performed to model the interaction of metal and olivine phases under conditions of changing *P* and *T*. Olivines were synthesized by a two-stage method (table 2). Initially, impurity-free ferromagnesian olivine were synthesized in a high-frequency heating unit. Mixtures of oxides were placed in a container, and the heater was a graphite ring in a high-frequency field. The experiments were carried out in a nitrogen atmosphere. Subsequently, the metal and olivine phases were reacted at pressures from 20 to 70 kbar and temperatures of 1100 to 2000° C in a modified "Bridgman anvil" type of unit. Mixtures used for the experiment consisted of the previously prepared, impurity-free olivine and metallic nickel or nickel monoxide. Nickel was used as the reagent for carrying out the exchange reaction.

$$\mathrm{Me} + (\mathrm{Mg, Fe})\ \mathrm{Si_{0.5}O_2} = \mathrm{Fe} + (\mathrm{Mg, Me})\ \mathrm{Si_{0.5}O_2}$$

Nickel was chosen because, of all the transition metals, it especially produces appreciable concentrations in the metallic phase of mete-

Table 3.—*Dependance of the Composition of the Products of the Exchange Reaction of the Conditions of the Synthesis*

Synthesis P(kbar)	Conditions T(°C)	Initial charge	Composition of the Products Olivine Fe wt %	Olivine Ni wt %	Ni-Fe alloy Fe wt %	Ni wt %
20		Olivine with 5.5-wt %	5.4	0.016	2.1	97.8
50	1100	iron	5.2	0.018	3.6	96.1
70		Metallic nickel constitutes	3.8	0.021	4.0	95.9
		5.5-wt % of weight of				
20		entire charge	3.5	0.041	5.0	94.8
50	1500		3.1	0.072	5.9	94.1
70			2.8	0.110	6.2	93.4
20		Oilvine with 11-wt %	7.6	0.410	3.0	96.1
50	2000	metallic nickel (5.5 per-	6.7	0.542	4.0	94.6
70		cent of charge weight)	5.1	0.621	10.6	88.1
20		Olivine with 11-wt % iron	6.9	2.211	2.3	97.1
50	2000	Nickel monoxide consti-	5.5	2.902	3.2	95.6
70		tutes 7.0 percent of	4.2	3.846	Finely dispersed	
		weight of entire charge			phase not	
					analyzed	

orites and in meteorite and terrestrial silicates. In addition, the calculated volumetric effect for the substitution of iron in the olivine structure by other transition metals is at a maximum, in absolute value for nickel: − 1.4 cm³/mole, compared with − 0.39 for cobalt and + 0.85 for manganese.

The ratios of the metallic and silicate portions were selected based on the composition of pallasite. Thus, metallic nickel was 5.5 wt %, which corresponds to the second group of pallasites in the classification of Yavnel' (ref. 5). When nickel was incorporated in the mixture in the oxide form, the amount of nickel monoxide was 7 wt %. Evaluation of the experimental conditions showed that the error in determination of pressure in the reaction chamber is not over 10 percent of the nominal value at temperatures from 1100 to 1500° C. The temperatures were measured with a tungsten-rhenium thermocouple, and the accuracy of determination of sample temperature was ± 20° C, with allowance for thermal gradients in the chamber. The oxidation-reduction conditions in the chamber were estimated indirectly from the reaction minerals present at the boundary with the graphite container (iron carbides and pyroxenes), which were determined by X-ray diffraction and X-ray spectral microanalysis. This is evidence that oxygen was removed from the system and, consequently, that the conditions in the synthesis were reducing.

Microanalysis of the synthesized olivines demonstrated their uniformity (coefficient of variation is not over 5 percent), indicating achievement of equilibrium in the system.

Study of the distribution of iron and nickel in the olivine-metal system in synthetic samples at temperatures from 1100 to 2000° C and pressures up to 70 kbar has shown that the nickel content in olivine increases with increasing pressure. Thus, with increasing pressure (from 20 to 70 kbar at 1500° C), the content of nickel in olivine increases from 0.04 to 0.11 wt % (see table

3). With increasing temperature to 2000° C, the nickel concentration in olivine increases from 0.41 to 0.62 wt % at a similar increase in pressure. At low temperatures (1100° C) diffusion processes are hampered, and the trace element content in olivine increases negligibly (from 0.016 to 0.021 wt %).

The content of oxygen in the system strongly affects the course of the exchange reaction. In experiments where nickel was incorporated into the reaction mixture in the form of the monoxide, the olivines obtained were strongly enriched in nickel (up to 3.85 wt %), which is never encountered in nature. The highest concentration of iron in the melt has been found in samples subjected to pressures of 70 kbar (up to 10.6 percent at $T = 2000°$ C).

In scanning photos of samples synthesized at $T = 2000°$ C and pressures of 20 kbar (fig. 1) and 70 kbar (fig. 2), it is evident that in the exchange reaction between metallic and olivine phases, iron in the olivine is replaced by nickel. In this case, the iron forms an alloy with unreacted nickel.

In scanning photos using reflected electrons (figs. 1a and 2a), white drops of metal of different sizes stand out from the light gray background of the silicate portion. In photos using the characteristic X-rays of nickel and iron (figs. 1 and 2), it is seen that the metal drops are a nickel-iron alloy.

Photos in the characteristic X-rays of silicon (fig. 1c) and magnesium (fig. 2c) confirm the absence of silicate inclusions in the metallic phase. The scanning photos (figs. 1b and 2b) show that nickel is distributed through the entire silicate portion of the samples, which is evidence of the completeness of the nickel-ferromagnesian olivine exchange reaction, both in the case where the reagent was nickel monoxide and in the case where metallic nickel was used. This is evidence of the possibility that the exchange reaction occurs without additional amounts of oxygen.

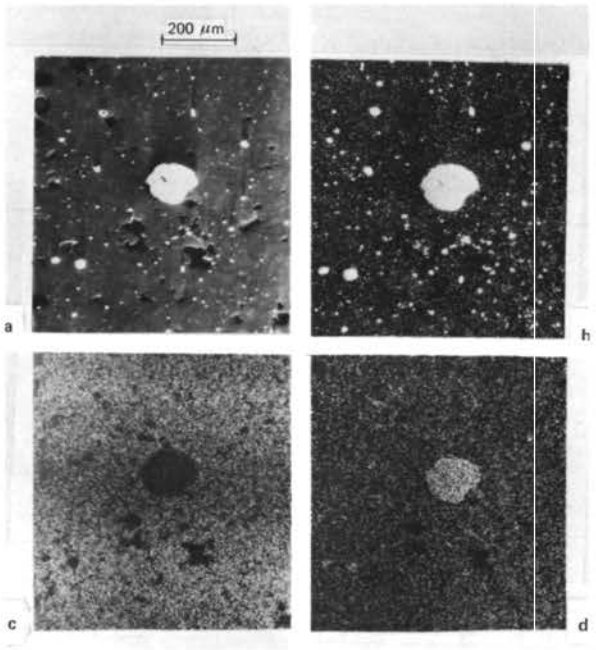


Figure 1.—*Scanning photographs of synthetic sample, produced at* T = *2000° C and* P = *20 kbar (starting materials were olivine + NiO): (a) in reflected electrons; (b) in characteristic* Ni_{K_a} *X-radiation; (c) in characteristic* Si_{K_a} *X-radiation; and (d) in characteristic* Fe_{K_a} *X-radiation.*

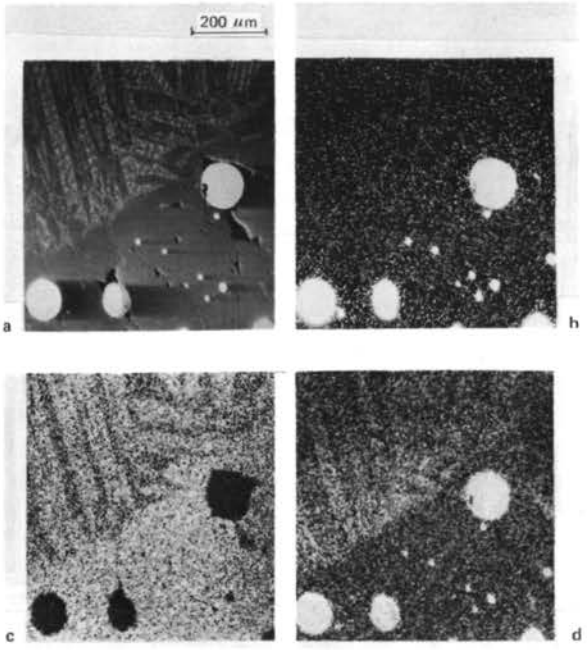


Figure 2.—*Scanning photographs of synthetic samples, produced at* T = *2000° C and* P = *70 kbar (starting materials were olivine + Ni): (a) in reflected electrons; (b) in characteristic* Ni_{K_a} *X-radiation; (c) in characteristic* Mg_{K_a} *X-radiation; and (d) in characteristic* Fe_{K_a} *X-radiation.*

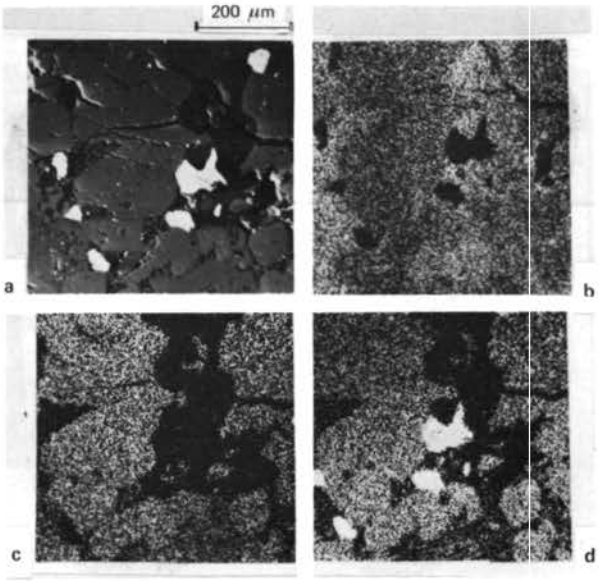


Figure 3.—*Image of Nikol'skoye chondrite structure before the experiment: (a) in reflected electrons; (b) in characteristic Si_{K_a} X-radiation; (c) in characteristic Mg_{K_a} X-radiation; and (d) in characteristic Fe_{K_a} X-radiation.*

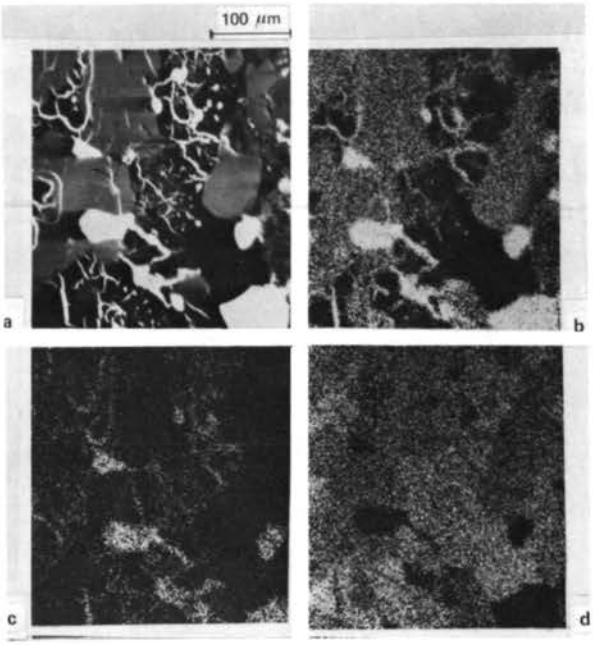


Figure 4.—*Image of Nikol'skoye chondrite structure after the experiment* (T = *1500°C and* P = *70 kbar): (a) in reflected electrons; (b) in characteristic Fe_{K_a} X-radiation; (c)in characteristic Ni_{K_a} X-radiation; and (d) in characteristic Si_{K_a} X-radiation.*

Besides the tests with synthetic mixtures, chondrite material was used to model the differentiation processes in the mantle of the Earth. Olivine-hypersthene (Kaande) and olivine-bronzite (Nikol'skoye) chondrites were held at pressures from 60 to 150 kbar and temperatures of 1000 to 1500° C. Comparison of the scanning images of the microstructure of the chondrites before and after the experiment (fig. 3) shows that a great change took place in the meteorite structure. In the scanning photos, traces of metal flowage are seen (fig. 4), and emulsion structures of sulfides and nickel iron are frequently observed on rapid cooling (fig. 5).

Interesting results were obtained by holding the Kaande chondrite at a pressure of 150 kbar and $T = 1000°$ C for a period of 10 min. Diamond was formed from the graphite that diffused into the chondrite material from the reaction chamber, with the metallic phase of the chondrite serving as a catalyst for the process. Changes occurred in the olivine composition: the amount of nickel increased and the manganese content

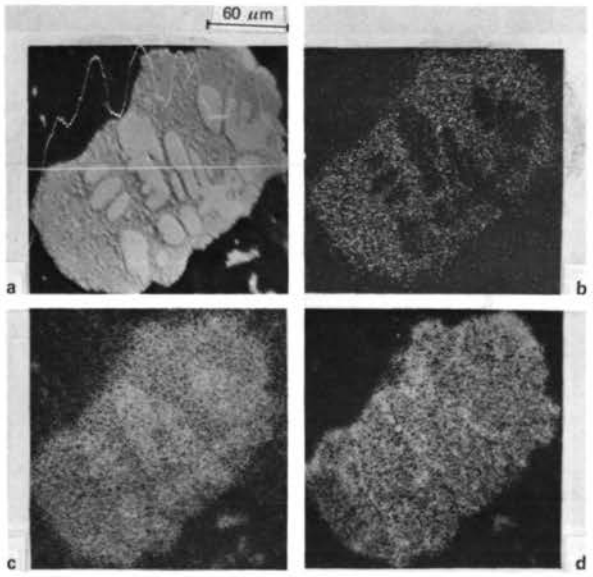


Figure 5.—*Image of Kaande chondrite structure after the experiment* (T = *1100°C and* P = *150 kbar): (a) in reflected electrons; (b) in characteristic Si_{K_a} X-radiation; (c) in characteristic Fe_{K_a} X-radiation; and (d) in characteristic Ni_{K_a} X-radiation.*

decreased somewhat, but all these processes are negligible, most likely because the low temperature restricted diffusion.

The experimentally confirmed tendency of nickel to enter into the olivine structure at high pressures allows calculation of the metal-olivine phase equilibrium conditions, not only for pallasites, chondrites, and achondrites, but also for rocks of the Earth's mantle.

Calculation of Equilibrium Conditions for the Metal-Olivine System in Natural Materials

On the basis of data on the content of trace elements in olivines as well as data on the composition of the metallic phase, one can calculate the equilibrium constant for exchange reactions of the type

$$\mathrm{Me} + (\mathrm{Mg, Fe})\mathrm{Si}_{0.5}\mathrm{O}_2 = \mathrm{Fe} + (\mathrm{Mg, Me})\mathrm{Si}_{0.5}\mathrm{O}_2 \qquad (1)$$

where iron group elements are the metal which is isomorphically replacing iron in olivine and forming solid solutions with iron in the metallic phase of meteorites. The equilibrium constant is shown below

$$K = \frac{(\gamma_{\mathrm{Fe}}^{\mathrm{alloy}})(X_{\mathrm{Fe}}^{\mathrm{alloy}})(\gamma_{\mathrm{MeSi}_{0.5}\mathrm{O}_2}^{\mathrm{olivine}})(X_{\mathrm{MeSi}_{0.5}\mathrm{O}_2}^{\mathrm{olivine}})}{(\gamma_{\mathrm{Me}}^{\mathrm{alloy}})(X_{\mathrm{Me}}^{\mathrm{alloy}})(\gamma_{\mathrm{FeSi}_{0.5}\mathrm{O}_2}^{\mathrm{olivine}})(X_{\mathrm{FeSi}_{0.5}\mathrm{O}_2}^{\mathrm{olivine}})}$$

where $\gamma_{\mathrm{Fe}}^{\mathrm{alloy}}$ and $\gamma_{\mathrm{FeSi}_{0.5}\mathrm{O}_2}^{\mathrm{olivine}}$ are the activity coefficients of a given component in the metallic and olivine phases, respectively, and $X_{\mathrm{Fe}}^{\mathrm{alloy}}$ and $X_{\mathrm{FeSi}_{0.5}\mathrm{O}_2}^{\mathrm{olivine}}$ are the mole fractions of the components.

It is known that iron-magnesium, iron-nickel, and magnesium-nickel olivines, as well as iron-nickel binary solid solutions, differ little from ideal solid solutions at temperatures of about 1000° C and above. There-

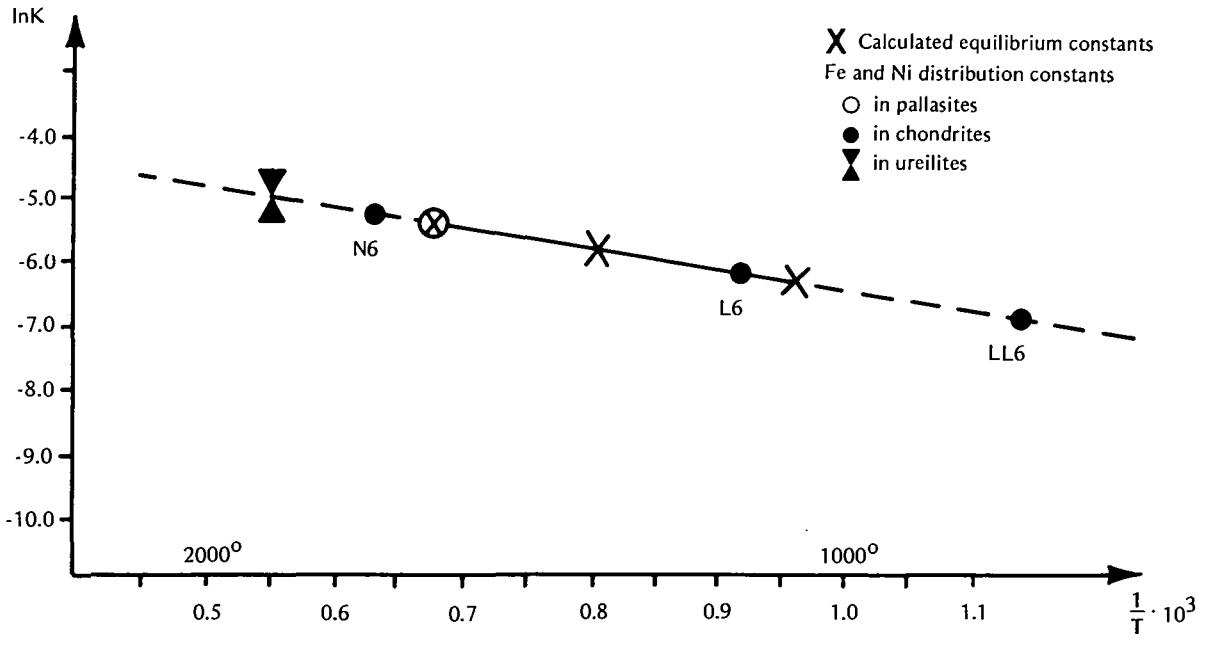


Figure 6.—*Equilibrium constants versus temperature for reaction* $Ni + FeSi_{0.5}O_4 = Fe + NiSi_{0.5}O_4$ *(at* P = *1 atm).*

fore, using methods of calculation for ideal solutions, the equilibrium constant can be calculated for the reaction

$$Ni + (Mg, Fe)Si_{0.5}O_2 = Fe + (Mg, Ni)Si_{0.5}O_2 \quad (2)$$

knowing only the ratio of the mole fractions of the components and taking the activity coefficients of the components in nearly ideal solid solution to be unity. Thus,

$$K = \frac{X_{Fe}^{alloy} \times X_{FeSi_{0.5}O_2}^{olivine}}{X_{Ni}^{alloy} \times X_{NiSi_{0.5}O_2}^{olivine}}$$

Using the thermochemical data presented in references 6 and 7, we calculated the values of the free energy of the exchange reaction at temperatures from 1100 to 1500 K, as well as the equilibrium constants of this reaction. On the basis of the calculations, a graph was plotted of the logarithm of the equilibrium constant versus temperature (fig. 6). The distribution coefficients for iron and nickel between the metallic and olivine phases were plotted on this graph for pallasites, ureilites, and chondrites of groups H6, L6, and LL6, as calculated from the analytical data in this paper. As is seen, the distribution factors for pallasites and chondrites of groups H6 and L6 fit well in this temperature range.

For all the pallasites studied, the equilibrium temperatures are close together and correspond to a temperature of 1500 K (at a pressure of 1 atm). In group H6 chondrites the equilibrium between the metal and olivine phases corresponds to a temperature of 1600 K; in group L6 chondrites, the equilibrium corresponds to a temperature of 1200 K. Lower temperatures characterize the equilibrium in group LL6 chondrites (900 K), and higher temperatures, up to 1900 K, are characteristic in achondrites.

An approximate calculation of the distribution factor between olivines from ultrabasic terrestrial rocks and metal, containing 8 percent Ni on the average, gives values that differ sharply from the equilibrium constants of the reactions, as calculated for atmospheric pressure. This suggests that other factors affect the interactions of the metallic and silicate phases during early stages of formation of the Earth's mantle from chondrite material.

Shift of the metal-olivine equilibrium in the direction of formation of olivines with a high nickel content may be due to two factors besides temperature, i.e., total pressure and the oxygen fugacity in the system. However, there is not sufficiently reliable information at the present time on the fugacity of oxygen at various depths.

The effect of pressure on the distribution constant can be expressed in the following manner:

$$P'' - P' = -\frac{2.3\,RT}{\Delta V} \log \frac{K''}{K'}$$

where P'' and P' express the change in pressure and K'' and K' the change in distribution constants. In the $\sim$ 100-kbar pressure region, $P'' >> P'$, and the formula is simplified to the form:

$$P'' = -\frac{2.3\,RT}{\Delta V} \log \frac{K''}{K'}$$

Using data on the nickel and iron concentrations in olivines from peridotite inclusions in kimberlite pipes and considering the inadequacy of the oxidation-reduction conditions in different parts of the mantle, the pressure for garnet peridotites can be estimated (at a temperature of 1800° C) to be approximately 100 kbar.

Conclusions and Discussion of Results

The data obtained allow determination of the relationship between the trace element content in olivines and the conditions of formation of rocks containing these minerals.

The highest concentrations of nickel and lowest concentrations of manganese are observed in the deepest rocks, garnet peridotites, which are characterized by maximum pressures and high temperatures of formation. In proportion to decreasing pressure in the series of mantle inclusions—achondrites, lunar rocks, chondrites—there occurs a de-

crease in the amount of nickel and an increase in the amount of manganese.

Chromium does not follow the regularities noted for nickel and manganese. Its maximum concentration is found in olivines from carbon- and diamond-containing achondrites and lunar soil.

High chromium content in lunar olivines also has been noted in work (ref. 8). The Cr_2O_3 concentration (up to 0.4 percent) of lunar olivines exceeds even that of olivines included in diamonds from kimberlite pipes (up to 0.06 to 0.09 percent) (refs. 9 and 10).

A sharp increase in chromium concentration, under conditions known to be reducing, is evidence that this element can be used as an indicator of the oxidation-reduction conditions of mineral formation.

Variations in the measured cobalt concentrations in meteorite and mantle olivines are negligible and cannot be considered as reliable indicators of the formation conditions.

The behavior of iron is also very nonunique in conformance with the diversity of factors which can change the concentrations of this macrocomponent. According to a large amount of experimental data, there is a strong dependence of the iron content in olivine on oxidation-reduction conditions, pressure, and temperature of the process.

Earlier, Vinogradov (ref. 11) examined the question of the cause of differentiation of trace elements between the metal and oxide phases in the protoplanetary cloud. It was shown that elements whose oxygen partial pressure of the reversible equilibrium of metal with the oxide is lower than in the Fe-FeO system at the melting temperature of iron (1803 K) can be oxidized to an oxide and do not dissolve in the metallic Fe-Ni phase. Manganese and chromium are among these elements. Chemical elements requiring higher oxygen partial pressures (P_{O_2}) for their oxidation will remain predominantly in the metallic phase. Nickel and cobalt are among these elements. Thus, at an early stage of differentiation of the protoplanetary material, oxidation-reduction conditions played a decisive part, and maximum concentrations of Mn and Cr, with minimum Ni and Co contents, were actually observed in the olivines of chondrites which are analogs of the primary material.

Subsequent differentiation in solid bodies is caused by a set of physical-chemical factors whose roles are still difficult to distinguish. Attention should be given first to the specific physical-chemical properties of the transition elements of the iron group. The main feature of these elements is variable valence. Change in valence of the transition metals depends on the ratio of the values of the successive ionization potentials. For chemical elements with comparatively low ionization potentials such as the transition elements, a small increase in temperature leads to a transition to a more highly ionized state, i.e., to an increase in valence. This concerns Fe and Cr first of all, because the low values of the first, second, and third ionization potentials, as well as the differences between them, are characteristic (the difference between the second and third ionization potentials for iron and chromium are minimal, 14.66 and 14.51 eV, respectively).

With change in oxidation-reduction conditions or temperature fluctuations, Fe and Cr will first change valence and move from one phase (mineral) to another, as shown for example by the increase in valence of these elements in the series metal-silicate-chromium spinel. Therefore, Cr and Fe can serve as indicators of the temperature and oxidation-reduction conditions.

For transitions of Ni and Mn to higher valence states, considerably more additional energy of ionization is required, 18.01 and 18.05 eV, respectively, and for Co, 16.44 eV. It can be assumed that their differentiation among phases is determined by other factors. In addition to the effect of the oxygen partial pressure (P_{O_2}) already noted, one such factor is the volumetric effect of the substitution reaction.

It is evident from table 4 that the greatest volume gain occurs for the substitution of manganese for iron in the olivine structure; that the least effect is observed for substitution by Ni; and that there is very little effect for Co. The substitution of Mn for Fe is posi-

Table 4.—*Volumetric Effects of Substitution Reaction*

Reaction	$Me + MgSi_{0.5}O_2 = Mg + MeSi_{0.5}O_2$	$Me + FeSi_{0.5}O_2 = Fe + MeSi_{0.5}O_2$
Metal	$\Delta V \frac{cm^3}{mole}$	$\Delta V \frac{cm^3}{mole}$
Mn	+ 9.06	+ 0.85
Fe	+ 8.21	—
Co	+ 7.82	− 0.39
Ni	+ 7.77	− 1.44
Mg	—	− 8.21

tive, i.e., it leads to an increase in volume of the olivine unit cell by expanding of the crystal structure.

In this manner one may use the physical-chemical factors considered to qualitatively explain the regularities of distribution of the transition elements Fe, Ni, Co, Cr, and Mn between metal and silicate phases established in this work; that is, increasing Ni and decreasing Mn contents in olivines from rock formed at high pressures and the concentration of Cr in rocks formed under reducing conditions.

Comparison of the analytical data of iron group transition element content in olivines of various origins, with the experimental results of modeling the interactions of the "metal-olivine" phases under conditions of high pressure and temperature as well as with thermodynamic calculations, permits the very specific conclusion that there is a sharp difference between the conditions of differentiation of the protoplanetary material during the formation of meteorites and asteroids and the conditions of differentiation of the planets and the Moon into concentric layers.

References

1. BROWN, H. AND C. PATTERSON, The Composition of Meteoritic Matter, 3; Phase Equilibria, Genetic Relationship and Planet Structure. *J. Geol.*, Vol. 56, No. 2, 1948.
2. LOVERING, J., Pressures and Temperatures within a Typical Parent Meteorite Body. *J. Geol.*, Vol. 12, No. 3, 1957.
3. VINOGRADOV, A. P., Origin of the Material of the Earth's Crust. *Geokhimiya*, Vol. 1, 1961.
4. PESHKOVA, V. M., V. M. BOCHKOVA AND L. I. LAZAREVA, Spectrophotometric Determination of Traces of Pure Nickel in Pure Indium and Aluminum. *Zhurn. Anal. Khim.* Vol. 15, 1960, p. 610.
5. YAVNEL', A. A., Classification of Meteorites by Composition. *Meteorities*, Vol. 15, 1958.
6. CAMPBELL, F. AND R. ROEDER, The Stability of Olivine and Pyroxene in the Ni-Mg-Si-O System. *Am. Mineralogist*, Vol. 53, 1968, pp. 1–2.
7. WILLIAMS, R., Reaction Constants in the System $Fe\text{-}MgO\text{-}SiO_2\text{-}O_2$ at 1 atm between 900 and 1300°C: Experimental Results. *Am. J. Sci.* Vol. 270 No. 5, 1971.
8. HAGGERTY, S. et al., Opaque Minerals and Olivine in Lavas and Breccias from Mare Tranquillitatis. *Geochimica et Cosmochimica Acta*, Supplement 1, Vol. 1, 1970.
9. SOBOLEV, N. V., Z. V. BARTOSHINSKIY, E. S. YEFIMOVA, YU. G. LAVRENT'YEV AND L. N. POSPILOVA, Olivine-Garnet-Chromium Diopside Association From a Yakut Diamond. *Dokl. Akad. Sci SSSR*, Vol. 192, No. 6, 1970.
10. MEYER, H. O. AND F. R. BOYD, Composition and Origin of Crystalline Inclusions in Natural Diamonds. *Dokl. Sci. Akad. SSSR*, Vol. 36, No. 11, 1972.
11. VINOGRADOV, A. P., High Temperature Protoplanetary Processes. *Geokhimiya* Vol. 11, 1971.

Page intentionally left blank

Page intentionally left blank

The Chemical Composition of the Cores of the Terrestrial Planets and the Moon

O. L. Kuskov and N. I. Khitarov
V. I. Vernadsky Institute of Geochemistry and Analytical Chemistry Academy of Sciences, Moscow, U.S.S.R.

Using models of the quasi-chemical theory of solutions, the activity coefficients of silicon are calculated in the melts Fe-Si, Ni-Si, and Fe-Ni-Si. The calculated free energies of solution of liquid nickel and silicon in liquid iron in the interval 0 to 1400 kbar and 1500 to 4000 K, shows that Fe-Ni-Si alloy is stable under the conditions of the outer core of the Earth and the cores of the terrestrial planets. The oxidation-reduction conditions are studied, and the fugacity of oxygen in the mantles of the planets and at the core-mantle boundary are calculated. The mechanism of reduction of silicon is analyzed over a broad interval of P and T. The interaction between the matter of the core and mantle is studied, resulting in the extraction of silicon from the mantle and its solution in the material of the core. It is concluded that silicon can enter into the composition of the outer core of the Earth and Venus, but probably does not enter into the composition of the cores of Mercury, Mars, and the Moon, if in fact the latter possesses one.

The question of the composition and mechanism of formation of the cores of the Earth and the terrestrial planets is still open. Among the various approaches to the solution of this problem, one of the most significant is analysis of a number of processes from the physical-chemical standpoint. In the first approximation they can be reduced to the following questions: (1) what were the redox conditions in the protoplanetary cloud; (2) what are the redox conditions in the mantle and at the core-mantle boundary; (3) what is the possibility of formation of alloys of iron with other chemical elements upon condensation from the protoplanetary cloud; (4) what is the possibility of solution of chemical elements in the liquid iron core; and (5) what is the possibility that equilibrium exists between the core and mantle.

The experimental data currently available allow sufficiently accurate calculation of processes occurring under the P–T conditions corresponding to the interior of the Earth.

After experimental studies (refs. 1 and 2) on the dynamic compressibility of iron-nickel alloy confirmed the hypothesis of Birch (ref. 3) about the inconsistency of the concepts of formation of a core of this composition, it became conclusively clear that in addition to the basic iron-nickel components the core contains other, lighter substances which reduce its density by 10 to 20 percent in comparison to the density of nickel-containing iron under the same conditions.

MacDonald and Knopoff (ref. 4) and Ringwood (ref. 5) suggested that such substance might be silicon.

It is the purpose of the present work to analyze the following problems: (1) the possibility of solution of silicon and nickel in liquid iron over a broad interval of P and T; (2) the mechanism for inclusion of silicon in the cores of the planets due to its reduction in the mantle; and (3) the mechanism

for inclusion of silicon in the cores of the planets due to interaction between the material of the core and mantle.

Solubility of Silicon and Nickel in Liquid Iron

Information on the inclusion of impurities in the core can be produced by calculating the free energy of solution of a chemical element or compound in liquid iron, which consists of the free energy of the process at a constant temperature and the contribution of high pressure:

$$\Delta G_T^P = G_T^\circ + \int_0^P \Delta V dP$$

The first term in the right-hand portion of the equation can be obtained experimentally or found theoretically using well-founded models of the theory of solutions. The second term is the difference between the partial molar volume of a component in a solution and the volume of the pure component at the same pressure.

THERMODYNAMIC PROPERTIES OF MELTS IN THE FE-NI-SI SYSTEM AT 1 ATM.

Metals similar in their properties to iron form nearly ideal solutions (quasi-ideal solutions) with iron.

Consider a dilute solution

$$Ni_{(l)} = [Ni] \text{ in } Fe_{(l)}$$

For one mole of dissolved material, the change in partial free energy between its initial state in the form of a pure component and its final state in the form of an ideal solution is

$$\Delta G_T^\circ \text{ soln.} = G_i - G_i^\circ = RTlna_i = RTlnX_i \quad (3)$$

where X_i is the molar fraction of the dissolved material.

The calculated values of ΔG_T° (soln.) with a content of 10 wt. % Ni in the solution are presented in table 1.

Liquid alloys of iron and silicon do not follow the regularities of ideal solutions, but are described in terms of stricter theories in which the close order, as well as the temperature and concentration dependence of the energies of the interatomic interaction, must be considered in melts (refs. 6 and 7).

The activity of silicon in melts at various temperatures has been calculated by an asymmetrical version of the quasi-chemical theory of solutions (ref. 7). The method of calculation and initial thermodynamic characteristics were described in detail in reference 8.

The activity of silicon in Fe-Si and Ni-Si melts at $X_{Si} = 0.2$, which corresponds to 11.2 wt. % Si, was calculated by two methods. In

$$\ln a_2 = \ln X_2 + 1/RTX_1^2 (X_1 \Delta\bar{G}_2^{o(E)} + X_2 \Delta\bar{G}_1^{o(E)})(1 + \eta + X_2 \frac{\partial\eta}{\partial X_2})$$

$$+ X_1^2 X_2 (1 + \eta) 1/RT (\Delta\bar{G}_1^{o(E)} - \Delta\bar{G}_2^{o(E)}) + \tfrac{1}{2} Z \left\{ \left[X_2 - X_1\eta + X_1X_2(1 + \eta \right.\right.$$

$$\left.\left. - X_1 \frac{\partial\eta}{\partial X_2}) \right] \ln \frac{X_2 - X_1\eta}{X_2} - X_1^2 (1 + \eta + X_2 \frac{\partial\eta}{\partial X_2}) \ln \frac{X_1 - X_2\eta}{X_1} \right.$$

$$\left. + 2X_1^2 (1 + \eta) \ln(1 + \eta) + 2X_1^2 X_2 \frac{\partial\eta}{\partial X_2} \ln(1 + \eta) \right\} \quad ; \quad (5)$$

$$\frac{\partial\eta}{\partial X_1} = -\frac{\partial\eta}{\partial X_2} = \frac{1 + \eta}{1 - \eta} \left\{ \frac{\eta\ (X_2 - X_1)}{X_1X_2} + \frac{2(\Delta\bar{G}_2^{o\,(E)} - \Delta\bar{G}_1^{o\,(E)})}{ZRT} \right.$$

$$\left. \times \left[\eta - X_1X_2(1 + \eta)^2 \right] \right\}. \quad (6)$$

the first case, calculations were made using the equation

$$\ln a_2 = \frac{X_1 Q_{12}(1+\eta)}{RT(1-\eta)}$$
$$(X_1 - X_{2\eta}) + \ln X_2 + \tfrac{1}{2}Z\ln\left[\frac{X_2 - X_1\eta}{X_2}\right] +$$
$$+ \tfrac{1}{2}ZX_1(X_1 - X_{2\eta})\left(\frac{1+\eta}{1-\eta}\right)$$
$$\ln\frac{X_1X_2(1+\eta)^2}{(X_1 - X_{2\eta})(X_2 - X_1\eta)}, \qquad (4)$$

where η is the close order parameter; $Q'_{12} = Q_{12} + (ZRT\ln 2)/2$ takes into account the dependence of mixing energy on temperature, where

$$-Q_{12} = \Delta\bar{H}^{\circ}_1 + qX_1 = -\Delta\bar{H}^{\circ}_2 - qX_2,$$
$$q = \Delta\bar{H}^{\circ}_2 - \Delta\bar{H}^{\circ}_1;\ X_1 \text{ and } X_2$$

are the molar fractions of the first and second components. In the second case, equations 5 and 6, found on the preceding page, were used.

The value of the close order parameter η, considering the deviation in distribution of atoms in a binary solution from random distribution, can be determined from the equation

$$(B-1)(1+\eta_{12})^2X_1X_2 - B\eta_{12} = 0 \qquad (7)$$

The probability parameter B was calculated by two methods:

$$B = \exp\left(-\frac{2Q_{12}}{ZRT}\right) \qquad (8)$$

and

$$B = exp\left[\frac{2(X_1\Delta\bar{G}_2^{o(E)} + X_2\Delta\bar{G}_1^{o(E)})}{ZRT}\right] \qquad (9)$$

where $\Delta G^{(E)} = \Delta G - \Delta G^{(\text{ideal})}$,

and Z is the mean coordination number.

Calculation of the averaged values of log γ_{Si} using equations (4) and (5) by the method of least squares in the interval 1500 to 4000 K leads to the following equations.

In the Fe-Si system

$$\log\gamma_{Si} = -\frac{4588}{T} + 0.656 \qquad (10)$$

In the Ni-Si system

$$\log\gamma_{Si} = -\frac{7268}{T} + 0.71 \qquad (11)$$

Let us now estimate the influence of 10 percent Ni on γ_{Si}, a_{Si}, and the free energy of solution of silicon in the ternary system Fe-Ni-Si. In the first approximation, this calculation can be expressed by the equation

$$\log\gamma_{Si}{}_{(Fe\text{-}Ni\text{-}Si)} = X_{Fe}\log\gamma_{Si}{}_{(Si\text{-}Fe)} + X_{Ni}\log\gamma_{Si}{}_{(Si\text{-}Ni)} \qquad (12)$$

Combining the earlier calculated data on γ_{Si} in liquid binary systems, we produce:

$$\log\gamma_{Si}{}_{(Si\text{-}Fe\text{-}Ni)} = -\frac{4856}{T} + 0.661 \qquad (13)$$

When 10 percent Ni is added to a melt, the values of γ_{Si} and a_{Si} decrease. However, this reduction is slight and the differences in free energies of solution of liquid silicon in liquid iron and in liquid nickel-iron are also not great, amounting to approximately 1.2 kcal through the entire temperature interval.

Calculation of the errors of thermodynamic parameters of Fe-Si, Ni-Si, and Fe-Ni-Si melts was described in an earlier work (ref. 8).

INFLUENCE OF HIGH PRESSURE ON SOLUBILITY OF NICKEL AND SILICON IN LIQUID IRON

In order to calculate the free energy of the process of solution at high pressures, information is required on the volumes of the pure liquid metals and the partial molar volumes of the metals dissolved in liquid iron.

In earlier works (refs. 1, 2, and 9 through 12), results are presented from studies of the dynamic compressibility of pure metals, iron-nickel, and iron-silicon alloys up to megabar pressures. From these data, the partial molar volumes of Ni and Si were calculated at pressures of 300, 500, 1000, and 1400 kbar (ref. 8).

The values of free energy of solution of liquid nickel (10 wt. %) and silicon ($\sim$ 10 wt. %) in liquid iron as functions of P and T are presented in table 1.

Table 1.—*Free Energies of Dissolution of Liquid Nickel (10 wt. %) and Liquid Silicon (10 wt. %) in Liquid Iron*

	$Ni_{(l)} = [Ni]$ (in $Fe_{(l)}$)					$Si_{(l)} = [Si]$ (in $FeNi_{(l)}$)				
T,K P,bar	1	3.10^5	5.10^5	10^6	$1.4.10^6$	1	3.10^5	5.10^5	10^6	$1.4.10^6$
1500	−7 000	−5 070	−5 450	1 130	3 370	−22 480	−44 060	−52 350	−76 970	−106 800
2000	−9 330	−7 400	−7 780	−1 200	1 040	−22 570	−44 150	−52 440	−77 060	−106 890
2500	−11 660	−9 730	−10 110	−3 530	−1 290	−22 660	−44 240	−52 530	−77 150	−106 980
3000	−14 000	−12 070	−12 450	−5 870	−3 630	−22 750	−44 330	−52 620	−77 240	−107 070
3500	−16 330	−14 400	−14 780	−8 200	−5 960	−22 840	−44 420	−52 710	−77 330	−107 160
4000	−18 660	−16 730	−17 110	−10 530	−8 290	−22 930	−44 510	−52 800	−77 420	−107 250

The free energy of solution of nickel decreases with increasing temperature (this follows from equation (1)), since the partial molar volume of nickel is greater than the volume of the pure element, i.e., $\Delta V > 0$. As composition changes, ΔG_T^P changes in a rather complex manner.

Figure 1 shows the change in free energy of solution of liquid nickel in liquid iron as a function of concentration of Ni at various temperatures at a constant pressure of 1400 kbar. The extremes on the curves result from the dependence of the partial molar volume of nickel in the melt on concentration of nickel. At parameters characteristic for the core-mantle boundary ($\sim$ 1400 kbar), the free energy has a minimum, indicating the stability of the Fe-Ni melt with nickel concentration $\simeq$ 10–18%.

The data produced indicate that up to pressures on the order of 500 kbar, nickel is dissolved in liquid iron at all of the temperatures studied. At pressures of 1000 to 1400 kbar, its solution is possible if the temperature is over 2000 K (table 1).

Table 2 presents certain data that allow us to judge the distribution of temperatures and pressures in the terrestrial planets and the Moon. At the core-mantle boundary of Mercury, Mars, and the Moon[1], the pressures do not exceed 300 kbar. The positive value of the contribution $\int \Delta V dP$ to the value of ΔG_T^P is not great; the free energy of solution is a negative value and nickel may therefore be included in the composition of the cores of

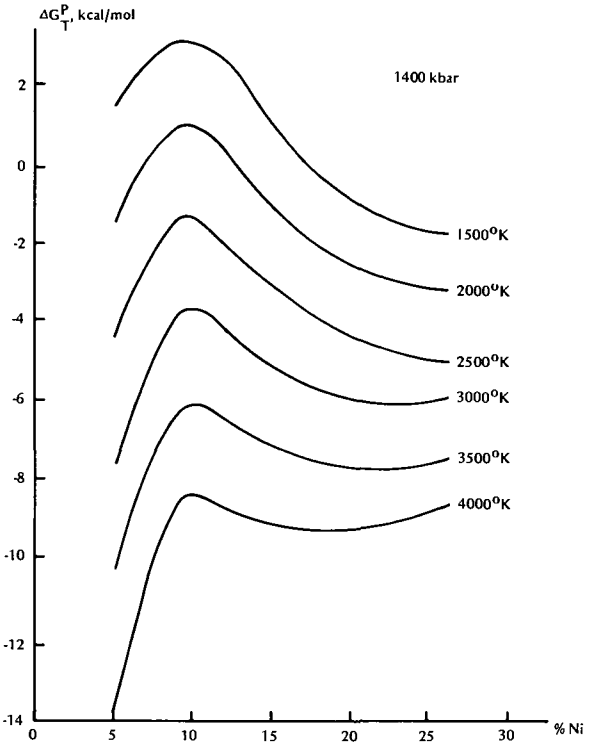


Figure 1.—*Change in free energy of solution of liquid nickel in liquid iron as a function of concentration of nickel in Fe-Ni system at 1400 kbar and various Temperatures.*

[1] It is not clear if the Moon has a core. The latest data presented at the Soviet-American Conference on the Cosmochemistry of the Moon and Planets did not clear up the question. Our calculations show that iron-nickel alloy is stable under the P–T conditions of the interior of the Moon, but they neither study nor answer the question of the existence of a core.

Table 2.—*Assumed P–T Conditions at the Core-Mantle Boundary for Earth-Type Planets*

Planet	Mean Radius of Planet (km)	Mean Radius of Core (km)	Pressure at Core-Mantle Boundary (kbar)	Temperature at Core-Mantle Boundary (K)
Mercury	2437	1700–2000	~ 100	1400–2000
Venus	6054	~ 3000	~ 1400	~ 4000
Earth	6371	3471	~ 1400	~ 4000
Mars	3386	500–1000	250–300	1000–1500
Moon	1737	200–300	~ 50	1000–1500

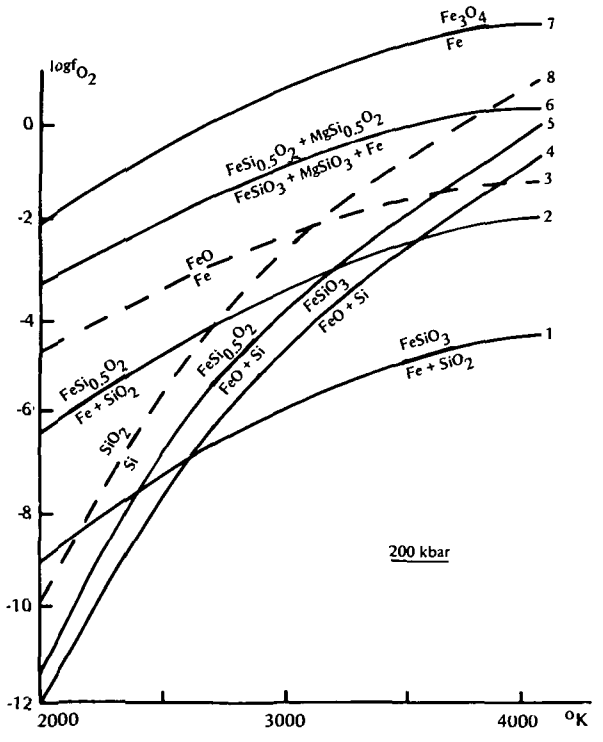


Figure 2a.—*Dependence of oxygen fugacity on temperature in the mantle of the Earth.* P = *200 kbars. Reactions:*

1. $FeSiO_3(s) = SiO_2(st.s) + Fe(l) + \frac{1}{2}O_2$
2. $FeSi_{0.5}O_2(sp.s.) = \frac{1}{2}SiO_2(st.s) + Fe(l) + \frac{1}{2}O_2$
3. $FeO(s) = Fe(l) + \frac{1}{2}O_2$
4. $FeSiO_3(s) = FeO(s) + Si(l) + O_2$
5. $FeSi_{0.5}O_2(sp.s) = FeO(s) + \frac{1}{2}Si(l) + \frac{1}{2}O_2$
6a. $FeSi_{0.5}O_2(sp.s) + MgSi_{0.5}O_2(sp.s) = MgSiO_3(s) + Fe(l) + \frac{1}{2}O_2$
6b. $2FeSi_{0.5}O_2(sp.s) = FeSiO_3(s) + Fe(l) + \frac{1}{2}O_2$
6c. $FeSi_{0.5}O_2(sp.s) + MgO(s) = MgSi_{0.5}O_2(sp.s) + Fe(l) + \frac{1}{2}O_2$
6d. $FeSiO_3(s) + MgO(s) = MgSiO_3(s) + Fe(l) + \frac{1}{2}O_2$
7. $\frac{1}{4}Fe_3O_4(s) = \frac{3}{4}Fe(l) + \frac{1}{2}O_2$
8. $SiO_2(st.s) = Si(l) + O_2$

these celestial bodies. At the core-mantle boundary of the Earth and Venus, the pressure is approximately 1400 kbar, but insofar as the temperature at the boundary is greater than 2000 K, the total change of the value $\Delta G_T^P < 0$ and Fe-Ni cores are not stable.

Thus, calculations show that Fe-Ni melts are stable in the ranges of temperatures and pressures characteristic for the terrestrial planets and the Moon.

The free energy of solution of liquid silicon and liquid iron is practically independent of temperature (due to the increase in activity), but decreases quite sharply with increasing pressure (due to high negative volume change), i.e., an increase in pressure facilitates the process of dissolution, table 1.

Calculations show that throughout the entire interval of P, T, and concentrations, the ΔG_T^P for the solution of silicon in liquid iron or nickel-iron has a large negative value. This indicates the stability of Fe-Si and Fe-Ni-Si melts under the conditions of the outer core of the Earth and the P–T conditions of the cores of terrestrial planets.

The stability of Fe-Si melts at the temperatures and pressures of the core of the Earth and the other planets is a necessary but not sufficient condition since we do not know even the principal means and mechanism of inclusion of silicon in the core. In order to understand this, we must study the redox reactions in the mantle of the Earth and the other planets.

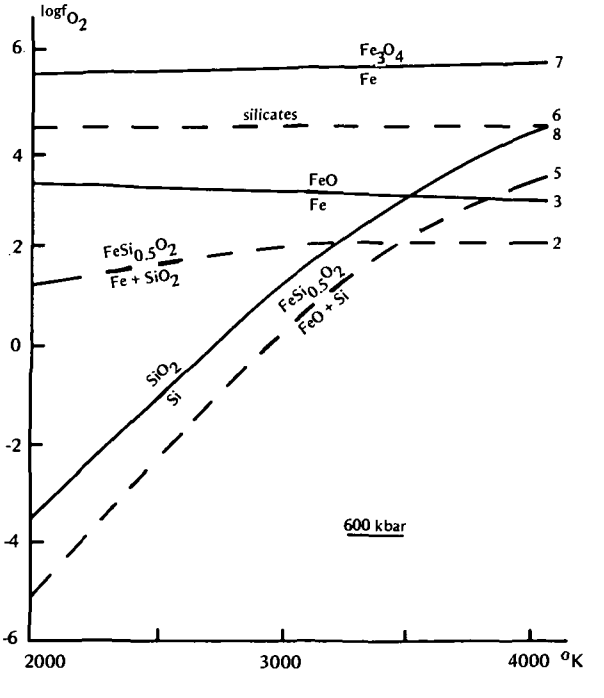


Figure 2b.—*Dependence of oxygen fugacity on temperature in the mantle of the Earth.* P = *600 kbars.*

Redox Reactions in the Interiors of Terrestrial Planets

The fugacity of gases in the mantle in the early stage of evolution of a planet (after its formation from the protoplanetary cloud, but before the descent of iron into the core) can be calculated on the basis of equilibria of metallic iron with ferromagnesium silicates and oxides. We will consider the fugacity of oxygen (f_{O_2}) as an indicator of the redox situation (refs. 13, 14, and 15).

For the reaction $aA + bB = cC + dD + O_2$, the nature of the change of fugacity as a function of phase composition, P, and T and is determined by the expression:

$$\log f_{O_2} = \log f^{o}_{O_2} + a\log a_A + b\log a_B - c\log a_C - d\log a_D - \frac{1}{2.303RT}\int_{o}^{P} \Delta V_s dP$$

where $f^{o}_{O_2}$ is the equilibrium fugacity of oxygen for a reaction in which all components are in the standard state; ΔV_s is the change in volume of the condensed phases; and a_i is the activity of the iron-containing component in the solid solution. In the calculations we assume $a_i \equiv 0.1$. All calculations were performed with consideration of compressibility data.

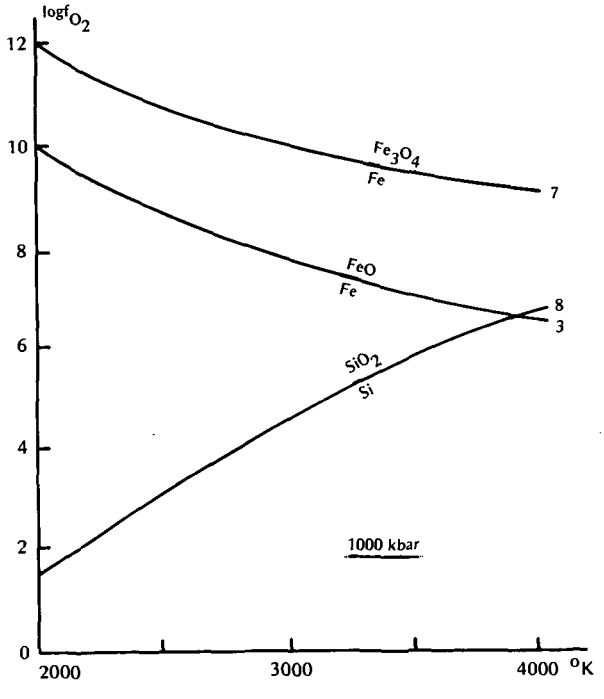


Figure 2c.—*Dependence of oxygen fugacity on temperature in the mantle of the Earth.* P = *1000 kbars.*

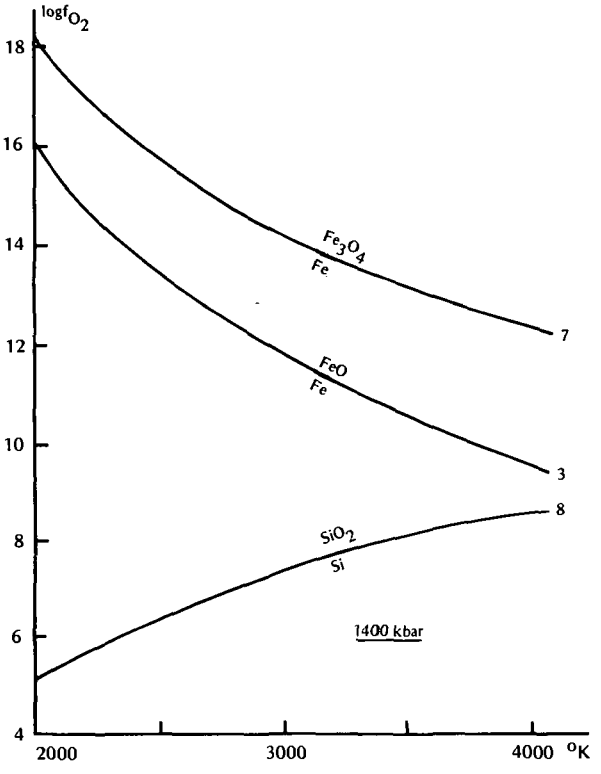


Figure 2d.—*Dependence of oxygen fugacity on temperature in the mantle of the Earth.* P = *1400 kbars.*

The results of calculating the fugacity of oxygen for a number of limiting buffer reactions in the interval 200 to 1400 kbar and 2000 to 4000 K are presented in figures 2a, 2b, 2c, and 2d.

EARTH, VENUS

Interpretation of the results of calculations is based on available information on the composition and structure of the concentric layers of the Earth, obtained from

experimental laboratory data at high pressures and seismology. Information on the structure of the other planets is quite sparse. Therefore, analogy is assumed between the chemical composition of the Earth and the terrestrial planets; it is also assumed that all planets have iron cores.

Let us study the limiting buffer reactions which controlled the fugacity of oxygen at various depths in the Earth during the early stages of its development.

At 200 kbar ($\sim$ 600 km), the lower limit of f_{O_2} was controlled by reaction (2) for reduction of spinel to Fe and stishovite (fig. 2a). At lower values of f_{O_2}, ferromagnesium silicates are reduced to Fe + SiO_2 or FeO + Si, contradictory to the seismic data which indicate that the transition layer of the mantle consists of Fe and Mg silicates.

The upper limit of f_{O_2} is probably controlled by the equilibrium of iron and magnetite, while the optimal value of f_{O_2} is that which changes according to curve (6) which reflects the Fe-Mg, silicate-Fe equilibrium and essentially combines four reactions (6a, b, c, d).

We can see from figure 2a that the reduction of liquid silicon and its formation of a melt with iron can occur under conditions corresponding to the intersection of reactions (2) and (5), i.e., at $\log f_{O_2} \geq -2.8$ and $T \geq 3200$ K.

However, these temperatures are significantly higher than the melting point of iron and of silicate matter (refs. 16, 17, and 18) and, judging from known thermal models, planetary interiors probably never reached such values. Consequently, the reduction of silicates to silicon at these depths could not have occurred.

Calculations show that the process of reduction becomes possible at pressures of over 400 kbar ($\sim$ 1000 km).

The Birch-Magnitsky hypothesis presumes that the lower mantle basically consists of the oxides FeO and MgO (NaCl-type structure) and SiO_2 (stishovite). Recently, this has been experimentally confirmed in experiments on the decomposition of Mg_2SiO_4 to periclase and stishovite at 330 kbar (ref. 19).

We can therefore accept the buffer equilibrium between stishovite and silicon as the lower limit of f_{O_2} in the lower mantle of the Earth, although we cannot exclude the possibility of conversion of the rutile-like modification of SiO_2 into the fluorite-like modification and we can accept the Fe-Fe_3O_4 equilibrium (7) as the upper limit (figs. 2b, 2c, and 2d).

The mass of the current terrestrial core is about one-third of the mass of the planet; consequently, it is obvious that the system Fe-FeO should have controlled f_{O_2} in the lower mantle of the Earth and of any other planet until the iron sank into the core. In other words, this system was responsible for the distribution of oxygen in the mantle, and all other systems were of secondary significance.

At a pressure of 600 kbar ($\sim$ 1400 km), T_m (Fe) = 3100 K (ref. 16). The reduction of stishovite becomes possible at $T \geq 3500$ K and $\log f_{O_2} \geq 3.1$ (fig. 2b). Under these conditions, liquid silicon is dissolved in the iron core forming an Fe-Si melt, which later forms the outer core. At 1000 kbar ($\sim$ 2200 km) and 1400 kbar ($\sim$ 2900 km), T_m (Fe) $\simeq$ 3600 K and 4100 K, and the reduction of silicon could have occurred at $T \geq 3900$ K and 400 K (fig. 2c, 2d). Calculations of the thermal history of the Earth show that such temperatures were reached during the first hundreds of millions of years of its evolution.

Calculations of the thermal history of Venus (refs. 20, 21, and 22) show that the distribution of temperatures in the interior of Venus differs little from the terrestrial values and allows us to assume the presence of an iron core (ref. 23). We will probably not be far off if we assume that the reduction of silicon in the core of Venus occurs at the same P–T parameters as on Earth.

As was pointed out in the first section, the free energy of solution of silicon in iron or nickel-containing iron is negative (table 1), which indicates the formation of Fe-Ni-Si melts in the lower mantle of the Earth and Venus. If we accept the scheme of Elsasser (ref. 24), this melt has an unstable equilibrium and descends, forming the outer core.

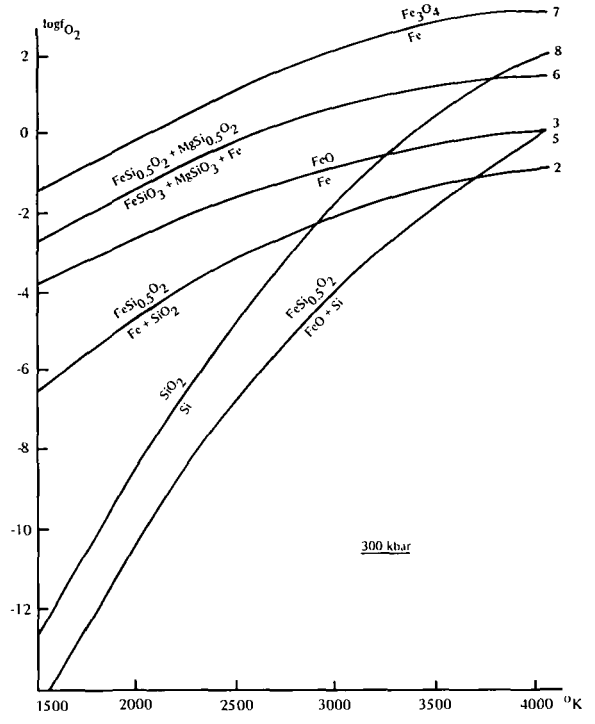


Figure 3.—*Oxygen fugacity as a function of temperature at the presumed core-mantle boundary of Mars.*

MARS

Calculations of models of Mars with an iron core show that the core amounts to not over 4 percent (ref. 25) or 9 to 10 percent (ref. 26) of the mass of the planet. Calculations of the thermal history of Mars, as a function of the concentration of radioactive elements, show that either the interior of the planet below 300 km is at the present time partially or fully molten or 50 percent of the volume of Mars is in the molten state, while the central parts remain solid (ref. 27). In the opinion of Sharma (ref. 28), modern Mars should have lower temperatures than the Earth at the same depths and should contain no liquid core. On the other hand, calculations of the thermal history performed by Toksoz (ref. 23) indicate a solid mantle and molten core.

The pressure at the core-mantle boundary of Mars is approximately 300 kbar (refs. 29 and 30).

Figures 2a and 3 show the results of calculation of the fugacity of oxygen for a number of reactions at 200 and 300 kbar.

At 200 kbar, the mantle of Mars consists of solid solutions of silicates and, as was noted earlier, the lower limit of reduction of silicon corresponds to a temperature of $\geq$ 3200 K.

At a pressure of 300 kbar, two versions are possible: either a silicate or an oxide mantle. In the former case, the reduction of silicates and formation of Fe-Si melt is possible at log $f_{O_2} \geq -1.2$ and $T \geq 3650$ K (at the intersection of reactions 2 and 5), the second case is possible where log $f_{O_2} \geq -0.5$ and $T \geq 3200$ K (at the intersection of reactions 3 and 8).

Study of the thermal history of Mars does not allow us to judge whether such temperatures were reached in the early stages of its development. Processing of data produced by Mariner 6 and 7 allowed Anderson (ref. 31) to propose that the entire core of the planet was not separated from the mantle. This means that the heating of Mars was insufficient to melt all of the available iron, of which the core is made. Analogy with the Earth also gives us reason to believe that temperatures of 3200 to 3600 K have not been reached in the interior of Mars.

Thus, using the currently available information on the thermal history and models of Mars, we can conclude that the reduction of silicates and stishovite to silicon has not occurred in the interior of the planet and, consequently, silicon should not enter into the composition of the core.

MERCURY, MOON

The high mean density of Mercury indicates that it has an iron core amounting to some 60 to 70 percent of the mass of the planet (refs. 25 and 32). According to the calculations of Plagemann (ref. 33), the core of Mercury has a radius of 2112 km. Processing of the data from Mariner 10 has indicated that Mercury has a magnetic field and that the presumed diameter of the core is

rather large, approximately equal to that of the Moon (ref. 34).

Iron is practically free of radioactive elements, and, therefore, their concentration in the material of Mercury should be significantly less than in the material of other planets. Calculations of the thermal history with an initial temperature at the center of 1000 K show that the temperature in the interior never rose above 2300 K, which is insufficient for melting and the formation of a core (ref. 20). On the other hand, with a higher initial temperature, say 1100 K, we find that the core might be either liquid or solid (ref. 23).

In spite of the many studies of specimens of lunar soil, measurements of heat flux, and interpretation of seismic data, the existence of a lunar core is still problematical. If a core exists, its radius does not exceed 200 to 300 km, with a temperature in the core of about 1500° C (ref. 35).

The characteristics of the material composition of the Moon and Mercury are not clear. We can assume, by analogy with Earth, that their interiors consist of ferromagnesium silicates. The pressure at the center of the Moon is about 46 kbar; at the core-mantle boundary of Mercury about 100 kbar (ref. 25). As the available calculations show, the reduction of silicates to silicon can occur at such pressures at temperatures of over 2500 to 3000 K.

Since these temperatures are apparently unrealistic for these celestial bodies, we can conclude that silicon should not enter in the composition of their cores.

Anderson (ref. 31), based on thermodynamic calculations of the condensation of the protoplanetary cloud, states his opinion that the Moon accumulated from Al, Ca, and Ti compounds such as gehlenite ($CaAl_2SiO_7$), spinel ($MgAl_2O_4$), and perovskite ($CaTiO_3$), which formed the primary condensate; it also cannot be excluded that Mercury is rich in refractory compounds, in addition to iron, and poor in the silicates of iron and magnesium. However, in this case silicon also should not be included in the composition of the core.

In summary, as a result of processes of reduction and high temperatures in the lower mantles of Earth and Venus in the early stage of their evolution, silicon might have dissolved in the liquid iron or nickel-iron, and this alloy might form the outer cores of the planets. In the interior of Mars, Mercury, and the Moon, the temperatures were insufficient for reduction of silicon, and it should not be included in the cores of these celestial bodies.

In preceding sections, we have studied the possibility of formation of an iron-silicon melt, which forms the cores of planets in the initial period of their evolution.

However, these processes do not limit the possible entry of silicon into the composition of the core. There is also another possibility; namely, the entry of silicon into the composition of the core as a result of interaction of the matter of the core and mantle, which exists at the present time.

Interaction Between Core and Mantle

Seismic data show that at the present time the mantle of the Earth is in the solid state and its outer core is in the liquid state. The interaction between the matter of the mantle and core can be represented in the form of the interaction between stishovite and liquid iron or nickel-iron:

$$SiO_2\ (st.\ 5) + 2Fe\,(l) = 2FeO\,(5) + [Si]$$

where [Si] represents a silicon solution (11.2 wt. %) in liquid iron or nickel-iron.

The values of free energies of solution of silicon are presented in table 1; the free energies of reaction are calculated according to the data of Tret'yakov (ref. 36), Robie and Waldbaum (ref. 37), and Kubashewski et al., (ref. 38).

The results of calculating the free energy of the reaction (ΔG_P^T) in the interval 2000 to 4000 K and 300 to 1400 kbar are presented in figure 4.

Free energy is a negative quantity in the pressure interval in question if the tempera-

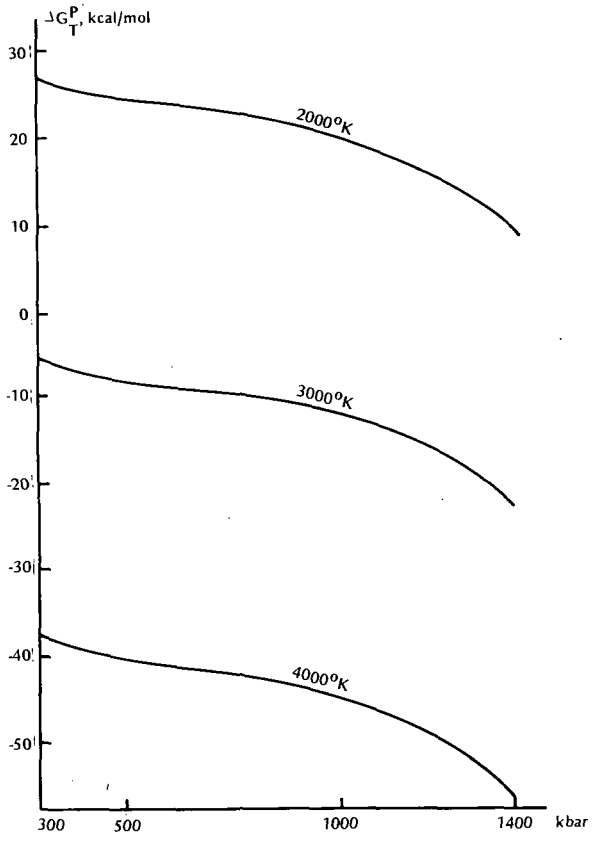


Figure 4.—*Change in free energy of the reaction* $SiO_2(st.s) + 2Fe(l) = 2FeO(s) + [Si]$*(in* $Fe(l)$*) as a function of pressure at 2000, 3000, and 4000 K.*

ture is over ~ 3000 K, i.e., in this case the reaction will be shifted to the right. The pressure at the core-mantle boundary of the Earth and Venus is ~ 1400 kbar, the temperature ~ 4000 K, and the free energy of the reaction — 55.3 kcal/mol. Under these conditions, the core extracts silicon from the mantle; this may explain its growth.

The temperature in the interior of Mars is probably not over 1500 to 2000° C (ref. 26), while the pressure at the core-mantle boundary is approximately 250 to 300 kbar. Therefore, if its mantle consists of oxides, the temperatures are insufficient for the occurrence of this reaction.

The pressure in the interior of the Moon and Mercury is insufficient for the formation of stishovite (but it is possible that coesite is formed), and the mechanism of interaction between the core and the mantle just studied is unsuitable for these bodies.

Conclusions

There are therefore two possible versions of inclusion of silicon in the composition of the iron-nickel cores of the planets. The first proposes the reduction of stishovite, with subsequent formation of an iron-silicon melt which, due to the unstable equilibrium in the gravity field of the planet, sinks to the center. The second possibility is found in the current interaction of the core and mantle, as a result of which silicon is extracted from the mantle and dissolved in the material of the core. Both versions are realized only for the Earth and Venus. The temperatures and pressures in the interior of Mars, Mercury, and the Moon are insufficient for inclusion of silicon in their cores. It is possible that the inclusion of other elements must be studied in this case, for example sulfur or carbon. Only strict quantitative calculations can serve as proof.

References

1. AL'TSHULER, L. V., G. V. SIMAKOV AND R. F. TRUNIN, *Izv. AN SSSR*, Earth Physics Series, No. 1, 1968.
2. MCQUEEN, R. G. AND S. P. MARSH, *J. Geophys. Res.*, Vol. 71, No. 6, 1966.
3. BIRCH, F., *J. Geophys. Res.*, Vol. 57, 1952, p. 227.
4. MACDONALD, G. J. F. AND L. KNOPOFF, *The Geophys. J. Roy. Astron. Soc. Geophys.*, Supplement M. N. R.A.S., Vol. 1, No. 4, 1958.
5. RINGWOOD, A. E., *Geochimica et Cosmochimica Acta*, Vol. 15, No. 4, 1959.
6. VAGNER, K., *The Thermodynamics of Alloys*, Metallurgizdat Press, Moscow, 1957.
7. GEL'D, L. V., B. A., BAUM AND M. S. PETRUSHEVSKIY, *Ferroalloy Production Melts*, Metallurgiya Press, Moscow, 1973.
8. KUSKOV, O. L., *Geokhimiya*, No. 11, 1974.
9. KORMER, S. B. AND A. I. FUNTIKOV, *Izv. AN SSSR*, Earth Physics Series, No. 5, 1965.
10. PAVLOVSKIY, M. N., *Fiz. Tv. Tela.*, Vol. 9, No. 2, 1967.
11. CLARK, S., *Handbook of the Physical Constants of Rock*, Mir. Press, Moscow, 1969.

12. BALCHAN, A. S., AND G. R. COWAN, *J. Geophys. Res.*, Vol. 71, No. 14, 1966.
13. KHITAROV, N. I. AND O. L. KUSKOV, *IASPEI Symposium*, Lima, Peru, 1973.
14. KHITAROV, N. I. AND O. L. KUSKOV, In: *Solutions Solides en Mineralogie*, Vol. 1, Colloque International, Orleans, France, May 27–30, 1974.
15. KUSKOV, O. L. AND N. I. KHITAROV, *Geokhimiya*, No. 1, 1974.
16. ZHARKOV, V. N., *Izv. AN SSSR*, Geophysics Series, No. 3, 1959.
17. UFFEN, R. J., *Trans. Am. Geophys. Union*, Vol. 33, No. 6, 1952.
18. HIGGINS, G. AND G. C. KENNEDY, *J. Geophys.* Vol. 76, No. 8, 1971.
19. KUMAZAWA, M. et al., *Nature*, Vol. 247, No. 5440, 1974.
20. MAYEVA, S. V., *Physics of the Moon and Planets*, Nauka Press, Moscow, 1972.
21. LEE, W. H. K., *Earth Planet. Sci. Letters*, Vol. 4, No. 4, 1968.
22. FRICKER, P. E. AND R. T. REYNOLDS, *Icarus*, Vol. 9, No. 2, 1968.
23. TOKSOZ, M. N., this collection.
24. ELSASSER, W. M., Early History of the Earth. In: *Earth Science and Meteorites*, 1963.
25. KOZLOVSKAYA, S. V., *Physics of the Moon and Planets*, Nauka Press, Moscow, 1972.
26. BINDER, A. B. AND D. R. DAVIS, *Phys. Earth Planet. Interiors*, Vol. 7, No. 4, 1973.
27. MAYEVA, S. V., *Dokl. AN SSSR*, Vol. 159, No. 3, 1964.
28. SHARMA, J. P., *J. Geophys. Res.*, Vol. 78, No. 23, 1973.
29. KOZLOVSKAYA, S. V., *Astron. Zhurn.*, Vol. 43, No. 5, 1966.
30. KOSLOVSKAYA, S. V., *Izv. AN SSSR*, Earth Physics Series, No. 7, 1972.
31. ANDERSON, D. L., *The Moon*, Vol. 8, Nos. 1 and 2, 1973.
32. REYNOLDS, R. T. AND A. E. SUMMERS, *J. Geophys. Res.*, Vol. 74, No. 10, 1969.
33. PLAGEMANN, S., *J. Geophys. Res.*, Vol. 70, No. 4, 1965.
34. NESS, N. R. et al., this collection.
35. LATHEM, G. et al., this collection.
36. TRET'YAKOV, YU. D., *The Thermodynamics of Ferrites*, Khimiya Press, Leningrad, 1967.
37. ROBIE, R. A. AND D. R. WALDBAUM, *U.S. Geol. Survey Bull.*, No. 1259, 1968.
38. KUBASHEWSKI, O., E. L. EVANS AND C. B. ALCOCK, *Metallurgical Thermochemistry*, 1967.

To the Problem About the Origin of Lunar Maria And Continents (Mössbauer Investigations)

T. V. Malysheva
V. I. Vernadskiy Institute of Geochemistry and Analytical Chemistry Academy of Sciences, Moscow, U.S.S.R.

A comparative study of Mossbauer spectra of regolith returned by the Luna 16 and Luna 20 spacecraft has shown that the distribution of iron among the mineral phases is quite characteristic of the landing sites. The overall fractions of regolith measured had the following grain sizes: 0.200 to 0.450 mm, 0.127 to 0.200 mm, 0.083 to 0.127 mm, and $\leq$0.083 mm.

The Mossbauer spectra of the mare regolith of Luna 16 differ significantly for all fractions from the spectra for the same fractions of continental regolith (Luna 20).

The total quantity of iron is 1.85 times greater in the mare regolith. There is 2.4 times less olivine in the mare region than in the continental region and it is higher in iron content (by 1.85 times). The pyroxene component of the mare regolith is less homogeneous in composition (contains more augite and glass) and is present in larger quantities. Ilmenite was found only in the mare regolith. In the continental region, the predominant titanium-containing phase is ulvospinel. The mare regolith contains more metallic iron, which is more finely dispersed and contains less nickel. Troilite is found in the maria region.

Based on these differences, it is concluded that the formation of continental rocks occurred at an earlier stage of crystallization from the melt and at higher temperatures and higher partial pressures of oxygen. The mare basalts crystallized from a more reduced magma, apparently in a later process.

Results

The distribution of iron among the mineral phases in the lunar rocks depends both on the physical conditions of crystallization of the minerals and on the chemical composition of the initial magma. Therefore, it is very important to do comparative phase analysis of lunar material that comes from various regions of the Moon and has not been subjected to any physical and chemical effects. The method of Mossbauer spectroscopy allows the material to be studied without preliminary separation. The overall regolith fractions returned by the Luna 16 and Luna 20 probes were measured on a Mossbauer spectrometer with a Co 57 source (refs. 1 and 2 and Malysheva, 1972 and 1974).

Measurements were performed at room temperature and at liquid nitrogen temperature. The analytical data were processed on a BESM–3m and a BESM–4 computer by the least-squares method assuming a Lorentz shape for the Mossbauer absorption line. The regolith fractions analyzed had the following grain sizes: 0.200 to 0.450 mm, 0.127 to 0.200 mm, 0.083 to 0.127 mm, and 0.083 mm.

The Mossbauer spectra of the fine regolith fractions (grain size 0.083 mm) are pre-

sented in figure 1. The same quantity of sample was measured under identical conditions in order to allow direct comparison of both spectra. The comparison of the fine regolith fractions is more obvious, due to the distinct peaks of metallic iron. One can see from the figures that the total area beneath the Mossbauer peaks for iron-containing minerals from the Luna 16 regolith is greater than for the Luna 20 regolith (according to the relative total peak areas, 1.85 times). The basic iron-containing minerals are identical in both fractions (two main peaks) and are silicates: olivine, pyroxene, and glass. Figure 2 presents the Mossbauer spectra of the same fractions of Luna 16 and Luna 20 regolith measured with lower rates of movement of the source relative to the absorber. In the middle part of the spectrum we clearly see the disappearance of peaks belonging to ilmenite in the regolith of Luna 20. In place of ilmenite there are peaks belonging to ulvospinel.

Table 1 shows the parameters of the olivine component of the Mossbauer spectra of the Luna 16 and Luna 20 regolith. We can see that the quadrupole splitting Δ decreases with decreasing grain size from 2.94 to 2.88 mm/s for Luna 16 and from 3.00 to 2.93 mm/s for Luna 20, indicating an increase in

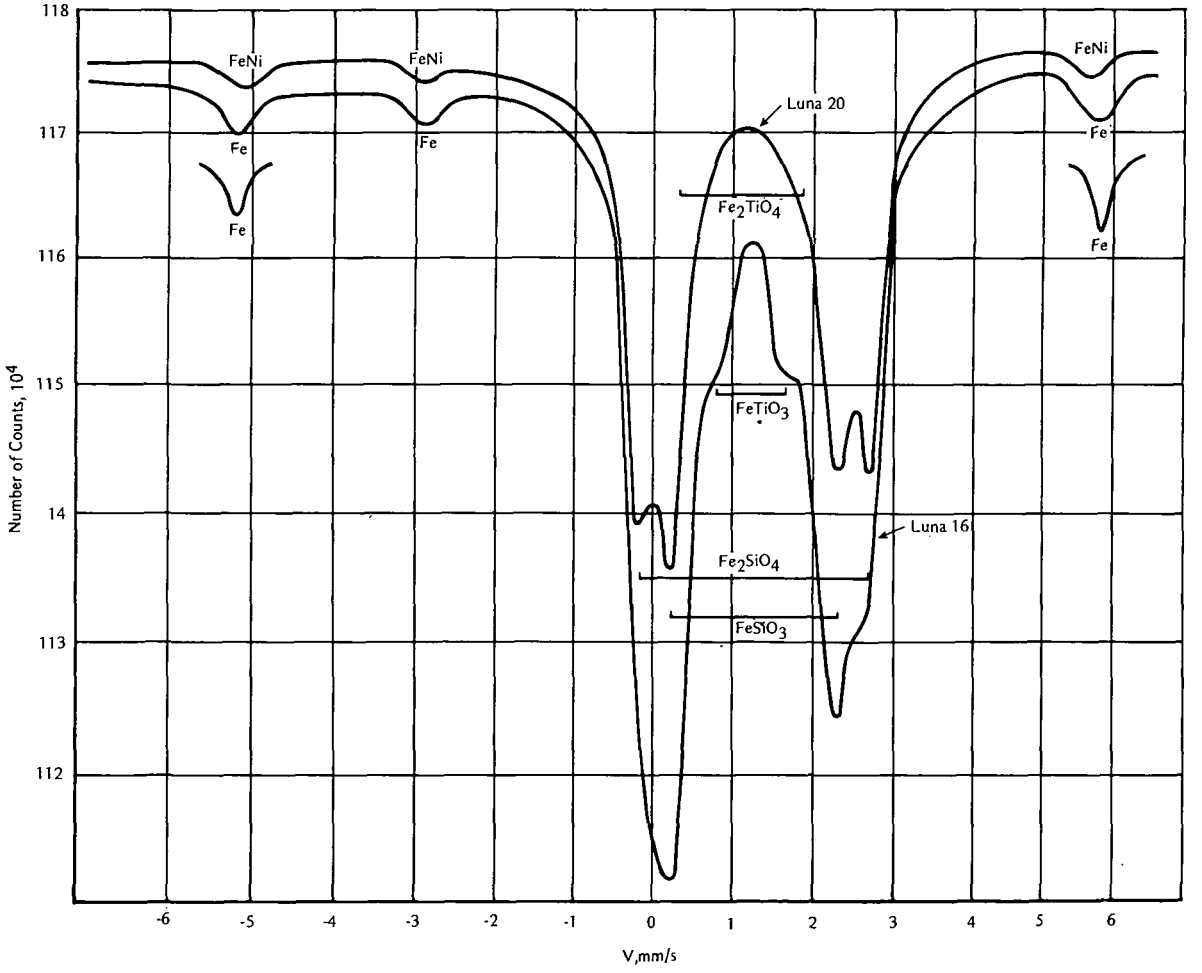


Figure 1.—*Mössbauer spectra of fine fractions of regolith returned by the Luna 16 and Luna 20 spacecraft (high speed of motion of source relative to absorber).*

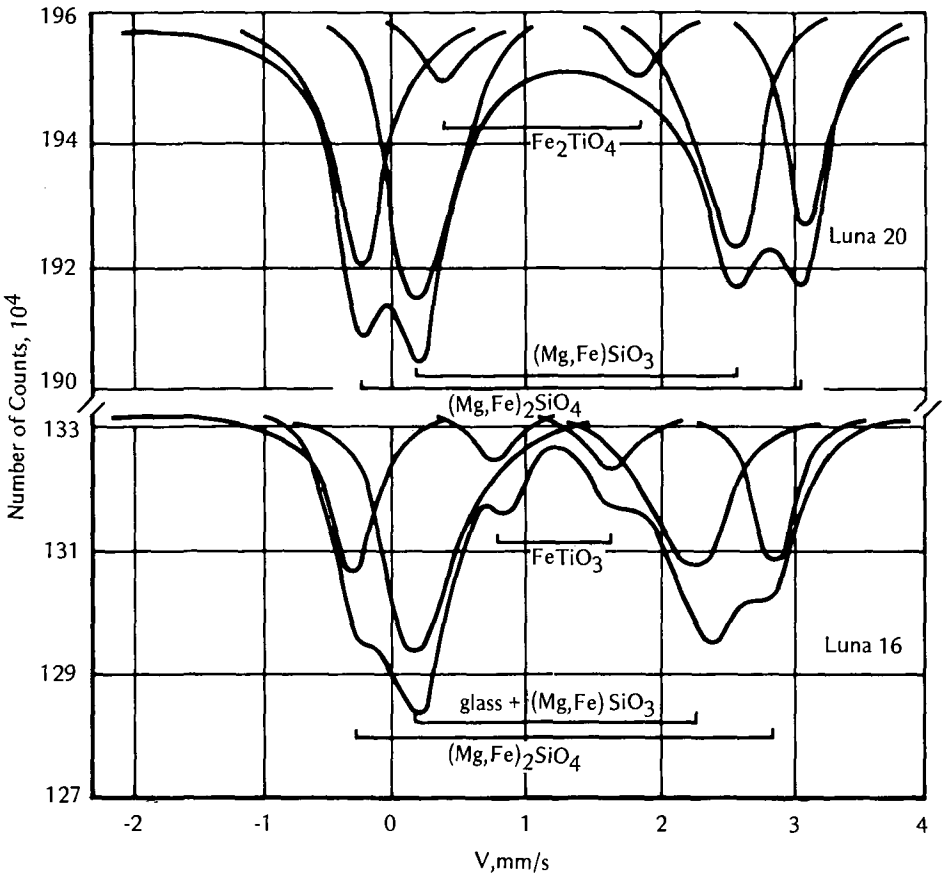


Figure 2.—*Mössbauer spectra and fine fractions of Luna 16 and Luna 20 regolith (low speed of relative motion).*

the iron content of the olivine with decreasing grain size both for the continental olivine and for the olivine from Mare Fecunditatis. The dependence of the quadrupole splitting on the fayalite content of olivine for terrestrial specimens forms a straight line (fig. 3).

If we place the data produced for the olivines of Luna 16 and Luna 20 on this line, we see that the fayalite content of olivines from Mare Fecunditatis lies within 50 and 80 percent, whereas for specimens from the continental region the fayalite content is lower (20 to 50 percent). Thus, the mean content of fayalite in the olivine is 1.85 times less for the Luna 20 regolith than for the Luna 16 regolith. The total iron content in the Luna 20 regolith (see above) is also 1.85 times less than in the Luna 16 regolith. A comparison of the fayalite content of olivines with the total iron content of the rocks returned by Apollo 11 and 12 yields similar results (Mason et al., 1971). The ratio FeO/(FeO + MgO) for the specimens of Apollo 11 was 41 mol. % and for the specimens of Apollo 12, 43 mol. %, corresponding to an olivine composition of 26 to 60 mol. % Fe_2SiO_4, or an average of 41 percent. The agreement of the fayalite content of olivine with the total iron content of the rock is evidence of a second generation of phenocrysts (Stanik, 1970).

The widths of the Mossbauer lines Γ (table 1) for olivines from the Luna 20 regolith are less than for Luna 16 olivines indicating their more homogeneous composition and slower cooling.

Table 1.—*Parameters of the Mossbauer Spectra for the Olivine Component of the Luna 16 and Luna 20 Regoliths*

Grain Size	δ mm/s		Δ mm/s		Γ mm/s		Γ mm/s	
					Luna 16		Luna 20	
	Luna 16	Luna 20	Luna 16	Luna 20	left peak	right peak	left peak	right peak
0.200–0.450	1.27 ± 0.02	1.29 ± 0.005	2.94 ± 0.01	3.00 ± 0.005	0.310 ± 0.003	0.422 ± 0.003	0.290 ± 0.005	0.360 ± 0.005
0.127–0.200	1.26 ± 0.02	1.275 ± 0.002	2.92 ± 0.01	2.998 ± 0.008	0.364 ± 0.005	0.426 ± 0.005	0.336 ± 0.003	0.360 ± 0.004
0.083–0.127	1.26 ± 0.02	1.275 ± 0.003	2.90 ± 0.01	2.984 ± 0.001	0.325 ± 0.002	0.417 ± 0.004	0.325 ± 0.002	0.357 ± 0.002
0.0–0.083	1.25 ± 0.005	1.26 ± 0.005	2.88 ± 0.005	2.93 ± 0.01	0.340 ± 0.005	0.596 ± 0.005	0.335 ± 0.002	0.360 ± 0.002

NOTES: δ = chemical shift relative to Co^{57} source in stainless steel
Δ = quadrupole splitting
Γ = line width

Table 2.—*Parameters of Mossbauer Spectra for the Pyroxene Component of Luna 16 and Luna 20 Regoliths*

Grain Size	δ mm/s		Δ mm/s		Γ		mm/s	
					Luna 16		Luna 20	
	Luna 16	Luna 20	Luna 16	Luna 20	low velocity peak	high velocity peak	low velocity peak	high velocity peak
0.200–0.450	1.21 ± 0.03	1.28 ± 0.005	2.06 ± 0.04	2.130 ± 0.005	0.61 ± 0.01	0.83 ± 0.01	0.47 ± 0.005	0.510 ± 0.005
0.127–0.200	1.24 ± 0.01	1.257 ± 0.002	2.05 ± 0.01	2.126 ± 0.002	0.61 ± 0.01	0.82 ± 0.01	0.440 ± 0.004	0.495 ± 0.006
0.083–0.127	1.24 ± 0.01	1.263 ± 0.002	2.05 ± 0.01	2.140 ± 0.001	0.59 ± 0.01	0.68 ± 0.01	0.442 ± 0.002	0.495 ± 0.005
0.0–0.083	1.24 ± 0.004	1.25 ± 0.01	2.03 ± 0.003	2.100 ± 0.002	0.580 ± 0.003	0.601 ± 0.008	0.445 ± 0.003	0.503 ± 0.006

NOTES: δ = chemical shift relative to Co^{57} source in stainless steel
Δ = quadrupole splitting
Γ = line width

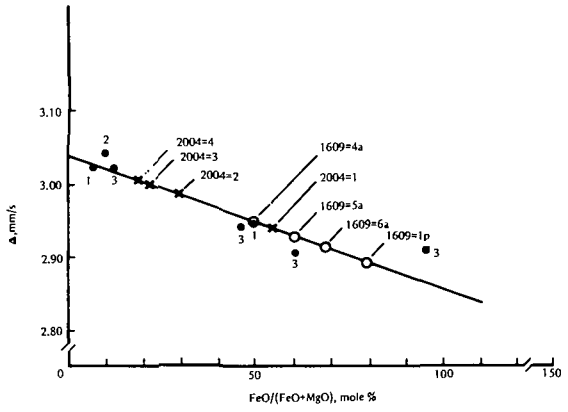


Figure 3.—*Quadrupole splitting as a function of iron content of olivine,* $f = \frac{FeO}{FeO + MgO}$ *mole %. Point 1 is from reference 3, point 2 is from reference 4, and point 3 is from reference 5. Luna 20 regolith specimens, 2004–4, 2004–3, 2004–2, and 2004–1 have grain sizes 0.250–0.400, 0.127–0.250, 0.083–0127, and ≤ 0.083mm, respectively. Luna 16 regolith samples, 1609–4a, 1609–5a, 1609–6a, and 1609–1p have grain sizes 0.250–0.400, 0.127–0.250, 0.083–0.0127, and ≤ 0.083mm, respectively.*

The parameters of the Mossbauer spectra of the pyroxenes are presented in table 2. Comparison of the line widths of the pyroxene component of the regolith of Luna 16 and Luna 20 shows that Γ for the Luna 20 pyroxene is approximately 1.5 times less than for the Luna 16 pyroxene. This indicates a more homogeneous composition of the pyroxene component of Luna 20. At the same time, the quadrupole splitting and chemical shifts are greater for the Luna 20 pyroxene. The combination of these factors indicates that in the Luna 20 regolith there is less glass and augite, which agrees with the data of X-ray spectroscopy (personal communication from Ye. S. Makarov).

In all fractions of the Luna 16 regolith, peaks are easily identified with parameters $\delta = 1.20$–1.24 mm/s and $\Delta = 0.66$–0.71 mm/s which belong to ilmenite (the internal peaks in fig. 2). However, no ilmenite is found in the continental specimens (Luna 20). Ilmenite, although widespread in lunar mare specimens (from 5 to 20 percent) (Thiel et al., 1972) is not characteristic for the lunar continent.

In the fine fractions of the Mossbauer spectra of the regolith of Luna 16 and Luna 20, given equal amplitudes and widths of doublet lines, one can identify ulvospinel Fe_2TiO_4 with the following parameters: $\delta = 0.69 \pm 0.08$ mm/s; $\Delta = 1.79 \pm 0.07$ mm/s (Luna 20) and $\delta = 0.91 \pm 0.03$; $\Delta = 1.82 \pm 0.03$ mm/s (Luna 16). These quantities agree well with the values for ulvospinel in Ono et al. (1968).

The ulvospinel found in significant quantities is the end member in the ulvospinel-chromite series, a new mineral series which is specific for lunar specimens. Chromite, $FeCr_2O_4$, has not been identified in the Mossbauer spectra of the lunar regolith within the limits of measurement accuracy.

The Mossbauer spectra of the Luna 20 regolith, as well as Luna 16 regolith, show three of the six peaks due to the superfine magnetic splitting of metallic iron (fig. 1).

When we compare the positions of the extreme peaks of the superfine splitting of metallic iron of the finest regolith fractions (table 3), we see that the position of the extreme peaks for specimen 9-1*r* (Luna 16) coincides with the position of the peaks for pure metallic iron; whereas for specimen 4-1 (Luna 20), the peaks are shifted inward in the spectrum, i.e., the superfine magnetic field on the iron nucleus in this specimen is 1.013 times less than in pure metallic iron.

This indicates that in the regolith of Luna 20, metallic iron is present as an alloy with nickel. In a study of lunar anorthosites from the regolith of Apollo 11 (Dickey 1970), it was also shown that metallic iron in the

Table 3.—*Position of Extreme Peaks of Superfine Magnetic Splitting for Metallic Iron in Fine Fractions of Luna 16 and Luna 20 Samples*

Specimen	Left Peak	Right Peak
2004–1 (Luna 20)	112.99 ± 0.17	450.48 ± 0.18
1609–1 (Luna 16)	115.50 ± 0.36	147.24 ± 0.85
Pure Metallic Iron	112.48 ± 0.14	449.96 ± 0.15

anorthosites contains from 6 to 20 percent Ni (kamasite and taenite), while the metal in the basalts is present almost as pure iron. However, determination of the composition and quantity of the metallic phase (20 to 30 percent Ni) against the background of a complex spectrum is impossible. This is true since at these concentrations the particles of iron do not produce magnetic splitting and only the paramagnetic peak is present in the spectrum (Azano, 1969) and its position coincides with the low-velocity peak of the silicate doublet. Furthermore, the presence of finely dispersed iron in the metallic phase, with sufficiently small particle size, may cause paramagnetic lines to develop in place of superfine magnetic splitting when the superparamagnetic relaxation becomes sufficiently fast and comparable to the rate of Larmor precession of nuclei in a superfine field. The position of the paramagnetic peak of finely dispersed iron also corresponds to the low-velocity peak of the quadrupole doublet, caused by iron in silicate. The presence of finely dispersed iron in the lunar regolith was determined in X-ray-electron spectra of Luna 16 and Luna 20 specimens (refs. 6 and 7). Housley et al., (1972), calculated the transition temperatures between ferromagnetism and superparamagnetism in the Mossbauer spectra for particles of various sizes: for $\phi = 134$ Å at 295 K, for $\phi = 85$ Å at 77 K, and for $\phi = 75$ Å at 11 K.

Both in the specimens of Luna 16 and in the specimens of Luna 20, the area of the left peak (low-velocity peak) is greater than the area of the right peak (high-velocity peak) (ref. 1). This difference increases with decreasing particle size. The asymmetrical nature of the Mossbauer spectrum was noted (Duchesne et al., 1971) in a study of the regolith of Apollo 12. The authors related this to the presence of finely dispersed paramagnetic iron with particle size less than 1 μ.

In order to determine the presence of finely dispersed iron, measurements were performed at liquid nitrogen temperatures using the fine fractions (particle size 0.083 mm) from the Luna 16 and Luna 20 regolith. The area of the peaks belonging to metallic iron for the Luna 16 regolith increased to 10.7 percent relative to the other iron-containing minerals. Consequently, at least 4.85 percent of the iron (about half) is in the finely dispersed state with particle size of 85 to 134 Å. The area of peaks due to metallic iron in the Luna 20 regolith remained almost unchanged (6.12 percent), indicating the absence of any significant quantity of finely dispersed iron in specimens from the continental region of the

Table 4.—*Distribution of Iron Among Primary Mineral Phases in Regolith Returned by Luna 16 and Luna 20 in Percent of the Total Area of the Mossbauer Spectrum*

Minerals	Luna 16				Luna 20			
	Grain Size				Grain Size			
	0.25–0.400	0.127–0.200	0.083–0.127	≤0.083	0.250–0.400	0.127–0.200	0.083–0.127	0.083
Olivine	15.8	16.2	22.6	22.0	38.0	35.6	34.8	36.0
Pyroxene + Glass	79.3	75.8	71.0	55.0	60.07	64.4	65.5	56.8
Ilmenite	4.9	4.9	5.8	5.72	1	1	1	1
Ulvospinel	1	1	1	6.25	2.1	1	1	6.6
Metallic Iron								
300 K	3.5	3.3	3.1	5.85	1	2	4.5	5.65
80 K	—	—	—	10.7	—	—	—	6.12
Troilite	1	1	2.8	2.0	1	1	1	1

Table 5.—*Distribution of Iron Among Mineral Phases in Weight Percent of the Total Quantity of Minerals*

Mineral	Luna 16		Luna 20	
	Particle Size 0.250–0.400	≤0.083	Particle Size 0.250–0.400	≤0.083
Olivine	4.6	5.3	15	8.1
Pyroxene and Glass	53.6	50.0	24.0	31.0
Ilmenite	1.0	1.8	0.05	0.05
Ulvospinel	0.05	1.4	0.2	0.82
Metallic Iron				
T_{meas} = 300 K	0.28	0.6	0.05	0.35
T_{meas} = 80 K	—	1.1	—	0.38
Troilite	0.05	0.6	0.05	0.05
Plagioclase	40	40	60	60

Moon. Apparently, the difference in areas of the right and left peaks of the silicate component for the Luna 20 regolith can be explained by the presence of 5 percent Fe3+.

The distribution of iron in the mineral phases as a percent of the total area of the Mossbauer spectra is presented in table 4.

The distribution of iron among mineral phases in weight percent is given in table 5. Calculations were made based on the following assumptions:

1. The resonant absorption is identical for all minerals.
2. The iron content of pyroxene and glass, $f = 20 \frac{FeO}{FeO + MgO}$ mol.%.
3. The iron content of olivine (fig. 3) for the Luna 16 regolith is 50 percent and 80 percent for fractions with grain size 0.250 to 0.400 and 0.083, respectively. For the Luna 20 regolith f = 20 percent and 50 percent for fractions of the same size.
4. The ilmenite and ulvospinel contain no magnesium.
5. The content of nickel in the iron was ignored.
6. The quantity of plagioclase was estimated on the basis of mineralogical and petrological work (Albee et al., 1972; Steel et al., 1972; Tarasov et al., 1973).

According to tables 4 and 5, the distribution of iron among the mineral phases is different and is representative for each sampling area (ref. 8). Therefore, based on the data produced we can draw general conclusions concerning the main differences between distinguishing features of mare and continental regoliths. On the other hand, the composition of regolith may be characteristic of the composition of the lunar rock of that region (ref. 9). Consequently, we can draw general conclusions about the characteristics of mare and continental areas of the Moon. The basic distinguishing features found from the Mossbauer studies are as follows:

1. The total content of iron is twofold greater in the mare regions.
2. There is 2.4 times less olivine in the mare regions than in the continental regions and it is twofold higher in iron content.
3. The pyroxene component of the mare regolith is less homogeneous in composition (contains more augite and glass)

and is present in twofold larger quantities than in the continental region.

4. Ilmenite was detected in the mare regolith.
5. In the continental region, the predominant titanium-containing phase is ulvospinel.
6. In the mare regolith, there is more metallic iron, which is more finely dispersed and contains less nickel.
7. There is more troilite in the mare regions.

These differences may result from differences in the chemical composition of the inital material or may reflect the physical conditions of crystallization of the minerals.

Let us study the relationship of the basic components in the regolith of Luna 16 and Luna 20 (ref. 9) (table 6).

If the decrease in the quantity of ilmenite in the continental region can be explained by an increase in the FeO/TiO_2 ratio, the increase in the olivine component relative to pyroxene (table 5) cannot be explained by differences in chemical composition because the $\frac{FeO+MgO}{SiO_2}$ ratio becomes less or remains unchanged if we consider the increase in the quantity of plagioclase.

In connection with this, we must note the differences in physical conditions of crystallization of rocks from the magma.

Since the mean iron content of olivine in the continental rocks is two times less than for the mare rocks, its crystallization must apparently have occurred at higher temperatures ($\sim$ 1300° C). If we use calculations of the minimum partial pressure of oxygen f_{O_2} necessary for the equilibrium composition of spinel at 1300°C (Haggerty, 1972), then for the mare basalts enriched in olivine we obtain $f_{O_2} = 10^{-13}$ atm, and for the continental rocks containing ulvospinel, $f_{O_2} = 10^{-11}$ atm.

The petrological, X-ray, and micro-X-ray studies confirm that the mare basalt of Luna 16 and Apollo 11 were formed by rapid, one-event surface crystallization of rocks at an oxygen partial pressure of 10^{-13} atm (Bence et al., 1972).

In summary, one can propose that the formation of continental rocks occurred in an earlier stage of crystallization from a melt and at a higher temperature and higher partial pressure of oxygen. The same conclusions were reached by Hubbard et al. (1973) by analysis of the content of Eu, Sr, and Al_2O_3 in continental rocks. Obviously, the conditions of increased temperature and pressure are related to greater depths. The mare basalts were crystallized from more reduced magma (progressive loss of volatiles) in a later process.

The formation of the mare basalts under more reduced conditions is also confirmed by data on the composition of olivine. According to Tarasov et al. (1973), the mare olivines contain more chromium than the continental olivines, while thermodynamic studies (ref. 10) have shown that the content of chromium in olivine increases with increasing reducing conditions.

Table 6.—*Ratio of Certain Oxides in the Regolith of Luna 16 and Luna 20*

	Luna 16	Luna 20
$\frac{FeO}{TiO_2}$	5	12.5
$\frac{FeO}{SiO_2}$	0.38 0.63	0.16 0.41
$\frac{Mg}{SiO_2}$	0.25	0.25

References

1. MALYSHEVA, T. V., Mossbauer Spectroscopy of Lunar Regolith Returned by the Luna 20 Spacecraft. *Geokhimiya*, No. 7, 1973, pp. 1079–1084.
2. MALYSHEVA, T. V. AND V. V. KURASH, Mossbauer Spectroscopy of Lunar Specimens. *Geokhimiya*, No. 1, 1973, pp. 120–125.
3. MALYSHEVA, T. V., V. V. KURASH AND A. N. YERMAKOV, *Geokhimiya*, No. 2, 1969.
4. MALYSHEVA, T. V., V. V. KURASH AND A. N. YERMAKOV, Proceedings of the Conference on Mossbauer Spectrometry. *Drosden*, 1971, p. 267.

5. BANCROFT, G. M., A. G. MADDOCK AND R. C. BURNS, *Am. Minerol.*, Vol. 52, Nos. 7 and 8, 1967.
6. VINOGRADOV, A. P., V. I. NEFEDOV, V. S. URUSOV AND M. M. ZHAVORONKOV, X-Ray–Electron Study of Lunar Regolith From the Sea of Fertility and Sea of Tranquility. *DAN SSSR*, Vol. 201, No. 4, 1971, p. 957.
7. VINOGRADOV, A. P., V. I. NEFEDOV, V. S. URUSOV AND M. M. ZHAVORONKOV, X-Ray–Electron Studies of Metallic Iron in Lunar Regolith. *DAN SSSR*, Vol. 207, No. 3, 1972, p. 433.
8. VINOGRADOV, A. P., The Genesis of the Regolith of the Moon. *Lunnyy Grunt Iz Morya Izobiliya*, 1974.
9. VINOGRADOV, A. P., Preliminary Data on Lunar Soil Returned by the Luna 20 Spacecraft. *Geokhimiya*, No. 7, 1972.
10. IL'IN, N. P. AND A. N. KOLOMEYTSEVA, Influence of Temperature and Pressure on the Distribution of Iron Group Elements Among Metal-Silicate Phases in the Process of Differentiation of Matter. *Abstracts of the Soviet-American Lunar Conference*, Moscow, 1974.

Other references cited in the text were not provided by the author.

Page intentionally left blank

Page intentionally left blank

The Surface Abundance and Stratigraphy of Lunar Rocks From Data About Their Albedo

V. V. Shevchenko
Shternberg State Astronomical Institute, Moscow, U.S.S.R.

The data of ground-based studies and surveys of the lunar surface by the Zond and Apollo spacecraft have been used to construct an albedo map covering 80 percent of the lunar sphere. Statistical analysis of the distribution of areas with various albedos shows several types of lunar surface. Comparison of albedo data for maria and continental areas with the results of geochemical orbital surveys allows us to identify the types of surface with known types of lunar rock. The aluminum/silicon and magnesium/silicon ratios as measured by the geochemical experiments on the Apollo 15 and Apollo 16 spacecraft were used as an indication of the chemical composition of the rock. The surveys had a surface resolution of about 150 km, which is comparable in order of magnitude to the resolution of the albedo map, which is equal to 50 km on the lunar surface. This dependence allowed a preliminary estimate to be made of the distribution of rocks of various types over the surface of the Moon. The relationship of the relative aluminum content to the age of crystalline rocks allows a direct dependence to be constructed between the mean albedo of areas and the age of the rocks of which they are composed.

The nature of the spatial distribution of optical parameters of the lunar surface indirectly reflects the peculiarities of the current nature and genesis of the Moon. Furthermore, it is possible, on the basis of territorial unity, to compare optical parameters with structural peculiarities and chemical composition of the covering material. Establishment of reliable qualitative and quantitative dependences allows, in turn, extension of data obtained for the limited areas where spacecraft operated, to larger areas of the visible and back hemispheres of the Moon.

It is particularly interesting to investigate the mean regularities, using data that encompass a large portion of the lunar surface. In this connection, an albedo map covering 80 percent of the entire lunar surface was used (fig. 1) as the primary information. The map was constructed in an original scale of 1:10 million based on the results of processing Earth-based and orbital surveys. The albedo of the areas of the back hemisphere was determined from measurements made on photographs produced by the Zond 6 and Apollo 13 spacecraft (ref. 1). The measured values of brightness were reduced to true full Moon. On the map is a system of isolines drawn with an interval of values $\rho_0 = 1.0$ percent, showing the distribution of albedo in the range from < 6 percent to > 18 percent.

The reliability of the results of comparison depends to a great extent on the agreement of the spatial resolution of the data studied. Therefore, in order to study the dependence of albedo on chemical composition of the surficial material, data were used from the selenochemical orbital survey. The indicators of chemical composition of rocks used in this case were the relative contents of aluminum and magnesium along selected flight paths.

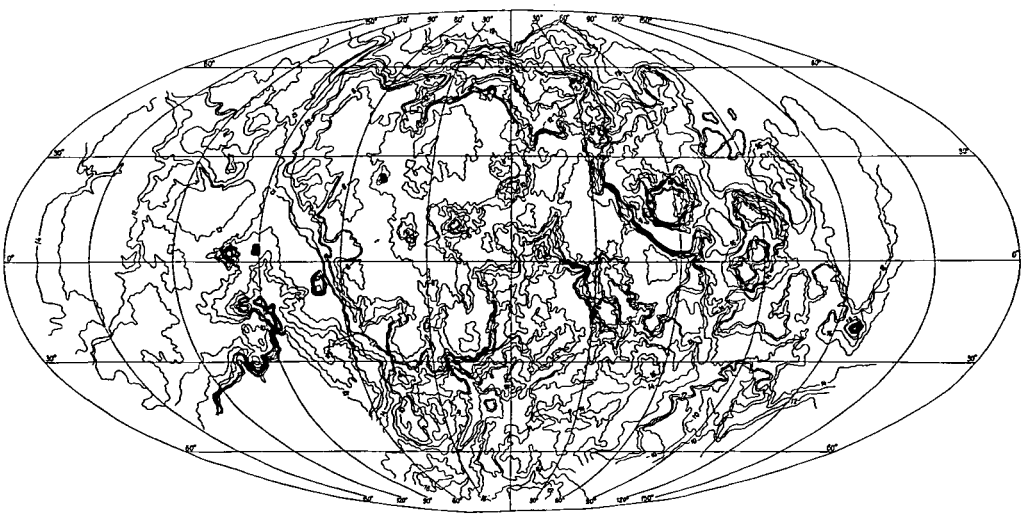


Figure 1.—*An albedo map for 80 percent of the lunar surface, drawn according to data from Earth-based studies and Zond and Apollo spacecraft.*

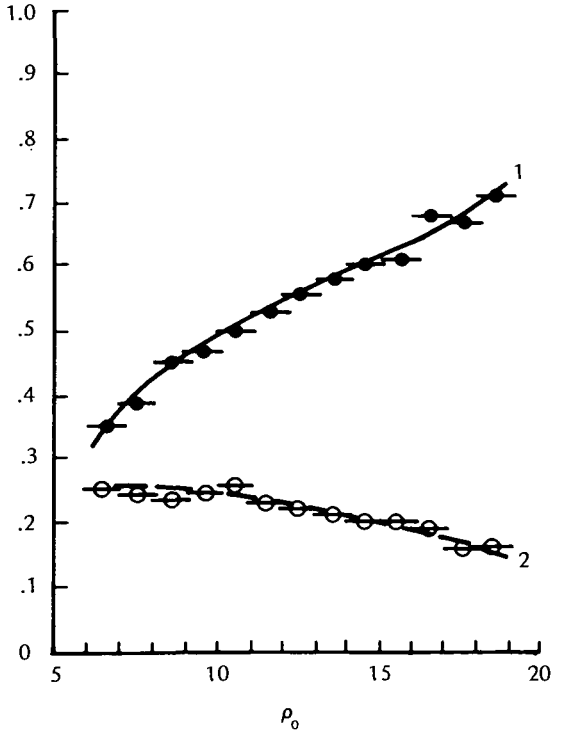


Figure 2.—*Curves showing the dependence of albedo on Al/Si (curve 1) and Mg/Si (curve 2).*

Figure 2 presents curves of the dependence of albedo on Al/Si (1) and Mg/Si (2). Curve (1) uses the mean values of Al/Si for the corresponding intervals of albedo ρ_0. The values of Al/Si are presented on the basis of individual measurements, representing the combined data from preliminary processing of the results of selenochemical surveying by the Apollo 15 and Apollo 16 spacecraft (refs. 2 and 3). In table 1 we present the number of individual measurements and the mean square deviations for the corresponding albedo intervals.

For the interval 17–18, the mean value of Al/Si was produced by use of two measurements with deviations of $\pm$ 0.040; interval 18–19 in this case corresponds to one measurement. Thus, curve (1) on figure 2 is the mean dependence of albedo on aluminum content in relationship to silicon with a mean deviation of individual Al/Si measurements of $\pm$ 0.040. Curve (2) corresponds to the dependence of albedo on relative content of magnesium (Mg/Si). The values of Mg/Si were taken from reference 4. The points used to construct curve (2) are mean values of Mg/Si for each albedo interval.

Table 1.—*The Mean Square Deviations and the Number of Measurements for Corresponding Albedo Intervals,* $\Delta\rho_0$

$\Delta\rho_0$	M	δ
6–7	29	± 0.049
7–8	29	.039
8–9	12	.040
9–10	6	.022
10–11	3	.030
11–12	6	.030
12–13	5	.037
13–14	9	.040
14–15	15	.058
15–16	10	.037
16–17	9	.059

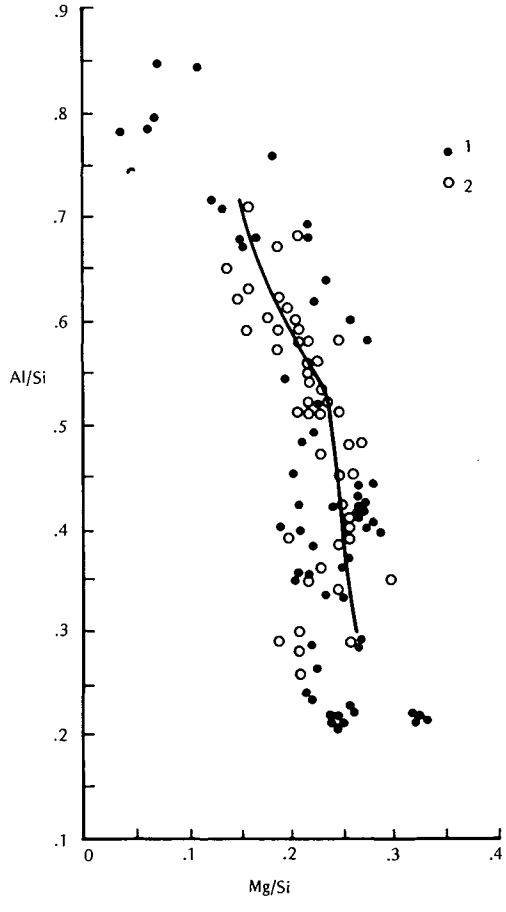


Figure 3.—*A curve showing the dependence of the relative contents of Al and Mg for surface rocks of identical albedo. The filled circles are for the analyses of returned samples and the open circles are for orbital data.*

One confirmation of the fact that albedo is a recognition indicator for rocks is the comparison in figure 2 of the dependence between the Al/Si and Mg/Si ratios and the results of selenochemical studies. Figure 3 presents a curve corresponding to the dependence of the relative contents of aluminum and magnesium for surface rocks of identical albedo (using the data of fig. 2). The individual points show the same relationship as do results of chemical analyses of specimens returned to Earth (filled circles "1") (refs. 5–13) and as do the results of selenochemical orbital study of individual sections (open circles "2") (ref. 4). Figure 3 shows that this curve actually reflects the mean relationship between Al/Si and Mg/Si. Consequently, the normal albedo can be considered a statistical mean indicator of rock type. This fact allows us to judge the distribution of lunar rocks of various types for 80 percent of the entire surface of the lunar sphere, i.e., that area covered by the measurements of normal albedo. Figure 4 shows a histogram of the albedo distribution. The histogram was constructed on the basis of a sample made from

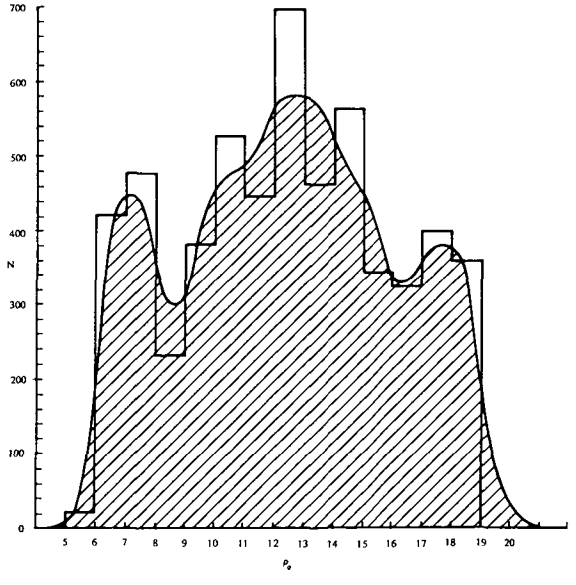


Figure 4.—*A histogram of the albedo distribution.*

Table 2.—*An Attempt to Identify the Maxima in Figure 4 With Known Rock Types, Using the Correlation Between Albedo and Al/Si Ratios*

Type of Rock	Al/Si	ρ_0 (percent)	S (percent)
Maria basalts	< 0.40	< 8	16.4
Norites	0.40–0.55	8–12	28.0
Anorthositic Gabbro	0.55–0.65	12–16	36.4
Gabbroic Anorthosites	0.65–0.85	> 16	19.2

the albedo map by using an ideal system of points to create an even distribution of readings over the scale. The ordinate shows the number of points; the abscissa shows the corresponding normal albedo intervals. The smooth curve clearly shows four maxima within the distribution presented. Table 2 shows an attempt to identify the maxima with known types of lunar rock on the basis of the connection established above between albedo and chemical composition (with respect to relative aluminum content). The same table presents preliminary data on the area of the lunar surface within which the rock types mentioned are found. Anorthosites, for which Al/Si > 0.85, occupy a comparatively small area, amounting to less than 6 percent of the entire surface.

Actually, the result produced relates only to the thin upper layer of lunar soil. Reflected radiation in the visible area of the spectrum, like fluorescence, radiation in the X-ray area, comes from the upper layer of lunar soil, less than 1 millimeter thick.

However, the heterogeneity of the surface structure of the lunar regolith practically means that the radiation recorded contains information on the material of deeper layers, which has been exposed or has been carried to the surface by crater-forming processes. It can be shown that the variations in albedo over significant areas reflect the peculiarities of the deep (down to several tens of kilometers) structure of the Moon. We know that on the global scale, areas of lunar matter with higher density occur in large depressions in the surface. In particular, it has been established that the level of areas of mascons averages 4 km below the level of the continents (ref. 14). Consequently, if there is a correlation between the reflectivity of matter and the absolute heights of the corresponding structures, the assumption stated above can be considered well founded. In one work (ref. 15), based on brightness measurements in the western portions of the Ocean of Storms made from the Zond 8 photographs, it was shown that along several profiles, each 500–600 km in length, there is a correlation between albedo and absolute altitude with a correlation factor of 0.790. A similar study was performed along the profile from the topographic survey, made with a laser altimeter (ref. 16) in the area from 140° E to 160° W (including the visible hemisphere) with the albedo map (fig. 1). Calculations of the correlation factor for 50 data points distributed at equal intervals along the profile yielded a value of $r = 0.798 \pm 0.051$.

The relationships between albedo of the lunar matter and chemical composition, as well as surface and depth distribution of lunar rock, allow us to use the reflectivity of lunar material as a stratigraphic indicator. In reference 1, data on the chemical composition and absolute age of specimens returned from various regions of the lunar surface have been used to produce a dependence between relative aluminum content in the rock and its crystallization time. Using the relationship of Al/Si with albedo, we can reveal the relationship between the albedo and the age of structures. Both of these dependences are presented in figure 5 (the abscissa has a double scale: top scale—albedo; bottom scale —relative aluminum content). The position of individual points on the graph in most cases corresponds to the mean data for the region when samples were collected. Thus, it is possible to determine a probable age of surface rock in various areas of the visible and back sides of the Moon. Since the described dependences are statistical in nature, the results are correct for structures covering significant areas. Small formations such as individual craters, aureoles, and ray systems are exceptions to the general rule.

Basing our deductions on the overall struc-

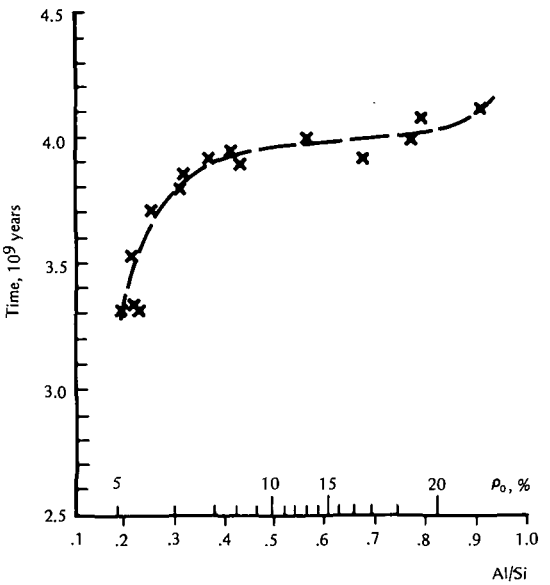


Figure 5.—*The age of lunar structures versus the Al/Si ratio and albedo.*

ture of the surface of the lunar sphere and considering the interrelationship of albedo, rock type, and crystallization time, we can draw the following preliminary conclusions. The contemporary lunar maria were formed within areas with predominantly noritic rock. At the present time, practically all maria are surrounded by zones of "dark" continental rock of probable noritic composition. Direct contact of the maria surface with light continental complexes, consisting of rocks of anorthositic type, is encountered very rarely. Within the limits of any given mare, sectors may be observed with variations of age of several hundreds of millions of years, eliminating the hypothesis of the catastrophic formation of the maria. This peculiarity indicates a very long and multiphased process of development of the maria areas. A general idea of the distribution of active processes on the Moon during various periods in history is given in figure 6. The integral curve of frequencies, constructed on the basis of the accumulated frequencies of albedo distribution (ordinate), based on the relationship of albedo to age (abscissa), shows the fraction of the entire lunar surface formed earlier than a given rock age. Figure 6 indicates that in the era before 4.0 billion years ago, active processes, accompanied by the melting of lunar matter with subsequent crystallization, covered the entire surface of the lunar sphere. During this time, the continental rocks of the anorthositic complex were primarily formed. During the next 0.1–0.2 billion years (formation time of norites), the active zone was gradually reduced, and during the last 3.0–3.5 billion years it has not exceeded a fraction of 1 percent of the entire surface of the moon.

The above-presented dependences of albedo on chemical composition and crystallization age are statistical in nature and are correct, as we have noted, for large territories. As concerns individual formations and small areas of the lunar surface, these dependences can be used for preliminary estimation only. Even in this case, however, the information is apparently of great interest for regions which have not been studied in detail by direct methods.

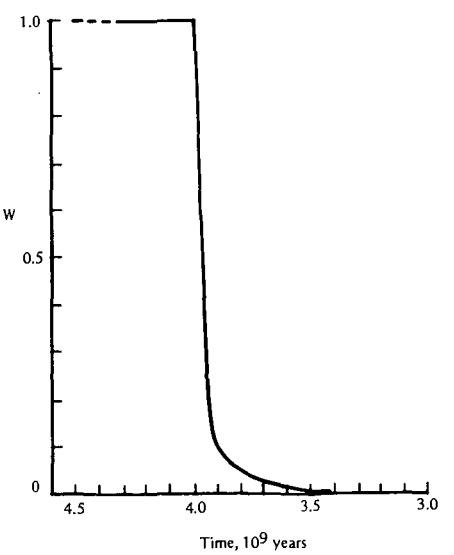


Figure 6.—*The distribution of active processes on the Moon during various periods in lunar history.*

References

1. SHEVCHENKO, V. V., *Astron. Zhurn.* In press.
2. ADLER, I., J. TROMBKA et al., *Science*, Vol. 175, No. 4020, 1972.
3. ADLER, I., J. TROMBKA et al., *Science*, Vol. 177, No. 4045, 1972.
4. ADLER, I., J. TROMBKA, et al., *The Moon*, Vol. 7, Nos. 3 and 4, 1973.
5. VINOGRADOV, A. P., *Geokhimiya*, No. 3, 1971.
6. VINOGRADOV, A. P., *Geokhimiya*, No. 7, 1972.
7. WOOD, J. et al., *Smithsonian Astrophysical Observatory, Special Report 307*, 1970.
8. WOOD, J. et al., *Smithsonian Astrophysical Observatory, Special Report 333*, 1971.
9. Summary of Apollo 11 Lunar Science Conference. *Science*, Vol. 167, No. 3918, 1970.
10. Preliminary Examination of Lunar Samples from Apollo 12. *Science*, Vol. 167, No. 3923, 1970.
11. Preliminary Examination of Lunar Samples from Apollo 14. *Science*, Vol. 173, No. 3998, 1971.
12. The Apollo 15 Lunar Samples: A Preliminary Description. *Science*, Vol. 175, No. 4020, 1972.
13. The Apollo 16 Lunar Samples: Petrographic and Chemical Description. *Science*, Vol. 179, No. 4068, 1973.
14. LEYKIN, G. A., M. P. POPOVA AND ZH. F. RODIONOVA, *Astron. Tsirk.*, No. 755, 1973.
15. LIPSKIY, YU. N., S. V. LANDAU, M. F. SHAVANOV AND V. V. SHEVCHENKO, *Kosmich. Issled.* In press.
16. WOLLENHAUPT, W. R. AND W. L. SJOGREN, *The Moon*, Vol. 4, Nos. 3 and 4, 1972.

New Data for the Lunar 20 Core and a Survey of Published Chemical Data

N. J. Hubbard
Johnson Space Center
Houston, Texas

A. P. Vinogradov, G. I. Ramendik, and M. S. Chupakhin
V. I. Vernadskiy Institute of Geochemistry
and Analytical Chemistry
Academy of Sciences,
Moscow, U.S.S.R.

The new analyses were obtained at Vernadsky Institute using a spark source mass spectrometer and a new method of analysis. About 10 mg of sample was pressed in an Al cup without the addition of an electrically conducting material (ref. 1). The opposing electrode was of Ta and served as the cathode. The analyses were corrected with the assistance of a device to cut off the arc stage of the discharge (refs. 2 and 3). This provides simpler spectra because of the resulting large reduction of complex ions and also provides stabilization of the sensitivity coefficients from sample to sample. Intersample precision is considered to be ± 5 to 15 percent.

At the start of analyses, three lunar soil samples—10084, 12070, and 14163—were chosen as control samples and geological samples W–1, BCR–1, and AGV–1 were to be standards. However, the first round of analyses demonstrated that only the lunar soil samples could serve as standards because the sensitivity coefficients for the geological standards often had prohibititively large scatter. Therefore the new data were taken relative to 12070. The new and published data for the fine fraction of the Luna 20 core are given in table 1 so that the readers can draw their own conclusions about the quality and interlaboratory biases of the results. Figure 1 shows the subdivision of the Luna 20 core, the corresponding Soviet sample numbers, and the relative position of the American sample. All samples analyzed in the U.S.S.R. were from the less than 83μ fraction, while the American samples were from the less than 125μ fraction.

The analytical results for the four zones of the Luna 20 core suggest that the core is nonuniform with depth (fig. 2). The higher concentrations of Ce, Sc, Ba, La, Co, Sr, and Zr in zone 2001 may be connected with the presence in this zone of a basaltic rock type seldom seen in the other zones (ref. 13). That is, about half of the basaltic fragments in the large size fractions in zone 2001 are of a specific porphyritic breccia-like type. Anorthositic fragments containing a noteable amount of metallic iron are basically limited to zone 2004 and probably explain the lower concentrations of Ce, Rb, Ba, La, and perhaps Co in this zone.

We also confirm the high concentrations of Ag and Ce found by Laul and Schmitt (ref. 7) and also by Morgan et al. (ref. 8). Although Ag is at nearly the same concentration in all four zones of the core, Cd in the core is the result of local enrichment. In particular, in zone 2004 the concentration of Cd may be as high as 10 ppm in a sample size of 0.01 mg.

Table 1.—*New Spark Source Mass Spectrometric Data for the Four Zones of the Luna 20 Core Tube and a Survey of Published Data*

Element	Helmke et al. (ref. 5)	Jerome and Philpotts (ref. 6)	Laul and Schmitt (ref. 7)	Morgan et al. (ref. 8)	Nava and Philpotts (ref. 9)	Bansal et al. (ref. 10)	Best Values 1–6	Surkov et al. (ref. 11) 2004	Yakovlev et al. (ref. 12) 2004	New Trace Element Data [ω]			
										Zone 2001	Zone 2002	Zone 2003	Zone 2004
	1	2	3	4	5	6	7	8	9	10	11	12	13
SiO_2	—	—	—	—	45.4	—	—	—	—	—	45.8	—	44.4
FeO	—	7.78	8.1	—	7.37	—	—	—	—	—	7.02	—	7.03
Al_2O_3	—	22.73	22.8	—	23.44	—	—	—	—	—	21.6	—	22.9
MgO	—	—	10	—	9.19	—	—	—	—	—	9.85	—	9.70
CaO	—	15.81	14.2	—	13.38	—	—	—	—	—	14.9	—	15.2
TiO_2	—	0.43	0.49	—	0.47	0.47	0.47	—	—	—	0.533	—	0.56
Na_2O	—	0.38	0.334	—	0.29	0.41	—	—	—	—	0.46	—	0.55
K_2O	—	—	0.076	—	0.0666	0.0691	—	—	—	—	0.10	—	0.10
P_2O_5	—	—	—	—	0.06	—	—	—	—	—	0.17	—	0.14
MnO	—	0.105	0.104	—	0.10	—	0.10	—	—	—	0.13	—	0.12
S	—	—	—	—	—	—	—	—	—	—	0.08	—	0.08
Sc	16	16.2	16.5	—	—	—	16.2	20	—	18.5	15	16.3	15.5
Co	26	34	27	—	—	—	27	25	—	32	40	24	18.6
Ni	—	—	260	—	—	—	—	—	—	315	262	243	280
Zn	35 ± 14	—	21.0	21.5	—	—	21	—	—	14.4	21.4	16	28
Rb	2.0	—	1.6	1.5	1.6	1.6	1.6	—	—	1.35	1.31	1.49	0.86
Sr	—	—	—	—	144	140	142	—	—	231	150	145	162
Zr	—	—	—	—	94	115	110	—	—	143	109	87	167
Y	—	—	—	—	—	—	—	—	—	22	15.8	19.8	18.0
Ba	—	—	—	—	93.8	87.3	90.6	—	—	134	116	126	85
La	6.7	6.4	6.2	—	—	6.13	6.13	6.0	6.5	6.9	5.8	5.5	4.3
Ce	15.8	20.3	16	—	16.1	17.7	17.0	15	13.7	21.4	19.7	19.9	14.8
Pr	—	—	—	—	—	—	—	2.1	2.06	—	—	—	—
Nd	10.5	11.1	—	—	10.6	10.3	10.5	12	11.4	—	—	—	—

Sm	3.23	3.2	3.1	—	2.98	2.97	2.93	3.0	2.68	—	—	—	—
Eu	0.94	0.96	0.92	—	0.94	0.922	0.931	0.88	0.88	1.00	0.93	1.12	0.71
Gd	4.4	—	—	—	3.81	3.80	3.81	4.0	4.02	—	—	—	—
Tb	0.68	0.66	0.63	—	—	—	0.66	0.6	0.66	—	—	—	—
Dy	4.48	—	4.0	—	4.08	4.23	4.16	3.7	4.2	—	—	—	—
Ho	0.85	—	—	—	—	—	—	0.9	0.86	—	—	—	—
Eu	3.0	—	—	—	2.40	2.66	2.53	2.4	2.77	—	—	—	—
Tm	—	0.35	—	—	—	—	—	0.35	0.48	—	—	—	—
Yb	2.38	2.30	2.6	—	2.36	2.54	2.40	1.9	2.65	—	—	—	—
Lu	0.349	0.37	0.43	—	0.38	0.375	0.37	0.36	0.34	—	—	—	—
Cr	1370	1250	1232	—	953	1663	—	—	—	—	—	—	—
Sb	—	—	0.760	0.0098	—	—	—	—	—	—	—	—	—
In	—	—	0.010	0.0039	—	—	—	—	—	—	—	—	—
Hf	2.9	2.1	2.5	—	2.7	—	2.6	—	—	—	—	—	—
Cs	0.05	—	0.07	0.07	—	—	0.070	—	—	—	—	—	—
Br	—	—	—	0.140	—	—	—	—	—	—	—	—	—
Se	—	—	0.200	0.209	—	—	0.205	—	—	—	—	—	—
Ge	—	—	—	0.430	—	—	—	—	—	20.4	18.2	30.2	18.2
V	—	—	47 ± 7	—	—	—	—	—	—	—	—	—	—
Cd	—	—	19.4	1.74	—	—	—	—	—	0.3	1.8	0.81	0.61
Ag	—	—	0.72	3.08	—	—	—	—	—	0.1	0.18	0.18	0.22

NOTE: (1) Data for major elements (SiO_2 through S) for zones 2002 and 2004 are from Vinogradov (ref. 4).

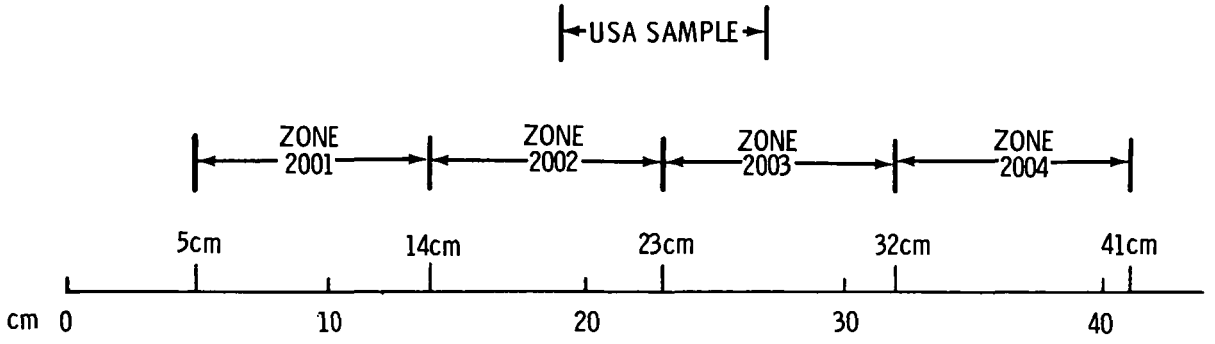


Figure 1.—*This figure shows the relative positions of the four zones of the Luna 20 core tube and the Soviet numbers for those zones relative position of the American sample. The centimeter values refer to distance along the tray into which the core was extruded, not to depths in the core tube.*

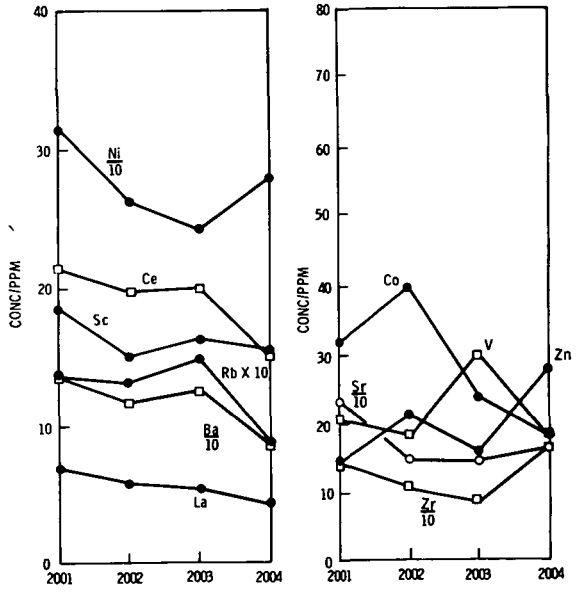


Figure 2.—*The concentrations of several elements in the four zones of the Luna 20 core tube.*

References

1. CHUPAKHIN, M. S., O. I. KRYUCHKOVA AND G. I. RAMENDIK, *Analytical Capabilities of Spark Mass Spectrometry*, Atomizdat Press, Moscow, 1972.
2. RAMENDIK, G. I., M. S. CHUPAKHIN, YU. G. TATSIY AND V. I. DERZHIYEV, *Zh Anal. Khim.*, Vol. 29, 1974, p. 238.
3. CHUPAKHIN, M. S., G. I. RAMENDIK, V. I. DERZHIYEV, YU. G. TATSIY AND M. A. POTAPOV, *Dokl. Akad. nauk SSSR*, Vol. 210, 1973, p. 1074.
4. VINOGRADOV, A. P., *Geokhimiya*, Vol. 7, 1972, p. 763.
5. HELMKE, P. A., D. P. BLANCHARD, J. W. JAKOBS, L. HASKIN AND A. HASKIN, *Geochimica et Cosmochimica Acta 37*, 1973, p. 869.
6. JEROME, D. Y. AND J. C. PHILPOTTS, *Geochimica et Cosmochimica Acta*, 1973, p. 909.
7. LAUL, J. C. AND R. A. SCHMITT, *Geochimica et Cosmochimica Acta*, 1973, p. 927.
8. MORGAN, J. W., U. KRÄHENBÜHL, R. GANAPATHY AND E. ANDERS, *Geochimica et Cosmochimica Acta*, 1973, p. 953.
9. NAVA, D. F. AND J. A. PHILPOTTS, *Geochimica et Cosmochimica Acta*, 1973, p. 963.
10. BANSAL, B. M., S. E. CHURCH, P. W. GAST, N. J. HUBBARD, J. M. RHODES AND H. WIESMANN, *Earth Planet. Sci. Letters*, Vol. 17, 1972, p. 29.
11. SURKOV, YU. A., G. M. KOLESOV AND F. F. KIRNOZOV, *Geokhimiya*, Vol. 1, 1974, p. 3.
12. YAKOVLEV, YU. V., N. N. DOGADKIN, A. Z. MIKLISHANSKIY, O. V. STEPANETS AND B. V. SAVEL'YEV, *Collection of Materials Connected to the Study of Luna 20*. In press.
13. TARASOV, L. S., K. P. FLORENSKIY, A. V. IVANOV AND O. D. RODE, *Geokhimiya*, Vol. 9, 1973, p. 1175.

Chemical Composition of Crystalline Rock Fragments From Luna 16 and Luna 20 Fines

A. Cimbálníková and M. Palivcová
Geological Institute, Czechoslovak Academy of Sciences
Prague-Suchdol, Czechoslovakia

J. Frána and A. Maštalka
Institute of Nuclear Physics
Czechoslovak Academy of Sciences,
Řež, Czechoslovakia

This paper deals with the chemical composition (bulk, rare earth, and trace elements) of the Luna 16 mare regolith and Luna 20 highland regolith, as shown by 14 basaltic rock fragments (Luna 16) and 13 rock fragments of the ANT suite (Luna 20). On the basis of bulk composition, two types of basaltic rocks have been differentiated and defined in the Luna 16 regolith: mare basalts (fundamental crystalline rocks of Mare Fecunditatis) and high-alumina basalts. The bulk analyses of rock fragments of the ANT suite also enabled distinction of two rock types: anorthositic norites and troctolites and/or spinel-troctolites (the most abundant crystalline rocks of the highland region, the landing site of Luna 20), and anorthosites. The chemical composition of Luna 16 and Luna 20 regolith samples is compared. Differences in the chemistry of the Luna 16 mare regolith and that of mare basalts are discussed. The chemical affinity between the Luna 20 highland regolith and (a) anorthositic norites and (b) troctolites and/or spinel-troctolites has been ascertained.

The Soviet Luna 16 automatic station collected soil samples in the typical lunar mare region (Mare Fecunditatis) and Luna 20 in the typical highland region, between Mare Fecunditatis and Mare Crisium, near Apollonius C Crater, about 120 km north of the sample collection of Luna 16 (ref. 1). Examination of the two samples makes it possible to compare the rocks of these lunar regions of different geological character.

In Czechoslovakia, the lunar soil samples of Luna 16 and Luna 20 (both whole samples and their rock fragments) were subjected to interdepartmental studies. The fragments were handpicked from the fraction of above 100 μm and were preliminarily characterized under a stereomicroscope. The results of chemical analyses and petrographic studies of some lunar rock fragments (primary and secondary) from the Luna 16 soil have been published, for example, in Adam et al. (ref. 2), Cimbálníková et al. (ref. 3), and Cimbálníková et al. (in press, 1974) (ref. 4).

This paper presents the chemical composition of other lunar crystalline rock fragments obtained from the Luna 16 mare regolith samples—14 fragments of basaltic rocks, including four analyses of basaltic fragments (see table 1). The analyses were published in Adam et al., 1973 (ref. 1). This paper also presents analyses from the Luna 20 highland regolith (13 rock fragments of the ANT suite) (see table 2). The nondestructive neutron activation analysis (INAA) was used for the study; and the weight of the samples analyzed ranged from 0.097 to 4.764 mg.

The purpose of our study was (1) to determine the chemistry of crystalline rock types from Luna 16 and Luna 20 soils (by their bulk composition) and to compare them; (2)

Table 1.—*Chemical Composition of Soil and*

		Luna 16 Soil	Mare Basalts							
			1012 [1]	1007 [1]	1008 [1]	2005 [1]	1029	1651	1652	1653	1654
		mg	2.660	0.670	0.366	0.724	0.545	1.880	0.719	1.337	1.990
Wt. %	Si	20.0	16.5	17.2	24.3	20.6	< 33.0	22.5	21.8		27.6
	Ti	1.9	2.2	2.3	2.5	2.5	2.1	3.2	2.9	3.2	2.9
	Al	8.7	4.6	4.7	4.7	4.9	4.8	6.9	6.9	7.0	7.2
	Cr	0.20	0.21	0.20	0.24	0.18	0.14	0.19	0.17	0.25	0.18
	Fe	13.7	19.9	20.0	19.6	18.0	17.3	18.8	15.5	16.8	17.7
	Mn	0.20	0.23	0.22	0.20	0.21	0.18	0.22	0.25	0.21	0.23
	Mg	5.3	3.3	3.4	2.5	2.9	6.2	3.8	5.2	5.7	4.7
	Ca	9.2	6.5	6.2	6.2	6.7	8.8	8.6	7.4	8.3	7.8
	Na	0.32	0.42	0.50	0.47	0.40	0.30	0.33	0.30	0.35	0.35
	K	0.12	0.17		0.22	0.19	0.18	0.14	0.16		0.14
ppm	Sc	60	89	83	88	83		70	55	76	70
	V	90	55	51	68	60	65	89	81	104	89
	Co	30	22	27	27	30	30	24	60	25	22
	Sr	350	500	754	741		560	800	1100		1000
	Ba	250	280	410	243	294	330	400	400	460	400
	La	15					10	20	20	16	21
	Ce	45	59	79	66	56		65	65	58	70
	Nd	40						50	60	70	62
	Sm	7	15	19	17	14	11	15	16	15	15
	Eu	2	5	6	5	5	2	4	3.5	4	5
	Tb	1.7						2.8	2.5	2.5	3
	Dy	12	17.3	31.6	26	31.9	14	20	24	14	21
	Ho	2.2						4	4	3	5
	Tm							2.6	2.8	2.7	1.6
	Yb	6						9	9	7	10
	Lu	1						1.5	1.4	1.1	1.5
	Hf							13	10	11	14
	Th	1.1						1.1	1.2	—	1.2
	U	0.7	0.9								1
Wt. %	SiO_2	42.8	35.3	36.8	52.0	44.1		48.1	46.6		59.1
	TiO_2	3.17	3.7	3.8	4.2	4.2	3.5	5.3	4.8	5.3	4.8
	Al_2O_3	16.4	8.7	8.8	8.9	9.3	9.1	13.1	13.0	13.2	13.6
	Cr_2O_3	0.29	0.31	0.29	0.35	0.26	0.21	0.28	0.25	0.37	0.26
	FeO	17.6	25.6	25.7	25.2	23.1	22.5	24.2	19.9	21.6	22.7
	MnO	0.26	0.29	0.28	0.26	0.27	0.23	0.28	0.32	0.27	0.29
	MgO	8.8	5.5	5.6	4.2	4.8	10.3	6.3	8.6	9.5	7.8
	CaO	12.9	9.1	8.7	8.7	9.4	12.3	12.0	10.4	11.6	10.9
	Na_2O	0.43	0.56	0.66	0.62	0.53	0.40	0.44	0.40	0.46	0.46
	K_2O	0.144	0.20		0.26	0.23	0.21	0.17	0.19		0.17

NOTE: (1) Adam et al. (ref. 2).

Basaltic Fragments From Luna 16 Fines

Mare Basalts—Continued				High-Alumina Basalts				
1656	1659	Average	Range	1028	1657	1662	Average	Range
0.327	0.599			1.092	0.320	0.344		
21.5			16.5 – 27.6	40.0	24.0	18.5		18.5 – 24.0
2.5	3.8	2.7	2.1 – 3.8	1.4	2.4	1.6	1.8	1.4 – 2.4
5.0	7.2	5.8	4.6 – 7.2	8.6	7.5	9.7	8.6	7.5 – 9.7
0.12	0.20	0.19	0.12 – 0.25	0.20	0.14	0.19	0.18	0.14 – 0.20
13.7	16.1	17.6	16.1 – 20.0	12.1	11.1	10.1	11.1	10.1 – 12.1
0.21	0.23	0.20	0.18 – 0.25	0.17	0.20	0.16	0.18	0.16 – 0.20
4.2	5.3	4.3	2.5 – 6.2	5.7	5.2	5.1	5.3	5.1 – 5.7
7.5	9.8	7.6	6.2 – 9.8	9.2	8.7	9.7	9.2	8.7 – 9.7
0.40	0.35	0.38	0.30 – 0.50	0.27	0.30	0.25	0.27	0.25 – 0.30
0.15	0.14	0.17	0.14 – 0.22		0.12	0.10	0.11	0.10 – 0.12
57		75	55 – 89	50	55	45	50	45 – 55
67	107	76	51 – 107	105	105	67	92	67 – 105
	25	29	22 – 60	45	100	30	58	30 – 100
	500	744	500 – 1100	300	—	—	300	
420	400	371	243 – 460	170	360	400	310	170 – 400
22	20	18	10 – 22	11	15	12	13	11 – 15
73	60	65	59 – 79	66	50	35	50	35 – 66
65	60	61	50 – 70	27	20	30	26	20 – 30
17	15	15	11 – 19	7	12	10	10	7 – 12
4.6	4	4.4	2 – 6	2	4	2.5	2.8	2 – 4
2.5	3	2.7	2.5 – 3		2	1.3	1.6	1.3 – 2
26	22	22.5	17.3 – 31.9	11	20	12	14	11 – 20
4	4.2	4	3 – 5		3.5	2	2.8	2 – 3.5
2.4		2.4	1.6 – 2.8		1.9	1.2	1.6	1.2 – 1.9
9	9	9	7 – 10	5.5	7	6	6	5.5 – 7
1.5	1.3	1.4	1.1 – 1.5	0.7	1	0.8	0.8	0.7 – 1
13	13	12	10 – 14		8	6	7	6 – 8
1.7	1.5	1.3	1.1 – 1.7		1.1	1.7	1.4	1.1 – 1.7
		1	0.9 – 1					
46.0			35.3 – 59.1		51.4	39.6		39.6 – 51.4
4.2	6.3	4.6	3.5 – 6.3	2.3	4.0	2.7	3.0	2.3 – 4.0
9.6	13.6	11.0	8.7 – 13.6	16.25	14.2	18.3	16.2	14.2 – 18.3
0.13	0.29	0.28	0.18 – 0.37	0.29	0.21	0.28	0.26	0.21 – 0.29
17.6	20.7	22.6	17.6 – 25.7	15.6	14.3	13.0	14.3	13.0 – 15.6
0.27	0.29	0.28	0.23 – 0.32	0.22	0.26	0.20	0.23	0.20 – 0.26
7.0	8.8	7.1	4.2 – 10.3	9.5	8.6	8.5	8.9	8.5 – 9.5
10.5	13.7	10.7	8.7 – 13.7	12.9	12.2	13.6	12.9	12.2 – 13.6
0.53	0.46	0.50	0.40 – 0.66	0.36	0.40	0.33	0.36	0.33 – 0.40
0.18	0.17	0.20	0.17 – 0.26		0.14	0.12	0.13	0.12 – 0.14

Table 2.—*Chemical Composition of Soil and Rock*

		Luna 20 Soil	Anorthosites						
			20001	20002	20010	20012	20013/15	Average	Range
		mg	0.518	0.622	0.410	0.213	0.233		
Wt. %	Si	20.0	23.0	14.8	20.0	24.0	21.0		14.8 – 24.0
	Ti	0.28	—	—	—	—	—	—	
	Al	12.5	18.8	20.9	20.1	17.5	19.7	19.5	17.5 – 20.9
	Cr	0.11	180(1)	50(1)	18(1)	10(1)	38(1)	29(1)	10(1) – 50(1)
	Fe	5.1	1.90	0.30	0.14	0.17	0.25	0.22	0.14 – 0.30
	Mn	83(1)	400(1)	84(1)	50(1)	100(1)	80(1)	78(1)	50(1) – 100(1)
	Mg	5.7	1.9	1.3	1.2	1.2	1.7	1.4	1.2 – 1.7
	Ca	10.3	14.0	14.7	16.2	13.7	13.5	14.5	13.5 – 16.2
	Na	0.26	0.35	0.37	0.20	0.22	0.30	0.27	0.20 – 0.37
	K	0.05	—	560(1)	300(1)	<800(1)	610(1)	490(1)	300(1) – 610(1)
ppm	Sc	15	5	1.5	0.2	0.3	0.6	0.7	0.2 – 1.5
	V	43							
	Co	28	45	31	47	90	90	64	31 – 90
	Sr	<120	435	400	300	<450	360	353	300 – 400
	Cs	240							
	Ba	170	80	10	200	140	150	125	10 – 200
	La	8	1.1	0.6	1.7	2	2	1.6	0.6 – 2
	Ce	18	2.7	2.1	4	4	5	3.8	2.1 – 5
	Nd	20							
	Sm	3.5	0.5	0.33	0.5	1	0.5	0.6	0.3 – 1
	Eu	1	0.7		1.8	0.8	1.5	1.4	0.8 – 1.8
	Tb	0.6		0.1					
	Dy	5	1	0.9	0.8	1	0.5	0.8	0.5 – 1
	Ho	1.3							
	Yb	2.5	0.5	0.3				0.3	
	Lu	0.4	0.05	0.05				0.05	
	Hf	0.3	0.3	0.3					
	Th	0.9	0.17						
	U	0.75							
Wt. %	SiO_2	42.8	49.2	31.7	42.8	51.4	45.0		31.7 – 51.4
	TiO_2	0.47	—	—	—	—	—	—	—
	Al_2O_3	23.6	35.5	39.5	38.0	33.1	37.2	36.95	33.1 – 39.5
	Cr_2O_3	0.16	260(1)	73(1)	26(1)	14(1)	55(1)	42(1)	14(1) – 73(1)
	FeO	6.6	2.4	0.38	0.18	0.22	0.32	0.28	0.18 – 0.38
	MnO	0.10	520(1)	108(1)	65(1)	130(1)	103(1)	101(1)	65(1) – 130(1)
	MgO	9.5	3.15	2.16	1.99	1.99	2.80	2.24	1.99 – 2.80
	CaO	14.4	19.6	20.6	22.7	19.2	18.9	20.4	18.9 22.7
	Na_2O	0.35	0.47	0.50	0.27	0.29	0.40	0.36	0.27 – 0.50
	K_2O	0.06		670(1)	360(1)		735(1)	590(1)	360(1) – 735(1)

NOTE: (1) In parts per million.

Fragments of the ANT Suite From Luna 20 Fines

Anorthositic Norites and Troctolites and/or Spinel-Troctolites									
20003	20004	20005	20023	20026/28	20032	20142	20143	Average	Range
2.829	0.483	0.258	0.097	0.227	0.140	4.764	0.773		
20.7	23.0		18.0	13.7	20.0	24.0	24.0		13.7 – 24.0
0.09	0.16	0.17	0.25		0.18	0.27	0.28	0.20	0.09 – 0.28
11.9	14.0	12.1	15.3	13.3	10.9	12.7	14.8	13.1	10.9 – 15.3
0.10	0.11	0.18	0.18	900 (1)	990 (1)	0.12	0.12	0.12	0.09 – 0.18
5.0	4.5	3.4	6.0	3.8	4.2	5.9	5.3	4.8	3.4 – 6.0
650 (1)	650 (1)	500 (1)	0.1	515 (1)	600 (1)	850 (1)	850 (1)	700 (1)	0.05 – 0.1
10.5	11.7	8.6	10.3	7.3	9.5	6.2	5.3	8.7	5.3 – 11.7
9.2	10.7	9.1	12.8	10.4	8.6	10.8	12.3	10.5	8.6 – 12.8
0.25	0.37	0.40	0.20	0.47	0.15	0.30	0.25	0.30	0.15 – 0.47
						0.10	550 (1)	780 (1)	550 (1) – 0.1
6	7.5	4.3	12	5.8		13	15	9.1	4.3 – 15
34	31	51	90	27		34	56	46	27 – 90
29	50	90	250	90	150	22	45	91	29 – 250
< 140						190	320	255	190 – 320
< 10		31							
100	100	220	290	300	160	200	150	190	100 – 300
1.3	1.5	3.4	1.5	2.9	3	19	8.5	5.1	1.2 – 19
4.2	6	8	5.6	8	7	40	20	12.3	4.2 – 40
0.6	0.65	1.4	0.9	1.1	1.2	8	4	2.2	0.6 – 8
0.8	0.6	0.8	0.7	1.2	1	1.5	1.4	1.0	0.6 – 1.5
		0.25				1.4	0.5		
1.2	1.3	2.7	4	1.6	2.8	10	6.4	3.7	1.2 – 10
			0.14			2	1.5		
0.6	0.8	1	0.7	1.4	1.6	6	2.8	1.9	0.6 – 2.8
0.08	0.07	0.16	0.10	0.12	0.20	0.90	0.40	0.25	0.07 – 0.90
						5.5	2.5		
						2.5	1		
						0.8			
44.3	49.2		38.5	29.3	42.8	51.4	51.4		29.3 – 51.4
0.15	0.26	0.28	0.41		0.30	0.45	0.47	0.33	0.15 – 0.47
22.5	26.5	22.8	28.9	25.1	20.6	24.0	28.0	24.8	20.6 – 28.9
0.14	0.16	0.26	0.26	0.13	0.14	0.18	0.18	0.18	0.13 – 0.26
6.4	5.8	4.3	7.7	4.9	5.4	7.6	6.8	6.1	4.3 – 7.7
840 (1)	840 (1)	645 (1)	0.13	665 (1)	775 (1)	0.11	0.11	0.09	645 (1) – 0.11
17.40	19.40	14.27	17.10	12.11	15.77	10.29	8.80	14.40	8.8 – 19.40
12.9	15.0	12.7	17.9	14.6	12.0	15.1	17.2	14.7	12.0 – 17.9
0.34	0.50	0.54	0.27	0.63	0.20	0.40	0.33	0.40	0.20 – 0.63
						0.12	0.06		

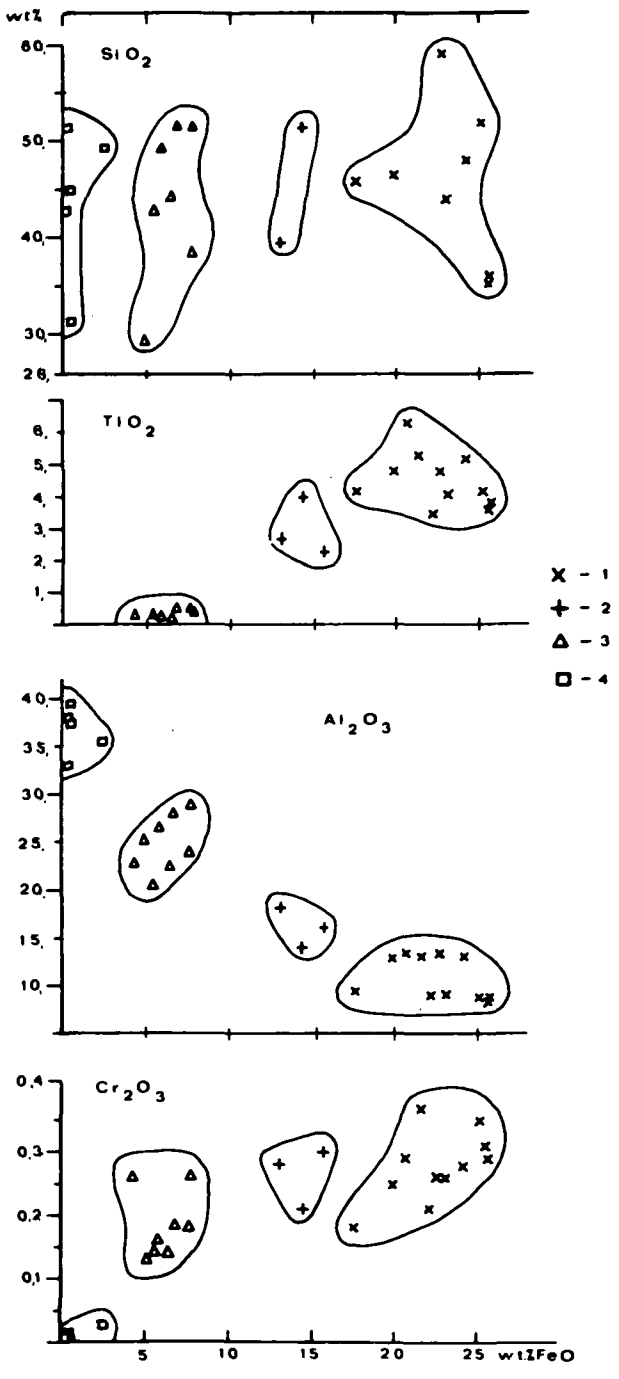


Figure 1.—*Plots of SiO_2, TiO_2, Al_2O_3, and Cr_2O_3 versus FeO in mare basalts and high-alumina basalts from Luna 16 soil and in rocks of the ANT suite from Luna 20 soil (1—mare basalts; 2—high-alumina basalts; 3—anorthositic norites and troctolites, and/or spinel-troctolites; and 4—anorthosites).*

in extending the number of analyzed fragments of lunar crystalline rocks, to contribute to a wider chemical basis for the statistical treatment of the data obtained, and thus to a more detailed and unbiased description of characteristics of the lunar rock types, and to the recognition of their genetic relations; and (3) to assess the differences in the chemistry of Luna 16 and Luna 20 soils and in that of the major and most abundant types of their crystalline rocks.

The fragments of crystalline rocks separated from the regolith samples are a more objective source of information on the nature of lunar rocks than the study of several more or less randomly collected samples. The study of local rock types typical of mare and highland lunar regions makes it possible to characterize these units of different geological nature. In contrast, the admixture of exotic rock types that are invariably present in the regolith and are derived from greater depths or distant places enables description of an overall characteristic of lunar rocks. The regolith can thus be regarded as a representative of the Moon rocks.

Experimental Studies

The preparation of samples for analysis, the irradiation method used in the nondestructive neutron activation analysis, and the evaluation of chemical composition have been described by Adam et al. (ref. 2). In this procedure the lower limits for quantitative determination are as follows:

Short-time irradiation:

Si	10 %
Ca, Ni	1 %
Ti, Pd, K, Rb, Mo	0.1%
Cl, Cu, Sr, Sn, Al, Ba, Te	100 ppm
Na, V, Sb, Co, Ga, As, Br, I, Cs, La, W	10 ppm
Mn, Sm, Re, Au, U	1 ppm
In, Eu, Dy	0.1 ppm

Long-time irradiation:

Fe, Ni, Zr	0.1%
K, Zn, Rb, Sn, Ce, Pr	100 ppm
Na, Cr, Mo, Ag, Te, La, Gd	10 ppm
Ca, Ga, As, Br, I, Ba, Tb, Mo,	

Tm, Yb, Hf, Ta, W, Re, Th, U	1	ppm
Se, Sb, Nd, Sn, Lu	0.1	ppm
Ir, Au	0.01	ppm

Results

Chemical compositions of analyzed crystalline rock fragments from Luna 16 and Luna 20 soils are summarized in tables 1 and 2. Figures 1 and 2 show the plots of the FeO content versus some other major elements.

Tables 1 and 2 and figures 1 and 2 show that the crystalline rock fragments from Luna 16 and Luna 20 soils form four groups, markedly differing in chemistry, which correspond to the following rock types:

1. Rocks of the ANT suite (anorthosite-norite-troctolitic suite) comprising (a) anorthosites and (b) anorthositic norities and troctolites and/or spinel-troctolites
2. Basaltic rocks involving two subgroups: (a) mare basalts and (b) high-alumina basalts.

For the designation of rocks, the nomenclature and chemical classification proposed by Prinz et al. (ref. 5) have been used.

All fragments of basaltic rocks were obtained from the Luna 16 mare regolith; rock fragments of the ANT suite were collected from Luna 20 highland regolith. Fragments of anorthositic rocks also occur in Luna 16 regolith as they do in all lunar maria sampled so far, but they were not analyzed by the INAA method, since they are rare, very brittle and light. Analogously, the Luna 20 highland regolith contained sporadic rock fragments identical with mare basalts.

ROCKS OF THE ANT SUITE

These constitute the dominant crystalline rock type of the Luna 20 highland regolith. Under a stereomicroscope they are white—milky- or icy-white; yellow olivines and pinkish-brown spinels are discernible in some specimens. The milky-white fragments of the ANT suite are either coarser grained (of

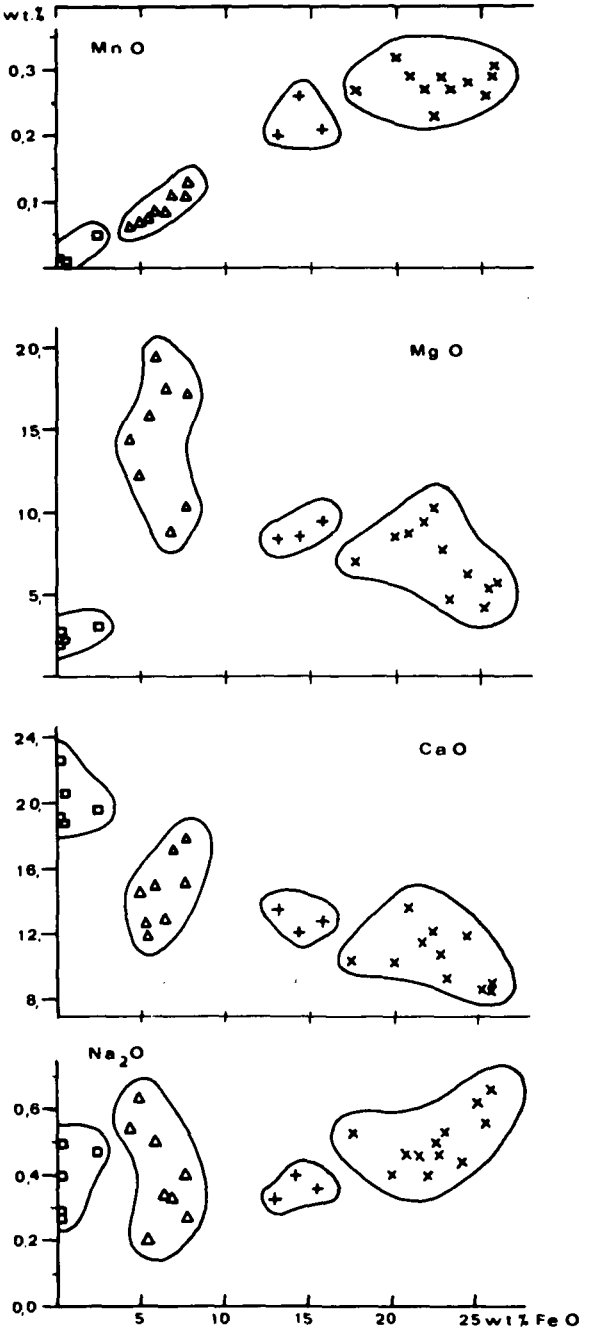


Figure 2.—*Plots of MnO, MgO, CaO, and Na_2O versus FeO in mare basalts and high-alumina basalts from Luna 16 soil and in rocks of the ANT suite from Luna 20 soil.*

depth derivation or recrystallized) or very fine grained (effusive or affected by shock or other alterations).

The rocks of the ANT suite are chemically characterized by a high Al_2O_3 content and low FeO and TiO_2. The Al_2O_3 invariably exceeds 22 weight percent.

From table 2 and figures 1 and 2 it is apparent that the rock fragments of the ANT suite do not constitute a compositionally continuous rock series ranging from anorthosites through noritic and troctolitic anorthosites (such a continuous series was determined by Prinz et al. (ref. 5) from the analyses of a much larger number of fragments (157) from Luna 20), but rather two separate groups. The rocks of the first group correspond in their chemical composition to anorthosites; the second group corresponds to anorthositic norites and troctolites and/or spinel troctolites.

Anorthosites (5 fragments) are virtually monomineral feldspathic rocks (> 90 percent plagioclases (refs. 6 and 5)). For their chemical composition, see table 2. They are characterized by average contents of Al_2O_3 (36.9 wt.%), FeO (0.3 wt.%), and MgO (2.2 wt.%). They are also characterized by ratios of CaO/Al_2O_3 (0.6), Fe/Al (0.01), and Fe/Mg (0.2).

Anorthosites differ from anorthositic norites and troctolites or spinel-troctolites in having higher Al and Ca and Eu (of microelements) and appreciably lower Cr, Fe, Mn, and Mg (7–10 times) and the following microelements: Sc, Co, Ce, Sm, Dy, Yb, Lu (2–4 times), and La. The differences in the content of elements of the two groups in the ANT suite are apparent from figure 3 (macroelements) and figure 4 (microelements). The values obtained for fragment 20001 have not been involved in the computation of average contents (Table 2), because it has somewhat higher Fe, Cr, and Mn relative to other anorthosites. Owing to this, it could be assigned more readily to noritic and troctolitic anorthosites, but its content of Al and Ca is too high for these rocks.

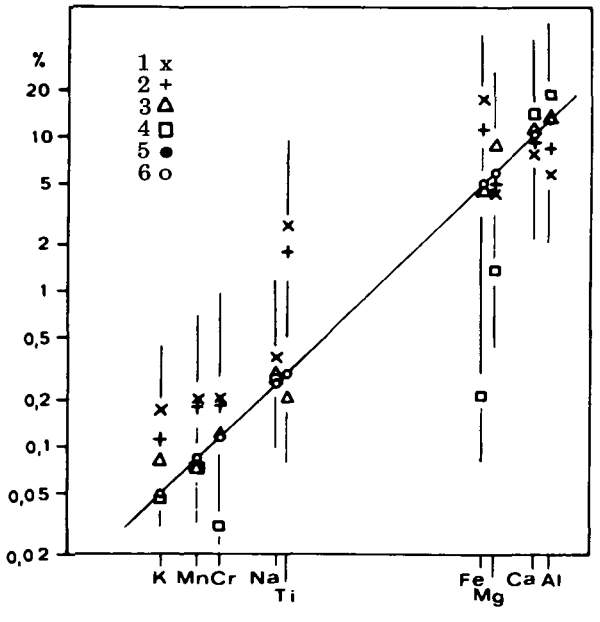


Figure 3.—*Plots of macroelement content in Luna 20 soil (on the straight line (6)) in mare basalts (1), high-alumina basalts from Luna 16 (2), in anorthositic norites and troctolites and/or spinel-troctolites (3), and in anorthosites from Luna 20 soil (4).*

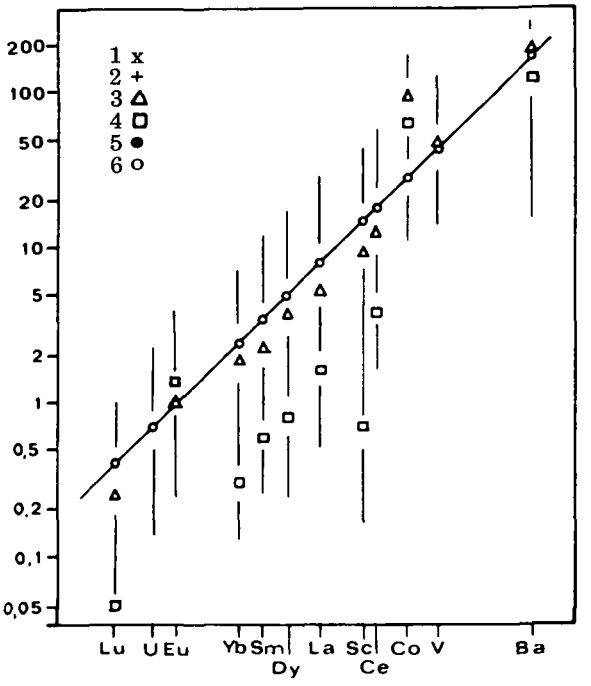


Figure 4.—*Plots of microelement content in Luna 20 soil (on the straight line) and in rocks of the ANT suite from Luna 20.*

Anorthositic norites and troctolites and/or spinel-troctolites (8 fragments) have a higher proportion of mafic minerals, which distinguish them chemically from the anorthosites.

The study of the lunar highland samples has shown that anorthositic norites and troctolites are the most abundant rocks of lunar highlands (refs. 7, 8, 9, 10, 1, and others). Prinz et al. (ref. 5) also identified rocks of spinel-troctolite type in the Luna 20 highland regolith and consider them to be the major highland rock type.

Most of the rock fragments of the ANT suite that we analyzed are compositionally equivalent to anorthositic norite and troctolite types.

Their average contents are as follows:

	Wt.%
Al_2O_3	24.8
FeO	6.1
MgO	14.4
Cr_2O_3	0.2
CaO	14.7

The mean ratios are $CaO/Al_2O_3 = 0.6$; $Fe/Al = 0.4$, and $Fe/Mg = 0.6$.

The average contents of macroelements are near the values given by Prinz et al. (ref. 5) for anorthositic norites and troctolites, except for MgO, which is higher and practically identical with that given by Prinz for spinel-troctolites. On the basis of bulk composition (table 2), fragments 20142, 20143, and probably also 20005 and 20026/28 may be regarded rather as anorthositic norites or troctolites, whereas fragments 20003, 20004, 20023, and 20032 are more likely to be regarded as troctolites. The former have a high TiO_2 content and comparatively lower MgO, while the latter show a strikingly high MgO. The contents of Al_2O_3, CaO, Cr_2O_3, FeO, and MnO do not allow an unequivocal differentiation of the two types in individual fragments. A more precise discrimination of the fragments of this group will be possible only by conducting a petrographical study of their thin sections.

Fragments with Al_2O_3 content corresponding to noritic and troctolitic anorthosites have so far not been found among our materials (except for fragment 20001, whose assignment is unclear). A compositional hiatus thus appears within the group of ANT suite rocks (figs. 1 and 2), which results in the existence of two separate subgroups (anorthosites and anorthositic norites and troctolites and/or spinel-troctolites). The fact that we have not safely established rocks of noritic and troctolitic anorthosite type may be caused by a small number of analyzed fragments, but it provides indirect evidence of the predominance of anorthositic norites and troctolites in the highland region sampled by Luna 20.

BASALTIC ROCKS

These are the major and most abundant crystalline rocks of the Luna 16 mare regolith. In a stereomicroscope, coarser grained microgabbro and fine-grained basalt are easily distinguishable (refs. 11 and 12). Chemically, the rocks have higher FeO and TiO_2 and lower Al_2O_3 than the highland rocks of the ANT suite. Table 1 and figures 1 and 2 show that basalts of two compositionally different types, i.e., mare basalts and high-alumina basalts, are represented in the 14 fragments of Luna 16 mare soils.

Mare basalts (11 fragments) are major crystalline rocks of Luna 16 soil. Like all basalts from the lunar mare terrains so far sampled, they are distinguished by high FeO —invariably above 20 wt.% (22.6 wt.% on the average, except for fragment 1656)—and a low Al_2O_3 content (11.0 wt.% on the average, with a maximum of 13.6 wt.%). The TiO_2 content is also high, averaging 4.6 wt.%. The average ratios are as follows: $CaO/Al_2O_3 = 1.0$; $Fe/Al = 3.0$; $Fe/Mg = 4.1$; and $TiO_2/Al_2O_3 = 0.4$. The chemical compositions of mare basalt fragments are presented in table 1. In regard to chemical composition, the chemistry of Luna 16 mare basalts and its relation to some secondary rocks of this regolith were discussed in more detail by Adam et al. (ref. 2).

In relation to other mare basalt fragments,

sample 1012 has a strikingly low FeO (table 1, figs. 1 and 2), only 17.6 wt.%. Its position in the graphs (figs. 1 and 2) at the mare basalt and high-alumina basalt boundary did not show clearly in which groups it should be placed. Since, however, the ratios of Fe/Al = 3.0, TiO_2/Al_2O_3 = 0.4, and CaO/Al_2O_3 = 1.0 are invariably higher than those of high-alumnia basalts, the fragment fits well into the group of mare basalts.

High-alumina basalts (3 fragments) were safely determined in the Luna 20 highland soils by Prinz et al. (ref. 5), who defined them as rocks transitional to anorthositic norites and troctolites. Compared with other rocks of the ANT suite, they have higher TiO_2, Cr_2O_3, FeO, MnO, K_2O, and P_2O_5, and lower Al_2O_3 and CaO. In relation to alkalic high-alumina basalts (KREEP), they are poorer in alkalies and REE. The authors named above believe these high-alumina basalts to be an important group of highland rocks that are genetically related to the rocks of the ANT suite.

Table 1 and figures 1 and 2 clearly show that the chemical composition of basaltic rock fragments 1028, 1657, and 1662 from mare regolith is near to that of high-alumina basalts described by Prinz et al. (ref. 5). The fragments we have studied have the following average contents:

	Wt.%
Al_2O_3	16.2
MgO	8.9
CaO	12.9
TiO_2	3.0

The average ratios are Ca/Al_2O_3 = 0.8, Fe/Al = 1.3, and Fe/Mg = 2.1.

The fragments are richer in Al_2O_3, MgO, and CaO, and poorer in FeO, Na_2O, and K_2O than the mare basalts (fig. 5). Of microelements, Sc, Sm, Dy, and particularly Sr occur in smaller amounts, whereas the V content is somewhat higher (fig. 6). The ratios of Fe/Mg, Fe/Al, TiO_2/Al_2O_3, and CaO/Al_2O_3 are lower than the ratios of mare basalts.

Basalts of KREEP type have not been found in the Luna 16 rock samples.

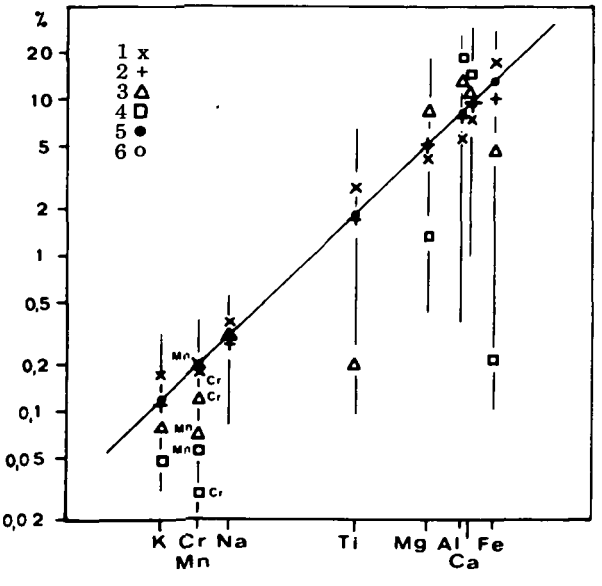


Figure 5.—*Plots of macroelement content in Luna 16 soil (on the straight line (5)), in mare basalts and high-alumina basalts from Luna 16, in anorthositic norites and troctolites and/or spinel-troctolites, and in anorthosites from Luna 20 soil.*

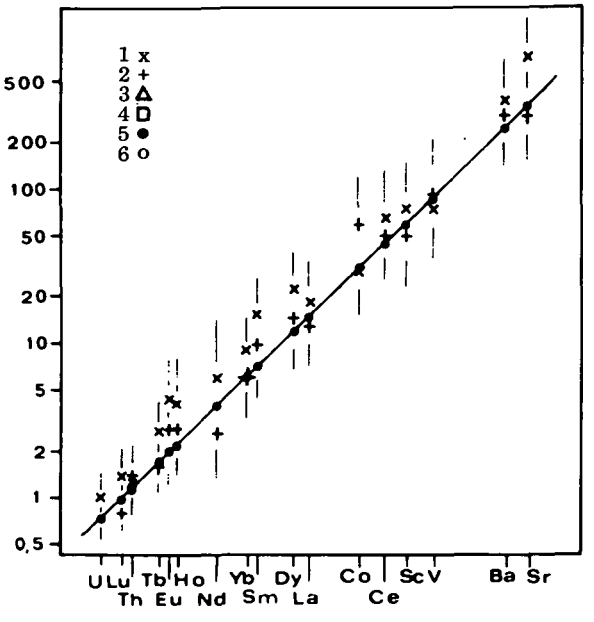


Figure 6.—*Plots of microelement content in Luna 16 soil (on the straight line) and in mare basalts and high-alumina basalts from Luna 16.*

CHEMICAL DIFFERENCES BETWEEN LUNA 16 AND LUNA 20 SOILS AND BETWEEN THEIR MAJOR OR MOST ABUNDANT CRYSTALLINE ROCK TYPES

Mare regolith—mare basalts

Compositional differences between the Luna 16 mare regolith and its basaltic rock fragments are shown in figure 5 (macroelements) and figure 6 (microelements). Compared with its major crystalline rocks, i.e., mare basalts, the Luna 16 regolith has lower Ti, Fe, Na, and K, and higher Al, Mg, and Ca; of microelements, Th, REE (La, Ce, Nd, Sm, Eu, Dy, Ho, Yb, and Lu), Sc, Ba, and Sr occur in smaller amounts, and V content is larger. The contents of Mn, Cr, and Co are very similar.

These differences are caused by an admixture of highland rocks. Figure 5 demonstrates that the deviations in the chemistry of the mare regolith, in relation to those of mare basalts, are more affected by anorthositic norites and troctolites than by anorthosites. This is exemplified especially by Mg (fig. 5), the content of which is higher in anorthositic norites and troctolites and lower in anorthosites than in mare basalts. The Mg amount in the regolith is still higher than in mare basalts and thus nearer to that in anorthositic norites and troctolites. As a result of deviations in the composition of the regolith caused by a proportion of anorthositic norites and troctolites, the chemistry of the Luna 16 mare regolith is closer to the composition of high-alumina basalts than to that of the mare basalts (fig. 5).

Highlands regolith—rocks of the ANT suite

The compositional relationships between the Luna 20 regolith and the ANT suite rocks are shown in figure 3 (macroelements) and figure 4 (microelements). In general, the composition of the Luna 20 highlands regolith shows a close affinity to anorthositic norites and troctolites, whereas it differs from the composition of anorthosites. Small deviations in the composition of the regolith and of anorthositic norites and troctolites are due rather to the presence of basaltic rock fragments than to that of anorthosites. Owing to basalt admixture, the Luna 20 highlands regolith has higher contents of Mn, Ti, and Fe, and lower amounts of Mg, Ca, and Al. On the whole, the Cr content remains unchanged. This chemical affinity between the Luna 20 highlands regolith and anorthositic norites and troctolites provides additional indirect evidence for the predominance of anorthositic norites and troctolites in the highland regolith.

Mare regolith—highlands regolith

The chemical data we have obtained for the Luna 16 and Luna 20 regolith samples (tables 1 and 2, respectively) are on the whole in agreement with the data given for both regoliths by Vinogradov (ref. 1).

For easier correlation, the relationships between the contents of elements from Luna 20 highland soils and Luna 16 mare soils are plotted in figure 7 (macroelements) and figure 8 (microelements). The latter have higher contents of K, Mn, Cr, Na, and especially Ti and Fe, and lower amounts of Mg, Ca, and Al than the former.

Conclusions

1. On the basis of bulk composition, two types have been differentiated in basaltic rock fragments from the Luna 16 mare soil: mare basalts and high-alumina basalts.

In relation to mare basalts, the high-alumina basalts have higher contents of Al_2O_3 (an average value of 16.2 versus 11.0 wt. %), MgO, and CaO, and lower content of FeO (an average value of 14.3 versus 22.6 wt.%), TiO_2, MnO, Na_2O, and K_2O.

2. Two rock groups have been distinguished in the rock fragments of the ANT

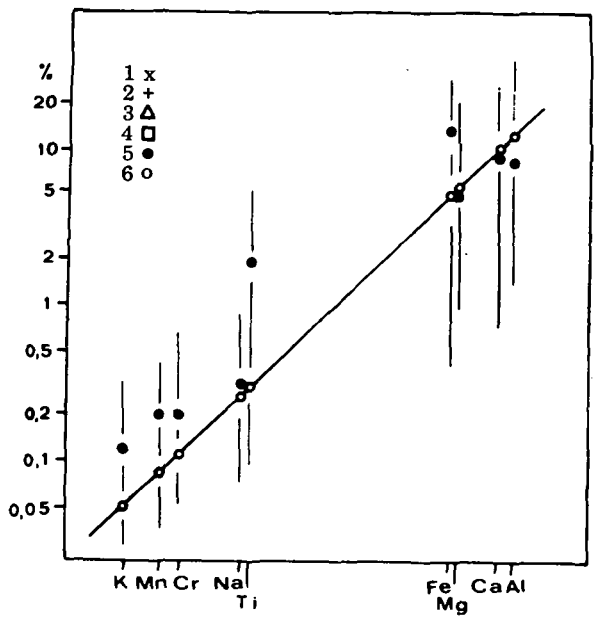


Figure 7.—*Plots of macroelement content in Luna 20 soil (on the straight line) and in Luna 16 soil.*

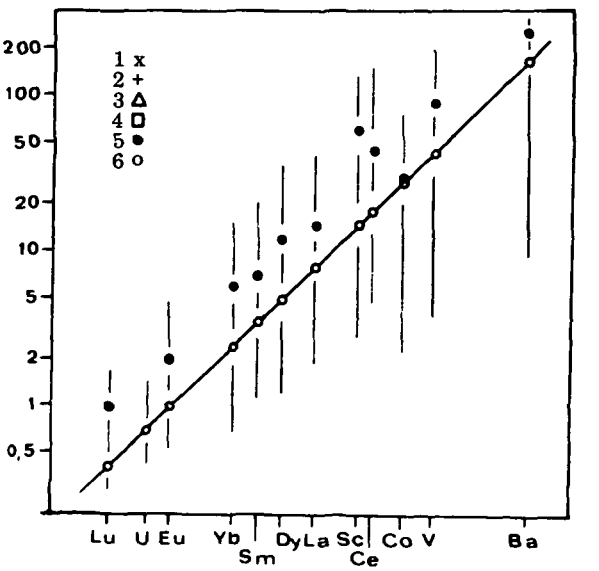


Figure 8.—*Plots of microelement content in Luna 20 soil (on the straight line) and in Luna 16 soil.*

suite from Luna 20 highlands regolith: anorthositic norites and troctolites and/or spinel-troctolites, and anorthosites.

Anorthositic norites and troctolites possess larger amounts of MgO (an average value of 14.4 versus 2.2 wt.%), TiO_2, Cr_2O_3, FeO, and MnO, and less Al_2O_3 (an average value of 24.8 versus 36.9 wt.%) and CaO, in comparison with anorthosites.

3. In relation to the major crystalline rocks, i.e., mare basalts, the Luna 16 mare regolith has lower contents of Ti, Fe, Na, and K; lower contents of microelements Th, REE, Sc, Ba, and Sr; and higher contents of Al, Mg, Ca, and V (of microelements). These compositional deviations are due to the admixture of fragments of anorthositic norite and troctolite rock types. The predominance of anorthositic norites and troctolites even in highland fragments of Luna 16 mare regolith is thus confirmed. The finding is in keeping with the view that anorthositic norites and troctolites are the most abundant rock types of lunar highlands.

4. The chemical composition of the Luna 20 highlands regolith is very close to that of anorthositic norites and troctolites. Deviations are accounted for by the admixture of basaltic rocks; their small size suggests a slight contamination.

References

1. VINOGRADOV, A. P., Preliminary Data on Lunar Soil Collected by the Luna 20 Unmanned Spacecraft. *Geochimica et Cosmochimica Acta*, Vol. 37, 1973, pp. 719–720.
2. ADAM, J., J. FRÁNA, A. MAŠTALKA, A. CIMBÁLNÍKOVÁ AND M. PALIVCOVÁ, Determination of Macro- and Micro-element Content in Lunar Soil Supplied by the Automatic Station Luna 16. *Geokhimiya*, No. 9, 1973, pp. 1287–1293.
3. CIMBÁLNÍKOVÁ, A., A. MAŠTALKA AND M. PALIVCOVÁ, Textures of Lunar Basaltic Rocks of the Luna 16 Automatic Station. *Čas. Miner. Geol.* Vol. 18, No. 2, 1973, pp. 113–129.
4. CIMBÁLNÍKOVÁ, A., M. PALIVCOVÁ, J. FRÁNA AND A. MAŠTALKA, Textures of Fragments of Lunar Breccias From Luna 16 Regolith. *Geokhimiya*, No. 8, 1974. In press.
5. PRINZ, M., E. DOWTY, K. KEIL AND T. E. BUNCH, Mineralogy, Petrology and Chemistry of Lithic Fragments From Luna 20 Fines: Origin of the Cumulate ANT Suite and Its Relationship to High-Alumina and Mare Basalts. *Geochimica et Cosmochimica Acta*, Vol. 37, 1973, pp. 979–1006.

6. WOOD, J. A., J. S. DICKEY, U. B. MARVIN AND B. N. POWELL, Lunar Anorthosites and a Geophysical Model of the Moon. *Proc. Apollo 11 Lunar Science Conference, Geochimica et Cosmochimica Acta*, Supplement 1, Vol. 1, 1970, pp. 965–988.
7. PRINZ, M., T. E. BUNCH AND K. KEIL, Composition and Origin of Lithic Fragments and Glasses in Apollo 11 Samples. *Contrib. Mineral. Petrol.*, Vol. 32, 1971, pp. 211–230.
8. PRINZ, M., T. E. BUNCH AND K. KEIL, *Electron Microprobe Analyses of Lithic Fragments and Glasses From Apollo 11 Samples.* Univ. New Mexico, Institute of Meteoritics, Spec. Publication No. 2, 1971, p. 13.
9. KURAT, G., K. KEIL, M. PRINZ AND C. E. NEHRU, Chondrules of Lunar Origin. *Proc. Third Lunar Science Conference, Geochimica et Cosmochimica Acta*, Supplement 3, 1972, pp. 707–721.
10. SCHONFELD, E. AND CH. MEYER, JR., The Abundances of Components of the Lunar Soils by a Least-Squares Mixing Model and the Formation Age of KREEP. *Proc. Third Lunar Science Conference, Geochimica et Cosmochimica Acta*, Supplement 3, 1972, p. 1397.
11. VINOGRADOV, A. P., Preliminary Data on Lunar Soil Collected By the Luna 16 Unmanned Spacecraft. *Geokhimiya*, No. 3, 1971, pp. 261–273.
12. IVANOV, A. V., L. S. TARASOV, O. D. RODE AND K. P. FLORENSKY, Comparative Characteristics of Regolith Samples Delivered From the Lunar Mare and Highland Regions By the Automatic Stations Luna 16 and Luna 20. *Geochimica et Cosmochimica Acta*, Supplement 4, 1973, pp. 351–364.

Page intentionally left blank

Page intentionally left blank

Investigation of the Composition of the Luna 16 Lunar Sample

L. Bakos, M. Chayka, L. Cher, A. Cheke, N. N. Dogadkin, A. Elek, K. Kulchar, A. Nagy, D. L. Nagy, E. Szabo, B. Forzats, and E. Zemplen
Central Institute of Physical Research
Hungarian Academy of Sciences
Budapest, Hungary
and
V. I. Vernadskiy Institute of Geochemistry
and Analytical Chemistry
Academy of Sciences,
Moscow, U.S.S.R.

The concentrations of aluminum, manganese, sodium, chromium, iron, cobalt, and 12 rare earth elements were determined by neutron activation analysis using slow neutrons, and oxygen and silicon were determined using a fast-neutron generator.

Mössbauer spectroscopy was used to investigate iron compounds in Luna 16 regolith samples from the upper part of the core.

A Luna 16 lunar sample was received in 1971 from the Institute of Geochemistry and Analytical Chemistry of the U.S.S.R Academy of Sciences for study of its composition. The sample consisted of small particles and was taken from the upper part of the lunar soil (from a depth of 7 cm), which has been called zone A (ref. 1). The following investigations were carried out at Central Institute of Physical Research:

1. Neutron activation analysis was used to determine the content of rare earth elements and those elements which cause the major radioactivity of the irradiated sample.
2. The oxygen and silicon concentrations were determined by activation analysis using a neutron generator.
3. Iron compounds were determined by Mössbauer spectroscopy.

Activation Analysis Using a Nuclear Reactor Apparatus

The samples were irradiated in a type VVR–SM nuclear reactor, with a slow-neutron flux of 2×10^{13} n · cm^{-2} · s^{-1}. Prolonged irradiations were done in the vertical channels of the reactor; short irradiations in channels serviced by pneumatic shuttles.

Gamma spectra were measured by a gamma spectrometer using a GeLi detector with a working volume of 45 cm^3 and a resolution of 3.5 keV, at an energy of 1332 keV (^{60}Co).

Determination of Aluminum, Manganese, Sodium, Chromium, Iron, and Cobalt

The above-listed elements account for most of the radioactivity after irradiation and

were determined by nondestructive methods. Sample sizes were 2 to 10 mg. Concentrations of Al, Mn, and Na were determined after 2-minute irradications using ^{28}Al, ^{56}Mn, and ^{24}Na and counting after cooling periods of 2 minutes, 1 hour, and 1 day, respectively. Concentrations of chromium, iron, and cobalt were determined using the isotopes ^{51}Cr, ^{59}Fe, and ^{60}Co after a 24-hour irradiation and a 2-week cooling period.

The results of nondestructive analysis are presented in table 1.

Table 1.—*The Concentration of Elements in Luna 16 Samples*

Element	Content %
Al	7.1 ± 1.0
Mn	0.17 ± 0.02
Na	0.28 ± 0.01
Cr	0.22 ± 0.03
Fe	14.3 ± 1.9
Co μg/g	32.5 ± 0.4

NOTE: The measurement error designates the maximum deviation from the average value.

Determination of Rare Earth Elements

The rare earth elements are very similar to one another in chemical properties and are of great interest from the point of view of the history of the lunar soil. Determination of the concentration of individual elements was specially important. For this purpose, 10-mg samples were irradiated for a period of 10 hours. The rock was fused with sodium peroxide in the presence of a lanthanum carrier, and the rare earth fraction was extracted from dilute hydrochloric acid in the form of oxalates.

Then, after various decay times, the gamma spectra of the resulting precipitates were measured. The content of 12 rare earth elements in the lunar rock was determined by this method (ref. 2); the analytical results are presented in table 2. Also indicated are certain data that characterize the analytical conditions.

Table 2.—*The Concentration of Rare Earth Elements in the Luna 16 Sample (ref. 1)*

Element	Isotope	Cooling Time (days)	Peak Used for Analysis (keV)	Concentration (μg/g)
La	^{140}La	0, 1, 4	486.8, 815.5, 1595.4	12.3 ± 0.4
Ce	^{141}Ce	5, 8, 20	145.4	32.4 ± 1.4
Pr	^{142}Pr	0, 1	1575.5	4.6 ± 2.5
Nd	^{147}Nd	8, 20	91.4	25.4 ± 2.5
Sm	^{153}Sm	5, 8	103.2	8.5 ± 0.3
Eu	^{152m}Eu	1, 4	841.6	2.20 ± 0.11
	^{152}Eu	20	344.2	
Gd	^{159}Gd	1	363.5	7.3 ± 1.2
Tb	^{160}Tb	8, 20	298.6	1.6 ± 0.2
Ho	^{166}Ho	0, 1	80.6	1.9 ± 0.2
Er	^{171}Er	0, 1	308.1	5.5 ± 0.6
Yb	^{175}Yb	5, 8, 20	282.6, 396.1	6.0 ± 0.3
Lu	^{177}Lu	5, 8, 20	208.4	0.86 ± 0.05

NOTE: The measurement error designates the standard error, calculated statistically.

We also investigated the uniformity of distribution of the rare earth elements in the rock by determining the europium and dysprosium concentrations. Six samples were used in this test and each was irradiated for 10 minutes. Then the rock was dissolved in a mixture of perchloric acid and hydrofluoric acid, and the rare earth elements were extracted with dilute hydrochloric acid by a previously prepared precipitate of lanthanum oxalate (ref. 3). The gamma spectra of the precipitates were taken several times, and the europium and dysprosium concentrations were calculated from several peaks of the ^{152m}Eu and ^{165}Dy isotopes.

The analytical results for each sample, as well as the average europium and dysprosium concentrations, are presented in table 3. Standard rock BCR 1 was taken as a material containing uniformly distributed rare earth elements, and the results of analyzing this sample are also given. As is evident from the table, the lunar sample contains both these elements in a rather uniform distribution because no significant differences in reproducibility of results between the lunar and standard rocks are obtained by using this method.

Activation Analysis Using a Neutron Generator Apparatus (ref. 4)

A neutron generator, with a neutron output of 10^{10} n $\times$ s^{-1}, was used as the fast neutron source. The gamma spectrometer had a NaI/Tl detector 75 cm $\times$ 75 cm in size.

Determination of Silicon and Oxygen

In these measurements, a 77.2 mg sample was used. Silicon was determined from the isotope ^{28}Al (irradiation 30 s, measurement 420 s) and oxygen, from the isotope ^{16}N (irradiation 8 s, measurement 15 s). The average value and standard error of the mean were calculated from the series of measurements: 20.6 $\pm$ 2.0 weight percent for silicon and 41.2 $\pm$ 1.2 weight percent for oxygen.

Mössbauer Measurements

The lunar dust sample that we measured weighted 60 mg. Sample thickness was 40

Table 3.—*Uniformity of the Europium and Dysprosium Distribution in Rocks*

	BCR1			Luna 16	
Sample (mg)	Eu (μg/g)	Dy (μg/g)	Sample (mg)	Eu (μg/g)	Dy (μg/g)
6.168	2.215	6.51	6.865	2.329	10.23
6.909	2.159	6.08	6.837	2.414	10.71
6.191	2.171	6.74	3.186	2.230	10.70
4.033	2.138	6.26	2.571	2.201	10.26
6.062	2.137	6.22	12.861	2.399	10.64
3.702	2.162	6.37	8.450	2.537	10.31
Mean	2.16	6.36	Mean	2.35	10.53
Root Mean Deviation	0.03	0.22	Root Mean Deviation	0.11	0.20

Table 4.—*Mössbauer Results*

Components	Concentration (atom %)	Hyperfine Magnetic Field (KO.)	Quadrupole Splitting (mm/s)	Chemical Shift (mm/s)
Metallic iron	4.5 ± 0.5	331.4 ± 1.0	− 0.021 ± 0.031	0.181 ± 0.015
Silicates (M1)	− 28.5 ± 0.9	—	2.748 ± 0.006	1.321 ± 0.002
Silicates (M2)	59.5 ± 1.8	—	1.956 ± 0.005	1.243 ± 0.006
Ilmenite	7.3 ± 0.4	—	0.71 (fixed)	1.202 ± 0.006

mg/cm^2. Twenty-five millicuries of ^{57}Co in Cr was the source of resonance gamma rays. The measurements were conducted at room temperature. A constant acceleration Mössbauer unit was used (ref. 5). The spectrum consisted of one hyperfine sextuplet and three poorly resolved quadrupole doublets. The parameters obtained are presented in table 4.

The values of the parameters indicate that the components of the spectrum correspond to metallic iron, ilmenite, and the M1 and M2 lattice sites of iron-containing silicates.

Acknowledgment

The authors thank academician A. P. Vinogradov for providing the sample of lunar material.

References

1. VINOGRADOV, A. P., *Geokhimiya*, Vol. 3, 1971, p. 261.
2. ELEK, A., G. PERENESZKI AND E. SZABO, *Geokhimiya*, Vol. 15, 1973, p. 123.
3. CSAJKA, M., *Radiochem. Radioanal. Letters*, Vol. 13, 1973, p. 151.
4. NAGY, A., A. CSÖKE, L. BAKOS AND E. SZABO, *Radiochem. Radioanal. Letters*, Vol. 11, 1972, p. 321.
5. SERF, E., L. VÁRHALMI AND E. KISS, To be published.

section 2

Thermal History of the Moon

Page intentionally left blank

Page intentionally left blank

In-Situ Measurements of Lunar Heat Flow

Marcus G. Langseth and Stephen J. Keihm
Lamont-Doherty Geological Observatory
Columbia University
Palisades, New York

During the Apollo program two successful heat-flow measurements were made in situ on the lunar surface. At the Apollo 15 site a value of 3.1×10^{-6}W/cm^2 was measured, and at the Apollo 17 site a value of 2.2×10^{-6}W/cm^2 was determined. Both measurements have uncertainty limits of ± 20 percent and have been corrected for perturbing topographic effects. The apparent difference between the observations may correlate with observed variations in the surface abundance of thorium. Comparison with earlier determinations of heat flow, using the microwave emission spectrum from the Moon, gives support to the high gradients and heat flows observed in situ.

There has long been an interest in the rate at which heat is escaping from the Moon. The Moon is a planetary-sized body that represents a significant sample of the solar system in the region of the terrestrial planets. On the other hand, the Moon is a small enough body so that there is reason to believe that during its 4.6-b.y. history it has lost a significant portion of its initial heat and, as a result, that the present heat flux mainly results from heat generated by radio isotopes in the interior to a depth of about 300 km.

Petrological and geochemical evidence gained from surface samples indicates that the Moon was radially differentiated early in its history. During this differentiation the long-lived, heat-generating isotopes of ^{238}U, ^{235}U, ^{40}K, and ^{232}Th were purged from the interior and concentrated in the outer layer of the Moon. As a result, the surface heat flow from the Moon should very nearly reflect the total abundance of isotopes in the Moon and thereby provide a valuable chemical constraint on the Moon's bulk composition.

Prior to the Apollo missions, lunar heat-flow determinations were based on Earth-based observations of thermal emissions from the Moon in the microwave band. Because of the partial transparency of lunar material to electromagnetic waves longer than 1 mm, the emission spectrum at wavelengths greater than 1 mm depends on temperatures in the subsurface. If the electrical properties of lunar soil are known, the subsurface temperature profile can be determined from the emission spectrum.

The most comprehensive effort to detect heat flow from the interior by this technique has been made by Troitsky and colleagues (refs. 1 and 2) at the Radiophysical Research Institute, Gorky, U.S.S.R. Their well-known curve, shown in figure 1, indicates an increase in brightness temperature with wavelength of about 0.6°C/cm. Using electrical and thermal properties deduced from microwave observations in the 1-mm to 3-cm range, Tikhonova and Troitsky (ref. 2) interpreted this spectral gradient in terms of a heat flow of 3×10^{-6} to 4×10^{-6}W/cm^2. Such a heat flow is approximately one-half the mean of observed heat-flow values on the Earth.

[1] Lamont-Doherty Geological Observatory Contribution No. 2141

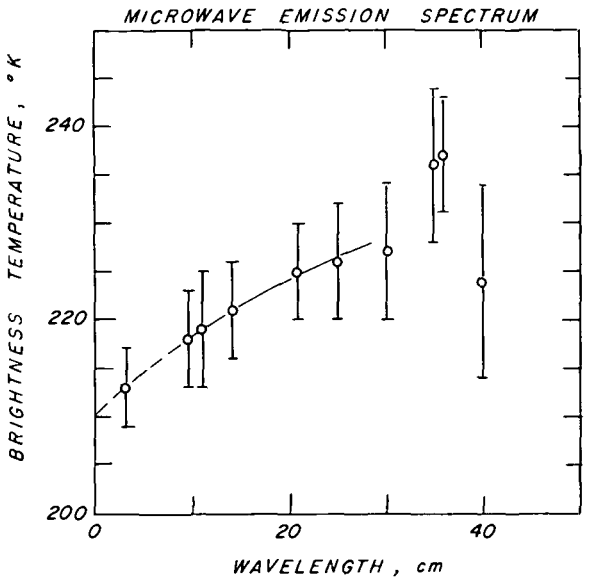


Figure 1.—*Data from microwave observations made in the Soviet Union between 1961 and 1964 using the "artificial Moon" technique (refs. 1 and 2). The plot shows microwave brightness temperature versus wavelength of the radiation.*

In-Situ Measurements During the Apollo Program

The manned lunar landings of the Apollo program provided an opportunity to make direct measurements in the lunar surface layer relevant to the heat flow through the surface. Successful measurements were made at two of the landing sites: Hadley Rille, near the edge of the Imbrium basin—visited on Apollo 15—and Taurus-Littrow, a narrow embayment on the southeastern margin of Serenitatis—visited on Apollo 17 (see figure 2).

At each location the astronauts buried two probes in the lunar soil to measure the temperature and thermal conductivity of the soil. At the Apollo 15 site the probes were buried to depths of 1.0 and 1.4 m; at Apollo 17 both probes were buried to a depth of 2.3 m. Each probe contains eight platinum resistance thermometers and four thermocouples which detect temperature at 11 different levels in the subsurface. Four thermometers on each probe are surrounded by heaters which can be turned on by command from Earth. These heaters are used to make in-situ determinations of thermal conductivity. The range and accuracy of measurements made by the heat-flow experiment are shown in table 1. The platinum resistance thermometers were carefully tested to demonstrate that they would retain their calibrations after experiencing the mechanical and thermal shocks of the lunar mission. Temperature data from all the thermometers are relayed to Earth every 7.2 min. At the Apollo 15 site we presently have more than 2½ yr of data and more than 1 yr of data at the Apollo 17 site.

A Summary of Results

The experiments installed on the Moon provide extensive information on the temperature and thermal properties of the lunar surface layer to a depth of 3 m, including surface temperature variations, near-surface thermal properties, subsurface temperature

Table 1.—*Heat-Flow Experiment Temperature Measurements*

Measurement	Range	Accuracy
Platinum Resistance Thermometers: Absolute Temperature	190–270 K	±0.05 K
Temperature Difference	±2 K	±0.001 K
Cable Thermocouples: Absolute Temperature	70–400 K	±0.5 K

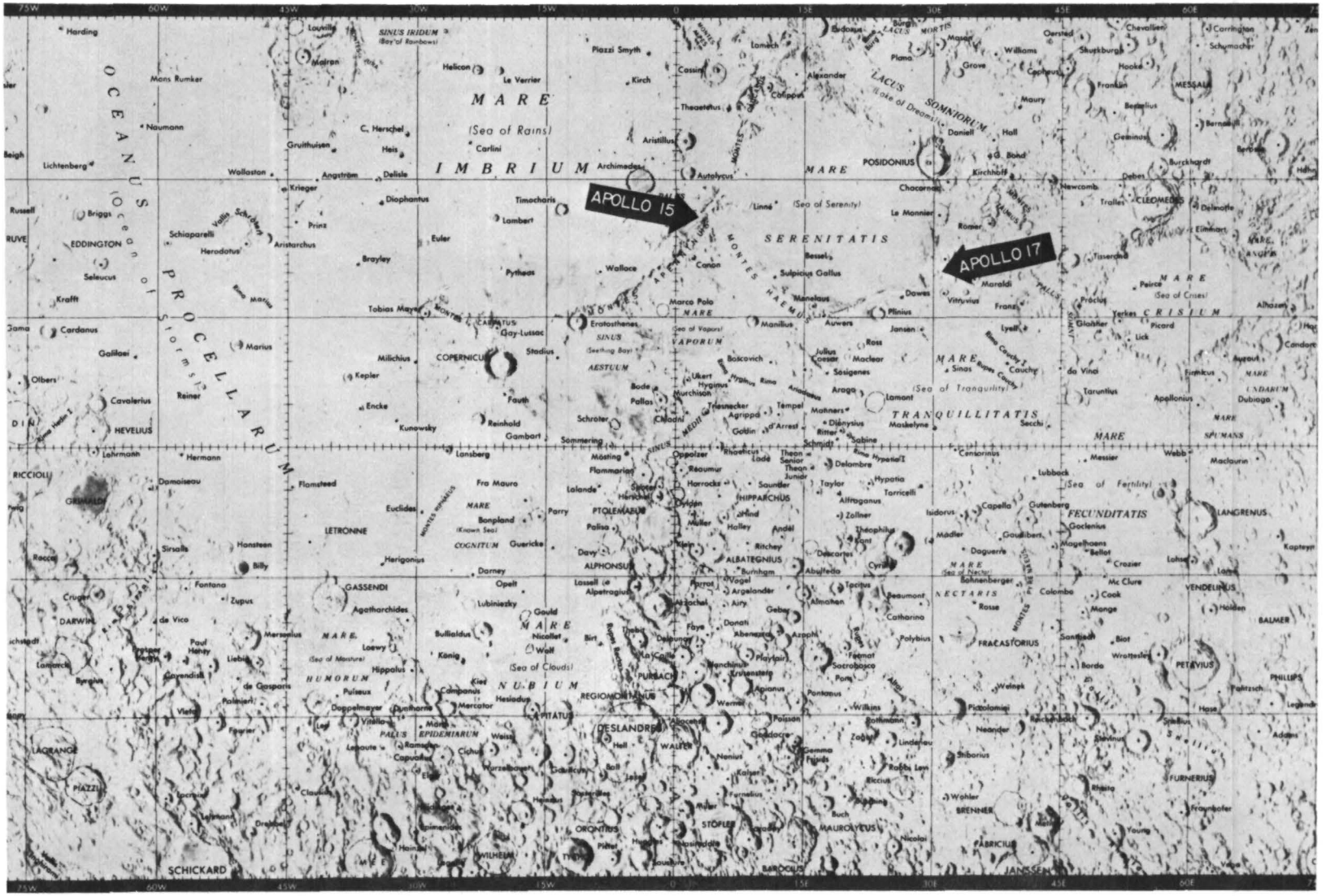


Figure 2.—*A lunar map showing the locations of the two successful heat-flow measurements.*

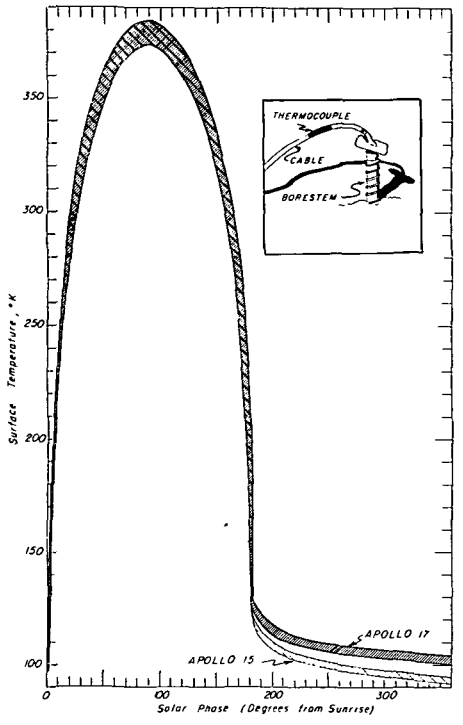


Figure 3.—*The calculated surface temperature throughout a lunation based on the temperature of a thermocouple inside a cable (see inset) which is exposed above the surface.*

variations, and thermal conductivity. All of this information is essential to understand the total heat budget near the lunar surface and the contribution of the flux from the interior.

SURFACE TEMPERATURE VARIATIONS

Measurements by thermocouples in cables above the lunar surface provide information on the surface temperature variation. The cable is in radiative equilibrium with the lunar surface, except during times when the temperature is changing rapidly, as during an eclipse or at terminator crossing. The lunar surface temperature can be readily computed from laws governing thermal radiation. In figure 3 we show the surface temperature variation at the Apollo 17 site during a complete lunation. During lunar day, the temperature deductions have large errors because of uncertainties in the amount of solar radiation reflected from the lunar surface, but at night the errors are small. Similarly, surface temperatures can be deduced quite accurately from thermocouple data during the umbral phase of an eclipse.

In a manner similar to the classical methods of Wesselink (ref. 3) and Jaeger (ref. 4), the cool-down of the surface after sundown and during an eclipse can be used to deduce the thermal properties of the regolith to a depth of about 15 cm. For analysis of the in-situ data we use a thermal model that includes many layers with thermal properties that vary with depth and temperature. To explain the observed temperature variations at lunar night and during an eclipse, the conductivity and density must vary with depth. The variations of density and conductivity shown in figure 4 will explain the surface temperature variations during the lunar night almost exactly, but these de-

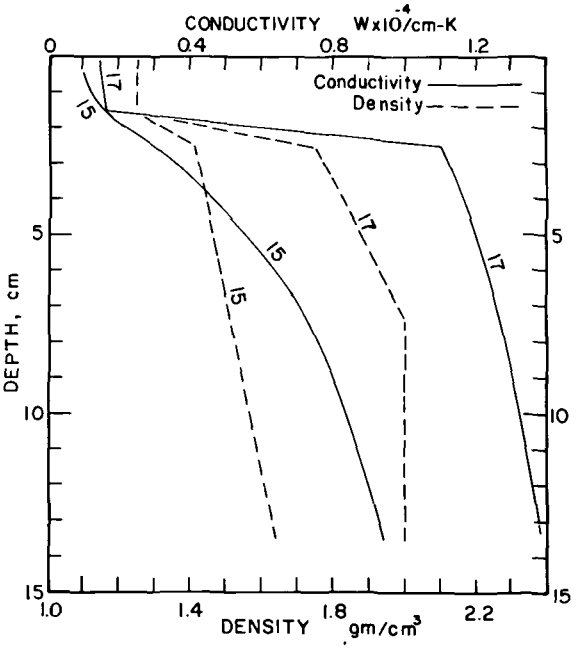


Figure 4.—*Profiles of thermal conductivity and density, with depth in the lunar regolith that will explain the observed surface temperature variations shown in figure 3. Conductivity values shown are those appropriate to the mean temperature at each depth.*

duced profiles are not necessarily unique. Two features of the profiles shown are essential to explain the data:

1. The upper 1 to 2 cm must have an extremely low thermal conductivity, and this conductivity must be temperature-dependent. The conductivity at the mean surface temperature (216 K) is approximately 1.5 × 10^{-5}W/cm-K, which is in good agreement with measurements on returned lunar fines.
2. At a depth of about 2 cm, the conductivity must increase greatly to values 5 to 7 times greater than the surface value.

THE NEAR-SURFACE MEAN TEMPERATURE GRADIENT

One of the most interesting features of the subsurface temperature measurements is the very large difference in mean temperature (i.e., the temperature averaged over one lunation) between the surface and depths of a few centimeters. At the Apollo 15 site the mean temperature 35 cm below the surface is 45 K higher than at the surface; the difference at the Apollo 17 site is 40 K. This large increase in mean temperature is due primarily to the temperature dependence of thermal conductivity in the top 1 to 2 cm, which results from the nonlinear behavior of radiative heat transfer. These large differences require that the ratio of the radiative component to conductive component at 350 K be about 2 to 3. Figure 5, from Keihm and Langseth (ref. 5), shows the variation of mean temperature and the amplitude and phase of variations of lunation period with depth in the regolith, based on the models shown in figure 4.

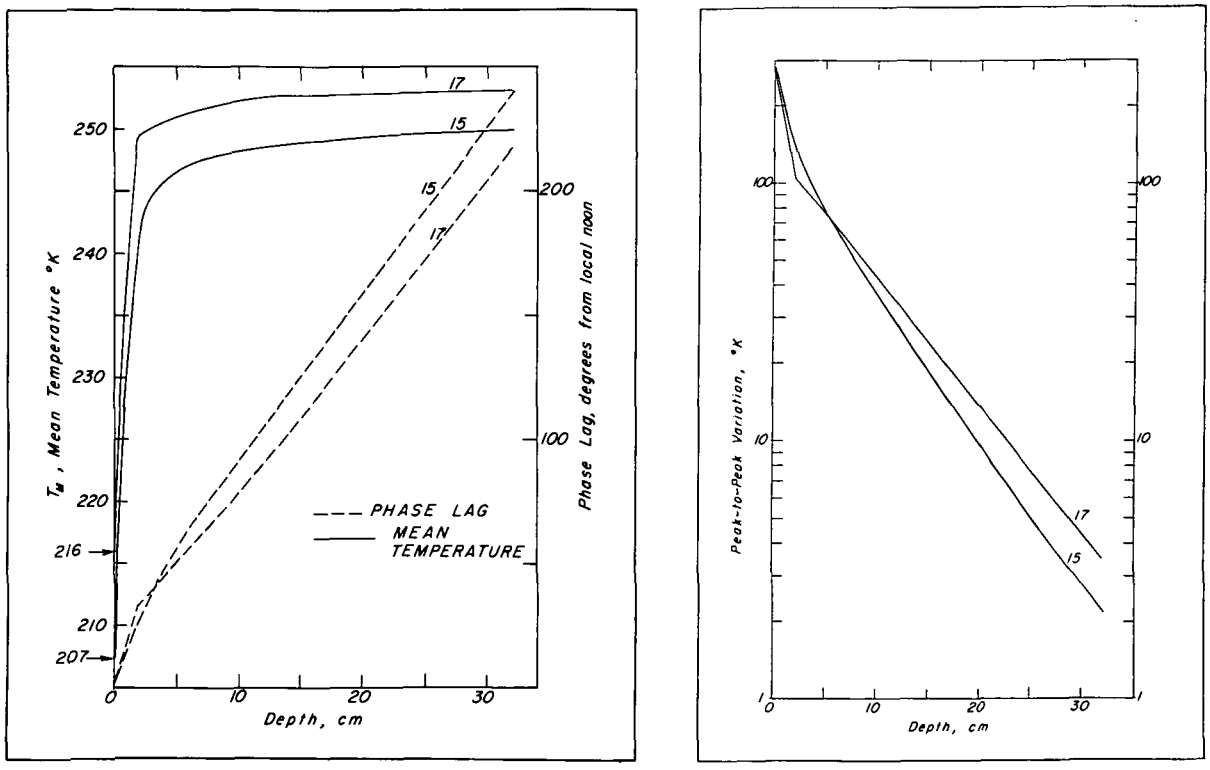


Figure 5.—*In the right plot, the expected peak-to-peak monthly variation of temperature as a function of depth. The left-hand plot shows mean temperature and phase lag of the monthly variation versus depth. These results are based on the conductivity and density models shown in figure 4.*

Subsurface Temperature Profiles

The probes are inserted inside the hollow fiberglass tubing which is drilled into the lunar soil. Figure 6 shows Charles Duke, an Apollo 16 astronaut, drilling one of the heat-flow holes. Figure 7 shows the temperature history of one of the probes after insertion into the tube. The probes require approximately 1 month to reach within a few thousandths of a degree of thermal equilibrium with the surrounding regolith. The thermometers buried below 80-cm depths do not see any perceptible variation due to the monthly temperature cycle, and temperature gradients should reflect heat flowing from the lunar crust. The temperature profiles at four of the probes are shown in figure 8. Very small corrections have been added to these data to account for thermal shunting effects of the fiberglass tubes and probes, so that these profiles should represent true undisturbed regolith temperatures.

THERMAL CONDUCTIVITY

Thermal conductivity of the regolith can be deduced from three different effects. First, and most important, were measurements made by in-situ experiments. The effects of heaters turned on for a period of 36 hours at low power were measured. From



Figure 6.—*An astronaut drilling sections of fiberglass tubing into the Moon for the heat-flow probes.*

the rate of rise of temperature after 20 hours it is possible to determine the conductivity. Second, the initial cool-down of the probes from high temperatures permits determination of conductivity based on the initial energy input into the hole. Cool-down estimates can be made at all the gradient sensors, i.e., at eight different depths in each hole. Third, temperature variations with a monthly period penetrate to approximately 80 cm, and the annual variation of surface temperature is felt at all depths. The attenuation of these variations with depth depends in part on the thermal conductivity of the surrounding material. However, because of radiative transfer along the fiberglass tubing, the attenuation data are difficult to interpret. Our analysis requires a thermal conductivity between 1 and 2 $\times$ 10^{-4}W/cm-K to reproduce the attenuation observed. The conductivities measured by the first two techniques are shown versus depth in figure 9. We note that the thermal conductivity of the lunar soil lies between 1.4 and 3.0 $\times$ 10^{-4}W/cm-K; this is approximately a factor of 10 higher than the conductivity at the surface. The increase of conductivity at about a 2-cm depth appears to be mainly

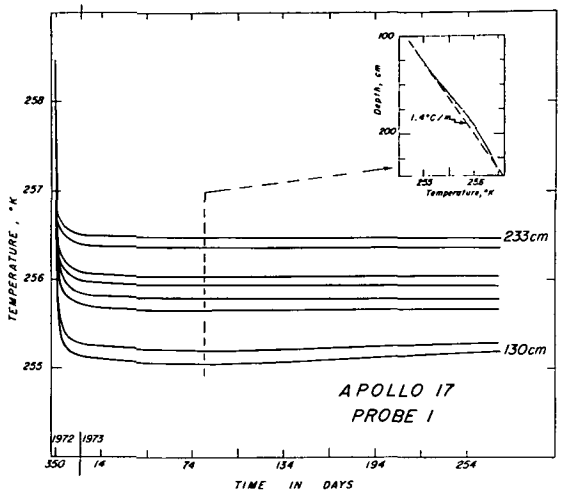


Figure 7.—*The 10-month temperature history of eight thermometers on one of the probes at the Apollo 17 site. The inset shows the temperature depth profile after 75 days.*

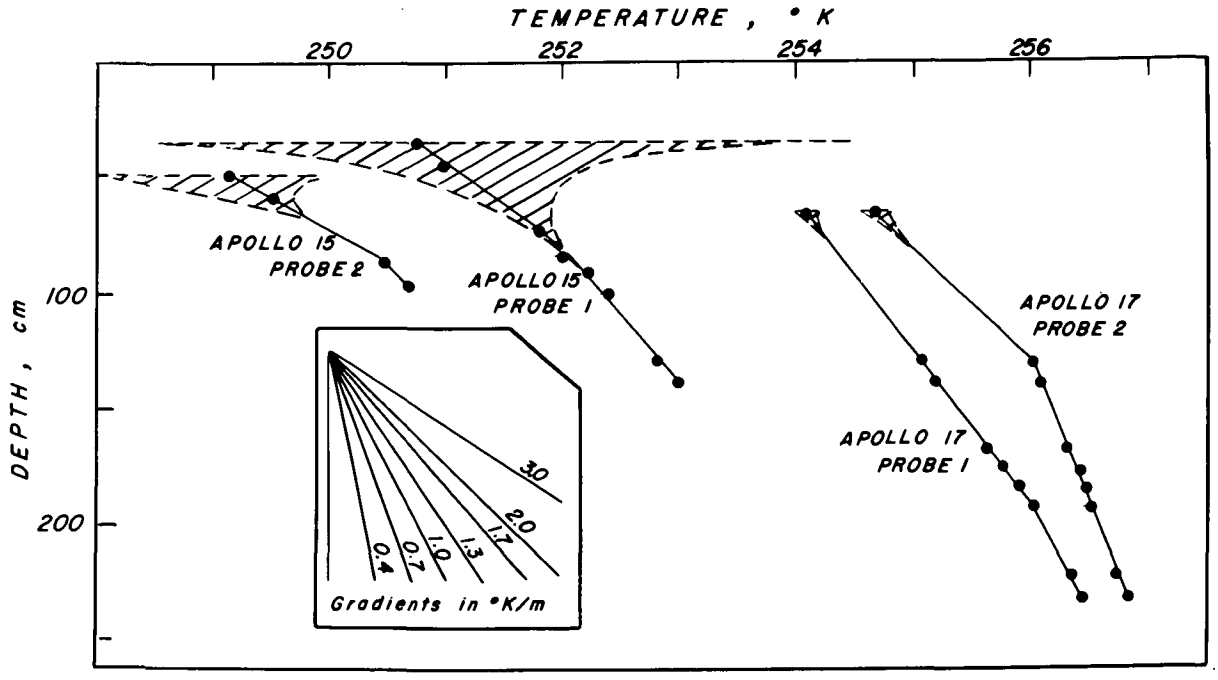


Figure 8.—*Temperature depth curves for the four lunar heat-flow measurements. The hatched areas above 70 cm are the envelopes of monthly variations.*

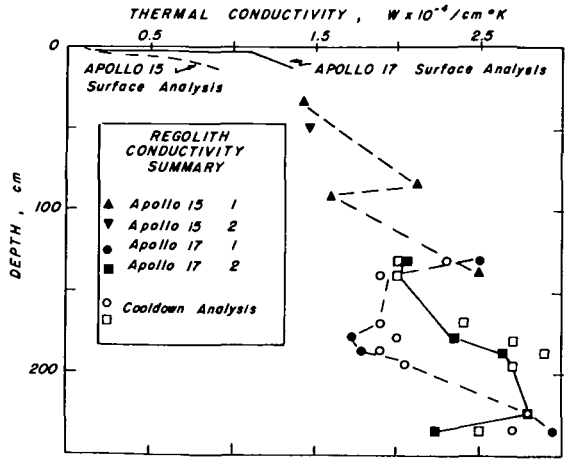


Figure 9.—*A summary of thermal conductivity determinations at the heat-flow site. At the top of the plot the lines are the same as in figure 4. Deeper points are results of in-situ measurements and analysis of probe cool-down data.*

due to a large increase in the soil compaction and grain boundary contacts with depth. It is likely that at this 2-cm depth the disruptive effects of micrometeorite bombardment give way to compactive effects. Conductivity values for regolith fines as high as 2×10^{-4} W/cm-K have not been duplicated in the laboratory, and further tests of highly compacted lunar soil should be made.

HEAT FLOW IN SITU

When the conductivity and gradient observations are combined, the heat-flow values shown in table 2 result. The best value of heat flow at the Hadley Rille site is 3.1×10^{-6}W/cm^2 and at Taurus-Littrow 2.8×10^{-6}W/cm^2.

Temperature measurements at probe 2 at the Apollo 17 site require special attention (see fig. 8). The profile indicates a very large decrease in gradient with depth at 130 cm which, because the conductivity is relatively uniform, must reflect a change in heat flow with depth. Also, the heat flow in the lower part of the hole, about 1.9 W/cm^2, is considerably lower than that at the other two locations. These results suggest that heat flow is locally disturbed, perhaps by a large rock buried very near where the probe is emplaced. The heat flow, using the temperatures at 67 and 234 cm, gives a heat flow of 2.5×10^{-6}W/cm^2, which is in reasonable agreement with the value at probe 1.

Possible Disturbance to the Heat Flow

How representative are the measurements of the average heat loss from the Moon? The answer to this question depends on whether there are significant regional and local disturbances. Certain disturbing effects, such as that of local topography, can be estimated and corrected for.

The amounts of radioisotopes in the crust may be anomalous in the region where the heat-flow observations are made. We have orbital data on the distribution of thorium and uranium on the surface that can be applied to this problem.

Table 2.—*Summary of Lunar Heat-Flow Results*

	Gradient K/m	Conductivity W x 10^{-4}/cm K	Heat Flow W x 10^{-6}/cm^2
Apollo 15			
Probe 1	1.75	1.78	3.1
Apollo 17			
Probe 1	1.36	2.06	2.8
Probe 2	1.30	2.00	2.5

NOTE: The estimated error of heat-flow determination is ±20 percent.

Other effects, such as thermal conductivity contrasts in the subsurface which can refract the heat-flow lines, are not directly observable, but geological observations can be used as a guide for assuming subsurface conductivity geometries. From these assumptions an appreciation of whether the measurements are anomalous may be obtained.

TOPOGRAPHY

Significant disturbances of heat flow will occur in the vicinity of craters having a diameter-to-depth ratio of 6 or less. The dominant effect of such craters is to increase the heat flow just outside the crater rim due to the slightly higher mean temperature in the crater floor. In the upper part of figure 10 we show the heat-flow anomaly over a crater with a diameter-to-depth ratio of 6 as a function of radius. It can be seen that the anomaly decreases very rapidly with distance from the rim. By and large the astronauts were successful in setting up the experiment far from craters larger than 1 m in diameter. At the Apollo 17 site, topographic maps show three craters which we estimate have a combined effect that increases the heat flow by 0.3 W/cm^2. That is, a correction of about −10 percent should be applied to the Taurus-Littrow values for the effect of craters. At the Hadley Rille site there were no craters in the vicinity of the probes which would have a significant effect on the heat flow. Consequently, no correction has been applied.

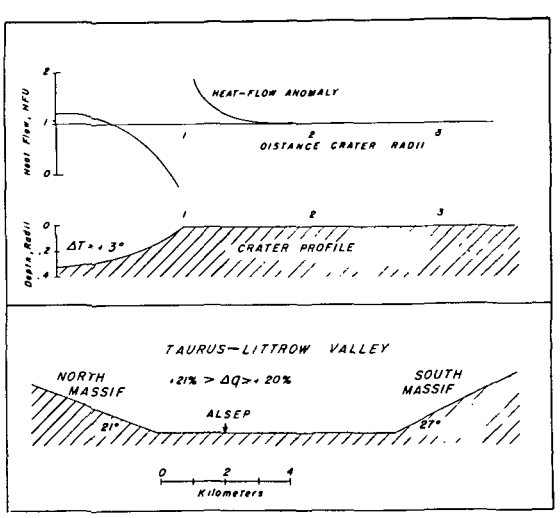


Figure 10.—*In the upper part of the figure, the heat-flow anomaly expected over a crater with an aspect ratio of 1.6. The lower part shows schematically a cross section of Taurus-Littrow and the estimated effect on the heat flow,* Δq.

At Hadley Rille both the rille and the Apennine Front will affect the heat flow, but in opposite ways. Both effects are on the order of 5 percent and, thus, appear to be self-cancelling. Therefore, it appears that the best value for the heat flow at Hadley Rille is the uncorrected value, 3.1×10^{-6}W/cm^2, with an estimated uncertainty of ± 20 percent.

The massifs that bound the Taurus-Littrow Valley on the north and south have a significant effect on the heat flow. We have estimated the correction to be applied using a method developed by Lachenbruch (ref. 6). The valley is modeled as shown at the bottom of figure 10. Based on this model, we estimate that a correction of −15 to −20 percent should be applied to the Apollo 17 measurement. Applying all corrections, the best value for heat flow in the Taurus-Littrow region is 2.2×10^{-6}W/cm^2, with an estimated uncertainty of ± 20 percent.

SURFACE RADIOACTIVITY

When topographic effects are taken into account, the heat flow at Taurus-Littrow is 25 to 30 percent lower than at Hadley Rille. The results of the orbiting gamma-ray experiment reported by Metzger (ref. 7) gave evidence of substantial variations in radioactive elements on the surface. One of the regions with the highest concentrations in radioactivity is the Hadley Rille area of Mare Imbrium. There the counts per second are about twice those at Taurus-Littrow and three to four times those observed over much of the lunar farside. The difference in heat flow between these two sites may therefore

reflect a real variation in radioactive heat production in the lunar crust. A similar correlation between surface heat flow and radioactive heat production of surface rocks is observed on the Earth. A most significant implication is that two in-situ measurements may overestimate global heat flow, especially if the results of the gamma-ray experiment over the farside and nearside highlands are representative, since the observed concentrations of radioactive isotopes are much lower there.

POSSIBLE SUBSURFACE EFFECTS

Both sites where the heat-flow experiments were installed are at the margins of large mascon basins. These basins have been flooded by basaltic lavas early in the Moon's history. As a result, it is possible that a conductivity contrast exists between the mare basalt and the underlying basin floor and adjacent highlands. It is not likely that the bulk conductivity of the basalt will be as high as that measured on returned solid samples. The active seismic experiments by Kovach and Watkins (ref. 8) indicate that these flows are highly fractured. Extensive fracturing of rocks in vacuum will decrease their conductivity appreciably. It may be possible to entertain a conductivity contrast of mare fill material to underlying basin floor material of 10.

Our observations, located at the margin of basins, may see an edge effect as a consequence of this contrast. If they lie within the basin as the Apollo 15 site appears to, an edge effect heat-flow anomaly would add to the observed heat flow. If, on the other hand, the observation is outside the basin rim as might be the case at Taurus-Littrow, the observed heat flow would be disturbed toward lower values. Uncertainties do not at this time permit an accurate assessment of disturbance due to buried contacts between rocks of different thermal conductivity. The best estimate of the size of such an effect is by comparison with other estimates of heat flow from the Moon; e.g., those made from Earth-based microwave measurements.

Comparison With Earth-Based Microwave Measurements

To compare our measurements with microwave measurements, we return to the set of measurements of lunar brightness temperature between 3 and 70 cm made by Troitsky and colleagues. Waves from 5 to 20 cm are emitted from depths comparable to those measured by the heat-flow experiment. We will compare the spectral gradient in this band of wavelengths with that expected from a lunar surface layer, having the temperatures and thermal properties we measured in situ. The greatest uncertainty in such a comparison is the value of the power absorption length, l_e, of electromagnetic waves. In figure 11 we show the microwave data compared with theoretical results using different absorption lengths. The model has the parameters given in the table at the top of the figure. The lowermost curve has a power absorption length that is a function of λ, i.e., $l_e = 5.8\ \gamma^{1.48}$, which is an empiri-

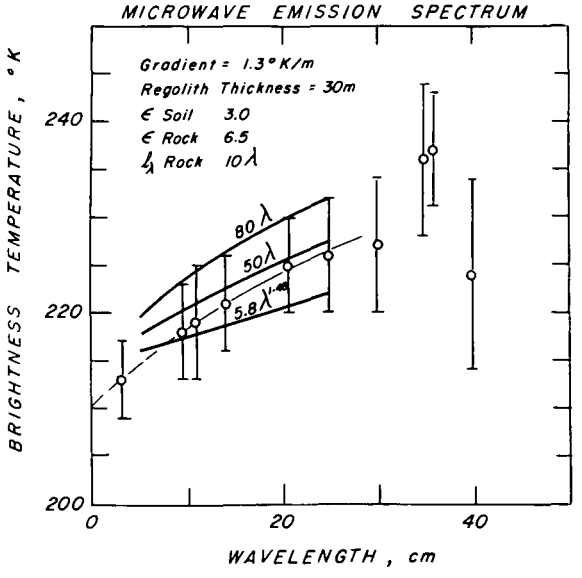


Figure 11.—*The data shown in figure 1, compared with theoretical emission spectra based on the thermal properties models at the Apollo 15 site. Three different relations between absorption length and wavelength were used and are noted on the curves.*

cal fit to the experimental results. This relation produces a good fit to radiotelescopic observations of the attenuation of the variations of microwaves over a monthly period in the range from 1 mm to 3.2 cm. The result is an increase in brightness temperature that fits within the error bars but is a poor fit to the observed spectral gradient. The temperature gradient in the lunar surface layer would have to be larger to better fit the microwave data using this relation. The middle curve corresponds to an l_e of 50λ, which is near the mean of values reported by Gold et al. (ref. 9), based on measurements of lunar samples at a wavelength of 68 cm. The best fit to the spectral gradient would be obtained for an l_e of 80λ. The principal result of this comparison at this point in our knowledge is that gradients of 1.3°C/m or higher, as observed in situ, are supported by microwave observations. The heat flows deduced by Tikhonova and Troitsky from 2.9×10^{-6} W/cm^2 to 4×10^{-6}W/cm^2 are in close agreement with our results.

Future Work

Several lines of future work can be proposed. First, more laboratory measurements of the electromagnetic power absorption length of lunar fines in the wave band from 5 to 20 cm would greatly improve the comparisons made above. Second, further Earth-based measurements of microwave emissions in the wavelength range from 5 to 30 cm would be extremely valuable. Measurements with sufficient resolution to detect variations in emission spectra over the lunar disk would be especially significant. Third, other in-situ measurements in highland regions, using an automated lander, would be extremely important. Finally, microwave observations from lunar orbit could possibly map heat flow variation over the entire Moon.

Acknowledgment

Columbia University's participation in the Lunar Heat-Flow Program was made possible through NASA contract NAS 9–6037. The experiment would not have been possible without the efforts of many people at the Bendix Aerospace Systems Division, Ann Arbor, Mich.; Arthur D. Little, Inc., Cambridge, Mass.; Martin Marietta Corporation, Denver, Colo.; Gulton Industries, Inc., Albuquerque, N. Mex.; and Rosemount Engineering Co., Minneapolis, Minn. The assistance of John Chute, Jr., and K. Peters in the analysis of the data is gratefully acknowledged. The drafting and manuscript were patiently done by A. Trefzer.

References

1. Krotikov, V. D., and V. S. Troitsky, Detecting Heat Flow From the Interior of the Moon. *Soviet Astron.*, Vol. 7, No. 6, 1964, pp. 822–826.
2. Tikhonova, T. V., and V. S. Troitsky, Effect of Heat From Within the Moon on its Radio Emission for the Case of Lunar Properties Which Vary With Depth. *Soviet Astron.*, Vol. 13, No. 1, 1969, pp. 120–128.
3. Wesselink, A. F., Heat Conductivity and Nature of the Lunar Surface Material. *Bull. Astron. Inst. of Netherlands*, Vol. 10, 1948, p. 351.
4. Jaeger, J. C., The Surface Temperature of the Moon. *Australian J. Phys.*, Vol. 6, 1953, p. 10.
5. Keihm, S. J., and M. G. Langseth, Jr., Surface Brightness Temperatures at the Apollo 17 Heat Flow Site: Thermal Conductivity of the Upper 15 cm of Regolith. *Proc. Fourth Lunar Science Conference, Geochimica et Cosmochimica Acta*, Supplement 4, Vol. 3, 1973, pp. 2503–2513.
6. Lachenbruck, A. H., Rapid Estimate of the Topographic Disturbance to Surficial Thermal Gradients. *Rev. Geophys.*, Vol. 6, No. 3, 1968, pp. 365–400.
7. Metzger, A. E., J. I. Trombka, L. E. Peterson, R. C. Reedy, and J. R. Arnold, Lunar Surface Radioactivity: Preliminary Results of the Apollo 15 and Apollo 16 Gamma Ray Spectrometer Experiments. *Science*, Vol. 179, 1973, pp. 800–803.
8. Kovach, R. L., and J. S. Watkins, The Velocity Structure of the Lunar Crust. *The Moon*, Vol. 7, 1973, pp. 63–75.
9. Gold, T., E. Bilson, and M. Yerbury, Grain Size Analysis and High-Frequency Electrical Properties of Apollo 15 and 16 Samples. *Lunar Science*, Vol. IV, Lunar Science Institute, Houston, 1973, pp. 293–295.

Page intentionally left blank

Page intentionally left blank

The Evolution of the Moon and the Terrestrial Planets

M. Nafi Toksöz and David H. Johnston
Department of Earth and Planetary Sciences
Massachusetts Institute of Technology
Cambridge, Massachusetts

The thermal evolutions of the Moon, Mars, Venus, and Mercury are calculated theoretically starting from cosmochemical condensation models. An assortment of geological, geochemical, and geophysical data are used to constrain both the present-day temperatures and the thermal histories of the planets' interiors. Such data imply that the planets were heated during or shortly after formation and that all the terrestrial planets started their differentiations early in their history.

Initial temperatures and core formation play the most important roles in the early differentiation. The size of the planet is the primary factor in determining its present-day thermal state. The Moon, smallest in size, is characterized as a differentiated body with a crust, a thick solid mantle, and an interior region which may be partially molten. It is presently cooling rapidly and is relatively inactive tectonically.

Mercury, which probably has a large core, may have a 500-km-thick solid lithosphere and a partially molten core, if it is assumed that some heat sources exist in the core. If this is not the case, the planet's interior temperatures are everywhere below the melting curve for iron. The thermal evolution is dominated by the core separation and the high conductivity of iron that makes up the bulk of Mercury.

Mars, intermediate in size, is assumed to have differentiated an Fe-FeS core. While the formation of an early crust is evident, large-scale melting and differentiation of the mantle silicates has occurred at least up until 1 b.y. ago. Present-day temperature profiles indicate moderate tectonic activity at the present time.

Venus is characterized as a planet not unlike the Earth in many respects. Core formation has occurred probably during the first billion years after the formation. The present-day temperatures indicate a partially molten upper mantle overlain by a 100-km-thick lithosphere and a molten Fe-Ni core. We can expect that today Venus may have tectonic processes similar to the Earth's.

The evolution of a planetary body is very strongly controlled by its thermal regime. Differentiation, volcanism, tectonic activity, and even magnetic field are all processes controlled by the internal temperatures and the thermal history. The calculation of the thermal evolution, however, requires strong constraints if it is to be realistic. In recent years significant new data from lunar and planetary missions have become available. For the Moon these have provided constraints both on the present-day temperatures and the past history of the thermal state of the lunar interior. For Mars, Venus, and Mercury, the thermal constraints are primarily qualitative. The purpose of this paper is to review these data and the thermal evolution models of the Moon and the terrestrial planets.

An extensive number of studies on thermal history of the Moon and planets have been carried out (refs. 1 through 34).

In the early studies, the Moon and the planets were generally modeled with chondritic compositions and radioactivity. With the successful lunar missions and new geo-

chemical data, it became necessary to revise the constraints used in lunar thermal calculations. The models generated since 1971 have incorporated these new data and in general give similar results. Generally, calculations for the other planets reflect this new knowledge about the chemistry of the solar system.

In this paper, then, we present thermal evolution models for the Moon, Mars, Venus, and Mercury for a comparative study. We use similar computational techniques and thermal factors associated with melting, differentiation, and core formation. These are discussed first. The thermal evolution of the Moon, with appropriate constraints, is then presented, followed by a discussion of the thermal evolution of the planets.

Computational Procedure and Model Parameters

For the theoretical calculations of thermal evolution in a planetary body, it is necessary to specify the initial conditions, heat sources, heat transport mechanisms, and a number of other parameters such as specific heat, density, and melting temperatures, as well as variations of these with temperature and pressure inside the planet. Generally, not all of these parameters can be determined and theoretical calculations cannot define thermal models uniquely.

The first input in theoretical calculations is the initial conditions assumed. Included in this is the heating due to accretion, tidal forces, induced electric currents, and short-lived radioactivity, although the relative importance of each may vary. Next is the definition of the long term heat sources that are important throughout the age of the planet. These include heating due to the decay of radioactive isotopes and the possibility of long term heating due to tidal dissipation and electrical currents. Finally, using the above inputs combined with other physical parameters, the conservation of energy equation must be solved numerically with the addition of certain perturbations designed to simulate melting, differentiation, and convection.

In this section we first describe the input parameters and then discuss the computational procedures involved in solving the thermal evolution problem.

MODEL PARAMETERS

Initial Temperature

The initial temperature of a planet is a function of both its mode of formation and its immediate environment during and shortly after its origin. As will be discussed in the following sections, constraints on lunar and planetary thermal evolution favor initially hot and possibly molten models. This is especially true for the Moon. Energy sources which might have provided the heat to raise the temperature of the planets to solidus or near-solidus levels include gravitational energy due to accretion, tidal dissipation, solar wind flux, short-lived radioactivity, and heating due to adiabatic compression. The temperature rise due to adiabatic compression amounts to only a few tens of degrees in the Moon, but increases with the increasing size of the planet. The effect of short-lived radioactivity depends on the time between nucleogenesis and lunar formation. Also, Schramm et al. (ref. 35) have shown that Al^{26}, the most likely heat source in the early history of the solar system (ref. 36), had little effect on the initial heating of the Moon and meteorites.

Tidal dissipation and solar wind flux could have been effective under special circumstances. The amount and the distribution of heat is difficult to quantify in both cases. For the Moon, as an example, the effects of tidal dissipation would be small (ref. 37), unless the Moon's orbit was originally much closer to the Earth. This might have occurred shortly after a capture event or after the Moon formed in close proximity to the Earth (ref. 38). Hallam (ref. 39) has calculated that tidal dissipation, even with $Q = 10$, raises the internal temperature by only 50–

100K in 1.5 b.y. Even if the Moon was once close to the Roche limit, it would recede so rapidly that the effect of tidal heating would be negligible.

Heating by electric currents produced by a unipolar generator driven by the solar wind might have been significant if the Sun had passed through a T-Tauri stage (ref. 40). This effect is difficult to calculate and include explicitly in any thermal model. However, combinations of all the above effects may contribute to the initial temperatures. We considered these effects by means of a "base" temperature added to accretional thermal profiles discussed below.

The most promising initial heat source for the terrestrial planets is the gravitational energy of accretion. Classically this effect is described by the equilibrium of added gravitational potential energy with black body radiation and internal heat:

$$\rho\frac{GM(r)}{r}dr = \varepsilon\sigma(T(r)^4 - T_b^4)\,dt + \rho C_p(T(r) - T_b)\,dr \qquad (1)$$

where t is time, ρ is the density of the accreting particles, G is the gravitational constant, $M(r)$ is the mass within radius r, σ is the Stefan-Boltzmann constant, C_P is the specific heat, and ε is the emissivity (taken to equal 1). $T(r)$ is the temperature at radius r, and T_b is the base temperature or the temperature of the accreting particles, including any effects of short-lived radioactivity. By specifying the accretion rate dr/dt and the physical parameters ρ, C_p, and T_b, temperature versus depth for an accreted body can be calculated from equation (1). An accretion rate suggested by Hanks and Anderson (ref. 15) and Mizutani et al. (ref. 41) is used in this paper and is given by:

$$\frac{dr}{dt} = ct^2 \sin \gamma t \qquad (2)$$

The constants c and γ are determined from the planet's final radius and the duration of accretion. Although the accretion rate is difficult to establish, it is a fair statement of the presumption that the rate grows as the accreted body grows, and that the rate then tapers off as primary material is depleted.

The accretion time is considered arbitrary, except that it is assumed to be longer for larger planets. Generally the accretion time and T_b are adjusted to provide an initial temperature profile consistent with the constraints that require initial differentiation. For the Moon, it can be shown from equations (1) and (2) that the temperature will never reach the basalt solidus for accretion times greater than 1000 years, unless the emissivity of the lunar surface is decreased. This conclusion was reached independently by Mizutani et al. (ref. 41) from a more detailed study of the accretion process.

Heat Sources

The most important long term heat source in thermal history calculations is the heat generated from the decay of the long half-life radioactive isotopes U^{238}, U^{235}, Th^{232}, and K^{40}. Abundances of these isotopes have been measured in many Earth rocks and returned lunar samples (refs. 42 through 48, and others), and indirectly by lunar orbital γ-ray spectrometers (ref. 49). While surface concentrations vary greatly, we may conclude that these values must be much higher than those in the interior of the Earth or the Moon (ref. 50, and others). The distribution of the isotopes in space and time are difficult to constrain, however, due to complex melting and crystal-liquid fractionation processes.

Figure 1 shows total K and U abundances measured for Apollo samples (including crystalline rocks, soils, and breccias), some meteorites, and terrestrial rocks. Figure 2 shows Th/U versus U for the same suite of measurements. Although there are small and systematic deviations, the K/U ratio for lunar material averages around 2000, compared with 10 000 for terrestrial rocks and 80 000 for chondrites. The low lunar K/U ratio is consistent with general depletion of volatile elements (refs. 42 and 52). From this, it is clear that neither terrestrial nor chondritic abundances can be used as the bulk radioactivity for the Moon. Furthermore, using

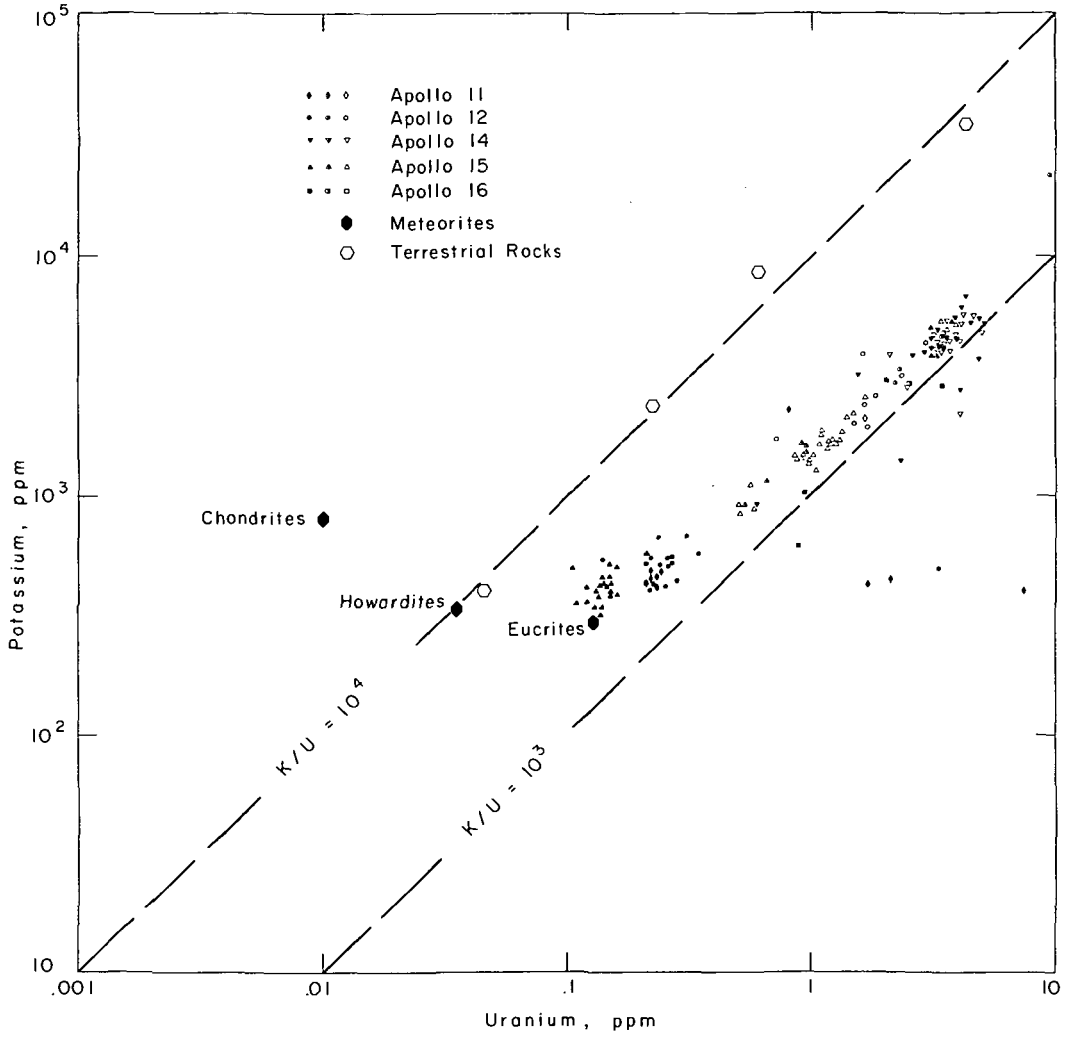


Figure 1.—*Potassium and uranium concentrations in selected meteorites, lunar samples, and terrestrial rocks. Lunar rocks are separated into three categories: crystalline rocks represented by filled symbols, breccias shown by half-filled symbols, and fines shown by empty symbols. Points for average chondrites, howardites, and eucrites are from Mason (ref. 51). Sources for lunar values are given in the text.*

Rb abundances for a model of the primitive lunar material (ref. 18), we can also reject chondrites. The Th/U ratio is consistently between 3.0 and 4.0 for terrestrial, lunar, and meteoritic material.

It is essential, then, to determine or estimate the bulk radioactive concentrations for each of the planets. In the case of the Moon, given that chondrites and terrestrial rocks are not good approximations of the bulk radioactivity, we turn to achondrites—specifically howardites and eucrites. A genetic relationship between achondrites and the Moon has been suggested by several investigators (refs. 53, 54, and 55). Howardites have, on the average, a uranium concentration of 35 ppb, with K/U = 9800, while brecciated eucrites, enriched in refractory elements, have U = 130 ppb, with K/U = 2300 (ref. 51). It is interesting to note that the K/U ratio for eucrites is close to that of the lunar material, while the ratio for howardites is somewhat higher.

If we take K/U for the bulk radioactive

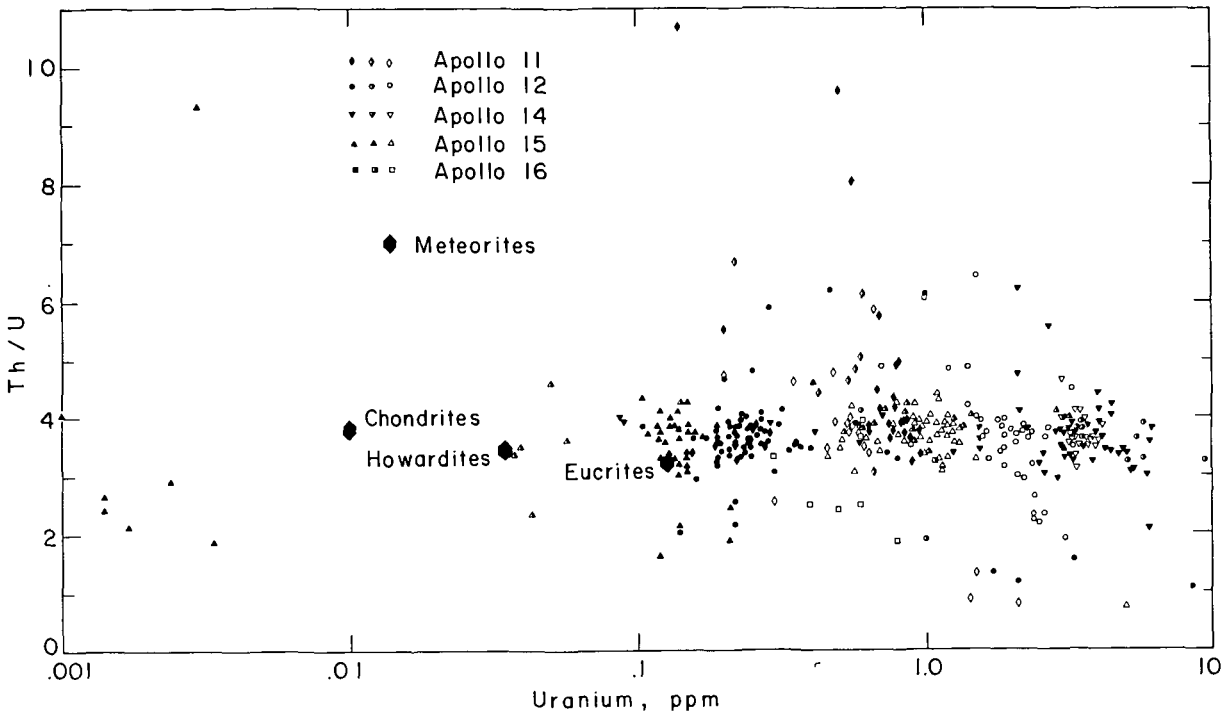


Figure 2.—*Th/U ratio versus uranium concentration for selected lunar rocks and meteorites. Lunar rocks are divided into crystalline rocks, breccias, and fines, with the same notation as in figure 5. Points for average chondrites, howardites, and eucrites are from Mason (ref. 51). Sources for lunar values are given in the text.*

concentration of the Moon to be 2000 and Th/U to be 3.5, then the average radioactivity of the Moon is a function of the bulk uranium content. Given the measured Apollo 15 and 17 heat flows of about 30 ergs/cm^2-s (refs. 56 and 57), Toksöz and Solomon (ref. 30) have shown that the bulk uranium concentration must be 60 $\pm$ 15 ppb to match the heat flow value. In this paper, then, we let U = 60 ppb, with K/U = 2000 and Th/U = 3.5 for the Moon.

For Mars, Venus, and Mercury, we will utilize values based on condensation models of the solar nebula (refs. 54, 58, and 59). These are shown in table 1. In the calculations we consider variations for individual cases as discussed in later sections. However, we expect that for Venus terrestrial abundances are a good approximation. For Mars we use values between terrestrial and chondrite abundances (ref. 32). For Mercury the uranium values are close to those of the Moon, but the planet is most likely lacking in K^{40} (ref. 33). The relevant decay constants, decay energies, and isotopic abundances are taken from Clark (ref. 60).

Distribution of Heat Sources

In most cases, the thermal models presented in this paper assume an initially homogeneous distribution of heat sources. However, the constraints on the internal temperatures rule out, at least for the Moon, a present-day uniform distribution of heat sources. When melting occurs, one would expect the magma to be enriched in U, Th, and K and to subsequently transfer these heat sources to the surface. To account for this, at discrete time steps the heat sources from the molten zones are differentiated upwards, leaving primordial radioactive abundances in any solid region below the zone. Heat

Table 1.—*Parameters Used in Thermal History Calculations*

	Mercury	Venus	Moon	Mars
Radius (km)	2439	6050	1738	3389
Mean Density (g/cm³)	5.43	5.25	3.34	3.96
C/Ma²	—	—	0.394	0.377
Surface Temperature (°C)	77	327	−20	−40
Uranium, ppb	44	31	60	31 [a]
K/U ratio	[a]	10,000	2000	10,000 [a]
Th/U ratio	4	4	3.6	4
Specific Heat (silicates) (J/g°C)	1.2	1.2	1.2	1.2
Heat of Fusion (silicates) (J/g)	400	400	400	400

NOTE: (1) See text.

sources differentiated toward the surface are allowed to decrease exponentially with depth so that

$$H(r) = A_0 \exp\left[-\frac{(R-r)}{h}\right] \quad (3)$$

where A_0 is the surface abundance, R is the radius, and $H(r)$ is the radioactive abundance at radius r. Such a distribution has been formulated for the Earth (ref. 61). The skin depth h decreases with time and is adjusted so that the present-day surface radioactivity, if known, is approximated.

Thermal Conductivity and Other Parameters

In a differentiating planet, heat is transported by conduction and by convection. At temperatures far below solidus, the role of convective flow is small and heat transport is governed by thermal conductivity. This quantity is temperature-dependent and is taken to be the sum of two terms, lattice (or phonon) conductivity and radiative conductivity. The relative dominance of each term is of crucial importance in solving the conduction problem of the planets. Although effective thermal conductivities have been measured for terrestrial and lunar materials (fig. 3), these do not always represent the bulk properties of the Moon or planetarv interiors. MacDonald's (ref. 8) theoretical formulation of conductivity as a function of temperature assumed the opacity to be constant, resulting in a cubic temperature dependence of the radiative term and, thus, its dominance over all temperatures. However, Schatz and Simmons (ref. 64) proposed that for a hypothetical dunite, radiative transfer is suppressed by grain-boundary extinction, resulting in an increase in the opacity with temperature. At low temperatures, then, the effective conductivity is dominated by the lattice term that decreases with increasing temperature. At higher temperatures, the radiative term, increasing roughly linearly with temperature, becomes dominant. This model has been used in previous thermal history calculations at MIT (refs. 23 and 30). For the Moon, however, upon examination of figure 3 and values of conductivity in many previous lunar models, one could just as well take the effective conductivity to be a constant. In some of the lunar models and for Mercury's mantle we shall treat it thus, with $K = 0.45 \times 10^6$ ergs/cm-s °C, while other calculations assume the model of Schatz and Simmons (ref. 64). The total conductivity, K, is given by

$$K = K_L + K_R$$

where K_L = lattice conductivity and K_R = radiative conductivity. As functions of temperature, T, these are given by

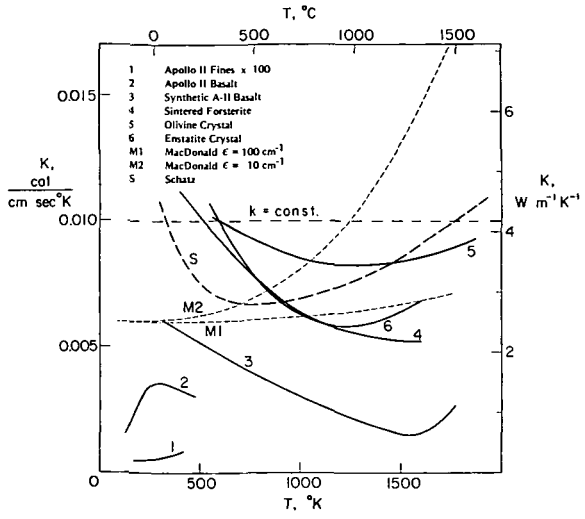


Figure 3.—*Thermal conductivity of selected materials. Sources of measured data (solid lines) are Cremers (ref. 62) for Apollo 11 fines, sample density 1.64 g/cm³; Horai et al. (ref. 63) for Apollo 11 basalt; Murase and McBirney (1970) for synthetic Apollo 11 basalt; Schatz and Simmons (ref. 64) for sintered, polycrystalline forsterite and for single crystal olivine (Fo_{88} Fa_{14}) and enstatite. Theoretical (dashed) curves include those of MacDonald (ref. 8) for two different values of the opacity ε, and one proposed by Schatz and Simmons (ref. 62) for polycrystalline olivine of approximate composition $Fo_{90}Fa_{10}$. The Schatz and Simmons curve, labeled* S *above and* K = *constant, was employed in this paper.*

$$K_L = \frac{4.184 \times 10^7}{30.6 + 0.21T}$$

and

$$K_R = \begin{cases} 0 \text{ for } T \leq 500°\text{K} \\ 230(T\text{-}500) \text{ for } T > 500°\text{K} \end{cases}$$

Other physical parameters required for the calculations are the melting curve, surface temperature, specific heat, heat of fusion, and density. A summary of the parameters common to all models is given in table 1. Appropriate melting curves are used for each planet, taking into account the composition and pressure.

COMPUTATIONAL TECHNIQUES

In this section we describe the thermal calculations for a spherically symmetric planet, taking into account conduction, melting, simulated convection of molten material, and differentiation.

Conductive Models

Assuming that conduction is the only mode of heat transfer in solid material (an approximation to convection will be discussed later), thermal evolution models are calculated using the finite difference solution of the heat conduction equation:

$$\rho C_p \frac{\partial T}{\partial t} = \frac{1}{2}\frac{\partial}{\partial r}\left(r^2 K \frac{\partial T}{\partial r}\right) + H(r,t) \quad (4)$$

where C_p is the specific heat, T is the temperature, r is the radius, K is the thermal conductivity, and $H(r,t)$ is the heat source term. The latter two quantities were discussed above.

The details of the calculations are described fully in the appendix of Toksöz et al. (ref. 23) and are stated here briefly. The finite difference analog of equation (4) which conserves heat flux is

$$T_n^{m+1} = T_n^m + \frac{\alpha}{n^2 p^2}\left[\left(n+\frac{1}{2}\right)^2 \frac{(K_{n+1}^m + K_n^m)}{2}(T_{n+1}^m - T_n^m) - \left(n-\frac{1}{2}\right)^2 \frac{(K_n^m + K_{n-1}^m)}{2}(T_n^m - T_{n-1}^m)\right] + \alpha H_n^m \quad (5)$$

where $\rho = \Delta r$, $r = np$, $t = m\Delta t$, $\alpha = \Delta t/\rho C_p$, and $T_n^m = T(np, m\Delta t)$. The stability condition relating the time increment and the grid spacing is

$$\Delta t < \frac{C_p \rho \Delta r^2}{2 K_{\max}} \frac{n^2}{\left(n+\frac{1}{2}\right)^2} \quad (6)$$

where $K_{\max}$ is the maximum value of the conductivity at a given time step. Δt is computed at each iteration using equation (6), with a factor of 4 instead of 2 in the denominator. A grid spacing, Δr, of 20 km is used.

Boundary conditions for the problem require the surface temperature of the planet to be constant, and $T_1^m = T_2^m$, where T_1^m is the

temperature at $r_1 = \Delta r$ and T_2^m is the temperature at $r_2 = r_1 + \Delta r$. The solution starts at $r = \Delta r$ to avoid a singularity at $r = 0$. Surface heat flux is calculated by adding the heat flow at the boundary between the upper two finite difference cells to the steady-state heat flow due to heat production in the uppermost half cell.

Simulation of Melting and Convection

The effects of melting and convection of molten material on temperature within the body can be modeled following the technique described by Reynolds et al. (ref. 65). In this method the temperature at each grid point at each time step is compared to the melting temperature at the respective grid point. If the temperature is greater than the melting point, the difference divided by the density and specific heat gives the heat equivalent, ΔH. If ΔH is less than or equal to the heat of fusion, ΔH_f, the material at that grid point is considered partially molten, and the temperature is set equal to the melting point. This process is continued at each iteration until the accumulated ΔH is greater than ΔH_f. At this point in time, the material is considered to be completely molten and the temperature is allowed to rise above the solidus. The same process allows completely molten material to solidify, releasing heat equal to ΔH_f.

In simulating convection of molten material, the same technique as outlined above is followed, with the exception that the temperature of the completely molten material is constrained to the melting curve. Any increase in temperature that would raise the temperature above the melting point is converted to its heat equivalent, transferred upward to the next grid point, and considered to be a temperature rise due to convection. The conversion to heat equivalents is necessary due to the increase in the volume element with increasing radius. The advantage of this approximation to convection is that it does not require the inclusion of mass transfer terms in the heat conduction equation. This scheme is not limited to convection of completely molten material. Convection of partially molten material is easily approximated by reducing the heat of fusion. Convection by solid-state creep requires techniques different from those described above. Various attempts at approximating solid-state convection and determining its relative effect on the thermal evolution of the Moon and planets are discussed in the following section.

SOLID STATE CONVECTION

The question of whether or not thermal models calculated assuming conduction mechanisms are unstable to solid-state convection motions has been discussed in many papers, most recently by Tozer (refs. 24 and 25), Turcotte et al. (ref. 66), Cassen and Reynolds (refs. 29 and 67), and Schubert et al. (ref. 34). Much of this work has been motivated by Schubert et al. (ref. 68). Using a number of conduction temperature profiles for the planets, these investigators applied a linear stability analysis and concluded that thermal convection would occur in each case. Earlier, Runcorn (refs. 69 and 70) attempted to explain departures of the lunar surface from hydrostatic equilibrium by employing convection. Whether or not convection has played a dominant role in the evolution of the planets, however, is still debatable. The question is not easily answered, since the presence (or absence) of convection is a complex function of the temperature and the rheology of the planetary material. Futhermore, in the case of the Moon, the characteristics of the mare basins and their possible filling with basalts by gravitational upwelling of magma implies the presence of more complicated geometries than the simple cellular convection pattern postulated by some investigators. Such upwelling type heat transport is well approximated in our calculations described earlier. Also, the attenuation of shear waves and the presence of deep moonquakes in the lunar interior, as discussed in the following section, present

difficulties for those who hypothesize that solid-state convection occurs in the Moon.

The strongest advocate for the dominance of solid-state creep in the Moon and planets has been Tozer (refs. 24, 25, and 26). In all his papers, Tozer has postulated that convection is at least as important as conduction for any planetary body of radius greater than a few hundred kilometers. This theory, based on the assumption that at any finite temperature an arbitrarily small nonhydrostatic stress produces some permanent deformation of the material, suggests that at some viscosity, or range of viscosities, this motion, or rate of creep, becomes "fast" enough to provide a very efficient method of heat transfer.

In this paper we do not go into detailed convection calculations. In some cases, however, we include models that approximate solid-state creep by arbitrarily raising the thermal conductivity of material with temperatures above a certain threshold value.

Thermal Evolution of the Moon

CONSTRAINTS ON THERMAL EVOLUTION

Thermal evolution calculations generally require boundary conditions that would indicate directly or indirectly the temperatures at certain times inside the planetary body. In addition to these, data are needed to specify material behavior, heat transport mechanisms, and heat sources. Normally, insufficient data and constraints are available. Thus, calculations generally are carried out with a set of initial conditions and assumptions, and the conditions are modified if the temperature models fail to satisfy available constraints.

Data and samples from Apollo missions imposed some strong constraints on the thermal evolution of the Moon. Some of these, such as heat flow, electrical conductivity, seismic velocities, attenuation, and tectonism, pertain to present-day temperatures. Some others, such as the presence of a differentiated lunar crust and chronology of lunar igneous and magmatic activity, indicate the thermal state early in the lunar history.

Lunar Heat Flow

Two heat flow measurements have been made on the Moon, one each at the Apollo 15 (Hadley Rille) and Apollo 17 (Taurus-Littrow) sites. The experiments and their results are described by Langseth et al. (ref. 57). The heat fluxes have been determined by measuring temperature gradients and thermal conductivities in bore holes to a maximum depth of 234 cm. In that depth range, temperature gradients in the lunar regolith are between 1.3 and 1.7 °K/m, and the thermal conductivity is in the range 1.7×10^{-4} and 2.0×10^{-4} W/cm-°K. The heat flow through the surface based on the measured temperature gradients and conductivity is 31 ergs/cm^2-s at the Apollo 15 site and 28 ergs/cm^2-s at the Apollo 17 site (ref. 57). In each case the estimated uncertainty is about $\pm$ 20 percent.

The Taurus-Littrow and Hadley Rille sites are located in the basalt-flooded valleys at the rims of the Serenitatis and Imbrium basins, respectively. There are no direct data to suggest that the thermal characteristics of these sites are any different from other parts of the Moon. Thus, an average heat flow value of about 30 ergs/cm^2-s will be adopted for the Moon in these calculations. This value is about one-half the average heat flow of the Earth (63 ergs/cm^2-s). If we assume steady-state conditions for both bodies and take into account the differences in the radii (average radii: $R_{Moon} = 1738$ km, $R_{Earth} = 6371$ km), surface area ($S_{Moon}/S_{Earth} = 0.074$), and volume ($V_{Moon}/V_{Earth} = 0.02$), we find that the lunar heat flow is higher by about a factor of 2 compared to the Earth. As was discussed earlier in this paper, this implies higher heat generation and radioactive sources inside the Moon than inside the Earth.

Another important measurement arising from the heat flow experiments is the value

of the near-surface temperature. At a depth of about 70 cm, the measured average ambient lunar temperature is 253 K. This will be used as the surface temperature in our calculations.

Electrical Conductivity and Inferred Temperatures

Three magnetometers deployed on the lunar surface, one each at the Apollo 12, 15, and 16 sites, have recorded the magnetic fields induced in the Moon by large-scale transient events. In addition to these, the ambient and time-dependent magnetic fields in the lunar environment are measured by the Explorer 35 satellite magnetometer which is orbiting the Moon.

The analysis of the transient fields recorded simultaneously by the Explorer 35 magnetometer and the surface magnetometer has made it possible to calculate the electrical conductivity inside the Moon (refs. 71 through 74). The Moon responds to transient magnetic events which induce eddy currents in the lunar interior. The response or transfer function is computed from the induced field at the Moon's surface and the forcing (source) function recorded by the Explorer 35 magnetometer.

These results are interpreted by calculating the theoretical response of the Moon with radially varying conductivity. Although there are some limitations of the theoretical calculations and some difficulty in matching all the available data, the results definitely show an increase of electrical conductivity with depth into the Moon. To a depth of about 1000 km the conductivity profile can be characterized by three layers (ref. 72) or by a greater variety of models including current layers (ref. 74). The resolving power of the data is not sufficient to detail the conductivity below this depth.

Conductivity depth profiles given by Dyal et al. (ref. 72) and the three-layer model (a good representation for the average models) of Sonett et al. (ref. 74) are shown in figure 4. Basically, the models require very low conductivity ($\sigma_1 \leq 10^{-9}$ mho/m) for the outer 50 km of the Moon. For the intermediate layer ($1100 < R \leq 1700$ km; R is radius), the conductivity is in the range of $\sigma_2 = 1$ to 7×10^{-4} mho/m. For the deeper interior there is a greater discrepancy. While Sonett et al. (ref. 74) give a value of about $\sigma_3 \simeq 10^{-3}$ mho/m for $R < 1200$ km from the sunlit side data, Dyal et al. (ref. 72) give $\sigma_3 \simeq 10^{-2}$ for $R \leq 1000$ km.

From the conductivity profiles, the temperatures inside the Moon can be estimated if the composition and temperature depen-

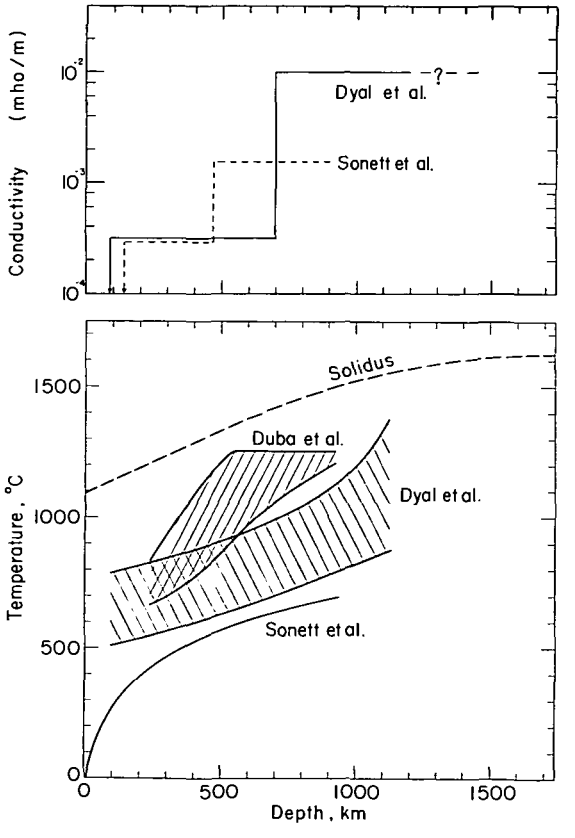


Figure 4.—*Lunar electrical conductivity profiles of Sonett et al (ref. 74) and Dyal et al. (ref. 72) and some estimates of present-day temperatures in the Moon inferred from these measurements. Included are the temperature curve of Sonett et al. (ref. 73), an interpretation of the Sonett et al. (ref. 73) conductivity distribution using the temperature-conductivity relation of an olivine with little or no Fe^{3+} (ref. 28), and the estimates by Dyal et al. (ref. 71) based on their conductivity models.*

dence of conductivity are known. For a given composition, conductivity, σ_T, increases with temperature: $\sigma_T = \sigma_0 \exp\left(-\frac{A}{kT}\right)$, where A = activation energy, k = Boltzmann constant, T = absolute temperature, and σ_0 is a constant dependent on the material. If olivine were assumed for a composition and a lower bound on the conductivity of olivine is used, a temperature of about 1000°C is estimated for the Moon at about 700 km depth (refs. 72 and 74). If newer laboratory data on pyroxenes and olivines—the most likely candidates for mantle composition (refs. 28, 75, and 76)—are used, higher temperatures (i.e., 1000°C at 400 km and 1400° at 800 km depth) are estimated (refs. 28 and 77). Some bounds on temperature models are shown in figure 4; in all cases temperatures are below the solidus to a depth of about 600 to 700 km. At greater depths, temperatures either approach or exceed the solidus, or some changes in the composition increase the conductivity. Another feature of this deep region is that both conductivity and temperature profiles flatten.

Structure of the Lunar Interior and Seismic Wave Attenuation

Seismic studies of the Moon have revealed much valuable information on the structure and the rheological properties of the lunar interior. The presence of a layered structure indicates differentiation and melting in the past. The attenuation characteristics of seismic waves may be explained in terms of increased temperatures or partial melting at the present.

The seismic velocity structure for the outer 150 km of the Moon has been determined from the analysis of manmade impact seismograms recorded by the Lunar Seismic Network (refs. 78, 79, and 80). This structure shows the presence of a lunar crust overlying a mantle. Over the mare the crust may be two layered (the upper layer being mare basalt), with a total thickness of about 60 km. In the highlands and on the backside, the crust may be somewhat thicker. The compositional inferences that can be made from the velocities and other data suggest that the crust is chemically different from the mantle and that it may have formed by the upward differentiation of the lighter minerals.

Below the crust the lunar mantle may extend to a depth of about 1000 km, probably with nearly constant compressional velocities (refs. 81 and 82). Data from moonquakes and meteorite impacts specify the properties of the mantle. The recording of well-defined shear waves from the deep moonquakes implies that the mantle must be sufficiently rigid to 700 or 1000 km depth to prevent appreciable shear-wave attenuation.

Seismic shear waves from farside impacts and farside moonquakes that have penetrated deeper into the Moon than about 700 km are attenuated (refs. 82, 83, and 84). This indicates a possible "softening" of the material in the central region of the Moon below about 700 or 1000 km. Any softening that would reduce Q to less than about 500 would explain the observations. This could be achieved by temperatures approaching the solidus, by a very small amount of partial melt, or by other mechanisms (such as perhaps an increase in the amount of volatiles in the deep lunar interior or a different bulk composition).

If we assume that the attenuation is due to temperature effects, this would place some limits, within the compositional constraints, on the temperatures below 700 km in the Moon. For a pyroxene-olivine-rich composition this is 1600°C. If the Moon has an Fe-FeS-rich core (see ref. 85 for a discussion), the minimum temperature for it would be about 1000°C, given by the Fe-FeS eutectic. Thus, the present-day lunar "core" temperatures range from about 1000 to 1600°C.

Constraints Implied by Lunar Viscosity, Seismicity, and Mascons

The lunar interior described in the previous section and shown in figure 5 can be divided into three units: a crust, a relatively rigid 1000-km-thick "lithosphere," and a

relatively soft deep interior "asthenosphere."

The crust and the lithosphere have supported lunar mass anomalies ("mascons") for over 3 b.y. This requires that (1) at the time of the mascon formation and mare flooding the lunar lithosphere was thick enough to support the loads (ref. 86) and (2) the viscosity of the lithosphere must be greater than about 10^{26} poise (refs. 87 and 88). This high viscosity requires temperatures significantly lower than the melting curve in the outer few hundred kilometers of the Moon.

Another important constraint on the present-day thermal state is that the lunar interior is the very low level of seismic activity in the Moon. Total seismic energy release in the Moon is about 10^{11} ergs/yr, 13 orders of magnitude lower than that of the Earth (refs. 83, 89, and 90). All moonquakes are very small, and those whose focal depths can be determined have hypocenters between 700 and 1200 km depth. These indicate that if there is any convection or tectonic motion taking place in the Moon today, it must be below about 700 to 1000 km.

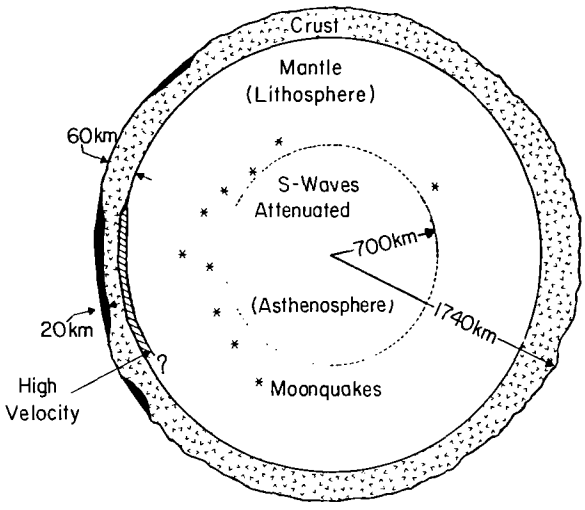


Figure 5.—*Schematic diagram of the structure of the Moon as inferred from lunar seismic data (ref. 80).*

Chronology of Lunar Igneous Activity

The time history of differentiation and igneous activity imposes the strongest constraints on the early thermal state of the Moon. The chronology of the lunar igneous activity starts from the formation of the original crust about 4.6 b.y. ago as deduced from model ages of lunar rocks and soils (refs. 91 through 94). More recently a Rb-Sr age of 4.6 b.y. has been obtained for an Apollo 17 dunite fragment (72415) by Albee et al. (ref. 95). To create a 60-km-thick feldspathic crust described in the previous section requires the total or partial melting and differentiation of at least one-half of the total volume of the Moon (ref. 96). This requirement strongly constrains the initial temperature of the lunar interior.

Following the formation of the initial crust, the chronology of lunar rocks (an excellent summary has been compiled by Doe (ref. 97)) is defined by three episodes in the lunar evolution:

1. The period 4.4 to 4.0 b.y. ago was characterized by continuing igneous activity, brecciation by meteoritic bombardments, and metamorphism of the older rocks. Because of the subsequent events, the detailed record of this episode has been largely obscured. Available data include ages of anorthosites (4.1 b.y. for lunar rock 15415) (ref. 98), the formation ages of KREEP basalts (refs. 50 and 99), and a number of the "recrystallization" ages of the metamorphosed breccias from the Apollo 12, 14, 16, and 17 and Luna 20 sites (see ref. 97 for a compilation). These are shown in figure 6.
2. Episode of basin excavation (4.0 to 3.9 b.y. ago) is characterized by intense bombardment, resetting of the geologic clocks, and excavation of the major basins such as Imbrium, Tranquillitatis, Serenitatis, Nectaris, etc. (refs. 94 and 100).
3. During the episode of mare flooding (3.9 to 3.16 b.y. ago), the basins

formed were filled with mare basalts. The ages of these lunar basalts are well documented by dating samples from the Apollo 11, 12, 15, and 17 and Luna 16 missions (refs. 18, 92, 93, 101 through 104, and others).

The failure to discover lunar igneous rocks younger than about 3.16 b.y. is an extremely important constraint in the lunar thermal history. Since basalts were probably derived from sources to about 400 km depth, the termination of lunar magmatic activity represents the end of melting or partial melting in the upper mantle of the Moon.

During the past 3.0 b.y., the lunar surface has continued to evolve as a result of meteorite impacts and cratering. There have been local melting and metamorphism in this period. There is no direct evidence for extensive volcanic activity or basalt flooding in the past 3.0 b.y.

Magnetism of Lunar Rocks

Although the Moon does not have a measurable dipole magnetic field at present, the lunar crust is extensively magnetized. This

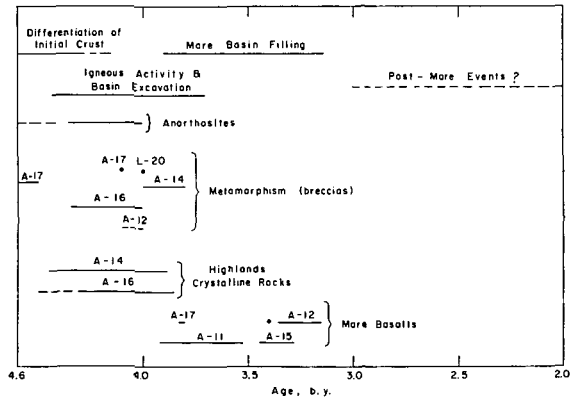


Figure 6.—*A summary of early lunar evolution and igneous activity at the surface, based on Rb-Sr, Ar^{39}-Ar^{40}, and concordia ages of returned lunar samples. Samples from different missions are designated by "A" for Apollo (A–11 is Apollo 11) and "L" for Luna. Sources for this summary are presented in the text.*

remanent magnetization has been verified by magnetic field measurements from the orbiting Apollo subsatellites (ref. 105), on the surface (ref. 71), and from the remanent magnetization of returned lunar samples (refs. 106 through 109, and others). This stable remanent magnetization was most likely acquired on the Moon as the rocks cooled through the Curie point of iron in the presence of a magnetic field. The intensity of the ambient magnetic field at the time of the formation of these rocks is estimated to be greater than 1000 gammas, and probably as high as a few thousand gammas (ref. 110).

The origin of the ancient magnetic fields which magnetized the initial lunar crust and the lunar rocks is one of the most important and as yet unresolved problems in lunar studies. From the ages of the crust and the rocks, the magnetizing field must have been present at least from 4.6 to 3.2 b.y. ago. The hypothesis of an external magnetizing field is not favored because of the difficulties associated with having a steady field of 1000 gammas or more near the Moon for a period of 1.5 b.y.

The favored hypothesis of the internally generated magnetizing field would require either a lunar dynamo or magnetized lunar interior (refs. 111, 112, and 113). In the dynamo model, it is necessary for the Moon to have a conducting iron or Fe/FeS core of sufficient size early in its history. The formation of such a molten core requires high internal temperatures early in the lunar history. In the case of a highly magnetized model of the lunar interior (refs. 111 and 113), it is required that the temperatures below a few hundred kilometers depth remain below the Curie temperature (about 760°C), while all the magmatic activity and differentiation take place at shallower depths. Such a model would put severe requirements on the thermal evolution models and also require a high magnetizing field at the time of the lunar accretion.

Thus, the magnetic history of the Moon according to the above models would require either extensive melting and differentiation

of the core at the onset of lunar evolution or temperatures less than about 800°C for the first 1.5 b.y. in the lunar mantle.

TEMPERATURE MODELS FOR THE MOON

In this section we present several specific models for the thermal evolution of the Moon which illustrate the effect of varying initial conditions and bulk radioactivities. Previous papers (refs. 23, 30, and 86) have discussed many of the models presented here and have assessed their ability to satisfy the constraints listed in the previous section. In this section we divide the models into three subgroups: initially homogeneous, convective, and inhomogeneous models.

Initially Homogeneous Models

We begin by considering a rather unrealistic model: initially cold (T = 0°C everywhere). This is a valuable exercise in the respect that it provides a verification of the computational scheme. Figure 7 shows three present-day temperature profiles each for the given present-day bulk uranium concentrations. Clearly, none of the models shown here satisfies the constraint of near-surface melting in the first billion years of the Moon's history. In fact, the basalt solidus (dashed line) is not reached at any point in time in the lunar evolution. Furthermore, while reasonable uranium concentrations of greater than 37 ppb provide present-day melting in the lunar interior, these models cannot generate enough heat to satisfy the above constraint. Since radioactive decay alone cannot provide the heat necessary for early melting and differentiation, we must consider models with high initial temperatures.

In an earlier section it was stated that one might consider the effects of early heating by tidal dissipation and/or solar wind flux as the Sun passed through a T-Tauri stage by investigating an initially completely molten Moon. Such a model is shown

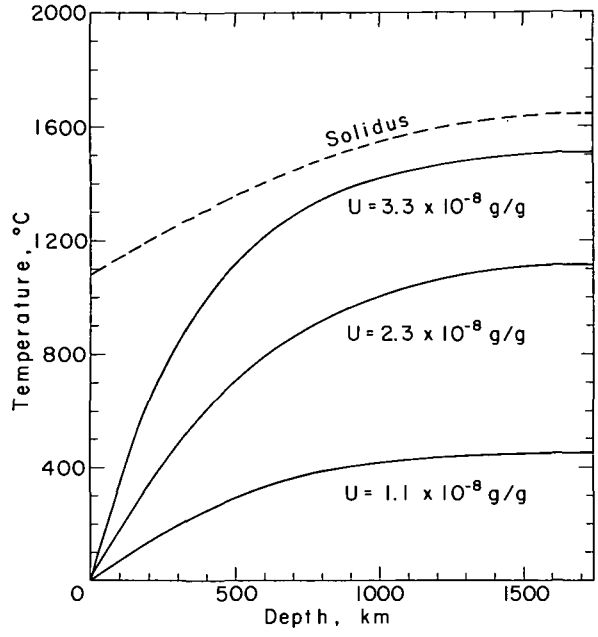


Figure 7.—*Present-day temperature profiles for an initially cold Moon (0°C everywhere), as a function of present-day uranium concentration. The solidus of anhydrous mare basalt (ref. 114) is also shown.*

in figure 8. In this case, all the radioactive heat sources are immediately differentiated and concentrated toward the surface. The formation of a dense core (ref. 86) composed of iron or FeS would easily be accomplished. Because of the depletion of heat sources in the lunar interior and the very effective heat transport in the convecting molten regions, this model cools rapidly and is completely solid after 2 b.y. At the present time it is completely solid and continuing to cool. With an average uranium composition of 60 ppb, the heat flow value is 29 erg/cm²-s, within the reported range of the Apollo 15 and 17 measurements. Although this model satisfies the constraints of early initial melting and heat flow, it does not allow for a small partially molten core as implied by the seismic data.

Since the normal process of accretion can produce initial near-surface partial melting without employing some catastrophic event, we now consider a model of lunar thermal evolution with initial temperatures calcu-

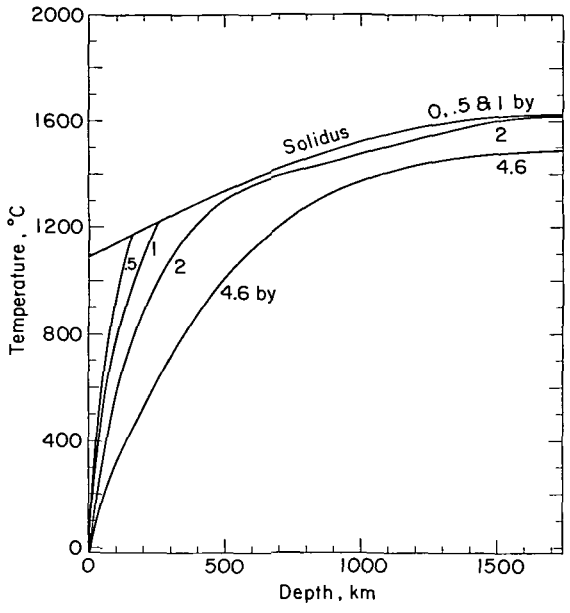


Figure 8.—*A model for thermal evolution as a function of time in an initially molten Moon. Time, in billions of years since lunar origin, is indicated by the number adjacent to each temperature profile. On this and later figures, the Moon is partially or completely molten at those depths where the temperature profile lies along the solidus.*

lated according to equations (1) and (2). This then allows for early segregation of the lunar crust and differentiation of the radioactive heat sources.

A model that satisfies all the major constraints presently known is shown in figure 9. The initial temperature is calculated from the accretion model, with an accretion time of 100 yr and a base temperature of 800°C, which allows for early heating by sources other than accretion. Initial melting extends to a depth of about 800 km, giving sufficient volume to differentiate a primordial lunar crust. The present-day uranium concentration averages to 60 ppb. The thermal conductivity is taken to be constant at 0.45×10^6 erg/cm-s-°C.

It can be seen from figure 9 that this model cools at the surface, giving a solid lithosphere growing at a rate of about 220 km per b.y. During the period of mare filling, the upper extent of melting progresses from 140 to 280 km, in agreement with the depth of origin of mare basalts (ref. 114) and with the necessity of maintaining a thick, cool lithosphere to sustain the stresses associated with mascon gravity anomalies. Shortly after 1 b.y., a convecting core develops due to undifferentiated heat sources of nearly primordial radioactive abundances near the center of the Moon. The core has a maximum radius of 1340 km at 1.5 b.y. and then slowly cools by conduction through the lithosphere. At present, this model is molten below 1000 km. This is in agreement with S-wave attenuation in the core region and with the occurrence of moonquakes at 700 to 800 km depth. The surface heat flow is 30 erg/cm^2-s, consistent with the measured values.

Convective Models

We now consider an approximation to solid-state convection in the Moon. We propose to simulate the efficient heat transport

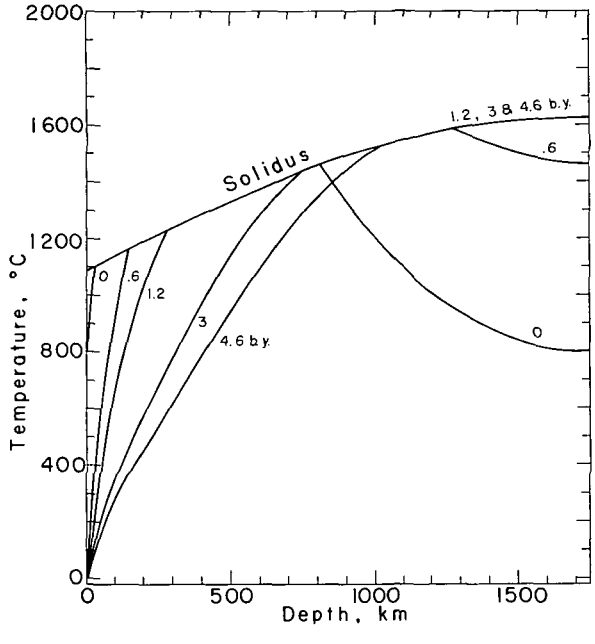


Figure 9.—*Thermal evolution in a Moon accreted in 100 yr at a base temperature of 800°C, with an average present-day uranium concentration of 60 ppb. Symbols are explained in the caption to figure 8.*

of convection by raising the thermal conductivity by a factor of 10 on a grid point that has a temperature greater than a critical temperature of 1000°C. This is equivalent to Tozer's steady-state "core" temperature. Otherwise, the conductivity follows the scheme of Schatz and Simmons (ref. 64). We permit this enhanced conduction after 1 b.y., i.e., after rapid differentiation is completed and a lithosphere has formed. As in the case of convection of molten material, this approximation does not include mass transport phenomena, nor is it a statement on any particular solid-state creep mechanism. It only enhances the heat transport.

Figure 10 illustrates a model with convection as described above. The initial conditions and present-day bulk uranium concentration are the same as for the previous model (fig. 9). The evolution proceeds as before until 1 b.y. At this point, convective processes dominate, and the conductivity is raised for temperatures above 1000°C. At the present, a convecting core of radius 1100 km and temperature nearly 1000°C underlies a nonconvecting, cool, rigid lithosphere. The present heat flow is 29 erg/cm²-s. The features of this model are essentially the same as Tozer's models.

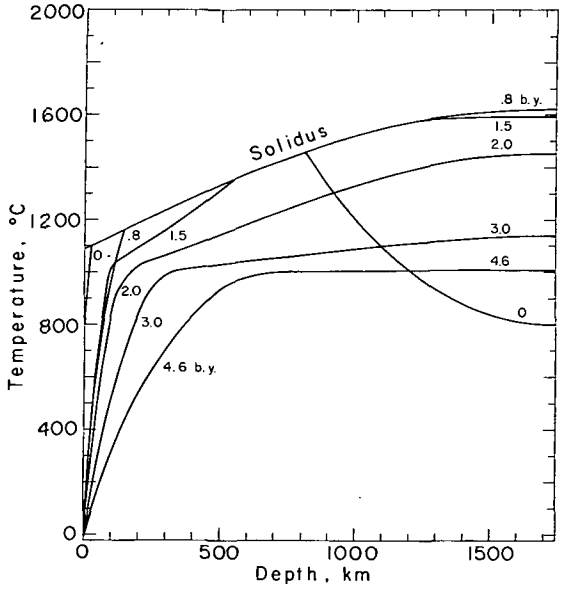


Figure 10.—*The effect of convection by solid state creep on the thermal evolution of the Moon (see text). The initial parameters for this model are the same as for figure 8.*

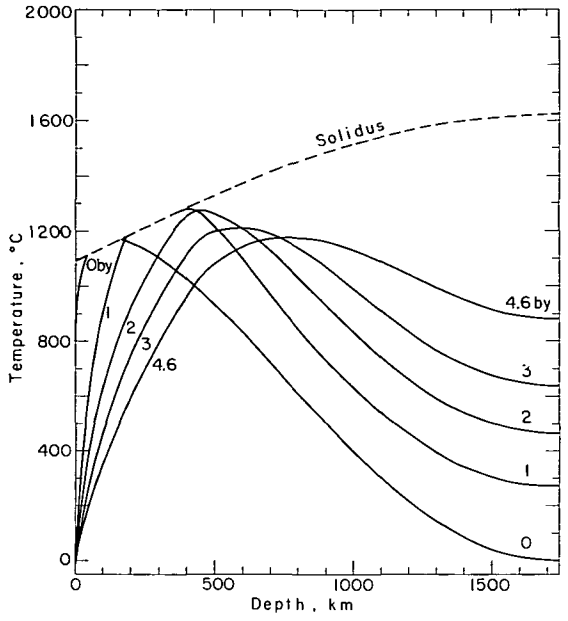


Figure 11.—*Thermal evolution in a Moon derived from inhomogeneous accretion (ref. 30). The initial temperature profile assumes a cold (0°C) accretion over a 1000-yr time interval. Primary zoning of radioactivity is assumed (see text).*

Inhomogeneous and "Blanketed" Models

We have considered up until this point models which assume an initially homogeneous distribution of heat sources in the Moon. The only exception was that of the molten Moon in which all the radioactive isotopes were initially differentiated to the surface. One type of model that allows relatively cool interior temperatures and satisfies the heat flow constraint without invoking solid-state convection has been suggested by several investigators (refs. 115, 116, and others). This involves a decrease in the concentration of radioactivity in the Moon, with depth as a primary feature associated with inhomogeneous accretion.

Figure 11 shoes a thermal history model

from Toksöz and Solomon (ref. 30) similar in many respects to the one proposed by McConnell and Gast (ref. 22). The initial temperature profile assumes accretion in 1000 yr, with a base temperature of 0°C. We assume that the radioactivity is stratified such that the present-day uranium abundance is 120 ppb in the uppermost 200 km, 50 ppb in the next 250 km, and 10 ppb in the remainder of the Moon. This gives a bulk uranium concentration of 53 ppb. The K/U and Th/U ratios are fixed with values given in table 1. The conductivity follows the Schatz and Simmons (ref. 64) model. Although the initial temperature barely exceeds the solidus between 40 and 140 km depth, shorter accretion times would provide initial melting at greater depths as in the previous models presented in this paper. With differentiation allowed for in four discrete time steps between 0 and 0.9 b.y., the evolution of the upper few hundred kilometers is similar to that in figures 9 and 10. The present-day heat flow is 32 erg/cm^2-s, and the interior of the Moon has temperatures well below the solidus.

The difference between this model and the others discussed earlier is that the interior of the Moon is depleted in radioactive elements at cold temperatures and, thus, heats slowly so that the Moon is everywhere solid at present. Whether or not a cold accretion can accompany primary chemical layering is debatable; however, such an origin is incompatible with a molten iron-rich core early in the Moon's history. Furthermore, as in the case of solid-state convection, the present-day temperature profile does not seem to satisfy the constraint implied by the attenuation of S-waves in the deep interior.

We finally examine the effect of a low thermal conductivity "blanket" layer on the Moon. Measurements of the effective thermal conductivity of uncompressed lunar soils (ref. 62) indicate values more than two orders of magnitude less than that assumed for the interior (see fig. 3). Some investigators have argued that the widespread distribution of these lunar fines following the large impact events 4 b.y. ago might have produced localized melting at shallow depths. Figure 12 compares such a model with that of figure 9, 100 m.y. after the soils are assumed to have been scattered. Since we are interested in the maximum possible effect of such an event, we will assume the lunar regolith to extend to a depth of 10 km, with a thermal conductivity of 0.45×10^4 erg/cm-s-°C. Both values are probably overestimates. The depth of dense fracturing in the lunar crust has been estimated to be less than 10 km by Toksöz et al. (ref. 80). Thermal conductivity increases rapidly with compression of the soils, and in-situ conductivity measurements made at the Apollo 15 and 17 heat flow sites (ref. 57) yield values only about 1 order of magnitude lower than the conductivity assumed for the bulk of the Moon. In any case, the maximum effect shown in figure 12 amounts to a rise in temperature of only about 180°C at 25 km. Thus, it can be confidently concluded that a uniform thermal "blanket" would have had

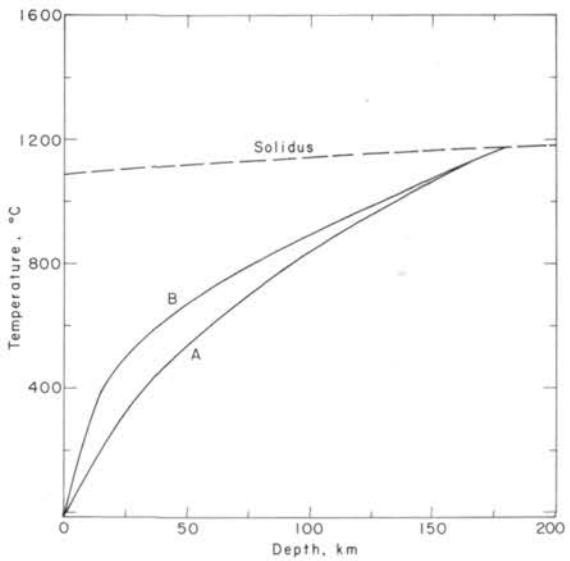


Figure 12.—*The maximum effect of a thermal "blanket" layer on near-surface lunar temperatures 100 m.y. after the presumed time of the Imbrium event (600 m.y. after lunar origin). Curve B represents a model with initial conditions the same as figure 9, but with the introduction of a low-conductivity, 10-km layer at 600 m.y. Curve A is the near-surface temperature profile for the model in figure 9, with no blanket layer.*

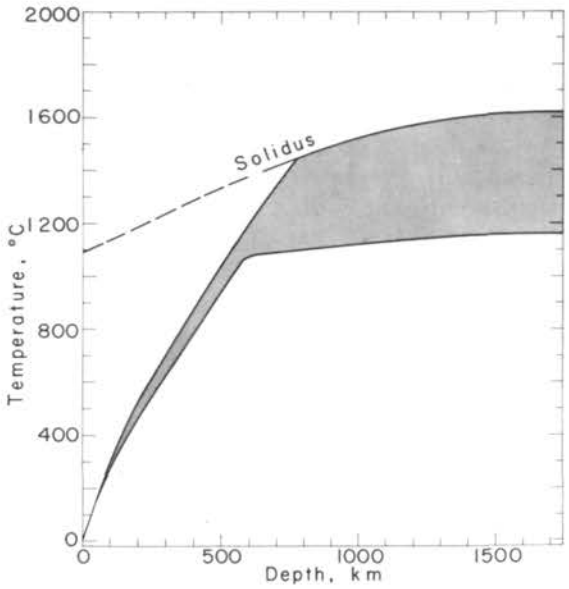


Figure 13.—*Range of present-day temperature profiles for theoretical thermal history calculations. The upper bound is from Toksöz and Solomon (ref. 30), while the lower bound is the convection solution of Turcotte et al. (ref. 66).*

a minimal effect on the early evolution of the Moon.

While the models discussed above are limited in number, they do serve to demonstrate the importance of initial conditions, geophysical constraints, and heat transport mechanisms in determining the thermal history of the Moon.

The range of present-day temperature profiles inside the Moon that satisfy the main constraints listed previously is shown in figure 13. One encouraging aspect of this figure is that regardless of how the temperatures are calculated, whether conduction or convection mechanisms are prevalent, the present-day temperatures are relatively narrow. Hopefully, with additional data, not only will the present-day temperature limits be narrowed, but also the early history of the Moon will be better understood.

EVOLUTION OF THE MOON

The thermal state of the lunar interior as a function of time is shown in figure 14, along with major episodes in lunar evolution. During the first 2 b.y., the lunar upper mantle undergoes sufficient melting to account for the differentiation of the crust and the subsequent lunar volcanism and mare filling. The zone of melting deepens with time. The lithosphere thickens at the rate of about 220 km/b.y. during this period. In particular, the shallowest melting progresses from 140 to 280 km depth during the period of mare filling, in agreement with the depth of origin of mare basalts (ref. 114) and with the need for a reasonably thick lithosphere to sustain the stresses associated with mascon gravity anomalies. The disappearance of melting in the mantle coincides roughly with the termination of magmatic events. At present the whole Moon is cooling. The deep interior, below a depth of 1000 km, may be hot enough for partial melting. This will explain the S-wave attenuation in this zone as described previously.

If indeed partially molten, the rheologic properties of the deep lunar interior may be

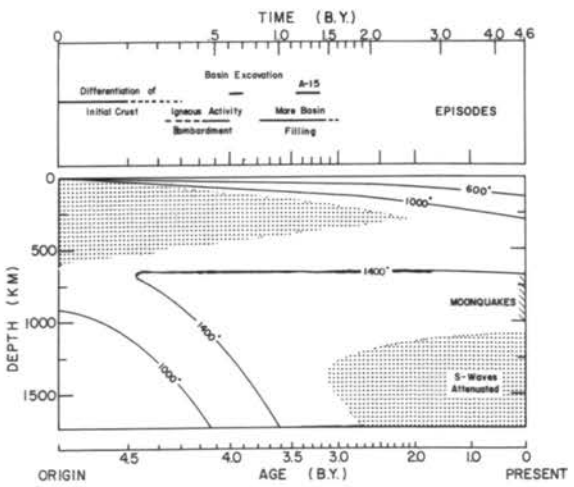


Figure 14.—*Thermal evolution of the lunar interior as a function of time, based on the temperature calculations shown in figure 9. Major episodes of differentiation and igneous activity are shown on top and are based on lunar sample ages. Isotherms are in 0° C. Fine and coarse shading denote regions of partial and extensive melting, respectively. Zones of moonquake activity and high attenuation of S-waves shown on the figure apply to the present.*

similar to the Earth's asthenosphere and may have convective motions. Such convection may exert small stresses at the bottom of the lithosphere where the moonquakes occur, but it could not induce sufficient stresses in the thick lunar lithosphere to cause large moonquakes or active tectonic motions.

Present-day temperatures shown in figure 13 and 14 generally exceed the melting temperatures of Fe or Fe/FeS combinations in the deep lunar interior. Thus, if there were a concentration of Fe or Fe/FeS in the center, it would be molten, and the Moon would have a molten core.

Thermal Evolution of Mars, Venus, and Mercury

In this section we calculate thermal history models for planets Mars, Venus, and Mercury. The Earth has been excluded from these calculations. Its evolution history is similar to that of Venus and is generally well understood. Its present-day temperatures are strongly constrained by the data, and models can be tailored to meet these requirements. New data that became available for Mars, Venus, and Mercury from recent planetary missions, however, justify a reexamination of the thermal histories of these planets.

For the calculations we use the numerical techniques described previously and follow a procedure similar to that used for the Moon. Since there are many fewer data for the planets, the calculated thermal models are less rigidly constrained than the lunar models.

MARS

The thermal history of Mars is not as strongly constrained as for the Moon or Earth. However, new data, primarily from the Martian Orbiter Mariner 9, provide information that places some conditions on its evolution and internal structure. We will now present several theoretically calculated thermal evolution models from Johnston et al. (ref. 32).

Structure and Constraints

The two main pieces of data regarding the composition and structure of the interior of Mars are its mass (M) and moment of inertia factor ($I/M\bar{R}^2$). These roughly determine the density variation within the planet and may indicate the presence (or absence) of a high-density core.

Using values of J_2 and the mean radius as determined from Mariner 9 experiments (ref. 117), we calculate $I/M\bar{R}^2 = 0.377 \pm 0.001$, indicating a distinct density increase with depth. This increase could easily be explained by a high-density core. Recent results from the U.S.S.R. Mars probe indicate that Mars maintains a relatively weak dipole magnetic field (ref. 118), giving further credence to the idea of a core.

The presence of a core places a fairly strong constraint on the thermal evolution. For core formation to take place, temperatures within the planet must have been nearly everywhere above a core material melting curve at one time. If Mars evolved in a manner similar to that of the Earth and Moon, the differentiation of core and mantle most likely took place relatively shortly after origin. It thus seems to be the case with Mars that volcanism and, therefore, differentiation have been active since early in the Martian history (ref. 119).

We assume that Mars has retained sulfur during its condensation and, thus, has an Fe-FeS core (refs. 58 and 120), and that potassium is partitioned into the sulphide phase (refs. 121 and 122), thus providing a heat source in the core by the decay of K^{40}. This model leads to early differentiation of Mars and early core formation, without requiring high initial temperatures necessary for the reduction of Fe or Si. This is possible due to the low and relatively pressure-independent Fe-FeS eutectic at 990°C (ref. 123).

Many new data concerning the evolution of Mars were obtained from the Mariner 9 photographs. The general picture was a planet much more dynamic than was previously thought. From the geologic interpre-

tation of these photographs (refs. 119, 124, 125, and 126), generally four regions of prominence stand out: an ancient cratered terrain, younger volcanic plains, large volcanic constructs such as shield volcanoes, domes, and craters, and extensive sedimentary deposits.

The Martian evolution inferred from the above features can be summarized as follows (ref. 126):

1. Roughly 4.6 b.y. ago Mars accreted. An intense bombardment of the surface took place at, or somewhat later than, the final stages, resulting in the heavily cratered, oldest terrain.
2. Volcanism, and probably the differentiation of the core, followed shortly thereafter.
3. Intense volcanic and tectonic activity characterized by basalt plains, uplifted, faulted, and eventually eroded, was apparently the next stage of Martian evolution. It was in this stage that the volcanic shields such as Nix Olympica began to develop.
4. The next stage featured large-scale tectonic activity and the completion of the shield volcanoes.
5. The final stage of evolution, lasting until the present, shows evidence of moderate tectonic and volcanic activity and wind and possibly water erosion and deposition.

Although no absolute ages are available for these stages of Martian evolution, they are valuable in constraining thermal history models. We know that an initial crust must have differentiated and the core formation must have occurred early in the Martian history, with volcanism, implying mantle melting, beginning shortly after and proceeding to the present time.

Heat Sources and Input Parameters

The thermal evolution models of Johnston et al. (ref. 32) are calculated in the manner described previously, with the exception that the formation of an Fe-FeS core and the differentiation of K^{40} into the core are specifically allowed.

As before, the most important heat source in the thermal history calculations is the heat generated by the decay of the long half-life radioactive isotopes U^{238}, U^{235}, Th^{232}, and K^{40}. No surface measurements of the abundances of these isotopes have been made for Mars, so we are forced to look at the only available data: those from the Earth, the Moon, and meterorites. The radioactive abundances for the Moon and some meteorites were discussed in an earlier section. The use of lunar, howarditic, or eucritic compositions in Mars, however, results in present-day temperatures too hot for any reasonable model.

The "chondritic coincidence" for the Earth has long been recognized (ref. 3), giving U = 11 ppb, but this requires the depletion of potassium in the crust relative to chondrites. Although putting the potassium in an Fe-FeS core can eliminate this problem, if all the excess potassium is put in the core, this increases the temperature significantly. In the other extreme, assuming no potassium in the core and K/U = 10 000, McDonald (ref. 7) recalculated the absolute uranium abundance for the Earth's mantle, constraining the heat production under steady-state conditions to match the average terrestrial heat flow. His uranium concentration, reduced to a homogeneous planet, is about 31 ppb. One might, therefore, place bounds on the Earth's absolute abundances, with U from 11 to 31 ppb and K/U from 80 000 to 10 000.

Recent models of the chemistry involved in the condensation of the solar nebula (refs. 59 and 127) indicate that a number of refractory trace elements, including the rare earths, will crystallize along with Ca-Al-rich assemblages at about 1500 K. This is before the condensation of magnesium silicates and metallic iron. Potassium and other volatiles will condense at lower temperatures (between 1100 K and 1200 K). Since these temperatures are higher than the condensation temperature for Mars ($\approx$ 450 K), we might expect that the planet retained solar propor-

tions of U, Th, and K. This amounts to a bulk uranium content of 15 ppb, with K/U = 50 000 and Th/U = 4. We have assumed, however, a bulk radioactive abundance equivalent to MacDonald's Earth model; i.e., U = 31 ppb, and K/U = 10 000. It is important to note, however, that the total heat production of these abundances is the same as that obtained with solar proportions. The only difference in the thermal modeling arises in the percentage of potassium allowed to enter the sulphide phase of the core. For solar abundances, this necessarily requires less potassium than is assumed in this paper (to be discussed later), but since little is know quantitatively about the partitioning of potassium, and given uncertainties in solar abundances, we believe this to be a minor effect.

The thermal conductivity of the Martian mantle is assumed to be temperature-dependent and described by the empirical equation derived by Schatz and Simmons (ref. 64). The silicate melting curve is taken to be an extrapolated peridotite solidus (ref. 128). Melting, convection of molten material, and differentiation of the radioactive isotopes are modeled as before.

The formation of the Fe-FeS core begins when temperatures in some portion of Mars exceed the Fe-FeS eutectic of 990°C and is completed when the temperatures for the bulk of the planet are above the liquidus for an assumed composition of iron and sulfur. In the calculations, core formation is modeled as both a continuous and discrete event. When the temperatures exceed the eutectic at a grid point, a small amount of excess heat, equivalent to the mass fraction of core material, is diverted to the next lower grid point and converted to its temperature equivalent. Thus, the core material effectively melts its way into the interior. Also, a specified percentage of the available potassium is released from the silicates in one discrete step and allowed to enter the core. Internal heating is also slightly enhanced by the gravitational settling of the molten metal. The temperature field is reset to an adiabatic gradient when the internal temperature rises above the Fe-FeS liquidus where it is believed sufficient mass transfer has occurred to warrant this action. The gravitational separation of the core is irreversible, and, once formed, the core does not react with the mantle.

We have assumed that the Fe-FeS eutectic and liquidus are unaffected by high-pressure phase changes of FeS. While this is apparently not the case (ref. 129), we maintain that the thermal models and conclusions presented in this paper remain essentially unchanged.

Parameters used in the thermal calculations may be found in table 1.

Thermal Models

Figure 15, taken from Johnston et al. (ref. 32), shows the effect of varying uranium concentrations. In the figure, the present-day temperatures in a uniform, initially cold ($T = 0°C$ everywhere) Mars are shown as a function of the present-day concentration of uranium. The terrestrial value of K/U = 10 000 is assumed. Also shown are the Fe-FeS eutectic, the Fe-FeS liquidus for 85 wt%

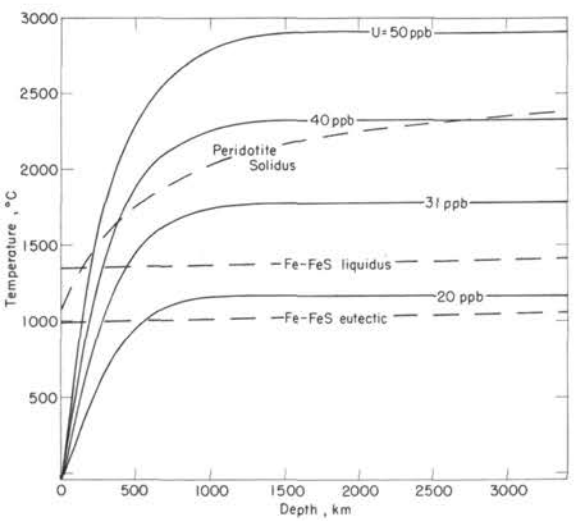


Figure 15.—*Present-day temperatures for an initially cold (0° C) Mars, as a function of uranium concentration. Also shown are the Fe-FeS eutectic and liquidus and the extrapolated peridotite solidus used in this paper (ref. 32).*

Fe, and the extrapolated peridotite solidus. No melting or differentiation is allowed. For $U \leq 37$ ppb, the temperatures are below the solidus. Clearly, these models do not satisfy the boundary condition that melting and differentiation of the silicates has occurred. For $U = 20$ ppb, the temperatures do not even exceed the Fe-FeS liquidus, prohibiting the completion of a core. To satisfy the boundary conditions, with the assumed radioactive heat production, higher initial temperatures must be used.

A thermal model that satisfies the major constraints on the evolution of Mars is shown in figure 16 (model "B" of ref. 32). The initial temperature is calculated from the accretion model, with an accretion time, τ, of 10^5 yr and a base temperature of 500°C. The core begins to form immediately and is completely formed by 1.0 b.y. Dry silicates begin to melt at 2 b.y. This zone of partial melt expands and works its way into the interior. The surface cools slowly by conduction, so that at the present time the dry solidus is reached at a depth of 1800 km. The calculated heat flow for this model is 43 erg/cm²-s, which is between the average measured heat flows for the Earth and Moon. The core is presently molten.

The evolution of Mars and the extent of melting is shown schematically for this model

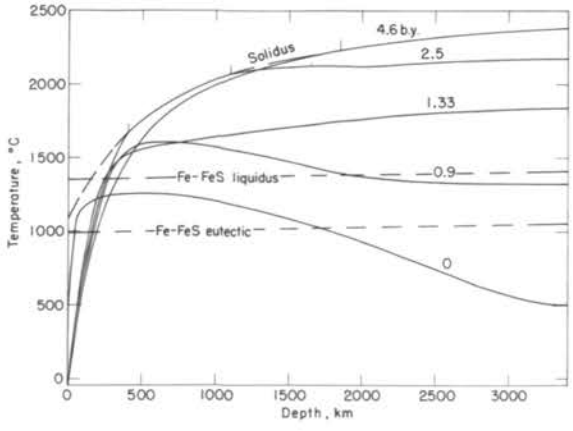


Figure 16.—*Thermal evolution of a Mars accreted in 10^5 yr, with T^b = 500°C. U = 31 ppb, with K/U = 10 000 (ref. 32).*

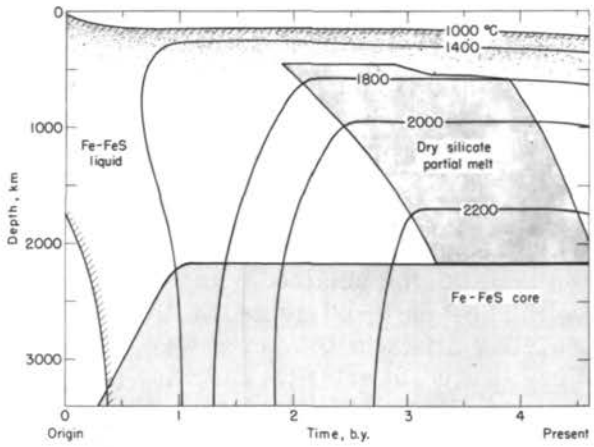


Figure 17.—*The evolution of the Martian interior as a function of time, based on the temperature calculations shown in figure 16. Isotherms are in ° C. The light shading above the dry silicate partial melt indicates the region where a small partial pressure of water would result in partial melt.*

in figure 17. Temperature and melting are plotted as functions of depth and time since origin. The light shading above the dry silicate melt shows regions where the introduction of a small partial pressure of water would result in a partial melt. Two episodes of Martian evolution are apparent from the figure. The first is the early differentiation of a crust due to partial melting in the near-surface regions and the formation of an Fe-FeS core. The formation of the crust is crucial in the understanding of the surface geology. Early volcanism, evident from Mariner photographs and the age of many regions inferred from crater densities, implies the formation and maintenance of a crust early in the Martian history. This is followed by upper mantle melting and differentiation probably resulting in extensive surface volcanism. The region of mantle partial melt progresses toward the interior as the surface slowly cools by conduction.

The presence of water and its relation to present-day tectonic activity is discussed in Johnston et al. (ref. 32). It was found that even for models such as the one discussed in this paper, where the anhydrous solidus is not reached until a depth of 1800 km, par-

tial melting can occur in the upper mantle. It is therefore concluded that one could expect moderate tectonic activity at the present time. A 200-km-thick lithosphere obtained for this model is consistent with the depth required by hydrostatics to elevate magma to the summit of volcanoes like Nix Olympica—about 23 km above the mean Martian sphere—and with the gravitational roughness of the planet.

Although the above temperature model is not a definitive statement about the present thermal state of Mars, it is adequate in the sense that all of the specified boundary conditions on thermal evolution are met. Hopefully, data from the future missions will provide additional constraints, and, thus, thermal models will be better specified.

VENUS

Venus is perhaps the most unconstrained planet as far as theoretically calculated thermal models are concerned. It can be supposed, however, that from size considerations alone, the evolution of Venus might be similar to the Earth's. There are, however, several important differences. Condensation models of the solar nebula imply that Venus retained little or no sulfur, thus eliminating the possibility of FeS or potassium in a core (ref. 58). Therefore, proceeding on the bias of early differentiation, we must require high initial temperatures in order to form a core within the first billion or so years. If one takes the moment of inertia factor for Venus to be equivalent to the Earth's (a rather strong assumption) it gives a core of radius about 2900 km for a composition of an Fe-Ni alloy. Lewis (ref. 58) also suggests that this core is surrounded by a massive mantle of Fe^{II}-free magnesium silicates. A crust, similar in composition to the Earth's, might also be expected.

Radar maps of the Venusian surface indicate relief of several kilometers (ref. 130). Considering the density and velocity of the atmosphere, we believe these features to be subject to extensive erosion and therefore young and probably of tectonic origin. Davidson and Anderson (ref. 131) have proposed that the rate of volcanism and tectonic activity is greater on Venus than on the Earth. Weertman (ref. 132), however, believes this not to be the case. Resolution of this conflict might be found from thermal models. Certainly, though, if the stresses associated with the nonhydrostatic state of Venus are not supported statically, we would have to expect convective motions in the upper mantle.

We now present a theoretical thermal model for Venus (fig. 18). The computational parameters for this model may be found in table 1. The initial temperature profile is calculated from equations (1) and (2), with an accretion time of 0.25×10^5 yr taken to ensure core differentiation within 1.0 b.y. The effect of adiabatic compression on the initial temperature is also included. The total heat production due to radioactive decay is essentially chondritic, having assumed uranium and potassium abundances equivalent to MacDonald's (ref. 7) Earth mantle values, i.e., U = 30 ppb, and K/U = 10 000 at the present day. This is consistent with theories on the condensation of the solar nebula (ref. 59). The bulk uranium concentration for

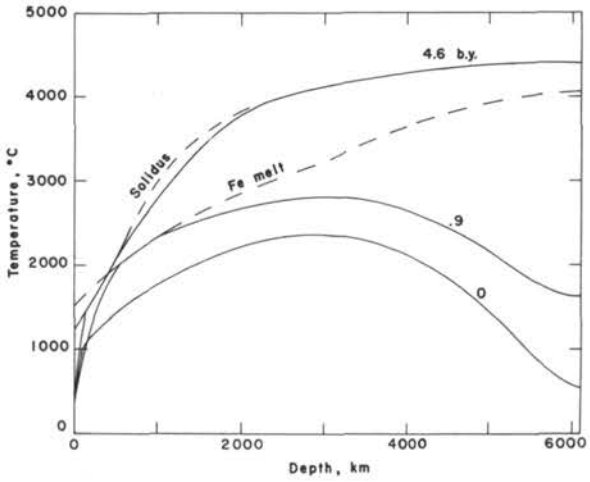


Figure 18.—*A model for the thermal evolution of Venus. The accretion time is 0.25 × 10⁵ yr, and the effect of compressional heating is included in the initial temperature. Input parameters for this model are described in the text.*

Venus might actually be slightly higher than the Earth's, due to the fact that it has not retained sulfur and, thus, has a lower mean atomic weight (ref. 58). The thermal conductivity of the undifferentiated planet and of the differentiated mantle is from the Schatz and Simmons (ref. 64) model.

Core formation is initiated when the temperatures within the interior exceed the Fe melting curve calculated for a homogeneous planet (ref. 133). At this point (about 1.0 b.y.), it is assumed that the rate of inflow of molten iron to the core is sufficient so that the gravitational energy due to core separation (refs. 134 and 135) allows for immediate core formation and temperatures in the interior are raised by the heat equivalent. We reset the temperature profile to an adiabatic gradient after core formation, due to the extensive mass transfer that has presumably taken place. Radioactive isotopes originally in the core region are displaced and distributed homogeneously throughout the mantle.

The temperature rise due to core infall is sufficient to initiate mantle melting immediately after core formation. The mantle melting curve is derived from Lindemann's equation which can be written in a form so that $T_m = \text{const}\ \phi$, where T_m is the melting temperature and ϕ is the seismic parameter (D. H. Chung, personal communication). Using measured values of ϕ for the Earth, this equation provides an adequate estimate for the mantle melting curve for Venus. Convection of molten material and differentiation of the radioactive isotopes are modeled as described previously.

Present-day temperatures are shown in the curve labeled 4.6 b.y. The iron melting curve shown in figure 18 is calculated for a differentiated planet. Notable features of this model are the thin (100-km) lithosphere, partially molten upper mantle, solid lower mantle, and molten core. Despite the molten core, the absence of a magnetic field for Venus can be explained by the lack of heat sources in the core and the slow rotation rate of the planet. Calculated heat flux is 98 ergs/cm^2-s.

Figure 19 shows schematically the evolution of Venus as a function of time. Isotherms are in degrees centigrade. As noted before, core formation takes place at 1.0 b.y., and present-day conditions indicate a region of high fractional partial melt (shaded area) in the upper mantle (higher than expected in the Earth), overlain by a lithosphere about 100 km thick. Although the degree of partial melt may be a function of the high surface temperature (presumably due to the atmosphere which may not have been in existence throughout the history of Venus), we have computed thermal models with the surface temperature arbitrarily set at 0°C. This results in a change of partial melt only in the upper few grid points. We therefore believe that any stresses associated with hydrostatic disequilibrium are supported within Venus by strong convective motions in the upper mantle. This points directly to the possibility of plate motion, similar to the Earth's and likely at a higher rate, and leads us to expect significant tectonic activity at the present time.

MERCURY

The knowledge of the planet Mercury has increased significantly since the Mariner 10 mission of April 1974. Preliminary results of television reconnaissance of the planet's

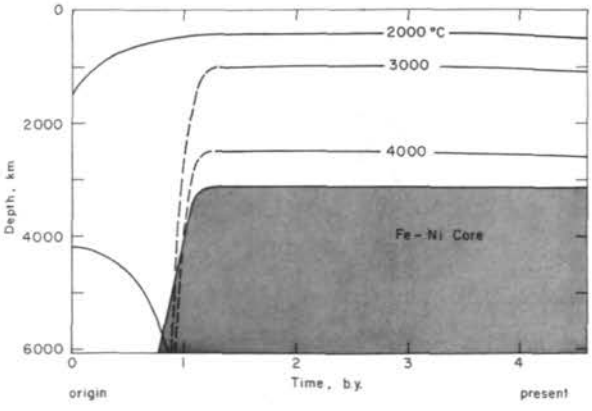


Figure 19.—*The evolution of Venus as a function of time, showing core formation and mantle melting (shaded region). Isotherms are in ° C.*

surface (ref. 136) show it to be remarkably similar to the lunar highlands. Regions resembling lunar mares have been observed, implying volcanic activity during Mercury's history. The presence of a magnetic field (ref. 137) could imply a molten iron core. We propose, then, that Mercury, as the other terrestrial planets, differentiated early, forming a crust similar to the Moon's and an iron core.

Siegfried and Solomon (ref. 33), using methods similar to those described earlier in this paper, have calculated several thermal and density models for Mercury. They point out, however, that Mercury is different from the other planets in the respect that condensation models of the solar nebula imply enrichment in refractory elements such as uranium and thorium and retention of little or no potassium and other volatiles. Furthermore, the thermal evolution is dominated by the high conductivity of iron, which makes up approximately 69 percent of the planet by weight.

Using appropriate initial temperatures, Siegfried and Solomon have shown that Mercury can indeed differentiate and form a core. Difficulties arise, however, if one assumes no heat source in the core and differentiation takes place earlier than about 3.0 b.y. These difficulties occur because the core is presently solid, with temperatures several hundred degrees lower than the iron melting curve calculated following Higgins and Kennedy (ref. 133). This is in apparent conflict with the presence of a magnetic field, if such a field is indeed due to an active core dynamo. Furthermore, differentiation at times earlier than 1.0 to 1.5 b.y. seems to be required from the nature of Mercury's surface.

We have therefore calculated a thermal model for Mercury (fig. 20), assuming the presence of some sort of heat source in the core. We have chosen this to be, as a matter of convenience, the decay of K^{40}. The initial temperature profile is calculated from the accretion model, with $\tau = 10^3$ yr, and $T_b = 1127°C$ (1400K), which provides initial iron melting to a depth of about 900 km. Thus, core formation and mantle melting are initiated immediately. Other model parameters such as uranium and thorium abundances are taken from Seigfried and Solomon (ref. 33) and may be found in table 1. Mantle conductivity is taken to be constant and equivalent to that used for the lunar thermal model presented in this paper ($K = 0.45 \times 10^6$ erg/cm-s °C).

As shown in figure 20, temperature profiles indicate a solid lithosphere 200 km thick at 2 b.y. and about 500 km thick at the present time. The core is presently partially molten and therefore might be able to sustain convective motions required to maintain a magnetic field. The lithosphere is probably thick enough to ensure a low level of tectonic activity. We would conclude from this model, however, that the regions on Mercury's surface that appear like the lunar mare may actually be younger, with tectonic activity having been prevalent on the planet for a longer period of time. We have also found that a K^{40} concentration of 0.156 ppm at the present time provides a minimum value required to maintain a partially molten core. The calculated heat flux is 60 ergs/cm²-s.

For comparison we show a thermal model of Mercury in figure 21 that contains no heat source in the core. Other model parameters are the same as those described above. In this case, although the mantle and core differentiate, the entire planet has temperatures

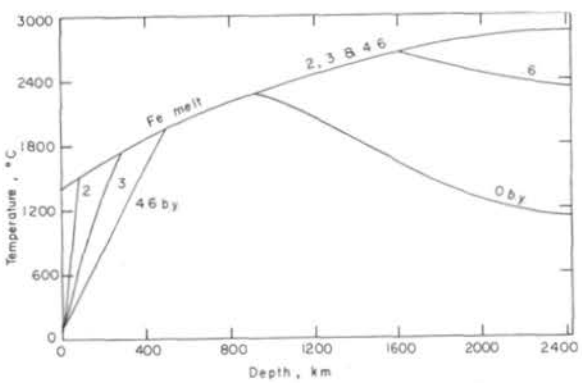


Figure 20.—*A thermal model of Mercury, with a heat source assumed in the core. Input parameters for this model are described in the text.*

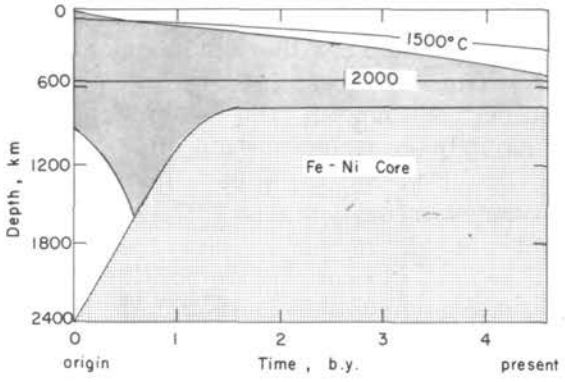


Figure 21.—*The thermal history of Mercury, with the same parameters as for the model in figure 20, except that the core is assumed to be free of heat sources.*

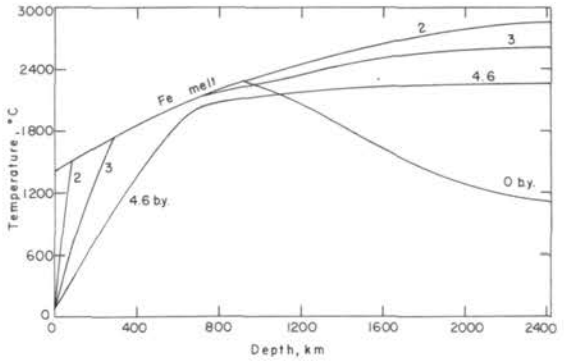


Figure 22.—*The evolution of Mercury as a function of time. Shading above the core region indicates mantle melting. Isotherms are in ° C.*

below the melting curve at the present time.

Figure 22 shows the evolution of Mercury as a function of time for the model in figure 20. Given the parameters used in this model, we conclude that Mercury could have a molten iron core if internal heat sources are assumed, and that present-day temperatures and the thickness of the lithosphere limit the tectonic activity to very low levels, if there is, in fact, any activitv.

Discussion and Conclusions

The thermal history models calculated for the Moon, Mars, Venus, and Mercury are representative of the whole spectrum of sizes and compositions of the terrestrial planets. The evolution histories are shown together in figure 23 for a comparative analysis. It is clear from this figure that although the initial temperatures are similar for these planets the evolution histories and present-day temperatures are quite different. The size (radius) of the planet more than any other factor seems to control its evolution and present-day thermal state. For the Moon and Mercury, the two smallest bodies, the evolution and differentiation took place relatively early in their histories. At present, both have thick lithospheres and are mostly solid. Venus, on the other hand, seems to be still at the peak of its evolution. Mars falls in between.

A good illustration of the comparison of evolutionary history of the planets can be obtained from the value of the total thermal energy of the planet as a function of time given by:

$$E(t) = (\int_v \rho C_p T(t)\,dV + Q(t))/M$$

where $E(t)$ is energy in ergs per gram, $T(t)$ the absolute temperature, and $Q(t)$ the heat that goes into fusion at time t. M is the mass, and V the volume of the planet. This is illustrated for the planets examined in this paper in figure 24.

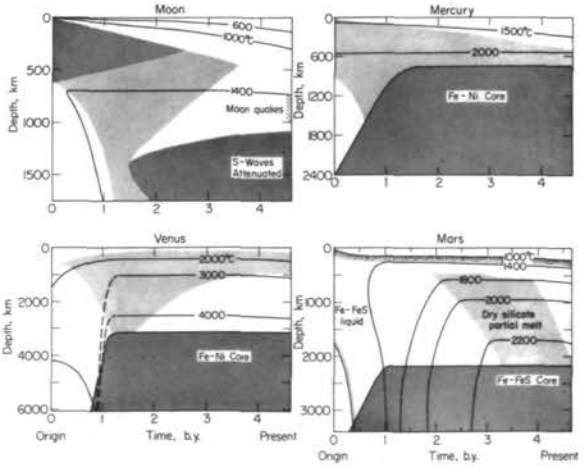


Figure 23.—*A comparison of the evolution of the planets.*

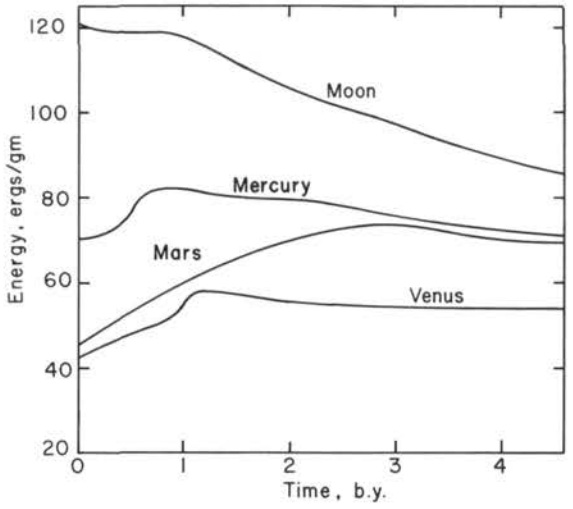


Figure 24.—*Total thermal energy as a function of time for the Moon, Mars, Mercury, and Venus.*

Several conclusions may be drawn from this figure. First, the maximum energy corresponds to the peak of the evolutionary process. Second, the rate of cooling is dependent primarily on the planet's size and somewhat on composition (that is, thermal conductivity).

For example, the Moon, which is the smallest planet, has a peak of thermal energy during the first billion years after formation. This corresponds roughly to the period of large-scale magmatic activity as evidenced by the mare basin filling. Afterwards, the energy level decreases rapidly as the Moon cools. At the present time we would expect the Moon to be relatively inactive tectonically. This is illustrated by a simple comparison with the Earth, which appears to be at the peak of its evolution at present. The terrestrial lithosphere is about 100 km thick, while that of the Moon is about 700 km. The Earth is tectonically active, with seismic energy release of about $E_s = 10^{25}$ ergs/yr, while the Moon is inactive with $E_s \simeq 10^{11}$ ergs/yr (ref. 90). While three-fourths of the Earth's surface is covered with rocks of 500 m.y. or younger, the youngest crystalline rock found on the Moon is 3.16 b.y.

Mercury, the next smallest planet, also reaches its peak of evolution early in its history. We would expect, upon examining figure 24 (with thermal energy calculated for the model shown in figure 20), that the bulk of the tectonic activity occurred before 2.0 b.y. The sharp increase in thermal energy is due to core formation. After 2.0 b.y. the energy decreases, showing that the planet is presently cooling and is probably dormant. If one does not include heat sources in the core, as in figure 21, the slope of $E(t)$ would be greater at the present time and the planet would obviously be cooler, heat transfer being dominated by the high conductivity of iron.

Mars, intermediate in size among the terrestrial planets, reached its peak of evolution around 3 b.y., maintained a relatively constant level of thermal energy for about a billion years, and is now beginning to cool. From this we can conclude that, while magmatic and tectonic activity have existed on Mars since early in its history, most of the volcanism and tectonics probably occurred in the last 2 b.y. We also expect a moderate level of tectonic activity at the present time.

Venus, in many respects similar to the Earth, differentiated a core early and has maintained a fairly constant level of thermal energy throughout its history. It can be considered to still be at its peak in evolution. Thus, we can expect tectonic processes in Venus similar to those observed on the Earth.

In interpreting the above results, one must be careful to note that the thermal energies calculated for each planet were taken from one nonunique thermal history model. These models, however, are reasonable in that they satisfy most of the constraints on the evolution of the planets known at the present time. Since they represent a bias toward early differentiation of all the terrestrial planets, the thermal energy turns out to be a useful tool to examine the effect of planetary size on the durations of high evolutionary and therefore tectonic activity.

In summary, we conclude the following:

1. The terrestrial planets were heated in some manner during or shortly after accretion.

2. This initial heating allowed for early core formation and/or differentiation. Early differentiation is evident from rock ages for the Earth and Moon and from photographic interpretation of Mars and Mercury surface features.
3. For planets with large cores such as the Earth, Venus, and Mercury, the energy released upon core separation is a large portion of the total heat budget of the planet.
4. The Moon is characterized as a differentiated body which evolved early in its history. The models that satisfy the constraints define a relatively narrow range for the temperatures in the outer several hundred kilometers, regardless of conduction and convective type calculations. Below 1000 km, the control on temperatures is not as great. Temperatures at the center of the Moon may be anywhere between 1000° and 1600°C. At these temperatures the Moon could have a partially molten (or, if Fe and FeS are differentiated, a totally molten) core.

   Acceptable evolution models require extensive differentiation and upward concentration of radioactive heat sources early in lunar history. This differentiation most likely is a product of extensive melting, although differentiation due to inhomogeneous accretion cannot be ruled out. A model of the Moon which is initially hot and extensively or totally molten can best satisfy the constraints.
5. Thermal models for Mars, assuming an Fe-FeS core composition, indicate formation of the core and the differentiation of an early crust within the first billion years after origin in order to satisfy the given constraints on the thermal evolution. These models involve large-scale differentiation of the mantle silicates in the past 2 b.y. This would be accompanied by volcanism and outgassing of volatiles at the surface. The inclusion of water in the upper mantle system leads to partial melting at a depth of about 22 km or greater at the present time.
6. Venus, while not as strongly constrained as the Moon or Mars, is characterized as a planet not unlike the Earth in many respects. Core formation is allowed to occur by 1.0 b.y., and present-day temperature profiles indicate a partially molten upper mantle overlain by a lithosphere approximately 100 km thick and a molten Fe-Ni core.
7. Mercury is taken to be similar to the Moon except for its large iron core. Thermal models with an assumed heat source in the core yield a planet that has a solid mantle to about 500 km depth, with a partially molten core. Those with no heat sources in the core have present-day temperatures well below the melting curve for iron, heat transfer being dominated by the high thermal conductivity of the iron.
8. The examination of total thermal energy as a function of time for each planet provides a method for determining the effect of planetary size on the durations of high tectonic activity. The Moon, smallest in size, is presently cool and tectonically inactive. Mercury is probably inactive at the present time, but its peak of activity lasted longer than the Moon's. Mars, intermediate in size, reached its peak in evolution in the past several billion years, but is probably moderately active at the present time. Venus, having been able to retain its thermal energy throughout its history, may today have tectonic processes similar to the Earth's.

Acknowledgment

The authors wish to thank Robert W. Siegfried and Dr. Sean C. Solomon for valuable discussions and the use of their computer program for Mercury and Eileen Schaffer for her contribution to the computations.

This research was supported by NASA grants NGL 22–009–187 and NSG–7081 (BASIC) and Contract No. 66437B under NASA Contract NAS1–9703.

References

1. UREY, H. C., The Origin and Development of the Earth and Other Terrestrial Planets. *Geochimica et Cosmochimica Acta*, Vol. 1, 1951, pp. 209–277.
2. UREY, H. C., *The Planets, Their Origin and Development*, Yale University Press, New Haven, Connecticut, 1952.
3. UREY, H. C., The Cosmic Abundances of Potassium, Uranium and Thorium and the Heat Balances of the Earth, Moon, and Mars. *Proc. Natl. Acad. Sci. U.S.*, Vol. 41, 1955, pp. 127–144.
4. UREY, H. C., Boundary Conditions for Theories of the Origin of the Solar System. *Physics and Chemistry of the Earth, 2*, L. H. Ahrens, F. Press, K. Rankama, and S. K. Runcorn, eds., Pergamon Press, New York, 1957, pp. 46–76.
5. UREY, H. C., Origin and History of the Moon. *Physics and Astronomy of the Moon, 1st Ed.*, Z. Kopal, ed., Academic Press, New York, 1962, p. 481.
6. LUBIMOVA, H., Thermal History of the Earth With Consideration of the Variable Thermal Conductivity of Its Mantle. *Geophys. J.*, Vol. 1, 1958, p. 115.
7. MACDONALD, G. J. F. Calculations on the Thermal History of the Earth. *J. Geophys. Res.*, Vol. 64, 1959, pp. 1967–2000.
8. MACDONALD, G. J. F., The Deep Structure of Continents. *Rev. Geophys.*, Vol. 1, 1963, p. 587.
9. LEVIN, B. J., Thermal History of the Moon. *The Moon*, Z. Kopal and Z. K. Mikhailov, eds., Academic Press, New York, 1962, p. 157.
10. ANDERSON, D. L., AND R. A. PHINNEY, Early Thermal History of the Terrestrial Planets. *Mantles of the Earth and Terrestrial Planets*, S. K. Runcorn, ed., Interscience, London, 1967, pp. 113–126.
11. FRICKER, P. E., R. T. REYNOLDS, AND A. L. SUMMERS, On the Thermal History of the Moon. *J. Geophys. Res.*, Vol. 72, 1967, p. 2649.
12. FRICKER, P. E., R. T. REYNOLDS, AND A. L. SUMMERS, On the Thermal Evolution of the Terrestrial Planets. *The Moon*, Vol. 9, 1974, pp. 211–218.
13. MCCONNELL, R. K., JR., L. A. MCCLAINE, D. W. LEE, J. R. ARONSON, AND R. V. ALLEN, A Model for Planetary Igneous Differentiation. *Rev. Geophys.*, Vol. 5, 1967, p. 121.
14. LEE, W. H. K., Effects of Selective Fusion on the Thermal History of the Moon, Mars, and Venus. *Earth Planet. Sci. Letters*, Vol. 4, 1968, p. 277.
15. HANKS, T. C., AND D. L. ANDERSON, The Early Thermal History of the Earth. *Phys. Earth Planet. Interiors*, Vol. 2, 1969, pp. 19–29.
16. MAJEVA, S. V., The Thermal History of the Terrestrial Planets. *Astrophys. Letters*, Vol. 4, 1969, p. 11.
17. UREY, H. C., AND G. J. F. MACDONALD, Origin and History of the Moon. *Physics and Astronomy of the Moon, 2nd Ed.*, Z. Kopal, ed., Academic Press, New York, 1971, pp. 213–289.
18. PAPANASTASSIOU, D. A., AND G. J. WASSERBURG, Lunar Chronology and Evolution From Rb-Sr Studies of Apollo 11 and 12 Samples. *Earth Planet. Sci. Letters*, Vol. 11, 1971, pp. 37–62.
19. HAYS, J. F., Radioactive Heat Sources in the Lunar Interior. *Phys. Earth Planet. Interiors*, Vol. 5, 1972, pp. 77–84.
20. WOOD, J. A., Thermal History and Early Magmatism in the Moon. *Icarus*, Vol. 16, 1972, pp. 229–240.
21. REYNOLDS, R. T., P. E. FRICKER, AND A. L. SUMMERS, Thermal History of the Moon. *Thermal Characteristics of the Moon*, J. W. Lucas, ed., MIT Press, Cambridge, 1972, pp. 303–337.
22. MCCONNELL, R. K., JR., AND P. W. GAST, Lunar Thermal History Revisited. *The Moon*, Vol. 5, 1972, pp. 41–51.
23. TOKSÖZ, M. N., S. C. SOLOMON, J. W. MINEAR, AND D. H. JOHNSTON, Thermal Evolution of the Moon. *The Moon*, Vol. 4, 1972, p. 190, and Vol. 5, 1972, p. 249.
24. TOZER, D. C., The Moon's Thermal State and an Interpretation of the Lunar Electrical Conductivity Distribution. *The Moon*, Vol. 5, 1972, pp. 90–105.
25. TOZER, D. C., The Present Thermal State of the Terrestrial Planets. *Phys. Earth Planet. Interiors*, Vol. 6, 1972, pp. 182–197.
26. TOZER, D. C., The Internal Evolution of Planetary Size Objects. *The Moon*, in press, 1973.
27. HANKS, T. C., AND D. L. ANDERSON, Origin, Evolution and Present Thermal State of the Moon. *Phys. Earth Planet. Interiors*, Vol. 5, 1972, pp. 409–425.
28. DUBA, A., AND A. E. RINGWOOD, Electrical Conductivity, Internal Temperatures and Thermal Evolution of the Moon. *The Moon*, Vol. 7, 1973, pp. 356–376.
29. CASSEN, P., AND R. T. REYNOLDS, The role of Convection in the Moon. *J. Geophys. Res.*, Vol. 78, 1973, pp. 3203–3215.
30. TOKSÖZ, M. N., AND S. C. SOLOMON, Thermal History and Evolution of the Moon. *The Moon*, Vol. 7, 1973, pp. 251–278.

31. TOKSÖZ, M. N., AND D. H. JOHNSTON, The Evolution of the Moon. *Icarus*, Vol. 21, in press, 1974.
32. JOHNSTON, D. H., T. R. MCGETCHIN, AND M. N. TOKSÖZ, The Thermal State and Internal Structure of Mars. *J. Geophys. Res.*, in press, 1974.
33. SIEGFRIED, R. W., AND S. C. SOLOMON, Mercury: Internal Structure and Thermal Evolution. *Icarus*, in press, 1974.
34. SCHUBERT, G., AND R. E. YOUNG, Internal Temperature of Mars. *EOS, Trans. Am. Geophys. Union*, Vol. 55, 1974, p. 343.
35. SCHRAMM, D. N., F. TERA, AND G. J. WASSERBURG, The Isotopic Abundance of Mg^{26} and Limits of Al^{26} in the Early Solar System. *Earth Planet. Sci. Letters*, Vol. 10, 1970, pp. 44–59.
36. FISH, R. A., G. G. GOLES, AND E. ANDERS, The Record of the Meteorites: III. On the Development of Meteorites in Asteroidal Bodies. *Astrophys. J.*, Vol. 132, 1960, pp. 143–256.
37. KAULA, W. M., Thermal Effects of Tidal Friction. *The Earth-Moon System*, B. G. Marsden and A. G. W. Cameron, eds., Plenum Press, New York, 1966, pp. 46–51.
38. SINGER, S. F., Origin of the Moon by Capture and Its Consequences. *EOS, Trans. Am. Geophys. Union*, Vol. 51, 1970, pp. 637–640.
39. HALLAM, M., Heat Sources for Early Differentiation of the Lunar Interior (abs.). *EOS, Trans. Am. Geophys. Union*, Vol. 54, 1973, p. 344.
40. SONETT, C. P., AND D. S. COLBURN, The Role of Accretionally and Electrically Inverted Thermal Profiles in Lunar Evolution. *The Moon*, Vol. 1, 1970, pp. 483–484.
41. MIZUTANI, H., T. MATSUI, AND H. TAKEUCHI, Accretion Process of the Moon. *The Moon*, Vol. 4, 1972, pp. 476–489.
42. LSPET (Lunar Sample Preliminary Examination Team), *Science*, Vol. 175, 1972, p. 363.
43. LSPET (Lunar Sample Preliminary Examination Team), *Science*, Vol. 179, 1973, p. 23.
44. O'KELLEY, G. D., J. S. ELDRIDGE, E. SCHONFELD, AND P. R. BELL, Primordial Radionuclide Abundances, Solar Proton and Cosmic-Ray Effects and Ages of Apollo 11 Lunar Samples by Non-Destructive Gamma Ray Spectrometry. *Proc. Apollo 11 Lunar Science Conference*, Vol. 2, A. A. Levinson, ed., 1970, pp. 1403–1423.
45. CLARK, R. S., AND J. E. KEITH, Determination of Natural and Cosmic Ray Induced Radionuclides in Apollo 16 Lunar Samples. *Proc. Fourth Lunar Science Conference (abs.)*, 1973, pp. 146–147.
46. SILVER, L. T., Uranium-Thorium-Lead Isotopic Characteristics. *Proc. Fourth Lunar Science Conference (abs.)*, 1973, pp. 673–674.
47. TATSUMOTO, M., P. D. NUMES, AND R. J. KNIGHT, U-Th-Pb Systematics of Some Apollo 16 Samples. *Proc. Fourth Lunar Science Conference (abs.)*, 1973, pp. 705–707.
48. PERKINS, R. W., L. A. RANCITELLI, J. A. COOPER, J. H. KAYE, AND N. A. WOGMAN, Cosmogenic and Primordial Radionuclide Measurements in Apollo 11 Lunar Samples by Nondestructive Analysis. *Proc. Apollo 11 Lunar Science Conference*, Vol. 2, A. A. Levinson, ed., 1970, pp. 1455–1469.
49. METZGER, A. E., J. I. TROMBKA, L. E. PETERSON, R. C. REEDY, AND J. R. ARNOLD, A First Look at the Lunar Orbital Gamma-Ray Data. *Proc. Third Lunar Science Conference*, Vol. 3, D. R. Criswell, ed., frontispiece, 1972.
50. PAPANASTASSIOU, D. A., AND G. J. WASSERBURG, Rb-Sr Ages of Igneous Rocks From the Apollo 14 Mission and the Age of the Fra Mauro Formation. *Earth Planet. Sci. Letters*, Vol. 12, 1971, pp. 36–48.
51. MASON, B., *Handbook of Elemental Abundances in Meteorites*, Gordon and Breach, New York, 1971.
52. LSPET (Lunar Sample Preliminary Examination Team), *Science*, Vol. 165, 1969, p. 1211.
53. DUKE, M. B., AND L. T. SILVER, Petrology of Eucrites, Howardites and Mesosiderites. *Geochimica et Cosmochimica Acta*, Vol. 31, 1967, pp. 1637–1665.
54. ANDERSON, D. L., The Composition and Origin of the Moon. *Earth Planet. Sci. Letters*, Vol. 18, 1973, pp. 301–316.
55. WÄNKE, H., H. BADDENHAUSEN, G. DREIBUS, M. QUIJANO-RICO, H. PALME, B. SPETTEL, AND F. TESCHKE, Multielement Analysis of Apollo 16 Samples and About the Composition of the Whole Moon. *Lunar Science*, Vol. IV, J. W. Chamberlain and C. Watkins, eds., Lunar Science Institute, Houston, 1973, pp. 761–763 and 767–769.
56. LANGSETH, M. G., JR., S. P. CLARK, JR., J. L. CHUTE, JR., S. J. KEIHM, AND A. E. WECHSLER, The Apollo 15 Lunar Heat-Flow Measurement. *The Moon*, Vol. 4, 1972, pp. 390–410.
57. LANGSETH, M. G., J. L. CHUTE, AND S. KEIHM, Direct Measurements of Heat Flow From the Moon. *Lunar Science*, Vol. IV, J. W. Chamberlain and C. Watkins, eds., Lunar Science Institute, Houston, 1973, pp. 455–456.
58. LEWIS, J. S., Metal/Silicate Fractionation in the Solar System. *Earth Planet. Sci. Letters*, Vol. 15, 1972, p. 286.
59. GROSSMAN, L., and J. W. LARIMER, Early Chemical History of the Solar System. *Rev. Geophys. and Space Phys.*, Vol. 12, 1974, p. 71.
60. CLARK, S. P., JR., Handbook of Physical Constants. *Geol. Soc. Am. Memoir 97*, 1966.
61. LACHENBRUCH, A. H., Preliminary Geothermal

Model of the Sierra Nevada. *J. Geophys. Res.*, Vol. 73, 1968, p. 6977.

62. CREMERS, C. J., Density, Pressure and Temperature Effects on Heat Transfer in Lunar Material. *AIAA J.*, Vol. 9, 1971, p. 2180.
63. HORAI, K., G. SIMMONS, H. KANAMORI, AND D. WONES, Thermal Diffusivity, Conductivity and Thermal Inertia of Apollo 11 Lunar Material. *Proc. Apollo 11 Lunar Science Conference*, Vol. 3, A. A. Levinson, ed., 1970, pp. 2243–2249.
64. SCHATZ, J. F., AND G. SIMMONS, Thermal Conductivity of Earth Materials at High Temperatures. *J. Geophys. Res.*, Vol. 77, 1972, pp. 6966–6983.
65. REYNOLDS, R. T., P. E. FRICKER, AND A. L. SUMMERS, Effects of Melting Upon Thermal Models of the Earth. *J. Geophys. Res.*, Vol. 71, 1966, pp. 573–582.
66. TURCOTTE, D. L., A. J. HSUI, K. E. TORRANCE, AND E. R. OXBURGH, Thermal Structure of the Moon. *J. Geophys. Res.*, Vol. 77, 1972, pp. 6931–6939.
67. CASSEN, P., AND R. T. REYNOLDS, *Convection in the Moon: Effect of Variable Viscosity.* In press, 1973.
68. SCHUBERT, G., D. L. TURCOTTE, AND E. R. OXBURGH, Stability of Planetary Interiors. *Geophys. J. R. Astr. Soc.*, Vol. 18, 1969, p. 441.
69. RUNCORN, S. K., Convection in the Moon. *Nature*, Vol. 195, 1962, pp. 1150–1151.
70. RUNCORN, S. K., Convection in the Moon and the Existence of a Lunar Core. *Proc. Roy. Soc. London, Ser. A*, Vol. 296, 1967, pp. 270–284.
71. DYAL, P., C. W. PARKIN, and P. CASSEN, Surface Magnetometer Experiments: Internal Lunar Properties and Lunar Field Interactions With the Solar Plasma. *Proc. Third Lunar Science Conference*, Vol. 3, D. R. Criswell, ed., 1972, pp. 2287–2307.
72. DYAL, P., C. W. PARKIN, AND W. D. DAILY, Surface Magnetometer Experiments: Internal Lunar Conductivity Profile and Steady Field Measurements. *Lunar Science*, Vol. IV, J. W. Chamberlain and C. Watkins, eds., Lunar Science Institute, Houston, 1973, p. 205.
73. SONETT, C. P., D. S. COLBURN, P. DYAL, C. W. PARKIN, B. F. SMITH, G. SCHUBERT, AND K. SCHWARTZ, Lunar Electrical Conductivity Profile. *Nature*, Vol. 230, 1971, pp. 359–362.
74. SONETT, C. P., B. F. SMITH, D. S. COLBURN, AND K. SCHWARTZ, The Induced Magnetic Field of the Moon: Conductivity Profiles and Inferred Temperature. *Proc. Third Lunar Science Conference*, Vol. 3, D. R. Criswell, ed., 1972, pp. 2309–2336.
75. HOUSLEY, R. M., AND F. J. MORIN, Electrical Conductivity of Olivine and the Lunar Temperature Profile. *The Moon*, Vol. 4, 1972, pp. 35–38.
76. OLHOEFT, G. R., A. L. FRISILLO, D. W. STRANGWAY, AND H. SHARPE, Electrical Properties of Lunar Solid Samples. *Lunar Science*, Vol. IV, J. W. Chamberlain and C. Watkins, eds., Lunar Science Institute, Houston, 1973, p. 575.
77. ANDERSON, D. L., AND T. C. HANKS, Is the Moon Hot or Cold? *Science*, Vol. 178, 1972, pp. 1245–1249.
78. TOKSÖZ, M. N., F. PRESS, K. ANDERSON, A. DAINTY, G. LATHAM, M. EWING, J. DORMAN, D. LAMMLEIN, G. SUTTON, F. DUENNEBIER, AND Y. NAKAMURA, Lunar Crust: Structure and Composition. *Science*, Vol. 176, 1972, pp. 1012–1016.
79. TOKSÖZ, M. N., F. PRESS, A. DAINTY, K. ANDERSON, G. LATHAM, M. EWING, J. DORMAN, D. LAMMLEIN, G. SUTTON, AND F. DUENNEBIER, Structure, Composition and Properties of Lunar Crust. *Proc. Third Lunar Science Conference*, Vol. 3, D. R. Criswell, ed., 1972, pp. 2527–2544.
80. TOKSÖZ, M. N., A. M. DAINTY, S. C. SOLOMON, AND K. R. ANDERSON, Velocity Structure and Evolution of the Moon. *Lunar Science*, Vol. IV, J. W. Chamberlain and C. Watkins, eds., Lunar Science Institute, Houston, 1973, pp. 734–736.
81. NAKAMURA, Y., G. LATHAM, D. LAMMLEIN, M. EWING, F. DUENNEBIER, AND J. DORMAN, Deep Lunar Interior Inferred From Recent Seismic Data. *Geophys.*, 1974.
82. TOKSÖZ, M. N., A. M. DAINTY, S. C. SOLOMON, AND K. R. ANDERSON, Structure of the Moon. *Rev. Geophys. and Space Phys.*, in press, 1974.
83. LATHAM, G., J. DORMAN, F. DUENNEBIER, M. EWING, D. LAMMLEIN, AND Y. NAKAMURA, Moonquakes, Meteoroids and the State of the Lunar Interior. *Lunar Science*, Vol. IV, J. W. Chamberlain and C. Watkins, eds., Lunar Science Institute, Houston, 1973, pp. 457–459.
84. NAKAMURA, Y., D. LAMMLEIN, G. LATHAM, M. EWING, J. DORMAN, F. PRESS, AND M. N. TOKSÖZ, New Seismic Data on the State of the Deep Lunar Interior. *Science*, Vol. 181, 1973, p. 49.
85. SOLOMON, S. C., Density Within the Moon and Implications for Lunar Composition. *The Moon*, in press, 1973.
86. SOLOMON, S. C., AND M. N. TOKSÖZ, Internal Constitution and Evolution of the Moon. *Phys. Earth Planet. Interiors*, Vol. 7, 1973, pp. 15–38.
87. BALDWIN, R. B., Absolute Ages of the Lunar Maria and Large Craters: II. The Viscosity of the Moon's Outer Layers. *Icarus*, Vol. 13, 1970, pp. 215–225.
88. ARKANI-HAMED, J., Viscosity of the Moon: I.

After Mare Formation. *The Moon*, Vol. 6, 1973, pp. 100–111.

89. LATHAM, G., M. EWING, J. DORMAN, D. LAMMLEIN, F. PRESS, M. N. TOKSÖZ, G. SUTTON, F. DUENNEBIER, AND Y. NAKAMURA, Moonquakes and Lunar Tectonism. *The Moon*, Vol. 4, 1972, pp. 373–382.
90. LAMMLEIN, D., G. LATHAM, J. DORMAN, Y. NAKAMURA, AND M. EWING, Lunar Seismicity, Structure and Tectonics. *Rev. Geophys. and Space Phys.*, in press, 1973.
91. SILVER, L. T., Uranium-Thorium-Lead Isotopes in Some Tranquillity Base Samples and Their Implications for Lunar History. *Proc. Apollo 11 Lunar Science Conference*, Vol. 2, A. A. Levinson, ed., 1970, pp. 1533–1574.
92. WASSERBURG, G. J., AND D. A. PAPANASTASSIOU, Age of an Apollo 15 Mare Basalt; Lunar Crust and Mantle Evolution. *Earth Planet. Sci. Letters*, Vol. 13, 1971, pp. 97–104.
93. TATSUMOTO, M., C. E. HEDGE, B. R. DOE, AND D. M. UNRUH, U-Th-Pb and Rb-Sr Measurements on Some Apollo 14 Lunar Samples. *Proc. Third Lunar Science Conference*, Vol. 2, D. Heymann, ed., 1972, pp. 1531–1555.
94. TERA, F., D. A. PAPANASTASSIOU, AND G. J. WASSERBURG, A Lunar Cataclysm at ~3.95 ae and the Structure of the Lunar Crust. *Lunar Science*, Vol. IV, J. W. Chamberlain and C. Watkins, eds., Lunar Science Institute, Houston, 1973, pp. 723–725.
95. ALBEE, A. L., A. A. CHODOS, R. F. DYMEK, A. J. GANCARZ, D. S. GOLDMAN, D. A. PAPANASTASSIOU, AND G. J. WASSERBURG, Dunite From the Lunar Highlands: Petrography, Deformational History, Rb-Sr Age. *Lunar Science*, Vol. V, Lunar Science Institute, Houston, 1974, p. 3.
96. WOOD, J. A., J. S. DICKEY, JR., U. B. MARVIN, AND B. N. POWELL, Lunar Anorthosites. *Science*, Vol. 167, 1970, p. 602.
97. DOE, B., Lunar Chronology. Written Communication, 1973.
98. HUSAIN, L., O. A. SCHAEFFER, AND J. F. SUTTER, Age of a Lunar Anorthosite. *Science*, Vol. 175, 1972, pp. 428–430.
99. SCHONFELD, E., AND C. MEYER, JR., The Abundances of Components of the Lunar Soils by a Least Squares Mixing Model and the Formation Age of KREEP. *Proc. Third Lunar Science Conference*, Vol. 2, D. Heymann, ed., 1972, pp. 1397–1420.
100. TERA, F., AND G. J. WASSERBURG, Lead Isotopic Evidence on Lunar Evolution. *EOS, Trans. Am. Geophys. Union*, Vol. 54, 1973, p. 355.
101. PAPANASTASSIOU, D. A., AND G. J. WASSERBURG, The Rb-Sr Age of a Crystalline Rock From Apollo 16. *Earth Planet. Sci. Letters*, Vol. 16, 1972, pp. 289–298.
102. MURTHY, V. R., M. M. EVENSEN, B. JAHN, AND M. R. COSCIO, JR., Apollo 14 and 15 Samples: Rb-Sr Ages, Trace Elements and Lunar Evolution. *Proc. Third Lunar Science Conference*, Vol. 2, D. Heymann, ed., 1972, pp. 1503–1514.
103. TURNER, G., J. G. HUNEKE, F. A. PODOSEK, AND G. J. WASSERBURG, Ar^{40}-Ar^{39} Systematics in Rocks and Separated Minerals from Apollo 14. *Proc. Third Lunar Science Conference*, Vol. 2, D. Heymann, ed., 1972, pp. 1589–1612.
104. HUSAIN, L., O. A. SCHAEFFER, J. FUNKHOUSER, AND J. SUTTER, The Ages of Lunar Material From Fra Mauro, Hadley Rille, and Spur Crater. *Proc. Third Lunar Science Conference*, Vol. 2, D. Heymann, ed., 1972, pp. 1557–1567.
105. COLEMAN, P. J., JR., B. R. LICHTENSTEIN, C. T. RUSSELL, L. R. SHARP, AND G. SCHUBERT, Magnetic Fields Near the Moon. *Proc. Third Lunar Science Conference*, Vol. 3, D. R. Criswell, ed., 1972, pp. 2271–2286.
106. FULLER, M., Lunar Magnetism. *Rev. Geophys. and Space Phys.*, Vol. 21, 1974, p. 23.
107. NAGATA, T., R. M. FISHER, F. C. SCHWERER, M. D. FULLER, AND J. R. DUNN, Rock Magnetism of Apollo 14 and 15 Materials. *Proc. Third Lunar Science Conference*, Vol. 3, D. R. Criswell, ed., 1972, pp. 2423–2447.
108. PEARCE, G. W., D. W. STRANGWAY, AND W. A. GOSE, Remanent Magnetization of the Lunar Surface. *Proc. Third Lunar Science Conference*, Vol. 3, D. R. Criswell, ed., 1972, pp. 2449–2464.
109. COLLINSON, D. W., S. K. RUNCORN, A. STEPHENSON, AND A. J. MANSON, Magnetic Properties of Apollo 14 Rocks and Fines. *Proc. Third Lunar Science Conference*, Vol. 3, D. R. Criswell, ed., 1972, pp. 2343–2361.
110. GOSE, W. A., A Determination of the Intensity of the Ancient Lunar Magnetic Field. *The Moon*, Vol. 7, 1973, pp. 196–201.
111. RUNCORN, S. K., AND H. C. UREY, A New Theory of Lunar Magnetism. *Science*, Vol. 180, 1973, pp. 636–638.
112. RUNCORN, S. K., D. W. COLLINSON, W. O'REILLY, A. STEPHENSON, M. H. BATTEY, A. J. MANSON, AND P. W. READMAN, Magnetic Properties of Apollo 12 Lunar Samples. *Proc. Roy. Soc. London*, Ser. A., Vol. 325, 1971, pp. 157–174.
113. STRANGWAY, D. W., H. N. SHARPE, W. A. GOSE, AND G. W. PEARCE, Magnetism and the Early History of the Moon. *Lunar Science*, Vol. IV, J. W. Chamberlain and C. Watkins, eds., Lunar Science Institute, Houston, 1973, pp. 697–699.
114. RINGWOOD, A. E., AND E. ESSENE, Petrogenesis of Lunar Basalts and the Internal Constitution of the Moon. *Science*, Vol. 167, 1970, pp. 607–610.

115. GAST, P. W., The Chemical Composition and Structure of the Moon. *The Moon*, Vol. 5, 1972, pp. 121–148.
116. GREEN, D. H., A. E. RINGWOOD, N. G. WARE, AND W. O. HIBBERSON, Experimental Petrology and Petrogenesis of Apollo 14 Basalts. *Proc. Third Lunar Science Conference*, Vol. 1, E. A. King, ed., 1972, pp. 197–206.
117. LORELL, J., G. H. BORN, E. J. CHRISTENSEN, J. F. JORDAN, P. A. LAING, W. L. MARTIN, W. L. SJOGREN, I. I. SHARPIO, R. D. REASONBERG, AND G. L. SCLATER, Mariner 9 Celestial Mechanics Experiment: Gravity Field and Pole Direction of Mars. *Science*, Vol. 175, 1972, p. 317.
118. DOLGINOV, S. S., Y. G. YEROSHENKO, AND L. N. ZHUZGOV, *The Magnetic Field in the Very Close Neighborhood of Mars According to Data From the Mars 2 and Mars 3 Spacecraft*. Goddard Space Flight Center, Report X–690–72–434, 1972.
119. CARR, M. H., Volcanism on Mars. *J. Geophys. Res.*, Vol. 78, 1973, p. 4049.
120. ANDERSON, D. L., Internal Constitution of Mars. *J. Geophys. Res.*, Vol. 77, 1972, p. 789.
121. LEWIS, J. S., Consequences of the Presence of Sulfur in the Core of the Earth. *Earth Planet. Sci. Letters*, Vol. 11, 1971, p. 130.
122. GOETTEL, K. A., Partitioning of Potassium Between Silicates and Sulphide Melts: Experiments Relevant to the Earth's Core. *Phys. Earth Planet. Interiors*, Vol. 6, 1972, p. 161.
123. BRETT, R., and P. M. BELL, Melting Relations in the Fe-Rich Portion of the System Fe-FeS at 30 kb Pressure. *Earth Planet. Sci. Letters*, Vol. 6, 1969, pp. 479–482.
124. MCCAULEY, J. F., M. H. CARR, J. A. CUTTS, W. K. HARTMANN, H. MASURSKY, D. J. MILTON, R. P. SHARP, AND D. E. WILHELMS, Preliminary Mariner 9 Report on the Geology of Mars. *Icarus*, Vol. 17, 1972, pp. 289–327.
125. CARR, M. H., H. MASURSKEY, AND R. S. SAUNDERS, A Generalized Geologic Map of Mars. *J. Geophys. Res.*, Vol. 78, 1973, p. 4031.
126. MASURSKEY, H., An Overview of Geological Results From Mariner 9. *J. Geophys. Res.*, Vol. 78, 1973, pp. 4009–4030.
127. GROSSMAN, L., Fractionation of Refractory Elements in the Solar Nebula (abs.). *Meteoritics*, Vol. 8, 1973, p. 41.
128. GREEN, D. H., and A. E. RINGWOOD, Mineralogy of Peridotitic Compositions Under Mantle Conditions. *Phys. Earth Planet. Interiors*, Vol. 3, 1969, p. 359.
129. USSELMAN, T. M., Composition and Temperature of an Fe-Ni-S Core of the Earth (abs.). *EOS, Trans. Am. Geophys. Union*, Vol. 55, 1974, p. 337.
130. CAMPBELL, D. B., R. B. DYCE, R. P. INGALLS, G. H. PETTENGILL, AND I. I. SHAPIRO, Venus: Topography Revealed by Radar Data. *Science*, Vol. 175, 1972, p. 514.
131. DAVIDSON, G. T., AND A. D. ANDERSON, Venus: Volcanic Eruptions May Cause Atmospheric Obscuration. *Science*, Vol. 156, 1967, p. 1729.
132. WEERTMAN, J., Venus: Tectonic Activity. *Science*, Vol. 156, 1967, p. 395.
133. HIGGINS, G., AND G. C. KENNEDY, The Adiabatic Gradient and the Melting Point Gradient in the Core of the Earth. *J. Geophys. Res.*, Vol. 76, 1971, p. 1870.
134. BIRCH, F., Energetics of Core Formation. *J. Geophys. Res.*, Vol. 70, 1965, p. 6217.
135. FLASAR, F. M., AND F. BIRCH, Energetics of Core Formation: A Correction. *J. Geophys. Res.*, Vol. 78, 1973, p. 6101.
136. TRASK, N. J., Preliminary Results of Television Reconnaissance of Mercury (abs.). *EOS, Trans. Am. Geophys. Union*, Vol. 55, 1974, p. 340.
137. BEHANNON, K. W., R. P. LEPPING, N. F. NESS, K. H. SCHATTEN, AND Y. C. WHANG, Magnetic Field Observations With Mariner 10 (abs.). *EOS, Trans. Am. Geophys. Union*, Vol. 55, 1974, p. 340.

Page intentionally left blank

Page intentionally left blank

Heat Flow and Thermal History of the Moon

Ye. A. Lyubimova
O. Yu. Schmidt Institute of Earth Physics
Academy of Sciences,
Moscow, U.S.S.R.

An analysis is made of current heat flow data and thermal models of lunar evolution which satisfy the diverse information that has accumulated on internal processes.

Direct measurements of the heat flux were made in drill holes at the Hadley Rille (Apollo 15) and Taurus-Littrow (Apollo 17) regions located on the margins of Mare Serenitatis and Mare Imbrium, which apparently have mascons. These measurements resulted in comparatively high values of the heat flux,

3.1×10^{-6} W/cm^2 $\left(0.74 \times 10^{-6} \frac{\text{cal}}{\text{cm}^2\text{sec}}\right)$

(Apollo 15) and

2.8×10^{-6} W/cm^2 $\left(0.67 \times 10^{-6} \frac{\text{cal}}{\text{cm}^2\text{sec}}\right)$

(Apollo 17), which differ from the wide spread earlier concept of a much lower heat flow from a Moon of chondrite composition. Only a small number of earlier works predicted a high heat flow. Those were the data on the thermal emission of the Moon in the microwave region (ref. 1) and the results of certain calculations of the thermal history of the Moon (ref. 2). Current interpretation of the high heat flow requires a high average concentration of uranium for the Moon—60 ppb—as well as an initial surface temperature sufficient to melt the upper several hundred kilometers, including the lunar crust and lithosphere.

The crust of the Moon is a discrete layer several-dozen-kilometers thick, bears traces of magmatic fractionation that occurred during the period of intensive melting of the uppermost layers of the Moon (hundreds of kilometers deep), and has been reworked by the impacts of meteorites.

Among the sources of initial melting are the following: accretional heating during accumulation of the Moon, possible electrical heating by an early strong solar wind, tidal friction when the Moon was close to the Earth, and the effect of short-lived isotopes. All the sources are problematical. The thermal effect due to collisions of protomoons during accretion appears to be adequate to melt the rocks in the area of impact, but not at great depth (refs. 3 and 4).

At this stage of investigation of the thermal state of the Moon, the following problems are the most significant.

What was the cause of the rapid early melting and differentiation?

To what extent can heat fluxes obtained close to the margin of a mascon be represented as global values? To what extent can an average, presently uniform concentration of uranium be responsible for the surface heat flux that undoubtedly results from irregular distributions of uranium and thorium with depth, due to the rapid fractionation during the accretionary stage? To what extent can coarse numerical modeling of the thermal history of the Moon, where the first step in the calculation grid is 20 km in size (refs. 5 and 6) or where even the smallest is 5 km (ref. 7), reflect the fine structure of the uniquely low thermal conductivity of the upper few meters?

Before the Luna and Apollo flights to the Moon, a lunar model of chondrite composition

was widely used (refs. 2 and 8 through 13). A drastic reexamination of these models was required after study of the chronology of the lunar samples and determination that the lunar K/U ratio was 2000 instead of 80 000 as for chondrites and 10 000 as for the Earth. The low lunar K/U ratios are in agreement with the overall depletion of the Moon in volatile elements.

A comparative study of the energy balance of the Earth and the Moon by Lyubimova (ref. 2) showed that the integral heat loss $Q_{\mathbb{C}}$ for the lifetime of the Moon, the integral heat generation $H_{\mathbb{C}}$, and the total heat content at the melting point of the planet $\Lambda_{\mathbb{C}}$ are in the relationship $\Lambda_{\mathbb{C}} < H_{\mathbb{C}} \approx Q_{\mathbb{C}}$ for the Moon. This means that the energy losses from the surface of the Moon predominate (in distinction from the Earth) over internal heat generation and heat content for the state of complete melting, i.e., the Moon is cooling down. The heat flux at the surface is assumed to be close to the upper limit established by lunar surface radio emission methods (refs. 14 and 15). According to thermal history calculations, the integral heat flux of the Moon should amount to $Q = 1.9 \times 10^{36}$ ergs, while the heat content of a completely molten Moon is $\Lambda_{\mathbb{C}} = 1.6 \times 10^{36}$ ergs (ref. 2). It was concluded that even in the case of a quite low concentration of radioactive elements, in agreement with the chondritic model, the energy is completely sufficient to convert the lunar interior to the molten state.

Direct measurements of the heat flux during Apollo 15 and Apollo 17 permit one to return to discussion of the energetic state of the Moon. They also make it possible, together with radioastronomers, to refine models of the structure of the uppermost layers of the Moon (refs. 16 and 17). Serious limitations on the thermal history of the Moon were introduced as a result of a seismic experiment on the Moon (ref. 18). They indicate the necessity for a high temperature of the lunar interior and the existence of an asthenosphere below 1000 km. On the other hand, the internal temperature derived from the electrical conductivity profile indicates that the temperature of the lunar interior should be less than the solidus temperature (ref. 19). The existence of mascons also requires this because the thickness of the lithosphere must be sufficient to sustain a load corresponding to the mascons. Correspondingly, the viscosity of the lunar interior is assumed to be very high, up to 10^{26} poise (ref. 20). The chronology of lunar volcanic activity shows that all episodes of volcanic activity and excavation of the mare must have ended 3 b.y. ago (refs. 21 and 22). The magnetic history of the Moon indicates that there was an old magnetic field which is responsible for the remanent magnetism of the Moon (ref. 23). This again entails the conclusion that there was intense melting in the initial stages of evolution of the Moon. In this manner, the factual materials returned by the Luna and Apollo missions indicate that the Moon evolved quickly.

In this article, we examine the parameters of lunar thermal models, calculation techniques that consider melting and effective convection, and the expected regional corrections to the heat flux.

Evolution of a Homogeneous Moon

In a number of the most recent works, the heat flux from the lunar interior is compared with an average uniform concentration of uranium (refs. 5, 6, and 23) in a homogeneous Moon.

A strict analytical solution for a body of spherical shape (the Moon in particular) with uniform distribution of heat sources, thermal diffusivity k, density ρ, and heat capacity C, was given by Lyubimova (refs. 2, 24, and 25), in the form:

$$T_{\mathbb{C}}(r,t) = \frac{1}{C\rho}\int_0^t H(\tau)\, d\tau - \frac{RC}{C\rho r}\int_0^t H(t) \times \left[erfc\left(\frac{R-r}{\sqrt{4k(t-\tau)}}\right) - erfc\left(\frac{R+r}{\sqrt{4k(t-\tau)}}\right)\right] d\tau \qquad (1)$$

where $R_\mathbb{C}$ is the radius of the Moon and r is the variable radius

$$erfc\ x = 1 - erfx;\ erfx = \frac{1}{\sqrt{\pi}} \int_0^x e^{-\alpha^2} d\alpha$$

The bracket in (1) is the first term of the series of the determinate Green's function (1.6) (see Appendix I):

$$G\ (t,r,t',r') = \sum_{n=0}^{\infty} \left\{ erfc \left[\frac{(2n+1)\ R - r}{\sqrt{4k\ (t-\tau)}} \right] - erfc \left[\frac{(2n+1)\ R + r)}{\sqrt{4k\ (t-\tau)}} \right] \right\}$$

The first term in the expression for temperature gives the temperature of the central region and the second gives the region of heat outflow to the surface. The region of outflow begins at depth:

$$D = R - r \leq 3 \cdot \sqrt{4kt} \qquad (2)$$

If there is no convection, the region of outflow, D, for Earth, Mars, and Venus does not reach the center, while D for the Moon reaches the center.

Analysis of uniform source models of the Moon, with a variable initial temperature $T_0\ (r)$, is useful in searching for the required models of lunar accretion that would provide a high early temperature of the upper layers of the Moon. This analysis should give the required age of the mare basalts and should provide rapid melting and rapid differentiation of the upper few hundred kilometers and a relatively cold lithosphere at the present time. The mineralogy of the lunar rocks indicates a phase of high temperature and low pressure as suggested by Ringwood (ref. 26) in a semiqualitative conclusion (even before the Apollo missions) that the initial temperature curve had maximum values in the upper 200 to 300 km and a gradual drop toward the center (figs. 1, 2). This curve was used in the calculation of Kaula (ref. 29) during interpretation of the lunar gravitational field. Ringwood (ref. 30) intuitively predicted a curve that is close to the curve for $T_0(r)$ given by Hanks and Anderson (ref. 31).

Homogeneous models of the Moon, with such nonuniform initial curves with maxima,

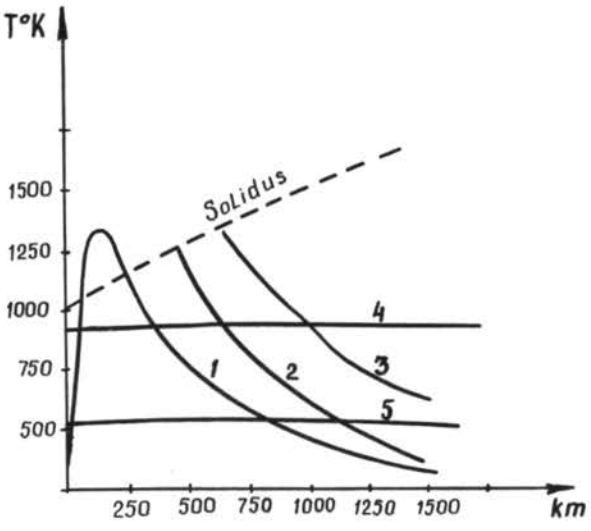


Figure 1.—*Variants of initial temperature distributions in the primitive moon: 1—from Ringwood (ref. 30), 2—from Mizutani (ref. 27), 3—from Hanks and Anderson (ref. 31), 4—MacDonald (ref. 9), Ruskol (ref. 3) (estimated as the result of collision of protomoons), 5—Urey and MacDonald (ref. 28).*

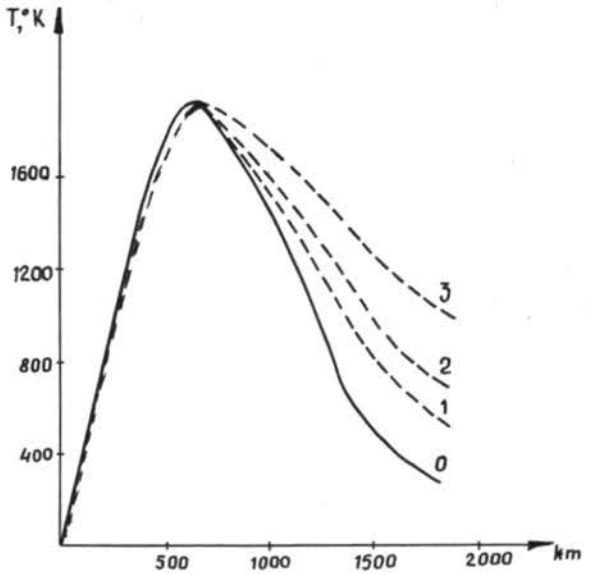


Figure 2.—*Effect of Resorption of Initial Heat with Passage of Time in the Lunar Interior in Absence of Convection (curve 1, fig. 1 is taken as T_0).*

indicate a possible thermal evolution that is dependent on the influence of initial processes. In particular, they permit understanding of the slowness of the disappearance of the maximum $T_0(r)$ and the slowness of propagation of the initial heat inward to the planet. The latter conclusion follows from examination of equation (2), which gives the rate of penetration of temperature by means of heat conductivity in the absence of convection. Initially, the interior of the Moon apparently was cold. The task consists of ascertaining the manner in which the temperature of the central regions of the Moon below 1000 km could reach at the present moment high values sufficient for formation of the aseismic "asthenosphere," the level at which deep moonquakes stop, according to data from low-frequency seismometers (ref. 18).

Evolution of A Heterogeneous Moon

Having selected a uranium content corresponding to the observed heat flux, U = 0.05 ppm in the lithosphere and 0.5 ppm in the crust, we obtain the following models of the lunar thermal history (fig. 3). The temperature curves are compared with the solidus curve of mare basalts, as determined by Ringwood and Essene (ref. 26), in the zone from 100 to 700 km, assuming no convection. The lithosphere thickens for 1.2 b.y. at a rate of 160 km/b.y. Melting proceeds from shallow depths to great depths during the filling of the mare (3.4–3.1)–(3.8–3.6 AE), in agreement with the depth of origin for mare basalts, according to petrogenetical theory (ref. 32). Moreover, a sufficiently thick lithosphere is provided as required to support the stresses connected with the mascon gravitational anomalies. Between 1 and 2 AE there occurred conditions for the existance of a convecting core of undifferentiated lunar material which contained approximately the original concentrations of radioactive elements. The core grew to a radius of 1200 km at 3 AE, then slowly decreased because the concentration of heat sources decreased with time. The chronology, mineralogy, and petrography of the lunar mare basalts indicate a definite sequence of events in differentiation and fractionation of the material. For example, the mare basalts evidently had to be formed during the second thermal cycle, if there was one, i.e., 3.4 to 3.7 b.y. ago, at depths on the order of 200 to 300 km as a result only of endogenous factors. Crater formation apparently mainly ended during the first, most intensive, phase of differentiation and fractional crystallization.

The heterogeneity of the internal structure of the current Moon is demonstrated by the low-frequency seismic experiment, data on the electrical conductivity distribution in the Moon, the existence of an ancient magnetic field, and gravitational data. A schematic section of the heterogeneous Moon was given by Anderson (ref. 33). The Moon consists of a crust, lithosphere, asthenosphere, and, possibly, a core. The upper layer of the crust is composed of mare basalts. The lower layer of the crust is composed of gabbroic anorthosites; under them is a layer of refractory crystals, and even plagioclase or pyroxenes, at depths of 60 to 80 km (ref. 34). The requirement for the absence of large-scale melting in the upper 1000 km imposes significant limitations on the thermal evolution of the Moon (ref. 6).

The chronology of volcanic activity and the concentration of radioactive elements toward the surface are evidence of intensive differentiation at an early stage of lunar development (ref. 35). There are two points of view on the differentiation process. Differentiation may be the result of a relatively rapid accretion and subsequent general melting or of initial chemical stratification during the accretion process.

If the measured values of the heat flux 0.74–0.67 $\times$ 10^{-6} cal/cm^{2}sec (ref. 36) represent the average heat loss characteristic of the entire Moon, the average uranium concentration in the lunar lithosphere must be in the 50- to 80-ppb range.

Attenuation of seismic waves depends strongly on temperature, showing a rapid

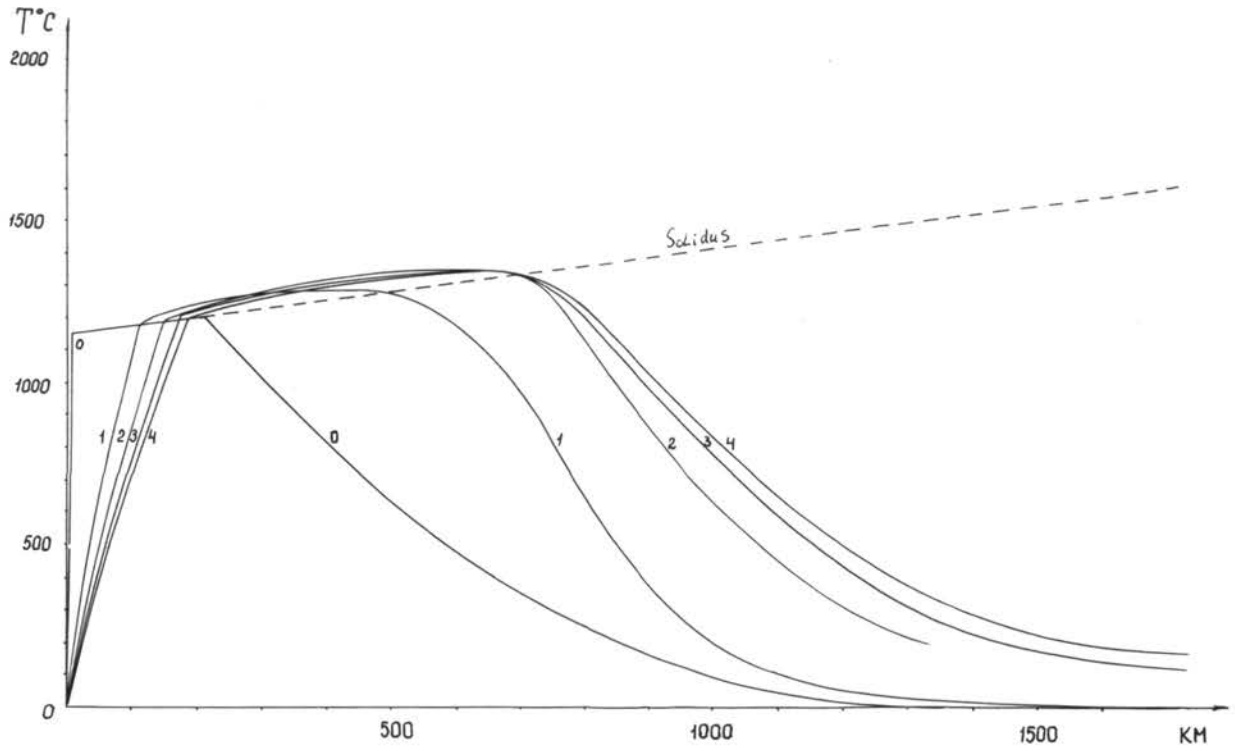


Figure 3.—*Thermal evolution model for a heterogeneous Moon (this work) K/U-2000, Th/U = 4, U = 0.5 ppm in crust and U = 0.05 ppm in lithosphere. Initial temperature taken from Ringwood (ref. 30).*

increase with temperature and a sharp increase with the onset of melting (refs. 23 and 37). Partial melting, with several percent of melt, can explain existing seismic data (ref. 23). The foci of moonquakes for which the depths were determined (18 cases) are concentrated in the 800- to 1000-km range; i.e., there is a concentration of lunar seismic activity in a zone 200 km thick.

The silicate interior of the Moon has a solidus temperature from 1620 K to 1950 K at depths from 100 km to the center. This is compared with some thermal models (ref. 23).

Geological and geochemical processes on the Moon are considerably more primitive than the processes of crustal formation on the Earth. Magmatic activity on the Moon leads to eruption of magma and formation of gabbro-basalt-type rocks similar to the magmatic rocks of the Earth. Differences are connected with the enrichment of the Moon with lithophile, refractory element, and the loss of a part of the siderophile elements. The depths of formation of magma chambers on the Moon, the rate of rise of magma, the temperature, and the diversity of surface crystallization conditions are reflected in the structure and texture of the rock (ref. 38). High concentrations of FeO, TiO_2, and other elements reduce the crystallization temperature of the magma. The ratios of close isomorphic pairs of chemical elements K/Rb, Ca/Sr, Th/U approach the same ratios as in the tholeiite basalts of the Earth (refs. 22 and 39).

One of the hypotheses of the origin and evolution of the heterogeneity of the Moon which deserves attention is the hypothesis of convection (ref. 40). The following expression for liquid flow of a cellular structure is obtained between the Nusselt (Nu) and Rayleigh (Ra) criteria which describe convective heat transfer:

$$\mathrm{Nu} = 0.205\ \mathrm{Ra}^{1/4}$$

$$\mathrm{Nu} = \frac{\alpha l}{\lambda};\ \mathrm{Ra} = \frac{g\beta}{\nu a} A l^4; \qquad (3)$$

α is the heat transfer coefficient, l is the thickness of the liquid layer, λ is the thermal conductivity coefficient, a is the thermal diffusivity coefficient, ν is the kinematic viscosity coefficient, β is the bulk expansion coefficient, g is the acceleration of gravity, and A is the temperature gradient in the layer.

Experiments with various liquids at $4000 < \mathrm{Ra} < 10^5$ have shown that equation (3) describes the test data well. The value of Ra_{crit} (which determines the start of the convective process) proved to be 3100 according to the experimental data. Thus, the convective process starts at the moment when $l \geq l_{crit}$, where

$$l_{crit} = \sqrt[4]{\frac{3100\ \nu a}{g\ \beta\ A}} \qquad (4)$$

Let the wall temperature be T_1 and T_2 and $(T_1 \leq T_2)$. The magnitude of the heat flux from the hotter wall will be

$$Q = \alpha\ (T_1 - T_2) \qquad (5)$$

On the other hand,

$$Q = \lambda_{ef} \times A \qquad (6)$$

The quantity A can be assumed to be equal to the melting temperature gradient, since it is known from geochemistry that moving melts are not superheated. Besides, this follows also from physical considerations, since the values of T_1 and T_2 are essentially the melting temperatures of rocks.

Thus, we write relationship (3) in the form

$$Q = lA\alpha \qquad (7)$$

Then, from relationships (3, 6, and 7) we obtain

$$\lambda_{ef}/\lambda = 0.205\ \mathrm{Ra}^{1/4} \qquad (8)$$

The values of λ_{ef}/λ were calculated for a melt under Earth, Mars, and Moon conditions.

Parameters adopted in the CGS system are shown in Table 1.

Table 1.—*Parameters for Calculation by Equation (8)*

		a = 0.01; $A = 3\times10^{-4}$		
	g, 10^3	β, 10^{-5}	l_{crit}, (km) $\nu = 10^{19}$	$\nu = 10^{20}$
Earth	1	2.0	47	84
Moon	0.16	4.0	64	113
Mars	0.39	3.5	52	93

Parameters of Thermal Models

The basic parameters of thermal models are the coefficients of heat transfer, heat capacity, latent heat of phase transitions, and the heat sources. The coefficient of heat transfer includes the coefficient of molecular (phonon) heat conductivity of a solid $\lambda\phi$, radiant heat transfer λ_r, as well as the effective heat transfer by convection λ_{ef}. A family of $\lambda\phi$ and $\lambda\phi + \lambda_r$ curves for the presumed rocks of the Moon are presented in figure 4. At high temperatures, the coefficients change between the bounds of 0.003 and 0.012 cal/cm · s · K, and it is very likely that, deep in the interior of the lunar lithosphere, the value of the thermal conductivity is close to constant, at 0.07 cal/cm · s · K = 2.8 W · m^{-1} · K^{-1}.

The unique thermal properties of the low-conduction surface layer of the Moon must play a significant role in the heat balance

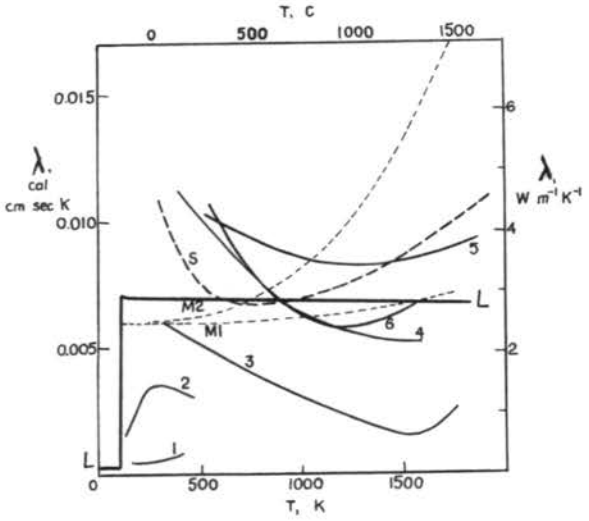


Figure 4.—*Thermal conductivity coefficients for lunar rock (curves 1–6 correspond to Toksöz and Solomon (ref. 23); curve L, this work).*

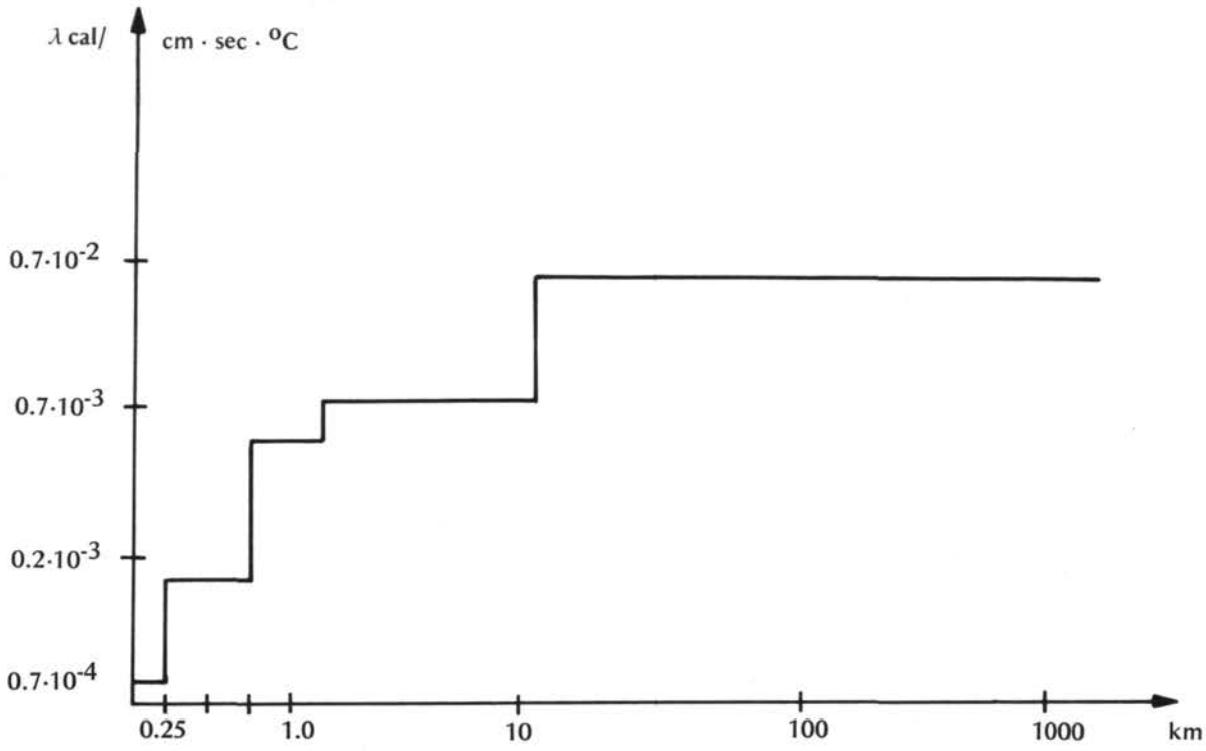


Figure 5.—*Model of step wise change in thermal conductivity used in calculations of evolution of heterogeneous Moon.*

and evolution of the heat flux. In connection with this, we have studied in greater detail than has been done previously the thermal conditions of contemporary models of the Moon, with the sharp change in thermal conductivity taken into account by means of the maximum possible decrease in the interval of temperature calculations close to the surface. Our initial model of thermal conductivity distribution is given in figure 5 and table 2:

The thermal isolation layer at the surface of the Moon is of significant value for prolonged retention of the melt in the interior of the Moon. If λ = const = 0.007 cal/cm · s · deg., it persists for 300 m.y.; if λ is according to table 2, it persists for 1.3 AE.

Table 2.–*Initial Model of Thermal Conductivity Distribution*

Depth, km	Thermal Conductivity λ, cal/cm • s • deg.
0–0.250	7×10^{-5}
0.250–0.750	7×10^{-4}
0.750–1.000	7×10^{-3}
1km–10km	7×10^{-2}
10km–1000km	7×10^{-2}
1000km–1740km	7×10^{-1}

The model of heat generation in the interior of the Moon is determined by the content of uranium, thorium, and potassium. The Luna and Apollo missions demonstrated that the chondrite model of the Moon is not correct (ref. 22). Several variants of U, Th, and K content were tried in numerical calculations.

For the case of uniform distribution of heat sources, variants with the maximum B and minimum A in content were taken:

A: U = 0.5 ppm
B: U = 0.8 ppm

After formation of a crust with layers 20 and 60 km thick and a lithosphere (1000 km), redistribution of sources leads to approximately a twentyfold depletion of uranium, according to the model of Vinogradov (ref.

22). According to these data, the concentrations of the elements in the upper 20 km was:

$U = 2.3 \times 10^{-7}$ g/g; Th $= 0.9 \times 10^{-7}$ g/g; $K = 0.83 \times 10^{-3}$%.

After stratification, the following remained in the lithosphere:

$U = 0.43 \times 10^{-8}$ g/g; Th $= 0.38 \times 10^{-7}$ g/g; $K = 0.83 \times 10^{-3}$%.

During melting, the physical parameters of the phase transition boundaries are disrupted. This disturbs the stability of the calculation schemes, if special smoothing procedures are not used. The effects of melting and convection on temperature were modeled using a technique described by Budak et al. A smoothing function of the physical parameters at the phase transition boundary was introduced. When the temperature T^M (r,t) becomes higher than the melting temperature, the thermal conductivity coefficient is replaced by an effective heat transfer coefficient $\lambda_{ef} = 0.1$–0.05 cal/cm · s · ° C, symbolizing convection.

The heat sources are the most important in calculations of the thermal history. The abundance of isotopes measured in lunar samples and by means of orbital gamma-ray observations (ref. 41) leads to the conclusion that the concentrations of uranium and thorium in the surface layers of the Moon are increased over those in the deep layers and are generally higher than on Earth. At the same time, the Moon is depleted in volatiles, including potassium. While for Earth K/U = 10 000 and for chondrites K/U = 80 000, we have only K/U = 2000 for the Moon. Using the ratio K/U = 2000, we obtain the average generation of heat $H(r,t)$ in the interior of the Moon as a simple function of the bulk uranium content $U(t_0)$:

$$H(r,t) = \rho\, U(\tau_0)\, 1.35\, [0.73 + 0.20\, Th/U + + 0.25 \times 10^{-4}\, K/U]$$

$\rho = 3.34$ g/cm³

$U_0 = 7.3 \cdot 10^{-6}$ g/g $= 7.3$ ppm

After stratification during the first billion years, the crust of the Moon consists of 20 km of basalts and 40 km of andesites; the Moon is considered to be three-layered, according to Anderson (ref. 33).

The average content of uranium is between those of howardites and eucrites and determines the average value of the global heat flux which is 33 erg/cm² · s (ref. 42). The decay constants, decay energy, and isotope abundances are taken in accordance with reference 43. We disregard the value of tidal friction, including it in $T_0(r)$.

Direct and Indirect Determination of Heat Flux and Structure of the Lunar Crust

Before the flights to the Moon of the Luna and Apollo 15, 16, and 17 spacecraft, the heat flux on the Moon was determined by study of its natural radio emission and extraction of the constant components that determine the temperature gradient in the interior. Precision measurements of the constant component of the radio temperature, at two wavelengths, μ_1 and μ_2, perpendicular to the surface, give an expression for the temperature gradient (refs. 15 and 44).

$$\text{grad } T(z) = \frac{dT_{e0}}{d\mu} \frac{1}{(1 - R_\perp)\, m l_t}$$

where T is the average effective temperature over the disk, depending on μ; $R_\perp$ is the albedo; and l_e/l_t is the ratio of the depth of penetration of electromagnetic and thermal waves, $\delta_1/\mu = m$.

The quantity l_e, the depth of penetration of electromagnetic waves, is proportional to wavelength μ and inversely proportional to tan Δ, the tangent of the loss angle (ref. 44):

$$l_e = \mu/(2\pi \sqrt{\varepsilon}\, tan\Delta) = \tilde{a}\, \mu$$

where ε is the dielectric constant and $\tilde{a}$ is a proportionality coefficient, depending on the properties of the substance in which

$$\tan \Delta = 2\sigma/\varepsilon f$$

Here, σ is the effective electrical conductivity at a given frequency f. Multiplying grad T by the thermal conductivity coefficient λ, we obtain the heat flux,

$$q_{\mathbb{Q}} = \frac{dT_{e0}}{d\mu} \frac{\sqrt{\pi}}{(1 - R_\perp)\, m\gamma \sqrt{t}}$$

Using the model of heterogeneous lunar surface structure (rocks with ρ_1 covered by a porous layer with ρ_2), Tikhonova and

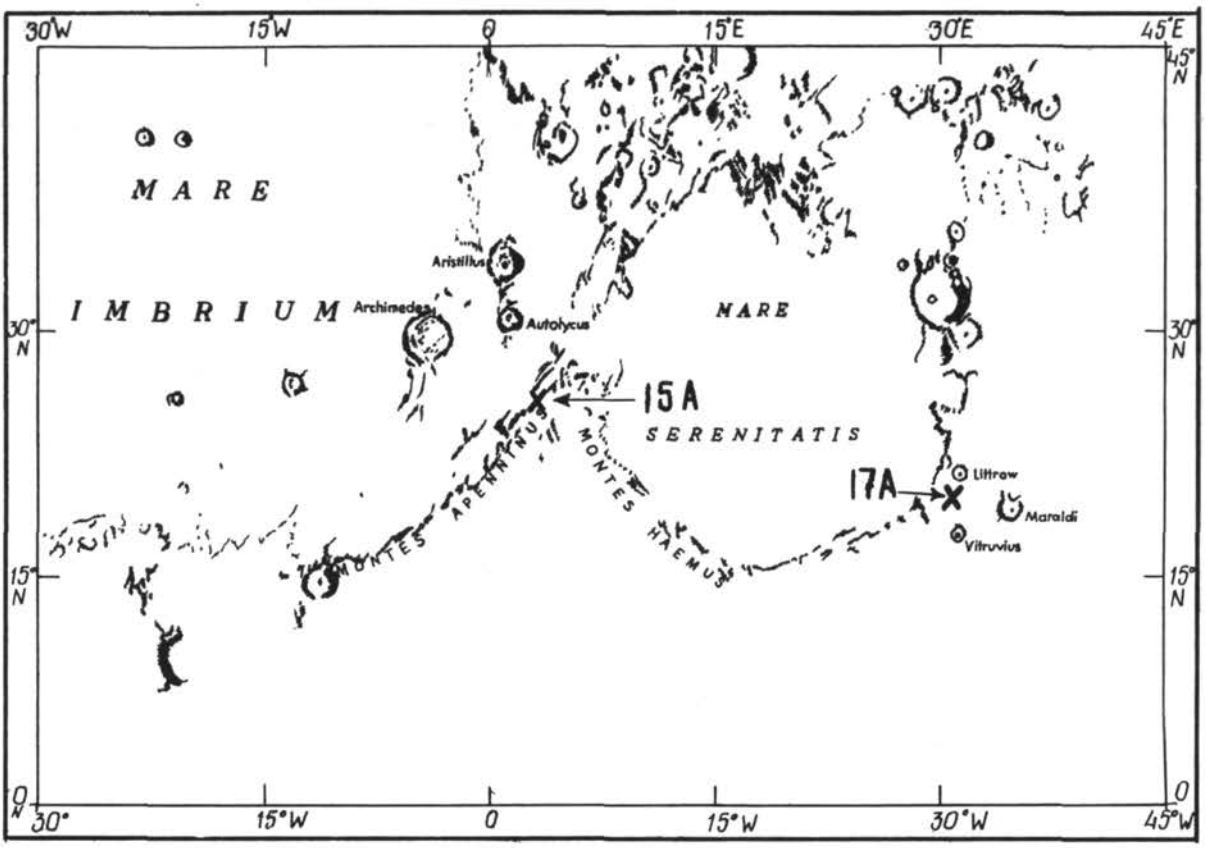


Figure 6.—*Location of heat-flux measurements by the Apollo 15 and Apollo 17 programs.*

Troitskiy (ref. 15) predicted the relatively high value of the heat flux from the interior of the Moon: $0.7 \times 10^{-6} < q_{\mathbb{C}} \leq 0.95 \times 10^{-6}$ cal/cm^2 · s.

Direct measurements of the heat flux in boreholes provide significant information on the heat balance and evolution of the Moon. Direct measurements of the heat flux from the interior of the Moon, with and without introduction of regional corrections (Apollos 15 and 17), showed that the value of the heat flux is at the upper limit of the expected values given on the basis of geochemical models, the intensity of radio emission, and calculations of the thermal history of the Moon. The two groups of measurements indicated were made at the margins of Mare Serenitatis and Mare Imbrium, at the boundary of the assumed mascon basins (fig. 6). The thick lunar crust contains significant irregularities. Particularly large irregularities are concentrated on the visible side of the Moon.

Similar boundaries are connected with change in the physical-chemical properties. In this connection, it is natural to expect a change in the thermophysical properties in the transition from the mare regions to the highlands. In fact, investigations by Luna 21 (Lunkhod 2) in the region of the eastern margin of Mare Serenitatis (as well as Lunokhod 1 in Mare Imbrium) showed that, according to the data of the RIFMA–M instrument, the iron content in the highlands is less than in the mare. According to radar observations, the region of measurement of the thermal flux was close to a "black spot region." The blue tint of these spots also is evidence of a high concentration of iron and titanium ions, with which variations in the coefficient of thermal conductivity and refraction of the heat flux may be connected. Terrestrial ex-

perience with heat flux measurements indicates the unreliability of judgments as to the average heat loss, q, on the basis of one or two measurements.

On the other hand, the absence of even a small region of water and appreciable tectonic activity permits one to assume that local variations in the heat flux on the Moon will be less than on Earth. However, the specific factors of disintegration and erosion of the surface of lunar rock (meteorite impacts, thermoelastic stresses as a result of fluctuations of the surface temperature, the effect of the mascons as inclusions of extraneous thermal conductivity) could be reflected in the history of the heat flux. The phenomena of disintegration of the lunar surface rocks by meteorite impacts should have introduced local changes in the energy balance of the surface.

The places of measurement of the heat flux in the boreholes on the Moon are presented in figure 6. They are located at the edges of Mare Serenitatis and Mare Imbrium. The Apollo 15 borehole is in the region of the Appennine Mountains, between Mare Serenitatis and Mare Imbrium and distant from three craters, Autolycus, Aristillus, and Archimedes. The landing site of Apollo 17 is located in the Taurus-Littrow Valley. There is a cross section of the latter, according to seismic sounding data, given in figure 7 (ref. 45). We made an attempt to determine the shape of the heat flux anomaly at the edges of the mascon, on the basis of numerical modeling of a two-dimensional structure, containing inclusions with high or low thermal conductivity as functions of varying degrees of burial (fig. 8). Data on thermal conductivity of the lunar rock and observed variations in them were used. Two mascon models were used (figs. 8 and 9), with and without allowance for the relief. In accordance with conclusions from the data of Luna 10, it was assumed that the surrounding surface rock of the Moon was basaltic.

The heat-flux anomaly has the appearance of sign-changing curves on the boundaries of trough-shaped (fig. 9) and rectangular (fig. 8) irregularities. With movement of an inclusion to the surface, a false anomaly at its edge can exceed 20 percent, with a threefold thermal conductivity drop. The size of the anomaly can increase due to a sudden increase in uranium concentration. On the lunar highlands and mare, Langseth et al. (refs. 16 and 17) used the observed q and more accurately determined the structure of the cover.

The absence of water and of noticeable

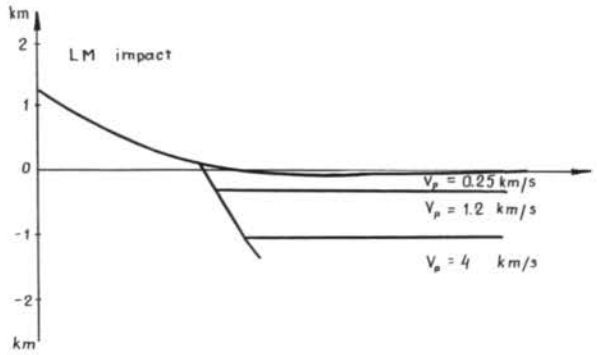
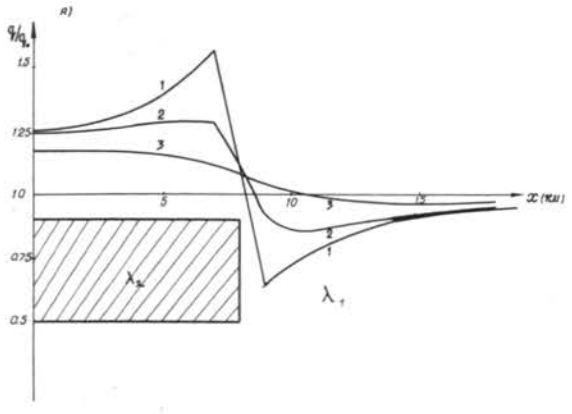


Figure 8.—*Change in relative value of heat flux* q/q_0 *above horizontal conducting inclusion (A) (cross hatched) with thermal conductivity* λ_2 *three times the thermal conductivity* λ_1 *of the surrounding rock, and above a thermal insulating inclusion (B). Curves 1, 2, and 3 correspond to depths of burial: (1)* H = 0, *(2)* H = 1 km,, *(3)* H = 2 km.

Figure 7.—*Cross section of the structure of the lunar crust in Apollo 17 landing region, from seismic data; line A–B, assumed fracture (ref. 45).*



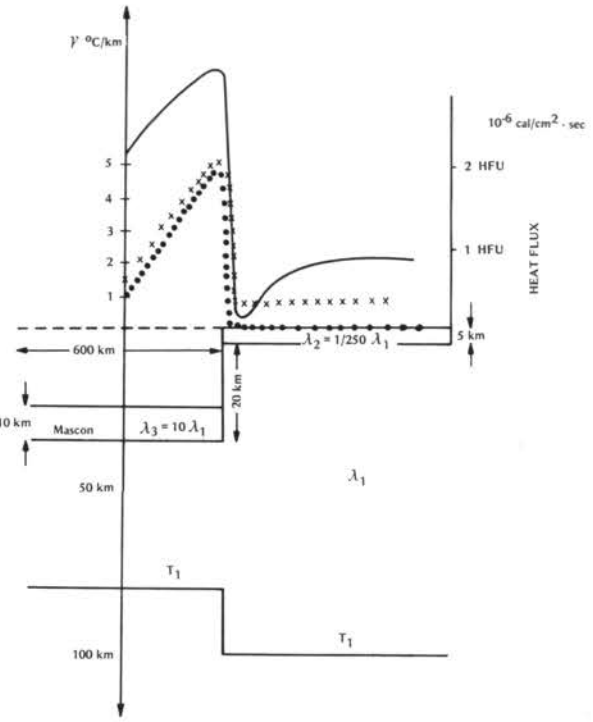


Figure 9.—*The thermal effect of a conducting mascon ($\lambda_3 = 10\ \lambda_1$), buried 20 km in a poorly conducting layer ($\lambda_2 = \lambda_1/250$) and with a high temperature T_1 at the level of the compensating layer.*

tectonic activity on the surface of the Moon allows one to assume that local variations in the heat flux on the Moon will be less than on Earth. However, disintegration and erosion of the surface layers by meteoritic impacts has severely disrupted the surface layer. Whether or not the direct measurements of the heat flux (refs. 16 and 17) by Apollo 15, 16, and 17 are representative involves data on the structure of the upper layer.

Research of Troitskiy et al., (ref. 44), Tikhonova and Troitskiy (ref. 15), and Langseth and Keihm (refs. 16 and 17) was devoted to study of the nature of the material and its density and heat conductivity. Significant change in the heat conductivity of the regolith and deep underlying layers was demonstrated in these researches by independent methods. In the work of Langseth and Keihm (ref. 36), the condition of a 15-cm layer of the regolith is studied in detail. At the same time, in work on the thermal history of the Moon, one studies the distribution of the thermal parameters on a considerably rougher scale which is unsatisfactory for calculation of the heat flux.

Calculation Procedure

The analytical solution for temperature and heat flux presented in Appendix I is a general solution that is universal for spherical planets of any radius, for stages when the distribution of heat sources and thermophysical parameters can be assumed to be uniform but, permitting change with time (e.g., a decrease in the concentration of radioactive elements because of their continuous decay).

In all later stages of development of planetary bodies, with the exception perhaps of the asteroids, the distribution of properties and of heat sources in particular is irregular, and differentiation, melting, and convection are included. The problem is solved with computers, using the method of finite differences. Any temperature distribution given by a computer is a partial solution. In principle, there can be an infinite number of such solutions from the point of view of thermal conductivity theory. In our numerical examples, the thermal conductivity equation was approximated by a finite difference scheme, with steps h along the axis r and along the time axis t (Appendix II). During melting, part of the thermal energy must have been absorbed as the latent heat of fusion.

Thermal conductivity problems, with phase transitions on the moving interface of two phases taken into consideration, are known in thermophysics as the "Stefan problem." Current models of the thermal evolution of the surface molten layer of the Moon (refs. 23 and 13) show that this layer is gradually displaced inward, with melting occurring on the lower boundary, while solidification and crystallization occur on the upper. In this manner, we must consider the Stefan problem for two moving boundaries: the upper $z = x_1\ (t)$ and the lower $z = x_2\ (t)$. It is controlled by the heat balance conditions in the form

$$L\rho\frac{dx_1(t)}{dt} = \lambda_1\frac{\partial T_1}{\partial z}\bigg|_{z=x1} - \lambda_2\frac{\partial T_2}{\partial z}\bigg|_{z=x2}$$

$$L\rho\frac{dx_2(t)}{dt} = -\lambda_2\frac{\partial T_2}{\partial z}\bigg|_{z=x2} + \lambda_3\frac{\partial T_3}{\partial z}\bigg|_{z=x2}$$

where z is the depth; λ_1 and λ_3 are the thermal conductivities above and below the molten layer; λ_2 is the coefficient of heat transfer or effective thermal conductivity inside the molten layer, possibly with inclusion of convective transport; L is the latent heat of fusion; and T_1 is the temperature in the upper solid layer, satisfying the boundary conditions:

$$T_1(z)\big|_{z=0} = 0$$

$$T_1(z)\big|_{z=x1(t)} = T_m\,[x_1\,(t)]$$

$$T_m = T_0 + \gamma_2 z$$

Here, T_m is the melting temperature, and γ_2 is the melting temperature gradient. Let T_2 be the temperature inside the molten layer, satisfying the conditions:

$$T_2(z,t)\big|_{z=x1} = T_m\,[x_1\,(t)]$$

$$T_2(z,t)\big|_{z=x2} = T_m\,[x_2\,(t)]$$

T_3 is the temperature in the lower layer below the level of the melt, satisfying the conditions:

$$T_3(z,t)\big|_{z=x2} = T_m\,[x_2\,(t)]$$

$$\frac{\partial T_3}{\partial z}\bigg|_{z=x2} = \gamma_2$$

The initial conditions for the moving boundary are the following:

$$x_1(t)\big|_{t=0} = a, \qquad x_2\,(t)\big|_{t=0} = b$$

The Stefan problem is nonlinear. The nonlinearity increases if the dependence of thermal conductivity on temperature is taken into consideration. In order to carry out automatic soothing of jumps in the physical parameters on the phase transition boundaries, we use the smoothing method of Budak et al. and we introduce a change of the variables

$$T = U + T^*$$

and the specific heat content function (see Appendix III)

$$H\,(u,r) = \int_0^u [c(\zeta)\rho(\zeta) + .L\rho\delta(\zeta - T^*)]\,d\zeta$$

The difference analog of the thermal conductivity equation is given in Appendix III. The value of the latent heat is assumed to be $L = 400$ J/g. The surface temperature is assumed to be constant during the life of the Moon and equal to $-20°$ C.

The temperature distribution should be satisfied by the data of a comparatively high heat flux (refs. 16 and 17). The value of q, previously calculated from theory for the present and with the age of the Moon being 4.6×10^9 yr, is 0.36×10^{-6} cal/cm^2 · s (ref. 2). A molten layer forms at 2.1×10^9 yr, at a depth of 500 km, with a 150-km width and, at 3.2×10^9 yr, the melting level reaches 300 km and is maintained up to the present time.

The hot state of the Moon could be explained in this manner, but the model does not completely satisfy the heat flux and the heterogeneous seismic structure. Better agreement with the seismic model and geochemical evolution is obtained by assuming higher uranium content up to a value of 60 ppb in a homogeneous Moon, which corresponds to the models of Toksöz et al. (ref. 46) and Toksöz and Solomon (ref. 23). In figure 3, with an initial formation of a melt, the effect of the latent heat on the phase transition boundaries was taken into account: absorption of 400 cal/g at the upper boundary and emission on the lower boundary of the melt, in accordance with Stefan's law for a moving boundary. The latent heat was incorporated in the thermal conductivity equation through the specific heat content by the method of Budak, and the solution of Stefan's problem then has the form of Appendix III. At the onset of melting, the heat transfer increases, and the coefficient λ increases tenfold. If one assumes differentiation at the very start and a crustal thickness of 60 km with uranium concentration 0.4×10^{-6} g/g, then a melt forms in the lithosphere at a depth of 100- to 600-km and quickly expands, and the greatest heat flux reaches 1.17×10^{-6} cal/cm^2 · s (1 AE) and is 0.6×10^{-6} cal/cm^2 · s at present, which is in agreement with the heat flux predicted by Tikhonova and Troitskiy (ref. 15) and measured by Langseth and Keihm (refs. 16, 17, and 36).

Consequences of the Thermal History of the Moon

Study of moonquakes and lunar tectonics by high-frequency seismometers has shown that thousands of very small lunar signals recorded by the Apollo 14, 15, and 16 stations are correlated with meteorite impacts, as well as with the sunrise and sunset periods. This correlation of micromoonquakes with the thermal cycle on the surface indicates that a considerable fraction of the micromoonquakes are of a thermal nature (ref. 47). There are two likely mechanisms of such periodic thermal moonquakes: (a) fracturing of the lunar rock and (b) slippage of lunar soil along slopes, caused by the periodic thermal stresses. The moonquake signals recorded by high-frequency seismometers are completely different from locally generated moonquakes. In conformance with current seismic models of the structure of the Moon, deep moonquakes arise at the base of a thick elastic shell (lithosphere), immediately above the boundary of the relatively weak central zone of the asthenosphere. Surface tectonic characteristics indicate the possibility of a slight tension on the lithosphere of the Moon in the past when the interior of the Moon became warmer. However, the absence of moonquakes at shallow and intermediate depths at present leads to the assumption that no appreciable compression or dilation rates exist now. Therefore, the Moon should be close to thermal equilibrium, and the rate of heat loss by radiation of heat from its surface should be approximately compensated by the rate of internal heat generation.

Seismic and tectonic activity of the Moon is extremely low compared with Earth. The Moon is characterized by an inactive outer layer 1000 km thick. The seismic hypothesis can be tested from the point of view of thermal processes by calculation of the thermoelastic state of the Moon, with allowance for the fact that its upper layer has already passed through a molten state and that the central layers are now in a softened state close to partial melting or the beginning of melting, i.e., the solidus.

The great thickness of the lunar lithosphere, compared with that of Earth, most likely explains the strongly differing tectonics of these planets.

An estimate of the propagation of elastic deformations and stresses that result from heating and cooling of the Moon can be carried out for models of an elastic, spherical layer placed on the surface of a molten layer.

For a maximum estimate of the expansion of the perimeter of the Moon, the elastic model can be used. The change in radius of an elastic Moon during its thermal history can be estimated by the formula

$$\frac{dR_{\mathbb{C}}}{dt} = \frac{\alpha}{c\rho}\left(- q_{\mathbb{C}} + \frac{HRa_{\mathbb{C}}}{3}\right)$$

where q is the heat flux at the surface, α is the coefficient of thermal expansion, and H is the heat generation. In 1960, the rate of expansion of the Moon was estimated by MacDonald, and in 1968 by Lyubimova, on the basis of chondrite models of the Moon and of a comparatively low heat flux taken from calculations of the thermal history. We have available at present independent, directly measured values of $q_{\mathbb{C}}$ and U. We substitute the following values of the flux $q_{\mathbb{C}} = 28$ erg/cm^2 · s, according to Langseth et al. (refs. 16 and 17) and heat generation based on the average uranium content U = 60 ppm and the value $\alpha = 3 \times 10^{-5}$ deg^{-1} (ref. 23). By substituting these numerical values, we obtain 10^{-6} cm/yr for the maximum rate of change in radius of the Moon in the last billion years of its evolution. The rate of change in the radius of the Moon was greater in the past than now. Deformation u and tangential stresses and τ on the surface $r = R$, in the presence of a molten layer, can be determined from the equation of elastic equilibrium in a spherical layer bounded on the inside ($r = a$) and outside ($r = R$) by spherical boundaries. The following are conditions on these boundaries: the upper one is free, and a normal stress is assumed on the lower one, designated conventionally by γ. For a given temperature distribution, we obtain deformation

$$(1 - s)\frac{du}{dr} + 2s\frac{u}{r}\Big|_R = 0$$

and also,

$$(1-s)\frac{du}{dr}+2s\frac{u}{r}\Big|_a=\frac{\gamma}{E}(1+s)(1-25)$$

i.e., the increase in radius u (R) and tangential stress $\tau(R)$ on the surface

$$u(R)=\frac{R}{R^3-a^3}\int_a^R d(r)T(r)r^2dr-\frac{\rho gR^2(1-2s)}{5E}\left[1+\frac{3(3-s)}{4(1-2s)}\cdot\frac{a^3(R^2-a^2)}{R^2(R^3-a^3)}\right]+\frac{\delta(a)T(a)(1-s)}{2(1-s)}\frac{a^3R}{(R^3-a^3)}-\frac{3}{2}\frac{\delta}{E}(1-s)\frac{a^3R}{R^3-a^3};$$

$$\tau(R)=-\frac{E}{2(1-s)}\frac{1}{R^3-a^3}\int_a^R\alpha(z)T(r)r^2dr+\frac{\rho gR(1-2s)}{10(1-s)}\left[1+\frac{3(3-s)}{4(1-2s)}\frac{a^3(R^2-a^2)}{R^2(R^3-a^3)}\right]-\frac{E\alpha(a)T(a)}{4(1-2s)}\frac{a^3}{R^3-a^3}+\frac{3}{4}\gamma\frac{a^3}{R^3-a^3}$$

from which we have

$$\tau(R)=-\frac{E}{2(1-s)R}u(R)$$

The formation of fractures on the surface of the Moon is possible only upon reaching τ, the limit of the strength of the material. From the relationship between u and τ just obtained, the magnitude of the fractures can be estimated, if the value of the critical stess τ_{crit} is substituted in the left side. We assume that on the boundary $r=a$ $\sigma_{rr}=\gamma$. Since the radial component of the stress in a liquid is given by the formula

$$s_{rr}=-p+2\nu\rho_l\left[\frac{\partial v_r}{\partial z}-\frac{1}{3}\operatorname{div}\vec{v}\right]$$

$$v_0=v_a=0$$

on the boundary, $r=a$ and $\sigma_{rr}=\gamma$

$$\gamma=p(a)=2\nu\rho_l\left(\frac{\partial v_r}{\partial z}-\frac{1}{3}\operatorname{div}\vec{v}\right)$$

where ρ_l is the density of the melt. The formula for determination of the increase in perimeter of the Moon will have the form:

$$\frac{u(R)}{R}=\frac{1}{R^3}\int_a^R\alpha Tr^2dr+\frac{\alpha(a)T(a)a^3}{3R^3}-\frac{\rho gR(1-2s)}{5E}\left(1-\frac{a^5}{R^5}\right)+\frac{s(1-s)\nu\rho_0(\bar{v}+\bar{v}_\tau)ab}{ER^3}\left[1+\frac{2\alpha_l\theta}{3(1+\alpha_l)\theta}\frac{(\bar{v}+\bar{v}_\tau)b}{\kappa_0}\right]\left[\frac{1}{1-\exp\frac{(\bar{v}+\bar{v}_\tau)(a-b)}{\kappa_0}}\right]$$

Calculations show that the perimeter of the Moon increased during the first half billion years and then began to decrease until the time of formation of the asthenosphere. If the assumption of the existence of the strong convective heat transfer in the region of the partially molten asthenosphere of the Moon is introduced, an increase in the perimeter again resulted 2 to 3 b.y. ago. It is as though the molten layer expands the Moon from inside, and the increase in the perimeter ensures formation of crustal fractures through which the magma erupts.

Conclusions

The principal attention has been given in this work to an effort to relate the values of the observed heat fluxes to the thermal evolution of the Moon, considering the fine structure of the outer crust which has the properties of a uniquely insulating material.

In calculations of the history of the heat flux, extremely small depths (steps in the calculation network of 250 m in all) were introduced into analysis of the numerical determinations of temperature differences (on the order of hundreds of meters), with allowance for abrupt differentiation in the thermophysical properties and for heat generation.

In this work, initial melting of the upper 250 km was assumed, with allowance for abrupt stepwise differentiation of the thermophysical properties and heat generation, as well as for the rapid fractionation of matter. The analysis included the effects of absorption and emission of heat at the boundaries of a moving, molten layer, with effective internal convection and rapid transport of the excess heat from the upper boundary to the lower one.

A new technique based on the Stefan equation is introduced for calculation of the absorption and emission of heat that results from the effect of the latent heat of fusion of phase transitions occurring at two moving boundaries of a melt.

From the analysis presented in this paper, the following preliminary conclusions are made:

1. The introduction of thermal conductivity, decreasing toward the surface, increases the thermal insulation effect of the upper cover of the Moon and facilitates retention of the melt in the interior of the Moon for a period of 1.3 b.y., rather than 300 m.y. as for a uniform thermal conductivity of 0.007 cal/cm · s · °C.
2. A uniform distribution of uranium with a concentration of 60 ppm does not reflect the observed values of the heat flux because γ-spectrometry data indicate a sharp concentration of radioactive elements in the crust and their enrichment in the lunar highlands.
3. A distorting effect of the mare basin mascons on the observed heat fluxes is not excluded due to the different nature of these basins whose substance is more heat conducting and contains increased percentages of iron and titanium. The greatest distortions are expected near the edge of such basins where the heat-flux measurements were made. It is presently difficult to accurately predict the magnitude of the expected anomalies because of the shortage of data on the thermal conductivity coefficient of the matter making up the mascons.
4. The thermoelastic history of the Moon, analyzed with allowance for the expanding effect of the molten layer below the lithosphere, shows that the increase in the Moon's perimeter was sufficient for the formation of deep fractures through which lavas erupted and filled the mare basins. The eruption of lava was stimulated in the early history of the Moon by bombardment of the surface with meteorites.
5. During the life of the Moon, the emission of heat into space has gradually declined. At 1 AE after formation of the Moon, the heat flux reached 1.17×10^{-6} cal/cm^2 · s; after 3 AE, it decreased to 0.64×10^{-6} cal/cm^2 · s and almost stabilized. Since then subsequent decrease has not exceeded 10 to 15 percent.

Appendix 1: Analytical Solution

Heat calculations are carried out using a nonstationary thermal conductivity equation for a spherically symmetric planetary body (Moon, Mars, Mercury, asteroids, etc.), containing internal heat sources

$$C_p\rho \frac{\partial T}{\partial t} = \frac{1}{r^2}\frac{\partial}{\partial r}\left[r^2(\lambda_{cp} + \lambda_r)\frac{\partial T}{\partial r}\right] + H(r,t) \quad (1.1)$$

where C_p is the specific heat capacity, T is the temperature at point (r,t), ρ is the density, and $H(r,t)$ is a function of the heat source, which usually implies the long-lived, naturally radioactive isotopes U^{238}, U^{235}, Th^{232}, and K. The energy of gravitational differentiation given off in the process of evolution of the Earth, the latent heat of phase transitions, and other things can also be included in $H(r,t)$ (ref. 2).

The physically based boundary conditions are

$$\left.\begin{aligned} T(r = R,t) &= \text{Const} \\ \frac{\partial T}{\partial r}(r = 0,t) &= 0 \\ T(r,t = 0) &= T_0(r) \end{aligned}\right\} \quad (1.2)$$

For these conditions, the classical form of solution applicable to the radius of the Earth was obtained by Lowan (1936), Urey (ref. 7), and Kopal (ref. 48).

The expression for the temperature inside a sphere of radius R obtained by these researchers is presented in the form of an infinite series by trigonometric functions and, as Van Orstrand showed (ref. 49), the series converges very slowly. The use of Green's function, with application of the method of sequential reflections, gives considerably

more rapid convergence of the series. It also represents the temperature inside the sphere and the thermal flux on the surface in the form of a formula, permitting a clear physical interpretation. Construction of a solution for temperature is carried out in the following manner. The substitution of variables is

$$u = r \times T(r,t) \tag{1.3}$$

The boundary conditions will then be

$$u(z,0) = 0;\ u(R,t) = 0;\ u\ (0,t) = 0 \tag{1.4}$$

The expression for $u\ (r,t)$ is expressed through Green's function G:

$$u(r,t) = \int_0^t \int_0^R G(r,t,r',\tau)\ \frac{H(\tau)r'}{c\rho}\ dr'd\tau \tag{1.5}$$

where $G(r,t,r',\tau)$ is Green's function for the segment $[0,R]$

$$G(r,t,r'\tau) = \sum_{n=-\infty}^{\infty} [G_0(r,t,2nR+r',\zeta) - G_0(r,t,2nR-r'\tau)] \tag{1.6}$$

in which

$$G_0(r,t,r',\tau) = \frac{1}{2\sqrt{\pi\kappa(t-\tau)}}\ \exp\left[-\frac{(r-r')^2}{4\kappa(t-\tau)}\right] \tag{1.7}$$

Further, the variables are replaced,

$$r \pm 2nR \pm r' = y \tag{1.8}$$

and the expression for the temperature inside a spherical body takes the form

$$T(r,t) = \frac{1}{c\rho\sqrt{4\pi\kappa}}\ \frac{1}{r}\int_0^t \frac{H(\tau)}{\sqrt{(t-\tau)}} \left\{ \sum_{n=0}^{\infty} \int_{(2n-1)\ R-r}^{(2n+1)\ R-r} (r - 2nR + y)\exp\left[-\frac{y^2}{4\kappa(t-\tau)}\right] dy + \sum_{n=1}^{\infty} \int_{(2n+1)\ R-r}^{(2n+1)\ R+r} (r + 2nR - y)\exp\left[-\frac{y^2}{4\kappa(t-\tau)}\right] dy \right\} d\tau \tag{1.9}$$

After transformation of the sums and integrals, we have

$$T(r,t) = \frac{1}{c\rho}\int_0^t \mathrm{H}(\tau)\,dr - \frac{1}{c\rho}\ \frac{R}{r}\int_0^t H(\tau) \left[\sum_{n=0}^{-\infty} erfc\ \frac{(2n+1)R-r}{4\kappa(t-\tau)} - erfc\ \frac{(2n+1)R+r}{4\kappa(t-\tau)}\right] d\tau$$

The first term defines the temperature in the center; the second the magnitude of the outflow of the heat to the surface. Analysis of the convergence permits determination of the number of terms of the series $n \geq m$, starting with which, all subsequent terms of the series, with $m \geq 3\sqrt{Kt/R}$, can be discarded.

With thermal diffusivity of the rock on the order of $K = 0.01$ cm²/s, it holds true for the terrestrial planets and for intervals of time less than 5×10^9 yr that it is sufficient to take only one term of the series with $n = 0$, if the radius of the body is greater than $R = 1700$ km.

The temperature in the center of the planet or asteroid of any radius and at any moment of time is given by the expression

$$\mathrm{T}(r = o,t) = \lim_{r\to 0} T(r,t) = \frac{1}{c\rho}\int_0^t H(\tau)\,d\tau - \frac{R}{c\rho}\ \frac{1}{\sqrt{\pi}}\int_0^t \frac{H(\tau)}{\sqrt{K(t-r)}} \sum_{n=0}^{\infty} \exp\left[-\frac{(2n+1)^2\ R^2}{4K(t-\tau)}\right] d\tau$$

where

$$H(\tau) = \Sigma\, H_0^i\ \exp(-\lambda_i(t-\tau_0))$$

Appendix 2: Numerical Solution Without Consideration of Melting

The schemes commonly used previously had the shortcoming that, with small steps along the radius, too much machine time was required. Therefore, for example, MacDonald (ref. 8) had to limit the radius steps h to the order of 50 km; Toksöz and Solomon (ref. 23) and Mayeva (ref. 50) to a value $h = 20$ km; and Ornatskaya (ref. 13) to about 5 km. In this case, the fine structure of the lunar crust and the unique nature of the low coefficients of thermal conductivity of the outer crust of the Moon actually drop out of the analysis. Calculations of the surface heat flux at such h is extremely inaccurate. In this case, the effect of the irregular structure of the crust of the Moon is ignored. Limitations on stability are weakened by the use of implicit finite difference schemes. The error is

small for great depths, but it increases near the surface. In order to obtain a denser location of points near the surface, one can substitute variables

$$r = 1-x^2 \qquad (2.1)$$

Then the thermal conductivity equation will be approximated by the scheme described for equal new variable steps. The calculation involves use of the standard trial-run method, a convenient method for solution of the resulting system of linear equations "linked" to each other. The finite difference analog of the thermal conductivity equation, with irregular distribution of heat sources $H(r,t)$ and variable physical parameters ρ,λ,C_p at each point of the calculation network, has the form

$$T_i^{j+1} = \frac{1}{c(r_i)\rho(r_i)} \left\{ c(r_i)\rho(r_i) - \frac{\tau}{h^2 r_i} \left[r_{i+1}\lambda \left(\frac{T_{i+1}^j + T_i^j}{2}; \frac{r_{i+1}+r_i}{2} \right) + r_{i+1}\lambda \left(\frac{T_i^j + T_{i-1}^j}{2}; \frac{r_i + r_{i+1}}{2} \right) \right] T_i^j + \frac{\tau}{h^2 r_i} \left[r_{i+1}\lambda \left(\frac{T_{i+1}^j + T_i^j}{2}; \frac{r_{i+1}+r_i}{2} \right) T_{i+1}^j + r_{i-1}\lambda \left(\frac{T_i + T_{i-1}}{2}; \frac{r_i + r_{i-1}}{2} \right) T_{i-1}^j \right] + \tau H(r_i, t_j) \right\} \qquad (2.2)$$

Appendix 3: Consideration of the Latest Heat of Fusion.

The difference analog of the thermal conductivity equation, containing a change in heat content due to absorption or emission of the latent heat of fusion at the phase transition boundaries, has the form in dimensionless variables

$$H'(Rr_i'; u_i^{j+1} \quad \frac{u_i^{j+1} - u_i^j}{2} = \frac{\kappa}{r_i^{j2}} \frac{1}{h} \left[\left(r'_i + \frac{h_{i+1}}{2} \right)^2 \lambda \left(\frac{u_{i+1}^{j+1} + u_i^{j+1}}{2}, R(r'_i + \frac{h_{i+1}}{2}) \right) \right] \frac{u_{i+1}^{j+1} - u_i^{j+1}}{} - \left[\left(r'_i - \frac{h_i}{2} \right)^2 \lambda \left(\frac{u_i^{j+1} + u_{i-1}^{j+1}}{2}, R(r_i - \frac{h_i}{2}) \right) \right] \frac{u_i^{j+1} - u_{i-1}^{j+1}}{h_i} \right]$$

$$+ H(Rr'_i, Lt_i^{j+1})L$$

where $t' = t/L$, $r' = r/R$

$$h_i = r'_i - r'_{i-1}$$

$$h_i = \frac{h_i + h_{i+1}}{2}$$

$$\Sigma h_i = 1, \quad \kappa = L/R^2$$

References

1. TIKHONOVA, T. V., AND V. S. TROITSKY, Determination of the Heat Flux From the Interior of the Moon with the Heterogeneous Structure of Its Surface Layer. *Fizika Luny i Planet*, 1972, pp. 78–182.
2. LYUBIMOVA, YE. A., *Thermals of the Earth and Moon*, 1968.
3. RUSKOL, YE. L., Model of Accretion of the Moon Compatible with Data on the Composition and Age of Lunar Rock. *The Moon*, Vol. 6, 1973, pp.176–189.
4. KAULA, W. M., *Mechanical Processes Affecting Differentiation of Proto-Lunar Material.* This collection.
5. SOLOMON, S. C. AND M. N. TOKSÖZ, Internal Constitution and Evolution of the Moon. *Phys. Earth Planet. Interiors*, Vol. 7, 1973, pp. 15–38.
6. TOKSÖZ, M. N. AND D. H. Johnston, The Evolution of the Moon and the Terrestrial Planets. *Soviet-American Conference on the Cosmochemistry of the Moon and the Planets*, Moscow, June 4–8, 1974. This collection.
7. ORNATSKAYA, O. I., YA. I. AL'BER, AND I. L. RYAZANTSEVA, *Calculations of the Thermal History of the Moon with Various Concentrations of Radioactive Elements, Considering Differentiation of Matter in Melting.* This collection.
8. MACDONALD, G. J. F., Calculations on the Thermal History of the Earth. *J. Geophys. Res.*, Vol. 64, 1959, pp. 1967–2000.
9. MACDONALD, G. J. F., *Space Sci. Rev.* Vol. 2, 1963, p. 473.
10. UREY, H. C., Origin and History of the Moon. *Physics and Astronomy of the Moon*, 1962, p. 481.
11. LEVIN, B. YU., Thermal History of the Moon. *The Moon*, 1962, p. 157.
12. MAYEVA, S. V., Some Calculations of the Thermal History of Mars and the Moon. *Izv. Komiza Po Fizike Planet*, No. 5, 1965, pp. 49–70.
13. LYUBIMOVA, YE. A., Theory of the Thermal State of the Earth's Mantle. *The Earth's Mantle*, No. 4, 1967.
14. TROITSKIY, V. S., *Izv. VUZ Radiofizika*, Vol. 10, No. 8, 1967.

15. TINHONOVA, T. V., AND V. S. TROITSKY, Determination of the Heat Flux From the Interior of the Moon with the Irregular Structure of Its Surface Layer. *Fizika Luny i Planet*, 1972, pp. 178–183.
16. LANGSETH, M. G., S. J. KEIHM, AND J. L. CHUTE, JR., Direct Measurements of Heat Flow From the Moon. *Lunar Sci.*, 1973, pp. 445–456.
17. LANGSETH, M. G., S. J. KEIHM, AND J. L. CHUTE, JR., Heat Flow Experiment Apollo 17. *Preliminary Sci. Report, NASA*, 9–1, 9–24, 1973.
18. LATHAM, G., J. DORMAN, F. DUENNEBIER, M. EWING, D. LAMMLEIN, AND Y. NAKAMURA, Moonquakes, Meteoroids and the State of the Lunar Interior. *Lunar Sci. IV*, 1973, pp. 457–459.
19. ANDERSON, D. L., AND T. C. HANKS, The Moon. *Science*, Vol. 178, 1972, p. 1245.
20. ARKANI HAMED, J., Viscosity of the Moon. 1: After Mare Formation. *The Moon*, Vol. 6, 1973, pp. 100–111.
21. WOOD, J. A., Thermal History and Early Magmatism in the Moon. *Icarus*, Vol. 16, 1972, pp. 229–240.
22. VINOGRADOV, A. P., *Differentiation of Lunar Material.* This collection.
23. TOKSÖZ, N. M. AND S. C. SOLOMON, Thermal Evolution of the Moon. *The Moon*, Vol. 7, 1973, pp. 251–278.
24. LYUBIMOVA, YE. A., The Role of Radioactive Decay in the Thermal Regime of the Earth. *Izv Akad nauk SSSR Geofiz, Serial 2*, 1952, pp. 3–17.
25. LYUBIMOVA, YE. A., "Thermal History of the Earth with Consideration of the Variable Thermal Conductivity of Its Mantle." *Geophys. J. Roy. Astron. Soc.*, Vol. I, No. 2, 1958.
26. RINGWOOD, A. E., AND E. ESSENE, Petrogenesis of Lunar Basalts and the Internal Constitution of the Moon. *Science*, Vol. 167, 1970, pp. 607–610.
27. MIZUTANI, H., T. MATSUI, AND H. TAKEUCHI, Accretion Process of the Moon. *The Moon*, No. 4, 1972, pp. 476–489.
28. UREY, H. C., AND G. J. F. MACDONALD, Origin and History of the Moon. *Physics and Astronomy of the Moon*, No. 4, 1971, pp. 213–289.
29. KAULA, W. M., Interpretation of the Lunar Gravity Field. *Phys. Earth Planet. Interiors*, Vol. 4, 1971, pp. 185–192.
30. RINGWOOD, A. E., Evolution of the Solar System. *Geochimica et Cosmochimica Acta*, 1966.
31. HANKS, T. C., AND D. L. ANDERSON, Origin, Evolution and Present Thermal State of the Moon. *Phys. Earth Planet. Interiors*, Vol. 5, 1972, pp. 409–425.
32. HAYS, T. F., AND D. WALKER, *Lunar Igneous Rocks and the Nature of the Lunar Interior.* This Collection.
33. ANDERSON, D. L., The Composition and Origin of the Moon. *Earth Planet. Sci. Letters*, Vol. 18, 1973, pp. 301–316.
34. WOOD, J. A., J. DICKEY, V. B. MARVIN, AND B. N. POWELL, Lunar Anorthosites. *Science*, Vol. 167, 1970, p. 602.
35. TAYLOR, S. R., Chemical Evidence for Lunar Melting and Differentiation. *Nature*, Vol. 245, 1973, pp. 203–205.
36. LANGSETH, M. G. AND S. J. KEIHM, In Situ Measurements of Lunar Heat Flow. *Soviet-American Conference on the Cosmochemistry of the Moon and the Planets*, Moscow, June 4–8, 1974. This collection.
37. ANDERSON, D. L., The Interior of the Moon. *Phys. Today*, Vol. 4, 1974, p. 49.
38. TRIFONOV, V. G., AND P. V. FLORENSKIY, Discrete Dimensions of Round Mare and Thalassoids of the Moon. *Phys. Today*, Vol. 4, pp. 191–195.
39. WOOD, J. A., *Science*, Fourth Lunar Science Conference, Vol. 181, No. 4100, 1973, pp. 615–622.
40. SHURERT, G., D. L. TURCOTT, AND E. R. OXRURGH, Stability of Planetary Interiors. *Geophys. J. Rev. Astron. Soc.* Vol. 18, 1969, p. 441.
41. SURKOV, YU. A., AND G. A. FEDOSEYEV, *Radioactivity of the Moon, Planets and Meteorites.* This collection.
42. LANGSETH, M. G., JR., S. P. CLARK, JR., G. L. CHUTE, JR., S. J. KEIHM, AND A. E. WECHSLER, The Apollo 15 Lunar Heat Flow Measurement. *The Moon*, Vol. 4, 1972, pp. 390–410.
43. CLARK, S. P., JR., Handbook of Physical Constants. *Geol. Soc. Am. Memoir*, 1966, p. 97.
44. TROITSKIY, V. S., O. B. SHCHUKO, V. N. GOL'DBERG, AND L. V. DROBOVA, Determination of the Density of the Outer Crust of the Moon by Specified Temperatures of the Surface During Eclipses and the Lunar Night. *Izv. VUZ Radiofizika*, Vol. 10, No. 8, 1972, pp. 48–52.
45. SCHMITT, H. H., AND E. A. CERNAN, A Geological Investigation of the Taurus-Littrow Valley. *Apollo 17 Prelim. Sci. Report, NASA*, 5–1;–5–21, 1973.
46. TOKSÖZ, M. N., S. C., SOLOMAN, J. W. MINEVE, AND D. H. JOHNSTON, Thermal Evolution of the Moon. *The Moon*, Vol. 4, 1972, pp. 190–213.
47. KOVACH, R. L., J. S. WATKINS, AND P. TALWANI, Lunar Seismic Profiling Experiment Apollo 17. *Prelim. Sci. Report, NASA*, 10–1;–10–12, 1973.
48. KOPAL, Z., *The Moon*, 1962.
49. VAN ORSTRAND, C. E., Geothermal Methods of Estimating the Age of the Earth. *Geophys.*, Vol. 5, 1940.
50. MAYEVA, S. V., The Thermal History of the Terrestrial Planets. *Astrophys. Letter*, Vol. 4, 1968, pp. 11–16.

Calculations of the Moon's Thermal History At Different Concentrations of Radioactive Elements, Taking Into Account Differentiation on Melting

O. I. Ornatskaya, Ya. I. Al'ber, and I. L. Ryazantseva
Scientific Research Institute of Radio Physics
Gorky, U.S.S.R.

Calculations of the thermal history of the moon were carried out by solving the thermal conductivity equation for the case in which the heat sources are the long-lived radioactive elements Th, U, and K^{40}. The concentrations of these elements were adjusted to give four variations of the heat flow: 1.35×10^{-6} and 0.91×10^{-6} cal cm^{-2} s^{-1} (I and I**), 0.61×10^{-6} (variant II, the terrestrial mixture of Lyubimova and Starkova), and 0.236×10^{-6} (variant III, the chondrite model of Urey and MacDonald). In the same calculations, we considered layering of the differentiated material with transport to the surface of the radioactive elements after the temperature of the layer rose to 200 K above the melting temperature, which is considered in five variants that differ in the amount of transported radioactive elements: 100 percent ($n = 1$), 80 percent $n = 0.8$), 40 percent, 20 percent ($n = 0.6$, 0.4, 0.2). During fusion the heat capacity and heat conductivity were changed.

We considered two variants of an initially cold (273 K) and hot (900 K) Moon. Calculations show that the interior of the Moon was heated to melting during the first 0.7 to 2.3×10^9 years. The maximum fusion involved practically the entire Moon to a distance from 15 to 45 km beneath the surface, and started 3.5 to 4.0×10^9 years ago (I, I**), or 2.5 to 3.0×10^9 years ago (II, III) and continued for 1 to 2×10^9 years. Today the Moon is cooling. The current thickness of the solid crust is from 150 to 200 km and the heat flow exceeds the stationary value 1.5 fold. Apparently the most realistic variant is II (terrestrial mixture) for an initially hot Moon, and gives, regardless of the moderate concentration of radioactive elements, a heat flow of 0.9 to 0.95×10^{-6} cal cm^{-2} s^{-1}, which agrees with the radioastronomical measurements of Troitsky and Krotikov and with the Apollo 15 data.

Papers by Urey, MacDonald, Lubimova, Levin, Mayeva, Fricker, Reynolds and Summers, Iriyama and Shimazu, Anderson and Phinney, Hanks and Anderson, MacConnel, Toksöz and Solomon, et al. (refs. 1–21) investigated the Moon's thermal history by solving the heat conductivity equation with given values for the parameters of lunar material and for the initial and boundary conditions, and with radioactive elements with the given concentrations as the heat sources. Our papers (refs. 21 and 22) are devoted to the same problem. Up to 1966–1967, homogeneous and layered lunar models were considered separately. In 1966–1967 we took into account in the calculations the differentiation of lunar material and convection of radioactive elements to the surface on melting. Working independently, P. Fricker, R. Reynolds, and A. Sommers conducted similar studies. The consideration of continuous differentiation in the calculation permits one to investigate the Moon's thermal history in more detail. In 1971 differentiation was also taken into account by Mayeva (ref. 13) and in 1973 by Toksöz and Solomon (ref. 21).

Thus, at the present time computer calculation schemes of lunar thermal history are

sufficiently fully developed and many new results have been obtained. However, interest in this problem has not yet decreased, but rather has increased. This is associated with the large uncertainty in the lunar parameters that enter into the heat conductivity equation. This applies also to the uncertainty in the values for density, heat capacity, and heat conductivity, and their dependence on the state of lunar material (for example, during melting). Also involved is uncertainty in the melting curve and the initial conditions (in particular, the initial temperature) and in the Moon's age. However, the determining factor in the Moon's thermal history is the accepted concentration of radioactive elements in the Moon and their redistribution with time in the lunar interior.

In the above papers, except for references 22 and 23, the concentration of radioactive elements is taken to be that of chondritic meteorites (for example, references 1–5, or of the Earth (refs. 7–13), or of a "terrestrial mixture," that lead to values of the heat flux through the lunar surface on the order of (0.3 to 0.6) $\times 10^{-6}$ cal cm^{-2} s^{-1}. At the same time radio astronomical investigations by V. S. Troitsky and V. D. Krotikov (refs. 24 and 25) give a flux value equal to 0.85 to 0.95 $\times 10^{-6}$ cal cm^{-2} s^{-1} which was long considered to be rather doubtful but was confirmed by the recent analyses of the lunar regolith by Apollo 15 (ref. 26). As a result, it is necessary to calculate the Moon's thermal history for concentrations of the radioactive elements that may account for such a large heat flux.

The first attempt at this calculation was made in our papers in 1966–1967 (refs. 22 and 23) where we used four variants of the concentration of radioactive elements, two of which correspond to concentrations used by Levin and Mayeva (ref. 8) (variant "C" uses the mean terrestrial value of Urey and MacDonald). The other two use relatively large concentrations which give heat flux values close to the radio astronomical values. An exponential differentiation of radioactive elements was assumed to occur on melting. Since the large concentration of radioactive elements was close to the surface of the Moon (in 10–20 km they weakly influence the temperature of the main lunar mass, which quickly cooled). As a result, the thickness of the solid crust in these variants was equal to 600–700 km, i.e., larger than for the mean (Levin) and the low (Urey, MacDonald) concentrations where the thickness was 250 km and 400 km.

In our studies (refs. 21 and 22), we used the exponential model for transport of the radioactive elements to the surface on differentiation which corresponds in some degree to the so-called "sudden differentiation." This model permits one to determine the main physical peculiarities of the thermal history related to differentiation; yet it limits the number of variable parameters. In this respect, the layered differentiation proposed by Fricker et al. (ref. 14) appears to be closer to the real processes. Therefore, in the present paper we have used a layered differentiation of radioactive elements on melting with different portions of the elements (from 20 percent up to 100 percent) transported from layer to layer. The concentration variants of radioactive elements were the same as in our 1966–1967 papers (refs. 22 and 23).

It should be noted that we are not specialists in geophysics and have no right to discuss questions of the Moon's origin and its chemical composition. For this reason, for calculations we have taken parameters either from the expected values of the heat flux (at given concentrations of radioactive elements) or from papers by other authors. Thus, the initial temperatures (273 K and 900 K) were taken on the basis of references 14 and 16, and the heat capacity on the basis of the papers by Mayeva (refs. 11 and 12), where a sharp change in the heat capacity at the time of melting is considered. Remarks by Lubimova (ref. 6) are taken into account on the possibility of the flux increasing at moderate concentrations of radioactive elements by means of the contribution from the exciton component of the heat conductivity and from amplification of the efficiency of the radiational component.

$$C[T,r(T)] = \begin{cases} C_o = 0.25 \ \dfrac{\text{cal}}{\text{g}^\circ \text{K}}, \text{ at } T \leq T_{\text{in.m.}} \text{ and } T \geq T_{\text{in.m.}} + \Delta T, \\ C_o + \dfrac{4L}{(\Delta T)^2}\,(T - T_{\text{in.m.}}) \text{ at, } T,\ T_{\text{in.m.}} < T < T_{\text{in.m.}} + \Delta T/2, \\ C_o - \dfrac{4L}{(\Delta T)^2}(\text{T} - T_{\text{in.m.}}) + \dfrac{4L}{\Delta T} \text{ at, } \left(T_{\text{in.m.}} + \dfrac{\Delta T}{2}\right) < T < T_{\text{in.m.}} + \Delta T \end{cases} \quad (1)$$

$$\text{f}(T) = A/T;\ A = 10.3 \times 10^7 \frac{\text{cal.}}{\text{cm year}}, \text{ at } T \leq T_{\text{in.m.}} \text{ and } T \geq T_{\text{in.m.}} + \Delta T;$$

$$\text{f}(T) = 0.04 \times 10^7 \frac{\text{cal}}{\text{cm year}} = \text{const, at } T_{\text{in.m.}} < T < (T_{\text{in.m.}} + \Delta T).$$

Consideration is given to the considerable idealization, primarily of the layering process, and therefore, the results obtained are correct only within the limits of our mathematical model.

Statement of the Problem

As is the custom, the Moon is assumed to be a sphere with the radius r = 1735 km, of homogeneous density $p = 3.34$ g/cm³, with heat capacity C and the heat conductivity K, defined according to Lubimova (ref. 6) (heat conductivity) and Mayeva (refs. 11 and 12) (heat capacity) as follows.

The heat capacity is shown in equation (1). $L = 100$ cal/g is the heat of fusion; $\Delta T = 200$ K;

r = in cm, $T = in$ K.

$T_{\text{init. melt}} = 1373 + 500\ (1 - r^2/r.^2.)$ is the beginning of melting of the silicate material (ref. 3).

Expression (1) considers the gradual absorption of the heat of fusion in the melting interval ΔT (the effective heat capacity in the interval ΔT first increases linearly and then decreases).

The heat conductivity is given by the expression:

$$\text{K} = \text{f}(T) + \frac{16n^2\delta T^3}{3\varepsilon} + 1.76\ T^2 \left[\left(\frac{E}{\text{k}T} + 2\right)^2 + 2\right] \text{e}^{-\frac{E}{\text{k}T}} \quad (2)$$

In (2) the lattice (phonon), radiational (photon) and exciton components of the heat conductivity (ref. 6) are taken into account.

Phonon heat conductivity outside the melting interval varies in inverse proportion to the temperature; during melting it sharply increases (see ref. 27) and remains constant as shown in the equation above.

Photon and exciton components of the heat conductivity are defined by the well-known relations where $n^2 = 3$ is the refractive index, $\delta = 4.27 \times 10^{-5}$ cal/cm² grad⁴ year is the Stephan-Boltzmann constant, $\varepsilon = 25$ cm⁻¹ is the absorption coefficient of the material, and $E = 5.17 \times 10^{-20}$ cal is the activation [1] energy of excitons.

For the assumption of a homogeneous distribution of heat sources and location of the initial coordinate in the center of the sphere, the heat conductivity equation has the form:

$$\rho c \frac{\partial T}{\partial t} = \frac{1}{r^2} \frac{\partial}{\partial r}\left(\text{K} r^2 \frac{\partial T}{\partial r}\right) + H, \quad (3)$$

where H is the heat due to the long-lived radioactive elements uranium, thorium, and potassium 40.

$$H = \sum_{j=1}^{3} H\,;\ e^{-\lambda_j t} F(r,t)\ \rho\alpha_j, \quad (4)$$

where the function F (r,t) defines the distribution of radioactive elements as a function of the radius at different times. Indexes $j = 1,2,3$ refer to uranium, thorium, and potas-

[1] The values are taken for pyrolite (a mixture of basalt and periodotite) lunar composition, which is similar to the Earth's mantle (see ref. 28).

Table 1.—*The* U, Th, *and* K *Concentrations in Several Variants of the Bulk Lunar Composition and the Stationary Heat Flow Values for These Variants*

Variants		Concentration of Radioactive Elements [g/g]			q_{stat} cal cm^{-2} s^{-1}
		Uranium $H_1^{t_0}$	Thorium $H_2^{t_0} - 4H_1^{t_0}$	Potassium^{+40} $H_3^{t_0}$	
Basalt 14% Peridotite 73% Iron 13% $(K^{40}/U) = 1.6$	I	11.55×10^{-8}	46.7×10^{-8}	18.5×10^{-8}	1.35×10^{-6}
Basalt 10% $(K^{40}/U) = 1.13$	I^{++}	8.50×10^{-8}	34.0×10^{-8}	9.6×10^{-8}	0.91×10^{-6}
Basalt 5% Variant by Levin $K^{40}/U = 1.6$	II	5.20×10^{-8}	21.0×10^{-8}	8.4×10^{-8}	0.61×10^{-6}
Chondrite Model Variants by Urey and MacDonald	III	1.16×10^{-8}	4.67×10^{-8}	9.35×10^{-8}	0.236×10^{-6}

sium 40, respectively, $\lambda_1 = 1.54 \times 10^{-10}$ year^{-1}, $\lambda_2 = 5 \times 10^{-11}$ year^{-1}, $\lambda_3 = 5.7 \times 10^{-10}$ year^{-1}, the heat released by one gram of the radioactive element is $\alpha_i = 0.805$ cal g^{-1} year^{-1}, $\alpha_2 = 0.193$, $\alpha_3 = 0.224$ and values of H_j^0, the concentration at the beginning are defined on the basis of the expected present concentration of $H_j^{t_0}$ according to the formula

$$H_j^0 = H_j^{t_0} e^{-\lambda_j t_0} \text{ where } t_0 = 4.7 \times 10^9 \text{ years}$$

is the age of the Moon. Let us consider four variants of the concentrations of radioactive elements given in table 1. The concentrations of radioactive elements were chosen on the basis of the stationary heat fluxes equal to 1.35 and 0.91 cal cm^{-2} s^{-1} for variants I and I^{++} and correspond to the radio astronomical data by Krotikov and Troitsky (ref. 24) and to the Apollo 15 data (ref. 26) Stationary heat fluxes 0.61 and 0.236 cal cm^{-2} s^{-1} for variants II and III coincide with one of the variants of Levin and Mayeva (ref.8) (II) and are close to concentrations taken by Urey and MacDonald (III). The ratio of thorium to uranium is taken equal to 4 (see ref. 8). The uranium concentration used in variants I, I^{++}, and II is based on the pyrolite lunar composition and the chondrite composition in variant III. The assumption of the pyrolite lunar composition is based on the similarity of the composition of the Moon to the Earth's mantle noted by Anderson (ref. 29) (for example, the mean atomic weight of the Earth's mantle is $\overline{M} = 22.4$, which refers to eruptive rocks and carbonaceous, ordinary, and enstatite chondrites and has the same mean atomic weight as lunar material—22.0).

The assumption of pyrolite lunar composition also is based on the data from Surveyor V and on the papers by McCrea (ref. 30) and Reynolds and Summers (ref. 15). From all these data it follows that the Moon

Rocks:	Granite	Basalt	Eclogite	Peridotite	Dunite	Chondrites
U x 10^{-8}	400	80	4.3	0.6	0.1	1.1
K^{40}/U	1.05	1.13	1.44	1.2	1.2	9

consists of silicates (for example, basalt) similar to those in the Earth's mantle.[1] The above table gives uranium concentrations and the ratio of K^{40} to uranium for different rocks.

From this table and the given stationary fluxes we chose the variants I, I^{++} and II with the content of basalt equal to 14 percent, 10 percent, and 5 percent, respectively; with periodotite equal to 73 percent, 77 percent, and 82 percent, respectively; and iron, 13 percent (ref. 15) with an impoverished content of radioactive elements (iron has U = 0.1×10^{-8} g/g, Th = 0.4×10^{-8}, and K^{40} = 0) and the ratio of K^{40}/U = 1.6, 1.13, and 1 6, respectively (see refs. 9 and 6). Variant III is the chondrite model (Urey and MacDonald). Note that variant II corresponds to variant "C" with the mean content of radioactive elements that of the Earth (see refs. 31 and 6[1]).

As initial conditions we take two variants of the "cold" and the "hot" models for the formation of the Moon with initial temperatures of 273° K and 900° K. These are the same initial conditions taken by Urey, MacDonald, Iriyama, Shimazu, and Fricker[2] based on the different hypothesis of the Moon's origin and the time of its accumulation and initial heating, on which we will not dwell.

The boundary condition ($r = r_o$) is defined by the following relation

$$K\left(\frac{\partial T}{\partial r}\right)_{r=r_o} = \partial T^4 - \mathrm{B}$$

where $B = 0.9 \times 10^{-2}$ cal cm^{-2} s^{-1} considers heating the Moon by solar radiation. On calculation this condition leads to practically the same results as does the more simple condition $T = 273°$ K = const.

THE MECHANISM OF DIFFERENTIATION

The mechanism of differentiation is defined by the function for the distribution of radioactive elements $F(r,t)$ which is given as follows. At first, we considered a homogeneous model for the distribution of radioactive elements, i.e., $F(r,t) = 1$ (analogous to refs. 22 and 23) for the first stage of the calculation. Then, after reaching at the moment t_1, at the point r_1, the temperature corresponding to the beginning of melting $T_{\text{init. melt}}$, the distribution of temperature obtained up to the time $t_2 = t_1 + \Delta t$ (where Δt is the time of melting (see below) is taken as the new initial distribution, and the distribution of radioactive elements is assumed to be layered; namely, radioactive elements from the layer $r_1 \pm \Delta r$ are transferred to the adjacent upper layer ($r_2 \pm \Delta r$) and the calculation is carried out with the depleted layer ($r_1 \pm \Delta r$). However, for the time Δt defined by the necessity of heating the layer by $\Delta T = 200°$ K, deeper layers have reached the melting temperature (since $T_{\text{init. melt.}}$ increases with the depth, i.e., with the decrease of r). Radioactive elements from these layers go to the layer $r_1 \pm \Delta r$, i.e., their content in this layer is equalized and so on, until the lower layers no longer melt. Such layered differentiation (similar to that used by Fricker, Reynolds, and Summers) is defined by five variants that differ in the value n which is the fraction of radioactive elements removed from the layer. We accept $n = 1$ (complete removal), 0.8 (80 percent of the radioactive elements are removed from the layer), 0.6, 0.4, and 0.2. In this way,

[1] It does not necessarily follow that the hypothesis is true for formation of the Moon by fusion from the Earth, since even interstellar material contains grains of refractory silicates (see reference 30).

[1] Running ahead, we note that this variant especially gives the flux corresponding to Apollo 15 data and the radio astronomical data, i.e., evidently, the terrestrial composition of the Moon is rather probable.

[2] Mayeva (ref. 13) used a parabolic temperature distribution with a value at the Moon's centre of 500° K.

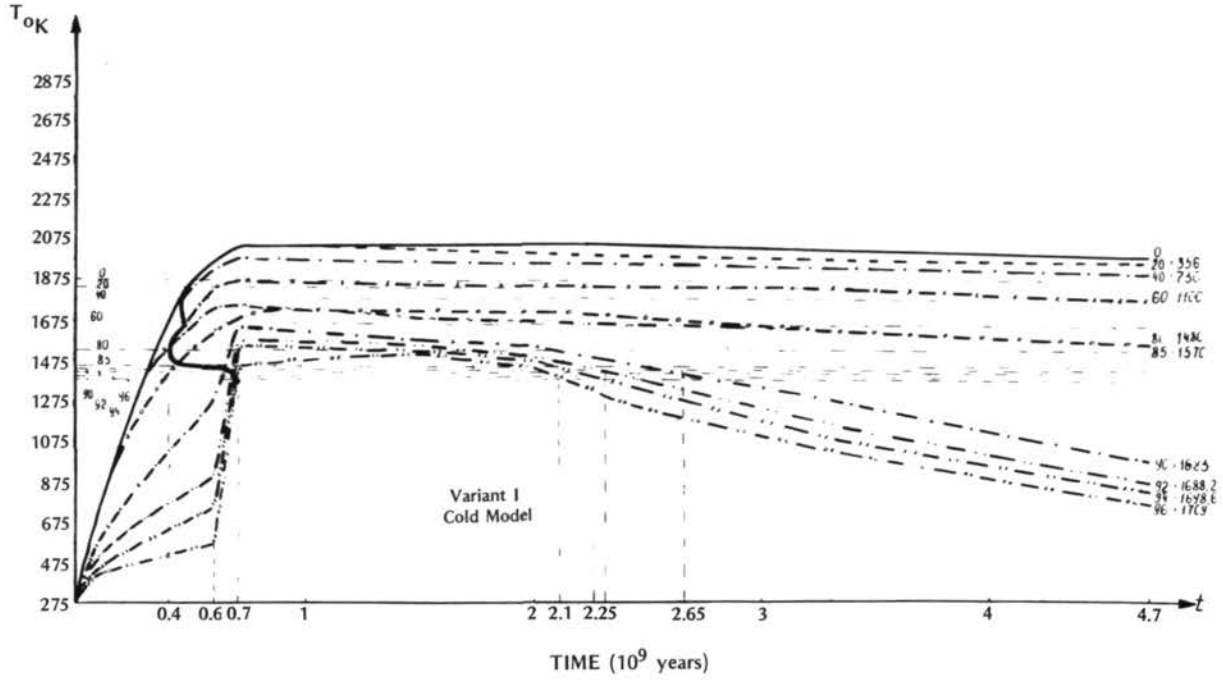


Figure 1.—*The time dependence of temperature in different layers of the Moon for n = 1 (along the radius, starting from the center, O, layer 20 = 356 km, 40,60—96 = 1709 km). The melting temperature corresponding to each layer is shown (dashed lines), as is the time dependence of the start of melting (heavy solid line). The times of initial melting of the Moon, the end of melting of the outer layers, as well as the start of differentiation are shown on the abscissa.*

after differentiation in each of the melted layers, there remains from 0 to 80 percent of the content of radioactive elements in the nondifferentiated material (note that in the latest paper by Mayeva (ref. 13) the residue was from 2 to 20 percent, i.e., $n \geq 0.8$).

The present paper does not consider the possibility of the melted material's penetrating into the external solid layer as was done in the paper by Mayeva (ref. 13), since the concentration of radioactive elements in the thin surficial layer leads, in reality, to more rapid cooling of the Moon and to the greater thickness of the hard crust, as obtained in the model of exponential differentiation considered in detail in references 22 and 23.

The Method of Calculation

For the numerical solution of the heat conductivity equation we use the method of line coordinates where the section $[0,r_o]$, (where $_o$ is the radius of the Moon) is divided into 100 layers and only the differentials in the *spatial* coordinate were replaced by difference relations ratio. Thus the solution of the boundary problem is reduced to a solution of the Cauchy problem for the system of ordinary differential equations. It should be noted that the approximation error is larger, the closer the layer is to the surface. That is why a non-uniform grid is used in the calculation: the layer thickness close to the surface ($\approx$ 5 km) is several times smaller in comparison with the depth layer ($\approx$ 18 km). The system obtained is solved by the approximation method, which provides an accuracy of the temperature calculation (at each step in time) of the order of 10^{-3}. All calculations are made by the computer BESM–6.

Results of Calculation

Results of the calculation are given in figures 1 through 12 and in tables 2 and 3.

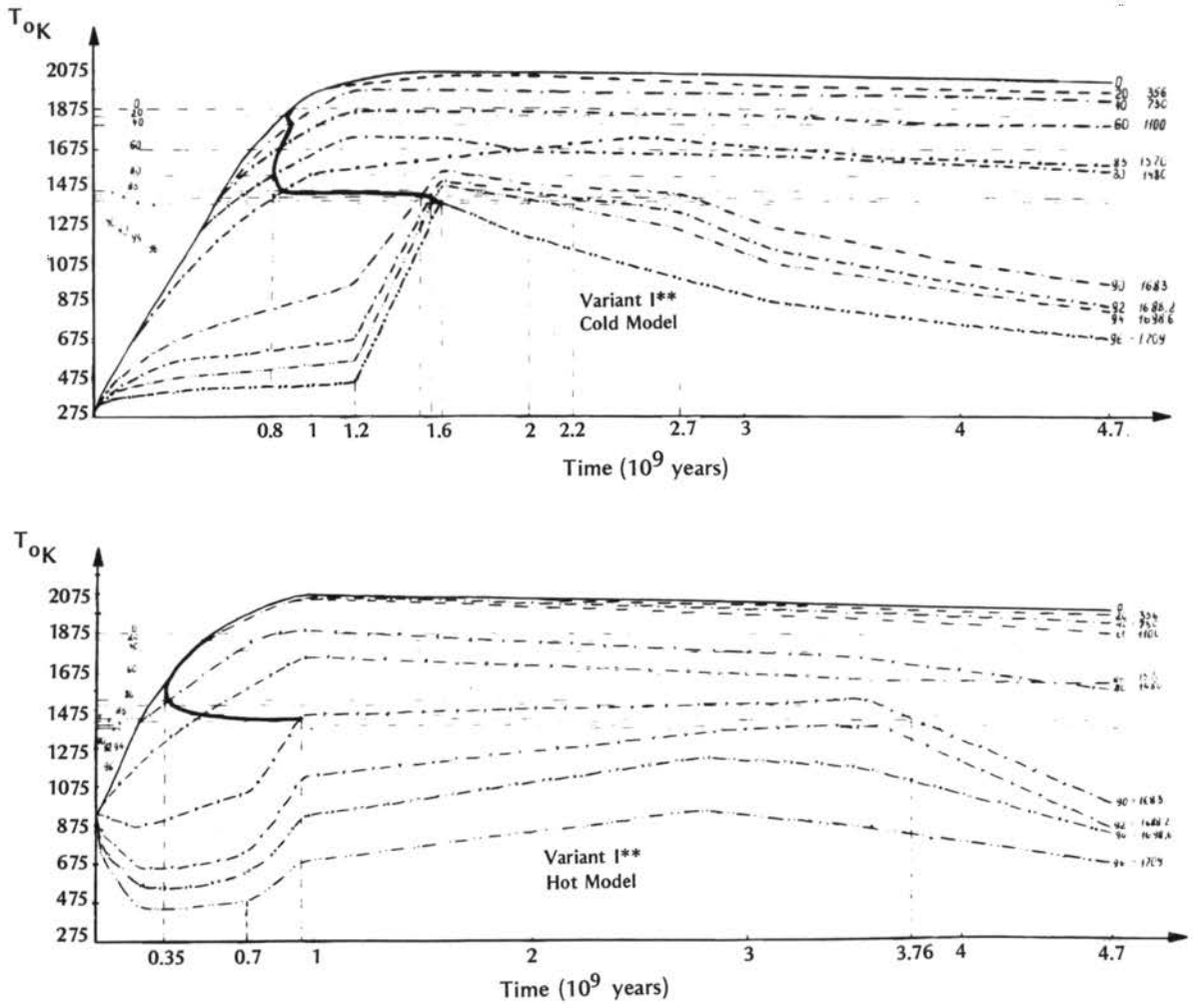


Figure 2.—*The time dependence of temperature in different layers of the Moon.*

THE PROCESS OF MELTING AND DIFFERENTIATION

Figures 1 through 4 show the time dependence of temperature in different layers of the Moon (along the radius beginning from the centre 0) for all variants at $n = 1$. Temperatures at the beginning of melting are plotted for each layer and the time dependence of the beginning of melting in different layers. From figures 1 through 4 it is seen that melting begins in layer 80[1] for all variants, about 1500 km from the center (i.e., at the depth $\approx$ 250 km under the surface) during the period from 0.4 to 1.5 billion years from the beginning of lunar history. Rapidly (in 0.1 to 0.3 billion years) the region of melting propagates to the center and to the Moon's surface. In the layer where melting first begins, differentiation of the material begins after 0.2 to 0.5 billion years. The region of melting at the start of differentiation ($t_{\text{init. dif.}}$) reaches 1600 km; at the same time there is a sharp temperature increase in the layers close to the surface. As a result the temperature in these layers is close to or exceeds $T_{\text{init. melt.}}$. This is understandable since the melted radioactive elements are moved by convection to these layers from deeper layers. The deep layers (at a depth of more

[1] Altogether there are 100 layers.

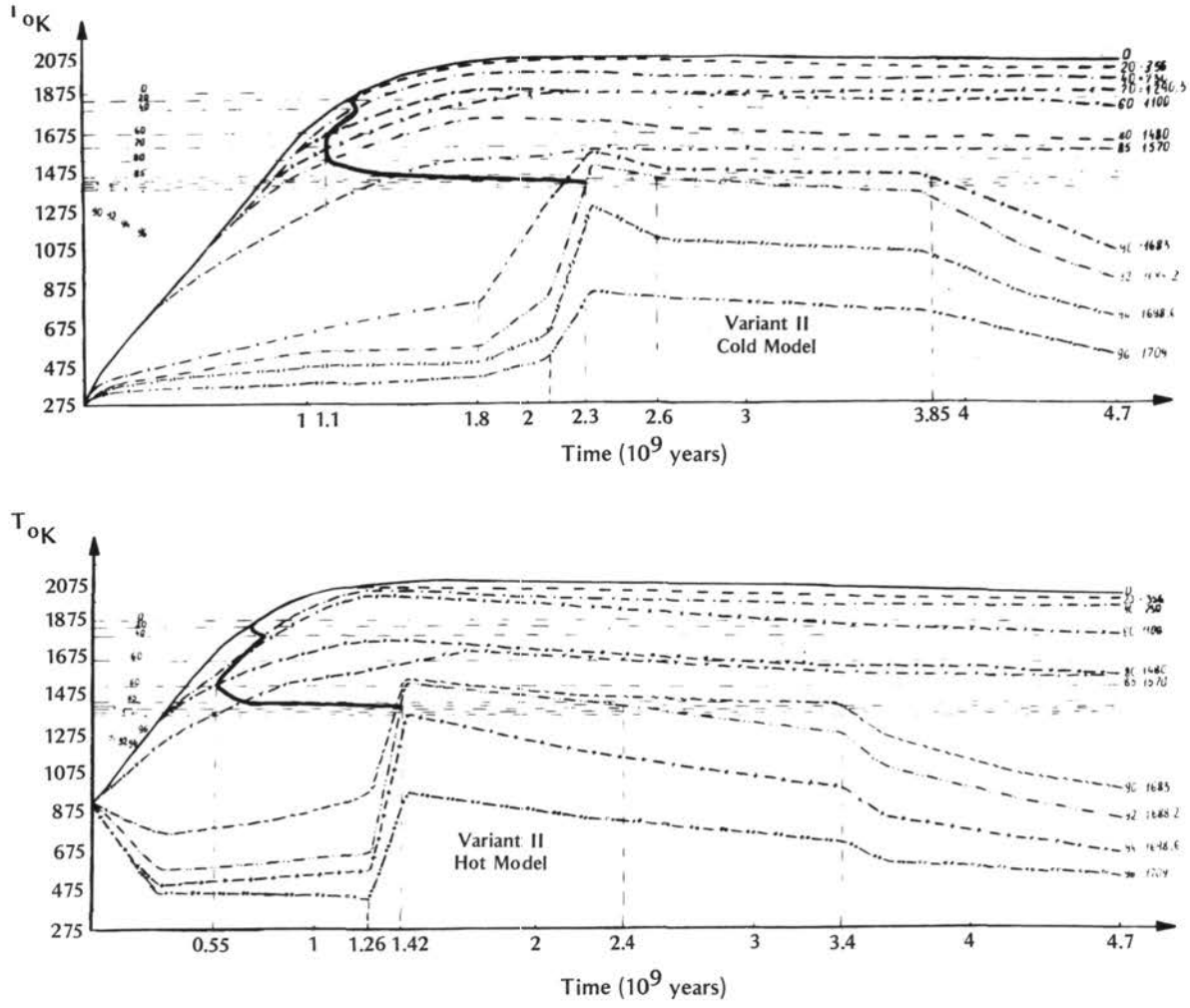


Figure 3.—*The time dependence of temperature in different layers of the Moon.*

than 500–600 km, i.e., r = 1100–1200 km) prior to differentiation have been heated above $T_{\text{init. melt.}}$ and are now slowly cooling due to the convection of radioactive elements to the upper layers[2]. From figures 5 through 7 it is seen that in this way almost simultaneous heating of lunar material occurs up to depths of 200–250 km under the surface. Layers which are closer to the surface heat more slowly and the thickness of these layers increases with time. Numerical data are given in tables 2 and 3.

[2] Differentiation occurs in all variants except for III (cold model), where the energy of radioactive elements is not sufficient for the beginning of differentiation.

THE BEGINNING AND THE DURATION OF THE MAXIMUM MELTING OF THE INTERIOR

Figures 8 through 11 give the time dependence for the radius of melting. From these figures it is seen that in all variants the period of the maximum melting continues for 1 to 2 billion years (depending on the variant —see tables 2 and 3) and begins in the interval from 0.7 to 2.3 billion years from the beginning of lunar history. Naturally, for large concentrations and "hot" models the maximum melting begins earlier than for low concentrations and "cold" models. So for the

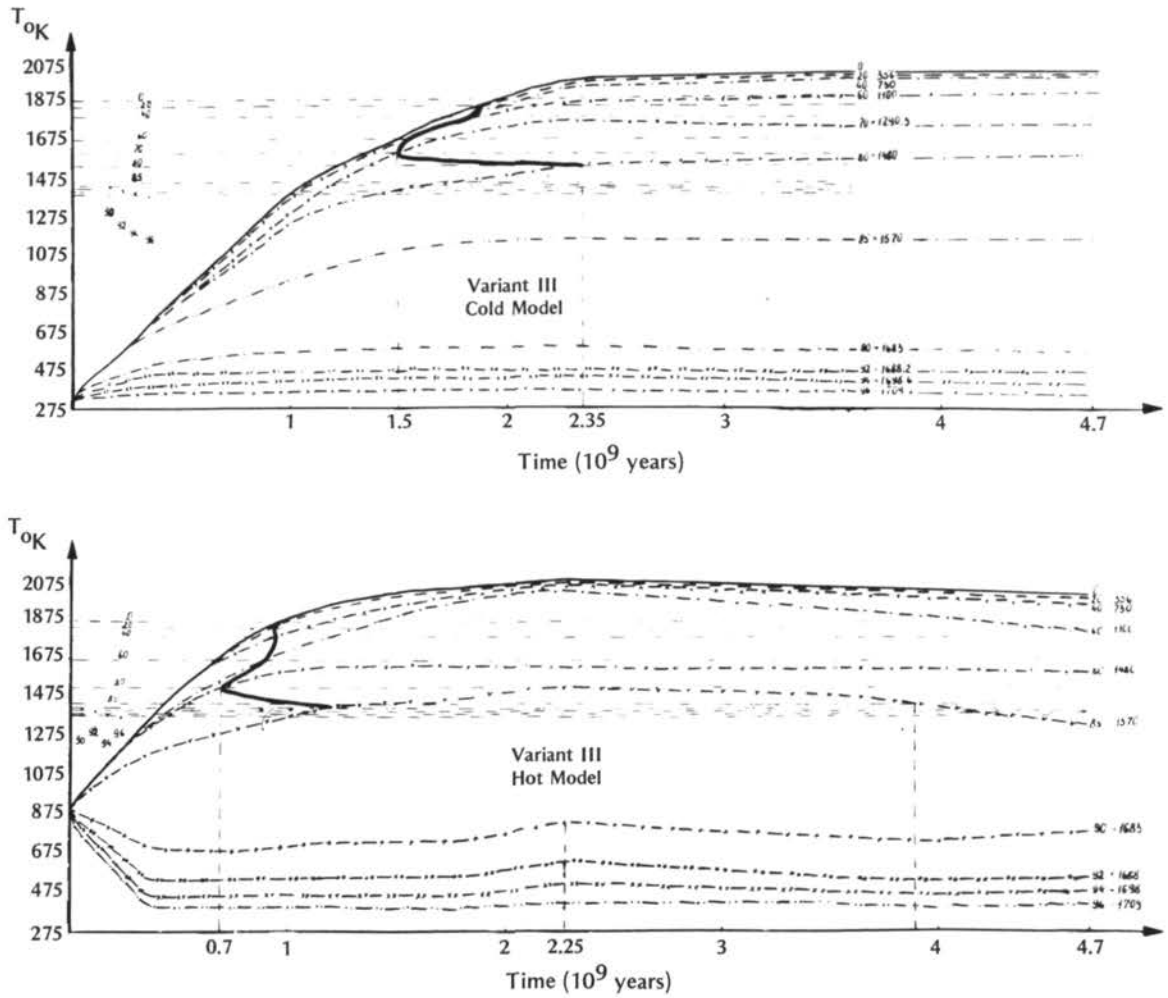


Figure 4.—*The time dependence of temperature in different layers of the Moon.*

variants I and I^{++} the maximum melting begins approximately 3.5 to 4 billion years prior to the present time and continues for 1.5 to 1 billion years. In the case of low (variant III) and intermediate concentrations and large convection ($n \geq 0.8$) of radioactive elements (variant II) the maximum melting begins from 2.5 to 3 billion years prior to the present and continues for 1.5 to 2 billion years, i.e., it begins later and continues longer, as expected[1]). A special case is variant II ("cold" model), which has a low degree of convection of radioactive elements ($n \leq 0.6$). In this case the period of maximum melting begins 2.5 billion years prior to the present and continues to the present time. Here a specific combination of conditions occurs. The concentration of radioactive elements is not so large and the process of differentiation is not so effective that a fast convection of radioactive elements to the surface occurs. Thus their influence on further history is small, but not sufficiently small for the natural cooling of the Moon.

Consequently, in all variants except for the above-mentioned II ($n \leq 0.6$) the Moon is presently cooling.

[1] The smaller the concentration, the more quietly the processes occurred.

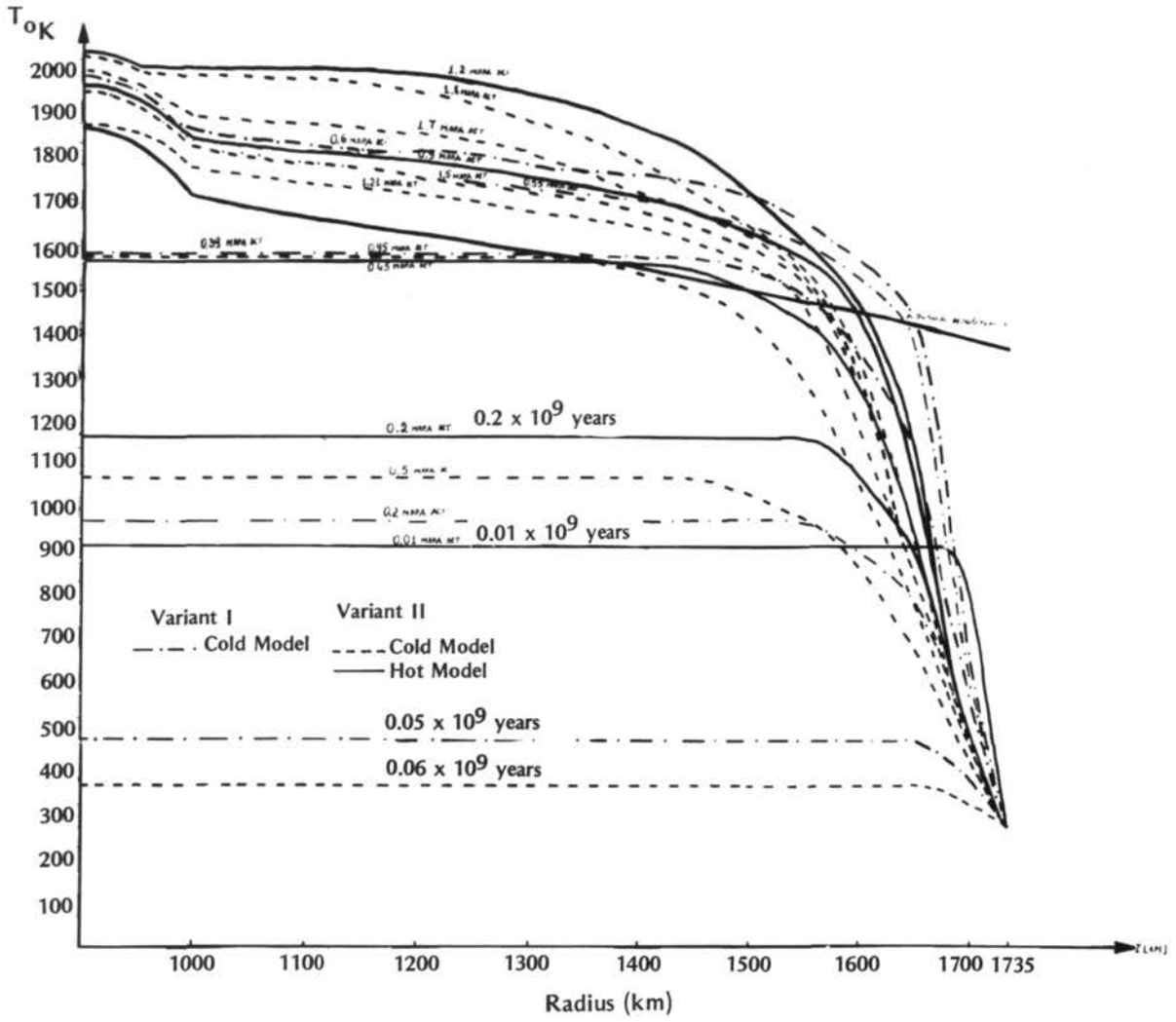


Figure 5.—*The temporal variation of temperature in the lunar interior.*

THE THICKNESS OF THE CRUST

As it is seen from figures 8 through 11 and tables 2 and 3, the thickness of the crust at the period of maximum melting ranges in variants I, I^{++}, II, and III from 15 to 20 km, from 25 to 30 km, from 35 to 45 km, and from 100 to 200 km, respectively; i.e., from 1 to 2.5 billion years ago the Moon was almost completely melted (in variant II with $n \leq 0.6$, the Moon even now should be melted up to the depth of about 45 km under the surface). Then cooling began and presently the crustal thickness in all variants is from 150 to 250 km (except for the above-mentioned "special case"). The same thing follows from figure 12, where the temperature distribution is given in the Moon for the present time.

THE HEAT FLUX THROUGH THE LUNAR SURFACE

Figure 12 gives the time dependence of the heat flux through the lunar surface. From these curves it is seen that at the period of maximum melting of the Moon the flux, as could be expected, is also maximum and ex-

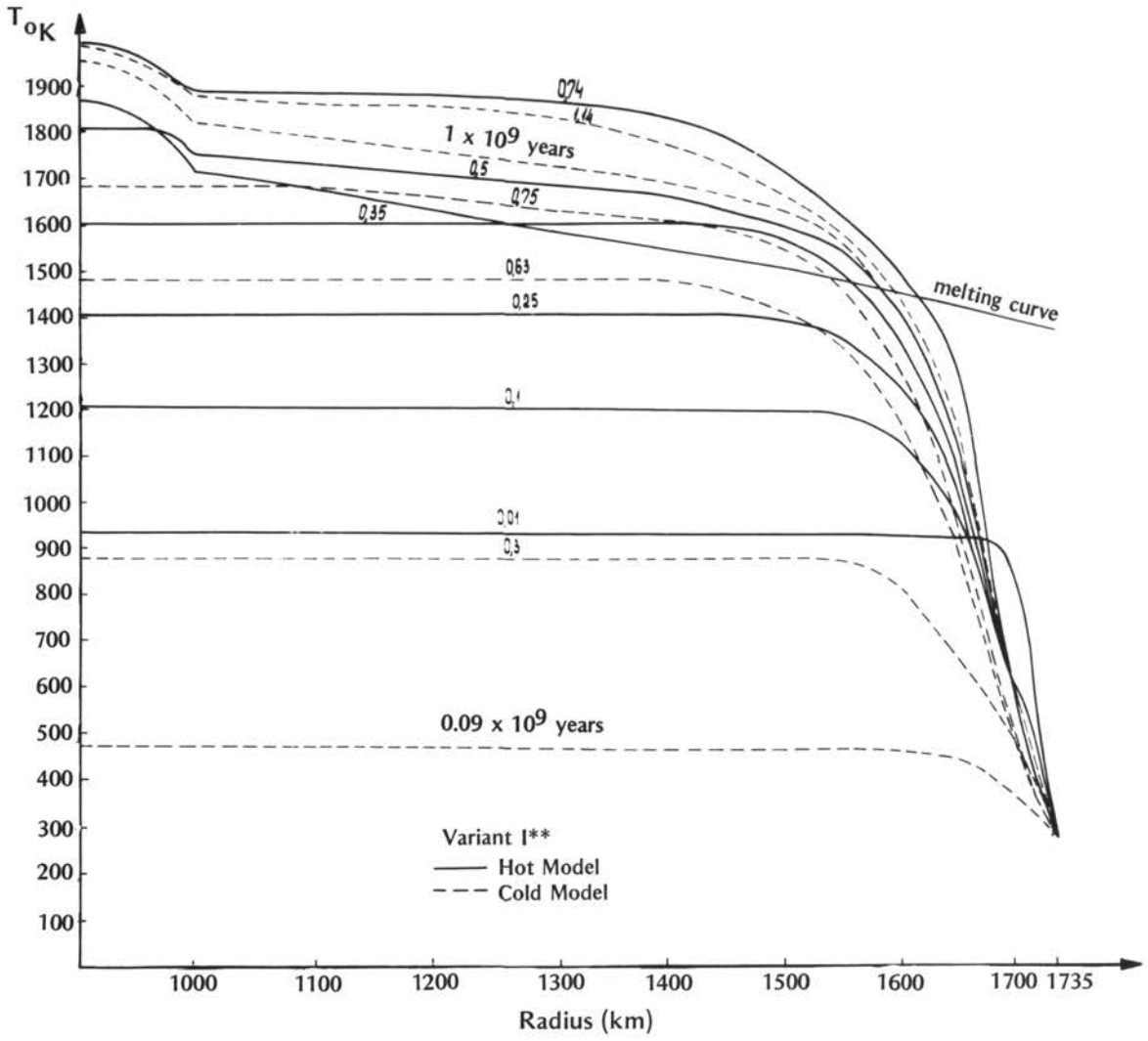


Figure 6.—*The temporal variation of temperature in the lunar interior.*

ceeds 2 to 3 times the stationary value for the given concentration of radioactive elements. At the present time for all variants (except for II with $n \leq 0.6$), the flux is decreasing and is approaching the stationary value $q_{stat.}$, yet even now the flux is nearly 1.5 times $q_{stat.}$. The flux value in variants I, I^{++}, II ($n \geq 0.8$), and III is equal to 1.8×10^{-6} cal cm^{-2} s^{-1}, 1.27×10^{-6} cal cm^{-2}s^{-1}, and 0.9 to 0.95×10^{-6} cal cm^{-2} s^{-1}, respectively. In variant III ("cold" and "hot" models) it is 0.28 and 0.55×10^{-6} cal cm^{-2} s^{-1} and variant II ($n \leq 0.6$) has a rather large flux equal to 1.6×10^{-6} cal cm^{-2} s^{-1}, which is associated with the continuation of melting in this variant up to the depth of 45 km.

Thus fluxes close to those measured by radio astronomical methods and obtained by Apollo 15 are realized in variants I^{++} and II ($n \geq 0.8$), i.e., for the terrestrial or "mantle" pyrolite compositions of lunar material.

Conclusion

Calculations are given for different concentrations of radioactive elements corresponding to a chondritic composition (III), to

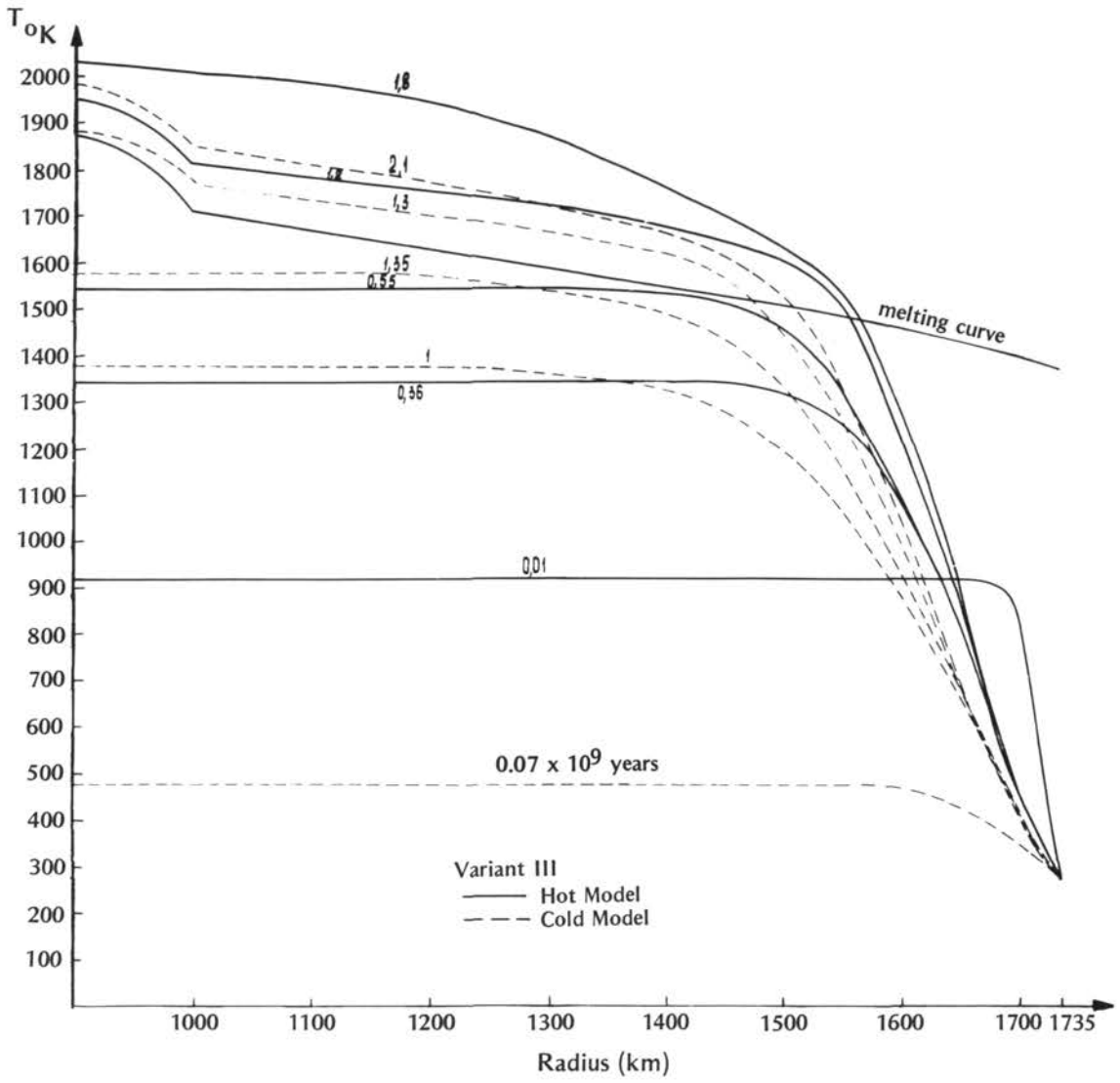


Figure 7.—*The temporal variation of temperature in the lunar interior.*

a terrestrial composition (II), and a terrestrial mantle-pyrolite composition (I and I^{++}). Differentiation of material and the convection of radioactive elements to the surface due to melting are taken into account in the calculation by a scheme similar to that used by Fricker, Reynolds, and Summers. The calculations show that the Moon's interior has been heated to melting during the first 0.7 to 2.3 billion years after its formation. The maximum melting of the Moon covered practically the entire Moon up to a depth of 15 to 45 km below its surface and began from 3.5 to 4 billion years ago, if one assumes a pyrolitic composition of the Moon; or 2.5 to 3 billion years ago, if one assumes a terrestrial or chondritic composition of the Moon. This maximum melting continued for 1 to 2 billion years and at present the Moon is cooling (true, there is an improbable variant of weak differentiation for the "terrestrial" composition of the Moon when melting is

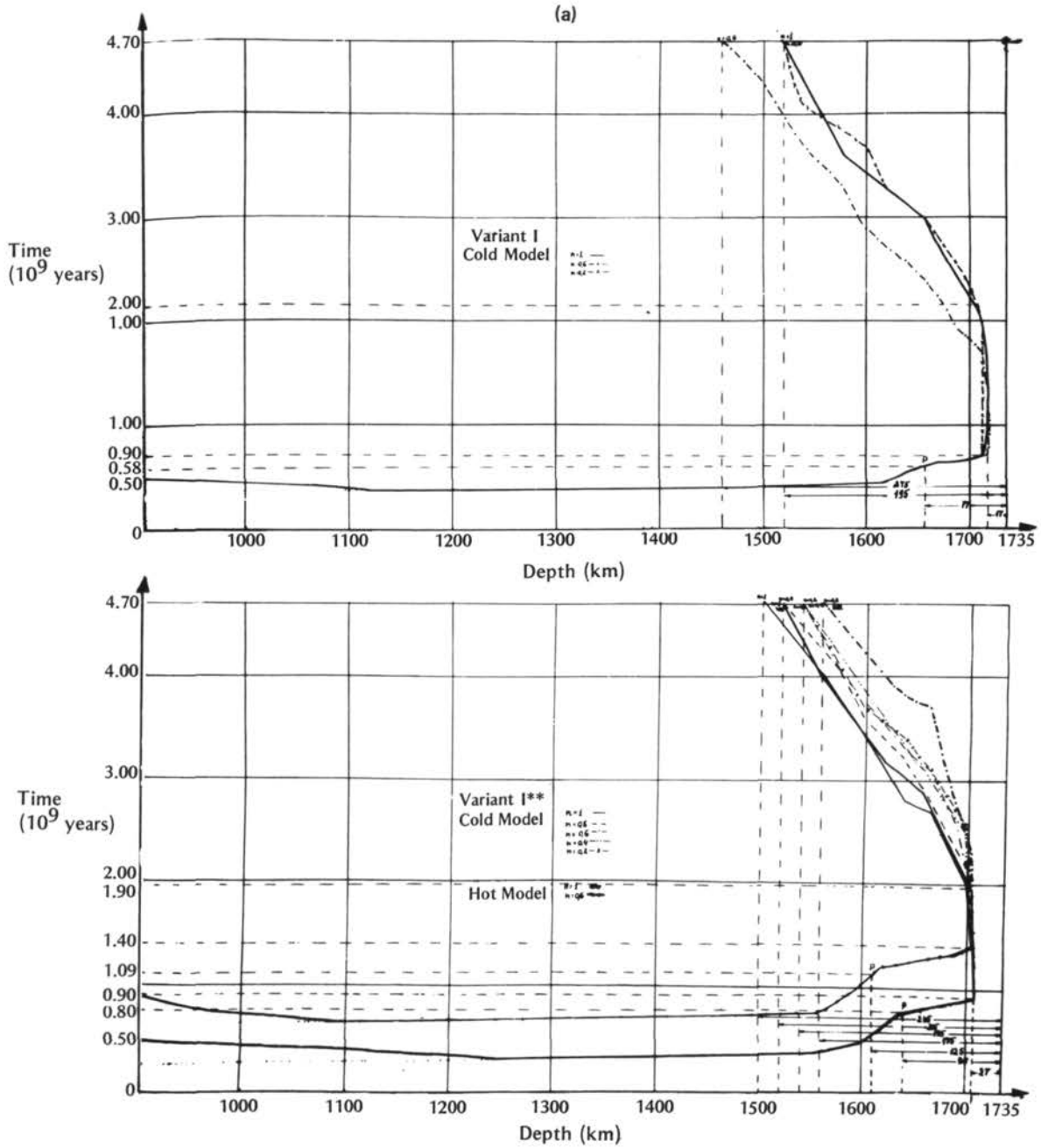


Figure 8.—*The time dependence of the depth of melting for various values of n.*

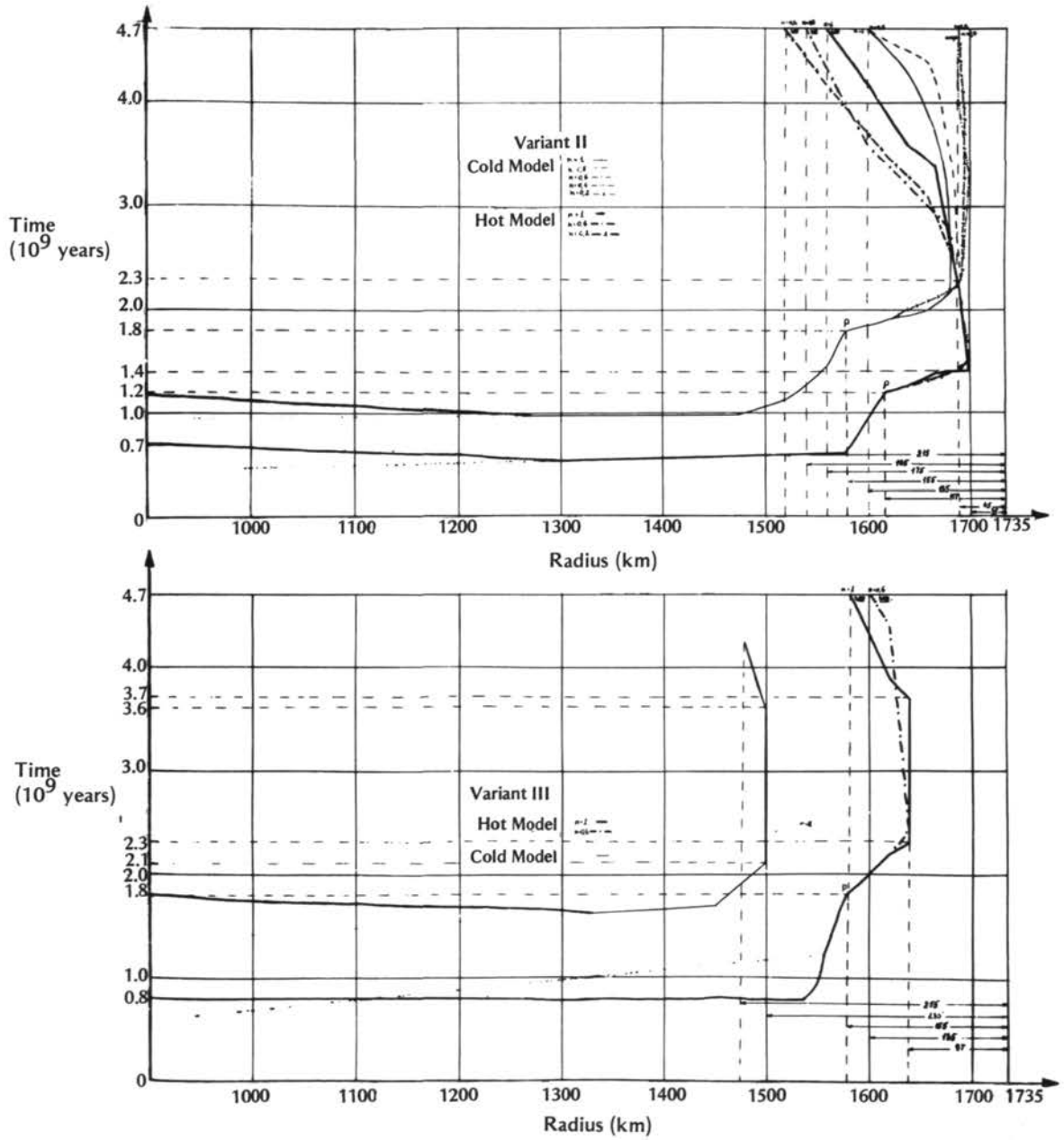


Figure 9.—*The time dependence of the depth of melting for various values of n.*

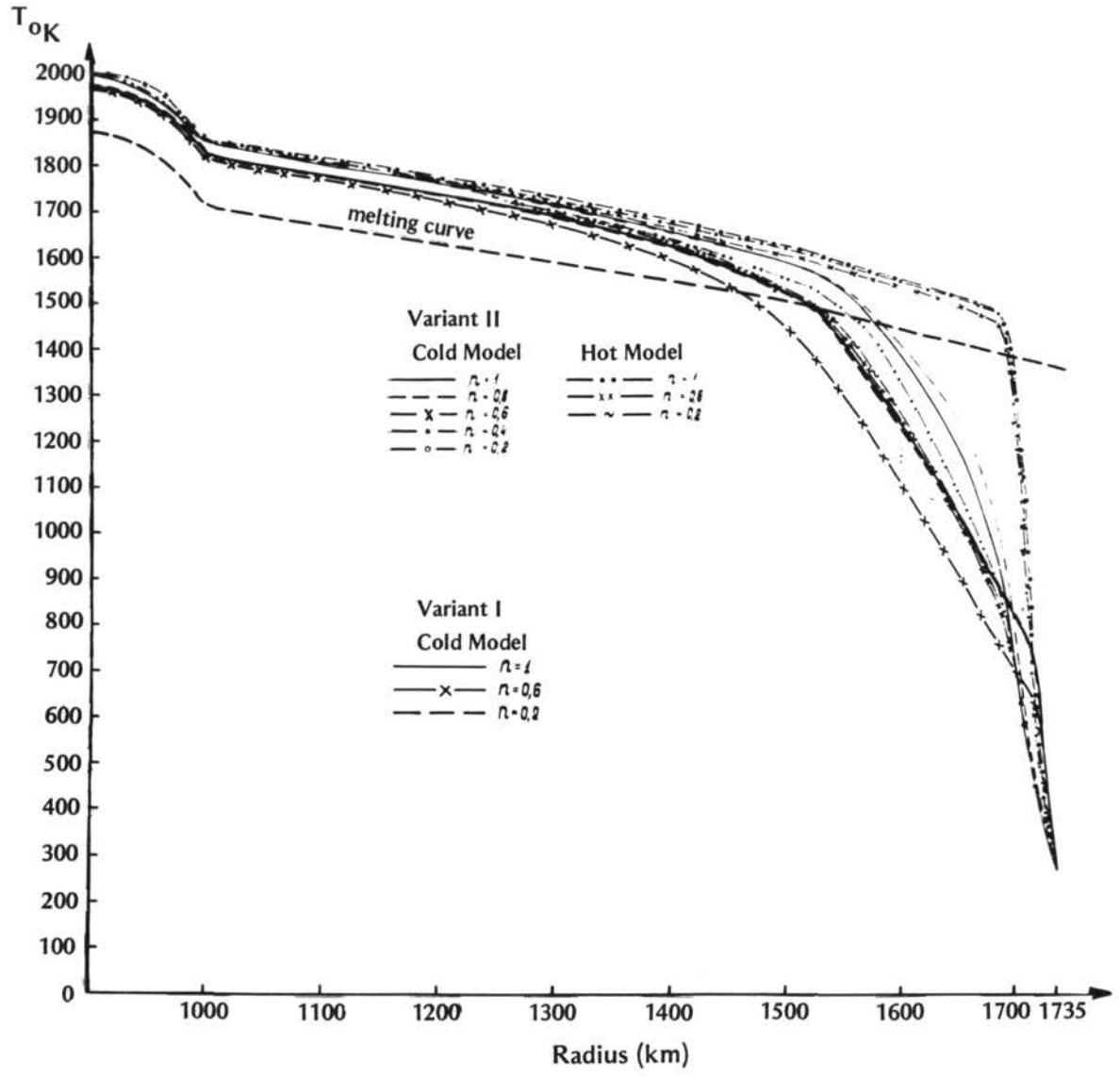


Figure 10.—*The distribution of present temperatures for various values of n.*

occurring even now). The present thickness of the crust is 150 to 250 km and the heat flux exceeds the approximately 1.5 times stationary value. The flux value for variants I, I^{++}, II, and III is equal to 1.8, 1.27, 0.9 to 0.95, and 0.28 to 0.55 $\times$ 10^{-6} cal cm^{-2} s^{-1}, respectively.

From tables 2 and 3 it follows that in the most probable variants with the pyrolite-"mantle" (I^{++}) and terrestrial (II) composition of the initially "hot" Moon, the maximum melting of the Moon began 3.3 to 3.8 billion years ago, which corresponds to the age of mare basalts and mascons (3.16 to 3.71 billion years). These data testify to the volcanic activity that was completed aproximately 2.7 to 3 billion years ago—evidence in agreement with the absence of lunar samples younger than 3 billion years (refs. 32, 33, and 34), when the activity stopped. Thus, limitations stated recently by Toksöz and Solomon (ref. 21) are satisfied, yet the thick-

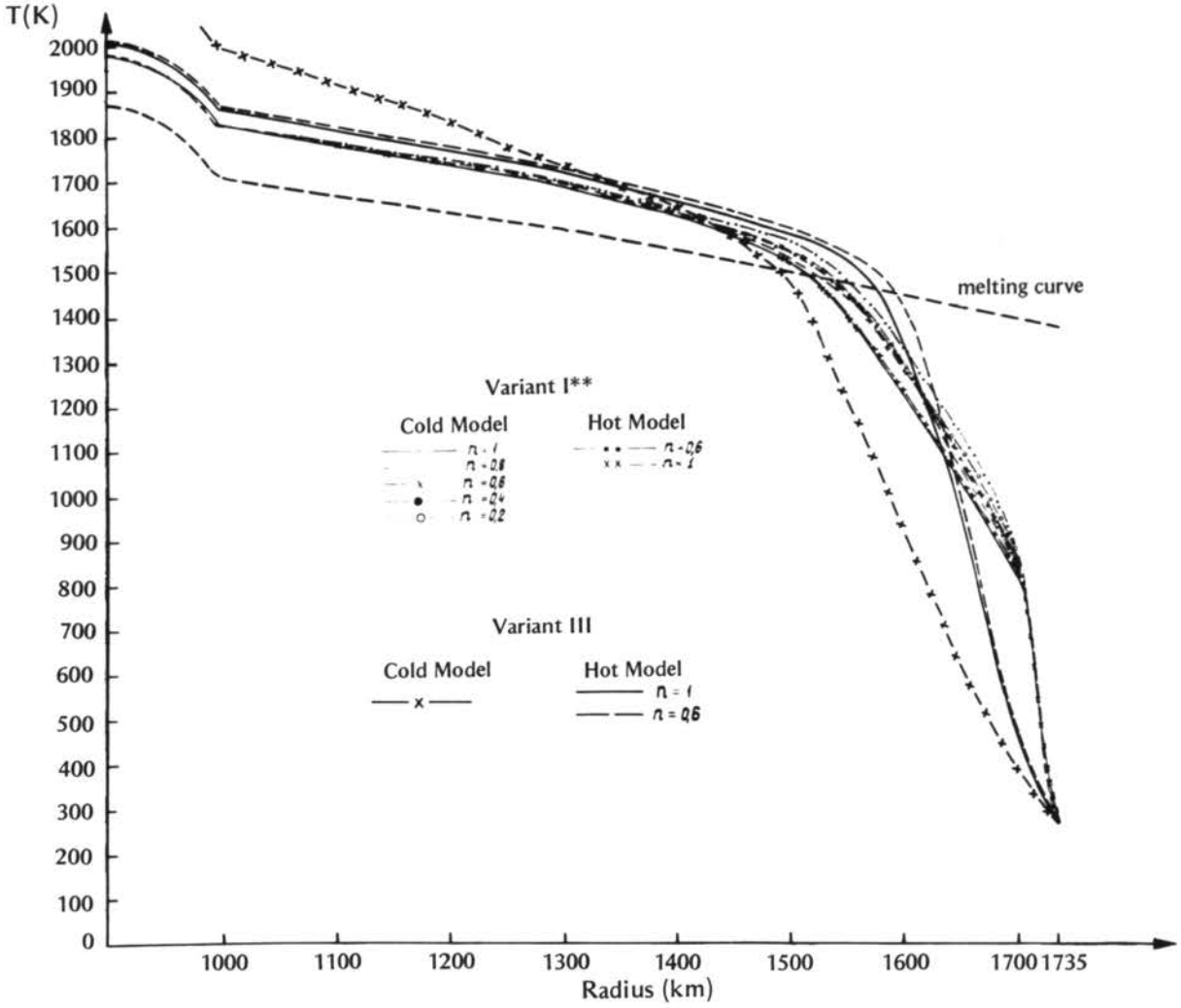


Figure 11.—*The distribution of present temperatures in the Moon as a function of n.*

ness of the crust obtained by our calculations is essentially small (ref. 21)—a crust 600 km thick.

It should be noted that the most realistic variant uses a "terrestrial" composition for the Moon (composition "C" according to Starkova), which gives, in spite of its moderate concentration of radioactive elements, a sufficiently large heat flux[1] that corresponds to the radio astronomical measurements and Apollo 15 data, i.e., to obtain the large observed flux it is not necessary to have high concentrations of radioactive elements.

[1] This possibility was noted by Lubimova in reference 6.

Acknowledgment

The authors are grateful to Professor V. S. Troitsky and Professor N. M. Tseitlin for their interest in the present paper and for useful discussions. Gratitude also is expressed to M. V. Ostrovskaya for help in the construction of numerous graphs.

References

1. UREY, H. C., *Geochimica et Cosmochimica Acta*, Vol. I, 1951, p. 209.
2. UREY, H. C., *Proc. Natl. Acad. Sci. U.S.*, Vol. 41,

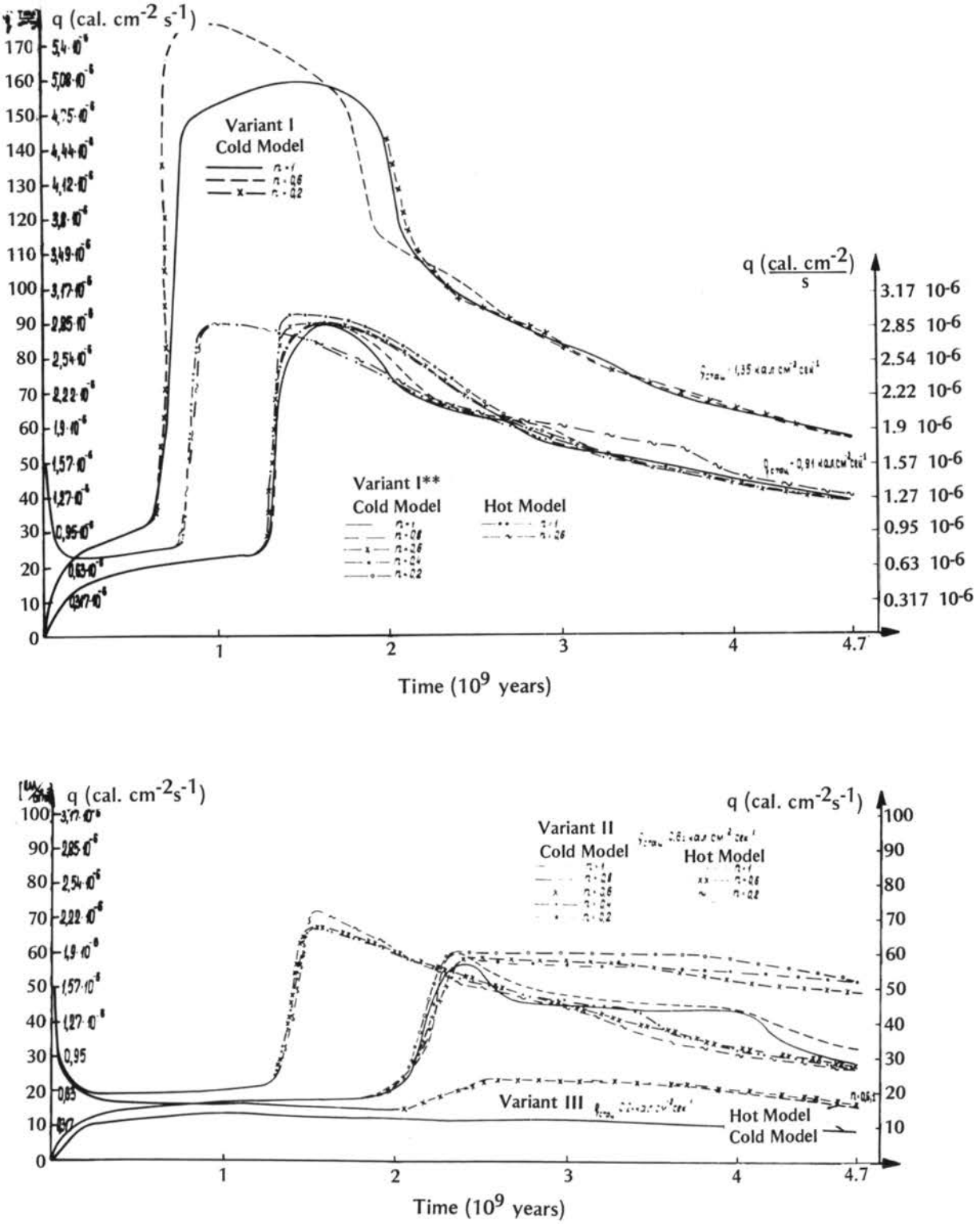


Figure 12.—*The time dependence of heat flow through the lunar surface.*

Table 2.—*Some Thermal Parameters and Calculated Results for the Various Thermal Model Variants*

Variant	n	Flux q 10^{-6} cal cm^{-2} s^{-1}			Time t Billion Years			Distance r km				
										solidification		
		q_{stat}	q_{max}	q_o	$t_{init\ melt}$ / $t_{init\ diff}$	$t_{max\ melting}$	$t_{max\ q}$	$r_{init\ mel\ diff}$ / $r_{mel\ init\ diff}$	$r_{max\ melting}$	r^ohard	$r_{h\ min}$	r crust
I Cold Model	I	1.35	5	1.8	(0.4) / 0.6	0.7–2.2	0.8–2	1500 / 1600	1720	1540	15–20	195
	0.6		5.5			0.7–1.8	0.7–1.8		1715	1460		275
	0.2					0.7–2.2	0.8–2			1540		195
I^{++} Cold Model	I	0.91	2.85	1.27	(0.85) / 1.15	1.4–2	1.4–2	1500 / 1610	1710	1500	25–30	235
	0.8									1520		215
	0.6								1705	1540		195
	0.4									1540		195
	0.2									1540		195
I^{++} Hot Model	I	0.91	2.85	1.27	(0.35) / 0.8	0.9–2	0.9–1.5	1500 / 1640	1710	1520	25–30	215
	0.6								1705	1560		175
II Cold Model	I	0.61	1.85	0.95	1.2	2.3–3.5	2.3–2.6	1500 / 1580	1695	1600	40–45	135
	0.8					2.3–3.5	2.3–2.6			1600		135
	0.6				1.8	2.3–4.7	2.3–4.7		1690	1690		45
	0.4			1.6		2.3–4.7	2.3–4.7			1690		45
	0.2					2.3–4.7	2.3–4.7			1690		45
II Hot Model	I	0.61	2.1	0.88	0.55 / 1.2	1.4–2.5	1.5–2	1500 / 1620	1700	1560	35–40	175
	0.6								1695	1540		195
	0.2									1520		215
III Exponential Model		0.236	0.41	0.28	1.55	2.1–3.6		1300	1500	1480	235	255
III Hot Model	I	0.236	0.73	0.55	(0.7) / 1.8	2.3–3.7	2.5–3.7	1500 / 1580	1635	1580	95–100	155
	0.6									1600		135

Table 3.—*Calculated Results for Various Thermal Model Variants*

Variant	(cal cm^{-2} sec^{-1}) 10^{-6}			$t_{init\ dif}$ Billion Years	t_{max} mel flux Billion years	r melt init dif (1) (km)	Δr crust min (km)	Δr^o crust (km)
	q_{stat}	q_{max}	q_o					
I	1.35	5.5	1.8	0.6 (0.4)	0.7–2	1660	15–20	200–250
I^{++}	0.91	2.85	1.27	0.8 (0.5)	1 –2	1630	25–30	180–220
			Cold $n \geq 0.8$ Hot		Cold $n \geq 0.8$ Hot			Cold $n \geq 0.8$ 135
II	0.61	2	0.9–0.95 Cold $n < 0.8$ 1.6	1.5 (0.9)	1.5–2+ 2.5–3.5	1600	35–45	Hot 200 Cold $n < 0.8$
					Cold $n < 0.8$ 2.3 + 4.7			45
III	0.24	cold hot 0.4 – 0.7	cold hot 0.28 – 0.55	hot 1.8 (1.1)	2.3–3.7	hot 1600	cold hot 235 100	hot cold 250 150

Note: (1) $r_{init\ melt}$ and $r_{init\ diff}$ = 1500 km.

1955, p. 127.
3. UREY, H. C., *Physics and Astronomy of the Moon*, 1962, p. 481.
4. MACDONALD, G. J. F., *J. Geophys. Res.*, Vol. 64, 1959, p. 1967.
5. MACDONALD, G. J. F., *Space Sci. Rev.*, Vol. 2, 1965, p. 473.
6. LUBIMOVA, E. A., *Termica of the Earth and the Moon*, 1968.
7. LEVIN, B. YU., AND E. A. LUBIMOVA, *Nature*, No. 10, 1955, p. 81.
8. LEVIN, B. YU., AND S. V. MAYEVA, *DAN SSSR*, Vol. 133, 1960, p. 44.
9. LEVIN, B. YU., New About the Moon. *AC SSSR*, 1963, p. 118.
10. LEVIN, B. YU., *Vulcanism and the Denth Construction of the Earth*, 1966.
11. MAYEVA, S. V., *DAN SSSR*, Vol. 159, 1694, p. 2,
12. MAYEVA, S. V., *Izv Commission on Physics of Planets*, No. 5, 1965.
13. MAYEVA, S. V. *Physics of the Earth, Izv As SSSR*, No. 3, 1971, p. 3.
14. FRICKER, P. E., R. T. REYNOLDS, AND A. L. SUMMERS, *J. Geophys. Res.*, Vol. 72, 1967, p. 2649.
15. REYNOLDS, R. T., AND A. L. SUMMERS, *J. Geophys. Res.* Vol. 74, No. 10, 1969, p. 2494.
16. IRIYAMA, J., AND I. SHIMAZU, *Icarus*, Vol. 6, 1967, p. 3.
17. ANDERSON, D. L., AND R. A. PHINNEY, Mantles of the Earth and Terrestrial Planets. *Interscience*, 1967, p. 113, and Amer. Astron. Soc. Pub., *Phys. Moon*, 1967, pp. 161–179.
18. HANKS, T. S., AND D. L. ANDERSON, *Phys. Earth Planet. Interiors*, Vol. 2, 1969, p. 19, and *Phys. Earth Planet. Interiors*, Vol. 5, 1972, p. 409.
19. ANDERSON, D. L., AND T. C. HANKS, *Science*, Vol. 3, 178, 1973, p. 1245.
20. MACCONNEL, R. K., L. A. MACCLAINS, D. W. LEE, J. R. ARONSON, AND R. V. ALLEN, *Rev. Geophys.*, Vol. 2, 1967, p. 12.
21. TOKSÖZ, M. N., AND S. C. SOLOMON, *The Moon*, Vol. 7, Nos. 3 and 4, 1973.
22. ORNATSKAYA, O. I., AND YA. I. AL'BER, *Izv. V Radiofizika*, Vol. 9, No. 3, 1965.
23. ORNATSKAYA, O. I., AND YA. I. AL'BER, *Astron. Zhurn.*, Vol. 44, No. 1, 1967, p. 158.
24. KROTIKOV, V. D., AND V. S. TROITSKY, *UFN*, Vol. 31, 1962, p. 4.
25. TROITSKY, V. S., *Izv. VUZ. Radiofizika*, Vol. 10, No. 8, 1967.
26. LANGSETH, M. G., S. P. CLARK, J. L. CHUTE, S. J. KEIHM, AND A. E. WECHSLER, *The Moon*, Vol. 4, 1972, p. 390.
27. TIKHONOV, A. N., E. A. LUMBIMOVA, AND VLASOV, *DAN SSSR*, Vol. 188, No. 2, 1969.
28. RINGWOOD, A. E., *Advances in Earth Science*, 1966, pp. 237–356.
29. ANDERSON, D. L., *Applied Optics*, Vol. 8, No. 7, 1969, p. 1271.
30. MCCREA, W. B., *Nature*, Vol. 223, No. 5203, 1969, p. 1271.
31. STARKOVA, A. G., *Meteoritics*, p. 13–19.
32. PAPANASTASSIOU, D. A., AND G. J. WASSERBURG, *Earth Planet. Sci. Letters*, Vol. II, p. 37, and Vol. 12, p. 36, 1971.
33. PAPANASTASSIOU, D. A., AND G. J. WASSERBURG, *Earth Planet. Sci. Letters*, Vol. 16, 1972, p. 289.
34. WASSERBURG, G. J., AND D A. PAPANASTASSIOU, *Earth Planet. Sci. Letters*, Vol. 13, 1971, p. 97.

Riddles About the Origin and Thermal History of the Moon

B. Yu. Levin and S. V. Mayeva
O. Yu. Schmidt Institute of Earth Physics
Academy of Sciences,
Moscow, U.S.S.R.

Analyses of lunar rocks have confirmed that the interior of the Moon has been subjected to magmatic differentiation, as has been determined by calculation of the thermal history of the Moon. However, it appears that differentiation occurred so early that it could not have been related to heating by long-lived radioactive elements, but rather indicates a high initial temperature of the Moon. The reasons for the high initial temperature remain unknown. The presence of a central, partially melted area revealed by seismic observations forces us to reject convective models of the Moon, while the dimensions of this area, together with the measured heat fluxes from the interior, serve as "boundary conditions" for any new calculations of the thermal history for a two-layered differentiated model of the Moon operative over the past 3.5 billion years. If we start with the early differentiation of the Moon and the high content of long-lived radioactive elements in it, explanation of its current thermal properties represents no difficulty. But these prerequisites themselves remain unexplained.

Due to the continuing controversy concerning the true nature of the process of magmatic differentiation of the Moon, estimation of the composition of the entire Moon on the basis of analyses of surface rock remains unreliable, and use of these estimates to clarify the origin of the Moon is premature. Existing hypotheses concerning the origin of the Moon encounter dynamic difficulties, as well as difficulties with explanation of the high initial temperature, to say nothing of the difficulty involved in explaining the proposed differences in the composition of the Earth and Moon.

New data on the Moon produced by its direct investigation have confirmed some important conclusions drawn earlier on the basis of thermal history (ref. 1) calculations. In particular, they have confirmed that the Moon has undergone magmatic differentiation and that even at present its interior is partially melted.

However, direct investigations have also led to several very important changes in earlier concepts about the evolution of the Moon. Some of these changes have generated new difficulties for hypotheses about the origin of the Moon, whereas the influence of the rest depends on the results of discussions concerning their interpretation. It is not yet possible to propose a new scheme of the origin and evolution of the Moon that considers all the new data and agrees with our concepts of the origin of the other members of the solar system. It is in this much broader area, the overall area of planetary cosmogony, that the current situation is most unclear and contradictory.

New Data About the Moon and Earlier Calculations of its Thermal History

THE HIGH INITIAL TEMPERATURE OF THE MOON

The petrological and chemical composition of the lunar samples returned to Earth has

confirmed that the Moon underwent partial melting and magmatic differentiation. However, measurement of the ages of lunar samples has shown that the differentiation did not occur 2 to 3 b.y. ago, as was obtained by calculations of the thermal history of an initially cold Moon with chondritic radioactivity (refs. 2 through 10), but significantly earlier —possibly even during the formation of the Moon. Such early magmatic differentiation requires a high initial temperature of the Moon or very rapid heating immediately after formation. This is a new and very difficult "boundary condition" that must be considered by any hypothesis of the origin of the Moon.

About 3 years ago, when the great thickness of the lunar crust was still unknown, it seemed necessary to assume not only a high initial temperature of the Moon, but also a very surprising radial temperature distribution with a maximum near the surface. This last assumption was related to the fact that the anorthositic lunar crust was formed simultaneously or nearly simultaneously with the formation of the entire Moon, while the maria basalts flowed out about a billion years later. The idea developed that the crust was formed as a result of differentiation of the outer few hundred kilometers, which were initially heated, whereas the basalts were separated from deeper areas, which were initially colder and only later were heated by radiogenic heat. Attempts were made to explain this temperature distribution by the liberation of gravitational energy during accumulation (ref. 11). The released gravitational energy, i.e., the energy per unit of falling mass, does increase as an accumulating body grows. But, in order that the energy released on the surface will not be lost to space but will heat the Moon, unacceptably rapid accretion is required. According to the calculations of Mizutani et al. (ref. 12), Toksöz et al. (refs. 13 and 14), and Toksöz and Solomon (ref. 15), the accumulation could not have lasted more than a few hundred years. Although these calculations were made for highly artificial models of the process of accumulation, they can be considered as satisfactory estimates of the order of magnitude of the duration of accumulation necessary to heat the Moon due to gravitational energy.

When seismic observations showed that the thickness of the lunar crust is about 65 km (refs. 16 and 14), the proponents of the idea of its formation as a result of differentiation of the outer layers of the Moon alone were forced to come up with the additional hypothesis that these layers were from the very beginning rich in calcium and aluminum minerals, i.e., to set forth the hypothesis of heterogeneous accumulation of the Moon. In this case, as noted by Wood (ref. 17), why should the lower temperature condensates accumulate first, followed by material rich in calcium and aluminum which should have condensed earlier?

Many researchers preferred another model. In it, the composition of the Moon is assumed to have been initially homogeneous, and the crust is considered to be a product of primary differentiation of all or almost all of the Moon, whereas the maria basalts are considered a product of later differentiation of the matter that remained deep in the Moon after separation of the crust. In recent years, petrographic and chemical data have accumulated in favor of this second point of view as against the hypotheses of heterogeneous accumulation. They are summarized and literature references given in the article of Brett (ref. 18).

If the lunar crust arose as a result of differentiation of all or almost all of an initially homogeneous Moon, one escapes the requirement of the surprising initial distribution of temperature with its maximum near the surface. Perhaps a high initial temperature for the entire lunar interior would be sufficient. Some calculations of Mayeva for this initial temperature are presented in an article by Levin (ref. 1). However, in any case the explanation of the high initial temperature of the Moon encounters difficulties that are discussed in this same article. Levin has discarded the possibility of heating of the Moon by aluminum 26 or by an intensive solar wind possibly emitted by the young

Sun, as well as the possibility of accumulation of the Moon from hot particles (before the cooling of the protoplanetary cloud). He prefers heating by gravitational energy during accumulation and heating by tidal deformations, although both of these possibilities also encounter significant difficulties.

It should be recalled that the source of energy for early heating is a problem not only for the Moon, but also for the asteroids, which are the parent bodies of the meteorites (ref. 19). Neither heating by the gravitational energy liberated upon accumulation nor heating by tidal deformations can be utilized to explain the heating of the asteroids. We must consider here not only the heating of the interiors of asteriods to approximately 800 to 1000°C as required to explain the thermal metamorphism of the meteorites, but also the melting required to explain the presumed basalt cover of Vesta (ref. 20) and the lava flows on the surface of the parent asteroid of the Ibitira meteorite, which consists of vesicular basalt (ref. 21).

Quite recently, the surface of Mercury was photographed from closeup. These photographs, produced and transmitted to earth by Mariner 10, showed that there are solidified lava flows on the surface of Mercury[1]. It shows that magmatic differentiation occurred on Mercury, which does not agree with the model of the thermal history of this planet calculated a few years ago by Mayeva (ref. 22). Although the Mayeva model assumed a high initial temperature of Mercury, namely 1000 K, it was found that the interior of the planet, according to this model, was never heated to the melting point. Judging from the photographs of Mercury, the lava flows apparently were already occurring during the era of intensive bombardment and cratering. In this case, the initial temperature of Mercury was apparently even higher than was assumed in the model of Mayeva. A high content of radioactive elements (Mayeva assumed chondritic composition for the rocky portion of the matter) would produce melting of the interior of the planet too late, i.e., after the end of intensive cratering. Thus, the question of early heating applies to Mercury as well as to the Moon and the asteroids.

If we seek a single explanation of the early heating of the Moon and the asteroids, we must turn to the same three possibilities that were rejected by Levin (ref. 1) or seek some principally new path, which is presently escaping attention.

Among the possibilities rejected by Levin, the most promising means for heating the Moon and asteroids is heating by short-lived radioactive isotopes. Although the idea that heating by aluminum 26 played an important role during the time of formation of the solar system has now been rejected (refs. 23 and 24), there are continued attempts to confirm the past existence or superheavy radioactive isotopes in the "island of stability" near atomic number Z = 114 (refs. 25, 26, and 27). However, in order to heat small bodies, the half life of these isotopes would have to be on the order of 10^6 yr, and, at the same time, their initial abundance would have to be just enough to allow them to exist, in quantities sufficient for heating, for more than 10 half-life periods, i.e., more than 10^7 yr after their nucleosynthesis. (The so-called "formation interval," i.e., the interval of time between the last explosion of a supernova star, which added fresh nucleosynthesis products to the matter of the future solar system, and the beginning of retention of radiogenic isotopes is about 10^8 yr.) Thus, by the time of formation of the Moon and the asteroids, the radioactive isotopes capable of heating them should have almost completely decayed if they were formed during the supernova explosion just mentioned. At the same time, it is difficult to imagine that they could have formed as a result of nuclear reactions in the interstellar nebula.

A similar difficulty arises in attempts to attribute the heating to an intensive solar wind because the characteristic time of attenuation of the latter is on the order of 10^7 yr. Furthermore, induction of sufficiently strong electric currents in the Moon and the asteroids would require that their substance

[1] See the report of B. Murray et al., at this conference.

be initially heated to approximately 500°C in order to provide sufficient conductivity. Thus, yet another source of energy is needed. Doubling of this unknown "initial" heating is sufficient to entirely eliminate heating by the solar wind.

THE PRESENT PARTIALLY MELTED STATE OF THE CENTRAL PART OF THE MOON

Seismic studies of the Moon have shown that at the present time it has a partially molten central area, as was indicated earlier by most calculations of the thermal history for conductive models (ref. 2 through 10 and 28). These calculations give widely varying thicknesses of the outer solid layer for different models: from 120 km to a completely solid Moon. In the models that seemed most probable 10 to 15 years ago, the thickness of the solid layer was 500 to 700 km (refs. 2, 3, 6, 7, and 28), but later, after the presumed thermal conductivity of the interior of the Moon was halved (0.005 in place of 0.01), this thickness changed to 200 to 400 km (refs. 1 and 8). Seismic observations have shown that the thickness of the outer solid layer is about 1000 km (ref. 16), i.e., at present only about 20 percent of the volume of the Moon is partially molten.

This direct determination of the partially melted state of the central area of the Moon has great significance, since it confirms the correctness of using conductive models in calculating its thermal history. In convective models, which consider stable thermal convective models, which consider stable themal convection in solid matter, it is found that the interior of the Moon should be solid right to its center (refs. 29, 30, and 31). It would be surprising if the convective models were confirmed, since they make the quite unrealistic implicit assumption of chemical homogeneity of the mantle of the Moon. After general differentiation leading to the separation of the crust, the matter remaining in the mantle should also be somewhat differentiated. At the same time, a very slight concentration of the heavier substances toward the center is sufficient to completely prevent thermal convection. Now that the presence of the partially molten "core" of the Moon has been established by direct seismic observations, we can quite justifiably use conductive models of the Moon in the study of its thermal history.

THE HEAT FLUX AND THE CONTENT OF RADIOACTIVE ELEMENTS NECESSARY TO PROVIDE IT

Measurements of the heat flow at the landing sites of Apollo 15 and 17 (refs. 32 and 33) have shown that it amounts to 28–30 erg/cm² s, i.e., about 0.7×10^{-6} cal/cm² s; whereas the models with chondritic radioactivity give 10–20 erg/cm² s, i.e., $(0.25–0.45) \times 10^{-6}$ cal/cm² s (refs. 6, 7, and 8) (see also refs. 4 and 5). At the same time, chondritic models yield a satisfactory picture of the Earth's thermal history (ref. 34). If the heat flow measured at two points on the lunar surface is typical for the entire Moon, then in order to explain it we must assume an average generation of radiogenic heat per unit of mass approximately three times greater than in the chondritic meteorites (refs. 13, 15, and 33). The results of Troitskiy indicate it is valid to extrapolate the heat flow measured at only two surface points to the entire Moon. Based on his measurements of thermal radio radiation from the entire visible hemisphere of the Moon, he obtained almost the same value of heat flow $(0.85 \pm 0.2) \times 10^{-6}$ cal/cm² s = 35 erg/cm² s (ref. 36)[2].

[2] The numerical value of heat flow depends on the value of parameter $\gamma = (k\rho c)^{-1/2}$, determined from the same radio observations. Using the value $\gamma = 600$, Troitskiy obtained a value of heat flow of $(1.0 \pm 0.3) \times 10^{-6}$ cal/cm² s (refs. 35 and 36). Later, using $\gamma = 700$, he obtained the value of heat flow presented in the text. Using the same measurements, Linsky (ref. 37) used $\gamma = 1300$ to determine a significantly lowed flow of 0.34×10^{-6} cal/cm² s near the flow obtained in calculations for chondritic models. However, Troitskiy (ref. 36) stands by his high value of heat flow. In a report at the Kiev Symposium (1968), he presented the following limits for heat flow, based on two models of the structure of the surface layer: from 0.7×10^{-6} to 0.95×10^{-6} cal/cm² s (ref. 38).

Nevertheless, the situation with heat flow remains unclear. On the one hand, suspicions exist that the thickness of the crust is twice as great on the back side of the Moon as on the visible side. (This would explain the shift of the center of the geometric figure of the Moon relative to its center of mass.) If the content of radioactive elements in the crust were uniform, the heat flow on the back side of the Moon would be even greater than on the front side. On the other hand, in the outermost layer of the Moon there are significant regional differences in the content of radioactive elements. Therefore, we cannot as yet eliminate the possibility that the large heat flows measured at the landing sites of Apollo 15 and 17 are local anomalies.

If we discard these doubts and consider the measured heat flow to be typical for the entire Moon, this is a new "boundary condition" that must be satisfied by calculations of the thermal history of the Moon. This condition restricts the present-day release of heat in the Moon's interior to very narrow limits. It must be three times greater than in the chondritic meteorites and also, apparently, in the Earth. Consequently, the long-lived radioactive elements, or at least some of them, must be present in the Moon in larger quantities than in meteorites and in the Earth. Although cosmochemists have set forth some ideas about this (see section titled "Proposed Differences in the Chemical Composition of the Earth and the Moon"), there is no cosmochemical foundation for these differences.

Model of the Moon's Thermal History Satisfying the New, Present Day–"Boundary Conditions"

Until recently, the present thickness of the outer solid layer of the Moon was determined by calculations of the thermal history or on the basis of the electrical conductivity profiles, which were nonuniquely determined from magnetic measurements. The thickness of the outer solid layer is now a reliable "boundary condition," known from seismic observations on the Moon.

If we consider the measured values typical for the entire Moon, we can use the heat flow from the interior as a second new boundary condition.

The measured heat flow requires the generation of approximately three times more heat in the Moon than in chondritic meteorites and, at the same time, the thickness of the outer solid layer has been found to be two- to four-times greater than that calculated for the chondritic models that had seemed most probable. Insofar as a large generation of heat hinders the cooling of the outer layers, it seems useful to calculate models of the lunar thermal history that satisfy both of the new boundary conditions.

The calculations of Toksöz and his colleagues (refs. 13, 14, and 15) were performed before seismic observations were used to determine the thickness of the solid layer. The main purpose of these calculations was to estimate the content of radioactive elements necessary to explain the measured heat flow. However, the current thickness of the solid layer in the models of these authors is half the true thickness. Furthermore, these authors utilize an initial temperature distribution with hot outer layers and cold interiors, in accordance with the first attempts to interpret the composition of lunar specimens. At the present time, this initial distribution of temperature is required only if we assume heterogeneous accumulation of the Moon. However, this assumption is not confirmed by a number of petrological and chemical properties of the lunar specimens (ref. 39) and, furthermore, does not agree with cosmogonic data, i.e., with the existing hypotheses for the origin of the Moon.

We have considered a simplified conductive model covering the last 3.5×10^9 yr of thermal history of the Moon and capable of giving an estimate of the distribution of radioactivity of the elements between the crust and mantle, as well as an estimate of the degree of partial fusion of the interior 3.5×10^9 yr ago. The complex and poorly known thermal evolution of the Moon for

the first 1×10^9 years of its existence was not studied. It was assumed that during this early period the interior of the Moon was subject to partial melting and magmatic differentiation due to the high initial temperature. As a result, the Moon was divided into a 63-km-thick homogeneous crust rich in radioactive elements and a homogeneous mantle poor in these elements. Then, the next 3.5×10^9 yr of the thermal history of this two-layer model were studied. During this entire time the model cools because the heat liberated in the crust can be easily lost into space. At the same time, this cooling occurs slowly since, as earlier calculations for differentiated chondritic models have shown (ref. 8), the heat flux through the surface is only 10- to 30-percent (depending on the model) greater than the equilibrium flow that corresponds to an equality between heat generation in the entire Moon and the total flux through the surface.

Since we were studying material that had already experienced differentiation in the interior, the temperature interval of melting was assumed to be 100°. The effective heat capacity was taken for this interval, considering the heat of fusion. Here, as before, we used a "triangular" dependence for the additional heat capacity with temperature (ref. 7).

The liquidus of anhydrous basalt (ref. 40) used was as the temperature of total melting, whereas in earlier calculations we used the old data of Wolf for the pressure-dependence of the melting point of dunite, which yields a smaller difference in melting temperatures between the center of the Moon and the surface.

The thermal conductivity of the lunar mantle and crust was taken as the sum of conductive and radiative thermal conductivities. However, the latter is of secondary importance, even at $\varepsilon = 10^{-1}$, since temperatures in the Moon are comparatively low.

The following "initial" temperature distribution was used: it was assumed that in the interior the temperature 3.5×10^9 yr. ago was 10 to 20° higher than the solidus temperature. With the "triangular approximation" of additional heat capacity, this corresponds to 2 to 8 percent of melted material. In the outer 200 km or so, the initial temperature dropped smoothly to the surface (more precisely speaking, to the subsurface) temperature of 230K in the equatorial zone and 90K at the poles.

In our calculations, we sought a combination of parameters to satisfy the following boundary conditions: the current thickness of the outer solid layer is about 1000 km, and the heat flux is about 30 erg/cm² s. One of the satisfactory combinations of parameters is presented in table 1. In this model, the content of uranium and thorium in the Moon's crust is nine times greater than the mean; in the mantle it is 19 times less than the mean. Thus, some 95 percent of the total quantity of these elements is concentrated in the crust. The crust also contains 90 percent of the potassium. It is assumed that 3.5 b.y. ago the temperature of the interior below 200 km depth was 20° higher than the temperature of the beginning of melting. In our model, this means that about 8 percent of the matter was melted at each point in the internal area.

As we can see from figure 1, the curve for the present-day temperature intersects the solidus curve at a very small angle, penetrating slightly into the temperature interval for

Table 1.—*Numerical Values of Parameters for One of the Satisfactory Models*

Crusted thickness	63 km		
Heat capacity	0.25 cal/g • deg		
Heat of melting	100 cal/g		
Melting interval	100°		
Heat conductivity at 0° C	0.01 cal/cm • s • deg		
Opacity	10 cm^{-1}		
Surface temperature			
at the equator	230K		
at the poles	90K		
Content of radioactive elements:			
	(Th/U = 4)		
	U (10^{-8} g/g)	K (10^{-4} g/g)	K/U
Mean	6.62	1.75	2 650
In crust	60	15	2 500
In mantle	0.35	0.34	10 000

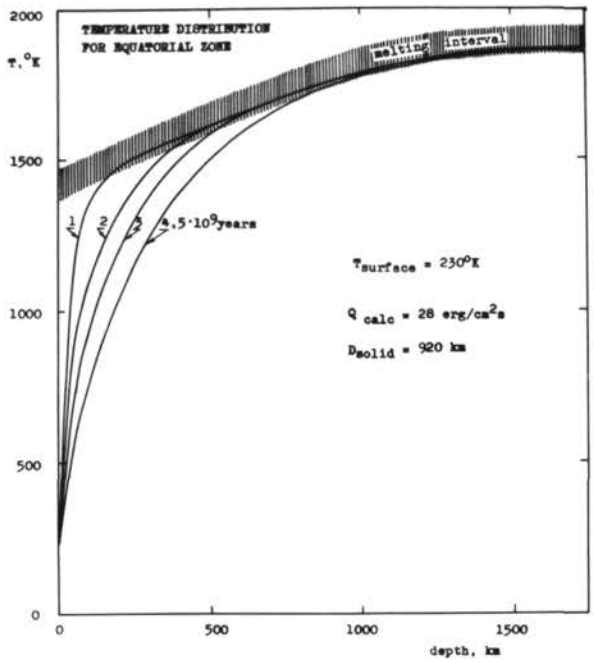


Figure 1.—*Distribution of temperature along radius for equatorial zone. Age of Moon assumed 4.5 × 10^9 yr, so that t = 4.5 × 10^9 corresponds to the present time. The curve for t = 1 × 10^9 illustrates the assumed "initial" temperature.*

partial melting. Thus, the boundary between the solid and partially melted areas of the lunar interior may be very vague. This probably corresponds to the great thickness of the layer where deep earthquakes originate on the Moon. With such a small angle between curves, the observed thickness of the solid layer determines the acceptable combination of parameters with great accuracy. An example in which the content of radioactive elements in the mantle is varied slightly is shown in figure 2.

The surface temperature in the polar areas of the Moon is significantly lower than in the equatorial areas. Therefore, as has already been shown in our earlier calculations of the thermal history for chondritic models of the Moon (refs. 6, 7, and 8), the thickness of the outer solid layer, as well as the heat flow, is greater in the polar areas than in the equatorial area (fig. 3). As a result, the central, partially molten area has a flattened, not a spherical, shape (fig. 4)[3]. Thus, the hypothesis of Levin, which attributes the flattening of the dynamic figure of the Moon to a decrease in surface temperature from the equator to the poles (refs. 4, 39, and 41), remains in force.

Our calculations show that if we start with an early melting of the Moon (i.e., a high initial temperature) and a high content of radioactive elements in the Moon, its modern thermal properties are explained without difficulty. However, both of these assumptions are riddles, related to the as yet unknown origin of the Moon.

Proposed Differences in the Chemical Composition of the Earth and the Moon

Many students of the Moon consider that in addition to different contents of radioactive elements shown by the high heat flux

[3] It is possible that the partially molten central area is not a spheroidal, but has a more complex form.

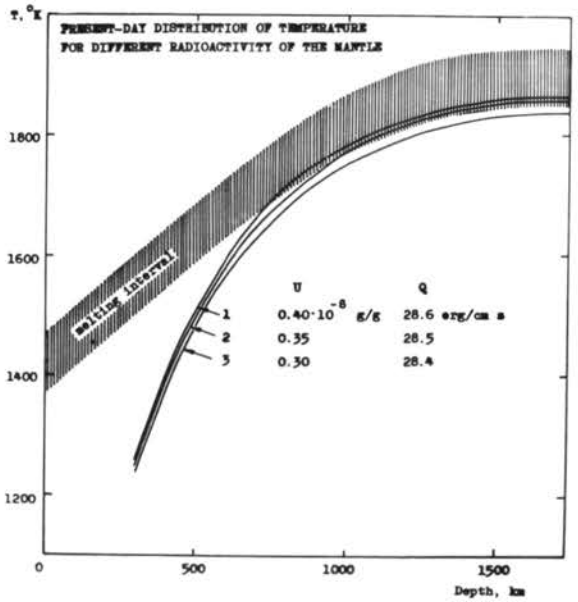


Figure 2.—*Current distribution of temperature with various contents of uranium and thorium in the mantle (Th/U = 4; content of potassium as shown in table 1).*

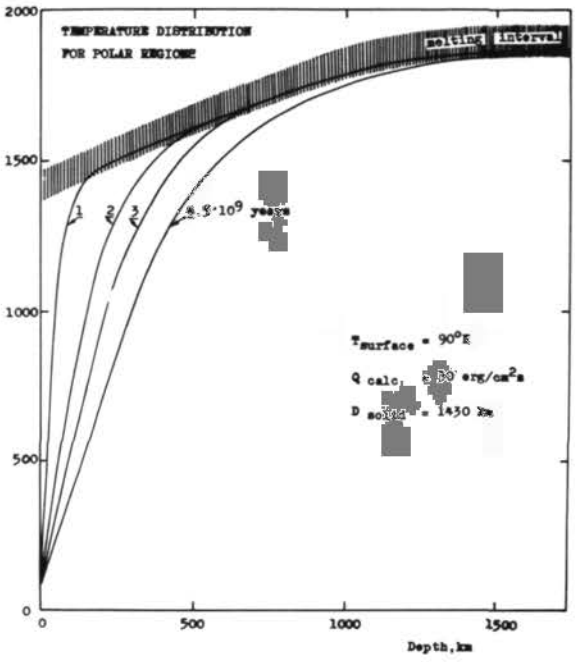
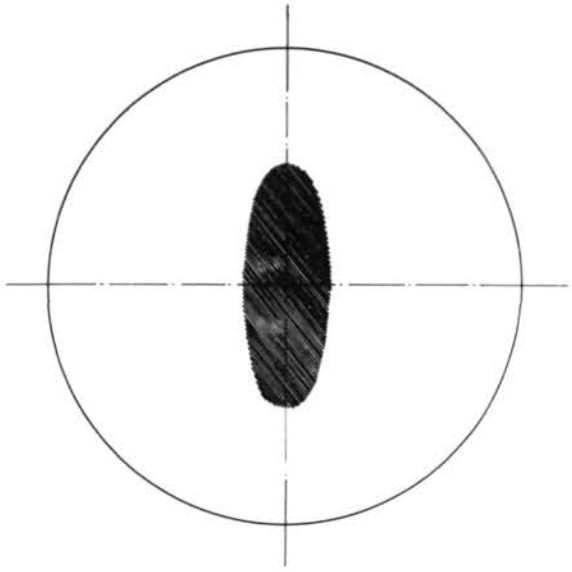


Figure 4.—*Schematic cross section of the Moon. Central partially molten area shaded.*

Figure 3.—*Distribution of temperature along radius for polar areas.*



of the Moon there are differences in the chemical composition of the Earth and Moon as well: a different content of iron; a shortage of volatile elements in the Moon; enrichment of the Moon with calcium and aluminum. However, none of these differences has been firmly established.

Based on analyses of a limited number of lunar samples taken at a small number of points on the surface and, in addition, distorted by processes accompanying the impact of bodies that have struck the Moon, it is a bit early yet to speak of impoverishment or enrichment of the entire Moon with various elements. It is particularly early to utilize these assumed impoverishments or enrichments as a basis for judgments about the origin of the Moon. Even the question as to how magmatic differentiation of the Moon occurred is a subject of intensive debate (e.g., see refs. 11, 18, 43, and 44). Apparently, Biggar et al. (ref. 43) are correct in stating that the "shadowing effect of near-surface processes, which have changed the composition of the lunar rock, prevents us from placing realistic limitations on the nature of the lunar interior, except for those already established on the basis of astronomical data. It is as yet impossible, on the basis of petrological or chemical data, to make a firm selection between formation of the Moon by separation at an early stage, capture or joint formation."

Silver, in his report to the seventh working group of COSPAR (April 1973), decisively rejected the possibility of judging the composition of the entire Moon on the basis of samples of surface rock currently available.

It is probably not by chance that the summary of the scientific results of the fourth conference on lunar science (March 1973), written by the Lunar Sample Analyses Team (ref. 32), contains no mention of the possible composition of the entire Moon or of its enrichment or impoverishment with various elements and compounds.

The authors of the present report are not competent to judge chemical and petrological data. We will limit ourselves to a few examples and comments.

DIFFERENCES IN IRON CONTENT

Since the dimensionless moment of inertia of the Moon, in spite of its light crust, is quite close to 0.4, it does not contain even a small iron core whose presence would be permissible from its low mean density (refs. 45 and 46). At present, no one doubts that the interior of the Moon has been subjected to magmatic and gravitational differentiation and, therefore, if there were any metallic iron alloy it would have sunk to form a core. If we accept the latest value of dimensionless moment of inertia (ref. 32), the mass of the

$$C/Mr^2 = 0.395\ ^{+0.005}_{-0.010}$$

iron core, if there is one, is not over 1 to 2 percent of the mass of the Moon.

Consequently, if we do assume that the Earth has an iron core, we reach the unavoidable conclusion that there is a significant difference in the content of iron in the Earth and in the Moon. However, one of the authors of the present report (Levin) remains a "heretic" and continues to prefer the hypothesis of a metalized core for the Earth (refs. 47 and 48). In this case, the Earth and Moon might have a similar or even identical iron content.

DEFICIENCIES OF VOLATILE ELEMENTS

Based on the depletion of volatile elements in the lunar basalts in comparison to analogous terrestrial basalts, some researchers believe that the entire Moon is poor in volatile elements, including such heavy elements as lead, bismuth, and thalium (refs. 49, 50, 51, and subsequent works). However, the history of thalium analyses can serve as an example of the dangers related to the insufficient number and variety of lunar samples.

All samples returned by Apollo 11, 12, and 14, which landed in mare areas of the lunar surface, were deficient in thalium. However, some of the anorthosite samples returned by Apollo 15 were found to be rich in thalium, and the majority of the anorthosites returned by Apollo 16 were rich in thalium (refs. 52 and 53).

One striking example of the sharply differing opinions is the debate concerning the origin of the mare basalts. Ringwood and his colleagues consider them to be a direct product of partial melting of the substance of the interior (refs. 54 and 55), whereas the English petrologists present them as supposedly convincing proof that the lunar mare were at one time lava lakes in which fractional crystallization occurred (ref. 43). They do not ascribe the deficit of volatile elements to a depletion of these elements in the whole Moon, but explain it by selective volatilization from hot lava issuing onto the surface, or, significantly more effective, from fire fountains accompanying the eruption of lava.

If we view the depletion of volatiles in the lunar basalts as a manifestation of an overall depletion throughout the Moon and attribute it to the accumulation of the Moon from matter that was still hot and condensing in the cooling protoplanetary cloud, Anders and his colleagues have found that the temperature of this matter must have been about 620K. However, since the duration of accumulation of the condensing matter could not have been much less than the duration of cooling of the cloud, the Moon, like the other bodies of the terrestrial planets, should consist of a mixture of matter that condensed at different temperatures, including low temperatures. Therefore, the meaning of the condensation temperature for lunar material found by Anders and his colleagues is not clear. Furthermore, these authors assume equilibrium condensation, whereas, as Arrhenius and Doe have recently shown (ref. 56), the conditions in the cloud must have been far from equilibrium, and condensation must have occurred with the temperature of dust particles much lower than the temperatures of the gas.

In all of the rocks returned from the surface of the Moon, the ratio of potassium to

uranium is less than in terrestrial rocks and much less than in the meteorites. However, both Urey (ref. 57) and Arnold (ref. 58) refrain from extrapolating this difference to the entire Moon. As Arnold notes, it is still not clear whether the loss of potassium occurred before the formation of the Moon, during its formation, or after its formation.

While emphasizing the absence of water in most lunar rocks, Urey (ref. 59) noted that at the Apollo 17 site some rocks contain volatiles which, in his opinion, might indicate the presence of volatiles in the deeper rocks of the Moon.

Thus, the entire range of questions related to the depletion of volatiles requires further investigation.

ENRICHMENT OF THE MOON WITH MINERALS RICH IN CALCIUM AND ALUMINUM

Since the continental areas of the Moon, which represent the greatest portion of its surface, consist of anorthositic rocks, there is no doubt as to the enrichment of the surface layers with minerals rich in Ca and Al. However, it is debatable to what extent this composition of the surface rocks indicates enrichment of the entire Moon with such minerals. These minerals, which are "early condensates" (see below) according to the theory of equilibrium condensation, are encountered as inclusions in the Allende meteorite and other type II and III carbonaceous chondrites.

Ringwood and Essene (ref. 55) proposed that the content of these minerals on the Moon was higher than that on Earth, but still moderate ($\sim$ 0.2 by mass). They considered that a higher content in the lunar interior would, as a result of their conversion into denser phases, cause a high mean density of the Moon, which does not agree with the observed density. Anderson (refs. 60, 61, and 62) proposes that the Moon consists almost entirely of these minerals and presents arguments (refs. 62 and 63) in favor of rejecting the limitations set forth by Ringwood and Essene. He bases his conclusions on the argument of Gast (ref. 64) who believed that the enrichment of the surface rock of the Moon with Ca and Al indicates enrichment of the source of this rock in these elements, i.e., enrichment of the interior. Wanke et al. (refs. 65 and 66) consider that the Moon consists of a mixture of matter similar to the inclusions in the Allende meteorite, plus the matter of the chondritic meteorites. Assuming that the ratio of potassium to lanthanum in the lunar samples is typical for the entire Moon and using their analyses of inclusions from Allende, they found that the content of matter similar to these inclusions amounts to 69 percent in the Moon, whereas in the Earth its content is found to be 22 percent, based on the same calculation. At the same time, Anders and his colleagues made similar calculations using not two, but five phases and found that the Moon contains 42 percent of material similar to the Allende (ref. 53) inclusions.

All of the above authors consider the minerals rich in calcium and aluminum to be "early condensates." Indeed, according to the theory of equilibrium condensation in a cooling protoplanetary cloud of solar composition, assuming identical temperatures for dust particles and gas, these minerals should condense at temperatures above 1300K, i.e., before iron and silicates (ref. 67). This is seemingly confirmed by Grey et al. (ref 68) who found that the Ca- and Al-rich chondrules from the Allende meteorite have the most primitive strontium isotopic composition known.

It should be noted that according to the theory of equilibrium condensation, uranium and thorium should be incorporated in the early condensates. This is confirmed by the high uranium content in the Allende inclusions (refs. 65 and 66). Due to this, in spite of the depletion of potassium, the total heat production in the early condensates is found to be greater than in chondritic material. Thus, the enrichment of the Moon with early condensates might explain the high heat flux from its interior.

However, the protoplanetary disk should have been transparent for infrared radiation

and, therefore, as Arrhenius and Doe have shown (ref. 56), the temperature of dust particles should have been hundreds of degrees or even a thousand degrees lower than the kinetic temperature of the gas. For many compounds, this does not change their sequence of condensation; but for some compounds, it makes a significant difference. Apparently, the course is that the hot gas should have been partially ionized, and in this case ionization potentials begin to play a role. According to Arrhenius (ref. 69), minerals rich in Ca and Al would condense at lower temperatures under these conditions, i.e. after iron and the silicates.

Onuma et al. (ref. 70) measured the differences in the isotopic composition of oxygen in terrestrial, lunar, and meteoritic specimens and interpreted them as the result of physical and chemical processes occurring at different temperatures. They considered that their measurements confirmed that the Ca- and Al-rich minerals from the Allende meteorite are actually high-temperature condensates. However, further measurements (ref. 71) have led to the conclusion that the peculiarities of the isotopic composition of oxygen in the carbonaceous chondrites are related not to chemical reactions but rather to the presence of an admixture of some "primitive" component (perhaps interstellar dust) very poor in O^{18} and O^{17}. Therefore, although it is impossible to determine the formation temperature of these inclusions, the presence of this admixture, like the results of Grey et al. (ref. 68) speaks against the conclusions of Arrhenius and in favor of the idea that the inclusions from Allende are not only early condensates, but also early "accumulates."

We know of two attempts—in our opinion unsuccessful—to explain the enrichment of the entire Moon with minerals rich in calcium and aluminum.

Anderson (refs. 60 and 61) proposed that the Moon consists almost entirely of early condensates and, therefore, differs greatly from the Earth. He also attempted to explain this difference by referring to the dependence of condensation temperature on pressure. He assumed that in contrast to the Earth, which accumulated near the central plane of the protoplanetary cloud, the Moon was somehow accumulated at some distance from this plane under lower pressure conditions. As a result of this, for some reason, the Moon includes only substances that condense before iron. Just exactly why remains unclear. Furthermore, the hypothesis of Anderson contradicts the laws of celestial mechanics, both for formation in circumsolar orbit significantly inclined to the ecliptic, and for formation in circumterrestrial orbit, even if perpendicular to the ecliptic. Twice in each revolution, the Moon would have to intersect the central plane of the protoplanetary cloud or the circumterrestrial swarm, and it is here, in the layer of maximum density of solid matter, that its main accumulation should occur. Later, Anderson (ref. 63) published a more detailed foundation for his idea that the Moon might consist entirely of early condensates, but the authors of the present report are unable to understand either his explanations as to where and how this might occur (ref. 65) or his answer (sec. 12, p. 56) to the objections of Cameron (ref. 72). Cameron himself, accepting the composition of the Moon according to Anderson, assumes that it was formed within the orbit of Mercury and later captured by the Earth. We also disagree with this hypothesis, since capture from an orbit differing greatly from the orbit of the Earth is practically impossible (see below).

Returning to the ideas of Anderson, we should note that he accepts the hypothesis of "accumulation during condensation," i.e., assumes that accumulation somehow occurred more rapidly than the cooling of the protoplanetary cloud. At the same time, he rejects the hypothesis of heterogeneous accumulation, preferring the idea of homogeneous initial lunar composition. True, he notes that the chemical stratification of the Moon, arising in his opinion as a result of early differentiation, is practically indistinguishable from that which would occur with heterogeneous accumulation.

Anders and his colleagues (ref. 53), considering that the moon contains 42 percent

"early condensates," whereas the Earth contains only 6 percent of these condensates according to their calculations, explain this by stating that the formation of the Earth and the Moon began with the formation of small "nuclei" consisting only of "early condensates" with masses of 6.3 percent and 0.5 percent of the contemporary mass of the Earth, respectively. Further accumulation of later condensates, namely chondrite-type condensates containing iron, increased the mass of the terrestrial protobody by a factor of 15, but the mass of the lunar protobody probably by only two times, leading to their variation in content of early condensates. Thus, it is implicitly assumed that by the moment of condensation of chondritic-type matter, all of the early condensates were already incorporated in the protobodies of the Earth and Moon, which were the only large bodies in the "Earth zone" of the protoplanetary cloud. However, the presumed cooling of the protoplanetary cloud should have occurred more rapidly than the accumulation of the condensation products, and, furthermore, the formation of the protobodies of the Earth and Moon should have been accompanied by the formation of many other bodies of similar dimensions and composition, later to be absorbed by the Earth and Moon. If they, as Anders and his colleagues believe, consisted of early condensates, their incorporation into the growing Earth and Moon during the stage of accumulation of chondritic matter would have continued to increase the content of early condensates in the Earth and Moon.

It must be added that Anders and his colleagues refer to the calculations of Öpik, who used a greatly simplified model to illustrate the differences in growth rate of two protobodies of different mass in similar orbits around the Sun. Thus, they implicitly refer to the point of view of the formation of the Moon by capture.

At the present time, it seems premature to attempt to determine the origin of the Moon on the basis of its proposed enrichment with minerals rich in Ca and Al. First we must determine whether any such enrichment actually exists and how great it is. We must better determine the mean thickness of the anorthosite layer for the entire Moon and the mechanism of its formation during the course of magmatic differentiation of the Moon. Only after this can we make any reliable judgment about the content of these minerals in the mantle of the Moon, which makes up 90 percent of the Moon's substance.

At the same time, we should turn our attention to clarification of the question of possible conditions of formation for these minerals—are they early or late condensates and are there still other ways to form them?

Origin of the Moon

At present, as before the beginning of direct investigation of the Moon, three main hypotheses of its origin continue to be discussed: (1) fission of the Moon from the Earth, (2) the capture hypothesis, and (3) the joint formation of the Earth and the Moon. The hypothesis of Öpik (ref. 57) recently appeared and combines the capture hypothesis with the hypothesis of the Moon's accumulation in the vicinity of the Earth.

Unfortunately, the new data on the Moon mentioned in the preceding sections of our report only increase the difficulties which stand before any attempt to explain its origin.

THE FISSION HYPOTHESIS

As was the case a few years ago, the hypothesis of fission of the Moon from the Earth remains without any mechanical foundation (ref. 1). The problem is not only that the calculations of past tidal evolution of the Moon indicate that the plane of the lunar orbit has never coincided with the plane of the Earth's equator; not only that the current total momentum of the Earth-Moon system is insufficient for rotational separation of an initially single body; and not only that a satellite which separated from the Earth, within the Roche limit, would have been destroyed by tidal forces. But, as has been demonstrated by Lyapunov

(ref. 73), Cartan, (refs. 74 and 75), and Littleton (refs. 76 and 77), even if rotational instability devolops, *smooth* separation of a satellite would be impossible. The onset of rotational instability leads not to separation, but rather to ejection of some of the material. If the ejection velocity were greater than the parabolic velocity, the material would depart forever. If it were less than the parabolic velocity, it would fall back to Earth. In the latter case, the ideal case, these ejections and returns would be repeated over and over forever. However, the return fall, occurring at high relative velocity, would be accompanied by explosive ejection of matter, and some of the clumps or "spray" would achieve hyperbolic velocities and, therefore, carry away the excess moment creating the rotational instability.

Fission hypotheses continue to be discussed in connection with the problem of the origin of close binary stars. In this case, in contrast to the problem of the Earth and the Moon, we are studying not idealized bodies of homogeneous density with solid-body rotation, but rather bodies of compressible gas which, therefore, have sharply increasing densities toward the center and, furthermore, not necessarily bodies with solid-body rotation. However, 20 years ago Littleton (ref. 74) believed that with centrally condensed bodies the situation is still worse than with homogeneous bodies. As we can see from the articles of Ostriker (ref. 78) and Leboviz (ref. 79), the possibility of fission of such bodies still remains hypothetical. It should be noted that the proponents of the fission of centrally condensed bodies limit themselves to discussion of the conditions for the onset of instability, without analyzing the question of to what this instability would lead, i.e., without studying the actual process of the supposed separation.

At first glance, the idea of the fission of the outer layers of the already differentiated Earth is attractive in that it could explain some of the supposed differences in the composition of the Earth and the Moon (refs. 80 and 81). However, we should not be misled by this, since contradictions would then arise with other geochemical data. For example, as Wanke believes (ref. 65), the difference in the values of the FeO/MnO ratio on Earth and on the Moon contradicts the hypothesis of separation of the Moon from the Earth. Furthermore, a contradiction would arise in geophysical data as well. The Moon and the Earth were formed practically simultaneously some 4.6×10^9 yr ago. If we assume that the Earth was already differentiated at the moment of separation from the Moon, we must assume a hot initial state, which is incompatible not only with the solid contemporary state of the entire mantle, but also with the small thickness of the terrestrial crust, indicating that it is a product of differentiation only of the upper mantle.

THE CAPTURE HYPOTHESIS

In its usual form, the capture hypothesis assumes the capture of the already formed Moon as a result of tidal friction during a close passage. However, this friction is so small that in order for capture to have occurred it is necessary that the geocentric orbit of the Moon before capture differ negligibly from a parabolic orbit, in order that its "velocity at infinity" be almost zero. This means that the probability of such a capture is negligible. Furthermore, this means that before capture the Moon must have moved around the Sun in an orbit almost identical to that of the Earth. Therefore, it is incorrect to think that the capture hypothesis provides a means of explaining the assumed differences in the composition of the Earth and the Moon, for example by allowing the formation of the Moon at some distance from the Earth, such as in the zone of the asteroids or within the orbit of Mercury, as Cameron suggests (ref. 72). Actually, the capture hypothesis requires formation of the Moon in the zone of formation of the Earth.

As Öpik has shown (ref. 57), the most probable form of capture of the Moon is capture of a portion of the matter of a large body broken off by tidal forces during pas-

sage (again also on a nearly parabolic geocentric orbit) within the Roche limit. Fragments of the hemisphere turned toward the Earth are captured, according to Öpik, in elliptical geocentric orbits, while fragments of the opposite hemisphere fly away, carrying with them a portion of the energy and moment of the captured fragments, as would be required for capture. If the fragments formed an absolutely homogeneous ring, tidal evolution would be impossible. However, unavoidable fluctuations in the distribution of the fragments around the Earth would result in tidal interaction with the Earth and their movement out beyond the Roche limit, where they would be combined into one or a few bodies. Thus, the hypothesis of Öpik combines the capture hypothesis with the hypothesis of accumulation of the Moon in the vicinity of the Earth.

A single body of lunar mass, if one could be present within the Roche limit, would move out beyond this limit in 5 years. If there were 1000 identical fragments with the same total mass, according to Öpik they would take thousands or tens of thousands of years to move out beyond the Roche limit.[1] However, if we consider that collisions between these fragments, occurring while still within the Roche limit, should be accompanied by fragmentation, i.e., increases in the total number, the time of movement to beyond the Roche limit would probably be still greater. Therefore, although the fragments should combine rapidly once beyond the Roche limit, the time of accumulation of a single Moon would be greater than 10^2 to 10^3 yr, the time necessary for its heating by gravitational energy. However, Öpik assumes the possibility of formation of several, for example, six, protomoons, whose later combination into a single Moon could result in its hot state.

Thus, Öpik's hypothesis about the formation of the Moon from fragments of a relatively large body captured by the Earth during passage within the Roche limit, with the resulting breakup by tidal forces, opens some possibilities for explanation of the high initial temperature of the Moon that are worthy of further study. However, this brings up many mechanical diffculties. Furthermore, as in the capture hypothesis for an already formed Moon, we are concerned here with the capture of a portion of the matter of a body moving in a *near-terrestrial orbit* and we do not as yet see any cosmogonically well-founded means for explaining the assumed (but as yet unproven) differences in composition between the Earth and the Moon.

THE HYPOTHESIS OF JOINT FORMATION OF THE EARTH AND MOON

According to the hypothesis suggested by Schmidt (refs. 82, 83, and 84), the Moon (as well as the regular satellites of the other planets) was accumulated in the vicinity of the growing Earth from the *circumterrestrial* swarm of bodies and particles, which was continually supplemented during the accumulation of the Earth from the *circumsolar* swarm of bodies and particles. According to this hypothesis, the formation of the Moon is a byproduct of the process of formation of the Earth.

In the vicinity of the growing Earth, inelastic collisions of bodies moving in circumsolar orbits had to occur. A certain fraction of the fragments then took on orbits around the Earth, i.e., formed a sparce circumterrestrial swarm. The particles of this swarm accumulated rapidly into the protomoon, but as long as rather intensive accumulation of the Earth continued, the existence of the circumterrestrial swarm was maintained by new collisions in the vicinity of the Earth.

The hypothesis of Schmidt is based on processes that must have occurred in the course of accumulation of the Earth, and it is most promising from the mechanical standpoint (ref. 85). Attempts at quantitative development of this hypothesis are contained in a number of papers by Ruskol

[1] In his preceding works, Öpik considered that the time of movement was proportional to the square root of the number of bodies (of identical mass). In his work of 1972, he indicated that this was an error and that actually it was directly proportional to the number of bodies.

(refs. 39, 86, 87, and 88). Unfortunately, new data on the Moon, its hot initial state, and possible differences in the composition of the Earth and Moon, might be a stumbling block for this hypothesis.

Actually, if the accumulation time of the Moon was as long as that of the Earth, the gravitational energy of accumulation, liberated primarily on the surface, would have been radiated out into space and could not have significantly increased the initial temperature of the Moon. As was noted earlier (ref. 1), the existence of a temporarily dust-filled atmosphere around the Moon during its accumulation might have prevented strong radiation and resulted in heating of the interior due to gravitational energy. However, if the greenhouse effect of the dusty atmosphere was so strong on the Moon, we would expect no less of a greenhouse effect on Earth, which leads to serious contradictions with our ideas concerning the thermal history of the Earth.

Ten years ago, MacDonald (ref. 89) wanted to lengthen the time scale for tidal evolution of the Moon and set forth the idea that in the past there were several protomoons around the Earth, which later combined into the contemporary Moon. Recently, Ruskol (ref. 90) attempted to apply the idea of several protomoons to explain the high initial temperature of the Moon. Actually, the merging of two or three protomoons might, if all of the gravitational energy were retained, result in significant heating of the interior. However, retention of the energy would require an almost head-on collision.

The possibility of early heating of the Moon by tidal deformations depends on the poorly known initial dynamic properties of the Earth-Moon system. The initial ellipticity of the lunar orbit is very important here. According to Alexander (ref. 91), this ellipticity in the past was not great, indicating that further studies in this direction are promising.

With a longer accumulation time for the Moon, as follows from the hypothesis of Schmidt, the liberation of energy by short-lived radioactive elements (if they were initially present) and electromagnetic heating by the intensive corpuscular radiation of the young Sun (if it passed through a T Tauri stage) should be significantly weakened or practically ended before the completion of formation of the Moon. These sources of energy could hardly have played a significant role in the initial heating of the lunar interior.

Within the framework of the hypothesis of Schmidt concerning the common formation of the Earth and Moon, it is natural to expect identical compositions for the Earth and Moon. The attempt by Ruskol (refs. 92 and 93) to prove that this hypothesis leads to a different composition of the two bodies seems dubious, both as concerns attempts to explain the supposed deficit of volatiles in the Moon, and as concerns attempts to explain the absence of an iron core in the Moon.

Ruskol attributes the depletion of volatiles to the fact that particles captured in the circumterrestrial swarm must have experienced an additional collision, the collision which caused their capture, in comparison to circumsolar particles which were directly included in the composition of the Earth. However, we are speaking here of a single additional collision, which could hardly have produced a significant effect. Furthermore, as Ruskol herself proved (ref. 93), it is possible that the Earth was also accumulated to a significant extent from particles that had been present in the circumterrestrial swarm.

Ruskol, following the idea of Orowan (ref. 94), attributes the absence of a lunar iron core to differences in the plastic properties of stony and iron particles. This difference should truly have played a role in the accumulation of tiny particles, however even the sign of the effect is unclear (ref. 95). However, in the gravitational accumulation of bodies hundreds of kilometers in diameter, the plastic properties of the particles should lose their meaning. Actually, it is this stage of accumulation that is most important, i.e., longest, in the formation of bodies of lunar and larger dimensions. Ruskol starts from

the physically unjustified assumption of linear growth of iron content, and therefore of density, as a function of the logarithm of the radius of a body in the range from 10^{-4} to 10^{8} cm. Therefore, her explanation of differences in the content of iron in the Earth and the Moon is purely formal.

We should once more emphasize that the hypothesis of Schmidt does not assume that a swarm sometimes existed around the Earth, and contained the entire mass of the contemporary Moon. But, if it did exist, then it is not difficult to show that its accumulation into one or a few large bodies would require less than 100 years. Consequently, the formation of such a swarm should have lasted at a maximum a few years, i.e., should have been practically instantaneous. Apparently, the only method capable of explaining such a "quasi-instantaneous" development of the circumterrestrial swarm is a collision of two comparatively large bodies (with total mass much greater than the mass of the Moon) moving in circumsolar orbits in the vicinity of the Earth. It is possible in principle that upon such a collision some of the fragments, with mass equal to the mass of the Moon, remained in circumterrestrial orbits. The accumulation of a swarm that developed in this manner into a single body should require no more than a few decades and would lead to heating of the Moon by gravitational energy. In addition to explaining the high initial temperature of the Moon, this method of formation also opens a path to explanation of the differences in the composition of the Earth and the Moon (if they are confirmed). The bodies whose collision generated the circumterrestrial swarm may have been formed at distances from the Sun differing somewhat from the distance at which the Earth was formed. In case of a significant dependence of the composition of a body on its distance from the Sun during its formation, we could attempt to explain in this manner those differences in the composition of the Earth and the Moon which will be established by future studies.

As we can see from the above, establishment of the high initial temperature of the Moon has not helped to explain its origin. Quite the opposite, attempts to explain the new data on the Moon bring up new and serious difficulties and riddles. Many of these riddles are made worse by the fact that attempts to solve lunar problems must be correlated with the explanation of the origin of the other planetary bodies in the solar system. Only in this manner can we avoid exaggerating the importance of ad hoc hypotheses and move forward to a proper understanding of the origin of the entire solar system.

References

1. LEVIN, B. J., Evolution of the Moon: Recent Modification of Previous Ideas. *The Moon, IAU Symposium No. 47*, 1972, pp. 441–449.
2. LEVIN, B. J., Thermal History of the Moon. *The Moon*, IAU *Symposium No. 14*, 1962, pp. 157–167.
3. LEVIN, B. J., The Thermal History of the Moon. *Novoye O Lune, MAC Symposium No. 14*, 1963, pp. 113–125.
4. LEVIN, B. J., The Structure of the Moon. *Proc. Caltech-JPL Lunar Planet. Conference*, 1966, pp. 61–76.
5. LEVIN, B. J., Thermal History of the Moon and the Development of Its Surface. *The Nature of the Lunar Surface*, Proc. 1965 IAU-NASA Symposium, 1966, pp. 267–271.
6. MAYEVA, S. V., Some Calculations of the Thermal History of Mars and the Moon. *Dokl. SSSR*, Vol. 159, No. 2, 1964, pp. 294–297.
7. MAYEVA, S. V., Some Calculations of the Thermal History of Mars and the Moon. *Izv. Komiss. Po Fizika Planet*, No. 5, 1965, pp. 49–70.
8. MAYEVA, S. V., The Thermal History of the Moon. *Fizika Zemli*, No. 3, 1971, pp. 3–10.
9. FRICKER, P. E., R. T. REYNOLDS, AND A. L. SUMMERS, On the Thermal History of the Moon. *J. Geophys. Res.*, Vol. 72, No. 10, 1967, pp. 2649–2663.
10. FRICKER, P. E., R. T. REYNOLDS, AND A. L. SUMMERS, Possible Thermal History of the Moon. *The Moon*, IAU Symposium No. 47, 1972, pp. 384–391.
11. WOOD, J. A., Thermal History and Early Magmatism in the Moon. *Icarus*, Vol. 16, No. 2, 1972, pp. 229–240.
12. MIZUTANI, H., T. MATSUI, AND H. TAKEUCHI, Accretion Process of the Moon. *The Moon*, Vol. 4, Nos. 3 and 4, 1972, pp. 476–489.
13. TOKSÖZ, M. N., S. C. SOLOMON, J. N. MINAR AND

D. H. JOHHSTON, Thermal Evolution of the Moon. *The Moon*, Vol. 4, Nos. 1 and 2, 1972, pp. 190–213.

14. TOKSÖZ, M. N., F. PRESS, K. ANDERSON, A. DAINTY, G. LATHAN, M. EWING, J. DORMAN, D. LAMMLEIN, Y. NAKAMURA, G. SUTTON, AND F. DUENNEBIER, Velocity Structure and Properties of the Lunar Crust. *The Moon*, Vol. 4, Nos. 3 and 4; 1972, pp. 490–504.
15. TOKSÖZ, M. N., AND S. C. SOLOMON, Thermal History and Evolution of the Moon. *The Moon*, Vol. 7, Nos. 3 and 4, 1973, pp. 251–278.
16. LATHAM, G., M. EWING, J. DORMAN, Y. NAKAMURA, F. PRESS, N. TOKSÖZ, G. SUTTON, F. DUENNEBIER, AND D. LAMMLEIN, Lunar Structure and Dynamics—Results from the Apollo Passive Seismic Experiment. *The Moon*, Vol. 7, Nos. 3 and 4, 1973, pp. 396–421.
17. WOOD, J. A., The Moon's Feldspatic Crust: Early Differentiation or Heterogeneous Accretion. *Meteoritics*, Vol. 8, No. 1, 1973, pp. 467–468.
18. BRETT, R., The Lunar Crust: A Product of Heterogeneous Accretion or Differentiation of a Homogeneous Moon. *Geochimica et Cosmochimica Acta*, Vol. 37, No. 12, 1973, pp. 2697–2703.
19. LEVIN, B. YU., AND S. V. MAYEVA, The Possibility of Heating of the Asteroids by Short-lived Radioactive Isotopes. *Meteoritics*, No. 31, 1972, pp. 18–23.
20. MCCORD, T. B., J. B. ADAMS, AND T. V. JOHNSON, Asteroid Vesta: Spectral Reflectivity and Compositional Implications. *Science*, Vol. 168, 1970, pp. 1445–1447.
21. WILKENING, L. L., AND E. ANDERS, The Ibitira Meteorite: A Vesicular Basalt. *Geochimica et Cosmochimica Acta*. In press.
22. MAYEVA, S. V., The Thermal History of the Terrestrial Planets. *Astrophys. Letter*, Vol. 4, 1969, pp. 11–16.
23. SCHRAMM, D. N., Nucleosynthesis of Al^{26} in the Early Solar System and in Cosmic Rays. *Astrophys. and Space Sci.*, Vol. 13, No. 1, 1971, pp. 249–266.
24. SCHRAMM, D. N., F. TERA, AND G. J. WASSERBURG, The Isotope Abundances of Mg^{26} and Limits on Al^{26} in the Early Solar System. *Earth Planet. Sci. Letters*, Vol. 10, No. 1, 1970, pp. 44–59.
25. ANDERS, E., AND D. HEYMANN, Elements 112 to 119: Were They Present in Meteorites? *Science*, Vol. 164, No. 3881, 1969, pp. 821–823.
26. DAKOWSKI, M., The Possibility of Extinct Superheavy Elements Occurring in Meteorites. *Earth Planet Sci. Letters*, Vol. 6, No. 2, 1969, pp. 152–154.
27. YORK, D., Extinct 129I, 244 Pu and Superheavy Elements in the Early History of the Solar Systems. *Comm. Earth Sci. Geophys.*, Vol. 2, No. 1, 1971, pp. 14–21.
28. LEVIN, B. YU, AND S. V. MAYEVA, Some Calculations of the Thermal History of the Moon. *Dokl. Akad. nauk. SSSR*, Vol. 133, No. 1, 1960, pp. 44–47.
29. TOZER, D. C., The Moon's Thermal State and an Interpretation of the Lunar Electrical Conductivity Distribution. *The Moon*, Vol. 5, Nos. 1 and 2, 1972, pp. 90–105.
30. TURCOTTE, D. L., AND E. R. OXBURGN, Implications of Convection Within the Moon. *Nature*, Vol. 223, No. 5203, 1969, pp. 250–251.
31. IRIYAMA, J., Thermal Structure Within the Convecting Moon. *J. Phys. Earth*, Vol. 21, pp. 77–96.
32. Lunar Sample Analysis Planning Team. *Proc. Fourth Lunar Science Conference, Science*, Vol. 181, No. 4160, 1973, pp. 615–622.
33. LANGSETH, M. G., S. P. CLARK, J. L. CHUTE, S. J. KEIHM, AND A. E. WECHSLER, The Apollo 15 Lunar Heat Flow Measurement. *The Moon*, Vol. 4, Nos. 3 and 4, 1972, pp. 390–410.
34. MAYEVA, S. V., The Thermal History of the Earth. *Fizika Zemli*, No. 3, 1967, pp. 3–17.
35. TROITSKIY, V. S., Investigation of the Surface of the Moon and Planets by Thermal Radiation. *J. Res. NBS, 69D*, No. 12, 1965, pp. 1585–1611.
36. TROITSKIY, V. S., Investigation of the Surfaces of the Moon and Planets by Means of Thermal Radiation. *Proc. Roy. Soc. 296A*, No. 1446, 1967, pp. 366–398.
37. LINSKY, J. L., Models of the Lunar Surface Including Temperature-Dependent Thermal Properties. *Icarus*, Vol. 5, No. 6, 1966, pp. 606–634.
38. TIKHONOVA, T. V., AND V. S. TROITSKIY, Determination of the Heat Flux From the Interior of the Moon with the Heterogeneous Structure of Its Surface Layer. *Fizika Luny i Planet*, 1972, pp. 78–182.
39. RUSKOL, YE. L., The Origin of the Moon; Formation of the Circumterrestrial Cluster of Bodies. *Astron. Zhurn.*, Vol. 37, No. 4, 1960, pp. 690–702.
40. COHEN, L. H., K. ITO, AND G. C. KENNEDY, Melting and Phase Relations in an Anhydrous Basalt to 40 Kilobars. *Am. J. Sci.*, Vol. 265, 1967, pp. 475–518.
41. LEVIN, B. J., A New Hypothesis for the Non-equilibrium Figure of the Moon. *Nature*, Vol. 202, No. 4938, 1964, pp. 1201–1202.
42. LEVIN, B. J., Thermal Effects on the Figure of the Moon. *Proc. Roy. Soc., A 296*, No. 1446, 1967, pp. 266–269.
43. BIGGAR, G. M., M. J. O'HARA, D. J. HUMPHRIES, AND A. PECKELT, Maria Lavas, Mascons, Layered Complexes, Achondrites and the Lunar Mantle. *The Moon, IAU Symposium No. 47*, 1972, pp. 129–164.
44. MITLER, H. E., The Cambridge Cosmochemistry Symposium, *Icarus*, Vol. 20, No. 1, 1973, pp.

54–71.

45. LEVIN, B. J., On The Internal Constitution of the Moon. *Preprint of a Report Presented at COSPAR Session*, Tokyo, 1967.
46. NAKAMURA, Y., AND G. V. LATHAM, Internal Constitution of the Moon: Is the Lunar Interior Chemically Homogeneous? *J. Geophys. Res.*, Vol. 74, No. 15, 1969, pp. 3771, 3780.
47. LEVIN, B. YU., *Sostav Zemli. Trudy Geofiz. Inst. AN SSSR*, No. 26 (153), 1955, pp. 11–38.
48. LEVIN, B. J., Origin of the Earth; The Upper Mantle. *Tectonophysics*, Vol. 13, Nos. 1–4, 1972, pp. 7–29.
49. KEAYS, R. R., R. GANAPATHY, J. C. LAUL, E. ANDERS, G. F. HERZOG, AND P. M. JEFFERY, Trace Elements and Radioactivity in Lunar Rocks: Implications for Meteorite Infall, Solar Wind Flux and Formation Conditions of the Moon. *Science*, Vol. 167, No. 3918, 1970, pp. 490–493.
50. GANAPATHY, R., R. R. KEAYS, J. C. LAUL, AND E. ANDERS, Trace Elements in Apollo 11 Lunar Rocks: Implications for Meteorite Influx and Origin of the Moon. *Proc. Apollo 11 Lunar Science Conference, Geochimica et Cosmochimica Acta*, Supplement 1, 1970, pp. 1117–1142.
51. ANDERS, E., R. GANAPATHY, R. R. KEAYS, J. C. LAUL, AND J. W. MORGAN, Volatile and Siderophile Elements in Lunar Rocks: Comparison with Terrestrial and Meteorite Basalts. *Proc. Second Lunar Science Conference, Geochimica et Cosmochimica Acta*, Supplement 2, 1971, pp. 1021–1036.
52. KRÄHENBÜHL, U., R. GANAPATHY, J. W. MORGAN, AND E. ANDERS, Volatile Elements in Apollo 16 Samples: Possible Evidence for Outgassing of the Moon. *Science*, Vol. 180, No. 4088, 1973, pp. 858–861.
53. KRÄHENBÜHL, U., R. GANAPATHY, J. W. MORGAN, AND E. ANDERS, Volatile Elements in Apollo 16 Samples: Implications for Highland Volcanism and Accretion History of the Moon. *Proc. Fourth Lunar Science Conference*, Vol. 2, 1973, pp. 1325–1348.
54. RINGWOOD, A. E., Petrogenesis of Apollo 11 Basalts and Implications of Lunar Origin. *J. Geophys. Res.*, Vol. 75, 1970, pp. 6453–6479.
55. RINGWOOD, A. E., AND E. ESSENE, Petrogenesis of Apollo 11 Basalts: Internal Constitution and Origin of the Moon. *Proc. Apollo 11 Lunar Science Conference, Geochimica et Cosmochimica Acta*, Supplement 1, 1970, pp. 769–800.
56. ARRHENIUS, G., AND B. R. DOE, Equilibrium Condensation in a Solar Nebula. *Meteoritics*, Vol. 8, No. 4, 1973, pp. 297–313.
57. ÖPIK, J., Comments on Lunar Origin. *Irish. Astron. J.*, Vol. 10, Nos. 5 and 6, 1972, pp. 190–238. *Contr. Armagh Obs.*, No. 79.
58. ARNOLD, J. R., The Chemist's Moon. *Bull. Atom. Sci.*, Vol. 29, No. 9, 1973, pp. 22–25.
59. UREY, H. C., The Moon and Its Origin. *Bull. Atom. Sci.*, Vol. 29, No. 9, 1973, pp. 5–10.
60. ANDERSON, D. L., The Origin of the Moon. *Nature*, Vol. 239, No. 5370, 1972, pp. 263–265.
61. ANDERSON, D. L., The Composition and Origin of the Moon. *Earth Planet. Sci. Letters*, Vol. 18, No. 2, 1973, pp. 301–316.
62. ANDERSON, D. L., Removal of a Constraint on the Composition of the Lunar Interior. *J. Geophys. Res.*, Vol. 78, No. 17, 1973, pp. 3222–3225.
63. ANDERSON, D. L., The Moon as a High Temperature Condensate. *The Moon*, Vol. 8, No. 1 and 2, 1973, pp. 33–57.
64. GAST, P. W., The Chemical Composition and Structure of the Moon. *The Moon*, Vol. 5, pp. 121–148.
65. WANKE, H., Chemistry of the Moon. *Top. Curr. Chem.*, Vol. 44, 1974, pp. 115–154.
66. WANKE, H., H. BADDENHAUSEN, G. DREIBUS, E. JAGOUTZ, H. KRAUSE, H. PALME, B. SPETTEL, AND F. TESCHKE, Multielement Analyses of Apollo 15, 16 and 17 Samples and the Bulk Composition of the Moon. *Proc. Fourth Lunar Science Conference, Geochimica et Cosmochimica Acta*, Supplement 4, Vol. 2, 1973, pp. 1461–1481.
67. GROSSMAN, L., Condensation in the Primitive Solar Nebula. *Geochimica et Cosmochimica Acta*, Vol. 36, No. 5, 1973, pp. 597–619.
68. GREY, M., D. A. PAPANASTASSIOU, AND G. J. WASSERBURG, The Identification of Early Condensates From the Solar Nebula. *Icarus*, Vol. 20, pp. 213–239.
69. ARRHENIUS, G., Chemical Effects in Plasma Condensation. *From Plasma to Planet*, Nobel. Symposium, 1972, pp. 117–129.
70. ONUMA, N., R. N. CLAYTON, AND T. K. MAYEDA, Cosmothermometer. *Geochimica et Cosmochimica Acta*, Vol. 36, No. 2, 1972, pp. 169–188.
71. CLAYTON, R. N., L. GROSSMAN, AND T. K. MAYEDA, A Component of Primitive Nuclear Composition in Carbonaceous Chondrites. *Science*, Vol. 182, 1973, pp. 485–488.
72. CAMERON, A. G. W., Properties of the Solar Nebula and the Origin of the Moon. *The Moon*, Vol. 7, Nos. 3 and 4, 1973, pp. 377–383.
73. LYAPUNOV, A., Sur les figures d'Equilibre Peu Differentes des Ellipsoides dune Masse Liquide Homogene Douee d'un Mouvement de Rotation. *Petirsbourg*, 1906–1914.
74. CARTAN, E., *Bull. Sci. Math.*, Vol. 46, 1922, p. 332.
75. CARTAN, E., Sur la Stabilite Ordinaire des Ellipoides de Jacobi. *Proc. International Mathematical Congress*, Toronto, Vol. 2, 1924, pp. 9–21.
76. LYTTLETON, R. A., *Stability of Rotating Liquid Masses*. Cambridge Univ. Press, 1953, p. 150.

77. LYTTLETON, R. A., The Theoretical Basis of the Fission Theory of Binary Stars. *Trans. Int. Ast., Univ.*, Vol. 8, 1954, pp. 717–721.
78. OSTRIKER, J. P., Fission and the Origin of Binary Stars. *Stellar Rotation*, IAU Colloq., 1970, pp. 147–155.
79. LEBOVITZ, On the Fission Theory of Binary Stars. *Astrophys. J.*, Vol. 175, No. 1, Part 1, 1972, pp. 171–183.
80. O'KEEFE, J. A., The Origin of the Moon: Theories Involving Joint Formation With the Earth. *Astrophys. and Space Sci.*, Vol. 16, No. 2, 1972, pp. 201–211.
81. O'KEEFE, J. A., After Apollo: Fission Origin of the Moon. *Bull. Atom. Sci.*, Vol. 29, No. 9, 1973, pp. 26–29.
82. SCHMIDT, O. YU., Development of the Planets and Their Satellites. *Izv. AN SSSR*, Physics Series, Vol. 14, No. 1, pp. 29–45. *Trudy Geophys. Inst.*, No. 11, (138), 1950, pp. 1–20.
83. SCHMIDT, O. YU., *Four Lectures on the Theory of the Origin of the Earth*, Acad. Sci. U.S.S.R. Press, 1950.
84. SCHMIDT, O. YU., *A Theory of the Origin of the Earth, Four Lectures, Lawrence and Wishart.*, London, 1959.
85. KAULA, W. M., Dynamical Aspects of Lunar Origin. *Rev. Geophys. Space Phys.*, Vol. 9, No. 2, 1971, pp. 217–238.
86. RUSKOL, YE. L., The Origin of the Moon II. The Growth of the Moon in the Circumterrestrial Satellite Cluster, *Astron. Zhurn.*, Vol. 40, No. 2, 1963, pp. 288–296.
87. RUSKOL, YE. L., The Origin of the Moon III. Some Problems of the Dynamics of the Circumterrestrial Cluster. *Astron. Zhurn.*, Vol. 48, No. 4, 1971, pp. 819–829.
88. RUSKOL, YE. L., The Formation of the Moon From the Circumterrestrial Cluster. *Izv. AN SSSR, Fizika Zemli*, No. 7, 1972, pp. 99–108.
89. MACDONALD, G. J. F., Tidal Friction. *Rev. Geophys.*, Vol. 2, No. 3, 1964, pp. 467–541.
90. RUSKOL, E. L., On the Model of the Accumulation of the Moon Compatible with the Data on the Composition and Age of Lunar Rocks. *The Moon*, Vol. 6, Nos. 1 and 2, 1973, pp. 190–201.
91. ALEXANDER, M. E., The Weak Friction Approximation and Tidal Evolution of Close Binary Systems. *Astrophys. and Space Sci.*, Vol. 23, No. 2, 1973, pp. 459–510.
92. RUSKOL, YE. L., Possible Differences in the Chemical Composition of the Earth and the Moon During the Formation of the Moon in the Circumterrestrial Cluster. *Astron. Zhurn.*, Vol. 48, No. 6, 1971, pp. 1336–1338.
93. RUSKOL, YE. L., On the Initial Distance of the Moon Forming in the Circumterrestrial Swarm. *The Moon, IAU Symposium No. 47*, 1972, pp. 402–404.
94. OROVAN, E., Density of the Moon and Nucleation of Planets. *Nature*, Vol. 222, No. 5196, 1969, p. 867.
95. KERRIDGE, J. F., AND J. F. VEDDER, Accretionary Processes in the Early Solar System: An Experimental Approach. *Science*, Vol. 177, No. 4044, 1972, pp. 161–163.

Page intentionally left blank

Page intentionally left blank

section 3

Lunar Magnetism and Gravity

Page intentionally left blank

Page intentionally left blank

Results From the Apollo Passive Seismic Experiment [1]

Gary Latham, Yosio Nakamura, James Dorman,
Frederick Duennebier, Maurice Ewing,
and David Lammlein
Marine Science Institute
Division of Solid Earth
and Planetary Geophysics
University of Texas
Galveston, Texas

Recent results from the Apollo Seismic Network suggest that (1) primitive differentiation occurred in the outer shell of the Moon to a depth of approximately 300 km and (2) the central region of the Moon is presently molten to a radius of between 200 and 300 km. If early melting to a depth of 300 to 400 km was a consequence of accretional energy, very short accretion times are required. The best model for the zone of original differentiation appears to be a crust 40 to 80 km thick, ranging in composition from anorthositic gabbro to gabbro, and overlying an ultramafic cumulate (olivine-pyroxene) about 250 km thick. The best candidate for the molten core appears to be iron or iron sulphide. A new class of seismic signals has recently been identified that may correspond to shallow moonquakes. These are rare, but much more energetic than the more numerous, deep moonquakes.

Five seismic stations have been placed on the Moon by the astronauts of Apollo missions 11, 12, 14, 15, and 16. The Apollo 11 station, powered by solar cells and intended for operation only during the lunar day, failed after exposure to the first nighttime period. The remaining four stations, powered by radio isotope thermal generators (RTG), have operated continuously since their initial activation. These four stations constitute the Apollo Seismic Network. The locations and installation dates of these stations are given in table 1.

The network was completed as of April 1974, with the installation of the fourth station in the Descartes region of the southern highlands during mission 16. It is estimated that the maximum lifetime of each station will be about 10 yr, corresponding to the useful lifetime of the RTG power source. Each station contains four seismometers. Three of these seismometers form a triaxial set (one sensitive to vertical motion and two sensitive to horizontal motion), with sensitivity to ground motion sharply peaked at .45 Hz. The fourth seismometer is sensitive to vertical motion, with peak sensitivity at 8 Hz. These instruments can detect vibrations of the lunar surface as small as ½ Å at maximum sensitivity.

Table 1.—*Locations and Installation Dates of the Stations of the Apollo Seismic Network*

Station	Date of Installation	Location	
		Latitude	Longitude
12	Nov. 19, 1969	3.04°S.	23.42°W.
14	Feb. 5, 1971	3.65°S.	17.48°W.
15	July 31, 1971	26.08°N.	3.66°E.
16	April 21,1972	8.97°S.	15.51°E.

[1] Contribution No. 44 of the Marine Science Institute, Division of Solid Earth and Planetary Geophysics, University of Texas, Galveston, Texas.

Owing to the extreme quiet of the lunar surface, the instruments can be operated at peak magnification of approximately 20 million. This is two to three orders of magnitude higher than can normally be used on Earth. All but two of the 16 separate seismometers are presently operating. The short-period seismometer at station 12 has failed to operate since initial activation, and the long-period vertical component seismometer at station 14 became unstable after 1 yr of operation.

The following section summarizes the major findings from earlier work for the benefit of the reader unfamiliar with these results. A recent review of the results has been presented by Lammlein et al. (ref. 1).

Brief Review of Previous Results

Prior to the first lunar landings, the seismic experiment team had anticipated that moonquakes, if extant, might originate along the large rill-like features that crisscross the lunar surface or along the fracture systems associated with the large maria basins. High-frequency signals that are possibly shallow moonquakes have, in fact, been recorded and are among the largest of the signals recorded to date. However, these high-frequency signals are extremely rare; 11 such events have been identified over a period of 3 yr. Much more numerous, but very small in magnitude (maximum Richter magnitudes of about 2), are moonquakes that occur at great depth. These are concentrated in a relatively thin zone at depths of between about 600 and 800 km. A third category of moonquakes has been recognized. These are small events that can be detected at each station at maximum ranges of a few tens of kilometers. The frequency of occurrence of these events is closely correlated with the lunar surface temperature cycle. These are almost certainly of thermal origin. Slumping of material along steep slopes or dislocations along fracture or bedding planes of material very near the surface caused by thermal stresses have been suggested as possible source mechanisms (ref. 2). These will not be discussed further here, except to remark that the mechanism leading to thermal moonquakes may represent an important erosional process on the lunar surface. The total annual energy release from moonquakes is estimated to be less than 10^{15} ergs per year. This is about nine orders of magnitude lower than that of the Earth. If the sensitivities of the lunar seismographs were limited to the levels of their terrestrial counterparts, we would have recorded no moonquakes at all. Our conclusion would have been that the Moon is totally devoid of internal activity leading to quakes. Signals are recorded from several hundred meteoroid impacts per year at each station. By using the impacts from the third stages of the Saturn boosters as calibrations and a statistical method developed by James Dorman (described in ref. 3), the present meteoroid flux in the vicinity of the Moon has been estimated to be

$$\log N = -1.62 - 1.16 \log m$$

where N is the cumulative number of meteoroids of mass m (in grams) and greater which strike the Moon per year per square kilometer. This flux estimate is one to three orders of magnitude lower than those derived from earlier Earth-based measurements. However, it is in agreement with estimates derived from the distribution of crater sizes on the youngest lunar maria, assuming a plausible decrease in meteoroid flux between the time of maria formation and the present. Indeed, Wetherill (ref. 4) has pointed out that previous Earth-based flux estimates were too high by a factor of about 35 to be consistent with the crater size distributions observed on the maria. We estimate that a meteoroid of mass 7 to 10 kg can be detected by the Apollo Seismic Network from any point on the Moon. Thus, the Moon, when attached to a seismometer, has proven to be an unexpectedly good "sounding board" for the detection of meteoroid impacts. This results from a combination of two factors: the extremely high instrument sensitivities possible on the lunar surface and the unusually high efficiency of seismic wave propagation throughout most of the lu-

nar interior. The major weakness in the method thus far is the availability of only one calibration point (S–IVB) impact energy). Obviously, a larger number of manmade impacts covering a wide range of impact energies would be highly desirable. Gault (personal communication) has pointed out that we may need to increase our flux estimate by a factor of 2 to correct for the probability of nonnormal angles of impact. It should also be noted that attempts to use near-range seismic sources (thumper, etc.) as calibrations for meteoroid impact signals recorded by the SPZ component lead to higher meteoroid flux estimates (ref. 2). The discrepancy between these two methods remains to be resolved.

Lunar seismograms differ markedly from typical Earth recordings. The most striking feature of lunar signals is their long duration. Examples are shown in figure 1. Impact-generated lunar signals have emergent beginnings, increase gradually to a maximum, and then slowly decay. Following the first one or two cycles of the P-wave, ground motion is very complex, with little or no correlation between any two components. The onset of the shear wave from near impacts (ranges less than 1000 km) cannot be identified with certainty. Coherent surface wave trains displaying dispersion have not been recognized in any recordings to date, although scattered surface waves undoubtedly contribute to the signals. The direction of propagation can rarely be determined from the particle motion at a single station. Thus, many analysis techniques found useful in terrestrial seismology cannot be applied to lunar signals. Signals from the deep moonquakes are generally less complex in the early part of the wave train than those from impacts. The largest amplitudes are clearly associated with the shear waves; however, the exact onset of the shear waves is difficult to identify. These unusual characteristics of lunar signals appear to be accounted for by assuming a high degree of heterogeneity, resulting in intensive scattering, and very low absorption of seismic wave energy in a thin surficial zone, referred to as the scattering zone. Nakamura (ref. 5) has successfully described the envelope characteristics of lunar signals by using diffusion theory. His analysis shows that most of the scattering occurs in the outer few hundred meters of the Moon in which the Q of the medium must range between about 3000 and 5000. In fact, the extremely low absorption of seismic waves in this material is the dominant factor leading to the characteristics of lunar seismograms described above. Many

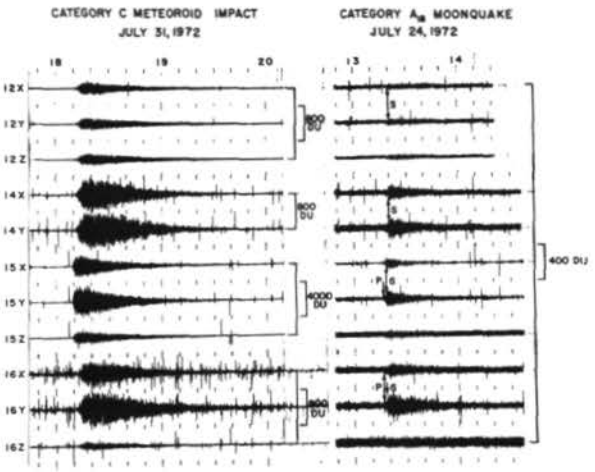


Figure 1.—*Compressed time-scale records of long-period (LP) components for two natural seismic events recorded at four seismic stations. X and Y refer to the horizontal component seismometers; Z refers to the vertical component seismometers. Each successive trace deflection of an LP compressed time-scale record represents the sum of the absolute values of the differences between 40 successive data samples during consecutive, nonoverlapping 6-s time intervals. Successive deflections are plotted on opposite sides of the zero baseline. The relative amplitudes of the signals are indicated by the brackets following each record. Tick marks are 10 min apart, and hours are labeled. The category A moonquake zone is located at the eastern border of Mare Serenitatis. For category A moonquakes, the direct shear wave S is prominent on seismograms from the horizontal seismometers. The direct compressional wave P is observed on seismograms of the largest category A moonquakes. The category C meteoroid impacted roughly 500 km north of station 15. The onsets of the direct compressional and shear waves can rarely be identified on LP seismograms of category C events.*

terrestrial seismograms would possess the same characteristics as those of lunar seismograms if the absorption of seismic energy were reduced to lunar values. There is a growing body of laboratory data supporting our earlier contention that this marked contrast in absorption can be ascribed to the nearly complete absence of volatiles, principally water, in the outer shell of the Moon.

A seismic velocity model for the upper 150 km of the Moon has previously been defined (refs. 3 and 6) on the basis of observed traveltimes and amplitudes of body waves from nine impacts of S–IVB and LM space vehicles, combined with data from laboratory measurements on returned lunar samples. Seismic signals from these impacts were recorded at ranges from 9 km to 1750 km. Figure 2 shows a first-order model for the variation in the velocity of compressional waves, with depth consistent with the traveltimes of seismic waves from these manmade impacts and a meteoroid impact that occurred within the array. The most important feature of this model is the abrupt increase in velocity in the depth range between 50 and 55 km. By analogy with the Earth, we refer to the zone above this discontinuity as the crust and to the zone below as the mantle. Near the surface the velocity increases rapidly from a value of about 100 m/s measured in the regolith, reaching a value of between 6.3 and 7.0 km/s at the base of the crust. The rapid increase in velocity near the surface can be explained by the progressive compaction of materials so thoroughly fragmented that the velocity of propagation through them is determined primarily by its mechanical state rather than by its chemical composition. Velocities in the range from 6 to 7 km/s are appropriate for, but not restricted to, the rock types found to predominate in the lunar highlands (anorthositic gabbros and aluminous basalts). At the mantle boundary, the compressional wave velocity increases to about 8.1 km/s—a value appropriate for rocks of olivine-pyroxene composition. As shown by Kovach and Watkins (ref. 7), the velocity variation in the outer crust may be stepwise in some areas where flows (ash or lava) have escaped complete obliteration, but the smooth variation shown in figure 2 appears to be a good approximation of the stepwise increase they infer for the region of the Apollo 17 landing site.

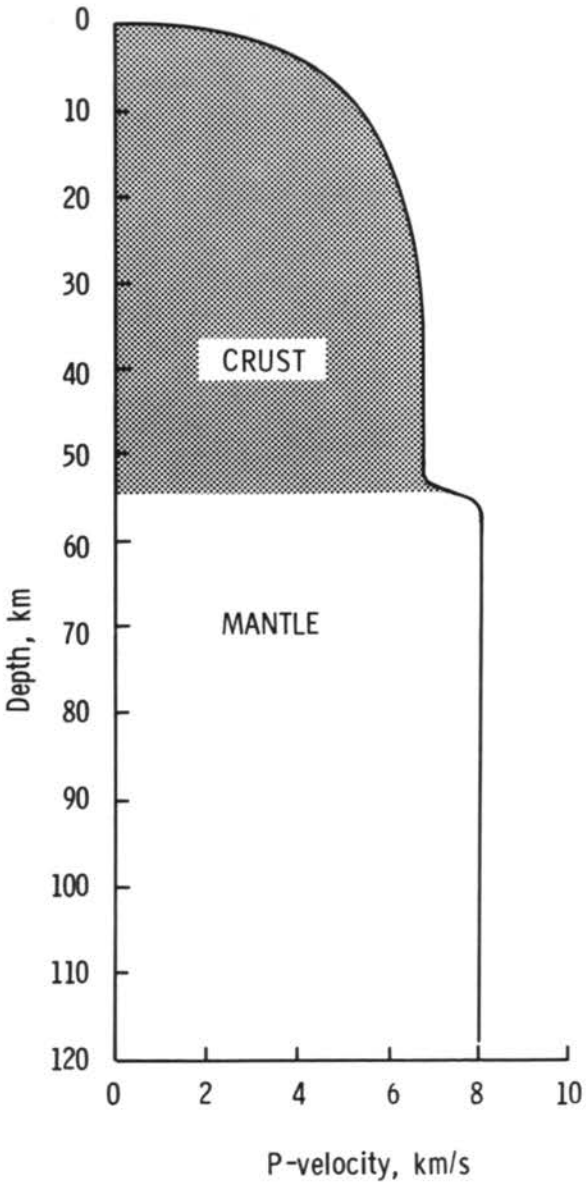


Figure 2.—*Compressional wave velocity model based on seismic data from nine manmade impacts and one near meteoroid impact.*

It was found soon after the installation of station 12 that moonquake signals could be grouped into sets, with members of each set having waveforms that match one another in detail. Moonquakes in each group occur at regular intervals, normally once per month, and at specific times during the lunar orbit. In some cases as many as three or four moonquakes of a given set will occur during a monthly cycle, but such multiple events occur over a relatively short interval of a few days or less. The repetitious character of these events strongly supports the hypothesis that they are moonquakes, each group of matching signals corresponding to an active zone or focus within the Moon at which the repeating moonquakes originate. Forty-one sets of signals, corresponding to 41 active foci, have been identified to date. Since the total number of moonquakes in the matching groups represent only about 10 percent of the several thousand moonquakes recorded to date, it is quite probable that many other active foci exist. However, the signals recorded from them are too small to permit detailed analysis of their waveforms.

Two tidal periodicities have been recognized in the moonquake activity patterns (variations in times-of-occurrence and amplitudes): 13.6 days and 206 days. The shorter period variation corresponds to the nodical or draconic month. The longer period is introduced by solar perturbation of the lunar orbit, which results in a cyclical variation of the Earth-Moon separation at times of perigee. A third periodicity, corresponding to the successive synchronizations of the anomalistic and nodical months and having a period of about 6 years, appears to be present. However, the sample length is not yet long enough to confirm this. It is evident that tides play a dominant role in the generation of moonquakes. However, with very few possible exceptions, the polarities of seismic signals from a given source are identical. This implies that the dislocation is progressive and not periodically reversed. Progressive dislocation suggests secular accumulations of strain periodically released by moonquakes. Weak convection within the deep lunar interior or relaxation of tidal deformation as the Moon recedes from the Earth have been suggested as possible sources of secular accumulation of strain.

Using the velocity model described above, extrapolated to the depths of moonquakes, 27 of the active foci have been located. The epicentral locations are shown in figure 3. In nine cases the depth of focus was assumed in the calculation. The moonquake foci are concentrated in two narrow belts. Both belts are 100 to 300 km wide, about 2000 km long, and 600 to 800 km deep. (Earlier estimates placed the depth of the moonquake zone at between 800 and 1000 km.) Whether the apparent alignment into belts is real or a mirage that will disappear as more epicenters are located is not known. However, the distribution is certainly not random. The epicenters lie approximately along arcs of great circles that intersect at an angle of about 80 degrees. This pattern cannot be explained as a natural consequence of the distribution of seismic stations, nor do we know of any tidal stress component that would lead to such a pattern. In addition, no systematics in the relative times of occurrence of the moonquakes within a given belt have been discerned, except that peaks in the combined activity detected from all foci occur at average intervals of 13.6 days and are approximately in phase at all stations.

Only one moonquake epicenter has been located on the farside of the Moon. For signals from this source, it was noticed that shear waves were missing in the seismogram recorded at the most distant station for which the signal could be detected (station 14). Since shear waves from moonquakes are normally prominent at station 14, this observation remained a mystery until the phenomenon of missing, or greatly delayed, shear waves was observed in the records from a distant impact. Although other interpretations are possible, Nakamura et al. (ref. 8) found that these observations could be explained by assuming that partial melting begins in the present-day Moon at a depth of about 1000 km. (This boundary must be moved upward to a depth of about

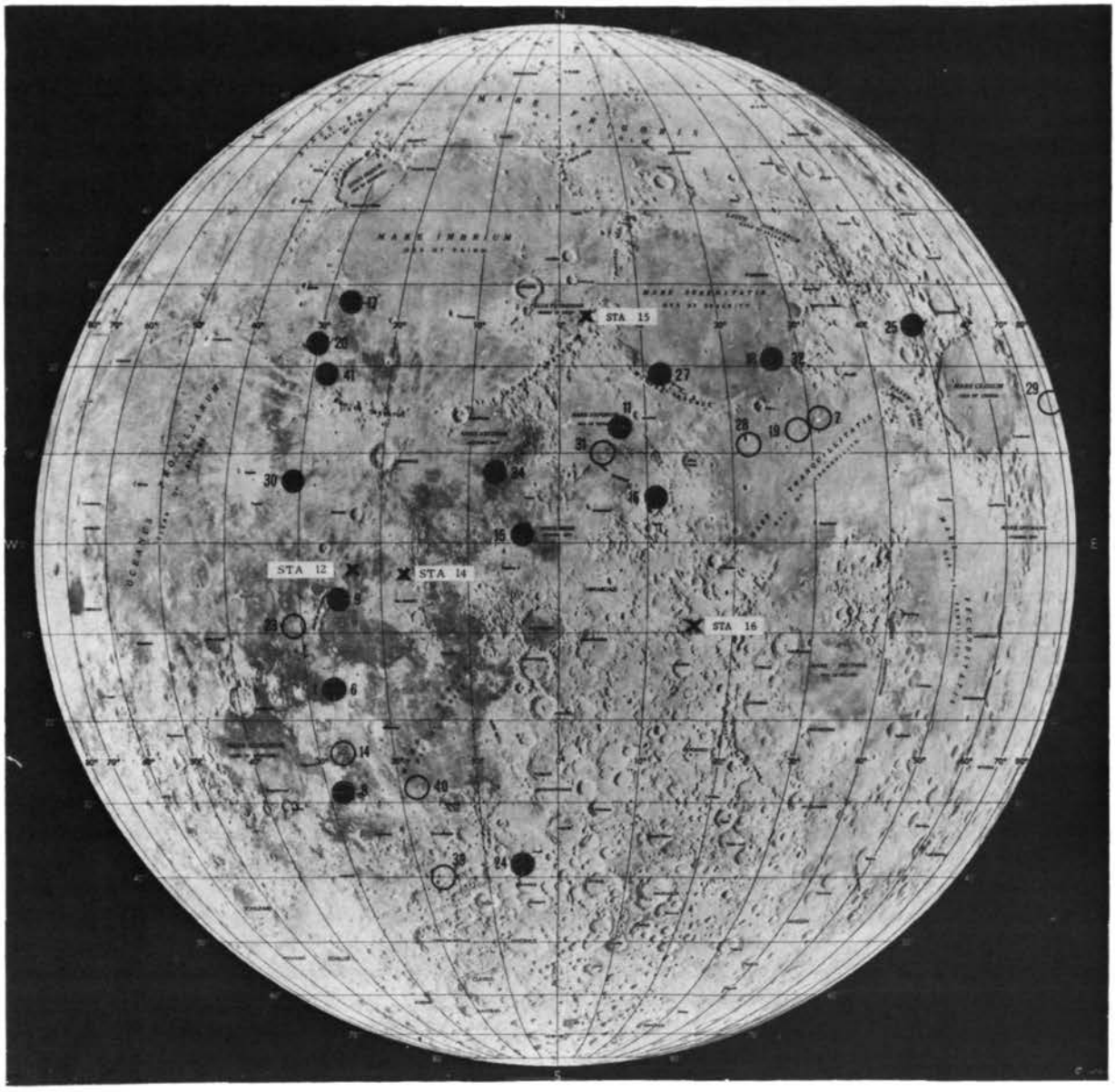


Figure 3.—*Map of the nearside of the Moon locating the Apollo 12, 14, 15, and 16 seismic stations (table 1) and the category A moonquake epicenters. Solid circles indicate the foci for which the depth can be determined. Open circles correspond to cases in which data are not sufficient for determination of depth. In these cases a depth of 800 km was assumed to locate the epicenter. Note that epicenters 1 and 6 and 18 and 32 are so closely spaced that their separation cannot be distinguished at the scale plotted. One focus occurs on the farside of the Moon.*

800 km according to the more recent results presented here.) Following the same line of reasoning, significant melting cannot be present in the crust and mantle at depth shallower than the moonquake zone, since high-frequency shear waves are prominent in the seismograms from all nearside moonquakes. Since little or no seismic activity has been detected above the moonquake zone and subsolidus temperatures are inferred, we refer to this dynamically inactive outer shell as the lithosphere and to the "weaker" central zone, in which partial melting is inferred, as the asthenosphere.

Recent Results

HIGH-FREQUENCY TELESEISMIC EVENTS

A set of seismic signals with unusual characteristics has recently been identified (ref. 9). They are distinguished from all other signals recorded at comparable ranges (greater than 1000 km) by their high-frequency content. Only 11 signals of this type, designated high-frequency teleseismic (HFT) signals, have been identified in the 3-year period for which data are available. Some of these are among the largest signals detected. Recordings for one of these events are shown in figure 4, along with representative signals from a moonquake and a meteroid impact. The relatively high-frequency content of the HFT signal can be seen in this figure by comparing the amplitudes recorded by the long-period seismometers (LPX,Y,Z) with those recorded by the short-period seismometers (SPZ). The relatively large amplitude of the SPZ record for the HFT event indicates that most of the signal energy is at frequencies above 1 Hz; whereas frequencies below 1 Hz are dominant in signals for distant moonquakes and impacts. This comparison is made for a larger number of events in figure 5, where the ratio of the maximum signal amplitudes recorded by the SPZ and LPY (one of the long-period horizontal components) seismometers is plotted

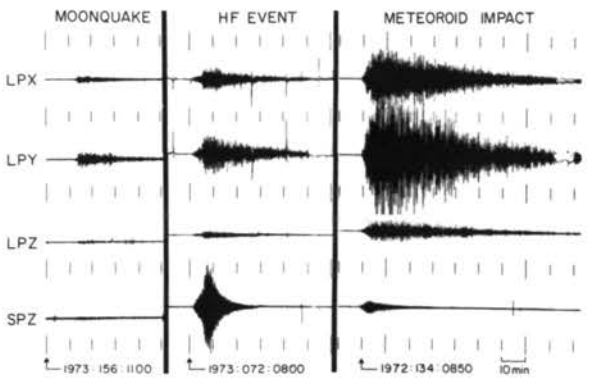


Figure 4.—*Seismogram of a high-frequency teleseismic (HFT) event detected on March 13, 1973 (center), compared with those of a moonquake detected on June 5, 1973 (left: category A_1), and a meteoroid impact detected on May 13, 1972 (right). All of these seismograms were recorded at the Apollo 16 station. LPX, LPY, and LPZ stand for three orthogonal components of a long-period instrument peaked at about 0.45 Hz. SPZ stands for a short-period vertical component peaked at 8 Hz. Note the relatively impulsive beginning of P- and S-wave arrivals of the HFT event, similar to those of the moonquake, and the large SPZ amplitude of the HFT event.*

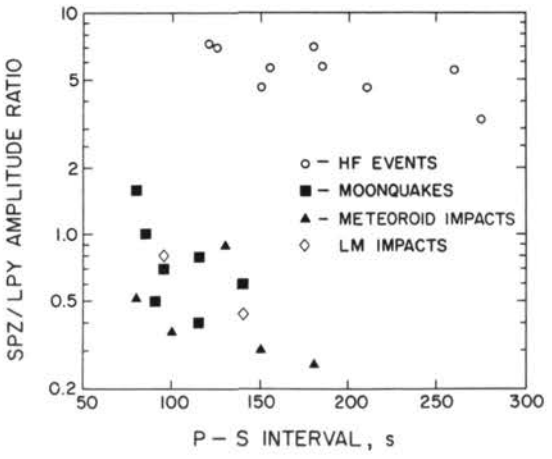


Figure 5.—*SPZ/LPY amplitude ratio versus S–P time interval for the HFT events and selected other events recorded by the Apollo 14 station. A large amplitude ratio means a greater high-frequency content of a signal. Increasing S–P time corresponds to increasing distance from the station.*

versus the time interval between the P-wave and S-wave arrivals for each signal. This time interval is a function of distance between the source and the seismic station—increasing time interval corresponding to increasing distance. The distinctive character of the HFT signals is evident in this plot.

The beginnings of the P-wave and S-wave trains are much more impulsive for HFT signals than those of typical meteoroid impact signals, suggesting that scattering near the source is much less for the HFT events than for normal surface sources. On the other hand, the predominance of shear waves in the signals from the most distant HFT events requires that the source be shallower than 300 km (ref. 9).

Several source mechanisms for these unusual signals are suggested: either they are generated by meteoroids that penetrate the scattering zone into more competent material below (200 to 300 meters), they are generated by impacts in areas where unusally competent and structurally homogeneous material lies close to the surface, or they are shallow moonquakes. The latter interpretation is favored. It is difficult to conceive of any process that would preserve isolated patches of the lunar surface relatively undisturbed by meteoroid impacts. If such regions do exist, gradational cases would be expected, resulting in a broad spectrum of signal characteristics instead of the sharp division between signal classes observed. On the other hand, the existence of some shallow moonquake activity in a cooling planet would be expected.

STRUCTURE AND STATE OF THE DEEP LUNAR INTERIOR

Information on the structure and state of the deep lunar interior is derived principally by analysis of seismic signals from distant impacts and moonquakes. As noted above, meteoroid impact signals are so emergent that it is rarely possible to pick the onset of the P-wave with certainty, and the onset of shear waves can be separated out from the compressional wave train only in the signals from distant impacts. Signals from four of the largest impacts and two of the HFT events have been selected as suitable for the present analysis. The traveltime curves for these events, as given by Nakamura et al. (ref. 10), are shown in figure 6. These data can be inverted by the Wiechert-Herglotz method to give seismic velocities as a function of depth, assuming that velocity gradients are not so large as to invalidate the method. However, several points can be made by inspection of these curves without further analysis. First, we note that the curve for shear (S) waves departs markedly from the curve for compressional (P) waves at a range of about 85° (2600 km), corresponding to maximum depths for the S-wave ray path of about 300 to 400 km. The velocity of shear waves must begin to decrease sharply (i.e., Poisson's ratio begins to increase) in this depth range. Secondly, the P-wave traveltime for the most distant point is delayed by about 120 s from the value expected by smooth extrapolation of the curve. This indicates that the velocity of P-

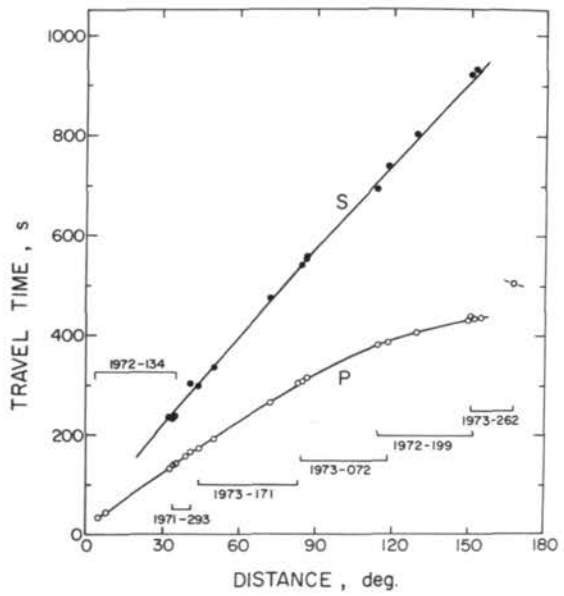


Figure 6.—*Travel-time data for compressional (P) and shear (S) waves recorded from four distant impacts and two HFT events.*

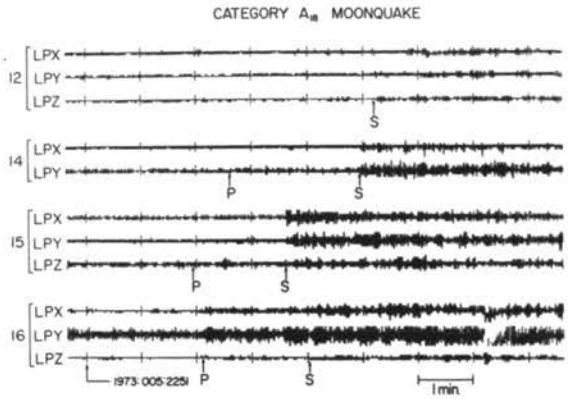


Figure 7.—*Four-station expanded time scale playouts of a category A_{1s} moonquake detected at 22:53 hours on January 5, 1973. X and Y refer to LP horizontal component seismometers; Z to the LP vertical component seismometers. Tick marks are 1 min apart. These signals are typical of moonquakes recorded at each of the stations. The direct shear wave (S) is prominent on the horizontal component seismograms at all of the stations. The direct compressional wave (P) is also observed at stations 14, 15, and 16.*

waves decreases abruptly at depths of between 1380 and 1570 km.

Below the zone of abrupt shear-wave decrease, the Wiechert-Herglotz method cannot be applied for shear waves with confidence, and signals from moonquakes that originate beneath this zone must be used. Signals from one of the moonquakes used in this analysis are shown in figure 7. Combining the traveltime data from deep moonquakes with the data of figure 6, the model shown schematically in figure 8 has been derived. For purposes of discussion, it is convenient to divide the lunar interior into five major zones:

Zone 1—The Crust

Zone 1 represents a layer approximately 55 km thick in the region of stations 12 and 14. If the crust is a global feature, as suggested by several lines of evidence (ref. 1), it is probably quite variable in thickness, with thickness of the backside crust substantially greater than that of the nearside (ref. 11). The crustal velocities are appropriate for the plagioclase-rich materials inferred from sample analysis, possibly grading from anorthositic material at the top to more gabbroic material at depth.

Zone 2—The Upper Mantle

Zone 2 is approximately 250 km thick, with a compressional wave velocity of about 8.1 km/s at the top, decreasing to about 7.8 km/s at the bottom. Possible compositions of this zone can be inferred from the velocities and densities corresponding to the model of figure 8. Based upon geochemical considerations (ref. 12), olivine and pyroxene are the most probable constituents of the rocks of the upper mantle. Curves of velocity versus density for these minerals are given in figure 9, along with the values derived from our preliminary model, assuming a uniform composition for the upper mantle (i.e., the velocity decrease with depth in the upper mantle is due to increasing temperature with depth). The experimental values

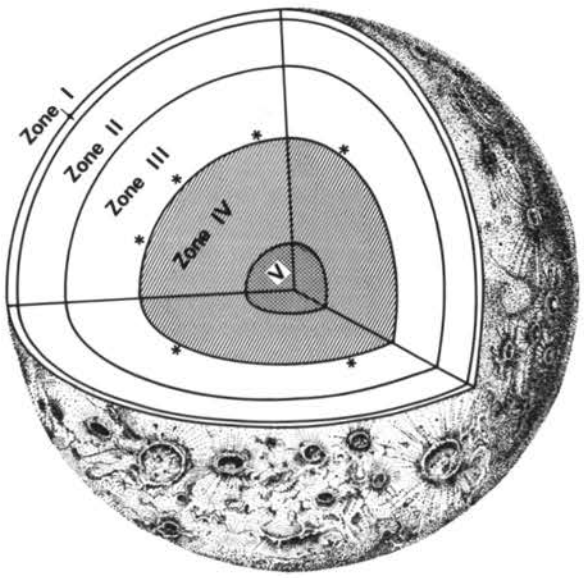


Figure 8.—*Pictorial representation (drawn approximately to scale) of the internal structure of the Moon as described in the text. X marks indicate the zone of deep moonquakes.*

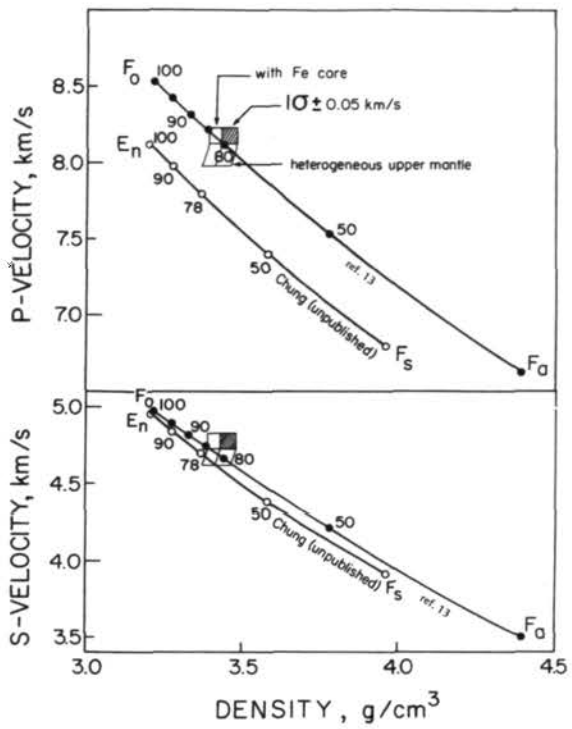


Figure 9.—*Density versus velocity (corrected to standard temperature and pressure) calculated from the seismic data of figure 6 for the upper mantle (zone 2) of the Moon. Compressional- and shear-wave data for the olivine (Fo—Fa) series (ref. 13) and the orthopyroxene (En—Fs) series (Chung, personal communication, 1974) are shown for comparison. The calculations permit variations in the various lattice dynamical parameters over ranges approximate for rocks of mafic composition. Calculations have been made for two cases. (1) The crosshatched block corresponds to the assumption that the composition of the upper mantle is uniform throughout, i.e., that the effects of temperature and pressure balance to give the experimentally determined velocity-depth functions. This requires a velocity gradient of 4 to 5° C/km in the upper mantle, (2) The open block below shows the change introduced by decreasing the temperature gradient to between 2 and 3° C/km. For this case, the intrinsic velocity and density must decrease slightly with depth. From this comparison, a composition close to the magnesian end of the olivine series (80 percent forsterite) is suggested for the upper mantle. For both cases described above, the effect of including an iron core (zone 5) of density 7.5 g/cc and a maximum radius of 360 km is also shown.*

for the upper mantle thus derived are in good agreement with the olivine data (80 to 85 percent forsterite). The calculated points are shifted slightly to the left if an iron-sulphide core (zone 5) is assumed. The assumption of constant composition requires a temperature gradient of 4 to 5°C/km for the upper mantle. Alternatively, the traveltime data can be satisfied by assuming a variation from magnesium olivine at the top to more pyroxenitic material below and reduction of the temperature gradient to between 2 and 3°C/km. Walker et al. (ref. 14) have pointed out that a mafic cumulate of thickness corresponding to that inferred here for the upper mantle (about 250 km) might be expected if a plagioclase-rich crust 50 to 60 km thick is present.

Zone 3—The Middle Mantle

This zone, extending from about 300 to 800 km, is characterized chiefly by the reduced velocity of shear waves (3.6 to 4.0 km/s) within it. It is likely that the compressional wave velocity is also decreased slightly in this layer, but this cannot be resolved with the available data. Thus, the material of zone 3 must have a high Poisson's ratio (0.34 to 0.35) compared to that of the material above in which the Poisson's ratio is approximately 0.25. One possible interpretation is that this zone represents primitive lunar material below the zone of initial melting that produced zones 1 and 2. Mare basalts may have been produced by partial melting within zone 3, 3.2 to 3.8 b.y. ago in accordance with the proposals of Duba and Ringwood (ref. 12) and others. Moonquakes are concentrated within a relatively thin zone at the base of zone 3, in a depth range of from 600 to 800 km. Because high-frequency shear waves are recorded from all of these sources (except the farside focus), we can say immediately that widespread melting in zones 1, 2, and 3 is not possible, i.e., temperatures in these zones must be subsolidus. In addition, there is little or no scattering of seismic waves in zone 3. Thus, if

this represents an accumulation of primitive materials, either individual blocks are small compared to a wavelength (less than about 1 km in dimension), the elastic properties of the individual blocks do not vary appreciably, or any inhomogeneities have been removed by subsequent melting.

There is some evidence that the transition from zones 2 to 3 may be relatively sharp. A prominent phase, designated R in figure 10, has been identified in the wavetrains of the largest moonquake signals. The relative arrival times for this phase can be explained by assuming that the phase is generated by conversion from S to P at an interface located at a depth of about 300 km, the approximate depth for the boundary between zones 2 and 3 derived from shear-wave travel-time data. Similar mode conversions have been tentatively identified in records from deep earthquakes (ref. 16).

Zone 4—The Lower Mantle

This zone is characterized chiefly by the absence of identifiable shear waves for events in the distance range for which shear waves would enter this zone. This can be ascribed to (1) a sharp decrease in shear-wave velocity at the top of the zone, leading to a shadow zone for shear waves, or (2) high attentuation of shear waves within this zone. The latter interpretation is favored for the following reasons. First, we must explain the concentration of moonquake activity, closely correlated with lunar tides, immediately above this zone. Calculation of tidal energy density as a function of depth shows that a sharp maximum is introduced in the depth range of moonquakes if a zone of much "weaker" material (zone 4) is introduced below (ref. 16). Second, the velocity of P-waves cannot decrease more than 0.2 to 0.3 km/s within this zone. A greater decrease in compressional wave velocity would be expected to accompany the sharp decrease in the shear-wave velocity required to produce an optical shadow zone. To explain these observations, Nakamura et al. (ref. 8) have argued that partial melting is probable in the lunar mantle. If so, a temperature of approximately 1500°C is inferred for the top of zone 4, assuming a mafic composition.

Zone 5—The "Core"

This zone is characterized by a sharp decrease in the velocity of P-waves beginning at a depth of from 1380 to 1570 km. The inferred P-wave velocity for this zone is about 5 km/s, suggesting that the material of this zone is completely molten. Unless the material of zone 5 is more dense than that of zone 4, convective instability between zones

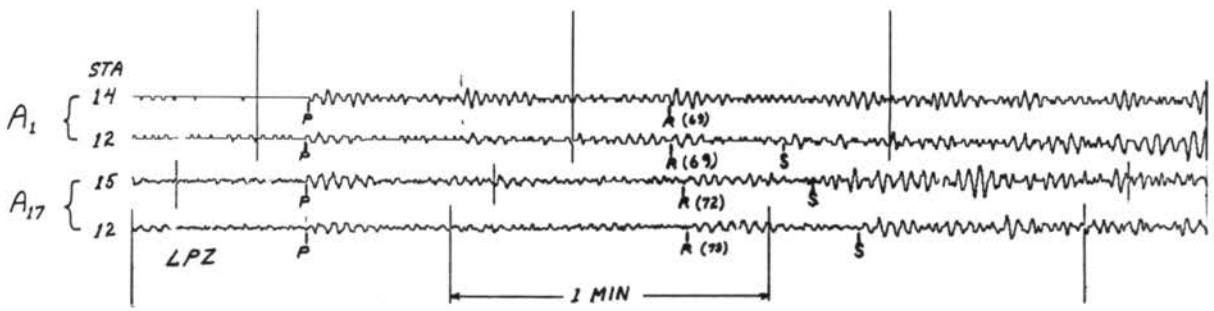


Figure 10.—*Seismograms from the long-period vertical component for two moonquakes, showing a phase (R) that may correspond to conversion from shear wave (S) energy to compressional wave (P) energy at an interface at a depth of about 300 km (the boundary between zones 2 and 3).*

4 and 5 would result. It is suggested that zone 5 represents a molten core of iron sulphide in accordance with the models earlier suggested on geochemical grounds by Brett (ref. 17) and Duba and Ringwood (ref. 12). If the composition of the core is iron sulphide, it represents less than 1 percent of the total mass of the Moon and falls easily within moment-of-inertia constraints. However, this interpretation must be regarded as quite tentative pending the acquisition of more seismic data pertinent to the properties of this zone.

Conclusions

An iron sulphide core of radius 200 to 300 km, as suggested by present seismic data, may have been the source of an early dipole field that magnetized lunar surface rocks.

If accretional energy were responsible for melting the outer shell of the Moon to a depth of about 300 to 350 km to produce the crust and upper mantle, very short accretion times are required—probably less than 10 000 years (ref. 12).

The low level of lunar seismicity and its concentration at great depth compared to the Earth now appear to be explained by the differences in thickness of the lithospheric shells and internal thermal energy of these two planets. The lunar lithosphere is simply too thick (about 800 km) to be disrupted by the relatively weak convective motion that might be induced by temperature gradients below. In the absence of this source of seismic activity, i.e., collisions between lithospheric plates, dislocations induced by tidal deformation of the Moon, are the dominant mechanisms for generation of quakes. Assuming that the Moon is cooling (contracting) slightly at present, as suggested by the thermal models of Toksöz and Solomon (ref. 18), the accumulation of compressional stress in the lithosphere would be expected to result in moonquakes at shallow depth. The few, relatively energetic events of unusually high-frequency (HFT) signals that have been detected may be explained in this way.

Acknowledgment

This research was supported by the National Aeronautics and Space Administration under contract NAS 9–13143.

References

1. LAMMLEIN, D., G. LATHAM, J. DORMAN, Y. NAKAMURA, AND M. EWING, Lunar Seismicity, Structure, and Tectonics. *Rev. Geophys. and Space Phys.*, Vol. 12, 1974, pp. 1–21.
2. DUENNEBIER, F., AND G. SUTTON, Thermal Moonquakes. *J. Geophys. Res.*, Vol. 79, in press, 1974.
3. LATHAM, G., M. EWING, J. DORMAN, Y. NAKAMURA, F. PRESS, T. TOKSÖZ, G. SUTTON, F. DUENNEBIER, AND D. LAMMLEIN, Lunar Structure and Dynamics—Results from the Apollo Passive Seismic Experiment. *The Moon*, Vol. 7, 1973, pp. 396–421.
4. WETHERILL, G., Of Time and the Moon. *Science*, Vol. 173, 1971, pp. 383–392.
5. LATHAM, G., M. EWING, F. PRESS, G. SUTTON, J. DORMAN, Y. NAKAMURA, N. TOKSÖZ, R. WIGGINS, J. DERR, AND F. DUENNEBIER, Apollo 11 Passive Seismic Experiment. *Geochimica et Cosmochimica Acta*, Supplement 1, Vol. 34, 1970, pp. 2309–2320.
6. TOKSÖZ, N., F. PRESS, A. DAINTY, K. ANDERSON, G. LATHAM, M. EWING, J. DORMAN, D. LAMMLEIN, G. SUTTON, F. DUENNEBIER, AND Y. NAKAMURA, Velocity Structure and Properties of the Lunar Crust. *The Moon*, Vol. 4, 1972, pp. 490–504.
7. KOVACH, R., AND J. WATKINS, Apollo 17 Seismic Profiling: Probing the Lunar Crust. *Science*, Vol. 180, 1973, pp. 1063–1064.
8. NAKAMURA, Y., D. LAMMLEIN, G. LATHAM, M. EWING, J. DORMAN, F. PRESS, AND N. TOKSÖZ, New Seismic Data on the State of the Deep Lunar Interior. *Science*, Vol. 181, 1973, pp. 49–51.
9. NAKAMURA, Y., J. DORMAN, F. DUENNEBIER, M. EWING, D. LAMMLEIN, AND G. LATHAM, High-Frequency Lunar Seismic Events. *Proc. Fifth Lunar Science Conference*, in press, 1974.
10. NAKAMURA, Y., G. LATHAM, J. DORMAN, F. DUENNEBIER, M. EWING, AND D. LAMMLEIN, Seismic Evidence on the Structure of the Deep Lunar Interior—A Progress Report. *Geophys. Res. Letters*, in press, 1974.
11. KAULA, W., G. SCHUBERT, R. LINGENFELTER, W. SJOGREN, AND W. WOLLENHAUPT, Lunar Topography from Apollo 15 and 16 Laser Altimetry. *Geochimica et Cosmochimica Acta*, Supplement 4, Vol. 3, 1973, pp. 2811–2819.

12. DUBA, A., and A. RINGWOOD, Electrical Conductivity, Internal Temperatures, and Thermal Evolution of the Moon. *The Moon*, Vol. 7, 1973, pp. 356–376.
13. CHUNG, D., Elasticity and Equations of State of Olivines in the Mg_2SiO_4-Fe_2SiO_4 System. *Geophys. J. R. Astron. Soc.*, Vol. 25, 1971, pp. 511–538.
14. WALKER, D., T. GROVE, J. LONGHEI, E. STOLPER, AND J. HAYS, Origin of Lunar Feldspathic Rocks. *Earth Planet. Sci. Letters*, Vol. 20, 1973, pp. 325–336.
15. JORDAN, T., Crust and Upper Mantle Structure From SP Phases. *Trans. Am. Geophys. Union*, Vol. 55, 1974, p. 359.
16. LAMMLEIN, D., AND G. LATHAM, Moonquakes and Tides. *Geological Soc. Am. Abs.*, Vol. 6, No. 3, 1974, p. 299.
17. BRETT, R., Sulphur and the Ancient Lunar Magnetic Field, *Trans. Am. Geophys. Union*, Vol. 53, 1972, p. 723.
18. TOKSÖZ, N., AND S. SOLOMON, Thermal History and Evolution of the Moon. *The Moon*, Vol. 7, 1973, pp. 251–278.

Page intentionally left blank

Page intentionally left blank

Lunar Mascons

V. N. Zharkov and A. P. Trubitsyn
O. Yu. Schmidt Institute of Earth Physics
Academy of Sciences,
Moscow, U.S.S.R.

In 1968, Muller and Sjogren discovered large positive anomalies in the gravitational field of the Moon and introduced the concept of mascons as the sources of these anomalies. In our review, we shall attempt to summarize ideas set forth in the literature and related in some manner to lunar mascons.

Mascons are found on the visible side of the Moon and near the limb, with the majority of them being colocated with the major circular mare (Mare Imbrium, Mare Serenitatis, Mare Nectarius, Mare Crisium, and Mare Humorum). Existing methods of observation do not allow the detection of mascons on the back side of the Moon. However, the fact that there are no large circular mare on the back side allows one to suppose that there are no large mascons there.

The distribution of mascons in the body of the Moon and their structure cannot, in principle, be uniquely solved without the use of additional data and, therefore, has been extensively discussed in the literature. However, it is now understood that the anomalous masses are located in the outer layers of the Moon and are well described by disc-shaped models. The magnitudes of the anomalous masses can be estimated either by analysis of test bodies placed at various depths or by the theorem of Gauss. The largest mascons correspond to anomalous masses of approximately 20×10^{-6} times the mass of the Moon, or about 10^{21} g. If we assign the anomalous masses to the surface of the Moon, all the large mare have approximately the same excess mass per unit area—800 to 900 kg/cm^2. This would be equivalent to an additional layer of basalt 3 km thick, with a density of 3.0 g/cm^3. If a mascon were formed by material located at the surface with a density of 0.3 g/cm^3 greater than the density of the crust, the thickness of the layer of displacing material would have to be 30 km.

Mascons are located in topographical depressions related to geologically ancient formations. Insofar as the circular mare are genetically related to the impact of large bodies on the surface of the Moon, these same events played an important role in the formation of the mascons. The impact of these bodies and the filling of the circular mare were separated by considerable intervals of time, on the order of hundreds of millions of years. The possibility that the mascons were formed by the impacting bodies themselves seems at present improbable. Therefore, the origin of the mascons is related to the transport of matter within the Moon and, apparently, requires the following chain of events, independent of the specific mechanism of mascon formation.

In the early stage of its development, the Moon developed a thick crust with a density less than the density of the underlying mantle. Apparently during this era the outer layers of the Moon were sufficiently hot to be highly plastic and possibly in a state of near hydrostatic equilibrium. Impacts of large bodies on the surface of the Moon resulted in the formation of large craters at the locations of the future circular mare, which then became in some manner isostatically equilibrated. Following this, the Moon entered a comparatively quiet period during which

formation of its lithosphere continued as a result of cooling of the outer layers. Apparently during this era the Moon acquired and retained an equilibrium shape. During this same era, the outer layers of the Moon acquired strength sufficient both to retain its shape and to support mascons. The formation of the lunar lithosphere was followed by the filling of the circular mare leading to the formation of the mascons.

Mascons represent the same kind of nonequilibrium feature on the Moon as does its figure, only on a smaller spacial scale. Apparently, the simultaneous theoretical study of the conditions of mascon formation and the figure of the Moon can reveal lunar dynamics during the epoch when the lunar lithosphere was formed. The lunar dynamics at this time are of fundamental scientific interest because they provide important boundary conditions for the formation of the Moon and the first stage of its existence.

The presence of mascons and the nonequilibrium figure (the latter is also reflected in the displacement of the geometric center of the Moon relative to the center of mass by up to several kilometers) leads to a displacement of the Moon's core from hydrostatic conditions and produces stresses on the order of 100 bars. This situation must be kept in mind when constructing various types of thermal histories for the Moon.

From the point of view of isostasy, there are two types of models for lunar mascons, nonisostatic and isostatic. A nonisostatic mascon corresponds to an actual excess of mass in the outer layer of the Moon. In the case of an isostatic mascon, the concentration of mass at the surface is compensated by a deficit of mass at a depth on the order of some hundreds of kilometers, leading to a density inversion. The isostatic model seems less satisfactory to us because it requires the existence of an area of reduced density at a considerable depth. Furthermore, this model strongly concentrates the stresses in the area between the two anomalous masses, increasing the maximum stresses in comparison to the nonisostatic models by five to ten times.

The presence of circular mare on one side of the Moon indicates that during their formation this side was physically isolated. It was assumed at one time that this was related to the fact that collisions of the Moon with large bodies occurred on one side of the Moon with greater probability. This was physically explained by the Moon's being in synchronous rotation and in the process of tidal evolution of its orbit when it caught up with smaller satellites of the Earth, which preferentially struck one of the lunar hemispheres and created the circular mare.

Presently, the impression is growing that the presence of circular mare and mascons on one side of the Moon is related not to an asymmetry of collisional processes, but rather to asymmetry of the lunar crust. It is thought that the thickness of the crust on the back side of the Moon is distinctly greater than it is on the visible side. The impact of large bodies on the visible side of the Moon significantly weakened the thin crust there and caused subsequent lava flows; whereas, with the thicker crust of the back side of the Moon, lava did not reach the surface.

So far, one cannot provide a unique interpretation for the mechanism of formation of lunar mascons. According to one point of view, the mascons are the remainders of bodies which struck the surface of the Moon and formed the circular mare. We have already noted that this is improbable. Although the impact mechanism of a large body with the surface of the Moon is insufficiently clear, there is no doubt that in a high-velocity impact the mass ejected from the crater is many times greater than the mass of the impacting body. The mascon of Mare Orientale is clearly connected with a high velocity impact, in which case the primary body would hardly remain in the crater.

There are several different hypotheses explaining the formation of the mascons by the transport of material in the Moon. Hypotheses related to local mass transfer require that there be a shortage of mass in the vicinity of the mascons and, consequently, a negative gravitational anomaly. The mas-

con of Mare Orientale is actually surrounded by a ring of negative anomalies. The question of the actual existence of such anomalies around other mascons has not yet been definitely answered. In hypotheses related to global transport of material in the Moon, the mass deficit is distributed over a great portion of the body of the Moon and does not lead to negative anomalies.

In one hypothesis of local mass transfer, a mascon is formed by denser matter rising from the mantle into the impact depressions in the lunar crust until an isostatic equilibrium is achieved, followed by subsequent filling of the remaining topographic depression with lava. In this case, the anomalous mass is created by the plug intruding into the crust from the mantle, and the mascon is located at the base of the crust. In other such hypotheses, the mascon is created by filling of the depressions with lava which is denser than the material of the crust. Some hypotheses attempt to explain the mascons by processes of chemical differentiation, without utilizing the concept of impact origin for the circular mare; however, these hypotheses seem as yet insufficiently developed.

In hypotheses related to global transport of material in the Moon, a source of excess pressure must be found which is capable of forcing the dense matter of the lunar interior into the impact-weakened areas of the crust beyond the limits of isostatic compensation. The excess pressure might be created by cooling and thermal compression of the outer parts of the Moon, which were heated by impacts during the final stages of its formation. This process would apparently lead to a global system of faults in the lunar crust. The excess pressure might also be created by expansion of the central areas of the Moon during the early stages of lunar history. During the time of formation of the mascons, the Moon was significantly closer to the Earth, and it is not ruled out that tidal stresses in the body of the Moon made a significant contribution to the expulsion of matter from the lunar interior into the lunar crust.

The problem of lunar mascons brings up a number of questions which still require an answer. A key unknown is the detailed structure of the lunar crust. This information might significantly narrow the range of uncertainty in our understanding of mascons. The history of formation of the lunar lithosphere and the history of stresses in it are insufficiently developed. We do not know the mechanism of formation of the noncircular lunar mare or their subsequent evolution. It is not fully understood why the flowing of lava into these mare did not result in the formation of mascons. It is not clear whether mascons subsided during the course of subsequent lunar history.

For a better clarification of the structure of the lunar mascons and selection among various mechanisms for their formation, it would be interesting to perform a series of experiments on the surface of the Moon. Since the mascons are ancient formations and the regions where they are located should be characterized by stable heat flow, it would be interesting to measure the heat flow and compare it with the heat flow in other areas of the lunar surface. It would also be desirable to perform detailed gravimetric surveying in several different regions of a circular mare. Gravimetric surveying on the lunar surface itself would help, in particular, to answer the questions of the negative anomalies around mascons. Finally, it would be worthwhile to perform deep electromagnetic soundings and to obtain a detailed seismic profile in the region of a circular mare.

We see that the problem of lunar mascons is related to the most important questions of the structure and evolution of the Moon. The remaining uncertainties show clearly that further and more detailed studies of the Moon by spacecraft are needed.

Page intentionally left blank

Page intentionally left blank

Some Geologic Observations Concerning Lunar Geophysical Models

James W. Head
Department of Geological Sciences
Brown University
Providence, Rhode Island

The distribution of lunar geologic units in space and time and their mode of origin provide significant data which bear on a number of current problems in lunar geophysics. Observations and problems discussed here deal with the characterization of the upper 25 km of the lunar crust; the tectonic style of the crust; the formation of mascons within major basins; analysis of lunar magnetic anomalies; and the history of the lunar crust.

A number of geological observations provide important insights into, and in some cases constraints on, current problems in lunar geophysics. These observations are predominantly in the form of (1) morphological characterization and classification of lunar surface geologic units and structural features; (2) the areal distribution of these features on the lunar surface; and (3) the distribution of these features in geologic time. The purpose of this paper is to examine relevant geologic observations which bear on a number of specific geophysical problems.

Characterization of the Upper 25 km of the Lunar Crust

APPROACH

A seismic velocity profile for the lunar crust has been constructed by the use of traveltimes and amplitudes of seismic waves generated primarily by artificial impacts (refs. 1–5). The profile is centered on the Fra Mauro-Apollo 12 region in the eastern Oceanus Procellarum-Mare Cognitum area and is summarized in figure 1. The seismic velocities in the upper portion of the crust (upper 25 km) lie within the velocity range of lunar basalts and this upper crustal layer has often been interpreted to be similar in composition to the basaltic rocks found at the surface. Since this profile applies primarily to the geographic area indicated, the geology

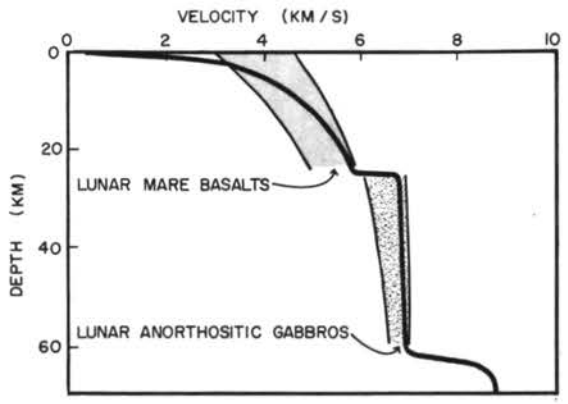


Figure 1.—*Seismic velocity profile for the lunar crust (after Toksöz et al., ref. 48). The velocity model is shown by a heavy line. The lunar basalts for which velocities have been measured include samples from different sites. The anorthositic gabbro region is bounded by Apollo 16 aluminous rocks 68415 at the high-velocity bound and 62295 and 65015 at the low-velocity bound (from Wang et al., ref. 49).*

of that region may provide some evidence for the stratigraphy and structure in the upper 25 km of the lunar crust which would bear on rock composition and physical properties.

OBSERVATIONS

The basaltic mare surface on which the Apollo 12 lunar module landed was deposited subsequent to the deposition of a regional ejecta blanket (Fra Mauro Formation) derived from the Imbrium basin to the north (fig. 2). The Apollo 14 mission explored the surface of this ejecta blanket in an area about 180 km to the east of the Apollo 12 site. There is considerable evidence that the Fra Mauro Formation originally blanketed most of the area around the Imbrium basin at radii from the basin center comparable to that of the Apollo 12 site (ref. 6). Therefore, the Fra Mauro Formation is believed to underlie the mare basalts at the Apollo 12 site. Since the Fra Mauro Formation represents an ejecta blanket deposited on preexisting topography, its regional surface elevation is largely a function of preexisting topography. Since mare lavas tend to pond in low areas, the areas of the Fra Mauro Formation which have been subsequently flooded represent low areas which



Figure 2.—*Earth-based telescopic view of the Apollo 12–14 region in eastern Oceanus Procellarum-northern Mare Cognitum. Crater in upper left is Lansberg, about 36 km in diameter. See figure 4 for location of Apollo 12 and 14 sites. From Consolidated Lunar Atlas, contributions of the University of Arizona Lunar and Planetary Laboratory No. 4.*

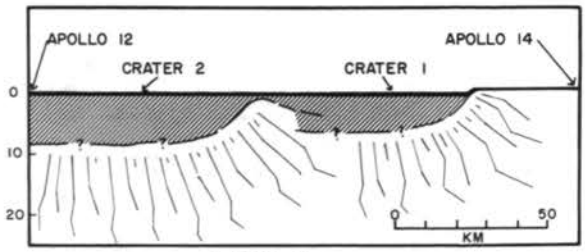


FIGURE 3

Figure 3.—*Schematic cross section of the upper 25 km of the lunar crust in the Apollo 12–14 region, showing dominant effects of large craters 100 to 200 km in diameter. Vertical exaggeration is 2:1. Heavy line at surface is combined thickness of mare and Fra Mauro Formation or Fra Mauro only where appropriate. Slanted lines are deposits related to the major craters including fallback, slump, crater fill, and autochthonous breccias. Exact base of these deposits is uncertain. Radiating lines define region of gradational zone of shock effects in deposits subjacent to the crater.*

existed prior to the deposition of the Imbrium ejecta blanket. This is supported by the lack of any deformation in the Fra Mauro Formation that might suggest major post-Imbrium downfaulting or downwarping.

Another characteristic of this region is that the small hills which are mapped as part of the Fra Mauro Formation are preserved as small islands in much of the area flooded by mare (ref. 7 and fig. 2). This suggests that the Fra Mauro covers the area under the maria and that the thickness of the maria is generally less than the elevation of these domes (which are up to several hundred meters in height). In mapping the Apollo 12 region, Pohn (ref. 8) assumed that the premare surface dipped away from the exposed highlands to the west at a 1-percent eastward slope, and predicted a thickness of 170 m for the mare material.

Therefore, the youngest regional unit deposited in this area is the mare material, and its thickness does not appear to exceed several hundred meters (fig. 3).

Specific sources for mare lavas are not easily identifiable because of their tendency to pond in low regions and to cover their own sources. Lavas must have reached the

surface along some type of conduits. These could form a subsurface network of dikes of unknown density and could affect the seismic velocities in this region.

The next oldest unit in this region is the Fra Mauro Formation and its average thickness at this radial distance from the center of Imbrium is approximately 100–150 meters (refs. 9, 10, and 11). The characteristics of this unit are compatible with its interpretation as a thermally metamorphosed major basin ejecta blanket (refs. 12–15).

Contributions from other multi-ringed basins at the Apollo 12/Apollo 14 sites appear slight (ref. 9) with only Humorum and Nubium approaching 50 m in average thickness of potential contribution. This is beyond the edge of continuous deposition for all the basins considered, so any contribution would lie in the form of secondaries which would be mixed with local material in the manner outlined by Oberbeck et al. (ref. 16).

Because of the erosive and blanketing effects of the deposition of a major multiringed basin ejecta blanket (refs. 9, 16, and 17), pre-ejecta blanket stratigraphy and structure are often difficult to decipher in specific areas. In general, evidence is gained from the detection of "ghost" or buried crater rims and structures (ref. 18). No major pre-Imbrium craters have been described in this area in the mapping of the region between the Apollo 12 and Apollo 14 sites (refs. 7 and 8), although several have been mapped to the south (ref. 7).

Analysis of photography of the region at a variety of scales and lighting angles reveals several possible pre-Imbrium craters between 30 and 200 km in diameter (fig. 4). Crater 1, the oldest of the three described here, is about 125 km in diameter and lies between the Apollo 14 and 12 landing sites. Crater 2, the next youngest of the three, is about 190 km in diameter and underlies the Apollo 12 site. Its ring remnant can be seen within crater 1 (figs. 2 and 4) establishing its younger age. Crater 3, about 30 km in diameter, lies within crater 2 and is therefore younger. These three craters are blanketed by Fra Mauro Formation and are therefore older than the Imbrium event. Three major units should be associated with craters: (1) impact melts and highly metamorphosed breccias concentrated on the crater interiors; (2) less intensely thermally metamorphosed breccias, unconsolidated ejecta, and local material excavated by secondary cratering events (refs. 16, 19, 20, and others), distributed in decreasing thickness outward from the crater rim (ref. 9); and (3) autochthonous breccias underlying the crater floor grading into crustal rocks showing progressively less shock deformation with depth. The pre-Imbrium craters described here would therefore make significant contributions to the outer portion of the lunar crust (fig. 3). Associated rock types would include pure impact melts (perhaps similar to 14310; see reference 21), extremely coherent breccias, weakly coherent breccias, and noncohesive ejecta.

The autochthonous breccias underlying a lens of crater floor fallback breccias and the subjacent gradational zone of shocked material could be several tens of kilometers thick for a crater such as 2.

Wilhelms and McCauley (ref. 6) have mapped a large multiringed basin in this region centered just east of the crater Copernicus. If this basin exists, then it predates craters 1, 2, and 3, since they are superposed on a ring of this structure. The role of this structure is difficult to assess, but if the ma-

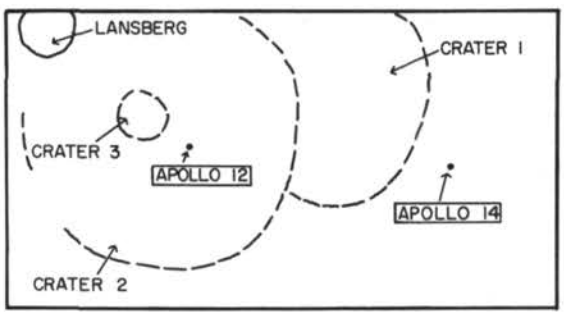


Figure 4.—*Sketch map covering same area pictured in figure 2, and showing location of pre-Imbrian craters 1 (about 125 km), 2 (about 190 km), and 3 (about 30 km). Cross section extends from the Apollo 12 to the Apollo 14 site (depicted in figure 3).*

jor part of the area lies within a multiringed basin, the impact-induced melting characteristic of these deposits (ref. 21) could produce a large volume of rocks with seismic velocities similar to crystalline rocks such as basalts. However, subsequent events (such as the formation of craters 1, 2, and 3) would have obliterated much of these deposits.

MODEL

On the basis of these observations, the most reasonable model for the upper 25 km of the crust in the Apollo 12/14 region (fig. 3) is one characterized by less than a km of basalt and Imbrium basin ejecta underlain by deposits associated with large craters (100 to 200 km in diameter) down to depths probably approaching 25 km. There is little evidence that basalts of the type found at the surface are abundant at depth in the same mode. In addition, lack of abundant typical mare basalt lithologies in highland breccia clasts argues against extensive pre-Imbrium surface volcanism of similar lithology. Finally, the geometry of the large craters seen in the region indicates that they would have destroyed early layered deposits during their formation.

The progressive increase in seismic velocity with depth may be a direct function of the progressive decrease in intensity of shock metamorphic effects, such as microfracturing, in the gradational zone of shock effects typical of subcrater deposits. These gradational zones have been noted in terrestrial craters (refs. 19, 22, 23, 24, and others). In particular, craters in the range of 100 to 200 km in diameter, such as those shown in figure 4, would certainly alter the physical properties of subjacent rocks down to 25 km depth. Abundance of similar large old craters on the lunar surface suggests that the velocity profile may be similar elsewhere.

Thus the seismic velocity profile of the outer portion of the crust probably represents progressive increase in velocities in an anorthositic gabbro crust due to progressive decrease in shock effects, rather than material of basaltic composition.

Todd et al. (ref. 25) and Simmons et al. (ref. 26) have studied the physical properties of terrestrial and lunar rocks. Their results show that shock-induced microcracks are significant in the outer 25 km of the Moon and support the geologic framework presented here for the characteristics of the outer crust.

Tectonic Style of the Lunar Crust

APPROACH

The morphologic characteristics of and distribution of planetary surface topographic features can provide much evidence for the tectonic style of a particular planet in space and time.

OBSERVATIONS

A surprisingly small variety of lunar surface morphologic features have been attributed to lunar tectonism or structural evolution. These include linear rilles, large graben, mare ridges, basin rings, and lineaments (refs. 27–31). Linear rilles generally take the form of flat-floored, steep-walled troughs, ranging up to several kilometers in width, and to tens (and often hundreds) of kilometers in length. The flat floors and linear walls suggest that the rilles are fault-bounded down-dropped blocks or grabens, and their generally constant width over different topographic levels indicates steep dips.

Several large linear graben-like valleys are associated with the major multiringed basins and are oriented in a radial direction. The best known example is the Alpine Valley associated with the Imbrium basin. These structures seem to occur preferentially in quadrants of the basin where they parallel lunar grid directions. They are interpreted to be major graben valleys which develop where

radial multiring basin fractures coincide with lunar grid fractures (ref. 32).

Lineaments are abundant on the lunar surface and their distribution and origin have long been a matter of controversy. Structural lineaments are often associated with major multiringed basins in radial and concentric orientations. In many cases, multiring basin-associated lineaments are enhanced in lunar grid directions (ref. 32) suggesting that the lineaments preferentially form along pre-basin planes of weakness. Many lineaments may also be related to structural trends from ancient, subsequently obliterated basins. However, the bulk of the lineaments seem more likely to be related to lunar grid patterns. Fielder (ref. 30), Strom (ref. 33), and Elston et al. (ref. 34), have discussed the global lineament systems and have concluded that they represent a stress field with the maximum principal stress axis oriented N–S with strike-slip movement developed 45° to the E and W and tension fractures developed N–S, producing the primary grid patterns.

Mare ridges and their analogous structures in the highlands have often been related to intrusive and extrusive igneous activity (ref. 35). However, evidence cited by Howard and Muehlberger (ref. 36), Bryan (ref. 37), Head (ref. 32), and Muehlberger (ref. 38) suggests that many of these structures are related to structural deformation which occurred primarily subsequent to the deposition of the main mare sequence. In many cases they appear to be layers of material which have been overthrust onto the surface for short distances.

The stratigraphic distribution of these structural features provides information on the time span of lunar tectonic elements. Major graben valleys appear to be associated with the formation of multiringed basins, smaller linear rilles with the period of mare filling, mare ridges with readjustments during and after mare fill, and lineaments and lunar grid structures with early highland crust formation, perhaps rejuvenated by tidal interaction with the Earth. There is virtually no evidence for extensive tectonic activity in the past 3.0 billion years of lunar history.

MODEL

Immediately obvious in a model of lunar structural deformation is the virtual lack of any evidence of analogs to terrestrial plate tectonics which might indicate major lateral crustal movement on the Moon. Major structural features are related either (1) to a background basement fracture system produced early in lunar history, or (2) to the formation of major multiringed basins or their subsequent filling. For the major part of lunar history, the lunar crust appears to have acted as a prestressed and fractured, but essentially passive and rigid layer, with deformation essentially being localized to the regions of large-scale basin excavation and filling.

Mascon Basins

APPROACH

Observations on the characteristics of Orientale, a young (about 3.85 b.y.; see ref. 39) relatively unflooded basin may provide insight into the cause of gravity anomalies in other older basins.

OBSERVATIONS

The Orientale basin (figs. 5 and 6) formed as a result of impact into lunar highland crustal rocks. In a recent study (ref. 21), the crater rim is shown to be closely represented by the position of the outer Rook Mountain ring, approximately 620 km in diameter. The inner Rook Mountains form a central peak ring within the crater. The Cordillera ring, 900 km in diameter, is a fault scarp which formed in the terminal stages of the cratering event as a large portion of the crust collapsed inward toward the recently excavated crater, forming a megaterrace. This collapse pushed the wall of the Orientale crater inward, distorting it and slightly decreasing its radius. The inward

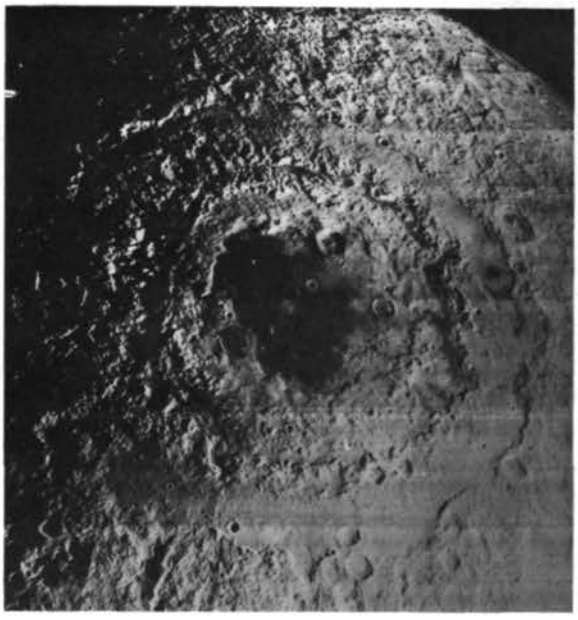


Figure 5.—*Orientale basin, about 900 km in diameter. Portion of Lunar Orbiter IV frame 194M.*

collapse was almost certainly aided by the upwelling of subcrater material since the present basin is relatively shallow (maximum height of rings and peaks is about 4.5 km above the surrounding plain; maximum depth must be near this figure).

Analysis of the facies provides evidence for the timing of the upwarping. A domical facies (fig. 6) is almost exclusively developed between the Cordillera and outer Rook rings. The domical facies is interpreted to be radially textured ejecta which was disrupted and modified to a jumbled domical texture by seismic shaking associated with the formation of the mega-terrace. The plains and corrugated facies pre-date the mare fill and lie within the Orientale crater. They are interpreted to have been deposited contemporaneously with the cratering event as partial and total impact melts which collected on the floor of the crater during the terminal stages of the event. The lack of major deformation associated with the crater floor (other than cooling and contraction cracks) strongly suggests that the floor was in its present shallow configuration prior to the final cooling of the corrugated and plains

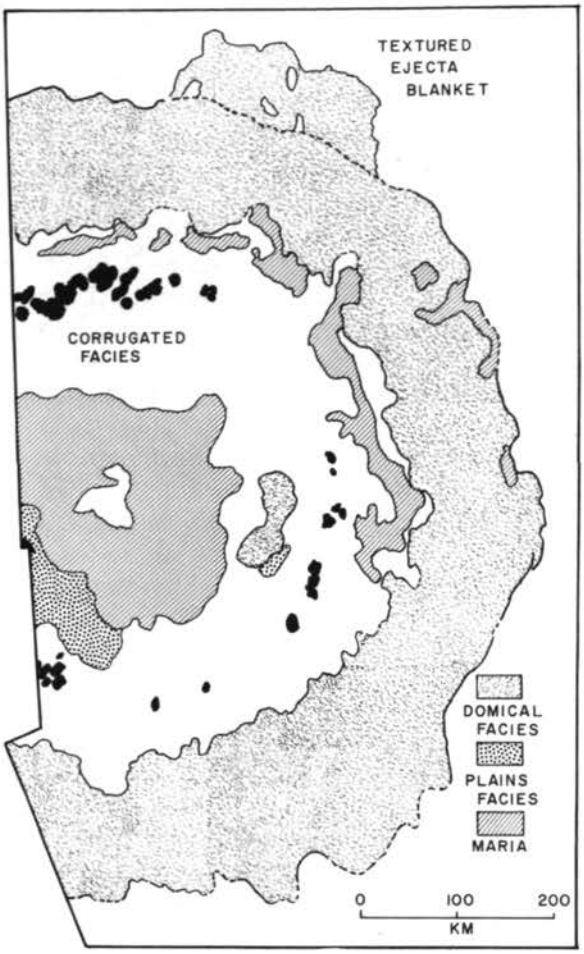


Figure 6.—*Major facies or geologic units in the Orientale basin (from Head, ref. 21).*

facies. Therefore, rebound and upwelling of the crater floor were coincident with the terminal stages of the cratering event.

Subsequent to the formation of the Orientale crater a small amount of mare material (when compared to other mare basins) was deposited in the central portion of the basin (about 50 000 km^2 in Mare Orientale), around its margin along the base of the outer Rook (Mare Veris, about 12 500 km^2), and along the base of the Cordillera (Mare Autumni, about 5000 km^2).

Sjogren et al. (ref. 40) have mapped a mascon associated with the Orientale basin and concentrated within the inner Rook Mountain ring. Since there is little evidence

of subsequent structural modification of the crater or extensive mare fill, this implies that the Orientale mascon formed in relation to the cratering event, rather than at a later time. As pointed out by Phillips et al. (ref. 41), a multiringed basin which was formed in low-density crust (in an area of a crust-mantle configuration of zero anomalous gravity) and which was isostatically compensated by upwelling of a mantle plug (as in the model of Wise and Yates, (ref. 42)), would show a negative gravity anomaly in the analyses of Phillips et al. In this case the gravity effect would be due to the zero density of the unfilled basin. Filling of the basin with material of crustal density tends to produce a positive anomaly due to the mantle plug. Filling of the basin with material of greater than average crustal density (mare basalts) produces a positive anomaly in which mantle plug and basin fill contribute to the effect. The mascon would then be composed of both these elements.

The model for the origin of the Orientale basin (ref. 21) is relevant in differentiating these effects. The model suggests that the present shallow basin configuration is very nearly the same as at its time of origin, and that only a small amount of mare material has flooded the basin. The Orientale mascon cannot be due to the small amount of mare material alone. Therefore, the anomaly may be related to upwelling of a higher density mantle plug and to filling of the topographic depression created by the ejection of material during the cratering event. The Orientale model suggests that these two factors may be dynamically related to the cratering event, rather than separate and occurring at different times. The size of the Orientale crater (620 km in diameter) and its shallowness suggest that it excavated relatively deep in the crust but rebounded in the terminal stages of the event, perhaps *pulling* the mantle plug up with it. Thus, the formation of the mantle plug seems to be related to the process of rebound at the time of the event, rather than to be a simple upwelling to reach isostatic equilibrium. This implies that the Orientale positive anomaly is primarily due to a mantle plug which in excess of equilibrium and which lies above the normal crust-mantle interface. In addition, the topographic depression (basin of excavation) is reduced by movement of material of crustal density into the basin in the terminal stages of the cratering event. This consists of ejecta fallback, upwelling of crater floor crustal material, and inward slumping of the crater walls (which forms a huge megaterrace bounded by the Cordillera Mountains).

If Orientale were flooded by mare material (denser than surrounding crust) to the same extent as that in the Imbrium basin (virtually covering the crater interior with additional shallower flooding out to the Apennine fault scarp), an additional contribution to the anomaly would be made. The thicker mare plate within the crater would also tend to broaden the positive anomaly so that it more closely corresponded to the crater rim, as is the case with the Imbrium anomaly (see Sjogren et al., ref. 43).

MODEL

On the basis of a model of the origin of the young multiringed Orientale basin (ref. 21), the Orientale mascon is thought to be due primarily to a mantle plug pulled up to form a positive anomaly during rebound associated with the cratering event. The Orientale gravity effect is enhanced by filling of the excavated crater during the impact event largely by material of density similar to the surrounding crust. Subsequent mare filling of the crater, such as has occurred in the Imbrium basin, tends to add to the mascon and broaden its distribution.

The gravitational history of mare basins therefore includes the following elements: (1) an initial crater of excavation, with circumferential ejecta deposition, causing a mass deficiency; (2) upward displacement of denser mantle material which brings the crater up to or above an equilibrium state in the terminal stages of the cratering event; (3) fallback of ejecta, inward slumping of multiple rings, and upwarping of the crater

floor due to rarefaction, which contribute to a super-isostatic configuration; and (4) in the case of the Imbrium basin, later extrusion and deposition of higher density mare flows, which cause a further increase in the mass excess, broadening the mascon distribution by laterally extending the high-gravity region.

Lunar Magnetic Anomalies

APPROACH

Numerous magnetic anomalies have been noted at Apollo sites (Dyal et al., ref. 44, and from lunar orbit (Russell et al., ref. 45) (reviewed by Fuller, ref. 46). Their correlation with geologic surface units may provide important information on their origin.

OBSERVATIONS

The remanent magnetic fields measured in the Descartes region (Apollo 16 landing site) are the largest extraterrestrial fields yet measured in situ (ref. 44). Four magnetic readings (generally large with downward components) were taken on the regionally flat Cayley plains surface. An additional reading (large and upward) was obtained on the slopes of Stone Mountain, which is a portion of low mountains bounding the Cayley plains in an arc-like manner. Thus, the plains and surrounding mountains appear to have differing characteristics. Strangway et al. (ref. 47) have suggested that the differences may be due to edge effects and consider that the Cayley plains represent breccia blankets which were deposited at temperatures above 770°C by a mechanism such as volcanic or impact base surge. An alternative model for the history of the site (ref. 18) supports the concept of an edge effect but attributes the formation of the Cayley plains and surrounding mountains to floor material and wall material, respectively, of an old 60-km diameter crater centered about 25 km west of the Apollo 16 site. In this model, the magnetism associated with the Cayley plains is believed to have been caused by cooling of impact melts concentrated on the crater floor of the 60-km diameter crater in the presence of a magnetic field. The crater wall (Stone Mountain) bears less intensely shocked ejecta and pre-crater material.

MODEL

The association of the strong magnetic field at the Apollo 16 site with the floor of an old large crater suggests that many localized anomalies may be caused by cooling of impact melts on crater floors in the presence of a magnetic field.

History of the Lunar Crust

A summary of the structural history of the lunar crust as inferred from photogeologic evidence is as follows: (1) formation of lunar crustal rocks and formation of lunar grid patterns; no apparent lateral offset associated with grid patterns (their origin is unknown); (2) formation of large multiringed basins (undoubtedly coincident with (1) in part, but youngest basins formed in crust which contained grid); (3) initial filling of many multiringed basins with mare material; tensional deformation of this material as many basin interiors subside to form linear and arcuate rilles; (4) continued filling of major basin interiors; little tensional deformation; and (5) compressional deformation associated primarily with mare basins and basin margins, and evidenced by mare ridges and associated structures. This latter phase may be associated with final mare subsidence or shrinking of crustal regions due to cooling of mare source areas. Except for mare ridges, there appears to be virtually no evidence for extensive tectonic activity in the past three billion years of lunar history.

References

1. TOKSÖZ, M. N., ET AL., Lunar Crust. Structure and Composition. *Science*, Vol. 176, 1972, pp. 1012–1016.
2. TOKSÖZ, M. N., ET AL., Structure, Composition, and Properties of Lunar Crust. *Proc. Third Lunar Science Conference*, Vol. 3, 1972, pp. 2527–2544.
3. LATHAM, G., ET AL., Moonquakes. *Science*, Vol. 174, 1971, pp. 687–692.
4. LATHAM, G., ET AL., Passive Seismic Experiment. *Apollo 16 Preliminary Science Report*, NASA SP–315, 1972, pp. 9–1 to 9–29.
5. SOLOMON, S. C., AND M. N. TOKSÖZ, Internal Constitution and Evolution of the Moon. *Phys. Earth Planet. Interiors*, Vol. 7, 1973, pp. 15–38.
6. WILHELMS, D., AND J. MCCAULEY, Geologic Map of the Near Side of the Moon. U.S. Geol. Survey, Misc. Geol. Inv., Map I–703, 1971.
7. EGGLETON, R. E., Geologic Map of the Riphaeus Mountains Region of the Moon. U.S. Geol. Survey, Misc. Geol. Inv., Map I–458, 1965.
8. POHN, H. A., Geologic Map of the Lansberg P Region of the Moon, U.S. Geol. Survey, Misc. Geol. Inv., Map I–627, 1971.
9. MCGETCHIN, T. R., M. SETTLE, AND J. W. HEAD, Radial Thickness Variations in Impact Crater Ejecta: Implications for Lunar Basin Deposits. *Earth Planet. Sci. Letters*, Vol. 20, No. 2, 1973, pp. 226–236.
10. EGGLETON, R. E., AND T. W. OFFIELD, Geologic Maps of the Fra Mauro Region of the Moon. Apollo 14 Pre-Mission Maps, U. S. Geol. Survey, Geologic Atlas of the Moon, Map I–708, 1970.
11. KOVACH, R. L., J. S. WATKINS, AND T. LANDERS, Active Seismic Experiment. *Apollo 14 Preliminary Science Report*, NASA SP–272, 1971, pp. 163–174.
12. LSPET (Lunar Sample Preliminary Examination Team), Preliminary Examination of Lunar Samples. *Apollo 14 Preliminary Science Report*, NASA SP–272, 1971, pp. 109–131.
13. SWANN, G. A., ET AL., Preliminary Geologic Investigations of the Apollo 14 Landing Site. *Apollo 14 Preliminary Science Report*, NASA SP–272, 1971, pp. 39–86.
14. WARNER, J. L., Metamorphism of Apollo 14 Breccias. *Proc. Third Lunar Science Conference*, Vol. 1, 1972, pp. 623–643.
15. WILSHIRE, H. G., AND E. D. JACKSON, *Petrology and Stratigraphy of the Fra Mauro Formation at the Apollo 14 Site*. U.S. Geol. Survey Prof. Paper 785, 1972.
16. OBERBECK, V. R., ET AL., *Emplacement of the Cayley Formation*. NASA TM X–62,302, 1973.
17. HEAD, J. W., Origin of Morphologic Components of the Hevelius Formation: Lunar Orientale Basin (abs.). *Geol. Soc. Am. 1973 Ann. Mtg.*, 1973, p. 661.
18. HEAD, J. W., Stratigraphy of the Descartes Region (Apollo 16): Implications for the Origin of Samples. *The Moon*, in press, 1974.
19. DENCE, M. R., Shock Zoning at Canadian Craters: Petrography and Structural Implications. In *Shock Metamorphism of Natural Materials*, B. M. French and N. M. Short, eds., Mono Book Corp., Baltimore, 1968.
20. SHORT, NICHOLAS M., Anatomy of a Meteorite Impact Crater: West Hawk Lake, Manitoba, Canada. *Geol. Soc. Am. Bull.*, Vol. 81, 1970, pp. 609–648.
21. HEAD, J. W., Orientale Multi-Ringed Basin Interior and Implications for the Petrogenesis of Lunar Highland Samples. Submitted to *The Moon*, 1974.
22. STÖFFLER, DIETER, Zones of Impact Metamorphism in the Crystalline Rocks of the Nördlinger Ries Crater. *Contr. Mineral. and Petrol.*, Vol. 12, 1966, pp. 15–24.
23. CHAO, E. C. T., Pressure and Temperature Histories of Impact Metamorphosed Rocks—Based on Petrographic Observations. In *Shock Metamorphism of Natural Materials*, B. M. French and N. M. Short, eds., Mono Book Corp., Baltimore, 1968.
24. ENGELHARDT, W. VON, AND D. STÖFFLER, Stages of Shock Metamorphism in Crystalline Rocks of the Ries Basin, Germany. In *Shock Metamorphism of Natural Materials*, B. M. French and N. M. Short, eds., Mono Book Corp., Baltimore, 1968.
25. TODD, T. E., D. A. RICHTER, G. SIMMONS, AND H. WANG, Unique Characterization of Lunar Samples by Physical Properties. *Proc. Fourth Lunar Science Conference*, Vol. 3, 1973, pp. 2639–2662.
26. SIMMONS, G., T. TODD, AND H. WANG, The 25–km Discontinuity: Implications for Lunar History. *Science*, Vol. 182, 1973, pp. 158–161.
27. BALDWIN, R. B., The Face of the Moon. University of Chicago Press, 1949.
28. BALDWIN, R. B., The Measure of the Moon. University of Chicago Press, 1963.
29. FIELDER, G., *Structure of the Moon's Surface*. Pergamon Press, 1961.
30. FIELDER, G., Lunar Tectonics. *Geol. Soc. London Quart. J.*, Vol. 119, No. 473, Pt. 1, 1963, pp. 65–69.
31. FIELDER, G., *Lunar Geology*. Butterworth Press, London, 1965.
32. HEAD, J. W., Morphology and Structure of the Taurus-Littrow Highlands (Apollo 17): Evidence for Their Origin and Evolution. *The Moon*, in press, 1973.
33. STROM, R. G., Analysis of Lunar Lineaments, I-Tectonic Map of the Moon. *Arizona Univ.*

Lunar and Planetary Lab. Commun., Vol. 2, No. 39, 1964, pp. 205–221.

34. ELSTON, W. E., ET AL., Lunar Near-Side Tectonic Patterns From Orbiter IV Photographs. *J. Geophys. Res.*, Vol. 76, 1971, pp. 5670–5674.
35. STROM, R. G., Lunar Mare Ridges, Rings, and Volcanic Ring Complexes. IAU Symposium No. 47, *The Moon*, 1972, pp. 187–215.
36. HOWARD, K. A., AND W. R. MUEHLBERGER, Lunar Thrust Faults in the Taurus-Littrow Region. *Apollo 17 Preliminary Science Report*, 1973, pp. 31–22 to 31–29.
37. BRYAN, W. B., Wrinkle-Ridges as Deformed Surface Crust on Ponded Mare Lava. *Proc. Fourth Lunar Science Conference*, Vol. 1, 1973, pp. 93–106.
38. MUEHLBERGER, W. R., Structural History of Southeastern Mare Serenetatis and Adjacent Highlands (abs.). *Lunar Science*, Vol. V, Lunar Science Institute, Houston, 1974, pp. 531–533.
39. SCHAEFFER, O. A., AND L. HUSAIN, Chronology of Lunar Basin Formation and Ages of Lunar Anorthositic Rocks. *Lunar Science*, Vol. V, Lunar Science Institute, Houston, 1974, pp. 663–665.
40. SJOGREN, W. L., P. M. MULLER, AND W. R. WOLLENHAUPT, S-Band Transponder Experiment. *Apollo 16 Preliminary Science Report*, NASA SP–315, 1972, pp. 24–1 to 24–7.
41. PHILLIPS, R. J., ET AL., Mascons: Progress Toward a Unique Solution for Mass Distribution. *J. Geophys. Res.*, Vol. 77, No. 35, 1972, pp. 7106–7114.
42. WISE, DONALD U., AND M. T. YATES, Mascons as Structural Relief on a Lunar "Moho". *J. Geophys. Res.*, Vol. 75, No. 2, 1970, pp. 261–268.
43. SJOGREN, W. L., W. R. WOLLENHAUPT, AND R. N. WIMBERLY, Lunar Gravity Via the Apollo 15 and 16 Subsatellites. In *The Moon*, Vol. 8, 1973.
44. DYAL, P., ET AL., Lunar Surface Magnetometer Experiment. *Apollo 16 Preliminary Science Report*, NASA SP–315, 1972, pp. 11–1 to 11–14.
45. RUSSELL, C. T., P. J. COLEMAN, JR., B. R. LICHTENSTEIN, G. SCHUBERT, AND L. R. SHARP, Subsatellite Measurements of the Lunar Magnetic Field. *Proc. Fourth Lunar Science Conference*, Vol. 3, 1973, pp. 2833–2845.
46. FULLER, M., Lunar Magnetism. *Rev. Geophys. Space Phys.*, Vol. 12, No. 1, 1974, pp. 23–70.
47. STRANGWAY, D. W., ET AL., Lunar Magnetic Anomalies and the Cayley Formation. *Nature*, in press, 1974.
48. TOKSÖZ, M. N., ET AL., Velocity Structure and Evolution of the Moon. *Proc. Fourth Lunar Science Conference*, Vol. 3, 1973, pp. 2529–2547.
49. WANG, H., T. TODD, D. RICHTER, AND G. SIMMONS, Elastic Properties of Plagioclase Aggregates and Seismic Velocities in the Moon. *Proc. Fourth Lunar Science Conference*, Vol. 3, 1973, pp. 2663–2671.

Magnetic and Dielectric Properties of Lunar Samples

D. W. Strangway, G. W. Pearce, and G. R. Olhoeft
Departments of Geology and Physics
University of Toronto
Toronto, Canada

The dielectric properties of lunar soil and rock samples show a systematic character when careful precautions are taken to ensure there is no moisture present during measurement. The dielectric constant (K) above 10^5 Hz is directly dependent on density according to the formula $K = (1.93 \pm 0.17)^{\rho}$ where ρ is the density in g/cc. The dielectric loss tangent is only slightly dependent on density and has values less than 0.005 for typical soils and 0.005–0.03 for typical rocks. In addition to a density dependence, the loss tangent appears to be directly related to the metallic ilmenite content. These results are in good agreement with the results of the Surface Electrical Properties Experiment carried on Apollo 17. It showed a surface layer of dielectric constant 3.8 and a loss tangent of 0.008. This is presumed to be a layer of compact soil about 7 m thick, overlying a medium with a dielectric constant of roughly 7.5 and a loss tangent interpreted to be 0.035. The medium is presumed to be bedrock. These results are compatible with seismic results.

The magnetic properties of lunar samples can be used to study the distribution of metallic and ferrous iron which shows systematic variations from soil-type to soil-type and a general tendency to increasing Fe°/Fe^{++} distribution in the more highly rewelded breccias. The other magnetic characteristics can also be used to determine the distribution of grain sizes. There are a number of ways of interpreting the origin of the stable remanent magnetization in lunar samples, but several lines of evidence suggest that it is of thermal origin and was acquired at a time when the igneous rocks and breccias cooled from above 800°C in the presence of an ancient field.

In this paper we review the electrical and magnetic properties of lunar samples and discuss the relevance to a number of problems of lunar interest. These problems include determining the history of the lunar magnetic field, studying the distribution of iron (metallic and ferrous) on the lunar surface, and establishing the relevance of magnetic properties to orbital magnetic mapping and surface electromagnetic sounding.

Dielectric Constant and Loss Tangent

Radar sounding of the Moon and planets has been conducted for some years now and provides a part of the basic data for the interpretation of planetary surfaces. A recent review paper (ref. 1) summarizes the results of the large number of measurements made on lunar samples in a number of laboratories. The results measured at frequencies above 10^5 Hz on samples treated with great care with respect to water content are summarized in figures 1 and 2. Samples which have only a small amount of moisture have a dielectric constant that is nearly independent of frequency and which, to a first approximation, is dependent only on the packing fraction. Simple equations relating the bulk density (ρ) and the dielectric constant (K) can be derived as illustrated in figure 1 [$K = (1.93 \pm 0.17)^{\rho}$].

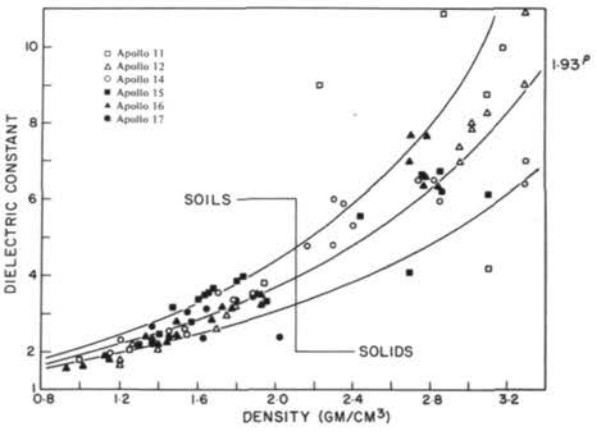


Figure 1.—*Dielectric constant (K) above 10^5 Hz as a function of density for lunar samples. Solid line is a least squares fit to the soil data and is of the form* $K = (1.93 \pm 0.17)^{\rho}$, *where* ρ *is the density in* g/cm^3. *Dashed lines represent the uncertainty limit.*

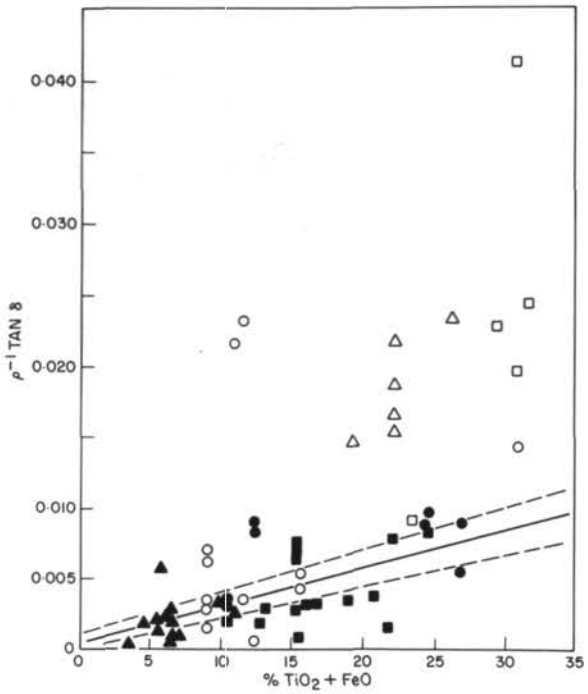


Figure 2a.—*Loss tangent (tan δ) measurements as a function of density for samples which have been extensively vacuum-dried by heating (symbols as in fig. 1). Solid line is a least squares fit to the soil data and is of the form* $\tan \delta = (0.00053 \pm 0.00056) + (0.00025 \pm 0.00009)\ C\ \rho$, *where C is the content of FeO + TiO₂. The loss tangent in all cases represents values above 10^5 Hz. On dry samples the values are nearly frequency-independent at or above this frequency.*

The more difficult measurement is the loss tangent which was found to be extremely sensitive to even minute amounts of moisture. Nevertheless, good results were obtained when careful measurements using high vacuum systems were made, and most results reported in the literature from lunar missions beyond Apollo 14 are considered to be reliable. Again, however, it is possible to fit this to a simple mixing formula that involves the volume fraction of material and that of sample. This given by $\tan \delta = [(0.00053 \pm 0.00056) + (0.00025 \pm 0.00009)\ C]\ \rho$ where C is the content of FeO + TiO_2. The fit is remarkably good and implies that for soils the typical loss tangent (tan δ) is less than 0.005, while solid rocks have somewhat higher loss tangents with values between 0.005 and 0.03. The range of loss tangents is dependent then on the content of ilmenite, a metallic phase, as well as the density.

From the sample studies alone, therefore, there is an implication that the dielectric properties and loss tangents of a typical lunar regolith are as illustrated in figure 3. The density profile used in this model is reported in detail by Olhoeft and Strangway (ref. 1) and is in general consistent with the results obtained during the lunar program soil experiments. Where the regolith gives way to solid bedrock, the dielectric constant will jump to a value of about 7.7, the intrinsic value of the dielectric constant. The loss tangent will jump to a value ranging between 0.005 to 0.03, depending upon the ilmenite content.

Ilmenite is present in varying amounts and is of course the main metallic conducting mineral present in lunar samples. Although this appears to have very little effect on the dielectric constant, the equation above shows a direct correlation between the ilmenite content and the loss tangent. Thus, the loss tangent can be expected to vary directly with

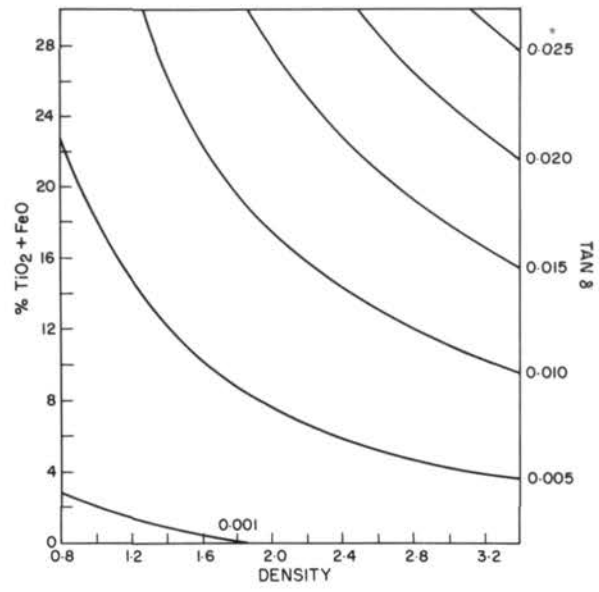


Figure 2b.—*The equation shown plotted as contours of loss tangent in a plane showing density versus FeO + TiO₂. This is roughly equivalent to the ilmenite content.*

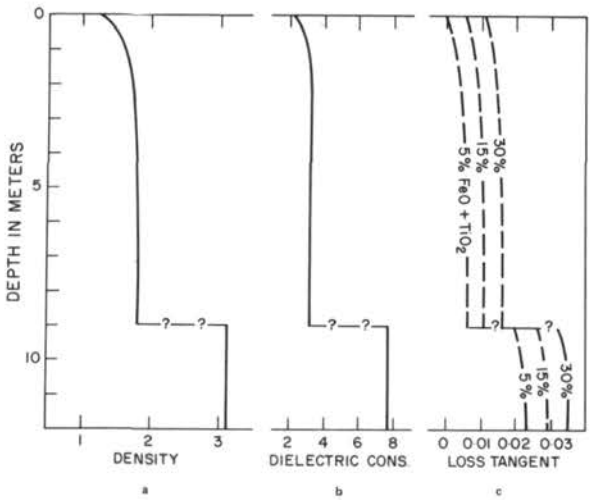


Figure 3.—*(a) An equation for density as a function of depth in the lunar soil given as* $Z = 0.01(-1 + \Sigma A_i be^{tP})$. *(b) The dielectric constant as a function of depth for the density profile of (a). The sharp change between soil and rock illustrated by ——? ——? ——— occurs at an unknown depth. (c) The loss tangent as a function of depth for the density profile of (a). The three curves correspond to 5-, 15-, and 30-percent FeO + TiO₂.*

the amount of metallic mineral present, at least up to the limit of about 25 percent observed in the lunar samples. Figure 3 is a rather generalized profile of the predicted dielectric properties from the surface of the Moon and shows values of the loss tangent that would be predicted for various ilmenite contents. Presumably these results are comparable to those that would be obtained on any planetary body totally free of moisture and having a regolith (ref. 1).

There have been a number of experiments conducted over the years which throw light on this problem. Remote observations of the lunar surface, as recently reviewed by Hagfors (ref. 2), have shown that the surface of the Moon has a dielectric constant in the general range of 1.5 to 3.0. Estimates of the loss tangent are model-dependent, but, choosing reasonable models, values in the range of 0.005 seem to be appropriate. More recently Tyler and Howard (ref. 3) detected Apollo spacecraft communication signals on Earth which had been reflected from the Moon. This permitted them to determine the electrical properties of the surface of the Moon. These observations are also in general agreement with the earlier Earth-based observations, although there is an implication of dielectric layering in the upper few centimeters of the Moon.

During the Apollo 17 mission, a specific experiment to measure the dielectric properties of lunar material in place was carried. This experiment has been described in the literature (refs. 4 and 5). The method used is illustrated in figure 4 and consists of the measurement of field strength as a function of distance from a transmitter. The fields transmitted are from two orthogonal dipole antennas laid on the lunar surface and operating at 1, 2, 4, 8, 16, and 32 mHz. These signals were received on the Rover by three orthogonal coils and recorded on tape together with navigation information. It was thus possible to produce plots of field strength versus distance at each of several frequencies. Some of these are shown in figure 5. In general, the information derived from this experiment consists of the interference patterns

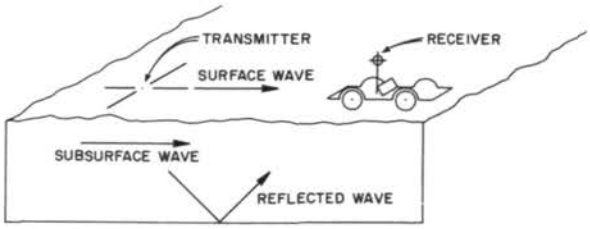


Figure 4.—*Sketch illustrating the principle of the surface electrical properties experiment. Field strengths were measured on the Rover as a function of distance from an electric dipole antenna on the lunar surface. Energy traveling at the speed of light above the interface interferes with the energy traveling below the interface to give a measure of the dielectric constant and loss tangent of the surface layers. Further interferences are generated by reflections from dielectric layering and/or scattering bodies.*

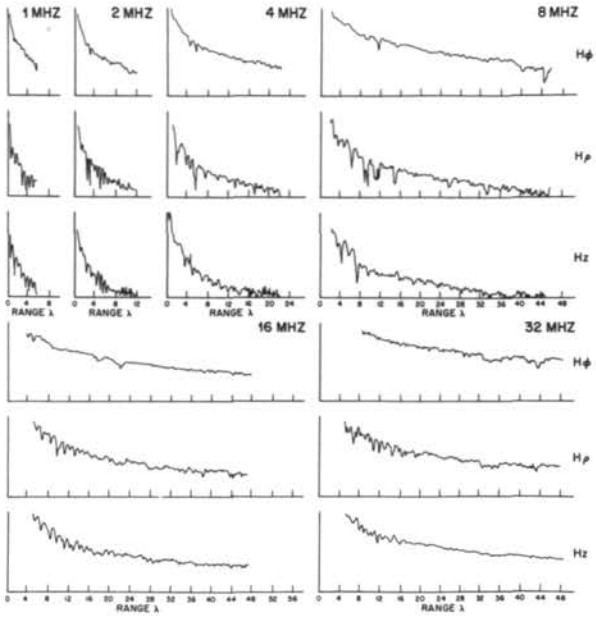


Figure 5.—*Field strength versus distance (in wavelength) plots for data recorded at 1, 2, 4, 8, 16, and 32 mHz. Components shown are the end-fire, maximum-coupled* H_ϕ *component and broadside, maximum-coupled* H_z *and* H_ρ *components where the coordinates are as illustrated in figure 4. The field strength is given in db.*

resulting from one or more of the following waves interfering with the surface wave: (a) subsurface waves, (b) waves reflected from layered electrical property contrasts, and (c) waves reflected from irregular, scattering bodies.

From (a) we can derive the dielectric constant and loss tangent at any frequency not affected by the other interfering effects.

Examining the plots shown in figure 5, a number of conclusions can be drawn. First of all, the $H\phi$ component is maximum-coupled, but the bulk of the energy from the end-fire antenna represented here travels above the surface. The result is that this component is relatively smooth when there is little scattering present either from the surface topography or from the subsurface. It can readily be seen that this component is fairly smooth at all frequencies from 1 to 32 mHz. This clearly implies that there are few scattering bodies in the subsurface. Since the free space wavelength ranges between 300 and 10 m, it is implied that there are not many boulders larger than a few meters present in the soil. Considering the dielectric constant of the medium, this means that there are few scatterers with a scale of 5 m or more. The lack of scattering bodies is in complete contrast to our previous studies on glaciers which we feel are the nearest available terrestrial analogs (refs. 5 and 6). In temperate glaciers the scattering is small at 1, 2, and 4 mHz, but at 8 mHz and above the scattering becomes large and dominates the results. The lack of scattering means that the lunar observations should be interpretable in terms of relatively simple models at all frequencies.

The second observation that can be made by observing figure 5 is that to a rough approximation the data show a rapid falloff relative to wavelength at 1 mHz and a slow falloff relative to wavelength at 32 mHz. This means simply that at 1 mHz the medium behaves much like a dielectric halfspace, and little energy is reflected to the surface, while at 32 mHz the medium is layered, and energy is trapped in the layer and reflected.

The third observation that can be made is that at 1 mHz the frequency of the inter-

ference corresponds very closely to the case of a halfspace with a dielectric constant of 7.5 ± 0.5 and a loss tangent of roughly 0.035 ± 0.025. These values are remarkably similar to the values reported on solid lunar samples and imply that at depths below the surface there is relatively solid rock present. The situation is analogous to that at the Apollo 15 landing site where bedrock a few meters below the surface was observed in the walls of Hadley Rille. This layer probably corresponds to the layer characterized by a seismic velocity of about 280 m/s (refs. 7 and 8). This is an extremely low velocity and implies the presence of rock that is strongly dominated by extensive fracturing. In figure 6, a sketch showing the inferred seismic structure at the Taurus-Littrow landing site is given.

At shallow depths (relative to a wavelength in the medium at 1 mHz) there is, however, considerable structure present. We have not yet been able to offer a unique interpretation of these results. It appears, however, that at 16 mHz and 32 mHz the results can be fitted reasonably well with a two-layer case consisting of a layer 7 ± 1 m thick, with a dielectric constant of 3.8 ± 0.2 and a loss tangent of 0.008 ± 0.004 as shown in figure 6. These dielectric properties are remarkably similar to those reported for dry samples of lunar soil. The dielectric constant is slightly high, which implies that the average density of the top 7 m is about 2.0 g/cc, a value not inconsistent with models of the density of the lunar surface (see fig. 3).

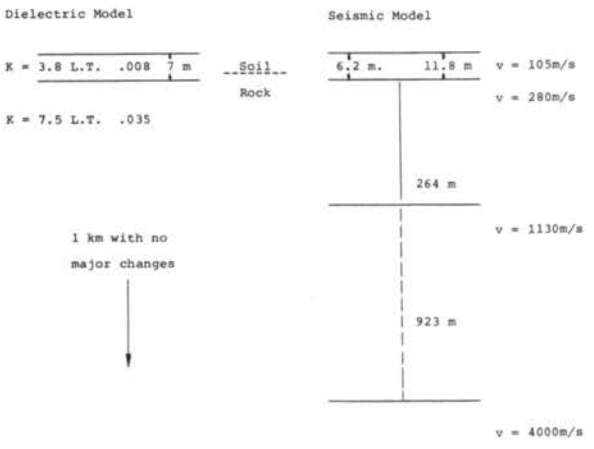


Figure 6.—*Cross section at the Taurus-Littrow landing site determined from the surface electrical properties experiment and from the lunar seismic profiling experiment.*

In summary, the measurements of the dielectric constant and loss tangent of lunar soils and rocks give values that can be used to predict the electrical structure of the lunar surface. Soil samples have a dielectric constant which to a first approximation is dependent only on the density. The loss tangent is only weakly dependent on the density, but it is directly proportional to the ilmenite content. Solid rock samples have a higher dielectric constant that is typically around 7.7. The values quoted for the soil are in good agreement with the results of remote radar and of passive thermal observations of the lunar surface from Earth-based observations.

An experiment carried on the Apollo 17 mission to determine the electrical structure shows that the top 7 m are composed of material with a dielectric constant of 3.8, presumably corresponding to fairly compact soil of average density 2.0 g/cc. Beneath this, the dielectric constant jumps to a value of about 7.5, a value which is typical of lunar rock samples. This regolith thickness is in close agreement with the values determined seismically. Low seismic velocities reported for the bedrock are in agreement with the high dielectric constant, provided the low velocity is the result of extensive fracturing of the bedrock.

Magnetic Properties of Lunar Samples

There are now a number of review articles on the subject of lunar magnetism, and no attempt will be made here to review the subject in depth. Rather, the reader is referred to an excellent treatise on the subject by Fuller (ref. 9) and an earlier paper by Strangway et al. (ref. 10). In the present

paper, we will discuss the major points of lunar magnetic properties and elaborate on some of the ramifications.

In making measurements on lunar samples, the magnetic hysteresis loop at room temperature is usually measured and can be utilized to determine a number of important parameters. The only ferromagnetic material present in any quantity in lunar materials is metallic iron, sometimes alloyed with nickel and/or cobalt. There have been isolated reports of minute amounts of oxidized phases such as magnetite and goethite, but these are very limited. It is therefore possible to make quite accurate magnetic measurements of the content of metallic iron. A histogram of observations on lunar samples is shown in figure 7. In all cases, the mare basalts have less than 0.1-percent metallic iron by weight and, in general, there is only about 0.05 to 0.06 percent. The few samples of anorthosite that have been measured have even less metallic iron than this. Thus, the major lunar igneous rock types are not highly reduced chemically since they also have considerable amounts of Fe^{++} present in iron silicates.

Soils from the various missions have also been examined, and it is found that the metallic iron content is much higher than that in any of the igneous rocks. This in itself is remarkable since the soil is largely derived from the rocks present. It was thought at one time that this was the result of excess iron added by iron meteorites. It is now known that this is not the case, since most of the metallic iron present is not nickel-rich kamacite.

Breccias which are derived largely as a result of impacts into soils show spreads of values of iron content between those of soils and igneous rocks, and in some cases have contents higher than the soils. We have somewhat arbitrarily used an additional group, here referred to as highland crystalline rocks. These are the highly remelted rocks collected from the Apollo 16 highland landing site. Again the range of metallic iron content is quite large, as with the less severely reworked breccias.

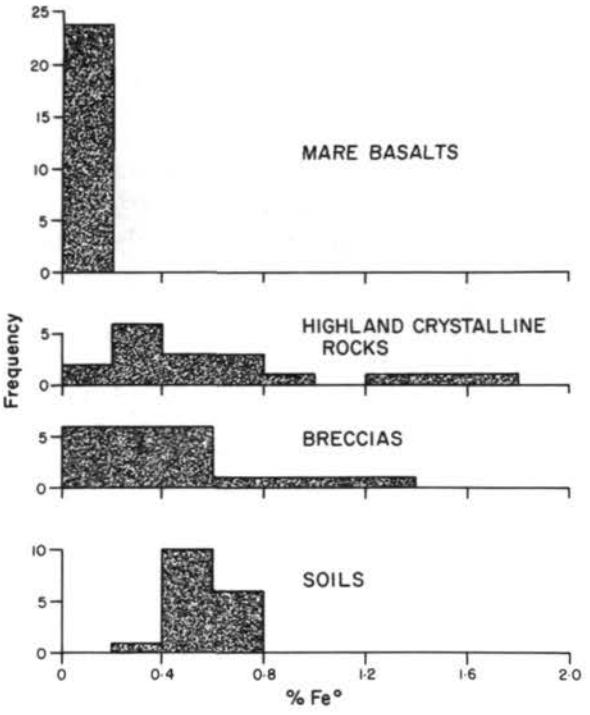


Figure 7.—*Metallic iron content in lunar samples of various types. Data represent a fairly complete compilation up to Apollo 16 from all laboratories as reported in Pearce et al. (ref. 11) and amplified with data from our laboratory on Apollo 17, as reported in Pearce et al. (ref. 12) and from reports in the Proceedings of the fourth Lunar Science Conference and the Lunar Science V abstract.*

It is also possible to determine the ferrous iron content from magnetic hysteresis studies by determining the slope of the paramagnetic portion of the curve. This method gives a good approximation to the true ferrous iron content present in the lunar silicates (refs. 11 and 13) provided there is not a large amount of superparamagnetic iron present. Superparamagnetic iron has grain sizes less than about 150 Å and is sufficiently thermally unstable to be unable to carry a remanence. In general, particles of about 150 to 300 Å are considered to be single domain. These are extremely stable magnetically and are able to carry very stable remanence. In grain sizes over 300 Å, iron is presumably

multidomain and can carry a remanence which is often quite soft and easily altered. The lunar soils and the low-grade breccias (refs. 14 and 15) have a significant amount of superparamagnetic iron present (size fractions less than about 160 Å). In such cases the paramagnetic susceptibility systematically overestimates the true iron content by a few percent. This fine-grained iron has led to an interesting study, since the lunar samples are almost unique in their complex range of ferromagnetic grain sizes, permitting the study of the full range of magnetic properties from superparamagnetic to single domain to multidomain in a single suite of samples. In addition to the normal hysteresis loops, it is well known that superparamagnetic particles can acquire a strong Viscous Remanent Magnetization (VRM) simply by being exposed to a field for a period of time. A number of studies of this have been reported (refs. 14, 15, and 16). Multidomain grains can also acquire VRM, but the character is quite different although it has not been studied in detail.

Information on other magnetic parameters for a number of samples is illustrated in figures 8 and 9. In figure 8 a plot of the magnetically determined ferrous iron (Fe^{++}) and the metallic iron (Fe^{o}) is illustrated using as an example the Apollo 17 rocks after Pearce et al. (ref. 12). By and large the mare basalts group in a small region with 16 to 18 percent of total iron and about 0.1-percent metallic iron. These samples have been little modified since emplacement, and it is tempting to speculate that this ratio is a norm for igneous processes in the lunar environment. Although the results from other missions are not shown in this figure, the few basalt samples for which these determinations have been made from other missions give comparable results. The dunite clast from 72415 shows a similar ratio, suggesting that it may not have suffered extensive surface modifications after it was formed.

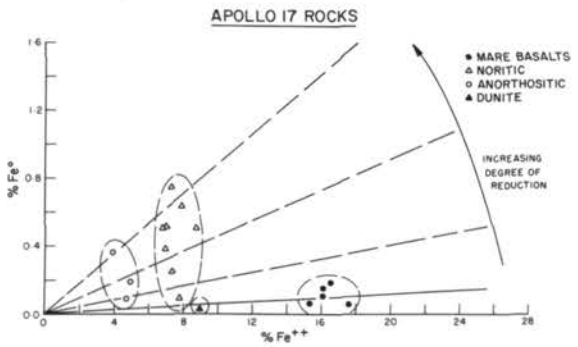


Figure 8.—*Cluster diagram of Fe^{o} versus Fe^{++} content (both determined magnetically) for rock samples from Apollo 17. Note the distinct groupings by rock type and the spread in the ratio for the anorthositic and noritic breccias. This corresponds to different degrees of chemical reduction.*

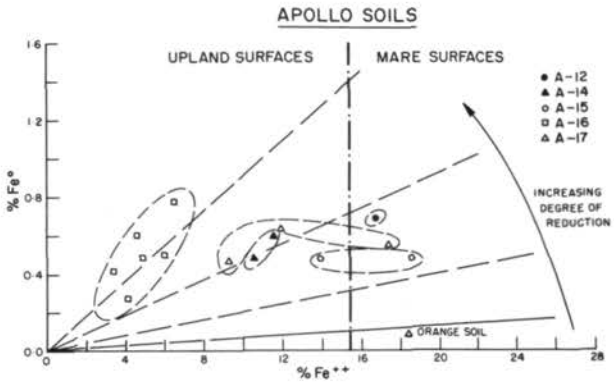


Figure 9.—*Cluster diagram of Fe^{o} versus Fe^{++} content for soils from all Apollo landing sites. Note distinct groupings for different soils and that the mare soils are generally high in Fe^{++} and are less reduced than highland soils.*

The anorthositic samples are much lower in total iron as expected, but they tend to be enriched in metallic iron. The same is true for the noritic samples from the Apollo 17 mission. It is hard to escape the conclusion that these latter samples, which are in reality chips from the highland breccias of the north massif, have undergone reheating in the lunar vacuum and that chemical reduction of iron from the silicates has been one of the consequences. This process has been demonstrated in the laboratory by Pearce et al. (ref. 17), and Pearce and Simonds (ref. 18) have shown that the

Apollo 16 rocks are similar to the Apollo 17 rocks in this respect.

The precise cause of the reduction involved remains unclear. Housley et al. (refs. 19 and 20) propose micro-meteorite bombardment that leads to local melting in the presence of samples enriched by reducing solar wind gases. Pearce et al. (ref. 17) and Cisowski et al. (ref. 21) propose that the process takes place as the result of larger impact processes. Pearce et al. suggest that the excess iron is primarily generated in the associated ejecta blanket including gas cloud and regions of local melting. Cisowski et al. (ref. 22) attribute it directly to the effect of shock rather than the associated ejecta blanket heating. In any event, there seems to be little question that surface processes which are the result of impacts generate the excess iron found in the lunar soils and breccias. Housley et al. (ref. 19) have particularly drawn attention to the fact that much of the excess metallic iron in the soils is present in the form of spherules within glass particles and that these spherules are quite accurately spherical.

We illustrate in figure 9 plots of Fe^{++} versus Fe^{o} for soils from the different Apollo missions. It should be noted that the magnetically determined Fe^{++} is the quantity used. As stated earlier, this is a systematic overestimate. The samples plotted are taken from the table given by Pearce et al. (ref. 12) for convenience, but the conclusions are similar when data from other laboratories are examined. The least reduced samples are the young mare soils from Apollo 12, 15, and 17. The number of samples plotted is not large, but the trend is unmistakable. At Apollo 15 and 17 highland samples were also collected. These have much less total iron and are relatively more reduced, probably as a result of the greater age of these surfaces. The proximity of mare surfaces at these two sites suggests that considerable mixing between old highland surfaces and young mare surfaces may have taken place. Samples from Apollo 14 are quite reduced, while the low iron content samples from the oldest site, Apollo 16, are by far the most reduced. Thus, there is a correlation between the amount of reduction and the exposure of the various sites to the continuing bombardment of the lunar surface by impacts of varying sizes during the early active period of lunar history.

The orange soil from the Apollo 17 site is quite anomalous in this sense. In agreement with other studies (ref. 23), it may be concluded that it was formed in a somewhat more oxidizing atmosphere than the bulk of lunar soils. It may well be that this environment was similar to that in which the basalts themselves were formed. Subsequent bombardment then caused chemical reduction of most of the soils. The orange soil, however, has remained relatively untouched by bombardment since its formation and so is not as reduced. There is undoubtedly much yet to be learned about the systematics of iron distribution and the controlling influences. Lunar surface processes will be better understood as we gain this insight.

In addition to the distribution of metallic iron, it is possible to determine a great deal about the grain sizes from a study of the magnetic hysteresis loop properties. Two such parametric representations are illustrated in figures 10 and 11. In figure 10, the saturation remanence (J_{rs}), which is a measure of the capacity of a sample to retain a memory, is normalized against the saturation magnetization (J_s), which is a direct measure of the total metallic iron. This plot is a histogram of results previously tabulated by Pearce et al. (ref. 11), and data from Apollo 17 (ref. 12) has been added. Most notable in this plot is the fact that the crystalline rocks are invariably the least able to carry a strong memory. This is due simply to the presence of multidomain iron (> 300 Å) and very little single-domain iron (150–300 Å). The crystalline rocks can be used for ancient field studies, but they have a large proportion of magnetically soft iron and are therefore extremely difficult to work with. Soils have distinct higher values of the ratio J_r/J_s and a greater spread. The mare soils tend to have the greatest ability to carry a memory, with values of J_r/J_s approaching 0.1. The breccias, as in previous indicators, tend to be

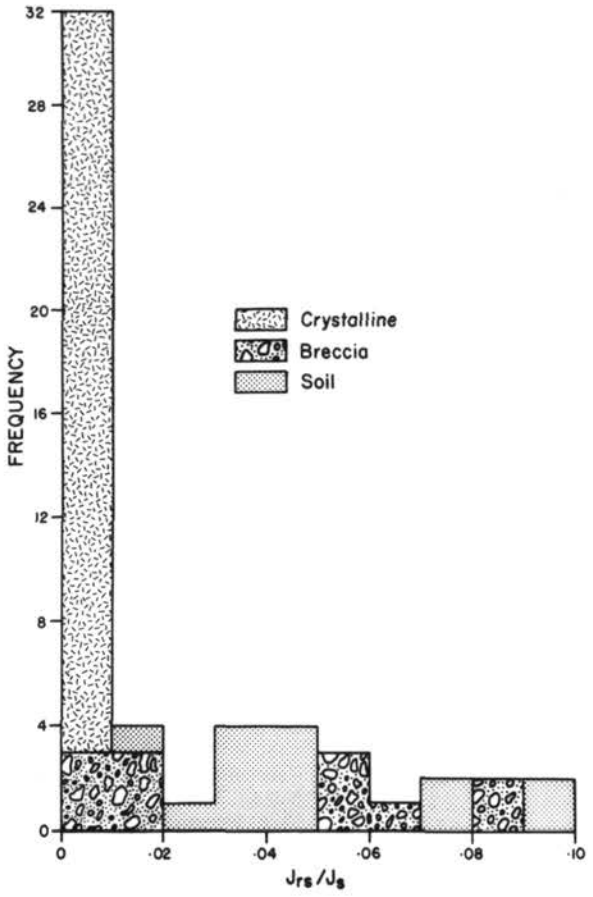


Figure 10.—*Histogram of values of* J_{rs}/J_s *for different types of lunar samples. Small values of this quantity imply multidomain materials which are magnetically soft.* (J_{rs} = *saturation remanence;* J_s = *saturation magnetization.*)

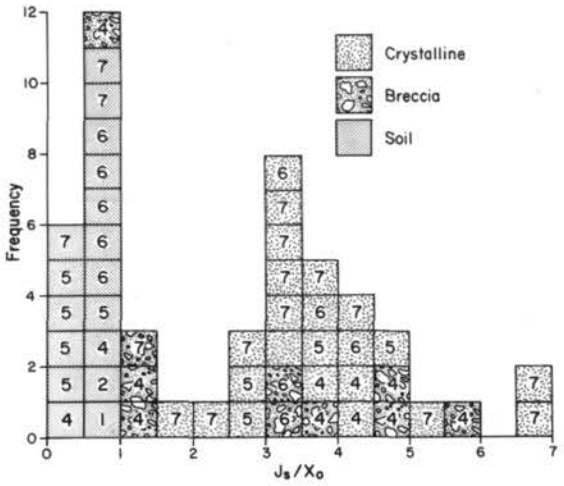


Figure 11.—*Histogram of values of* J_s/X_o *for different types of lunar samples. Small values of* X_o *(the initial susceptibility) imply the presence of multidomain material, while larger values imply single-domain materials. This grades into the largest values for superparamagnetic materials.*

mixed with values ranging from those for the true igneous rocks to those for the least developed soils.

A second parameter, the ratio of the saturation magnetization (J_s) to the initial susceptibility (X_o), is shown in figure 11. The initial susceptibility is a measure of the shape of the hysteresis loop. When the value of J_s/X_o is small, the material tends to have a high proportion of superparamagnetic and single-domain material; when it is large, it implies the presence of multidomain materials. Even though any one sample undoubtedly contains volume fractions of all these, it is interesting to examine the systematics. The soils are almost invariably characterized by low values, implying thereby that they are rich in superparamagnetic or single-domain material. The crystalline rocks tend to have high values, thereby implying that they are rich in multidomain materials. Again the breccias are spread between these and represent intermediate distributions of grain sizes.

It is therefore abundantly clear that not only is the iron content and oxidation state highly variable on the lunar surface, but there are systematic variations in the grain sizes. Mechanisms considered for generating the excess iron appear to create excess fine-grained material which is dominant in the glasses (refs. 19 and 20). Subsequent processes appear to lead to the coarsening of grain sizes as the samples are lithified into breccias and heated to temperatures often approaching the melting temperature (ref. 24).

This is characterized by the plots of figure 12 that use a scheme like the one developed by Wasilewski (ref. 25) for classification of the magnetic properties of basalts and used by Fuller (ref. 9) for lunar samples. Here it

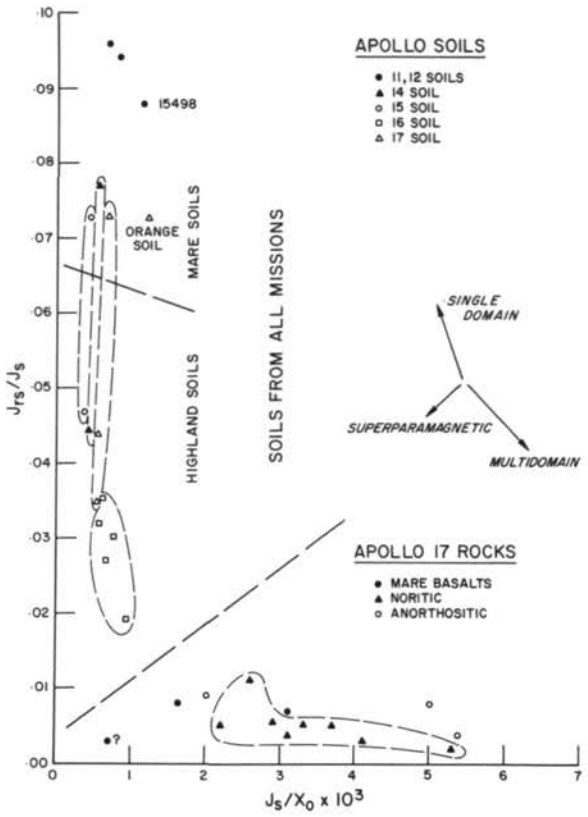


Figure 12.—*Cluster diagram of data from figures 10 and 11 showing character of soils from all missions and character of rocks from Apollo 17. Note that the mare soils tend to be rich in superparamagnetic and single-domain materials (high J_r/J_s and low J_s/X_0). Highland soils tend to be lower in single-domain materials and have more multidomain grains. Mare basalts and the high-grade noritic and anorthositic breccias tend to be low in single-domain materials and rich in multidomain materials.*

is shown that the basalts fall into a characteristic region of the plot just as the soils do. There are characteristic variations in the soil properties depending especially on whether they are of mare or of highland origin. The anorthosites and noritic rocks from Apollo 17 tend to show the coarsening of grain size and are intermediate between soils and mare.

Added to figure 12 are the data for sample 15498 which led to a useful paleointensity determination (ref. 26). Notice that this sample is rich in single-domain iron.

Natural Remanent Magnetization (NRM)

The intensity of remanent magnetization in lunar samples covers a wide range of values. Tabulated data for a large number of samples are shown in figure 13 (ref. 11). These data include most observations up to the time of the Apollo 16 mission.

A distinct peak for mare basalts occurs at

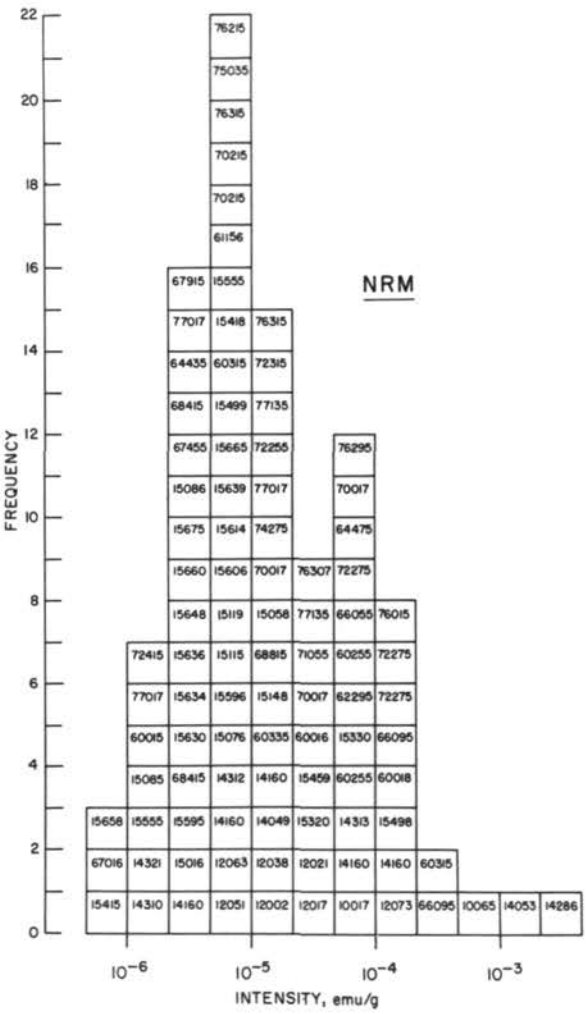


Figure 13a.—*Natural remanent magnetization (NRM) as measured on returned lunar samples. Figure from reference 11, with new data from references 13 and 27 through 32.*

about 10^{-5} emu/g. When the samples are demagnetized at 100 Oe as shown in figure 13, a large soft component is removed from most of the mare basalts and some of the breccias. This gives a peak of stable NRM at about 10^{-6} emu/g. A limited number of samples, however, retain their strong magnetization and form a small group at about 10^{-4} emu/g. Most of these samples are breccias. It seems likely that only this type of material can give the magnetic fields detected on the lunar surface.

One of the most important observations that must be the focus of more studies is the determination of the ancient lunar field intensity. To date only a few generally unsatisfactory observations have been made. The full Thellier-Thellier technique has proven to be difficult to apply since the samples change character on heating. One observation by Gose et al. (ref. 26) on a sample rich in single-domain particles gave a value of 2100 gammas. Heating in vacuum to 650°C showed no mineralogic changes, but at 700°C the sample changed irreversibly. Watson et al. (ref. 33) have reported measurements on breccias and basalts that gave intensity values of about 1100 gammas. Their heating was done in a controlled oxygen fugacity system. They were able to heat a basalt to 700°C with no apparent changes, although heating to 800°C caused generation of excess iron. A breccia sample started to alter even at temperatures less than 550°C. They attribute this to the presence of very fine-grained iron with a large ratio of surface area to volume.

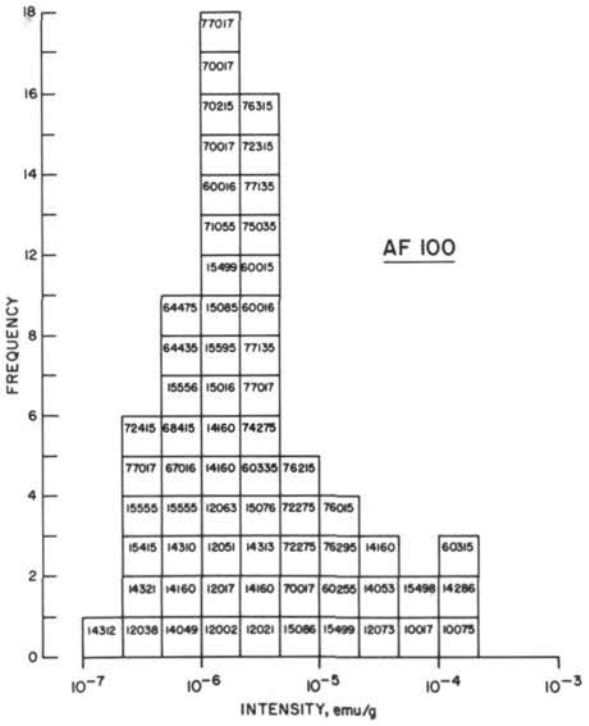


Figure 13b.—*Natural remanent magnetization after cleaning samples in alternating fields of 100 oe.*

The heating question is the central dilemma for paleointensity studies, and other workers have tried other approaches, including measurements of anhysteretic remanent magnetization. Stephenson and Collinson (ref. 34) report on a number of samples measured in this way which give apparent paleointensities of around 10 000 to 120 000 gammas. Heating to 500°C was reported (ref. 28). Above this, changes again took place. The subject requires much more careful study because, as pointed out by Dunlop et al. (ref. 35), the viscous effects in some samples can probably only be removed by heating to above about 300°C. Any information acquired without thermal demagnetization is likely to have a strong VRM effect. This means that the most important temperaature range to study (300°C to the Curie point) is only barely accessible to us. It is also worth noting that lunar samples are especially difficult to work with because, in general, they have a large soft component of magnetization which can introduce spurious effects unless extreme precautions are exercised. The presence of large soft components of NRM in lunar samples is one of the unsolved problems. At least some of this component may be of nonlunar origin, as shown by Pearce and Strangway (ref. 36). They returned an Apollo 12 sample to the Moon on Apollo 16. This sample had the soft component removed before flight, but it had acquired a large, soft component on return,

presumably from spacecraft fields of a few oersteds. However, some of the soft component may be of lunar origin.

History of the Magnetic Field of the Moon

There is of course a high degree of importance to study of ancient lunar magnetic fields in view of the importance this has in determining something about the history and evolution of the Moon. The impact of magnetic studies on terrestrial studies is well known since it ushered in the new generation of the Earth sciences. While it may play the same role in lunar studies, it is important to understand the origin of the fields which magnetized the lunar samples. This same magnetization has been dramatically confirmed by the study of lunar surface fields (ref. 37) at a few places and by lunar orbital fields (ref. 38). There seems to be little question that large volumes of lunar material are present on the Moon, magnetized in a sufficiently coherent manner that they can give rise to detectable anomalies even at orbital heights. One model for this has been proposed by Strangway et al. (ref. 39) who call on the deposition of Cayley-type breccias in a coherent manner. Although only a small portion of the Moon has been studied by orbital mapping, there are several genuine anomalies and several inferred ones. This type of anomaly was also detected by the Apollo 16 subsatellite when it was at low altitude (ref. 38) and by the study of electron mirroring from the Moon (refs. 20 and 40). The Russians have reported on the presence of fields observed on the Lunokhod. By comparison with terrestrial studies, it is interesting to note that at comparable altitudes detectable crustal features are very weak (refs. 41, 42, and 43) relatively speaking, when the large magnetic field of the Earth is considered.

There are many unknowns about the nature and origin of lunar fields, but with the presence of lunar magnetic anomalies there can be no doubt that portions of the crust carry a memory of some early field. The geometry and the time duration of this field are unknown, and many speculations have been put forward as reviewed by Fuller (ref. 9). As we have already indicated, there are some highly magnetic samples on the Moon, and these are the most likely cause of the field observed from orbit. Since these samples are generally breccias, it has been considered that the magnetization they carry is somehow related to the impact that created them. These samples appear to carry a stable remanence, and there are many indications that they were heated well above the Curie point of iron. Many lines of evidence support this view as reviewed by Williams (ref. 44). The remanence in these samples would therefore be a Thermoremanence Magnetization (TRM) acquired on cooling in the presence of a field. As reviewed by Wasilewski (ref. 45), those regions around an impact not heated above the Curie temperature could acquire a Partial Thermoremanence Magnetization (PTRM).

Because of the similarity of this process to the comparable terrestrial process, we briefly review here the observation made on terrestrial impact structures and their related melts. Studies of the remanent magnetism of a number of terrestrial craters have been made. These include the Ries crater (ref. 46), the Rochechouart structure (ref. 47), the Mistastin Lake structure (ref. 48), the Manicouagan structure (refs. 49 and 50), the Charlevoix structure (ref. 51) and Meteor Crater (ref. 52). The findings can be very simply summarized. Wherever impactites containing glass are found so that the temperature clearly approached the melting temperatures, there is a consistent report of unusually strong, unusually stable, and unusually well-grouped paleomagnetic results. There seems to be no question that the materials cooled slowly enough that any transient magnetic fields associated with the impact had no influence on the resulting magnetization. Rather, the materials acquired a TRM which is considered to be an unusually accurate record of the ambient Earth's field. It seems likely that a similar

mechanism operated on the Moon. The larger impacts caused heating to above the Curie temperature; in many cases the temperature approached melting. On cooling, the transient field effects of the impact were gone, and portions of the lunar crust acquired a coherent remanence governed by the ambient lunar field. Where heating does not reach the Curie point it is likely that scatter will be introduced just as is found in the low-temperature portions of terrestrial ash flows (ref. 53). In most cases, the softer portions of any preexisting remanence can, of course, be modified by shock, as at Meteor Crater.

If this explanation is correct and the terrestrial analog is relevant, we have yet to account for the origin of the original field controlling the process. Many models have been proposed, and we select no favorites in this paper. However, the discovery of a significant field on Mercury (ref. 54) and the strong indication of a field on Mars (ref. 55) suggest that these bodies also retain a memory of something that happened early in the history of the solar system. It seems to us that it is necessary to create models of the Moon and other nondynamo planets that have the ability to acquire a coherent magnetization at some time in the past.

Future mapping of the intrinsic magnetic field of planets and asteroids continues to be an important goal in understanding the early solar system.

Acknowledgment

This work was supported by NRC grants to D. W. Strangway and G. W. Pearce. The authors have benefited greatly from laboratory assistance by R. Schmidt and D. Redman and extensive discussions with their colleagues J. Carnes and W. Gose.

References

1. OLHOEFT, G. R., AND D. W. STRANGWAY, Dielectric Properties of the First 100 Metres of the Moon. Submitted to *Earth Planet. Sci. Letters*, 1974.
2. HAGFORS, T., Remote Probing of the Moon by Infrared and Microwave Emissions and by Radar. *Radio Science*, Vol. 5, 1970, pp. 189–226.
3. TYLER, G. L., AND H. T. HOWARD, Dual Frequency Bistatic Radar Investigations of the Moon With Apollo 14 and 15. *J. Geophys. Res.*, Vol. 78, 1973, pp. 4852–4874.
4. SIMMONS, G., D. W. STRANGWAY, L. BANNISTER, R. BAKER, D. CUBLEY, G. LA TORRACCA, AND R. D. WATTS, The Surface Electrical Properties Experiment. *Lunar Geophysics*, Lunar Science Institute, Houston, 1972.
5. STRANGWAY, D. W., G. SIMMONS, G. LA TORRACA, R. WATTS, L. BANNISTER, R. BAKER, J. D. REDMAN, AND J. R. ROSSITER, Radio Frequency Interferometry—A New Technique for Studying Glaciers. *J. Glaciology*, Vol. 13, 1974, pp 123–132.
6. ROSSITER, J. R., D. W. STRANGWAY, A. P. ANNAN, AND R. D. WATTS, Detection of Thin Layers by Radio Interferometry. *Geophysics*, in press, 1974.
7. KOVACH, R. L., AND J. S. WATKINS, The Structure of the Lunar Crust at the Apollo 17 Site. *Proc. Fourth Lunar Science Conference, Geochimica et Cosmochimica Acta*, Supplement 4, 1973, pp. 2549–2560.
8. WATKINS, J. S., AND R. L. KOVACH, Seismic Investigations of the Lunar Regolith. *Proc. Fourth Lunar Science Conference, Geochimica et Cosmochimica Acta*, Supplement 4, 1973, pp. 2561–2574.
9. FULLER, M. D., Lunar Magnetism. Rev. *Geophys. and Space Phys.*, Vol. 12, 1974, pp. 23–70.
10. STRANGWAY, D. W., W. A. GOSE, G. W. PEARCE, AND J. G. CARNES, Magnetism and the History of the Moon. *Proc. 18th Annual Conference on Magnetism and Magnetic Materials, Am. Inst. Phys. Conference Proc.*, Vol. 10, 1973, pp. 1178–1196.
11. PEARCE, G. W., W. A. GOSE, AND D. W. STRANGWAY, Magnetic Studies on Apollo 15 and 16 Lunar Samples. *Proc. Fourth Lunar Science Conference, Geochimica et Cosmochimica Acta*, Supplement 4, 1973, pp. 3045–3076.
12. PEARCE, G. W., D. W. STRANGWAY, AND W. A. GOSE, Magnetic Properties of Apollo Samples and Implications for Regolith Formation. *Proc. Fifth Lunar Science Conference*, in press, 1974.
13. NAGATA, T., R. M. FISHER, F. C. SCHWERER, M. D. FULLER, AND J. R. DUNN, Magnetic Properties and Natural Remanent Magnetization of Apollo 15 and 16 Materials. *Proc. Fourth Lunar Science Conference, Geochimica et Cosmochimica Acta*, Supplement 4, 1973, pp. 3019–3043.
14. NAGATA, T., AND B. J. CARLETON, Natural Rema-

nent Magnetization and Viscous Magnetization of Apollo 11 Lunar Materials. *J. Geomag. and Geoel.*, Vol. 22, 1970, pp. 491–506.

15. GOSE, W. A., AND J. G. CARNES, The Time-Dependent Magnetization of Fine-Grained Iron in Lunar Samples. *Earth Planet. Sci. Letters*, Vol. 20, 1973, pp. 100–106.
16. STEPHENSON, A., Single Domain Grain Distributions; I. A Method for the Determination of Single Domain Grain Distributions. II. The Distribution of Single Domain Iron Grains in Apollo 11 Lunar Dust. *Phys. Earth Planet. Interiors*, Vol. 4, 1971, pp. 353–360, 361–369.
17. PEARCE, G. W., R. J. WILLIAMS, AND D. S. MCKAY, The Magnetic Properties and Morphology of Metallic Iron Produced by Subsolidus Reduction of Synthetic Apollo 11 Composition Glasses. *Earth Planet. Sci. Letters*, Vol. 17, 1972, pp. 95–104.
18. PEARCE, G. W., AND C. H. SIMONDS, Magnetic Properties of Apollo 16 Samples and Implications for Their Mode of Formation. *J. Geophys. Res.*, Vol. 79, 1974, pp. 2953–2959.
19. HOUSLEY, R. M., R. W. GRANT, AND N. E. PATON, Origin and Characteristics of Excess Fe Metal in Lunar Glass Welded Aggregates, *Proc. 4th Lunar Science Conference, Geochimica et Cosmochimica Acta*, Supplement 4, 1973, pp. 2737–2749.
20. HOUSLEY, R. M., E. H. CIRLIN, AND R. W. GRANT, Solar Wind and Micrometeorite Alteration of the Lunar Regolith. *Lunar Science*, Vol. V, Lunar Science Institute, Houston, 1974, pp. 360–362.
21. CISOWSKI, S., M. FULLER, M. F. ROSE, AND P. J. WASILEWSKI, Magnetic Effects of Experimental Shocking of Lunar Soil. *Proc. Fourth Lunar Science Conference, Geochimica et Cosmochimica Acta*, Supplement 4, 1973, pp. 3003–3017.
22. CISOWSKI, S., M. FULLER, M. F. ROSE, AND P. J. WASILEWSKI, Impact Processes and Their Effect on Lunar Magnetism. *Lunar Science*, Vol. V, Lunar Science Institute, Houston, 1974, pp. 123–125.
23. MAO, H. K., D. VIRGO, AND P. M. BELL, Analytical and Experimental Study of Iron and Titanium in Orange Glass From Apollo 17 Soil Sample 74220. *Proc. Fourth Lunar Science Conference, Geochimica et Cosmochimica Acta*, Supplement 4, 1973, pp. 397–412.
24. USSELMAN, T. M., AND G. W. PEARCE, The Grain Growth of Iron: Implications for the Thermal Conditions in a Lunar Ejecta Blanket. *Proc. Fifth Lunar Science Conference*, in press, 1974.
25. WASILEWSKI, P. J., Magnetic Hysteresis Classification for the Lunar Surface. *The Apollo 15 Lunar Samples*, Lunar Science Institute, Houston, 1972.
26. GOSE, W. A., D. W. STRANGWAY, AND G. W. PEARCE, The Determination of the Intensity of the Ancient Lunar Magnetic Field. *The Moon*, Vol. 7, 1973, pp. 196–201.
27. NAGATA, T., N. SUGIURA, R. M. FISHER, F. C. SCHWERER, M. D. FULLER, AND J. R. DUNN, Magnetic Properties and Natural Remanent Magnetization of Apollo 16 and 17 Lunar Materials. *Lunar Science*, Vol. V, Lunar Science Institute, Houston, 1974.
28. COLLINSON, D. W., A. STEPHENSON, AND S. K. RUNCORN, Magnetic Properties of Apollo 15 and 16 Rocks. *Proc. Fourth Lunar Science Conference, Geochimica et Cosmochimica Acta*, Supplement 4, 1973, pp. 2963–2976.
29. RUNCORN, S. K., D. W. COLLINSON, AND A. STEPHENSON, Magnetic Properties of Apollo 16 and 17 Rocks—An Interim Report. *Lunar Science*, Vol. V, Lunar Science Institute, Houston, 1974.
30. BRECHER, A., D. J. VAUGHAN, R. G. BURNS, AND K. R. MORASH, Magnetic and Mössbauer Studies of Apollo 16 Rock Chips 60315, 51 and 62295, 27. *Proc. Fourth Lunar Science Conference, Geochimica et Cosmochimica Acta*, Supplement 4, 1973, pp. 2991–3001.
31. BRECHER, A., AND K. R. MORASH, Inferences From Comparative Magnetic Studies of Some Apollo 17 Basalts, Breccias and Soils. *Lunar Science*, Vol. V, Lunar Science Institute, Houston, 1974.
32. BANNERJEE, S. K., K. HOFFMAN, AND G. SWITS, Reversed Polarity Remanent Magnetization in a Layered Boulder Near South Massif. *Lunar Science*, Vol. V, Lunar Science Institute, Houston, 1974.
33. WATSON, D. E., E. E. LARSON, AND R. L. REYNOLDS, Microscopic and Thermomagnetic Analysis of Apollo 17 Breccia and Basalt; Feasibility of Obtaining Meaningful Paleointensities of the Lunar Magnetic Field. *Lunar Science*, Vol. V, Lunar Science Institute, Houston, 1974, pp. 727–829.
34. STEPHENSON, A., AND D. W. COLLINSON, The Determination of Lunar Magnetic Field Paleointensities. *Lunar Science*, Vol. V, Lunar Science Institute, Houston, 1974, pp. 735–737.
35. DUNLOP, D. J., W. A. GOSE, G. W. PEARCE, AND D. W. STRANGWAY, Magnetic Properties and Granulometry of Metallic Iron in Lunar Breccia 14313. *Proc. Fourth Lunar Science Conference, Geochimica et Cosmochimica Acta.*
36. PEARCE, G. W., AND D. W. STRANGWAY, *Cause of Secondary Magnetization in Lunar Samples.* National Aeronautics and Space Administration, SP-315, 1973, pp. 7–55 to 7–58.
37. DYAL, P., G. W. PARKIN, AND W. D. DAILY, Surface Magnetometer Experiments: Internal Lunar Properties. *Proc. Fourth Lunar Science Conference, Geochimica et Cosmochimica Acta,*

Supplement 4, 1973, pp. 2925–2945.

38. RUSSELL, C. T., P. J. COLEMAN, B. R. LICHTENSTEIN, G. SCHUBERT, AND L. R. SHARP, Subsatellite Measurements of the Lunar Magnetic Field. *Proc. Fourth Lunar Science Conference, Geochimica et Cosmochimica Acta*, Supplement 4, 1973, pp. 2833–2845.
39. STRANGWAY, D. W., W. A. GOSE, G. W. PEARCE, AND R. K. MCCONNELL, Lunar Magnetic Anomalies and the Cayley Formation. *Nature, Phys. Sci.*, Vol. 246, 1973, pp. 112–115.
40. ANDERSON, K. A., H. C. HOWE, R. P. LIN, R. R. MCGUIRE, L. M. CHASE, AND J. E. MCCOY, Observation of Energetic Electron Mirroring From the Lunar Remanent Magnetic Field. *Lunar Science*, Vol. V, Lunar Science Institute, Houston, 1974, pp. 18–19.
41. ZIETZ, I., G. E. ANDREASEN, AND J. C. CAIN, Magnetic Anomalies From Satellite Magnetometer. *J. Geophys. Res.*, Vol. 75, 1970, pp. 4007–4015.
42. CAIN, J. C., Geomagnetic Models From Satellite Surveys. *Rev. Geophys. and Space Phys.*, Vol. 9, 1971, pp. 259–273.
43. BENKOVA, N. P., SH.SH. DOLGINOV, AND T. N. SIMONENKO, Residual Magnetic Field From the Satellite Cosmos 49. *J. Geophys. Res.*, Vol. 78, 1973, pp. 798–803.
44. WILLIAMS, R., The Lithification and Metamorphism of Lunar Breccias. *Earth Planet. Sci. Letters*, Vol. 16, 1972, pp. 250–256.
45. WASILEWSKI, P. J., Shock Remagnetization Associated With Meteorite Impacts at Planetary Surfaces. *The Moon*, Vol. 6, 1973, pp. 264–291.
46. POHL, J., AND G. ANGENHEISTER, Anomalien des Erdmagnetfelds und Magnetisiering der Gesteine in Nordlinger Ries. *Geol. Bavaria*, Vol. 561, 1969, p. 327.
47. POHL, J., AND H. SOFFEL, Paleomagnetic Age Determination of the Rochechouart Impact Structure (France). *Zietschrift fur Geophysik*, Vol. 37, 1971, pp. 857–866.
48. CURRIE, K. L., AND A. LAROCHELLE, A Paleomagnetic Study of Volcanic Rocks From Mistastin Lake, Labrador, Canada. *Earth Planet. Sci. Letters*, Vol. 6, 1969, pp. 309–315.
49. LAROCHELLE, A., AND K. L. CURRIE, Paleomagnetism of Igneous Rocks From the Manicouagan Structure, Quebec. *J. Geophys. Res.*, Vol. 72, 1967, pp. 4163–4169.
50. ROBERTSON, W. A., Manicouagan, Quebec, Paleomagnetic Results. *Can. J. Earth Sci.*, Vol. 4, 1967, pp. 641–649.
51. HARGRAVES, R. B., AND D. N. ROY, Paleomagnetism of Anorthosites in and Around the Charlevoix Crypto-Explosion Structure, Quebec. *Can. J. Earth Sci.*, Vol. 11, 1974, pp. 854–859.
52. HARGRAVES, R. B., AND W. E. PERKINS, Investigation of the Effect of Shock on Natural Remanent Magnetization. *J. Geophys. Res.*, Vol. 74, 1968, pp. 2576–2589.
53. STRANGWAY, D. W., J. SIMPSON, AND D. YORK, *Paleomagnetic Studies of Volcanic Rocks From the Mogollon Plateau Area of Arizona and New Mexico*. New Mexico Press, in press, 1974.
54. NESS, N. F., K. W. BEHANNON, R. P. LEPPING, Y. C. WHANG, AND K. H. SCHATTEN, Magnetic Field Observations Near Mercury; Preliminary Results From Mariner 10. *Science*, Vol. 185, 1974, pp. 151–160.
55. DOLGINOV, SH.SH., YE. G. YEROSHENKO, AND L. N. ZHUGOV, Magnetic Field in the Very Close Neighborhood of Mars, According to Data From Mars 2 and Mars 3 Spacecraft. *J. Geophys. Res.*, Vol. 78, 1973, pp. 4779–4786.
56. HOWE, H. C., R. P. LIN, R. E. MCGUIRE, AND K. A. ANDERSON, Energetic Electron Scattering From the Lunar Remanent Magnetic Field. *Geophys. Res. Letters*, Vol. 1, 1974, pp. 101–104.

Page intentionally left blank

Page intentionally left blank

Magnetic Field in Le Monnier Bay According to Data of Lunokhod 2

Sh. Sh. Dolginov, Ye. G. Yeroshenko, L. N. Zhuzgov, and V. A. Sharova
Institute of Terrestrial Magnetism, The Ionosphere and Radio Wave Propagation Academy of Sciences, Moscow, U.S.S.R.

G. A. Vnuchkov, B. A. Okulessky, and A. T. Bazilevsky
Institute for Space Research, Academy of Sciences, Moscow, U.S.S.R.

The results of the first traverse measurement of the magnetic field on the surface of the Moon are analyzed. The mean value of the magnetic field in the portion of Le Monnier Bay investigated is estimated at 20–30 gammas. An anomaly of the field (10–15 gammas) was disclosed, which is confined to craters that exceed 50 meters in size.

Experiment Task

Magnetization of the lunar rocks, discovered by the Apollo missions (ref. 1), coupled with the observed absence of a uniform field on the Moon during the present (refs. 2–4), is one of the enigmas of the history of the Moon.

Investigation of the distribution of magnetic field sources from low-flying satellites is the most appropriate means of studying the global distribution of magnetic anomalies on the Moon. However, since extrapolation of the fields to the lunar surface is difficult, the necessity arises for supplementing the investigation of magnetization of the Moon from satellites with investigations on the surface of the Moon. The magnetic characteristics of individual regions, with different topographic relief characteristics (craters, faults, fields of rocks, etc.), can be studied only by a magnetic survey on the surface. Local anomalies of the field, which may be connected with these features, quickly decrease with altitude. A comparison of the magnetic data with the data of other physicochemical and geological investigations is an additional possibility in the study of the origin of the anomalies, and in understanding the nature and origin of the magnetization of the lunar rocks.

Investigation of the magnetic field on the surface of another celestial body, by means of a self-propelled vehicle, is a technical question, since a Lunokhod-type vehicle cannot be constructed without electromagnetic devices, which create interference with the operation of the onboard magnetometer. Lunokhod 2 was not intended specially to conduct magnetic studies.

Apparatus and Measurements

A three-component fluxgate magnetometer, with automatic range extension, permitting measurement of three components of the field with uniform sensitivity, in the $\pm$ 580

gamma range, was installed aboard Lunokhod 2.

The magnetometer sensors were located remotely from the body of Lunokhod by 1.5 meters. The three sources of magnetic contamination are:

a. Permanently magnetized material and circulating electrical currents
b. Moving magnetic material in the wheels
c. Thermoelectric currents, determined mainly by the heat flow in the housing and support of the magnetometer sensor.

Elimination of these sources from the onboard magnetogram data was carried out by specially planned maneuvers of Lunokhod 2 in selected sections of the traverse, on the basis of data from ground tests and the data of instruments determining the course of the Lunokhod. It was estimated that elimination of these fields was accomplished with an absolute error of $\pm$ 3 gammas for the horizontal components. The zero point of the vertical component could not be tested on the surface of the Moon. The relative error in determination of this component was about three gammas. The estimates of errors were tested by repeated measurements along the same traverse.

General Characteristics of the Field in Le Monnier Bay

A map of the route of Lunokhod 2, on which the magnetic measurements were performed, is presented in figure 1. It is clear that, geologically-morphologically, the mea-

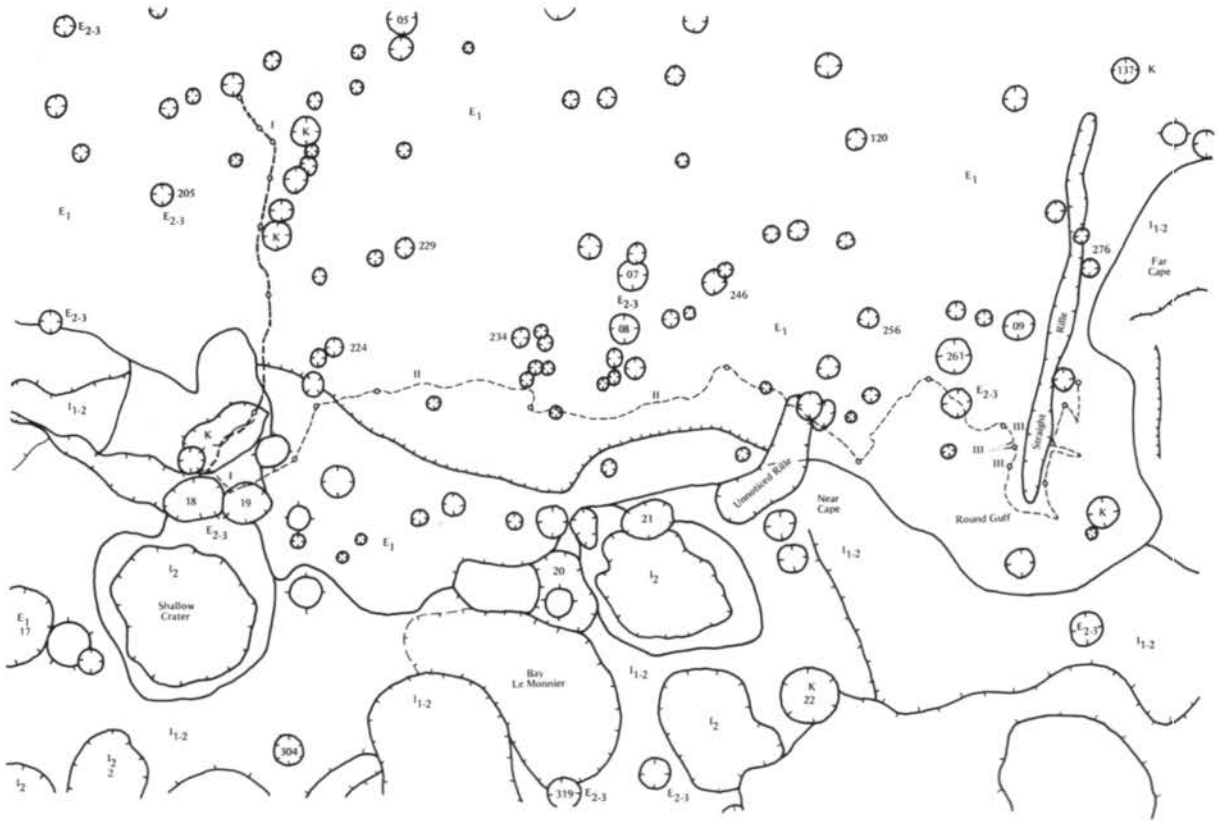


Figure 1.—*Map diagram of Lunokhod 2 route.*

surements were carried out in three characteristic types of terrain:

a. On the mare plain of the bottom of Le Monnier crater
b. In the elevated, hilly plain, which is a type of highland
c. In the vicinity of a tectonic fault crossing the bottom of Le Monnier

Examination of the magnetogram shows that the scalar value of the horizontal component of the field H changes from 2 or 3 to 30 gammas. The vertical component of the field, the absolute value of which is known no more accurately than 10 gammas, changed from − 10 gammas to + 40 gammas. Thus, the average value of the field in Le Monnier Bay is low. The value of the horizontal component, in a number of cases, was comparable to the field of the external sources: the field of the magnetic tail of the Earth, the transition zone, and the perturbed interplanetary field.

Introduction of corrections for the effect of the external sources is necessary, since such an important characteristic as the direction of the field can be strongly distorted in a number of cases. The procedure for taking account of the external sources has not yet been completely carried out.

For the measurements made in February and April 1973, the magnitude and direction of the field of the solar wind were estimated from Pioneer 8 and Pioneer 9 data (ref. 5). For a preliminary estimate of the magnitude of the field in the magnetosheath, the average characteristics of the field in the sheath were used (ref. 6), with the location of the Moon in the sheath taken into account. We hope that, as a result of the forthcoming exchange of data with Sonett and Coleman on Explorer 35, the effect of the external field in those sections of the route in which there were simultaneous measurements by Lunokhod 2 and Explorer 35 will be successfully taken into account.

In the magnetograms presented below, both the initial values of the field vectors and those corrected for the external sources are indicated.

Considering what has been reported above, it can be noted that, on the whole, the horizontal component of the field, in the portion of Le Monnier Bay investigated, is directed primarily to the southwest and south.

Concerning the vertical component, as has already been mentioned, only relative measurements could be carried out. If one assumes a zero value of this component of + 10 gammas, estimated on Earth under different measuring conditions, it can be concluded that the vertical component is directed upward, i.e., "north magnetism" acts in Le Monnier Bay.

Magnetic Field of Individual Regions

As follows from figure 1, the route of Lunokhod 2 lay across sections with different geological structures. Although the magnetic measurements were made over the entire route, data on three sections are discussed in this report. Routes over the three sections are designated by roman numerals in figure 1.

Section I–I. Lunokhod moved in the north-south direction. This section, the total extent of which is about 7 km, includes a mare-type lava plain (about 5 km) and an elevated hilly plain of the highland type (2 km). These surfaces are complicated by craters of various sizes. The average thickness of the regolith in the mare portion of the section is 2–3 m and over 5 m in the highland portion.

Magnetograms of this section are presented in figure 2 (A and B).

In the northern (mare) portion of this route, sections 1–1, 1–2, and 2–3 differ somewhat with respect to the direction of the horizontal component.

In the first section, 1–1, H has a southwest direction and a value of 20–25 gammas. The vertical component Z is of the order of 20 gammas. In the second section, 1–2, vector H is directed toward the west-southwest, and its value is about 10 gammas; the vertical component is 30 gammas.

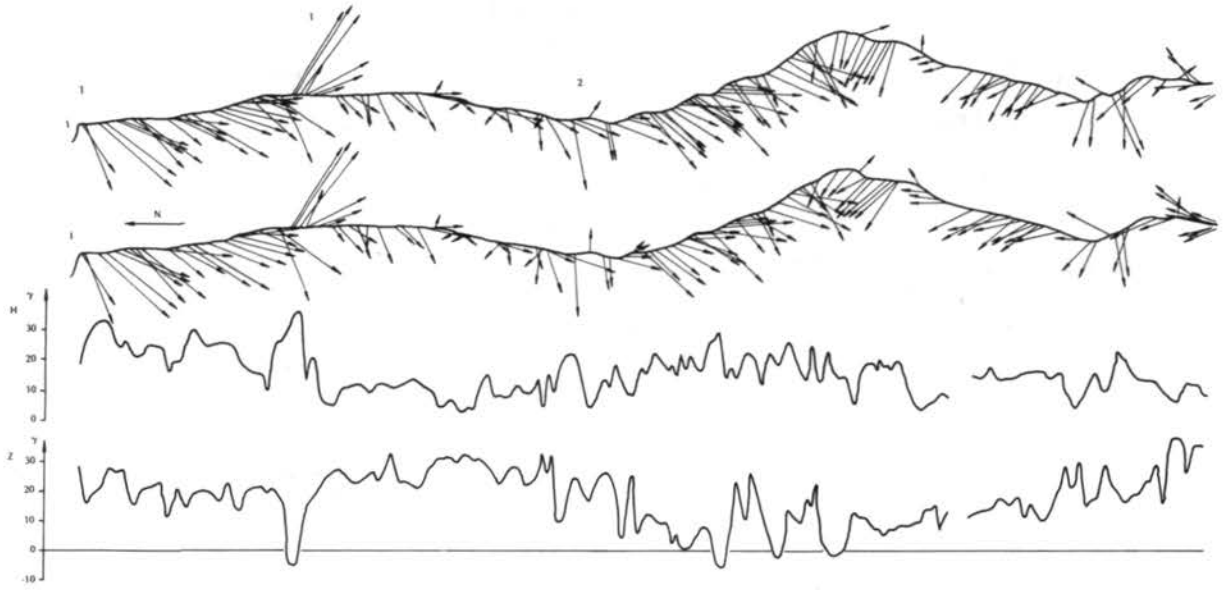


Figure 2A.—*Lunokhod 2 magnetograms in section I–I: (a) horizontal component* H *vector, taking external field into account; (b) horizontal component* H *vector, not taking external field into account; and (c) scalar value of horizontal and vertical components, taking account of external field.*

In section, 2–3, the field vector changes direction from the southwest to the northwest in a distance of 2 km. In this case, the value of H is about 20 gammas, and Z changes between 10 and 30 gammas. In this section, the route passes across a mare surface complicated by small craters which are not plotted in figure 1.

In the southern highland section of the route, 3–4, vector H is directed to the west and has a value of 10 gammas, and Z is of the order of 30 gammas. Thus, portion 3–4 is similar to portion 1–2 according to the magnetograms.

Section II–II. Lunokhod 2 moved in the west-east direction. Section II–II is located entirely on a mare-type lava plain, complicated by craters smaller than 500 m. The average regolith thickness is 2–3 m. The magnetograms of this section are presented in figure 3.

In sections where there are no craters penetrating through the regolith of the rocky base, vector H has primarily a south direction and a value of 20 gammas; Z has a value of 10–15 gammas.

Section III–III. Section III–III is on the west side of Straight Rille. Lunokhod initially moved about 500 m away from the rille to the west-southwest and then returned to the rille, approaching to within 10–20 m of the edge of the rille. The probable distance from the main tectonic fault, which formed the west side of the rille is 50–100 m. The terrain structure distant from the rille is similar to the structure of other mare-type sections. In the edge zone of the rille, the regolith thickness decreases to 1–1.5 m. Tectonic cracks, connected with the main faults, are possible here, in the rock of the basement.

The magnetograms of section III–III are presented in figure 4. Both traverses reveal agreement in direction (southwest) and magnitude (H = 20 gammas) of the field. The vertical component Z averages 20 gammas. The field is quite uniform overall.

Appreciable changes in the direction of H (from the southwest to the east-northeast) and magnitude of H (from 20 to 10 gammas) and of Z (from 20 to 5 gammas), are observed in direct proximity to the edge of the

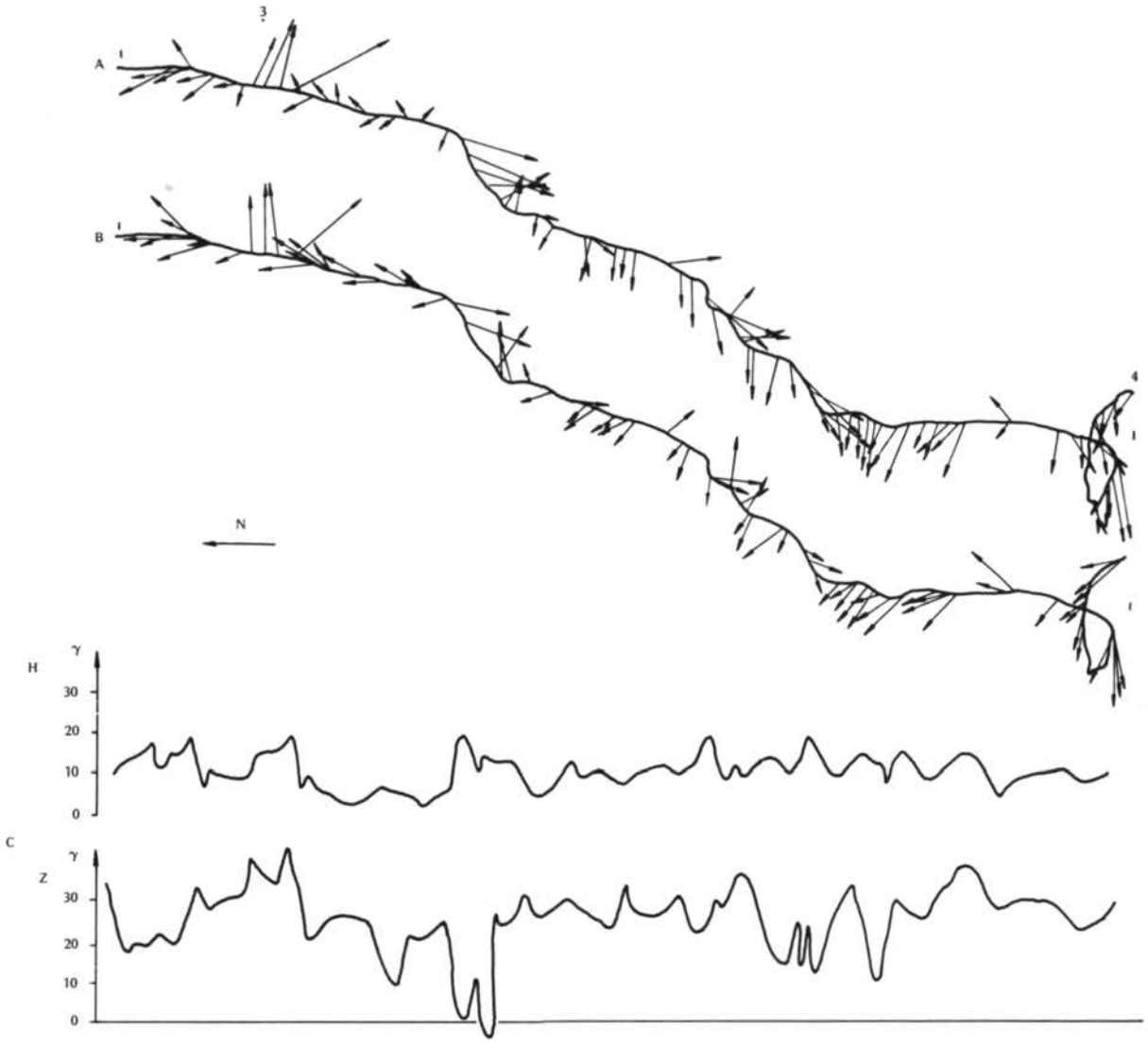


Figure 2B.—*Continuation of figure 2A.*

rille, at the beginning and end of section III–III.

On the scales of the route surveys on the Moon, it naturally is desirable to identify sections with fields of different characteristics and to determine their relationship to geological structures.

It is evident from what has been reported above that differences in the magnetic characteristics are small. Nevertheless, on routes oriented differently, lying on the mare sections and 5–10 km distant from each other, some similarity in behavior of the field is noted (see sections I–I, II–II, III–III).

Measurements in Craters

Magnetograms obtained while Lunokhod crossed craters penetrating through the regolith of the rocky base are presented in figure 5.

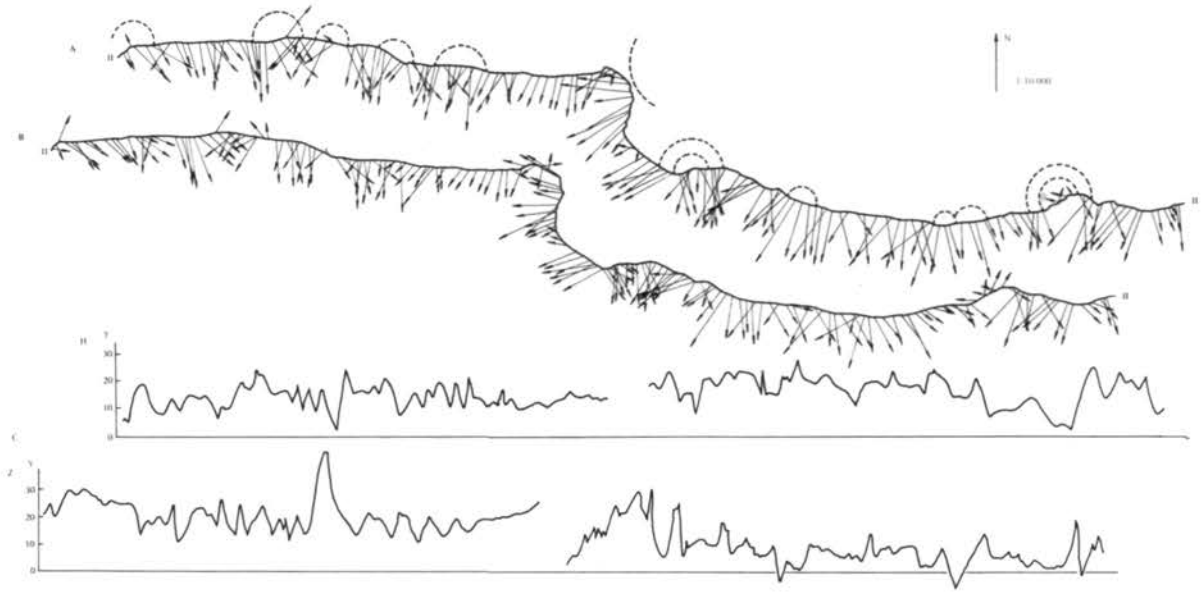


Figure 3.—*Lunokhod 2 magnetograms in section II–II: designations same as in figure 2.*

As is evident from the figure, the magnetograms are quite diverse, but some common properties can be noted:

a. The scalar value of the field magnitude T above the crater reveals noticeable changes within up to 10 gammas.
b. The greatest changes are observed above the edge of the crater.
c. The nature of changes in field components H and Z is quite diverse, but three basic types can be distinguished: A—above the center of the crater; Z—minimum; and H—maximum; B: above the center of the crater, Z is at a maximum and H, minimum; C: Z is at a maximum and H is at a minimum above the edge of the crater.

It should be noted that type C was observed in section II–II, where the route crossed a chain of craters located close together.

The craters discussed above have diameters of over 50 m and are in classes VS and S, i.e., their ratio of the diameter to the depth is 1/10 and 1/1.5, respectively, and the inclination is not over 7°. The effect of craters of smaller sizes, with the measurement accuracy noted, could not be detected.

The question arises, What is the origin of the field anomalies connected with the craters? All these craters are considerably younger formations than Le Monnier Bay. The change of field in the craters is close to or only a little less, in absolute value, than the average value of the field in the section of LeMonnier Bay examined. They can be connected, either with destruction of existing magnetization by impacts or with magnetization by impacts, which is proposed by Hide (ref. 7). Although details of this mechanism have not been described, it apparently cannot be effective without an external field. The existence of craters with types A and B magnetization would be easier to understand, if it is assumed that the external field was different in sign, and the magnetization was thermoremanent.

Beyond these speculations, we do not have the experimental data available which would permit a choice between possible mechanisms of magnetization. It is possible that the most important result is proof of confinement of the anomalies to craters of such sizes.

The SG–70 magnetometer with automatic range extension, installed aboard Lunokhod

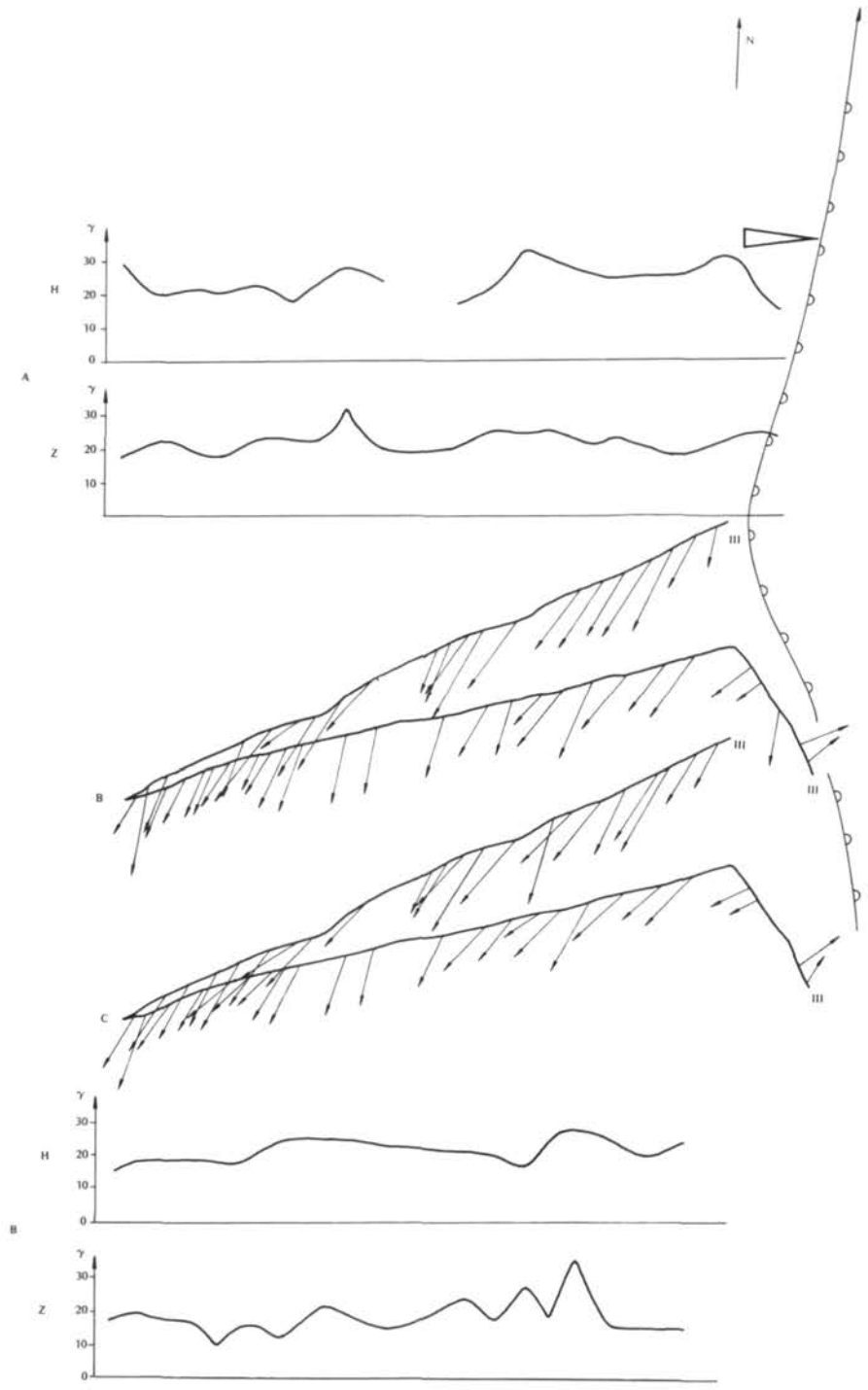


Figure 4.—*Lunokhod 2 magnetograms in section III–III at Straight Rille: (a) scalar values of* H *and* Z, *taking account of external field during departure from rille; (b) horizontal component* H *vector, taking account of external field; (c) horizontal component* H *vector, not taking account of external field; and (d) scalar values of* H *and* Z, *taking account of external field in approaching rille.*

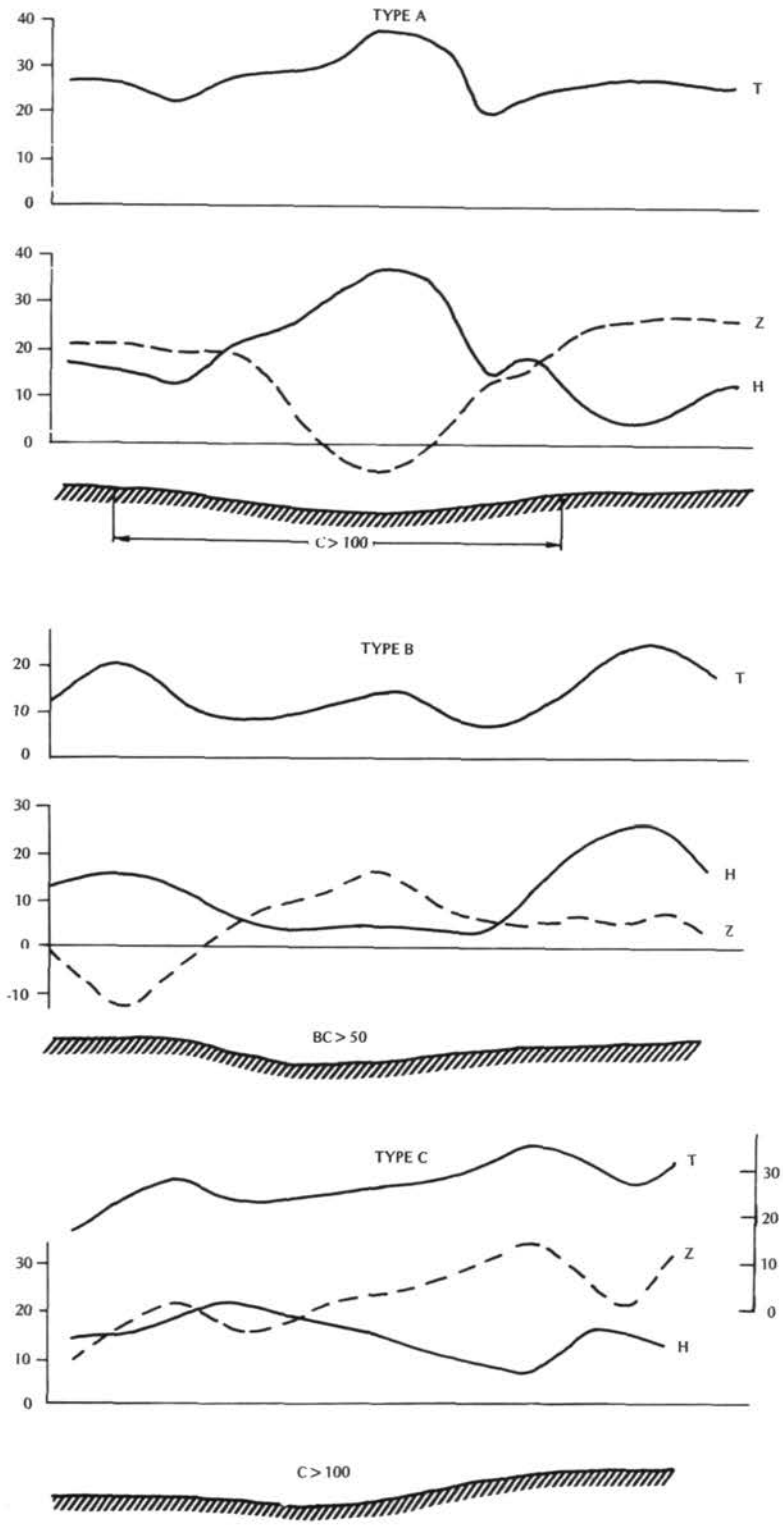


Figure 5.—*Magnetograms of horizontal* H *and vertical* Z *components above craters; angular dimensions in crater profiles given in scale.*

2, was designed and built in the Special Construction Brigade "Geologorazvedka," Ministry of Geology, U.S.S.R.

The laborious work of elimination of the magnetic deviations was carried out by laboratory workers V. M. Agafonnikova, L. B. Vinogradova, I. P. Lyannaya, Ye. Ye. Kanonidi, T. S. Tikhonova, and L. I. Ulanova.

Acknowledgment

The authors wish to thank the organizations and persons who organized the Lunokhod 2 experiment, which ensured obtaining the experimental data. They also express their gratitude to the crew of Lunokhod 2.

The authors are indebted to B. V. Nepoklonov for assistance in cartographic correlation of the magnetic data, and to A. N. Pushkov, A. Kh. Frunze, and E. B. Faynberg, for assistance in machine processing of the data.

References

1. RUNCORN, S. K., D. W. COLLINSON, W. O'REILLY, A. STEPHENSON, N. N. GREENWOOD AND M. N. BATTEY, *Science*, Vol. 167, p. 697.
2. DOLGINOV, SH. SH., YE. G. YEROSHENKO, L. N. ZHUZGOV AND N. V. PUSHKOV, *Dokl. Akad. nauk SSSR*, Vol. 170, No. 3, 1966, p. 574.
3. NESS, N. F., ET AL., *J. Geophys. Res.*, Vol. 72, No. 23, 1967, p. 5769.
4. SHARP, L., P. J. COLEMAN, B. R. LICHTENSTEIN, C. T. RUSSELL AND G. SHUBERT, *The Moon*, Vol. 7, Nos. 3 and 4, 1973, p. 322.
5. NESS, N. F., *Solar Geophys. Data*, 1973.
6. MIHALOV, J. D. AND C. F. SONETT, *J. Geophys. Res.* Vol. 73, No. 21, 1968, p. 6837.
7. HIDE, R., *The Moon*, Vol. 7, Nos. 3 and 4, 1973.

Page intentionally left blank

Page intentionally left blank

Deep Electromagnetic Sounding of the Moon With Lunokhod 2 Data

L. L. Van'yan, I. V. Yegorov, and E. B. Faynberg
Institute of Space Research
Academy of Sciences,
Moscow, U.S.S.R.

Fluctuations of the frozen-in magnetic field in the solar plasma induce electric currents in the conducting interior of the Moon. The magnetic field of these currents is too weak to overcome the dynamic force of the solar wind and form a shock wave ahead of the Moon. It diffuses into the solar plasma, dying away exponentially as $\exp(-\omega_0 Z/c)$, where ω_0 is the electron plasma frequency; c is the speed of light; and Z is the distance from the surface of the Moon. As is evident, the depth of penetration of the field depends only on the density of the plasma, and it usually is a few kilometers. In comparison with the depth of penetration of fluctuations of the magnetic field into the material of the Moon, measured in hundreds of kilometers, it can be considered that the Moon is surrounded by an ideal conductor on the illuminated side. Therefore, on the illuminated side, the induced magnetic field turns out to be compressed between the conducting interior of the Moon and the solar plasma, which leads to a severalfold increase in its intensity.

On the other hand, on the darkside of the Moon a cavity forms with a very low plasma density, where the induced magnetic field propagates as in a vacuum. On the lateral surfaces of the cavity and on the illuminated side of the Moon, as in an ideal conductor, the normal component of the induced magnetic field reverts to zero: $H_{ni} = 0$. Consequently, the vertical component on the illuminated side of the lunar surface reflects the behavior of the external field and does not depend on the structure of the Moon (ref. 1).

Let us consider a two-layer model of the Moon in which the outer layer, in conformance with measurements of electrical conductivity of samples, is assumed to be an insulator, and the inner one, with radius a, is assigned a spherical impedance $Z(\omega,n)$. Then, in the region formed by the outer layer of the Moon and the cavity, the magnetic field intensity satisfies the wave equation and propagates with the speed of light. Since the length of the lunar cavity is not over 3×10^3 km, the delay time is measured in hundredths of a second and can be disregarded for fluctuations having periods of tens of seconds. Consequently, in the region being examined the wave equation is converted into a Laplace equation, with the following boundary conditions:

$$H_n = H_{ne} + H_{ni} = H_{ne}$$

where H_e is the frozen-in magnetic field moving past the Moon, with a velocity equal to or exceeding the velocity of the solar wind. Although fluctuations of the interplanetary magnetic field can arbitrarily change with time, it is convenient to examine the problem for a time-harmonic of the type $\exp(-i\omega t)$.

If a solution of the Laplace equation is sought in the form of an expansion by spherical harmonics, we have for their amplitudes $h_r = h_{re}$ on the surface separating the Moon from the solar plasma, and

$$\frac{h_r}{h_\theta} = \frac{n(n+1)\ Z\ (\omega,n)}{-i\omega\mu a}$$

on the surface of the inner conducting sphere. Here, h_r is the spatial amplitude of the radial variations; h_θ is the meridional magnetic variation; n is the number of spherical harmonics; and $Z(\omega,n)$ is the impedance of the inner sphere (ref. 2).

A numerical solution of the formulated problem (ref. 3) allows the following conclusions to be made:

1. If the wavelength of the exciting field exceeds 15×10^3 km, it can be considered, with satisfactory accuracy, that it changes cophasally everywhere.
2. On the illuminated side around the subsolar point, there is a region where the magnetic field depends slightly on the length of the lunar cavity.

Consequently, keeping in mind the observations on the illuminated side, a simplified model can be used in which the time of propagation of the solar wind past the Moon is disregarded.

The induced magnetic field carries information on the deep electrical conductivity of the Moon. There are two basic methods for extracting this information. The first method is study of the impedance, i.e., the ratio of the components of the electrical and magnetic fluctuations tangential to the lunar surface. Although this is widely used under terrestrial conditions, it has not yet been used on the Moon because of technical difficulties.

In the second method, one uses the ratio of the horizontal magnetic component on the lunar surface to its unperturbed value, as measured by a satellite of the Moon. As shown by experiment (ref. 1), the horizontal magnetic field increases threefold to fivefold in the harmonic mode for fluctuation periods of about 20 to 30 s, and drops to 1 for periods of about an hour. This drop reflects gradual penetration of the electromagnetic field into the interior of the Moon. If the interplanetary magnetic field changes by steps, a similar process is observed where the induced currents practically completely decay and the magnetic gain approaches unity a few minutes after arrival of the step change at the Moon.

Discontinuities propagating from the Sun have one important characteristic: the magnetic field in them usually is linearly polarized. This makes it possible to use the ratio of the horizontal and vertical magnetic components on the surface of the Moon, normalizing it to unity for $t \to \infty$. This procedure was used in analysis of a number of magnetic pulses recorded by the Lunokhod 2 magnetometer. An example of the meridional and vertical components of a magnetic field pulse, recorded at 0 hours 31 min 35 s on 23 March 1973, is shown in figure 1. The vertical component has the form of a trapezoid, which approaches a steady value in approximately 16 s. The horizontal component initially increases sharply, then decreases, and after 3 min it also settles at a constant level.

The pulse of 23 March was recorded at a solar wind velocity over 730 km/s, according to the data from the Prognoz and Pioneer 9 satellites. This means that for a Fourier harmonic with a period exceeding 20 s, the effect of the finite time of passage of the solar wind past the Moon on the electromagnetic induction can be disregarded.

If a change in the vertical component re-

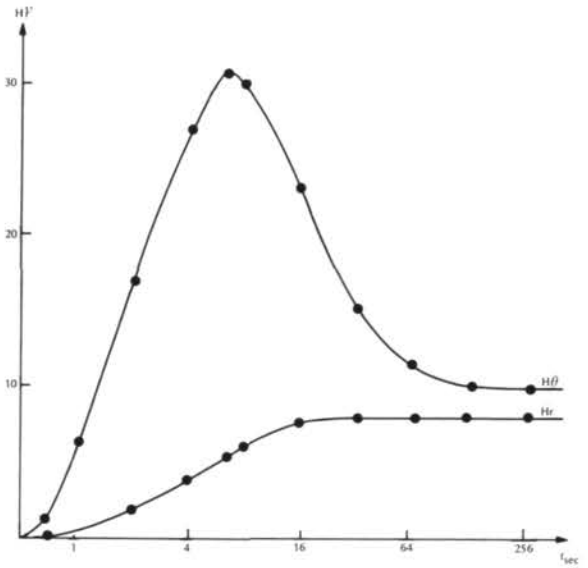


Figure 1.—*Meridional and vertical components of unsettled magnetic field, from Lunokhod 2 data.*

flecting the behavior of the induced field had the form of an ideal rectangular step, the transitional characteristic of the Moon could be determined from the ratio $H_\theta(t)/H_\theta(\infty)$. However, the impulse of the vertical component differs significantly from a rectangular step. To allow for the shape of the pulse H_r, it is convenient to change to spectra; for example, to use the Laplace transform $h(p) = \int_0^\infty H\ (t)\ e^{-pt}dt$.

In this case, instead of $H_\theta(t)/H_\theta(\infty)$, we have:

$$\tilde{h}(p) = \frac{h_\theta(p)}{h_\theta(o)} : \frac{h_r(p)}{h_r(o)}$$

The increase in the tangential magnetic field was determined in the interval $5 \times 10^{-3}\ s^{-1} \leq p \leq 2\ s^{-1}$. It contains all the information on the deep electrical conductivity of the Moon which there was in the pulse being analyzed.

However, before attempting to extract this information, we must consider the effect of the lunar cavity. This effect differs at different points on the surface of the Moon; therefore, it is convenient to introduce corrections that take the symmetry of the cavity into consideration. Calculations have shown that for the point at which the pulse being analyzed was recorded, the observed gain decreases to 1.5 times that of a symmetric model when the solar plasma surrounds the Moon on all sides.

$\tilde{h}_{asym}$	$\tilde{h}_{sym}$	$\frac{\tilde{h}_{sym}}{\tilde{h}_{asym}}$
2.7	3.9	1.5
2.2	2.6	1.2
1.7	1.9	1.1
1.4	1.4	1.0

From the corrected values of the gain, the apparent resistivity $\rho_a = 9.5 \times 10^5 p/\tilde{h}^2(p)$ was calculated. It is a convenient form for presenting the sounding results (ref. 4). The values of the apparent resistivity are shown by black dots in figure 2, as a function of the parameter $p^{-1/2}$, which characterizes the depth of penetration of the field into the Moon. It must be noted that at $p^{-1/2} > 10$, the apparent resistivity stops reflecting the change in conductivity with depth and approaches an asymptote, characterizing decay of the currents induced in the Moon.

For interpretation of the experimental graph of the apparent resistivity, a series of theoretical curves was calculated for the following parameters:

Model 1.	$\rho_1 > 10^8$ ohm·m	$d_1 = 100$ km
	$\rho_2 = 10^4$	$d_2 = 800$
	$\rho_3 = 10^2$	
Model 2.	$\rho_1 > 10^8$	$d_1 = 250$
	$\rho_2 = 10^4$	$d_2 = 800$
	$\rho_3 = 10^3$	
Model 3.	$\rho_1 > 10^8$	$d_1 = 180$
	$\rho_2 = 10^4$	$d_2 = 300$
	$\rho_3 = 10^5$	$d_3 = 300$
	$\rho_4 = 10^3$	

Model 3 demonstrates the best agreement with experimental data, which support the existence of a layer having increased conductivity in the 200- to 500-km-depth interval

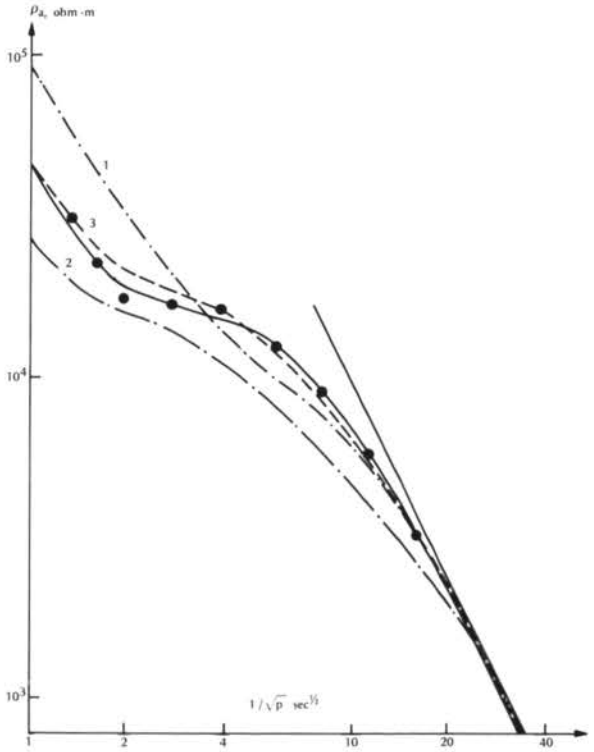


Figure 2.—*Comparison of experimental and theoretical apparent resistance curves.*

that was first found by the results of Apollo 12 (ref. 1).

However, the results of electromagnetic sounding most reliably distinguish an outer high-resistance shell about 200 km thick.

The results obtained permitted Fadeyev to make a preliminary petrological interpretation of the layers of the Moon (ref. 4). Their origin is probably a consequence of differentiation of the initial periodotite material. Upon melting, 20 to 40 percent of the material melts and is removed to form a high-resistance basaltic shell, underlain by a layer of spinel periodotites enriched in divalent iron oxides and having a reduced resistance, as shown by experiments. As is known, spinels are stable in the pressure range from 10 to 20 kbars, which corresponds to depths of 200 to 400 km; i.e., it is in agreement with the zone of reduced resistance. If one relies on the laboratory measurements of the electrical conductivity of terrestrial periodotites, the resistivity of 10^4 ohm·m found at depths of 400 to 500 km corresponds to a temperature of 600° to 700°C. This gives an average value of the temperature gradient of about 1.5 deg/km.

Acknowledgment

The authors are indebted to Sh. Sh. Dolginov, Ye. G. Yeroshenko, and L. N. Zhuzgov for furnishing the results of the magnetic measurements by Lunokhod 2, as well as to K. I. Gringauz and A. P. Remizov for furnishing the results of the plasma measurements by the Prognoz satellite.

References

1. SONETT, C. P. et al., *Science*, Vol. 172, 1971, pp. 256–258.
2. BERDICHEVSKIY, M. N., L. L. VAN'YAN, AND E. B. FAYNBERG, *Geomagnetism i Aeranomiva*, Vol. 2, 1967.
3. VAN'YAN, L. L., AND I. V. YEGOROV, *Kosmich. Issled.*, Vol. 6, 1973.
4. VAN'YAN, L. L. et al., *Ann. Geophys.*, Vol. 29, 1973, pp. 367–374.

Lunar Electrical Conductivity, Permeability, and Temperature from Apollo Magnetometer Experiments

P. Dyal
NASA/Ames Research Center
Moffett Field, California

C. W. Parkin
University of Santa Clara
Santa Clara, California

W. D. Daily
Brigham Young University
Provo, Utah

Magnetometers have been deployed at four Apollo sites on the Moon to measure remanent and induced lunar magnetic fields. Measurements from this network of instruments have been used to calculate the electrical conductivity, temperature, magnetic permeability, and iron abundance of the lunar interior. The measured lunar remanent fields range from 3 gammas (γ) minimum at the Apollo 15 site to 327 γ maximum at the Apollo 16 site. Simultaneous magnetic field and solar plasma pressure measurements show that the remanent fields at the Apollo 12 and 16 sites interact with, and are compressed by, the solar wind. Remanent fields at Apollo 12 and Apollo 16 are increased 16 γ and 32 γ, respectively, by a solar plasma bulk pressure increase of 1.5×10^{-7} dynes/cm^2. Global lunar fields due to eddy currents, induced in the lunar interior by magnetic transients, have been analyzed to calculate an electrical conductivity profile for the Moon. From nightside magnetometer data in the solar wind it has been found that deeper than 170 km into the Moon the conductivity rises from 3×10^{-4} mhos/m to 10^{-2} mhos/m at 1000-km depth. Recent analysis of data obtained in the geomagnetic tail, in regions free of complicating plasma effects, yields results consistent with nightside values. Conductivity profiles have been used to calculate the lunar temperature for an assumed lunar material of olivine. In the outer layer ($\sim$ 170 km thick) the temperature rises to 110° C, after which it gradually increases with depth to 1500° C at a depth of $\sim$ 1000 km. Simultaneous measurements by magnetometers on the lunar surface and in orbit around the moon are used to construct a whole-moon hysteresis curve, from which the global lunar magnetic permeability is determined to be $\mu = 1.012 \pm 0.006$. The corresponding global induced dipole moment is 2×10^{25} gauss-cm^3 for typical inducing fields of 10^{-4} gauss in the lunar environment. Lunar free iron abundance corresponding to the global permeability is determined to be 2.5 ± 2.0 wt. %. Total iron abundance (sum of iron in the ferromagnetic and paramagnetic states) is calculated for two assumed compositional models of the lunar interior. For a free iron/orthopyroxene lunar composition the total iron content is calculated to be 12.8 ± 1.0 wt. %; for a free iron/olivine composition, total iron content is 5.5 ± 1.2 wt. %. Other lunar models with an iron core and with a shallow iron-rich layer are also discussed in light of the measured global lunar permeability. Velocities and thicknesses of the Earth's magnetopause and bow shock have been estimated from simultaneous magnetometer measurements. Average speeds are determined to be about 50 km/s for the magnetopause and 70 km/s for the bow shock, although there are large variations in the measurement for any particular boundary crossing. Corresponding measured boundary thicknesses average about 2300 km for the magnetopause and 1400 km for the bow shock.

Magnetometers placed on the lunar surface and in orbit about the Moon have returned a wealth of information about the Moon which was not anticipated prior to the Apollo manned lunar missions. Earlier measurements, by U.S.S.R. and U.S magnetometers on unmanned spacecraft, indicated that the Moon might be electromagnetically inert; during that time investigators often concentrated on the interactions of the Moon with the solar wind plasma (refs. 1–4) rather than on magnetic studies of the lunar interior. Studies of the lunar interior prior to the Apollo landings (e.g., see refs. 2 and 5–9) were constrained by the lack of high resolution measurements of whole body induction fields near the Moon.

The measurement of magnetic fields in the vicinity of the Moon began in January 1959, when the U.S.S.R. spacecraft Luna 1 carried a magnetometer to within several hundred kilometers of the Moon. In September 1959, Luna 2, also equipped with a magnetometer, impacted the lunar surface. The instrument aboard Luna 2 set an upper limit of 100 gammas (1 gamma = 10^{-5} gauss) for a possible lunar field at an altitude of about 50 km above the Moon's surface (ref. 10). In April 1966, Luna 10 carrying a magnetometer 10 times more sensitive than that aboard Luna 2, was successfully placed in a lunar orbit that came to within 350 km of the Moon. The Luna 10 magnetometer recorded a time-varying magnetic field in the vicinity of the Moon, which was at that time interpreted as indicating the existence of a weak lunar magnetosphere (ref. 11), although later studies modified this interpretation.

A year later (July 1967) the United States placed the Explorer 35 satellite, with two magnetometers aboard, in orbit around the Moon. In its orbit the satellite passed to within 830 km of the Moon's surface. Explorer 35 successfully measured magnetic properties of the solar-wind cavity downstream from the Moon, but it did not detect the lunar magnetosphere indicated by Luna 10 measurements nor the lunar bow shock and induced-field configuration previously suggested by Gold (ref. 12). In an analysis of the Explorer 35 results, Sonett et. al. (ref. 13) concluded that if a permanent lunar field exists at all, its magnitude would be less than two gammas at an altitude of 830 km and therefore ≤ 4 gammas at the surface for a global permanent dipole field. The upper limit on the global permanent dipole moment was set at 10^{20} gauss-cm^3, i.e., less than 10^{-5} that of the Earth. In studies of the solar wind interaction with the lunar body (refs. 1 and 2), investigators found the solar wind field magnitude to be ~ 1.5 gammas greater in the diamagnetic cavity on the Moon's antisolar side than in the solar wind.

Surveyor spacecraft, used in the first U.S. unmanned lunar landings, carried no magnetometers. Permanent magnets were carried aboard the Surveyor 5 and 6 spacecraft, however, which demonstrated that soils at those two landing sites contain less than 1 percent (by volume) ferromagnetic iron (ref. 14).

During the early manned Apollo missions it was determined that the Moon is much more interesting magnetically then had been expected. Natural remanent magnetization in lunar samples was found to be surprisingly high at all U.S. Apollo sites and at the U.S.S.R. Luna 16 site (see, for example, refs. 15–21). Such high natural remanent magnetism implies that at some time in the past there existed an ambient surface magnetic field considerably higher than that which now exists on the Moon (refs. 16 and 22).

The first lunar surface magnetometer (LSM), deployed at the Apollo 12 site in November 1969, made the first direct measurement of an intrinsic lunar magnetic field (ref. 23). The 38-gamma field measurement showed that not only are individual rocks magnetized but also that magnetization in the lunar crust can be ordered over much larger regions of 2-km to 200-km scale sizes (refs. 23 and 24). The permanent and induced fields measured by the Apollo 12 magnetometer provided the impetus to develop portable surface magnetometers and satellite magnetometers for later Apollo missions. Permanent mag-

netic fields were subsequently measured at four other landing sites: Apollo 14 (103 γ maximum), Apollo 15 (3 γ), Apollo 16 (327 γ maximum), and more recently at several positions along the U.S.S.R. Lunokhod II traverse. The surface fields were attributed to local magnetized sources ("magcons"); their discovery prompted a reexamination of Explorer 35 magnetometer data by Mihalov et al. (ref. 25), who found indirect evidence that several magnetized regions exist in the lunar crust. Direct field measurements from Apollo 15 and 16 subsatellite magnetometers, activated in August 1971 and April 1972, respectively, yielded maps of some of the larger magnetized regions in the lunar crust (refs. 26 and 27) which confirmed the existence of magnetized regions over much of the lunar surface. Subsatellite magnetometer measurements have also placed an upper limit of 4.4×10^{13} gauss-cm^3 on the global permanent magnetic dipole moment (ref. 28).

Investigations of simultaneous surface magnetometer data and solar wind spectrometer data show that the surface remanent magnetic fields interact with the solar wind when on the dayside of the moon (refs. 29, 30, and 31). The interaction is interpreted as a compression of the surface remanent fields by the solar wind; the magnetic pressure at the surface increases in proportion to the dynamic bulk pressure of the solar wind plasma.

In addition to measuring permanent lunar fields, the network of lunar surface and orbiting magnetometers measured fields induced in the lunar interior by extralunar magnetic fields, allowing investigation of deep interior properties of the Moon. Behanon (ref. 8) placed an upper limit of 1.8 on the bulk relative magnetic permeability by studying Explorer 35 magnetometer measurements in the geomagnetic tail. Subsequently, simultaneous measurements of Explorer 35 and Apollo 12 magnetometers have been used to yield the more accurate value of 1.012 $\pm$ 0.006 (refs. 32 and 33). Recent Apollo 15 subsatellite magnetometer measurements have indicated the existence of a possible lunar ionosphere, which could affect the whole-Moon permeability calculations (ref. 34); effects of a lunar ionosphere on iron abundance determinations are considered by Parkin et al. (ref. 32).

The electrical conductivity of the lunar interior has been investigated by analyzing the induction of global lunar fields by time-varying extralunar (solar or terrestrial) magnetic fields. Since temperature and conductivity of geological materials are related, calculated conductivity profiles have been used to infer temperature of the lunar interior. Early estimates of bulk lunar electrical conductivity were made from lunar-orbiting Explorer 35 data by Colburn et al. (ref. 1) and Ness (ref. 7). For homogeneous-conductivity models of the Moon, Colburn et al. placed an upper limit of 10^{-6} mhos/m for whole-Moon conductivity, whereas Ness' upper limit was 10^{-5} mhos/m. These investigators also stated that their measurements were consistent with a higher conductivity lunar core surrounded by an insulating crust.

Theoretical studies of the electrodynamic response of the Moon to time-dependent external fields have been undertaken by many authors. Two types of whole-Moon magnetic induction fields have been treated: a poloidal field due to eddy currents driven by time-varying external magnetic fields, and a toroidal field due to unipolar currents driven through the Moon by the motional solar-wind $V \times B$ electric field.

The toroidal induction mode, first suggested to be an important process in the Moon by Sonett and Colburn (ref. 5), was later developed in detail theoretically for a lunar model totally confined by the highly conducting solar wind (refs. 35, 36, and 37). However, analysis of simultaneous Apollo 12 and Explorer 35 magnetometer data later indicated that for the Moon, toroidal induction is negligible in comparison to poloidal induction; upper limits on the toroidal field mode were used to calculate an upper limit of 10^{-9} mhos/m for electrical conductivity of the outer 5 km of the lunar crust (ref. 38). In subsequent analysis of lunar electromagnetic induction, toroidal induction has been assumed to be negligible relative to poloidal induction.

The eddy-current response of a homogeneous sphere in a vacuum to time-varying magnetic fields has been described by Smythe (ref. 39) and Wait (ref. 40). Early theoretical application of vacuum poloidal induction to studies of the lunar interior were presented by Gold (ref. 12) and Tozer and Wilson (ref. 41). Poloidal response theory for a lunar sphere totally confined by a highly conducting plasma was developed by Blank and Sill (ref. 42), Schubert and Schwartz (ref. 36), and Sill and Blank (ref. 37).

Since deployment of the Apollo 12 magnetometer in November 1969, electrical conductivity analysis has been developed with two basic approaches: a time-dependent, transient-response technique (refs. 43, 44, and 45) and a frequency-dependent, Fourier-harmonic technique (refs. 44 and 46–49). Past analyses have all used magnetometer data recorded at times when global eddy-current fields were asymmetrically confined by the solar wind plasma (refs. 45 and 50–53). The asymmetric confinement of lunar fields is particularly complex to model theoretically (ref. 54); indeed, the general time-dependent asymmetric induction problem has not been solved at the time of this writing. To avoid these complications, recent conductivity analysis has used field data recorded in the geomagnetic tail, which is relatively free of plasma and asymmetric confinement effects. Preliminary results of this analysis will be presented in this paper.

The purpose of this paper is to review the application of lunar magnetic field measurements to the study of properties of the lunar crust and deep interior. Following a brief descriptive section on lunar magnetometers and the lunar magnetic environment, measurements of lunar remanent fields and their interaction with the solar plasma will be discussed. The magnetization induction mode will be considered with reference to lunar magnetic permeability and iron abundance calculations. Electrical conductivity and temperature calculations from analyses of poloidal induction, for data taken in both the solar wind and in the geomagnetic tail, will be reviewed. Finally, properties of the Earth's magnetopause and bow shock measured by lunar magnetometers will be discussed.

The Apollo Surface Magnetometers

LUNAR SURFACE MAGNETOMETER (LSM)

Lunar surface magnetometers, designed to measure and transmit data continuously to Earth for at least one year, have been deployed at three sites on the moon: Apollo 12 (coordinates 3.0° south latitude, 23.4° west longitude), Apollo 15 (26.1° N, 3.7° E), and Apollo 16 (9.0° S, 15.5° E). A photograph of the LSM fully deployed and aligned at the Descartes landing site is shown in figure 1 and the Apollo 16 LSM characteristics are given in table 1. (A detailed description of this instrument is provided by Dyal et al., ref. 55).

Mechanical and Thermal Subsystems

In the exterior mechanical and thermal configuration of the Apollo LSM, the three fluxgate sensors are located at the ends of three 100-cm-long orthogonal booms that separate the sensors from each other by 150 cm, and position them 75 cm above the lunar surface (fig. 2). Orientation measurements with respect to lunar coordinates are made with two devices. A shadowgraph and bubble level are used by the astronaut to align the LSM and to measure azimuthal orientation with respect to the Moon-to-Sun line to an accuracy of 0.5°. Gravity-level sensors measure instrument tilt angles to an accuracy of 0.2° every 4.8 seconds.

In addition to the instrument normal mode of operation in which three vector field components are measured, the LSM has a gradiometer mode in which commands are sent to operate three motors, which rotate the sensors such that all simultaneously align in a parallel manner, first to one of the three boom axes, then to each of the other two boom axes in



Figure 1.—*The Apollo lunar surface magnetometer (LSM) deployed on the Moon at the Apollo 16 Descartes site. Magnetic field sensors are at the top ends of the booms and approximately 75 cm above the lunar surface.*

Table 1.—*Apollo Surface Magnetometer Characteristics*

Parameter	Apollo 16 Stationary Magnetometer (LSM)	Apollo 16 Portable Magnetometer (LPM)
Ranges, Gammas (each sensor)	0 to ± 200 0 to ± 100 0 to ± 50	0 to ± 256
Resolution, Gammas	0.1	1.0
Frequency Response, Hz	dc to 3	dc to 0.05
Angular Response	Cosine of angle between field and sensor	Cosine of angle between field and sensor
Sensor Geometry	3 orthogonal sensors at ends of 100-cm booms	3 orthogonal sensors in 6-cm cube
Analog Zero Determination	180° flip of sensor	180° flip of sensor
Power, Watts	3.5	1.5 (battery)
Weight, kg	8.9	4.6
Size, cm	63 x 28 x 25	56 x 15 x 14
Operating Temperature, °C	−50 to +85	0 to +50
Commands	10 ground: 1 spacecraft	—

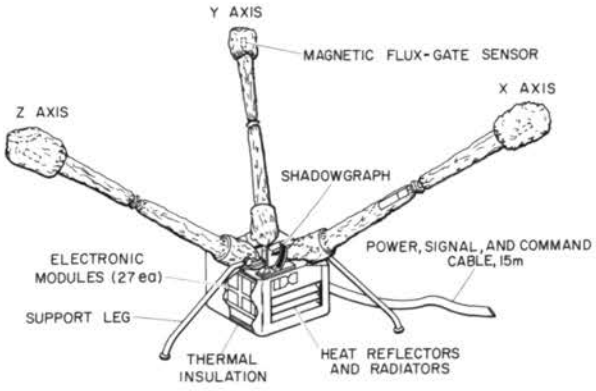


Figure 2.—*Schematic diagram of the lunar surface magnetometer (LSM) without the sunshade shown in figure 1. Sensors are at the top ends of the booms and approximately 75 cm above the ground. The electronics and motor drive assembly are located in the box, encased in a thermal blanket. Heat rejection during lunar day and retention during lunar night are controlled by a parabolic reflector array on two sides of the electronics box. The astronaut bubble level and azimuthal shadowgraph are shown on top of the box. Power, digital signals, and commands are provided through the ribbon cable which connects to the central station telemetry receiver and transmitter.*

turn. This rotating alignment permits the vector gradient to be calculated in the plane of the sensors, and also permits an independent measurement of the magnetic field vector at each sensor position.

The thermal subsystem is designed to allow the LSM to operate over the complete lunar day-night cycle. Thermal control is accomplished by a combination of insulation, control surfaces, and heaters that operate collectively to keep the electronics between 267 K and 319 K. A plot of the temperature of the X sensor and the electronics for the first post-deployment lunation is shown in figure 3 for the Apollo 16 LSM.

Electronics

The electronic components for the LSM are located in the thermally insulated box. The operation of the electronics is illustrated in figure 4. Long-term stability is attained by extensive use of digital circuitry, by internal calibration of the analog portion of the instrument every 18 hours, and by mechanical rotation of each sensor through 180° to determine the sensor zero offset. The analog output of the sensor electronics is internally processed by a low-pass digital filter and a telemetry encoder; the output is transmitted to Earth via the central-station S-band transmitter.

The LSM has two data samplers: the analog-to-digital converter (26.5 samples/second) and the central-station telemetry

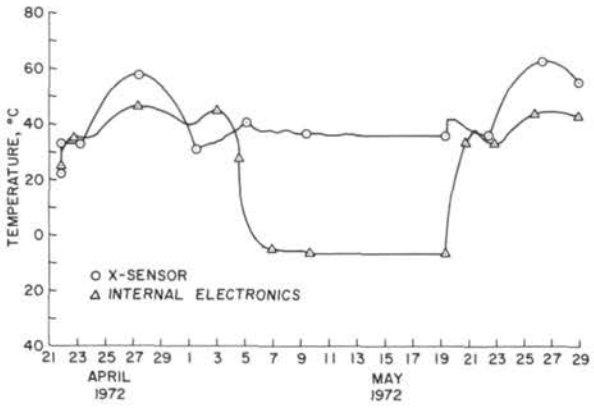


Figure 3.—*Temperature inside one of the Apollo 16 LSM flux-gate sensors and inside the electronics box during the first postdeployment lunation of the Apollo 16 instrument.*

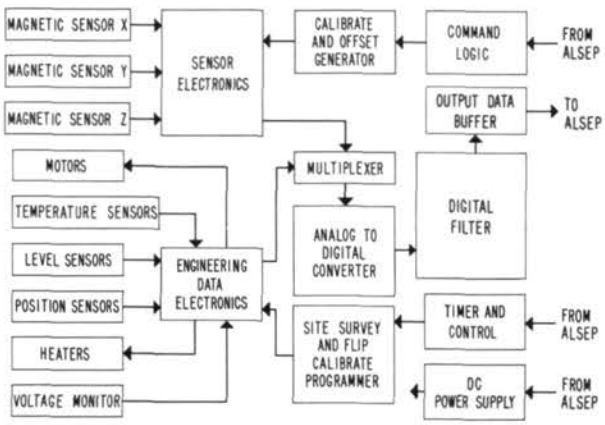


Figure 4.—*Functional block diagram for the Apollo LSM electronics.*

encoder (3.3 samples/second). The pre-alias filter following the sensor electronics has attenuations of 3 dB at 1.7 Hz, 64 dB at 26.5 Hz, and 58 dB at the Nyquist frequency (13.2 Hz), with an attenuation rate of 22 dB/octave. The four-pole Bessel digital filter limits the alias error to less than 0.5 percent and has less than 1 percent overshoot for a step function response. This filter has an attenuation of 3 dB at 0.3 Hz and 48 dB at the telemetry-sampling Nyquist frequency (1.6 Hz). The phase response is linear with frequency. The response of the entire LSM measurement system to a step function input is shown in figure 5. The digital filter can be bypassed by ground command in order to pass higher frequency information.

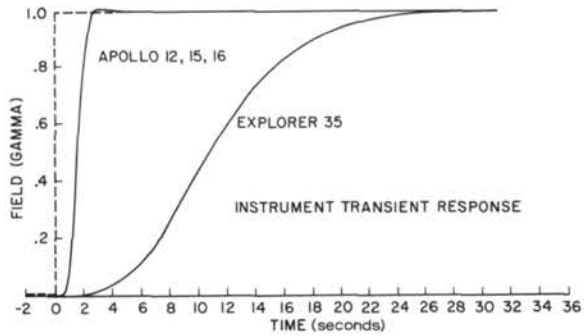


Figure 5.—*Laboratory measurements comparing instrument transient responses of the Apollo 12, 15, and 16 lunar surface magnetometers with the Explorer 35 lunar orbiting magnetometer for a 1.0-γ step change in the input magnetic field.*

Fluxgate Sensor

Three orthogonal vector components of the magnetic field are measured by three fluxgate sensors designed and fabricated by the U.S. Naval Ordnance Laboratory (ref. 56). The sensor shown schematically in figure 6 consists of a toroidal Permalloy core that is driven to saturation by a sinusoidal current having a frequency of 6000 Hz. The sense winding detects the superposition of the drive-winding magnetic field and the total lunar surface field; as a result, a second har-

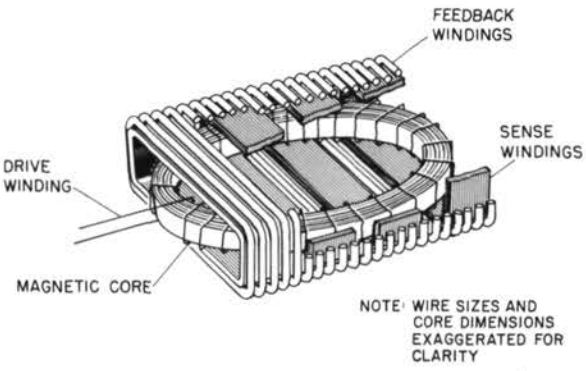


Figure 6.—*Simplified view of the ring core magnetometer sensor developed jointly by the U.S. Naval Ordnance Laboratory and NASA/Ames Research Center.*

monic of the driving frequency is generated in the sense winding with a magnitude that is proportional to the strength of the surface field. The phase of the second harmonic signal with respect to the drive signal indicates the direction of the surface field with respect to the sensor axis. This output signal is amplified and synchronously demodulated to drive a voltage to the analog-to-digital converter and then through the central-station radio to Earth.

Data Flow and Mission Operation

The LSM experiment is controlled from the NASA/Johnson Space Center (JSC) by commands transmitted to the Apollo lunar surface experiments package (ALSEP) from remote tracking stations. The data are recorded on magnetic tape at the remote sites and are also sent directly to JSC for real-time analysis to establish the proper range, offset, frequency response, thermal control, and operating mode.

The Apollo 12 LSM returned useful scientific information from the time of its deployment on day 323 of 1969 to day 256 of 1971. The Apollo 15 LSM operated from its deployment on day 212 of 1971 to day 264 of 1972. The Apollo 16 LSM was deployed on day 112 of 1972 and continues to return useful information at the time of this writing.

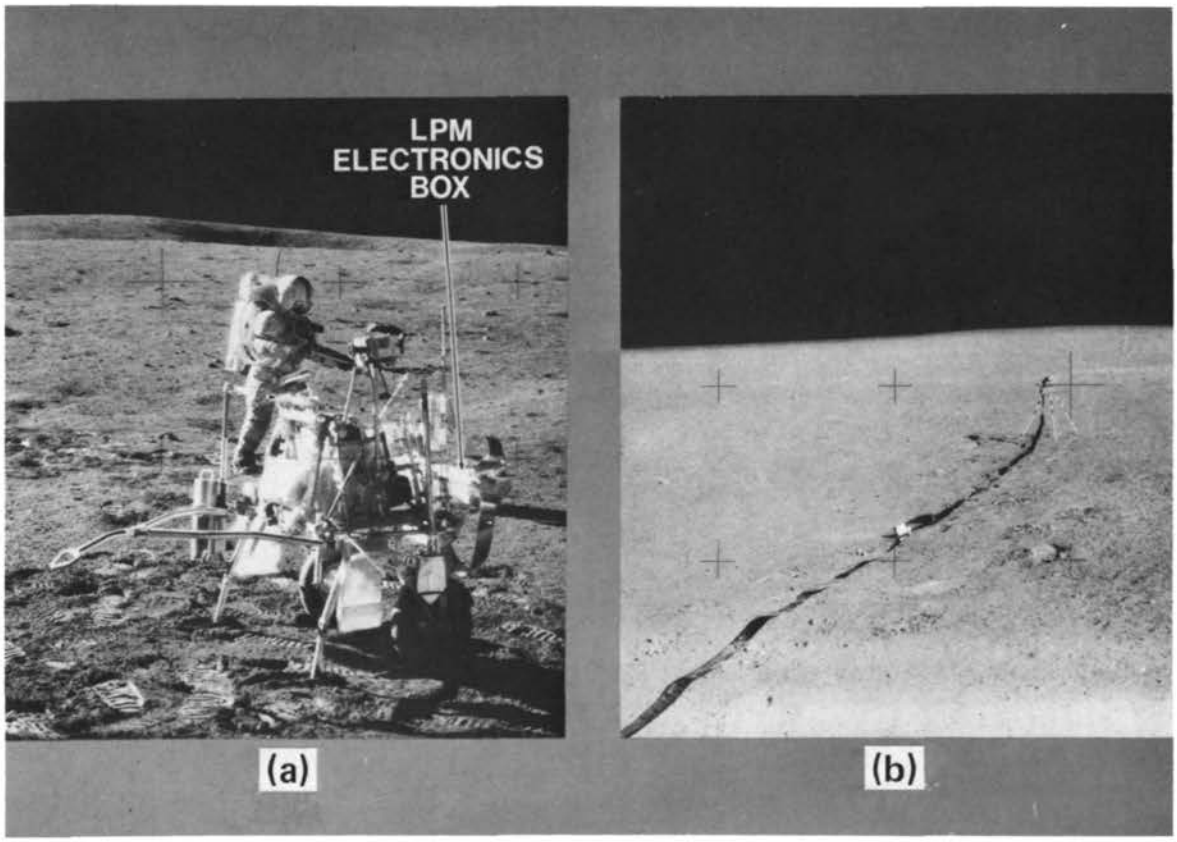


Figure 7.—*The Apollo 14 lunar portable magnetometer (LPM), shown (a) stowed aboard the mobile equipment transporter and (b) deployed during a magnetic field measurement. The sensor-tripod assembly is deployed 15 meters from the electronics box, which remains on the mobile equipment transporter so that magnetic fields of the astronaut's suit and other equipment will not be measured by the LPM.*

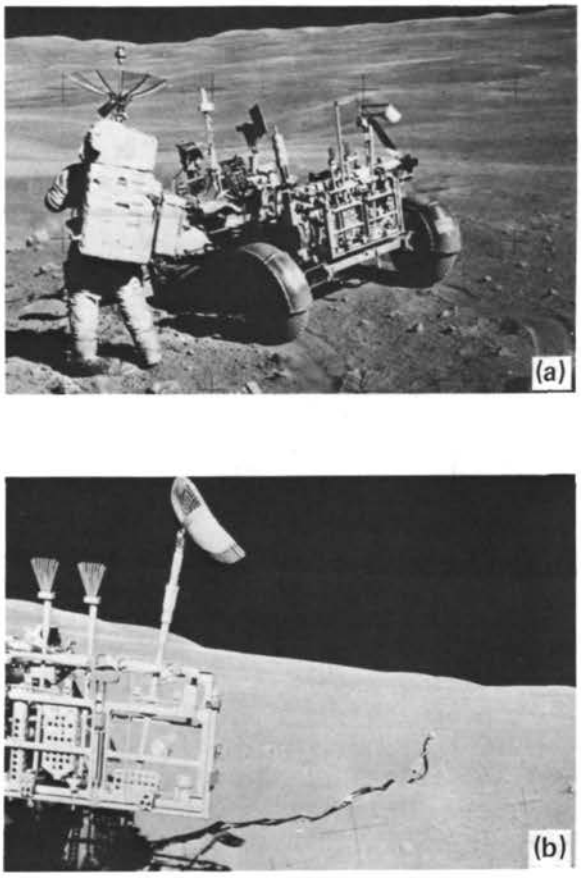


Figure 8.—*The Apollo 16 LPM (a) stowed on the lunar roving vehicle and (b) deployed during a magnetic field measurement.*

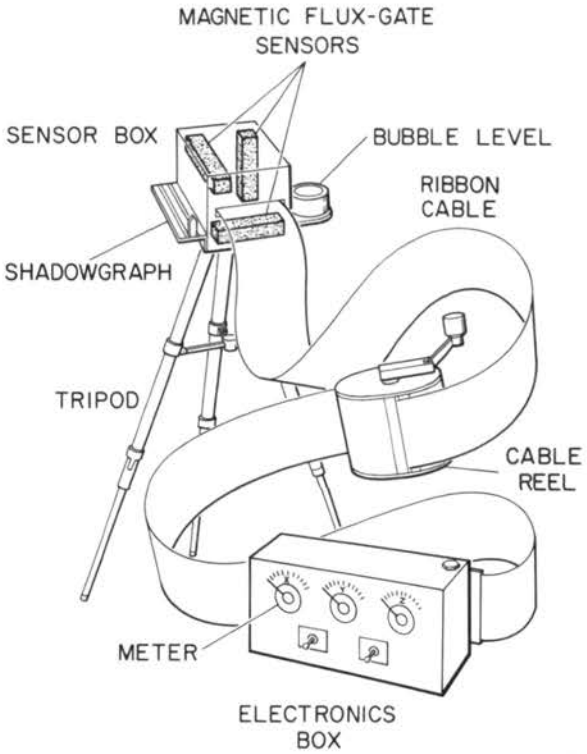


Figure 9.—*Schematic diagram of the Apollo 14 LPM. The sensor-tripod assembly is connected by means of a 15-meter ribbon cable to the electronics box, which contains a battery pack, electronics, and visual displays for three magnetic field vector components. Meter displays are used for the Apollo 14 LPM, and digital displays are used for the Apollo 16 LPM.*

LUNAR PORTABLE MAGNETOMETER (LPM)

The self-contained LPM is used to measure the steady magnetic field at different points along the lunar traverse of the astronauts. Two portable magnetometers have been deployed on the moon by the Apollo astronauts: one at the Apollo 14 site (3.7° S, 17.5° W) shown in figure 7, and one at the Apollo 16 landing site (9.0° S, 15.5° E) shown in figure 8.

The LPM field measurements are a vector sum of the steady remanent field from the lunar crust and of the time-varying ambient fields. The LSM simultaneously measures the time-varying components of the field; these components are later subtracted from the LPM measurements to give the desired resultant steady field values caused by the magnetized crustal material. The LPM consists of a set of three orthogonal fluxgate sensors mounted on top of a tripod (fig. 9); the sensor-tripod assembly is connected by means of a 15-m ribbon cable to the electronics box, which is mounted on the mobile equipment transporter (Apollo 14) or the lunar roving vehicle (Apollo 16).

The 15-m cable length was determined from magnetic properties tests of the mobile equipment transporter and lunar roving vehicle. The LPM was calibrated by using magnetic reference instruments directly traceable to the U.S. National Bureau of Standards. The pertinent LPM characteristics are listed in table 1.

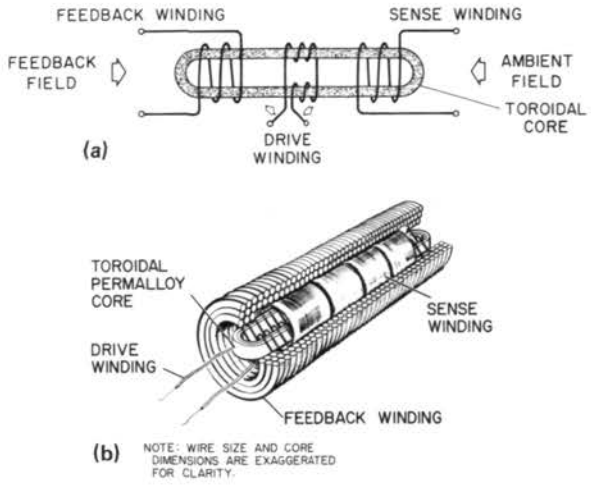


Figure 10.—*The fluxgate used in the LPM to measure each of three components of the magnetic field, (a) Functional schematic. (b) Cutaway view of the sensor windings and high-permeability core.*

Fluxgate Sensor

The fluxgate sensor, shown schematically in figure 10 is used to measure the vector components of the magnetic field in the magnetometer experiment. Three fluxgate sensors (refs. 56 and 57) are orthogonally mounted in the sensor block as shown in figure 9. Each sensor (see fig. 10) weighs 18 g and uses 15 mW of power during operation. The sensor consists of a flattened toroidal core of Permalloy that is driven to saturation by a square wave at a frequency f_o = 7250 Hz. This constant-voltage square wave drives the core to saturation during alternate half cycles and modulates the permeability at twice the drive frequency. The voltage induced in the sense windings is equal to the time rate of change of the net flux contained in the area enclosed by the sense winding. This net flux is the superposition of the flux from the drive winding and the ambient magnetic field. The signal generated in the sense winding at the second harmonic of the drive signal will be amplitude modulated at a magnitude proportional to the ambient magnetic field. The phase of this second harmonic signal with respect to the drive waveform indicates the polarity of the magnetic field. The sensor electronics amplifies and filters the 2 f_o sense-winding signal and synchronously demodulates it to derive a voltage proportional to the ambient magnetic field. After demodulation, the resulting signal is amplified and used to drive the feedback winding to null out the ambient field within the sensor. Operating at null increases thermal stability by making the circuit independent of core permeability variations with temperature.

The sensor block, mounted on the top of a tripod, is positioned 75 cm above the lunar surface. The tripod assembly consists of a latching device to hold the sensor block, a bubble level with 1° annular rings, and a shadowgraph with 3° markings used to align the device along the Moon-to-Sun line.

Electronics

The magnetometer electronics box is self-contained with a set of mercury cells for power and three digital displays for visual readout of the magnetic field components. A block diagram of the instrument is shown in figure 11. The sensors are driven into saturation by a 7.25-kHz square wave, and a 14.5-kHz pulse is used to demodulate the second harmonic signal from the sense windings. The amplifier output is synchronously demodulated, producing a direct-current output voltage proportional to the amplitude of the ambient magnetic field. This demodulated output is used to drive the feedback wind-

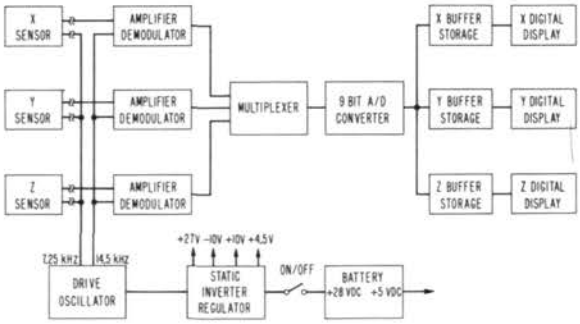


Figure 11.—*Functional block diagram of the LPM electronics.*

ing of the sensor so that the sensor can be operated at null conditions. The demodulated output from each channel is passed through a low pass filter with a time constant of 20 seconds.

Three meters were used to read the electronics output of the Apollo 14 LPM. The Apollo 16 LPM was actuated by a READ switch which caused the filtered analog signal to be converted to a digital 9-bit binary number. In system operation, the output of the analog-to-digital converter then goes to a storage register for display by the light-emitting diode numeric indicator. Three numeric indicators are used for each axis and read out in octal from 000 to 777 for magnetic field values from − 256 to + 256 γ.

Deployment and Operation

The astronaut operation was crucial to the execution of this experiment. The following measurement sequence was conducted: leaving the electronics box on the mobile equipment transporter (Apollo 14) or lunar roving vehicle (Apollo 16), the astronaut deployed the sensor-tripod assembly about 15 meters away, leveling and azimuthally aligning the instrument by bubble level and shadowgraph. The astronaut then returned to the electronics box, turned the power switch on, read the sensor meters (or digital displays) in sequence, and verbally relayed the data back to Earth. At the first deployment site only, two sets of additional readings were taken with the sensor block first rotated 180° about a horizontal axis and then rotated about a vertical axis. These additional readings allowed determination of a zero offset for each axis.

Explorer 35 Magnetometer

The ambient steady-state and time-dependent magnetic fields in the lunar environment are measured by the Explorer 35 satellite magnetometer. The satellite has an orbital period of 11.5 hrs., an aposelene of 9390 km, and a periselene of 2570 km (fig. 12). Two magnetometers are carried aboard Explorer 35, one provided by NASA/Ames Research Center and the other provided by NASA/Goddard Space Flight Center. Since most of the analysis of lunar internal properties has been carried out with the Ames magnetometer, its characteristics will be considered here. The Explorer 35 Ames magnetometer measures three magnetic field vector components very 6.14 seconds and has an alias filter with 18-dB attenuation at the Nyquist frequency (0.08 Hz) of the spacecraft data-sampling system. This instrument has a phase shift linear with frequency, and its step-function response is slower than that of the Apollo LSM instrument (fig. 5). Further information about the Explorer 35 magnetometer is given by Sonett et al. (ref. 58). Figure 12 also shows the orbit of the Apollo 16 particles and fields subsatellite which carried a magnetometer, and the three lunar surface magnetometers. Additional information on the subsatellite magnetometer is reported by Coleman et al. (refs. 59 and 60).

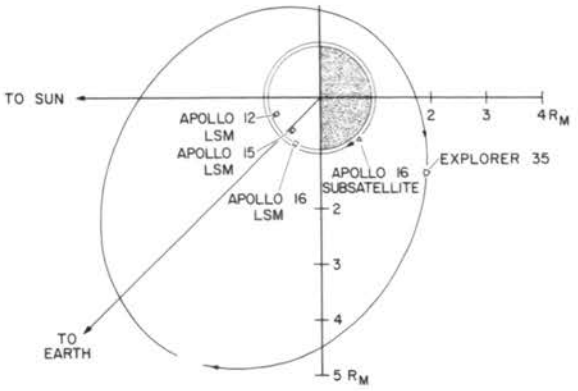


Figure 12.—*The Explorer 35 orbit around the Moon, projected onto the solar ecliptic plane. The period of revolution is 11.5 hrs. The Apollo 12, 15, and 16 surface instrument positions and Apollo 16 subsatellite trajectory are shown.*

The Lunar Magnetic Environment

In different regions of a lunar orbit, the magnetic environment of the Moon can have

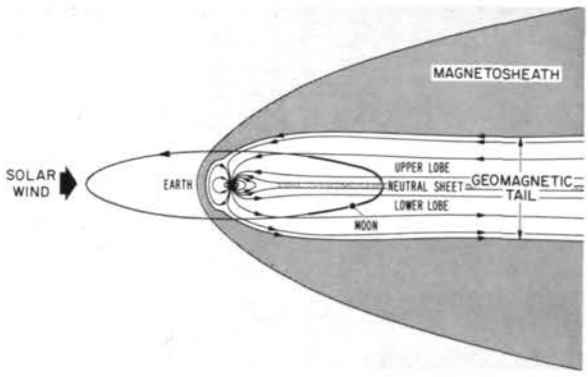


Figure 13.—*Magnetic environment of the Moon during a complete lunar orbit, with emphasis on the geomagnetic tail region. The plane of the lunar orbit very nearly coincides with the ecliptic plane of the Earth's orbit. The Earth's permanent dipole field is swept back into a cylindrical region known as the geomagnetic tail; at the lunar distance the field magnitude is ~ 10 gammas or 10^{-4} oersteds. Substructure of the tail consists of two "lobes"; the upper or northward lobe has its magnetic field pointing roughly toward the Earth, whereas the lower lobe field points away from the Earth. The Moon is immersed about four days of each orbit in the tail; the Moon can pass through either or both lobes (accented portion of orbit), depending upon the characteristics of the particular orbit.*

distinctly different characteristics (see figure 13). Average magnetic field conditions vary from relatively steady fields of magnitude ~ 10 γ in the geomagnetic tail to mildly turbulent fields averaging ~ 5 γ in the free-streaming solar plasma region, to turbulent fields averaging ~ 8 γ in the magnetosheath. Average solar wind velocity is ~ 400 km/s in a direction approximately along the Sun-Earth line.

Various induced lunar and plasma-interaction fields are assumed to exist at the lunar surface; for reference, we write the sum of these fields as

$$\underline{B}_A = \underline{B}_E + \underline{B}_R + \underline{B}_\mu + \underline{B}_P + \underline{B}_T + \underline{B}_D + \underline{B}_F \quad (1)$$

Here $\underline{B}_A$ is the total magnetic field measured on the surface by an Apollo lunar surface magnetometer; $\underline{B}_E$ is the total external (solar or terrestrial) driving magnetic field measured by the Explorer 35 and Apollo 15 subsatellite lunar orbiting magnetometers while outside the antisolar lunar cavity; $\underline{B}_R$ is the steady remanent field at the surface site; $\underline{B}_\mu$ is the magnetization field induced in permeable lunar material; $\underline{B}_P$ is the poloidal field caused by eddy currents induced in the lunar interior by changing external fields; $\underline{B}_T$ is the toroidal field corresponding to unipolar electrical currents driven through the Moon by the $V \times \underline{B}_E$ electric fields; $\underline{B}_D$ is the field associated with the diamagnetic lunar cavity; and $\underline{B}_F$ is the field associated with the hydromagnetic solar wind flow past the Moon.

The interaction of the solar wind with the Earth's permanent dipole field results in formation of the characteristic shape of the Earth's magnetosphere; the solar wind in effect sweeps the Earth's field back into a cylindrical region (the geomagnetic tail) on the Earth's antisolar side. The Earth's field magnitude is about 30 000 γ at the equator; in the geomagnetic tail the field decreases with distance from the earth with a radial dependence expressible as $R^{-0.736}$ (ref. 61). At the distance where the Moon's orbit intersects the tail, the field magnitude is ~ 10 γ. The Moon is in the geomagnetic tail for about four days of each 29.5-day lunation (period between successive full Moons). Substructure of the tail consists of two "lobes": the upper or northward lobe has its magnetic field pointing roughly toward the Earth, whereas the lower lobe field points away from the Earth. The Moon can pass through either or both lobes, depending upon the characteristics of the particular orbit, the geomagnetic dipole axis orientation, and perturbations of the geomagnetic field by solar wind pressures. When the Moon is passing through a quiet region of the geomagnetic tail, solar wind interaction fields ($\underline{B}_T$, $\underline{B}_D$, and $\underline{B}_F$) and the induced poloidal lunar field $\underline{B}_P$ are negligible, and the total field at the lunar surface is

$$\underline{B}_A = \underline{B}_E + \underline{B}_\mu + \underline{B}_R \quad (2)$$

The induced magnetic field $\underline{B}_\mu$ is dependent on the relative magnetic permeability distribution of the lunar sphere and is proportional to the external magnetic field $\underline{B}_E$.

Therefore, when $B_E = 0$, $B_A = B_R$ and the Apollo magnetometer measures the steady remanent field alone. Once B_R is known, the relative magnetic permeability of the Moon μ/μ_o can be calculated.

A different set of field terms in equation (1) is dominant when the Moon is immersed in free-streaming solar wind and the magnetometer is on the lunar sunlit side. $B_D \rightarrow 0$ outside the cavity, and the global fields B_μ and B_T can be neglected in comparison to B_P (ref. 38). The interaction field B_F has been found to be important during times of high solar wind particle density (ref. 29); therefore the interaction term B_F is not to be assumed negligible in general, and equation (1) becomes

$$B_A = B_P + B_E + B_R + B_F \qquad (3)$$

At low frequencies ($\leq 3 \times 10^{-4}$ Hz), $B_P \rightarrow 0$ and the interaction field B_F can be investigated.

When the magnetometer is located on the dark (antisolar) side of the Moon, it is generally isolated from solar plasma flow and $B_F \rightarrow 0$. Then for dark side data, equation (3) reduces to

$$B_A = B_P + B_E + B_R \qquad (4)$$

where cavity effects (B_D) are neglected to a

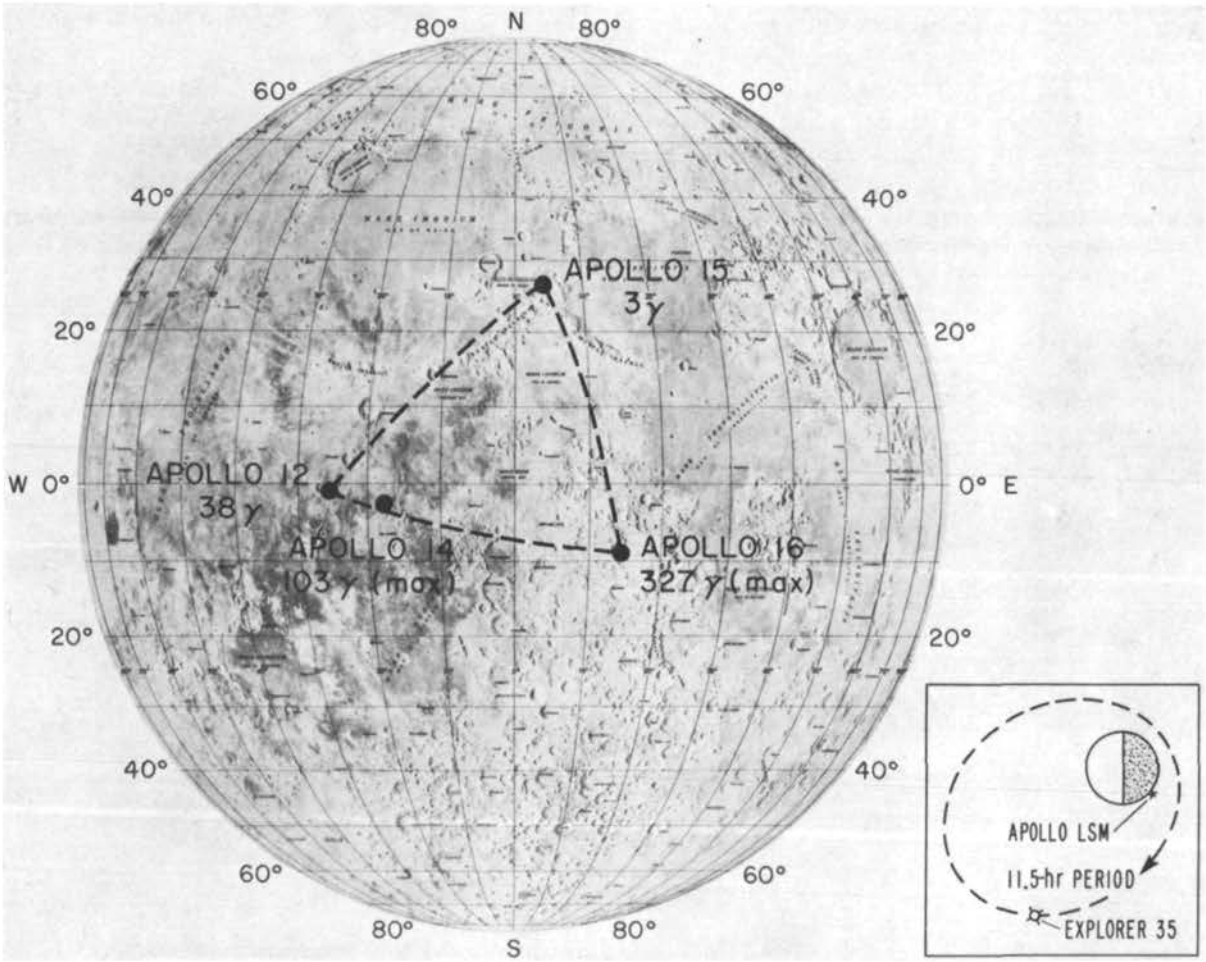


Figure 14.—*Apollo magnetometer network on the lunar surface. Maximum remanent magnetic fields measured at each landing site are shown.*

first approximation for measurements made near lunar midnight (ref. 38). After $\underline{B}_R$ has been calculated from geomagnetic tail data, only the poloidal field $\underline{B}_P$ is unknown. Equation (4) can then be solved for certain assumed lunar models, and curve fits of data to the solution determine the model-dependent conductivity profile σ (R). Furthermore, electrical conductivity is related to temperature, and the lunar interior temperature can be calculated for assumed lunar material compositions.

Lunar Remanent Magnetic Fields

The permanent magnetic fields of the Moon have been investigated by use of surface magnetometer measurements at four Apollo sites (see fig. 14) and the U.S.S.R. Lunokhod II site; orbital measurements from Explorer 35 and two Apollo subsatellite magnetometers; and natural remanent magnetization measurements of returned lunar samples. Lunar remanent field measurements by Apollo surface magnetometers will be emphasized in this paper. Sample magnetization measurements have been reviewed elsewhere (refs. 62–65); orbital results have been reported by Mihalov et al. (ref. 25), Sonett and Mihalov (ref. 66), Coleman et al. (refs. 26, 59, and 60), Sharp et al. (ref. 27), and Russell et al. (refs. 28 and 34).

SURFACE SITE FIELD MEASUREMENTS

Analyses of Apollo 11 lunar samples first demonstrated the presence of a natural remanent magnetization (NRM) in the lunar surface material. This magnetization ranges from 10^{-3} to 10^{-7} gauss cm^3 g^{-1} and most likely arises from the thermoremanent magnetization of metallic iron grains (ref. 65). The discovery of NRM in the lunar samples, which was a surprise to most scientists, did not lead to the expectation that the magnetization would be ordered on sufficiently large scale to produce localized magnetic fields. Also, measurements from orbiting magnetometers had not been interpreted as indicating the presence of permanent lunar fields

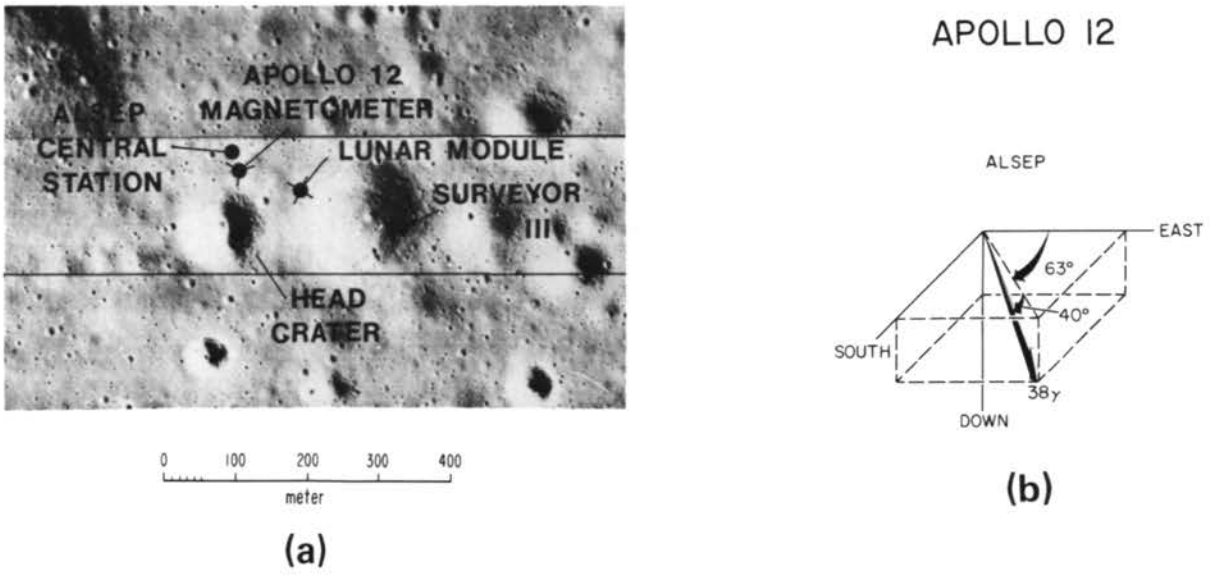


Figure 15.—*Lunar remanent magnetic field measured at the Apollo 12 site in Oceanus Procellarum. (a) Lunar Orbiter photograph showing the Apollo 12 landing site and location of the surface magnetometer where the remanent field measurements were made. (b) Magnitude and orientation of the measured vector magnetic field.*

prior to the Apollo 12 landing in November 1969.

However, a local remanent magnetic field was measured by the first (Apollo 12) lunar surface magnetometer, which was deployed on the eastern edge of Oceanus Procellarum. The permanent field magnitude was measured to be 38 ± 3 gammas and was attributed to local sources composed of magnetized subsurface material (refs. 23 and 24; see fig. 15). A remanent field this large was generally unexpected, and the origin of magnetized regions on the Moon yet remains a central problem in lunar magnetism. Subsequent to this measurement of an intrinsic lunar magnetic field, surface magnetometers have measured fields at the Apollo 14, 15, and 16 sites. Fields of 103 ± 5 and 43 ± 6 gammas, at two sites located about a kilometer apart, were measured by the Apollo 14 Lunar Portable Magnetometer (LPM) at Fra Mauro (see fig. 16). A steady field of 3.4 ± 2.9 gammas was measured near Hadley Rille by the Apollo 15 LSM (see fig. 17). At the Apollo 16 landing site both a portable and stationary magnetometer were deployed; magnetic fields ranging between 112 and 327 gammas were measured at five different locations over a total distance of 7.1 kilometers at the Descartes landing site. These are the largest lunar fields yet measured. A schematic representation of the measured field vectors is shown in figure 18. All the vectors have components pointing downward except the one at Site 5 near Stone Mountain, which points upward. This suggests, among other possibilities, that the material underlying Stone Mountain has undergone different geological processes than that underlying the Cayley Plains and North Ray Crater. In fact, Strangway et al. (ref. 67) proposed the possibility that the light-colored, relatively smooth Cayley formation is magnetized roughly vertically; the difference in the vertical component at site 5 was explained as an edge effect at the Cayley Plains-Stone Mountain boundary.

The similarities between the Apollo 12 and 14 field measurements (viz, all vectors are pointed down and toward the south, and have magnitudes that correspond to within a factor of 3) and the proximity of the two landing sites (see fig. 14) suggest that the two Apollo 14 sites and possibly the Apollo 12 site are located above a near-surface slab of material that was uniformly magnetized

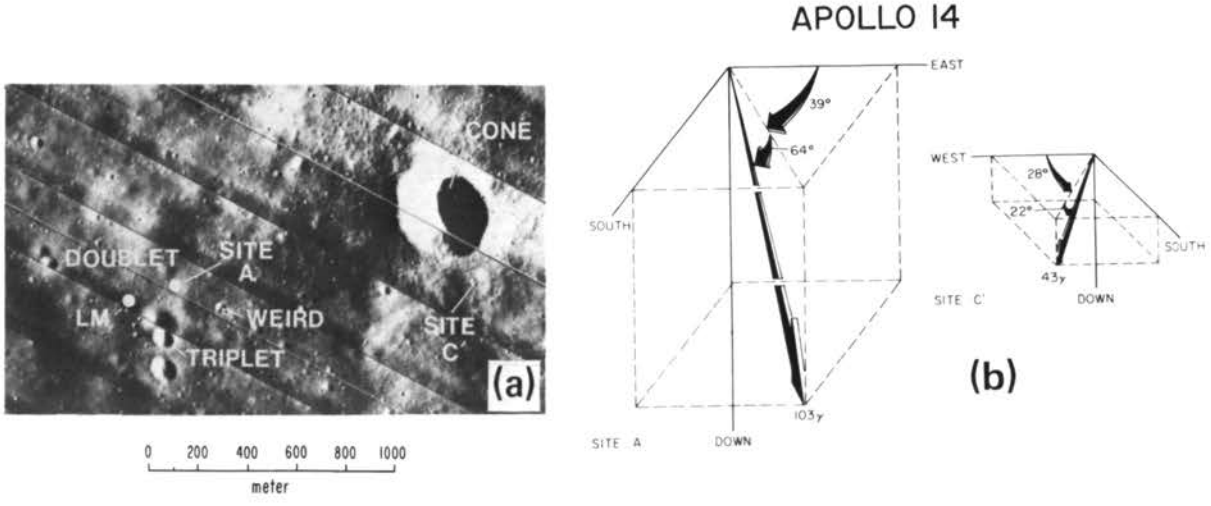


Figure 16.—*Lunar remanent magnetic fields measured at the Apollo 14 site at Fra Mauro. (a) Lunar Orbiter photograph showing the Apollo 14 landing site and the locations of sites A and C' where the lunar portable magnetometer measurements were made. (b) Magnitude and orientation of the measured remanent magnetic fields.*

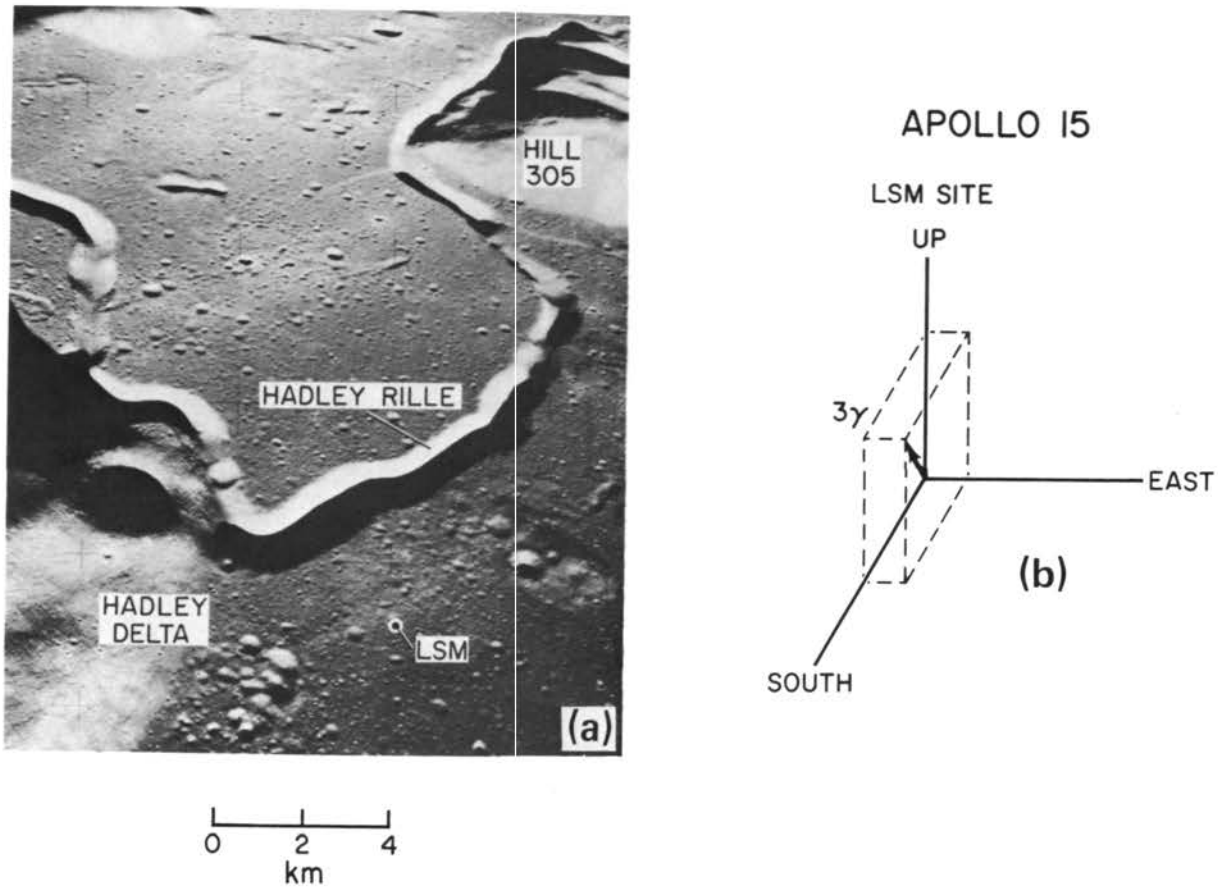


Figure 17.—*Lunar remanent magnetic field measured at the Apollo 15 site near Hadley Rille. (a) Photograph showing the Apollo 15 landing site and location of the surface magnetometer where the remanent field measurement was made. (b) Magnitude and orientation of the measured remanent magnetic field.*

at one time. Subsequently the magnetization in the slab was perhaps altered by local processes, such as tectonic activity or fracturing and shock demagnetization from meteorite impacts. This latter process is graphically illustrated in figure 19. The Apollo 12 and 14 steady magnetic fields could also originate in surface or subsurface dipolar sources, such as meteoroid fragments or ore bodies. Another possibility is that the region was subjected to a uniform magnetic field but that various materials with differing coercivities were magnetized to different strengths. Another model might involve a slow variation in the direction of the ambient field, causing regions that passed through the Curie temperature at different times to be magnetized in different directions. A summary of all remanent lunar fields measured by the magnetometers deployed on the surface is given in table 2, and the network of surface sites at which remanent fields have been measured is shown in figure 14.

Information on the scale sizes of the permanently magnetized regions near Apollo landing sites is given by gradient measurements of the lunar surface magnetometers, the spacing of vector measurements over the lunar surface, the known interaction properties of these remanent fields with the solar wind plasma, and limits imposed by satellite measurements. The field gradient in a plane parallel to the lunar surface is less than the instrument resolution of 0.13 gamma/meter

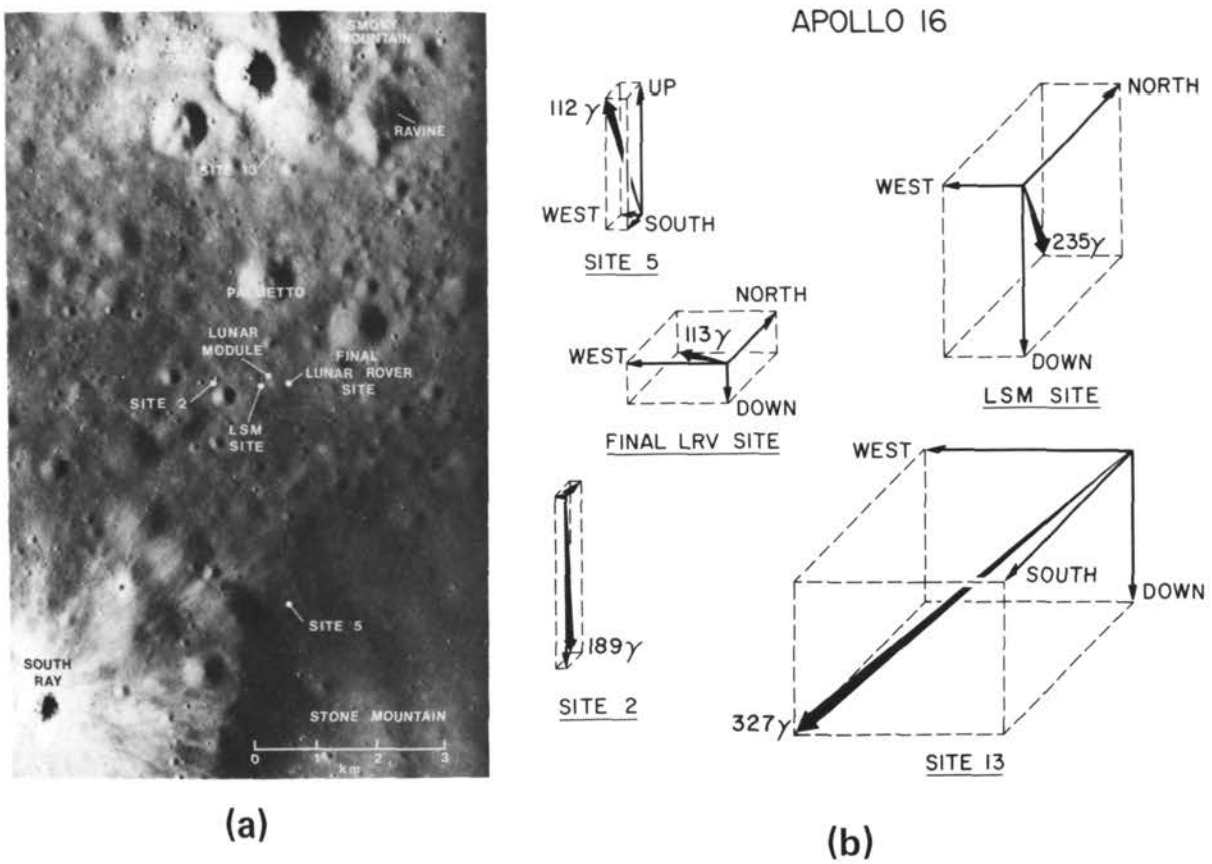


Figure 18.—*Lunar remanent magnetic fields measured at the surface Apollo 16 Descartes site. (a) Photograph showing the Apollo 16 landing site, the location of the surface magnetometer, and the traverse positions where the portable magnetometer was deployed. (b) Magnitude and orientation of the measured vector remanent magnetic fields.*

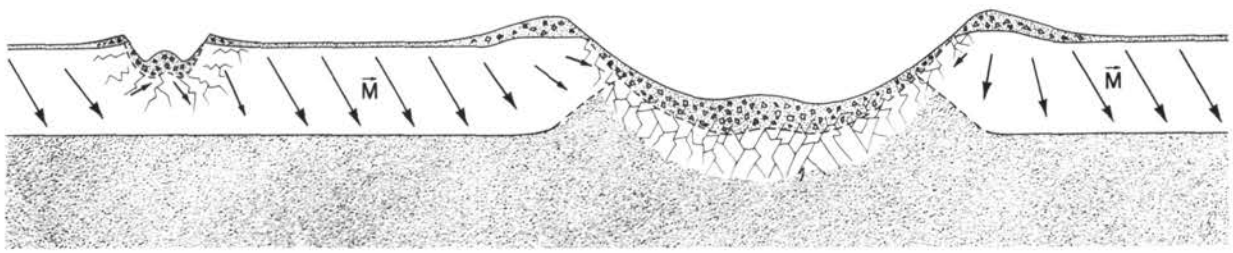


Figure 19.—*Conceptional diagram showing disruption of a previously uniformly magnetized subsurface layer by meteorite impact. The vectors* (M) *represent the direction and magnitude of remanent magnetization in the layer.*

Table 2.—*Summary of Lunar Surface Remanent Magnetic Field Measurements*

Site	Coordinates, Degrees	Field Magnitude, Gammas	Magnetic-Field Components, Gammas		
			Up	East	North
Apollo 16:					
ALSEP Site	8.9°S, 15.5°E	235 ± 4	−186 ± 4	−48 ± 3	+135 ± 3
Site 2		189 ± 5	−189 ± 5	+3 ± 6	+10 ± 3
Site 5		113 ± 4	+104 ± 5	−5 ± 4	−40 ± 3
Site 13		327 ± 7	−159 ± 6	−190 ± 8	−214 ± 6
LRV Final Site		112 ± 5	−66 ± 4	−76 ± 4	+52 ± 2
Apollo 15:					
ALSEP Site	26.1°N, 3.7°E	3.4 ± 2.9	+3.3 ± 1.5	+0.9 ± 2.0	−0.2 ± 1.5
Apollo 14:					
Site A	3.7°S, 17.5°W	103 ± 5	−93 ± 4	+38 ± 5	−24 ± 5
Site C′		43 ± 6	−15 ± 4	−36 ± 5	−19 ± 8
Apollo 12:					
ALSEP Site	3.2°S, 23.4°W	38 ± 2	−25.8 ± 1.0	+11.9 ± 0.9	−25.8 ± 0.4

at the Apollo 12 and 15 sites. At Apollo 14 a field difference of 60 γ was measured at two sites located 1.1 km apart. Gradient measurements and the absence of changes in the permanent field at the sites after lunar module ascent demonstrated that the field sources are not magnetized artifacts.

The scale size of the Apollo 12 remanent field has been calculated from local gradient and Explorer 35 measurements to be from 2 km to 200 km (ref. 29). For the Apollo 16 field, portable magnetometer measurements over the lunar roving vehicle traverse showed that the scale size for the field was greater than 5 km; the Apollo 16 subsatellite magnetometer showed no anomalous field attributable to the Descartes area at orbital altitude, implying a surface field scale size upper limit of 100 km. Therefore, the Apollo 16 remanent field scale size is between 5 and 100 km.

ORIGIN OF THE LUNAR REMANENT MAGNETIZATION

From the beginning of the Apollo missions the origin of the lunar remanent fields has been of great interest and there has been no shortage of mechanisms proposed to explain the origin of the lunar fields and remanence. Many authors have discussed various aspects of natural remanent magnetization (NRM) in the lunar surface material (e.g., refs. 22, 68, and 69). Possible source mechanisms for the remanent fields have been reviewed by Dyal et al. (refs. 70 and 72), Strangway et al. (ref. 71), and in detail by Fuller (ref. 65). Some of these possible mechanisms are discussed briefly here and displayed schematically in figures 20 and 21.

Large Solar or Terrestrial Field

The thermoremanent magnetization of the near-surface lunar material (such as might be responsible for the remanent fields measured by the surface and subsatellite magnetometers) was probably accomplished by the cooling of crustal material on a scale of tens of kilometers in a relatively steady external magnetic field of a few thousand gammas. It is possible that the Sun was the source of the external magnetic field (ref. 19). The early solar field may have been greatly en-

hanced during an early T-Tauri solar phase, as suggested by Sonett et al. (ref. 73), although at the lunar orbit such a field was probably even more variable than it is at the present time. A terrestrial field increase greater than 100 times its present value would probably be necessary to magnetize lunar material at the present-day lunar orbit. Such a large terrestrial field is not indicated by paleomagnetic studies. For an ancient terrestrial field of present-day magnitude, the Moon would have to have approached to within 2 to 3 Earth radii, close to the Roche limit (refs. 16 and 74) to be subjected to the necessary field strength. All of the alternatives for these hypotheses seem to have shortcomings.

Iron Core Dynamo

For this mechanism a whole-Moon field results from the self-generating dynamo action of a small iron core (refs. 75 and 76). The dynamo is assumed to have been active 3 to 4 billion years ago when surface rocks and breccias were formed. After the thermoremanent magnetization was established in the upper crust material, as it cooled through the Curie temperature, the dynamo turned off. Subsequently, meteorite impacts on the magnetized surface randomized the field's sources by a gardening process (see fig. 19) and destroyed the whole-body magnetization in the crust. The core dynamo hypothesis also has its shortcomings. In the first place it is not clear that even the most efficient dynamo mechanism in a lunar core of limited size would be self-sustaining at rotational speeds for which the Moon could hold together (ref. 77). In addition, it is doubtful that a dynamo, if ever operating, could produce the surface fields to explain the thermoremanent magnetization of some lunar samples (refs. 20 and 77).

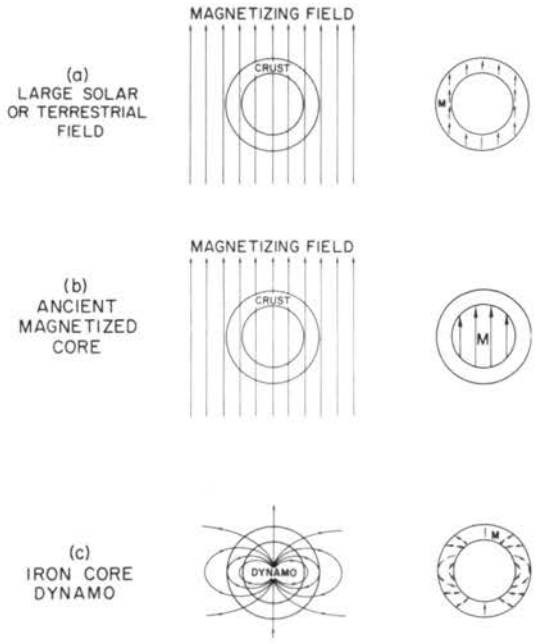


Figure 20.—*Schematic representation of some global mechanisms proposed to explain the origin of lunar remanent magnetic fields. (a) Large solar or terrestrial field. (b) Ancient magnetized core. (c) Iron core dynamo. Descriptions of the mechanisms are given in the text.*

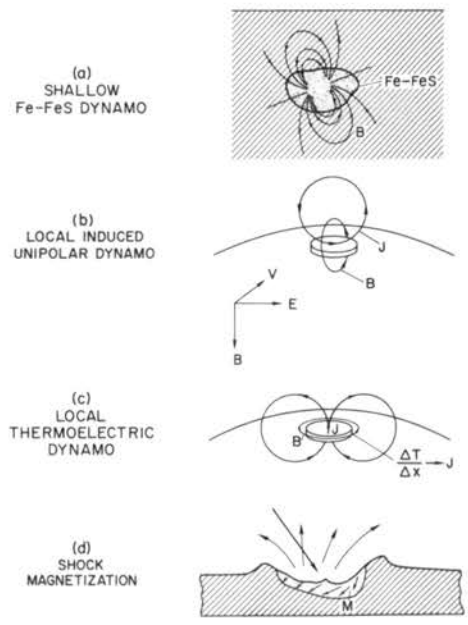


Figure 21.—*Schematic representation of some local mechanisms proposed to explain the origin of lunar remanent magnetic fields. (a) Shallow Fe-FeS dynamo. (b) Local induced unipolar dynamo. (c) Local thermoelectric dynamo. (d) Shock magnetization. Descriptions of the mechanisms are given in the text.*

Ancient Magnetized Core

Urey and Runcorn (ref. 78) and Strangway et al. (refs. 64 and 71) have suggested that near-surface material may have been magnetized by the field of a lunar core which had been previously magnetized by one of several possible means: (1) magnetization achieved isothermally by a strong transient field, (2) viscous remanent magnetization by a weak field applied over a long period, (3) depositional remanent magnetization during early lunar formation in a weak field, or (4) thermoremanent magnetization of the core by cooling through the Curie point in a weak field. If the Moon formed in a cold state, neither accretion nor radioactivity would necessarily have raised the temperature of the deep interior above the Curie point of iron, with accompanying loss of magnetization, until 4.1 to 3.2 billion years ago. In the outer shell, perhaps 200 to 400 km thick, partial melting could easily have been realized during later stages of accretion. During the crystallization of the crustal rocks in the magnetic field of the core, they obtained a thermoremanence. Subsequently, radioactive heating in the interior raised the core temperature above the Curie point, resulting in loss of the magnetization in the core.

Shallow Fe-FeS Dynamo

A model related to the lunar core dynamo is one hypothesizing small pockets of iron and iron sulfide (Fe-FeS) melt a few hundred kilometers below the surface (ref. 79) which act as small localized dynamos. The proponents of this mechanism suggest that these "fescons" are about 100 km in diameter. A variation of this local dynamo idea is suggested by Smolychowski (ref. 80) wherein a thin layer of molten basalt generates the field. The existence of such local source regions for magnetic field should be evident once the surface fields have been mapped over more of the lunar surface. However, the recently discovered asymmetry in the electromagnetic field fluctuations at the Apollo 15 landing site (ref. 81) could be due to such a highly conducting subsurface body.

Local Induced Unipolar Dynamo

The solar wind transports magnetic fields past the Moon at velocities V of approximately 400 km/s; the corresponding $V \times B$ electric field causes currents to flow along paths of high electrical conductivity (refs. 19 and 35) such as molten mare regions, with the highly conducting solar wind plasma completing the circuit back to the lunar interior. The fields associated with these currents magnetize the materials as they cool below the Curie temperature. Because this induction mechanism has the strongest influence while the hot region is sunlit, an average preferred direction is associated with V. However, the $V \times B$ induction model requires solar wind magnetic fields or velocities much higher than the present-day Sun provides.

Local Thermoelectrically Driven Dynamo

Dyal et al. (ref. 45) have proposed a mechanism of thermoelectrically driven currents to account for remanent fields. Thermoelectric potential is a function of the thermal gradient and electrical properties of the geological material. For the mechanism, a mare basin is modeled by a disk which has an axial temperature gradient. Thermal gradients in the cooling mare lava could produce a Thomson thermoelectromotive force which would drive currents axially through the mare disk. The solar wind plasma, highly conducting along magnetic field lines, could provide a return path to complete the electrical circuit from the top surface of the lava to the lunar surface outside the mare and back into the mare through the lunar interior. The upper limit of the fields generated in terrestrial materials by this process is a few thousand gammas. Such fields near a mare disk would produce thermoremanent magnetization in the Moon of magnitudes measured in lunar samples. This mechanism

awaits experimental verification using materials characteristic of lunar mare composition.

Shock Magnetization

Anisotropic compression of rocks by meteorite impacts is suggested by Nagata et al. (ref. 82) as a means of inducing a remanence in certain samples which they studied magnetically. This piezo-remanent magnetization can be significantly large even when the external field is very weak (e.g., the solar wind field) if the uniaxial compression is very large. This mechanism is appealing since it relies on a well-established lunar process and may explain some correlation between craters and magnetic anomalies (ref. 27), but the details remain undeveloped.

Local Currents from Charged Particle Transport

Any process which results in plasma flow near the lunar surface may generate strong local currents and magnetic fields. Cap (ref. 83), for example, has shown that ionized volcanic ash flows may produce fields up to 10^3 gammas. As another example, Nagata et al. (ref. 82) proposed the idea that lightning may be generated as a result of exploding dust clouds from meteorite impacts. The large currents associated with an electrical discharge could produce transient magnetic fields up to 10 or 20 gauss, resulting in isothermal remanent magnetization of local material.

At this time it is difficult to determine which of the above mechanisms is responsible for the lunar sample NRM. Of course, several (or none) of these hypotheses may explain the phenomenon. It seems to the authors that the locally active mechanisms are preferable over the global mechanisms because of the very low upper limit on the permanent global magnetic dipole moment and the apparently random nature of the local fields on the scale of tens of kilometers. Certainly a large amount of work remains to be carried out using the available lunar data, simulations in the laboratory, and future orbital measurements before preferred hypotheses can be identified with any degree of certainty.

REMANENT FIELD INTERACTION WITH THE SOLAR WIND

Compression of the remanent lunar magnetic field by the solar wind has been measured at the Apollo 12 and 16 sites. Simultaneous surface magnetic field and plasma data show, to first order, a compression of the remanent field in direct proportion to the solar wind pressure as schematically illustrated in Figure 22.

In order to study the compression of the remanent field, it is advantageous to define a field $\underline{\Delta B}$ as

$$\underline{\Delta B} = \underline{B}_A - (\underline{B}_E + \underline{B}_R), \qquad (5)$$

where $\underline{B}_A$ is the total surface magnetic field, measured by an Apollo lunar surface magnetometer; $\underline{B}_E$ is the extralunar (solar) driving magnetic field, measured by the lunar orbiting Explorer 35 magnetometer; and $\underline{B}_R$ is the steady remanent field at the site due to magnetized material. For low frequencies, i.e., 1-hour averages of magnetic

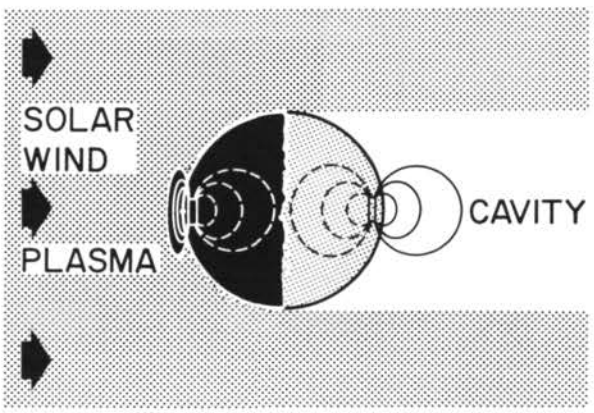


Figure 22.—*Schematic representation of remanent field compression by a high-density solar wind plasma. The remanent field is unperturbed during nighttime (antisolar side), while on the sunlit side it is compressed.*

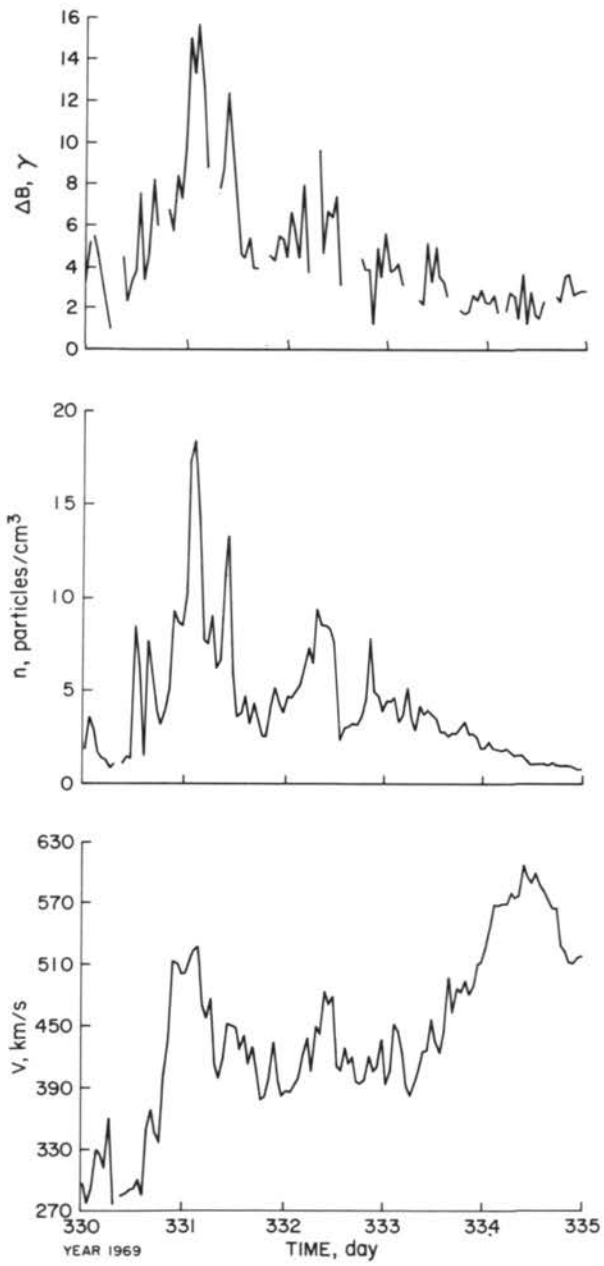


Figure 23.—*Simultaneous graphs of magnitude of the vector* $\Delta B = B_A - (B_E + B_R)$, *plasma density, and plasma velocity.* B_A *is the total surface field measured by the Apollo 12 lunar surface magnetometer,* B_E *is the extralunar field measured by lunar orbiting Explorer 35, and* B_R *is the remanent field at the Apollo 12 site.*

and solar wind data, the eddy-current poloidal field can be neglected and equation (5) contains all the vector fields, which are dominant at the lunar surface.

We shall show that to first order $\underline{\Delta B}$ is the vector change in the steady remanent field due to the solar wind pressure. Figure 23 shows simultaneous 1-hour average plots of the magnitude of the vector field difference $\underline{\Delta B}$, solar wind proton density n, and solar wind velocity magnitude V measured at the Apollo 12 site. All data are expressed in the surface coordinate system $(\hat{x}, \hat{y}, \hat{z})$ which has its origin at the Apollo 12 magnetometer site; $\hat{x}$ is directed radially outward from the surface while $\hat{y}$ and $\hat{z}$ are tangent to the surface, directed eastward and northward,

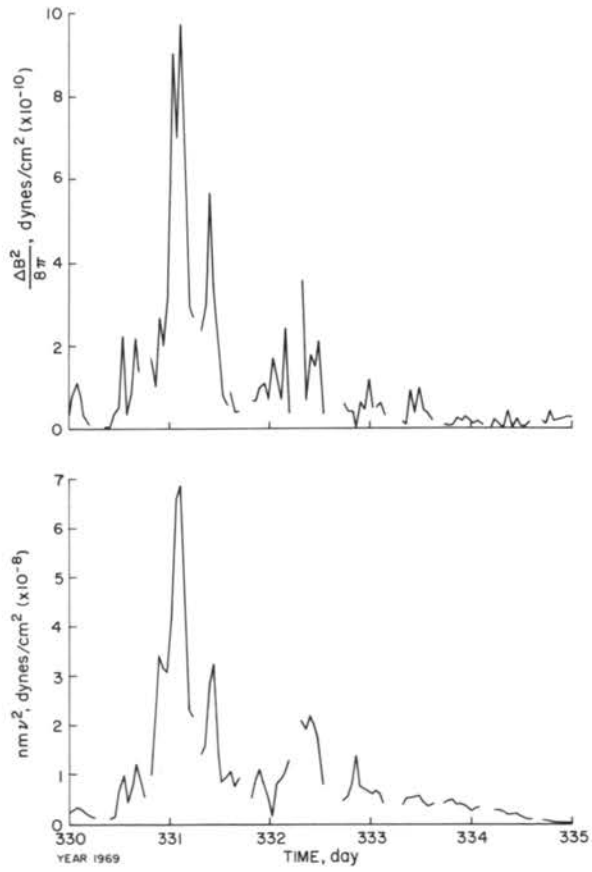


Figure 24.—*Simultaneous plots of the magnetic field pressure difference* $\Delta B^2/8\pi$ *and solar wind bulk pressure* $nm\mu^2$ *at the Apollo 12 surface site, showing the correlation between the pressures.*

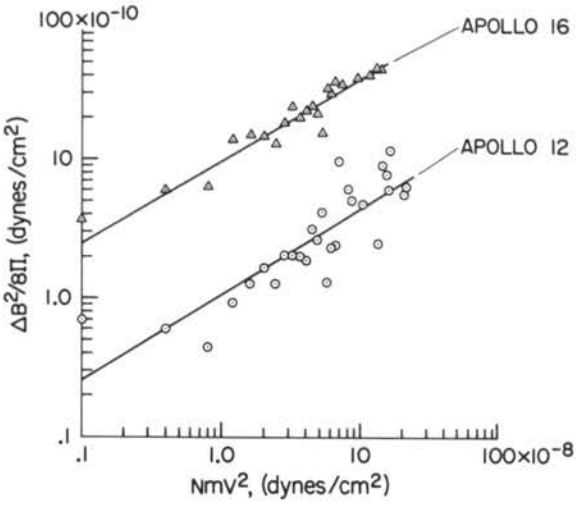


Figure 25.—*Magnetic energy density versus plasma energy density at two Apollo sites which have different remanent magnetic fields. Energies are defined in figure 24. Uncompressed remanent field magnitudes are 38 γ at Apollo 12 and 234 γ at Apollo 16. Apollo 12 magnetometer data are plotted versus Apollo 12 solar wind spectrometer (SWS) data, while Apollo 16 magnetometer data are plotted versus Apollo 15 SWS data. The SWS data are available by courtesy of C. W. Synder and D. R. Clay of the Jet Propulsion Laboratory.*

respectively. Components of the steady remanent field at the Apollo 12 site have been determined (ref. 38) to be $B_{Rx} = -25.8\ \gamma$, $B_{Ry} = +11.9\ \gamma$, and $B_{Rz} = -25.8\ \gamma$. By inspection we see a strong relationship between the magnitude ΔB and plasma proton density (n); no such strong correlation, however, is apparent between ΔB and velocity V alone.

The ratio of plasma pressure to total magnetic pressure is expressed

$$\beta = \frac{nmV^2}{B^2_{ST}/8\pi} \qquad (6)$$

where $\underline{B}_{ST} = \underline{B}_S + \Delta B$ is the total surface compressed field. During times of maximum plasma pressure shown in figure 24, we calculate $\beta = 5.9$; $\beta \leq 1$ would imply that the field had been compressed to the stagnation magnitude required to stand off the solar wind and possibly form a local shock. Compression of the remanent field alone therefore does not cause the stagnation condition to be reached during the time period of these data; however, at high frequencies the induced poloidal field $\underline{B}_P$ is also compressed ($\underline{\Delta B} = \underline{B}_P + \underline{B}_F$ in equation (3)), and thus it is possible that the stagnation pressure is reached for short time periods. Total surface fields of over 100 gammas have been observed (ref. 84) when large solar field transients pass the Moon; therefore a shock could be formed temporarily at the Apollo 12 site (as well as at the Apollo 14 and 16 sites).

The nature of the correlation between magnetic field and plasma pressures is further illustrated in figure 25, which shows data from several lunations at the Apollo 12 and 16 LSM sites. The pressures are related throughout the measurement range. The magnitudes of magnetic pressure changes at the Apollo 12 and Apollo 16 LSM sites are in proportion to their unperturbed steady field magnitudes of 38 γ and 234 γ, respectively.

Global Magnetization Induction: Magnetic Permeability and Iron Abundance

Magnetic permeability and iron abundance of the Moon are calculated by analysis of magnetization fields induced in the permeable material of the Moon. When the Moon is immersed in an external field it is magnetized; the induced magnetization is a function of the distribution of permeable material in the interior. Under the assumption that the permeable material in the Moon is predominately free iron and iron-bearing minerals, the lunar iron abundance can be calculated from the lunar permeability for assumed compositional models of the interior. Since the amount of iron present in the lunar interior should be consistent with the measured global magnetic permeability, the permeability in effect places a constraint on the physical and chemical composition of the Moon's interior.

GLOBAL MAGNETIC PERMEABILITY

Deployment of Apollo magnetometers on the lunar surface allowed simultaneous measurements of the external inducing field (by Explorer 25) and the total response field at the lunar surface (by an Apollo magnetometer). The total response field measured at the surface by an Apollo magnetometer is the sum of the external and induced fields:

$$\underline{B} = \mu \underline{H} = \underline{H} + 4\pi \underline{M} \qquad (7)$$

where $\underline{H}$ is the external magnetizing field and $\underline{M}$ is the magnetization field induced in the permeable lunar material (see fig. 26). The relative magnetic permeability is $\mu = 1 + 4\pi k$, where k is magnetic susceptibility in emu/cm³. Since the dipolar magnetization $\underline{M}$ is known to be below the Explorer 35 magnetometer resolution (ref. 8), it is assumed in the dual magnetometer analysis that Explorer 35 measures $\underline{H}$ alone.

For the two-layer lunar permeability model illustrated in figure 26 (which will be referred to later when iron abundance results are reviewed), the total field at the outer surface of the sphere is expressed

$$\underline{B} = H_x(1 + 2G)\hat{x} + H_y(1\text{-}G)\hat{y} + H_z(1\text{-}G)\hat{z} \qquad (8)$$

where

$$G = \frac{(2\eta + 1)(\mu_1 - 1) - \lambda^3(\eta - 1)(2\mu_1 + 1)}{(2\eta + 1)(\mu_1 + 2) - 2\lambda^3(\eta - 1)(\mu_1 - 1)} \qquad (9)$$

Here $\eta = \mu_1/\mu_2$; μ_1 and μ_2 are relative permeability of the shell and core, respectively. The permeability exterior to the sphere is $\mu_o = 1$, that of free space; $\lambda = R_c/R_m$; R_c and R_m are radius of the core and the Moon, respectively. Equation (8) expresses the total surface field in a coordinate system which has its origin on the lunar surface at an Apollo magnetometer site: $\hat{x}$ is directed radially outward from the lunar surface, and $\hat{y}$ and $\hat{z}$ are tangential to the surface, directed eastward and northward, respectively.

A plot of any component of equation (8) will result in a B–H hysteresis curve. Equation (9) relates the slope of the hysteresis curve to the lunar permeability. The average whole-Moon permeability μ is calculated from the hysteresis-curve slope by setting $\mu_1 = \mu_2 = \mu$ in equation (9):

$$G = \frac{\mu - 1}{\mu + 2} \qquad (10)$$

The hysteresis-curve method of permeability analysis was first employed by Dyal and Parkin (ref. 38) to calculate the whole-Moon permeability result 1.03 ± 0.13. Since then the error limits have been lowered by processing a larger number of simultaneous data sets and using more rigid data selection criteria (e.g., ref. 85).

In the most recent dual-magnetometer results (refs. 32 and 33), a hysteresis curve was constructed with 2703 data sets (see fig. 27). Since the external magnetizing field is so small (~ 10 gammas), the familiar "S" shape of the hysteresis curve degenerates to a straight line (ref. 86). The data were fit by a least-squares technique which yields the

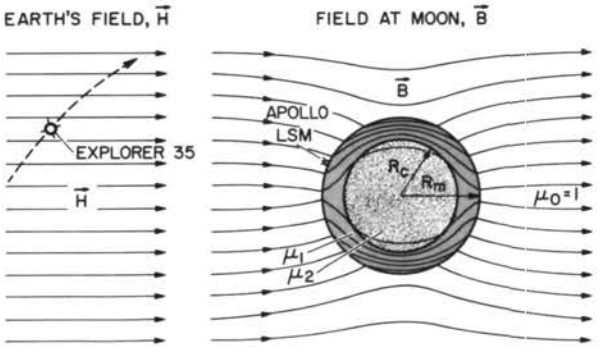


Figure 26.—*Magnetization induction in the Moon. When the Moon is immersed in a uniform external field* H *(in this case the steady geomagnetic tail field), a dipolar magnetization field* M *is induced in permeable material in the lunar interior, with the dipole axis of* M *aligned along the direction of* H. *The total magnetic field near the Moon is* B = H + 4 πM. *The magnetic permeabilities of the two layers are* μ_1 *and* μ_2, *and for regions outside the Moon,* $\mu = \mu_o = 1$ *(free space).* H *is measured by the lunar orbiting Explorer 35, whereas* B *is measured by an Apollo lunar surface magnetometer (LSM). Measurements of* B *and* H *allow construction of a* B-H *hysteresis curve for the sphere, from which permeability and iron abundance can be calculated.*

slope best-estimate of 1.008 ± 0.004. By use of this value with the radial (x) component of equation (8) and equation (10), the whole-Moon permeability was calculated to be $\mu = 1.012 \pm 0.006$ (2σ error limits). Both extremes are greater than 1.0, implying that the Moon, as a whole, acts as a paramagnetic or weakly ferromagnetic sphere. This result has been used to calculate the iron abundance of the Moon as discussed in the next section.

Russell et al. (ref. 34) have recently made permeability calculations using data from a single magnetometer, the Apollo 15 subsatellite magnetometer orbiting at an altitude about 100 km above the Moon. The results indicate that the relative permeability of the entire spherical volume enclosed by the satellite orbit is below 1.0, implying that the layer between the Moon and the satellite orbit is diamagnetic. The charged particles measured on the lunar surface by the Rice University suprathermal ion detector experiments (ref. 87) may be from a lunar ionosphere. If an ionosphere fills the entire region between the lunar surface and the subsatellite at 100 km altitude, the interior global lunar permeability would be higher than that calculated under the assumption of no ionosphere. The lunar permeability value of Parkin et al. (ref. 32) would be adjusted upward from 1.012 to 1.017, provided there exists a lunar ionosphere compatible with the measurements of Russell et al. (ref. 34). The corresponding free iron abundance value would be 3.9 instead of 2.5 wt.%. The existence of a lunar ionosphere is uncertain at present; further investigation is required, using both magnetic and plasma data.

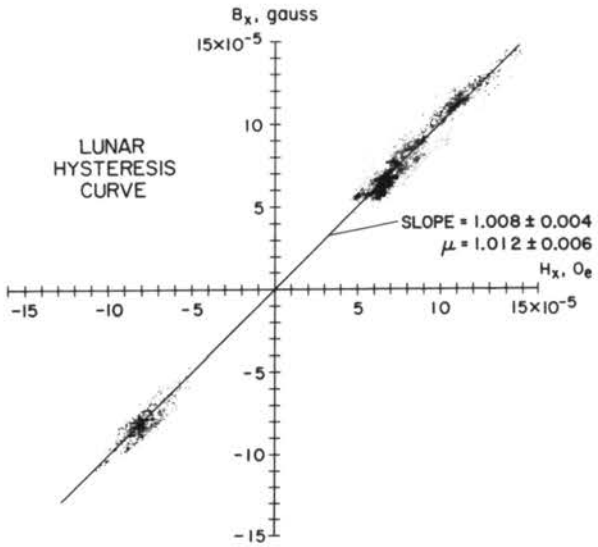


Figure 27.—*Hysteresis curve for the Moon. Data points are 2703 simultaneous 2-minute averages of radial components of the external geomagnetic field data* H *(measured by the lunar orbiting Explorer 35 Ames magnetometer) and total magnetic induction* $B = \mu H$ *(*B *is measured by the Apollo 12 lunar surface magnetometer). Data points are selected from four lunations of measurements made when the Moon is immersed in the uniform geomagnetic tail field, far from the neutral sheet in the tail. In this low-external-field regime (~ 10 gammas or 10^{-4} Oe), the hysteresis curve is linear and is fitted by a least-squares line of slope 1.008 ±0.004. This slope corresponds to a whole-Moon magnetic permeability of 1.012 ± 0.006. The least-squares line intersects the origin exactly in this figure because the vertical-axis intercept (the radial or* x*-component of the remanent field at the Apollo 12 site) was subtracted out after the least-squares fit was made.*

LUNAR IRON ABUNDANCE

Iron abundance calculations have been presented by various authors, in theoretical treatments based on geochemical and geophysical properties calculated for bodies of planetary size (refs. 88, 89, and 90) or on measured compositions of meteorites (ref. 91). Recently Parkin et al. (refs. 32, 33, and 85) have used a global lunar permeability measurement, determined from magnetic field measurements, to calculate lunar iron abundance for the Moon. In their calculations the Moon is modeled by a homogeneous paramagnetic rock matrix (olivine and orthopyroxene models are used), in which free metallic iron is uniformly distributed. Pyroxenes and olivines have been reported to be major mineral components of the lunar surface fines and rock samples (refs. 18, 92, and 93), with combined iron present as the paramagnetic Fe^{2+} ion. The ferromagnetic

component of lunar samples is primarily metallic iron which is sometimes alloyed with small amounts of nickel and cobalt (refs. 17 and 19). This free iron is thought to be native to the Moon (because of its low nickel content) rather than meteoritic in origin (ref. 71). Orthopyroxene and olivine models are consistent with geochemical studies (refs. 94–97) and geophysical studies (ref. 98).

Since the susceptibility of free iron changes several orders of magnitude at the iron Curie temperature (T_c), Parkin et al. have used a two-layer model with the core-shell boundary R_c at the Curie isotherm (see fig. 26). For $R > R_c$, $T < T_c$, and for $R \leq R_c$, $T > T_c$. Therefore, for $R > R_c$ any free iron is ferromagnetic while at greater depths where $T > T_c$, the free iron is paramagnetic. The Curie isotherm location is determined from the thermal profile used for a particular model. Three thermal models have been used in the calculations. For model profile T_1 the Curie isotherm is spherically symmetric and located at $R_c/R_m = 0.9$. Shell and core temperatures are 600° C and 1400° C, respectively. For the model profile T_2 the shell is 500° C and the core is 1300° C, while the Curie isotherm boundary is at $R_c/R_m = 0.85$. Temperatures are 300° C and 700° C for shell and core of model profile T_3, which has $R_c/R_m = 0.7$. In the outer shell there are both ferromagnetic and paramagnetic contributions to the total magnetic permeability $\mu_1 = 1 + 4\pi k_1$. The susceptibility of the shell is $k_1 = k_{1c} + k_{1a}$, where k_{1a} is "apparent" ferromagnetic susceptibility and k_{1c} is paramagnetic susceptibility. The ferromagnetic component is metallic free iron, assumed to be composed of multidomain, noninteracting grains; the paramagnetic component is Fe^{2+} combined in the orthopyroxene or olivine rock matrix. The measured ferromagnetic susceptibility of the shell material is an apparent value which differs from the intrinsic ferromagnetic susceptibility of the iron because of self-demagnetization of the iron grains and the volume fraction of iron in the shell. For $R < R_c$ the lunar material is paramagnetic only, with susceptibility $k_2 = k_{2c} + k_{2a}$; k_{2c} is the contribution of paramagnetic chemically combined iron, and k_{2a} is the apparent susceptibility of free paramagnetic iron above the Curie temperature.

Using the information described in the previous paragraphs, Parkin et al. (ref. 33) have generated the curves shown in figure 28, which relate free iron abundance (q) and total iron abundance (Q) to the hysteresis-curve slope. The results are summarized in table 3 and figure 29. The *minimum* total iron abundance consistent with the hysteresis curve can be calculated assuming the whole-Moon permeability corresponds

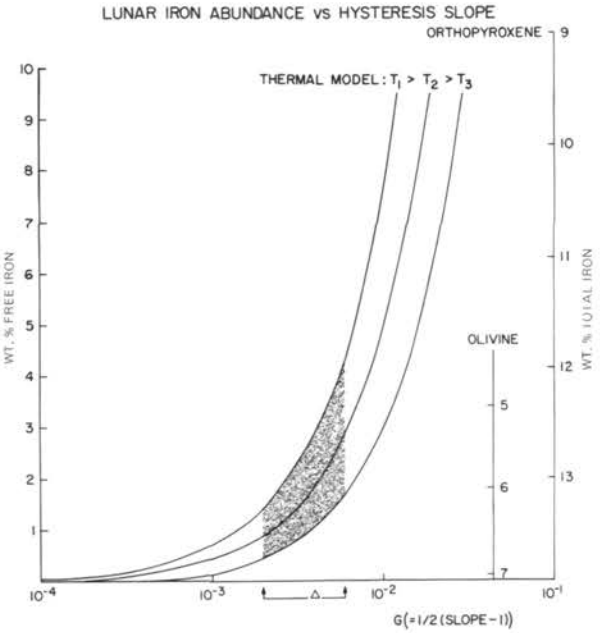


Figure 28.—*Iron abundance in the Moon as a function of global hysteresis curve slope. Free iron abundance (q) and total iron abundance (Q) versus the parameter G (hysteresis curve slope equals 2G + 1) for three temperature profiles described in the text. Total iron abundance is shown for two lunar composition models, orthopyroxene and olivine. Arrows below the horizontal axis show the range of the parameter G, experimentally determined from the hysteresis curve slope: G = 0.004 ± 0.002. The shaded region defines the allowed values of free and total iron abundances, bounded by hysteresis curve error limits and by thermal models T_1 and T_3.*

Table 3.—*Iron Abundance of the Moon as a Function of Thermal and Compositional Models*

Compositional Model \ Thermal Model	Free Iron Abundance, weight percent			Total Iron Abundance, weight percent		
	T_3	T_2	T_1	T_3	T_2	T_1
Orthopyroxene	1.0 ± 0.5	2.0 ± 1.0	3.0 ± 1.5	13.4 ± 0.3	13.0 ± 0.5	12.6 ± 0.6
Olivine	1.0 ± 0.5	2.0 ± 1.0	3.0 ± 1.5	6.5 ± 0.3	5.9 ± 0.7	5.3 ± 1.0

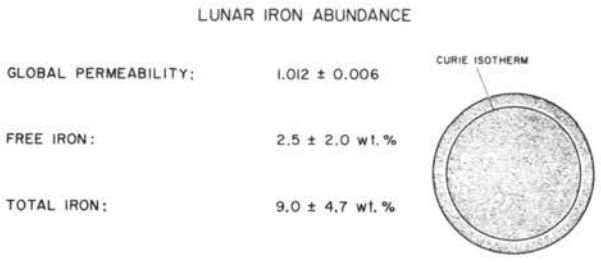


Figure 29.—*Summary of global lunar magnetic permeability, free iron abundance, and total iron abundance.*

entirely to ferromagnetic iron in the outer shell where the temperature is below the Curie point. For this case the bulk iron abundance is 0.9 + 0.5 wt.%. It is noted that the susceptibilities of both olivine and pyroxene are about an order of magnitude too small to account for the measured permeability without some ferromagnetic material present.

CONSIDERATIONS OF AN IRON CORE AND IRON-RICH LAYER

The whole-Moon permeability has also been used by Parkin et al. (ref. 32) to investigate the magnetic effects of a hypothetical iron core in the Moon. Density and moment of inertia measurements for the Moon limit the size of such a core to less than 500 km in radius (ref. 98). If this hypothetical iron core were entirely paramagnetic and the surrounding core were orthopyroxene of average temperature 1100° C the global permeability would be 1.0003. This value is small compared with the measured permeability of 1.012 ± 0.006, implying that if such a small paramagnetic iron core exists, its magnetization is masked by magnetic material lying nearer to the surface. Therefore, the hysteresis measurements can neither confirm nor rule out the existence of a small iron core in the Moon.

An iron-rich layer in the Moon has been considered by several investigators (refs. 94, 95, and 99). It is possible that early melting and subsequent differentiation of the outer several hundred kilometers of the Moon may have resulted in the formation of a high-density, iron-rich layer beneath a low-density, iron-depleted crust. Constraints have been placed on an iron-rich layer by Gast and Giuli (ref. 99) using geochemical and geophysical data (for example, measurements of lunar moments of inertia). One set of their models consists of high-density layers between depths of 100 km and 300 km. At a depth of 100 km the allowed layer thickness is 12 km; the thickness increases with increasing depth, to 50 km at 300-km depth. Also presented is a set of layers at 500-km depth. Using exactly the same considerations as were used in the iron abundance calculations, Parkin et al. have

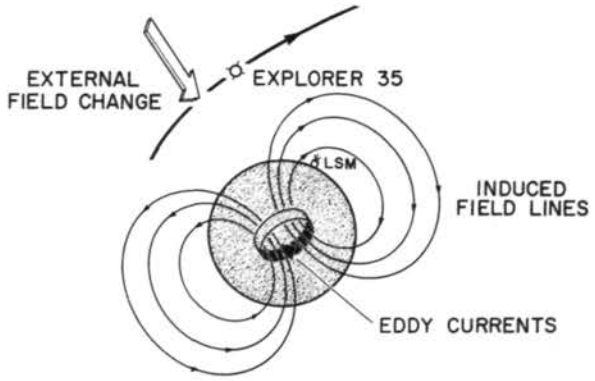


Figure 30.—*Global eddy-current induction: Moon in the geomagnetic tail. The induced poloidal field experiences greatly reduced plasma effects, especially in deep-lobe regions of the tail far from the neutral sheet. The poloidal field is considered to be an unconfined (vacuum) dipole field for analytical purposes.*

calculated whole-Moon permeabilities which would be expected from lunar models with these iron-rich layers. The calculations indicate that all iron-rich layers allowed by geophysical constraints as outlined by Gast and Giuli, if wholly above the iron Curie temperature, would yield global permeabilities of about 1.00006. As for the case of a small lunar iron core, the magnetization field of such paramagnetic layers would be masked by ferromagnetic materials elsewhere in the Moon, and the hysteresis curve measurements can neither confirm nor rule out these layers. This conclusion would particularly apply to the Gast-Giuli layers at 500-km depths, which are almost certainly paramagnetic. If the iron-rich layers are below the Curie temperature and therefore ferromagnetic, they yield global permeabilities of about 3.5. This is above the upper limit for the measured permeability of 1.012 ± 0.006 and the Gast-Giuli layers can be ruled out if they are cool enough to be ferromagnetic. It is important to realize that the high-density layers discussed by Gast and Giulu (ref. 99) can be thought of as limiting cases and that there are innumerable less dense and thinner layers which are allowed by geophysical, geochemical, and magnetic constraints.

Global Eddy-Current Induction: Electrical Conductivity and Temperature

Electrical conductivity and temperature of the Moon have been calculated from global eddy-current response to changes in the magnetic field external to the Moon. When the Moon is subjected to a change in the external field, an eddy-current field is induced in the Moon which opposes the change (see fig. 30). The induced field responds with a time dependence which is a function of the electrical conductivity distribution in the lunar interior. Simultaneous measurements of the transient driving field (by Explorer 35) and the lunar response field (by an Apollo surface magnetometer) allow calculation of the lunar conductivity. Since conductivity is related to temperature, a temperature profile can be calculated for an assumed compositional model of the lunar interior.

When the Moon is in the solar wind, lunar

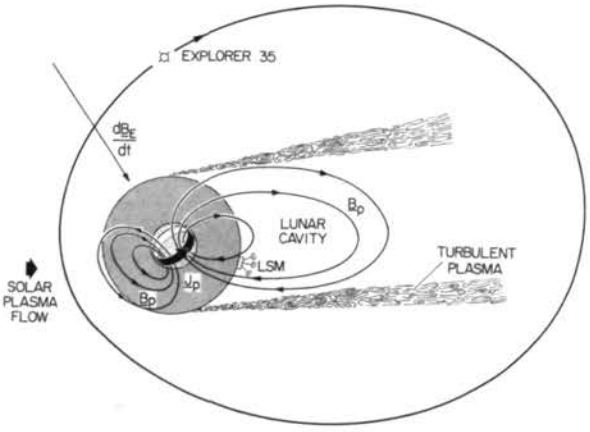


Figure 31.—*Global eddy-current induction: Moon in the solar wind. Eddy currents and corresponding poloidal magnetic fields are induced by response to time-dependent fluctuations in the external field* B_E. *The poloidal field has different characteristics, depending on the Moon's environment. When the Moon is in the solar wind, the global induced field is asymmetrically confined by the solar wind flowing past the Moon; the field is compressed on the day (sunlit) side and confined to the cavity region on the night (antisolar) side of the Moon.*

eddy-current fields form an induced lunar magnetosphere which is distorted in a complex manner due to flow of solar wind plasma past the Moon. The eddy-current field is compressed on the dayside of the Moon and is swept downstream and confined to the "cavity" on the lunar nightside (see fig. 31). Because of the complexity, early analysis included a theory for transient response of a sphere in a vacuum in order to model lunar response as measured on the lunar nightside (refs. 43, 44, and 100). The transient technique has subsequently been further developed to include effects of cavity confinement on nightside tangential data and to introduce analysis of magnetic step transients measured on the lunar dayside (refs. 45 and 51). Recently time-dependent poloidal response of a sphere in a vacuum has been applied to data measured in the geomagnetic tail (refs. 72 and 101) where plasma confinement effects are minimized. The poloidal response analysis has been used to determine the electrical conductivity and temperature profiles of the lunar interior.

ELECTRICAL CONDUCTIVITY ANALYSIS: MOON IN SOLAR WIND PLASMA

Lunar Nightside Data Analysis

The lunar electrical conductivity has been investigated by analysis of the lunar response to transients in the solar wind magnetic field. The response, measured by an Apollo

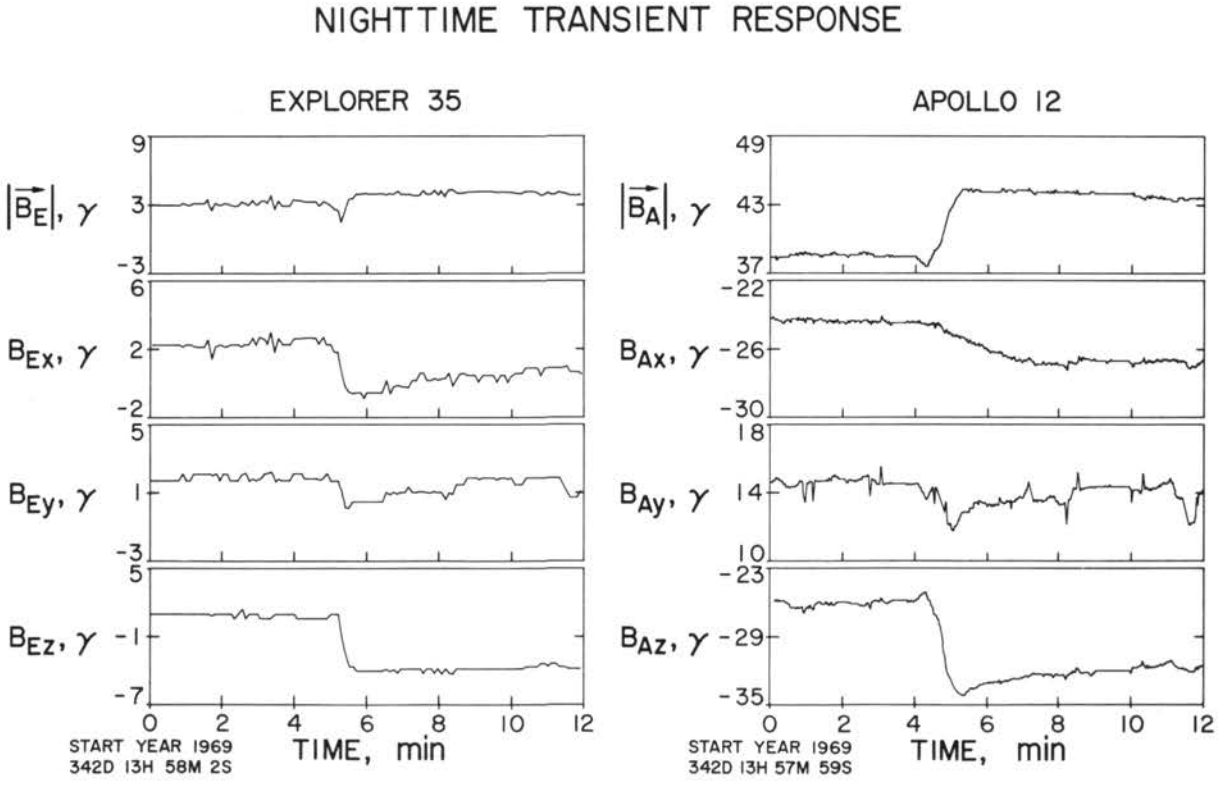


Figure 32.—*Nighttime transient response magnetic field data. A transient measured by an Apollo LSM while on the nighttime (antisolar) side of the Moon, showing simultaneous external solar wind field data measured by Explorer 35. Data are expressed in the surface coordinate system which has its origin at the Apollo 12 magnetometer site;* $\hat{x}$ *is directed radically outward from the surface, while* $\hat{y}$ *and* $\hat{z}$ *are tangent to the surface, directed eastward and northward, respectively.*

magnetometer on the nightside of the Moon, is theoretically approximated by the response of a conducting sphere in a vacuum. The theory has been developed by extending the work of Smythe (ref. 39) and Wait (ref. 40) for a radially varying lunar conductivity profile (ref. 102). Figure 32 shows an example of an event in which a transient in the external solar wind magnetic field is measured simultaneously by the Explorer 35 Ames magnetometer and an Apollo surface magnetometer. The transient is essentially a rotation in the external field, as indicated by the near-constancy of the field magnitude $|\underline{B}_E|$ measured by Explorer 35. Simultaneous field data ($\underline{B}_A$), measured on the nightside of the Moon by the Apollo 12 lunar surface magnetometer, are the vector sum of the external driving field $\underline{B}_E$, the induced eddy-current poloidal field $\underline{B}_P$, and the constant remanent field $\underline{B}_R$ (see equation (4)). Again, the field components are expressed in a coordinate system which has its origin located at the Apollo LSM site on the lunar surface; $\hat{x}$ is directed radially outward from the Moon, and $\hat{y}$ and $\hat{z}$ are tangential to the lunar surface, directed eastward and northward, respectively.

Figure 33 shows averages of radial components of the measured response field (B_{Ax}) for eleven normalized transient events of the type illustrated in figure 32. Error bars are standard deviations of the measured responses.

For models of the interior of the Moon a family of conductivity profiles (all of which monotonically increase with depth in the Moon), the theoretical response to a fast ramp is calculated and compared with the measured response. For this analysis the external field transient is represented by a ramp input function which falls from unity

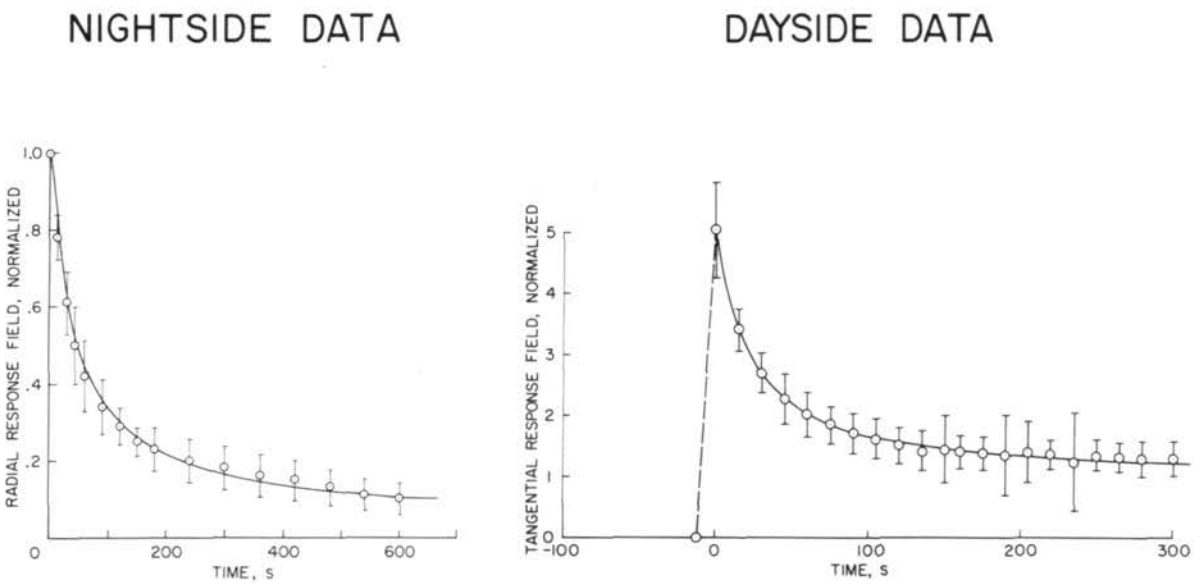


Figure 33.—*Normalized averages of transient response data, measured when Moon was in the solar wind. (a) Nightside transient response data, showing decay characteristics of the radial component of the total surface field* B_{Ax} *after arrival of a step transient which* reduces *the external magnetic field radial component by an amount* ΔB_{Ex}, *here normalized to one. The shape of the curve illustrates time characteristics of the decay of the induced poloidal eddy-current field. (b) Daytime transient response data, showing decay characteristics of tangential components* ($B_{Ay,z}$) *of the total surface field after arrival of a step transient which* increases *the external magnetic field tangential component by an amount* $\Delta B_{Ey,z}$, *here normalized to one. Shape of the curve again illustrates decay characteristics of the induced poloidal field. The overshoot maximum is amplified to* $\sim$ *5 by solar wind dayside compression; the theoretical overshoot maximum is 1.5 for an unconfined poloidal field.*

to zero in 15 seconds, a time characterizing convection of a solar wind dicontinuity past the Moon. (For a 400 km/s solar wind, this time is 10–20 seconds, depending on the thickness of the discontinuity and the inclination of its normal to the solar wind velocity.) The input field is constant before and after the field change. A particular set of conductivity profiles yield response functions which pass within all data error bars of figure 33. These profiles define the shaded region of figure 34 and are all consistent with the nightside response data.

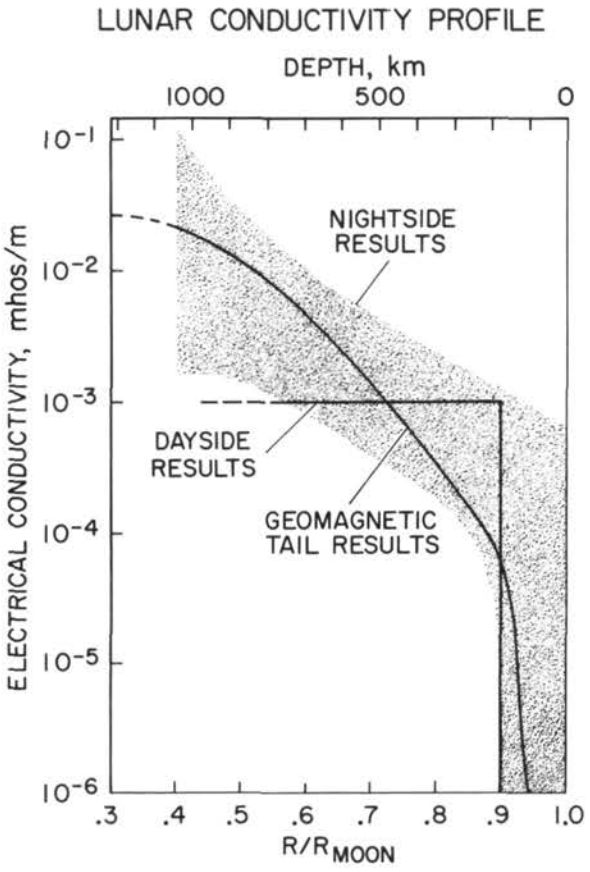


Figure 34.—*Electrical conductivity profiles for the lunar interior calculated from measurements in different regions of the lunar orbit around the Earth. The shaded region is from analysis of nightside transient data averages shown in figure 33 (a). The dayside conductivity profile is calculated by fitting totally confined two-layer Moon models to the dayside tangential component data illustrated in figure 33 (b). The curve labeled "geomagnetic tail results" is a profile consistent with analysis of transients in the geomagnetic tail lobes such as events illustrated in figures 37 and 39. Errors associated with this latter curve are approximately the same as the conductivity band shown for the nightside results.*

Lunar Dayside Data Analysis

Induced lunar eddy-current fields are confined, by the highly conducting solar wind, to the inside of the Moon and a small region above the lunar surface on the lunar dayside and to a "cavity" region on the nightside. Due to the complexity of the confinement, the conductivity analysis of transient magnetometer data measured on the lunar dayside has involved modeling the Moon by a sphere of homogeneous conductivity; the induced eddy-current field B_P is considered to be totally confined inside the lunar sphere (ref. 45). Figure 35 shows an example of a transient event in the solar wind magnetic field which is measured on the lunar dayside. Figure 33 shows averages of tangential components of response fields, measured on the lunar dayside, induced in response to rising fast-ramp transients in the free-streaming solar wind (error bars are standard deviations). The overshoot maximum is amplified by a factor of 5 over the external input field step change, by solar wind dayside confinement of the surface tangential field components. The data are fit by a lunar conductivity model with a homogeneous core of radius $R_c = 0.9\,R_m$ and conductivity $\sigma \sim 10^{-3}$mhos/m. This result is consistent with the nightside conductivity profile illustrated in figure 34 to depths allowed by the duration of the response data which is shown in figure 33.

The theoretical models outlined so far have all assumed spherical symmetry to describe lunar eddy-current response to changes in the external field. However, the nightside and dayside analyses have used data taken when the Moon was immersed in the solar wind plasma with asymmetric confinement of the inducing fields. The shortcomings of using spherically symmetric approximations to describe the induced lunar magnetosphere,

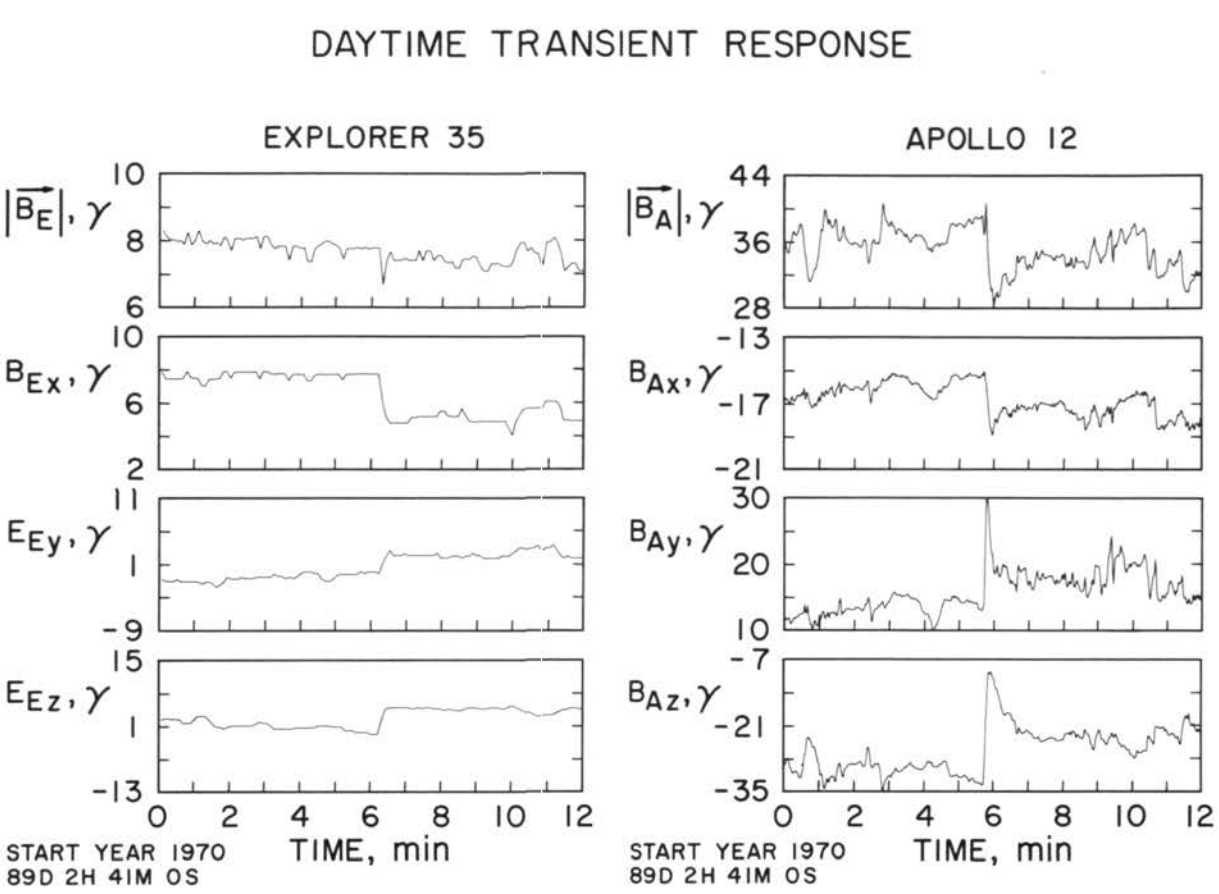


Figure 35.—*Daytime transient response magnetic field data, measured by an Apollo LSM while on the dayside (subsolar side) of the Moon, showing simultaneous external solar wind field data measured by lunar orbiting Explorer 35. The coordinate system is defined in the text. Note in particular the tangential components: dayside overshoot amplification is much higher relative to the Explorer-measured external step magnitudes than is nighttime amplification (shown in fig. 32).*

which is actually asymmetrically confined, have been pointed out in the literature for both the nightside vacuum approximation (see, e.g., ref. 52) and the dayside totally confined approximation (see e.g. ref. 51) Three-dimensional, dynamic asymmetric confinement presents a difficult theoretical problem which has not been solved at the time of this writing. Previous theoretical approximations of the asymmetric problem have included a two-dimensional approximation (ref. 50); three-dimensional static theory for a point-dipole source, with substantiating laboratory data (ref. 51); a three-dimensional dynamic theory for particular orientations of variations in the external field (ref. 103).

The confinement of the induced poloidal field by the highly conducting solar wind has been studied in the laboratory by considering a point-dipole field inside a superconducting cylinder (ref. 51). Two geometrical orientations of the point dipole have been considered: along the cylinder axis, and transverse to the cylinder axis. (See inserts in figure 36 for an illustration of these orientations.) The fields of the dipole-oriented transverse and axial with respect to the cylinder axis have been determined following Parker (ref. 104) and P. Cassen (private communication). The highly conducting solar wind plasma cavity is modeled by a thin lead superconducting capped cylinder and the instantaneous induced poloidal field is modeled by a small

dipolar samarium-cobalt magnet placed equidistant from the closed end and the side walls of the cylinder. The measured ratios of confined fields to unconfined fields are shown in figure 36. The theory and laboratory data presented in figure 36 represent to first order the effects of solar wind compression on a poloidal induced lunar field, as measured by a lunar surface magnetometer positioned at the antisolar point.

ELECTRICAL CONDUCTIVITY ANALYSIS: MOON IN THE GEOMAGNETIC TAIL

In order to circumvent the problem of asymmetry, recent analyses (refs. 72 and 101) have considered lunar eddy-current response during times when the Moon is in the geomagnetic tail where plasma interaction effects encountered in the solar wind (asymmetric confinement, remanent field compression, plasma diamagnetism, etc.) are minimal.

Poloidal Response of a Sphere in a Vacuum: Theory

In the conductivity profile analysis we assume that plasma effects are negligible in the lobe regions of the geomagnetic tail, and that the response of the Moon can be represented as that of a conducting sphere in a vacuum. To describe the response of a lunar sphere to an arbitrary input field in the geomagnetic tail, we define the magnetic vector potential $\underline{A}$ such that $\nabla \times \underline{A} = \underline{B}$ and $\nabla \cdot \underline{A} = 0$. We seek the response to an input $\underline{\Delta B_E} b(t)$, where $b(t) = 0$ for $t < 0$ and $b(t)$ approaches unity as $t \to \infty$. The direction of $\underline{\Delta B_E}$ is taken to be the axis of a spherical coordinate system (r,θ,ϕ). If the conductivity is spherically symmetric, the transient magnetic field response has no ϕ component,

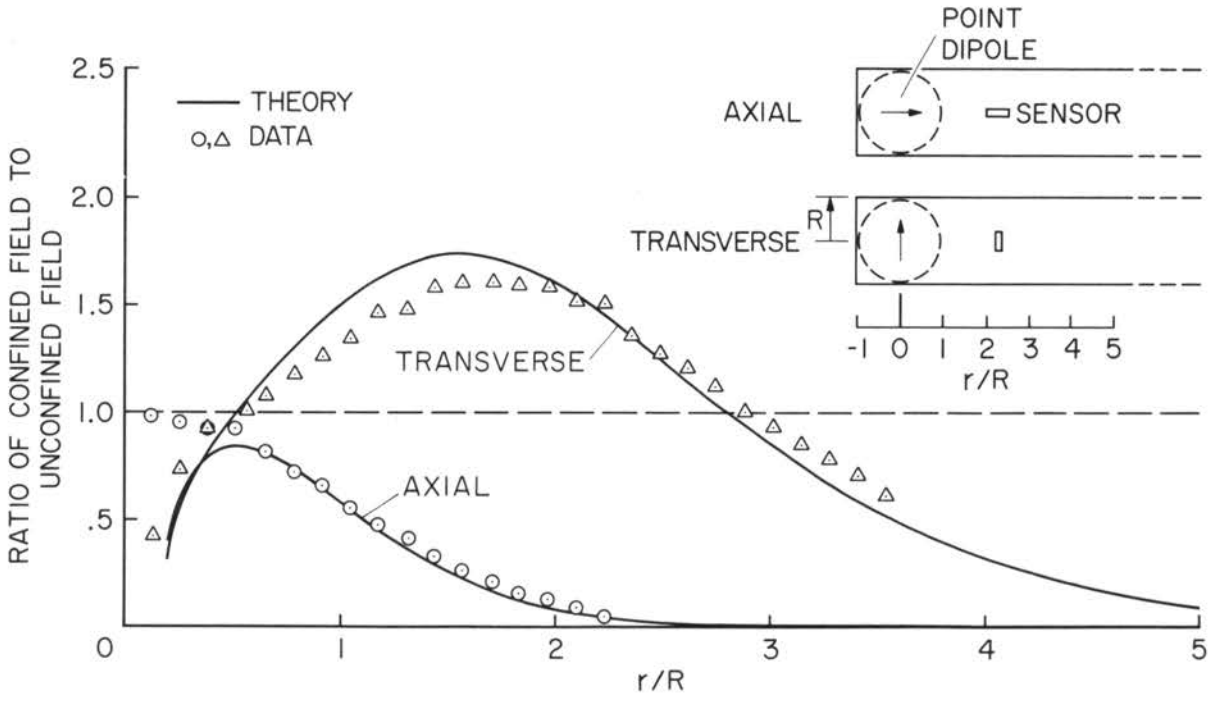


Figure 36.—*Confinement of a point dipole magnetic field, shown theoretically and experimentally. The inserts schematically show lunar confinement by the solar wind, approximated by a capped-cylinder superconductor enclosing a point dipole field. The theoretical curves show ratios of a confined to an unconfined dipolar field versus distance along the cylinder axis. Data are results of a laboratory experiment in which confinement of a small dipole magnet's field by a cylindrical superconductor is measured experimentally.*

and hence $\underline{A} = A\hat{e}_\phi$ and $\partial/\partial\ \phi = 0$. Under these conditions (and neglecting displacement currents) the laws of Faraday, Ampere, and Ohm combine to yield a diffusion equation (ref. 102) for the magnetic potential (in MKS units):

$$\Delta^2\ \underline{A}\ (r, \theta; t) = \mu\ \sigma\ (r) \frac{\partial\ \underline{A}}{\partial\ t} (r, \theta; t) \quad (11)$$

From magnetization induction analysis it is shown that $\mu \cong \mu_o$, that of free space (ref. 32). Then, for $t > 0$, the magnetic field must be continuous at the surface, so that $\underline{A}$ and $\partial\underline{A}/\partial r$ must always be continuous at $r = R_m$, the radius of the sphere. We also have the boundary condition $\underline{A}\ (0,t) = 0$ and the initial condition $\underline{A}\ (r, \theta, \phi) = 0$ inside the Moon. Outside the Moon, where $\sigma = 0$,

$$A = \Delta B_E \left(\frac{r}{2}\right) b(t)\ \sin\theta + \frac{\Delta B_E}{r^2} f\ (t)\ sin\theta. \quad (12)$$

The first term on the right is a uniform magnetic field modulated by $b(t)$; the second term is the (as yet unknown) external transient response, which must vanish as $r \to \infty$, and $t \to \infty$. Note that at $r = R_m$ where R_m is normalized to unity,

$$A = \Delta B_E \sin\theta \left(\frac{b(t)}{2} + f(t)\right) \quad (13)$$

and

$$\frac{\partial A}{\partial r} = \Delta B_E \sin\theta \left(\frac{b(t)}{2} - 2f(t)\right). \quad (14)$$

Therefore, at $r = R_m = 1$,

$$\frac{\partial A}{\partial r} = -2A + \frac{3}{2}\left(\Delta B_E \sin\theta\ b(t)\right). \quad (15)$$

Since the magnetic field is continuous at $r = r_m$, this is a boundary condition for the interior problem. Letting $G(r,t) = A/\ \Delta B_E \sin\theta$ and $\overline{G}(r,s)$ be the Laplace transform

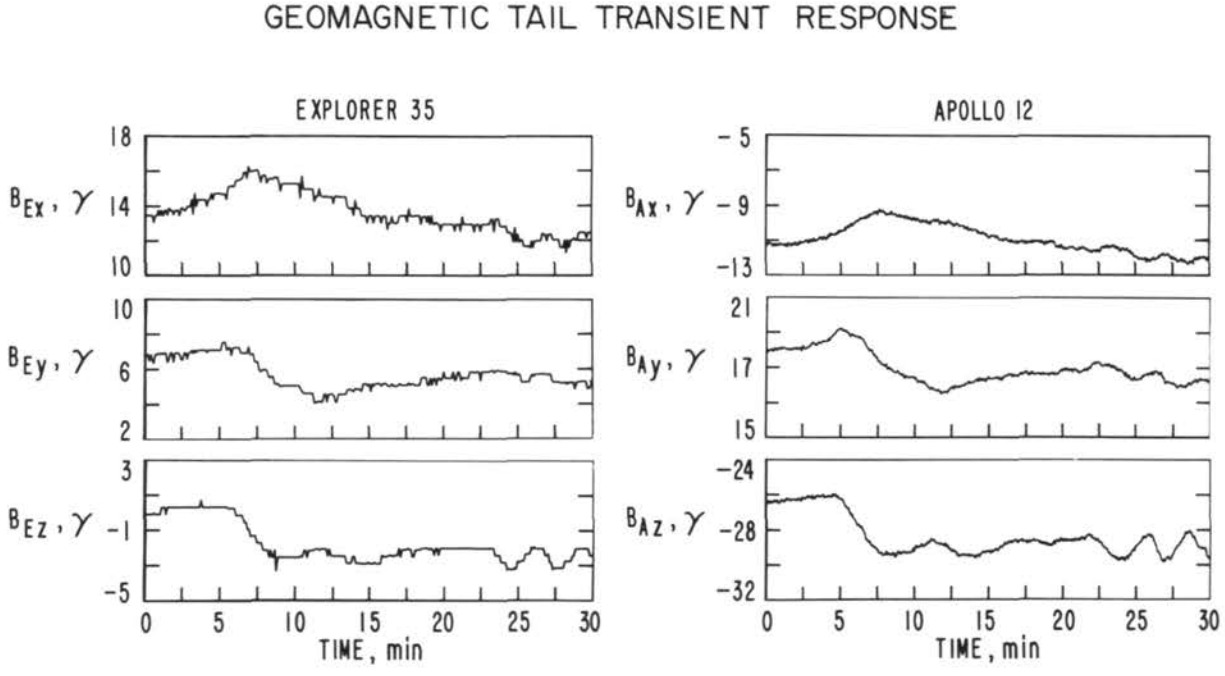


Figure 37.—*Magnetic transient event measured simultaneously by the Apollo 12 LSM and the Explorer 35 Ames magnetometer deep in the north lobe of the geomagnetic tail. Data are expressed in the surface coordinate system which has its origin at the Apollo 12 magnetometer site; x is directed radially outward from the surface, while y and z are tangent to the surface, directed eastward and northward, respectively. Due to poloidal field induction in the Moon, the Apollo 12 radial ($\hat{x}$) component is "damped" relative to the Explorer 35 radial component, whereas the Apollo 12 tangential ($\hat{y}$ and $\hat{z}$) field components are "amplified" relative to Explorer 35 data.*

of G, equation (1) becomes

$$\frac{1}{r}\left(\frac{\partial^2}{\partial r^2}(r\overline{G}) - \frac{2}{r}\overline{G}\right) = s\mu_o\sigma(r)\overline{G} \quad (16)$$

for the interior. The boundary conditions are

$$\frac{\partial \overline{G}}{\partial r} = -2\overline{G} + \frac{3}{2}\overline{b}(s) \quad (17)$$

at $r = R_m$ and $\overline{G} = 0$ (18)

at $r = 0$.

Since the governing equations are linear, the response to a general time-dependent input function can be found by superposition of solutions as follows. The individual input function (that is, external field transient event measured by Explorer 35) is approximated by a succession of ramp functions $b_i(t)$. For each $b_i(t)$ and the given conductivity profile $\sigma(r)$, the above system of equations is numerically integrated to obtain $\overline{G}_i(r,s)$ in the range $02 \leq r \leq R_m$. The function $\overline{G}_i(r,s)$ is then numerically inverse Laplace transformed to find the characteristic transient response $f_i(t)$ for the system. Then the individual functions $f_i(t)$ are superposed to calculate the final time response function $F(t)$ corresponding to the arbitrary input function and $\sigma(r)$. This calculated time series response is compared with the measured time series response (Apollo magnetometer data) and iterated with a different function $\sigma(r)$ until the error between the calculated $F(t)$ and the measured $F(t)$ is minimized.

Conductivity Results: Geomagnetic Tail Data Analysis

Figure 37 shows an example of a magnetic transient measured in the northward lobe of the geomagnetic tail. The data components are expressed in a coordinate system which has its origin on the lunar surface at the Apollo 12 magnetometer site. Again the x-component is directed radially outward from the lunar surface, while the y- and z-components are tangent to the surface, directed eastward and northward, respectively. The external (terrestrial) driving magnetic field is measured by Explorer 35, whereas the total response field is measured on the lunar surface by the Apollo 12 magnetometer.

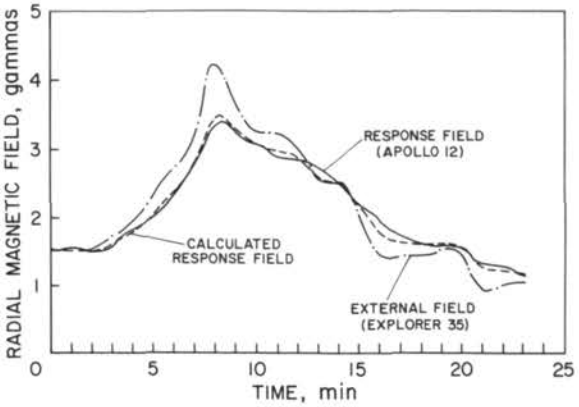


Figure 38.—*Electrical conductivity analysis for a transient event in the geomagnetic tail, deep in the north lobe. Shown are data from the radial component of the event of figure 37. Response to the Explorer 35 external field radial component is computed numerically for the conductivity profile shown in the insert of figure 40 and compared to the measured Apollo 12 response field. In the preliminary results of geomagnetic tail conductivity analysis, this selected conductivity profile, though not unique, yields a satisfactory fit of input and response data for this and thirteen other deep lobe tail events processed to date.*

Figure 38 shows an example of calculated response for the Explorer 35 x-axis (radial) input function of figure 37, using the geomagnetic tail electrical conductivity profile illustrated in figure 34. Superimposed is the actual response which is the Apollo 12 x-component of figure 37. This conductivity profile yields the best fit of eighty profiles which have been run to date, although it is not unique. The profile also yields theoretical responses which fit well for the measured tangential components of figure 37 and the components of fourteen other deep-lobe geomagnetic tail transients which have been processed to date.

Figure 39 illustrates an example of a neutral sheet crossing. Figure 40 shows analysis of the radial components of the magnetometer measurements, using the conductivity profile determined from deep-lobe measurements. A

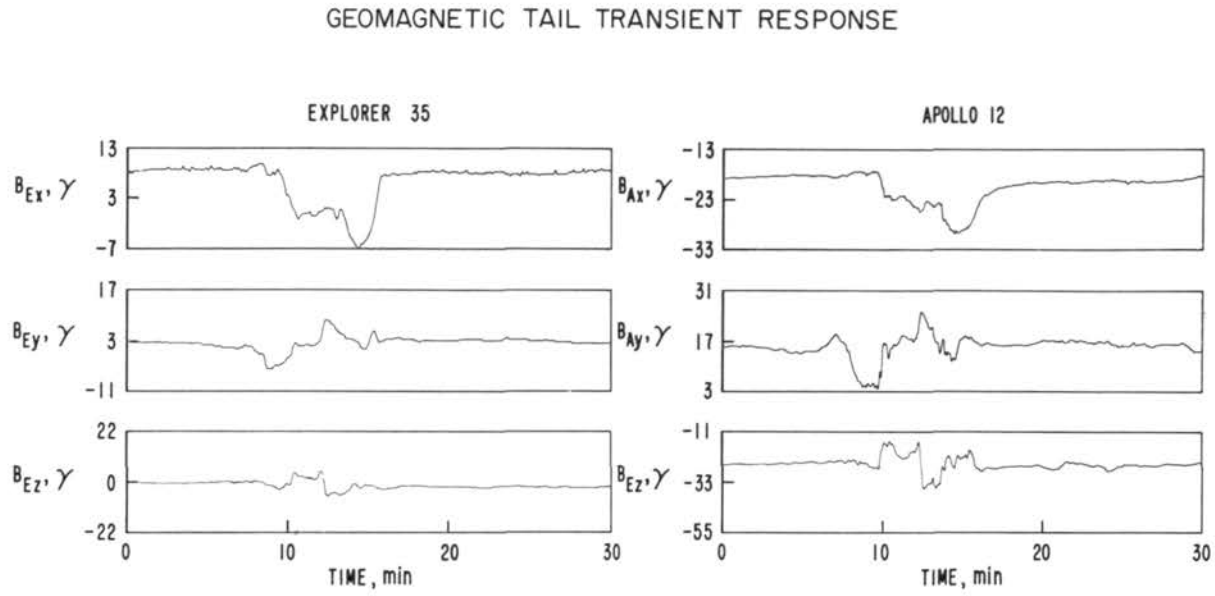


Figure 39.—*Another transient event, measured in the plasma sheet of the geomagnetic tail. Details concerning the data are given in the figure 37 caption.*

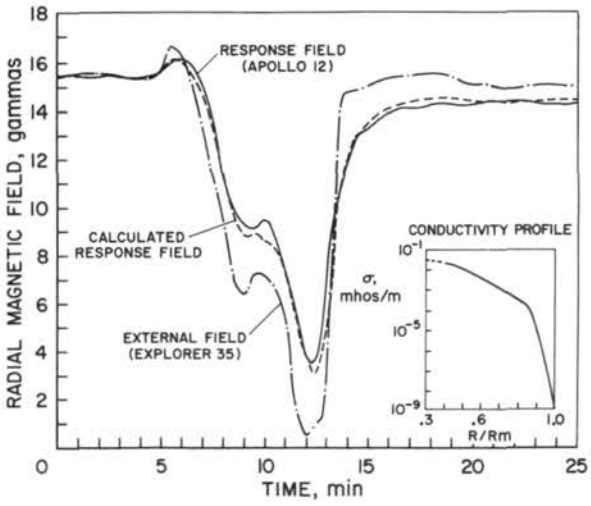


Figure 40.—*Electrical conductivity analysis for the transient event measured in the plasma sheet of the geomagnetic tail. Shown are data from the radial component of the event of figure 39. Response to the Explorer 35 external field radial component is computed numerically for the conductivity profile shown in the insert and compared with the measured Apollo 12 response field.*

qualitative fit of the data can be seen. It is surprising that these few selected neutral sheet data events are in such good agreement with the deep-lobe events. An explanation of this will require further analysis.

Figure 34 shows a plot of the conductivity profile derived from deep-lobe geomagnetic field transient events, superimposed on the conductivity profiles derived from nightside transient-response data in the solar wind (ref. 45). The results are in general agreement. The geomagnetic tail conductivity profile is not unique; rather, it is one of a family of profiles, which results from the geomagnetic tail transient response analysis. The range of profiles from the geomagnetic tail analysis is approximately that of the nightside analysis shown by the shaded region in figure 34. In the future many more geomagnetic transient events will be processed to determine a range of conductivity profiles consistent with a large data set.

LUNAR TEMPERATURE PROFILES FROM CONDUCTIVITY ANALYSES

From an electrical conductivity profile the internal temperature distribution of the Moon can be inferred for an assumed lunar material composition (ref. 105). Electrical conduc-

tivity measurements are particularly useful for determination of lunar temperature because of the strong dependence of conductivity on the temperature of geological materials. The conductivity σ and temperature T of geological materials can be described by an equation of the form

$$\sigma = \Sigma_i E_i \exp\ (-a_i/kT) \qquad (19)$$

where a_i represents the activation energies of impurity, intrinsic, and ionic conduction modes; E_i indicates material-dependent, temperature-independent constants; and k is Boltzmann's constant. Laboratory analyses relating conductivity to temperature for various minerals which are good geochemical candidates for the lunar interior, have been conducted by many investigators (e.g., refs. 106–110). These laboratory investigations have been designed to determine a_i and E_i of equation (19) and effects on these constants produced by the physical and chemical state of minerals. Duba (ref. 108) measured the conductivity of single olivine crystals as a function of temperature, pressure, and fayalite content. He concluded that conductivity was highly dependent on the oxidation state of the iron at temperatures below 1100° C. Later Duba and Nicholls (ref.111) reported that the conductivity of a single olivine crystal under an oxygen fugacity of 10^{-12} atm was almost three orders of magnitude lower than its conductivity measured in air. This decrease was attributed to the reduction of Fe^{3+} to Fe^{2+} in the sample. Duba et al. (ref. 110) measured the conductivity of olivine as a function of temperature up to 1440° C under controlled oxygen fugacity and found the measurements to be essentially pressure independent (up to 8 kbars). These recent measurements for olivine by Duba et al. were used to convert conductivity profiles in figure 34 labeled nightside results and geomagnetic tail results, respectively, to temperature profiles numbered 1 and 2 in figure 41. Also included in figure 41, for comparison, are profiles resulting from thermal history calculations of two other investigators. One must be aware that large uncertainties in the lunar temperature profile will remain until more definitive laboratory and space measurements are completed.

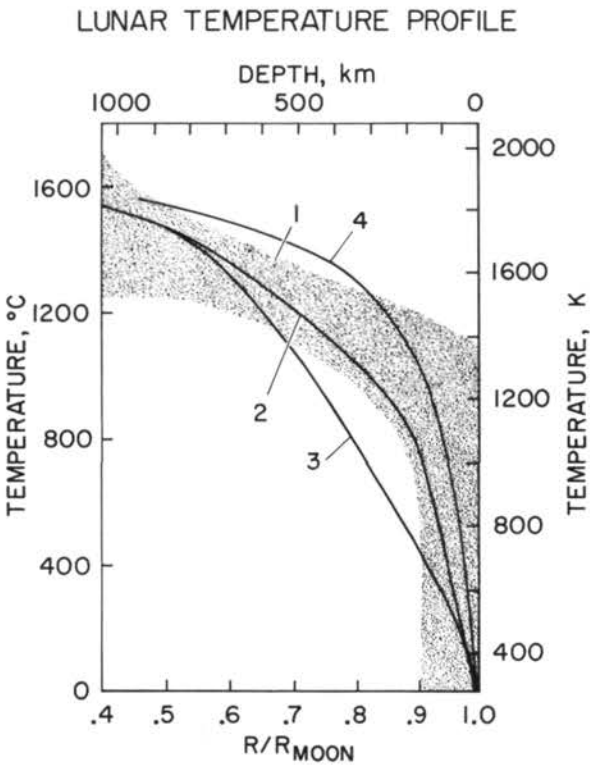


Figure 41.—*Comparison of lunar temperature profiles calculated by different investigators. 1: Temperature profile calculated from the "nightside" conductivity profile shown in figure 34, by use of laboratory data relating conductivity to temperature for olivine (ref. 110). 2: Profile calculated from the "geomagnetic tail" conductivity profile of figure 26 and the data from Duba et al. (ref. 110). 3,4: Temperature profiles from thermal history calculations of Toksöz (ref. 98) and Hanks and Anderson (ref. 119).*

Measurements of the Magnetopause and Bow Shock

With the use of simultaneous data from magnetometers on the lunar surface and in orbit around the Moon, the velocity and thickness of the Earth's magnetopause and bow shock (see fig. 42) have been measured at the lunar orbit. The boundary crossings are measured simultaneously by the Apollo 12

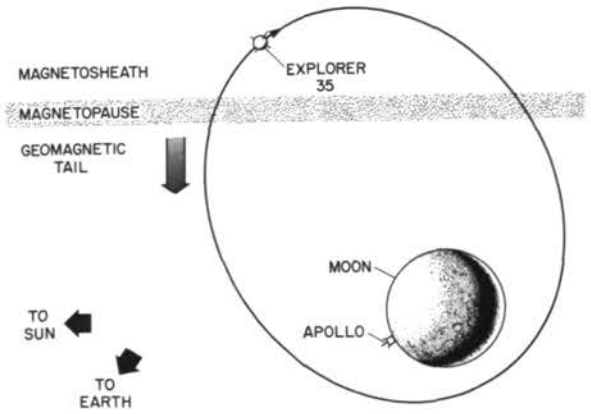


Figure 42.—*Schematic diagram depicting a crossing of the magnetosphere boundary layer (the magnetopause) past the Moon. Velocity of the layer is determined by using arrival-time difference measurements at the two instruments along with known distances between the instruments along the direction of travel of the magnetopause.*

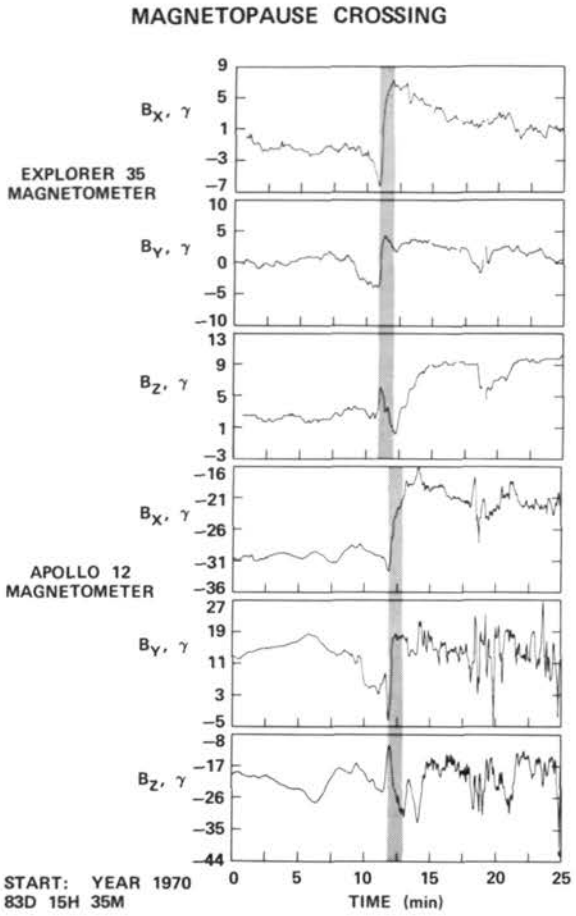


Figure 43.—*Magnetopause crossing, measured by the Apollo 12 lunar surface magnetometer and the lunar orbiting Ames Explorer 35 magnetometer. Data are expressed in the lunar surface coordinate system which has its origin at the Apollo 12 magnetometer site; x is directed radially outward from the surface, while* y *and* z *are tangent to the surface, directed eastward and northward, respectively. Shaded regions show arrival times at the two instruments.*

lunar surface magnetometer and the lunar orbiting Explorer 35 magnetometer (fig. 43 shows an example of a magnetopause crossing). Assuming that the plane of a passing boundary layer is perpendicular to the solar ecliptic plane and that the boundary layer moves along its normal at the lunar orbit, the velocity of the layer is measured from arrival-time difference measurements and the known separation of the two magnetometers. In addition, the thickness of the bow shock and magnetopause are estimated by use of the calculated boundary speeds and the signature of the boundary in the magnetometer data. Measurements of the magnetospheric boundaries at the lunar orbit are pertinent to a complete understanding of the magnetic and plasma environment during each part of the Moon's orbit. Of particular current interest, is the interaction of the solar plasma with the moon as a particle-absorbing body (refs. 112 and 113), with the lunar ionsphere (refs. 114, 115, and 116), with the lunar remanent magnetic fields (refs. 25, 29, and 117), and with the induced lunar magnetosphere (refs. 51, 53, and 54).

To date, analysis has been carried out on seven evening and fifteen morning magnetopause crossings, and one evening and ten morning bow shock crossings (ref. 118). There appear to be no significant differences in the measured properties of the morning and evening boundaries at the lunar orbit, although statistics are limited. Elapsed-time data for shock and magnetopause motions, as measured by the magnetometers separated from each other by as much as 10^4 km, indicate that these boundaries are nearly always in motion and can have highly variable velocities. The magnetopause has an average

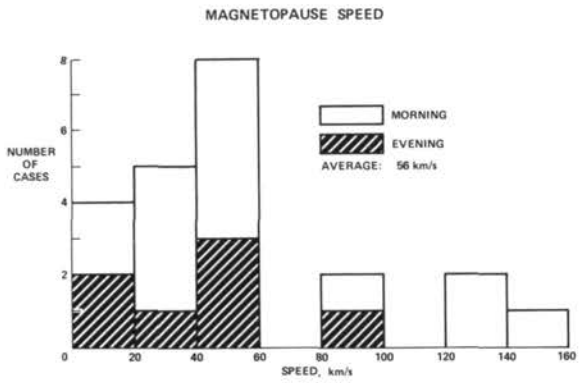


Figure 44.—*Magnetopause speed distribution for 15 morning and 7 evening magnetopause crossings.*

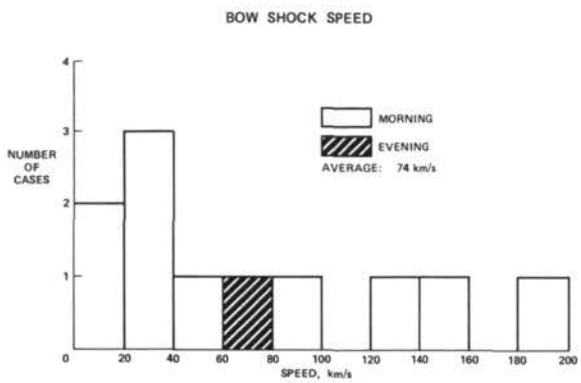


Figure 45.—*Bow shock speed distribution for 1 evening and 10 morning bow shock crossings.*

speed of about 50 kms/s but measurements vary from less than 10 km/s up to about 150 km/s (fig. 44). Similarly, the bow shock has an average speed of about 70 km/s but again there is a large spread in measured values from less than 10 km/s to about 200 km/s (fig. 45). The average measured magnetopause thickness is about 2300 km; however, individual magnetopause boundaries range from 500 km to 5000 km in thickness (fig. 46). The average bow shock thickness is determined to be about 1400 km, with a spread in individual values ranging from 220 km to 3000 km.

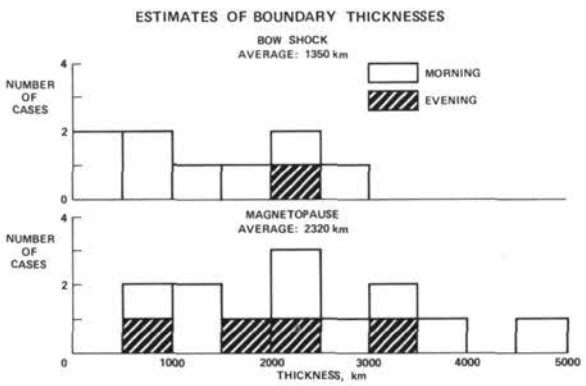


Figure 46.—*Boundary thickness distributions calculated for 9 bow shock and 13 magnetopause crossings.*

Summary

LUNAR REMANENT MAGNETIC FIELDS

Direct measurements of remanent fields have been made at nine sites on the lunar surface: 38 γ at Apollo 12 in Oceanus Procellarum; 103 γ and 43 γ at two Apollo 14 sites separated by 1.1 km in Fra Mauro; 3 γ at the Apollo 15 Hadley Rille site; and 189 γ, 112 γ, 327 γ, 113 γ, and 235 γ, respectively at five Apollo 16 sites in the Descartes region, over a distance of 7.1 km. Simultaneous data from Apollo surface magnetometers and solar wind spectrometers show that the remanent fields at the Apollo 12 and 16 sites are compressed by the solar wind. In response to a solar wind dynamic pressure increase of 1.5×10^{-7} dynes/cm^2, the 38-γ remanent field at the Apollo 12 LSM site is compressed to 54 γ, whereas the field at the Apollo 16 LSM site correspondingly increases from 235 γ to 265 γ. Scale sizes of fields at the Apollo 12 and 16 sites are determined from properties of the remanent field-plasma interaction and orbiting magnetometer measurements. The Apollo 12 field scale size L is in the range 2 km $\leq$ L $\leq$ 200 km, whereas for Apollo 16, 5 km $\leq$ L $\leq$ 100 km.

Measurements by Apollo lunar magnetometers, and remanance in the returned samples, have yielded strong evidence that the lunar crustal material is magnetized over

much of the lunar globe. The surface measurements indicate that fields tend to be stronger in highland regions than in mare regions. The origin of lunar remanent fields remains an enigma. Possibilities are generally grouped under three classifications: a strong external (solar or terrestrial) field, an ancient intrinsic field of global scale, and smaller localized field sources.

LUNAR MAGNETIC PERMEABILITY, INDUCED DIPOLE MOMENT, AND IRON ABUNDANCE

Simultaneous measurements by lunar magnetometers on the surface of the Moon and in orbit around the Moon are used to construct a whole-Moon hysteresis curve, from which the global lunar relative magnetic permeability is determined to be 1.012 $\pm$ 0.006. The global induced magnetization dipole moment corresponding to the permeability measurement is 2×10^{22}H cm^3 (where H is magnetizing field in gauss). For typical geomagnetic tail fields of H $\sim 10^{-4}$ gauss, the corresponding induced dipole moment is 2×10^{18} gauss-cm^3. Both error limits on magnetic permeability value are greater than 1.0, implying that the Moon as a whole is paramagnetic and/or weakly ferromagnetic. Assuming that the ferromagnetic component is free metallic iron of multidomain, noninteracting grains, the free iron abundance in the Moon is calculated to be 2.5 $\pm$ 2.0 wt.%. Total iron abundance in the moon is determined by combining free iron and paramagnetic iron components for two assumed lunar compositional models. For an orthopyroxene moon of overall density 3.34 g/cm^3 with free iron dispersed uniformly throughout the lunar interior, the total iron abundance is 12.8 $\pm$ 1.0 wt.%. For a free iron/olivine moon the total iron abundance is 5.5 $\pm$ 1.2 wt.%. Iron abundance results are summarized in table 3 and figure 29.

Lunar models with a small iron core and with an iron-rich layer have been investigated by using the measured global lunar permeability as a constraint. A small pure iron core of 500-km radius (the maximum size allowed by lunar density and moment of inertia measurements), which is hotter than the iron Curie point. ($T > T_c$), would not be resolvable from the data since its magnetization field would be small compared with the measured induced field. Similarly, an iron-rich layer in the Moon could not be resolved if the iron is paramagnetic, i.e., if the iron is above the iron Curie temperature. Gast and Giuli (ref. 99) have proposed a family of high-density-layer models for the Moon which are geochemically feasible. If these models are iron-rich layers lying near the lunar surface so that $T < T_c$, the ferromagnetic layers would yield a global permeability value well above the measured upper limit. Therefore, it is concluded that such shallow iron-rich-layer models are not consistent with magnetic permeability measurements.

LUNAR ELECTRICAL CONDUCTIVITY AND TEMPERATURE

The electrical conductivity of the lunar interior has been investigated by analyzing the induction of global lunar fields by time varying extralunar (solar or terrestrial) magnetic fields. An upper limit on the unipolar induction field has been determined which shows that at least the outer 5 km of the lunar crust is a relatively poor electrical conductor ($< 10^{-9}$ mhos/m) compared with the underlying material. Past conductivity analyses have used magnetometer data recorded at times when global eddy-current fields were asymmetrically confined by the solar wind plasma. A time-dependent, transient-response analytical technique has been used in the studies. Transient analysis using lunar nightside data yields a conductivity profile rising from a range of values lying between 1×10^{-4} and 2×10^{-3} mhos/m at 250-km depth in the Moon to values ranging between 2×10^{-3} and 8×10^{-2}/ mhos/m at 1000-km depth. Transient analysis of dayside data yields a conductivity profile generally compatible with nightside transient results.

Recent conductivity analysis has considered

lunar eddy-current response during times when the moon is in the geomagnetic tail, in order to minimize the analytical problems posed by asymmetric solar wind confinement of the induced lunar magnetosphere. Preliminary results show that the following conductivity profile, though not unique, is compatible with input and response data: the conductivity increases rapidly with depth, from 10^{-9} mhos/m at the surface to 10^{-4} mhos/m at 200-km, then less rapidly to 2×10^{-2} mhos/m at 1000-km depth. By use of the conductivity-to-temperature relationship for olivine reported by Duba et al. (ref. 110), a temperature profile is calculated from this conductivity profile: temperature rises rapidly with depth to 1100 K at 200-km depth, then less rapidly to 1800 K at 1000-km depth.

MAGNETOPAUSE AND BOW SHOCK PROPERTIES AT THE LUNAR ORBIT

Velocities and thicknesses of the Earth's magnetopause and bow shock at the lunar orbit have been estimated from simultaneous magnetometer measurements. Average speeds are about 50 km/s for the magnetopause and about 70 km/s for the bow shock, with large spreads in individual measured values. Average thicknesses are about 2300 km for the magnetopause and 1400 km for the bow shock, also with large spreads in individual measured values.

References

1. COLBURN, D. S., R. G. CURRIE, J. D. MIHALOV, AND C. P. SONETT, Diamagnetic Solar-Wind Cavity Discovered Behind the Moon. *Science*, Vol. 158, 1967, p. 1040.
2. NESS, N. F., K. W. BEHANNON, C. S. SCEARCE, AND S. C. CANTARANO, Early Results From the Magnetic Field Experiment on Explorer 35. *J. Geophys. Res.*, Vol. 72, 1967, p. 5769.
3. MICHEL, F. C., Magnetic Field Structure Behind the Moon. *J. Geophys. Res.*, Vol. 73, 1968, p. 1533.
4. SPREITER, J. R., M. C. MARSH, AND A. L. SUMMERS, Hydromagnetic Aspects of Solar Wind Flow Past the Moon. *Cosmic Electrodynamics*, Vol. 1, 1970, p. 5.
5. SONETT, C. P., AND D. S. COLBURN, Establishment of a Lunar Unipolar Generator and Associated Shock and Wake by the Solar Wind. *Nature*, Vol. 216, 1967, p. 340.
6. SONETT, C. P., AND D. S. COLBURN, The Principle of Solar Wind Induced Planetary Dynamo. *Phys. Earth Planet. Interiors*, Vol. 1, 1968, pp. 326–346.
7. NESS, N. F., Electrical Conductivity of the Moon (abs.). *Trans. Am. Geophys. Union*, Vol. 49, 1968, p. 242.
8. BEHANNON, K. W., Intrinsic Magnetic Properties of the Lunar Body. *J. Geophys. Res.*, Vol. 73, 1968, p. 7257.
9. NESS, N. F., *Electrical Conductivity and Internal Temperature of the Moon.* Goddard Space Flight Center Report X-616-69-191, 1969. (Also presented as paper k 11 at COSPAR, Prague, May 1969.)
10. DOLGINOV, SH. SH., E. G. EROSHENKO, L. N. ZHUZGOV, AND N. V. PUSHKOV, Investigation of the Magnetic Field of the Moon. *Geomagnetics and Aeronomy*, Vol. 1, 1961, p. 18.
11. DOLGINOV, SH. SH., E. G. EROSHENKO, L. N. ZHUZGOV, AND N. V. PUSHKOV, Measurements of the Magnetic Field in the Vicinity of the Moon by the Artificial Satellite Luna 10. *Akad. Nauk USSR, Doklady*, Vol. 170, 1966, p. 574.
12. GOLD, T., The Magnetosphere of the Moon. In *The Solar Wind*, R. J. Mackin, Jr., and M. Neugebauer, eds., Pergamon Press, New York, 1966.
13. SONETT, C. P., D. S. COLBURN, AND R. G. CURRIE, The Intrinsic Magnetic Field of the Moon. *J. Geophys. Res.*, Vol. 72, 1967, p. 5503.
14. DEWYS, J. N., Results and Implications of Magnetic Experiments on Surveyer 5, 6, and 7 Spacecrafts (abs.). *Trans. Am. Geophys. Union*, Vol. 49, 1968, p. 249.
15. STRANGWAY, D. W., E. E. LARSON, AND G. W. PEARCE, Magnetic Studies of Lunar Samples —Breccia and Fines. *Proc. Apollo 11 Lunar Science Conference, Geochimica et Cosmochimica Acta*, Supplement 1, Vol. 3, A. A. Levinson, ed., 1970, p. 2435.
16. RUNCORN, S. K., D. W. COLLINSON, W. O'REILLY, M. H. BATTEY, A. A. STEPHENSON, J. M. JONES, A. J. MANSON, AND P. W. READMAN, Magnetic Properties of Apollo 11 Lunar Samples. *Proc. Apollo 11 Lunar Science Conference, Geochimica et Cosmochimica Acta*, Supplement 1, Vol. 3, A. A. Levinson, ed., 1970, p. 2369.
17. PEARCE, G. W., D. W. STRANGWAY, AND E. E. LARSON, Magnetism of Two Apollo 12 Igneous Rocks. *Proc. Second Lunar Science Conference, Geochimica et Cosmochimica Acta*, Supplement 2, Vol. 3, 1971, p. 2451.

18. NAGATA, T., R. M. FISHER, F. C. SCHWERER, M. D. FULLER, AND J. R. DUNN, Magnetic Properties and Remanent Magnetization of Apollo 12 Lunar Materials and Apollo 11 Lunar Microbreccia. *Proc. Second Lunar Science Conference, Geochimica et Cosmochimica Acta*, Supplement 2, Vol. 3, 1971, p. 2461.
19. NAGATA, T., R. M. FISHER, F. C. SCHWERER, M. D. FULLER, AND J. R. DUNN, Rock Magnetism of Apollo 14 and 15 Materials. *Proc. Third Lunar Science Conference, Geochimica et Cosmochimica Acta*, Supplement 3, Vol. 3, 1972, p. 2423.
20. COLLINSON, D. W., A. STEPHENSON, AND S. K. RUNCORN, Magnetic Properties of Apollo 15 and 16 Rocks. *Proc. Fourth Lunar Science Conference, Geochimica et Cosmochimica Acta*, Supplement 4, Vol. 3, 1973, p. 2963.
21. PEARCE, G. W., W. A. GOSE, AND D. W. STRANGWAY, Magnetic Studies on Apollo 15 and 16 Lunar Samples. *Proc. Fourth Lunar Science Conference, Geochimica et Cosmochimica Acta*, Supplement 4, Vol. 3, 1973, pp. 3045–3076.
22. GOSE, W. A., D. W. STRANGWAY, AND G. W. PEARCE, A Determination of the Intensity of the Ancient Lunar Magnetic Field. *The Moon*, Vol. 7, 1973, pp. 196–201.
23. DYAL, P., C. W. PARKIN, AND C. P. SONETT, Apollo 12 Magnetometer: Measurement of a Steady Magnetic Field on the Surface of the Moon. *Science*, Vol. 169, 1970, p. 726.
24. BARNES, A., P. CASSEN, J. D. MIHALOV, AND A. EVIATAR, Permanent Lunar Surface Magnetism and its Deflection of the Solar Wind. *Science*, Vol. 171, 1971, pp. 716–718.
25. MIHALOV, J. D., C. P .SONETT, J. H. BINSACK, AND MOUTSOULAS, Possible Fossil Lunar Magnetism Inferred From Satellite Data. *Science*, Vol. 171, 1971, p. 892.
26. COLEMAN, P. J., JR., B. R. LICHTENSTEIN, C. T. RUSSELL, L. R. SHARP, AND G. SCHUBERT, Magnetic Fields Near the Moon. *Proc. Third Lunar Science Conference, Geochimica et Cosmochimica Acta*, Supplement 3, Vol. 3, D. R. Criswell, ed., 1972, pp. 2271–2286.
27. SHARP, L. R., P. J. COLEMAN, JR., B. R. LICHTENSTEIN, AND C. T. RUSSELL, Orbital Mapping of the Lunar Magnetic Field. *The Moon*, Vol. 7, 1973, p. 322.
28. RUSSELL, C. T., P. J. COLEMAN, JR., B. R. LICHTENSTEIN, G. SCHUBERT, AND L. R. SHARP, Subsatellite Measurements of the Lunar Magnetic Field. *Proc. Fourth Lunar Science Conference, Geochimica et Cosmochimica Acta*, Supplement 4, Vol. 3, W. A. Gose, ed., 1973, pp. 2833–2845.
29. DYAL, P., C. W. PARKIN, C. W. SNYDER, AND D. R. CLAY, Measurements of Lunar Magnetic Field Interaction With the Solar Wind. *Nature*, Vol. 236, 1972, pp. 381–385.
30. CLAY, D. R., B. E. GOLDSTEIN, M. NEUGEBAUER, AND C. W. SNYDER, Solar-Wind Spectrometer Experiment. *Apollo 15 Preliminary Science Report*, NASA SP–289, 1972, pp. 10–1 to 10–7.
31. DYAL, P., AND C. W. PARKIN, The Magnetism of the Moon. *Sci. Amer.*, Vol. 225, 1971, pp. 62–73.
32. PARKIN, C. W., W. D. DAILY, AND P. DYAL, Iron Abundance in the Moon. *Proc. Fifth Lunar Science Conference, Geochimica et Cosmochima Acta*, Vol. 3, 1974.
33. PARKIN, C. W., W. D. DAILY, AND P. DYAL, Lunar Iron Abundance From Magnetometer Measurements. *Lunar Science*, Vol. V, Part II, Lunar Science Institute, Houston, 1974, p. 589.
34. RUSSELL, C. T., P. J. COLEMAN, JR., B. R. LICHTENSTEIN, AND G. SCHUBERT, Permanent and Induced Magnetic Dipole Moment of the Moon. *Proc. Fifth Lunar Science Conference, Geochimica et Cosmochimica Acta*, Supplement 5, Vol. 3, W. A. Gose, ed., in press, 1974.
35. SCHWARTZ, K., AND G. SCHUBERT, Time-Dependent Lunar Electric and Magnetic Fields Induced by a Spatially Varying Interplanetary Magnetic Field. *J. Geophys. Res.*, Vol. 74, 1969, pp. 4777–4780.
36. SCHUBERT, G., AND K. SCHWARTZ, A Theory for the Interpretation of Lunar Surface Magnetometer Data. *The Moon*, Vol. 1, 1969, p. 106.
37. SILL, W. R., AND J. L. BLANK, Method for Estimating the Electrical Conductivity of the Lunar Interior. *J. Geophys. Res.*, Vol. 75, 1970, p. 201.
38. DYAL, P., AND C. W. PARKIN, The Apollo 12 Magnetometer Experiment: Internal Lunar Properties From Transient and Steady Magnetic Field Measurements. *Proc. Second Lunar Science Conference, Geochimica et Cosmochimica Acta*, Supplement 2, Vol. 3, 1971, p. 2391.
39. SMYTHE, W. R., *Static and Dynamic Electricity*. McGraw-Hill Book Co., New York, 1950.
40. WAIT, J. R., A Conducting Sphere in a Time Varying Magnetic Field. *Geophysics*, Vol. 16, 1951, p. 666.
41. TOZER, D. C., AND J. WILSON, The Electrical Conductivity of the Moon's Interior. *Proc. Roy. Soc. London*, Vol. A296, 1967, p. 320.
42. BLANK, J. L., AND W. R. SILL, Response of the Moon to the Time-Varying Interplanetary Magnetic Field. *J. Geophys. Res.*, Vol. 74, 1969, pp. 736–743.
43. DYAL, P., AND C. W. PARKIN, Electrical Conductivity and Temperature of the Lunar Interior From Magnetic Transient-Response

Measurements. *J. Geophys. Res.*, Vol. 76, 1971, pp. 5947–5969.

44. SILL, W. R., Lunar Conductivity Models From the Apollo 12 Magnetometer Experiment. *The Moon*, Vol. 4, 1972, pp. 3–17.
45. DYAL, P., C. W. PARKIN, AND W. D. DAILY, Surface Magnetometer Experiments: Internal Lunar Properties. *Proc. Fourth Lunar Science Conference, Geochimica et Cosmochimica Acta*, Supplement 4, Vol. 3, W. A. Gose, ed., 1973, pp. 2229–2945.
46. SONETT, C. P., G. SCHUBERT, B. F. SMITH, K. SCHWARTZ, AND D. S. COLBURN, Lunar Electrical Conductivity From Apollo 12 Magnetometer Measurements: Compositional and Thermal Inferences. *Proc. Second Lunar Science Conference, Geochimica et Cosmochimica Acta*, Supplement 2, Vol. 3, 1971, pp. 2415–2431.
47. SONETT, C. P., D. S. COLBURN, B. F. SMITH, G. SCHUBERT, AND K. SCHWARTZ, The Induced Magnetic Field of the Moon: Conductivity Profiles and Inferred Temperature. *Proc. Third Lunar Science Conference, Geochimica et Cosmochimica Acta*, Supplement 3, Vol. 3, 1972, p. 2309.
48. KUCKES, A. F., Lunar Electrical Conductivity Profile. *Nature*, Vol. 232, 1971, p. 249.
49. HOBBS, B. A., The Inverse Problem of the Moon's Electrical Conductivity. *Earth Planet. Sci. Letters*, Vol. 17, 1973, pp. 380–384.
50. REISZ, A. C., D. L. PAUL, AND T. R. MADDEN, The Effects of Boundary Condition Asymmetrics on the Interplanetary Magnetic Field-Moon Interaction. *The Moon*, Vol. 4, 1972, pp. 134–140.
51. DYAL, P., AND C. W. PARKIN, Global Electromagnetic Induction in the Moon and Planets. *Phys. Earth Planet. Interiors*, Vol. 7, 1973, p. 251.
52. SCHUBERT, G., K. SCHWARTZ, C. P. SONETT, D. S. COLBURN, AND B. F. SMITH, Lunar Electromagnetic Scattering II. Magnetic Fields and Transfer Functions for Parallel Propagation. *Proc. Fourth Lunar Science Conference, Geochimica et Cosmochimica Acta*, Supplement 4, Vol. 3, W. A. Gose, ed., 1973, pp, 2909–2923.
53. SMITH, B. F., D. S. COLBURN, G. SCHUBERT, K. SCHWARTZ, AND C. P. SONETT, Induced Magnetosphere of the Moon 2. Experimental Results From Apollo 12 and Explorer 35. *J. Geophys. Res.*, Vol. 78, 1973, pp. 5437–5448.
54. SCHUBERT, G., C. P. SONETT, K. SCHWARTZ, AND H. J. LEE, Induced Magnetosphere of the Moon I. Theory. *J. Geophys. Res.*, Vol. 78, 1973, pp. 2094–2110.
55. DYAL, P., C. W. PARKIN, AND C. P. SONETT, Lunar Surface Magnetometer. *IEEE Trans. on Geoscience Electrons*, Vol. GE–8(4), 1970.
56. GORDON, D. I., R. H. LUNDSTEN, AND R. A. CHIRADO, Factors Affecting the Sensitivity of Gamma-Level Ring-Core Magnetometers. *IEEE Trans. on Magnetics*, Vol. MAG–1(4), 1965, p. 330.
57. GEYGER, W. A., *Nonlinear-Magnetic Control Devices*. McGraw-Hill Book Co., New York, 1964.
58. SONETT, C. P., D. S. COLBURN, R. G. CURRIE, AND J. D. MIHALOV, The Geomagnetic Tail: Topology, Reconnection and Interaction With the Moon. In *Physics of the Magnetosphere*, R. L. Carovillano, J. F. McClay, and H. R. Radoski, eds., D. Reidel Publishing Co., Dordrecht, Holland, 1967.
59. COLEMAN, P. J., JR., G. SCHUBERT, C. T. RUSSELL, AND L. R. SHARP, The Particles and Fields Subsatellite Magnetometer Experiment. *Apollo 15 Preliminary Science Report*, NASA SP–289, 1972, pp. 22–1 to 22–9.
60. COLEMAN, P. J., JR., B. R. LICHTENSTEIN, C. T. RUSSELL, G. SCHUBERT, AND L. R. SHARP, The Particles and Fields Subsatellite Magnetometer Experiment. *Apollo 16 Preliminary Science Report*, NASA SP–315, 1972, pp. 23–1 to 23–13.
61. MIHALOV, J. D., D. S. COLBURN, R. G. CURRIE, AND C. P. SONETT, Configuration and Reconnection of the Geomagnetic Tail. *J. Geophys. Res.*, Vol. 73, 1968, p. 943.
62. HINNERS, N. W., The New Moon: A View. *Rev. Geophys. and Space Phys.*, Vol. 9, 1971, p. 447.
63. NAGATA, T., R. M. FISHER, AND F. C. SCHWERER, Lunar Rock Magnetism. *The Moon*, Vol. 4, 1972.
64. STRANGWAY, D. W., H. N. SHARP, W. A. GOSE, AND G. W. PEARCE, Magnetism and the Early History of the Moon. *Geochimica et Cosmochimica Acta*, Supplement 4, Vol. 37, in press, 1973.
65. FULLER, M., Lunar Magnetism. *Rev. Geophys. and Space Sci.*, in press, 1974.
66. SONETT, C. P., AND J. D. MIHALOV, Lunar Fossil Magnetism and Perturbations of the Solar Wind. *J. Geophys. Res.*, Vol. 77, 1972, p. 588.
67. STRANGWAY, D. W., W. A. GOSE, G. W. PEARCE, AND R. K. MCCONNELL, Lunar Magnetic Anomalies and the Clayey Formation. *Nature*, Vol. 246, 1973, p. 112.
68. WOOD, J. A., Thermal History and Early Magnetism in the Moon. *Icarus*, Vol. 16, 1972, pp. 229–240.
69. STRANGWAY, D. W., AND H. A. SHARP, Lunar Magnetism and an Early Cold Moon. *Nature*, Vol. 249, 1974, p. 227.
70. DYAL, P., C. W. PARKIN, C. P. SONETT, R. L. DUBOIS, AND G. SIMMONS, Lunar Portable Magnetometer Experiment. *Apollo 14 Preliminary Science Report*, NASA SP–272, 1971, pp. 227-237.

71. STRANGWAY, D. W., W. A. GOSE, G. W. PEARCE, AND J. G. CARNES, Magnetism and the History of the Moon. *Proc. 18th Annual Conference on Magnetism and Magnetic Material, J. Appl. Phys.*, in press, 1973.
72. DYAL, P., C. W. PARKIN, AND W. D. DAILY, Magnetism and the Interior of the Moon. Submitted to *Rev. Geophys. Space Phys.*, 1974.
73. SONETT, C. P., D. S. COLBURN, AND K. SCHWARTZ, Electrical Heating of Meteorite Parent Bodies and Planets by Dynamo Induction From Premain Sequence, T Tauri Solar Wind. *Nature*, Vol. 219, 1968, p. 924.
74. HELSLEY, C. E., Magnetic Properties of Lunar 10022, 10069, 10084, and 10085 Samples. *Proc. Apollo 11 Lunar Science Conference, Geochimica et Cosmochimica Acta*, Supplement 1, Vol. 3, 1970, p. 2213.
75. RUNCORN, S. K., D. W. COLLINSON, W. O'REILLY, A. STEPHENSON, M. H. BATTEY, A. J. MANSON, AND P. W. READMAN, Magnetic Properties of Apollo 12 Lunar Samples. *Proc. Roy. Soc. London, Ser. A*, Vol. 325, 1971, p. 157.
76. STRANGWAY, D. W., G. W. PEARCE, W. A. GOSE, AND R. W. TIMME, Remanent Magnetization of Lunar Samples. *Earth Planet. Sci. Letters*, Vol. 13, 1971, p. 43.
77. LEVY, E. H., Magnetic Dynamo in the Moon: A Comparison With Earth. *Science*, Vol. 178, 1972, p. 52.
78. UREY, H., AND S. K. RUNCORN, A New Theory of Lunar Magnetism. *Science*, Vol. 180, 1973, p. 636.
79. MURTHY, V. R., AND S. K. BANERJEE, Lunar Evolution: How Well Do We Know it Now. *The Moon*, Vol. 7, 1973, p. 149.
80. SMOLYCHOWSKI, R., Magnetism of the Moon. *The Moon*, Vol. 7, 1973, p. 127.
81. SCHUBERT, G., B. F. SMITH, C. P. SONETT, D. S. COLBURN, AND K. SCHWARTZ, Polarized Magnetic Field Fluctuations at the Site of Apollo 15: Possible Regional Influence on Lunar Induction. Submitted to *Science*, 1974.
82. NAGATA, T., Y. ISHIKAWA, H. KINOSHITA, M. KONO, Y. SYONO, AND R. M. FISHER, Magnetic Properties and Natural Remanent Magnetization of Lunar Materials. *Proc. Apollo 11 Lunar Science Conference, Geochimica et Cosmochimica Acta*, Supplement 1, Vol. 3, 1970, p. 2325.
83. CAP, F. F., Possible Production Mechanisms of Lunar Magnetic Fields. *J. Geophys. Res.*, Vol. 77, 1972, pp. 3328–3333.
84. DYAL, P., C. W. PARKIN, AND C. P. SONETT, Lunar Surface Magnetometer Experiment. *Apollo 12 Preliminary Science Report*, NASA SP–235, 1970, pp. 55–73.
85. PARKIN, C. W., P. DYAL, AND W. D. DAILY, Iron Abundance in the Moon From Magnetometer Measurements. *Proc. Fourth Lunar Science Conference, Geochimica et Cosmochimica Acta*, Supplement 4, Vol. 3, 1973, p. 2947.
86. ELLWOOD, W. B., A New Ballistic Galvanometer Operating in High Vacuum. *Rev. Sci. Inst.*, Vol. 5, 1934, pp. 300–305.
87. LINDEMAN, R., J. W. FREEMAN, JR., AND R. R. VONDRAK, Ions From the Lunar Atmosphere. *Proc. Fourth Lunar Science Conference, Geochimica et Cosmochimica Acta*, Supplement 4, Vol. 3, 1973, p. 2889.
88. UREY, H. C., *The Moon*. Z. Kopal and Z. K. Mikhailov, eds., Academic Press, 1962, p. 133.
89. REYNOLDS, R. T., AND A. L. SUMMERS, Calculations on the Composition of the Terrestrial Planets. *J. Geochim. Res.*, Vol. 74, 1969, p. 2494.
90. UREY, H. C., AND G. J. F. MACDONALD, Origin and History of the Moon. *Physics and Astronomy of the Moon*, Z. Kopal, ed., Academic Press, 1971, p. 213.
91. WÄNKE, H., H. BADDENHAUSEN, G. DREIBUS, M. QUIJANO-RICO, M. PALME, B. SPETTEL, AND F. TESCHKE, Multi-Element Analysis of Apollo 16 Samples and About the Composition of the Whole Moon. *Lunar Science*, Vol. IV, J. W. Chamberlain and C. Watkins, eds., Lunar Science Institute, Houston, 1973, pp. 761–763.
92. ZUSSMAN, J., The Minerology, Petrology and Geochemistry of Lunar Samples—A Review. *The Moon*, Vol. 5, 1972, p. 422.
93. WEEKS, R. A., Magnetic Phases in Lunar Material and Their Electron Magnetic Resonance Spectra: Apollo 14. *Proc. Third Lunar Science Conference, Geochimica et Cosmochimica Acta*, Supplement 3, Vol. 3, 1972, p. 2503.
94. UREY, H. C., K. MARTI, J. W. HANKINS, AND M. K. LIU, Model History of the Lunar Surface. *Proc. Second Lunar Science Conference, Geochimica et Cosmochimica Acta*, Supplement 2, Vol. 3, 1971, p. 987.
95. WOOD, J. A., J. S. DICKEY, U. B. MARVIN, AND B. J. POWELL, *Proc. Apollo 11 Lunar Science Conference, Geochimica et Cosmochimica Acta*, Supplement 1, Vol. 1, 1970, p. 965.
96. RINGWOOD, A. E., AND E. ESSENE, Petrogenesis of Lunar Basalts and the Internal Constitution and Origin of the Moon. *Science*, Vol. 167, 1970, pp. 607–610.
97. GREEN, D. H., A. E. RINGWOOD, N. G. WARE, W. O. HIBBERSON, A. MAJOR, AND E. KISS, Experimental Petrology and Petrogenesis of Apollo 12 Basalts. *Proc. Second Lunar Science Conference, Geochimica et Cosmochimica Acta*, Supplement 2, Vol. 1, A. A. Levinson, ed., 1971, pp. 601–615.

98. TOKSÖZ, M. N., Geophysical Data and the Interior of the Moon. *Ann. Rev. of Earth and Planet. Sci.*, Vol. 2, in press, 1973.
99. GAST, P. W., AND R. T. GIULI, Density of the Lunar Interior. *Earth Planet. Sci. Letters*, Vol. 16, 1972, p. 299.
100. DYAL, P., C. W. PARKIN, C. P. SONETT, AND D. S. COLBURN, *Electrical Conductivity and Temperature of the Lunar Interior From Magnetic Transient Response Measurements.* NASA TM X-62,012, 1970.
101. DYAL, P., C. W. PARKIN, AND W. D. DAILY, Temperature and Electrical Conductivity of the Lunar Interior From Magnetic Transient Measurements in the Geomagnetic Tail. *Proc. Fifth Lunar Science Conference, Geochimica et Cosmochimica Acta*, in press, 1974.
102. DYAL, P., C. W. PARKIN, AND P. CASSEN, Surface Magnetometer Experiments: Internal Lunar Properties and Lunar Surface Interactions With the Solar Plasma. *Proc. Third Lunar Science Conference, Geochimica et Cosmochimica Acta*, Supplement 3, Vol. 3, D. R. Criswell, ed., 1972, p. 2287.
103. SCHWARTZ, K., AND G. SCHUBERT, Lunar Electromagnetic Scattering, 1: Propagation Parallel to the Diamagnetic Cavity Axis. *J. Geophys. Res.*, Vol. 78, 1973, pp. 6496–6506.
104. PARKER, E. N., *Space Sci. Rev.*, Vol. 1, 1962, p. 62.
105. RIKITAKE, T., *Electromagnetism and the Earth's Interior.* Elsevier, Amsterdam, 1966.
106. ENGLAND, A. W., G. SIMMONS, AND D. STRANGWAY, Electrical Conductivity of the Moon. *J. Geophys. Res.*, Vol. 73, 1968, p. 3219.
107. DUBA, A., H. C. HEARD, AND R. N. SCHOCK, The Lunar Temperature Profile. *Earth Planet. Sci. Letters*, Vol. 15, 1972, p. 301.
108. DUBA, A., Electrical Conductivity of Olivine. *J. Geophys. Res.*, Vol. 77, 1972, p. 2483.
109. DUBA, A., AND A. E. RINGWOOD, Electrical Conductivity, Internal Temperatures and Thermal Evolution of the Moon. *The Moon*, Vol. 7, 1973, p. 356.
110. DUBA, A., H. C. HEARD, AND R. N. SCHOCK, Electrical Conductivity of Olivine at High Pressure and Under Controlled Oxygen Fugacity. *J. Geophys. Res.*, Vol. 79, 1974, p. 1667.
111. DUBA, A., AND I. A. NICHOLLS, The Influence of Oxidation State on the Electrical Conductivity of Olivine. *Earth Planet. Sci. Letters*, Vol. 18, 1973, pp. 59–64.
112. ANDERSON, K. A., L. M. CHASE, R. P. LIN, J. E. MCCOY, AND R. E. MCGUIRE, Solar-Wind and Interplanetary Electron Measurements on the Apollo 15 Subsatellite. *J. Geophys. Res.*, Vol. 77, 1972, pp. 4611–4626.
113. GEISS, J., F. BUHLER, H. CERUTTI, AND P. EBERHARDT, Solar Wind Composition Experiment. *Apollo 15 Preliminary Science Report*, NASA SP-289, 1972, pp. 15–1 to 15–7.
114. CRISWELL, D. R., Photoelectrons and Solar Wind/Lunar Limb Interaction. *The Moon*, Vol. 7, 1973, p. 202.
115. MANKA, R. H., AND F. C. MICHEL, Lunar Ion Energy Spectra and Surface Potential. *Proc. Fourth Lunar Science Conference, Geochimica et Cosmochimica Acta*, Supplement 4, Vol. 3, W. A. Gose, ed., 1973, pp. 2897–2908.
116. RICH, F. J., D. L. REASONER, AND W. J. BURKE, Plasma Sheet at Lunar Distance: Characteristics and Interactions With the Lunar Surface. *J. Geophys. Res.*, Vol. 78, 1973, pp. 8097–8112.
117. NEUGEBAUER, M., C. W. SNYDER, D. R. CLAY, AND B. E. GOLDSTEIN, Solar Wind Observations on the Lunar Surface With the Apollo 12 ALSEP. *Planetary and Space Sci.*, Vol. 20, 1972, pp. 1577–1591.
118. DAILY, W. D., P. DYAL, AND C. W. PARKIN, Magnetopause Velocity and Thickness From a Network of Apollo Magnetometers (abs.). *Trans. Amer. Geophys. Union (EOS)*, Vol. 55, 1974, p. 390.
119. HANKS, T. C., AND D. L. ANDERSON, Origin, Evolution, and Present Thermal State of the Moon. *Phys. Earth Planet. Interiors*, Vol. 5, 1972, pp. 409–425.

Page intentionally left blank

Page intentionally left blank

On the Mechanism of the Magnetic Dynamo of the Planets

Sh. Sh. Dolginov
Academy of Sciences,
Moscow, U.S.S.R.

Results of testing the effectiveness of the theory of precessional dynamos in the generation of the magnetic fields of the planets are presented. It is shown that the magnetic state of Earth and of the planets Mars, Jupiter, and Venus can be satisfactorily described by the formula

$$H_i = H_3 \frac{V_i}{V_3} \frac{T_3}{T_i} \frac{\Omega_i}{\Omega_3} \frac{\sin\alpha_i}{\sin\alpha_3}$$

where H, v, T, Ω, and α are the dipole fields, volumes of liquid cores, periods of rotation, rates of precession, and angles between precession vector and angular rotation, respectively, for the planets and Earth. The v_i corresponds to known models of the internal structure. It is shown that the magnetic state of Mercury satisfies this formula if the dynamic flattening of the planet $f = 5.7 \times 10^{-5} - 8.3 \times 10^{-5}$.

The idea that the magnetic field of the Earth is related to the operation of some sort of dynamo mechanism in its highly conductive liquid core has now been largely confirmed.

Modern kinematic models of the terrestrial magnetic dynamo have been found capable of describing the basic peculiarities of the terrestrial magnetic field (refs. 1 and 2). At the same time, no physical theory of the terrestrial field as yet presented considers the actual parameters and processes in the core of the Earth. This is particularly true concerning the uncertainty of the mechanism generating the terrestrial dynamo. Three mechanisms are known:

1. Convection in the core under the influence of thermal sources (refs. 3 and 4).
2. Convection under the influences of forces of gravity (ref. 5).
3. Convection in the core caused by precession of the axis of rotation of the Earth (refs. 6 and 7).

With a model of a purely iron-nickel core, the radioactive elements U and Th are forced out because of their chemical and physical incompatibility with iron at the pressures present in the core. Thermal sources in the core have been related to processes of continuing differentiation of matter in the Earth: the settling of heated iron, melted from the mantle (ref. 3) and the latent heat of melting, liberated upon crystallization of the outer core at the boundary with the inner solid core (ref. 4).

In order for thermal convection to occur in the liquid core of the Earth, the temperature gradient must exceed the adiabatic gradient. In a number of publications during 1971–1973 (ref. 8), concepts of the isothermal state of the core were discussed. A stable thermal state is incompatible with thermal convection in the core, to which the generation of the magnetic field is related. Ideas of the thermal conditions of the Earth's core have changed, on the basis of assumptions of the presence of radioactive potassium K^{40} in the core (ref. 9).

The effectiveness of thermal sources in any mechanism of generation of the magnetic field has been assumed to be low, because of the low efficiency of thermal machines. According to one hypothesis (ref. 5), the processes of differentiation of material indicated by Urey and Verhoogen are actually involved in the generation of the magnetic field, but only because of the gravitational energy released during these processes. Convection in the core is caused by direct upwelling of impurities of light silicon, accompanying the process of crystallization and sinking of heavy iron.

The hypothesis of the gravitational nature of the "motor" driving the Earth's dynamo encounters great difficulties in light of current hypotheses of the nonhomogeneous formation of the planets (refs. 10 and 11). As concerns thermal sources, their role is at least as great in the creation of the necessary conductivity and viscosity in the core.

Malkus suggested that the precession of the Earth was the motive force of the magnetic dynamo. The precession of the planets is caused by the action of the gravitational fields of the Sun and other celestial bodies on the equatorial bulge of the rotating planets. The presence of precession, at an angular velocity Ω, results in an additional angular acceleration $\Omega = [\Omega \times \omega]$ and an additional inertial force $F_\eta = -\rho[\bar{\Omega} \times \bar{\omega}] \times \bar{r}$. Malkus called this the Poincaré force, after the man who first solved analytically the problem of the motion of a fluid in a precessing spheroidal container. The experiments performed by Malkus showed that with certain relationships of $\bar{\omega}$ and $\bar{\Omega}$ in the precessing liquid, turbulent flow arises, which is not predicted by classical theory.

The rate of precession of the planet is directly proportional to its dynamic flattening, and independent of its radius and mass. Since the core and mantle of the Earth have somewhat differing dynamic flattening, the gravity fields of the Sun and the Moon create different torques on the core and mantle, causing stress both in the core and in the mantle, which tend to equalize the rates of the two precessions. These stresses act on the liquid in the core, leading to the motion necessary for the operation of the dynamo. In the final analysis, the energy of the magnetic dynamo is taken from the kinetic energy in the Earth's rotation.

The details of the precessional mechanism generating the magnetic field have not been worked out. There are contradictory opinions concerning its effectiveness. Braginskiy (ref. 12) turned his attention to the fact that the speed of the liquid under the influence of the Poincaré force fluctuates with the frequency of the main rotation ω and therefore cannot directly influence slow processes in the dynamo. On the other hand Dolginov (ref. 13) notes that the precession of a liquid in a nonspherical envelope results in the appearance of flows of a spiral nature that are similar to tidal flows. Flows of a spiral nature facilitate the generation of magnetic fields (ref. 14).

At the present time, the magnetic fields of the Earth, Venus, Mars, Jupiter, and Mercury have been studied. For the first four planets, certain models of the internal structure are known (refs. 15–20), as well as the parameters of rotation and dynamic flattening (refs. 21 and 22), and magnetic fields (refs. 23–27).

This paper presents a model and results of a test of the effectiveness of the mechanism of the precessional dynamo in the generation of the magnetic fields of the Earth, Mars, and Jupiter. Furthermore, conditions are studied under which the magnetic states of Venus and Mercury can be explained, on the basis of the hypothesis of precession as the motive force of the planetary dynamo.

The approach is based on the following assumptions:

1. The processes of generation of the field in the planets are similar in terms of modeling and are determined by a number of dimensionless parameters.
2. The magnetic fields are proportional to the volumes of the liquid cores of the planets (ref. 28).
3. The rates of convection of matter are proportional to the Poincaré force F_η

$\sim [\bar{\omega} \times \bar{\Omega}] \times \bar{r}$, where ω is the angular velocity of rotation, and Ω is the angular velocity of precession.

4. Under these conditions, a simple dependence between the dipole fields of two planets 1 and 2 is assumed to exist:

$$\gamma_{1\text{-}2} \sim \frac{V_1}{V_2} \cdot \frac{T_2}{T_1} \cdot \frac{\Omega_1}{\Omega_2} \cdot \frac{\sin \alpha_1}{\sin \alpha_2}, \quad (1)$$

where γ is the ratio of the dipole fields $\frac{H_{01}}{H_{02}}$ on the surface at the magnetic equator; α is the angle between vectors ω and Ω; V is the volume of the liquid core, and T the rotation period. Volume V_1 is the liquid core of the Earth, and is assumed known (ref. 19).

Earth, Mars, Jupiter

We present below the values of the parameters T, Ω, α, and H_0 of three rapidly rotating planets.

Formula (1) has one unknown, V_2, the volume of the liquid core of the second planet. The dimensions of the core of Mars have been very approximately determined. The measured values of radius, mass, and moment of inertia are satisfied in various models with significantly differing core dimensions R_c. In the model of Kozlovskaya (ref. 15), $R_c = 960$ km; in the model of Ringwood (ref. 16), $R_{c_{ext}} = 1720$ km and $R_{c_{int}} = 1510$ km; in the model of Binder and Davis (ref. 17), $R_c = 1250$ km; in the model of Anderson (ref. 18), $R_c = 1350$ km; and in the model of Johnston and Toksöz (ref. 19), $R_c = 1300$ km. The ratios of volumes of the cores of the Earth and Mars which they obtain are 45, 26, 20, 16, and 18, respectively.

The dimensions of the magnetically active area of Jupiter are determined primarily by the depth at which hydrogen is converted to the metallic state. According to Zharkov et al. (ref. 19), this occurs at depths of $r/R_J = 0.8$. The magnetically active area apparently begins at a point ranging from $r/R_J = 0.7$ to $r/R_J = 0.15$. The volume of the magnetically active area of Jupiter, with these dimensions, exceeds the volume of the liquid core of the Earth by some 1600 times. Now, formula (1) and the data of table 1 lead to the following values of calculated and measured field strength ratios between the Earth and Mars ($\gamma_{e\text{-}m}$ using the various models), Jupiter and Earth ($\gamma_{j\text{-}e}$); $\gamma_{e\text{-}m} =$ 315, 180, 140, 110, and 130, respectively, while measured $\gamma_{e\text{-}m} = 470$. Calculated $\gamma_{j\text{-}e} = 22$, while measured $\gamma_{j\text{-}e} = 13$.

We note the moderately good degree to which the measured and calculated values of dipole field ratios of the three rapidly rotating planets agree with this tremendous difference in volumes and fields.

Venus

The planet Venus apparently does not have a magnetic field of its own which exceeds 10 gammas (refs. 24 and 27). It is natural to expect that formula (1) will take note of this fact with some accuracy. According to the data from the trajectory measurements on Mariner 5 and radar studies of the planet, the radius of Venus $R_V = 6052.5 \pm 2.5$ km (ref. 29).

The period of rotation, as determined by Dyce et al. (ref. 30), is 245.1 ± 0.7 days; according to the data of Carpenter (ref. 31), it is $\sim 243 \pm 1$ days.

The inclination of the axis of rotation relative to the pole of the orbit, according to Dyce et al. (ref. 30), is $\sim 3.3 \pm 0.4°$; according to Carpenter (ref. 31), $\sim 2.2°$. Trajectory measurements of Mariner 5 (ref. 32)

Table 1.—*Parameters of Rapidly Rotating Planets*

	T	Ω	α	H_0, gammas
Earth	23h 56m 04s	50.25 ″/yr	23.5°	30 000
Mars	24h 37m 23s	7.40 ″/yr	23.2°	64
Jupiter	9h 50m 56s	2.34 ″/yr	3°	400 000

have been used to estimate the degree of dynamic flattening $f = 1/100$ of this terrestrial planet. This value has been confirmed by the data from Mariner 10 ($f = 1/30\,000$). The precession of Venus results from the influence of the dipole gravitational field of the Sun. The rate of presession of Venus, with $f = 1/30\,000$, is $\Omega_v = 122''$/yr. We can further assume that the volume of the liquid core of Venus is equal to or only slightly less than the volume of the liquid core of Earth (ref. 20). Then formula (1) gives us, with $\alpha = 2.2°$ and $3.3°$, a field intensity $H_0 \leq 20$–30 gammas in comparison with the terrestrial magnetic field.

Thus, proceeding from formula (1), there is no need to postulate any difference in the internal structure of Venus from that of Earth, except on the basis of the fact that it has no significant magnetic field (refs. 33 and 34).

Mercury

For Mercury, data on most of the parameters included in formula (1) are quite indefinite. Nevertheless, there is reason to use (1) to estimate the limits of dynamic flattening of the planet Mercury. The flight of Mariner 10 produced new experimental data on the parameters of rotation and, we can hope, in the near future it will be possible to compare results and take into consideration the new experimental results.

For the value of the dipole magnetic field, assuming that it is intrinsic to the planet (ref. 26), there are at present two values available: 227 gammas and 380 gammas. The first of these values corresponds to the theoretical dipole, somewhat inclined to the axis of rotation and displaced from the center by 0.47 km, to achieve best agreement with the experimental data. The second value is produced from the data of the gasdynamic model of solar wind flow around the planet. The shock front was intersected in this experiment at an angle of $\sim 110°$ with respect to the direction to the Sun.

It is now generally accepted that Mercury rotates with a period of 58 days. For the angle of inclination of the axis of rotation to the plane of the orbit, widely different values have been given. According to radar data (ref. 30), an angle of $\alpha \simeq 28°$ is given. According to terrestrial photographs of Mercury (ref. 35), the axis of rotation is perpendicular to the plane of the orbit with an accuracy of $\sim 3°$. It is assumed (ref. 26) that the axis of the dipole makes an angle of $80 \pm 10°$ with the plane of the ecliptic. The orbital plane of Mercury makes an angle of $\sim 7°$ with the plane of the ecliptic.

Studies of the internal structure of Mercury, based on determinations of mass and radius, lead to comparatively large dimensions for the core of Mercury. Plageman (ref. 36) indicates $R_c = 2112$ km, and Kozlovskaya (ref. 37) indicates $R_c = 1730$ km.

With the existing uncertainties of most parameters, there is reason to take certain arbitrary parameters and estimate from them, the order of magnitude of a quite unknown quantity, the dynamic flattening. Let us take $H_0 = 250$ gammas, $R_c = 1800$ km, $\alpha = 20°$. Then, comparing with the Earth, from formula (1) we can estimate the rate of precession of Mercury: $\Omega_{\text{Merc}} = 190''$/yr. The dynamic flattening of Mercury f_{Merc} can be estimated by comparing the rate of precession of Mars and Mercury, since both planets precess under the influence of the gravitational field of the Sun.

$$f_{\text{Merc}} = \frac{R^3\sigma}{R^3_{\text{Merc}}} \cdot \frac{T\sigma}{T_{\text{Merc}}} \cdot \frac{\Omega_{\text{Merc}}}{\Omega\sigma} \cdot f\sigma$$

Then where

$H_0 = 250$ gammas, $f_{\text{Merc}} = 5.7 \cdot 10^{-5}$
$H_0 = 380$ gammas, $f_{\text{Merc}} = 8.3 \cdot 10^{-5}$

These values are somewhat greater than those for the dynamic flattening of Venus.

Thus, even with the current uncertainty for a number of parameters of Mercury, formula (1) indicates that the fact of the existence of a magnetic field of Mercury (ref. 26) is not too surprising.

Correspondence of the Dynamo Model

1. In the theory of the terrestrial dynamo, the inclination of the axis of the dipole is not

considered to be a chance phenomenon, but rather a fact directly related to the mechanism of generation of the field (ref. 12).

Paleomagnetologists, on the other hand, consider the current orientation of the magnetic dipole to be a brief (in the geological scale) deviation from the position of symmetry (ref. 38).

The magnetic dipoles of Jupiter, Mars, and—apparently—Mercury, are inclined in relation to their axes of rotation. Furthermore, for Jupiter, as for Earth, the dipole is eccentric. The eccentricity of the dipole appears to be particularly great for Mercury.

2. Mercury, Earth, Mars, and Jupiter have direct rotation. However, the polarity of the magnetic fields of Mars and Jupiter is the reverse of the polarity of the current fields of Earth and Mercury. In kinematic models of the terrestrial dynamo, the sign of the field is not directly related to the direction of rotation, and the possibility of field reversals is explained by the action of instabilities in the mechanism of generation. The possible relationship of terrestrial field reversals with precession of its axis has been indicated by (ref. 39).

Experiments in the third decade of the space age should clarify the degree of regularity of the connections revealed between the planets' parameters of rotation, their structure, and their magnetic fields.

References

1. BRAGINSKIY, S. I., *Izvestiya AN SSSR, Fizika Zemli*, No. 10, 1972.
2. Origin of the Geomagnetic Field in World Magnetic Survey 1957–1969. *JACA Bulletin*, No. 28, 1971.
3. UREY, H. C., *The Planets*. Yale Univ. Press, 1952.
4. VERHOOGEN, J., *Geophys. J. R.A.S.*, Vol. 4, No. 276, 1961.
5. BRAGINSKIY, S. I., *Geomagnetizm I Aeronomiya*, Vol. 4, No. 5, 1964.
6. MALKUS, W. V. R., *J. Geophys. Res.*, No. 68, 1963, p. 2871.
7. MALKUS, W. V. R., *Science*, Vol. 160, No. 3825, 1968.
8. KENNEDY, G. G., AND G. H. HIGGINS, *The Moon*, Vol. 7, Nos. 1 and 2, 1973.
9. VERHOOGEN, J., *Phys. Earth Planet. Interiors*, No. 7, 1973, pp. 47–58.
10. TUREKIAN, K. K., AND S. P. CLARK, *Earth Planet. Sci. Letters*, No. 6, 1969, p. 346.
11. VINOGRADOV, A. P., *International Geochemical Congress*, 1971 Collection, Vol. 1.
12. BRAGINSKIY, S. I., *Geomagnetizm i Aeronomiya*, Vol. 4, No. 4, 1964.
13. DOLGINOV, A. Z., *Astron. Zhurn.* Vol. 51, No. 2, 1974.
14. LILLEY, F. E., *Pros. Rou. Soc.*, A. 316, No. 525, 1970, p. 153.
15. KOZLOVSKAYA, S. V., *Izvestiya AN SSSR, Fizika Zemli*, No. 7, 1972.
16. RINGWOOD, A. E., AND S. P. CLARK, *Nature*, Vol. 234, No. 5324, 1971.
17. BINDER, A. B., AND DAVIS, *Phys. Earth Planet. Interiors*, Vol. 7, 1973, p. 477.
18. ANDERSON, D. L., *Comments on Earth Sci. Geophys.*, Vol. 1, No. 5, 1971.
19. JOHNSTON, D. H., T. R. MCGETCHIN, AND M. F. TOKSÖZ, *Preprint*, April, 1974.
20. ZHARKOV, V. N., V. P. TRUBITSIN AND L. V. SAMSONENKO, *Fizika Zemli i Planet*, 1971, p. 383.
21. LORELL, J., et al., *Icarus*, Vol. 28, No. 2, 1973, p. 304.
22. KOVALEVSKY, J., *Surface and Interiors of Planets and Satellites*, 1970.
23. DOLGINOV, SH. SH., YE. G. EROSHENKO, AND L. N. ZHUZGOV, *DAN SSSR*, Vol. 207, No. 6, 1972. DAN, 1974. (In press).
24. DOLGINOV, SH. SH., YE. G. EROSHENKO, AND L. N. ZHUZGOV, *Kosmich. Issled.*, 1967.
25. SMITH, E. J., L. J. DAVIS, D. E. JONES, D. S. COLBURN, P. J. COLEMAN, P. DYAL, AND C. P. SONETT, *Science*, Vol. 183, 1974, p. 305.
26. NESS, N. F., K. W. BEHANNON, R. P. LEPPING, Y. C. WHANG, AND K. H. SCHATTEN, *Science*, 1974. In press.
27. NESS, N. F., K. W. BEHANNON, R. P. LEPPING, Y. C. WHANG, AND K. H. SCHATTEN, *Science*, Vol. 183, 1974, p. 1301.
28. KERN, J. W., AND E. H. VESTINE, *Space Science Reviews*, 1963, p. 136.
29. ANDERSON, J. D., *J. Atmosph. Sci.*, Vol. 25, No. 6, 1968.
30. DYCE, R. B., G. H. PETTENGILL, AND I. SHAPIRO, *Astron. Zhurn.* Vol. 72, No. 3, 1967, p. 371.
31. CARPENTER, R. L., *Astron. Zhurn.* Vol. 71, No. 9, 1966.
32. ANDERSON, J. D., L. EFRON, AND G. E. PEASE, *Astron. Zhurn.*, Vol. 73, No. 10, Part 2, 1968.
33. HENDERVARI, P., *Observatory 86*, No. 953, 1966.
34. RUNCORN, S. K., *Geophys, J. Roy. Astron. Soc.*, Vol. 15, Nos. 1 and 2, 1968.
35. MURRAY, J. B., A. DOLLFUS, AND B. SMITH, *Icarus*, Vol. 17, No. 3, 1972.
36. PLAGEMAN, S., *J. Geophys. Res.*, Vol. 70, No. 4, 1965.

37. KOZLOVSKAYA, S. V., Physics of the Moon and Planets, International Symposium, October 15–22, 1968, Kiev, 1972.
38. STACY, *Fizika Zemli*, 1972.
39. KALININ, YU. D., *IFSO Preprint*, 2 F, 1972.

The Intensity of the Ancient Lunar Field From Magnetic Studies on Lunar Samples

A. Stephenson, D. W. Collinson, and S. K. Runcorn
Department of Geophysics and Planetary Physics
School of Physics,
The University, Newcastle-upon-Tyne, England

Palaeointensity determinations on Apollo 11, 16, and 17 rocks have indicated that from 3.9 to 4.0 AE ago the strength of the surface lunar magnetic field was about 1.3 Oe, while there is evidence from younger rocks that a field of about one quarter of this value was present at a later time (3.6 AE).

One of the objectives of magnetic studies on lunar samples is the determination of the intensity of the ancient lunar field present when the rocks were formed. Rocks containing hard components of magnetization have been found by many investigators, suggesting that this is a primary magnetization acquired at the time of formation; but estimates of the strength of the field which was present have been relatively few in number (refs. 1–4).

The usual method for estimating palaeointensities is by using the Thellier method, which involves a comparison of the natural remanent magnetization (NRM) lost by thermal demagnetization and the partial thermoremanent magnetization (PTRM) gained in a known field in the same temperature interval. A further method which can be used to estimate palaeointensities is one using anhysteretic remanent magnetization (ARM). The way in which this has been used here is similar to the Thellier method except that field replaces temperature. Thus the NRM lost by alternating field (AF) demagnetization is compared with the ARM gained in a known direct field for various values of peak alternating field. Provided that the coercivity spectrum of ARM is the same as TRM (and that the NRM is a TRM) and if the ratio f′ of the relative strengths of TRM to ARM acquired in the same direct field is known, the ancient lunar field can be estimated.

To enable the same tumbling system to be used for alternating field demagnetization and for building up ARM, a perspex holder was used to provide the unidirectional field. The holder contained a fixed magnet system into which the sample fitted. This was then placed in the tumbling system within the demagnetizing coil, the coercivity of the magnets being high enough to be unaffected by the maximum peak demagnetizing field (1360 Oe). The unidirectional field was originally 4 Oe, but was later reduced to 1.8 Oe to reduce nonlinearities between ARM and direct field. A fuller description of the method is given in another paper (Ref. 5) together with the determination of the factor f′ from TRM measurements on a synthetic multidomain iron sample and Apollo 11 basalt sample 10050,33. These gave values for f′ of 1.28 and 1.40, respectively, an average value of 1.34 being used in the palaeointensity determinations.

The factor f′ may theoretically have any value greater than unity and thus it is possible that values significantly different from 1.3 may occur in some samples. However, provided that a significant fraction of the NRM is carried by grains with blocking

temperatures less than about 670° C (ref. 5), f′ is expected to be within a few tens of percent of the above value. A direct determination of f′ from the thermal demagnetization curve of the NRM of 62235 yielded a value of about 1.3 in agreement with the expected value.

Results

Figure 1 shows the result of a determination on 62235,53 by the Thellier method in an applied field of 0.5 Oe. The necessary heating was carried out in a continuously pumped enclosure to minimize the effects of oxidation, and from the slope of the graph the ancient field intensity is 1.2 Oe (ref. 3). Using the ARM method (fig. 2) where the NRM lost up to a particular field value is plotted against the ARM gained in the same peak field, gives a palaeofield h_p of 1.4 Oe (i.e., $h_p = \frac{\text{slope}}{1.34} \times h_A$) where h_A is the applied direct field (in this case 1.8 Oe). The initial nonlinearity between NRM and ARM may be explained by partial demagnetization of the NRM by solar heating during the lunar day, and this is consistent with the virtually constant direction obtained (fig. 3) during the AF demagnetization of the major part of

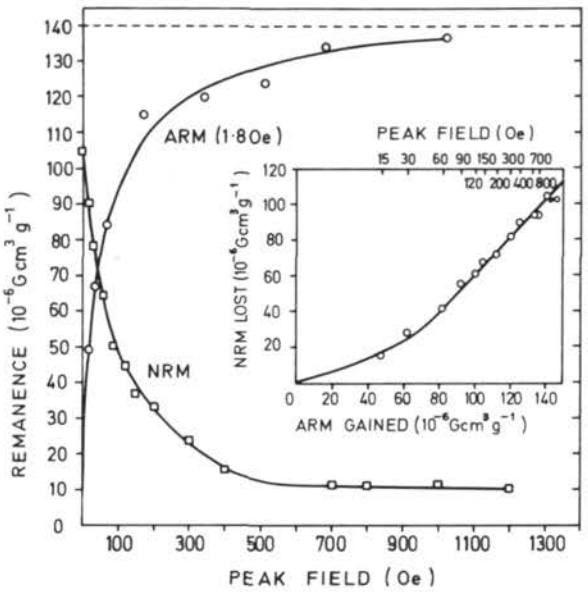


Figure 2.—*Determination of palaeointensity (1.4 Oe) on sample 62235,53 by ARM method.*

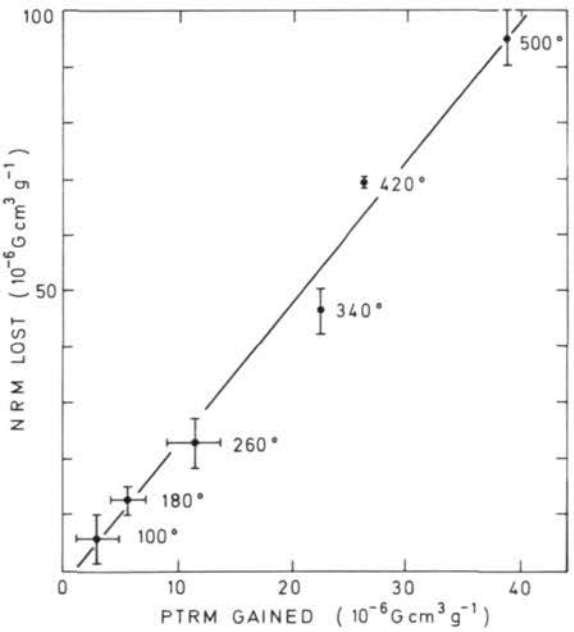


Figure 1.—*Determination of palaeointensity (1.2 Oe) on sample 62235,53 by Thellier method.*

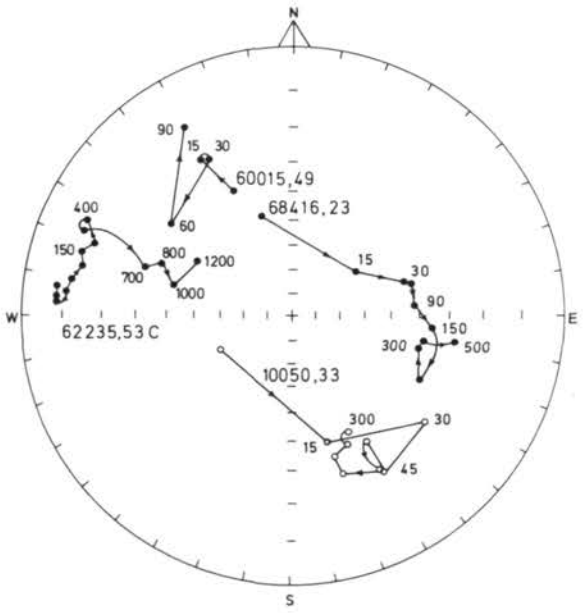


Figure 3.—*Direction changes of the NRM of samples during AF demagnetization. Peak field values are indicated.*

the remanence. These two determinations by different methods suggest very strongly that the NRM is of thermoremanent origin and was acquired in a surface field of about 1.3 Oe at 3.9 AE, this being the time at which this KREEP basalt crystallized (ref. 6).

Further evidence for a surface field of this magnitude at this time comes from a field determination using ARM on sample 68416,23, which is a gabbroic anorthosite. The result (fig. 4) clearly indicates that two components approximately opposed to one another are present in this rock, since on initial demagnetization of the NRM an increase in intensity is observed. If it is assumed that the primary component is the harder of the two, then since a straight line is obtained in the NRM–ARM plot above a peak demagnetizing field of 150 Oe, it appears that this slope (which yields a palaeointensity of about 1.2 Oe) must represent this component. This interpretation is also consistent with the observation that the direction remains constant above 150 Oe (fig. 3). Evidence that the moderately hard secondary component almost opposed to the primary may be a partial TRM acquired on subsequent heating to a temperature less than the Curie point of iron (770° C) comes from studies of the thermal history of the rock. It has been found that while the crystallization age of

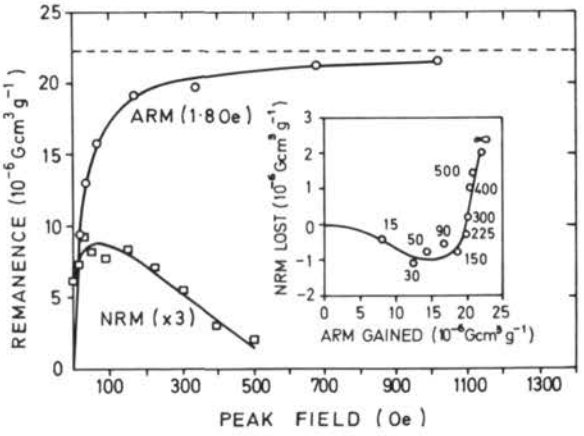


Figure 4.—*Determination of palaeointensity (1.2 Oe) on primary component of sample 68416,23 by ARM method.*

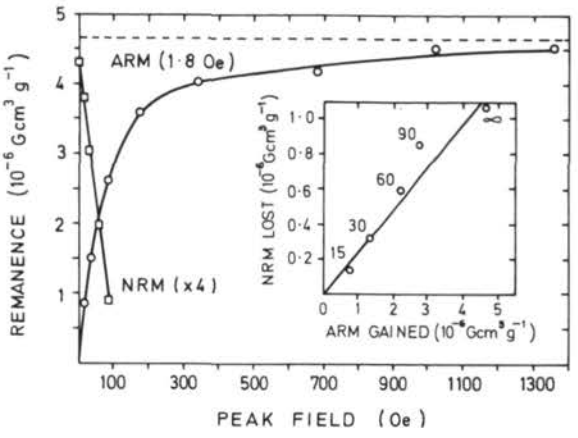


Figure 5.—*Determination of palaeointensity (0.33 Oe) on sample 60015,49 by ARM method.*

the rock is 4.0 AE (ref. 7), secondary reheating has taken place some 150 My after its formation (ref. 8). This suggests that at this later time a field which was comparable to 1.2 Oe must have been present, and that either the field or the rock must then have been in almost reverse orientation. The palaeointensity of 1.2 Oe determined from the primary component (4.0 AE) is very similar to the 1.3 Oe average field determined from 62235,53 above (3.9 AE).

A determination using ARM on an anorthosite sample 60015 yielded a paleointensity of 0.33 Oe. Although this was based only on an initial demagnetizing curve up to 90 Oe peak field (fig. 5), there was no change in direction during this procedure and the extrapolated total loss of magnetization at infinite field also lay on the slope of the NRM-lost-ARM-gained plot. This means that the NRM is indistinguishable from TRM. The age of this sample is 3.58 AE (ref. 9).

A determination on an Apollo 11 basalt sample 10050,33 yielded a field of 0.38 Oe after removal of a large secondary component (fig. 6). Direction changes on demagnetization also support this interpretation. This sample is probably of similar age to 10057, which is a basalt of age 3.63 AE (ref. 10) and which gave a tentative field value of 0.14 Oe.

Other samples which for various reasons did not yield satisfactory results (ref. 11)

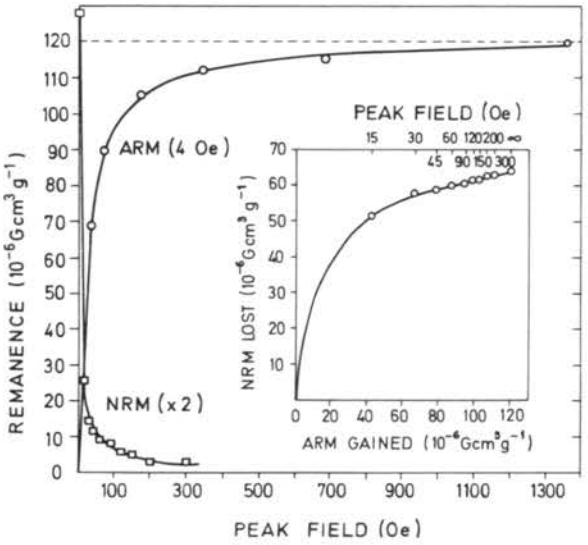


Figure 6.—*Determination of palaeoinstensity (0.38 Oe) on sample 10050,33 after removal of large secondary component.*

were 76315 and 77035. Another two samples which gave results of doubtful validity were 70215 and 70017. Although little confidence could be placed in the results, the samples gave very similar palaeointensity values by two different methods. Sample 70017,78 gave 0.5 ± 0.2 Oe by the Thellier method, and 0.3 Oe with the use of ARM. Sample 70215,45 gave a field of 0.04 Oe to within a factor of 2 by the Thellier method compared with 0.06 Oe with the use of ARM.

Conclusion

There is strong evidence from these results that some 4.0 AE ago the surface field was as high as 1.3 Oe and that at 3.6 AE it was somewhat less than this. Whether this apparent decrease occurred gradually or whether it was part of more random variations is a question which at present cannot be answered. The presence of a strong field does, however, have important implications regarding lunar history.

If a convecting lunar core was responsible for the field, then in terms of the magnetic moment per unit volume of core, the lunar core would have to be much more efficient than that of the Earth, assuming that a lunar core cannot exceed about one-fifth of the lunar radius. Permanent magnetization of the Moon acquired in some way during the formation process could not lead to such a high surface field unless the concentration of iron increases considerably toward the center, since to produce 1.3 Oe at the surface, the average magnetization of the Moon would exceed the saturation remanent magnetization of typical lunar basalts.

It is clear that further plaeointensity studies on lunar samples are necessary to evaluate the behavior of the ancient lunar field with time.

References

1. Helsley, C. E., Magnetic Properties of Lunar 10022, 10069, 10084 and 10085 Samples. *Proc. Apollo 11 Lunar Sci. Conference, Geochimica et Cosmochimica Acta*, Supplement 1, Vol. 3, 1970, pp. 2213–2219.
2. Gose, W. A., D. W. Strangway, and G. W. Pearce, A Determination of the Intensity of the Ancient Lunar Magnetic Field. *The Moon*, Vol. 7, 1973, pp. 198–201.
3. Collinson, D. W., A. Stephenson, and S. K. Runcorn, Magnetic Properties of Apollo 15 and 16 Rocks. *Proc. Fourth Lunar Science Conference, Geochimica et Cosmochimica Acta*, Supplement 4, Vol. 3, 1973, pp. 2963–2976.
4. Fuller, M., Lunar Magnetism. *Rev. Geophysics & Space Physics*, Vol. 12, 1974, pp. 23–70.
5. Stephenson, A., and D. W. Collinson, Lunar Magnetic Field Palaeointensities Determined by an Anhysteretic Remanent Magnetization Method. *Earth Planet. Sci. Letters*, in press, 1974.
6. Nyquist, L. E., N. J. Hubbard, P. W. Gast, B. M. Bansal, H. Wiesmann, and B. Jahn, Rb-Sr Systematics for Chemically Defined Apollo 15 and 16 Materials. *Proc. Fourth Lunar Science Conference, Geochimica et Cosmochimica Acta*, Supplement 4, Vol. 2, 1973, pp. 1823–1846.
7. Kirsten, T., P. Horn, and J. Kiko, ^{39}Ar-^{40}Ar Dating and Rare Gas Analysis of Apollo 16 Rocks and Soils. *Proc. Fourth Lunar Sci. Conference, Geochimica et Cosmochimica Acta*, Supplement 4, Vol. 2, 1973, pp. 1757–1784.
8. Huneke, J. C., E. K. Jessberger, F. A. Podesek, and G. J. Wasserburg, ^{40}Ar/^{39}Ar Measurements in Apollo 16 and 17 Samples and the Chronology of Metamorphic and Volcanic Ac-

tivity in the Taurus-Littrow Region. *Proc. Fourth Lunar Science Conference, Geochimica et Cosmochimica Acta*, Supplement 4, Vol. 2, 1973, pp. 1725–1756.

9. TATSUMOTO, M., P. D. NUNES, AND R. J. KNIGHT, U-Th-Pb Systematics of Some Apollo 16 Samples. In *Lunar Science IV*, J. W. Chamberlain and C. Watkins, eds., Lunar Science Institute, Houston, 1973, pp. 705–707.
10. PAPANASTASSIOU, D. A., G. J. WASSERBURG, AND D. S. BURNETT, Rb-Sr Ages of Lunar Rocks From the Sea of Tranquility. *Earth Planet. Sci. Letters*, Vol. 8, 1970, pp. 1–19.
11. STEPHENSON, A., D. W. COLLINSON, AND S. K. RUNCORN, Lunar Magnetic Field Palaeointensity Determinations on Apollo 11, 16 and 17 Rocks. *Proc. Fifth Lunar Science Conference, Geochimica et Cosmochimica Acta*, in press, 1974.

☆ U.S. GOVERNMENT PRINTING OFFICE: 1977 O—592–572